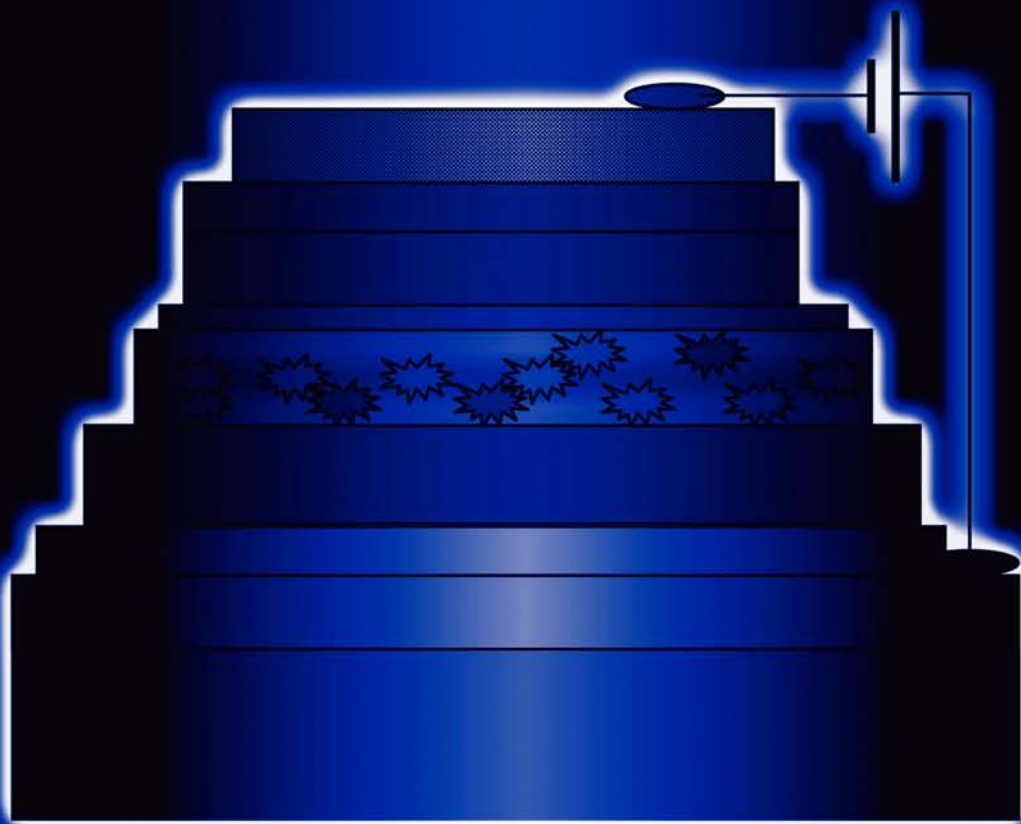


Organic Light-Emitting Materials and Devices



Edited by
Zhigang Li
Hong Meng



Taylor & Francis
Taylor & Francis Group

Organic Light-Emitting Materials and Devices

OPTICAL SCIENCE AND ENGINEERING

Founding Editor

Brian J. Thompson

University of Rochester

Rochester, New York

1. Electron and Ion Microscopy and Microanalysis: Principles and Applications, *Lawrence E. Murr*
2. Acousto-Optic Signal Processing: Theory and Implementation, *edited by Norman J. Berg and John N. Lee*
3. Electro-Optic and Acousto-Optic Scanning and Deflection, *Milton Gottlieb, Clive L. M. Ireland, and John Martin Ley*
4. Single-Mode Fiber Optics: Principles and Applications, *Luc B. Jeunhomme*
5. Pulse Code Formats for Fiber Optical Data Communication: Basic Principles and Applications, *David J. Morris*
6. Optical Materials: An Introduction to Selection and Application, *Solomon Musikant*
7. Infrared Methods for Gaseous Measurements: Theory and Practice, *edited by Joda Wormhoudt*
8. Laser Beam Scanning: Opto-Mechanical Devices, Systems, and Data Storage Optics, *edited by Gerald F. Marshall*
9. Opto-Mechanical Systems Design, *Paul R. Yoder, Jr.*
10. Optical Fiber Splices and Connectors: Theory and Methods, *Calvin M. Miller with Stephen C. Mettler and Ian A. White*
11. Laser Spectroscopy and Its Applications, *edited by Leon J. Radziemski, Richard W. Solarz, and Jeffrey A. Paisner*
12. Infrared Optoelectronics: Devices and Applications, *William Nunley and J. Scott Bechtel*
13. Integrated Optical Circuits and Components: Design and Applications, *edited by Lynn D. Hutcheson*
14. Handbook of Molecular Lasers, *edited by Peter K. Cheo*
15. Handbook of Optical Fibers and Cables, *Hiroshi Murata*
16. Acousto-Optics, *Adrian Korpel*
17. Procedures in Applied Optics, *John Strong*
18. Handbook of Solid-State Lasers, *edited by Peter K. Cheo*
19. Optical Computing: Digital and Symbolic, *edited by Raymond Arrathoon*
20. Laser Applications in Physical Chemistry, *edited by D. K. Evans*
21. Laser-Induced Plasmas and Applications, *edited by Leon J. Radziemski and David A. Cremers*
22. Infrared Technology Fundamentals, *Irving J. Spiro and Monroe Schlessinger*
23. Single-Mode Fiber Optics: Principles and Applications, Second Edition, Revised and Expanded, *Luc B. Jeunhomme*
24. Image Analysis Applications, *edited by Rangachar Kasturi and Mohan M. Trivedi*
25. Photoconductivity: Art, Science, and Technology, *N. V. Joshi*
26. Principles of Optical Circuit Engineering, *Mark A. Mentzer*
27. Lens Design, *Milton Laikin*

28. Optical Components, Systems, and Measurement Techniques, *Rajpal S. Sirohi and M. P. Kothiyal*
29. Electron and Ion Microscopy and Microanalysis: Principles and Applications, Second Edition, Revised and Expanded, *Lawrence E. Murr*
30. Handbook of Infrared Optical Materials, *edited by Paul Klocek*
31. Optical Scanning, *edited by Gerald F. Marshall*
32. Polymers for Lightwave and Integrated Optics: Technology and Applications, *edited by Lawrence A. Hornak*
33. Electro-Optical Displays, *edited by Mohammad A. Karim*
34. Mathematical Morphology in Image Processing, *edited by Edward R. Dougherty*
35. Opto-Mechanical Systems Design: Second Edition, Revised and Expanded, *Paul R. Yoder, Jr.*
36. Polarized Light: Fundamentals and Applications, *Edward Collett*
37. Rare Earth Doped Fiber Lasers and Amplifiers, *edited by Michel J. F. Digonnet*
38. Speckle Metrology, *edited by Rajpal S. Sirohi*
39. Organic Photoreceptors for Imaging Systems, *Paul M. Borsenberger and David S. Weiss*
40. Photonic Switching and Interconnects, *edited by Abdellatif Marrakchi*
41. Design and Fabrication of Acousto-Optic Devices, *edited by Akis P. Goutzoulis and Dennis R. Pape*
42. Digital Image Processing Methods, *edited by Edward R. Dougherty*
43. Visual Science and Engineering: Models and Applications, *edited by D. H. Kelly*
44. Handbook of Lens Design, *Daniel Malacara and Zacarias Malacara*
45. Photonic Devices and Systems, *edited by Robert G. Hunsberger*
46. Infrared Technology Fundamentals: Second Edition, Revised and Expanded, *edited by Monroe Schlessinger*
47. Spatial Light Modulator Technology: Materials, Devices, and Applications, *edited by Uzi Efron*
48. Lens Design: Second Edition, Revised and Expanded, *Milton Laikin*
49. Thin Films for Optical Systems, *edited by Francoise R. Flory*
50. Tunable Laser Applications, *edited by F. J. Duarte*
51. Acousto-Optic Signal Processing: Theory and Implementation, Second Edition, *edited by Norman J. Berg and John M. Pellegrino*
52. Handbook of Nonlinear Optics, *Richard L. Sutherland*
53. Handbook of Optical Fibers and Cables: Second Edition, *Hiroshi Murata*
54. Optical Storage and Retrieval: Memory, Neural Networks, and Fractals, *edited by Francis T. S. Yu and Suganda Jutamulia*
55. Devices for Optoelectronics, *Wallace B. Leigh*
56. Practical Design and Production of Optical Thin Films, *Ronald R. Willey*
57. Acousto-Optics: Second Edition, *Adrian Korpel*
58. Diffraction Gratings and Applications, *Erwin G. Loewen and Evgeny Popov*
59. Organic Photoreceptors for Xerography, *Paul M. Borsenberger and David S. Weiss*
60. Characterization Techniques and Tabulations for Organic Nonlinear Optical Materials, *edited by Mark G. Kuzyk and Carl W. Dirk*
61. Interferogram Analysis for Optical Testing, *Daniel Malacara, Manuel Servin, and Zacarias Malacara*
62. Computational Modeling of Vision: The Role of Combination, *William R. Uttal, Ramakrishna Kakarala, Spiram Dayanand, Thomas Shepherd, Jagadeesh Kalki, Charles F. Lunskis, Jr., and Ning Liu*
63. Microoptics Technology: Fabrication and Applications of Lens Arrays and Devices, *Nicholas Borrelli*
64. Visual Information Representation, Communication, and Image Processing, *edited by Chang Wen Chen and Ya-Qin Zhang*
65. Optical Methods of Measurement, *Rajpal S. Sirohi and F. S. Chau*

66. Integrated Optical Circuits and Components: Design and Applications, *edited by Edmond J. Murphy*
67. Adaptive Optics Engineering Handbook, *edited by Robert K. Tyson*
68. Entropy and Information Optics, *Francis T. S. Yu*
69. Computational Methods for Electromagnetic and Optical Systems, *John M. Jarem and Partha P. Banerjee*
70. Laser Beam Shaping, *Fred M. Dickey and Scott C. Holswade*
71. Rare-Earth-Doped Fiber Lasers and Amplifiers: Second Edition, Revised and Expanded, *edited by Michel J. F. Digonnet*
72. Lens Design: Third Edition, Revised and Expanded, *Milton Laikin*
73. Handbook of Optical Engineering, *edited by Daniel Malacara and Brian J. Thompson*
74. Handbook of Imaging Materials: Second Edition, Revised and Expanded, *edited by Arthur S. Diamond and David S. Weiss*
75. Handbook of Image Quality: Characterization and Prediction, *Brian W. Keelan*
76. Fiber Optic Sensors, *edited by Francis T. S. Yu and Shizhuo Yin*
77. Optical Switching/Networking and Computing for Multimedia Systems, *edited by Mohsen Guizani and Abdella Battou*
78. Image Recognition and Classification: Algorithms, Systems, and Applications, *edited by Bahram Javidi*
79. Practical Design and Production of Optical Thin Films: Second Edition, Revised and Expanded, *Ronald R. Willey*
80. Ultrafast Lasers: Technology and Applications, *edited by Martin E. Fermann, Almantas Galvanauskas, and Gregg Sucha*
81. Light Propagation in Periodic Media: Differential Theory and Design, *Michel Nevière and Evgeny Popov*
82. Handbook of Nonlinear Optics, Second Edition, Revised and Expanded, *Richard L. Sutherland*
83. Polarized Light: Second Edition, Revised and Expanded, *Dennis Goldstein*
84. Optical Remote Sensing: Science and Technology, *Walter Egan*
85. Handbook of Optical Design: Second Edition, *Daniel Malacara and Zacarias Malacara*
86. Nonlinear Optics: Theory, Numerical Modeling, and Applications, *Partha P. Banerjee*
87. Semiconductor and Metal Nanocrystals: Synthesis and Electronic and Optical Properties, *edited by Victor I. Klimov*
88. High-Performance Backbone Network Technology, *edited by Naoaki Yamanaka*
89. Semiconductor Laser Fundamentals, *Toshiaki Suhara*
90. Handbook of Optical and Laser Scanning, *edited by Gerald F. Marshall*
91. Organic Light-Emitting Diodes: Principles, Characteristics, and Processes, *Jan Kalinowski*
92. Micro-Optomechatronics, *Hiroshi Hosaka, Yoshitada Katagiri, Terunao Hirota, and Kiyoshi Itao*
93. Microoptics Technology: Second Edition, *Nicholas F. Borrelli*
94. Organic Electroluminescence, *edited by Zakya Kafafi*
95. Engineering Thin Films and Nanostructures with Ion Beams, *Emile Knystautas*
96. Interferogram Analysis for Optical Testing, Second Edition, *Daniel Malacara, Manuel Sercin, and Zacarias Malacara*
97. Laser Remote Sensing, *edited by Takashi Fujii and Tetsuo Fukuchi*
98. Passive Micro-Optical Alignment Methods, *edited by Robert A. Boudreau and Sharon M. Boudreau*
99. Organic Photovoltaics: Mechanism, Materials, and Devices, *edited by Sam-Shajing Sun and Niyazi Serdar Saracftci*
100. Handbook of Optical Interconnects, *edited by Shigeru Kawai*
101. GMPLS Technologies: Broadband Backbone Networks and Systems, *Naoaki Yamanaka, Kohei Shiimoto, and Eiji Oki*

102. Laser Beam Shaping Applications, *edited by Fred M. Dickey, Scott C. Holswade and David L. Shealy*
103. Electromagnetic Theory and Applications for Photonic Crystals, *Kiyotoshi Yasumoto*
104. Physics of Optoelectronics, *Michael A. Parker*
105. Opto-Mechanical Systems Design: Third Edition, *Paul R. Yoder, Jr.*
106. Color Desktop Printer Technology, *edited by Mitchell Rosen and Noboru Ohta*
107. Laser Safety Management, *Ken Barat*
108. Optics in Magnetic Multilayers and Nanostructures, *Štefan Višňovský*
109. Optical Inspection of Microsystems, *edited by Wolfgang Osten*
110. Applied Microphotonics, *edited by Wes R. Jamroz, Roman Kruzelecky, and Emile I. Haddad*
111. Organic Light-Emitting Materials and Devices, *edited by Zhigang Li and Hong Meng*
112. Silicon Nanoelectronics, *edited by Shunri Oda and David Ferry*
113. Image Sensors and Signal Processor for Digital Still Cameras, *Junichi Nakamura*
114. Encyclopedic Handbook of Integrated Circuits, *edited by Kenichi Iga and Yasuo Kokubun*
115. Quantum Communications and Cryptography, *edited by Alexander V. Sergienko*
116. Optical Code Division Multiple Access: Fundamentals and Applications, *edited by Paul R. Prucnal*

Organic Light-Emitting Materials and Devices

**Edited by
Zhigang Li
Hong Meng**



Taylor & Francis

Taylor & Francis Group

Boca Raton London New York

CRC is an imprint of the Taylor & Francis Group,
an informa business

CRC Press
Taylor & Francis Group
6000 Broken Sound Parkway NW, Suite 300
Boca Raton, FL 33487-2742

© 2007 by Taylor & Francis Group, LLC
CRC Press is an imprint of Taylor & Francis Group, an Informa business

No claim to original U.S. Government works
Printed in the United States of America on acid-free paper
10 9 8 7 6 5 4 3 2 1

International Standard Book Number-10: 1-57444-574-X (Hardcover)
International Standard Book Number-13: 978-1-57444-574-9 (Hardcover)

This book contains information obtained from authentic and highly regarded sources. Reprinted material is quoted with permission, and sources are indicated. A wide variety of references are listed. Reasonable efforts have been made to publish reliable data and information, but the author and the publisher cannot assume responsibility for the validity of all materials or for the consequences of their use.

No part of this book may be reprinted, reproduced, transmitted, or utilized in any form by any electronic, mechanical, or other means, now known or hereafter invented, including photocopying, microfilming, and recording, or in any information storage or retrieval system, without written permission from the publishers.

For permission to photocopy or use material electronically from this work, please access www.copyright.com (<http://www.copyright.com/>) or contact the Copyright Clearance Center, Inc. (CCC) 222 Rosewood Drive, Danvers, MA 01923, 978-750-8400. CCC is a not-for-profit organization that provides licenses and registration for a variety of users. For organizations that have been granted a photocopy license by the CCC, a separate system of payment has been arranged.

Trademark Notice: Product or corporate names may be trademarks or registered trademarks, and are used only for identification and explanation without intent to infringe.

Library of Congress Cataloging-in-Publication Data

Organic light-emitting materials and devices / Zhigang Li and Hong Meng.

p. cm. – (Optical science and engineering ; 111)

Includes bibliographical references and index.

ISBN 1-57444-574-X (alk. paper)

1. Light emitting diodes. 2. Polymers--Electric properties. 3. Electroluminescent devices--Materials.

I. Li, Zhigang R., 1958- II. Meng, Hong, 1966- III. Optical science and engineering (Boca Raton, Fla.) ; 110.

TK7871.89.L53O735 2006
621.3815'22--dc22

2006002545

Visit the Taylor & Francis Web site at
<http://www.taylorandfrancis.com>

and the CRC Press Web site at
<http://www.crcpress.com>

Preface

Organic light-emitting diodes (OLEDs) possess a number of advantages over conventional display devices, such as high brightness and contrast, high luminous efficiency, fast response time, wide viewing angle, low power consumption, and light weight. In addition, the new technologies offer the potential of low manufacturing cost. OLED displays can be fabricated on large area substrates (including flexible substrates) and offer a virtually unlimited choice of colors. The technological promise of these unique characteristics puts OLEDs at the forefront of research efforts of a number of government agencies, industries, and universities. Many major industrial electronics giants and many newcomers have invested heavily in OLED research and development. As a result, a stream of new OLED products has reached the marketplace and a number of large-scale manufacturing facilities are under construction. Though the field is growing rapidly and its impact is both pervasive and far-reaching, major challenges still remain, especially the lack of highly efficient, stable organic light-emitting materials, the insufficient operational lifetimes of the devices, and technical hurdles in large-scale manufacturing yields of the OLED displays. Overcoming these drawbacks will require further multidisciplinary studies.

In recent years, several books on related topics have provided the readers with essential information in the field of organic electroluminescence. However, none of these could serve as a comprehensive guide. Our aim is to provide readers with a single source of information covering all aspects of OLEDs, including the systematic investigation of organic light-emitting materials, device physics and engineering, and so on. In this spirit, we titled this book *Organic Light-Emitting Materials and Devices*, a compilation of the progress made in recent years and of the challenges facing the future development of OLED technology.

Eleven chapters by internationally recognized academic and industrial experts in their respective fields offer a broad perspective of interdisciplinary topics uniting organic materials synthesis with device physics and engineering. Chapter 1 introduces the history, fundamental physics, and potential applications of OLEDs. OLEDs can be divided into two categories: small molecule and polymer-based light emitting diodes (SMOLEDs and PLEDs). From the basic structure point of view, both devices employ multilayered architectures with anode, hole transporting, emissive and electron transporting layers, and cathodes. Developing high-efficiency OLEDs poses a great challenge for material scientists, requiring an understanding of the physics beyond device operation, and structure–property relationships to allow for new material design. From this perspective, Chapter 2 through Chapter 6 provide a comprehensive review of the synthesis, properties, and device performance of electroluminescent materials used in OLEDs. Chapter 2 deals with polymer light-emitting materials, subdivided into its most important classes: poly (*p*-phenylenevinylene)s (PPVs), polyfluorenes (PFs), polythiophenes (PTs), and other conjugated and nonconjugated electroluminescent polymers. It describes the progress and the current state of understanding of molecular design in the field, exemplifying over 600 light-emitting polymers, and highlighting the most efficient materials and devices. Chapter 3 reviews small molecules-based OLEDs, specifically describing hole and electron injection and transport materials, electron- and hole-blocking materials, sensitizers, and fluorescent and phosphorescent light emitters. Solution-processable phosphorescent polymer LEDs are described in Chapter 4, which starts with a brief discussion of the energy transfer processes. Chapter 5 depicts the progress of polarized OLEDs. Chapter 6 is dedicated to anode materials and focuses on novel transparent anode materials with a brief

review of other actively investigated anode materials used in transparent OLED devices. Chapter 7 and Chapter 8 provide readers with well structured information on two main manufacturing techniques employed in OLED fabrication: vapor deposition and printing processes. Chapter 9 describes the application of α -Si-based backplane technology for organic light-emitting displays. Chapter 10 describes microstructural characterization and performance measurement techniques currently used in the OLED field. Finally, Chapter 11 presents the patent statuses of the currently investigated organic light-emitting materials. The book includes numerous diagrams, device configurations, and molecular structures clearly illustrating the described ideas. Within space limitations, this book provides a comprehensive overview of the field and can serve as a primary reference source to those needing additional information in any particular subarea in organic electroluminescence. Furthermore, the described materials and principles of device physics have broad applications in other areas of organic electronics. A balance between the academic and industrial points of view is presented, enhanced by the diverse background of the contributing authors. This book should attract the attention of multidisciplinary researchers (e.g., materials scientists, synthetic chemists, solid-state physicists, electronic device engineers) and industrial managers and patent lawyers engaged in OLED-related business areas.

The successful birth of the book is attributed to the hard work of our author teams. We take this opportunity to thank all contributors for their excellent work. It is a great pleasure to acknowledge Dalen. E. Keys, Kurt L. Adams, Curtis R. Fincher, and Charles R. Ginnard for their strong support during editing of the book. Thanks also to our friends (D. Perepichka, Z. Bao, M. Zilch, Y. Bai, L. Zhong, Z. Cai, J. Yang, Q. Liang, J. Huang, W. Huang) and colleagues (F. Sun, M. Goldfinger, G. Johansson, C. DuBois) for their encouragement and help in various forms. We would like to thank Richard Dekker, the CEO of Marcel Dekker (acquired by CRC Press, now Taylor & Francis group, the current publisher), for his personal support of this project and the staff of CRC Press for helping to translate our ideas into this book. Finally, our hearts go out to our families for their continuous support and encouragement; this book would never have appeared if so many hours in last three years had not been stolen from them.

Editors

Zhigang-Rick Li is a research associate at DuPont Central Research and Development, Wilmington, Delaware. He is a member of the Microscopy Society of America, the author or coauthor of more than 70 professional publications and book chapters, and the editor of a book about the microstructural studies of materials. Dr. Li is the recipient of the Sino-France Abroad Study Awards (1982–1986) and the Kazato Research Foundation of Japan Award (1986).

Dr. Li earned a B.S. (1982) in optics from the Beijing Institute of Technology, China, and a Ph.D. in physics from the Laboratoire d'Optique Electronique du C.N.R.S., Toulouse, France. Since joining the DuPont Company, he has worked on many industrially important projects, including the research and development of new OLEDs. His main interest is to establish the relationship of the process conditions, microstructures, and performances of these devices.

Hong Meng is a research chemist in the Central Research and Development area at E.I. DuPont Company in Wilmington, Delaware. His research interests are design and synthesis of conjugated organic materials and their applications in organic electronics, particularly, organic thin film transistors, and organic light-emitting diodes. He has contributed to over 40 peer-reviewed journal articles, 25 conference papers, 4 book chapters, and has filed several patents.

Dr. Meng was awarded a Ph.D. from the University of California, Los Angeles, under the supervision of Professor Fred Wudl in 2002. Before joining DuPont Company, he pursued internship training at Lucent Technologies, Bell Laboratories under Professor Zhenan Bao (now at Stanford University) in the field of organic electronics.

Contributors

Sue A. Carter

Physics Department
University of California
Santa Cruz, California

Norman Herron

DuPont Company
Wilmington, Delaware

Yongtaek Hong

EECS Department
University of Michigan
Ann Arbor, Michigan

Jerzy Kanicki

EECS Department
University of Michigan
Ann Arbor, Michigan

Zhigang-Rick Li

Experimental Station
DuPont Central Research &
Development
Wilmington, Delaware

Mang-Mang Ling

Department of Chemical Engineering
Stanford University
Stanford, California

Hong Meng

Experimental Station
DuPont Central Research &
Development
Wilmington, Delaware

Jeff Meth

Experimental Station
DuPont Central Research & Development
Wilmington, Delaware

Dmitrii F. Perepichka

Department of Chemistry
McGill University
Montréal, Québec, Canada

Igor F. Perepichka

L. M. Litvinenko Institute of Physical
Organic and Coal Chemistry
National Academy of Sciences of Ukraine
Donetsk, Ukraine

Daniel Steiger

Global Research Center
General Electric Company
Niskayuna, New York

Jian Wang

Institute of Polymer Optoelectronic
Materials and Devices
South China University of Technology
Guangzhou, China

Manxue Wang

Experimental Station
DuPont Central Research & Development
Wilmington, Delaware

Michael S. Weaver

Universal Display Corporation
Ewing, New Jersey

Christoph Weder

Department of Macromolecular Science
and Engineering
Case Western Reserve University
Cleveland, Ohio

Fred Wudl

Department of Chemistry and Biochemistry
University of California
Los Angeles, California

Gang Yu

Diode Solutions
Goleta, California

Furong Zhu

Institute of Materials Research and
Engineering
Singapore

Table of Contents

Chapter 1 Organic Light-Emitting Devices and Their Applications for Flat-Panel Displays	1
<i>Gang Yu and Jian Wang</i>	
Chapter 2 Light-Emitting Polymers.....	45
<i>Dmitrii F. Perepichka, Igor F. Perepichka, Hong Meng, and Fred Wudl</i>	
Chapter 3 Organic Small Molecule Materials for Organic Light-Emitting Diodes	295
<i>Hong Meng and Norman Herron</i>	
Chapter 4 Phosphorescent Polymer Light-Emitting Diodes	413
<i>Dmitrii F. Perepichka, Hong Meng, and Mang-Mang Ling</i>	
Chapter 5 Polarized Light Emission from Organic Light-Emitting Diodes.....	451
<i>Daniel Steiger and Christoph Weder</i>	
Chapter 6 Transparent Electrode for OLEDs.....	483
<i>Furong Zhu</i>	
Chapter 7 Vapor-Deposited Organic Light-Emitting Devices	527
<i>Michael S. Weaver</i>	
Chapter 8 Print-Based Manufacturing Technologies for Organic Light-Emitting Displays	567
<i>Sue A. Carter</i>	
Chapter 9 Amorphous Silicon Thin-Film Transistor Active-Matrix Organic Light-Emitting Displays	583
<i>Jerzy Kanicki and Yongtaek Hong</i>	
Chapter 10 Microstructural Characterization and Performance Measurements.....	617
<i>Zhigang-Rick Li and Jeff Meth</i>	
Chapter 11 Patent Position of Emerging Companies in Organic Light-Emitting Materials.....	639
<i>Manxue Wang</i>	
Index	655

1 Organic Light-Emitting Devices and Their Applications for Flat-Panel Displays

Gang Yu and Jian Wang

CONTENTS

1.1	Introduction	1
1.2	Conjugated Polymers in PLEDs	4
1.3	PLED Structures, Processes, and Performance.....	10
1.4	Novel Devices and Novel Functions in Thin-Film Polymer Devices.....	18
1.4.1	Dual-Function Polymer Device and Display Matrices	18
1.4.2	Polymer Light-Emitting Electrochemical Cells	20
1.4.3	PLED with Stable Cathode Electrode.....	22
1.4.4	PLED and PLEC in Surface Cell Configuration	23
1.4.5	Optocouplers Made with Semiconducting Polymers.....	24
1.5	Flat-Panel Displays Made with Solution-Processible Organic Semiconductors	25
1.5.1	SMOLEDs and PLEDs as Emitter Elements in Flat-Panel Displays	25
1.5.2	PMOLED Displays versus AMOLED Displays.....	26
1.5.3	Monochrome AMPLEDs Made with Solution-Processible Polymers	29
1.5.4	Full-Color AMPLED Modules.....	30
1.5.5	Performance Simulation for Full-Color AMOLEDs	32
1.5.6	AMOLED for Graphic and Motion Picture Applications.....	34
1.6	Summary and Remarks	35
	Acknowledgment.....	36
	References	36

1.1 INTRODUCTION

The electroluminescence (EL) phenomenon was first discovered in a piece of carborundum (SiC) crystal by H.J. Round in 1907 [1]. Commercial research into light-emitting diodes (LEDs) technology started in early 1962, when Nick Holonyak Jr. created the first inorganic LED [2,3]. Work on gallium arsenide phosphide (GaAsP) led to the introduction of the first commercially mass-produced 655 nm red LEDs in 1968 by Hewlett-Packard and Monsanto. In 1950s, Bernanose first observed EL in organic material by applying a high-voltage alternating current (AC) field to crystalline thin films of acridine orange and quinacrine [4,5]. The direct current (DC) driven EL cell using single crystals of anthracene was first demonstrated by Pope and his coworkers following the discovery of LEDs made with III–V compound semiconductors [6]. In 1975, the first organic electroluminescence (OEL) devices made with a polymer polyvinyl carbazole (PVK) were demonstrated [7].

In early attempts to develop organic EL devices, the driving voltage was on the order of 100 V or above in order to achieve a significant light output [8–10]. Vincett et al. achieved an operating voltage below 30 V by using a thermally deposited thin film of anthracene [11]. The research focused mainly in the academic field until Dr. C.W. Tang and his coworkers at Kodak Chemical showed for the first time efficient organic light-emitting devices in multilayer configuration with significant performance improvement [12]. Nowadays, small molecule organic light-emitting diodes (SMOLEDs) made by means of a thermal deposition process have been used for commercial display products. Pioneer Corporation has commercialized OEL display panels for consumer electronics applications, such as car audio systems, CD/MP3 players, A/V receivers, etc., since 1999. One of the recent products from Pioneer Electronics is an in-car CD player featuring a blue OEL display made in passive matrix (PM) configuration [13]. Kodak Company and Sanyo Electric Company Limited demonstrated the first full-color 2.4-in. active matrix (AM) SMOLED displays in 1999. Their joint manufacturing venture, SK Display Corporation, produced the world's first AM SMOLED displays for a Kodak digital camera (Model LS633) [14]. Recently, Sony Corporation announced mass production of SMOLED displays for its CLIE PEG-VZ90 personal entertainment hand-held devices, starting in September 2004 [15].

Another type of organic semiconductor, conjugated polymer, was discovered in 1977 by Alan J. Heeger, Alan G. MacDiarmid, and Hideki Shirakawa [16,17]. In addition to the focus on its novel physical and chemical properties in heavily doped states, great attention was paid to its intrinsic properties in the undoped semiconducting phase, its nonlinear optical properties under photoexcitation [18,19] and its interfacial behaviors with metal contacts. Schottky diodes made with polyacetylene film were demonstrated in metal–semiconductor polymer–metal configurations [20,21]. Their optoelectric and electro-optical properties were studied. Although significant photosensitivity was demonstrated, the electroluminescent property of this system was intrinsically weak due to its electronic structure. Extensive studies of conjugated polymers in the early and middle 1980s focused on searching and developing new materials with solution processibility. A popular, well-studied system was a polythiophene derivative, of which poly(3-alkyl)thiophene (P3AT) was one (Figure 1.1). Solution-processed metal/P3AT/metal thin-film devices were demonstrated at the University of California at Santa Barbara in 1987 [22]. Following the first demonstration of light-emitting device with unsubstituted poly(*p*-phenylenevinylene) (PPV) (Figure 1.1) by R.H. Friend's group at Cambridge University, [23] a high efficient polymer light-emitting diode (PLED) device was made with a solution-processible polymer, poly[2-methoxy-5-(2'-ethyl-hexyloxy)-1,4-phenylene vinylene] (MEH-PPV) (Figure 1.1), by Heeger's group in Santa Barbara, California [24]. As discussed in later chapters, the current commercialized soluble PPV derivatives are based on a synthesis approach originally developed by Fred Wudl's group in Santa Barbara in 1988 [25,26] and later modified by UNIAX Corporation in the mid-1990s and Aventis Research & Technologies GmbH (now Covion Organic Semiconductors GmbH) in the late 1990s. Soluble PPV derivatives synthesized following this approach not only have high molecular weights, but also show excellent solubility in common organic solvents. Most importantly, these materials have intrinsically low charged impurity (typically below 10^{14} per cm^3) and high photoluminescent efficiency (typically in the range of 20–60%) [25–28]. PLEDs made with such PPV films show high electroluminescent efficiency, low operation voltage, and long device lifetime [29–31]. Displays made with PPV emitters were first commercialized in 2002 by Philips (Norelco electric razor: Spectra 8894XL).

Although the energy gap in a PPV derivative can be increased by reducing conjugation and planarization between the phenyl group and the vinyl group (as observed in PPVs with phenyl groups attaching at 2 or 5 positions or both sites) [27,32,33], it is not large enough to produce saturated blue color needed for full-color displays. Conjugated polymers with optical

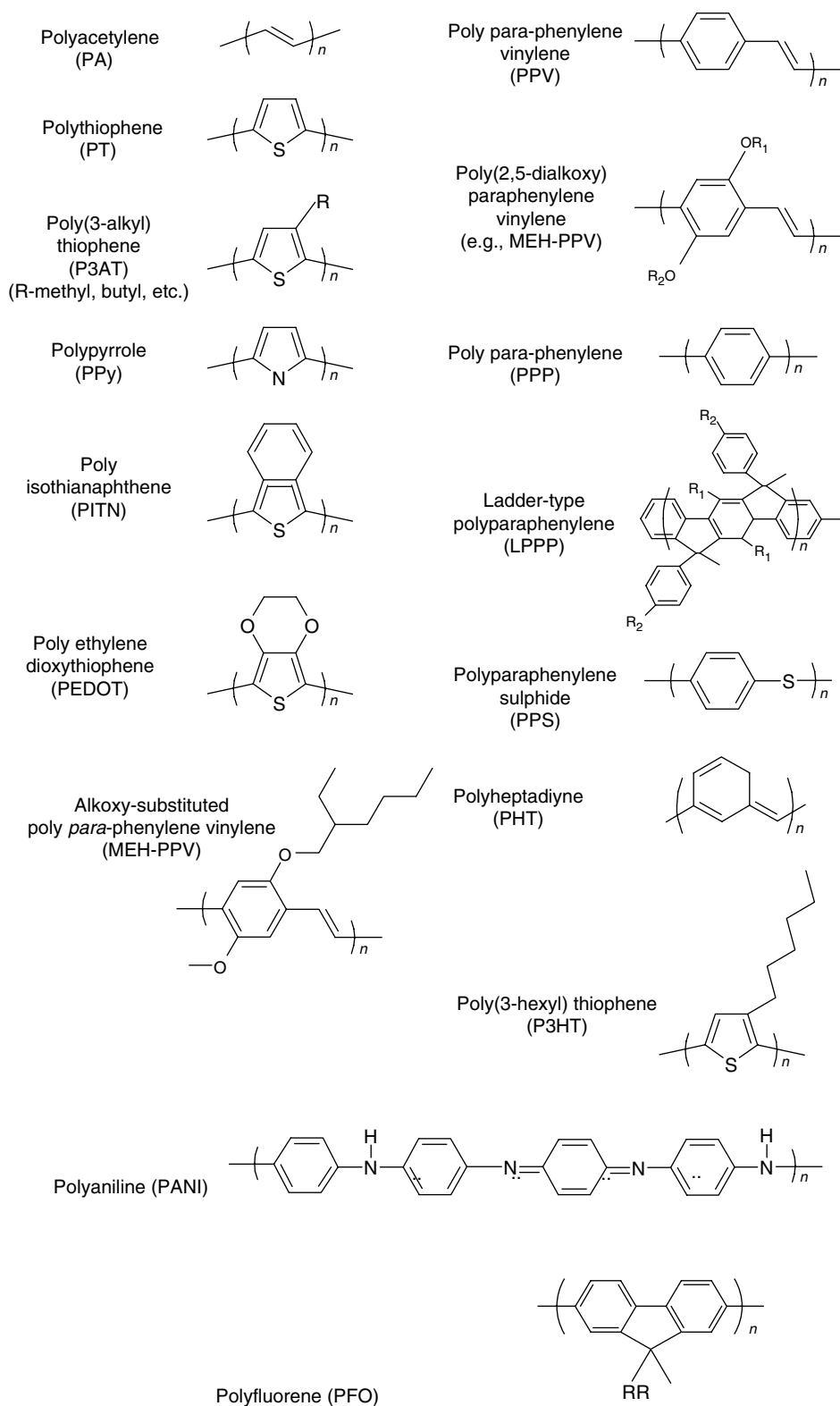


FIGURE 1.1 Molecular structures of popular conjugated polymers.

energy gaps (>2.9 eV) are needed for PLEDs with blue emission. Significant efforts have been made on searching and developing wide energy gap polymers (such as poly(*p*-phenyl) and their functional derivatives) [34–46]. In addition to its use as making blue emitters, the same building blocks can also be utilized for making red and green emitters (as the host) by copolymerizing them with a proper emitter group (as the guest) [47–49]. The red, green, and blue material sets developed by several companies (including Covion and Dow Chemical) are all soluble in common organic solvents with high optoelectric performance and good film-forming properties [49,50].

PLED-based displays are attractive due to their processing advantages in device manufacture. The organic materials used are soluble in common organic solvents or in water. Large-sized, uniform, and pinhole-free thin films can be cast from solutions at room temperature by means of spin coating or other coating techniques commonly seen in printing and painting industries. Because of the large elongation at rupture characteristic of polymers, they are flexible and can be easily fabricated onto rigid or flexible substrates in flat or curved shapes. Solution processing is also promising for forming patterned color pixels in full-color displays. Different EL polymers can be deposited onto predefined locations by means of a printing technique, such as inkjet printing [51,52], screen printing [53,54], or photolithographic patterning [55]. Full-color PLED displays made with an inkjet process or laser-induced thermal transfer process have demonstrated excellent image qualities [56,57].

Section 1.2 gives a brief review of conjugated polymers in semiconducting and metallic phases. Section 1.3 discusses device architectures and their corresponding processes. Section 1.4 introduces some novel devices and their functions in thin-film polymer devices. Section 1.5 is devoted to technical merits of SMOLEDs and PLEDs used as emitter elements in flat-panel displays.

1.2 CONJUGATED POLYMERS IN PLEDs

Conjugated polymers represent a novel class of semiconductors that combine the optical and the electronic properties of semiconductors with the processing advantages and mechanical properties of polymers. The molecular structures of several popular conjugated polymers are shown in Figure 1.1. Before the revolutionary discovery of conjugated polymers, polymer science and technology had focused on saturated polymers, i.e., conventionally nonconductive polymers (a term for macromolecules with repeat structural units). In saturated polymers, the valence electrons of the carbon atoms in the main chain are hybridized in sp^3 configuration, and each carbon atom is bonded to four other atoms. As a result, the electronic orbitals are fully saturated. Due to their electronic structures, saturated polymers have wide energy gaps and are electrically insulating.

The fundamental difference between the saturated polymers and the conjugated polymers is the electronic configuration. Figure 1.2 compares the molecular and the electronic structures of saturated (nonconjugated) polyethylene and conjugated polyacetylene. In a conjugated polymer, the carbon orbitals are in the sp^2p_z configuration, which leads to one unpaired electron (the π electron) per carbon atom. As each carbon atom is covalently bonded to only three other atoms, and p_z orbitals of successive carbon atoms along the backbone overlap, the delocalized π bands are therefore formed. As a result, conjugated polymers exhibit semiconducting or metallic properties, depending on whether the bands are filled or partially filled. The number of π bands is determined by the number of atoms within the repeat unit. In the case of PPV, as the repeat unit contains eight carbons, the π band is split into eight sub-bands. Each sub-band can hold only two electrons per atom, so the four π sub-bands with the lowest energy are filled, and the four π^* sub-bands with the highest energy are empty.

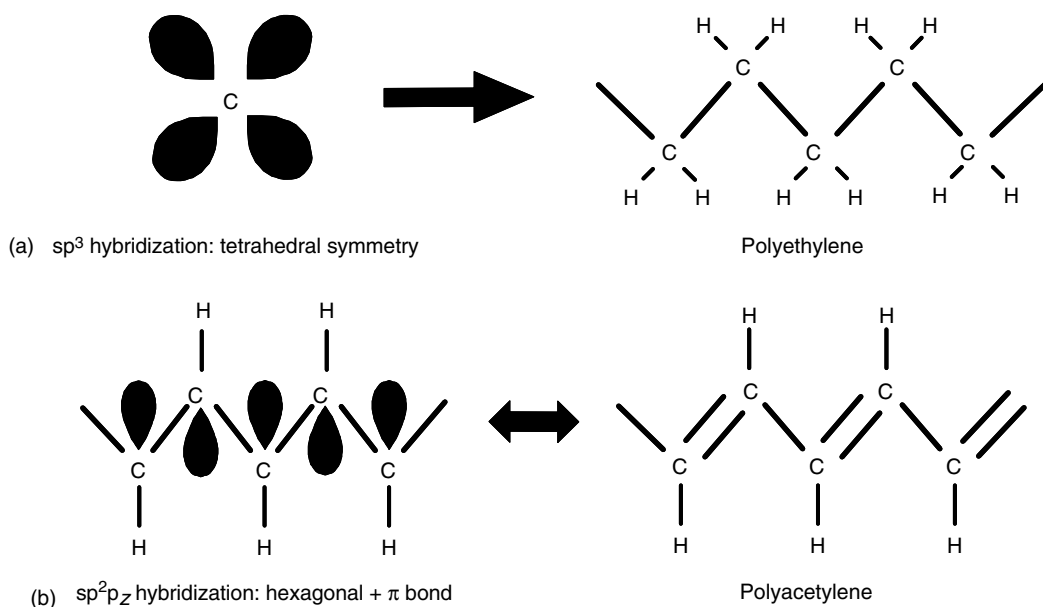


FIGURE 1.2 Electronic and molecular structures of (a) polyethylene and (b) polyacetylene.

The energy difference between the highest occupied π sub-band and the lowest unoccupied π^* sub-band defines the π – π energy gap E_g .

One of the advantages of organic semiconductors is that their mechanical and processing properties can be modified, retaining their electric and optical properties. For example, PPV is a semiconductor with $E_g \sim 2.5$ eV. It is insoluble in any organic solvent after conversion from its precursor to a conjugated form [23,58]. However, by attaching alkyl groups to the 2,5 positions of its benzyl group, alkyl-PPV derivatives are formed. The alkyl-PPV derivatives possess similar energy band gap and luminescent emission profile as those of PPV, but are soluble in most nonpolar organic solvents (such as xylene or toluene) and processible in conjugated form [59]. Another advantage of organic semiconductors is that the energy band gap of a given system can be tuned, retaining its processing capability. For example, by replacing the alkyl groups of PPV derivatives with alkoxy groups on the 2 and 5 positions (for example, MEH-PPV, Figure 1.1), the energy band gap can be reduced from 2.5 to 2.1 eV. Figure 1.3 shows the absorption and electroluminescent spectra for a series of PPV derivatives. The energy gaps are in the range of 2.5 to 1.9 eV, providing a spread of 0.6 eV. These engineering flexibilities are especially promising for optoelectric and electro-optic device applications. Along with the change of the energy band gap, luminescent profile and emission color also change, as shown in Figure 1.3b.

Photonic devices are often classified into three categories: light sources (LEDs, diode lasers, etc.), photodetectors (photoconductors, photodiodes, etc.), and energy conversion devices (photovoltaic devices, solar cells, etc.) [60]. Most of the photonic phenomena known in conventional inorganic semiconductors have been observed in these semiconductor polymers [29,61], including luminescence and photosensitivity. Photoluminescence (PL) describes the phenomenon of light generation under optical radiation. An incoming photon with energy larger than the band gap excited an electron from the filled π band to the unoccupied π^* band to form an electron–hole pair (exciton), which subsequently recombines to emit a photon. In semiconductor polymers used for light emission applications, the photoluminescent quantum efficiency is typically in the 10–60% range. Photoconductivity

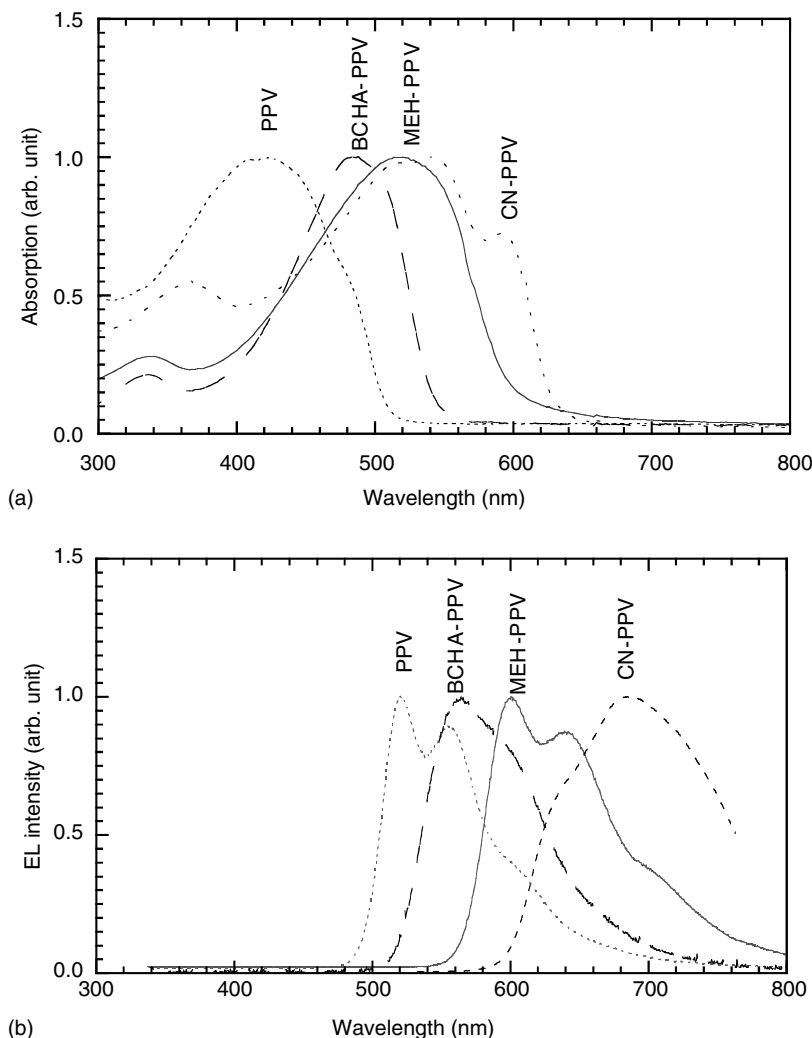


FIGURE 1.3 Absorption (a) and electroluminescence (b) of PPV derivatives. The energy band gap ranges from 2.5 (~ 500 nm) to 1.9 eV (640 nm).

describes the process of photogeneration of the electric current. The electron-hole pairs generated by light illumination can migrate under electric field and be collected at the electrodes. Opposite to the light-emitting process, photoconductivity offers promise for large-area photovoltaic and photosensing applications [62–64]. In the applications of light emission and photoconduction, the carrier mobility of the polymer plays an important role. Depending on the detailed molecular structures, the morphology and the electric field strength applied, carrier mobility in typical organic semiconductors is in the range of 10^{-7} to 10^{-2} $\text{cm}^2/(\text{V} \cdot \text{s})$.

In electroluminescent applications, electrons and holes are injected from opposite electrodes into the conjugated polymers to form excitons. Due to the spin symmetry, only the antisymmetric excitons known as singlets could induce fluorescent emission. The spin-symmetric excitons known as triplets could not decay radiatively to the ground state in most organic molecules [65]. Spin statistics predicts that the maximum internal quantum efficiency for EL cannot exceed 25% of the PL efficiency, since the ratio of triplets to singlets is 3:1. This was confirmed by the performance data obtained from OLEDs made with fluorescent organic

small molecules such as tris(8-hydroxyquinoline) aluminum (Alq_3). In PLEDs made with semiconducting MEH-PPV films, EL to PL efficiency ratio of $\sim 50\%$ was detected by Yong Cao and coworkers [66]. Since then, this phenomenon has been observed by other groups around the world and in other polymer systems [67]. It was suggested that, in conjugated polymers, the singlet cross section could be considerably larger than that of triplets by a factor of 3 to 4 [68,69]. The finding has triggered considerable interests in further enhancing the singlet recombination cross section and singlet populations in EL polymers. For instance, EL to PL ratio of $>75\%$ was reported recently by introducing perturbation of ferromagnetic exchange interaction near EL polymer chain [70]. Triplet excitons can also emissively recombine a phenomenon known as phosphorescence. The lifetime of triplet excitons is much longer, typically in the range of 10^{-7} to 10^{-3} s [71–74], than that of singlet excitons, typically in the range 10^{-10} to 10^{-9} s [75–78]. There has been considerable effort in fabricating SMOLED and PLED devices with triplet excitons for their potential high quantum efficiency [72,73,79–83]. A challenge in this approach is to prevent the long life triplet excitons from interacting with impurities in the organic layers. More rigorous requirements on material purity, charge blocking, and device encapsulation are anticipated.

The color of the EL from PLED devices can be selected by modifying the chemical structure of the polymer either through the main-chain molecular structures or through the side-chain structures, as in the example of PPV derivatives [23,24,31,34,37,84,85]. The EL color can also be tuned by doping the host polymer with luminescent emitters. The emitters could be fluorescent dyes [86–89], phosphorescent emitters [79,80,83], or other luminescent polymers [46,90–93]. In such blend systems, the host polymer has a wider energy gap while the dopant has a smaller energy gap. The excitation energy of the host was transferred to the guest molecules through the dipole–dipole interaction (Förster energy transfer), or the direct quantum mechanical electrons transfer (Dexter energy transfer). By selecting appropriate host and guest materials, and adjusting the weight ratio of the guest to the host, the white LEDs have also been successfully demonstrated [87,89,94]. To make a PLED-based full-color display through the host–guest approach, a stable wide band-gap polymer with high efficiency is a must. Therefore, blue EL materials and devices have been the focus of considerable attention in the field. The red and green emitters, besides formed by host–guest polymers, can also be formed by copolymerizing wider band-gap host molecular unit with one or more guest units with desired emission profiles [47–50,95]. Blue emitters being studied include poly(*p*-phenylene) (PPP) [37–39], ladder-type poly(*p*-phenylene) (LPPP) [40–44], polyfluorene (PF) [34–36,48,95,96], and their stereotype variations [50]. Their molecular structures are provided in Figure 1.1.

Chemical doping and electrochemical doping applied to these semiconducting conjugated polymers lead to a wide variety of interesting and important phenomena. For example, by doping polyaniline (PANI) with phorsulfonic acid (CSA), a conducting polymer with bulk conductivity of 100–300 S/cm can be fabricated [97]. Thin film of PANI–CSA complex in polyblends with poly(methyl methacrylate) (PMMA) shows optical absorption in infrared range (due to free-carrier absorption and polaron absorption) and in ultraviolet range (due to interband optical transition), while the film is optically transparent in most of visible spectroscopic region [98]. Similar phenomena have also been observed in poly(ethylenedioxythiophene)–polystyrene sulfonate (PEDOT–PSS) blends commercialized by Bayer Chemical (Batron-P) [99], and in polypyrrole (PPY) [100]. Figure 1.4 shows the optical transmission spectra of PANI–CSA and PEDOT–PSS. The infrared electric conductivity of PANI is shown in Figure 1.5 [101,102]. These data can be well described by heavily doped semiconductors in disordered or amorphous systems. Such doped conjugated polymers are a novel class of thin, transparent conducting films that can be cast on rigid or flexible substrates through solution process. These films have been widely used in PLED devices in single-layer anode form [98], or as a buffer layer between indium-tin-oxide (ITO) electrode and the EL

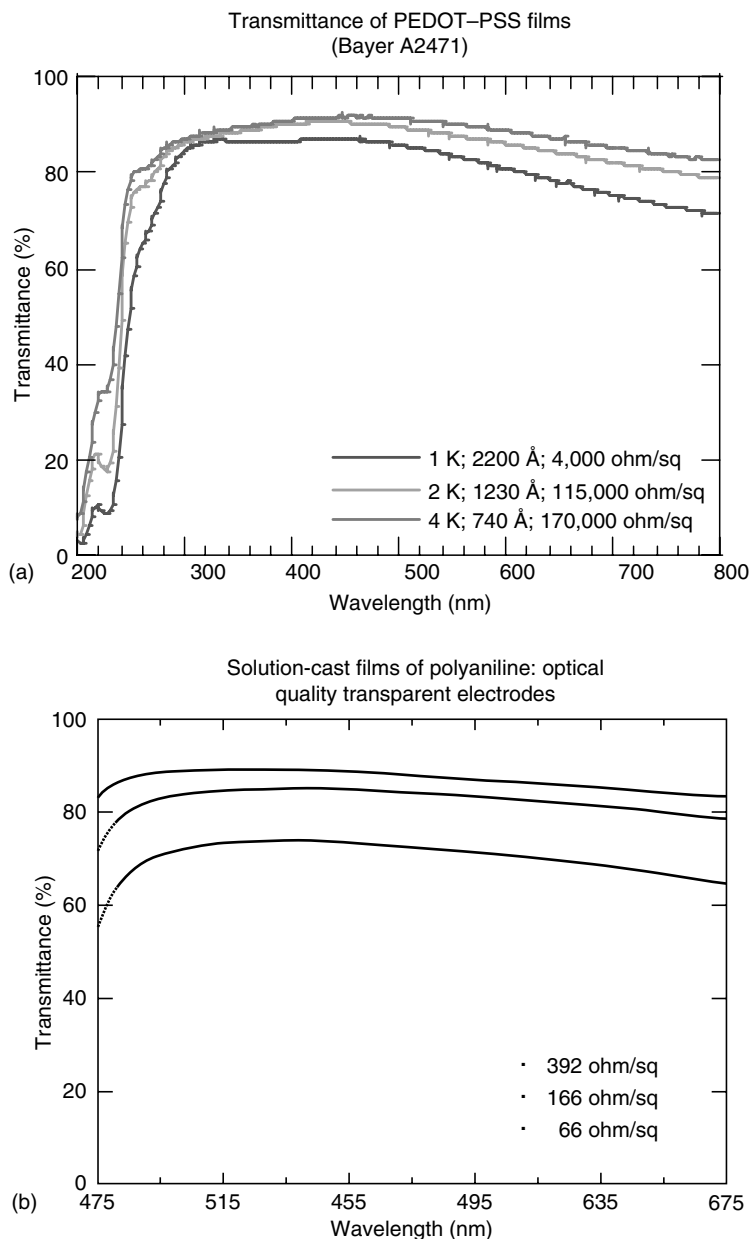


FIGURE 1.4 Optical transmission spectra of (a) PEDOT–PSS and (b) PANI–CSA.

layer [103]. In addition to optimizing the hole injection, this buffer layer also serves as a planarization layer to eliminate pin-holes in EL layer caused by the rough ITO surface. It also serves as a chemical buffer, preventing chemical impurities in the substrate and the transparent ITO electrode from reaching EL polymers, therefore, significantly improving the PLED operation lifetime [30].

The processible organic conductors, semiconductors, and insulators (not discussed in this chapter but well known historically for saturated polymers with sp^3 electronic configuration) form fundamental material set for device applications. In the following sections, we discuss how to construct a PLED with such material set.

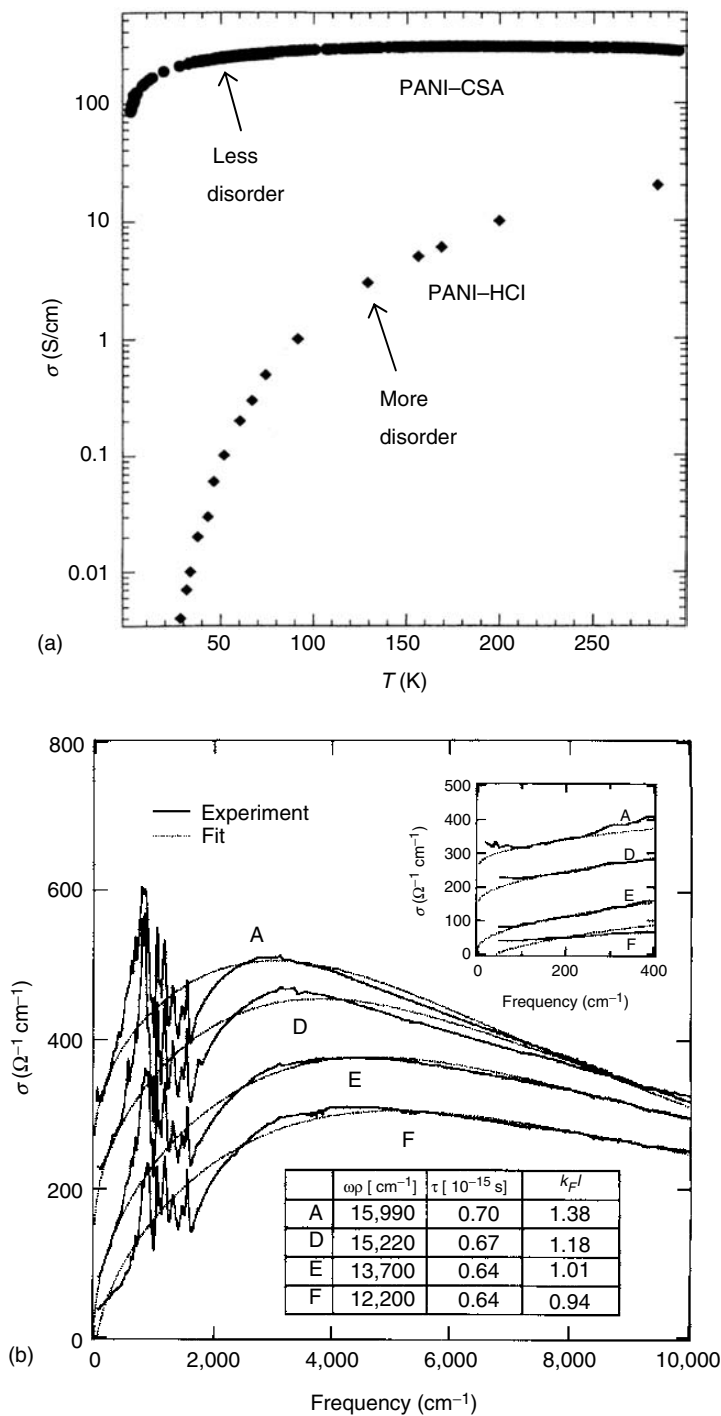


FIGURE 1.5 (a) Temperature dependence of electric conductivity; (b) infrared electric conductivity of PANI-CSA.

1.3 PLED STRUCTURES, PROCESSES, AND PERFORMANCE

The solution-processed PLED is typically prepared with a thin layer of semiconducting polymer film sandwiched between two charge injection contact electrodes, as shown in Figure 1.6. The device is generally made onto a glass substrate or a thin plastic film with partially coated transparent electrode (such as ITO). A thin, semiconducting, luminescent polymer film with thickness typically in 50–200 nm range is then coated. Finally, the device is completed by depositing a low-work-function metal (such as calcium) [24], as the cathode electrode. Although the PLED is a typical single-layer device, the SMOLED has a bilayer structure consisting of a hole transport layer (HTL) and an emissive electron transport layer (ETL), sandwiched between low-work-function cathode and transparent anode [12]. To improve the brightness and efficiency of the basic bilayer devices, extra layers are often introduced. A popular multilayer structure used in a phosphorescent OLED includes a hole injection layer, a hole transport layer, an electron-blocking layer, a light emission layer, a hole-blocking layer, an electron transport layer, and an electron injection layer (Figure 1.7). These layers help reduce the energy barriers at the electrode–organic interface, facilitate the transportation of the charged carriers, confine the opposite charges inside the emission layer, and therefore ultimately improve the power efficiency and operation lifetime of the device. In contrast, a PLED, a popular structure adopted by the whole industry for single-color displays, has only one semiconductor polymer layer between the anode and cathode electrode. This layer serves multiple functions including hole and electron transport and exciton recombination [61,104].

Due to the thin profile of the organic layers, the criteria for both the flatness of the transparent contact electrode and the film quality of the EL layer are rigorous. This was one of the concerns in early days of the SMOLED and PLED development. These requirements are significantly relieved in PLEDs by inserting a conducting polymer buffer layer between the ITO and the electroluminescent polymer layer [30,99,103]. Such a conducting polymer buffer layer provides multiple benefits to the PLED device: (1) it serves as a polymeric anode, and matches the highest occupied molecular orbital (HOMO) of the EL polymer to facilitate the

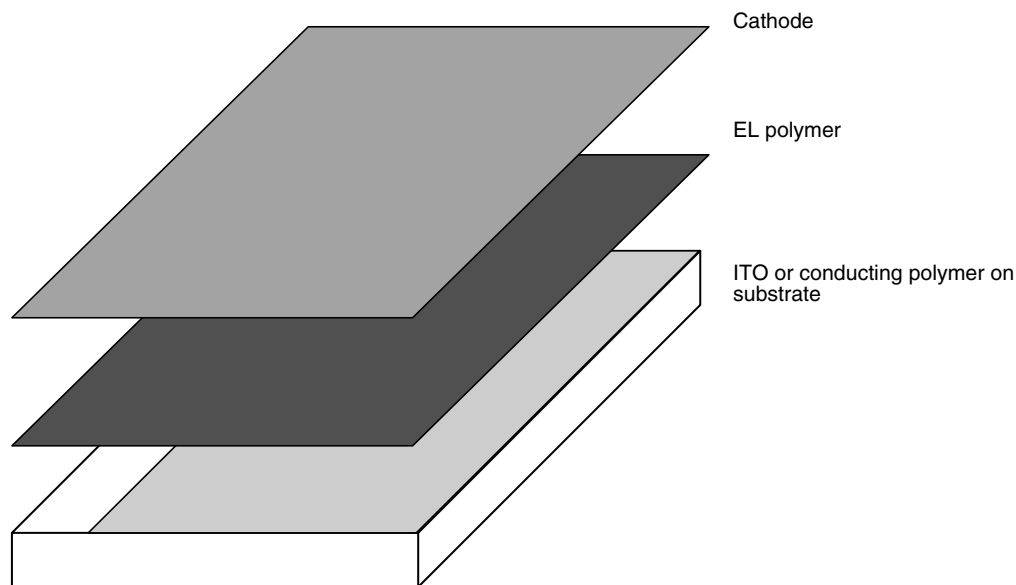


FIGURE 1.6 PLED in sandwich configuration.

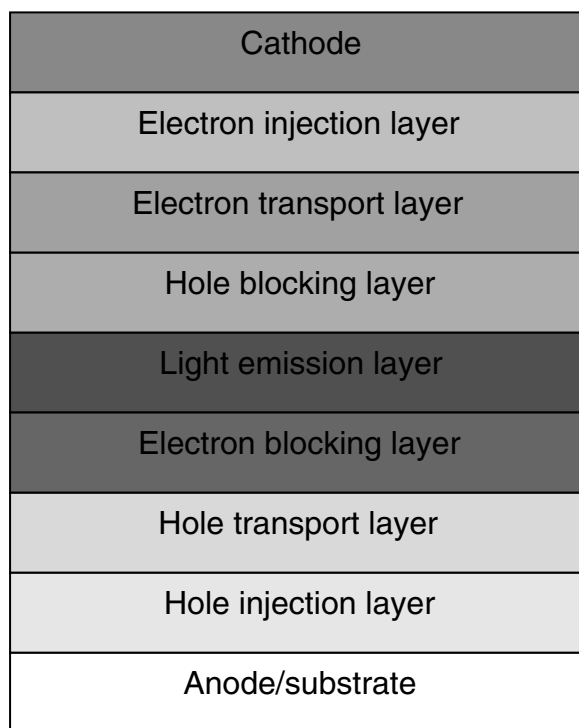


FIGURE 1.7 Multilayer small molecule OLED structure.

hole injection; (2) it serves as a planization layer smoothing the rough ITO surface and eliminating shorts due to sharp spikes on the ITO surface; and (3) it serves as a chemical barrier preventing inorganic atoms in the ITO layer (such as indium) from diffusing into the EL polymer layer. The device operation and shelf life have been dramatically improved, from about 10^2 h to longer than 10^4 h, by applying such buffer layer into PLED devices [29,30,61]. The so-called single-layer (single semiconducting layer between the bilayer anode and metal cathode) structure has achieved great success in PPV-based PLED devices as well as in PF- and PPP-based red, green emitters. It becomes more challenging to use such single-layer device structure for polymers with energy gap larger than 2.9 eV. This is similar to that encountered in SMOLED devices, in which the popular host material in the emitter layer (such as Alq₃ or bis-(2-methyl-8-quinolinolate)-4-(phenyl-phenolate)-aluminum, BAlq) has energy gap $\gg 2.5$ eV. Significant improvements in device efficiency and operation lifetime have been achieved in a blue PLED with an additional thin crosslinkable interlayer between the buffer layer and the EL layer [105]. After coating the interlayer from solution, it is cross-linked at an elevated temperature, and becomes insoluble during the process of the following EL layer. A sharp and clear interface could thus be formed. This layer serves as hole transport material from the anode to the EL layer. Since it separated the anode from the recombination zone in EL layer, it eliminated exciton quenching caused by contact electrode. With such an interlayer, 8.9 cd/A was demonstrated in a blue PLED made with PF provided by Dow Chemical. The extrapolated lifetime of such blue devices was reported to be over 70,000 h from initial luminance of 100 cd/m² at room temperature [106,107].

For PLEDs with relatively small active area, the anode can be made of a single layer of conducting polymers with relatively high bulk electric conductivity. Gustafsson and coworkers at UNIAX demonstrated a flexible PLED with conducting PANI-CSA anode, and

with MEH-PPV as the light emitting layer [108]. Conducting polymers with moderate bulk electric conductivity are generally favorable as the buffer layer on top of ITO, especially for the applications in segmented or pixelated displays. By proper selection of the bulk conductivity and the thickness of the buffer layer, one can control the lateral conductance between neighbor pixels, so that a continuous, nonpatterned buffer layer can be used in the display matrix, which provides sufficient conducting in vertical direction and sufficient insulating in lateral direction. This structure reduces manufactory process time and cost considerably.

The main difference in process between SMOLEDs and PLEDs is that SMOLEDs are commonly fabricated by vacuum deposition, whereas PLEDs are prepared by solution processing, which is a simpler and cheaper process. However, organic molecules with relatively low molecular weight can also be fabricated into solution-processible forms. In addition to adding flexible side chains to the luminescent molecule, molecules in oligomer and dendrimer forms have been demonstrated [109,110]. The first solution-processing made PLED was demonstrated at the University of California, Santa Barbara, right after the discovery of PLED [23,24]. In solution-processing methods, spin coating has been the most popular method in both research laboratory and industry for the buffer and EL polymer layers. PLED devices with low operation voltage, high efficiency, and long operation lifetime have been obtained by spin-coating method. To pattern fine structures for full-color displays, shadow masking is typically used in SMOLED fabrication. The shadow mask process becomes challenging for large-size display panels. In contrast, full-color PLED pixels can be patterned with such printing techniques as inkjet printing [51,52], screen printing [53,54], dye diffusion [53], laser-induced thermal transfer [111–113], or with the photolithographic process [55]. The solution process is typically carried out at low temperatures or at room temperature, allowing a device to be made onto a flexible, organic substrate [108]. As illustrated in Figure 1.6, the substrate (rigid or flexible) with or without ITO was spin-cast with a thin layer of buffer. On top of the buffer layer, an electroluminescent 50–200 nm polymer film was spin coated. During these two processing steps, postbaking is generally required to remove the residue solvent in the buffer and polymer layers. The cathode layers are typically prepared by physical vapor deposition (such as thermal deposition) under vacuum of 10^{-6} torr or below. Calcium, barium, and magnesium are commonly chosen as the cathode because of their low work functions. Since low-work-function metals are highly reactive, PLED devices must be hermetically sealed for long-operation life.

PLEDs are two-terminal, dual-carrier thin-film devices. They could be viewed as metal–insulator–metal (M–I–M) or metal–semiconductor–metal (M–S–M) devices with asymmetric metal contacts. The energy structure of a PLED can be approximated by a rigid band model as illustrated in Figure 1.8. This model is justified because the charge carrier concentration in undoped films is so low ($\leq 10^{14}$ per cm^3) that all of the free carriers are swept out by the field that arises from the difference in work functions of the two electrodes. The depletion depth of a high-quality PPV film is beyond microns, which is much larger than the thickness of the EL polymer layer in the PLED device. As a result, there is negligible band bending [18]. Under forward bias, the electrons are injected from the low-work-function cathode into the π^* band (conduction band) of the EL polymer, while the holes are injected from a high-work-function electrode into the π band (valence band) of the EL polymer. The oppositely charged carriers in the two different bands encounter each other within the EL polymer film, and recombine radiatively to emit light. The light emission process is an intrinsically fast process. The only delay is due to the transport of the holes and electrons from the electrodes to the emission zone. Thus, the PLED has a fast response time, typically in the range of $10\text{--}10^2$ ns, limited by the RC time constant, resulting from the geometric factors of the PLED device [114]. For comparison, the fastest response time of LCD displays available in the market is around 10 ms.

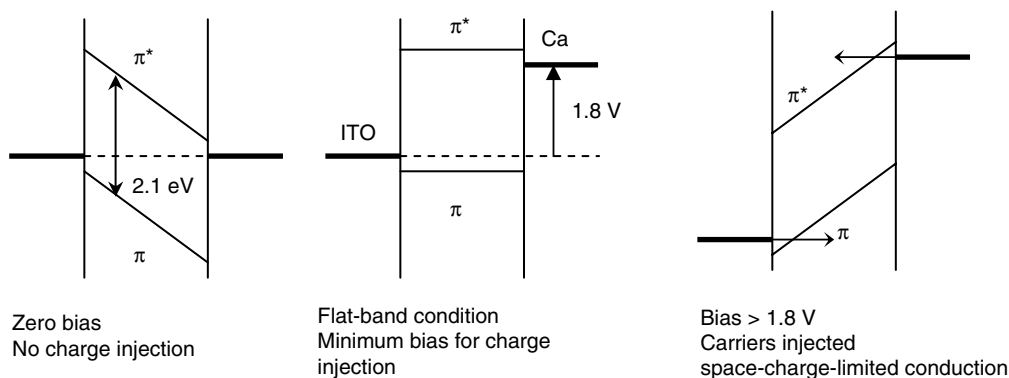


FIGURE 1.8 Energy band structure of a PLED in the configuration of ITO/MEH-PPV/Ca.

Ideally, the work function of the cathode is required to perfectly match the lowest unoccupied molecular orbital (LUMO) energy level of the EL polymer, and the work function of the anode is required to perfectly match the HOMO energy level of the EL polymer. In reality, when the electrode's work function lies within ~ 0.2 eV of the HOMO or the LUMO energy level, doping occurs at the contact between the electrode and the EL polymer interface, and p- or n-type polarons form at the corresponding interfaces. When the work function of the metal electrode is lower than the HOMO or higher than the LUMO of the EL polymer, doping occurs and an inverting layer is formed at the metal–polymer interface. The electrode's work function is thus closely linked to the LUMO or HOMO of the EL layer. This effect is similar to what is frequently observed in p–i–n devices fabricated with inorganic semiconductors [60]. In such semiconductors, ohmic contact is frequently observed at the polymer–metal interface, which is characterized by exponential behavior in I – V curves in forward bias near the corresponding E_g/e value. Figure 1.9 shows a data set taken from an ITO/PEDOT/EL polymer/cathode device. The EL polymer layer is made of Covion PDY with thickness of 70–90 nm. Its optical absorption and emission spectra are shown in Figure 1.10, with optical energy gap of ~ 2.3 eV and peak of emission profile at 560 nm. The anode contact of the device is made of a conducting PEDOT layer with a work function ~ 5.2 eV. The cathode contact is made of a thin barium layer with a thick aluminum cap [50,115]. The carrier injection occurs at flat band condition (Figure 1.8) at which the forward voltage is close to optical band gap of the EL polymer minus two polaron-binding energies, ~ 2 V in this example. Exponential I – V characteristic is typically seen in the voltage range close to that corresponding to the optical energy gap, similar to that seen in light-emitting devices made with inorganic III–V semiconductor crystals [60]. For current density higher than ~ 1 mA/cm², the I – V plot deviates from the exponential behavior, and becomes bulk limited. This device emits greenish-yellow light with CIE color coordinates at $x \sim 0.48$ and $y \sim 0.52$. It reaches 100 cd/m² at 2.4 V (typical luminance of a computer monitor), 1000 cd/m² for $V < 4$ V (typical luminance of a fluorescent lamp), and over 10,000 cd/m² for $V > 5$ V. These data suggest that conjugated polymer PLEDs are very efficient light emitters with low operating voltages. The external quantum efficiency of such device is $>5\%$ photons per electron (ph/el), and the luminous efficiency is >10 lm/W for 2–4 V. As the efficiencies indicated, PLED devices are one of the most efficient thin-film light sources. For comparison, the power efficiencies of ZnS-based thin-film electroluminescent devices are typically 2–4 lm/W [116].

When the work functions of the contact electrodes are not well matched to the bands of the EL polymers, energy barriers are formed at the respective interfaces. The height of the barrier for hole injection is determined by the difference between the work function of

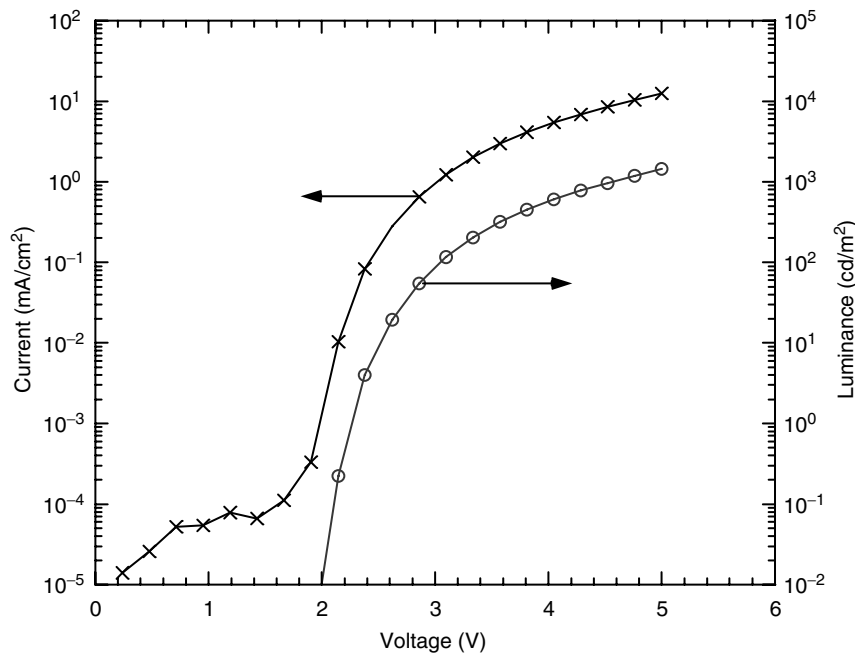


FIGURE 1.9 L - V and I - V characteristics of a PLED in the structure of ITO/PEDOT/Covion PDY/Ba/Al.

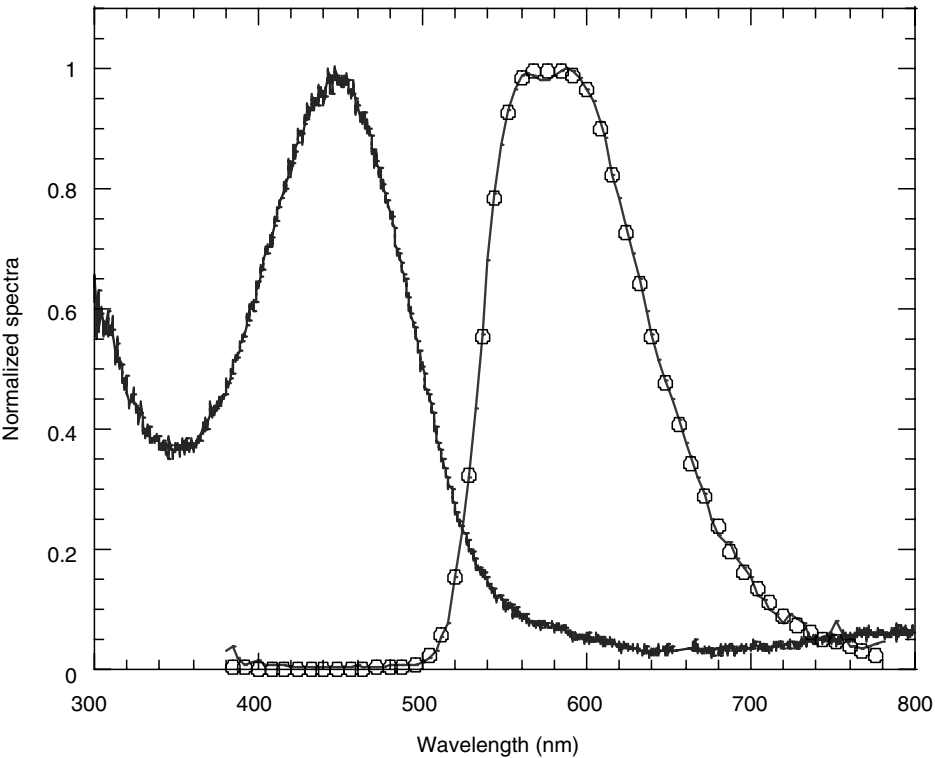


FIGURE 1.10 Optical absorption, photoluminescence and electroluminescence (circle) of Covion SY film.

the anode and the HOMO energy level. The height of the barrier for electron injection is determined by the difference between the work function of the cathode and the LUMO energy level. Carrier tunneling through the barrier can be described primarily by Fowler–Nordheim field emission tunneling: $I \propto V^2 \exp(-1/V)$ [117,118]. When the barrier heights are significantly less than 100 meV (comparable to thermal energy of room temperature), thermionic emission (thermal-assisted carrier tunneling) becomes the dominating mechanism. Thermionic emission in PLED device could be well described by Schottky emission where thermionic emission across the metal–insulator interface or the insulator–semiconductor interface is dominating [60,118,119]. In PPV devices with ohmic contacts and with relatively thick EL polymer layer (larger than 150 nm), the hole current is space-charge-limited and the electron current is trap limited [120,121]. The space-charge-limited hole current arises due to the higher mobility of holes than that of the electrons observed in some popular polymer systems [120,122,123]. The traps-limited electron current results from the defects with energy levels just below the conduction band due to disorder, structural imperfectness, or chemical impurities in the polymer. SMOLEDs and PLEDs are electric current driving devices. The intensity of light is proportional to the driving current (the number of charges flowing through the device in unit time), and when the number of injected holes and injected electrons are balanced, the light emission intensity follows same dependence as the current on the voltage. This is indeed observed in SMOLEDs and PLEDs with optimized structures and parameters. Figure 1.11 shows the luminous efficiency dependence of a PLED made with Covion PDY on the operating current. The luminous efficiency defined as emitting luminance per unit current is ~ 15 cd/A in broad current range without any sign of reduction at the highest testing current.

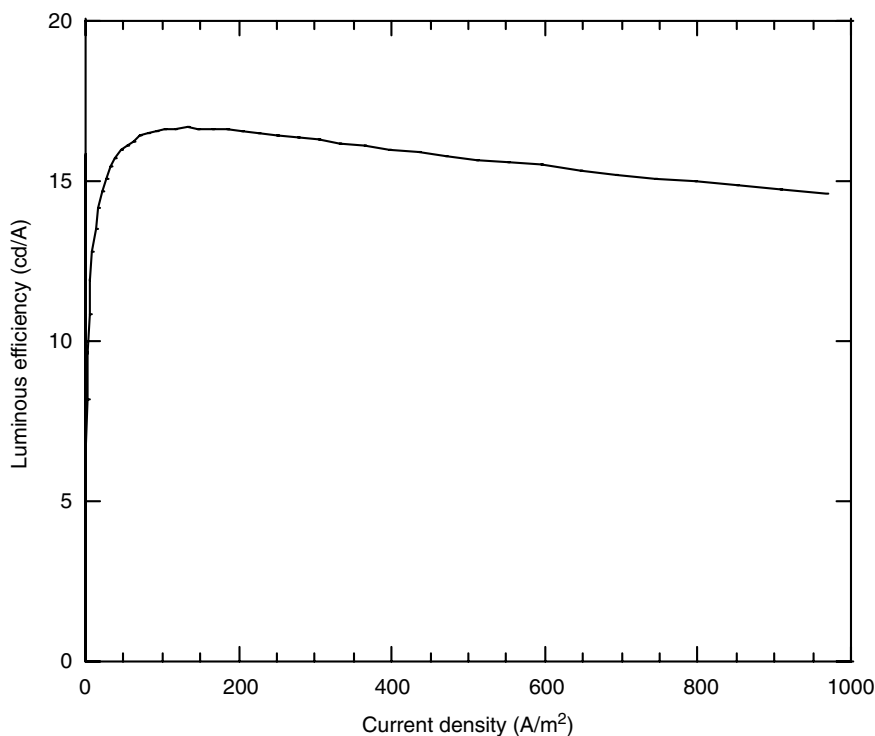


FIGURE 1.11 Luminous efficiency as a function of driving current in a PLED made with Covion PDY.

The operating lifetime, defined as the time for the light emission decaying to half of its initial value under continuous constant current operation, has been a principal concern for the practical application of PLED in the display industry: Can operating lifetimes sufficient for commercial display products be achieved using polymers processed from solution? There was skepticism during the early 1990s that solution-processed materials could achieve the level of purity required for semiconductor applications. The operating lifetimes of PLEDs during that time ranged from a few minutes to a few hundred hours at 100 cd/m² initial brightness, significantly less than the operating lifetimes of SMOLEDs for which over 20,000 h of operating lifetimes were achieved at a similar brightness level [124]. By inserting a conductive PANI layer between the ITO and MEH-PPV layers, UNIAX demonstrated the first polymer LEDs with an operating life longer than 10⁴ h [30,125,126]. At ~450 cd/m² initial brightness, the luminance of the PLED device drops only ~20% after 2000 h operation at 35 mA/cm². The extrapolated room temperature operation lifetime at 100 cd/m² was in excess of 10⁴ h, corresponding to a charge density of $\sim 3 \times 10^5$ C/cm² passing through the device. This number is still a significant number even at current stage.

Covion PDY and its early versions including MEH-PPV represent a class of EL polymers with high quantum efficiencies. Single-layer devices with band-matched electrodes exhibit low operation voltage (as a result of high carrier mobility), high quantum efficiency, and long-operation lifetime. With improved device engineering, PLEDs made with Covion PDY showed operation lifetime longer than 700 h under constant current driving with 200 cd/m² initial luminance at 80°C. Two data sets taken from two batches of devices (made over 9 months time period) at accelerated test conditions (3 mA/cm², 80°C) are shown in Figure 1.12. It is well known that the device operation lifetime at room temperature is approximately 32 to 35 times longer than that at 80°C [61,127]. The data suggest ~25,000 h operation lifetime under constant current driving, and ~35,000 h operation lifetime under 200 cd/m² constant luminance driving at room temperature. The voltage increase rate is constant over most of the stress period, ~1 mV/h at 80°C that corresponds to ~30 μ V/h at room temperature. It is worth mentioning that under the operating conditions at which the device heating is negligible, the operation lifetime of a given SMOLED or PLED is inversely proportional to the operation current density. In other words, the device operation lifetime can be represented by a universal number: the total charge passing through the device during its lifetime. For the device shown in Figure 1.12, the total passing charge at room temperature is approximate 3×10^5 C/cm², consistent with the value we found in the MEH-PPV device [126]. Thus, solution-processed PLEDs have met the requirements for commercial applications with operating lifetimes in excess of 10⁴ h at display brightness.

Under transient pulsed operation, PLEDs can emit light up to 10⁶ cd/m². Figure 1.13 provides a data set taken from a PLED made with MEH-PPV [61]. The PLED was fabricated in a microcavity configuration with semitransparent Au as anode electrode and Ca–Al as cathode electrode. The Au anode not only significantly reduced the contact resistance, but also allowed high current density (more than 100 A/cm²) passing through the device. The luminous efficiency was ~2 cd/A for current density between 1 and 50 mA/cm². At 100 A/cm², the luminance reached ~10⁶ cd/m² with efficiency ~1 cd/A. This result revealed that the luminous efficiency remained relatively constant for charge density running over five orders of magnitude. That no substantial emission spectral change was observed even at the highest operation current also deserves attention. Similar results were also obtained in other PPV derivatives in traditional ITO–EL polymer/cathode device configuration [128]. Emission intensity up to 5×10^6 cd/m² was observed in PPV and its copolymer.

Polymer laser diodes have been an attractive topic after the discovery of EL in conjugated polymers. Optical lasing in semiconducting luminescent polymer solutions was first

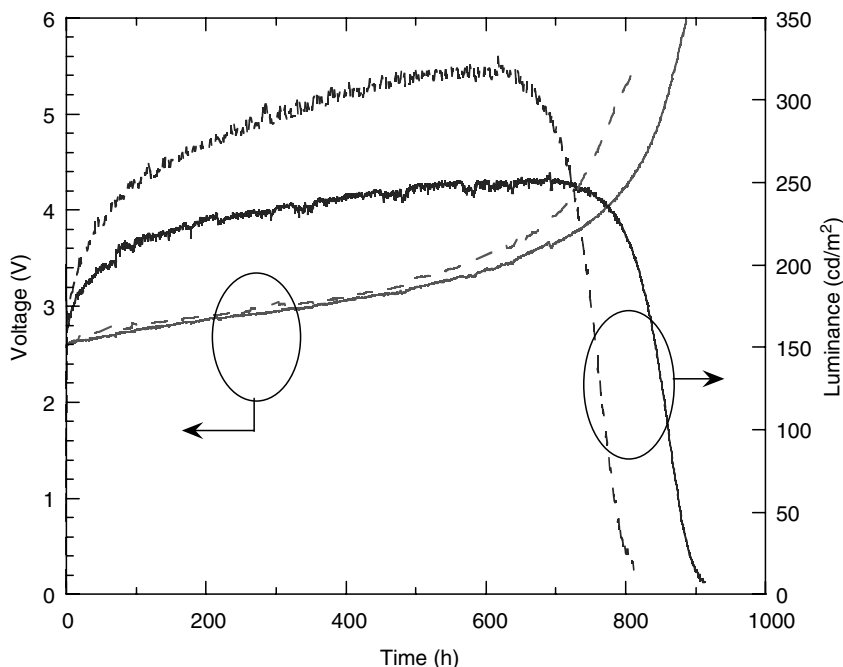


FIGURE 1.12 Operation lifetimes of two PLEDs made with Covion PDY polymer.

demonstrated by D. Moses at the University of California at Santa Barbara by replacing organic molecular dye with MEH-PPV solution [129]. Photopumped solid-state lasing from thin conjugated polymer films was then discovered in several groups in early 1996 [130–132]. Since then, considerable efforts have been devoted to the study of polymer and small molecule laser diodes [133]. However, no reliable lasing effects have been reported under direct electrical pumping even at 10^6 cd/m^2 (current density of 1000 A/cm^2) level. The challenges for the electrically pumped laser diodes include (but not limited) the following: (1) good electrode–polymer interfaces that can pass the needed current density; (2) low optical loss at the metal electrodes; (3) minimum charge-induced absorption; (4) incorporating contact electrode with high- Q mirrors; and (5) good thermal dissipation from junction area to the substrate or to a heat sink.

In a full-color display, each color pixel contains three subpixels with primary colors in red, green, and blue emission zones, respectively. A popular approach for fabricating such color pixels is fabricating each color subpixel with EL materials in corresponding emission spectra. Considerable efforts have been given in both SMOLEDs and PLEDs fields to develop red, green, and blue color emitters with performance sufficient for commercial display applications. Figure 1.14 shows a set of luminance–voltage data of polymer LEDs made with red, green, and blue emitters. Again, light emission occurs at forward bias corresponding to the photon energies of the emitting colors, similar to the fact known in inorganic LEDs. The operation voltages of red, green, and blue emitters at 200 cd/m^2 are 6.6 , 3.6 , and 5.4 V, respectively. The respective luminous efficiencies are 2.2 , 18 , and 6.0 cd/A . These numbers suggest that they are promising thin-film emitters with high luminous efficiencies and low operation voltages. As shown in Figure 1.15, the CIE color coordinates of these emitters have been improved to the level comparable to those in active matrix liquid crystal display (AMLCD) TV screens. The

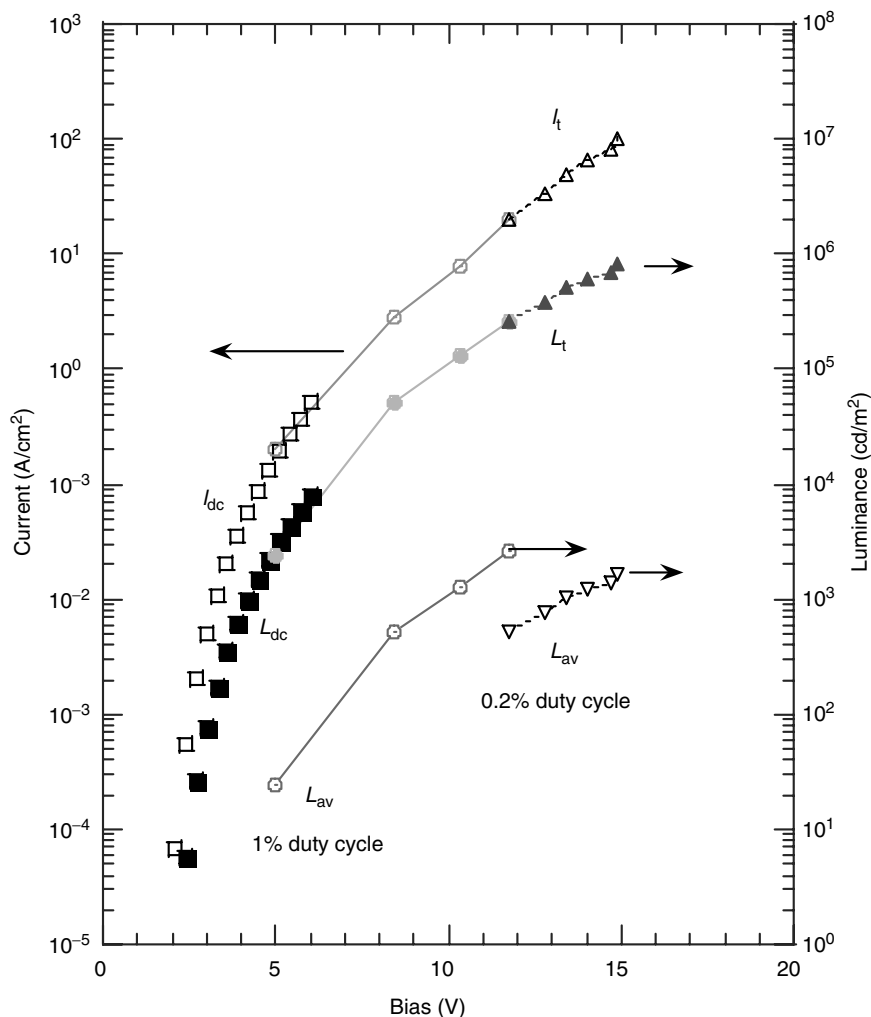


FIGURE 1.13 Light intensity of 106 cd/m^2 achieved in PLED.

operation lifetimes of these emitters have also been improved dramatically in the past years, approaching the level needed for initial market entry [106,134].

1.4 NOVEL DEVICES AND NOVEL FUNCTIONS IN THIN-FILM POLYMER DEVICES

1.4.1 DUAL-FUNCTION POLYMER DEVICE AND DISPLAY MATRICES

The thin-film device illustrated in Figure 1.6, made with a semiconducting polymer as the active layer, can function as both light-emitting device and light-detecting device (i.e., a photodetector) [135]. The asymmetric electrodes provide a built-in potential equal to the difference between their work functions. Thus, at zero or reverse bias, photogenerated electrons and holes are separated by the internal field and collected at the respective electrodes. The dual-function utility is illustrated in Figure 1.16 for an ITO/MEH-PPV/Ca device. At forward bias larger than 2 V, light emission becomes visible with the naked eye.

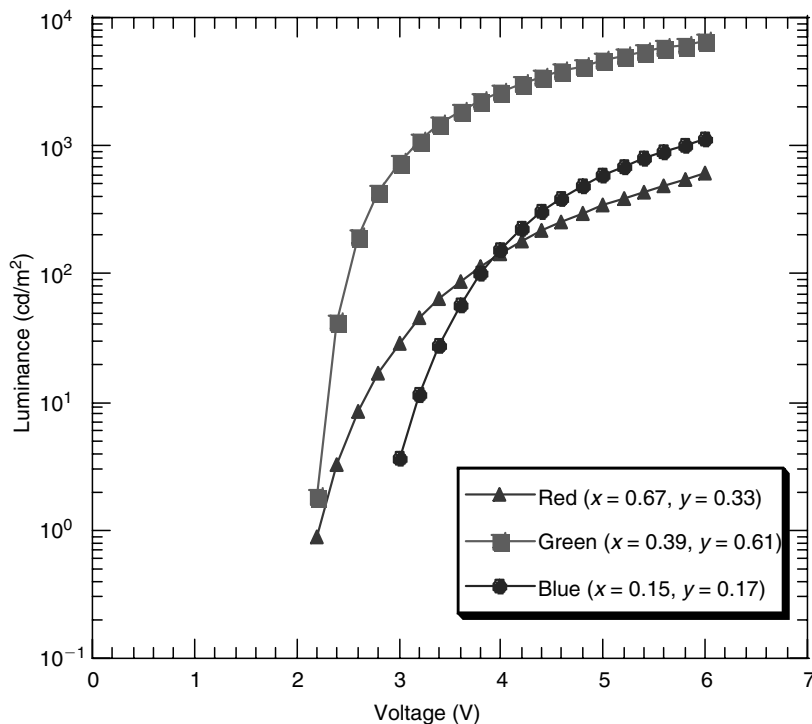


FIGURE 1.14 Luminance–voltage plots of red, green, and blue polymer emitters.

The luminance reaches 100 cd/m^2 at $\sim 2.5 \text{ V}$ with EL efficiency of $\sim 2.5 \text{ cd/A}$. The corresponding external quantum efficiency is about 2% ph/el. At -10 V bias, the photosensitivity at 430 nm is around 90 mA/W , corresponding to a quantum yield of $\sim 20\%$ el/ph [135]. The carrier collection efficiency at zero bias was relatively low in the order of 10^{-3} ph/el. The photosensitivity showed a field dependence with activation energy of 10^{-2} eV [135]. This value is consistent with the trap distribution measured in the PPV-based conjugated polymers [136,137].

While pure semiconductor polymer films often exhibit low photoconductivities, sensitizers have been used not only to increase the photosensitivity, but also to broaden the photoaction spectrum [138–140]. A model system is polymer doped with electron acceptor C_{60} and its functional derivatives. In polymer blends made with MEH-PPV- C_{60} in $\sim 1:1$ weight ratio, the PL in MEH-PPV is quenched by more than four orders of magnitude, while the photoconductivity increases 10 to 100 times [141]. In a device fabricated in sandwich configuration similar to that shown in Figure 1.6, the carrier collection efficiency at zero bias reaches 30–50% ph/el [63]. The power conversion efficiency reaches 3% at 430 nm. These studies in the early 1990s have opened a number of new opportunities for conjugated polymers. Photodetectors, image sensors, solar cells, and photovoltaic cells have since then been successfully demonstrated [63,64,142,143]. Recent studies along this direction have resulted in polymer photovoltaic cells with 3–5% power conversion efficiency under AM1.5 solar radiation [144–147].

The dual-function utility (photon emission in forward bias and photon detection in reverse bias) can be employed to fabricate smart display matrices [148]. By presetting the device in the photodetecting mode (zero or reverse bias), each pixel can sense an optical signal and transfer that signal to the memory in the driving circuit, similar to the process in a photodiode

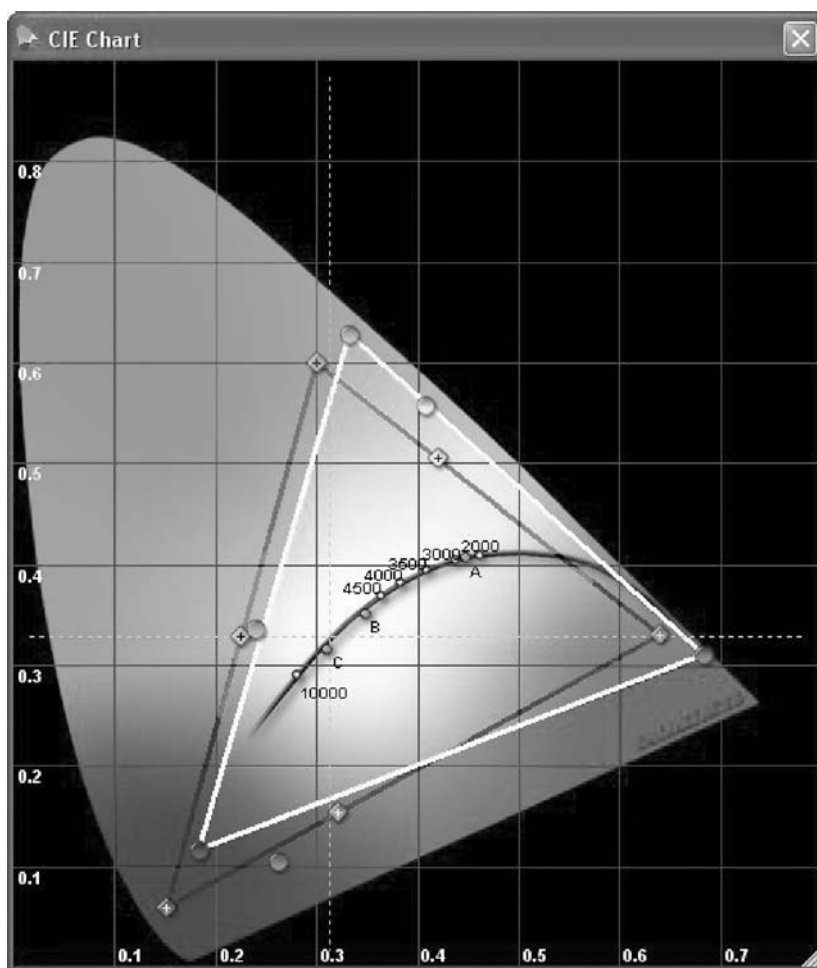


FIGURE 1.15 CIE coordinates of polymer RGB emitters.

array. Subsequently, the pixels that were addressed during the input cycle can be switched to the displaying mode (forward bias), thereby creating an emissive image of the input that was displayed on the same diode array.

1.4.2 POLYMER LIGHT-EMITTING ELECTROCHEMICAL CELLS

The polymer light-emitting electrochemical cell (LEC) is a new approach to light emission from semiconducting polymers [149,150]. By laminating a blend of a luminescent conjugated polymer and a solid state electrolyte (such as PEO:Li⁺) between two air-stable contact electrodes, a dynamic p-i-n junction could be created under external bias. The semiconducting polymer is electrochemically doped to p-type on one side and n-type on the other side. Light is emitted from the compensated insulating region at the center. Because the doped polymer becomes highly conductive, ohmic contacts are formed at the electrode-polymer interface. As a result, facile electron and hole injections are achieved with stable metals as electrodes, such as Au or Al. The *I-V* characteristic in PLEC is similar to that shown in PLED with optimized interfaces (such as that shown in Figure 1.9). This fact confirms the p-i-n structure in PLEDs with optimized interfaces.

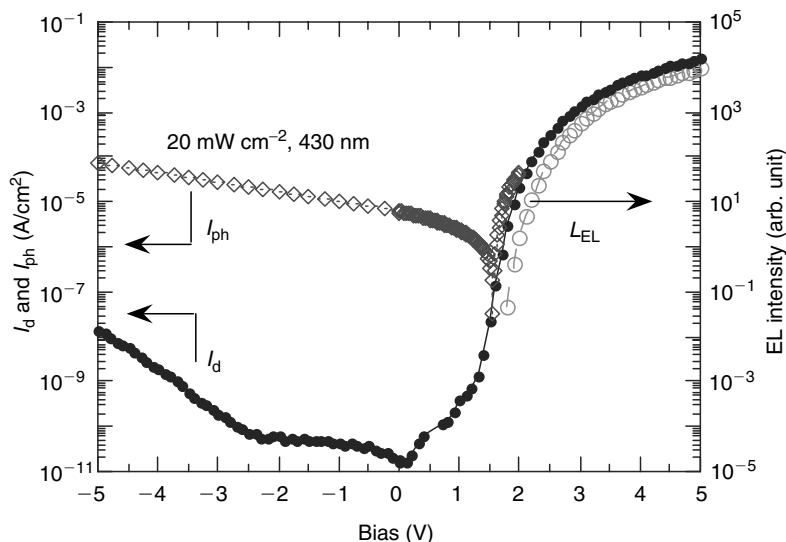


FIGURE 1.16 Dual-function utility of MEH-PPV device: light emission and photodetection.

The operating mechanism of the polymer LEC includes the following steps:

- (i) Electrochemical p-type and n-type doping in the regions adjacent to the anode and the cathode, respectively, upon application of voltage greater than the π - π^* energy gap of the semiconducting polymer
- (ii) Formation, *in situ*, of a p-n junction within the active layer
- (iii) Radiative recombination of the p- and n-type carriers within the compensated p-n junction

The speed of p- and n-type doping and that of p-n junction formation depend on the ionic conductivity of the solid electrolyte. Because of the generally nonpolar characteristics of luminescent polymers like PPV, and the polar characteristics of solid electrolytes, the two components within the electroactive layer will phase separate. Thus, the speed of the electrochemical doping and the local densities of electrochemically generated p- and n-type carriers will depend on the diffusion of the counterions from the electrolyte into the luminescent semiconducting polymer. As a result, the response time and the characteristic performance of the LEC device will highly depend on the ionic conductivity of the solid electrolyte and the morphology and microstructure of the composite.

A methodology for increasing the ionic conductivity within the layer and, simultaneously, for controlling the morphology of the phase-separated microstructure of the electroluminescent polymer–solid electrolyte composite has been successfully demonstrated [151]. The idea is to use a bifunctional (surfactant-like) liquid compound with a high boiling point as an additive to facilitate the phase separation to ensure maximum interfacial surface area between these two phases, and ideally, to support the formation of an interpenetrating bicontinuous network in the composite. If the additive compounds have, in addition, a relatively high dielectric constant, the ionic conductivity will also be enhanced. By the said method, the response time of the polymer LECs has been improved to milliseconds or even submilliseconds. This fast response allows LECs to be used as the emitters for x - y addressable display arrays in both PM and AM forms, and to be operated at video rate, e.g., 60 frames per second.

A set of data obtained from an LEC [ITO/MEH-PPV:PEO:Li + OCA/Al] is shown in Figure 1.17. Since the junction is created *in situ*, the doping profile reverses when the bias

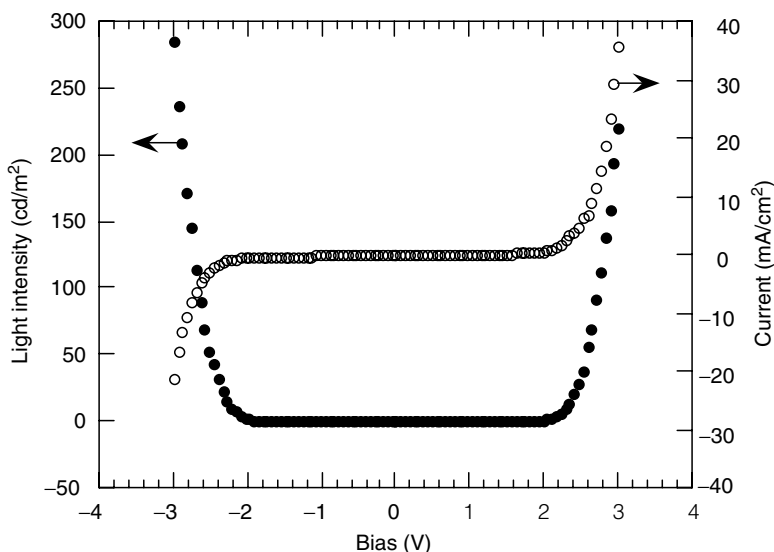


FIGURE 1.17 I - V (open circles) and L - V (solid circles) characteristics of a LEC fabricated as ITO/MEH-PPV:PEO:Li + OCA/Al. Forward bias is defined as positive bias with respect to JTO. (From Pei, Q., Yu, G., Zhang, C., Yang, Y., and Heeger, A.J., *Science*, 269, 1086, 1995. With permission.)

polarity is reversed. Consequently, light emission can be observed in both bias directions. By selecting polymers with proper energy gaps, red, green, and blue LECs have been demonstrated with external quantum efficiencies and luminous efficiencies close or even better than those in corresponding PLEDs with optimized parameters [152,153]. Due to its ease of operation to control the carrier injection and balance, single-layer LEC devices can, in fact, be employed to assess the intrinsic performance of an unknown polymer semiconductor.

On one hand, the ionic conductor was unique in creating dynamic junction in LEC. On the other hand, the slow ionic motion and irreversibly electrochemical doping under high biasing field were two of the challenges for polymer LECs to be used in practical applications. More recent works have been focusing on the following directions:

- (i) LEC with frozen junction operation [153,154]. With frozen p-i-n junction, the LEC device exhibited unipolar (rectifying) behavior and no hysteresis was observed in fast I - V scans. To freeze out ionic mobility, either lower temperature could be applied after the formation of the p-i-n junction, or an electrolyte with negligible ionic conductivity at room temperature could be used. In the latter method, the p-i-n junction was formed at elevated temperatures, and the device was operated at room temperature.
- (ii) LEC under pulsed operation with mean field below EC doping threshold and pulse width shorter than the response time of ionic charges [155]. This operation scheme allows the induced junction in a LEC to be stabilized, and to be used for emitters in a PM display (see the following section for PMPLED).

1.4.3 PLED WITH STABLE CATHODE ELECTRODE

To optimize the performance of SMOLEDs and PLEDs, it is important to choose electrodes whose work functions are well matched to the bands of EL organic materials in order to minimize the barriers for charge injections. Although cathodes made of low-work-function

metals are necessary to obtain adequate electron injection for high efficiency at low operation voltage, metals such as Ca, Ba, or Mg are air-sensitive, highly reactive, and difficult to handle. To achieve long storage life and long stress life, devices fabricated with low-work-function cathodes must be hermetically sealed.

To use air-stable metals with high work function as cathodes, the electron injection barriers have to be reduced. As proposed by Campbell et al., a change in barrier height can be induced by a self-assembled monolayer of oriented dipoles chemically attached to the electrode [156]. Cao and his coworkers have demonstrated that certain surfactant-like additives, such as anionic ether sulfates, $R(OCH_2CH_2)_nOSO_3Li$, dissolved or dispersed in the EL polymer significantly improve electron injection from relatively high-work-function metals such as Al [157,158]. The Al electrode is complexed with the ethylene oxide group of the surfactant molecule, thus the dipoles of the surfactant molecules orienting in the correct direction to reduce the barriers. The Li-NPTEOS-type compounds not only improve the PLEDs' quantum efficiency in single-layer device, but also enhance the performance of PLEDs and SMOLEDs in bilayer structures with Al as cathodes. With air-stable metals as cathodes, the devices can be stored in air for approximately 30 h without significant degradation.

1.4.4 PLED AND PLEC IN SURFACE CELL CONFIGURATION

Besides the commonly used sandwich structure, organic light-emitting devices could be fabricated in the metal–polymer–metal surface cell configuration, as illustrated in Figure 1.18 [61,159,160]. To make such devices, first, two symmetric electrodes are prepared onto a substrate with a gap in between. The metal can be deposited onto the substrate by thermal

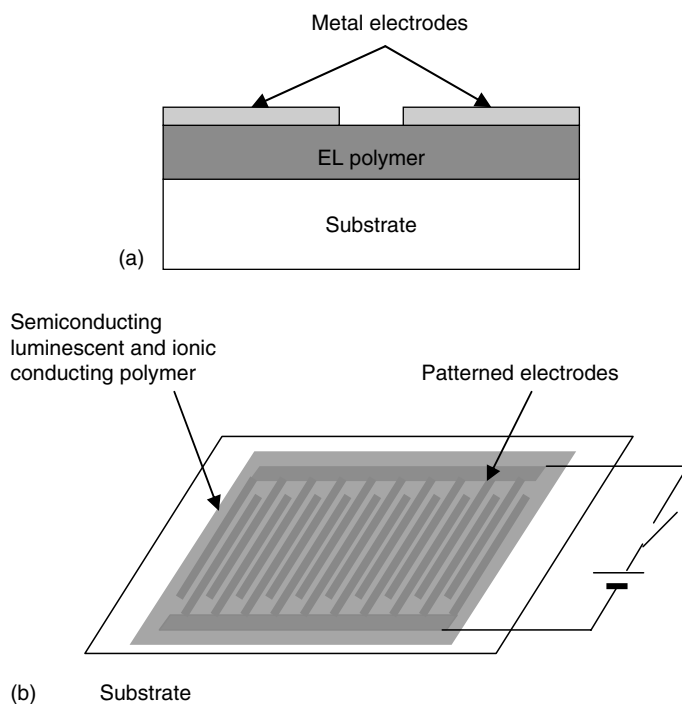


FIGURE 1.18 (a) Planar PLED and (b) planar PLEC in interdigitated cell configuration.

evaporation, electron beam evaporation, or sputtering. Patterning can be achieved by depositing through a shadow mask, by photolithography, by microcontact printing, or by screen printing. Since the n-type doped and p-type-doped regions in the LEC (under bias) have relatively low resistivity, the LEC in surface cell configuration exhibited similar performance parameters as those in sandwich configuration [149,151,161]. Contrary to LEC devices, the symmetric electrodes in the planar PLED devices made the carriers injection extremely difficult. For a planar PLED with a 20- μm gap between two gold electrodes and free standing PPV as the EL polymer layer, light emission was observed at 77 K, and an operation voltage of more than 500 V was required [159]. To reduce the operation voltage to normal level, a submicron gap of 0.41 μm was made by photolithography, resulting in a turn-on voltage of 35 V at room temperature [160].

The planar configuration allows the display to be hybridized with integrated circuits on a Si wafer and thereby enables new approaches to fabricate integrated electro-optical devices. The combination of conjugated polymer LEDs and LECs with silicon technology relies on the design of structures that allow efficient surface emission. For nontransparent substrates, e.g., Si, a planar device configuration compatible with standard photolithography is a promising approach. With interdigitated electrodes on transparent substrates, such as glass or polymer films, light emission can be viewed from both sides of the device. In addition to these novel features, the planar configuration has manufacturing advantages: (1) the electrodes can be prepared before the active polymer film is cast onto the substrate; (2) the device performance is insensitive to pinholes or other defects on the polymer films; (3) the device performance is relatively insensitive to the thickness of the active polymer layer; and (4) the planar emissive devices can be fabricated in a roll-to-roll process at room temperature without vacuum equipments.

1.4.5 OPTOCOUPLERS MADE WITH SEMICONDUCTING POLYMERS

Optocouplers are a class of devices with input current (I_i) and output current (I_o) coupled optically, but isolated electrically. They are used extensively in the automation industry and in laboratory equipments where large common-mode noise/voltage or hazardous electrical shocks are present in circuits between transducers–detectors and controlling equipments. The simplest optocoupler is composed of an LED (input) and a photodiode (output) as shown in Figure 1.19.

By coupling a PLED with external EL efficiency (η_{EL}) over 1% ph/el with a polymer photodiode with quantum yield (η_c) of >20% el/ph, a polymer optocoupler can be constructed with current transfer ratio I_o/I_i larger than 2×10^{-3} . The transfer ratio I_o/I_i is proportional to product of the LED's external EL efficiency and the photodiode's quantum yield, $A \times \eta_c \times \eta_{\text{EL}}$, where A is a coupling constant determined by the spectral and geometrical overlap of the LED and the photodiode. In Figure 1.19, I_o/I_i is plotted versus input current for an optocoupler made with a MEH-PPV LED and a P3OT photodiode [62]. The current transfer ratio is $\sim 2 \times 10^{-3}$ at -10 V bias, comparable to I_o/I_i of commercial optocouplers made with inorganic semiconductors. In recent years, both the efficiency of the PLED and the efficiency of the photodiode have been improved significantly over those in the devices used to generate the data in Figure 1.19. Using the improved devices currently available, such as SMOLEDs and PLEDs made with fluorescent emitters with η_{EL} of 5–7% or with phosphorescent emitters with η_{EL} of 10–15%, and photodiodes made with P3AT:PCBM blend [64] or PFO-BET:PCBM blend with η_c of 50–100% [146], a current transfer ratio of 0.1 is expected even when the PD is at 0 to -2 V bias. Thus, the polymer optocoupler could be a high transfer efficiency electric device for integrated circuits, optical interconnectors, or emitters, receivers, and modulators for telecommunication applications.

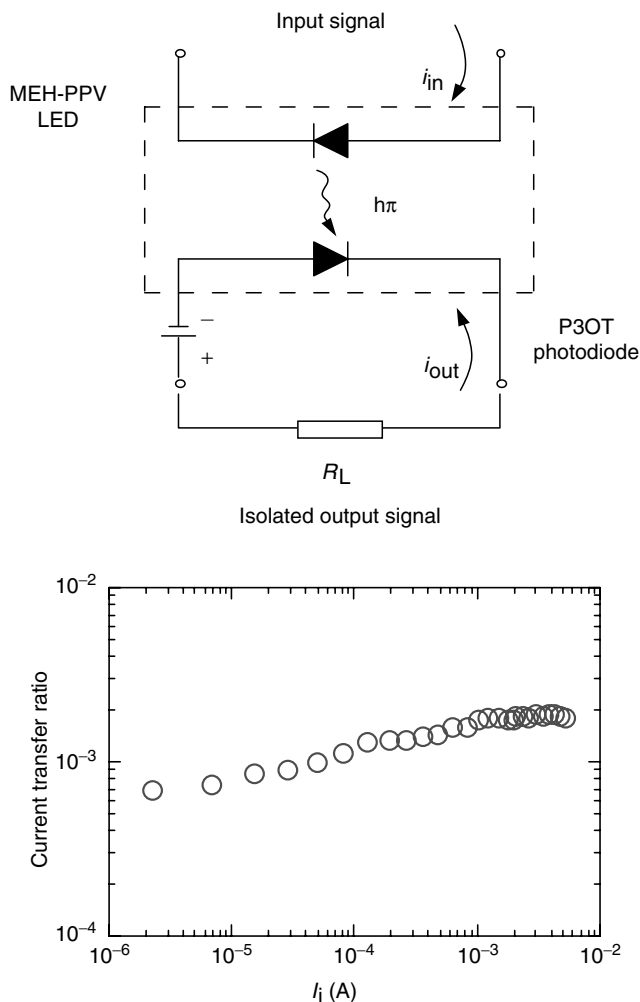


FIGURE 1.19 Circuit diagram (upper panel) and current transfer ratio, I_o/I_i (lower panel) of the polymer optocoupler. The photodiode was biased at -10 V.

1.5 FLAT-PANEL DISPLAYS MADE WITH SOLUTION-PROCESSIBLE ORGANIC SEMICONDUCTORS

1.5.1 SMOLEDs AND PLEDs AS EMITTER ELEMENTS IN FLAT-PANEL DISPLAYS

Offering lightweight, thin panel thickness, wide view angle (Lambertian emitter), high self-electroluminescent efficiencies, less power consumption, fast response time, and high-contrast, SMOLED and PLED technologies are considered as the next generation flat-panel display technology to replace liquid crystal. Low-temperature processes allow such SMOLED- and PLED-based displays to be made on plastic substrates in rigid or in flexible forms. Two kinds of processing technologies have been developed for high information content, full-color displays: vacuum deposition, suitable for processing organic molecules with low molecular weight [12], and solution casting and printing suitable for processing organic molecules soluble in common solvents [24]. The display development team at DuPont

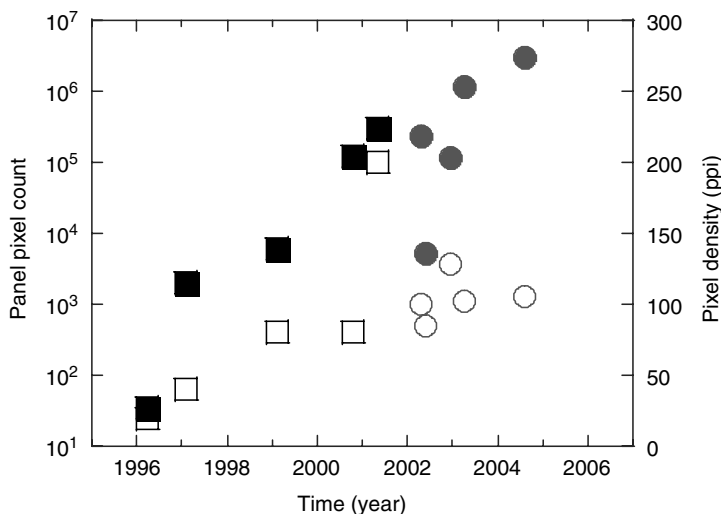


FIGURE 1.20 Development history on monochrome (squares) and full-color displays (circles) at DuPont Displays (formerly UNIAX Corporation): solid symbols denote total pixel counts; open symbols denote pixel density.

Displays (formerly UNIAX Corporation) has been focusing on pixelated display development with solution-processible EL polymers for more than 8 years. Display panel size, pixel density (number of pixels per inch), and total pixel counts have been improved gradually to the level needed for medium- to large-size high-definition television screens (Figure 1.20). 9" AMPLED in WVGA format ($800 \times \text{RGB} \times 480$), 7" AMPLED in HVGA format ($480 \times \text{RGB} \times 320$), and 14.1" AMPLED in WXGA format ($1280 \times \text{RGB} \times 768$) with over three million pixels have been successfully demonstrated recently [57,162,163].

1.5.2 PMOLED DISPLAYS VERSUS AMOLED DISPLAYS

Display pixels can be connected in the forms of segmental displays and column–row addressable displays. In the form of segmental displays, each display pixel is wired up individually and is addressed independently. Figure 1.21 shows a drawing of ITO pattern and cathode pattern for a seven-segment display. Such display is often operated under DC condition (with $\sim 100\%$ duty cycle), or operated in multiplexing mode with low duty cycle. Figure 1.22 shows a four-digit display system operating under $1/4$ duty cycle. Since the OLED pixels in segmental displays are operated at low duty cycle, the power efficiency of segmental displays is easy to be optimized.

Two kinds of driving schemes have been generally adopted in column–row addressable, pixelated OLED displays: PM and AM. Figure 1.23 shows their respective device structures. Since PLEDs are two-terminal, thin-film devices with rectifying I – V characteristics, a monochrome, PMPLED display can be made by laminating an unpatterned EL polymer layer between an array of anode electrodes (transparent ITO has been commonly used) and an array of cathode electrodes. In this way, only the electrode stripes need to be patterned, resulting in a device structure similar to that in TN- or STN-LCD displays. The manufacturing process is simple and its cost is relatively low. In AMPLED displays, each display pixel is addressed by the column and row electrodes (bus lines) on an AM backpanel, a common counter electrode can thus be used on the other side of EL film.

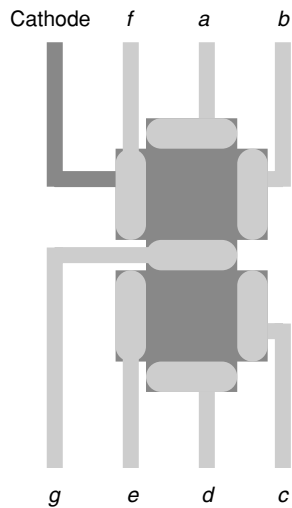


FIGURE 1.21 ITO pattern and cathode pattern of a seven-segment display.

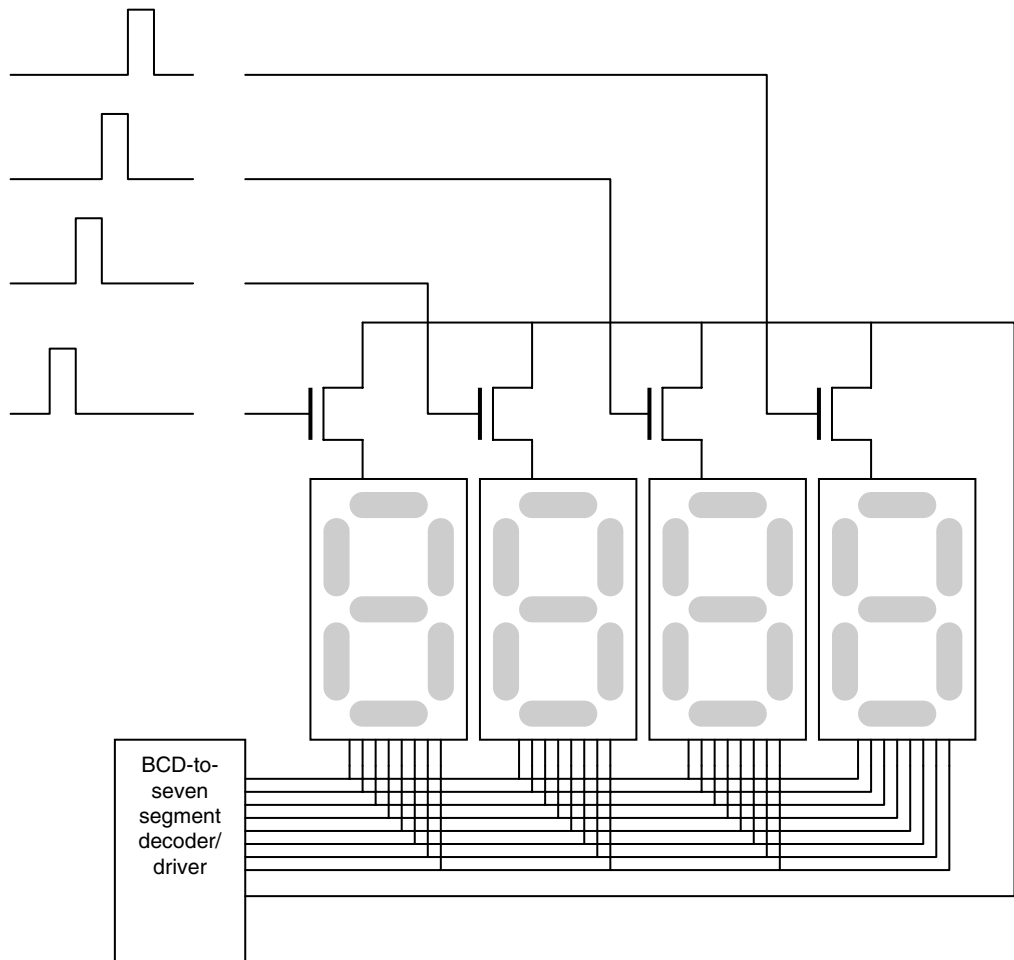


FIGURE 1.22 Multiplexing operation of a four-digit segmental display.

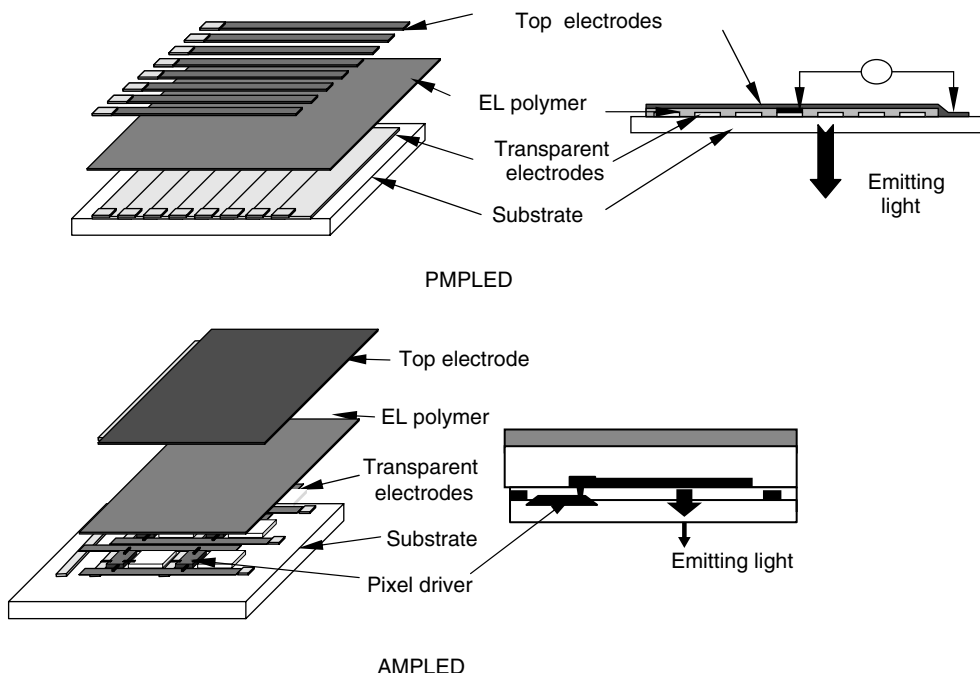


FIGURE 1.23 Cross-section views of the device structures of PMPLED (top) and AMPLD (bottom).

OLED pixel elements in PM displays are selectively turned on row by row with transient luminescent intensity N times brighter than the integrated intensity sensed by human eyes. The constraint of the maximum emitting intensity and the maximum operating voltage of the OLED pixels sets the limits on the duty cycle ($1/N$) of the PMOLEDs; in the past $1/32$ to $1/120$ have been demonstrated. The number of rows in PMOLEDs is equal to the reciprocal of the duty cycle when single scan is adopted, or twice of the reciprocal of the duty cycle when dual-scan driving scheme is adopted. Moreover, the resistance of the row and column power lines, the capacitance of the display pixel matrix, the requirement for the frame rate to achieve flicker-free operation, and the dielectric breakdown electric field over the organic EL film set additional limits on the number of rows and total number of the display pixels [164]. PMOLEDs are thus only practical for low or medium pixel count displays (typically less than 100,000 pixels). Figure 1.24 shows an engineering prototype for cellphone displays. It is a 96×64 PM display with 0.35-mm pitch size, made with Covion SY materials [165].

By means of a latchable switch made with thin-film-transistor (TFT) technology, the emitting pixels in AMOLED displays are operated continuously during a frame time (with analog driving scheme). Thus, the transient brightness of the emitting pixel is equal (or close) to the average brightness sensed by human eye. The pixel switch and the AM driving scheme also remove the limitations in PMOLED displays. High information content displays can thus be realized with such kind of driving scheme. Monochrome AMOLED in 4" VGA format (640×480 pixels, 200 ppi) [166], full-color AMOLED displays in 2.2" QCIF+ ($176 \times \text{RGB} \times 220$, 128 ppi) [167], 3.5–4" QVGA ($320 \times \text{RGB} \times 240$) [168], 9.1" WVGA ($800 \times \text{RGB} \times 480$) [162], 13" ($576 \times \text{RGB} \times 324$) [169], 13" WVGA ($852 \times \text{RGB} \times 480$) [170], 17" UXGA ($1600 \times \text{RGB} \times 1200$) [171], 15–20" WXGA ($1280 \times \text{RGB} \times 768$) [172], have been demonstrated with impressive image quality.



FIGURE 1.24 PM displays in 96 × 64 format made at DuPont Display.

1.5.3 MONOCHROME AMPLEDs MADE WITH SOLUTION-PROCESSIBLE POLYMERS

Monochrome AMPLED flat-panel displays have been made with performance parameters attractive for battery-powered portable applications. The AM backpanel was made of polysilicon material with integrated column and row drivers. Table 1.1 shows a data sheet for a 4" diagonal monochrome display with 960×240 pixels [173]. The resolution in horizontal direction was 300 ppi (85μm pitch size), while the resolution in vertical direction was 100 ppi (255 μm pitch size). With 100% pixels turned on at 200 cd/m², the entire AMPLED panel (including pixel drivers) only consumed electric power less than 500 mW (with 100% pixels on), which was

TABLE 1.1
Performance Parameters of a 4" Diagonal Monochrome
AMOLED Panel (without Circular Polarizer)

Active area	3.2 × 2.4" (81.6 × 61.2 mm)
Pitch size	85 × 255 μm
Color coordinates	x = 0.48, y = 0.53
Voltage	6.7 V
Panel current	71 mA
Pixel current	0.31 μA
Luminance	205 cd/m ²
Luminous efficiency	14.5 cd/A
Power efficiency	6.8 lm/W
Power consumption	0.47 W (100% pixels on)

the best number ever reported for AMPLEDs and AMOLEDs. The power efficiency reached 6.8 lm/W (without circular polarizer). These values are three to five times better than those of transfective AMLCDs with fluorescent backlight. Therefore, they are especially suitable for mobile, portable, and hand-held applications. The local emission intensity is 1/aperture ratio times the effective areal luminescence. For an AMPLED with aperture ratio of 50%, the display lifetime is approximately half that measured from a PLED backlight device. This relation has been confirmed in our monochrome AMPLED panels. Thus, the performance of monochrome AMPLEDs meets specifications for certain commercial applications.

When an AMOLED display panel is used for graphic or video applications, the average power consumption is only 20 to 50% of that consumed at 100% pixel light on at full intensity (depending on image content), reducing the power consumption further by two to five times [173,174]. It is worth mentioning that OLED displays exhibit superb performance at temperatures below the room temperature (with fast response time, sustaining EL efficiency, and longer operation lifetime), in contrast to AMLCDs' performances at low temperatures.

1.5.4 FULL-COLOR AMPLED MODULES

In manufacturing monochromatic OLED displays, the spin-coating process has been widely adopted for solution-based materials. To make a display with full-color images, each display pixel consists of three subpixels, each of which emits one of the three primary colors red, green, and blue, respectively. A reliable, cost-efficient, high throughput process for producing color subpixel is essential for commercializing full-color AMOLEDs, which has been one of the key focuses in AMOLED developments. For full-color AMOLED made of small molecules, thermal deposition with shadow masks has been widely adopted for patterning the EL molecule layer into three color subpixels. A known challenge for this process is to make large-size full-color display panel reliably, efficiently, and uniformly. Another challenge facing thermal deposition is to make full-color OLED displays with large mother glass sheet (Gen-3 to Gen-7 panel sizes are currently used for manufacturing AM backpanels). A popular process used in solution-processed full-color OLED to pattern color subpixels is printing, which is a scalable process, as demonstrated in paper printing industry. Inkjetting equipment capable of processing Gen-5 panel-size panels has been demonstrated by Seiko Epson Corporation for manufacturing color filters for AMLCDs. Thus, full-color process by means of inkjetting is attractive to manufacturing AMPLEDs.

By means of a proprietary printing process, DuPont Displays has been able to demonstrate full-color AMOLEDs at 100 ppi (4" QVGA and 9.1" WVGA) and 128 ppi (2.2" QCIF+). Table 1.2 provides data from a group of 4" QVGA panels [173]. A photo of such display panel is shown in Figure 1.25a. The total thickness of the display panel is less than 2 mm with a weight of only 26 g. Panel thickness less than 1 mm can also be made with modified packaging schemes. The AM backpanel was made with polysilicon technology,

TABLE 1.2
Performance of a Set of 4" Diagonal Full-Color AMOLED Made with Solution Process

Panel ID	Red η_{EL} (cd/A)	Green η_{EL} (cd/A)	Blue η_{EL} (cd/A)	White η_{EL} (cd/A)
A-DDD-G	1.15	9.2	0.69	1.89
A-DDD-C	0.92	4.7	0.80	1.68
A-DDD-F	0.56	6.6	0.43	1.1
A-DDD-F	0.94	5.07	1.34	2.08



FIGURE 1.25 Photo of a full-color AMOLED in 4" diagonal, QVGA format (a), and 14.1" diagonal WXGA (HDTV) format (b).

with integrated column and row drivers. It was driven with a customer-designed display controller in analog driving scheme. The equivalent white EL efficiency reaches 2.1 cd/A (without circular polarizer). The panel consumes ~260 mA with 100% pixels on at 115 cd/m² (white equivalent without circular polarizer). When running video images, peak luminescence

TABLE 1.3
Performance Parameters of a 14.1" WXGA Full Color AMOLED
Panel (Without Circular Polarizer)

Size	14.1"
Format	WXGA (1280 × 768)
Resolution	106 ppi
Contrast ratio	>10,000:1
Full white brightness	>600 cd/m ²
Power consumption	~20 W (100% pixel on at full white)
Color gamut	>60% NTSC
Luminance uniformity	>85%
Pixel count	~3 million

of 200 cd/m² was achieved. Again, when such a panel is used for video screen, the average power consumption is only 20–50% of the full power, lower than the power needed for the AMLCD panel with identical size and format.

The performance of AMOLEDs is improved drastically in the past years. In contrast to the data shown in Table 1.2 (which representing development stage in 2002), a set of recent data of a 14.1" WXGA AMLCD made with solution-processed OLED emitters is shown in Table 1.3 [163,175,176]. The color gamut is improved to over 60% with respect to NTSC. The luminous and power efficiencies at white point ($x \sim 0.28$, $y \sim 0.31$) are >8 cd/A and >5 lm/W. The power efficiency surpasses the performance of AMLCDs, plasma displays, and all other known flat-panel displays in commercial market or under development. A photo of the 14.1" AMOLED display is shown in Figure 1.25b.

1.5.5 PERFORMANCE SIMULATION FOR FULL-COLOR AMOLEDs

A simulation protocol has been developed for designing monochrome and full-color AMOLED panels. With input parameters of color coordinates, luminance–voltage, and current–voltage data of the red, green, and blue emitters, geometric dimensions and aperture ratio of the subpixels, and the numbers of rows and columns, one can predict the AMOLED panel performance including power consumption at a given brightness and luminous efficiency. In reverse, one can also extrapolate the minimum requirements for EL emitters for a given display format, display brightness, and power budget. Table 1.4 provides the power consumption of PLED portion for a series of display panels of popular formats. The data are obtained at panel's full brightness of 200 cd/m² without circular polarizer when all the pixels are fully turned on. Aperture ratio of 50% was assumed. Power consumptions were calculated based on three groups of polymer emitters available with different maturities. This simulation tool has been used for several AMOLED display panels and proven effective and accurate. Comparing the data in Table 1.4 with the testing results shown in Table 1.2, one can see that the performance of our 4" full-color AMOLED panels has passed the first performance target, approaching to the second one.

The simulation discussed above was based on full color produced by individual red, green, and blue emitters. Other full-color reproduction approaches have been proposed for OLED displays including color from blue emitter by means of energy down conversion fluorescent filter [177], and color from white emitters by means of transmission color filter sets similar to that used in LCD industry [178,179]. Table 1.5 compares the EL efficiency of equivalent white

TABLE 1.4
Power Consumption of AMOLEDs for Three Sets of OLED Emitters (Portion on Pixel Driver Is Excluded)

Format	Size	Power Consumption (PLED-1) ^a (W)	Power Consumption (PLED-2) ^b (W)	Power Consumption (PLED-3) ^c (W)	Targeting Applications
QCIF+220×RGB×176	2.2'' 128 ppi	0.605	0.214	0.141	Mobile phone, digital camera
QVGA 320×RGB×240	4.0'' 100 ppi	1.99	0.71	0.47	Hand PC, PDA, game console, web reader
WQVGA 480×RGB×240	5.4'' 100 ppi	2.97	1.04	0.70	DVD screen, GPS
VGA 640×RGB×480	8.0'' 100 ppi	7.92	4.2	1.86	Portable TV, PC monitors
WVGA 800×RGB×480	9.3'' 100 ppi	9.95	3.53	2.32	Portable TV, PC monitors
WXGA 1280×RGB×768	15'' 100 ppi	25.3	8.9	5.9	Table-top TV, PC monitors
UXGA 1600×RGB×1200	20'' 100 ppi	49.7	17.6	11.6	Table-top and Wall-mount TVs
WXGA 1280×RGB×768	40'' 37 ppi	182	64	42.4	Wall-mount TVs

^a Based on a set of polymer RGB emitters with EL efficiencies of 1 cd/A (R), 5 cd/A (G), and 1 cd/A (B), respectively.
^b Based on a set of polymer RGB emitters with EL efficiencies of 2 cd/A (R), 10 cd/A (G), and 2 cd/A (B), respectively.
^c Based on a set of polymer RGB emitters with EL efficiencies of 5 cd/A (B), 17 cd/A (G), and 3 cd/A (R), respectively.

generated by red, green, and blue subpixels from three different color reproduction approaches [180]. The data were based upon EL emitters with equal quantum efficiency (5% ph/el), and identical geometric pixel form factors. In the color-from-blue approach, energy down conversion efficiency of 70% was used for the fluorescent filers. The results suggest that the approach of full color reproduced from red, green, and blue color emitters has the best power efficiency, while the approach of full color reproduced from white emitter is the least efficient. The display panel operation lifetime (for given OLED efficiency and lifetime) follows the same trend as that discussed in the previous sections, due to different local brightness needed for achieving given panel brightness. It is also worth mentioning that the order of manufacturing simplicity is perhaps reversed in the three different color reproduction

TABLE 1.5
EL Efficiencies of Equivalent White Generated by Color Pixels Made by Three Different Color Reproduction Approaches

Full-Color Production Approach	Luminous Efficiency (cd/A)	Power Efficiency (lm/W)
Color from red, green, and blue emitters	11.2	11.8
Color from blue emitter with phorsphor filters	8.64	7.23
Color from white emitter with transmission filters	0.908	0.759

approaches. The choice of full-color manufacturing process can thus be selected differently based on market differentiation, display format and performance requirements, OLED lifetime, process cost, yield, and so on.

1.5.6 AMOLED FOR GRAPHIC AND MOTION PICTURE APPLICATIONS

The issue of power consumption of an OLED display panel changing with the information content has not been well addressed in the OLED field. For AMLCD display panel, the power consumption is almost independent of the information content. For an AMOLED or an AMPLD panel, the power consumption is directly proportional to the number of pixels lighting up. For each display pixel, the power consumption is nearly proportional to the level of brightness (gray level). Thus, AMOLED display only consumes the power necessary, without any waste. This effect is similar to the concept of Pay-Per-View developed in cable and satellite TV industries. Two direct consequences of the Pay-Per-View effect are:

- (1) Significant reduction of panel power consumption
- (2) Substantially extended display operation lifetime

To investigate the effectiveness of the Pay-Per-View for graphic and video applications, nine movies were selected randomly and were run with an AMPLD panel. The panel current and power were recorded with respect to the operation time. The total energy consumed for each movie and the respective average power consumption were then derived. An effective power saving factor (which can also be defined as a lifetime-enhancing factor) was calculated by dividing the full power corresponding to 100% pixels turned on at maximum brightness (provided in Table 1.1 and Table 1.4) by the average power consumed for each movie. The results are listed in Table 1.6. The results showed that

- (1) The power consumption of OLED display varies over a broad range for videos in different subjects and different categories and
- (2) The average power of an AMPLD panel for video applications is only 20–50% of the full power.

The average lifetime-enhancing factor over the nine movies is at least 3.3 times longer than that measured with full screen on at full brightness, e.g., a panel with 10,000 h operation life under maximum brightness has an effective operation lifetime $\sim 33,000$ h for video

TABLE 1.6
Effectiveness in Power Saving and Lifetime Extension

Movie	Operation Time (min)	Average Power (W)	Power Saving or Lifetime-Enhancing Factor
#1	87.5	0.763	2.13
#2	94.25	0.602	2.70
#3	94.33	0.535	3.03
#4	98.67	0.564	2.88
#5	24.87	0.674	2.41
#6	87.55	0.400	4.06
#7	77.62	0.244	6.65
#8	118.07	0.486	3.34
#9	94.53	0.697	2.33

applications. This statement is based upon the simple charge conservation mechanism discussed in earlier sections. It is worth mentioning that the operation lifetimes of the colored OLED emitters are proportional to $L^{-\beta}$ (in which $\beta = 1.3 - 2.2$ was frequently observed in both SMOLED and PLED) at the interesting brightness. Taking this superlinearity into consideration, the operation lifetime in video operation would be larger than the power-saving factor discussed above. Assuming the average intensity for movie operation is one third of the full intensity, the lifetime-enhancing factor would be 5.3 times that driving at full brightness. The Pay-Per-View effect makes OLED displays promising for motion image applications.

Another significance of this finding is the effective power saving (with the same factor as lifetime enhancement) for AMOLED displays used for graphic and video applications. This feature makes OLED displays attractive especially for battery-powered mobile and portable applications. Taking this power saving factor into account, the AMOLED displays with the performance parameters shown in Table 1.3 have already won over AMLCD for graphic and video applications. Recently DuPont and Samsung demonstrated a 14.1" diagonal, solution-processed full-color AMOLED display in HDTV format at SID05. The current efficiency and power efficiency were improved to over 8 cd/A and 5 lm/W [175,176]. AMOLED for video application also minimizes or eliminates the differential aging among emissive display pixels.

All these features above make AMOLED especially suitable for portable DVD players, digital cameras, portable TVs, and game players. The discussion in this section also suggests that the performance of a given OLED display can be maximized by proper design of display contents.

1.6 SUMMARY AND REMARKS

The development history of organic light-emitting device and OLED displays provides a great story on how scientific concepts and discoveries can be transformed into application technologies and eventually impact human life in many different ways. Within less than 20 years, the field of organic light emitters has come through concept demonstration, single device performance improvement, industrial development in matrix formation, color pixel formation, display architecture, and system integration. The performance parameters of OLED displays have been improved to the level better than other existing display technologies and better than that needed for many commercial applications. Products in both PMOLED and AMOLED forms have been in commercial markets for several years. More products based on OLED displays are to be introduced this year and in the coming years. The market of OLED display industry is expected to reach 4 billion dollars by 2008–2010 estimated by Display Research.

As mentioned in this review, AMPLDs are especially attractive for motion picture applications. The Pay-Per-View effect in OLED displays reduces power consumption and extends operation lifetime. Motion picture applications also minimize image retention and optimize display homogeneity. AMOLED has been widely viewed as a promising display technology in competing with AMLCD and plasma displays. The dream of using organic semiconductor films for optoelectronic device applications has become a reality.

In addition to light emission effect and its applications, other electric and optoelectronic effects and device applications in organic semiconductors have been well studied, including photovoltaic cells, photodiodes, image sensors, and thin-film transistors. The field of organic electronics has become one of the hottest areas in the past decade. Due to the excellent optoelectronic and electro-optical conversion efficiencies, and less demanding on charge mobilities in thin-film device configuration, significant progress was achieved in all

optoelectric and electro-optical applications. The performance parameters have been improved to the level comparable or substantially better than their inorganic counterparts, promising for a variety of practical applications.

ACKNOWLEDGMENT

We would like to thank our coworkers in DuPont Displays for numerous stimulating discussions and support.

REFERENCES

1. HJ Round, A note on carborundum, *Electron. World*, 19:309–310, 1907.
2. N Holonyak Jr. and SF Bevacqua, Coherent (visible) light emission from Ga(As_{1-x}P_x) junctions, *Appl. Phys. Lett.*, 1:82–83, 1962.
3. TS Perry, Red hot, *IEEE Spectrum*, June 3, 2003.
4. A Bernanose, M Comte, and P Vouaux, A new method of emission of light by certain organic compounds, *J. Chim. Phys.*, 50:64–68, 1953.
5. A Bernanose, The mechanism of organic electroluminescence, *J. Chim. Phys.*, 52:396–400, 1955.
6. M Pope, H Kallman, and P Magnante, Electroluminescence in organic crystals, *J. Chem. Phys.*, 38:2042–2043, 1963.
7. RH Partridge, Radiation Sources, U.S. Patent 3,995,299, 1976.
8. W Helfrich and WG Schneider, Recombination radiation in anthracene crystals, *Phys. Rev. Lett.*, 14:229–231, 1965.
9. J Dresner, Double injection electroluminescence in anthracene, *RCA Rev.*, 30:322–334, 1969.
10. DF Williams and M Schadt, DC and pulsed electroluminescence in anthracene and doped anthracene crystals, *J. Chem. Phys.*, 53:3480–3487, 1970.
11. PS Vincett, WA Barlow, RA Hann, and GG Roberts, Electrical conduction and low voltage blue electroluminescence in vacuum-deposited organic films, *Thin Solid Films*, 94:171–183, 1982.
12. CW Tang and SA VanSlyke, Organic electroluminescent diodes, *Appl. Phys. Lett.*, 51:913–915, 1987.
13. www.pioneerelectronics.com Press Release.
14. www.kodak.com Press Release.
15. www.sony.com Press Release, September 14, 2004.
16. CK Chiang, CR Fincher, YW Park, AJ Heeger, H Shirakawa, EJ Louis, SC Gau, and AG MacDiarmid, Electrical conductivity in doped polyacetylene, *Phys. Rev. Lett.*, 39:1098–1101, 1977.
17. H Shirakawa, EJ Louis, AG MacDiarmid, CK Chiang, and AJ Heeger, Synthesis of electrically conducting organic polymers: halogen derivatives of polyacetylene, (CH)_x, *Chem. Commun.*, 16:578–580, 1977.
18. MD McGehee, EK Miller, D Moses, and AJ Heeger, Twenty years of conducting polymers: from fundamental science to applications, in *Advances in Synthetic Metals: Twenty Years of Progress in Science and Technology*, P. Bernier, S. Lefrant, and G. Bidan, Eds., Elsevier, Amsterdam, 1999, pp. 98–205.
19. R Kiebooms, R Menon, and K Lee, Synthesis, electrical, and optical properties of conjugated polymers, in *Handbook of Advanced Electronic and Photonic Materials and Devices*, H.S. Nalwa, Ed., Academic Press, New York, 2001, pp. 1–102.
20. M Ozaki, DL Peebles, BR Weinberg, CK Chiang, SC Gau, AJ Heeger, and AG MacDiarmid, Junction formation with pure and doped polyacetylene, *Appl. Phys. Lett.*, 35:83–85, 1979.
21. BR Weinberg, SC Gau, and Z Kiss, A polyacetylene:aluminum photodiode, *Appl. Phys. Lett.*, 38:555–557, 1981.
22. H Tomozawa, D Braun, SD Phillips, AJ Heeger, and H Kroemer, Metal–polymer Schottky barriers on cast films of soluble poly(3-alkylthiophenes), *Synth. Met.*, 22:63–69, 1987.
23. JH Burroughes, DDC Bradley, AR Brown, RN Marks, K Mackay, RH Friend, PL Burns, and AB Holmes, Light-emitting diodes based on conjugated polymers, *Nature*, 347:539–541, 1990.

24. D Braun and AJ Heeger, Visible light emission from semiconducting polymer diodes, *Appl. Phys. Lett.*, 58:1982–1984, 1991.
25. F Wudl, P-M Allemand, G Srdanov, Z Ni, and D McBranch, Polymers and an unusual molecular crystal with NLO properties, in *Materials for Non-Linear Optics: Chemical Perspectives*, S.R. Marder, J.E. Sohn, and G.D. Stucky, Eds., American Chemical Society, Washington, 1991, pp. 683–686.
26. F Wudl and G Srdanov, Conducting Polymer Formed of Poly(2-Methoxy,5-(2'-Ethyl-Hexyloxy)-*p*-Phenylenevinylene), U.S. Patent 5,189,136, 1993.
27. H Spreitzer, H Becker, E Kluge, W Kreuder, H Schenk, R Demandt, and H Schöo, Soluble phenyl-substituted PPVs — new materials for highly efficient polymer LEDs, *Adv. Mater.*, 10:1340–1343, 1998.
28. H Becker, H Spreitzer, K Ibrom, and W Kreuder, New insights into the microstructure of gilch-polymerized PPVs, *Macromolecules*, 32:4925–4932, 1999.
29. G Yu and AJ Heeger, Semiconducting polymers as materials for device applications, in *The Physics of Semiconductors*, M. Schleffer and R. Zimmerman, Eds., World Scientific, Singapore, 1996, p. 35.
30. C Zhang, G Yu, and Y Cao, Long Operating Life for Polymer Light-Emitting Diodes, U.S. Patent 5,798,170, 1998.
31. H Becker, H Spreitzer, W Kreuder, E Kluge, H Schenk, ID Parker, and Y Cao, Soluble PPVs with enhanced performance — a mechanistic approach, *Adv. Mater.*, 12:42–48, 2000.
32. DM Johansson, G Srdanov, G Yu, M Theander, O Inganäs, and MR Andersson, Synthesis and characterization of highly soluble phenyl-substituted poly(*p*-phenylenevinylene)s, *Macromolecules*, 33:2525–2529, 2000.
33. DM Johansson, X Wang, T Johansson, O Inganäs, G Yu, G Srdanov, and MR Andersson, Synthesis of soluble phenyl-substituted poly(*p*-phenylenevinylene)s with a low content of structural defects, *Macromolecules*, 35:4997–5003, 2002.
34. Y Ohmori, M Uchida, K Muro, and K Yoshino, Blue electroluminescent diodes utilizing poly(alkylfluorene), *Jpn. J. Appl. Phys.*, 30:L1941–L1943, 1991.
35. M Uchida, Y Ohmori, C Morishima, and K Yoshino, Visible and blue electroluminescent diodes utilizing poly(3-alkylthiophene)s and poly(alkylfluorene)s, *Synth. Met.*, 55–57:4168–4173, 1993.
36. Q Pei and Y Yang, Efficient photoluminescence and electroluminescence from a soluble polyfluorene, *J. Am. Chem. Soc.*, 118:7416–7417, 1996.
37. G Grem, G Leditzky, B Ullrich, and G Leising, Realization of a blue-light-emitting device using poly(*p*-phenylene), *Adv. Mater.*, 4:36–37, 1992.
38. B Grem, G Leditzky, B Ullrich, and G Leising, Blue electroluminescent device based on a conjugated polymer, *Synth. Met.*, 51:383–389, 1992.
39. Y Yang, Q Pei, and AJ Heeger, Efficient blue polymer light-emitting diodes from a series of soluble poly(paraphenylene)s, *J. Appl. Phys.*, 79:934–939, 1996.
40. J Huber, K Müllen, J Salbeck, H Schenk, U Scherf, T Stehlin, and R Stern, Blue light-emitting diodes based on ladder polymers of the PPP type, *Acta Polym.*, 45:244–247, 1994.
41. J Grüner, PJ Hamer, RH Friend, HJ Huber, U Scherf, and AB Holmes, A high efficiency blue-light-emitting diode based on novel ladder poly(*p*-phenylene)s, *Adv. Mater.*, 6:748–752, 1994.
42. G Horowitz, P Delannoy, H Bouchriha, F Deloffre, J-L Fave, F Garnier, R Hajlaoui, M Heyman, F Kouki, P Valat, V Wintgens, and A Yassar, A high efficiency blue-light-emitting diode based on novel ladder poly(*p*-phenylene)s, *Adv. Mater.*, 6:752–755, 1994.
43. G Grem, V Martin, F Meghdadi, C Paar, J Stampfl, J Sturm, S Tasch, and G Leising, Stable poly(*para*-phenylene)s and their application in organic light emitting devices, *Synth. Met.*, 71:2193–2194, 1995.
44. S Tasch, A Niko, G Leising, and U Scherf, Highly efficient electroluminescence of new wide band gap ladder-type poly(*para*-phenylenes), *Appl. Phys. Lett.*, 68:1090–1092, 1996.
45. I Sokolik, Z Yang, FE Karasz, and DC Morton, Blue-light electroluminescence from *p*-phenylene vinylene-based copolymers, *J. Appl. Phys.*, 74:3584–3586, 1993.
46. C Zhang, H von Seggern, K Pakbaz, B Kraabel, H-W Schmidt, and AJ Heeger, Blue electroluminescent diodes utilizing blends of poly(*p*-phenylphenylene vinylene) in poly(9-vinylcarbazole), *Synth. Met.*, 62:35–40, 1994.

47. A Kraft, AC Grimsdale, and AB Holmes, Electroluminescent conjugated polymers — seeing polymers in a new light, *Angew. Chem. Int. Ed.*, 37:402–428, 1998.
48. M Bernius, M Inbasekaran, E Woo, W Wu, and L Wujkowski, Light-emitting diodes based on fluorene polymers, *Thin Solid Films*, 363:55–57, 2000.
49. M Bernius, M Inbasekaran, E Woo, W Wu, and L Wujkowski, Fluorene-based polymers — preparation and applications, *J. Mater. Sci. Mater. Electron*, 11:111–116, 2000.
50. H Becker, S Heun, K Treacher, A Büsing, and A Falcou, Materials and inks for full color PLED-displays, *SID Digest Tech. Pap.*, 33:780–782, 2002.
51. TR Hebner, CC Wu, D Marcy, MH Lu, and JC Sturm, Ink jet printing of doped polymers for organic light emitting devices, *Appl. Phys. Lett.*, 72:519–521, 1998.
52. S-C Chang, J Liu, J Bharathan, Y Yang, J Onohara, and J Kido, Multicolor organic light-emitting diodes processed by hybrid ink jet printing, *Adv. Mater.*, 11:734–737, 1999.
53. F Pschenitzka and JC Sturm, Three-color organic light-emitting diodes patterned by masked dye diffusion, *Appl. Phys. Lett.*, 74:1913–1915, 1999.
54. DA Pardo, GE Jabbour, and N Peyghambarian, Application of screen printing in the fabrication of organic light-emitting devices, *Adv. Mater.*, 12:1249–1252, 2000.
55. CD Müller, A Falcou, N Reckefuss, M Rojahn, V Wiederhirn, P Rudati, H Frohne, O Nuyken, H Becker, and K Meerholz, Multi-colour organic light-emitting displays by solution processing, *Nature*, 421:829–833, 2003.
56. SID 2002 Advance Program. <http://www.sid.org/conf/sid2002/sid2002.html>, 2002.
57. Samsung SDI, IMID Exhibition, Asia Display/IMID'04, Daegu, Korean, August 23–24, 2004.
58. RW Lenz, C-C Han, J Stenger-Smith, and FE Karasz, Preparation of poly(phenylene vinylene) from cycloalkylene sulfonium salt monomers and polymers, *J. Polym. Sci., Part A*, 26:3241–3249, 1988.
59. MR Andersson, G Yu, and AJ Heeger, Photoluminescence and electroluminescence of films from soluble PPV-polymers, *Synth. Met.*, 85:1275–1276, 1997.
60. SM Sze, *Physics of Semiconductor Devices*, John Wiley & Sons, New York, 1981.
61. G Yu, High performance photonic devices made with semiconducting polymers, *Synth. Met.*, 80:143–150, 1996.
62. G Yu, K Pakbaz, and AJ Heeger, Optocoupler made from semiconducting polymers, *J. Electron. Mater.*, 23:925, 1994.
63. G Yu, J Gao, JC Hummelen, F Wudl, and AJ Heeger, Polymer photovoltaic cells: enhanced efficiencies via a network of internal donor–acceptor heterojunctions, *Science*, 270:1789–1791, 1995.
64. G Yu, J Wang, J McElvain, and AJ Heeger, Large-area, full-color image sensors made with semiconducting polymers, *Adv. Mater.*, 10:1431–1434, 1998.
65. AR Brown, K Pichler, NC Greenham, DDC Bradley, RH Friend, and AB Holmes, Optical spectroscopy of triplet excitons and charged excitations in poly(*p*-phenylenevinylene) light-emitting diodes, *Chem. Phys. Lett.*, 210:61–66, 1993.
66. Y Cao, ID Parker, G Yu, C Zhang, and AJ Heeger, Improved quantum efficiency for electroluminescence in semiconducting polymers, *Nature*, 397:414–417, 1999.
67. J-S Kim, PKH Ho, NC Greenham, and RH Friend, Electroluminescence emission pattern of organic light-emitting diodes: implications for device efficiency calculations, *J. Appl. Phys.*, 88:1073–1081, 2000.
68. Z Shuai, D Beljonne, RJ Silbey, and JL Brédas, Singlet and triplet excitons formation rates in conjugated polymer light-emitting diodes, *Phys. Rev. Lett.*, 84:131–134, 2000.
69. M Wohlgenannt, K Tandon, S Mazumdar, S Ramasesha, and ZV Vardeny, Formation cross-sections of singlet and triplet excitons in π -conjugated polymers, *Nature*, 409:494–497, 2001.
70. B Hu, Y Wu, Z Zhang, S Dai, and J Shen, Effects of ferromagnetic nanowires on singlet and triplet exciton fractions in fluorescent and phosphorescent organic semiconductors, *Appl. Phys. Lett.*, 88:022114, 2006.
71. V Cleave, G Yahiolu, P Le Barny, RH Friend, and N Tessler, Harvesting singlet and triplet energy in polymer LEDs, *Adv. Mater.*, 11:285–288, 1999.
72. MA Baldo, ME Thomson, and SR Forrest, High-efficiency fluorescent organic light-emitting devices using a phosphorescent sensitizer, *Nature*, 403:750–753, 2000.

73. C Adachi, MA Baldo, SR Forrest, and ME Thompson, High-efficiency organic electrophosphorescent devices with tris(2-phenylpyridine)iridium doped into electron-transporting materials, *Appl. Phys. Lett.*, 77:904–906, 2000.
74. AP Monkman, HD Burrows, LJ Hartwell, LE Horsburgh, I Hamblett, and S Navaratnam, Triplet energies of π -conjugated polymers, *Phys. Rev. Lett.*, 86:1358–1361, 2001.
75. L Smilowitz, A Hays, AJ Heeger, G Wang, and JE Bowers, Time-resolved photoluminescence from poly[2-methoxy, 5-(2-ethyl-hexyloxy)-*p*-phenylene-vinylene]: solutions, gels, films, and blends, *J. Chem. Phys.*, 98:6504–6509, 1993.
76. M Yan, LJ Rothberg, F Papadimitrakopoulos, ME Galvin, and TM Miller, Spatially indirect excitons as primary photoexcitations in conjugated polymers, *Phys. Rev. Lett.*, 72:1104–1107, 1994.
77. NC Greenham, IDW Samuel, GR Hayes, RT Phillips, YARR Kessener, SC Moratti, AB Holmes, and RH Friend, Measurement of absolute photoluminescence quantum efficiencies in conjugated polymers, *Chem. Phys. Lett.*, 241:89–96, 1995.
78. SV Frolov, M Liess, PA Lane, W Gellermann, ZV Vardeny, M Ozaki, and K Yoshino, Exciton dynamics in soluble poly(*p*-phenylene-vinylene): towards an ultrafast excitonic switch, *Phys. Rev. Lett.*, 78:4285–4288, 1997.
79. J Kido, K Nagai, Y Okamoto, and T Skotheim, Electroluminescence from polysilane film doped with europium complex, *Chem. Lett.*, 20:1267–1270, 1991.
80. MD McGehee, T Bergstedt, C Zhang, AP Saab, MB O'Regan, GC Bazan, VI Srdanov, and AJ Heeger, Narrow bandwidth luminescence from blends with energy transfer from semiconducting conjugated polymers to europium complexes, *Adv. Mater.*, 11:1349–1354, 1999.
81. MA Baldo, DF O'Brien, Y You, A Shoustikov, S Sibley, ME Thompson, and SR Forrest, Highly efficient phosphorescent emission from organic electroluminescent devices, *Nature*, 395:151–154, 1998.
82. W Zhu, Y Mo, M Yuan, W Yang, and Y Cao, Highly efficient electrophosphorescent devices based on conjugated polymers doped with iridium complexes, *Appl. Phys. Lett.*, 80:2045–2047, 2002.
83. X Gong, JC Ostrowski, MR Robinson, D Moses, GC Bazan, and AJ Heeger, High-efficiency polymer-based electrophosphorescent devices, *Adv. Mater.*, 14:581–585, 2002.
84. D Braun, G Gustafsson, D McBranch, and AJ Heeger, Electroluminescence and electrical transport in poly(3-octylthiophene) diodes, *J. Appl. Phys.*, 70:564–568, 1992.
85. NC Greenham, SC Moratti, DDC Bradley, RH Friend, and AB Holmes, Efficient light-emitting diodes based on polymers with high electron affinities, *Nature*, 365:628–630, 1993.
86. J Kido, M Kohda, K Okuyama, and K Nagai, Organic electroluminescent devices based on molecularly doped polymers, *Appl. Phys. Lett.*, 61:761–763, 1992.
87. J Kido, K Hongawa, K Okuyama, and K Nagai, White light-emitting electroluminescent devices using the poly(*N*-vinylcarbazole) emitter layer doped with three fluorescent dyes, *Appl. Phys. Lett.*, 64:815–817, 1994.
88. CC Wu, JKM Chun, PE Burrows, JC Sturm, ME Thompson, SR Forrest, and RA Register, Poly(*p*-phenylene vinylene)/tris(8-hydroxy) quinoline aluminum heterostructure light emitting diode, *Appl. Phys. Lett.*, 66:653–655, 1995.
89. J Kido, H Shionoya, and K Nagai, Single-layer white light-emitting organic electroluminescent devices based on dye-dispersed poly(*N*-vinylcarbazole), *Appl. Phys. Lett.*, 67:2281–2283, 1995.
90. M Berggren, O Inganäs, G Gustafsson, J Rasmussen, MR Andersson, T Hjertberg, and O Wennerström, Light-emitting diodes with variable colours from polymer blends, *Nature*, 372:444–446, 1994.
91. C Zhang, S Höger, K Pakbaz, F Wudl, and AJ Heeger, Improved efficiency in green polymer light-emitting diodes with air-stable electrodes, *J. Electron. Mater.*, 23:453–458, 1994.
92. H Nishino, G Yu, AJ Heeger, T-A Chen, and RD Rieke, Electroluminescence from blend films of poly(3-hexylthiophene) and poly(*N*-vinylcarbazole), *Synth. Met.*, 68:243–247, 1995.
93. G Yu, N Nishino, AJ Heeger, T-A Chen, and RD Rieke, Enhanced electroluminescence from semiconducting polymer blends, *Synth. Met.*, 72:249–252, 1995.
94. S Tasch, EJW List, O Ekström, W Graupner, G Leising, P Schlichting, U Rohr, Y Geerts, U Scherf, and K Müllen, Efficient white light-emitting diodes realized with new processable blends of conjugated polymers, *Appl. Phys. Lett.*, 71:2883–2885, 1997.

95. MT Bernius, M Inbasekaran, J O'Brien, and W Wu, Progress with light-emitting polymers, *Adv. Mater.*, 12:1737–1750, 2000.
96. EP Woo, WR Shiang, M Inbasekaran, and GR Roof, 2,7-Aryl-9-Substituted Fluorenes and 9-Substituted Fluorene Oligomers and Polymers, U.S. Patent 5,708,130, 1998.
97. Y Cao, P Smith, and AJ Heeger, Counter-ion induced processability of conducting polyaniline and of conducting polyblends of polyaniline in bulk polymers, *Synth. Met.*, 48:91–97, 1992.
98. Y Cao, GM Treacy, P Smith, and AJ Heeger, Solution-cast films of polyaniline: optical-quality transparent electrodes, *Appl. Phys. Lett.*, 60:2711–2713, 1992.
99. Y Cao, G Yu, C Zhang, R Menon, and AJ Heeger, Polymer light-emitting diodes with polyethylene dioxythiophene polystyrene sulfonate as the transparent anode, *Synth. Met.*, 87:171–174, 1997.
100. J Gao, AJ Heeger, JY Lee, and CY Kim, Soluble polypyrrole as the transparent anode in polymer light-emitting diodes, *Synth. Met.*, 82:221–223, 1996.
101. K Lee, EK Miller, AN Aleshin, R Menon, AJ Heeger, JH Kim, CO Yoon, and H Lee, Nature of the metallic state in conducting polypyrrole, *Adv. Mater.*, 10:456–459, 1998.
102. R Menon, CO Yoon, D Moses, and AJ Heeger, Metal-insulator transition in doped conducting polymers, in *Handbook of Conducting Polymers*, T.A. Skotheim, R.L. Elsenbaumer, and J.R. Reynolds, Eds., Marcel Dekker, New York, 1998, pp. 27–84.
103. Y Yang and AJ Heeger, Polyaniline as a transparent electrode for polymer light-emitting diodes: lower operating voltage and higher efficiency, *Appl. Phys. Lett.*, 64:1245–1247, 1994.
104. H Wang and G Yu, Copolymers Having Tunable Energy Levels and Color of Emission, Patent Application, US03016853, 2003.
105. M Radler, Progress in Dow Polyfluorenes for Light Emitting Diodes, 23rd International Display Research Conference, September 15–18, 2003, Pointe South Mountain Resort, Phoenix, Arizona.
106. M Leadbeater, N Patel, B Tierney, S O'Connor, I Grizzi, and C Towns, Blue LEP-OLED with 30,000 hours lifetime for flat panel display applications, *SID Digest Tech. Pap.*, 35:162–163, 2004.
107. J Burroughes, PLEDs: A Display Technology, IMID 04 2004.
108. G Gustafsson, Y Cao, GM Treacy, F Klavetter, N Colaneri, and AJ Heeger, Flexible light-emitting diodes made from soluble conducting polymers, *Nature*, 357:477–479, 1992.
109. JM Lupton, IDW Samuel, R Beavington, PL Burn, and H Bässler, Control of charge transport and intermolecular interaction in organic light-emitting diodes by Dendrimer generation, *Adv. Mater.*, 13:258–261, 2001.
110. S-C Lo, EB Namdas, PL Burn, and IDW Samuel, Synthesis and properties of highly efficient electroluminescent green phosphorescent iridium cored dendrimers, *Macromolecules*, 36:9721–9730, 2003.
111. ST Lee, JY Lee, MH Kim, MC Suh, Tae Min Kang, YJ Choi, JY Park, JH Kwon, HK Chung, J Baetzold, E Bellmann, V Savvateev, M Wolk, and S Webster, A new patterning method for full-color polymer light-emitting devices: laser induced thermal imaging (LITI), *SID Digest Tech. Pap.*, 33:784–787, 2002.
112. MB Wolk, PF Baude, JM Florczak, FB McCormick, and Y Hsu, Thermal Transfer Element for Forming Multilayer Devices, U.S. Patent 6,114,088, 2000.
113. MB Wolk, PF Baude, FB McCormick, and Y Hsu, Thermal Transfer Element and Process for Forming Organic Electroluminescent Devices, U.S. Patent 6,194,119, 2001.
114. J Wang, RG Sun, G Yu, and AJ Heeger, Fast pulsed electroluminescence from polymer light-emitting diodes, *J. Appl. Phys.*, 91:2417–2422, 2002.
115. B Werner, J Posdorfer, B Webling, H Becker, S Heun, H Vestweber, and T Hassenkam, Polyaniline as hole injection layer for OLEDs and PLEDs, *SID Digest Tech. Pap.*, 33:603–605, 2002.
116. YA Ono, *Electroluminescent Displays*, World Scientific, Singapore, 1995.
117. RH Fowler and L Nordheim, Electron emission in intense electric fields, *Proc. R. Soc. Lond.*, 119:173–181, 1928.
118. ID Parker, Carrier tunneling and device characteristics in polymer light emitting diodes, *J. Appl. Phys.*, 75:1656–1666, 1994.
119. D Braun, Diodes Made from Soluble Semiconducting Polymers: Electrical Transport and Electroluminescence. Ph.D. dissertation, University of California at Santa Barbara, Santa Barbara, CA, 1991.

120. PWM Blom, MJM de Jong, and JJM Vleggaar, Electron and hole transport in poly(*p*-phenylene) devices, *Appl. Phys. Lett.*, 68:3308–3310, 1996.
121. PWM Blom and MCJM Vissenberg, Dispersive hole transport in poly(*p*-phenylene vinylene), *Phys. Rev. Lett.*, 80:3819–3822, 1998.
122. H Antoniadis, MA Abkowitz, and BR Hsieh, Carrier deep-trapping mobility — lifetime products in poly(*p*-phenylene vinylene), *Appl. Phys. Lett.*, 65:2030–2032, 1994.
123. DJ Pinner, RH Friend, and N Tessler, Transient electroluminescence of polymer light emitting diodes using electrical pulses, *J. Appl. Phys.*, 86:5116–5130, 1999.
124. SA VanSlyke, CH Chen, and CW Tang, Organic electroluminescent devices with improved stability, *Appl. Phys. Lett.*, 69:2160–2162, 1996.
125. G Yu, C Zhang, Q Pei, Y Cao, Y Yang, and AJ Heeger, Low-Voltage, High-Brightness Polymer Light-Emitting Diodes with Long Stress Life, MRS Spring Meeting, San Francisco, 1996.
126. G Yu and AJ Heeger, High efficiency photonic devices made with semiconducting polymers, *Synth. Met.*, 85:1183–1186, 1997.
127. ID Parker, Y Cao, and CY Yang, Lifetime and degradation effects in polymer light-emitting diodes, *J. Appl. Phys.*, 85:2441–2447, 1999.
128. NT Harrison, N Tessler, CJ Moss, RH Friend, and K Pichler, Peak current density and brightness from poly(*p*-phenylenevinylene) based light-emitting diodes, *Opt. Mater.*, 9:178–182, 1998.
129. D Moses, High quantum efficiency luminescence from a conducting polymer in solution: a novel polymer laser dye, *Appl. Phys. Lett.*, 60:3215–3216, 1992.
130. N Tessler, GJ Denton, and RH Friend, Lasing from conjugated-polymer microcavities, *Nature*, 382:695–697, 1996.
131. F Hide, MA Díaz-García, BJ Schwartz, MR Andersson, Q Pei, and AJ Heeger, Semiconducting polymers: a new class of solid-state laser materials, *Science*, 273:1833–1836, 1996.
132. SV Frolov, M Shkunov, and ZV Vardeny, Ring microlasers from conducting polymers, *Phys. Rev. B*, 56:R4363–R4366, 1997.
133. MD McGehee and AJ Heeger, Semiconducting (conjugated) polymers as materials for solid-state lasers, *Adv. Mater.*, 12:1655–1668, 2000.
134. DuPont Displays News Release, SID 03 2003.
135. G Yu, C Zhang, and AJ Heeger, Dual-function semiconducting polymer devices: light-emitting and photodetecting diodes, *Appl. Phys. Lett.*, 64:1540–1542, 1994.
136. M Meier, S Karg, K Zuleeg, W Brütting, and M Schwoerer, Determination of trapping parameters in poly(*p*-phenylenevinylene) light-emitting devices using thermally stimulated currents, *J. Appl. Phys.*, 84:87–92, 1998.
137. A Kadashchuk, Y Skryshevski, Y Piryatinski, A Vakhnin, EV Emelianova, VI Arkhipov, H Bässler, and J Shinar, Thermally stimulated photoluminescence in poly(2,5-dioctoxy *p*-phenylene vinylene), *J. Appl. Phys.*, 91:5016–5023, 2002.
138. Y Wang, Photoconductivity of fullerene-doped polymers, *Nature*, 356:585–587, 1992.
139. NS Sariciftci, L Smilowitz, AJ Heeger, and F Wudl, Photoinduced electron transfer from a conducting polymer to buckminsterfullerene, *Science*, 258:1474–1476, 1992.
140. KY Law, Organic photoconductive materials: recent trends and developments, *Chem. Rev.*, 93:449–486, 1993.
141. CH Lee, G Yu, D Moses, K Pakbaz, C Zhang, NS Sariciftci, AJ Heeger, and F Wudl, Sensitization of the photoconductivity of conducting polymer by C₆₀: photoinduced electron transfer, *Phys. Rev. B*, 48:15425–15433, 1993.
142. G Yu, K Pakbaz, and AJ Heeger, Semiconducting polymer diodes: large size, low cost photo-detectors with excellent visible-ultraviolet sensitivity, *Appl. Phys. Lett.*, 64:3422–3424, 1994.
143. NS Sariciftci, D Braun, C Zhang, VI Srdanov, AJ Heeger, and F Wudl, Semiconducting polymer–buckminsterfullerene heterojunctions: diodes, photodiodes and photovoltaic cells, *Appl. Phys. Lett.*, 62:585–587, 1993.
144. CJ Brabec, C Winder, NS Sariciftci, JC Hummelen, A Dhanabalan, PA van Hal, and RAJ Janssen, A low-bandgap semiconducting polymer for photovoltaic devices and infrared emitting diodes, *Adv. Funct. Mater.*, 12:709–712, 2002.

145. M Svensson, F Zhang, SC Veenstra, WJH Verhees, JC Hummelen, JM Kroon, O Inganäs, and MR Andersson, High-performance polymer solar cells of an alternating polyfluorene copolymer and a fullerene derivative, *Adv. Mater.*, 15:988–991, 2003.
146. Q Zhou, Q Hou, L Zheng, X Deng, G Yu, and Y Cao, Fluorene-based low band-gap copolymers for high performance photovoltaic devices, *Appl. Phys. Lett.*, 84:1653–1655, 2004.
147. www.siemens.com
148. AJ Heeger and G Yu, Dual Function Conducting Polymer Diodes, U.S. Patent 5,504,323, 1996.
149. Q Pei, G Yu, C Zhang, Y Yang, and AJ Heeger, Polymer light-emitting electrochemical cells, *Science*, 269:1086–1088, 1995.
150. Q Pei, Y Yang, G Yu, C Zhang, and AJ Heeger, Polymer light-emitting electrochemical cells: *in situ* formation of a light-emitting p–n junction, *J. Am. Chem. Soc.*, 118:3922–3929, 1996.
151. Y Cao, G Yu, AJ Heeger, and CY Yang, Efficient, fast response light-emitting electrochemical cells: electroluminescent and solid electrolyte polymers with interpenetrating network morphology, *Appl. Phys. Lett.*, 68:3218–3220, 1996.
152. Y Cao, MR Andersson, Q Pei, G Yu, and AJ Heeger, Light-emitting electrochemical cells using crown ether as solid electrolyte, *J. Electrochem. Soc.*, 144:L317–L320, 1997.
153. G Yu, Y Cao, M Andersson, J Gao, and AJ Heeger, Polymer light-emitting electrochemical cells with frozen p–i–n junction at room temperature, *Adv. Mater.*, 10:385–388, 1998.
154. J Gao, G Yu, and AJ Heeger, Polymer light-emitting electrochemical cells with frozen p–i–n junction, *Appl. Phys. Lett.*, 71:1293–1295, 1997.
155. G Yu, Y Cao, C Zhang, Y Li, J Gao, and AJ Heeger, Complex admittance measurements of polymer light-emitting electrochemical cells: ionic and electronic contributions, *Appl. Phys. Lett.*, 73:111–113, 1998.
156. IH Campbell, S Rubin, TA Zawodzinski, JD Kress, RL Martin, DL Smith, NN Barashkov, and JP Ferraris, Controlling Schottky energy barriers in organic electronic devices using self-assembled monolayers, *Phys. Rev. B*, 54:R14321–R14324, 1996.
157. Y Cao, G Yu, and AJ Heeger, Efficient, low operating voltage polymer light-emitting diodes with aluminum as the cathode material, *Adv. Mater.*, 10:917–920, 1998.
158. Y Cao, Electrically Active Polymer Compositions and Their Use in Efficient, Low Operating Voltage, Polymer Light-Emitting Diodes with Air-Stable Cathodes, U.S. Patent 5,965,281, 1999.
159. U Lemmer, D Vacar, D Moses, and AJ Heeger, Electroluminescence from poly(phenylene vinylene) in a planar metal–polymer–metal structure, *Appl. Phys. Lett.*, 68:3007–3009, 1996.
160. MD McGehee, D Vacar, U Lemmer, D Moses, and AJ Heeger, Microplanar polymer light-emitting diodes, *Synth. Met.*, 85:1233–1234, 1997.
161. G. Yu, Polymer Light-Emitting Electrochemical Cells in Surface Cell Configuration, U.S. Patent 5,677,546, 1997.
162. DuPont Displays, SID Exhibition, Baltimore, May 20–22, 2003.
163. DuPont Displays, SID Exhibition, Boston, May 22–27, 2005.
164. D Braun, J Rowe, and G Yu, Crosstalk and image uniformity in passive matrix polymer LED displays, *Synth. Met.*, 102:920–921, 1999.
165. DuPont Displays, SID Exhibition, May 2000; RiT Displays, SID Exhibition, May 2003.
166. DuPont Displays, SID Exhibition, San Jose, June 5–7, 2001.
167. Toshiba, SID Exhibition, May 2002; Seiko-Epson, SID Exhibition, May 2003; DuPont Displays, SID Exhibition, May 2003; Samsung, SID Exhibition, May 2003; SK Displays, SID Exhibition, May 2003.
168. DuPont Displays, SID Exhibition, May 2002; Samsung, SID Exhibition, May 2003.
169. Philips, SID Exhibition, Seattle, May 25–27, 2004.
170. SONY, SID Exhibition, Seattle, May 25–27, 2004.
171. Samsung SDI, SID Exhibition, Seattle, May 25–27, 2004.
172. Toshiba, SID Exhibition, May 2002; Samsung, SID Exhibition, May 2003; IDT/Chi-mei/IBM, SID Exhibition, May 2003.
173. G Yu, G Srdanov, B Zhang, M Stevenson, J Wang, P Chen, E Baggao, J Macias, R Sun, C McPherson, P Sant, J Innocenzo, M Stainer, and M O'Regan, Active-Matrix Polymer Displays Made with Electroluminescent Polymers, Cockpit Displays X, Orlando, Florida, 2003, pp. 192–199.

174. NCvd Vaart, EA Meulenkamp, ND Young, and M Fleuster, Next-generation active-matrix polymer OLED displays. Asia display/IMID '04, *Digest*, 337–342, 2004.
175. G Yu, Fabless Business Models for OLED Products. OLEDs 2004, San Diego, 2004.
176. AK Saafir, J Chung, I Joo, J Huh, J Rhee, S Park, B Choi, C Ko, B Koh, J Jung, J Choi, N Kim, K Chung, G Srdanov, C MacPherson, N Truong, M Stevenson, A Johnson, P Chen, T Cardellino, R Pflanzner, G Yu, A Goenaga, M O'Regan, and D Keys, A 14.1" WXGA Solution Processed OLED Display. SID 05, *Digest*, 968–971, 2005.
177. H Tokailin, C Hosokawa, and T Kusomoto, Electroluminescent Element, U.S. Patent 5,126,214, 1992.
178. TDK, SID Exhibition, May 2002 and May 2003; SK Displays, SID Exhibition, May 2003.
179. M Kashiwabara, K Hanawa, R Asaki, I Kobori, R Matsuura, H Yamada, T Yamamoto, A Ozawa, Y Sato, S Terada, J Yamada, T Sasaoka, S Tamura, and T Urabe, Advanced AM-OLED Display Based on White Emitter with Microcavity Structure. SID 04, *Digest*, 1017–1019, 2004.
180. J Wang and G Yu, Performance Simulation of Active-Matrix OLED Displays, Photonics Asia 2004: Light-Emitting Diode Materials and Devices, Beijing, China, 2004, pp. 32–44.

2 Light-Emitting Polymers

*Dmitrii F. Perepichka, Igor F. Perepichka, Hong Meng,
and Fred Wudl*

CONTENTS

2.1	Introduction	47
2.2	Poly(<i>p</i> -Phenylene Vinylenes)	51
2.2.1	Synthetic Routes to Poly(<i>p</i> -Phenylene Vinylenes)	52
2.2.2	Substituted Poly(<i>p</i> -Phenylene Vinylene) Homopolymers.....	57
2.2.2.1	Alkoxy-Substituted Poly(<i>p</i> -Phenylene Vinylenes).....	58
2.2.2.2	Alkyl-Substituted Poly(<i>p</i> -Phenylene Vinylenes).....	62
2.2.2.3	Silyl-Substituted Poly(<i>p</i> -Phenylene Vinylenes)	63
2.2.2.4	Aryl-Substituted Poly(<i>p</i> -Phenylene Vinylenes)	64
2.2.2.5	Poly(<i>p</i> -Phenylene Vinylene) Homopolymers with Electron-Withdrawing and Donating Substituents	69
2.2.3	Conjugated Poly(<i>p</i> -Phenylene Vinylene) Copolymers.....	73
2.2.3.1	Poly(<i>p</i> -Phenylene Vinylene) Copolymers with Electron Donor and Aryl Substituents	73
2.2.3.2	Poly(<i>p</i> -Phenylene Vinylene) Copolymers with Electron-Withdrawing Substituents.....	81
2.2.4	Poly(<i>p</i> -Phenylene Vinylene) Polyelectrolytes	88
2.2.5	Controlling the Conjugation in Poly(<i>p</i> -Phenylene Vinylene) Polymers	89
2.2.5.1	Formally Conjugated Systems with Twists, <i>Meta</i> -Links, and sp-Hybridized Atoms in the Backbone.....	89
2.2.5.2	Conjugated and Nonconjugated Poly(<i>p</i> -Phenylene Vinylene) Block Copolymers	92
2.2.5.3	Nonconjugated Polymer Containing Oligo(Phenylene Vinylene) Pendant Substituents	97
2.2.6	The Best Performing Poly(<i>p</i> -Phenylene Vinylene) Light-Emitting Polymers.....	98
2.3	Polyfluorenes.....	99
2.3.1	Characterizations Stability and Phase Behavior	99
2.3.2	Optical and Electronic Properties	120
2.3.3	General Methods in Synthesis of Polyfluorene Homopolymers	122
2.3.4	The Problem of Pure Blue Emission in Polyfluorenes: Excimer and Aggregate Formation or Fluorenone Defects?	124
2.3.5	Aromatic Ring-Substituted Polyfluorenes	128
2.3.6	Side-Chain Modifications in Polyfluorenes	129
2.3.7	End-Capped Polyfluorenes	139
2.3.8	3D Polyfluorenes	144
2.3.9	Blends of Polyfluorenes with Other Polymers	144
2.3.10	PF Copolymers.....	145
2.3.11	Color Tuning in Polyfluorene Copolymers	159

2.3.11.1	Doping with Low Molar-Mass Fluorescent Dyes	159
2.3.11.2	Alternating Copolymers	160
2.3.11.3	Random (Statistical) Copolymers.....	169
2.3.11.4	Copolymers with Three or More Comonomer Units	177
2.3.12	Polyfluorene-Based Polyelectrolytes	178
2.3.13	Conclusions	181
2.4	Polythiophenes	184
2.4.1	General Synthetic Routes to Polythiophenes.....	185
2.4.2	Light-Emitting Thiophene Homopolymers.....	187
2.4.2.1	Polythiophenes as Red-Light Emitters	187
2.4.2.2	The Effect of Regioregularity of Polythiophenes on Electroluminescence	190
2.4.2.3	Emission Color Tuning in Polythiophenes	192
2.4.3	Light-Emitting Thiophene Block Copolymers with Conjugation Break	199
2.4.4	Polythiophenes for Light-Emitting Electrochemical Cells	200
2.4.5	Blends of Polythiophenes.....	200
2.4.6	Polythiophenes for Structured and Polarized Polymer Light-Emitting Diodes	202
2.4.7	Electroluminescent Oligothiophenes	203
2.4.8	Thiophene-S,S-Dioxides as Emissive and Electron Transport Moieties	205
2.4.9	Copolymers of Thiophenes with Other Conjugated Moieties.....	207
2.4.9.1	Thiophene Copolymers with Aromatic Moieties	207
2.4.9.2	Thiophene Copolymers with Heteroaromatic Moieties	208
2.4.10	Conclusions.....	213
2.5	Miscellaneous Classes of Light-Emitting Polymers	214
2.5.1	Poly- <i>p</i> -Phenylenes	214
2.5.2	Ladder-Type Poly- <i>p</i> -Phenylenes	222
2.5.3	Poly(Phenylene Ethynylene)s	225
2.5.4	Substituted Polyacetylenes	227
2.5.5	Carbazole-Containing Polymers	228
2.5.6	Poly(Pyridine)s and Related Poly(N-Heterocycle)s	233
2.5.7	Oxadiazole, Oxazole, and Thiadiazole Polymers	238
2.5.8	Boron-, Silicon-, and Phosphorus-Containing Polymers	242
2.5.9	Conclusions.....	244
2.6	Conclusions and Outlook	244
2.7	Appendix.....	245
2.7.1	Syntheses of Poly(<i>p</i> -Phenylene Vinylene)s	245
2.7.1.1	The Wessling–Zimmerman (Thermoconversion) Precursor Route to PPV.	245
2.7.1.2	Gilch Polymerization Procedure.	247
2.7.1.3	Chlorine (Bromine) Precursor Route.....	248
2.7.1.4	Heck-Coupling Route.....	248
2.7.1.5	Knoevenagel-Coupling Route.....	249
2.7.2	Syntheses of Polyfluorenes.....	250
2.7.2.1	Synthesis of PF Monomers.....	250
2.7.2.2	Suzuki-Coupling Polymerization	252
2.7.2.3	Yamamoto Polymerization	253
2.7.3	Syntheses of Polythiophenes	255
2.7.3.1	Polymerization of Thiophene Monomers with FeCl ₃	255
2.7.3.2	Yamamoto Polymerization	255

2.7.3.3	McCullough Method of Preparation of Regioregular HT Poly(3-Alkylthiophenes)	256
2.7.3.4	Rieke-Zinc (Zn*)-Mediated Polymerization	257
2.7.3.5	Rieke-Nickel-Catalyzed Polymerization	259
2.7.4	Commercial Availability of Light-Emitting Polymers	259
	Acknowledgments	259
	References	259

2.1 INTRODUCTION

The origin of the field of electroluminescent (EL) polymers is connected with the 1990 article by Friend and coworkers [1] that describes an EL device based on conjugated poly(*p*-phenylene vinylene) (PPV), although some polymer EL devices based on poly(*N*-vinyl carbazole) (PVK) and doped with luminescent dyes had been reported by Partridge [2,3] long before. In the former paper, a single layer of PPV, placed between indium tin oxide (ITO) and Al electrodes, emitted green-yellow light under applied DC voltage. The device efficiency and relatively low turn-on voltage promised for a possible technological progress to a state of commercial application. It was clear that such progress would require not only improved device engineering techniques, but also sophisticated control of the materials' luminescence efficiency and electron-hole transporting properties, challenging the community of physical organic and polymer chemists.

Since the 1990s until now, light-emitting diodes (LEDs) are probably the most important application, maintaining the researchers' interest in conjugated (conducting) polymers, although in recent years we witnessed a growing interest in other relevant applications such as sensors and photovoltaics. Hundreds of academic research groups around the world have contributed to the development of EL polymers. An even more pronounced research activity is held in industries. Several newly born R&D companies such as Cambridge Display Technologies (CDT, spin-off from Cambridge University), Covion Organic Semiconductors (currently Merck OLED Materials) and UNIAX Corp. (spin-off from University of California of Santa Barbara (UCSB), currently DuPont Displays), are targeted at the development of high-efficiency, long-lifetime EL polymers. A huge commercial potential, connected with the possibility of solution fabrication of EL devices (particularly flat or flexible displays), attracted industrial giants such as Dow Chemical, DuPont, IBM, Kodak, and Philips [4].

Light-emitting polymers (LEPs) have been a subject of many review articles, which dealt with various aspects of the design, synthesis, and applications of different classes of LEPs (Table 2.1). Very insightful reviews of a general character have been presented by Holmes and coworkers (1998), Friend et al. (1999), and Mitschke and Bäuerle (2000) (Table 2.1). Among the recent papers, one of the most complete review was written by Akcelrud (2003, Table 2.1). However, none of the papers mentioned is comprehensive in covering different classes of EL polymers, and cannot be taken as a single source of information on this matter.

This chapter aims to be the most complete collection of references to the existing EL polymers, while discussing the problems of their design, synthesis, physical properties, and the resulting LED performance. In what follows, we describe main classes of LEPs that have been studied since about 1990 through mid-2004. Although it would not be possible to cover all the related literature in a single chapter (or even a separate book), an attempt has been made to cover all important polymeric EL materials that have been communicated in scientific journals (and, when relevant, in patents). However, considering the enormous number of publications appearing in a broad variety of journals each year, it is possible that some important papers describing a new LEP did not gain our attention. The chapter is written from the viewpoint of an organic materials chemist. It includes description of basic synthetic methods and, through a diversity of discussed structural variations influencing

TABLE 2.1
Reviews Covering the Synthesis and Application of Light-Emitting Polymers

Year	Title	Authors	Publication
1993	Conjugated polymer light-emitting diodes	A.R. Brown, N.C. Greenham, R.W. Gymer, K. Pichler, D.D.C. Bradley, R.H. Friend, P.L. Burn, A. Kraft, and A.B. Holmes.	<i>Intrinsically Conducting Polymers: An Emerging Technology</i> , NATO ASI Series, Series E: Applied Sciences 246: 87–106
1993	Conjugated polymer electroluminescence	D.D.C. Bradley	<i>Synth. Met.</i> 54: 401–415
1994	Light-emitting diodes fabricated with conjugated polymers—recent progress	D.R. Baigent, N.C. Greenham, J. Gruener, R.N. Marks, R.H. Friend, S.C. Moratti, and A.B. Holmes	<i>Synth. Met.</i> 67: 3–10
1996	Conjugated polymer electroluminescence	R.H. Friend and N.C. Greenham	<i>Physical Properties of Polymers Handbook</i> , J.E. Mark, Ed., AIP Press, New York, pp. 479–487
1997	Polymer electroluminescent devices	Y. Yang	<i>MRS Bull.</i> , June: 31–38
1997	Light-emitting polymers: increasing promise	W.C. Holton	<i>Solid State Technol.</i> , 40: 163–169
1997	Single- and heterolayer polymeric light emitting diodes based on poly(<i>p</i> -phenylene vinylene) and oxadiazole polymers	W. Rieß	<i>Organic Electroluminescent Materials and Devices</i> , S. Miyata and H.S. Nalwa, Eds., Gordon and Breach, Amsterdam, pp. 73–146
1997	Making polymer light emitting diodes with polythiophenes	O. Inganäs	<i>Organic Electroluminescent Materials and Devices</i> , S. Miyata and H.S. Nalwa, Eds., Gordon and Breach, Amsterdam, pp. 147–175
1997	Optically detected magnetic resonance (ODMR) studies of π -conjugated polymer-based light emitting diodes (LEDs)	J. Shinar	<i>Organic Electroluminescent Materials and Devices</i> , S. Miyata and H.S. Nalwa, Eds., Gordon and Breach, Amsterdam, pp. 177–202
1997	Thin film electroluminescent diodes based on poly(vinyl carbazole)	Z.-L. Zhang, X.-Y. Jiang, S.-H. Xu, and T. Nagatomo	<i>Organic Electroluminescent Materials and Devices</i> , S. Miyata and H.S. Nalwa, Eds., Gordon and Breach, Amsterdam, pp. 203–230
1998	Electroluminescent conjugated polymers—seeing polymers in a new light	A. Kraft, A.C. Grimsdale, and A.W. Holmes	<i>Angew. Chem. Int. Ed.</i> , 37: 402–428
1998	The chemistry of electroluminescent organic materials	J.L. Segura	<i>Acta Polym.</i> , 49: 319–344
1998	Design and synthesis of polymers for light-emitting diodes	A. Greiner	<i>Polym. Adv. Technol.</i> , 9: 371–389

TABLE 2.1 (continued)
Reviews Covering the Synthesis and Application of Light-Emitting Polymers

Year	Title	Authors	Publication
1998	Optical applications	M.G. Harrison and R.H. Friend	<i>Electronic Materials: The Oligomer Approach</i> , K. Müllen and G. Wegner, Eds., Wiley-VCH, Weinheim, pp. 515–558
1998	The chemistry and uses of polyphenylenevinylenes	S.C. Moratti	<i>Handbook of Conducting Polymers</i> , T.A. Skotheim, R.L. Elsenbaumer, and J.R. Reynolds, Eds., Marcel Dekker, New York, pp. 343–361
1998	Conjugated ladder-type structures	U. Scherf	<i>Handbook of Conducting Polymers</i> , T.A. Skotheim, R.L. Elsenbaumer, and J.R. Reynolds, Eds., Marcel Dekker, New York, pp. 363–379
1998	Electroluminescence in conjugated polymers	R.H. Friend and N.C. Greenham	<i>Handbook of Conducting Polymers</i> , T.A. Skotheim, R.L. Elsenbaumer, and J.R. Reynolds, Eds., Marcel Dekker, New York, pp. 823–845
1998	Fundamentals of electroluminescence in <i>para</i> -phenylene-type conjugated polymers and oligomers	G. Leising, S. Tasch, and W. Graupner	<i>Handbook of Conducting Polymers</i> , T.A. Skotheim, R.L. Elsenbaumer, and J.R. Reynolds, Eds., Marcel Dekker, New York, pp. 847–880
1999	Electro-optical polythiophene devices	M. Granström, M.G. Harrison, and R.H. Friend	<i>Handbook of Oligo- and Polythiophenes</i> , D. Fichou, Ed., Wiley-VCH, Weinheim, pp. 405–458
1999	Electroluminescence in conjugated polymers	R.H. Friend, R.W. Gymer, A.B. Holmes, J.H. Burroughes, R.N. Marks, C. Taliani, D.D.C. Bradley, D.A. Dos Santos, J.L. Brédas, M. Lögdlung, and W.R. Salaneck	<i>Nature</i> , 397: 121–127
1999	Polarized luminescence from oriented molecular materials	M. Grell and D.D.C. Bradley	<i>Adv. Mater.</i> , 11: 895–905
1999	Ladder-type materials	U. Scherf	<i>J. Mater. Chem.</i> , 9: 1853–1864
1999	Electroluminescence in organics	J. Kalinowski	<i>J. Phys. D: Appl. Phys.</i> , 32: R179–R250
2000	The electroluminescence of organic materials	U. Mitschke and P. Bäuerle	<i>J. Mater. Chem.</i> , 10: 1471–1507
2000	Progress in light-emitting polymers	M.T. Bernius, M. Inbasekaran, J.O'Brien, and W. Wu	<i>Adv. Mater.</i> , 12: 1737–1750
2000	Synthesis of conjugated polymers for application in light-emitting diodes (PLEDs)	R.E. Martin, F. Geneste, and A.B. Holmes	<i>C.R. Acad. Sci. Paris</i> , t. 1, Série IV: 447–470
2000	Blue light emitting polymers	D.Y. Kim, H.N. Cho, and C.Y. Kim	<i>Prog. Polym. Sci.</i> , 25: 1089–1139
2000	Fluorene-based polymers—preparation and applications	M. Bernius, M. Inbasekaran, E. Woo, W. Wu, and L. Wujk'owski	<i>J. Mater. Sci.: Mater. Electronics</i> , 11: 111–116

continued

TABLE 2.1 (continued)
Reviews Covering the Synthesis and Application of Light-Emitting Polymers

Year	Title	Authors	Publication
2000	Poly(aryleneethynylene)s: syntheses, properties, structures, and applications	U.H.F. Bunz	<i>Chem. Rev.</i> , 100: 1605–1644
2000	Semiconducting (conjugated) polymers as materials for solid-state lasers	M.D. McGehee and A.J. Heeger	<i>Adv. Mater.</i> , 12: 1655–1668
2001	Conjugated polymers. New materials for optoelectronic devices	R.H. Friend	<i>Pure Appl. Chem.</i> , 73: 425–430
2001	Conjugated polymers for light-emitting applications	L. Dai, B. Winkler, L. Dong, L. Tong, and A.W.H. Mau	<i>Adv. Mater.</i> , 13: 915–925
2001	Polyfluorenes: twenty years of progress	M. Leclerc	<i>J. Polym. Sci. Part A: Polym. Chem.</i> , 39: 2867–2873
2001	Polyfluorene homopolymers: conjugated liquid-crystalline polymers for bright emission and polarized electroluminescence	D. Neher	<i>Macromol. Rapid Commun.</i> , 22: 1365–1385
2002	Recent developments in light-emitting polymers	I.D. Rees, K.L. Robinson, A.B. Holmes, C.R. Towns, and R. O'Dell	<i>MRS Bull.</i> , June: 451–455
2002	Semiconducting polyfluorenes —toward reliable structure–property relationships	U. Scherf and E.J.W. List	<i>Adv. Mater.</i> , 14: 477–487
2003	Conjugated polymers as molecular materials: how chain conformation and film morphology influence energy transfer and interchain interactions	B.J. Schwartz	<i>Annu. Rev. Phys. Chem.</i> , 54: 141–172
2003	Synthesis of π -conjugated polymers bearing electronic and optical functionalities by organometallic polycondensations. Chemical properties and applications of the π -conjugated polymers	T. Yamamoto	<i>Synlett</i> : 425–450
2003	Carbazole-containing polymers: synthesis, properties and applications	J.V. Grazulevicius, P. Stroehriegl, J. Pielichowski, and K. Pielichowski	<i>Prog. Polym. Sci.</i> , 29: 1297–1353
2003	Electroluminescent polymers	L. Akcelrud	<i>Prog. Polym. Sci.</i> , 28: 875–962
2004	Recent development of polyfluorene-based RGB materials for light emitting diodes	W. Wu, M. Inbasekaran, M. Hudack, D. Welsh, W. Yu, Y. Cheng, C. Wang, S. Kram, M. Tacey, M. Bernius, R. Fletcher, K. Kiszka, S. Munger, and J. O'Brien	<i>Microelectron. J.</i> , 35: 343–348
2004	Synthesis of conjugated oligomers and polymers: the organometallic way	F. Babudri, G.M. Farinola, and F. Naso	<i>J. Mater. Chem.</i> , 14: 11–34

TABLE 2.1 (continued)
Reviews Covering the Synthesis and Application of Light-Emitting Polymers

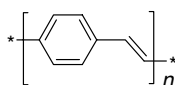
Year	Title	Authors	Publication
2004	Electron transport materials for organic light-emitting diodes	A.P. Kulkarni, C.J. Tonzola, A. Babel, and S.A. Jenekhe	<i>Chem. Mater.</i> , 16: 4556–4573
2004	Application of three-coordinate organoboron compounds and polymers in optoelectronics	C.D. Entwistle and T.B. Marder	<i>Chem. Mater.</i> , 16: 4574–4585
2005	Electron-transporting materials for organic electroluminescent and electrophosphorescent devices	G. Hughes and M.R. Bryce	<i>J. Mater. Chem.</i> , 15: 94–107

optoelectronic and EL properties, uncovers some general structure–property relationships in the described materials. A short description of LED structure is given along with the data on EL performance, whenever possible. However, the reader should be aware of limitations of a comparison of the EL data obtained by different groups (even for the same device structure). The conclusions on the practical values of different materials, beyond those given in the chapter, should be made with great care. In Section 2.6, we will list some of the best-performing LEPs and their future perspectives. Finally in the Appendix, the interested reader can find some practical synthetic methods for different classes of LEPs.

2.2 POLY(*p*-PHENYLENE VINYLENES)

Poly(*p*-Phenylene Vinylene) (PPV) **1** is a highly stable conjugated polymer (Chart 2.1). Its yellow color is due to an absorption band centered at ~400–420 nm (depending on the method of synthesis) with an onset corresponding to a band gap of ~2.5 eV [5]. The highest occupied molecular orbital (HOMO) and the lowest unoccupied molecular orbital (LUMO) levels in PPV can be accessed through cyclic voltammetry (CV) experiments that, under proper conditions, reveal chemically reversible oxidation and reduction waves (Figure 2.1). The deduced electrochemical gap corresponds reasonably well to the optical band gap. As a relatively good electron donor, PPV and its derivatives can be chemically doped by strong oxidizing agents and strong acids, affording highly conductive p-doped materials (with conductivity up to ~10⁴ S/cm [5]). The yellow-green fluorescence of PPV **1** results from a vibronically structured emission band with peak maxima at 520 and 551 nm (Figure 2.1).

The discovery of the EL in PPV in 1990 resulted in a tremendous growth of interest in polymer LEDs (PLEDs) [1]. Since then, numerous derivatives and analogs of PPV with tailored light-emitting properties have been synthesized, and a number of reviews and accounts described the synthesis and the EL properties of these materials [6–16]. Many new applications of PPV polymers, as solid-state lasing [17,18], photovoltaics [19], etc., have been



1, PPV

Chart 2.1

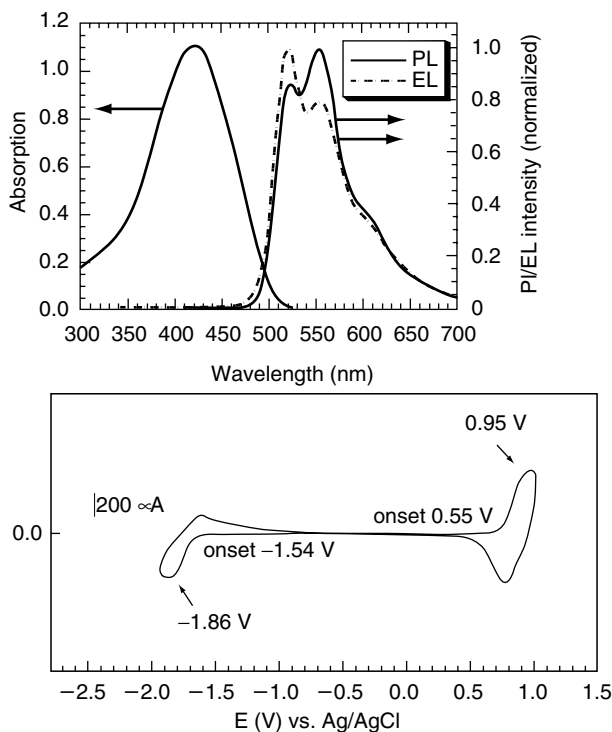


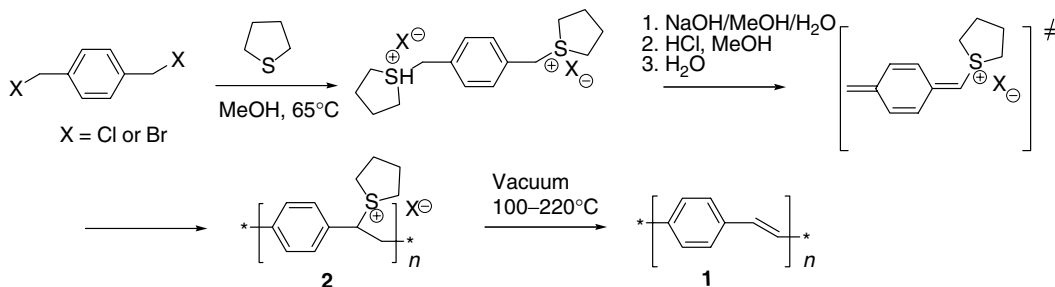
FIGURE 2.1 Top: Typical absorption, photo- and electroluminescence spectra of PPV (given for dialkyl-PPV **28**). (From Andersson, M.R., Yu, G., and Heeger, A.J., *Synth. Met.*, 85, 1275, 1997. With permission.) Bottom: Cyclic voltammetry of dialkoxy-PPV **13**. (From Kim, J.H. and Lee, H., *Chem. Mater.*, 14, 2270, 2002. With permission.)

explored but they are beyond the scope of this book. Below we give a general overview of the basic methods of synthesis of PPV derivatives and the design of PPV materials with controllable properties, as they were widely explored for the last 15 years in order to create high-performance PLEDs.

2.2.1 SYNTHETIC ROUTES TO POLY(*p*-PHENYLENE VINYLENES)

There are a number of synthetic strategies elaborated for preparation of PPV homo- and copolymers [20]:

1. Thermoconversion (Wessling–Zimmerman route)
2. Chemical vapor deposition (CVD)
3. Ring-opening metathesis polymerization (ROMP)
4. Gilch polycondensation
5. Chlorine precursor route (CPR) (Gilch modification)
6. Nonionic route (Gilch modification)
7. Knoevenagel polycondensation
8. Heck-coupling polymerization
9. Wittig(–Horner) condensation
10. Miscellaneous



SCHEME 2.1 The Wessling–Zimmerman precursor route to PPV. (From Wessling, R.A. and Zimmerman, R.G., Polyelectrolytes from Bis Sulfonium Salts, U.S. Patent 3,401,152, 1968.)

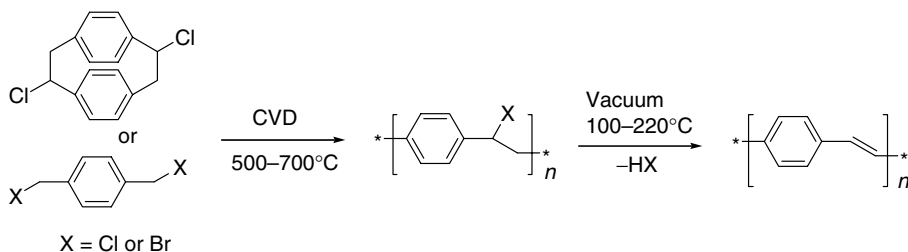
1. Thermoconversion (Wessling–Zimmerman route)

Since PPV itself is insoluble and difficult to process, the most widely used method, developed in the early 1960s by Wessling and Zimmerman, is thermoconversion of a processible sulfonium intermediate **2** (Scheme 2.1) [21]. The polymer **2** is soluble in methanol and can be spin coated to give a high-quality thin film, heating of which results in the formation of PPV **1** via the elimination of hydrogen halide and tetrahydrothiophene. Under proper conditions, the thermoconversion can give pinhole-free thin films of PPV suitable for PLED fabrication. The conversion temperature can be reduced to 100°C by using bromide derivatives instead of chlorides, thus enabling fabrication of PLED on flexible substrates [22].

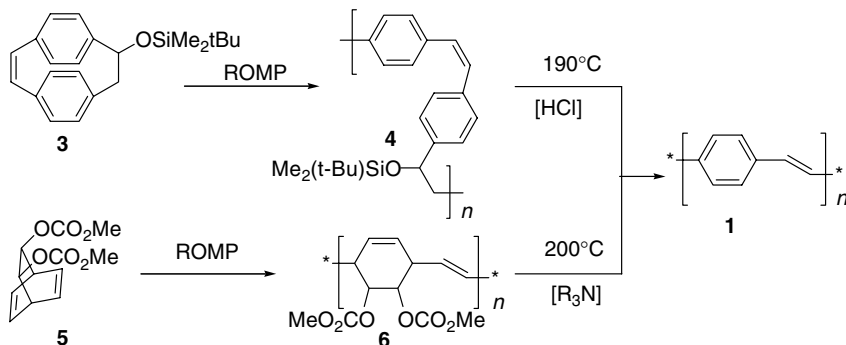
The issues of low stability of the precursor polymer **2** and extremely unpleasant odor of the sulfur-containing by-product can be resolved by the substitution of the sulfonium leaving groups with a methoxy group (under acid catalysis). The methoxy-substituted precursor polymer requires very harsh conditions for conversion to PPV (HCl gas at 220°C) [23]. On the other hand, the resulting PPV material showed significantly improved photophysical properties (more resolved vibronic structure of the absorbance, higher third-order nonlinearity), which were explained by a higher degree of order of the polymer chains [24]. Some other method modifications, such as employment of a xanthate-leaving group [25,26] or replacing the chloride ion (in precursor **2**) with dodecylbenzenesulfonate ion [27] were reported. For the latter, the long-chain counterion facilitates processing of the precursor polymer in Langmuir–Blodgett films.

2. Chemical vapor deposition (CVD)

Another synthetic method, applicable for processing PPV in thin films, is CVD of dichloro-*p*-[2.2]cyclophane [28] or dichloro-*p*-xylene [29] (Scheme 2.2). This method, though it can afford uniform and patterned thin films [30], requires heating at 500–700°C, which may give rise to by-product impurities. Such harsh conditions and difficulties of complete removal of the halogen (second stage) result in ill-defined material, which affords very low-performance PLEDs (maximum brightness of 20 cd/m²) [30].



SCHEME 2.2 Chemical vapor deposition route to PPV. (From Iwatsuki, S., Kubo, M., and Kumeuchi, T., *Chem. Lett.*, 20, 1971, 1991.)



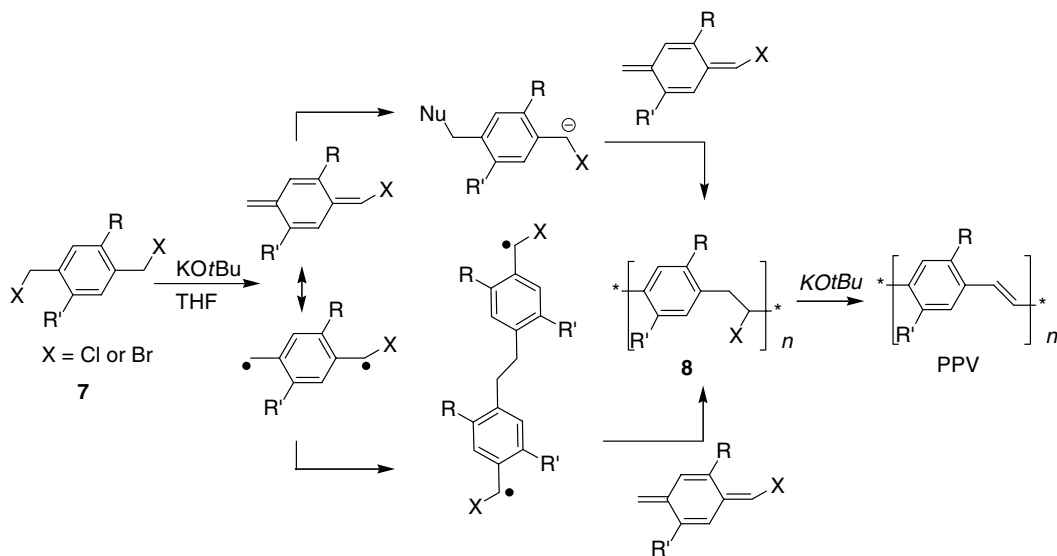
SCHEME 2.3 ROMP route to PPV. (From Miao, Y.-J. and Bazan, G.C., *J. Am. Chem. Soc.*, 116, 9379, 1994; Conticello, V.P., Gin, D.L., and Grubbs, R.H., *J. Am. Chem. Soc.*, 114, 9708, 1992.)

3. Ring-opening metathesis polymerization (ROMP)

The drawback of the CVD method is eliminated in ROMP, which is based on a catalytic (e.g., molybdenum carbene catalyst) reaction, occurring in rather mild conditions (Scheme 2.3). A living ROMP reaction of *p*-cyclophane **3** or bicyclooctadiene **5** results in soluble precursors of PPV, polymers **4** [31] and **6** [32], respectively, with rather low polydispersity. In spite of all *cis* (for **4**) and *cis* and *trans* (for **6**) configuration, these polymers can be converted into all-*trans* PPV by moderate heating under acid–base catalysis. However, the film-forming properties of ROMP precursors are usually rather poor, resulting in poor uniformity of the PPV films.

4. Gilch polycondensation

A general and most widely used method for the synthesis of PPV derivatives was introduced by Gilch and Wheelwright [33]. This method avoids high-temperature conditions and occurs through base-promoted 1,6-elimination of 1,4-*bis*(chloro/bromomethyl)benzenes **7** (Scheme 2.4). For device applications, the as-synthesized PPV materials need to be soluble

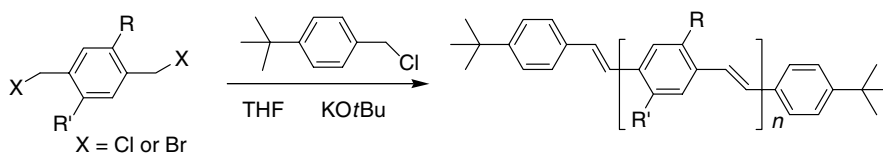


SCHEME 2.4 General synthetic route or Gilch route to solution-processable PPV derivatives (From Gilch, H.G. and Wheelwright, W.L., *J. Polym. Sci. Part A*, 4, 1337, 1966.)

in organic solvents, otherwise the as-formed polymer powder is completely unprocessable. Alkyl, alkyloxy, and other substituted monomers giving soluble PPVs have been employed in this reaction. The mechanism of the Gilch polymerization is still a subject of some controversy [34,35,36]. It is well accepted to proceed through a reactive quinodimethane intermediate, followed by either a radical or a living chain anionic polymerization. A molecular weight decrease upon the addition of chain transfer radical agent (2,2,6,6-tetramethylpiperidyl-1-oxyl (TEMPO)) was interpreted as a sign of the radical polymerization mechanism [37], although the same effect imposed by nucleophilic initiator (4-*tert*-butylbenzyl chloride) was taken as a confirmation of the nucleophilic chain growth mechanism [35]. In the absence of initiators, the latest evidence suggests the radical polymerization mechanism [34]. In both mechanisms, the regularity of the polymer conjugation chain is challenged by the possibility of side reactions, which are anomalous “head-to-head” (HH) or “tail-to-tail” (TT) couplings of the dehydrochlorinated intermediate. These reactions lead to the appearance of tolane-bisbenzyl (TBB) defects in the conjugation chain [38]. Although normally the amount of TBB is very low (<1–2%), certain substitution patterns (as sterically hindered phenyl-PPV, see below) can greatly enhance the defect formation. Note that (Scheme 2.4) a radical mechanism suggests the formation of at least one TBB defect in the middle of the polymer chain due to sterically preferable HH coupling of two monomer biradicals (although the further chain growth should proceed via normal head-to-tail, HT, coupling).

The molecular weight of the polymers can be controlled (from ca. 50,000 to above 1,000,000) by changing the reaction temperature and time, the solvent, the concentration of the monomer, and the amount of base [39,40]. High molecular-weight polymers and a high content of *trans* double bonds are the reasons for the wide usage of Gilch polymerization in the synthesis of PPV homo- and copolymers.

Hsieh et al. [35] used 4-*tert*-butylbenzyl chloride as an initiator and end-capping reagent to control the molecular weight of the Gilch synthesis of poly(2-methoxy-5-(2'-ethyl-hexyloxy)-1,4-phenylene vinylene) (MEH-PPV) (Scheme 2.5). Adding different amounts (0.6–60 mol%) of the end capper results progressively in a decrease in the molecular weight of the polymer ($M_n = 66,500$ for 6% of 4-*tert*-butylbenzyl chloride), suppressing the undesirable gel formation effect, as often observed in Gilch synthesis. However, the polymerization yield under these conditions was found to be rather low (35% for 6% of the initiator and below 20% for higher amount), which can be logically expected, considering possible side reactions of the initiator in the strongly basic media. Admitting the problem of self-coupling reaction of the benzyl chloride initiator, Neef and Ferraris [36] attempted to control the molecular weight of the polymer with 4-methoxyphenol as an anionic initiator. The authors claim that relatively small amounts of the phenolic initiator (1–2%) can decrease the M_n by more than a factor of 2, while keeping the polymerization yield above 50% (which is still essentially lower compared to 76% yield obtained in the absence of initiator). At the same time, a very low polydispersity, reported in this paper (1.04–1.52), is unexpected for this type of reaction and the reproducibility of the reported results seem to be a problem. Both approaches are based on an arguable hypothesis of anionic living polymerization and are of very limited practical



SCHEME 2.5 End-capping modification of the Gilch polymerization. (From Hsieh, B.R., Yu, Y., van Laeken, A.C., and Lee, H., *Macromolecules*, 30, 8094, 1997.)

applicability for controlling the molecular weight of PPV, although the use of these and similar reagents in small amounts, as end cappers, may be beneficial for improving the stability of the PPV material.

5. Chlorine precursor route (CPR)

An important modification of Gilch polymerization (also known as CPR), introduced by Swatos and Gordon in 1990, is based on using one equivalent of the base (instead of four in classical Gilch method) to stop the polymerization at the stage of formation of the precursor polymer **8** (Scheme 2.4) [39,41]. Polymer **8** is very much a soluble material and can be spin coated to afford high-quality films. Thermal annealing at 230–280°C results in the elimination of hydrogen chloride and affords the PPV material in high yield.

6. Nonionic route

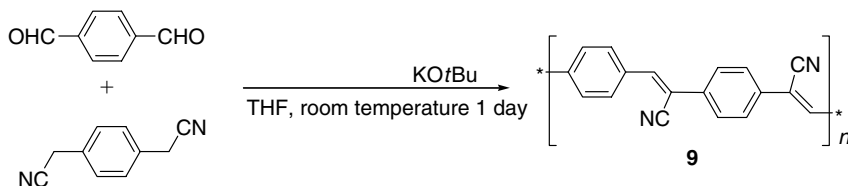
Another extension of the Gilch polymerization approach, similar to the CPR method, was developed by Vanderzande and coworkers [42]. They have substituted one of chlorine atoms in the monomer **7** with alkylsulfinyl group (BuS(O)), so that the resulting “precursor polymer” **8** would not contain any chlorine. The alkylsulfinyl group can be removed in the nonionic process by simply heating the polymer at ~110°C for a few hours. The process can be attractive for applications where the low halogen content is a critical issue, although the EL efficiency of PPV prepared by this method is a few times lower than that prepared by traditional Gilch polymerization (presumably due to defects in the polymer structure) [42].

7. Knoevenagel polycondensation

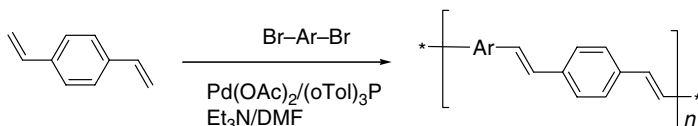
Knoevenagel condensation, based on the reaction of aldehyde group with active methylene component, was one of the first methods used for the synthesis of PPV derivatives [43]. In general, it requires strong electron acceptor substituents (such as cyano (CN) group) in the methylene component (Scheme 2.6). The method delivers the PPV containing cyano substituents on the vinylene units (**9**), and numerous substituted CN-PPV homo- and copolymers have been synthesized [44]. Recently, ruthenium-based catalysis ($\text{RuH}_2(\text{PPh}_3)_4/\text{dppe}$) was used to replace the strong base (as $\text{KO}t\text{Bu}$) in Knoevenagel-type synthesis of CN-PPV, which has the advantage of neutral and mild reaction conditions [45].

8. Heck-coupling polymerization

The PPV-polymer chain can also be constructed by Heck coupling of aromatic dihalides with a divinylbenzene. In contrast to the above-described methods, the Heck coupling is a Pd-catalyzed reaction occurring in very mild conditions. The polymerization normally leads to all-*trans* geometry with very few side reactions (Scheme 2.7) [46]. Although this method is somewhat complicated for the preparation of PPV homopolymers, the Heck-type synthesis of unsubstituted PPV and its methylated, trifluoromethylated, and phenylated derivatives from divinylbenzene and dibromobenzene, dibromobenzene and ethylene, or bromovinylbenzene (self-coupling) was demonstrated [47]. This method is of great utility in the preparation of alternating copolymers (see Section 2.3).



SCHEME 2.6 Knoevenagel condensation route to PPV. (From Lenz, R.W. and Handlovits, C.E., *J. Org. Chem.*, 25, 813, 1960; Moratti, S.C., Cervini, R., Holmes, A.B., Baigent, D.R., Friend, R.H., Greenham, N.C., Grüner, J., and Hamer, P.J., *Synth. Met.*, 71, 2117, 1995.)



SCHEME 2.7 Heck-coupling route to synthesis of PPV copolymers. (From Hilberer, A., Brouwer, H.-J., van der Scheer, B.-J., Wildeman, J., and Hadziioannou, G., *Macromolecules*, 28, 4525, 1995; Greiner, A. and Heitz, W., *Macromol. Chem. Rapid Commun.*, 9, 581, 1988.)

9. Wittig(–Horner) condensation

Wittig or Wittig–Horner condensation between substituted terephthalaldehydes and *p*-xylene-diylphosphonium salts is also extensively used in the preparation of alternating PPV copolymers, e.g., containing different substituents in adjacent phenylene units (Scheme 2.8) [48].

10. Miscellaneous

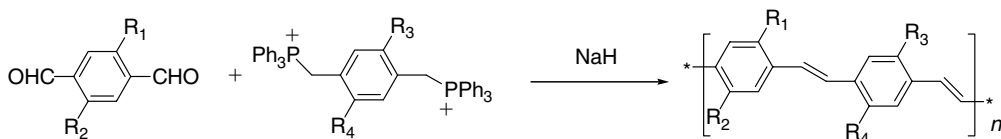
A totally different route based on dehydrogenation of a saturated polymer precursor was introduced by Francois et al. [49] (Scheme 2.9). The method is based on anionic copolymerization of cyclohexadiene with styrene, followed by oxidation with chloranil. Due to possible coupling of two styrene (or two cyclohexadiene) molecules, a block copolymer, containing oligo(phenylene vinylene) units separated by oligo(phenylacetylene) and oligo(phenylene) blocks, is obtained. To the best of our knowledge, it was, so far, used only in the synthesis of phenyl-substituted PPV **10**.

Ackelrud and coworkers [50] reported the preparation of acetoxy-PPV **11** via controlled potential electrolysis of $\alpha,\alpha,\alpha',\alpha'$ -tetrabromoxylene precursor on a mercury electrode in Et_4NBr /dimethylformamide (DMF) electrolyte solution (Scheme 2.10). However, the only structural characterization reported was UV–vis and fluorescence spectra.

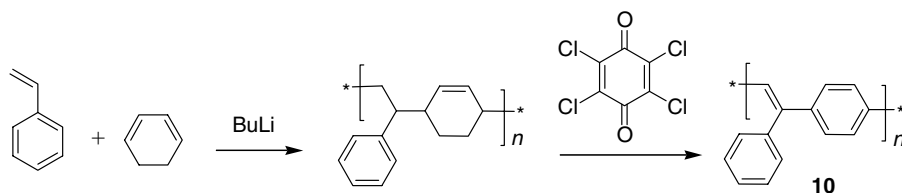
Below we describe the application of the described reactions to the synthesis of PPV derivatives with tailored properties for PLEDs.

2.2.2 SUBSTITUTED POLY(*p*-PHENYLENE VINYLENE) HOMOPOLYMERS

The first conjugated PLED was prepared by Friend and coworkers [1] by sandwiching unsubstituted PPV **1** (prepared by Wessling–Zimmerman reaction) between a transparent ITO anode and an Al cathode. It showed a maximum $\Phi_{\text{EL}}^{\text{ex}}$ of only 0.01% at room temperature (0.05% at 120 K), and required 14 V to turn on [1]. This low efficiency has several reasons, among which is an imbalance of hole–electron injection barriers. The efficiency could be improved to 0.1% by using a lower work-function electrode (Ca) [51]. However, Ca is a highly reactive metal, which complicates the fabrication process and reduces the device stability. Alternatively, the EL can be improved by a factor of 30 by placing an electron-transporting layer (ETL) (oxadiazole-based nonconjugated polymer) between PPV **1** and Al electrode [52]. On the way to electrically pumped lasers, Friend and coworkers [53] reported exceptionally high peak brightness PLEDs based on PPV **1**. Applying a short-pulsed voltage of $\sim 10\text{--}40\text{ V}$ (pulse width of 100–200 ns), a brightness of $5 \times 10^6\text{ cd/m}^2$ has been achieved for a device ITO/PEDOT/**1**/Al (PEDOT is poly(3,4-ethylenedioxythiophene), Chart 2.2). Although a



SCHEME 2.8 Wittig condensation route to PPV. (From McDonald, R.N. and Campbell, T.W., *J. Am. Chem. Soc.*, 82, 4669, 1960.)



SCHEME 2.9 Synthesis of phenyl-PPV by dehydrogenation route. (From Francois, B., Izzillo, S., and Iratçabal, P., *Synth. Met.*, 102, 1211, 1999.)

relatively high EL efficiency (2.8 cd/A) was found in this device, the authors mention that it is still the device efficiency, and not the brightness, which limits the laser action.

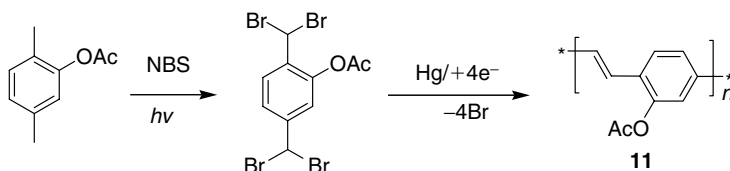
As will be shown throughout the chapter, the parent PPV **1** is extensively used as a hole-transporting layer (HTL) in combination with other EL polymers. Recently, improved photo-stability of organic–inorganic hybrid EL material, prepared by incorporating PPV **1** into zeolite capsules, was described [54]. However, the material showed only weak EL (at driving voltage of 2.5 V).

Modifications of the chemical structure of PPV provide various opportunities for tuning the optical properties of this material. The most explored modification was introducing the substituents in the benzene ring. These include alkyl-, alkoxy-, and silyl-substituents, aromatic functional side groups, and electron-releasing and -withdrawing groups, as discussed in detail in the following sections.

One should, however, bear in mind that not only molecular structure of the polymers but also their supramolecular organization defines the performance of a PLED. Thermal annealing of the films and other ordering techniques are widely used to control the properties of the polymers. Particularly, solvents used for casting the film and the casting procedure can substantially change the supramolecular organization of the polymer and, thus, the performance of PLED. Single molecule fluorescence correlation spectroscopy studies confirmed that the chain collapse and orientation of the single molecules of CN-PPV (**9**) and MEH-PPV (**13**) are highly influenced by the choice of the solvent: the production of oriented species is strongly favored in “poorer” solvents, where the polymer chains have more compact solution-phase structures [55].

2.2.2.1 Alkoxy-Substituted Poly(*p*-Phenylene Vinylenes)

The insolubility of the PPV **1** and the need for conversion of the precursor polymer on the last stage under rather harsh conditions are obvious drawbacks for a wide application of these materials. The obvious route to increase the solubility of the PPV would be introducing long-chain substituents. Although several groups synthesized and studied dimethoxy- and diethoxy-PPV derivatives starting from 1970, aiming at high-stability conducting polymers [56,57], only dihexyloxy derivative, DH-PPV **12**, prepared by Wudl and coworkers [58] by thermal treatment of the sulfonium salt, appeared to be soluble in common organic solvents (Scheme 2.11).



SCHEME 2.10 Synthesis of acetoxypoly(*p*-phenylene vinylene) (**11**) by electroreduction. (From Aguiar, M., Fugihara, M.C., Hümmelgen, I.A., Péres, L.O., Garcia, J.R., Gruber, J., and Akcelrud, L., *J. Lumin.*, 96, 219, 2002.)

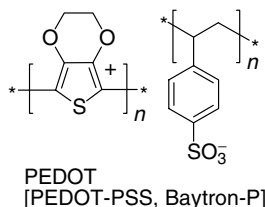
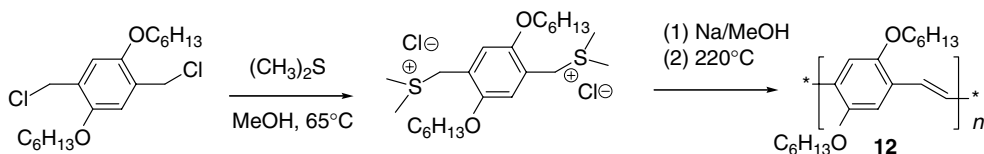


Chart 2.2

However, the solubility of this material at room temperature was still not high enough. The simple elongation of the substituents results in a “side-chain crystallization effect” and does not increase the solubility. To solve the problem, Wudl and Srdanov [59] came up with a highly asymmetric substituent pattern (methoxy/2-ethylhexyloxy) for the synthesis of polymer **13** (well-known as MEH-PPV) via the Gilch-polymerization route (Chart 2.3). The side-chain disorder brought about by two different substituents as well as nonplanar structure and optical isomers (due to stereogenic 2-ethylhexyloxy substituents) results in a high solubility of this polymer in common organic solvents (toluene, chloroform, tetrahydrofuran (THF), etc.) in spite of extremely high molecular weight ($>10^6$ Da). Such a high molecular weight can nevertheless result in gelation of the polymer, and several attempts of controlling the degree of polymerization by introducing end-capping reagents were undertaken [35,36]. Also, studies by Burn and coworkers [60] suggest that aggregation of MEH-PPV in solutions might affect the molecular weight determination, and lower M_n values have been obtained when analyzing highly diluted MEH-PPV solutions. A completely insoluble form of MEH-PPV, which can be useful for the preparation of multilayer PLEDs, was prepared by the same group via the CPR (using less than one equivalent of the base) [61].

MEH-PPV is a bright-orange material ($\lambda_{\max} \sim 490$ nm); upon photoexcitation, it produces a red-orange emission ($\lambda_{\text{PL}} \sim 590$ nm, PL is photoluminescence). For the last decade, MEH-PPV has been one of the most studied EL materials [62–73]. It was used as a standard LEP for the demonstration of several innovative concepts in the fabrication of PLEDs, including light-emitting electrochemical cells (LECs) [63], microstructuring the polymer layer for increased light output [69], application of transparent polymer electrodes (doped polyaniline (PANI) or PEDOT films) in place of ITO [65], nanocomposites with inorganic materials [67,69], etc. The first LEDs fabricated with this material were reported to show a $\Phi_{\text{EL}}^{\text{ex}}$ of 0.05% in ITO/**13**/In configuration and $\sim 1\%$ in ITO/**13**/Ca configuration [62]. An external quantum efficiency (QE) of 1% can also be achieved with Al electrode in an LEC device, using a blend of MEH-PPV, poly(ethylene oxide) (PEO), and electrolyte [63], whereas a QE of less than 0.4% was achieved by the same group in the same device using unsubstituted PPV **1** [64]. Numerous improvements of the EL performance of MEH-PPV by blending this polymer with different organic and inorganic materials were reported. Highly efficient PLEDs ($\Phi_{\text{EL}}^{\text{ex}}$ of 2%, maximum brightness of $10,000 \text{ cd/m}^2$) were fabricated by adding SiO_2 nanoparticles to the MEH-PPV layer (between ITO and Ca electrodes) [67]. A $\Phi_{\text{EL}}^{\text{ex}}$ of 1.3% was obtained by blending MEH-PPV



SCHEME 2.11 Synthesis of the first soluble PPV derivative, DH-PPV. (From Askari, S.H., Rughooputh, S.D., and Wudl, F., *Synth. Met.*, 29, E129, 1989.)

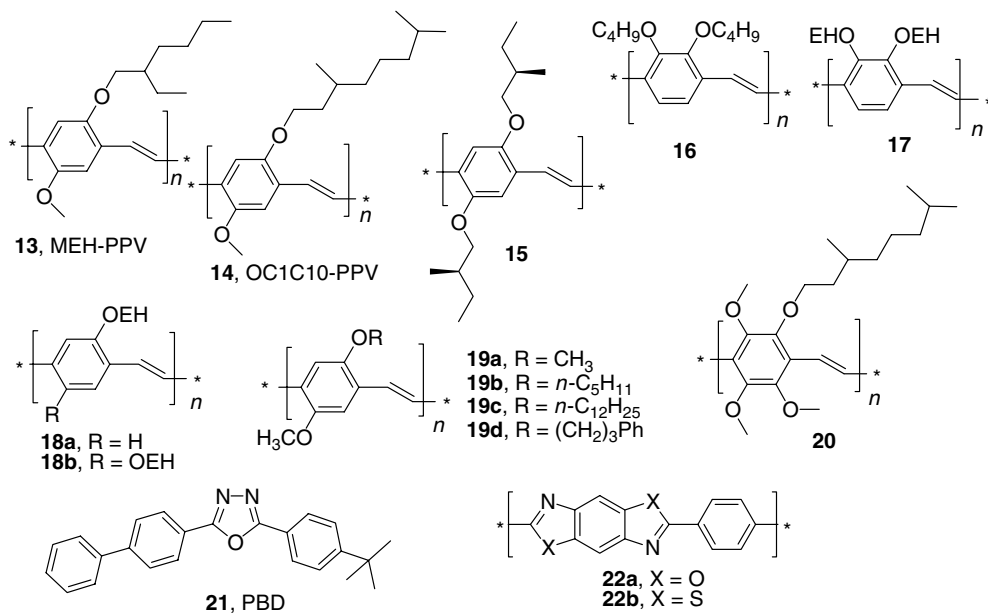


Chart 2.3

with an electron transport material, 2-(4-biphenyl)-5-(4-*tert*-butylphenyl)-1,3,4-oxadiazole (PBD **21**) [68]. More recently, an efficiency up to 2.5% was reported for multilayer PLEDs with additional polybenzobisazole (**22**) ETL (ITO/PEDOT/**13/22b**/Al) [71]. Very high QE values have been also obtained blending MEH-PPV with lithium organophosphonate surfactant (2.3% [65]) or carbazole–thiophene copolymers (3.8% [72]). Recent results from Wong and coworkers [73] show a two orders of magnitude increase of the EL efficiency (up to 2.7 cd/A, maximum brightness up to 5500 cd/m²) of the ITO/MEH-PPV/Al device upon simple dilution of the MEH-PPV with poly(ethylene glycol) (PEG).

The 2-ethylhexyl (EH) substituent became a very popular side-chain group for the synthesis of soluble conjugated polymers of different classes, but other branched alkyloxy substituents have also been introduced in the PPV backbone. For example, polymer **14** substituted with a 3,7-dimethyloctyl group showed a very similar electronic behavior to that of MEH-PPV, but an additional branching further improved its solubility and the film-forming properties [42,74]. PLEDs with an EL efficiency of 1.2 cd/A (with maximum brightness of 4000 cd/m²) [42] and even higher, 2.1 cd/A (2.5 lm/W) [74] and ~3 cd/A [75] have been fabricated with polymer **14**. A systematic study of lifetime and degradation effects in PLEDs was reported for this polymer [76]. At low brightness level of ~100 cd/m², half-lifetime around 20,000 h was achieved. The device stability strongly depends on the operating temperature (Figure 2.2), and the authors suggested that electron (rather than hole) injection and passage are primarily responsible for the device degradation. Very high $\Phi_{\text{EL}}^{\text{ex}}$ was demonstrated by Heeger and coworkers [68] for the polymer **14** blended with 20% of PBD (electron transport material). Increasing the operating temperature of the device from 25 to 85°C, the $\Phi_{\text{EL}}^{\text{ex}}$ values increased from 2 to 4%. Comparing these numbers with the PL quantum yield (PLQY) (~8%), measured by exciting the material-incorporated diodes, the authors reached an interesting, though somewhat speculative, conclusion that 50% singlet–triplet ratio is achieved in this material (which exceeds the widely accepted theoretical value of 25%). A related enantiomerically pure (*S*)-2-methylbutoxy- substituted PPV **15** has been used

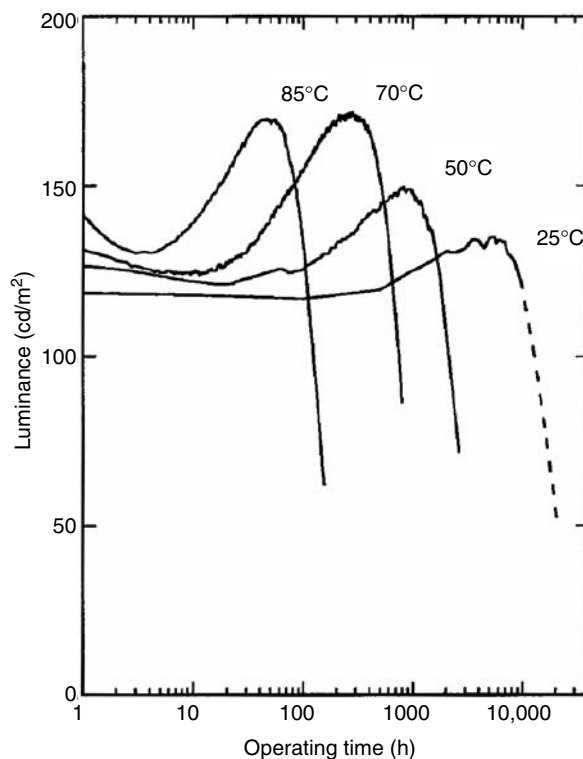


FIGURE 2.2 Operation lifetime of the device ITO/PANI/**14**/Ca/Al. (From Parker, I.D., Cao, Y., and Yang, C.Y., *J. Appl. Phys.*, 85, 2441, 1999. With permission.)

to create circularly polarized PLED, in which the polarization is brought about by molecular chirality of the polymer and does not require any molecular alignment [77].

Polymer **16** bears two alkoxy substituents at positions 2 and 3 of the benzene ring, which results in a notable blue-shifted absorption and emission bands ($\lambda_{\text{PL}} = 519$ nm, close to that of unsubstituted PPV) with about twice higher solid-state PL efficiency (40%) compared with 2,5-disubstituted PPVs (15–20%) [78]. The EL efficiency of 0.03 cd/A (for Al cathode) and 0.07 cd/A (for Ca cathode) at an operating voltage of 10–15 V were reported for a single-layer device, whereas in a double-layer PLED with PPV **1** as a HTL, the high efficiency of 0.68 cd/A was achieved at 7.5 V (and maximum brightness of 4500 cd/m²). Notably, a similar polymer **17** showed somewhat lower PL efficiency (28% vs. 40%), and the PLED device fabricated as ITO/PEDOT/**17**/Ca showed an EL efficiency of 0.13 cd/A (and maximum brightness of only 86 cd/A) [79].

Many other monoalkoxy-PPV (e.g., **18a** [80]) as well as symmetric (e.g., polymer **18b** [81] and **19a** [82]) and asymmetric (e.g., polymers **19b–d** [83]) dialkoxy-PPVs have been synthesized. Interestingly, the monoalkoxy-PPV **18a** demonstrated improved PLQY ($55 \pm 5\%$) compared to dialkoxy-PPVs, and the authors emphasized a key role of the synthetic conditions determining the photophysical properties of the polymer [80].

EL from tetraalkoxy-substituted PPV **20**, synthesized by Gilch polymerization, was recently reported [84]. A multilayer device ITO/PEDOT/**20**/PBD/LiF/Al with PBD as an ETL emits green-yellow light with a luminescent efficiency of 0.12 lm/W, a maximum brightness of 8200 cd/m², and a turn-on voltage of 5 V.

The most branched among the alkoxy-PPVs are cholestanoxo-substituted polymers **23** and **24**, developed by Wudl and coworkers [81,85–87] (Chart 2.4). The authors suggested that

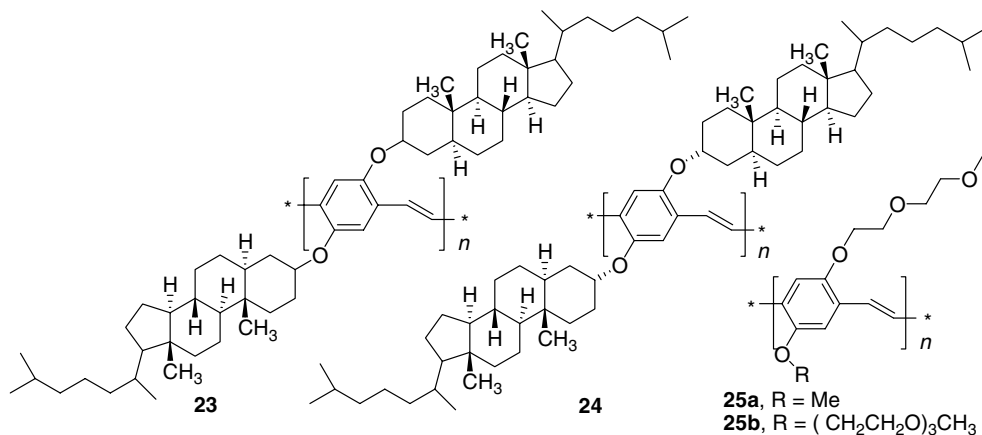


Chart 2.4

a highly amorphous nature, possessed by all known steroids, will result in highly soluble PPVs with very good film-forming properties. Indeed, the solid-state fluorescence efficiency for **23** was reported to be 53%, which is more than twice higher than that of MEH-PPV **13** measured in the same conditions [88].

Oligoethylenoxy-substituted PPVs **25** [89,90] are also known, but the PL efficiency of these in the solid state is very low (0.6% for **25a** and 8.8% for **25b** [90]), which is transmitted into a low efficiency of PLED (ITO/**25b**/Al: luminous efficiency of 0.04 lm/W).

A combined theoretical (AM1 and valence-effective Hamiltonian (VEH)) and experimental (ultraviolet photoelectron spectroscopy (UPS)) study of the effect of alkyl and alkoxy substituents on the electronic structure of PPV has been undertaken by Fahlman et al. [91]. The results suggest that strong influence of the substituents on the HOMO–LUMO levels (and the band gap) is primarily due to change in the torsion angle between the phenylene and vinylene groups. Interestingly, introduction of the alkoxy substituents does not cause significant steric hindrance and weak intramolecular O ··· H interactions (between the oxygen atom of alkoxy group and a vinylic proton) in dialkoxy-substituted PPV may even favor the planar backbone geometry. In contrast, the dialkyl-substituted PPV is predicted to have a large torsion angle of 34° in the gas phase, and in the solid state the intermolecular packing and planarization will result in a significant change of the band gap.

2.2.2.2 Alkyl-Substituted Poly(*p*-Phenylene Vinylenes)

A number of alkylated-PPV polymers have been reported, e.g., **26a** [57,82,92], **26b** [93], **27** [94] (Chart 2.5). The absorption of dialkylated PPVs is very close to that of unsubstituted PPV **1**

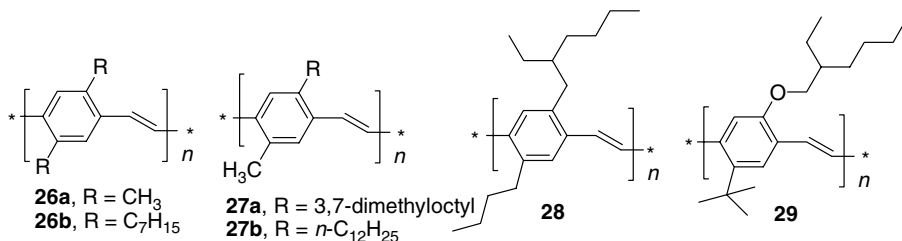


Chart 2.5

(**26b**: $\lambda_{\max} = 404$ nm (solution) [93]; **28**: $\lambda_{\max} = 422$ nm (film) [88]) and hypsochromically shifted with respect to dialkoxy-PPVs. It was demonstrated that dialkylated PPV **28** can be used as a new type of solid-state laser material [17,95]. As for PLEDs, the first devices ITO/polymer/Ca fabricated with polymers **27** emitted light with $\lambda_{\max} = 530$ –560 nm, but the reported $\Phi_{\text{EL}}^{\text{ex}} = 0.2\%$ was lower [94] compared with alkoxy-PPV (**13**) in the same device configuration [62]. Somewhat later, very high QE PLEDs were fabricated with *t*-butyl/2-ethylhexyloxy-PPV **29** [65]. The device in configuration ITO/PANI/**29**:surfactant/Al (where surfactant was lithium organophosphonate) emitted green light with $\Phi_{\text{EL}}^{\text{ex}}$ as high as 2.7% (turn-on voltage 10 V), although this high value is mostly due to the surfactant effect because a similar efficiency was obtained for a MEH-PPV **13**-based device in the same configuration.

2.2.2.3 Silyl-Substituted Poly(*p*-Phenylene Vinylenes)

Several PPV derivatives possessing trialkylsilyl substituents have been studied with the aim to control the band gap and the emission color of the polymer. The electronic influence of silicon substituents is somewhat difficult to predict. Judging from the variety of reported Hammett σ -constants of silyl substituent, it may act either as a weak electron donor or electron acceptor. Probably, more importantly in the case of substituted PPV, the bulky trialkylsilyl group increases the torsion angle between the phenylene and vinylene π -systems, thus enlarging the band gap of the polymer. The first Si-substituted PPV **30** was synthesized by Wudl's group [96] (Chart 2.6). Clearly, the trialkylsilyl substituent increases the band gap and shifts the emission to the blue region: thin films of **30** exhibit light-green EL emission with an $\Phi_{\text{EL}}^{\text{ex}}$ up to 0.3% [97].

A simple Si-containing polymer **31** was reported by Friend and coworkers [98]. The optical band gap of this material in thin films is almost 2.5 eV, and it emits light at λ_{PL} of 515 and 550 nm with a remarkable (as for PPV derivatives) PLQY of 60%. A single-layer PLED device reveals the same emission spectrum and the $\Phi_{\text{EL}}^{\text{ex}} = 0.05$ and 0.08% for ITO/**31**/Al and ITO/**31**/Ca structures, respectively. The QE can be significantly improved (to 0.2 and 0.5%, respectively), by introducing a hole-blocking and electron-injecting layer of PBD (in a blend with polystyrene) between the light-emitting layer and the cathode.

Holmes and coworkers studied silyl-substituted PPVs **31a** [99] and **32a** [100] and their copolymers with 2,3-dibutoxy-PPV **16** [79]. The solid-state PL efficiency of **31a** and **32a** is over 60%, which is significantly higher than that of PPV **1** (27%) and MEH-PPV **13** (15%). Polymer **31a** reveals bright-green EL with $\Phi_{\text{EL}}^{\text{ex}} = 0.05\%$ (in ITO/**31a**/Al configuration) and 0.1% (in ITO/**31a**/Ca configuration) [99]. Interestingly, the PLEDs synthesized from **32a** emit light at positive and negative bias, but the EL efficiency was not reported.

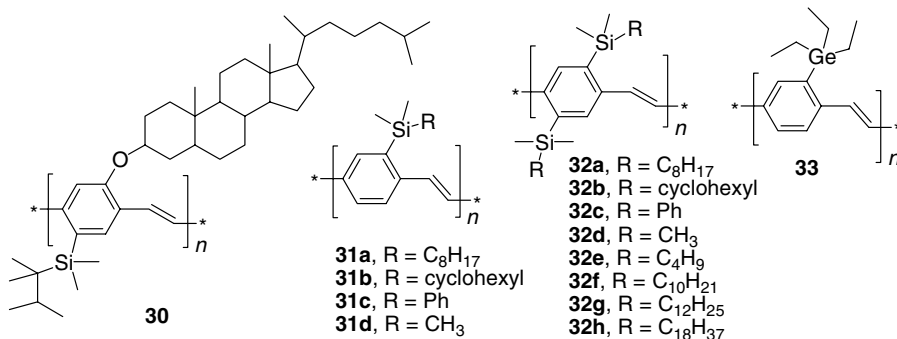


Chart 2.6

A systematic study of a series of *bis*-silyl-substituted PPVs **32d–h** with different side-chain lengths ranging from C1 to C18 was performed by Huang and coworkers [101]. The long-chain silyl-substituted PPVs show improved processability and film-forming properties and sharp emission bands, although the thermal stability of the polymer somewhat decreases for the longest chain substituents. The external QE of the device built with Al cathode (ITO/**32f**/Al) is modest ($\Phi_{\text{EL}}^{\text{ex}} = 0.05\%$) for this diode structure, but interestingly, only little improvement of the efficiency (to 0.08%) was observed when replacing the Al cathode with Ca.

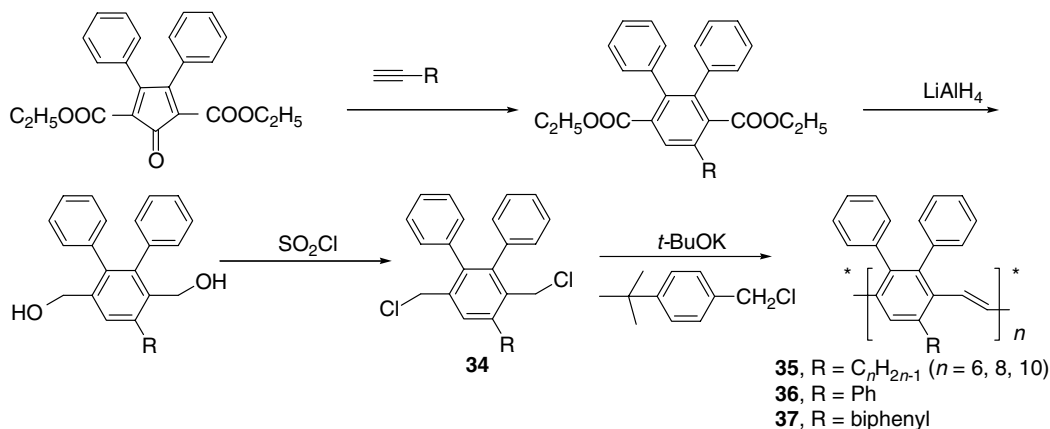
To improve the mechanical properties and the thermostability of the silyl-substituted PPVs, Shim and coworkers [102] replaced the long *n*-alkyl chains in silyl substituents with more sterically demanding cyclohexyl and phenyl groups (polymers **31b**, **32b** and **31c**, **32c**, respectively). The best results (processability and EL efficiency) have been achieved for monosubstituted polymers **31b** and **31c**, which had a high glass-transition temperature (T_g) ($\sim 125^\circ\text{C}$), were thermally stable (5% mass loss at $>430^\circ\text{C}$) and, due to high molecular weight ($M_n \sim 3 \times 10^5$), possessed good film-forming properties. The PLED fabricated with these polymers as ITO/PVK/**31c**/Al and ITO/PVK/**31b**/Al emitted green-yellow light ($\lambda_{\text{max}} \sim 520\text{ nm}$) with $\Phi_{\text{EL}}^{\text{ex}} = 0.08$ and 0.07%, respectively, and the maximum brightness of the device was also quite low (220 cd/m²).

Recently, Hwang et al. [103] reported the synthesis of germylated-PPV **33**. Due to insolubility of the material prepared by Gilch polymerization, the authors employed the thermoconversion route to prepare thin films of **33** from a nonconjugated methoxylated precursor polymer. The rationale beyond this synthesis was to increase steric hindrance (due to bulkier germanium atom) and to prevent the interchain quenching effect, but no essential improvement vs. silylated analogs has been found. The device fabricated as ITO/**33**/LiF/Al emitted green light ($\lambda_{\text{max}} = 514\text{ nm}$) with an efficiency of 0.015 lm/W and the maximum brightness of 600 cd/m² (cf. **31d**: [103] efficiency 0.025 cd/W, brightness 310 cd/m²). The turn-on voltage (13 V) was even somewhat higher than that for silylated-PPV **31** (10.5 V).

Generally, silyl substituents seem to retard the hole-transporting ability of PPV. As a result, devices fabricated from silyl-substituted PPVs suffer from a high turn-on voltage. To improve the EL efficiency of PLEDs fabricated from Si-PPVs, the introduction of additional hole injection layer or copolymerization with electron-rich comonomers is required.

2.2.2.4 Aryl-Substituted Poly(*p*-Phenylene Vinylenes)

Numerous studies have been devoted to PPV derivatives, possessing pendant aromatic groups. In 1998, Hsieh et al. [104] synthesized a series of soluble diphenyl-PPV derivatives via an ingenious route based on a Diels–Alder reaction of commercially available substituted cyclopentadienone with alkylacetylenes (Scheme 2.12). This is a very versatile method for the preparation of a variety of substituted monomers for PPV. In contrast to the classical route of chloromethylation of alkyl(alkoxy)-substituted benzenes, the Diels–Alder approach eliminates the problem of isomer formation. The polymerization of the monomer **34** was carried out either through the CPR for insoluble polymers **36** and **37** or via a modified Gilch route involving the end capping with 4-*tert*-butylbenzyl chloride for **35**. However, even with the latter, the extremely high molecular weight of the polymer (M_w exceeds 2×10^6 for 1:0.05 ratio, 4×10^5 for 1:1 ratio) was still an issue, affecting the material processability (which is also the case for MEH-PPV **13**). Due to significant steric factors of this substitution pattern, the emission of polymer **37** is blue-shifted to a λ_{max} of 490 nm, which is very low for fully conjugated PPVs. Furthermore, the solid-state PL efficiency also reached a very high value of 65%, which can be explained by preventing the intermolecular packing of highly distorted polymer chains.



SCHEME 2.12 Synthesis of 2,3-diphenyl-substituted PPVs (From Hsieh, B.R., Yu, Y., Forsythe, E.W., Schaaf, G.M., and Feld, W.A., *J. Am. Chem. Soc.*, 120, 231, 1998.)

The solubility of the phenyl-PPVs can be greatly improved by the introduction of alkoxy substituents into the pendant phenyl groups. Spreitzer and coworkers [105,106] first reported the alkoxyphenyl-substituted PPVs **38–42** and their numerous copolymers (see below) prepared through a modified Gilch route (Chart 2.7). These polymers exhibited high PLQY and PLEDs, fabricated using these alkoxy-substituted phenyl-PPVs, showed improved EL performance owing to their good film-forming properties. Thus, the green-emitting PLED ITO/**39**/Ca demonstrates $\Phi_{\text{EL}}^{\text{ex}} = 3.1\%$ (7.9 cd/A) [106,107].

However, it was later found that the phenyl-substituted PPVs have a significant level of defect TBB moieties built into the polymer chain [106]. The defects have moderate influence on the photophysical properties of polymers, but strongly affect the PLED device lifetime. In fact, the amount of TBB defects in phenyl-substituted PPVs is several times higher than in similarly prepared dialkoxy-PPVs (5–6% in phenyl-PPVs vs. 1.5–2.2% in dialkoxy-PPVs **13** or **14**). Considering the mechanism of TBB formation (Scheme 2.13), the monophenyl-substituted monomers should favor such defects. Due to similar acidity of both CH₂Cl groups, two types of quinone intermediate, A and A', can be formed. At the same time, the steric hindrance brought about by phenyl groups will favor the HH coupling of these monomers rather than a normal HT reaction. The amount of TBB defects can be significantly suppressed (to <0.5%) by introducing an additional methoxy substituent into phenyl-PPV monomer. This is especially important, as it has been shown that the lifetime of the phenyl-substituted PPVs in PLED is increased by over 30 times on lowering the TBB content from 6 to 3% [106].

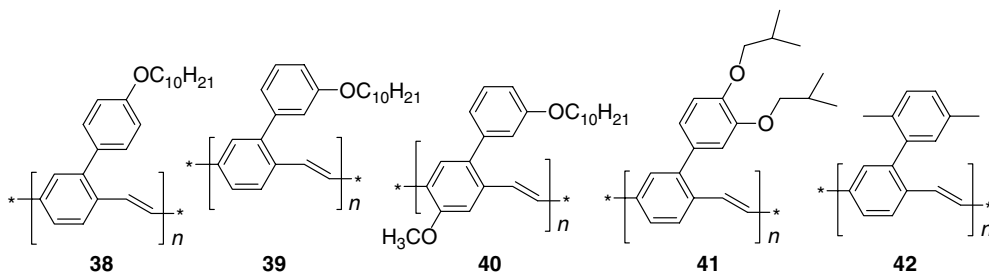
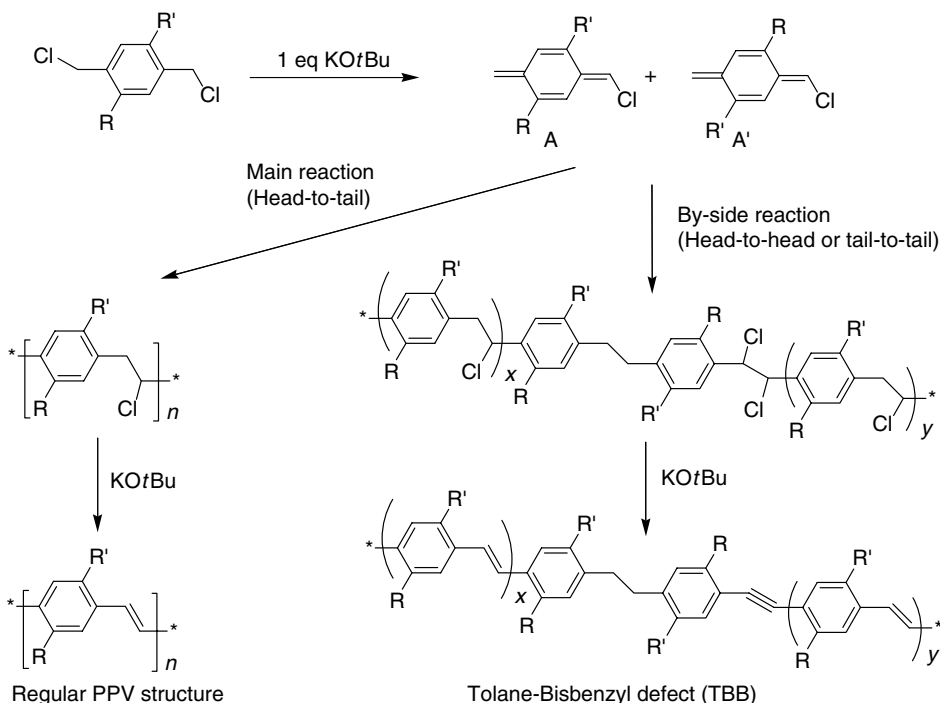


Chart 2.7



SCHEME 2.13 The mechanism of formation of TBB in the Gilch polymerization (From Becker, H., Spreitzer, H., Kreuder, W., Kluge, E., Schenk, H., Parker, I., and Cao, Y. *Adv. Mater.*, 12, 42, 2000.)

Introducing two alkoxy substituents in positions 2 and 5 of the phenyl side group can efficiently prevent the interchain-fluorescent quenching, as has been demonstrated in the polythiophene series [108]. Based on this observation, Andersson and coworkers [40,109] synthesized phenyl-substituted PPVs **43** and studied their properties and EL performance (Chart 2.8). As in other phenyl-substituted PPVs, the TBB defects were a major problem, although the amount of defects could be somewhat decreased by a careful control of the reaction conditions: the TBB content of 9% for the polymer prepared at 144°C reduces to 3% for the polymer prepared at 0°C. The highest $\Phi_{\text{EL}}^{\text{ex}} = 0.94\%$ was achieved with the polymer prepared at 66°C (in the PLED ITO/PEDOT/**43**/Ca). The same group has also synthesized similar polymers **44** and **45** [110]. As found earlier, the introduction of the alkoxy group in the phenyl-PPV backbone decreases the amount of TBB content. The polymer **45** showed a few times lower level of TBB defect compared with **44** and by performing the reaction at -35°C , the amount of TBB can be brought below 1%. This difference is clearly reflected in the PLED device performance. The external QE of PLEDs fabricated as ITO/PANI/polymer/Ba/Al is

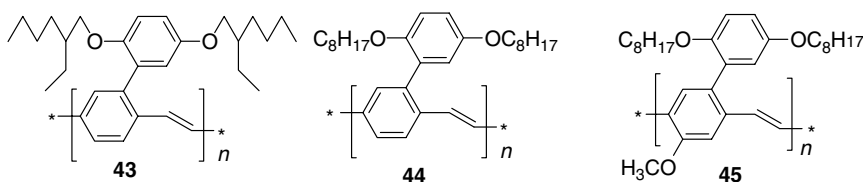


Chart 2.8

similar for both polymers (1.74% for **45** and 1.34% for **44**), but the operation lifetime of the low TBB content polymer **45** is prolonged by about five times.

Recently, Chen et al. [111] synthesized a series of dialkoxybiphenyl-substituted PPV polymers **46–48** and model alkoxyphenyl-PPVs **49** and **50** by the Gilch route (Chart 2.9). Additional phenyl rings were introduced in the side chain in order to investigate the effect of the steric interaction on the formation of TBB defects as well as to increase the thermal stability of the polymers. The authors described the observed variation of the TBB defect ($\sim 0.5\%$ for polymer **46** and $\sim 4\%$ for polymers **47** and **48**) as “expected,” although the influence of the structural variations between, for example **46** and **47**, is not obvious. The authors also demonstrated that using a more polar solvent, such as THF, during polymerization helps to suppress the TBB formation by a factor of 2, compared to *p*-xylene. These results were argued against the previous finding by Andersson and coworkers [40], who attributed the suppression of the TBB formation in THF vs. *p*-xylene solution solely to the lower temperature employed for the former. The green-emitting PLEDs fabricated in configuration ITO/PEDOT/polymer/Ba/Al showed the lowest turn-on voltage for polymer **46**, although the highest QE of 0.66% was achieved for **47** (0.37% for **46** and 0.25% for **48**).

The same group recently reported that the TBB defects can be brought below the nuclear magnetic resonance (NMR) detection limit by employing similar polymerization conditions (*t*-BuOK in THF at room temperature) in the synthesis of naphthyl-substituted PPVs **51–53** [112]. Although the absorption and PL spectra of all three polymers are similar, the EL can be finely tuned between 486 nm (for **52**) and 542 nm (for **53**). The external QE (studied for ITO/PEDOT/polymer/Ba/Al device) is also sensitive to the substituents pattern in the naphthyl pendant group: 0.08% for **51**, 0.02% for **52**, and 0.54% for **53**.

Jin et al. [113] attached a solubilizing trialkylsilyl substituent in the *meta*-position of the pendant phenyl group. The target polymer **54** was purified by membrane dialysis and revealed improved thermal (the decomposition temperature, $T_{\text{dec}} = 406^\circ\text{C}$) and color stability. The device fabricated as ITO/PEDOT/polymer/Al:Li emits light at $\lambda_{\text{max}} = 525$ nm with rather moderate performance: maximum $\Phi_{\text{EL}}^{\text{ex}} = 0.08\%$, maximum brightness of 570 cd/m^2 (at 43 V), and turn-on voltage as high as 14 V. The authors explained these discouraging results by a high-energy barrier between the HOMO band of **54** (-5.30 eV) and the ITO/PEDOT work function (-5.0 V), although 0.3 eV barrier can hardly be the only problem with the device. Nevertheless, the device performance was significantly improved by copolymerization with

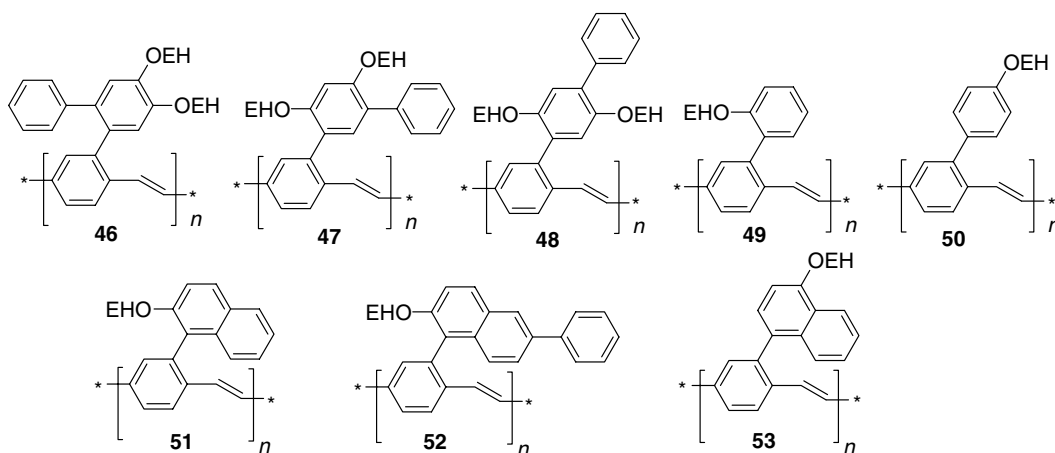
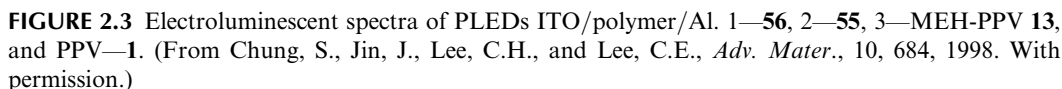


Chart 2.9



An important extension to phenyl-substituted PPVs was first reported by Tsutsui and co-workers [115], who used Gilch polymerization to synthesize fluorenyl-substituted PPVs (**57**, **58**, **59**) and studied their performance in PLEDs (Chart 2.11). Due to bulky but rigid fluorene substituents, these polymers have excellent solubility and yet are thermally stable up to 320°C and have a



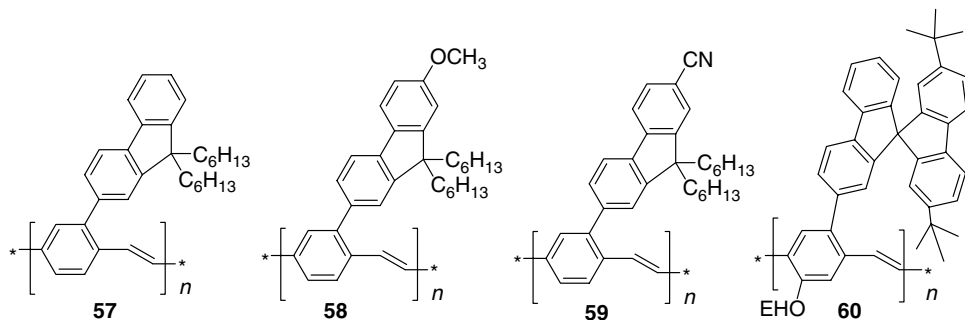


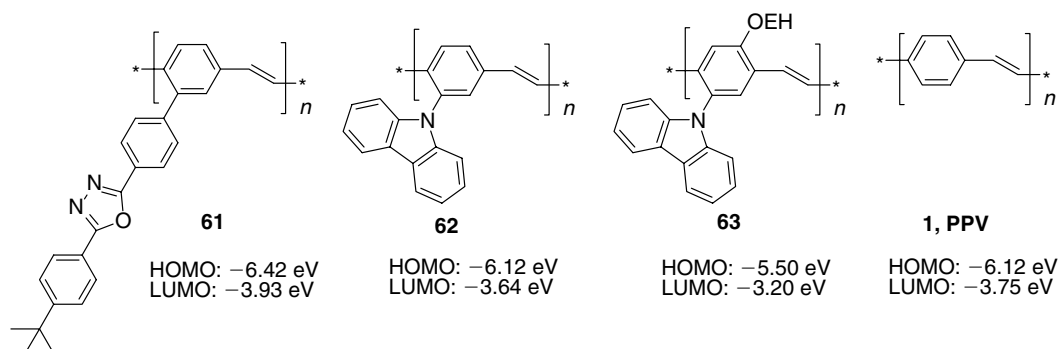
Chart 2.11

T_g of 113–148°C. The electron-donating methoxy group or electron-withdrawing cyano group was introduced to adjust the optical and electronic properties of the polymers. However, the influence of the substituents in the fluorene nucleus on the redox and fluorescent properties of polymers **57**–**59** was found to be very small, indicating that PPV backbone rather than the pendant fluorene unit determines the optoelectronic properties of the system. At the same time, as was shown later, the substituents in fluorene nucleus retard the hole mobility of the polymer [116]. In fact, the unsubstituted polymer **57** showed quite high hole mobility of $4.5 \times 10^{-4} \text{ cm}^2/(\text{Vs})$ (at electric field of $2.5 \times 10^5 \text{ V/cm}$), which is two orders of magnitude higher than that of MEH-PPV **13**.

All three polymers emit blue-green light with a maximum of around 500 nm and a shoulder of 532 nm with a PLQY of 68–71% (in solution). The PLEDs were fabricated with polymers **57**, **58**, and **59** as ITO/PEDOT/polymer/Ca. The EL performance of the device fabricated with **57** had the lowest turn-on voltage (2.8 V) and the highest luminescence efficiency (a maximum luminance of $12,000 \text{ cd/m}^2$ with a maximum $\Phi_{\text{EL}}^{\text{ex}} = 0.53\%$). The performance of the other two polymers **58** and **59** was similar, but the QE was 1.6 to 2.8 times lower than that of **57**. More recently Kwon and coworkers [117] synthesized even more hindered spiro-bifluorenyl-PPV **60**. Polymer **60** is highly soluble with T_g as high as 200°C, although its solid-state PL efficiency is not very high (26%). The PLED showed a turn-on voltage of 6 V and a maximum brightness of 1150 cd/m^2 at 12.5 V and a maximum power efficiency of 0.12 lm/W .

2.2.2.5 Poly(*p*-Phenylene Vinylene) Homopolymers with Electron-Withdrawing and Donating Substituents

One of the problems of application of conjugated PLEDs is a rather high-lying LUMO energy level, which requires an unstable low work-function metal electrode (as Ca) for efficient electron injection. The VEH calculations predict that introduction of an electron-withdrawing group onto either the phenyl ring or the vinyl unit of PPV lowers the HOMO and LUMO energies of the polymer [91]. Significant improvement of the EL efficiency can be achieved by blending dialkoxy-PPV polymers with electron-transporting materials (as PBD) [68]. In this regard, Jin and coworkers [118] compared the properties of PPV polymers carrying an electron acceptor 2,5-diphenyl-1,3,4-oxadiazole group (resembling PBD, a widely used electron transporter) and an electron donor carbazole group (an excellent hole transporter) (Scheme 2.14). In spite of the absence of long-chain substituents, polymers **61** and **62** are very soluble in common organic solvents, probably due to relatively low-molecular weight ($M_n = 24,000$ and $16,000$, respectively). Although the absolute efficiencies of the derived PLEDs were quite low ($\Phi_{\text{EL}}^{\text{ex}} < 0.004\%$) due to unoptimized device structure (ITO/polymer/Al), there is a clear dependence of the EL efficiency on the molecular orbital levels: the lower the barrier between the Al work function (-4.3 eV) and the LUMO of the polymer, the higher the efficiency: **61** > **1** > **62**



SCHEME 2.14 Tuning the energy levels of PPV by introducing pendant charge-transporting units. The HOMO defined as the $-I_p$ value (determined from the UPS experiments) and the LUMO was deduced by adding the optical gap to the HOMO value.

(Scheme 2.14). This suggests that the electron and hole injections (or transport) in PPV are unbalanced and holes are the dominant charge carriers.

On the other hand, in a later publication, the same group admitted that the charge-injection barrier is not the only consideration playing a role in maximizing the EL efficiency [119]. Surprisingly, the introduction of a donor alkoxy substituent into carbazole-PPV, which further raises the LUMO level (but also the HOMO and thus facilitates the hole injection), increases the EL efficiency. The same structure PLED, prepared with polymer **63** possesses 550-fold increase of external QE (0.01%), compared to polymer **62**. Furthermore, a very high-performance PLED can be fabricated with PEDOT-modified anode: the device ITO/PEDOT/**63**/Ca/Al shows an EL efficiency of up to 4.4 cd/A and maximum brightness in excess of 30,000 cd/m² [119]. The device half-lifetime was estimated to be 70 h at a brightness of 1000 cd/m².

In a similar approach, the HOMO level of PPV was controlled by the introduction of a dialkylamino donor group (polymer **64**) [120] (Chart 2.12). The dialkylamino groups render

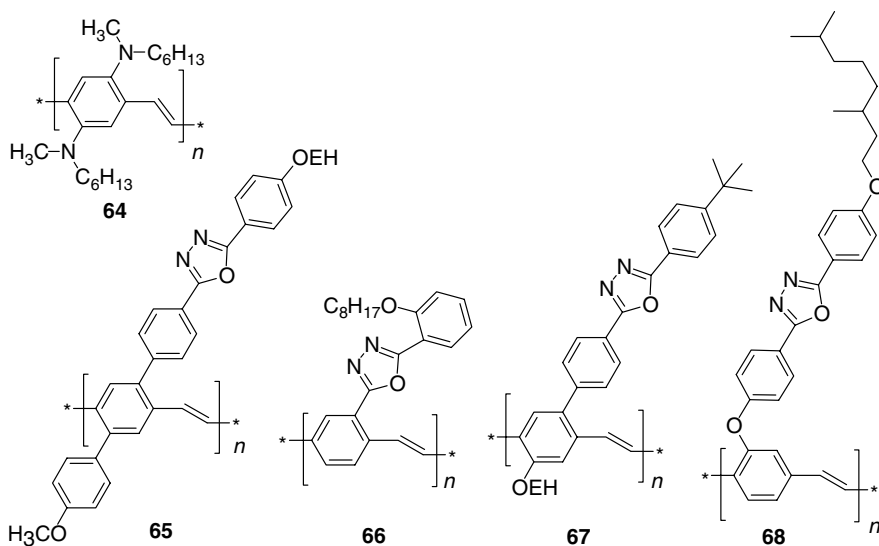


Chart 2.12

the material with high solubility and good film-forming properties and, similar to alkoxy groups, shift the emission maxima (~ 560 nm) to the red. The PLED ITO/**64**/Mg/Al showed moderate efficiency (0.3% at ~ 30 cd/m²; 0.2% (0.45 cd/A, 0.08 lm/W) at 300 cd/m²), but the turn-on voltage (>10 V) was rather high [120].

Balancing the charge transport via introduction of electron-transporting oxadiazole groups was further developed by Huang and coworkers [121,122], who synthesized the polymers **65** and **66** by Gilch polymerization. Surprisingly, the polymer **65** was completely insoluble, regardless of the preparation conditions (Gilch polymerization), which was explained by its very rigid structure [121]. This polymer is in drastic contrast with **61**, which does not even have long-chain 2-ethylhexyloxy substituent and can be due to higher molecular weight. Polymer **66**, where the *o*-alkoxyphenyl-substituted oxadiazole nucleus is directly connected to the PPV backbone, is a highly soluble material with moderate molecular weight of $M_n = 20,700$ and rather high T_g of 170°C. The PLEDs fabricated with this polymer in simple ITO/polymer/Al configuration showed improved charge-transport properties, as seen from the low turn-on voltage (4.0 V) at which the device starts to emit a yellow-orange light.

Jin and coworkers [123] synthesized PPV **67**, containing an oxadiazole and an alkoxy group. According to UPS study, the HOMO and LUMO levels in **67** (-6.32 and -3.98 eV) are within the band gap of the parent polymer **61** without alkoxy substituents (Scheme 2.14). The external QE of PLEDs based on polymer **67** is about one order of magnitude higher than that for **61** (0.045% for ITO/**67**/Li:Al) and a maximum brightness of up to 7570 cd/m² was achieved for this material (using Ca cathode).

The recently synthesized PPV **68**, in which the oxadiazole group is separated from the PPV backbone by an oxygen atom, is a very soluble material with optical band gap of 2.36 eV and yellowish-orange emission color (chromaticity coordinates by the Commission Internationale de l'Eclairage, CIE: $x = 0.50$, $y = 0.47$; $\lambda_{\max}^{\text{PL}} = 591$ nm) [124]. An extremely high-performance PLED was claimed for this polymer in a single-layer configuration (ITO/PEDOT/**68**/Al). The device is characterized by a low turn-on voltage of 5 V, achieves the maximum brightness of 19,400 cd/m² at 14 V, and demonstrates a luminance efficiency of 21.1 cd/A (at 5900 cd/m²), which ranks it among the best performing EL PPV materials.

Using CPR, Burn and coworkers introduced several electron-accepting moieties such as *p*-nitrostyryl (**69** [125]) and methylsulfonyl-phenyl (**70** [126]) groups as substituents in the PPV backbone. However, essentially no difference in EL performance (maximum QE 0.01% for ITO/polymer/Al) was found between polymers **70** and **71** and the authors concluded that the methylsulfonyl group in the pendant phenyl ring does not facilitate electron injection (Chart 2.13).

Similar materials containing electron-withdrawing cyano groups, also attached to pendant phenyl substituents, were recently synthesized by Shim and coworkers [127] via Gilch

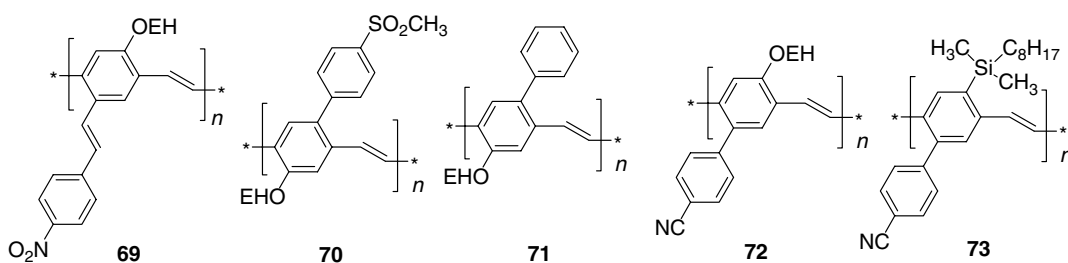


Chart 2.13

polymerization. Polymers **72** and **73**, soluble in organic solvents, show good thermal stability (less than 5% weight loss at 400°C) and very high T_g (192 and 180°C, respectively). The PL quantum efficiencies of **72** and **73** were 43 and 62%, respectively. PLEDs fabricated in ITO/PEDOT/polymer/LiF/Al configuration emitted greenish-yellow light (CIE: $x=0.455$, $y=0.532$) for **72** and very pure green light (CIE: $x=0.330$, $y=0.599$) for **73**, which is very close to the standard green color (CIE: $x=0.30$, $y=0.60$) used in high definition television (HDTV). According to electrochemical measurements, both polymers possess similar LUMO energy values (-2.72 eV for **72** and -2.75 eV for **73**, respectively), but their HOMO energy levels are different (-5.41 eV for **72** and -5.72 eV for **73**), reflecting the difference in electron-donating properties of alkoxy and trialkylsilyl substituents (and also steric, a factor of the trialkylsilyl substituent reducing conjugation). Interestingly, the HOMO energy level of **72** is closer to the work function of PEDOT (-5.0 eV), but its EL performance is lower: the maximum brightness of **73** is 2900 cd/m² at 10 V (maximum QE 0.65%), whereas polymer **72** reaches only 330 cd/m² at 10.5 V (maximum QE 0.025%). Once again, these results indicate a not well-understood, yet very beneficial effect of silyl substituents on the EL properties of PPV polymers.

Several groups have investigated the effect of fluorine electron-withdrawing substituents in PPV. The trifluoromethyl electron-withdrawing group (polymer **74**), attached directly to the phenylene units, improves the electron injection quite significantly, but probably also acts as a quencher. The PLQY of this polymer (5–7%) is much lower than that of the parent PPV (27%) [128]. As a result, single-layer LED devices ITO/**74**/Al and ITO/**74**/Ca showed almost the same Φ_{EL}^{ex} , which was one order of magnitude lower than that of ITO/PPV **1**/Ca (Chart 2.14).

Shim and coworkers [129] synthesized poly(2-fluoro-1,4-phenylene vinylene) **75** by the thermal conversion method. This polymer exhibits almost the same absorbance spectra as PPV **1** ($\lambda_{max} \sim 410$ nm), but the fluorescence band ($\lambda_{max} = 560$ nm) is red-shifted by ca. 20 nm. The LUMO level was shifted down by ca. 0.15 eV, facilitating electron injection but, in contrast to the above polymer **74**, no fluorescence quenching was observed. Consequently, the PLED devices fabricated as ITO/**75**/Al have about ten times higher EL efficiency than those fabricated with PPV **1** under identical conditions.

Comparative analysis of different fluorine-substituted PPVs **75–77** has been performed by Karasz and coworkers [130]. Polymers **75** and **76** exhibit slightly blue-shifted UV absorbance relative to PPV **1**, but remarkably, have substantially red-shifted PL and EL emission bands.

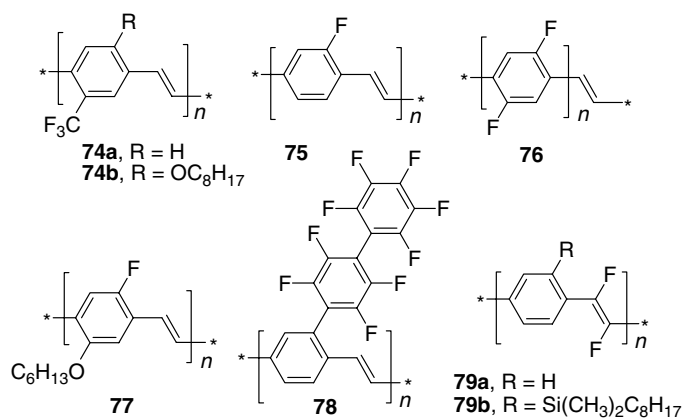


Chart 2.14

In push–pull polymer **77**, both the absorption and emission maxima are red-shifted relative to **1**. The LED performance of these materials appeared to be rather low (the EL efficiency of ~ 0.002 cd/A and the maximum luminance of ~ 100 cd/m² was achieved at 30 V), and the turn-on voltage for the push–pull polymer **77** (4 V) was lower than that in more electron-deficient polymers **75** and **76**.

Jang et al. [131] reported high electron affinity perfluorobiphenyl-substituted PPV **78**. This polymer was synthesized by the thermoconversion method. Single-layer PLED ITO/**78**/Al showed 64 times higher EL efficiency than that fabricated with unsubstituted PPV **1**. A further (380-fold) increase of efficiency was achieved in a bilayer device ITO/**1**/**78**/Al.

Fluorine has also been introduced into the vinylene fragment of PPV (**79a,b** [132]), resulting in blue shifts in PL (from 580 to 495 nm) and EL (from 565 to 540 nm; yellow to green) spectra. The turn-on voltage of ITO/PEDOT/**79**/Al devices was 3–4 V and for silyl-substituted **79b**, a rather high luminance of 2.7 cd/A (at 6.5 V) and a maximum brightness of 750 cd/m² (at 7.5 V) was achieved.

Chlorine substituents have also been introduced into PPV (in phenylene units), but no EL or PL properties of these materials have been reported [57].

2.2.3 CONJUGATED POLY(*p*-PHENYLENE VINYLENE) COPOLYMERS

2.2.3.1 Poly(*p*-Phenylene Vinylene) Copolymers with Electron Donor and Aryl Substituents

Due to higher variety of possible structures, copolymers allow a better control of the HOMO–LUMO levels necessary to optimize the EL properties of the PPV, compared to homopolymers. Often the optical and electronic properties in copolymers can be finely tuned by simply changing the feed ratio of comonomers (although the structure–property relationship in these systems is even more complex than in homo-PPV polymers). Using different comonomer units, various PPV-based materials with tuned optical and electronic properties have been prepared.

Although MEH-PPV **13** (at the time of discovery) was one of the most efficient soluble polymers for PLEDs application, its performance is not high enough for commercialization as LEP. One of the reasons is unbalanced hole–electron mobility in MEH-PPV (the mobility of holes is 100 times faster than the mobility of electrons) [133]. Copolymerization with other conjugated monomers, to some extent, can improve the electron-transporting properties and increase the EL performance.

The first realization of this approach was reported by the Cambridge group, which synthesized copolymers **80** containing phenylene vinylene and dialkoxy(phenylene vinylene) units by the thermoconversion method [23,134]. A 30-fold improvement in EL efficiency was observed for these copolymers compared with PPV **1** or MEH-PPV **13** devices fabricated in the same configuration (Chart 2.15).

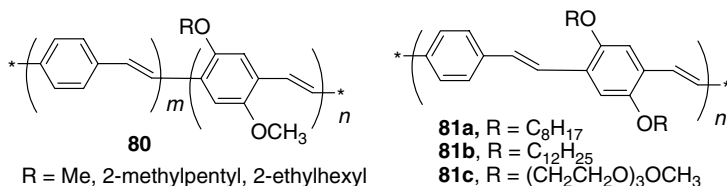


Chart 2.15

Since then, most research groups use the copolymerization approach to tune the properties of EL materials. The synthetic methods include the Wittig–Horner condensation, Gilch polymerization, Heck reaction, etc. A number of PPV copolymers similar to **80** were synthesized (e.g., **81a** [135], **81b** [136]). Most recently, Huang et al. [137] used a Wittig–Horner reaction to construct polymer **81c** with hydrophilic oligo(ethylene oxide) substituents for LECs. This copolymer is a yellow-green emitter, whose efficiency can be improved from 0.038 lm/W (in classical LED configuration ITO/polymer/Al) to 0.185 lm/W (in LEC ITO/polymer+LiOTf/Al).

The groups of Holmes and Friend reported a series of PPV copolymers containing alkoxy- and trialkylsilyl-substituted phenylene rings in random distribution (**82–83** [90], **84** [79], and **85** [138]). The authors mentioned that introduction of the trialkylsilyl group results in about a five-time increase of the luminous efficiency of copolymers **83a,b**, compared with corresponding dialkoxy-PPV homopolymers **25a,b** (0.2 lm/W for ITO/**83b**/Al). High ion affinity of the oligo(ethylene oxide) pendant group allows to create LECs with an efficiency of 0.5 lm/W (for ITO/**83b**+LiOTf/Al) [90].

EL from related polymers **84a,b**, containing more sterically demanding 2,3-dibutoxyphenylene units, have also been studied. Both copolymers are blue-green emitters ($\lambda_{\text{max}} \sim 545$ nm) with moderately high PLQY in the solid state, 35% for **84a** and 28% for **84b**. At the same time, EL from **84a** can only be observed with a Ca (but not Al) electrode, whereas a single-layer device ITO/PEDOT/**84b**/Al shows a current efficiency of 0.72 cd/A and a maximum luminance of 1380 cd/m² (turn-on voltage 4 V) [79] (Chart 2.16).

Synthesis of phenyl- or alkoxy-substituted PPV copolymers was first reported by Spreitzer et al. [74], who studied in detail the dependence of the EL on the comonomer ratio in **86** (Scheme 2.15) and other related phenyl-substituted PPV copolymers [105–107]. The polymerization was performed via the Gilch route using different comonomer feed ratios. All copolymers showed a high EL efficiency of above 10 cd/A and low-driving voltage (~ 3.5 V). In addition, very high emission brightness (10,000 cd/m²) was easily achieved by applying a very reasonable voltage of 6 to 8 V. The emission color of the phenyl-substituted PPV, **86a** is green (CIE: $x = 0.35$, $y = 0.61$), whereas increasing the ratio of dialkoxy(phenylene vinylene) unit results in a gradual red shift of the emission, through yellow (for **86e**, CIE: $x = 0.49$, $y = 0.50$) to orange color (for **86f**, CIE: $x = 0.60$, $y = 0.40$). Interestingly, the dialkoxy-PPV homopolymer

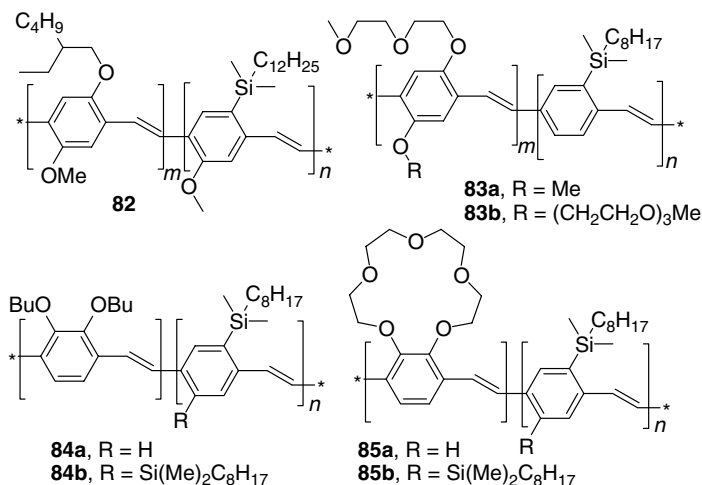
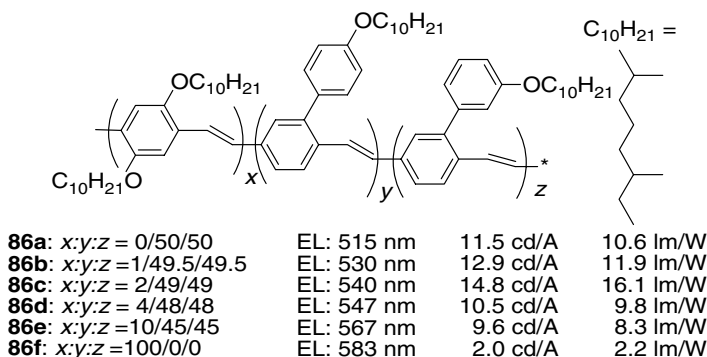


Chart 2.16

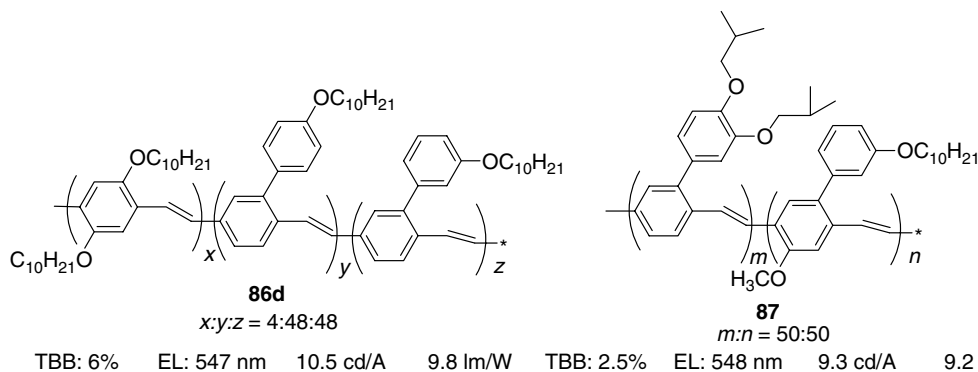


SCHEME 2.15 Dependence of the electroluminescence of alkoxyphenyl-PPV copolymers on the comonomers ratio (PLED configuration ITO/PEDOT or PANI/polymer/Ca or Yb/Ag).

86f revealed a significantly lower EL efficiency of 2 cd/A, but introducing the corresponding unit in the copolymer in small amounts (2%, based on feed ratio) allows to increase the luminous efficiency from 10.6 lm/W (for **86a**) to 16.1 lm/W (for **86c**).

As we mentioned before, phenyl substituents in PPV increase the amount of TBB defects in the Gilch synthesis, affecting the device stability. Becker et al. [106] showed that introducing a second substituent (alkoxy group) can significantly reduce the formation of TBB. The TBB suppression was observed with increasing the feed ratio of alkoxy-phenyl-substituted monomer. Scheme 2.16 shows the chemical structures of two greenish-yellow copolymers and their EL performance along with their TBB defects. These two copolymers have similar optical and electronic properties, but their TBB contents are different. Hence, the device fabricated from low TBB content copolymer **87** showed 30 times longer lifetime than the device made from high TBB content copolymer, even though their initial EL performance was nearly identical. Rather high lifetime of copolymers of type **87** made them attractive enough for industrial applications in PLEDs, as pursued by Philips and DuPont [139].

An extremely efficient PLED was fabricated with a similar phenyl-PPV copolymer **88** by the Cambridge group [140]. The PLED ITO/PEDOT/**88**/Ca could be turned on at only 2.2 V and shows $\Phi_{\text{EL}}^{\text{ex}}$ of amazing 6% (20 cd/A) (estimated internal QE of 15–20%, close to theoretical limit of 25%), which is still among the record values in electrofluorescent PPV materials. Although this significant improvement was greatly due to sophisticated engineering of the



SCHEME 2.16 The concentration of TBB defects and the initial EL performance of two related phenyl-PPV copolymers.

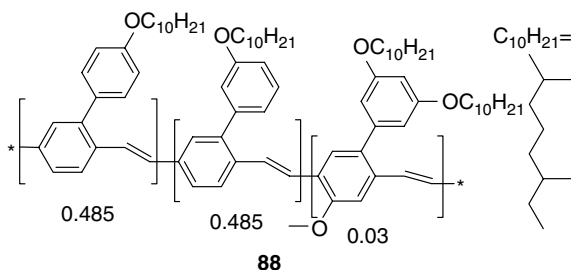


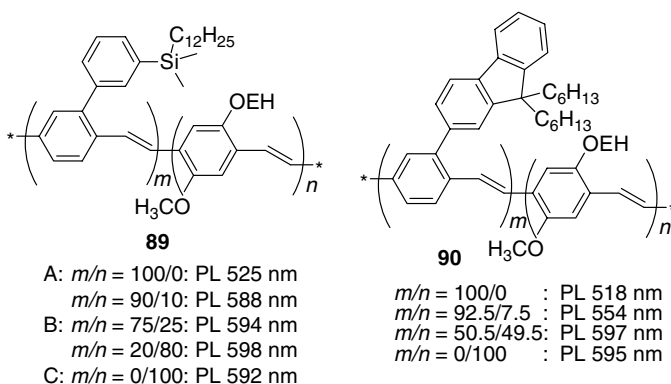
Chart 2.17

anode and EL polymer interface (ITO was modified by multilayer deposition of PEDOT-based materials), the dialkoxy-PPV homopolymer **14**, under the same conditions, showed essentially lower efficiency (1.8%, 2.6 cd/A) (Chart 2.17).

Scheme 2.17 illustrates some MEH-PPV random copolymers with trialkylsilylphenyl (**89** [113]) and dihexylfluorene (**90**, [141]) units, synthesized by Jin's group using the Gilch polymerization method. The HOMO–LUMO energy levels and the emission color of these copolymers can be finely tuned by adjusting the feed ratio of the comonomers (Scheme 2.17, Figure 2.4). The authors found a turn-on voltage dependence on the gap between the HOMO level and the work function of the ITO electrode and suggested that holes are the major carriers in these materials. A high efficiency red-orange-emitting ($\lambda_{\text{max}}^{\text{EL}} = 590$ nm) PLED has been fabricated with copolymer **89** using low work-function Al:Li alloy electrode [113]. The device ITO/**89**/Al:Li showed a low turn-on voltage of 2.3 V, a high maximum brightness of over 19,000 cd/m² (at 12 V), a high luminance efficiency of 2.9 lm/W, and a half-life of 120 h at 1000 cd/m², which significantly overrides the performance of similar devices prepared from the corresponding homopolymers.

Likewise, copolymers **90** have higher EL efficiency than homopolymers DHF-PPV **57** or MEH-PPV **13**, due to more balanced charge injection and transport properties. Copolymer **90** with 7.5 wt% loading of dialkoxyphenylene comonomer gave the highest QE. The device with an ITO/PEDOT/**90**/Ca configuration showed remarkably higher efficiency (2.4 cd/A) than devices fabricated with other copolymers in the series (0.65–1.0 cd/A) [141].

One of the problems in the design of organic (electro)luminescent materials is the decrease of the QE of fluorescence in the solid state due to the formation of π -aggregates. Earlier we



SCHEME 2.17 Tuning the emission maxima in random phenyl-PPV copolymers.

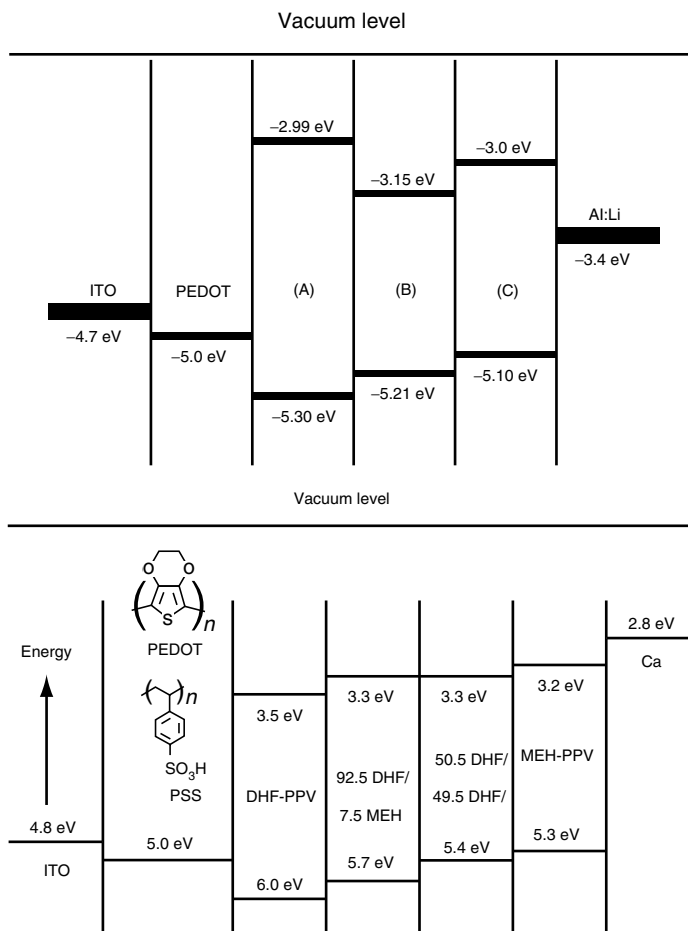


FIGURE 2.4 Energy diagrams of PLEDs based on polymers. Top: **89**(A,B,C). Bottom: **90**, with different feeding ratio (DHF stands for 9,9-dihexylfluorenyl). (From Jin, S., Jang, M., and Suh, H., *Chem. Mater.*, 14: 643, 2002. With permission. Sohn, B., Kim, K., Choi, D.S., Kim, Y.K., Jeoung, S.C., and Jin, J., *Macromolecules*, 35, 2876, 2002. With permission.)

described one approach to circumvent this problem by introducing bulky aromatic substituents into the PPV backbone to hinder intermolecular π -stacking. However, in homopolymers, very bulky substituents slow down the polymerization reaction, resulting in low-molecular-weight products. The problem can be solved by introducing a second, less sterically demanding comonomer unit. The polymer **91**, synthesized by Peng et al. [142] through Wittig–Horner reaction, is a highly fluorescent material with a PLQY (in films) of 61–82% (cf. 10% for dioctyloxy-PPV). Unfortunately, no EL data was reported for these copolymers.

Even more bulky substituents were introduced in copolymers **92** synthesized by Heck coupling [143]. These materials emit blue light with a maximum emission peak at 442 nm, which is among the shortest emission wavelengths of the formally conjugated PPV (although likely, it is more related to the oligophenylene substituents than to the PPV backbone). This high-energy emission was attributed to conjugation interruption caused by oligophenylene substituents, although, as mentioned above, the aromatic substituents can adopt a nearly orthogonal dihedral angle with respect to the PPV chain, minimizing the steric encumbrance.

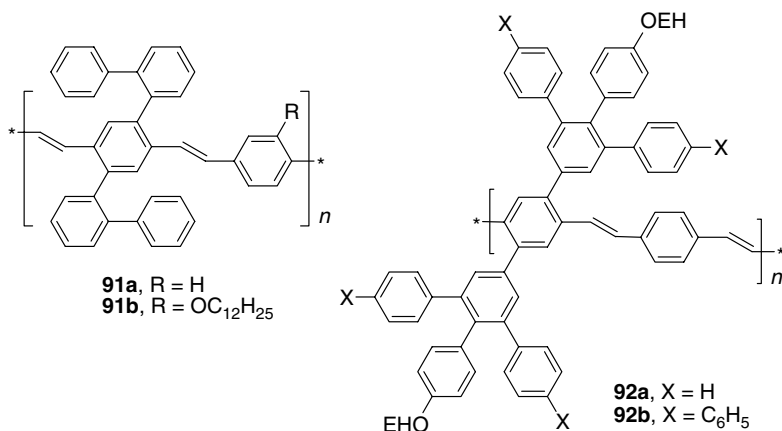


Chart 2.18

Interestingly, in spite of these bulky substituents, the fluorescence spectra of **92** in films differ from those of solutions by an additional longer wavelength shoulder at 512 nm, ascribed by the authors to aggregate emission (Chart 2.18).

The properties of PPV polymers can also be tailored by introducing additional aromatic units in the PPV chain. In 1995, Hadzioannou and coworkers [46] reported terphenylene-containing copolymer **93**, synthesized by the Heck reaction (Chart 2.19). A relatively poor conjugation brought about by the alkyl-substituted oligophenylene fragments (see Section 2.5), resulted in blue shift of the emission wavelength ($\lambda_{PL} = 440$ nm in films; solution $\Phi_{PL} = 89\text{--}90\%$). A nonoptimized single-layer PLED (ITO/**93**/Al) emitted blue light ($\lambda_{EL} \sim 450$ nm) with Φ_{EL}^{ex} up to 0.03%.

The related copolymer **94**, synthesized in the 1980s by Feast et al. [144], presents a rare example of a PPV-containing phenyl substituents on the vinylene unit. Apparently, the steric hindrance caused by phenyl substituents in **94** is not dramatic, and the optical properties of **94** are similar to those of other PPVs (green emission, $\lambda_{PL} \sim \lambda_{EL} \sim 530$ nm). An internal QE of up to 1% was reported with multilayer **94**-based PLEDs containing PPV **1** and PVK as HTL [145].

In the effort to make pure blue-emitting materials Shim and coworkers [146] synthesized a series of PPV-based copolymers containing carbazole (polymers **95** and **96**) and fluorene (polymers **97** and **98**) units via Wittig polycondensation. The use of trimethylsilyl substituents, instead of alkoxy groups, eliminates the electron donor influence of the latter and leads to chain distortion that bathochromically shifts the emission ($\lambda_{max} = 480$ nm for **95** and 495 nm for **97**). In addition, a very high PLQY was found for these polymers in the solid state (64 and 81%, respectively). Single-layer PLEDs fabricated with **95** and **97** (ITO/polymer/Al) showed EL efficiencies of 13 and 32 times higher than MEH-PPV, respectively (see also Ref. [147] for synthesis and PLED studies of polymers **99** and **100**) (Chart 2.20).

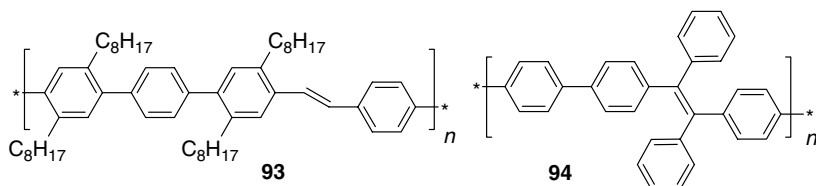


Chart 2.19

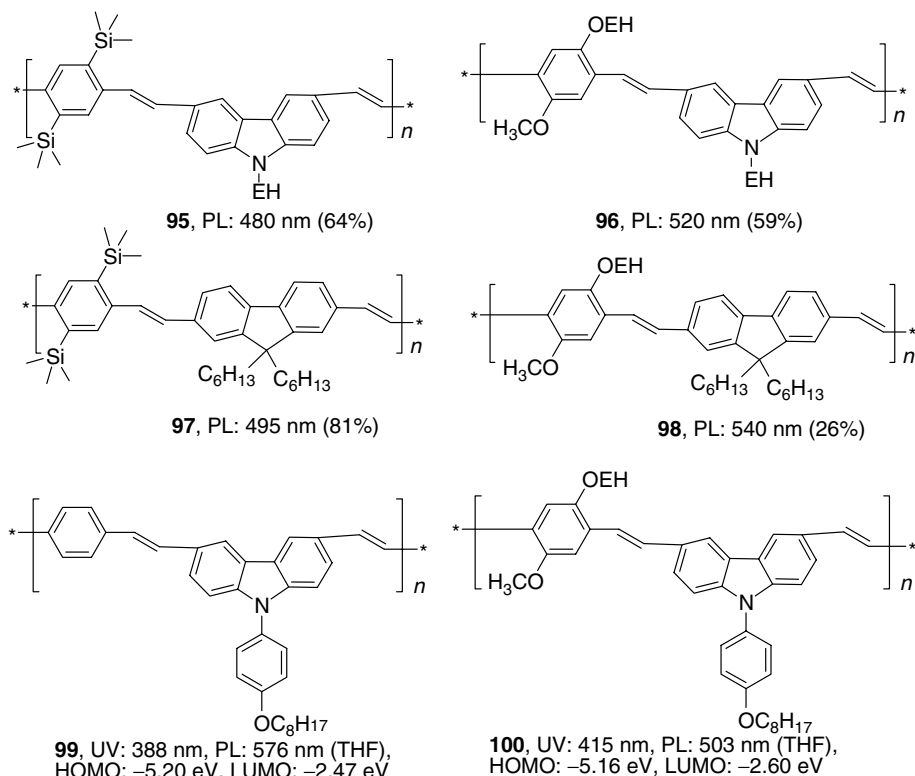


Chart 2.20

Similar PPV-based copolymers with carbazole and fluorene units in the backbone **101** and **102** (and also similar copolymers with oxadiazole substituents **103** and **104**) have been synthesized by Ree and coworkers [148]. Much lower PL efficiency in films was found in this case for carbazole-containing polymers **102** and **104** (1–4%), when compared to materials prepared by Shim (**95** and **96**, 59–64%) (Chart 2.21).

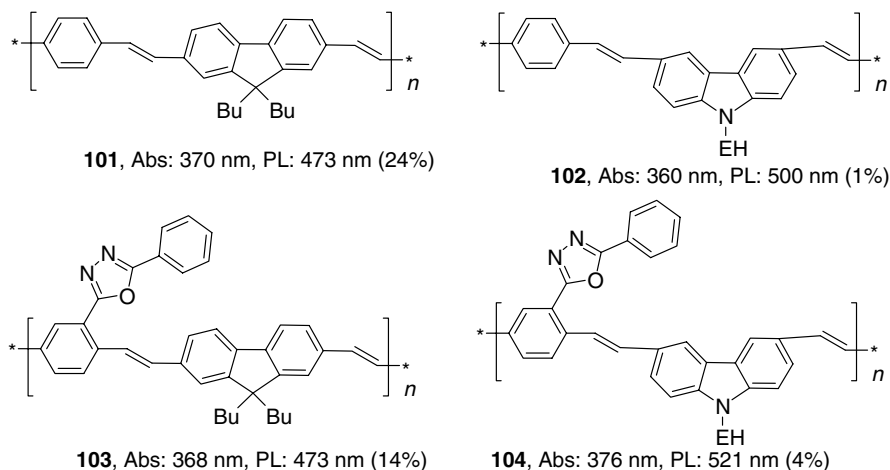


Chart 2.21

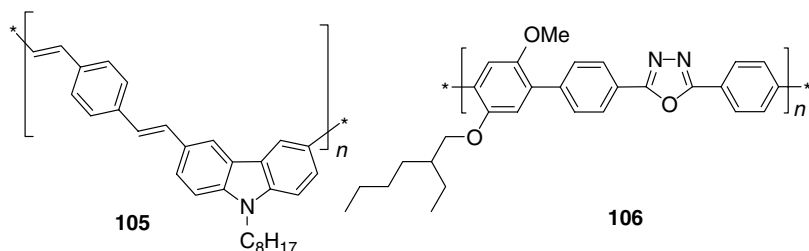


Chart 2.22

Blends of yellowish-green-light emissive carbazole-containing PPV-based copolymer **105** ($\lambda_{PL}=490, 520$ nm, $\lambda_{EL}=533$ nm) with blue-emissive oxadiazole-poly(*p*-phenylene) (PPP) copolymer **106** ($\lambda_{EL}=426$ nm) allowed to tune the emission of PLEDs (ITO/polymer blend/Al) from $\lambda_{EL}=533$ nm to $\lambda_{EL}=451$ nm, although the device turn-on voltage was essentially higher for the blends with increased content of **106** [149] (Chart 2.22).

The diphenylamino-substituted PPV **107**, with solubilizing alkoxy groups, was synthesized by Shi and Zheng [150] via Wittig–Horner reaction (Chart 2.23). Its PL (555 nm) is very similar to that of diamino-PPV **64** and dialkoxy-PPV **14** homopolymers. The PLQY is rather high in solution (80%), but it drops to only 8% in films. Consequently, only a moderate EL efficiency of 0.6 cd/A was obtained with this material (device ITO/PEDOT/**107**/Mg/Al) [150]. Almost simultaneously, Kido and coworkers [151] reported a similar diphenylamino-substituted PPV copolymer **108**, which affords very efficient PLEDs. The device ITO/PEDOT/**108**/Ca/Al

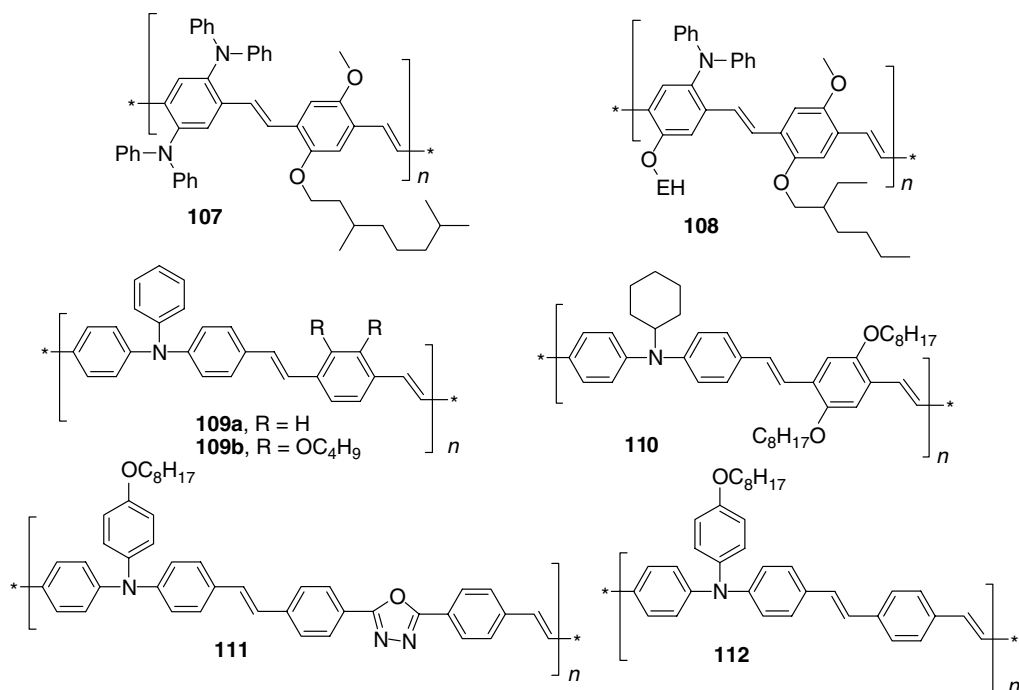


Chart 2.23

showed low turn-on voltage (3 V), high maximum brightness (29,500 cd/m²), and a power efficiency of 1.1 lm/W, which can be further improved to 3.0 lm/W, if cesium is used as a cathode.

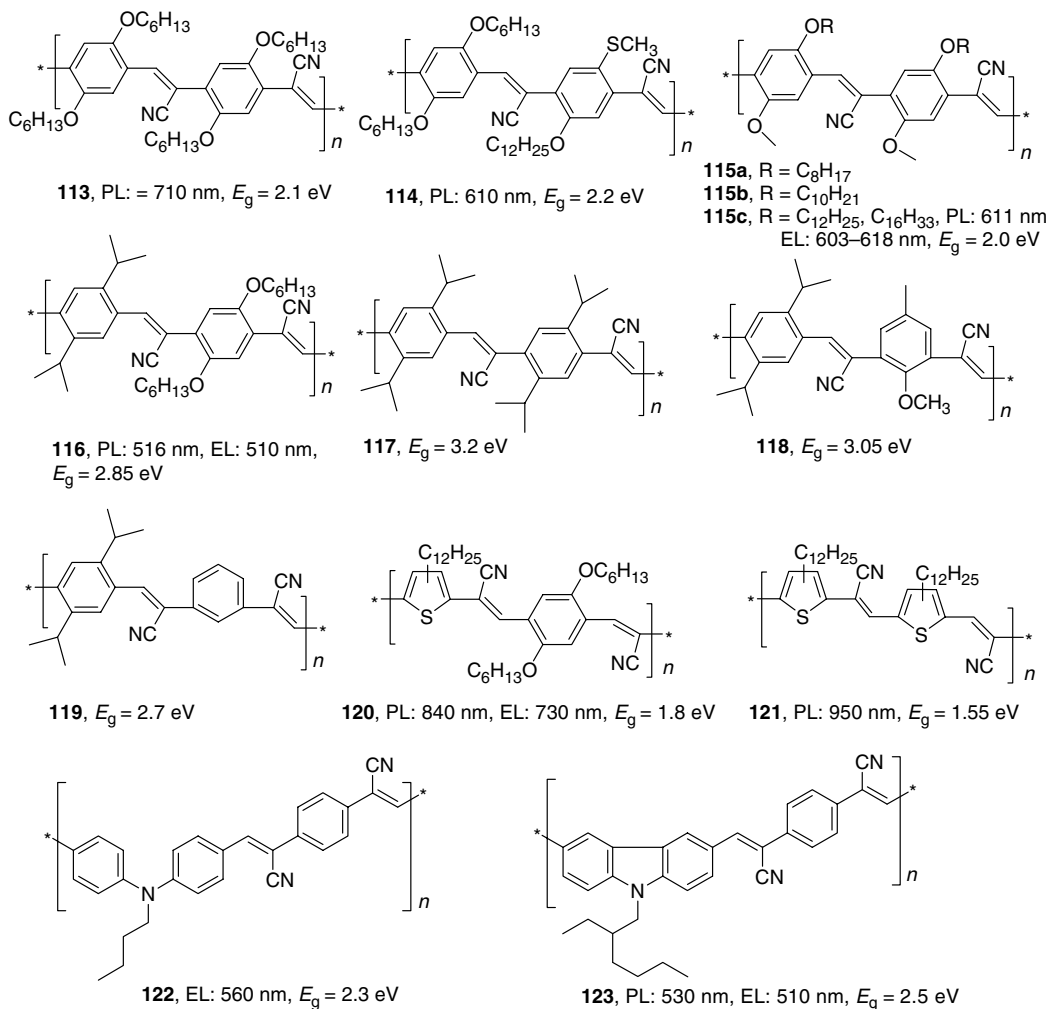
The amino group has also been introduced in the PPV backbone. Copolymers **109** and **110** (and some derivatives incorporating additional phenylene, naphthalene, or anthracene units in the main chain [152]) have been synthesized by Wittig–Horner reaction as green-emitting materials ($\lambda_{\text{PL}} \sim 530$ nm) with moderate PLQY (10–15% in films) [138]. Preliminary results showed improved hole-transport properties in these materials (manifested as a decrease of the turn-on voltage to 2.4–2.8 V, for ITO/PEDOT/**109b**/Ca(Al)), although the efficiency of the unoptimized device was very low (0.001 cd/A). An even lower turn-on voltage of 1.5 V was reported for PLED ITO/**109a**/Al [152]. Some related imino-substituted PPV copolymers with metal chelating azomethine site have been recently synthesized, but their applications as EL materials have not yet been explored [153].

Ma and coworkers [154] synthesized a bipolar luminescent PPV-based polymer **111**, which contained both donor triarylamine and acceptor oxadiazole moieties in the backbone. A device fabricated with this polymer (ITO/PEDOT/**111**/CsF/Al) showed a maximum brightness of 3600 cd/m² and a maximum luminescent efficiency of 0.65 cd/A ($\Phi_{\text{EL}}^{\text{ex}} = 0.3\%$), about 15 times brighter and more efficient than the device of the same configuration with a nonoxadiazole polymer **112**.

2.2.3.2 Poly(*p*-Phenylene Vinylene) Copolymers with Electron-Withdrawing Substituents

The first PPV, bearing a cyano group attached to vinylene fragment (**9**), was synthesized as early as 1960 as unprocessable and insoluble material, which could not be used in PLEDs [43]. Electron acceptor cyano substituents lower the HOMO and LUMO levels of the polymer by ca. 0.6 and 0.9 eV, respectively. In 1993, the Cambridge group reported the first soluble phenylene cyanovinylene (CN-PPV) copolymers (**113**, **114**), synthesized by Knoevenagel condensation polymerization [155]. Actually, the presence of two electron donor alkoxy substituents significantly reduced the electron-accepting effect of the cyano groups. Nevertheless, compared to the most widely used dialkoxy-PPVs, the electron injection (and transport) in **113** and **114** is facilitated, allowing the use of the less-reactive aluminum electrode instead of calcium in PLEDs (both give the same EL QE). On the other hand, the cyano groups reduce the hole-transporting properties of the diode, which had to be adjusted by introducing a second layer of a hole-transporting material (unsubstituted PPV **1**). The double-layer PLEDs ITO/PPV **1**/CN-PPV/Al emitted red (for **113**) or yellow-orange (for **114**) light with rather high (for the time) internal quantum efficiencies of 4 and 2%, respectively. Following this initial report, a series of other CN-PPV derivatives **115** [156] and **116–119** [44] and thiophene analogs **120** and **121** [44] have been synthesized by Knoevenagel polycondensation. This reaction appears to be a convenient way to prepare a number of different substituted PPVs with finely tuned band gap and emission wavelength (Scheme 2.18). Thus PLEDs with blue (**116–119**), red (**113**, **114**), and near-infrared (NIR) (**120**, **121**) emission have been fabricated with these polymers. Remarkably high (as for PPV) band gaps of over ~ 3 eV were achieved for *bis*(*i*-propyl)-substituted copolymers **116–119**, probably due to backbone distortion.

Knoevenagel coupling has also been used to synthesize CN-PPV copolymers with diphenylamino donor unit (**122**, Scheme 2.18) [157]. In spite of a short solubilizing group (butyl), **122** is a very soluble polymer, which is due to rather low molecular weight ($M_n = 5700$). A simple PLED ITO/**122**/Al can be turned on at 4.5 V emitting at $\lambda_{\text{max}}^{\text{EL}} = 560$ nm, but the efficiency of the device was not reported. A related donor–acceptor CN-PPV copolymer **123** was synthesized with essentially higher molecular weight ($M_n = 37,000$) (Scheme 2.18) [158]. The PLED device thereof was fabricated as ITO/**123**/Al, but its efficiency and brightness were not reported in the paper.



SCHEME 2.18 Band gap and emission tuning in cyano-substituted PPVs.

Heck- and Suzuki-coupling polymerization have been used to synthesize CN-PPV copolymers **124** [159] and **125** [160], respectively. As expected, decreasing the number of cyano groups, compared to CN-PPV **113** destabilizes the LUMO orbital increasing the band gap that turned out to be the same for both compounds (**124**: $E_g(\text{optical}) = 2.37$ eV; **125**: $E_g(\text{optical}) = 2.38$ eV, $E_g(\text{electrochemical}) = 2.37$ eV). The solid-state emission maxima are also identical (590 nm). The $\Phi_{\text{EL}}^{\text{ex}} = 0.025\%$ demonstrated by **124** in a simple device ITO/polymer/Al can be increased to 0.062% by applying a second layer of PPV **1** between the ITO and light-emitting layers. For the polymer **125**, a significantly lower EL efficiency was obtained, in spite of a more optimized device structure: the $\Phi_{\text{EL}}^{\text{ex}}$ of ITO/copper phthalocyanine HTL/**125**/Ca/Ag was only 0.011% (and the maximum brightness was 213 cd/m²) (Chart 2.24).

Hanack and coworkers [161] reported related cyano-substituted naphthalene vinylene derivatives **126** and **127**. Interestingly, replacing the phenylene unit in CN-PPV **113** with naphthalene in polymers **126** and **127** results in significant blue shift of the emission maxima from 710 to 595 nm (for **126a**) and 500 nm (for **127**). In addition, the efficiency, tested for double-layer device ITO/**1**/**127**/Mg:Al(3:97), was rather low ($\Phi_{\text{EL}}^{\text{ex}} = 0.017\%$).

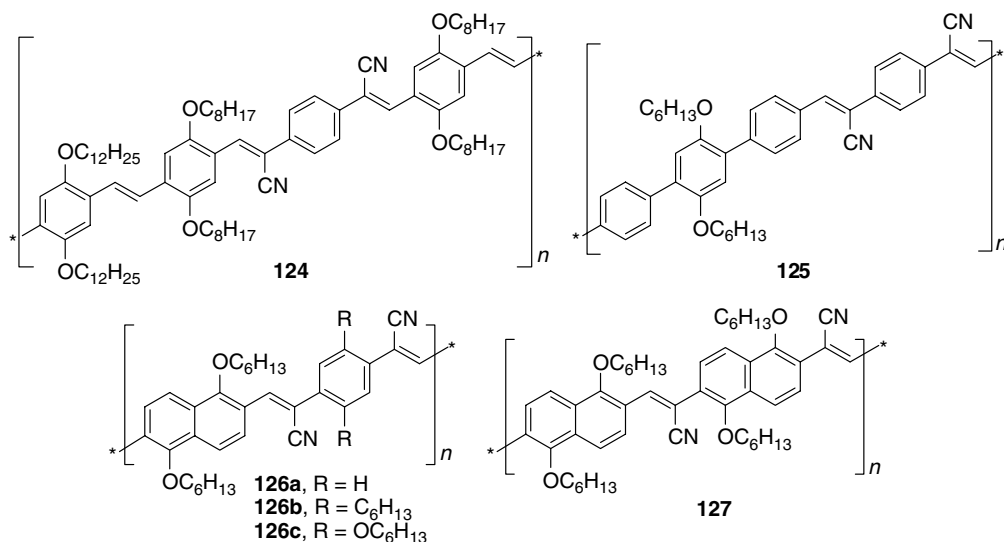
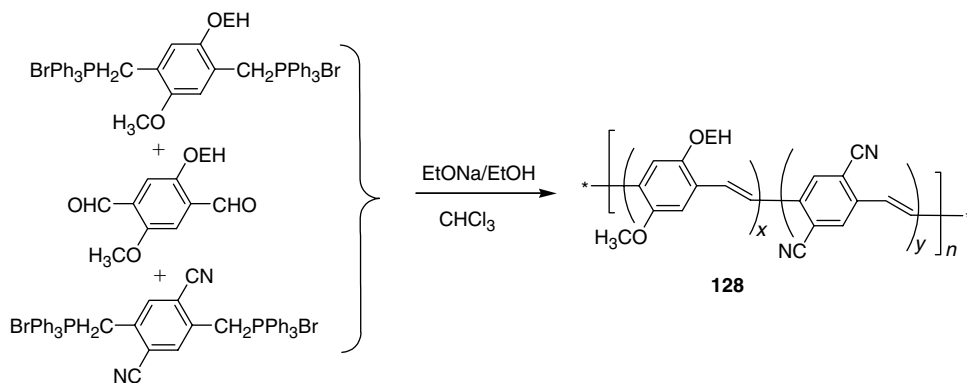


Chart 2.24

Following the CN-PPV series, another electron deficient copolymer **128**, in which the cyano groups are attached to the phenylene units has been synthesized by Huang and coworkers [162,163] (Scheme 2.19). Due to more efficient conjugation of two cyano groups within the phenylene unit, this polymer possesses a higher electron affinity than **113–121**. The copolymers **128** with different ratio of dicyanophenylene vinylene and dialkoxyphenylene vinylene units have been synthesized. Changing the feed ratio of comonomers, the HOMO–LUMO energy levels can be finely adjusted, and the electron affinity of the copolymer having a 1:1 ratio of dialkoxy- and dicyano-phosphonium monomers is higher than that of MEH-PPV by over 0.8 eV (cf. 0.4 eV for same ratio CN-PPV copolymer). A single-layer PLED (ITO/**128**($x=y$)/Al) emits pure red light ($\lambda_{\text{PL}} = 610$ nm), but no characteristics of the device except a low turn-on voltage (4–6 V) were reported [163].

The 2,5-dicyanophenylene unit has also been used by Jen and coworkers [164] in the synthesis of a series of polyfluorene (PF)–PPV copolymers **129–131** through Suzuki-coupling



SCHEME 2.19 Synthesis of dicyanophenylene vinylene copolymers by Wittig condensation.

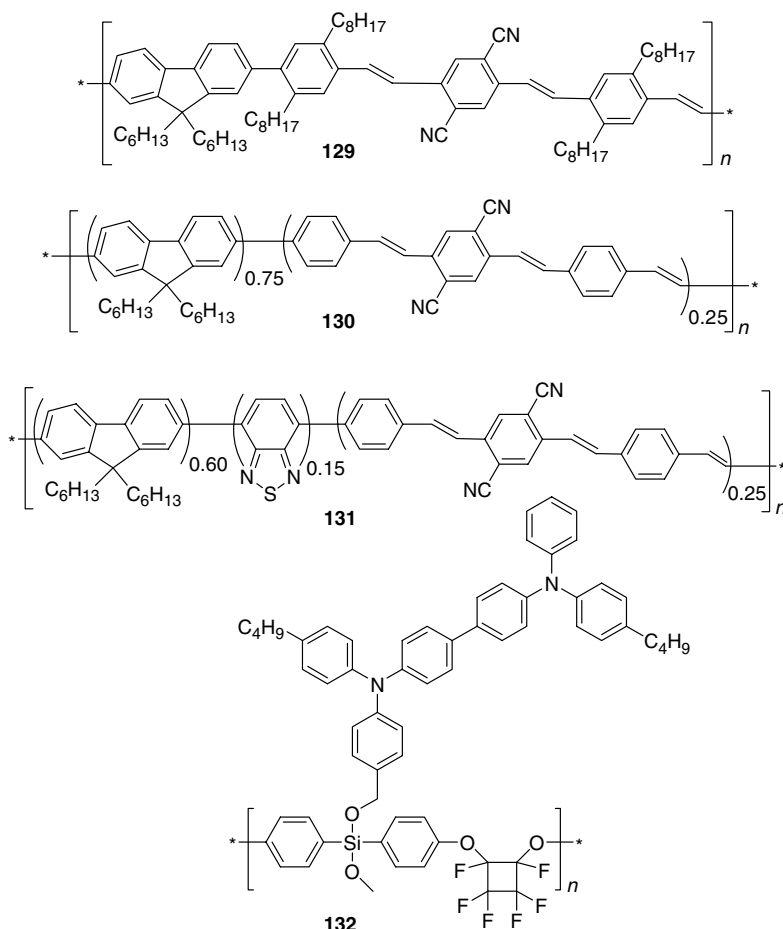


Chart 2.25

reactions. An important, although somewhat discouraging point discovered within this series was an observation of inverse correlation between the electron affinity and the PLQY (17% for **129**, 15% for **130**, and 10% for **131**), i.e., strong electron acceptor moieties tend to quench the PL. Nevertheless, the polymer **129** showed a quite respectable performance in a double-layer device containing a HTL of BTPD-PFCB polymer (**132**): ITO/HTL/**129**/Ca PLED had very low switching voltage (2.6 V), high $\Phi_{\text{EL}}^{\text{ex}} = 0.88\%$, and a brightness of 4730 cd/m² achieved at 1.62 A/cm² (Chart 2.25).

Neumann and coworkers [165] synthesized tetrafluorinated-PPV copolymer **133** and studied its light-emitting properties. However, this material was quite unsuccessful for LED applications: increasing the amount of fluorinated comonomer resulted in a dramatic decrease of the PLQY and the turn-on voltage of the devices was above 30 V (which could only be realized in ac mode due to device shorting). The quenching was less pronounced for an analogous copolymer with MEH-PPV (**134**), which showed an EL efficiency of up to 0.08 cd/A (in ITO/PEDOT/**134**/Ca diode) [166] (Chart 2.26).

As we already mentioned, electron-transporting properties of PPV polymers can be adjusted by introduction of an oxadiazole moiety in the polymer structure. A variety of PPV copolymers

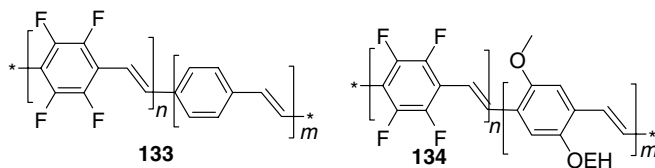


Chart 2.26

containing oxadiazole units as pendant groups have been synthesized. Among the first, in 1998, Bao et al. [135] reported copolymers **135**, containing phenyl (naphthyl)oxadiazole moieties separated from the PPV backbone by an oxymethylene bridge (Chart 2.27). The PL emission of **135** ($\lambda_{\text{PL}} = 580$ nm) is almost unperturbed by the presence of the oxadiazole moiety but the EL efficiency, measured with Al and Ca cathodes, suggests that the electron transport has been significantly improved in these materials, compared to dialkoxy-PPVs (e.g., $\Phi_{\text{EL}}^{\text{ex}} = 0.002\%$ for a related device ITO/**81c**/Al) [135]. In fact, $\Phi_{\text{EL}}^{\text{ex}}$ was higher with an Al cathode (0.02%) than with Ca (0.015%) and, in contrast to dialkoxy-PPV, adding PBD as an additional electron transport material only decreased the device efficiency (0.013%).

A year later, Peng and Zhang [136,167] reported PPV **136**, containing two oxadiazole substituents attached directly to the polymer backbone (to the phenylene unit). Compared to the previous oxadiazole-PPV, $\Phi_{\text{EL}}^{\text{ex}}$ in **136** was further improved to 0.045% (ITO/**136b**/Al) and a maximum brightness reached 1160 cd/m^2 . Even a higher brightness of 3000 cd/m^2 was achieved with polymer **137** (ITO/**137**/Al device) containing oxadiazole in both pendant groups and in the backbone ($\Phi_{\text{EL}}^{\text{ex}}$ was 0.07 and 0.15% for Al and Ca cathodes, respectively) [167].

Lee and coworkers [168] reported an efficient LEP, containing the oxadiazole groups attached to the vinylene units of PPV. Polymer **138** was synthesized by Heck polymerization of dialkoxy-divinylbenzene with an oxadiazole-containing aromatic dibromide. The PL efficiency of **138** ($\lambda_{\text{max}} = 560$ nm) in films was 6.5 times higher than that of MEH-PPV **13** and the energy levels were more favorable for electron transport: **138**, HOMO = -5.30 eV, LUMO = -3.10 eV; cf. MEH-PPV **13**, HOMO = -4.98 eV, LUMO = -2.89 eV (all determined electrochemically). The PLED device ITO/PEDOT/**138**/Al showed relatively high $\Phi_{\text{EL}}^{\text{ex}}$ of 0.34%, with a maximum brightness of 1450 cd/m^2 (at 13 V). Again, changing the Al electrode for Ca resulted in only a small increase of the QE (0.43%), suggesting that the charge-transport properties of **138** are relatively well-balanced (Chart 2.27).

Several groups introduced an oxadiazole moiety as a part of the PPV backbone (polymers **139a** [169,170], **139b** [171], **140** [172], **141** [169], and **142** [170]). Not unexpected, the oxadiazole moieties lowered the LUMO energy of these polymers (as demonstrated by CV measurements). The decreased electron injection barrier is manifested by lowered turn-on voltage (6 V for ITO/**139b**/Al) [171]. However, relatively low efficiency (0.15% for **139b** [171]) was reported for these copolymers (Chart 2.28).

Burn and coworkers [173] synthesized copolymer **143**, containing a similar electron deficient moiety (triazole) incorporated in the PPV backbone. They have reported an efficient blue emission from this polymer ($\lambda_{\text{PL}} = 466$ nm (solution), 486 nm (film), $\Phi_{\text{PL}} = 33\%$ (film)) although the efficiency of the PLED fabricated as ITO/PPV/**143**/Al was not very high ($\Phi_{\text{EL}}^{\text{ex}}$ reached 0.08% at a luminance of 250 cd/m^2).

Most recently, Jenekhe and coworkers [174] synthesized PPV copolymers with quinoxaline as pendants **144** and **145**, as well as a part of the chain (not shown here). These polymers showed reductions with onsets of -1.70 and -1.75 V vs. saturated calomel electrode (SCE),

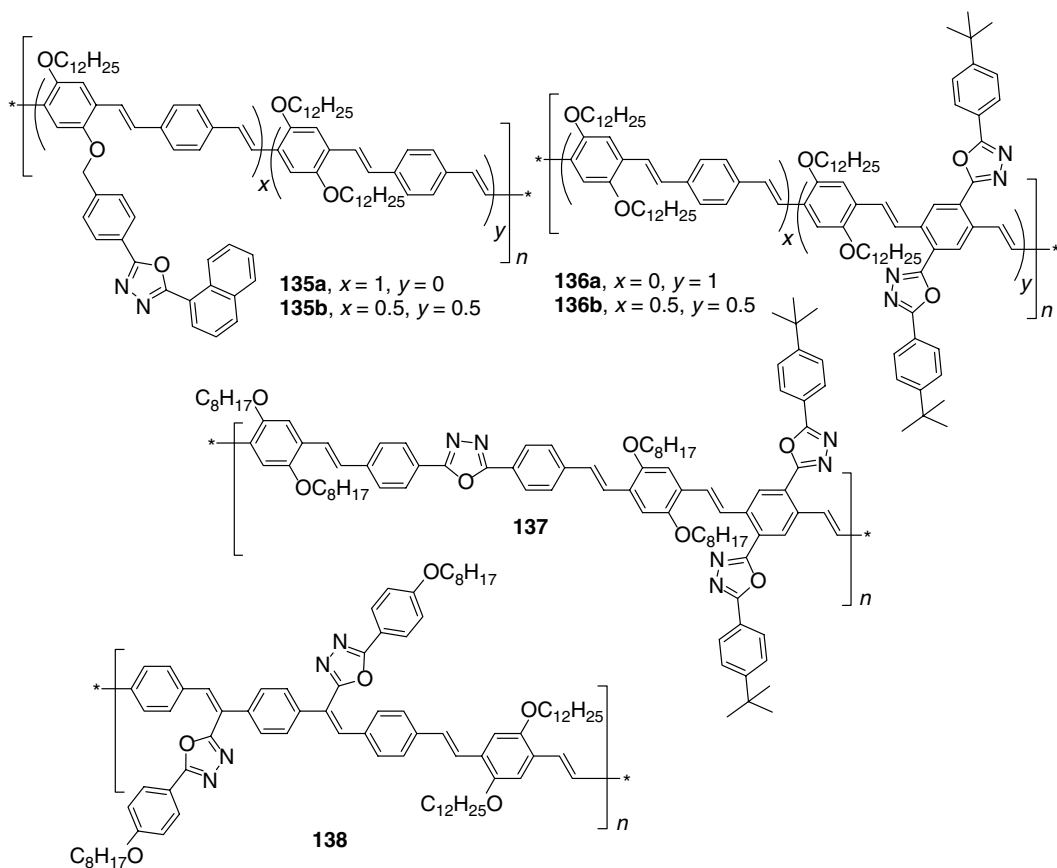


Chart 2.27

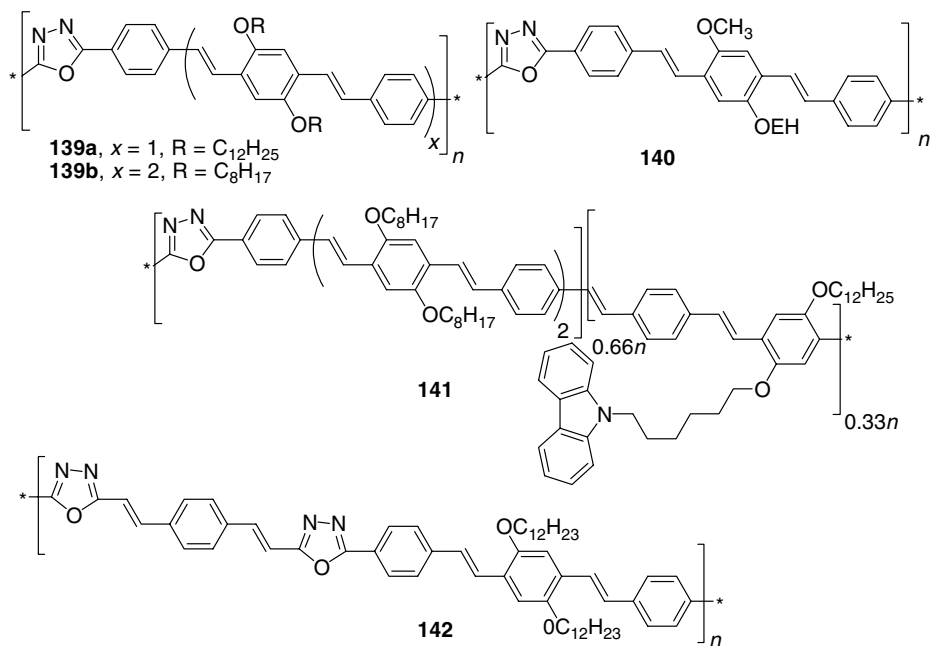


Chart 2.28

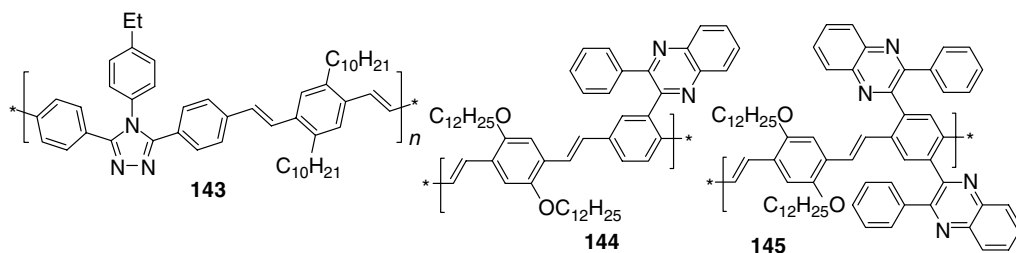


Chart 2.29

respectively ($E_A = 2.70$ and 2.65 eV) and greenish-yellow (**144**, $\lambda_{PL} = 563$ nm) or blue-green (**145**, $\lambda_{PL} = 470$ nm) fluorescence in films. An ITO/PEDOT/**144**/Al diode emitted yellow light ($\lambda_{EL} = 550$ nm) with a quite low maximum brightness of 35 cd/m^2 at 12 V (Chart 2.29).

Yu and Chen [175] studied copolymer **146**, incorporating a triphenyltriazole moiety as a pendant group (Chart 2.30). Increasing the proportion of electron-deficient triazole moieties ($n:m$) improved the electron transport properties of the material, as demonstrated by an increase of the EL efficiency from 0.2 cd/A (for $n:m=0:1$, MEH-PPV) to 3.1 cd/A (for $n:m=4:1$), for the ITO/PEDOT/polymer/Al device configuration. At the same time, for the devices ITO/PEDOT/polymer/Ca, where the electron transport is already improved by using a low work-function electrode, the device efficiency stayed at the level of $1\text{--}2 \text{ cd/A}$ for the whole range of polymer compositions ($n:m$). A very high brightness of $17,000\text{--}19,000 \text{ cd/m}^2$ was observed for these devices.

By analogy with Kodak's low molecular dyes, Kim and Lee [176] introduced an electron acceptor dicyanomethylenepyran moiety into the PPV copolymer chain. The PPV copolymer **147**, synthesized by Heck-coupling polymerization, revealed strong, pure red color emission (λ_{max} : 646 nm ; CIE: $x=0.67$, $y=0.33$). The downshifted orbital levels of **147** (HOMO: -5.44 eV , LUMO: -3.48 eV) compared with MEH-PPV **13** (HOMO: -4.98 eV , LUMO: -2.89 eV) resulted in more balanced hole–electron injection and the single-layer PLED fabricated as ITO/**147**/Al showed eight times higher EL efficiency than the PLED fabricated with MEH-PPV.

Porphyrine chromophore units have also been introduced to the PPV backbone but the PLQY of such materials decreased rapidly with increasing ratio of the porphyrine units and no EL devices have been reported [177,178].

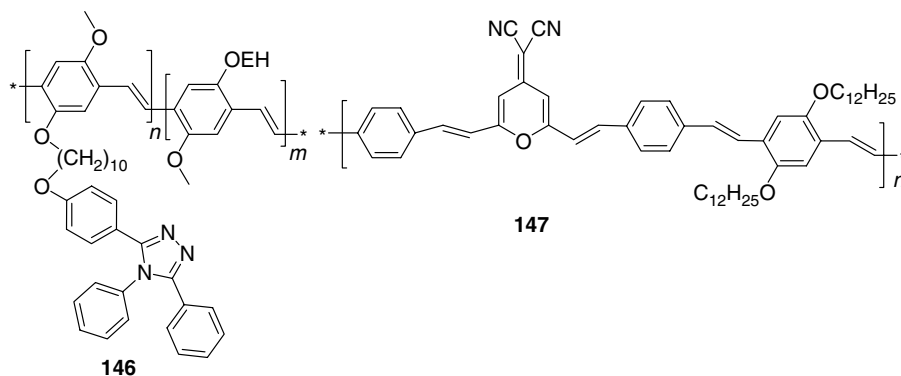


Chart 2.30

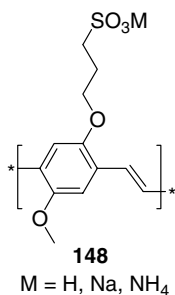


Chart 2.31

2.2.4 POLY(*p*-PHENYLENE VINYLENE) POLYELECTROLYTES

For developing a cost-effective and environment-friendly fabrication process as well as for possible applications in biological systems, it is desirable to have water-processible LEPs. In this line, Shi and Wudl [179] synthesized water-soluble PPV **148**, containing ionic sulfonate groups, isolated from the PPV backbone by an alkyl chain (Chart 2.31). This material appeared to be highly fluorescent with λ_{PL} in the range of 550–600 nm, depending on the solid-state structure (engineered by self-assembly of the anionic PPV **148** multilayers separated by counterion layers) [180]. A water solution of **148** (M = Na) was used together with a cationic LEP (**479**, see below) for a hybrid ink-jet printing of dual-color (blue and red) light-emitting pixels [181]. Taking advantage of good compatibility of polymer **148** with aqueous media and the known quenching amplification in conjugated polymers, highly efficient fluorescent biological sensors have been designed with this material [182]. Unfortunately, LEC devices with **148** have not been reported.

Anderson and coworkers [183–185] reported water-soluble polyrotaxanes **149** and **150**, containing sulfonated PPV chains surrounded by mechanically bound α - and β -cyclodextrin macrocycles (Chart 2.32). The cyclodextrin rings play the role of a “wire insulator,” preventing aggregation and interchain quenching. The effect was demonstrated by atomic force

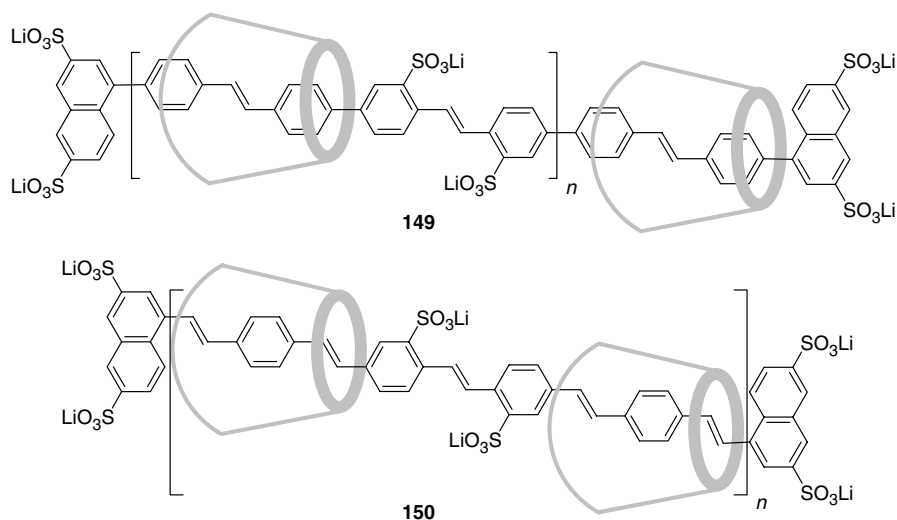


Chart 2.32

microscopy (AFM), which showed individual polymer chains for cyclodextrin-encapsulated polymer but not for the noncomplexed material. The PL (for **150** [185]) and EL efficiency (for **149** [183]) of the complexed material was $\sim 3\text{--}4$ times higher than that for noncomplexed polymer. However, the absolute value of $\Phi_{\text{EL}}^{\text{ex}} \sim 0.025\%$ was very low for practical application, which was not only due to unoptimized device structure (ITO/**149**/Ca), but also due to generally low PLQY of the polymer containing a sulfonate group directly attached to the backbone.

2.2.5 CONTROLLING THE CONJUGATION IN POLY(*p*-PHENYLENE VINYLENE) POLYMERS

So far, we have demonstrated that PPV derivatives are among the most popular materials for PLED and different color emission can be achieved by substitution but, with few exceptions [104,143], blue color is not available for fully conjugated PPV. Furthermore, a rigid-rod structure of the highly conjugated chain results in high crystallinity of many PPV materials, which is held responsible for the decrease of the PL efficiency in the solid state and pinhole defects in thin films. The following two sections present current approaches to the solution of this problem via control of the conjugation length in PPV materials.

2.2.5.1 Formally Conjugated Systems with Twists, *Meta*-Links, and *sp*-Hybridized Atoms in the Backbone

Intramolecular π -stacking can be effectively prevented by introducing a twist structure in the backbone of PPV that also reduces the conjugation along the chain and is expected to result in hypsochromic shift of the emission. This kind of twist was achieved by copolymerization with binaphthyl or biphenyl units (**151** [186] and **152** [187]). A twisted binaphthyl copolymer **151**-based PLED (fabricated with ITO and Al electrodes) exhibited blue-green light emission with $\Phi_{\text{EL}}^{\text{ex}}$ of 0.1% and a moderate driving voltage of 6 V. Similar results were found for biphenyl copolymer **152**. The PLEDs fabricated as ITO/PEDOT/**152**/Ca/Al emit green-blue light ($\lambda_{\text{max}}^{\text{EL}}$ of 485–510 nm, depending on substituent pattern) with $\Phi_{\text{EL}}^{\text{ex}} = 0.17\%$. The authors explained the lower QE of the copolymers to be due to increased nonradiative relaxation resulting from interruption of the conjugation by the twisted units. Importantly, in both cases, due to interrupted conjugation, the emission band undergoes a significant hypsochromic shift (Chart 2.33).

In fact, blue-emitting PPV materials are the subjects of significant research interest, as blue EL is the key for creating either white or full color EL displays. However, this is generally unavailable for conjugated PPVs due to relatively low band gap. Consequently, several strategies to decrease the effective conjugation length have been studied in search of blue-emitting PPVs. This can be achieved by introducing either nonconjugated blocks or sp^3 “defects” into the PPV chain (see conjugated and nonconjugated copolymers below) or changing the attachment mode of the phenylene unit in the chain. The synthesis of substituted poly(*m*-phenylene vinylene) and poly(*o*-phenylene vinylene) homopolymers were reported in

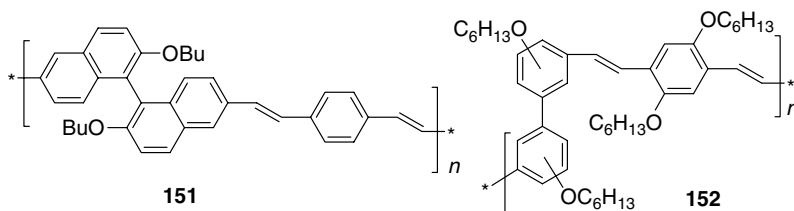


Chart 2.33

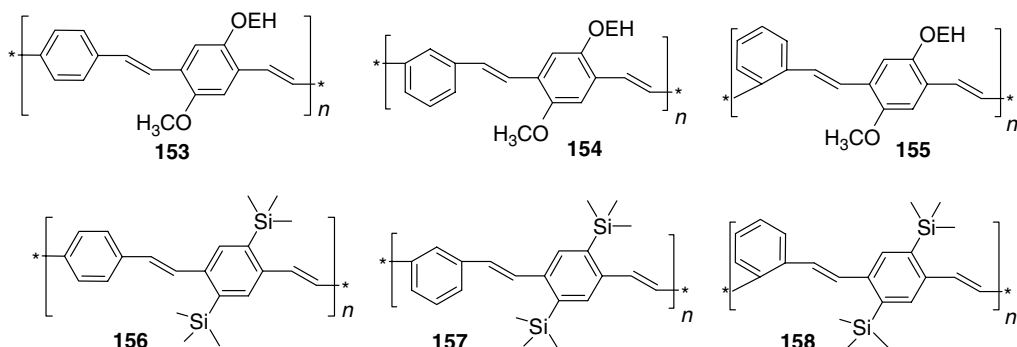


Chart 2.34

1993 by Leung and Chik [92], although with no connection to control the luminescent properties of the polymer. In 1999, Shim and coworkers [188] synthesized and studied a series of dialkoxy- and *bis*(trimethylsilyl)-substituted PPV copolymers with *o*-, *m*-, and *p*-phenylene linkages (**153–158**) (Chart 2.34). The *m*-phenylene unit does not allow for direct conjugation, resulting in a hypsochromic shift of both absorption and emission bands. The *ortho*-linking is formally conjugated but due to steric hindrance, the polymer chain has an effectively decreased conjugation length. Combining these structural changes with substituent variations, fine-tuning of the EL wavelength was achieved (Figure 2.5).

Almost simultaneously to the above report, Pang et al. [189] reported another PPV copolymer **159a** containing alternating *p*-phenylene and *m*-phenylene units, also synthesized via Wittig–Horner coupling (Chart 2.35). As expected, **159a** exhibits strong hypsochromic luminescence shift. In solution, the polymer emits blue light with $\lambda_{\text{max}}^{\text{PL}}$ of 444 and 475 nm and 60% PLQY, the latter is improved to 82% for the material containing *cis* defects (these are naturally produced in the synthesis, but can be converted to *trans* configuration by refluxing in toluene). However, strong aggregation in the solid state resulted in an emission maxima shift to 480 and 530 nm (shoulder). In spite of high PL efficiency, $\Phi_{\text{EL}}^{\text{ex}}$ of a PLED with **159a** was only 0.05% that still was an order of magnitude higher than that of a device with the parent PPV **1**, prepared under the same conditions.

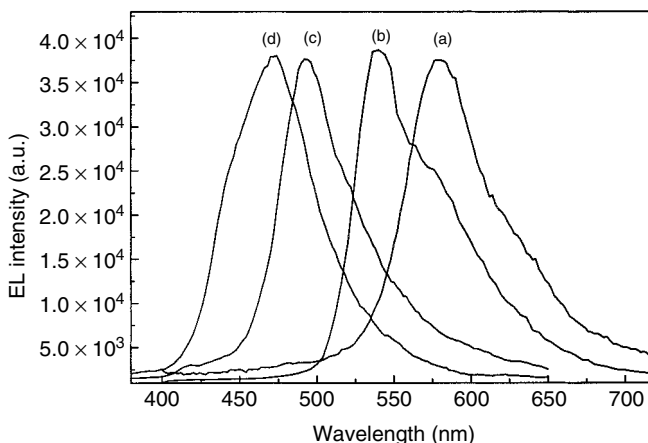


FIGURE 2.5 Tuning the electroluminescence in PPV copolymers through introducing nonconjugated kinks: (a) MEH-PPV **13**, (b) **153**, (c) **156**, and (d) **158**. (From Ahn, T., Jang, M.S., Shim, H.-K., Hwang, D.-H., and Zyung, T., *Macromolecules*, 32, 3279, 1999. With permission.)

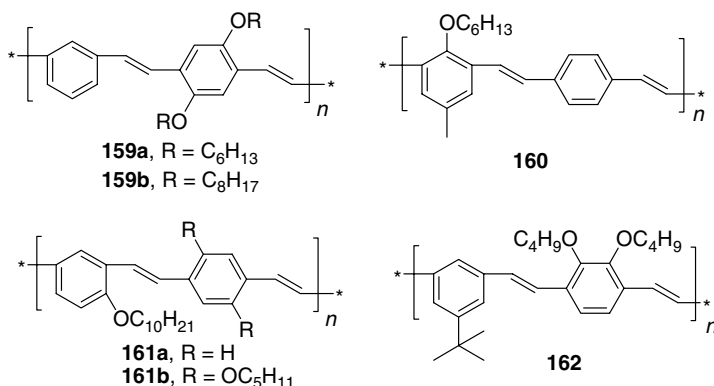


Chart 2.35

Other structural variations included copolymers **159a,b** [190], **160** [191], **161a,b** [192], and **162** [190]. Low switch-on voltage (4.3 V) and moderately high brightness (1000 cd/m²) were achieved for **161** [192], but the purity of blue color was still a problem. Even for the “most blue” copolymer **162**, the CIE coordinates ($x=0.188$, $y=0.181$) are still quite far from the pure blue emission ($x=0.15$, $y=0.06$) due to a green tail [190].

Several groups have studied introduction of phenylene ethynylene units into PPV backbones. The first material of this type, copolymer **163**, was reported by Bunz and coworkers [193] (Chart 2.36). The material displayed blue luminescence in solution ($\lambda_{\text{max}}^{\text{PL}} = 460$ nm), but due to the polymer's rigid-rod structure, very strong aggregation in the solid state gave rise to

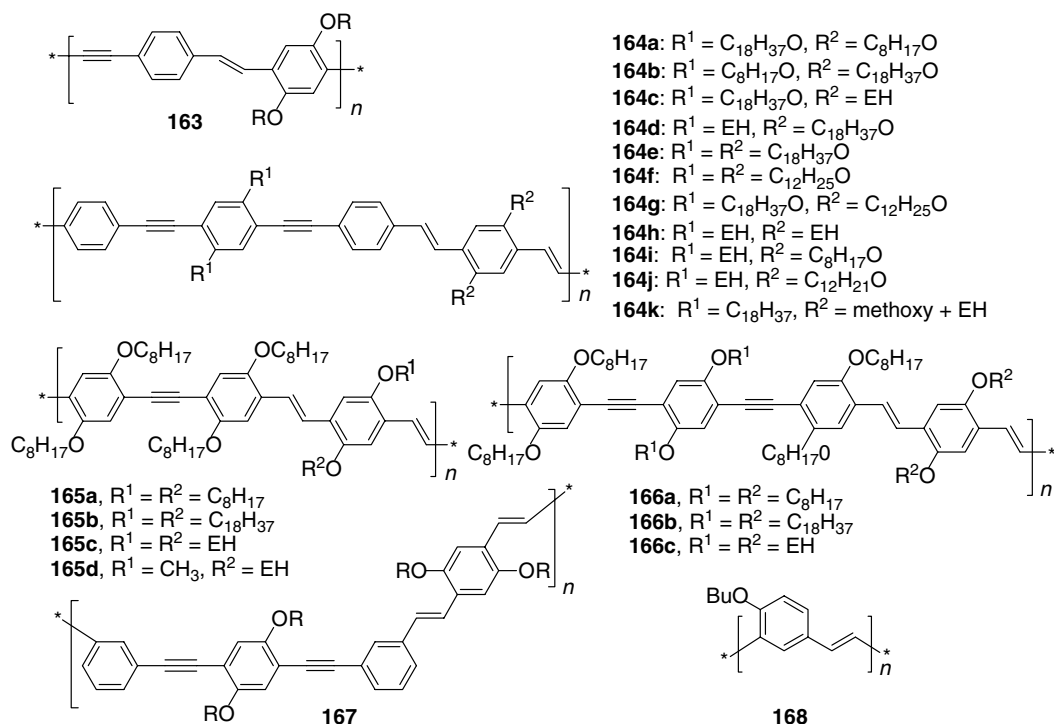


Chart 2.36

bathochromic shifts and the PLQY in films was only 5%. A series of alkyl- and alkoxy-substituted poly(phenylene vinylene/ethynylene) hybrids **164–166** have been recently reported by Egbe and coworkers [194–196]. Whereas all alkoxy-substituted polymers **164a–g** showed similar PL emission (λ_{PL} from 525 to 554 nm), the performance of the green-emitting PLEDs thereof (ITO/PEDOT/**164**/Ca; $\lambda_{\text{max}}^{\text{EL}}$ from 508 to 554 nm) strongly depended on the alkoxy substituents R^1 and R^2 in the copolymers. A large substituent effect was observed in polymers **164a–g** that showed $\Phi_{\text{EL}}^{\text{ex}}$ from 0.02% to 0.047% (0.085–0.20 cd/A; **164a–c,f**) to 0.89–0.95% (3.5–4.0 cd/A; **164d,e**) [195].

Comparisons between **165** and **166** series ($\lambda_{\text{abs}} \sim 468\text{--}475$ nm, $\lambda_{\text{PL}} \sim 519\text{--}528$ nm) showed that the conjugation pattern has very little effect on photophysical properties of these polymers in solution (blue shift in absorption and PL by only 4–7 nm from **165** to **166**). However, the performance of their PLED (ITO/PEDOT/polymer/Ca) differed drastically; cf. a brightness of 27.9 cd/m² and an external QE of 0.017% for **166b** and a brightness of 595–5760 cd/m² and an external QE of 0.22–2.15% for **165a–d** (the maximum values are for **165b**) [196]. Pang and coworkers [197] reported that a related polymer **167** possesses *m*-phenylene linking groups, which might reduce the aggregation effect (although this was not investigated). The PLED device ITO/PEDOT/**167**/Ca was reported to emit green light with $\Phi_{\text{EL}}^{\text{ex}} = 0.32\%$.

Very recently, Liang et al. [198] reported the first poly(*m*-phenylene vinylene) homopolymer **168**. Due to all-*meta*-linking of the phenylene units, the PL maxima (417 nm with a shoulder at 434 nm) of **168** is further shifted in the blue region and the emission band is very narrow, which promises to deliver a pure blue-emitting PLED (although a device fabrication was not yet reported).

2.2.5.2 Conjugated and Nonconjugated Poly(*p*-Phenylene Vinylene) Block Copolymers

Soon after the first demonstration of the EL of PPV **1** [1], it was shown that introducing saturated (nonconjugated) defects into PPV chains results in an emission blue shift and improves the film quality [23,25]. This could be achieved via modified Wessling–Zimmerman thermoconversion of a precursor polymer containing different (tetrahydrothiophene and methoxy) leaving groups, which can be selectively eliminated to give conjugated and non-conjugated (uneliminated) fragments (**169**) (Chart 2.37) [23,134,199]. A similar effect was obtained by controlled conversion of PPV precursor having ethylxanthate-leaving group (**170**) [25]. For the latter, the ethylxanthate group also favored the formation of *cis*-vinylene defects, preventing the intermolecular stacking effect (Figure 2.6). Due to very negligible crystallinity and good film-forming properties, the polymers **169** and **170** showed significantly

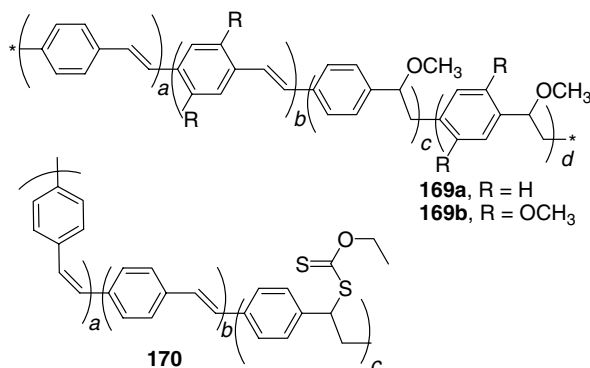


Chart 2.37

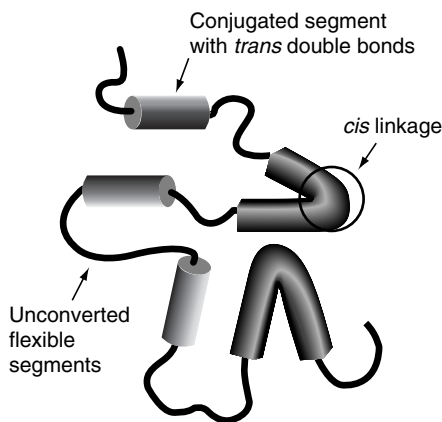


FIGURE 2.6 The schematic structure of rigid and flexible block PPV containing saturated (unconverted) units and *m*-vinylene links. (From Son, S., Dodabalapur, A., Lovinger, A.J., and Galvin, M.E., *Science*, 269, 376, 1995. With permission.)

improved EL efficiency ($\Phi_{\text{EL}}^{\text{ex}} = 0.44\%$) was demonstrated for the device ITO/**170**/PBD/Al [23,25]. Introduction of nonconjugated fragments (by partial substitution of the tetrahydrothiophenium-leaving group in the PPV precursor **2** with acetoxy group) was also demonstrated to increase the operation lifetime of the PLED (above 7000 h without noticeable degradation) [200].

However, due to random distribution of the conjugation length in these polymers, the emitted light was still essentially green. In 1993, Karasz and coworkers [201] developed the idea of preparing a PPV copolymer containing well-defined blocks of rigid conjugated oligo(phenylene vinylene) and flexible nonconjugated aliphatic units. Copolymer **171a**, synthesized by Wittig–Horner condensation, contained 2.5 phenylene vinylene fragments in each conjugated block and showed PL (and EL) maxima at ~ 465 nm (Chart 2.38). This low wavelength emission is achieved exclusively due to very short conjugation length, and increasing the latter by only one more phenylene vinylene unit (**171b** [202] and **171c** [189]) shifts the emission to $\lambda_{\text{max}} = 513$ nm, so that the PLED ITO/**171b**/Al emits green light with CIE coordinates ($x = 0.29$, $y = 0.47$) [202]. Sun et al. [203] have reported a dimethoxy-substituted analog **172**. The alkoxy substituents in the conjugated block result in a red shift of the emission maxima (vibronic band with peaks at ~ 500 , 540, and 590 nm (shoulder)), but remarkably, the PLQY in the solid state was as high as 90%. Several other block copolymers of this type (**173a–c**) having shorter nonconjugated block and different substituents in the phenylene vinylene unit have been synthesized [204]. The trimethylsilyl-substituted polymer **173a** showed the most blue PL (and EL) ($\lambda_{\text{max}}^{\text{PL}}$ 467, 490 nm), whereas alkoxy substituents result in bathochromic shift of the emission band.

The solubility of such PPV copolymers in both polar and nonpolar media can be dramatically improved when using the oligo(ethylene oxide) flexible block (copolymer **174**), which also allows application in LEC. The first compound of this series copolymer **174c** was synthesized by Sandman and coworkers [205] using low polydispersity PEG block (PEG-900), but no high-performance PLED could be fabricated with this material. Later, Feast and coworkers [206] reported the synthesis of copolymer **174b** as a bluish-green emitter with $\lambda_{\text{max}}^{\text{EL}}$ at 490 and 525 nm and moderately high PLQY (34%). The PLED ITO/**174b**/Al can be turned on at 6.5 V and shows a luminescence efficiency of 0.5 cd/A, and the maximum brightness of 2000 cd/m² [206]. Furthermore, the LEC design [63] (blending with LiOTf electrolyte) allows

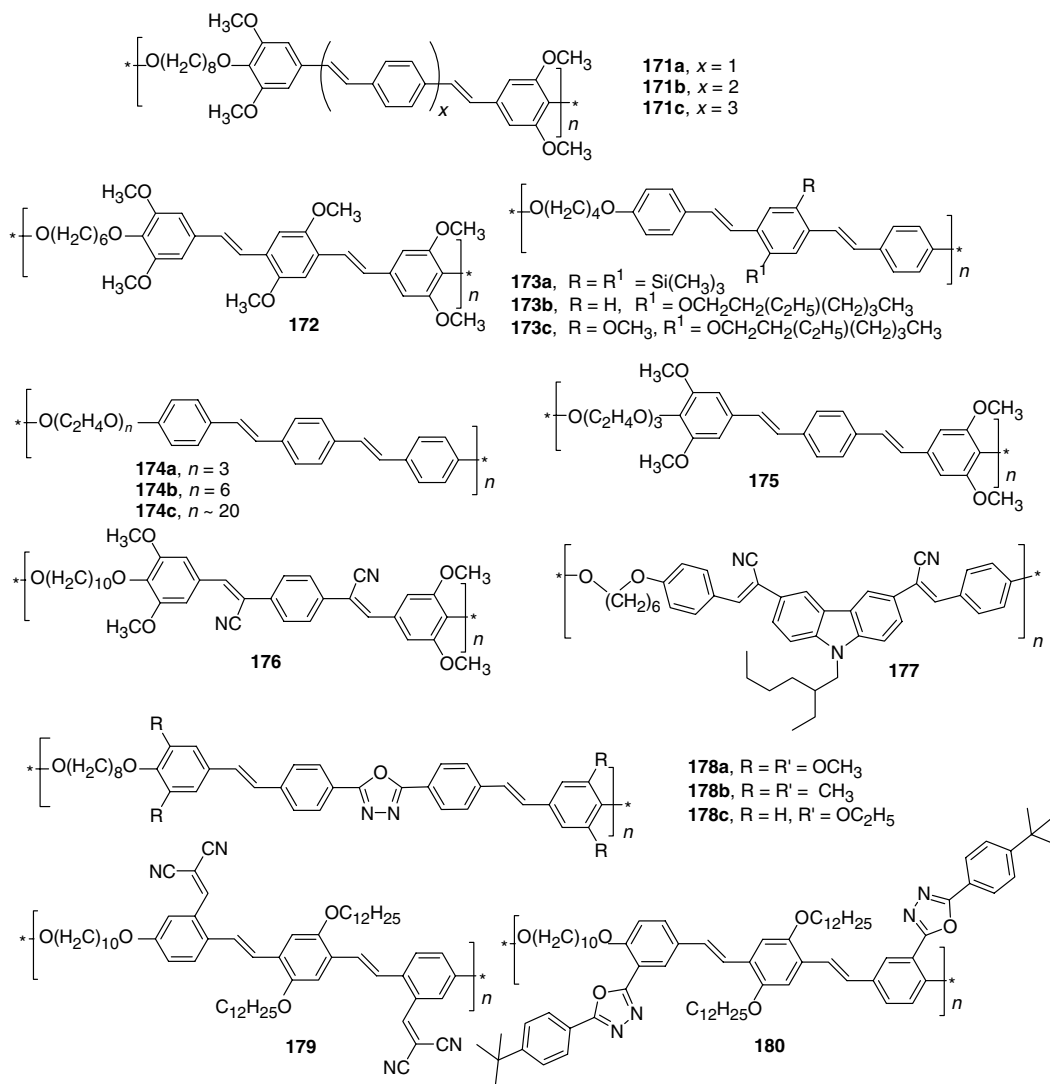


Chart 2.38

a decrease of the turn-on voltage to 3.8 V. A more pure blue color with a single emission peak at 490 nm has been reported with a similar compound **174a** having shorter nonconjugated block. The PLED turn-on voltage achieved with **174a** is lower (4.6 V) due to more complex device structure (ITO/PEDOT/**174a**/Alq3/Ca), but the device efficiency and brightness were very similar [207]. Alkoxy substituents have been introduced in this polymer structure, but the resulting copolymer **175** showed no improvement in the EL properties ($\lambda_{\text{EL}} = 475$ nm, maximum brightness of 36 cd/m² at 23 V) [208].

Introducing two cyano groups into the conjugated block (copolymer **176** [209] and **177** [158]) slightly alters the emission color ($\lambda_{\text{max}}^{\text{EL}} = 493$ nm for **176** and 518 nm for **177**), but also significantly improves the electron transport properties of the polymer. Nevertheless, even the double-layer (ITO/**176**/Al) PLEDs showed a modest luminescence efficiency of 0.17 cd/A and a maximum brightness of only 40 cd/m² [158]. Significantly higher brightness (2400 cd/m²) and $\Phi_{\text{EL}}^{\text{ex}} = 0.1\%$ were achieved for PPV block copolymer **178** containing an

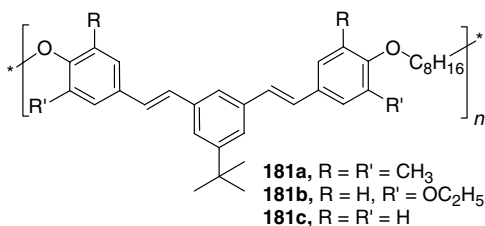


Chart 2.39

electron acceptor oxadiazole moiety in the backbone, although extending the conjugation through the oxadiazole moiety also resulted in some red shift of the emission maxima ($\lambda_{\text{max}}^{\text{EL}} = 480\text{--}509$ nm, depending on R) [210].

Electron acceptor dicyanovinyl and oxadiazole substituents have been recently introduced into phenylene units of the PPV block copolymers (**179**, **180**) [211]. Blue and blue-greenish PL emission was observed for **179** and **180**, respectively, but the PLQY was relatively low even in solution (13 and 24%) and no EL device has yet been reported.

Lahti and coworkers [212] reported a series of *meta*-linked oligo(phenylene vinylene) block copolymers **181a–c**. A *meta*-linked phenylene unit imposed an additional hypsochromic shift on the emission of these segmented polymers. The PL maxima were found at 399–416 nm, but a significant (ca. 70 nm) red shift was observed for EL spectra (ITO/polymer/Ca/Al) (Chart 2.39).

At Kodak, researchers used a rigid adamantane moiety to separate the luminescent oligo(phenylene vinylene) blocks (copolymers **182**, **183**) [213]. The EL color can be tuned from blue ($\lambda_{\text{EL}} = 470$ nm) to green ($\lambda_{\text{EL}} = 516$ nm) by replacing a phenylene unit in **182** for 2,7-naphthylene (**183**). A very low turn-on voltage of 5.5 V (as for this class of materials) was achieved in the device ITO/**182**/Mg:Ag, but no EL efficiency was reported (Chart 2.40).

Karasz and coworkers [214] have also synthesized a series of block copolymers **184–187**, having an *m*-xylenedioxy bridge as a flexible unit and studied their optical and electrochemical properties. By changing the substituents in the central ring of the phenylene vinylene block (polymers **184a–e**) or altering the conjugation by changing the aromatic unit in **185–187**, the emission band can be tuned between $\lambda_{\text{max}}^{\text{PL}}$ of 413 and 533 nm (Scheme 2.20, Figure 2.7). Breaking the conjugation in the oligo(phenylene vinylene) block by changing the substitution position (1,4-phenylene \rightarrow 1,2-phenylene \rightarrow 1,3-phenylene \rightarrow 9,10-anthracene

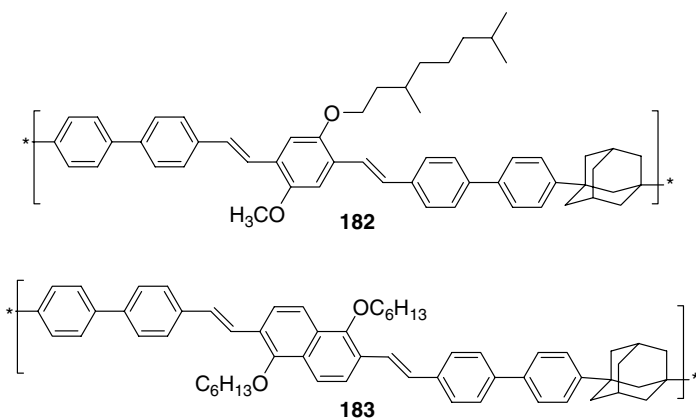
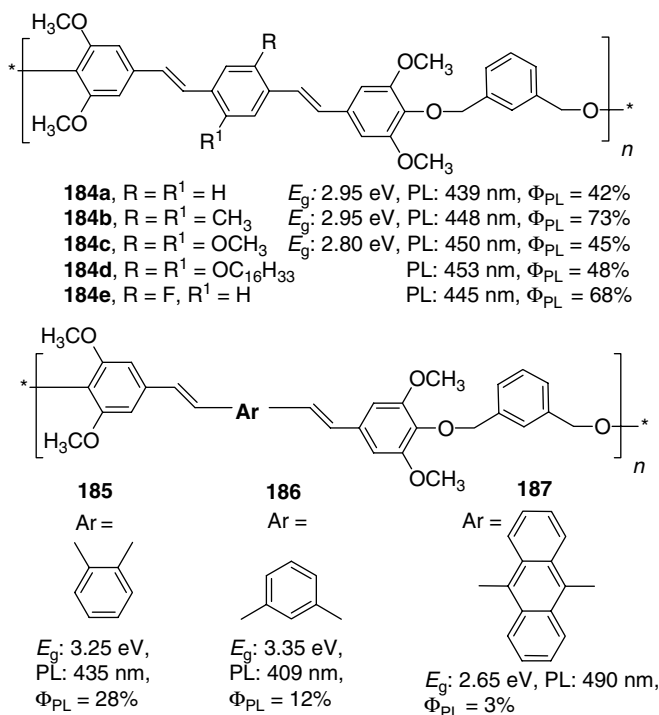


Chart 2.40



SCHEME 2.20 Tuning the band gap and the emission wavelength in PPV block copolymers **184–187** (in chloroform solution).

units) progressively increases the band gap of the polymer, and hypsochromically shifts the emission band (the longest wavelength absorption and emission peaks of **187** are due to isolated anthracene unit; based on the second phenylene vinylene absorption band, its

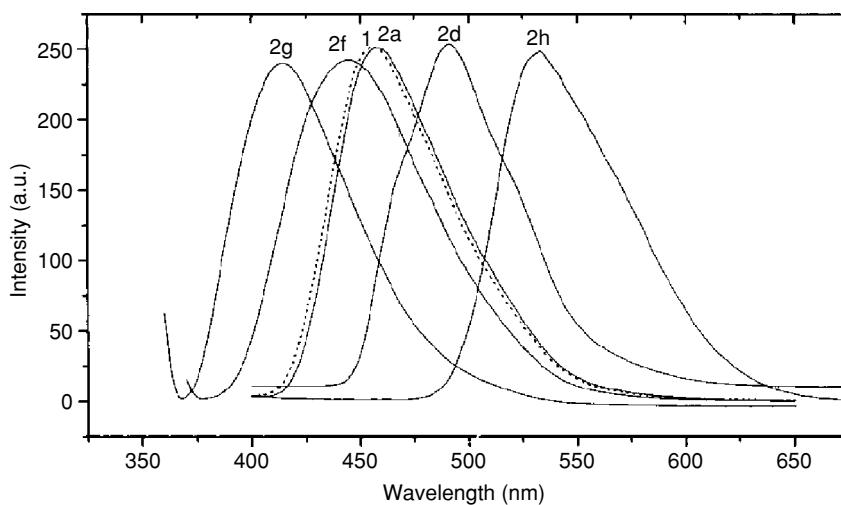


FIGURE 2.7 Tuning the solid state emission maxima in PPV block copolymers **184–187**: (1) **171**, (2a) **184a**, (2d) **184d**, (2f) **185**, (2g) **186**, and (2h) **187**. (From Zheng, M., Sarker, A.M., Gürel, E.E., Lahti, P.M., and Karasz, F.E., *Macromolecules*, 33, 7426, 2000. With permission.)

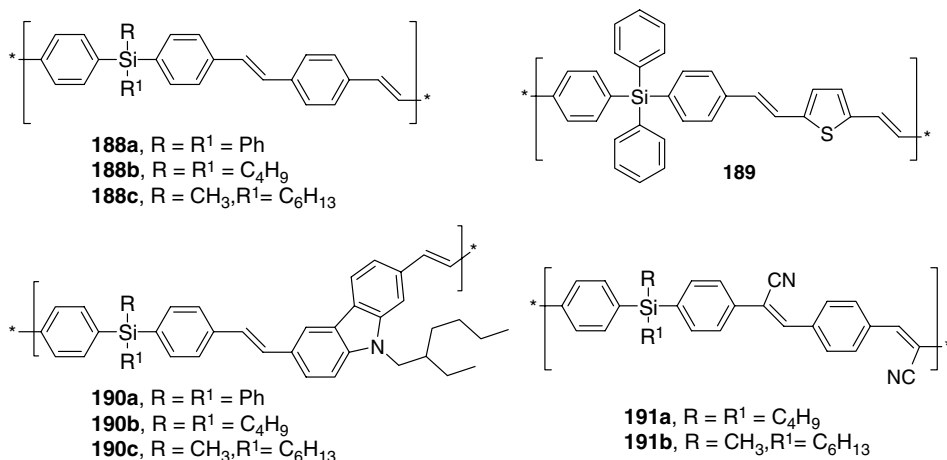


Chart 2.41

$E_g = 3.6$ eV). However, PL efficiencies of compounds **185–187** also drop down very significantly (Scheme 2.20), and no EL devices have been reported for this series.

Kim et al. have introduced silicon atoms in PPV block copolymers to confine the conjugation length and achieve blue EL materials. Copolymers **188–190** [215] and **191** [216] have been synthesized by Wittig–Horner and Knoevenagel condensation, respectively. The emission band in this series can be tuned between 410 and 520 nm, and ITO/polymer/Al PLEDs with turn-on voltages ~ 7 V have been reported (Chart 2.41).

Monodisperse analogs of such π -electron systems, PPV oligomers (molecular glasses) were studied by Bazan and coworkers [217]. The films prepared from **192** by solution casting showed completely amorphous structure due to a tetrahedral structure of the molecule and OLEDs ITO/PVK/**192**/Al-emitted green light with an efficiency up to 0.22 cd/A (Chart 2.42).

As we discussed above, nonconjugated blocks in PPV copolymers generally improve the film homogeneity. Furthermore, by changing the properties of the nonconjugated blocks, one can engineer the topology of the films. Introducing highly polar amide groups into nonconjugated blocks, Zhang et al. [218] prepared water-soluble copolymer **193** ($\lambda_{\text{max}}^{\text{PL}} = 509$ nm), which achieves nanophase separation of conjugated and nonconjugated domains in spin-coated films.

2.2.5.3 Nonconjugated Polymer Containing Oligo(Phenylene Vinylene) Pendant Substituents

The conjugation length and the emission color of PPV-type materials can be also controlled by using short oligo(phenylene vinylene) units as pendant substituents in nonconjugated polymer chain. The advantage of such an approach is the possibility to use well-established

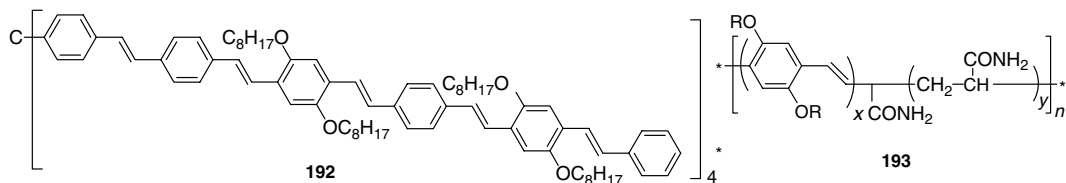


Chart 2.42

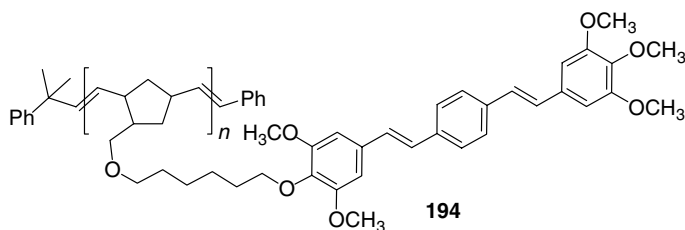
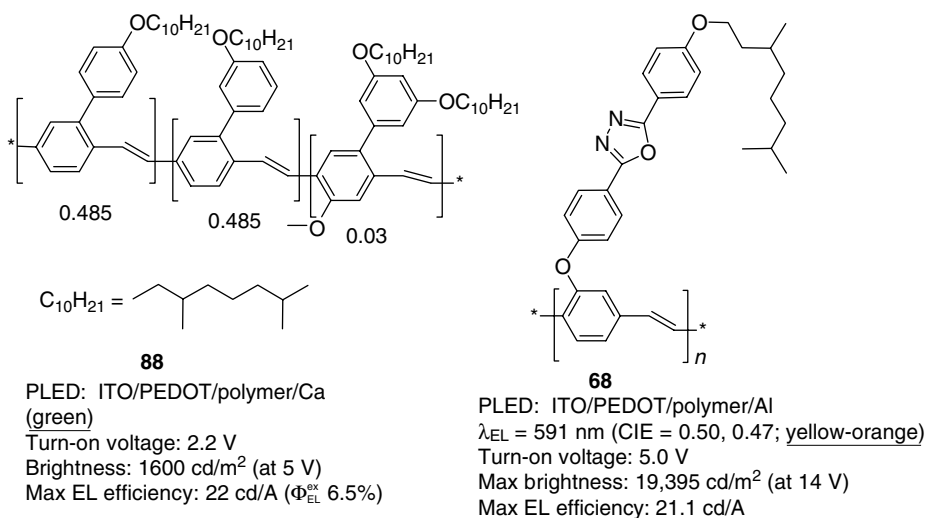


Chart 2.43

polymerization techniques, developed for nonconjugated systems in the last century. Thus, Schrock and coworkers [219] reported on high-yield (95%) synthesis of a well-defined polymer **194** ($n \approx 50$, polydispersity index (PDI) = 1.1) as a blue-emitting material (λ_{PL} (films) = 475 nm). A single-layer PLED ITO/**194**/Ca showed $\Phi_{\text{EL}}^{\text{ex}} = 0.3\%$ (turn-on voltage of 12 V), which can be improved to 0.55% by blending the polymer with electron transport material PBD (Chart 2.43).

2.2.6 THE BEST PERFORMING POLY(*p*-PHENYLENE VINYLENE) LIGHT-EMITTING POLYMERS

Thus, as we have seen, 15 years of chemical design in PPV materials, together with remarkable engineering progress, resulted in the creation of PLEDs of remarkable performance. Efficiencies in excess of 20 cd/A were achieved for polymers **88** [140] and **68** [124] (Scheme 2.21), which render them among the best performing green and orange EL polymers. Low-operating voltages, even with Al cathode, were achieved for PPV-based materials via introduction of electron-accepting fragments. Color tuning, in wide range, covering from blue to the NIR region, was demonstrated in PPV copolymers. The lifetime of the PPV-based PLEDs surpasses 20,000 h (for low brightness of ca. 100 cd/m²).



SCHEME 2.21 Best performing PPV electroluminescent polymers **88** (From Ho, P.K.H., Kim, J.-S., Burroughes, J.H., Becker, H., Li, S.F.Y., Brown, T.M., Cacialli, F., and Friend, R.H., *Nature*, 404, 481, 2000.) and **68** (From Jin, S., Kim, M., Kim, J.Y., Lee, K., and Gal, Y., *J. Am. Chem. Soc.*, 126, 2474, 2004.)

2.3 POLYFLUORENES

Fluorene (Fl) is a polycyclic aromatic compound, which received its name due to strong violet fluorescence arising from its highly conjugated planar π -electron system (Chart 2.44).

Positions 2 and 7 in Fl are the most reactive sites toward electrophilic attack, which allows construction of a fully conjugated rigid-rod polymer chain by substitution reactions, whereas the methylene bridge provides an opportunity to modify the processability of the polymer by substituents without perturbing the electronic structure of the backbone. The varieties, excellent optical and electronic properties, and high thermal and chemical stability of PFs make them an attractive class of materials for PLEDs. Different aspects of syntheses, properties, and LED applications of fluorene-based conjugated polymers and copolymers have been highlighted in several recent reviews [220–227]. In fact, PFs are the only class of conjugated polymers that can emit a whole range of visible colors with relatively high QE (Table 2.2).

2.3.1 CHARACTERIZATIONS STABILITY AND PHASE BEHAVIOR

Routine gel permeation chromatography (GPC) (size exclusion chromatography (SEC)) with calibration against polystyrene standard is a common method for the estimation of the molecular weights of PF. The PF homopolymers and copolymers obtained by different synthetic procedures, as will be described below, could substantially differ in molecular weight and polydispersity index, which also depend on the purification procedure. Generally, the M_n ranges from 10,000 to 200,000 with $PDI \approx 1.5$ –3, using polystyrene as a standard.

In principle, GPC with polystyrene standard overestimate the molecular weight of PFs because of their rigid-rod character [225]. Bradley and coworkers [228] determined an overestimation factor of 2.7 for poly(9,9-dioctylfluorene) by comparing the M_n values of coupled GPC and light scattering with those of GPC with polystyrene standard. Dynamic light-scattering experiments on narrow fractions ($PDI = 1.22$ to 1.67) of poly(9,9-*bis*(2-ethylhexyl)fluorene-2,7-diyl), prepared by preparative GPC fractionation have also displayed reduced absolute M_w values (50–70%), compared to polystyrene-calibrated SEC results [229]. Nevertheless, use of GPC with the same polystyrene standard throughout the majority of publications on PFs allows comparing more or less adequately the data for different polymers.

Generally, fluorene homo- and copolymers show excellent thermal stability: the T_{dec} of many PF exceeds 400°C (according to thermogravimetric analysis (TGA) analysis under inert atmosphere) [224].

Whereas poly(9,9-dihexylfluorene) (PDHF, **195**) is generally considered as amorphous, PF with longer octyl side chains, PFO **196**, is crystalline material. Many PFs — dioctyl (PFO **196** [228,230,231]) or *bis*(2-ethylhexyl) (**197** [232]) as well as some fluorene copolymers [233] exhibit liquid crystalline behavior, opening a possibility to fabricate polarized LEDs [224,234,235] (Chart 2.45).

PFO **196** is clearly crystalline with a melting point temperature around 150°C , above which a nematic mesophase exists up to ca. 300°C . Nanoscale crystallinity of PFO **196** was demonstrated by x-ray diffraction (XRD) experiments (Figure 2.8) [236,237]. For the crys-

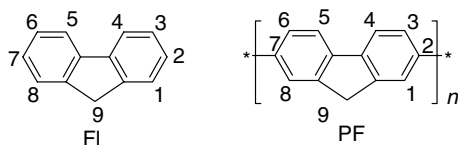


Chart 2.44

TABLE 2.2
Physical Properties of PFs

Polymer	M_n (g/mol) (PDI)	T_g (°C)	T_{dec} (°C)	λ_{max}^{abs} (nm) {Solution}	λ_{max}^{abs} (nm) {Film}	λ_{PL}^{max} (nm) {Solution} ^a [Φ_{PL} (%)]	λ_{PL}^{max} (nm) {Film} ^a [Φ_{PL} (%)]	E_g^{opt} (eV) ^b	HOMO–LUMO (eV) [CV Data]	EL Data	Ref.
195	35,700 (2.3)	75	421	385 { <i>p</i> -xy ene}	391	415 [82%]	425	2.91			320
195	24,300 (1.4)	103	390	379	385.5	415 (438, 469) [82%]	422 (444, 476) [74%]	2.86	–5.50/–2.37		379
195				382 {THF}		417, 436 [79%] {THF}		3.26	–5.87/–2.90		413
196	24,000 (2.3)	72	385	386 {CHCl ₃ }	391	422, 443 {CHCl ₃ }	422 [47%]	2.76	–5.77/–2.16	λ_{EL} : 456 nm, Φ_{EL}^x : 0.52%, CIE(0.20, 0.20)	353, 422
196	36,600 (2.81)			389 {CHCl ₃ }	394	414, 439, 471 [81%] {CHCl ₃ }	424, 448 [55%]	2.93		λ_{EL} : 425, 446 nm, CIE (0.17, 0.09)	390
196	41,600 (1.68)	113	418	389 {THF}	383	417, 439 [78%] {THF}	425, 447, 520 [40%]	2.9	–5.8/–2.9		342
196	40,000 (2.0)	78	426		380		420	2.93	–5.80/–2.87	CIE (0.17, 0.09)	408
197					380	[80%]	420	2.91	–5.79/–2.88	λ_{EL} : 419 nm, CIE (0.17, 0.12)	419, 431

201	5,600 (1.6)	130	407	374 {CHCl ₃ }	366	412 (436) [48%]	430	−5.65/−2.38	303
202	41,200 (4.3)	128	412	388 {CHCl ₃ }	380	420 (445) [93%]	434	−5.67/−2.30	303
205	20,700 (1.75)			389 {THF}			417 (439, 473)		272
207	20,300 (1.97)	108			~290	~425	~425, ~452	CIE (0.136, 0.162)	311
208	46,000 (3.6)	248	400	388 {CHCl ₃ }	419, 443	427, 448	420		313
209				385 {DCM}	413, 437	422, 446		CIE (0.189, 0.137)	314
210a	51,400 (2.01)	94	320	388 {THF}	388	414 [78%]	421, 446		315
210b	9,300 (1.66)	50	360	380 {THF}	382	411 [100%]	[25%] 418, 438		315
210c	4,400 (1.11)	10	320	340 {THF}	345	391 [41%]	[98%] 419br		315
211a	62,800 (2.22)	73	350	384 {THF}	388	411 [69%]	[15%] 417, 440		315
211b	26,200 (2.33)	48	290	383 {THF}	388	411 [92%]	[29%] 415, 438		315
211c	68,300 (2.21)	51	320	385 {THF}	388	411 [76%]	[46%] 416, 449		315
212a	3,900 (1.96)	78	340	372 {THF}	380	411 [53%]	[35%] 415, 438		315
212b	16,300 (2.46)	50	370	388 {THF}	388	419 [100%]	[12%] 419, 440		315
							[73%]		

continued

TABLE 2.2 (continued)
Physical Properties of PFs

Polymer	M_n (g/mol) (PDI)	T_g (°C)	T_{dec} (°C)	λ_{max}^{abs} (nm) {Solution}	λ_{max}^{abs} (nm) {Film}	λ_{max}^{PL} (nm) {Solution} ^a [Φ_{PL} (%)]	λ_{max}^{PL} (nm) {Film} ^a [Φ_{PL} (%)]	E_g^{opt} (eV) ^b	HOMO–LUMO (eV) [CV Data]	EL Data	Ref.
212c	11,900 (1.65)	49	360	374 {THF}	380	410 [84%]	414, 436 [56%]				315
213a	35,000 (1.9)	90	351	392 {THF}	394	419 (443) [92%]	424 (448) [26%]				316
213b	18,000 (2.2)	59	371	388 {THF}	392	418 (442) [99 %]	424 (448) [58%]				316
213c	15,000 (2.5)	56	360	380 {THF}	385	417 (439) [100%]	423 (446) [75%]				316
214a	46,700 (2.21)	103		~387 {THF}		420, 444					317
214b	131,000 (1.20)	73		~387		420, 444					317
214c	143,000 (1.19)	73		~370		415, 440					317
218	14,000 (3.3)	—	367	399		425, 446	418	2.94		CIE (0.17, 0.12)	318
219	32,000 { M_w }	121	400	~391 {toluene}		416 [91%] {toluene}	427				319
221	34,000 (2.2)	106	425	385 { <i>p</i> -xylene}	392	415 [82%]	425	2.91			320
222	77,000 (2.4)	110	427	386 { <i>p</i> -xylene}	391	415 [83%]	424	2.91			320

223	8,860 (1.76)							428, 452 [22%]		CIE (0.184, 0.159)	322
224a	7,000 (1.8)							410 (436), 538 {THF}			324
224b	13,500 (1.8)							410 (436) {THF}			324
240a	80,000	135						455 [79%] {THF}		$\Phi_{\text{EL}}^{\text{ex}}$: 0.17%	338
240b	89,000	136						454 [65%] {THF}		$\Phi_{\text{EL}}^{\text{ex}}$: 0.09%	338
240c	73,000	139						453 [61%] {THF}		$\Phi_{\text{EL}}^{\text{ex}}$: 0.08%	338
242a	4,200 (2.5)							~455		λ_{EL} : ~455 nm	341
242c	46,200 (1.92)	79	412	384 {THF}	383			417, 438 [74%] {THF}	2.9	-5.6/-2.7	342
242d	27,000 (1.80)		408	374 {THF}	383			417, 440 [81%] {THF}	3.0	-5.5/-2.5	342
243a	28,100 (2.21)	108	422	370 {THF}	365			413, 436 [72%] {THF}		-5.37/-2.07	343
243b	36,300 (4.02)	101	421	375 {THF}	370			413, 436 [74%]{THF}		-5.43/-2.12	343
243c	18,500 (2.30)	88	421	380 {THF}	375			414, 438 [74%] {THF}		-5.44/-2.13	343
244a	26,000 (2.29)	113	422	350 {THF}	346			397 [68%] {THF}		-5.33/-2.02	343
244b	35,900 (2.51)	108	421	367 {THF}	362			409, 431 [76%] {THF}		-5.34/-2.04	343
244c	31,000 (2.65)	98	420	372 {THF}	368			421, 435 [76%] {THF}		-5.39/-2.17	343
244d	13,100 (1.97)	86	422	375 {THF}	371			414, 438 [80%] {THF}		-5.42/-2.21	343

continued

TABLE 2.2 (continued)
Physical Properties of PFs

Polymer	M_n (g/mol) (PDI)	T_g (°C)	T_{dec} (°C)	λ_{max}^{abs} (nm) {Solution}	λ_{max}^{abs} (nm) {Film}	λ_{max}^{PL} {Solution} ^a [Φ_{PL} (%)]	λ_{max}^{PL} {Film} ^a [Φ_{PL} (%)]	E_g^{opt} (eV) ^b	HOMO–LUMO (eV) [CV Data]	EL Data	Ref.
245				381 {CHCl ₃ }	383	417, 440 [78%] {CHCl ₃ }	426, 448				346
253	10,000 (1.77)		344	378 {DCM}	378	462 [12%] {toluene}; 528 [<1%] {NMP}	497 [24%]				351
254a						433, 457 [51%] {toluene}; 466 [50%] {NMP}	443, 465 [51%]				351
254b						433, 457 [64%] {toluene}; 466 [60%] {NMP}	443, 465 [9%]				351
255a	14,000 (2.56)	107	394		406		429	2.88	–5.13/–2.25		352
255b	12,500 (3.02)	120	413		411		433	2.85	–5.10/–2.25		352
255c	12,300 (2.37)	65	401		411		433	2.85	–5.10/–2.25		352
256a	20,600 (2.0)	70	389	380 {CHCl ₃ }	380	420 {CHCl ₃ }	422 [30%]	2.79	–5.77/–2.19	λ_{EL} : 446 nm, Φ_{EL}^{ex} : 0.16%	353
256b	19,000 (1.9)	82	395	385 {CHCl ₃ }	383	420 {CHCl ₃ }	422 [28%]	2.79	–5.75/–2.19	λ_{EL} : 442 nm, Φ_{EL}^{ex} : 0.22%, CIE (0.19, 0.16)	353
256c	24,000 (2.6)	80	397	361 {CHCl ₃ }	380	418 {CHCl ₃ }	420 [51%]	2.90	–5.73/–2.22	λ_{EL} : 442 nm, Φ_{EL}^{ex} : 0.40%, CIE (0.17, 0.12)	353
256d	12,400 (2.2)	83	406	363 {CHCl ₃ }	370	420 {CHCl ₃ }	420 [60%]	2.90	–5.74/–2.26	λ_{EL} : 438 nm, Φ_{EL}^{ex} : 0.40%, CIE (0.17, 0.11)	353

256e	22,800 (1.5)	398	362 {CHCl ₃ }	380	418 {CHCl ₃ }	419 [49%]	2.97	−5.72/−2.27	λ _{EL} : 440 nm, Φ _{EL} ^{ex} : 0.45%, CIE (0.15, 0.08)	353
256f	15,600 (1.3)	93	340 {CHCl ₃ }	350	403 {CHCl ₃ }	413 [15%]	3.15	−5.36/−2.33	λ _{EL} : 424 nm, Φ _{EL} ^{ex} : 0.02%, CIE (0.21, 0.20)	353
257	13,000 (2.1)	213	390 {THF}	390	419 (444) [124%] {THF}	427 (452) [43%]		−5.76/−2.47	λ _{EL} : 428 nm, Φ _{EL} ^{ex} : 0.52%	354
258	11,000 (2.2)	166	440 {THF}	389 {THF}	420 (444) [95%] {THF}	426 (450) [42%]		−5.30/−2.54	CIE (0.193, 0.141), Φ _{EL} ^{ex} : 1.21%	356
259	4,900 (1.2)	119	398	321 {CHCl ₃ }	445 [15%] {CHCl ₃ }	447	3.14	−5.90/−2.70	λ _{EL} : 452 nm	357
260a	6,700 (1.7)	109	418	327 {CHCl ₃ }	405 [30%] {CHCl ₃ }	411	3.33	−5.97/−2.64	λ _{EL} : 408 nm	357
260b	14,800 (1.5)	125	421	329 {CHCl ₃ }	402 [39%] {CHCl ₃ }	407	3.32	−5.92/−2.60	λ _{EL} : 409 nm	357
260c	26,600 (2.8)	128	414	325 {CHCl ₃ }	404 [36%] {CHCl ₃ }	412	3.32	−5.93/−2.61	λ _{EL} : 423 nm	357
260d	24,500 (2.7)	85	410	322 {CHCl ₃ }	404 [31%] {CHCl ₃ }	409	3.33	−5.96/−2.63	λ _{EL} : 406 nm	357
260e	25,200 (2.6)	148	422	323 {CHCl ₃ }	430 [17%] {CHCl ₃ }	430	3.32	−5.74/−2.84	λ _{EL} : 431 nm	357
260f	12,200 (1.9)	120	407	323 {CHCl ₃ }	409 [26%] {CHCl ₃ }	415	3.33	−6.04/−2.71	λ _{EL} : 416 nm	357
260g	6,500 (1.7)	132	446	328 {CHCl ₃ }	410 [38%] {CHCl ₃ }	410	3.34	−5.95/−2.61	λ _{EL} : 417 nm	357
262	12,000 (2.28)	150	439	394 (372) {DCM}	402 (426) [73%] {DCM}					358
263	25,100 (2.50)	114	431	396 (380) {DCM}	420 (442) [75%] {DCM}					358
264	30,400 (2.70)	98	432	395 (381) {DCM}	422 (443) [72%] {DCM}					358

continued

TABLE 2.2 (continued)
Physical Properties of PFs

Polymer	M_n (g/mol) (PDI)	T_g (°C)	T_{dec} (°C)	λ_{max}^{abs} (nm) {Solution}	λ_{max}^{abs} (nm) {Film}	λ_{max}^{PL} {Solution} ^a [Φ_{PL} (%)]	λ_{max}^{PL} (nm) {Film} ^a [Φ_{PL} (%)]	E_g^{opt} (eV) ^b	HOMO–LUMO (eV) [CV Data]	EL Data	Ref.
265	21,600 (2.63)	127	430	396 (379) {DCM}		422 (444) [67%] {DCM}					358
266a	20,000 (1.71)	143							–6.4/–2.6		359
266b	11,000 (1.36)	263							–6.4/–2.6		359
266c	33,200 (2.4)	117									359
267a	38,600 (1.87)	95							–6.0/–2.8		359
267b	36,200 (1.25)	85							–6.0/–2.8		359
268a	8,700 (2.3)	137	399	366 {CHCl ₃ }	369	405 {CHCl ₃ }	414	3.02	–6.24/–3.01		360
268b	9,100 (2.2)	194	394	349 {CHCl ₃ }	352	428 {CHCl ₃ }	422	3.09	–6.38/–3.19		360
269a	21,800 (2.7)	119	411	350 (368) {DCE}	354 (373)	379, 396 (415) [41%]	403, 423 (447)	3.22	–6.32/–3.10		361
269b	27,600 (3.6)	118	411	352 (371) {DCE}	350 (369)	380, 396 (415) [90%]	399, 421 (447)	3.23	–6.27/–3.04		361
269c	11,700 (3.0)	71	352	353 (370) {DCE}	356 (376)	385, 403 (423) [86%]	394, 427 (443)	3.20	–6.08/–2.88		361
270	15,600 (1.63)			390 {THF}		404 (425) {THF}					362
271a					380		477	2.85	–5.74/–2.89	Φ_{EL}^{ex} : 0.50%	363
271b					328, 384		447	2.92	–5.90/–2.98	Φ_{EL}^{ex} : 0.057%	363

272				−378, 368		420, 448 [40%]	−5.66/−2.62	λ_{EL} : 420, 448 nm, $\Phi_{\text{EL}}^{\text{ex}}$: 0.60% $\Phi_{\text{EL}}^{\text{ex}}$: 0.12%	364, 365
274	11,600 (2.9)	105		379		452	2.88		366
275	3,800 (3.04)	105	435	375	413, 436 {THF}	440			367
276	12,800 (7.67)	144	440	381	414, 438 {THF}	429, 444		λ_{EL} : 423 nm, $\Phi_{\text{EL}}^{\text{ex}}$: 0.06%, CIE (0.173, 0.098)	367
277	4,600 (5.25)	93	430	378	415, 439 {THF}	435			367
278	6,400 (9.27)	90	445	381	414, 436 {THF}	427, 440			367
279a	13,800 (2.43)	236	449	345	398 (420) [73%] {THF}	399 (420) [38%]			368
279b	6,640 (1.15)	237	439	333	397 [92%] {THF}	402 (419) [65%]			368
279c	4,530 (1.67)	238	380	374	407 [99%] {THF}	414 (439) [82%]			368
280a	23,500 (1.52)	118	241	341		411 [32%]	2.95	λ_{EL} : 418 nm, $\Phi_{\text{EL}}^{\text{ex}}$: 0.43%	369
280b	24,200 (1.58)	110	243	341		408 [30%]	2.94	λ_{EL} : 419 nm, $\Phi_{\text{EL}}^{\text{ex}}$: 0.60%	369
280c	20,700 (1.61)	79	342	344		412 [32%]	2.94	λ_{EL} : 420 nm, $\Phi_{\text{EL}}^{\text{ex}}$: 0.41%	369
281a	14,100 (4.2)			396, 415	427, 447 {CHCl ₃ }	428			370
281b	11,600 (5.8)			394, 416	426, 447 {CHCl ₃ }	429			370
281c	9,800 (4.4)			387, 413	426, 447 {CHCl ₃ }	429			369

continued

TABLE 2.2 (continued)
Physical Properties of PFs

Polymer	M_n (g/mol) (PDI)	T_g (°C)	T_{dec} (°C)	λ_{max}^{abs} (nm) {Solution}	λ_{max}^{abs} (nm) {Film}	λ_{PL}^{max} (nm) {Solution} ^a [Φ_{PL} (%)]	λ_{PL}^{max} (nm) {Film} ^a [Φ_{PL} (%)]	E_g^{opt} (eV) ^b	HOMO–LUMO (eV) [CV Data]	EL Data	Ref.
281d	17,000 (3.6)			394, 412 {CHCl ₃ }	392, 416	426, 446 {CHCl ₃ }	434				370
281e	9,500 (5.4)			392, 412 {CHCl ₃ }	396, 424	427, 447 {CHCl ₃ }	434				370
282	19,500 (1.9)				360		428, 445 [44%]	2.97		λ_{EL} : 420, 446 nm, Φ_{EL}^{ex} : 0.82%	371
283a	2,320 (1.39)			361 {THF}	367	411 (428) [75%] {THF}	417 (440) [42%]				373, 374
283b	1,700 (1.35)					[36%] {THF}	[18%]				373
283c	2,780 (1.22)										373
284a	56,700 (1.56)		330	378 (408) {THF}	386 (410)	471 (427, 448) [22%] {THF}	484 (515)				374
284b	48,500 (1.59)		288	384 (411) {THF}	388 (424)	471 (426, 500) [16%] {THF}	492 (518)				374
284c	43,300 (1.76)		256	385 (408) {THF}	390 (416)	471 (429, 502) [15%] {THF}	479				374
285	35,200 (1.57)			385 {THF}	383	413 (435) {THF}	453, 477 (425)	2.88	E_{ox} : 1.39 V, E_{red} : −1.76 V (vs. SCE)		375
286	37,200 (1.49)			424, 448 {THF}	432, 459	463 (492) {THF}	521	2.52	E_{ox} : 1.01 V, E_{red} : −1.60 V (vs. SCE)		375
287	59,200 (1.92)			392, 409 {THF}	395, 425	424 (444) {THF}	477, 503 (439)	2.74	E_{ox} : 1.50 V, E_{red} : −1.67 V (vs. SCE)		375

289	14,000 (1.5)	185	429	352 {CHCl ₃ }	355	398, 419 {CHCl ₃ }	404, 425 [42%]		CIE (0.165, 0.128)	378
290a	9,400 (1.5)	50	390	326 {CHCl ₃ }	324	383 (403) [64%] {CHCl ₃ }	404 (389) [88%]	3.32	−5.66/−2.31	379
290b	5,050 (2.0)	72	377	370.5 {CHCl ₃ }	373.5	414 (436) [63%] {CHCl ₃ }	418 (414) [55%]	2.95	−5.38/−2.41	379
290c	22,800 (1.5)	123	410	355 {CHCl ₃ }	370	409.5 (432) [74%] {CHCl ₃ }	423.5 (443) [48%]	2.93	−5.78/−2.81	379
290d	48,100 (1.9)	111	376	353 {CHCl ₃ }	350.6	451 [35%] {CHCl ₃ }	443 [20%] [48%]	3.04	−5.76/−2.80	379
290e	8,900 (1.7)	145	390	348 {CHCl ₃ }	343	398 (417) [26%] {CHCl ₃ }	428 (406, 451) [10%]	3.06	−5.28/−2.47	379
290f	7,300 (1.6)	213	375	349 {CHCl ₃ }	349	418 [58%] {CHCl ₃ }	423.5 [23%]	3.05	−5.64/−2.42	379
290g	60,400 (2.0)	122		385 {CHCl ₃ }	395	416 (440, 475) [91%] {CHCl ₃ }	426 (447) [41%]	2.82	−5.69/−2.83	379
291	17,500 (2.4), 12,000 (1.8)	55			364	407 [87%] {CHCl ₃ }	425, 443 {cast}, 420, 442 {spin coated};	E_{ox} : 1.76 V, E_{red} : −2.44 V (vs. SCE)	λ_{EL} : 419 nm	380, 382 ^c
291	11,800 (1.7)		398	369.5 {CHCl ₃ }	371	408 (431.5) [85%] {CHCl ₃ }	422 (441, 470) [78%]	2.92	−5.36/−2.47	379
292	15,000 (2.2)	70			365	406 [72%] {CHCl ₃ }	424, 442 {cast}, 418, 440 {spin coated};	E_{ox} : 1.50 V, E_{red} : −2.40 V (vs. SCE)	λ_{EL} : 416 nm	380, 382

continued

TABLE 2.2 (continued)
Physical Properties of PFs

Polymer	M_n (g/mol) (PDI)	T_g (°C)	T_{dec} (°C)	λ_{max}^{abs} (nm) {Solution}	λ_{max}^{abs} (nm) {Film}	λ_{max}^{PL} (nm) {Solution} ^a [Φ_{PL} (%)]	λ_{max}^{PL} (nm) {Film} ^a [Φ_{PL} (%)]	E_g^{opt} (eV) ^b	HOMO–LUMO (eV) [CV Data]	EL Data	Ref.
293	2,700 (1.4)	60	224	374 {CHCl ₃ }	366	415 (438) [85%] {CHCl ₃ }	424		–5.56/–2.23		303
294a	6,800 (1.6); 10,000 (2.6)				438	496 [49%] {CHCl ₃ }	490, 515 {cast}, 485, 512 {spin coated}; 537		E_{ox} : 1.26 V, E_{red} : –2.40 V (vs. SCE)	λ_{EL} : 480 nm	380, 382
294b	15,000 (2.2)	70			384		469 {cast}, 460 {spin coated}		E_{ox} : 1.35 V (vs. SCE)	λ_{EL} : 468 nm	380
295	14,500 (3.0)	73		452, 470 {CHCl ₃ }	427	488 [30%] {CHCl ₃ }	563 {cast}, 548 {spin coated}; 599		E_{ox} : 1.11 V, E_{red} : –2.34 V (vs. SCE)	λ_{EL} : 545 nm	380, 382
295	19,000 (2.83)	93	426	452, 470 {CHCl ₃ }	458, 479	495, 530, 571 [20%]	511, 537, 577 [12%]	2.44	–5.41/–2.48	λ_{EL} : 539 nm, CIE (0.40, 0.58)	390
296	2,400 (1.3)	65	399	444 {CHCl ₃ }	446	498 (530) [30%] {CHCl ₃ }	510		–5.21/–2.53	λ_{EL} : 588 nm	303
297	12,700 (1.4)	129			444		495, 527 {cast}, 494, 526 {spin coated}		E_{ox} : 1.18 V (vs. SCE)	λ_{EL} : 536 nm	380

298	6,600 (1.9)	105	517	536, 574 {cast}, 532, 574 {spin coated}	E_{ox} : 1.22 V, E_{red} : -2.73 V (vs. SCE)	380
300	18,700 (1.4)	203 (T_m)	412	461 (490) [65%] {CHCl ₃ }	-5.39/-2.56	Φ_{EL}^{ex} : 0.64%
301	18,600 (1.6)	78	375.5	447 (473) [39%] {CHCl ₃ }	-5.63/-2.35; -5.53/-2.65	Φ_{EL}^{ex} : 0.37%
302a	15,200 (1.9)	63	403	482 (515) [31%] {CHCl ₃ }	-5.38/-2.45	Φ_{EL}^{ex} : 0.25%
302b	22,600 (1.7); 13,000 (1.67)	77	401; 396; 392	483 (520) [28%]; 32% {CHCl ₃ }	-5.40/-2.39; -5.30/-2.85; -5.29/-2.79	λ_{EL} : 493 (515) nm, CIE (0.24, 0.51), Φ_{EL}^{ex} : 0.30%
304	13,600 (1.80)	112	448, 471	478, 510, 554 [32%] {CHCl ₃ }	-5.38/-2.40	λ_{EL} : 515 nm, CIE (0.29, 0.63)
305			390	540 [64%]	-5.9/-3.2	λ_{EL} : 545 nm, Φ_{EL}^{ex} : 2.5%, CIE (0.394, 0.57)
306	16,800 (2.33)	162	339, 395	512 [45%]	-5.81/-2.98	Φ_{EL}^{ex} : 0.60%
307a	21,700 (1.53)	111	337, 399	508 [56%]	-5.74/-2.98	Φ_{EL}^{ex} : 1.56%
307b	25,600 (1.45)	80	336, 398	509 [59%]	-5.71/-2.93	Φ_{EL}^{ex} : 2.53%
308	10,600 (2.95)		415	481, 536	-5.76/-2.79	λ_{EL} : 480, 536 nm

continued

TABLE 2.2 (continued)
Physical Properties of PFs

Polymer	M_n (g/mol) (PDI)	T_g (°C)	T_{dec} (°C)	λ_{max}^{abs} (nm) {Solution}	λ_{max}^{abs} (nm) {Film}	λ_{max}^{PL} (nm) {Solution} ^a [Φ_{PL} (%)]	λ_{max}^{PL} (nm) {Film} ^a [Φ_{PL} (%)]	E_g^{opt} (eV) ^b	HOMO–LUMO (eV) [CV Data]	EL Data	Ref.
309a	10,600 (2.1)	173	415	417 {CHCl ₃ }	419	463 {CHCl ₃ }	507	2.6	–5.34/–2.75	λ_{EL} : 508 nm	399, 421
309a	100,000 (1.3)		~400		418		465, 506 (530)	2.56	–5.73/–3.13	λ_{EL} : 472 nm, CIE (0.23, 0.38)	401
309b	39,300 (2.28)	—	~450		420 (370)		[34%] 505 (480, 550)	2.55	–5.40/–2.85	λ_{EL} : 505	402
310	10,700 (3.33)	100	380		375		440, 465, (490), 540	2.85	–5.67/–2.82	λ_{EL} : 540 nm	403
311	18,800 (1.91)	149	395	404 {toluene}		658 {toluene}	664	2.05		λ_{EL} : 668 nm, CIE (0.682, 0.317)	150
315a	33,500 (2.00)	155	422		316, 412		592	2.39	–6.20/–3.79	λ_{EL} : 562 nm	405
315b	39,100 (1.83)	122	427		301, 404		584	2.40	–6.18/–3.75	λ_{EL} : 559 nm	405
315c	36,000 (1.14)	100	434		304, 406		580	2.42	–6.17/–3.72	λ_{EL} : 557 nm	405
316	13,100 (2.9)	114	411	399 {CHCl ₃ }	403	465 {CHCl ₃ }	476	2.66	–6.13/–3.08	λ_{EL} : 466 nm, Φ_{EL}^{ex} : 0.2%	406
317	13,000 (2.4)	121		500	500	556 (608) [3%]	610	2.2	–5.47/–3.30	λ_{EL} : 582 (610) nm	407
318	13,300 (3.08)		388	538 {CHCl ₃ }	563 (601)	616 [32%] {CHCl ₃ }	656 (702)	2.00	–5.32/–3.32		303
319	7,800 (1.54)	—	~450		440		535 (500)	2.38	–5.50/–3.12	λ_{EL} : 535 nm	402
320	11,000 (2.5)	106	370	302 {CHCl ₃ }	372	468 {CHCl ₃ }	525	2.74	–5.82/–3.08	λ_{EL} : 547 nm, CIE (0.40, 0.53)	408

321	18,000 (1.8)	112	391	439 {CHCl ₃ }	468	513 {CHCl ₃ }	555	2.28	-5.87/-3.59	λ_{EL} : 554 nm, CIE (0.48, 0.51)	408
322	21,000 (2.1)	113	400	516 {CHCl ₃ }	460	516 {CHCl ₃ }	602	2.21	-5.65/-3.44	λ_{EL} : 604 nm, CIE (0.63, 0.38)	408
323	14,000 (1.9)	118	407	530 {CHCl ₃ }	537	530 {CHCl ₃ }	674	1.95	-5.59/-3.64	λ_{EL} : 674 nm, CIE (0.66, 0.33)	408
324	4,430 (2.1)		367		419		591 [5.7%]			λ_{EL} : 599 (557), CIE (0.48, 0.48)	409
325	4,620 (2.9)		332		439		602 [14.7%]			λ_{EL} : 596, CIE (0.53, 0.44)	409
326	2,250 (2.0)		450		417		551 (580) [3.5%]			λ_{EL} : 557, 585, CIE (0.43, 0.45)	409
327	23,500 (1.52)	186	407		352, 457		662, 712 [7%]	2.22	-5.78/-3.57	λ_{EL} : 657 (702) nm, Φ_{EL}^{ex} : 0.27%	410
328	24,200 (1.58)	119	406		345, 435		641, 704 [5%]	2.32	-5.79/-3.54	λ_{EL} : 636 (694 nm), Φ_{EL}^{ex} : 0.38%	410
329	20,700 (1.61)	73	406		347, 438		641, 705 [4%]	2.30	-5.77/-3.53	λ_{EL} : 638 (696) nm, Φ_{EL}^{ex} : 0.21%	410
330					400, 780		1035	1.27		λ_{EL} : 970 nm, Φ_{EL}^{ex} : 0.03- 0.05%	411
335	11,090 (1.3)			328 {THF}	336	368, 386 [62%] {THF}	376, 384	3.26	-5.89/-2.63	λ_{EL} : 395 nm, Φ_{EL}^{ex} : 0.054%	413
338	55,000	90	>400				540				415
339a	38,000 (3.0)	85	>400		370, 465 376		466				415, 416

continued

TABLE 2.2 (continued)
Physical Properties of PFs

Polymer	M_n (g/mol) (PDI)	T_g (°C)	T_{dec} (°C)	λ_{max}^{abs} (nm) {Solution}	λ_{max}^{abs} (nm) {Film}	λ_{max}^{PL} (nm) {Solution} ^a [Φ_{PL} (%)]	λ_{max}^{PL} (nm) {Film} ^a [Φ_{PL} (%)]	E_g^{opt} (eV) ^b	HOMO–LUMO (eV) [CV Data]	EL Data	Ref.
339b	11,000	95	>400		374		481				415
339c	10,000	110	>400		390		510				415
341a	20,000 (2.3)		~300		380	[69%]	536		–5.72	λ_{EL} : 532 nm	418, 419
341b	15,000 (1.5)		~300		380	[57%]	544		–5.73	λ_{EL} : 535 nm	418, 419
341c	13,000 (2.5)		~300		380	[51%]	583		–5.72	λ_{EL} : 580 nm	418, 419
341d	22,000 (2.7)		~300		379	[34%]	620		–5.73	λ_{EL} : 630 nm	418, 419
342a	87,000 (1.4)		~400		418	470, 506 [36%]			–5.53/–2.93	λ_{EL} : 472 nm, CIE (0.23, 0.38)	401
342b	57,000 (2.1)		~400		419	470, 506 [36%]			–5.55/–2.95	λ_{EL} : 475 nm, CIE (0.23, 0.38)	
344a	11,900 (2.6)	176	410	415 {CHCl ₃ }	418	463 {CHCl ₃ }	576	2.57	–5.34/–2.75	λ_{EL} : 574 nm	421
344b	14,100 (1.9)	170	390	418 {CHCl ₃ }	421	464 {CHCl ₃ }	580	2.54	–5.36/–2.77	λ_{EL} : 576 nm	421
344c	11,400 (2.6)	172	385	418 {CHCl ₃ }	420	463 {CHCl ₃ }	589	2.54	–5.16/–2.62	λ_{EL} : 589 nm	421
344d	14,400 (3.0)	169	355	417 {CHCl ₃ }	422	463 {CHCl ₃ }	593	2.1	–5.09/–2.99	λ_{EL} : 592 nm	421
345a	14,000 (1.51)	74	400	383 {CHCl ₃ }	383	418 {CHCl ₃ }	422 [29%]		–5.77/–2.16	λ_{EL} : 422 nm, Φ_{EL}^{ex} : 0.36%	422
345b	19,000 (1.82)	76	400	375 {CHCl ₃ }	380	416 {CHCl ₃ }	421		–5.78/–2.17	λ_{EL} : 421 nm,	422

345c	17,000 (1.77)	79	406	{CHCl ₃ }	369	373	418 {CHCl ₃ }	[25%] 420	−5.80/−2.12	$\Phi_{\text{EL}}^{\text{ex}}$: 0.34% λ_{EL} : 420 nm, $\Phi_{\text{EL}}^{\text{ex}}$: 0.22% λ_{EL} : 419 nm, $\Phi_{\text{EL}}^{\text{ex}}$: 0.10% λ_{EL} : 417 nm, $\Phi_{\text{EL}}^{\text{ex}}$: 0.42%	422
345d	1,100 (1.96)	84	401	{CHCl ₃ }	350	350	415 {CHCl ₃ }	[18%] 419	−5.81/−2.12		422
345e	1,000 (2.18); 5400 (1.9)	125; 130	397	{CHCl ₃ }	336	343	405 {CHCl ₃ }; 381 / 37% {CHCl ₃ }	[23%] 410 [62%]	−5.89/−2.06		422, 423
348a	26,000 (2.56)					382		568 [27%]	−5.68/−2.22	λ_{EL} : 574 nm, $\Phi_{\text{EL}}^{\text{ex}}$: 0.81%, CIE (0.689, 0.314)	426
348b	28,000 (2.78)					374, 468		563 [21%]	−5.71/−2.21		426
348c	32,000 (3.15)					375, 469		579 [52%]	−5.70/−2.20	λ_{EL} : 582 nm, $\Phi_{\text{EL}}^{\text{ex}}$: 1.0%, CIE (0.698, 0.300)	426
348d	16,000 (2.04)					342, 487		595 [16%]	−5.79/−2.14	λ_{EL} : 600 nm, $\Phi_{\text{EL}}^{\text{ex}}$: 0.42%, CIE (0.706, 0.292)	426
349a	21,000 (2.23)				391 {CHCl ₃ }			423, 634 [33%]	−5.78/−3.62	λ_{EL} : 634 nm, $\Phi_{\text{EL}}^{\text{ex}}$: 0.56%, CIE (0.37, 0.34)	427
349b	60,000 (3.09)				391 {CHCl ₃ }			438, 645 [69%]	−5.76/−3.62	λ_{EL} : 645 nm, $\Phi_{\text{EL}}^{\text{ex}}$: 0.30%, CIE (0.61, 0.35)	427
349c	24,000 (2.46)				385, 556 {CHCl ₃ }			423, 647 [77%]	−5.80/−3.68	λ_{EL} : 657 nm, $\Phi_{\text{EL}}^{\text{ex}}$: 3.10%, CIE (0.64, 0.33)	427
349d	23,000 (2.32)				390, 559 {CHCl ₃ }			420, 656 [84%]	−5.76/−3.64	λ_{EL} : 659 nm, $\Phi_{\text{EL}}^{\text{ex}}$: 1.14%, CIE (0.67, 0.32)	427

continued

TABLE 2.2 (continued)
Physical Properties of PFs

Polymer	M_n (g/mol) (PDI)	T_g (°C)	T_{dec} (°C)	λ_{max}^{abs} (nm) {Solution}	λ_{max}^{abs} (nm) {Film}	λ_{max}^{PL} (nm) {Solution} ^a [Φ_{PL} (%)]	λ_{max}^{PL} (nm) {Film} ^a [Φ_{PL} (%)]	E_g^{opt} (eV) ^b	HOMO–LUMO (eV) [CV Data]	EL Data	Ref.
349e	18,000 (2.09)			389, 555 {CHCl ₃ }			421, 671 [53%]	2.95, 1.96	–5.74/–3.66	λ_{EL} : 662 nm, Φ_{EL}^{ex} : 0.35%, CIE (0.68, 0.31)	427
349f	8,000 (2.61)			353, 563 {CHCl ₃ }			422, 681 [34%]	2.95, 1.95		λ_{EL} : 672 nm, Φ_{EL}^{ex} : 0.22%, CIE (0.69, 0.30)	427
350a	23,000 (2.6)				382		635 [11.4%]		–5.72/–2.79	λ_{EL} : 628 nm, Φ_{EL}^{ex} : 0.5%, CIE (0.67, 0.32)	428
350b	35,000 (3.1)				382, 535		651 [12.5%]	2.08	–5.65/–2.72	λ_{EL} : 643 nm, Φ_{EL}^{ex} : 0.6%, CIE (0.70, 0.31)	428
350c	33,000 (2.7)				384, 536		655 [8.6%]	2.07	–5.61/–3.54	λ_{EL} : 652 nm, Φ_{EL}^{ex} : 0.9%, CIE (0.70, 0.30)	428
350d	34,000 (2.6)				382, 538		678 [7.9%]	2.03	–5.55/–3.54	λ_{EL} : 663 nm, Φ_{EL}^{ex} : 1.4%, CIE (0.70, 0.29)	428

350e	29,000 (2.4)	384, 542	678 [5.2%]	2.02	-5.50/-3.52	λ_{EL} : 669 nm, $\Phi_{\text{EL}}^{\text{ex}}$: 0.6%, CIE (0.70, 0.29)	428
350f	11,000 (1.7)	388, 551	685 [4%]	2.01	-5.47/-3.46	λ_{EL} : 674 nm, $\Phi_{\text{EL}}^{\text{ex}}$: 0.5%, CIE (0.70, 0.29)	428
351a	16,000 (2.7)	383	629 [88%]	2.91	-6.76/-2.85	λ_{EL} : 613 nm, $\Phi_{\text{EL}}^{\text{ex}}$: 0.65%, CIE (0.60, 0.38)	429
351b	15,000 (2.5)	382, 520	636 [75%]	2.09	-5.68/-3.59	λ_{EL} : 625 nm, $\Phi_{\text{EL}}^{\text{ex}}$: 1.02%, CIE (0.65, 0.35)	429
351c	67,000 (2.9)	381, 520	647 [69%]	2.07	-5.68/-3.61	λ_{EL} : 629 nm, $\Phi_{\text{EL}}^{\text{ex}}$: 1.10%, CIE (0.66, 0.34)	429
351d	18,000 (2.3)	378, 520	642 [70%]	2.06	-5.64/-3.58	λ_{EL} : 634 nm, $\Phi_{\text{EL}}^{\text{ex}}$: 1.45%, CIE (0.66, 0.34)	429
351e	3,000 (2.0)	371, 522	670 [50%]	2.06	-5.62/-3.56	λ_{EL} : 672 nm, $\Phi_{\text{EL}}^{\text{ex}}$: 0.42%, CIE (0.67, 0.33)	429
351f	4,000 (1.9)	369, 526	678 [44%]	2.03	-5.62/-3.59	λ_{EL} : 671 nm, $\Phi_{\text{EL}}^{\text{ex}}$: 0.31%, CIE (0.68, 0.32)	429

continued

TABLE 2.2 (continued)
Physical Properties of PFs

Polymer	M_n (g/mol) (PDI)	T_g (°C)	T_{dec} (°C)	λ_{max}^{abs} (nm) {Solution}	λ_{max}^{abs} (nm) {Film}	λ_{PL}^{max} (nm) {Solution} ^a [Φ_{PL} (%)]	λ_{PL}^{max} (nm) {Film} ^a [Φ_{PL} (%)]	E_g^{opt} (eV) ^b	HOMO–LUMO (eV) [CV Data]	EL Data	Ref.
351g	40,000 (2.1)				370, 525			2.06	–5.60/–3.54	λ_{EL} : 669 nm, Φ_{EL}^{ext} : 0.25%, CIE (0.68, 0.32)	429
352	2,840 (6.45)	167	324	328 {THF}	287	486 [43%] {THF}	490	2.76	–5.1/–2.4	λ_{EL} : ~490 nm, Φ_{EL}^{ext} : 0.10%, λ_{EL} : 480 nm, CIE (0.16, 0.32)	430
353a	7,650 (1.7)		~350		373	[84%] ^d	474	2.86	–5.38		431
353b	13,500 (2.0)		~350		373	[71%] ^d	480	2.81	–5.40/–2.59	λ_{EL} : 484, CIE (0.17, 0.37)	431
353c	9,400 (1.6)		~350		367	[37%] ^d	478	2.81	–5.40	λ_{EL} : 480, CIE (0.17, 0.33)	431
354	18,500 (1.7)				371		482	2.82	–5.40/–2.58	λ_{EL} : 482	432

^aThe data in the parentheses are the wavelengths of shoulders and subpeaks.

^b E_g stands for the band-gap energy estimated from the onset of the optical absorption.

^cFrom Marsitzky, D., Murray, J., Scott, J.C., and Carter, K.R., *Chem. Mater.*, 13, 4285, 2001.

^dQuantum yield relative to compound 197.

^eIn some cases, the same group in subsequent publications reported different properties for the given materials, in which case these are marked by italic font.

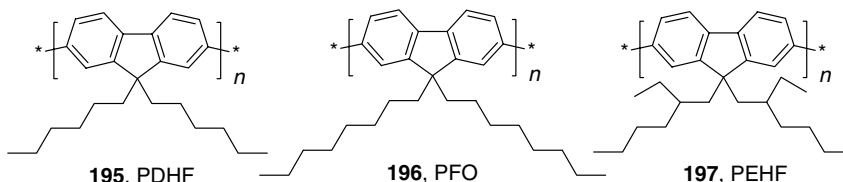


Chart 2.45

talline phase, a periodicity in the plane of the surface of 4.15 Å corresponded to half the fluorene ring repeat distance along the backbone [236,238]. Octyl chains (which are perpendicular to the direction of the PF backbone) of two neighboring polymer backbones are believed to intercalate, allowing a more efficient space filling. This side-chain packing may be responsible for an unusual ability of PFO **196** and related PF to undergo thermotropic alignment into monodomain structures [238]. PFO **196** is the most studied PF for its crystallinity and liquid crystallinity (LC) having the largest effects and most promising properties for polarized EL, although both LC and crystallinity were also reported for **195** [236,239]. It was also shown that high degree of alignment in PFO **196** can be achieved by the friction transfer technique with subsequent thermal treatments. Depending on cooling rate, liquid crystalline or crystalline films are formed [240].

Several reports on PF with optically active side chains imply possible helicity of the fluorene backbone (right- or left-handed 5/2 and 5/1 helical states) [241–244]. Because of the high tendency of PF to form ordered structures, solvent could have a large effect on the morphology and photophysical properties of PF films and consequently device performance. Bradley and coworkers [228] showed dramatic changes in the absorption spectra of PFO **196** resulting from certain treatment protocols (dissolution in moderately poor solvent such as cyclohexane, or exposing spin-coated films to toluene or THF vapor). Sirringhaus and coworkers [245] demonstrated that the highest degree of macroscopic order was observed in films that were cast from an aromatic solvent and annealed while still “wet,” which was attributed to the plasticizing effect of the solvent during the reorientation process. Ellipsometry was used to study the alignment properties of films cast from six different solvents. Maximum dichroic ratio (D_{\max}) was used as a measure of ordering: $D_{\max} = 14.6$ (isodurene), 3.7 (tetrachloroethane), 10.2 (*o*-xylene), 9.1 (*p*-xylene), 7.5 (toluene), 2.8 (chloroform). The ordering did not directly correlate

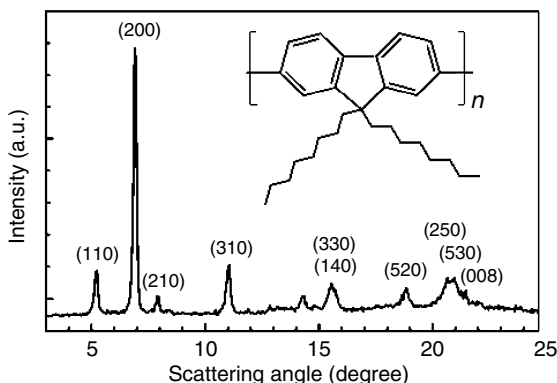


FIGURE 2.8 XRD powder pattern of highly crystalline thick-film PFO **196** specimen after extended heat treatments at elevated temperatures and stepwise cooled to room temperature. (From Chen, S.H., Chou, H.L., Su, A.C., and Chen, S.A., *Macromolecules*, 37, 6833, 2004. With permission.)

with the boiling point of the solvent (cf. D_{\max} for *o*-xylene and tetrachloroethane, which have the same boiling point). These results demonstrate that the choice of the solvent and casting, drying, and annealing techniques are very important for the device performance.

2.3.2 OPTICAL AND ELECTRONIC PROPERTIES

The electronic absorption spectra of dilute (typically 5–10 mg/l) solutions of poly(9,9-dialkylfluorenes) show a sharp peak with $\lambda_{\max} \sim 385\text{--}390\text{ nm}$ (3.2 eV) of $\pi\text{--}\pi^*$ electronic transition. Thin solid films (spin coated from 15 to 20 mg/ml solutions) reveal similar absorption with a slightly red-shifted ($\sim 10\text{ nm}$) and relatively broader peak (due to intermolecular interaction) (Figure 2.9) [246].

The PL spectra of the PFs show well-resolved structural features with maxima at 420, 445, and 475 nm assigned to the 0–0, 0–1, and 0–2 intrachain singlet transition, respectively (the 0–0 transition, the most intense) [247]. Due to the tail emission spectrum of PFs, the thin films emit bright sky-blue light. The QE of the PFs is very high, typically in the range of 40 to 80% and, as shown for PFO **196**, it depends substantially on the morphology of the polymer [248].

The effective conjugation length, estimated by Klaerner and Miller [249] for PDHF **195** from the absorption maxima of a series of monodisperse oligofluorenes (isolated from the mixture of oligomers by HPLC) is ca. 11.8 fluorene units (Figure 2.10) and similar conjugation length of 9–10 fluorene units was deduced by Tagawa and coworkers [250] from optical band gaps (i.e., red-edge of absorbance) in oligo(9,9-dihexylfluorenes) ($n = 1\text{--}5$). Similar estimation of the conjugation length for **197** ($\lambda_{\max} = 383\text{ nm}$) from the linear dependence of $1/\lambda_{\max}$ vs. $1/n$ for oligomers with $n = 2\text{--}7$ gave the conjugation length of 14 repeat units [251].

The band gap, determined as the onset of the absorption band in thin films is 2.95 eV (425 nm). Janietz et al. [252] used the onset of the redox waves in CV experiments to estimate the I_P and E_A energies of the dialkyl-PFs (Figure 2.11). The gap between the obtained energy levels (5.8 eV for I_P and 2.12 eV for E_A) $I_P - E_A \sim 3.8\text{ eV}$ is substantially higher than the optical band gap. Although optical absorption and electrochemistry test two physically different processes (vertical electron excitation and adiabatic ionization) and are not expected to be the same,

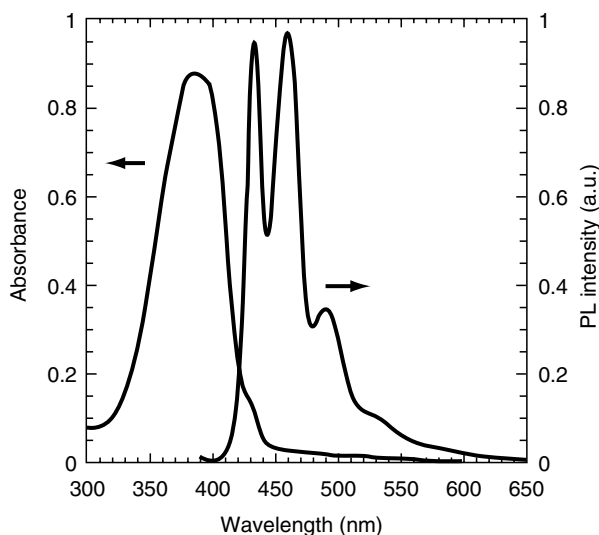


FIGURE 2.9 Typical absorption and emission spectra of polyfluorene in thin films (shown for poly(9,9-dioctylfluorene) **196**). (From Gong, X., Iyer, P.K., Moses, D., Bazan, G.C., Heeger, A.J., and Xiao, S.S., *Adv. Funct. Mater.*, 13, 325, 2003. With permission.)

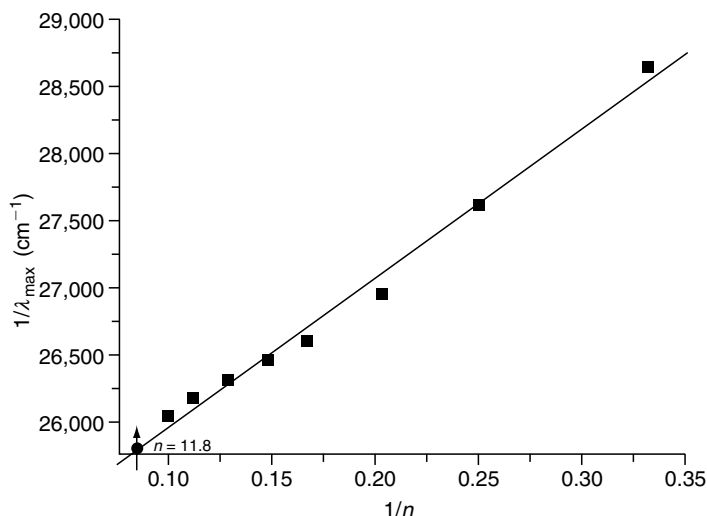


FIGURE 2.10 Plot of $1/\lambda_{\max}$ vs. $1/n$ for oligo(9,9-dihexylfluorenes) **195** in THF (n is the number of fluorene units); • is for the polymer with a degree of polymerization of 54, the absorption maximum of which (388 nm) corresponds to effective conjugation length $n = 11.8$. (From Klaerner, G. and Miller, R.D., *Macromolecules*, 31, 2007, 1998. With permission.)

very good agreement between the methods have been documented, particularly, for conjugated polymer systems. On the other hand, the I_P/E_A values derived from the electrochemical measurements in films should be taken with great caution, since they are often obtained under nonthermodynamic conditions (irreversible or quasireversible redox process) and may include a very significant kinetic factor, due to structural rearrangements and counterion diffusion. This is confirmed by comparison of the redox potential of PF in thin films and in solution, where the solution experiments gave significantly lower band gap, similar to the optical band gap [253].

The ultraviolet and x-ray photoelectron spectroscopy (UPS and XPS) measurements are used to calculate I_P of PFO at -5.6 ± 0.05 eV, and the band gap at 3.1 ± 0.1 eV, which is also much closer to the optical band gap than to the value deduced from the electrochemistry in films [254]. Thus, the HOMO–LUMO levels of PF can be reasonably well-matched by work functions of ITO/PEDOT (-5.1 eV) and Ca electrode (ca. -2.9 eV), respectively. However,

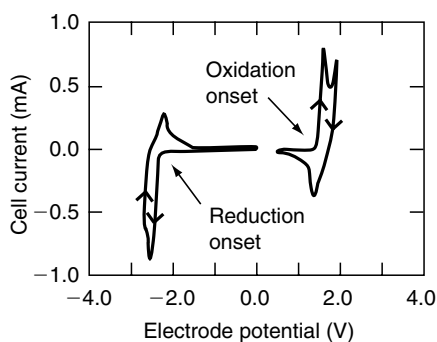


FIGURE 2.11 Cyclic voltammetry of PFO **196** in thin film (potentials vs. Ag/AgCl). (From Janietz, S., Bradley, D.D.C., Grell, M., Giebeler, C., Inbasekaran, M., and Woo, E.P., *Appl. Phys. Lett.*, 73, 2453, 1998. With permission.)

as shown by Lee and coworkers [255], the energy levels of PF can be shifted significantly in contact with active metals such as Ca, and should be taken with caution. It was also shown that an initial nonohmic PEDOT/PFO **196** contact in ITO/PEDOT/PFO/Al device can be made locally ohmic by electrical conditioning of the device at voltages higher than the EL onset voltage [256,257]. Ohmic injection of holes was also observed from plasma-cleaned ITO electrode or ITO electrode coated with PEDOT (for fluorene–triarylamine copolymer **249**) [258]. The possibility of tuning the HOMO–LUMO energy levels in PF is very important. Besides affecting the emission color, it facilitates the hole–electron injection (and also mobility) by matching the work functions of the electrodes, and thus improves the device performance.

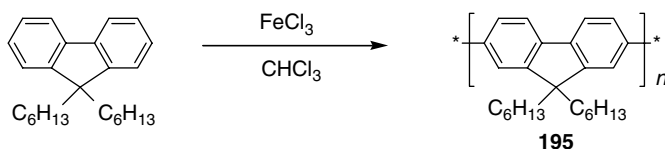
Beside the excellent optical properties and suitable HOMO–LUMO energy levels, the PFs possess great charge-transport properties. Time-of-flight (TOF) measurements of PFO showed nondispersive hole transport with a room temperature mobility of holes of $\mu_+ = 4 \times 10^{-4} \text{ cm}^2/(\text{V s})$ at a field of $E = 5 \times 10^5 \text{ V/cm}$ that is about one order of magnitude higher than that in PPV [259]. The polymer revealed only a weak-field dependence of the mobility, from $\mu_+ = 3 \times 10^{-4} \text{ cm}^2/(\text{V s})$ at $E = 4 \times 10^4 \text{ V/cm}$ to $\mu_+ = 4.2 \times 10^{-4} \text{ cm}^2/(\text{V s})$ at $E = 8 \times 10^5 \text{ V/cm}$.

Because of the great importance of PF as a class of conjugated polymers with excellent optical and electronic properties, several theoretical studies were performed to better understand the electronic structure and the photophysical processes, which occur in these materials [260–265].

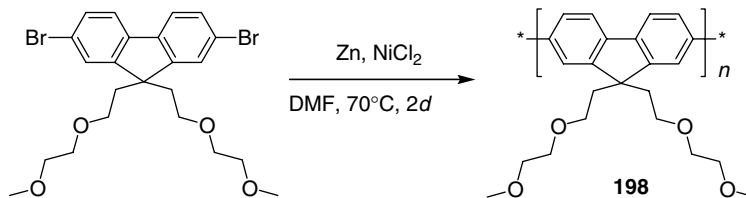
2.3.3 GENERAL METHODS IN SYNTHESIS OF POLYFLUORENE HOMOPOLYMERS

Parent (unsubstituted) PF was first synthesized electrochemically by anodic oxidation of fluorene in 1985 [266] and electrochemical polymerization of various 9-substituted fluorenes was studied in detail later [220,267]. Cyclic voltammogram of fluorene ($E_{\text{red}}^1 = 1.33 \text{ V}$, $E_{\text{ox}}^2 = 1.75 \text{ V}$ vs. Ag/Ag^+ in acetonitrile [267]) with repetitive scanning between 0 and 1.35 V showed the growth of electroactive PF film on the electrode with an onset of the p-doping process at $\sim 0.5 \text{ V}$ (vs. Ag/Ag^+). The unsubstituted PF was an insoluble and infusible material and was only studied as a possible material for modification of electrochemical electrodes. For this reason, it is of little interest for electronic or optical applications, limiting the discussion below to the chemically prepared 9-substituted PFs.

The first synthesis of poly(9,9-dialkylfluorene) with long-chain solubilizing hexyl groups (**195**) was carried out by Yoshino's group via an oxidative coupling reaction using ferric chloride in chloroform (Scheme 2.22) [268,269]. This resulted in polymers with relatively low molecular weights (M_n up to 5000). The regioregularity of the polymerization process in these conditions was rather poor due to nonregiospecific oxidation reactions resulting in some degree of branching and nonconjugative linkages through the positions other than 2 and 7. Some evidences of irregular coupling along the backbone were shown by NMR of soluble low molecular-weight fractions [247]. The PLED fabricated using this material gave relatively low QE, and in spite of a well-resolved vibronic structure of the PL band, the EL emission showed



SCHEME 2.22 Oxidative coupling synthesis of poly(9,9-dihexyl)fluorene **195**. (From Fukuda, M., Sawada, K., and Yoshino, K., *Jpn. J. Appl. Phys., Pt. 2 — Letters*, 28, L1433, 1989.)



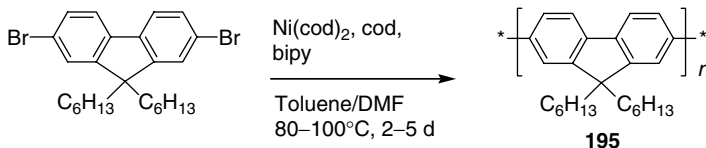
SCHEME 2.23 First Yamamoto synthesis of poly[9,9-*bis*(3,6-dioxaheptyl)fluorene]. (From Pei, Q. and Yang, Y., *J. Am. Chem. Soc.*, 118, 7416, 1996.)

a very broad band (maximum at 470 nm) [270]. A serious drawback of this synthetic method was also a significant amount of residual metal impurities, which dramatically affected the PLED performance.

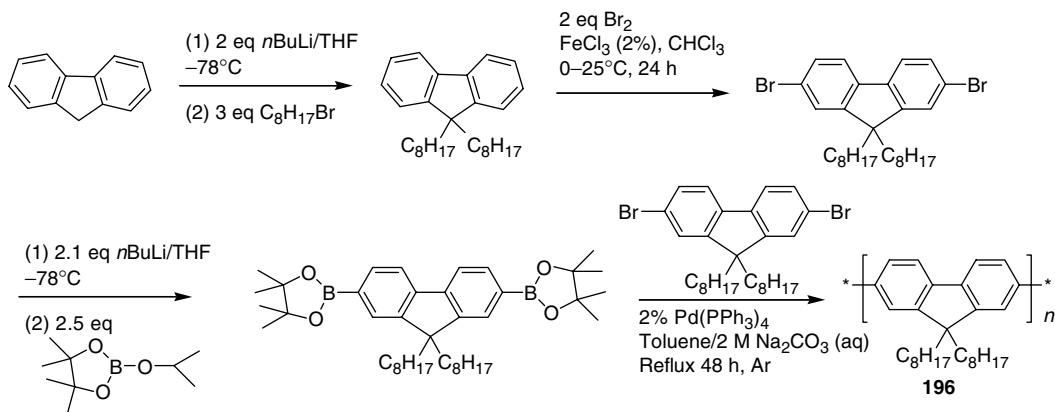
The next step toward soluble PF as materials for PLEDs, was an application of Yamamoto synthesis to polymerize various 2,9-dihalo-9,9- R^1, R^2 -fluorenes. Pei and Yang [271] at UNIAX Corporation first reported a reductive polymerization of 9,9-*bis*(3,6-dioxaheptyl)-fluorene in DMF using zinc as a reductant and reactive Ni(0) as a catalyst (generated from $NiCl_2$ salt), resulting in high molecular-weight PF **198** ($M_n = 94,000$ vs. polystyrene standard, $PDI = 2.3$), (Scheme 2.23). However, a patent application from Dow Chemicals Co., describing polymerization of various 9,9-disubstituted 2,7-dihalo fluorenes, Br or Cl as halogen, by the same Yamamoto synthesis in similar conditions was filed almost a year before that in July 1995 [272]. Later on, numerous patents from UNIAX [273,274] and Dow Chemicals [275–278] described the preparation of various PF by Yamamoto synthesis.

Although Ni-catalyzed reaction allowed improvement of the regiospecificity and minimization of cross-linking and mislinking reactions [247] compared to $FeCl_3$ oxidation method, it employs a large amount of metals (Ni, Zn) during the synthesis and the resulting polymer should be carefully purified to remove the metal impurities. In addition, because of the nonpolar hydrophobic nature of poly(9,9-dialkyfluorenes), the polymer chain growth in polar solvents (DMF or *N,N*-dimethylacetamide (DMA), which are used in Zn/ $NiCl_2$ reductive polymerization, is terminated by polymer precipitation from the reaction mixture, limiting the molecular weight. Thus, whereas relatively high molecular weight $M_n = 94,000$ can be achieved for PF **198**, containing hydrophilic 3,6-dioxaheptyl substituents, in cases of various alkyl substituents, the molecular weights are limited to $M_n \sim 14,000$ –60,000 [272–275].

Another example of Yamamoto-type polycondensation [279] was demonstrated by Miller and coworkers [249,280], who performed coupling of corresponding 2,7-dibromofluorenes using $Ni(cod)_2$ /cyclooctadiene/2,2'-bipyridyl in a toluene-DMF solvent mixture (Scheme 2.24). This method allows preparation of PFs with very high molecular weight M_n up to 250,000 (i.e., up to ~ 500 fluorene units) [281], and Scherf and List [225] noted that on the lab scale, the usage of $Ni(cod)_2$ as reductive transition metal-based coupling agent is very convenient.



SCHEME 2.24 Synthesis of PF by Yamamoto coupling with $Ni(cod)_2$. (From Klaerner, G. and Miller, R.D., *Macromolecules*, 31, 2007, 1998; Kreyenschmidt, M., Klaerner, G., Fuhrer, T., Ashenhurst, J., Karg, S., Chen, W.D., Lee, V.Y., Scott, J.C., and Miller, R.D., *Macromolecules*, 31, 1099, 1998.)



SCHEME 2.25 Synthesis of PF via Suzuki-coupling reaction. (From Ranger, M. and Leclerc, M., *Chem. Commun.*, 1597, 1997.)

Suzuki-coupling synthesis of PF, first reported by Leclerc and coworkers [282,283], could minimize the problem of metal impurities by employing catalytic amount of $\text{Pd}(\text{PPh}_3)_4$ (Scheme 2.25), and the use of a phase transfer catalyst gives higher molecular weights ($M_n \sim 50,000$ instead of 15,000) [282–284]. Although the molecular weights of PF achieved by Yamamoto coupling with $\text{Ni}(\text{cod})_2$ (up to $M_n \sim 100,000$ –200,000) are higher than those obtained by Suzuki coupling (ca. several 10,000 Da), reaching such high molecular weights is controlled not only by the method of the coupling but mainly by careful purification of the monomers and by optimization of the reaction conditions, as well as by the solubility of the polymer in the reaction mixture (determined by substituents on the fluorene nucleus).

Researchers at Dow Chemicals filed a patent, describing the preparation of a wide range of homo- and copolymers of a series of dialkylfluorenes by Suzuki- and Yamamoto-coupling polymerization [276]. Simultaneously and independently, an improved technological procedure for Suzuki coupling polymerization of dialkylfluorenes was also reported by Cambridge Display Technology (CDT) [285].

2.3.4 THE PROBLEM OF PURE BLUE EMISSION IN POLYFLUORENES: EXCIMER AND AGGREGATE FORMATION OR FLUORENONE DEFECTS?

The major problem in the application of PFs in blue PLEDs is color instability. As will be discussed below, the pure blue emission of PFs can be contaminated by the undesired contribution of a green emission band (at ca. 530 nm) upon thermal annealing of the polymer film or during the device operation. The initial hypotheses explained this phenomenon by formation of aggregates [286] or excimers [287–292], which act as energy or charge traps and emit in the long wavelength region. Indeed, the green emission increased during the thermal annealing and was not observed in polymer solution. This hypothesis has borne a tremendous amount of synthetic research activities based on the introduction of bulky substituents in the PF side chain or bulky fragments in the backbone of the polymer to prevent the formation of the excimers. Such modifications resulted, in some cases, in stabilization of blue emission that was, in turn, classified as confirmation of the hypothesis of excimeric nature of green emission in PF.

More recently, it was shown by List et al. [293–296] and later by Moses et al. [246] that the green emission of the PFs is due to fluoren-9-one defects in the polymer chain. This was confirmed by comparison of PL films annealed in an inert atmosphere and in air: a progressive additional band in the green region was observed on annealing in air (Figure 2.12) [246].

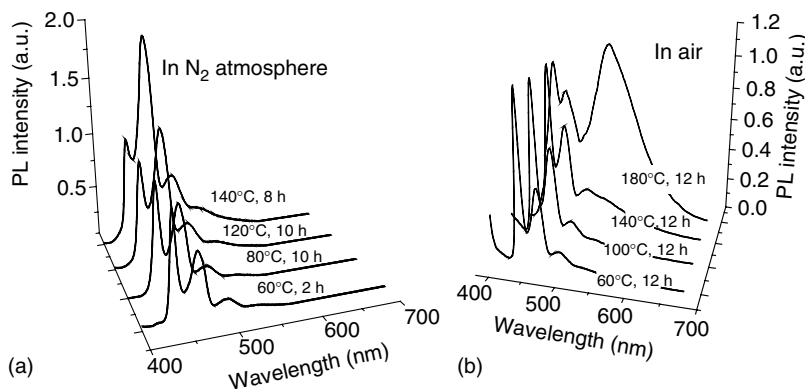


FIGURE 2.12 PL spectra of PFO **196** films after annealing at different temperatures: (a) in a nitrogen atmosphere, and (b) in air. (From Gong, X., Iyer, P.K., Moses, D., Bazan, G.C., Heeger, A.J., and Xiao, S.S., *Adv. Funct. Mater.*, 13, 325, 2003. With permission.)

A similar increase in the green PL peak was observed on photooxidation of the dialkyl-PF **199** film (Figure 2.13) [293]. Infrared (IR) spectra also indicate an appearance of fluorenone C=O peak on photooxidation [246,293] and the same peak in the green region appears in the EL spectra during the device operation.

The defects can be either introduced during synthesis or caused by photooxidation during the device preparation and operation. Moreover, the intensity of long wavelength emission is increased in the EL spectrum due to the fact that more electron-deficient fluorenone units can act as electron traps, increasing the probability of electron-hole recombination on the fluorenone defects. It was shown that less than 1% of the fluorenone defects can almost completely quench the blue fluorescence of the PF, transferring the excitation energy into the long wavelength region [297]. Importantly, as confirmed by theoretical calculations [262], the PF chain planarization and dense intermolecular packing facilitate energy transfer onto the fluorenone defects, which is much less efficient in solutions [265]. This explains the partial

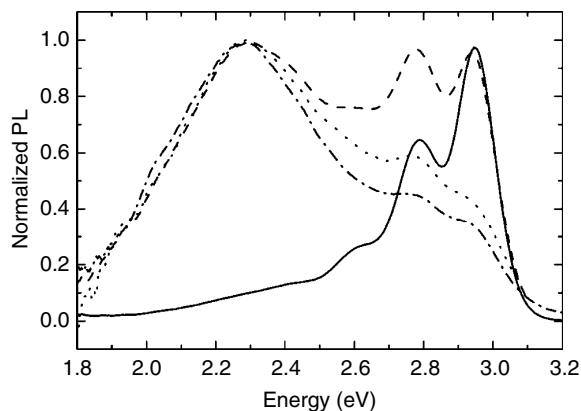


FIGURE 2.13 PL emission spectra of a pristine PF **199** film (solid line), and after photooxidation with a 1000 W xenon lamp under air for 2 min (dashed line), 4 min (dotted line), and 6 min (dashed-dotted line). (From List, E.J.W., Guentner, R., de Freitas, P.S., and Scherf, U., *Adv. Mater.*, 14, 374, 2002. With permission.)

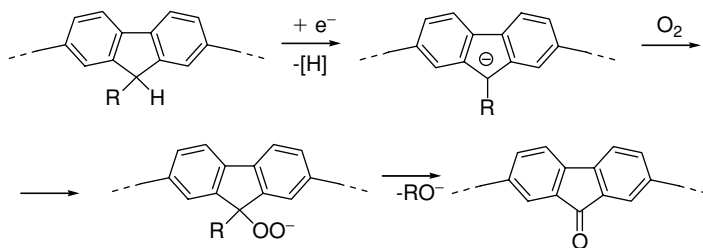
success of the strategy of introducing the bulky substituents, which hinders the energy transfer onto fluorenone defect sites.

Zhao et al. [298] compared the PL, photoexcitation, GPC, and Fourier transform infrared (FTIR) spectra of silsesquioxane end-capped poly(9,9-dioctylfluorene) in films and solution, before and after annealing. They found that air annealing of PF renders ~80% of the film insoluble, with stronger green emission from the insoluble part of the film. The soluble part of the film, showing negligible green emission in solution, develops the green band after recasting (though with twice lower intensity compared to the insoluble part). Some FTIR features led authors to believe that air annealing also results in β -hydrogen elimination in alkyl chains affording C=C alkene fragments. The latter can be responsible for the observed cross-linking rendering the annealed films insoluble and facilitating the interchain quenching. Another very detailed study of the origin of green emission was performed by Bradley and coworkers [299]. They agreed with List et al. on importance of fluorenone defects for the green emission in PF, which, however, in their opinion, originates from fluorenone-based excimers rather than from monomeric fluorenone π - π^* transition. On the basis of comparative studies of matrix-isolated PF chains with nondiluted PF films, the kinetics of PL decay and the effects of molecular fluorenone additions, they concluded that the green emission band arises from fluorenone-based excimers. Whatever the case, it is clear that solid-state packing plays an important role in the appearance of the green band in PF films.

The polarized emission experiments on partially photooxidized aligned PF films indicate that the emission from the keto defects exhibits a somewhat smaller polarization ratio than the blue emission from the defect-free chains [263]. This observation was explained with the support of quantum mechanical calculations, which showed that the polarization of the fluorenone emission is influenced by local disorder [263].

Although the exact mechanism of the fluorenone formation is not known, it is believed that the monoalkylated fluorene moieties, present as impurities in poly(dialkylfluorenes), are the sites most sensitive to oxidation. The deprotonation of rather acidic C(9)-H protons by residue on Ni(0) catalyst, routinely used in polymerization or by metal (e.g., calcium) cathode in LED devices form a very reactive anion, which can easily react with oxygen to form peroxides (Scheme 2.26) [293]. The latter are unstable species and can decompose to give the fluorenone moiety. It should also be noted that the interaction of low work-function metals with films of conjugated polymers in PLED is a more complex phenomenon and the mechanisms of the quenching of PF luminescence by a calcium cathode was studied by Stoessel et al. [300].

Meijer and coworkers [301] recently demonstrated that the purity of the 9,9-dialkylfluorene monomer is of great importance for the stability of the resulting polymer **200**. They performed additional purification of the monomer by treatment with potassium *tert*-butoxide in THF (to deprotonate the monoalkylated by-product) followed by filtration through dried



SCHEME 2.26 The mechanism for the generation of keto-defect sites as proposed by List et al. (From List, E.J.W., Guentner, R., de Freitas, P.S., and Scherf, U., *Adv. Mater.*, 14, 374, 2002.)

alumina (twice). The material, obtained by polymerization of thus treated monomer showed significantly less-pronounced green emission, compared to the polymer obtained from unpurified monomer (Figure 2.14). Furthermore, the device operated for 60 h showed no change in the EL spectrum (Chart 2.46).

In this context, a recently proposed procedure for alkylation of 2,7-dibromofluorene by alkylbromides in *t*BuOK/THF is advantageous over the widely used alkylation in aqueous NaOH or KOH as it could directly result in more pure monomers with good yields (see Appendix) [302]. The reaction can be easily monitored by a color change (from yellow to pink) and it is also more convenient than alkylation using BuLi, due to the low cost and ease of handling. In contrast to BuLi, an excess of *t*BuOK can be used to ensure the complete alkylation.

On the other hand, the stability of the dialkylfluorene moiety to photo- and electrooxidation cannot be postulated as well. The n-doping of PF (chemically from Ca cathode, or

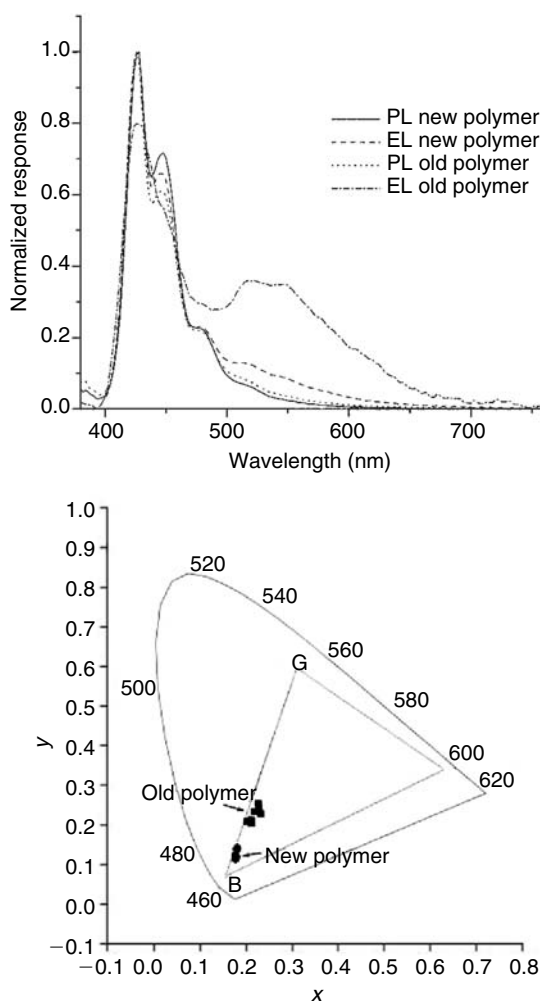


FIGURE 2.14 Electro- and photoluminescence (PL: excitation at 265 nm; EL: at 3.6 V (new polymer, i.e., obtained from purified monomer) and 4.0 V (old polymer, i.e., obtained from conventional monomer)) spectra of **200** (top) and CIE (1931) *x*-*y* color coordinates of old (squares) and new polymers (circles) from 4 to 6 V (bottom). (From Craig, M.R., de Kok, M.M., Hofstraat, J.W., Schenning, A.P.H.J., and Meijer, E.W., *J. Mater. Chem.*, 13, 2861, 2003. With permission.)

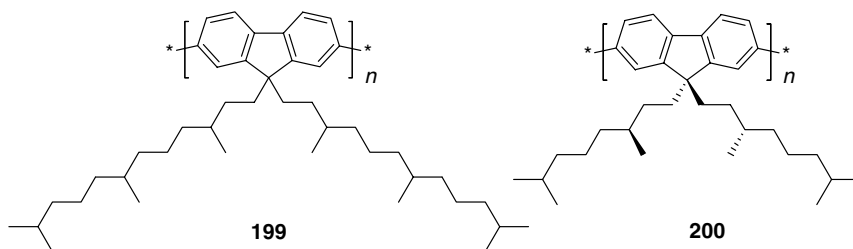


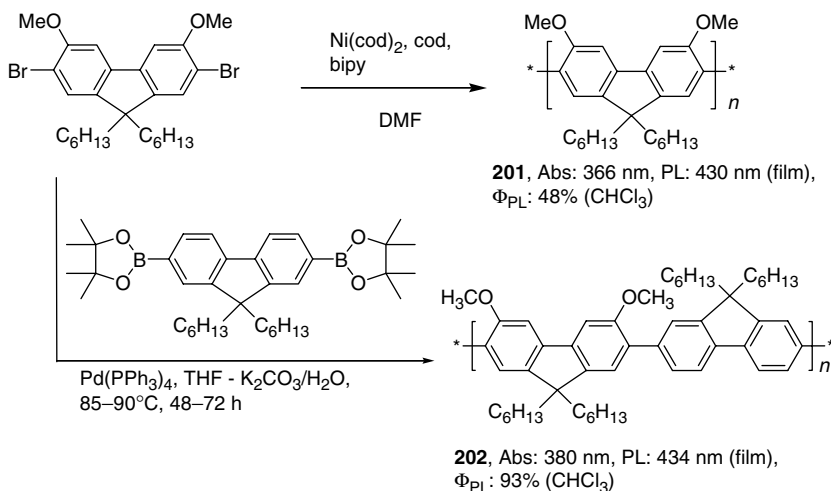
Chart 2.46

electrochemically during the device operation) forms radical anion species (see, e.g., theoretical studies of the effect of PF doping with Li atoms [260]), which are not expected to be stable toward oxygen. Thus, not only monomer and polymer purification, but also the device structure and operation should be optimized in order to achieve pure blue emission. In this line, Moses et al. [246] have shown that introducing a buffer layer between the PF and the cathode (Ca) layers block the metal diffusion in the polymer and inhibit fluorenone defect formation, which improves the color stability during the device operation.

The following sections will discuss the modifications of the chemical structure of PF through introduction of side-chain substituents and end-capping units, copolymerization with other conjugated units and polymer blends, aiming to achieve a pure blue LEP. After that, tuning of the emission color via the PF backbone and charge and energy transfer processes will be discussed.

2.3.5 AROMATIC RING-SUBSTITUTED POLYFLUORENES

Almost all modifications in PF homopolymers consist of variation of substituents at position 9 of the fluorene nucleus. Recently, Beaupré and Leclerc [303] reported a new synthetic strategy to polymers **201** and **202** with the aim to modulate the I_p of the PFs (for better injection of holes from the anode in LED) by introducing donor 3,6-dimethoxy substituents into the fluorene moiety (Scheme 2.27). The Φ_{PL} of polymer **201** is relatively low (48%), but it



SCHEME 2.27 Synthesis of PFs with 4,5-dimethoxy substituents in the fluorene rings. (From Beaupré, S. and Leclerc, M., *Macromolecules*, 36, 8986, 2003.)

can be increased to 93% by introducing a dihexylfluorene comonomer unit (copolymer **202**), which is probably due to partial release of the steric hindrances brought by 3,6-substituents.

2.3.6 SIDE-CHAIN MODIFICATIONS IN POLYFLUORENES

Many studies on side-chain modifications in PF were initially based on the idea of excimer formation, resulting in the green emission during LED operation or in solid-state PL on annealing PF films. This resulted in several proposed strategies for the design of fluorene side-chain homopolymers, where bulky substituents at position 9 of the fluorene moiety should sterically prevent (hinder) interchain interaction and thus improve the stability of blue emission.

The group of Miller [304] at IBM investigated the intensity of the long wavelength emission in 9,9-dialkyl-PFs with different length alkyl chains. Interestingly, differential scanning calorimetry (DSC) analysis reveals that while dihexyl-PF **195** is amorphous, dioctyl-PF **196** and even branched poly(9,9-*bis*(2-ethylhexyl)fluorene) **197** are crystalline. PL spectra of the polymer thin films show the appearance of a green emission band during thermal annealing (appearance of long wavelength emission), regardless of the crystallinity of the films, although the effect was somewhat less pronounced for polymers with larger substituents (**196** and **197**).

In addition to **195–200**, many other alkyl substituents and their derivatives have been introduced at position 9 of the fluorene nucleus in order to create a processible stable blue-emitting PF material, e.g., **203a–h** [273–275,305]. Chiral-substituted PFs **200** and **203g,h** have been synthesized to study their chiroptical properties [306], particularly interesting due to polarized emission in such materials (see Chapter 5 in this book) (Chart 2.47).

Patents of Dow Chemicals first described 9,9-diaryl-substituted PF homopolymers **204** and **205** by Yamamoto polymerization of the corresponding 2,7-dibromo monomers [272], although the methods for monomer preparation were not described. For unsubstituted fluorenone, a convenient method for its conversion into 9,9-(4-hydroxyphenyl)-[307–309] and 9,9-(4-alkoxyphenyl)fluorenes [310] was reported previously, which included condensation of fluorenone with phenol or its ethers in acidic conditions (dry HCl [308,309] or H₂SO₄ [307,311]) in the presence of β -mercaptopropionic or mercaptoacetic acids. Both polymers **204** and **205** showed similar $M_n \sim 21,000$ with PDI of 1.48 and 1.75, respectively, and spectral data typical for PF (**205**: $\lambda_{\text{abs}} = 389$ ($\epsilon = 50,000$ l/(mol cm)); $\lambda_{\text{PL}} = 417, 439$, and 473 nm (THF)) (Chart 2.48).

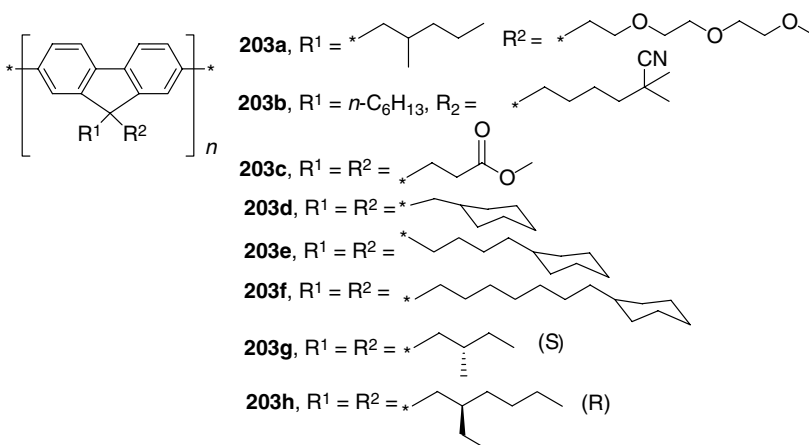


Chart 2.47

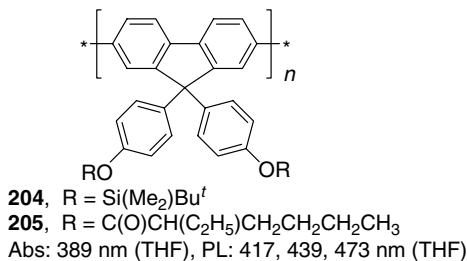
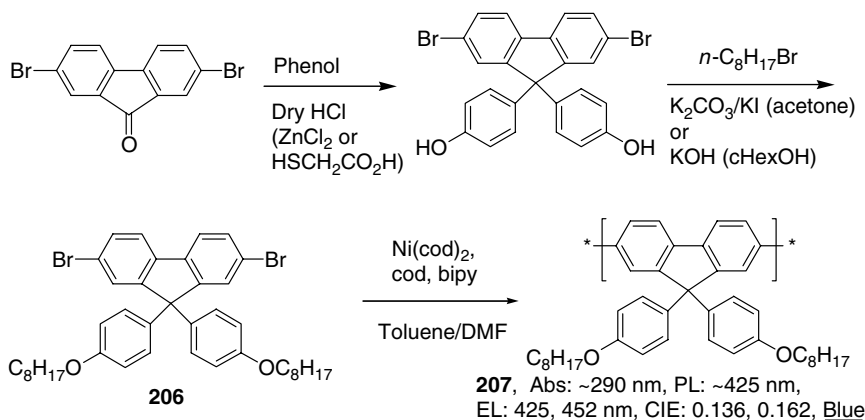


Chart 2.48

Polymer **207** obtained by Yamamoto polymerization of monomer **206** (Scheme 2.28) [311] showed bright-blue emission with PL maximum in a film at 430 nm. Its emission was found to be very stable toward thermal annealing. In contrast to poly(9,9-dialkyl)fluorenes [246], this polymer did not show the green component in the PL spectrum after annealing for 2 h at 180°C in air (Figure 2.15), and FTIR spectra also did not show a carbonyl peak after annealing, indicating good resistance of the polymer against oxidation [311]. The device ITO/PEDOT/**207**/Ca/Al showed a turn-on voltage of 3.7 V (~ 1 cd/m²), with a maximum brightness of 820 cd/m² and an EL efficiency of 0.03 cd/A (CIE: $x = 0.136$, $y = 0.162$). Similar increased stability of pure blue emission toward thermal annealing (compared to dialkyl-PF homopolymers) was also observed in random copolymers of monomer **206** with 2,7-dibromo-9,9-di(2-ethylhexyl)fluorene (absorption and PL spectra of which were very similar to those of homopolymers **207**). However, these showed somewhat lower values of luminous efficiency and maximum brightness, and slightly increased turn-on voltage [312].

Müllen's group [313] at Max-Planck Institute was the first to report using dendron substituents to sterically hinder the excimer formation, which delivers pure blue emission in substituted PF material. The dendron-containing monomer was obtained from 2,7-dibromofluorene in three elegant steps including (i) base-catalyzed alkylation of the fluorene methylene group, (ii) Pd(0)-mediated Hagihara–Sonogashira coupling introducing the acetylene functionality, and (iii) Diels–Alder cyclization producing the phenylene dendron (Scheme 2.29). The polymerization was achieved by Yamamoto coupling and the polymer chain was terminated by arylation with bromobenzene.



SCHEME 2.28 Synthesis of poly[9,9-di(4-octyloxyphenyl)fluorenes]. (From Lee, J.-H. and Hwang, D.-H., *Chem. Commun.*, 28, 2836, 2003.)

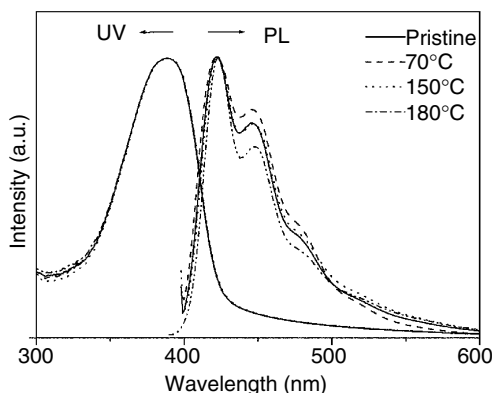
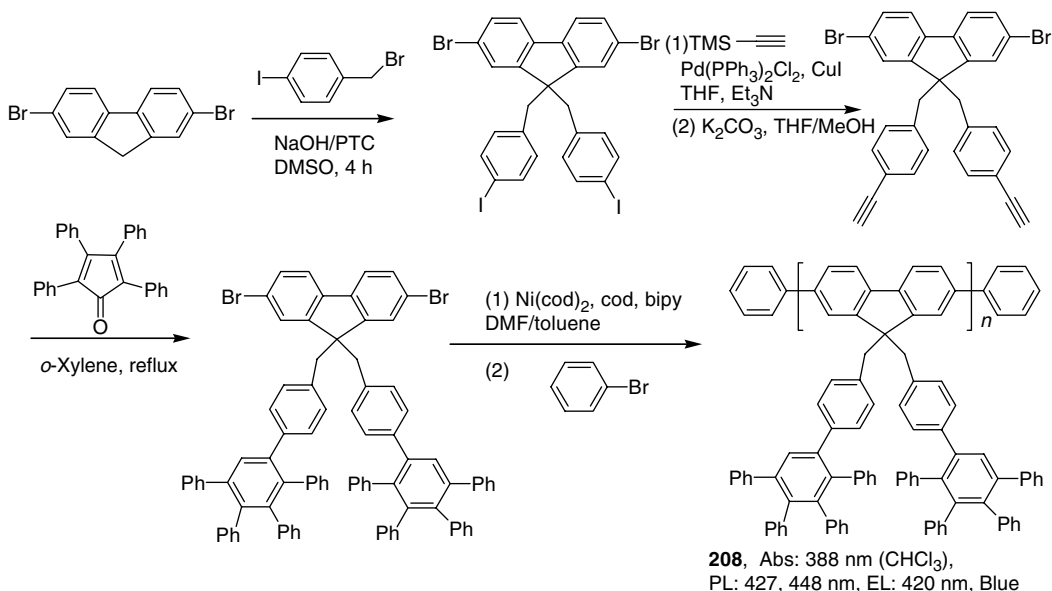


FIGURE 2.15 UV-vis absorption and PL emission spectra of film of **207** after thermal annealing for 2 h at different temperatures in air. (From Lee, J.-H. and Hwang, D.-H., *Chem. Commun.*, 21, 2836, 2003. With permission.)

The resulting polymer **208** is soluble in toluene, benzene, and chlorinated organic solvents and forms high-quality films. The molecular weight was determined by GPC analysis to be $M_n = 46,000$ g/mol (PDI = 3.6), which corresponds to ~ 40 repeat units. This polymer exhibits the same absorption and emission maxima as alkyl-substituted PFs, which implies that the bulky groups in position 9 do not alter the torsion angle of the conjugated backbone. Thin films of the oligophenylene-substituted PF emit pure blue color without any green emission tail, even after thermal annealing at 100°C for 1 day, confirming the impact of dendron substituents on suppression of the intermolecular aggregation. A PLED device fabricated in the structure of ITO/PEDOT/**208**/Ca/Al, gave a pure blue emission, and no green band



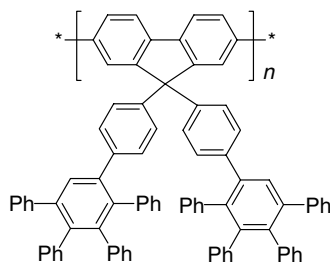
SCHEME 2.29 Synthesis of the phenylene-dendron-substituted PFs. (From Setayesh, S., Grimsdale, A.C., Weil, T., Enkelmann, V., Müllen, K., Meghdadi, F., List, E.J.W., and Leising, G., *J. Am. Chem. Soc.*, 123, 946, 2001.)

appeared at driving voltages up to 12 V. However, it was found that the device stability is relatively low due to photooxidation of the benzyl linkage group. This was improved by design of a modified polymer **209** having the phenylene dendron attached directly to the position 9 of PF, for which ITO/PEDOT/**209**/Ca/Al device showed blue emission (CIE: $x=0.189$, $y=0.237$) with a turn-on voltage of ~ 6 –7 V and a maximum efficiency of 0.06 lm/W at 7.8 V [314] (Chart 2.49).

A different type of a dendron was used by Carter's group at IBM. They demonstrated significant suppression of aggregation by inserting Fréchet-type ether dendrimer substituents at position 9 of PFs (Scheme 2.30) [315]. Due to their large size and flexibility, these substituents can act as encapsulators of the PF chain, hindering the aggregation and increasing the solubility.

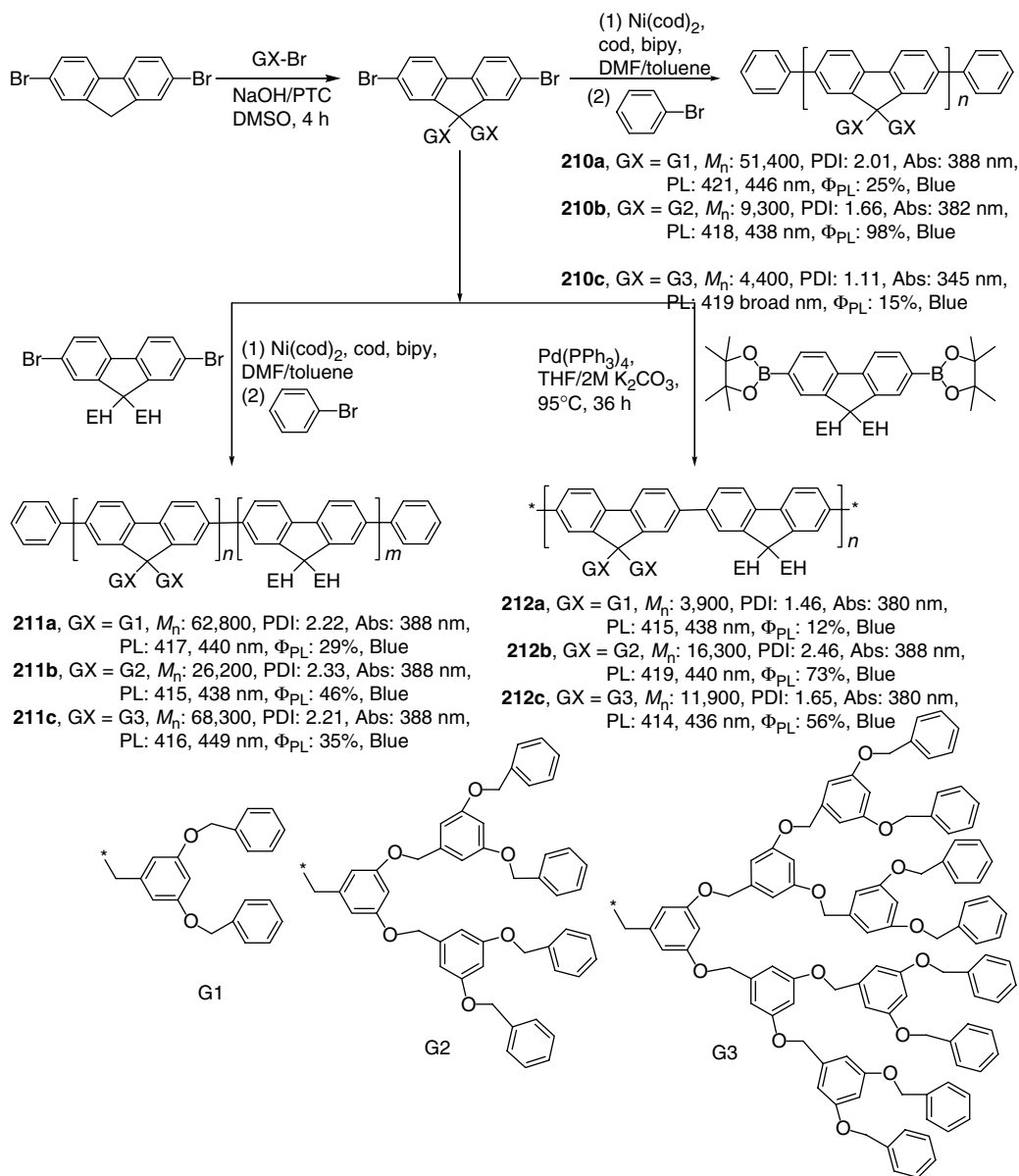
These PF dendrimers **210a–c** were synthesized by Yamamoto polymerization, followed by end capping with bromobenzene. A drastically decreased molecular weight (from $M_n=51,400$ g/mol for **210a** to 4400 g/mol for **210c**) and glass transition temperature (from $T_g=94^\circ\text{C}$ for **210a** to 10°C for **210c**) was observed. These polymers show a bright-blue fluorescence in both solution and solid state; spectral characteristics of **210a,b** are quite similar, whereas some blue shift is observed for **210c**. The polymer **210b** showed the highest QE close to 100% in both solution and in films, whereas **210a,c** displayed much weaker fluorescence (25 and 15%, respectively). Two types of fluorene copolymers, containing dendrimer substituents, have been prepared by Yamamoto (random end-capped polymers **211a–c**) and Suzuki-coupling polymerizations (alternating polymers **212a–c**). Some differences in properties of the two series of polymers were observed. For random polymers **211a–c**, the molecular weights ($M_n=26,200$ –68,300 g/mol) were generally higher than for alternating polymers **212a–c** ($M_n=3900$ –16,300 g/mol) and the less steric comonomer with a 2-ethylhexyl side chain allowed a high molecular weight to be achieved with the most bulky dendron **G3**, although the T_g (ranged from 48 to 78°C) for both series were similar (for given **GX**). Moreover, both absorption ($\lambda_{\text{abs}}=380$ –388 nm) and PL maxima ($\lambda_{\text{PL}}=414$ –419 and 436–440 nm) were also quite close. Again the highest PL QE was observed for second-generation dendron, containing polymers **211b** and **212b**. The results indicated that rather bulky dendron substituents (second or third generation) must be used in order to completely suppress the interchain interaction. Preliminary results show pure blue-light luminescence from PLEDs fabricated in configuration ITO/PEDOT/**210a–c**/Ca/Al, with driving voltage of 4.5–16 V (depending on the structure). However, nothing was reported on the stability of the devices, which is expected to be low due to possible (photo)oxidation of CH_2 group, as discussed above, and low T_g for the polymers.

A year later, Chou and Shu [316] reported Suzuki coupling of similar alternating fluorene copolymers containing Fréchet-type dendrimers as side chains. In contrast to the above



209, Abs: 385 nm (DCM),
PL: 422, 446 nm, CIE (0.189, 0.237), Blue

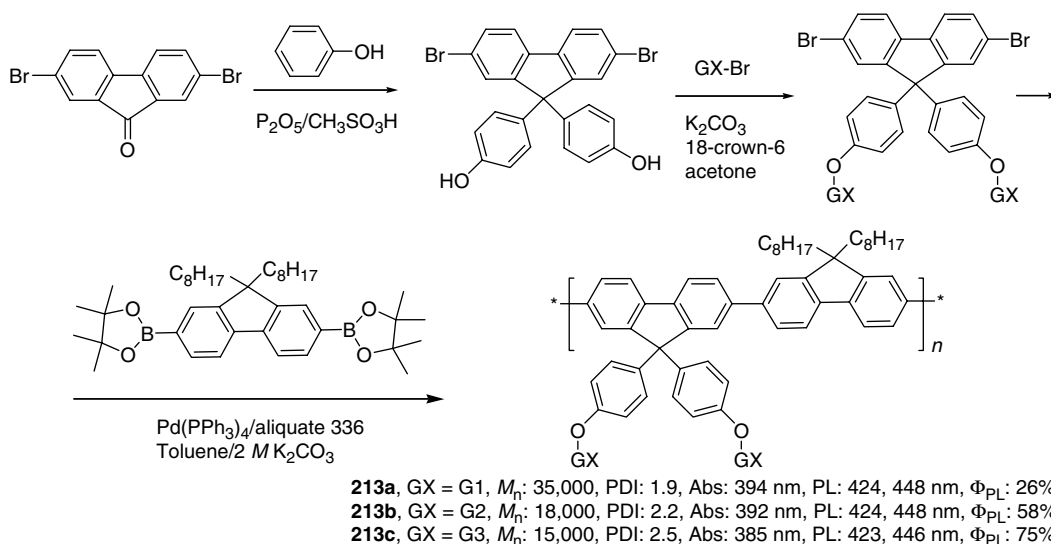
Chart 2.49



SCHEME 2.30 Synthesis of the Fréchet-type dendrimer-substituted PFs and fluorene random and alternating copolymers. (From Marsitzky, D., Vestberg, R., Blainey, P., Tang, B.T., Hawker, C.J., and Carter, K.R., *J. Am. Chem. Soc.*, 123, 6965, 2001.)

systems (Scheme 2.30) in polymers **213a–c**, the photooxidizable methylene group is separated from the photoactive PF chain by an additional phenylene moiety. The starting monomer was readily prepared from 2,7-dibromofluorenone by acid-catalyzed arylation with phenol, followed by Williamson alkylation of hydroxy groups (Scheme 2.31).

The highly branched dendronized PF copolymers are readily soluble in common organic solvents. All the three-generation copolymers showed high molecular weights of $M_n \approx$



SCHEME 2.31 Dendrimer-PF alternated copolymer synthesized by Suzuki coupling (same functional groups GX as in Scheme 2.30). (From Chou, C.-H. and Shu, C.-F., *Macromolecules*, 35, 9673, 2002.)

$1.5\text{--}3.5 \times 10^4$ g/mol with polydispersity in the range of 1.9–2.5 (by GPC analysis). The UV–vis spectra of **213a,b** in solution and in thin films showed the same spectra as dialkyl-PFs, but a somewhat hypsochromic shift was observed for **213c**. The result is the same as previously observed for the high generation dendronized PFs with a somewhat different degree of polymerization. The PL spectra of dendritic PFs **213a–c** exhibited the same emission maxima as PFO **196**. The emission spectra of annealed thin films follow the same trend as in homopolymers **210a–c**: the green emission is visible (though suppressed compared to PFO) for **213a**, but completely disappears starting from **213b**. Apart from a strong shielding effect, introduction of dendrimer side groups in PFs may also improve the thermal stability of the material, but no LED device performance was reported for these materials.

Recently, Bo and coworkers [317] reported on dendronized PF with carbazole end groups in the peripheral Fréchet-type dendrons **214a–c**. Polymers emitted blue light with high Φ_{PL} of 86–96% in solution for all three polymers **214a–c** (**G0–G2**). In the solid state, Φ_{PL} depended on the size of the attached dendron (29, 55, and 64% for **G0**, **G1**, and **G2**, respectively) (Chart 2.50).

Fujiki and coworkers [290] synthesized asymmetrically substituted PFs, bearing a bulky Fréchet-type dendron and a less bulky 3,6-dioxaoctyl group in position 9. The polymers **215–217** showed a pure blue PL emission with rather low green emission band (at 520 nm) for the films annealed at 200°C for 3 h (in vacuum) (Chart 2.51).

Furthermore, the green emission band for the films of asymmetric polymer **217** was much weaker than that of polymer **216** having two straight substituents, and even polymer **215**, having two bulky dendron substituents. The latter fact was attributed to the liquid crystalline properties of relatively well-defined polymer **215**, compared to more disordered asymmetrically substituted **217**. However, it can also be explained by the difficulties in complete dialkylation of fluorene with two bulky substituents (to completely convert the oxidizable C–H bonds). This makes the polymer vulnerable to oxidation and produces fluorenone-originated green emission band. The terminal end capping of polymers **215–217** with 9H-fluorene is likely to cause device instability. This is not seen during the annealing *in vacuo* (i.e., in the absence or at least very low concentration of oxygen), but is likely to show up during the operation of the PLED under atmospheric conditions.

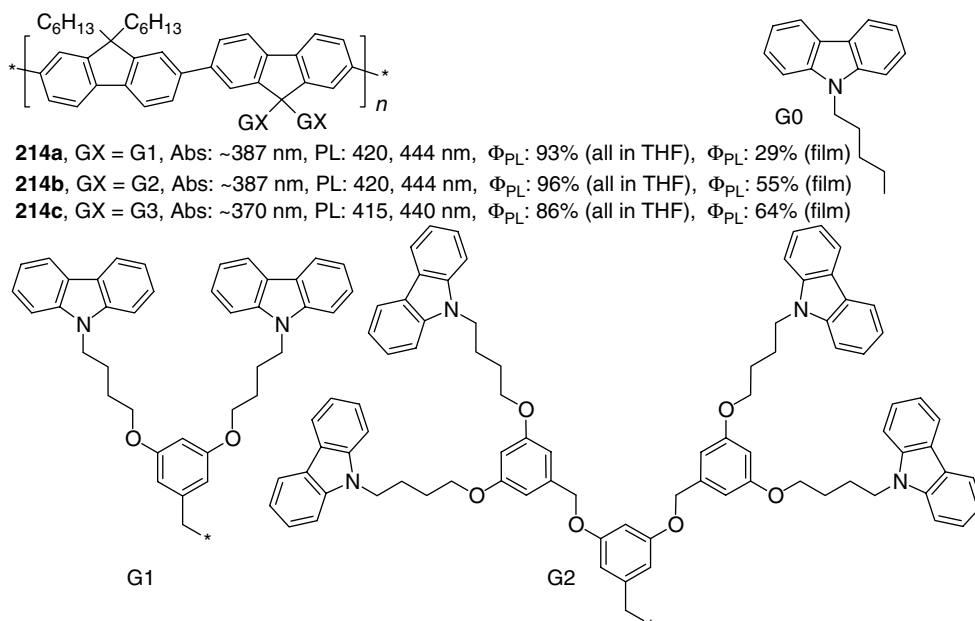


Chart 2.50

Kim and coworkers [318] reported PF derivatives **218** containing spiro-dihydroanthracene units in which the remote C-10 position of the anthracene moiety allows a facile substitution with alkyl groups for improving the solubility (Scheme 2.32). No clear phase transition, including T_g , up to T_{dec} ($T_{\text{dec}} = 367^\circ\text{C}$) was observed for this polymer. The polymer showed high spectral stability toward heat treatment, UV irradiation, and current (annealing at 200°C for 15 h did not show any signature of green band emission usually observed for poly(9,9-dialkylfluorenes) (Figure 2.16). The ITO/PEDOT/**218**/LiF/Ca/Ag device showed good color coordinates (CIE: $x = 0.17$, $y = 0.12$) and a maximum luminance of over 1600 cd/m^2 .

Another example of spiro-derivatized PF was demonstrated by Bo and coworkers [319], who synthesized soluble spiro-bifluorene-based polymer **219**. This polymer showed stable bright-blue PL ($\Phi_{\text{PL}} = 91\%$ in toluene), and showed no green emission in the annealed film (although no device preparation has been reported as yet) (Chart 2.52).

Shim and coworkers [320] synthesized cross-linked PF copolymers, containing siloxane bridges **221** and **222**. Ni-mediated copolymerization of 9,9-dihexyl-2,7-dibromofluorene in

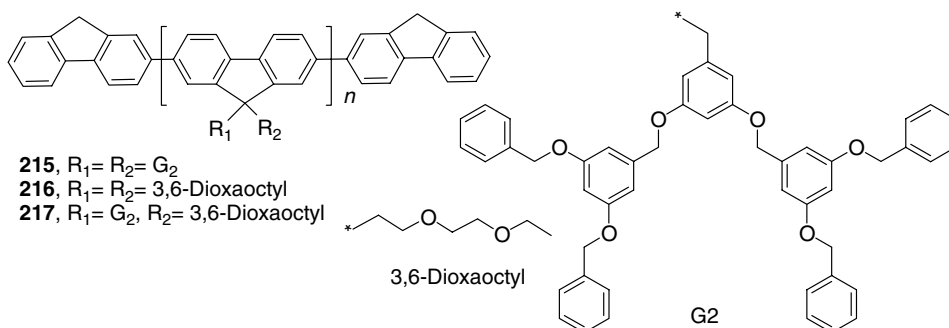
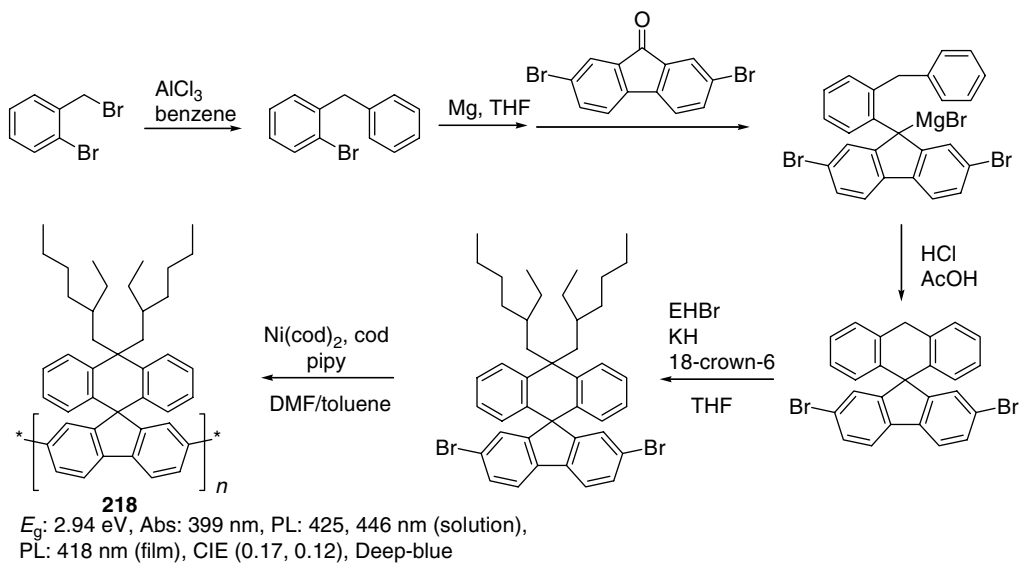


Chart 2.51



SCHEME 2.32 Synthesis of soluble spiro-anthracene-fluorene polymer. (From Vak, D., Chun, C., Lee, C.L., Kim, J.-J., and Kim, D.-Y., *J. Mater. Chem.*, 14, 1342, 2004.)

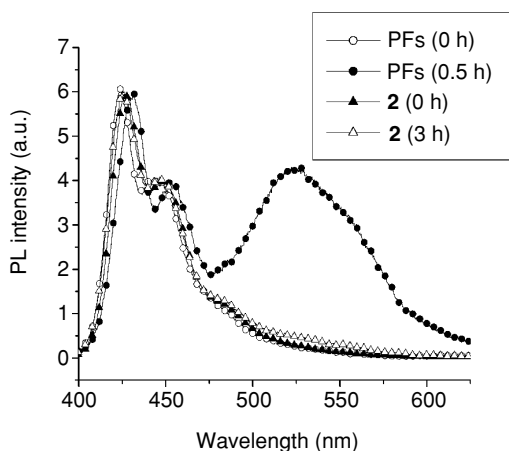
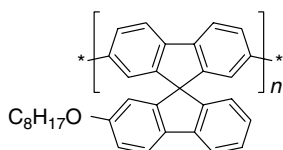


FIGURE 2.16 PL spectra of polymer **219** and poly(dialkylfluorene) (**2** and PFs in figure, respectively) in films before and after thermal annealing at 200°C for different times. (From Wu, Y., Li, J., Fu, Y., and Bo, Z., *Org. Lett.*, 6, 3485, 2004. With permission.)

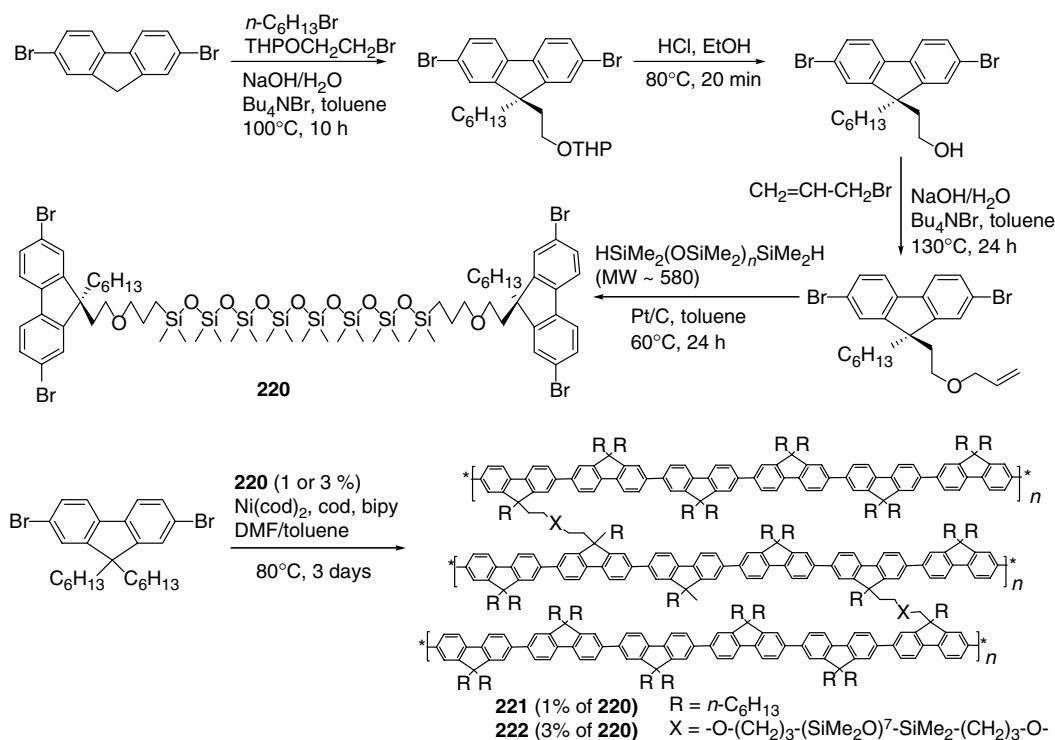


Abs: ~391 nm, PL: 416 nm, Φ_{PL} : 91% (toluene),
 PL: 427 nm (film), HOMO: -5.8 eV, LUMO: -2.9 eV, Blue

the presence of 1 or 3 mol% of bridged monomer **220** resulted in copolymers **221** and **222** in which PF backbones networked by siloxane chains (Scheme 2.33) [320]. Their electrochemical and spectral properties were close to that for PDHF **195**. On the other hand, the copolymers showed increased T_g values (106 and 110°C, respectively), compared to the parent PDHF **195** and almost pure blue emission, which is stable toward annealing (whereas full width at half-maximum (fwhm) for **195** after annealing of the film at 150°C for 4 h is increased to 85 nm, **221** and **222** showed an fwhm of only 52 and 51 nm, respectively) (Figure 2.17). Authors discussed these results in terms of hindered aggregation and excimer formation in such cross-linked PFs.

The approaches described above only dealt with structural modifications, improving the processability of the polymer and suppressing the undesirable aggregation tendency of PFs. For electronic applications, and particularly LEDs, even more important is balancing the charge-transport properties. For the best device performance, the transport of holes and electrons should be equalized without changing the HOMO–LUMO gap of PF (which determines the emission color). To achieve this, Scherf and coworkers [321] blended the light-emitting PF with triarylamine-based hole transport molecular compounds and demonstrated an increase of the device efficiency (up to 0.87 cd/A) and brightness (up to 800 cd/m²). Furthermore, a very substantial decrease of the green emission at 520 nm in these blends was observed.

However, a phase separation problem in the above two-component system may affect the device stability. To overcome the problem, Müllen and coworkers [322] introduced triphenylamine groups as side chains at the PF backbone. The triphenylamine substituents simultaneously improve the hole-transport properties of PF (facilitating the injection of holes),



SCHEME 2.33 Synthesis of cross-linked polyfluorenes with oligosiloxane bridge. (From Cho, H.-J., Jung, B.-J., Cho, N.S., Lee, J., and Shim, H.-K., *Macromolecules*, 36, 6704, 2003.)

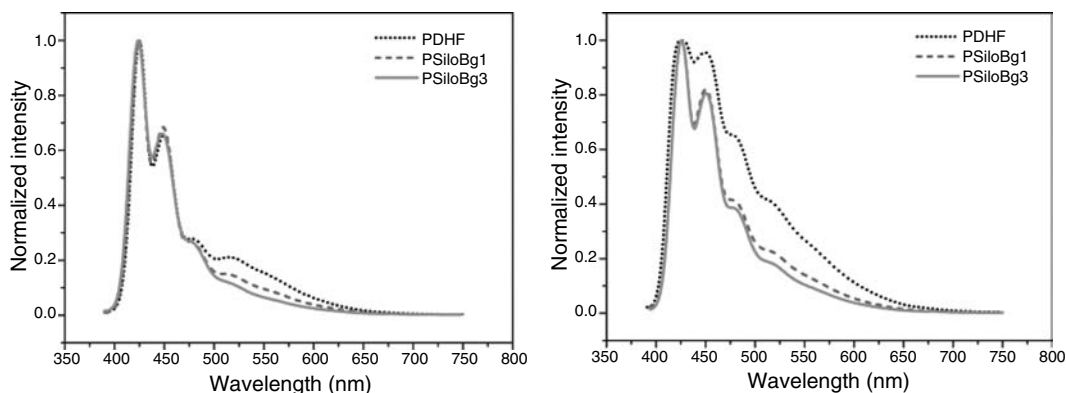
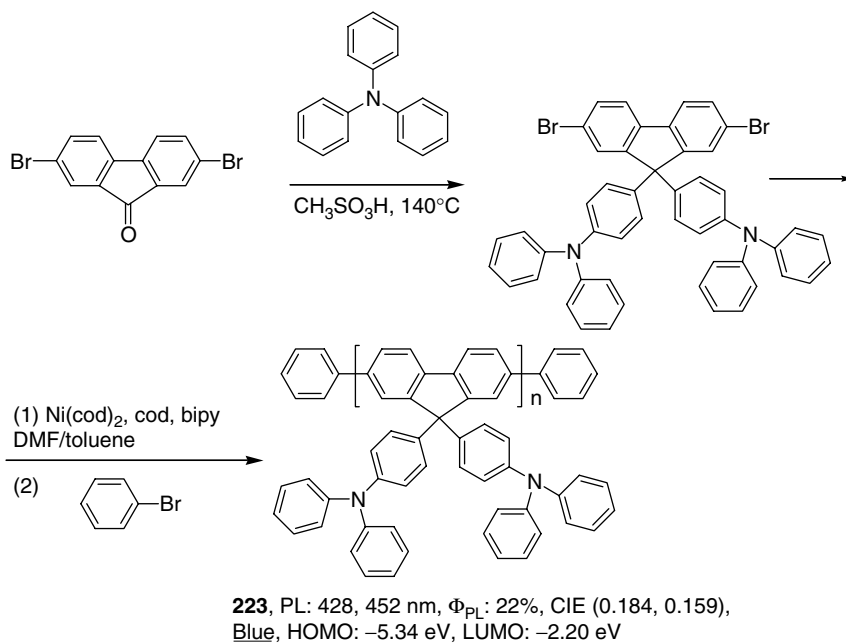


FIGURE 2.17 PL spectra of PDHF **195** (Homo PF), **221** (PsiloBg1), and **222** (PsiloBg3) as spin-coated films (1500 rpm, *p*-xylene) and annealed at 150°C for 30 min (left) and 4 h (right). (From Cho, H.-J., Jung, B.-J., Cho, N.S., Lee, J., and Shim, H.-K., *Macromolecules*, 36, 6704, 2003. With permission.)

prevent aggregate formation due to steric shielding effect, and bring high solubility to the material. Commercially available 2,7-dibromofluorenone was arylated with a large excess of triphenylamine in methanesulfonic acid followed by Yamamoto polymerization of the dibromo monomer. The polymer was end capped to give poly[9,9-*bis*(4-diphenylaminophenyl)-fluorene] **223** (Scheme 2.34). The obtained polymer has very good solubility in common organic solvents and has a polymerization degree of ca. 14 units in the chain ($M_n = 8860$, PDI = 1.76; GPC analysis against a polyphenylene standard). The polymer emits blue light in solution and in the solid state, with a QE of 22% in thin films, a value half of dialkyl-PF (~50% in the solid) [323], but the emission spectrum did not change after thermal annealing of the film.



SCHEME 2.34 Synthesis of triphenylamine-substituted PF. (From Ego, C., Grimsdale, A.C., Uckert, F., Yu, G., Srdanov, G., and Müllen, K., *Adv. Mater.*, 14, 809, 2002.)

The triarylamine groups in **223** improve the hole-transporting properties and reduce the diode turn-on voltage. A single-layer PLED ITO/PEDOT/**223**/Ba starts to emit blue light (CIE: $x = 0.184$, $y = 0.159$) at as low as 4 V (1 cd/m^2) and shows a maximum current efficiency of 0.67 cd/A (0.36 lm/W). The EL spectrum shows a nearly complete suppression of the green emission. The effect can be rationalized by a charge(hole)-trapping effect of the triarylamine moieties, which compete with electron trapping on the fluorenone defects, and minimize the emission from the defect sites. Introducing an additional HTL (PVK) allows a further improvement of the device performance: a maximum current efficiency of 1.05 cd/A was demonstrated by blue-emitting PLED ITO/PEDOT/PVK/**223**/Ba (CIE: $x = 0.19$, $y = 0.181$), although the maximum brightness demonstrated by both devices was relatively low (up to $200\text{--}300 \text{ cd/m}^2$).

Two PFs **224a,b** with 2,2'-bipyridyl side group were reported by Pei et al. [324]. In solution, both polymers show typical PF fluorescence (410, 436 nm), but in low polarity nonhydrogen bonding solvents, the hydroxy polymer **224a** has an additional weak emission at 500–650 nm. In solid films, this low-energy emission becomes dominant, which is not the case for alkylated polymer **224b**. This implies that the hydrogen bonding strengthens the intermolecular interactions in **224a**, changing the emission color from blue (in solutions) to yellow-orange (in films) (Chart 2.53).

2.3.7 END-CAPPED POLYFLUORENES

The very first and obvious reason for introducing the end groups, terminating the polymer chain, was to replace reactive functionalities (halogen, boronic acid, or metal-organic group), which can quench the fluorescence or decrease the stability of the material. Secondly, varying the feed ratio of the end-capping reagent, one can control the molecular weight of the polymer. Some examples of such utilization of the end-capping approach have been demonstrated in the previous section. The third important reason for end capping is tuning the optoelectronic properties of the polymer by electronically active end cappers. The most important examples of functional end-capped PFs, such as the hole transport or electron transport groups, dye moieties, and cross-linkable functionalities are given below.

The initial work introducing end-capping groups in PFs was reported by an IBM group [249]. They also systematically studied the stability of the polymers after end capping [288]. The end-capped polymers **225** and **226** have been synthesized by Yamamoto-coupling polymerization (Scheme 2.35). Comparison of the 9*H*-fluorene and 9,9-dihexylfluorene end-capped polymers unequivocally indicate higher color stability of the latter, which again confirms the fluorenone-based origin of the green band.

Miller and coworkers [325] reported using an anthracene end capper (which is twisted orthogonally in respect to the neighboring fluorene moiety) in PF **227** to enhance the color stability of PLEDs. However, the results show that the PLED fabricated with the anthracene

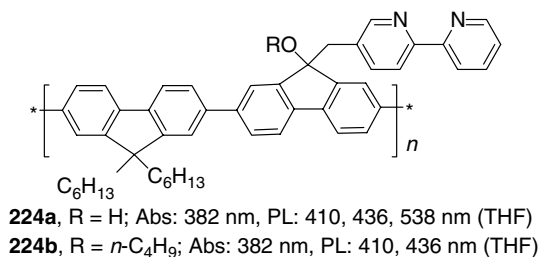
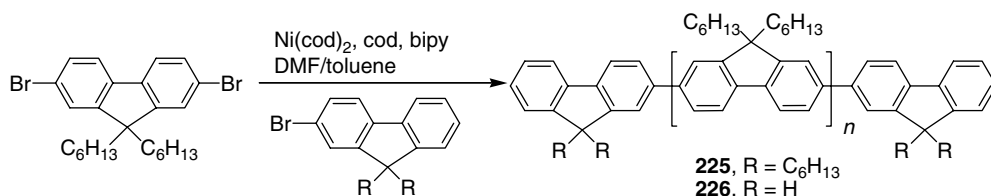


Chart 2.53



SCHEME 2.35 Synthesis of dihexyl-PF end capped with 2-fluorenyl groups. (From Klaerner, G. and Miller, R.D., *Macromolecules*, 31, 2007, 1998; Lee, J.-I., Klaerner, G., and Miller, R.D., *Chem. Mater.*, 11, 1083, 1999.)

end-capped polymer still suffer from the color instability (appearance of green emission band), unless the anthracene unit is also introduced as a comonomer (at 15% level) [288] (Chart 2.54).

A high-efficiency PLED with excellent color stability has been fabricated with PFs **228** and **229**, end capped with hole-transporting triarylamine moieties [253]. Rather high HOMO (-5.6 eV for **229** and -5.48 eV **228**) brought by triarylamine moieties facilitates the holes transport, although the authors claim that the current in devices ITO/PEDOT/polymer/Ca is still dominated by electron transport. The best performing material (maximum luminance of 1600 cd/m^2 at 8.5 V and EL efficiency of 1.1 cd/A) has been achieved at the feed ratio of the end capper (triarylamine) to the fluorene monomer of 4%. Compared with the nonend-capped polymer, the EL efficiency was increased by more than one order of magnitude without disturbing the electronic structure of the backbone. As in triarylamine-substituted PF **223**, the parasitic green emission in **228** and **229** was completely suppressed, giving pure blue color (CIE: $x = 0.15$, $y = 0.08$) at voltages above 4 V (Figure 2.18). This effect can be attributed to less effective electron-hole recombination on the green-emitting species (fluorenone defects) due to competing charge trapping on the hole-transporting units. A very high EL efficiency (up to 3 cd/A) can be obtained with polymer **228** in multistructured PLEDs, containing cross-linked HTL made of several triarylamine-based polymer layers with different HOMO levels [326] (Chart 2.55).

Very recently, Heeger's group [327] reported PF capping with a bulky polyhedral oligomeric silsesquioxane (POSS) group. The hybrid organic-inorganic polymers, containing POSS segments, have several advantages such as increased thermal stability and improved adhesion between the substrate and polymer layer. The molecular weight (M_w) of **230** (GPC vs. polystyrene) was as high as 10^5 g/mol . There is no essential difference in UV-vis and PL between **230** and PDHF **195**, but the PLED devices fabricated with the former showed increased $\Phi_{\text{EL}}^{\text{ex}}$ and somewhat improved blue color purity (which still suffered from residual green emission). Also, the silsesquioxane end-capped PF show much higher thermal stability (Chart 2.56).

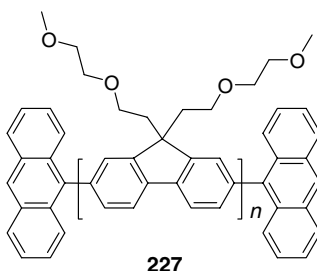


Chart 2.54

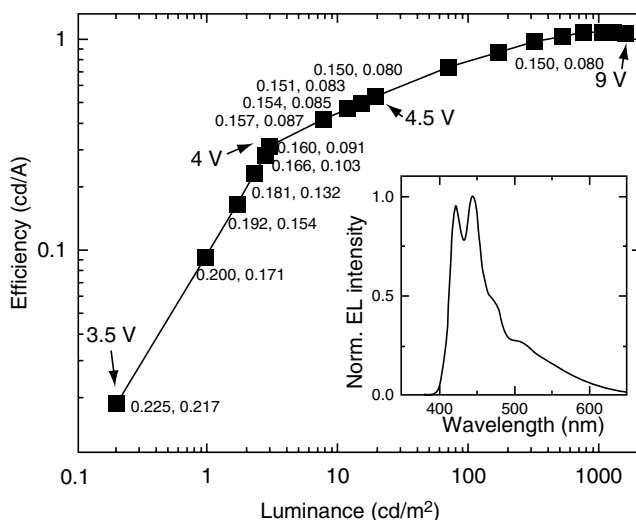


FIGURE 2.18 The efficiency–luminance plot for ITO/PEDOT/**228**/Ca device. The numbers along the curve are the CIE coordinates at the corresponding brightness levels. The insert shows the EL emission spectrum of a diode driven at 3.6 V. (From Miteva, T., Meisel, A., Knoll, W., Nothofer, H.G., Scherf, U., Müller, D.C., Meerholz, K., Yasuda, A., and Neher, D., *Adv. Mater.*, 13, 565, 2001. With permission.)

An interesting and important approach of using the end-capping styrene group for cross-linking the PF chains was reported by Miller and coworkers [328,329] (Scheme 2.36). The cross-linking during thermal annealing of the film renders an insoluble material **231**, which can be used as a substrate for spin casting the next layer in multilayer LEDs. In addition, cross-linking drastically increases the T_g temperature, thus suppressing the formation of aggregates and giving pure blue emission.

Styrene-containing polymer is completely soluble in common solvents such as CHCl_3 , THF, xylene, or chlorobenzene and can be spin cast as thin films that are easily cross-linked

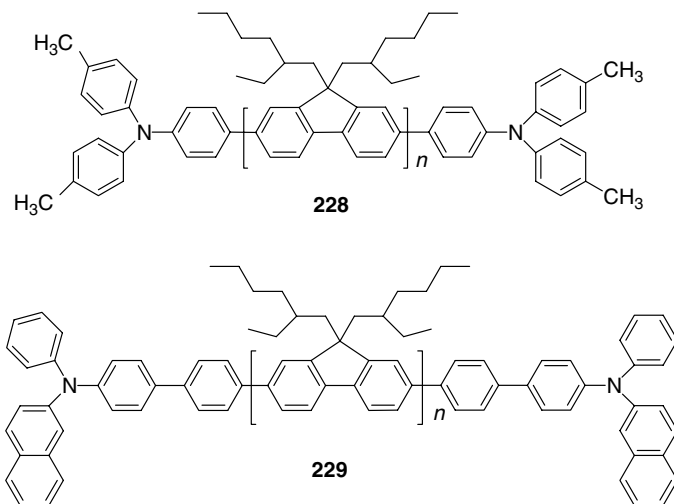


Chart 2.55

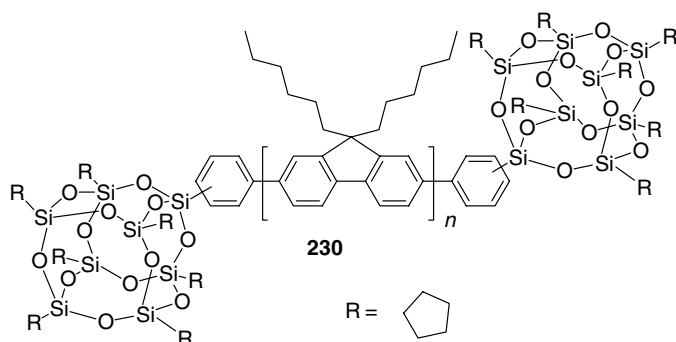
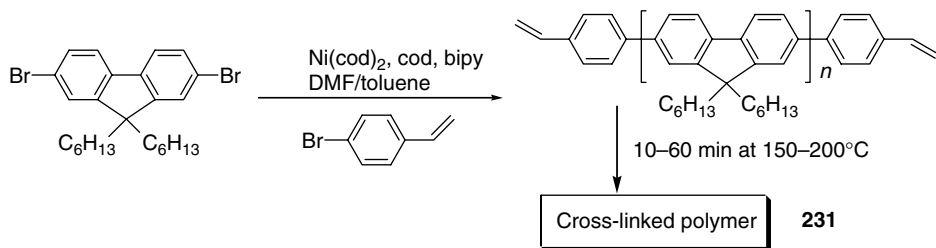


Chart 2.56

upon heating (as shown by FTIR spectroscopy) to deliver an insoluble material. A relatively high amount of cross-linkable units, however, is required to completely suppress the green emission band. It was achieved by adjusting the fluorene/styrene molar ratio from 85:15 to 67:33. The latter ratio delivered rather short polymer ($M_n = 3500$ g/mol, ca. 10 FI units in the chain), which upon cross-linking (200°C , 10 min), revealed no green band in either the PL or EL spectra. However, incorporating the cross-linkable units in the side chain of fluorene copolymers (in similar ratio) does not lead to complete suppression of green emission, although it does deliver an insoluble cross-linked polymer. The last finding suggests that an improved purity of the end-capped material (due to conversion of reactive chain ends), and not the aggregation suppression due to geometric constraints of cross-linked polymers, is responsible for the pure blue emission.

Some other PFs end capped with cross-linkable groups, such as benzocyclobutene, have been patented by Dow Chemicals [275–277]. For example, the thermal curing of spin-coated polymer **232** gave an insoluble pinhole-free film without alteration of the fluorescent properties (Chart 2.57).

End capping with hole-transporting triarylamine and electron-transporting oxadiazole moieties has been shown to tune the charge injection and transport, without altering the electronic properties of the semiconducting polymer. Comparative studies of polymers **233**, PFO **196** and **234** showed that the current density increased in the order of $234 < 196 < 233$ for “hole-only” devices and in the order of $233 < 196 < 234$ for “electron-only” devices (Figure 2.19) [330]. LEDs fabricated with these polymers reach their optimum efficiency whenever hole and electron densities are balanced [331]. Because the hole current measured in the “hole-only” devices was an order of magnitude larger than the electron current in the



SCHEME 2.36 Synthesis of cross-linked PF **231**. (From Klärner, G., Lee, J.-I., Lee, V.Y., Chan, E., Chen, J.-P., Nelson, A., Markiewicz, D., Siemens, R., Scott, J.C., and Miller, R.D., *Chem. Mater.*, 11, 1800, 1999.)

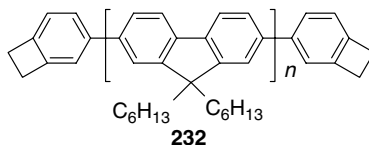


Chart 2.57

“electron-only” devices (Figure 2.19), improving the electron injection and transport should be more critical for the performance of a real “ambipolar” device. Devices fabricated with polymer **234** instead of PFO **196** demonstrated ca. 20% increase in brightness and luminance efficiency (Chart 2.58).

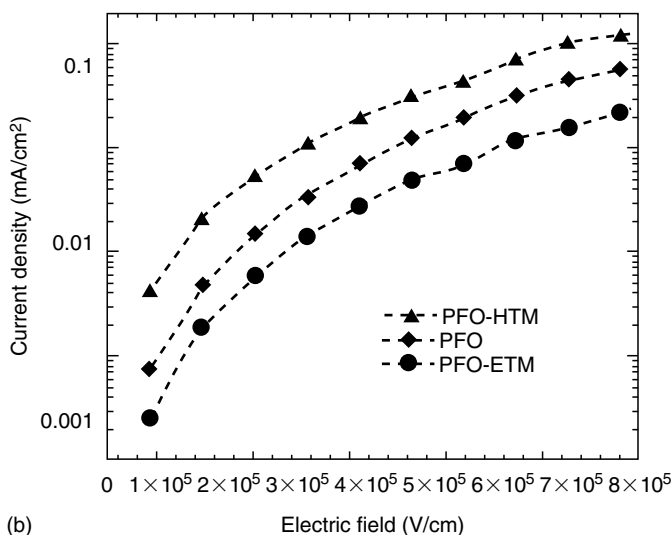
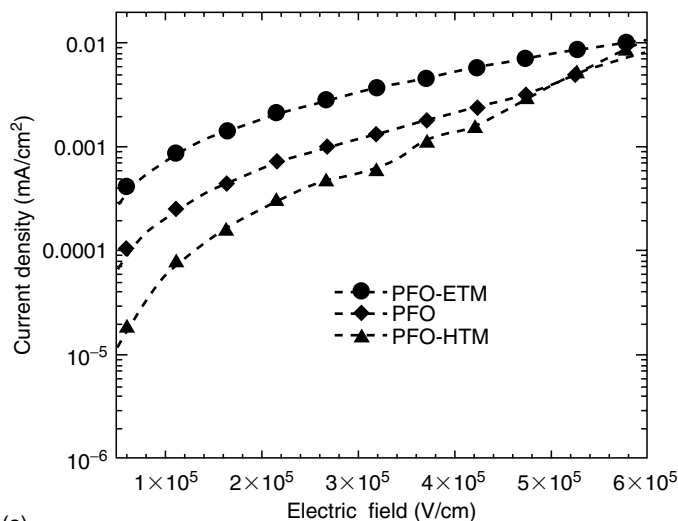


FIGURE 2.19 Current density vs. electric field for PLEDs based on **196** (PFO), **233** (PFO-HTM), and **234** (PFO-ETM). (a) “Electron-only” devices Yb/polymer/Ba/Al; (b) “hole-only” devices ITO/polymer/Au. (From Gong, X., Ma, W., Ostrowski, J.C., Bechgaard, K., Bazan, G.C., Heeger, A.J., Xiao, S., and Moses, D., *Adv. Funct. Mater.*, 14, 393, 2004. With permission.)

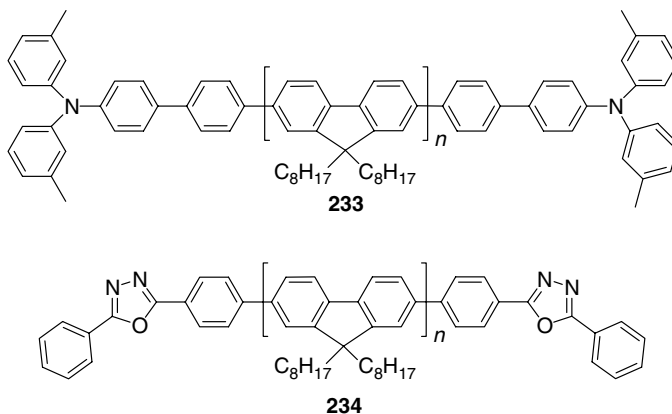


Chart 2.58

2.3.8 3D POLYFLUORENES

Networked materials with oligofluorene fragments were prepared by thermal treatment of oligofluorene–diboronic acids [332]. They exhibit high thermal (TGA: $T_{\text{dec}} = 363\text{--}420^\circ\text{C}$) and morphological (DSC: $T_g = 173\text{--}202^\circ\text{C}$) stability and emit violet-blue or blue light (depending on the number of fluorene units in the fragment). The cured films exhibit almost unchanged absorption and PL spectra even after heating at 150°C for 24 h, although the performance of double-layer devices ITO/CzBA/**235**/Mg/Al (CzBA = carbazole-3,6-diboronic acid, a hole-transporting material) was very poor (Chart 2.59).

Star-like PFs **236** with a silsesquioxane core have been prepared by Ni-mediated copolymerization of 2,7-dibromo-9,9-dioctylfluorene with octa(2-(4-bromophenyl)ethyl)octasilsesquioxane [333]. The polymer is thermally stable up to 424°C (TGA). In both chloroform solution and films, its absorption and PL spectra are very close to that for PFO **196**, although a somewhat higher PL efficiency is observed in films (64 and 55%, respectively). The polymer **236**, however, demonstrates a better PL color stability during thermal annealing. An ITO/PEDOT/**236**/Ca/Ag device can be turned on at 6.0 V, and shows a brightness of 5430 cd/m^2 (at 8.8 V) with $\Phi_{\text{EL}}^{\text{ex}} = 0.44\%$, almost twice as high as that for the corresponding PFO device (Chart 2.60).

2.3.9 BLENDS OF POLYFLUORENES WITH OTHER POLYMERS

It was shown that adding low oxidation potential material to PFs can stabilize the emission color and increase the device efficiency [321]. However, using low-molecular-weight organic dopants causes several problems such as phase separation and crystallization. These problems can be partially solved by using polymer blends. Cimrová and Výprachtický [334] reported

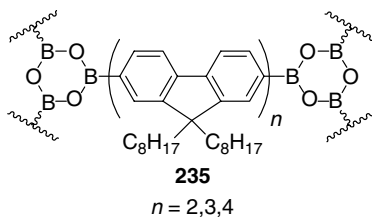


Chart 2.59

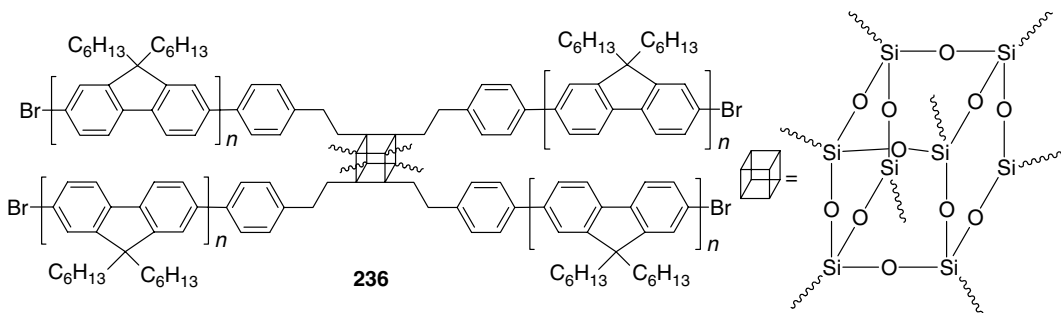


Chart 2.60

using low ionization potential ($I_P = 5.1\text{--}5.2\text{ eV}$) aromatic polysilane **238** as a blend polymer for poly(9,9-dihexadecylfluorene-2,7-diyl) (**237**) ($I_P = 5.8\text{ eV}$) (Chart 2.61).

Since the ionization potential of **238** matches closely the work function of PEDOT ($5.1\text{--}5.3\text{ eV}$) [335], the hole injection is dramatically improved. Accordingly, the device ITO/PEDOT/**237:238**(7:3)/Al has a significantly improved EL efficiency, $\eta_{EL} = 1.5\text{ cd/A}$, two orders of magnitude higher than that of single-layer PLED with **237**, six times higher than that of bilayer PLED with triarylamine polymer HTL, and almost twice as high as that of PF blends with low molecular triphenylamine HT materials (in device with Ca electrode) [321].

A highly stable blue EL was also achieved in single-layer PLEDs fabricated from the binary blends of conjugated PFO **196** with either stable poly(vinylidenediphenylquinoline) **239** or polystyrene as demonstrated by Kulkarni and Jenekhe [336]. PLEDs fabricated in the configuration of ITO/PEDOT/polymer blend/Al showed a brightness and an EL efficiency enhanced by a factor of 5–14, compared to neat PFO material. Besides, the color stability was also greatly improved, particularly for **239** blends (which possessed the highest T_g). The authors suggested that spatial confinement of the emissive excitons and improved electron–hole recombination in the “diluted” materials is responsible for the observed improvements.

Enhanced environmental stability was recently demonstrated for PLED with PFO **196**/gold nanoparticle (5–10 nm) nanocomposite-emitting layer [337]. In addition, the gold nanoparticle-doped PLEDs (1.5×10^{-5} volume fraction of Au) demonstrated improved luminescent lifetime and 2–3 times higher QE, compared with pure PFO-based PLED.

2.3.10 PF COPOLYMERS

Copolymerization of fluorene with other highly luminescent materials offers a possibility of fine-tuning the emitting and charge-transport properties of PF. Thus Miller and coworkers

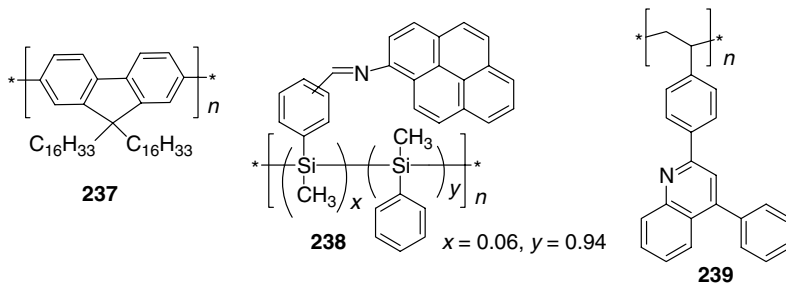
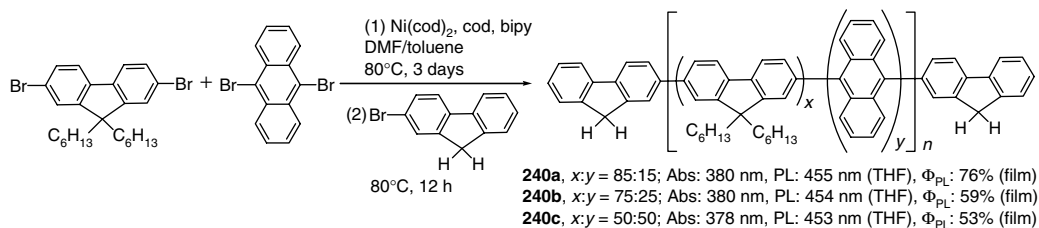


Chart 2.61



SCHEME 2.37 Synthesis of anthracene–fluorene copolymers. (From Klärner, G., Davey, M.H., Chen, E.-D., Scott, J.C., and Miller, R.D., *Adv. Mater.*, 13, 993, 1998.)

[338,339] used nickel-mediated copolymerization to synthesize random fluorene–anthracene copolymers **240a–c**, which showed high molecular weights ($M_n = 73,000\text{--}89,000$), good thermal stability ($T_{\text{dec}} > 400^\circ\text{C}$), high glass-transition temperatures ($T_g = 135\text{--}139^\circ\text{C}$), and a high QE of PL (53–76% in films) (Scheme 2.37). An increased stability of blue emission (for **240a** even after annealing at 200°C for 3 days) was explained in terms of preventing excimer formation due to incorporation of anthracene units that are orthogonal to the plane of the fluorenes in the backbone, although this can also be an effect of diminishing exciton migration toward fluorenone defects. The device ITO/PANI/**240a**/Ca/Al showed a stable blue EL emission (CIE: $x = 0.17$, $y = 0.25$) with an $\Phi_{\text{EL}}^{\text{ex}} = 0.17\%$ [338]. Similar fluorene–anthracene copolymers with 3,6-dioxaocetyl substituents on the fluorene moiety and different end-capping groups have also been reported [288,325].

Several groups studied carbazole derivatives as comonomers for blue-emitting PF materials. Carbazole has higher HOMO than fluorene, and many of its oligomers and polymers (e.g., well-known PVK) are good hole-transporting materials. Therefore, such modification of the fluorene polymers could improve the hole-transporting characteristics of PFs. Kim et al. [340] have reported one of the first alternating fluorene–carbazole polymers **241**, synthesized by Wittig reaction of carbazole-3,6-dialdehyde with the corresponding fluorene-2,7-*bis*-(triphenylmethylenephosphonium) salt. The PLED fabricated by sandwiching a spin-coated copolymer thin film between ITO and Al electrodes is a white emitter with a fwhm of 150 nm. Blending the polymer **241** with PVK in 4:1 ratio narrows the EL emission band ($\lambda_{\text{max}} = 460$ nm) to give pure blue color. However, the turn-on voltage for the LED is quite high (13 V) and $\Phi_{\text{EL}}^{\text{ex}}$ is only 0.002% (Chart 2.62).

Later, a random copolymer **242a,b** with slightly different substituent pattern was synthesized by Stéphan and Vial [341] by polymerization with Zn/NiCl₂ (see Appendix). Both

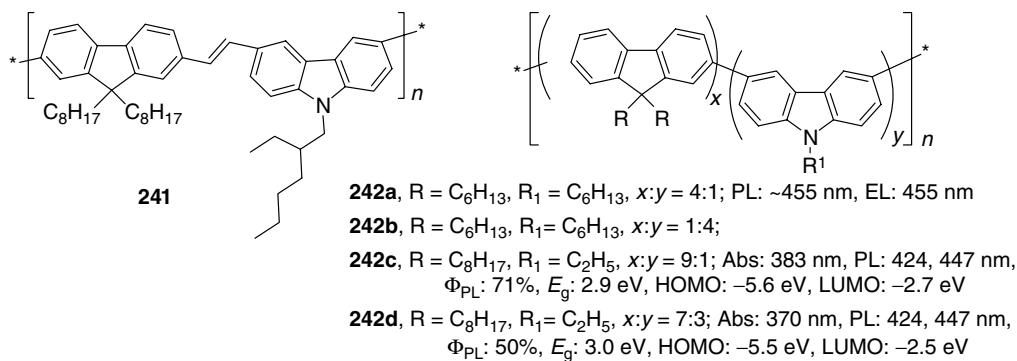


Chart 2.62

copolymers were soluble in organic solvents and had molecular weights of $M_n \sim 4000\text{--}5000$ g/mol (ca. 15 units). The PL spectrum of polymer **242a** is identical to that of the corresponding fluorene homopolymer and increasing the amount of carbazole units (from 1:4 to 4:1, **242b**) only results in decreasing emission intensity. The authors suggested that only the oligofluorene units are responsible for the emission and assumed the inhomogeneous distribution of comonomers, with relatively long homo-oligomer sections. Low QE for the polymers having high carbazole content can be due to interruption of conjugation, brought about by carbazole-3,6-diyl units (*meta*-substitution effect).

Similar random fluorene–carbazole polymers **242c,d**, synthesized by Yamamoto polymerization with $\text{Ni}(\text{cod})_2$ by Xia and Advincula [342] have much higher molecular weights ($M_n = 27,000\text{--}46,000$). Carbazole units in the backbone of the copolymers do not change emission of the copolymers in both solution and solid state, which corresponds well to that of PFO homopolymers **196**, but increase the solid state Φ_{PL} (especially for **242c**) and improve the PL color stability toward thermal annealing. This was attributed to a disorder in the polymer chain, brought about by carbazole units (Figure 2.20).

The effect of regularity in fluorene–carbazole copolymers was very recently studied by comparison of random and alternating copolymers **243** and **244** [343]. Both random and alternating copolymers showed progressive blue shifts in absorption with increasing carbazole content. A similar blue shift was observed in PL for copolymers **244** but all random copolymers **243** showed almost identical PL spectra, similar to that for PFO **196** (UV: 387 nm, PL: 420, 442 nm (film), E_g^{cv} : 3.25 eV, E_{HOMO} : 5.63 eV, conditions similar to the copolymers in Scheme 2.38). This difference between the alternating and regular copolymers was attributed to the longer fluorene sequences (>5 fluorene units) in random copolymers **243** and migration of the excitons to these segments where the emission occurs. The device

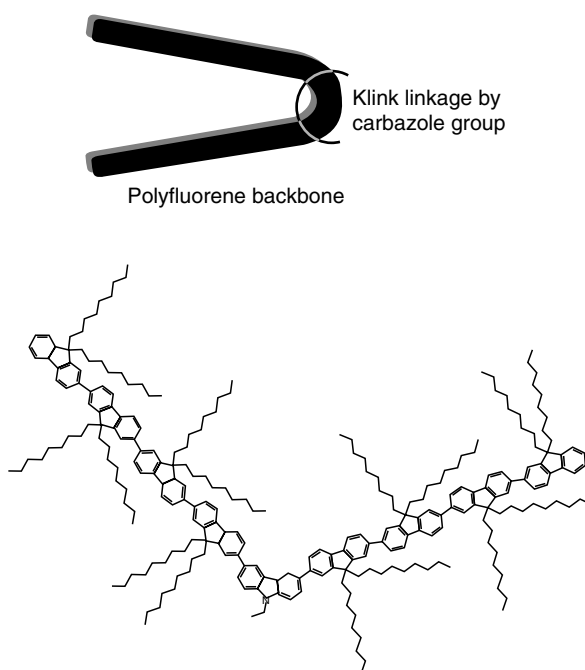
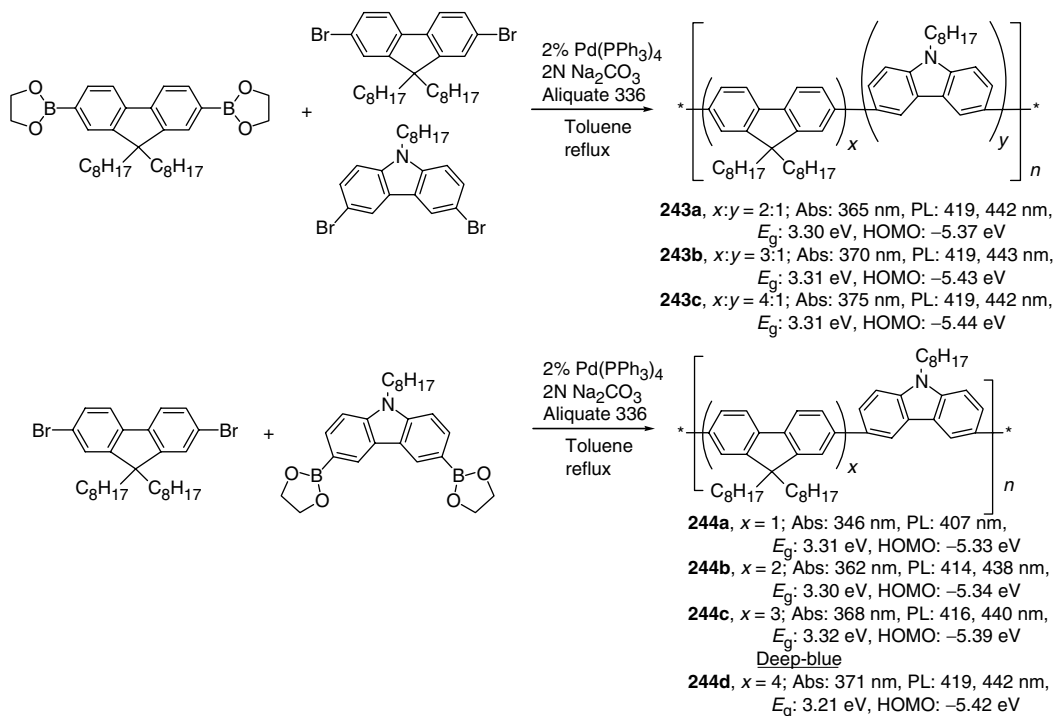


FIGURE 2.20 Schematic illustration of a disorder in polyfluorene introduced by carbazole-3,6-diyl unit in the main chain. (From Xia, C. and Advincula, R.C., *Macromolecules*, 34, 5854, 2001. With permission.)



SCHEME 2.38 Synthesis of random and alternating fluorene-carbazole copolymers. (From Li, Y., Ding, J., Day, M., Tao, Y., Lu, J., and D'orio, M., *Chem. Mater.*, 16, 2165, 2004.)

ITO/**244c**/F-TBB/Alq3/LiF/Al with 1,3,5-*tris*(4'-fluorobiphenyl-4-yl)benzene (F-TBB) as hole-blocking layer showed a maximum luminance of 350 cd/m² at 27 V and a luminance efficiency of 0.72 cd/A at a practical brightness of 100 cd/m², about double that for the device with **196** under the same conditions (160 cd/m² and 0.30 cd/A) [343,344]. Pure deep blue EL with narrow fwhm (39–52 nm) and negligible low-energy emission bands was observed for this device [344].

Leclerc's group [345,346] in Canada first synthesized PF copolymer **245** based on carbazole-2,7-diyl units that, in contrast to the above examples, is a fully conjugated system. Just as in carbazole-3,6-diyl copolymers, polymer **245** showed absorption and PL spectra similar to those of PFO **196**, with almost the same PL QE. However, there was no sign of the green emission band in this copolymer after thermal annealing (Chart 2.63).

Copolymerization of fluorene with triarylamine compounds was shown to increase the hole-transport properties of the polymers. Several copolymers of triarylamine and fluorene (**246–250**) synthesized by Suzuki coupling were reported by Bradley et al. [347,348]. The hole's

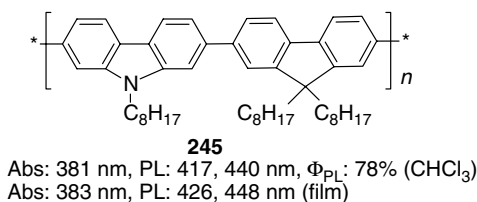


Chart 2.63

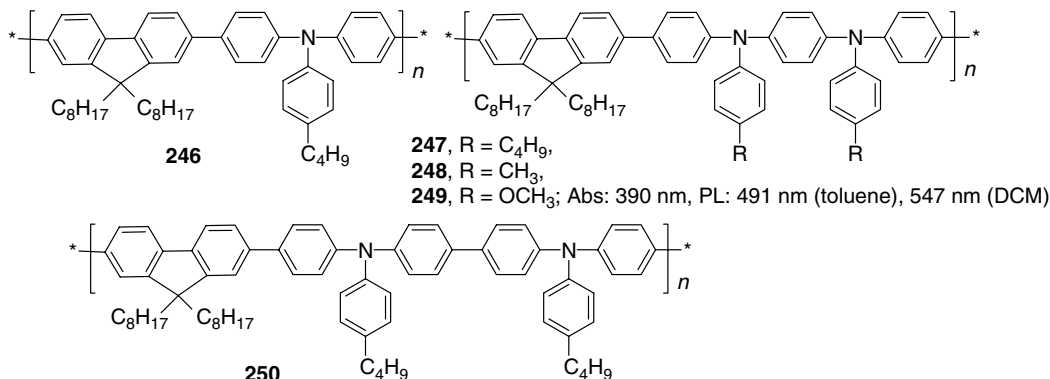


Chart 2.64

mobility of the copolymers was in the range of $3 \times 10^{-4} \text{ cm}^2/(\text{V s})$ to $3 \times 10^{-3} \text{ cm}^2/(\text{V s})$, and the I_p was as low as 5.0–5.3 eV (cf. 5.8 eV for PFO **196**), which is well-matched with the work function of the ITO/PEDOT electrode. Unfortunately, no PL or EL properties have been reported in the paper, although PLED devices based on blends of these copolymers with other PF have been patented by Dow Chemicals [349] (Chart 2.64).

Dow Chemicals group and coworkers [276,350] synthesized similar triarylamine–fluorene copolymers **251** and **252**, possessing carboxylic acid substituents, via hydrolysis of the corresponding ethyl ester polymers, prepared by Suzuki polymerization. Due to the very polar substituents, the copolymers **251** and **252** are only soluble in polar solvents such as DMF but not in aromatic hydrocarbons as toluene or xylene, which allowed simple fabrication of multilayer PLEDs by solution processes (Chart 2.65).

Fang and Yamamoto [351] reported on postpolymerization functionalization of triarylamine–fluorene copolymer **253**, resulting in copolymers **254a,b** with stilbene pendant groups. Whereas in the solid-state absorption and PL maxima of both polymers are essentially the same, PL in solution is strongly influenced by solvent (from 433 nm in toluene to 466 nm in *N*-methylpyrrolidone). Copolymer **254a** showed Φ_{PL} in the solid state of 51%, comparable to that of poly(9,9-dialkylfluorenes) (Chart 2.66).

Molecular triarylamine-based hole-transporting materials are usually synthesized by Ullmann-coupling or Pd-catalyzed amination, although polymerization using these reactions is difficult. Shim and coworkers [352] reported successful Pd-catalyzed copolymerization of dibromofluorene derivatives with anilines and obtained thermally stable, reasonably high molecular-weight ($M_n = 12,300$ – $14,000$, $\text{PDI} = 2.4$ – 3.0) copolymers **255a–c** (Scheme 2.39). The HOMO levels of these copolymers (ca. -5.1 eV) matched well with the ITO anode. The LEDs consisting of these polymers as buffer layer demonstrated a lower turn-on voltage, enhanced efficiency, and higher maximum luminance due to improved hole injection. For comparison, the devices consisting of ITO/**255a**/TPD/Alq₃/LiF/Al and

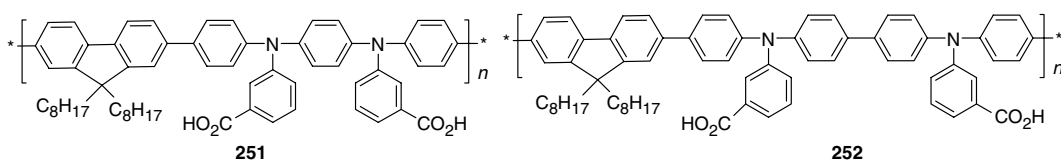


Chart 2.65

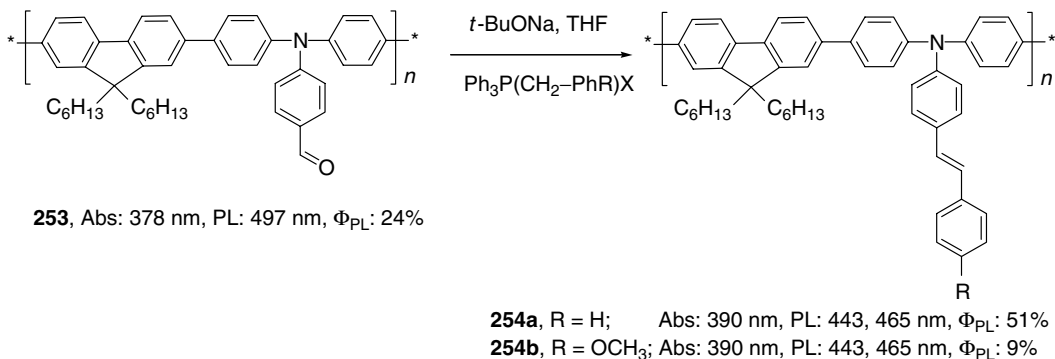
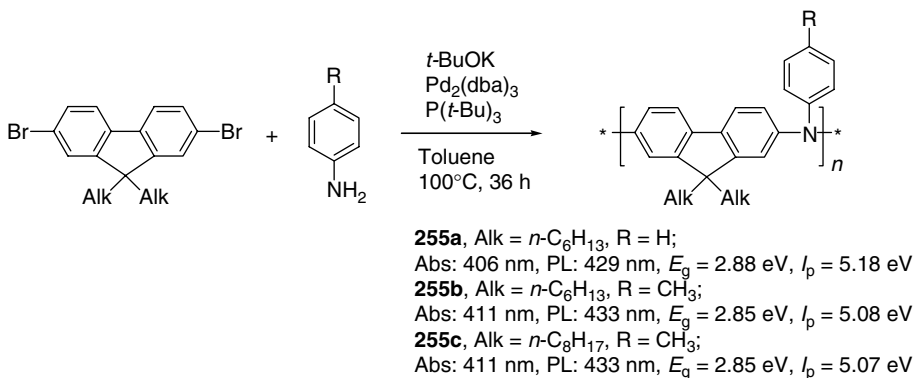


Chart 2.66

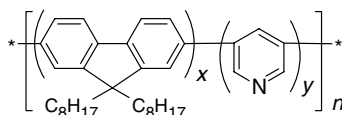
ITO/TPD/Alq₃/LiF/Al showed, respectively, a turn-on voltage of 2.2 and 3.6 V, a maximum luminance (at the highest current density) of 12,370 cd/m² (at 472 mA/cm²), and 5790 cd/m² (at 233 mA/cm²).

A series of random fluorene-pyridine copolymers **256a–f** have been prepared by Suzuki coupling of fluorene monomers with small amounts of 3,5-dibromopyridine (5, 10, 20, 30, 40, 50 mol%) [353]. The *meta*-linkage of the pyridine units is expected to interrupt conjugation but no regular spectral dependence was observed for different pyridine loadings. PL spectra for all copolymers are very close, except for copolymer **256f** (50:50 ratio), for which the PL and EL spectra are shifted by ~10–20 nm, compared to other copolymers. This could be a result of longer fluorene sequences in the random copolymers as discussed above for the fluorene-carbazole and fluorene-phenothiazine copolymers. All materials (except **256f**) showed narrow, pure blue EL emission and the devices with configuration ITO/PEDOT/**256a–e**/Ba/Al had a turn-on voltage of 5–6 V as well as moderately high $\Phi_{\text{EL}}^{\text{ex}} = 0.4\text{--}0.5\%$ (Chart 2.67).

The tuning of electron injection and transport in PF has been undertaken by Shu's group [354], who introduced electron-deficient oxadiazole units as pendant groups in fluorene copolymer **257**. The introduction of oxadiazole units into the PF can potentially improve the electron transport properties of the polymer, while their bulkiness can help to suppress aggregation effects (Chart 2.68).



SCHEME 2.39 Synthesis of fluorene-arylamine electron-rich copolymers. (From Jung, B.-J., Lee, J.-I., Chu, H.-Y., Do, L.-M., and Shim, H.-K., *Macromolecules*, 35, 2282, 2002.)

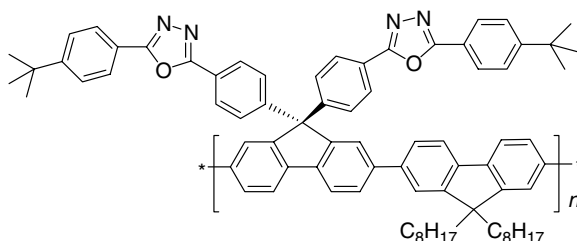


- 256a**, $x:y = 95:5$; Abs: 380 nm, PL: 422 nm, Φ_{PL} : 30%, EL: 446 nm, $\Phi_{\text{EL}}^{\text{ex}}$: 0.16%
256b, $x:y = 90:10$; Abs: 383 nm, PL: 422 nm, Φ_{PL} : 28%, EL: 442 nm, $\Phi_{\text{EL}}^{\text{ex}}$: 0.22%
256c, $x:y = 80:20$; Abs: 380 nm, PL: 422 nm, Φ_{PL} : 51%, EL: 442 nm, $\Phi_{\text{EL}}^{\text{ex}}$: 0.40%
56d, $x:y = 70:30$; Abs: 370 nm, PL: 420 nm, Φ_{PL} : 60%, EL: 438 nm, $\Phi_{\text{EL}}^{\text{ex}}$: 0.40%
256e, $x:y = 60:40$; Abs: 380 nm, PL: 419 nm, Φ_{PL} : 49%, EL: 440 nm, $\Phi_{\text{EL}}^{\text{ex}}$: 0.45%
256f, $x:y = 50:50$; Abs: 350 nm, PL: 413 nm, Φ_{PL} : 15%, EL: 424 nm, $\Phi_{\text{EL}}^{\text{ex}}$: 0.02%

Chart 2.67

Polymer **257** was readily soluble in common organic solvents such as THF, chloroform, chlorobenzene, and xylene. GPC analysis (vs. polystyrene standard) gave a molecular weight, M_n of 13,000 g/mol, with a PDI of 2.1. The polymer possessed excellent thermal stability with a very high T_g of 213°C. The electrochemically determined HOMO–LUMO levels of **257** were -5.76 and -2.47 eV, respectively, which are similar to those of PFO **196** (-5.8 and -2.6 eV), with only slightly improved electron affinity. The absorption spectrum of **257** in THF solution showed two major peaks at 297 and 390 nm. The former peak is attributed to the aromatic oxadiazole group and the latter to the $\pi-\pi^*$ transition of the polymer backbone. There is essentially no influence of the attached oxadiazole group on the conjugated backbone: the PL spectrum displays a blue emission with two sharp peaks at 419 and 444 nm, and a small shoulder at 469 nm, very similar to that of PFO **196**. The PL QE in solution was very high (124% vs. 9,10-diphenylanthracene as a standard; for the latter, an absolute fluorescence efficiency of $90 \pm 4\%$ was determined [355]), which dropped in thin film to a value of 43%, comparable to PFO (55%). Under thermal annealing of thin films at 150°C for 20 h, the PL spectrum of **257** remains almost intact with only a negligible long wavelength tail, resulting in very pure blue emission in PLED devices (fabricated as ITO/PEDOT/**257**/Ca/Ag). The devices showed a low turn-on voltage of 5.3 V and a luminance of 2770 cd/m² at 10.8 V with a current density of 1.12 A/cm². The maximum $\Phi_{\text{EL}}^{\text{ex}}$ was 0.52% at 537 cd/m² and 7.4 V. The device efficiency is much higher than that of a similar PFO-based device (maximum brightness of 600 cd/m² and $\Phi_{\text{EL}}^{\text{ex}} = 0.2\%$).

A recent paper reported a highly efficient blue color emission PF copolymer **258** incorporating both triphenylamine and oxadiazole pendant groups [356]. This statistical copolymer was designed to bring together good hole transporting (due to triphenylamine groups) and



- 257**, Abs: 298 nm, PL: 427 nm, Φ_{PL} : 43%, EL: 428 nm,
 Blue, HOMO: -5.76 eV, LUMO: -2.47 eV

Chart 2.68

electron-transporting properties (due to oxadiazole groups). The copolymer showed high solubility in organic solvents, good stability ($T_{\text{dec}} = 440^\circ\text{C}$, $T_g = 166^\circ\text{C}$) and high PL QE (95% in solution and 42% in films) with stable emission color (unchanged after thermal annealing). The electron-rich and electron-deficient substituents endow rather high HOMO (-5.30 eV) and relatively low LUMO (-2.54 eV)-energy levels that are expected to facilitate charge injection and transport. Indeed, the PLED device fabricated with the following configuration ITO/PEDOT/**258**/Ca/Ag, showed a low turn-on voltage of 4.4 V and maximum $\Phi_{\text{EL}}^{\text{ex}} = 1.21\%$ (achieved at 7.6-V driving voltage with a brightness of 354 cd/m^2), more than twice higher than that for PF **257**, containing only electron-deficient oxadiazole substituents [354]. In spite of minor additional emission bands at 580 and 660 nm (which increase at higher voltages), this PLED emission falls in the blue region (CIE: $x = 0.193$, $y = 0.141$) that, together with a high maximum luminance of 4080 cd/m^2 and an efficiency of 0.63 cd/A (0.19 lm/W), render **258** as a promising LEP (Chart 2.69).

A series of fluorene copolymers **259** and **260a–g** with oxadiazole pendant groups was recently synthesized by Sung and Lin [357]. The EL maximum for copolymer **259** (452 nm) is red-shifted, compared to **260a–g** (406–431 nm). The devices fabricated with these copolymers in ITO/PEDOT/polymer/Ca/Al configuration showed a relatively high turn-on voltage of 6.5–8.5 V and only moderate maximum brightness ($29\text{--}462\text{ cd/m}^2$) (Chart 2.70).

Oxadiazole units were also introduced into the backbone of fluorene-alternating copolymers (Scheme 2.40). The key monomer in the synthesis of a series of fluorene–oxadiazole copolymers was 2,7-bis(tetrazolyl)fluorene derivative **261** for the preparation of copolymers **262–265** [358]. This tetrazole route has several advantages over other oxadiazole ring formation reactions: fast and clean reaction, mild reaction conditions, high yields, and high polymer molecular weights. The copolymers showed excellent thermal stability ($T_{\text{dec}} > 430^\circ\text{C}$) and their T_g progressively increased from 98 to 150°C with increasing oxadiazole content in the polymer. Remarkably, the UV and PL spectra of the copolymers were all very similar to those of fluorene homopolymers with only slight red shifts in absorption (10–12 nm) and emission (5–7 nm) spectra. The copolymers also demonstrated high $\Phi_{\text{PL}} \approx 70\%$ (in DCM solution), typical for PFs. Several other fluorene–oxadiazole, fluorene–thiadiazole, and fluorene–triazole fully conjugated copolymers **266a–c** and **267a,b** have been prepared in the same way [359] (Chart 2.71).

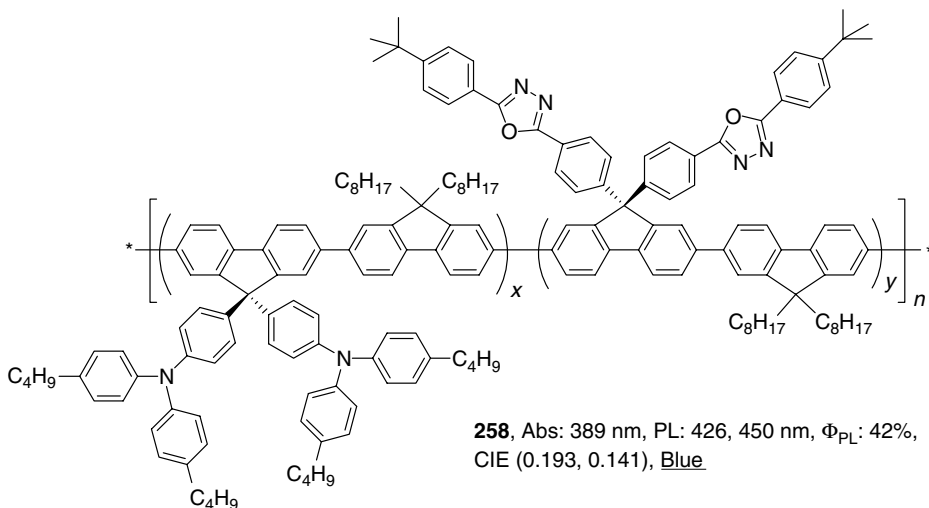


Chart 2.69

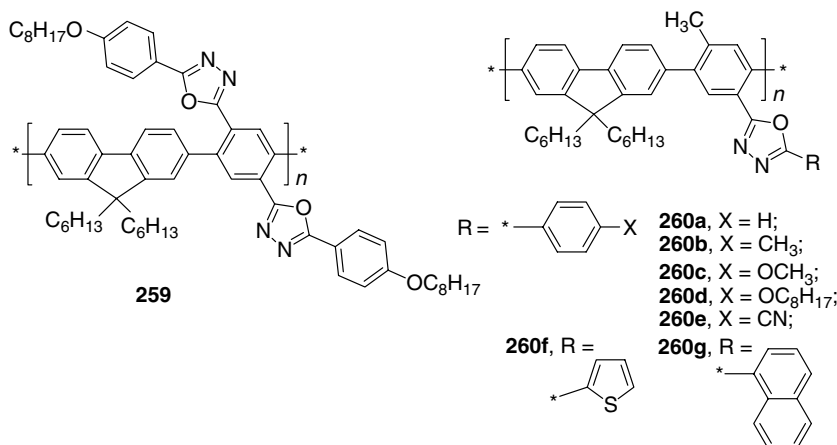
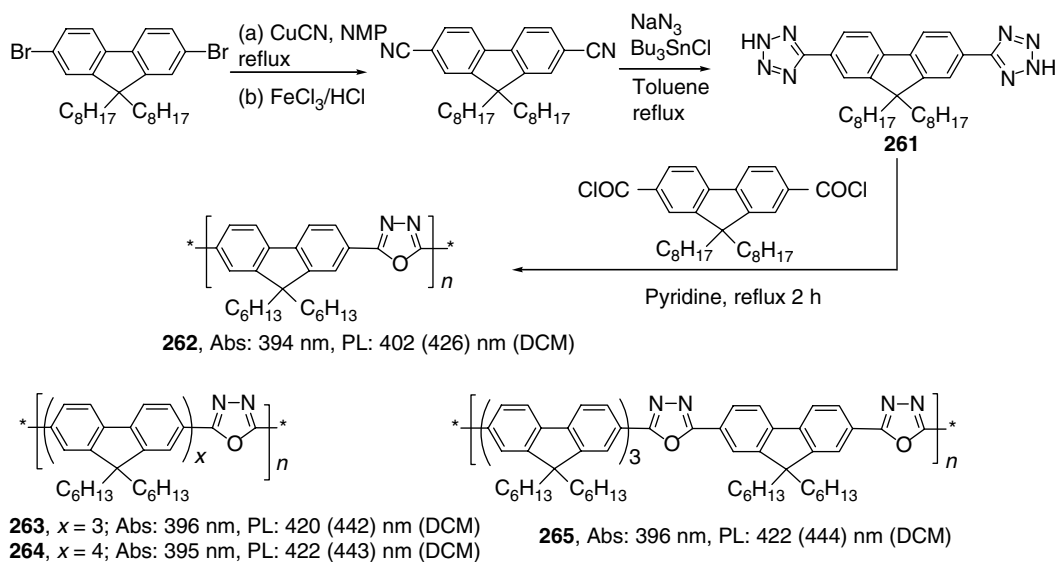


Chart 2.70

Other fluorene-oxadiazole copolymers, such as fully conjugated **268a,b** [360] or **269a-c**, with conjugation interrupted by σ -links [361], have been synthesized. For both series of polymers, emission was in the blue region at very similar wavelengths, but no LED device was reported.

Pei and coworkers [362] synthesized fluorene copolymer functionalized with imidazole ligands in the side chains (**270**). The PL emission of **270** was sensitive to the presence of metal cations in solution (particularly efficient quenching was due to Cu^{2+}), which makes it a promising material for fluorescent chemosensing.

Efficient blue emission and good electron affinity and electron-transporting properties were demonstrated for two fluorene copolymers with dicyanobenzene moiety in the main chain, **271a,b** (Scheme 2.41) [363]. Due to improved electron transport properties, the device



SCHEME 2.40 Synthesis of fluorene-oxadiazole copolymers. (From Ding, J., Day, M., Robertson, G., and Roovers, J., *Macromolecules*, 35, 3474, 2002.)

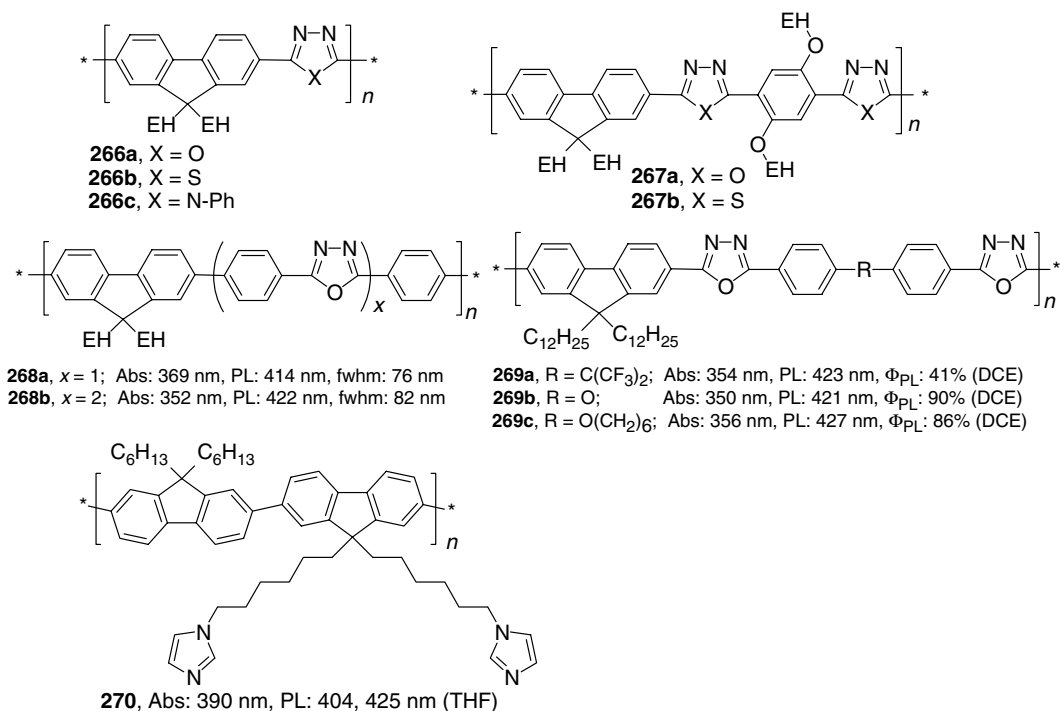
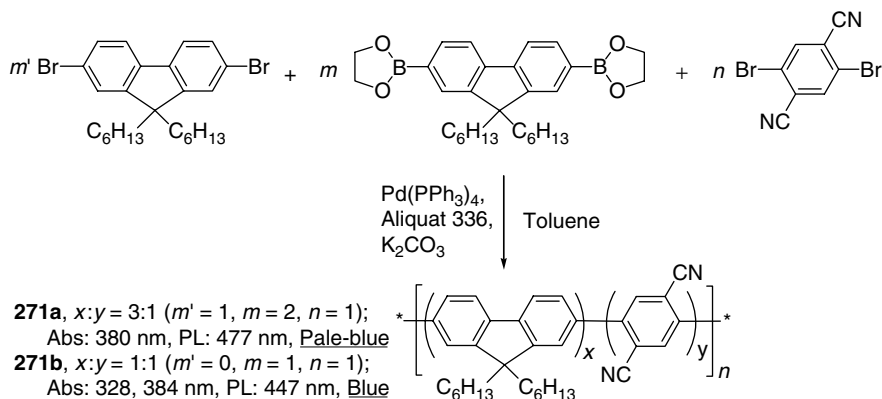


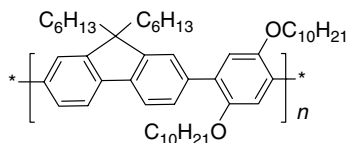
Chart 2.71

ITO/PEDOT/**271a**/Ca showed a low turn-on voltage (3.4 V), better Φ_{EL}^{ex} (0.5%), and high brightness (5430 cd/m²), compared to the PDHF **195** device in the same configuration.

Many other PF copolymers, which do not contain a particularly electron-active moiety, but nevertheless, can improve the performance of the material in PLED have been synthesized. The Huang group [364,365] at Institute of Materials Research and Engineering (IMRE, Singapore) synthesized deep-blue copolymer **272** by Suzuki copolymerization of fluorene–diboronic acid with dibromobenzene. The emission band of **272** has a peak at 420 nm and a well-defined vibronic feature at 448 nm with a fwhm of 69 nm, and virtually no green emission,



SCHEME 2.41 Synthesis of fluorene–(2,5-dicyanobenzene) copolymers via Suzuki coupling. (From Liu, M.S., Jiang, Z., Herguth, P., and Jen, A.K.-Y., *Chem. Mater.*, 13, 3820, 2001.)

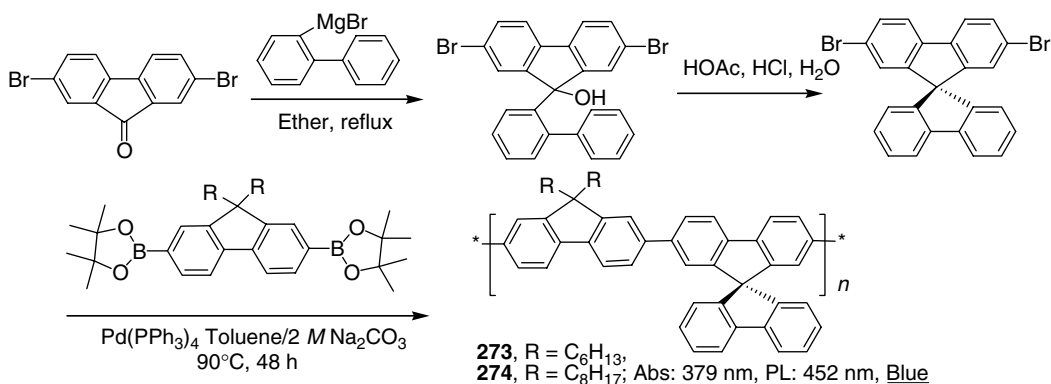


272, Abs: 378 nm, PL: 420, 448 nm, Φ_{PL} : ~40%,
HOMO: -5.66 eV, LUMO: -2.62 eV, Deep-blue

Chart 2.72

allowing for very pure deep blue fluorescence, compared to PDHF **195**. The PL QE of thin films was around 40%, similar to that of PDHF. The single-layer PLED device (ITO/**272**/Ca) and the multilayer devices (ITO/PANI/PVK/**272**/Ca and ITO/CuPc/PVK/**272**/Ca) gave identical deep blue EL emission ($\lambda_{\text{max}} = 420$ nm, fwhm = 53 nm) [364]. A maximum $\Phi_{\text{EL}}^{\text{ex}} = 0.6\%$ and a maximum luminance of 700 cd/m^2 were achieved for a multilayer PLED (Chart 2.72).

A spiro-bifluorene moiety was used to construct alternating copolymers **273** and **274** with dialkylfluorene units. The aim of this modification was to increase the T_g of the material, so that moderate heating during the device operation would not result in aggregate formation [366]. A 90° geometry of spiro-annulated bifluorene units prevents interchain aggregation, whereas the long-alkyl substituents in the second comonomer improve the solubility. The synthesis is given in Scheme 2.42. Grignard reaction of 2,7-dibromo-9-fluorenone with biphenyl-2-magnesium bromide, followed by acid-promoted cyclization affords the spiro-annulated monomer. The copolymers were synthesized by Suzuki coupling with commercially available (from Aldrich) dialkylfluorenediboronic esters. The copolymers **273** and **274** are only partially soluble in solvents such as THF and chloroform, but can be completely dissolved in chlorobenzene (used to spin cast the polymer films). The M_n , determined for the THF-soluble part of **274** is 11,600 g/mol, PDI = 2.9, although a higher molecular weight is expected for the THF-insoluble part. The DSC-determined T_g of **273** (105°C) is higher than that of PDHF **195** (75°C). Consequently, no long wavelength emission was found for films annealed at 100°C (in contrast to PDHF), although further annealing above T_g at 150°C does result in appearance of a strong emission band at 525 nm. Another feature of these copolymers is their narrow emission spectra compared to dialkylfluorene homopolymers, attributed to less dense molecular packing: for **274** and **195**, fwhm = 39 and 62 nm, $\lambda_{\text{onset}}^{\text{PL}} = 585$ and 610 nm, respectively [291]. A PLED device fabricated as ITO/**274**/Ca gave pure blue emission

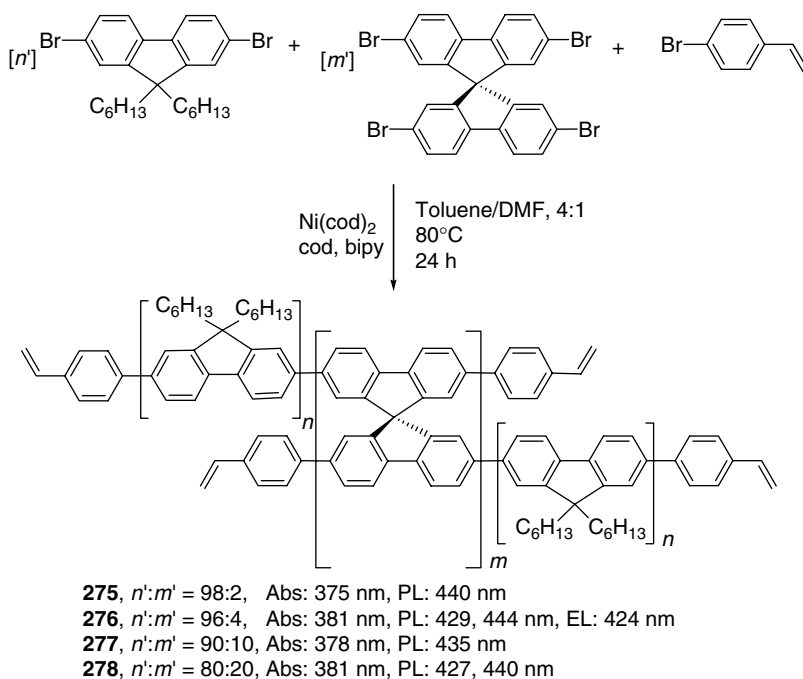


SCHEME 2.42 Synthesis of the PF spiro-copolymers. (From Yu, W.-L., Pei, J., Huang, W., and Heeger, A.J., *Adv. Mater.*, 12, 828, 2000.)

with a maximum $\Phi_{\text{EL}}^{\text{ex}} = 0.12\%$. Adding copper phthalocyanine (CuPc) as an HTL between the ITO and copolymer layers decreased the operating voltage from 16 to 7 V and increased the QE to 0.54% (maximum luminance 24 cd/m²).

Random copolymers **275–278** containing spiro-fluorene moieties were also reported by Carter and coworkers at IBM Almaden Research Center. They used spiro-bifluorene dibrominated at both fluorene moieties. Ni(0)-mediated random copolymerization of 9,9-dihexyl-2,7-dibromofluorene with this spiro-bifluorene monomer resulted in 3D-branched copolymers **275–278** (Scheme 2.43) [367]. Due to the expected insolubility of such materials at high degree of polymerization owing to the network formation, the molecular weight was controlled at $M_n \approx 3800\text{--}12,800$, by adding 4-bromostyrene as a terminating agent. The latter also serves as a cross-linkable unit that allowed to obtain an insoluble polymer film by heating of the soluble spin-coated polymer. The resulting amorphous polymers **275–278** demonstrated excellent thermal stability ($T_{\text{dec}} > 430^\circ\text{C}$) and their T_g values (105, 144, 93, and 90°C for **275–278**, respectively) were substantially higher than those of PDHF **195** (75°C). A series of PL measurements in films revealed blue emission that remains stable (no green component) after thermal treatment at 120°C for 30 min (in these conditions, the copolymers are cross-linked through the 4-phenylethenyl end groups rendering insoluble films) (Figure 2.21). A bilayer device ITO/PEDOT/x-HTPA/**275**/Ca/Al was fabricated by spin coating the cross-linkable poly(4-hexyl-triphenyl)amine (x-HTPA) as HTL, curing at 100°C for 1 h in a glovebox and repeating the process with **275**. The diode could be switched on at 3 V to emit blue light ($\lambda_{\text{EL}} = 424\text{ nm}$; CIE: $x = 0.168$, $y = 0.07$) and maximum $\Phi_{\text{EL}}^{\text{ex}} = 0.08\%$ was achieved at 9 V.

He and coworkers [368] synthesized a series of hyperbranched alternating copolymers of tetraphenyl(*p*-biphenyl)-methane and -silane with 9,9-dihexylfluorene by Suzuki coupling



SCHEME 2.43 Synthesis of random PFs with spiro-fluorene moieties. (From Marsitzky, D., Murray, J., Scott, J.C., and Carter, K.R., *Chem. Mater.*, 13, 4285, 2001.)

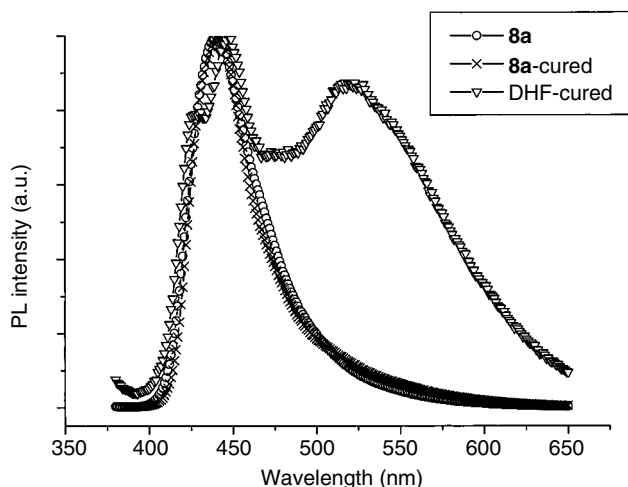


FIGURE 2.21 PL spectra of the uncured and cured amorphous spiro-PF **275** (**8a**) and a cured PDHF **195** (DHF). (From Marsitzky, D., Murray, J., Scott, J.C., and Carter, K.R., *Chem. Mater.*, 13, 4285, 2001. With permission.)

(**279a–c**). Remarkably, copolymers **279a–c** were soluble in common solvents, showed high T_g ($>200^\circ\text{C}$) and emitted in the blue region, slightly blue-shifted compared to poly(9,9-dialkylfluorenes). Due to their 3D structure preventing close packing of fluorene chains, these copolymers are less prone to self-aggregation in the solid state and, accordingly, no green emission was observed. A PLED ITO/PEDOT/polymer/LiF/Ca/Ag showed bright-blue emission peaking at 415 nm with $\Phi_{\text{EL}}^{\text{ex}} = 0.6\%$ and a turn-on voltage of 6.0 V (Chart 2.73).

Blue light-emitting copolymers **280a–c**, with interrupted conjugation due to *m*-phenylene linkages in the backbone, did not show the typical vibronic structure of PFs in their PL spectra. They possess an increased stability toward appearance of undesired green emission upon annealing. Fabrication of ITO/PEDOT/**280**/Ba/Al devices demonstrated turn-on voltages of 7.4–8.4 V and $\Phi_{\text{EL}}^{\text{ex}}$ in the range of 0.43–0.6% [369] (Chart 2.74).

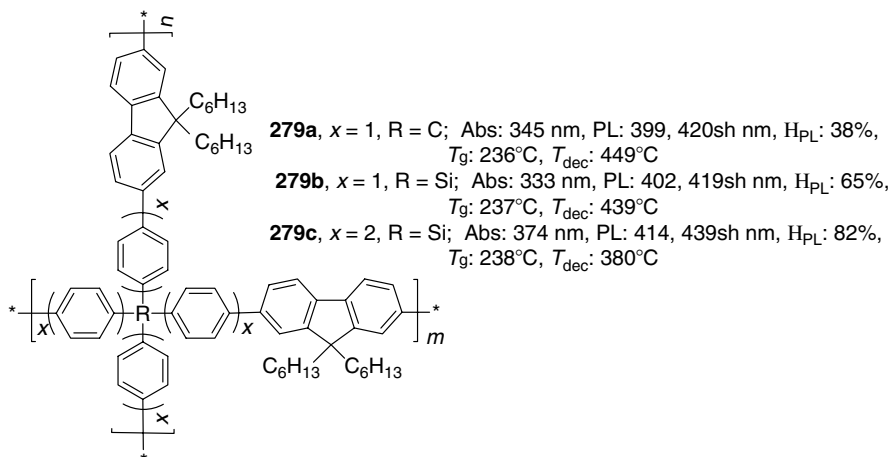
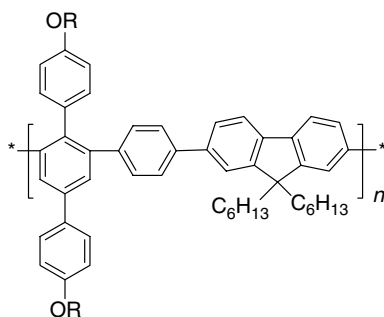


Chart 2.73



280a, R = C₆H₁₃; Abs: 341 nm, PL: 411 nm, Φ_{PL} : 32%, EL: 418 nm

280b, R = EH; Abs: 341 nm, PL: 408 nm, Φ_{PL} : 30%, EL: 419 nm

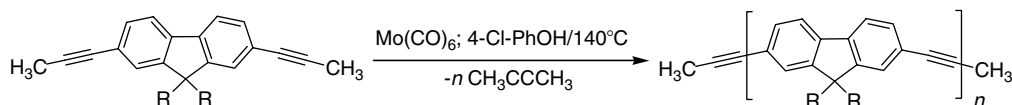
280c, R = C₁₂H₂₅; Abs: 344 nm, PL: 412 nm, Φ_{PL} : 32%, EL: 420 nm

Chart 2.74

An unusual synthetic approach to PF copolymers was demonstrated by Bunz and coworkers [370], who prepared poly(fluorene ethynylene) **281a–e** by metathesis polymerization reaction (Scheme 2.44) [370]. The aggregation of polymers **281** in concentrated solutions and in solid state is manifested in slight (up to 10–20 nm) red shift of the absorbance and emission peaks, although solutions and films emit pure blue light.

Jen and coworkers [371] reported a binaphthyl-containing random PF copolymer **282**, synthesized by Suzuki coupling. The twisted binaphthyl units control the effective conjugation length, and prevent fluorescence quenching in the solid state by hindering intermolecular π – π interactions. Accordingly, a pure blue emission (two peaks at 428 and 448 nm, blue-shifted compared to PFO **196**) and a relatively high PL efficiency (44%) were observed in solid films of this material. Multilayer PLEDs fabricated with CuPc or BTPD-PFCB (**132**) [372] HTL (ITO/HTL/**282**/Ca configuration) exhibited EL emission peaks at 420 and 446 nm with EL maximum brightness and $\Phi_{\text{EL}}^{\text{ex}}$ up to 3070 cd/m² and 0.82%, respectively (although an additional low-intensity emission band was observed for the most efficient devices using BTPD-PFCB as an HTL) [371,372] (Chart 2.75).

Recently, Lai and coworkers [373,374] reported fluorene copolymers, containing dithia[3.3]cyclophane as a repeating unit. The polymers **283a–c** and **284a–c** were synthesized by Suzuki-coupling fluorene borate derivatives with dibromocyclophane. The polymer **283a** shows pure blue fluorescence with rather high PLQY (75%), but no LED device performance was reported. Remarkably, introduction of either electron donor or electron acceptor substituents in the cyclophane moiety results in significant quenching of the fluorescence quantum yield (36% for **283b**, 0% for **283c**), which was explained by a transannular



281a, R = C₆H₁₃; Abs: 396, 415 nm, PL: 428 nm, Blue

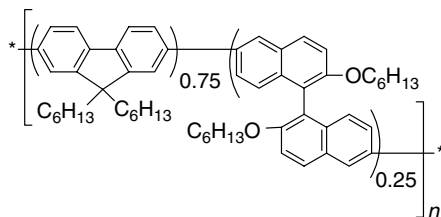
281b, R = C₈H₁₇; Abs: 394, 416 nm, PL: 429 nm, Blue

281c, R = C₁₂H₂₅; Abs: 387, 413 nm, PL: 429 nm, Blue

281d, R = 2-ethylhexyl; Abs: 392, 416 nm, PL: 434 nm, Blue

281e, R = (S)-3,7-dimethyloctyl; Abs: 396, 424 nm, PL: 434 nm, Blue

SCHEME 2.44 Metathesis polymerization synthesis of fluorene-ethynyl copolymer **281**. (From Pschirer, N.G. and Bunz, U.H.F., *Macromolecules*, 33, 3961, 2000.)



282, Abs: 360 nm, PL: 428, 445 nm, Φ_{PL} : 44%
EL: 420, 446 nm, E_g : 2.97 eV

Chart 2.75

charge-transfer effect [373]. Copolymers **284a–c** also showed lower quantum yields (15–22%) [374] (Chart 2.76).

Huang and coworkers [375] reported alternating fluorene copolymers **285–287**, containing 2,2'-bipyridyl fragments in the main chain using Suzuki, Wittig–Horner, and Heck coupling of 9,9-dioctyl-2,7-dibromofluorene, respectively. All three polymers were responsive to a wide variety of transition metal ions by an absorption spectral red shift (up to 40 nm) and fluorescence quenching (Chart 2.77).

Kong and Jenekhe [376] prepared triblock copolymers **288** by the ring-opening polymerization of γ -benzyl-L-glutamate *N*-carboxyanhydride using benzylamine end-capped PDHF (Scheme 2.45). The polymers retain the emissive properties of PF ($\lambda_{\text{max}}^{\text{abs}} = 380$ nm, $\lambda_{\text{max}}^{\text{PL}} = 424$ nm in CHCl_3) and show EL with a brightness comparable to PF homopolymers. Different nanostructured assemblies of the block copolymers **288** were observed by AFM depending on the copolymer composition and secondary structure (helix or coil) of the polypeptide blocks.

2.3.11 COLOR TUNING IN POLYFLUORENE COPOLYMERS

The above strategies were focused on creating highly stable PFs with pure blue emission. However, other emission colors can also be achieved through doping with fluorescent dyes or through a copolymerization strategy in either alternating or random PF copolymers. Through careful selection of suitable comonomers, considering their effect on HOMO–LUMO levels of the polymer, one can achieve a whole range of emission colors from PF-based materials.

2.3.11.1 Doping with Low Molar-Mass Fluorescent Dyes

The high-energy blue emission of PF polymers can be changed into virtually any color by adding a small amount of low energy-emitting materials. This approach, based on energy transfer, is of prime importance for phosphorescent PLEDs, although nonphosphorescent dyes

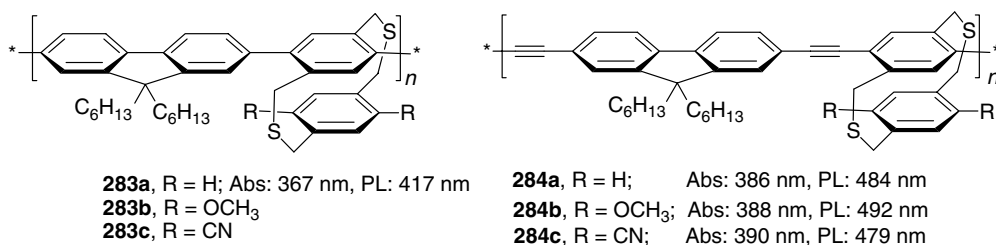


Chart 2.76

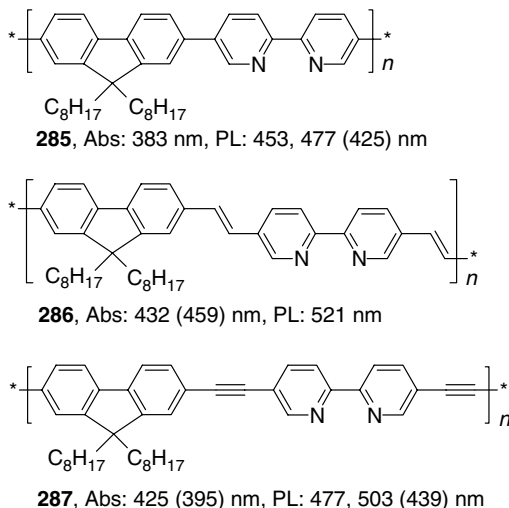
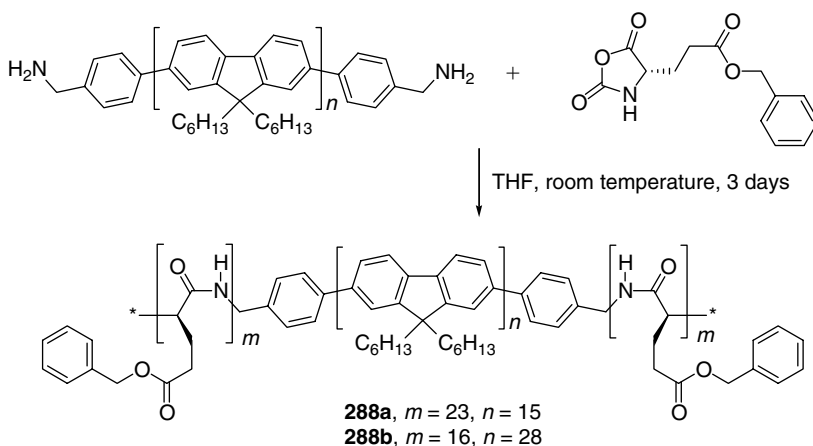


Chart 2.77

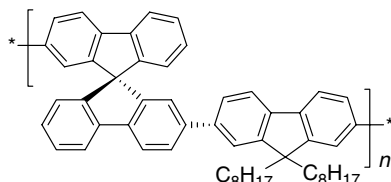
were used to tune the PF emission color. Thus, efficient Förster energy transfer from blue to red (typical for porphyrins) was demonstrated for tetraphenylporphyrin (TPP)-doped PFO **196**-based LED as a result of good overlap between the PF emission with the Soret absorption band of the porphyrin [377]. It was shown that for composites with 1–10% TPP, 95% of photo-generated excitons are transferred from the polymer to TPP. The ITO/**252**/**196**: TPP/Ca LED (**252** here plays the role of HTL) device showed $\Phi_{\text{EL}}^{\text{ex}} = 0.9\%$ at 33 V, corresponding to 0.18 cd/A and a luminance of 90 cd/m². The EL emission was identical to the PL emission of TPP, with CIE coordinates ($x = 0.65$, $y = 0.29$), representing a rather pure red color.

2.3.11.2 Alternating Copolymers

Wu et al. [378] have recently reported a new spiro-linked PF (**289**). Unlike the spiro-*co*-PF discussed in the previous section, the conjugation in **289** is completely interrupted by the spiro-bifluorene units. As a result, the copolymer showed significant blue-shifted absorption



SCHEME 2.45 Synthesis of triblock copolymers **288**. (From Kong, X. and Jenekhe, S.A., *Macromolecules*, 37, 8180, 2004.)



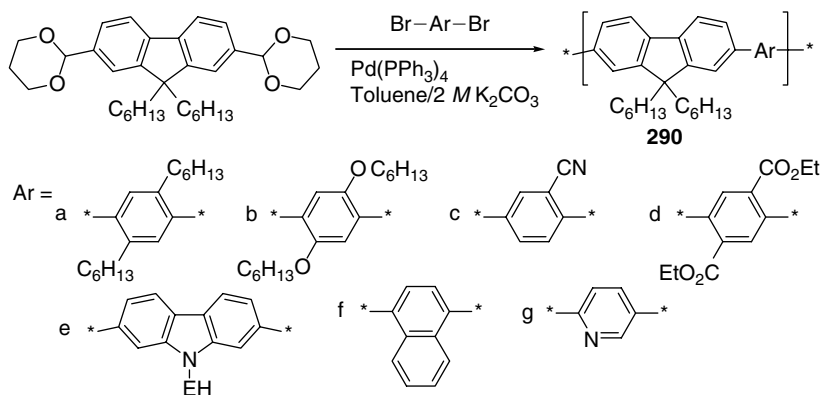
289, Abs: 355 nm, PL: 404, 425 nm, Φ_{PL} : 42%,
Purplish-blue, CIE (0.165, 0.128)

Chart 2.78

and emission spectra, compared with PFO **196**. The UV-vis absorption of thin films coated from a toluene solution has a maximum at 355 nm and the PL emission showed a vibronic fine structure with two sharp peaks at 400 and 422 nm. The QE of the polymer in thin films is 42%, comparable to PFO. This copolymer shows superb color stability: the thermal annealing of thin films has no effect on the emission. While the copolymer itself demonstrates a purple-blue emission at the UV limit of the visible region of the spectra (CIE: $x = 0.165$, $y = 0.128$), it can be used as an energy-transfer material with fluorescent dyes to achieve a desirable color. Thus, pure blue emission is easily achieved with ca. 1% of 2,5,8,11-tetra-*tert*-butylperylene (Chart 2.78).

Using Suzuki polymerization, Huang and coworkers [379] synthesized and studied optical and electronic properties of a series of fluorene-arylene alternating polymers **290a–g** (Scheme 2.46). These copolymers had a band gap ranging from 2.82 to 3.32 and emitted blue light ($\lambda_{\text{max}}^{\text{PL}}$ from 404 to 443 nm), whose PL efficiency varied substantially with the Ar moiety ($\Phi_{\text{PL}} \sim 10$ –88% in films). The polymers showed good thermal stability ($T_{\text{dec}} \sim 375$ –410°C) with wide variation in T_{g} (~ 50 –213°C). Electron-rich or electron-deficient arylene moieties in the backbone tuned the HOMO–LUMO levels of these materials (see Table 2.2).

Leclerc and coworkers [303,380–382] have efficiently tuned the emission from blue to green and yellow by introducing various phenylene and thiophene units in alternating fluorene copolymers **291–297**, although no simple correlation between the polymer structure and the EL color was found. Changing the nature of the comonomer unit from the relatively electron-deficient phenylene to very electron-rich *bis*(ethylenedioxy)thiophene affects the band gap of the polymer (and the emitting color) as well as the charge-transport properties, thus influencing the performance of the PLEDs (see also Ref. [383] on thermo- and solvatochromic properties of these copolymers). The highest brightness achieved for bithiophene-



SCHEME 2.46 Suzuki-coupling polymerization route to alternating fluorene-arylene copolymers **290**. (From Liu, B., Yu, W.-L., Lai, Y.-H., and Huang, W., *Chem. Mater.*, 13, 1984, 2001.)

based copolymer **295** was of 4.5 cd/m^2 for a neat copolymer and 18 cd/m^2 for a blend with 20% of hole-transport material tetraphenylbenzidine, TPD (**299**), values that are far too low for a practical application (Chart 2.79).

Huang's group [384–386] has systematically studied the structure–property relationships of fluorene–thiophene-based conjugated polymers **300–302**. In contrast to polythiophene (PT) homopolymers (see Section 2.3.11.3), the regioregularity of the bithiophene fragments in their copolymers show little influence on the optical band gap (**302a,b** respectively: $E_g = 2.49$ and 2.58 eV [385], or 2.57 and 2.60 eV [387,388]) or the emission maxima, but the HH copolymer **302b** was significantly more thermally stable (Chart 2.80).

All copolymers showed reversible n- and p-doping in CV experiments and a schematic diagram showing the HOMO and LUMO energy levels relative to the electrode's work function of EL devices are given in Figure 2.22 [388]. The single-layer ITO/**302b** (100 nm)/Ca device emitted green light (493, 515 nm) with a high turn-on voltage of 20 V. The introduction of PVK hole-transport layer decreased the turn-on voltage to 8 V and increased the maximum $\Phi_{\text{EL}}^{\text{ex}}$ from 0.05 to 0.6% [384,386] (although less pronounced increase was observed for other polymers of the series [388]). Later, this group reported a somewhat lower EL QE of 0.3% for the device ITO/PVK/**302b** (75 nm)/Ca/Al. The highest $\Phi_{\text{EL}}^{\text{ex}}$ in this series was reported for **300** (0.64% for ITO/PVK/**300**/Ca/Al device) and the lowest one was for **302a** (0.07% for ITO/PEDOT/**302a**/Ca/Al device) [388]. Note that this trend has no correlation with the polymer energy levels.

A series of alternating copolymers **303**, containing conjugated thiophene-2,5-diyl (A) and nonconjugated thiophene-3,4-diyl (B) units in different ratios was recently synthesized by Vamvounis and Holdcroft [389] via Suzuki coupling of fluorene–diboronic ester with mixtures of 2,5- and 3,4-dibromothiophenes. There is a significant progressive blue shift of the emission with increased feed ratio of the nonconjugated monomer B (from $\lambda_{\text{PL}} = 466, 482 \text{ nm}$

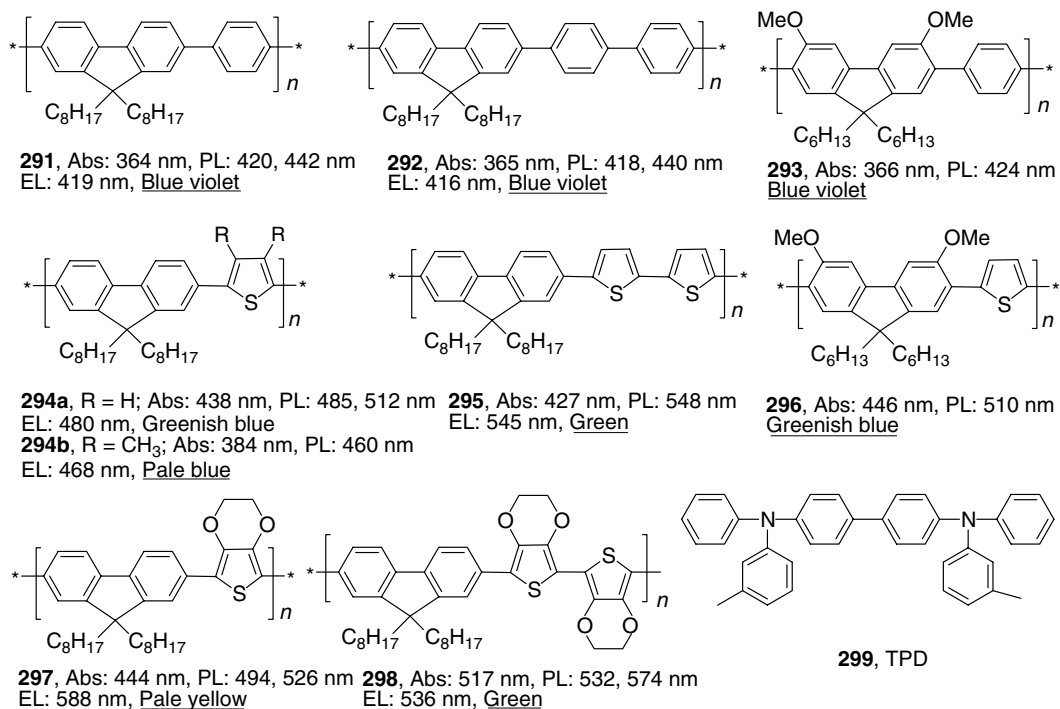


Chart 2.79

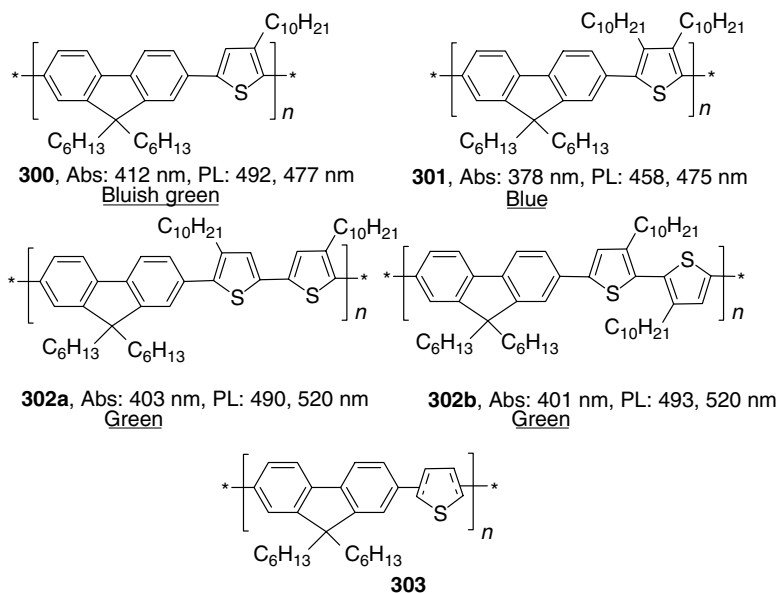


Chart 2.80

for 100% A-**303** to $\lambda_{\text{PL}} = 383, 482$ nm for 100% B-**303**). However, the most interesting finding was that using both of these comonomers allows the suppression of the fluorescence quenching in the solid state of **303**. The solid-state PLQY of a polymer with A:B ratio of 1:24 was almost as high as that in solution (43% vs. 57%), whereas a nearly tenfold decrease of the Φ_{PL} in the solid state was observed for copolymers **303** with only A or only B units.

An increase in the PL QE of the fluorene–thiophene copolymers can be achieved by introduction of *S*-oxidized thiophene units (although no efficient EL from such materials was reported). This aspect and the chemical structures of thiophene-*S,S*-dioxide–fluorene copolymers are discussed in more detail in Section 2.4.

A very efficient green-emitting fluorene copolymer **304** was synthesized by Shim and coworkers [390] via Suzuki coupling of dibromothiopheno[3,2-*b*]thiophene with dialkylfluorene-diboronic acid [390]. The authors compared the EL properties of this copolymer with PFO homopolymer **196** and PFO-bithiophene copolymer **295**. Both the absorption and emission spectra of **304** are red-shifted compared with PFO **196** but slightly blue-shifted compared to bithiophene-based copolymer **295**. PLEDs fabricated in the configuration ITO/PEDOT/**304**/LiF/Al showed a pure green emission (CIE: $x = 0.29, y = 0.63$) close to the

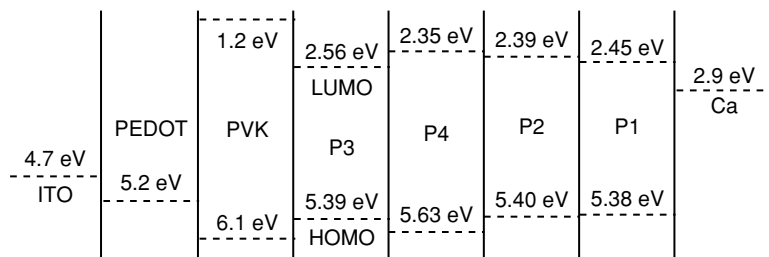


FIGURE 2.22 The schematic energy level structure for the devices with copolymers **300** (P3), **301** (P4), **302a** (P1), and **302b** (P2). (From Liu, B., Niu, Y.-H., Yu, W.-L., Cao, Y., and Huang, W., *Synth. Met.*, 129, 129, 2002. With permission.)

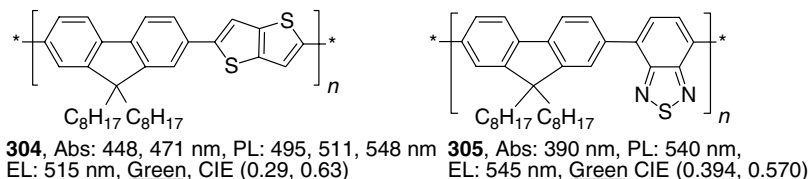


Chart 2.81

standard NTSC green color (CIE: $x=0.26$, $y=0.65$) (NTSC is National Television Systems Committee) with a very low turn-on voltage of 3.3 V. The low turn-on voltage is attributed to the better (compared to PFO) match between the HOMO (−5.38 eV) level and the work function of PEDOT (5.1–5.3 eV). Interestingly, although the PLQY of **304** (12% in films, similar to **295**) is lower than that of PFO (55%), the EL efficiency is much higher, which may reflect an improved balance of electron–hole transport in this copolymer. The maximum current efficiency of **304** is 0.32 cd/A at 0.78 A/cm², which exceeds the performance of similar devices fabricated with **295** or PFO **195** (which showed 0.20 cd/A at 143 mA/cm² and 0.06 cd/A at 25 mA/cm², respectively). The external QE of **304** (0.1%) was twice as high as for the former polymers (Chart 2.81).

A green-emitting fluorene–benzothiadiazole (BT) copolymer **305** was synthesized at Dow Chemicals by Suzuki coupling of fluorene–2,7-diboronic acid with dibromobenzothiadiazole [222,391]. A high-performance green emission PLED was demonstrated with this copolymer [392,393]. In contrast to other PFs, which demonstrate high-mobility nondispersive hole transport [259], copolymer **305** shows a weak and highly dispersive electron transport [394]. Since this copolymer has an electron-deficient moiety in the polymer backbone, a stable anode electrode such as Al can be used, although a thin (70 Å) HTL (TPD, **299**) should be introduced for optimal EL performance. A double-layer PLED device fabricated in configuration ITO/**299**/**305**/Al showed green emission with a turn-on voltage of 7.0 V. A maximum $\Phi_{\text{EL}}^{\text{ex}}$ as high as 3.86% (peak efficiency 14.5 cd/A) and a brightness of 5000 cd/m² were achieved at a current of 34 mA/cm². Even higher performance ($\Phi_{\text{EL}}^{\text{ex}} = 5\%$, efficiency > 20 lm/W, brightness 10,000 cd/m²) for this polymer was reported by Millard [395] at CDT, although the exact LED structure was not disclosed. The EL device with **305** exhibited excellent electrical stability even when operated at high current densities (>0.25 A/cm²). When blended with PFO **196**, an efficient Förster energy transfer from excited PFO segments to **305** chain is observed [396].

Green-emitting fluorene copolymers **306** and **307** were also obtained by introducing pyrazoline moieties into the backbone that completely interrupt the conjugation due to sp³ carbons in the ring [397]. These polymers emit green light with a PL efficiency of 49–59% in films. The PLEDs ITO/PEDOT/polymer/Ba/Ca showed bright-green emission at $\lambda_{\text{EL}} = 494\text{--}500$ nm with high $\Phi_{\text{EL}}^{\text{ex}} = 0.6\text{--}2.5\%$, low turn-on voltage (3.7–5.5 V), and a brightness of up to 2400 cd/m² (Chart 2.82).

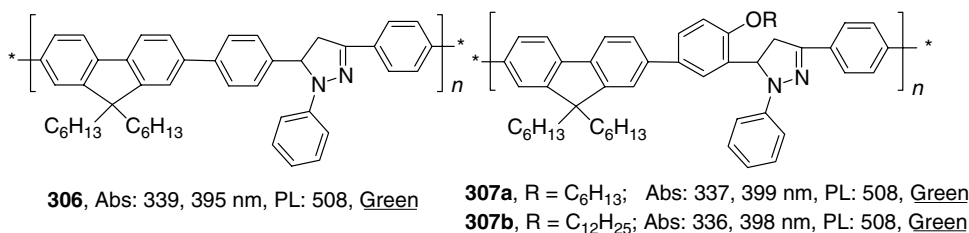


Chart 2.82

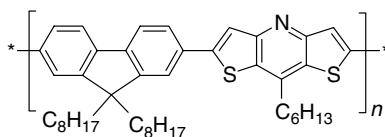
Introduction of electron-accepting bithieno[3,2-*b*:2',3'-*e*]pyridine units resulted in copolymer **308** with ca. 0.5 V lower reduction potential compared to the parent homopolymer PFO **195** [398]. Upon excitation at 420 nm ($\lambda_{\text{max}}^{\text{abs}} = 415$ nm), copolymer **308** exhibited blue-green emission with two peaks at 481 and 536 nm. Preliminary EL studies of an ITO/PEDOT/**308**/Al device showed two peaks positioned as in the PL spectra. The PLED exhibited low turn-on voltage (~ 4 V) but at higher voltages of 6–9 V, a slight increase in the green component was observed (Chart 2.83).

Various fluorene–phenylenevinylene alternating copolymers with different emission colors have been synthesized, e.g., **309a** [399–401], **309b** [402], **310** [403], **311** [149], **312–314** [404], and **315a–c** [405] (Scheme 2.47). Introducing electron-rich (as in polymers **312** and **314**), electron-deficient (as in compounds **310**, **315**, and **327–329**), or both of these units (as in compounds **311** and **313**) in the PF chain allow for precise tuning of the emission wavelength (Scheme 2.47), the HOMO–LUMO levels, and the charge injection and transport properties. However, no high-performance PLEDs based on the above copolymers have yet been reported. One of the best performing devices built in configuration ITO/PEDOT/**309a**/Ca/Al showed a maximum brightness of 870 cd/m² (at 10 V) and an EL efficiency of only 0.16 cd/A.

Several fluorene-containing arylene–vinylene copolymers with a cyano group attached to the vinylene fragment have been reported. The copolymer **316**, containing cyanovinylene–phenylene segments in the main chain, in contrast to the red-emitting copolymers CN-PPV [154], emitted a narrow band with blue light (fwhm = 71 nm) [406]. The ITO/PVK:**316**/Alq₃/Al device reached a brightness of 784 cd/m² at a bias voltage of 18 V and $\Phi_{\text{EL}}^{\text{ex}} = 0.2\%$ (at 123 mA/cm²).

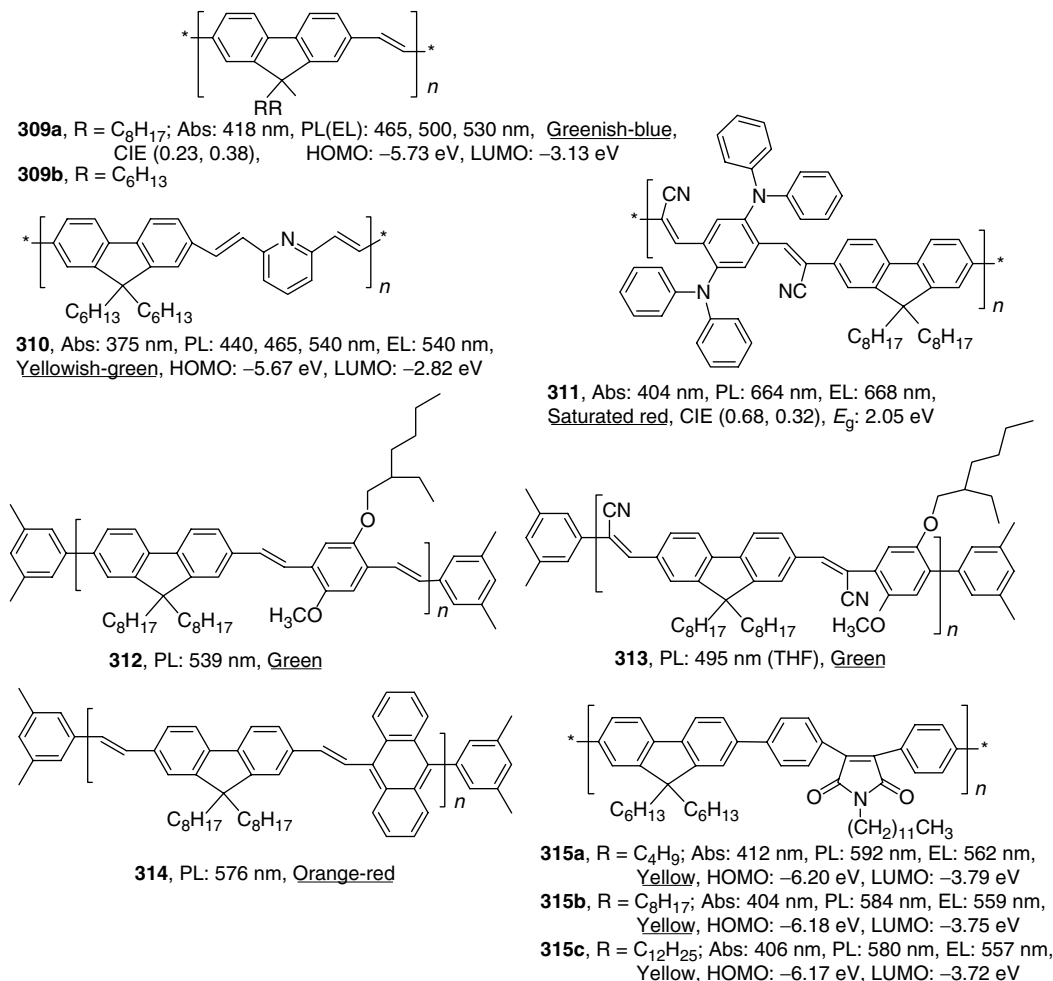
The structural analog **317** of copolymer **316**, in which the benzene ring was replaced with thiophene, showed substantial red shifts in both absorption (97 nm) and emission (134 nm) spectra and PLEDs based on this copolymer (ITO/LiF/**317**/PBD/LiF/Al/Ag) emitted red-orange light (brightness of 45 cd/m² at 10 V; turn-on voltage of 5 V) [407]. A further bathochromic shift in the PL (pure red emission) was observed in copolymer **318**, for which HOMO (−5.32 eV) and LUMO (−3.32 eV) energies were calculated from electrochemical data (both oxidation and reduction appeared as quasireversible processes) [303]. No devices were fabricated with this copolymer. Green-emitting polymer **319** ITO/PEDOT/**319**/Al devices showed a turn-on voltage of 4.8 V, a brightness of 600 cd/m² (at 5.8 V), and a maximum power efficiency of 0.85 lm/W (at 5.6 V) [402].

A series of four fluorene–phenylene vinylene copolymers **320–323** clearly demonstrates the effect of the exact position of CN groups in the vinylene fragment on the emission of the materials (Scheme 2.48) [408]. Substitution of benzene rings in copolymers **320** and **321** by thiophene results in red-shifted PL and EL, where copolymers **322** and **323** exhibit pure red emission with chromaticity values very close to the standard red (CIE: $x = 0.66$, $y = 0.34$), although no PLQY values were reported. The ITO/PEDOT/**322**/Ca/Al device showed a very



308, Abs: 415 nm, PL: 481, 536 nm
EL: 480, 536 nm, Blue-green

Chart 2.83

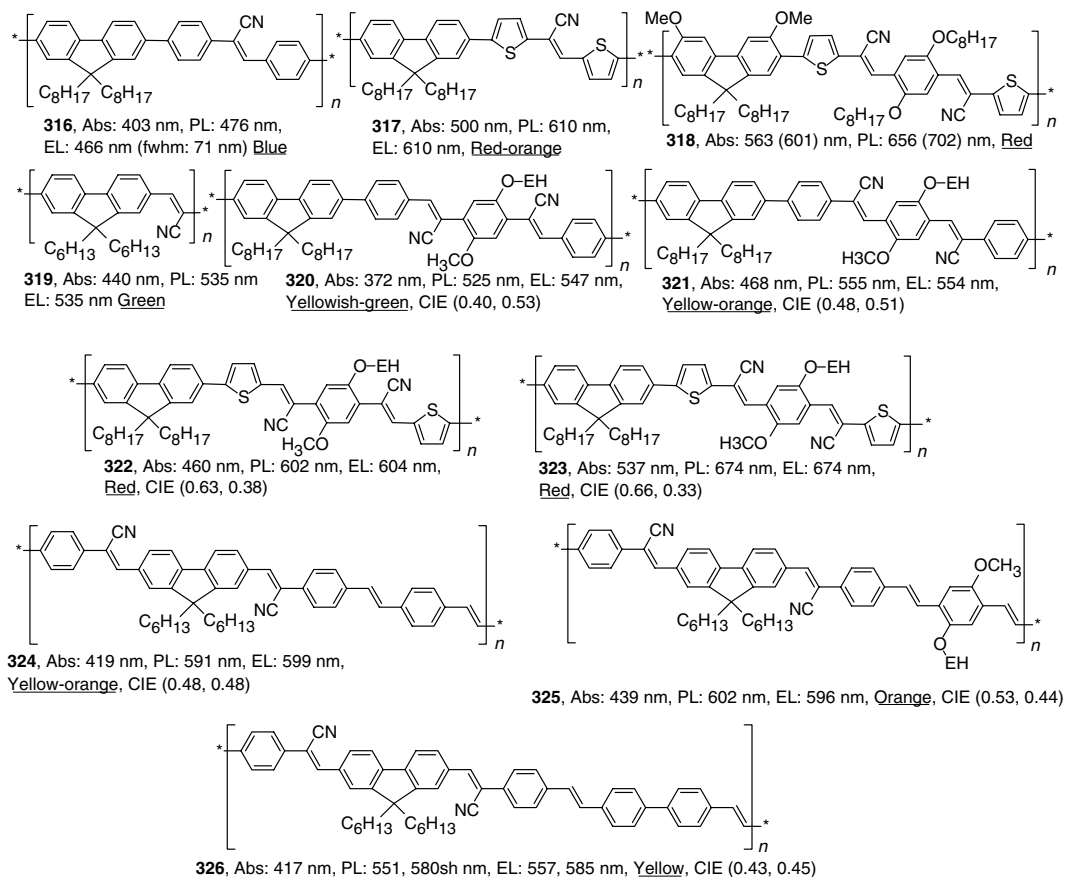


SCHEME 2.47 Fluorene-phenylene vinylene copolymers and their optical and electronic properties in the solid state.

low turn-on voltage of 2.6 V and a maximum brightness of 3100 cd/m² at 6 V. Its maximum $\Phi_{\text{EL}}^{\text{ex}}$ was 0.46% at 4 V, with a brightness of 652 cd/m².

Yellow to orange emission was observed in another series of fluorene-phenylene copolymers with CN groups in the vinylene fragment **324–326** (Scheme 2.48) [409]. The PLQY of the copolymers was relatively low (from 3.5% for **326** to 14.7% for **325**) and the best results in PLED testing were achieved for copolymer **325**. The device ITO/PEDOT/**325**/Al showed a turn-on voltage of 5.0 V and a maximum brightness of 7500 cd/m² at 20 V, with a maximum luminance efficiency of 0.21 lm/W at 6.7 V.

Another series of red-emitting fluorene-containing copolymers of arylene-vinylene type was obtained by introducing 4-dicyanomethylenepyrene-2,6-diyl moiety in the main polymeric chain (**327–329**) [410]. The PL and EL spectra revealed a broad band at 600–800 nm and no emission from the fluorene segments (expected at ~450 nm). The PLEDs fabricated as ITO/PEDOT/polymer/Ba/Al emitted red light with maximum $\Phi_{\text{EL}}^{\text{ex}} = 0.21\text{--}0.38\%$, quite high turn-on voltages (10.4–11.7 V), and a brightness of ~200–450 cd/m² at a bias voltage of ~16–18 V (Chart 2.84).



SCHEME 2.48 Fluorene-phenylene vinylene copolymers with CN groups at vinylene fragment, and their optical and electronic properties in the solid state.

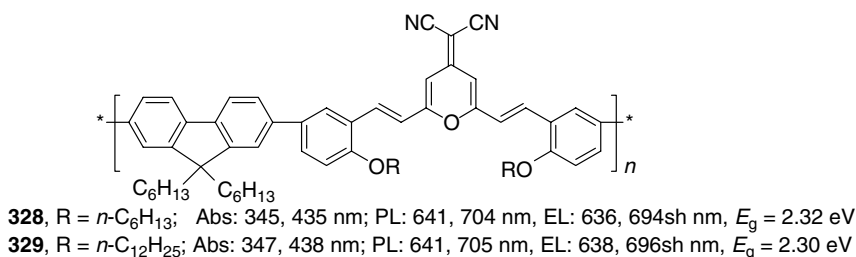
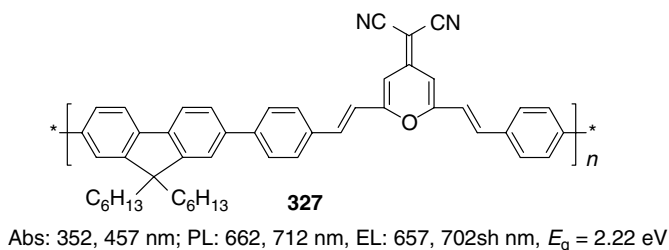
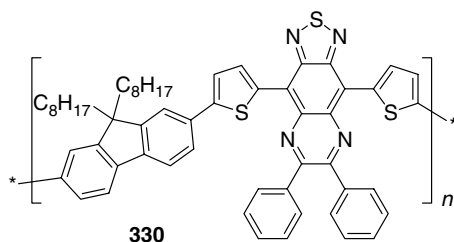


Chart 2.84



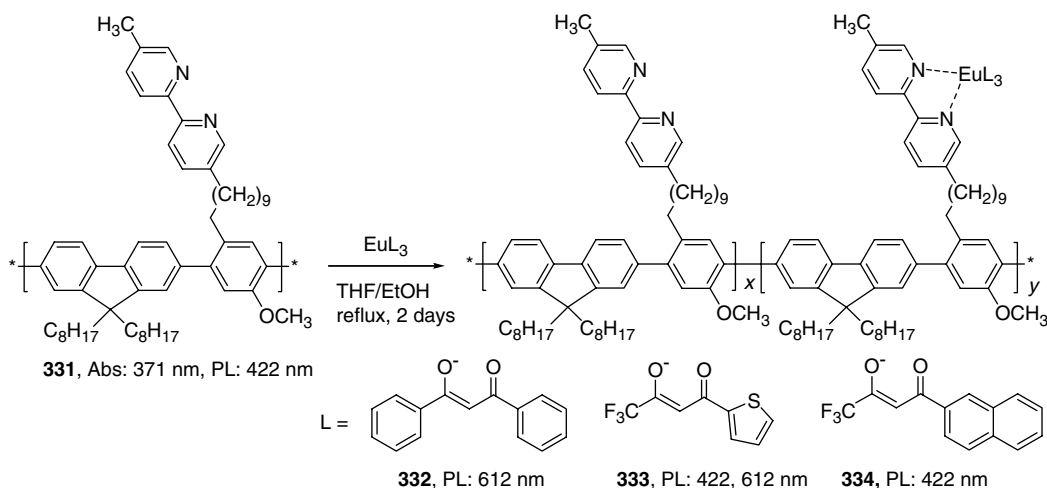
Abs: 400, 780 nm, PL: 1035 nm, EL: 970 nm, E_g : 1.27 eV

Chart 2.85

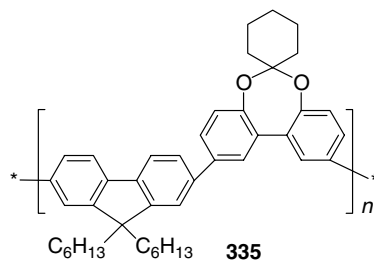
PL and EL emissions from a very low band-gap copolymer **330** ($E_g = 1.27$ eV) was demonstrated by Swedish researchers [411]. The material has two absorption peaks at 400 and 780 nm and emits light in the NIR region. The PL spectrum of thin films has one peak at 1035 nm, which is blue-shifted by ca. 60 nm on annealing at 200°C for 10 min. The ITO/PEDOT/**330**/Ca/Al diode was positively biased when the Al/Ca electrode was connected to lower potential and the EL emission became observable at 1.1 V ($\lambda_{EL} = 970$ nm). The Φ_{EL}^{ex} for a nonoptimized device was quite low (0.03–0.05%), nevertheless demonstration of EL from PLED in the NIR can be important for communication and sensor technologies (Chart 2.85).

Pei et al. [412] reported an alternating fluorene copolymer **331** with 2,2'-bipyridyl in a side chain that emitted at 422 nm. Treating this polymer with Eu^{3+} chelates formed the polymeric complexes **332**–**334**. Their emission was governed by intramolecular Förster energy transfer, whose efficiency depends on the structure of the ligands and the Eu^{3+} content (Scheme 2.49) [412]. The most effective energy transfer manifested itself in a single red emission band at 612 nm for the complex **332** with a maximum intensity achieved at ~25 mol% content of Eu^{3+} .

The color of fluorene copolymers can also be shifted into the UV, as exemplified by copolymer **335** [413]. Its PL spectrum in THF solution is blue-shifted by 49 nm compared to



SCHEME 2.49 Synthesis of Eu-containing chelated PFs. (From Pei, J., Liu, X.-L., Yu, W.-L., Lai, Y.-H., Niu, Y.-H., and Cao, Y., *Macromolecules*, 35, 7274, 2002.)



Abs: 328 nm, PL: 368, 386 nm, Φ_{PL} : 62% (all in THF)
EL: 395 nm, HOMO: -5.89 eV, LUMO: -2.63 eV

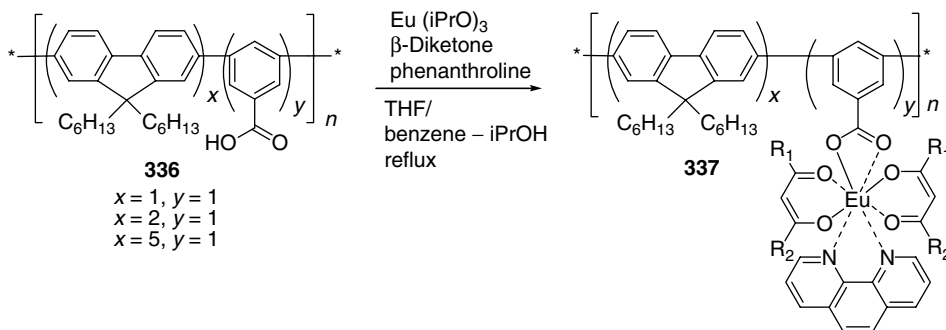
Chart 2.86

PDHF **195**, showing somewhat lower PLQY (62%). The ITO/PEDOT/**335**/Ba/Al device emits violet light with $\lambda_{\text{max}}^{\text{EL}} = 395$ nm. However, performance is poor (turn-on voltage 8 V, maximum $\Phi_{\text{EL}}^{\text{ex}} = 0.054\%$, brightness 10 cd/m^2). When it was blended with 5% PDHF **195**, $\Phi_{\text{EL}}^{\text{ex}}$ increased to 0.3% (slightly lower than for pure PDHF **195** measured in the same conditions) and the color purity (blue) was improved (CIE: $x = 0.18$, $y = 0.10$ at potentials 8–20 V), compared to pure PDHF **195** (CIE: $x = 0.21$, $y = 0.26$ at 5 V and $x = 0.26$, $y = 0.37$ at 10 V) (Chart 2.86).

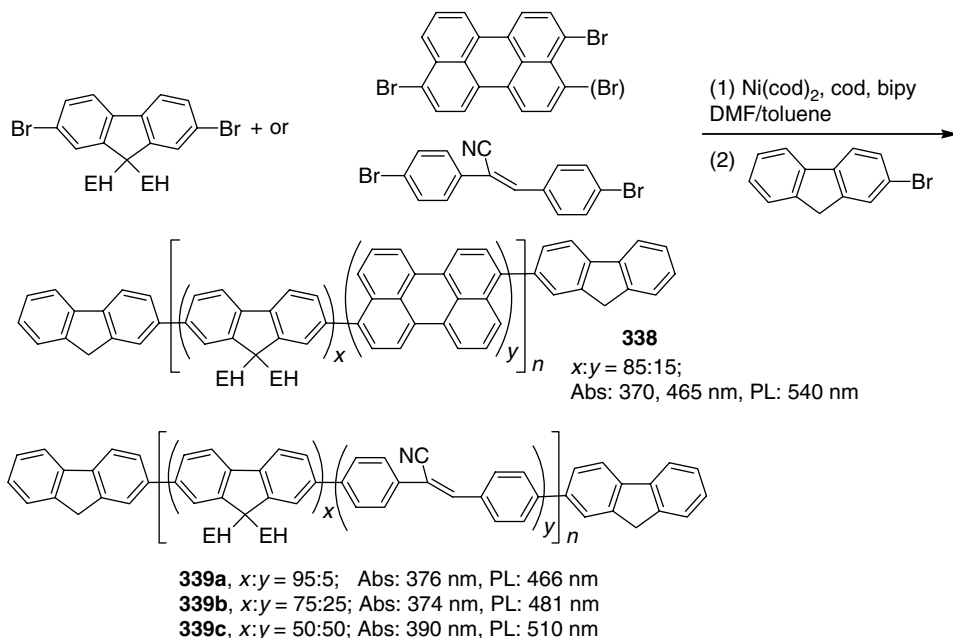
2.3.11.3 Random (Statistical) Copolymers

Another example of efficient Förster energy transfer in Eu^{3+} complexes of fluorene copolymers (similar to the alternating copolymers described in Scheme 2.49) was demonstrated by Huang and coworkers [414] for random copolymers. They synthesized copolymers **336** with a different ratio between the fluorene and the benzene units in the backbone and converted them into europium complexes **337** (Scheme 2.50) [414]. The complexes **337** were capable of both blue and red emission under UV excitation. In solution, blue emission was the dominant mode. However, the blue emission was significantly reduced or completely suppressed in the solid state and nearly monochromatic (fwhm ≈ 4 nm) red emission at 613 nm was observed.

Miller's group [415–417] at IBM reported two series of statistical PF copolymers using perylene and cyano-substituted phenylene vinylene chromophoric segments (Scheme 2.51).



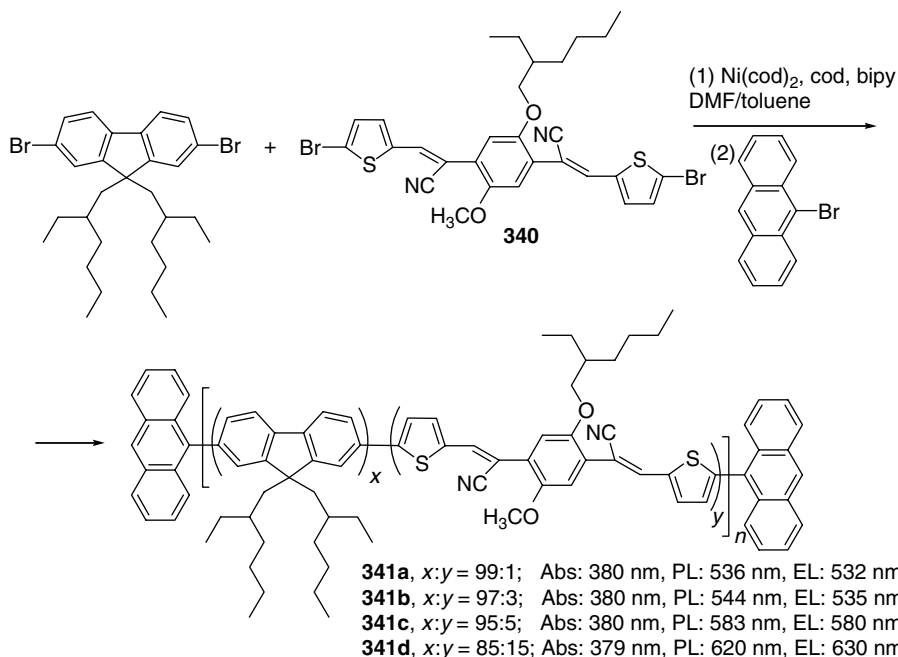
SCHEME 2.50 Synthesis of polymeric Eu complex **337**. β -Diketone ligands are the same as in complexes **332–334** (Scheme 2.49). (From Ling, Q.D., Kang, E.T., Neoh, K.G., and Huang, W., *Macromolecules*, 36, 6995, 2003.)



SCHEME 2.51 Synthesis of perylene–fluorene and α -cyanostilbene–fluorene copolymers via Yamamoto coupling. (From Klärner, G., Lee, J.-I., Davey, M.H., and Miller, R.D., *Adv. Mater.*, 11, 115, 1999.)

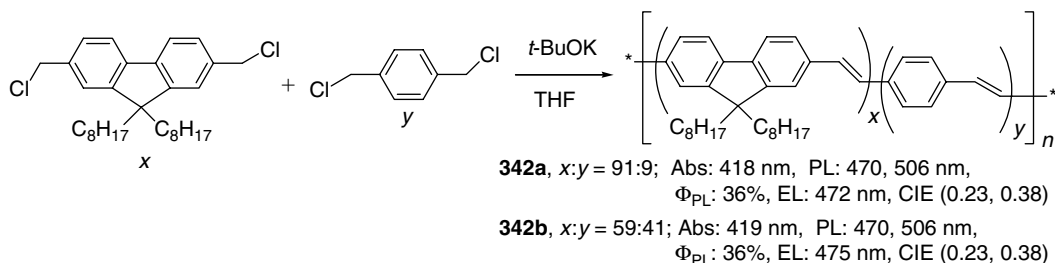
Copolymers **338** and **339a–c** are soluble in organic solvents and their molecular weights are in the range of $M_n \sim 10,000$ –55,000 g/mol. They are thermally stable and show no color change upon thermal annealing. The emission color is strongly dependent on the feed ratio of the comonomers. For example, in the case of copolymers **339**, the emission color can be turned from blue (**339a**, 466 nm) through blue-green (**339b**, 481 nm) to pure green (**339c**, 510 nm).

After Miller's report, Shim and coworkers [418,419] reported a series of random copolymers synthesized by Yamamoto coupling of 2,7-dibromo-9,9-bis(2-ethylhexyl)fluorene with **340** (Scheme 2.52). Varying the feed ratio of the thiophene comonomer from 1:99 to 15:85, green-, yellow-, and red-emitting copolymers were synthesized. The actual ratio of the comonomer, calculated from nitrogen analysis, is somewhat higher than the feed ratio, reflecting a higher reactivity of **340** monomer in the Yamamoto reaction ($y = 1.4, 3.1, 7.0$, and 17.5% for **341a,b,c,d**, respectively). All the copolymers are soluble in common organic solvents and a molecular weight (M_n) in the range of 13,000–22,000 g/mol ($\text{PDI} = 1.5$ –2.7) was reported. Interestingly, regardless of composition, all the copolymers showed a similar absorption with λ_{max} at ~ 380 nm, with the exception of a weak shoulder at ~ 470 nm, which is more intense for polymers with a higher ratio of the **340** unit. In contrast, their emission colors are progressively red-shifted with increasing comonomer **340** fraction. As a result, **341a** emits green (540 nm), **341b** emits yellow (585 nm), and **341c** emits bright-red (620 nm), all with reasonably high PLQY (34–69%). The EL spectra obtained from PLEDs fabricated as ITO/PEDOT/polymer/LiF/Al are almost identical to the PL spectra. As the feed ratio of **340** increases, the threshold voltage drops from 13 V to only 5 V, and the emission intensity at low voltages also increases, which suggests improved charge transport and balance in the material. As can be calculated from the current–voltage–luminance (IVL) plot, a luminous efficiency of ~ 0.7 cd/A (at 15 V), ~ 2.4 cd/A (at 12 V), and ~ 1.5 cd/A (at 9.5 V) is achieved with polymers **341a,b,c**, respectively.

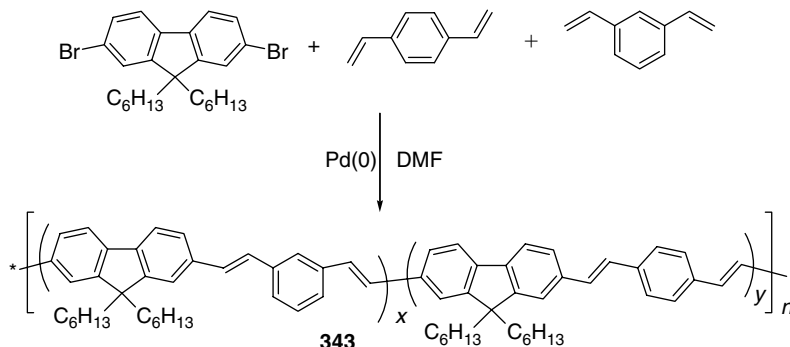


SCHEME 2.52 Synthesis of PF-PPV copolymers **341a–d** with tunable emission color. (From Hwang, D.-H., Cho, N.S., Jung, B.-J., Shim, H.-K., Lee, J.-I., Do, L.-M., and Zyung, T., *Opt. Mater.*, 21, 199, 2002; Cho, N.S., Hwang, D.-H., Lee, J.-I., Jung, B.-J., and Shim, H.-K., *Macromolecules*, 35, 1224, 2002.)

Hwang et al. [401] reported random copolymers of PF with PPV units in different feed ratios through Gilch polymerization (Scheme 2.53). The molecular weights of the obtained copolymers are in the range of 57,000–87,000 g/mol with PDI of 1.4 to 2.1. Interestingly, the copolymers **342** with different feed ratio $x:y$ showed the same optical properties as those of the corresponding fluorene–vinylene homopolymer ($y = 0$, **309a**). The UV–vis spectrum of the thin films showed a peak absorption at 418 nm with onset absorption of 485 nm and PL emission maximum at 470 nm plus well-defined vibronic bands at ~500, 530, and 560 nm. The PLED devices, consisting of ITO/PEDOT/**342**/Al, gave very similar EL emission spectra (CIE: $x = 0.23$, $y = 0.38$) and significantly improved device performance (0.71–1.05 cd/A), compared to the homopolymer **309** (0.13 cd/A). The latter was explained to be due to improved hole injection and transport, owing to the PPV segments. Indeed, the ionization



SCHEME 2.53 Gilch polymerization to synthesis of random copolymers. (From Hwang, D.-H., Lee, J.-D., Kang, J.-M., Lee, S., Lee, C.-H., and Jin, S.-H., *J. Mater. Chem.*, 13, 1540, 2003.)



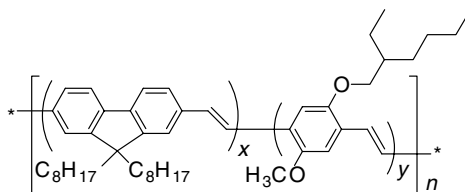
SCHEME 2.54 Random fluorene–divinylbenzenes copolymers by Heck polymerization. (From Cho, H.N., Kim, J.K., Kim, D.Y., Kim, C.Y., Song, N.W., and Kim, D., *Macromolecules*, 32, 1476, 1999.)

potential of the copolymers is around 5.53–5.55 eV, which is much closer to the HOMO level of PEDOT (5.2 eV), when compared to homopolymer (5.73 eV).

It is interesting that statistical copolymers **343**, containing *m*-phenylene linkages that are supposed to interrupt conjugation, showed a PL maximum of 475 nm, similar to **342**. Due to efficient energy transfer from the *meta*- to the *para*-linked chromophores, the emission maxima did not depend on the ratio of *m*- and *p*-divinylbenzenes, unless 100% loading of the *meta* units was used [420] (Scheme 2.54).

The emission wavelength of PF–PPV copolymer can be red-shifted and the band gap reduced by introducing alkoxy substituents, as demonstrated for compounds **344** [421]. Consequently, the transport of both holes and electrons is facilitated and the PLED built in the configuration ITO/PEDOT/**344**/Al produces an orange-red color ($\lambda_{\text{EL}} = 574\text{--}592\text{ nm}$) with a maximum brightness for **344b** of 1350 cd/m^2 and a luminous efficiency of 0.51 cd/A , at a rather low turn-on voltage of 2.5 V (Chart 2.87.)

Several random fluorene–thiophene copolymers such as **345a–e** [422,423], **346** [424], **347** [420,425] have been investigated. Because of the possible fine-tuning of the comonomer ratio, many of these have shown an EL performance far greater than that of the PF homopolymer or the corresponding alternating copolymers. Thus, the PLED ITO/PEDOT/**346**/Ba/Al showed a brightness of ca. 2600 cd/m^2 (at 8 V) and $\Phi_{\text{EL}}^{\text{ex}} = 1.25\%$. The “*meta*” linkage of



344a, $x:y = 95:5$; Abs: 418 nm, PL: 576 nm, EL: 574 nm, HOMO: -5.36 eV , LUMO: -2.77 eV

344b, $x:y = 90:10$; Abs: 421 nm, PL: 576 nm, EL: 576 nm, HOMO: -5.16 eV , LUMO: -2.62 eV

344c, $x:y = 80:20$; Abs: 420 nm, PL: 589 nm, EL: 589 nm, HOMO: -5.31 eV , LUMO: -2.77 eV

344d, $x:y = 50:50$; Abs: 422 nm, PL: 593 nm, EL: 592 nm, HOMO: -5.09 eV , LUMO: -2.99 eV

309a, $x:y = 100:0$; Abs: 419 nm, PL: 507 nm, EL: 508 nm, HOMO: -5.34 eV , LUMO: -2.75 eV

13, $x:y = 0:100$; Abs: 502 nm, PL: 582 nm, EL: 586 nm, HOMO: -4.90 eV , LUMO: -2.80 eV

Chart 2.87

Chart 2.88

Cao and coworkers synthesized three series of copolymers **348** [426], **349** [427], **350** [428], and **351** [429], exploiting random copolymerization of fluorene fragments with dibromoderivatives of Se,N and S,N heterocycles (Scheme 2.55). Fluorene–benzoselenadiazole

SCHEME 2.55 Synthesis of benzothiaselanazole-, naphthoselenathiazole-, and (thiophene-benzothiazole-thiophene)-fluorene copolymers via Suzuki coupling. (From Yang, R., Tian, R., Hou, Q., Yang, W., and Cao, Y., *Macromolecules*, 36, 7453, 2003; Yang, J., Jiang, C., Zhang, Y., Yang, R., Yang, W., Hou, Q., and Cao, Y., *Macromolecules*, 37: 1211, 2004; Hou, Q., Xu, Y., Yang, W., Yuan, M., Peng, J., and Cao, Y., *J. Mater. Chem.*, 12, 2887, 2002; Hou, Q., Zhou, Q., Zhang, Y., Yang, W., Yang, R., and Cao, Y., *Macromolecules*, 37, 6299, 2004.)

alternating copolymer **348** ($x:y=50:50$) showed substantial (55 nm) red shift in PL, compared to its BT analog **305** (595 nm [426] and 540 nm [300,392], respectively) because of a narrower $\pi-\pi^*$ gap of the benzoselenadiazole unit. Increasing the content of the fluorene moieties in the copolymers **348** results in a regular PL blue shift of (568 nm for $x:y=98:2$), though an irregular variations in Φ_{PL} (between 16 and 51% in films) was reported for this series of copolymers. Whereas the main PL in solution is observed in the region of 570–600 nm with a low-intensity short-wavelength band (due to fluorene emission), the latter is completely suppressed in films. PLEDs fabricated as ITO/PEDOT (or PVK)/**348**/Ba/Al showed orange-red emission ($\lambda_{\text{max}}^{\text{EL}}=573\text{--}600$ nm, depending on the $x:y$ ratio) with no blue emission, even at the lowest concentration (2%) of the heterocyclic units. Comparison of devices with two different HTL (PEDOT or PVK) showed that LEDs with a PVK layer (ITO/PVK/**348** ($x:y=85:15$)/Ba/Al) demonstrated a better $\Phi_{\text{EL}}^{\text{ex}}$ that reached a value of 1% ($\lambda_{\text{max}}^{\text{EL}}=582$ nm; CIE: $x=0.698$, $y=0.300$) [426].

A much more pronounced bathochromic shift in emission was achieved for copolymers **349**, which emit in the red with $\lambda_{\text{PL}}=634\text{--}681$ nm ($\Phi_{\text{PL}}=33\text{--}84\%$). Although blue emission at 423–438 nm from the fluorene fragments was also observed, its intensity decreased with decreasing $x:y$ ratio [427]. In EL spectra, the blue emission from the PF segment was completely quenched at very low naphthoselenadiazole content (0.5%), which could be due to efficient exciton and charge trapping on the narrow band gap naphthoselenadiazole sites. The highest $\Phi_{\text{EL}}^{\text{ex}}=3.1\%$ was reported for ITO/PEDOT/**349** ($x:y=99:1$)/Ba/Al diodes (although it corresponds to a relatively low luminous efficiency of 0.91 cd/A very likely due to insensitivity of the human eye to this particular spectral distribution) with a maximum brightness of up to 2100 cd/m² (CIE: $x=0.64$, $y=0.33$).

The last example of red-emitting fluorene copolymer in this series, the copolymers **350** and **351** contain both BT acceptor and thiophene donor units in the main chain [428,429]. As expected for donor–acceptor alternation in the main chain of the conjugated polymers, a substantial red shift in PL, compared to copolymer **305** or even **348**, was observed ($\lambda_{\text{PL}}=635\text{--}685$ nm (**350** [428]) 629–678 nm (**351b** [429]) in films for $x:y=99:1\text{--}65:35$). In dilute solution, additional emission from fluorene segments is completely suppressed by increasing the polymer concentration or the content of heterocyclic fragment in the polymer chain. ITO/PEDOT/**350**/Ba/Al devices showed $\Phi_{\text{EL}}^{\text{ex}}$ in the range of 0.5–1.4%. The highest efficiency of 1.4% and the luminance of 256 cd/m² at a bias of 5.1 V was achieved for the copolymer having $x:y=85:15$ ratio. This device reached a maximum luminance of 3780 cd/m² at 8.2 V. Even higher $\Phi_{\text{EL}}^{\text{ex}}=1.93\text{--}2.54\%$ was achieved with copolymers **351b** ($x:y=95:5\text{--}85:15$) for the device ITO/PEDOT/PVK/**351b**/Ba/Al [429]. These copolymers showed saturated red emission with $\lambda_{\text{EL}}=634\text{--}647$ ($x=0.66\text{--}0.67$, $y=0.33\text{--}0.34$).

Jenekhe and coworkers [430] synthesized a phenothiazine-containing alternating fluorene copolymer **352** by Suzuki coupling (Chart 2.89). The phenothiazine-3,7-diyl fragment in the polymer backbone interrupts the conjugation, and substantially blue shifts absorption

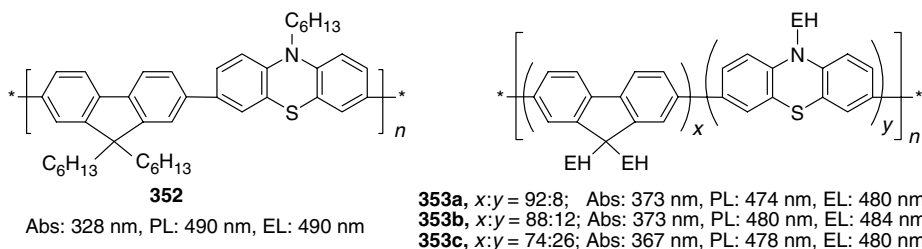
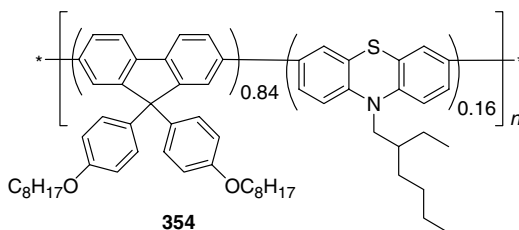


Chart 2.89

compared to PDHF homopolymer **195** (328 and 385 nm, respectively). Nevertheless, the ionization potential of **352** (estimated from the electrochemical data as $I_P = E_{\text{ox}}^{\text{onset}} + 4.4 \text{ V}$) is much higher (5.1 eV) than that for PDHF **195** due to the electron-rich phenothiazine unit, suggesting good hole-transport properties. Greenish-blue EL ($\lambda_{\text{max}}^{\text{EL}} = 490 \text{ nm}$) with a luminance of up to 320 cd/m^2 and a maximum $\Phi_{\text{EL}}^{\text{ex}} = 0.10\%$ at 12.5 V was observed for an ITO/PEDOT/**352**/Al diode. Similar random fluorene–phenothiazine copolymers **353a–c** showed close EL maxima but much better device performance (e.g., for **353b**: maximum brightness 4170 cd/m^2 , power efficiency 2.08 cd/A , turn-on voltage 3.8 V; CIE: $x = 0.17$, $y = 0.37$) [431].

Hwang et al. [432] studied EL from the devices fabricated using blends of similar blue-emissive fluorene–phenothiazine copolymer **354** with MEH-PPV (Chart 2.90). The maximum brightness of the devices ranged from 1580 to 2640 cd/m^2 with $\Phi_{\text{EL}}^{\text{ex}} = 0.3\text{--}0.4\%$. The inefficient energy transfer between these blue and red LEP enabled the production of white-light emission through control of the blend ratio; with an increasing amount of **354** in the blends, CIE coordinates of EL emission are shifted from $x = 0.19$, $y = 0.45$ (for 1% of **354**) to $x = 0.36$, $y = 0.51$ (for 3% of **354**), although even the most optimal blend (2.5% of **354**: $x = 0.19$, $y = 0.45$) is quite far from the real white point [433].

Müllen and coworkers [434] achieved efficient color tuning in PF via excitation energy transfer onto perylene dye fragments introduced as (i) randomly distributed comonomer in the PF chain, (ii) end-capping group, or (iii) side chain. Perylene compounds are known for their high stability, great QE, and large range of emission colors, achieved via introduction of different substituents. The random copolymers (**355–361**) were synthesized by Yamamoto coupling of dibromodialkylfluorenes with corresponding brominated perylenes (1–5%) (Chart 2.91). The M_n in the range of 30,000–140,000 (90–400 units in a chain) and very high polydispersity (4.1–7.7) observed in these polymers were explained by relatively low reactivity of bromoperylene comonomers. The PL spectra of the copolymers in solution were essentially identical to those of PF homopolymers, while in the solid state an efficient energy transfer onto the dye fragments occurred, giving rise to an additional red-shifted emission band, whose position depends on the perylene structure. The energy transfer appears to be as efficient with 1% of the dye as with 5%. Generally, the PL efficiencies of the copolymers in solid films varied from 38 to 56%, with the exception of material **359** that showed a PL efficiency of only 7%. The latter contains 3% of both perylene fragments. The low QE was explained by aggregation of the perylene units in the solid state. The devices made from these copolymers in configuration ITO/PEDOT/copolymer/Ca showed stable emission color with $\Phi_{\text{EL}}^{\text{ex}} = 0.2\text{--}0.6\%$ and an EL efficiency of $0.9\text{--}1.6 \text{ cd/A}$, which are rather high for nonoptimized devices. In contrast to PL spectra, there was a complete energy transfer in the EL spectra (no fluorene emission), and the emission color can be finely tuned by structural modifications in the perylene units (Table 2.3, Figure 2.23).



Abs: 371 nm, PL (EL): 482 nm, Blue,
 E_g : 2.82, HOMO: -5.40 eV , LUMO: -2.58 eV

Chart 2.90

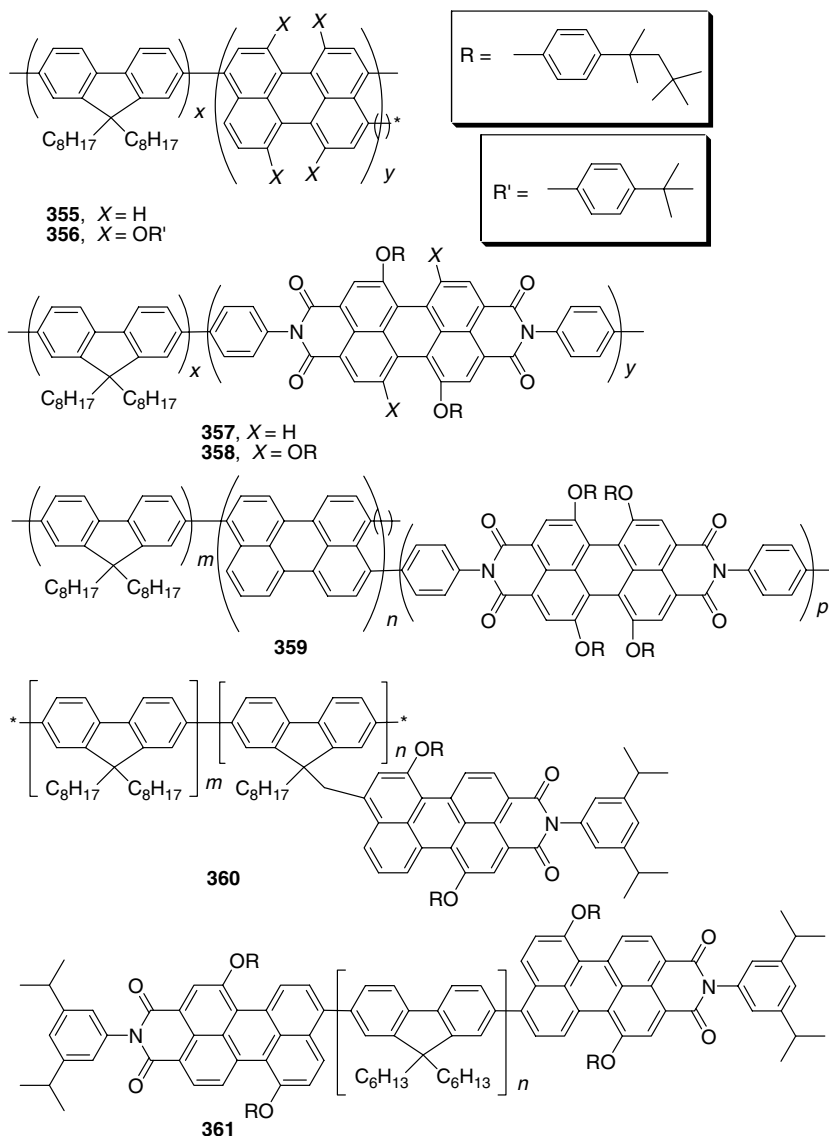


Chart 2.91

TABLE 2.3
Optical and Electronic Properties of the Fluorene–Perylene Copolymers

Polymers (% Dye), Emission Color	M_n (g/mol) (PDI)	Φ_{PL} (Film)	λ_{max}^{EL} (nm) [Φ_{EL}^{ex}], CIE (x , y)	Turn-On Voltage (V)	Luminous Efficiency (cd/A)
355 (3%), Bright-green	47,930 (4.1)	51%	520 [0.6%], (0.362, 0.555)	12	0.9
356 (5%), Yellow	32,300 (4.9)	40%	558 [0.2%], (0.414, 0.519)	11	0.4
357 (5%), Deep-red	63,510 (3.6)	33%	675 [0.5%], (0.636, 0.338)	8	1.6
358 (1%), Red-orange	142,500 (3.8)	42%	600 [0.3%], (0.590, 0.365)	15	1.4

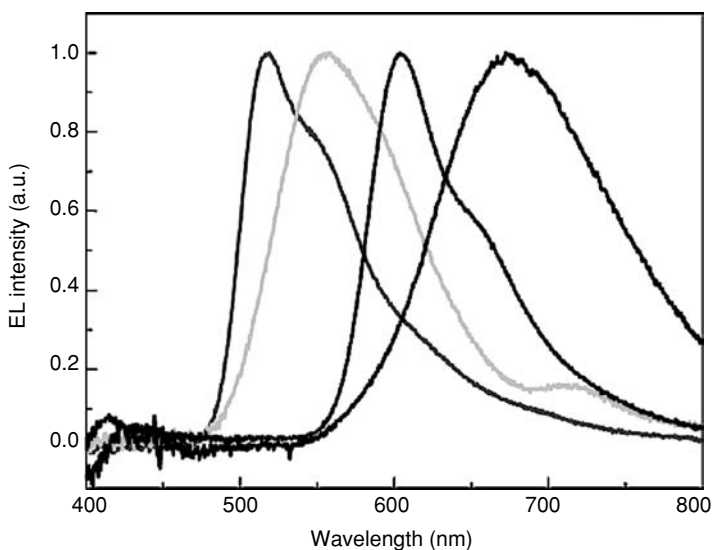


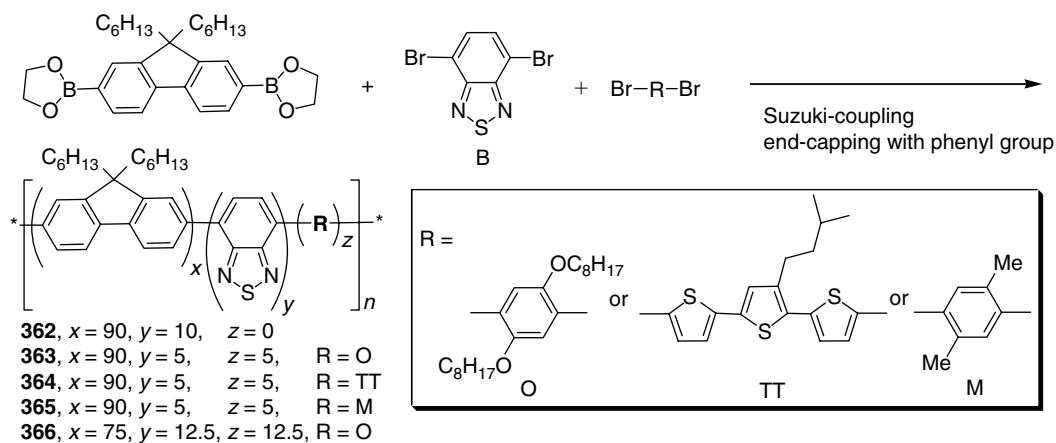
FIGURE 2.23 EL spectra of the copolymers (from left to right) **355**, **356**, **358**, and **357** in devices ITO/PEDOT/polymer/Ca/Al. (From Ego, C., Marsitzky, D., Becker, S., Zhang, J., Grimsdale, A.C., Müllen, K., MacKenzie, J.D., Silva, C., and Friend, R.H., *J. Am. Chem. Soc.*, 125, 437, 2003. With permission.)

A very efficient energy transfer (producing emission at 613 nm) was observed in PL spectra of the perylene end-capped polymer **361** in solid films. This material had the highest QE (>60%) among the fluorene–perylene polymers, although the performance of its PLED has not yet been reported [434].

Attaching perylene moieties as side groups allows achievement of high concentration without affecting the electronic structure of the polymer backbone. Putting 16% perylene moieties as side chains predictably results in more efficient energy transfer, observed with polymer **360**, both in solution and solid state (emission band at 599 nm). Although no PLED device with **360** has been reported, this material showed excellent performance in solar cells (external photovoltaic QE = 7%, in blend with PPV) [434].

2.3.11.4 Copolymers with Three or More Comonomer Units

Alex Jen's group [435] reported a series of highly efficient random conjugated copolymers **362–366**, containing dialkylfluorene and electron-deficient BT units, synthesized by Suzuki-coupling polymerization (Scheme 2.56). To balance the charge-transport and charge-injection properties, a third, electron-rich unit was introduced in the polymer. All of the copolymers showed very similar absorption spectra ($\lambda_{\text{max}} = 380$ nm). The luminescence properties of the copolymers are dominated by the BT unit; all the copolymers have similar red-shifted luminescence peaks at $\lambda_{\text{PL}} = 540$ nm ($\Phi_{\text{PL}} = 23\text{--}55\%$, depending on the monomer) and the third comonomer does not contribute to the emission spectra. This can be explained by a charge transfer or energy transfer process between the electron-rich segments and electron-deficient BT units. Although the luminescence properties of the copolymers are the same, their charge-transport properties are quite different. The authors studied current–voltage characteristics of metal–polymer–metal junctions, fabricated with metals of high and low work function. As expected, the highest hole conductivity belongs to terthiophene-containing polymer **364** (at the expense of the lowest electron conductivity). The highest electron conductivity was achieved with polymer **366**, having the highest ratio of electron-deficient BT component. Remarkably,



SCHEME 2.56 Synthesis of fluorene-benzothiadiazole copolymers. (From Herguth, P., Jiang, X., Liu, M.S., and Jen, A.K.-Y., *Macromolecules*, 35, 6094, 2002.)

the last polymer showed the best performance in LED devices, demonstrating that increasing the electron conductivity balances the charge-transport properties in PF materials. The PLEDs were fabricated in configuration ITO/HTL/copolymer/Ca (HTL was either PEDOT or BTPD-PFCB, **132**). The lowest performance was revealed by copolymer **364**, attributed to the oligothiophene units' quenching effect. The best device, fabricated in configuration ITO/BTPD-PFCB **132/366**/Ca/Al, had a remarkable $\Phi_{\text{EL}}^{\text{ex}}$ of 6.0% and a photometric power efficiency of 18.5 cd/A (an even higher efficiency of 28.6 cd/A for an unspecified device structure is reported in Section 2.6 [435]). The highest brightness of 59,400 cd/m² was achieved with this device at 15.2 V. Interestingly, when PEDOT was used in the same device structure, instead of BTPD-PFCB **132**, the PLED performance was lower: $\Phi_{\text{EL}}^{\text{ex}} = 1.5\%$, an EL current to light efficiency of 4.66 cd/A, and a maximum brightness of 21,000 cd/m². However, as seen in Figure 2.24, the higher performance of HTL **132** appears only at relatively high voltage (>12 V) and thus cannot be taken as a general rule for all PLEDs.

A further development of this approach with multicomponent PF copolymers for tuning the emission color was recently exemplified by fabrication of an red-blue-green (RGB) prototype display, where pure red, green, and blue colors were achieved by simple variation of the feed ratio of several monomers (Scheme 2.57) [436]. The resulting polymers were very soluble in organic solvents, had high molecular weight ($M_n \sim 50,000$), and revealed a respectable EL performance. The PLED fabricated as ITO/PEDOT/polymer/Ca/Al showed switch-on voltages of 4.5 V for blue emitter **367**, 3.8 V for green emitter **368**, and 7.5 V for red emitter **369** with a maximum EL efficiency of 3.0, 6.5, and 1.1 cd/A, respectively. The presence of a photopolymerizable (in the presence of photoacid) oxetane unit in the comonomer B renders insoluble cross-linked polymer upon photolithographic development, allowing solution process fabrication of the PLED display, bearing different emitting materials.

2.3.12 POLYFLUORENE-BASED POLYELECTROLYTES

Fluorene-[2,5-di(aminoethoxy)benzene] copolymers **370a,b** have been synthesized by Huang and coworkers [437,438] as precursors to the first water-soluble cationic PFs **371**, **372a-c** (Scheme 2.58). Whereas the neutral polymers **370a,b** readily dissolve in common organic solvents such as THF, chloroform, toluene, and xylene (but not in dimethyl sulfoxide (DMSO), methanol, or water); their quaternization produces material **371**, which is insoluble in chloroform or THF but completely soluble in DMSO, methanol, and water. For

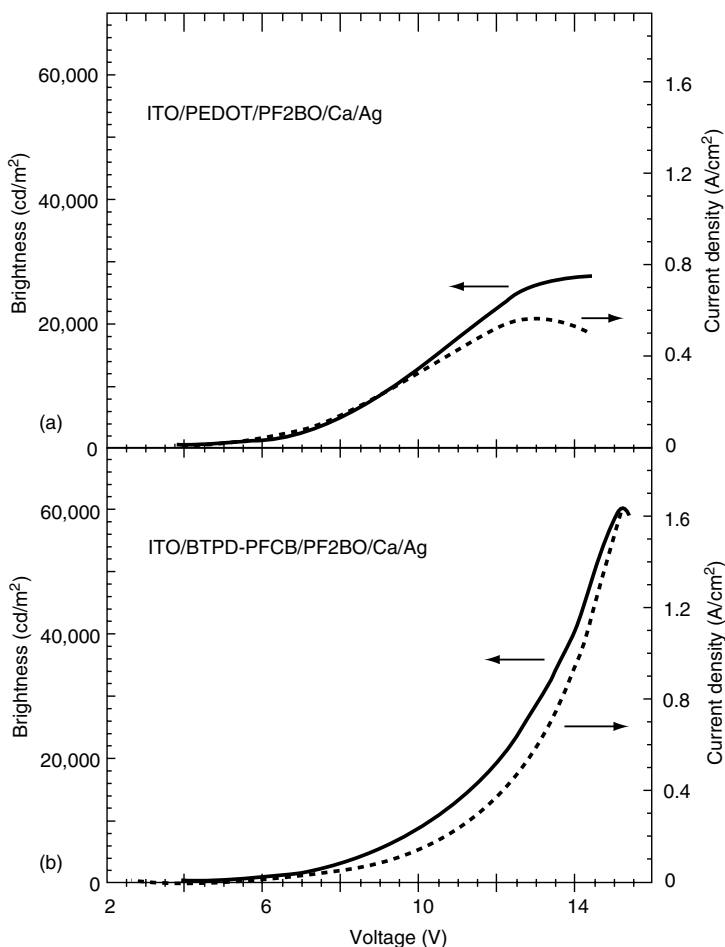
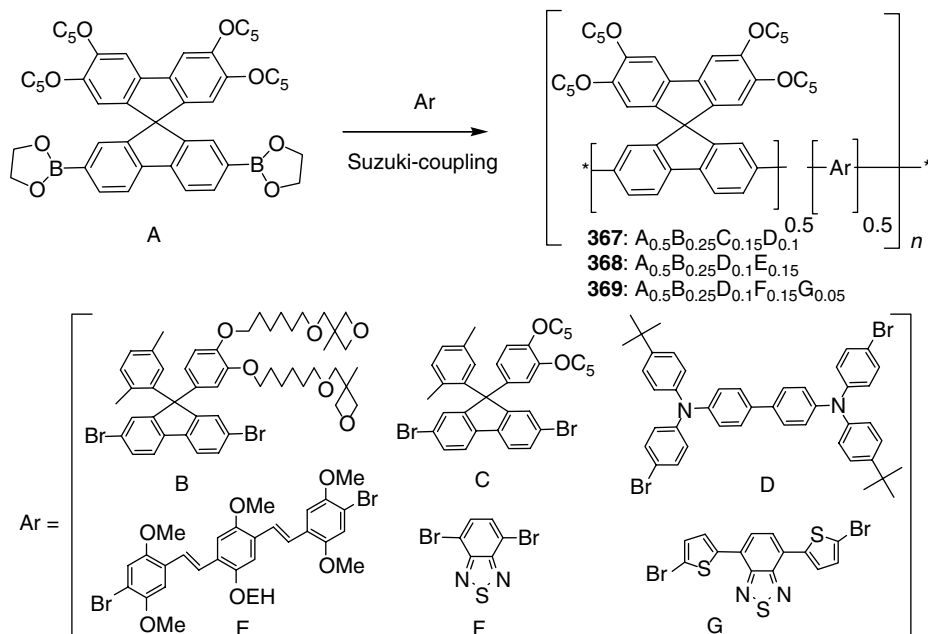


FIGURE 2.24 The plot of brightness (dashed line) and current density (dotted line) vs. applied voltage for PLEDs (a) ITO/PEDOT/**366**/Ca/Ag and (b) ITO/**132/366**/Ca/Ag. (From Herguth, P., Jiang, X., Liu, M.S., and Jen, A.K.-Y., *Macromolecules*, 35, 6094, 2002. With permission.)

copolymers **372a–c**, with partial degree of quaternization, the solubility is intermediate between the neutral and fully quaternized polymers. Whereas neutral polymers **370a,b** showed good thermal stability ($T_{\text{dec}} = 400$ and 340°C , respectively, in nitrogen), quaternized polymers **371** and **372a–c** begin to decompose at ca. 230°C [438], although a higher value of $T_{\text{dec}} = 300^{\circ}\text{C}$ was reported in the preliminary communication [437]. Both neutral and quaternized polymers absorb and emit in the region typical for PFs with only small variations (~ 10 nm) in PL depending on the structure and the solvent, e.g., **370a**: $\lambda_{\text{abs}} = 370.5$ nm, $\lambda_{\text{PL}} = 414, 428\text{sh}$ nm (tetrahydrofuran (THF)); **372a–c**: $\lambda_{\text{abs}} = 360.5$ nm, $\lambda_{\text{PL}} = 410$ nm (methanol). The Φ_{PL} in solutions is very high for both neutral (**370a**: 87% (CHCl_3); **370b**: 57% (THF)) and quaternized (**371**: 76% (methanol), 25% (H_2O)) polymers. The decrease of Φ_{PL} for **371** in water was attributed to the aggregation, and a further decrease in Φ_{PL} for this polymer was observed in films (4%). No EL devices with these copolymers were reported.

A series of fluorene copolymers with amino-functionalized side chains **373** and **374** has been prepared by the same group (Chart 2.92). Upon quaternization, they gave copolymers **375** and **376**, which were soluble in polar solvents (methanol, DMF, DMSO) [439]. Devices from the

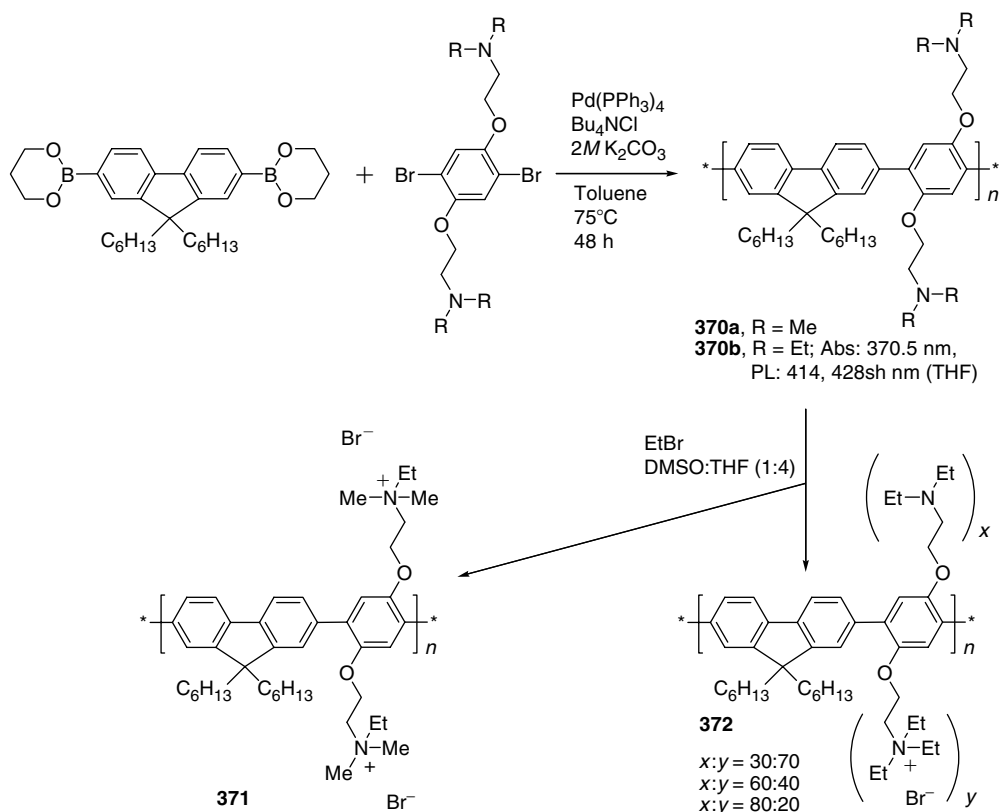


SCHEME 2.57 Suzuki synthesis of multicomponent copolymers for RGB PLED display. (From Müller, C.D., Falcou, A., Reckefuss, N., Rojahn, M., Widerhirn, V., Rudati, P., Frohne, H., Nuyken, O., Becker, H., and Meerholz, K., *Nature*, 421, 829, 2003.)

neutral copolymers **373** and **374** and the quaternized copolymers **375** and **376** showed similar absorption and PL spectra but very different EL spectra. For the neutral polymers, high-energy peaks observed in the PL spectra are replaced with a new broad low-energy peak. At the same time, the main peaks in the EL spectra of quaternized copolymers coincide well with PL emission, with only one additional shoulder around 492–497 nm that the authors assigned to excimer emission. Using **373** as an electron injection layer in ITO/PEDOT/MEH-PPV/**373**/Al configuration gave devices with a luminance of 3000 cd/m² and $\Phi_{\text{EL}}^{\text{ex}} = 2.3\%$.

When an electron-deficient BT unit was incorporated into the backbone of these polymers, an efficient energy transfer resulted in complete fluorescence quenching from the fluorene sites already at BT concentrations as low as 1% (for both neutral and quaternized copolymers, **377** and **378**) [440] (Chart 2.93). These macromolecules emit green (544–550 nm, **377**) to yellow (555–580 nm, **378**) light and can be processed from environment-friendly solvents such as alcohols. The PLED fabricated with these polymers showed high $\Phi_{\text{EL}}^{\text{ex}}$ over 3 and 1% for **377** and **378**, respectively (Al cathode).

Bazan and coworkers [441,442] reported similar water-soluble random cationic fluorene copolymers **379** and **380** with quaternary amine side groups attached at the C-9 position of the fluorene moiety (Chart 2.94). There was a progressive blue shift in absorption spectra of copolymers **379** with increasing amount of *meta*-linker in the polymer chain. Increasing the *para* content above 50:50 ratio, however, did not perturb the emission maxima, interpreted to be due to localization of excitons on the longest conjugated segments [441]. At low concentrations in solution, the absorption and emission spectra of **380** ($\lambda_{\text{max}}^{\text{abs}} = 380$ nm, $\lambda_{\text{PL}} \sim 400$ –500 nm; blue emission) is nearly identical to that of **379**, which lacks BT units. However, at concentrations $>10^{-6}$ M, the emergence of green emission ($\lambda_{\text{PL}} \sim 500$ –650 nm) characteristic of BT sites was observed, resulting from aggregation that leads to enhanced energy transfer to units containing lower energy BT chromophores [442].



SCHEME 2.58 Synthesis of water-soluble blue-emitting fluorene copolymers. (From Liu, B., Yu, W.-L., Lai, Y.-H., and Huang, W., *Chem. Commun.*, 551, 2000; Liu, B., Yu, W.-L., Lai, Y.-H., and Huang, W., *Macromolecules.*, 35, 4975, 2002.)

Whereas all above water-soluble PFs are tetra-alkylammonium-based salts, Burrows et al. [443] reported on anionic fluorene-based copolymer **381** that showed a blue shift in PL (from 424 to 411 nm) as well as a dramatic increase in the fluorescence quantum yield (from 10–15 to 60%) when incorporated into *n*-dodecylpentaoxyethylene glycol ether micelles [443].

2.3.13 CONCLUSIONS

Clearly, at present, PFs are the most promising class of blue-emitting materials. The original problem associated with the undesirable “green emission band” was shown to be a result of exciton trapping on the electron-deficient fluorenone defect sites. The color purity can be reestablished via (i) careful purification of the monomer (complete elimination of mono-substituted units), (ii) inserting a protecting layer between the PF and reactive cathode material, (iii) introducing hole-trapping sites (most commonly, triarylamine units), which would compete with fluorenone defects, minimizing the exciton formation on the latter, and (iv) introducing bulky substituents to the PF backbone that minimize the exciton trapping on fluorenone defects. Furthermore, introduction of different conjugated moieties to the PF backbone allows for efficient color tuning in these materials.

So far, the most efficient PLED based on PFs in terms of pure red, green, and blue emission can be summarized with the following examples (Chart 2.95).

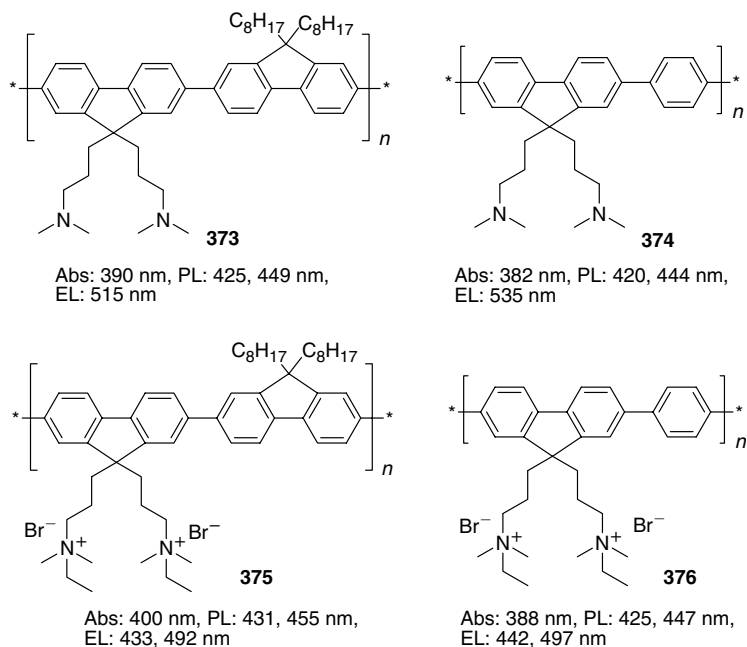


Chart 2.92

Blue emitter 228 [253]: A single-layer device ITO/PEDOT/**228**/Ca can be turned on at 3.5 V, emits blue light (CIE: $x = 0.150$, $y = 0.080$) with an EL efficiency of 1.1 cd/A (at 8.5 V; power efficiency of 0.40 lm/W) and a maximum brightness of 1600 cd/m². A multilayer device with a structured triarylamine-based HTL results in an EL efficiency of over 2.7 cd/A and higher (maximum brightness of 5000 cd/m²).

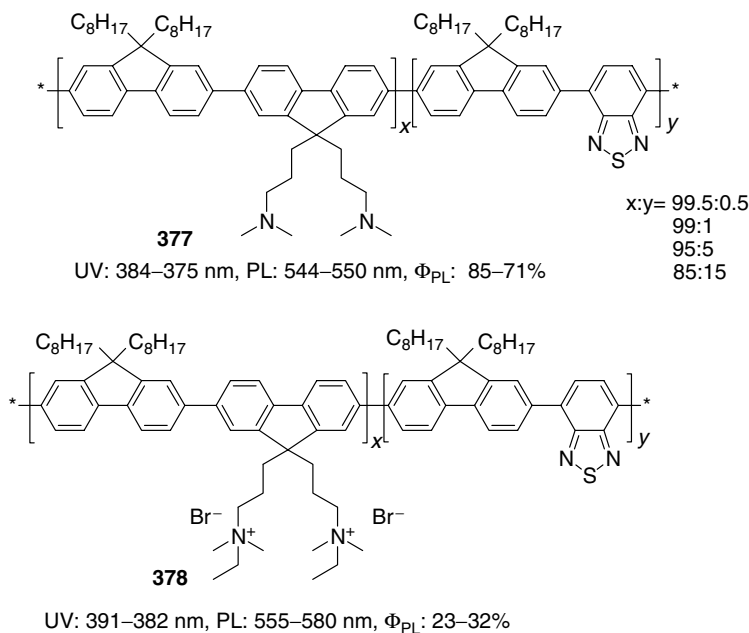


Chart 2.93

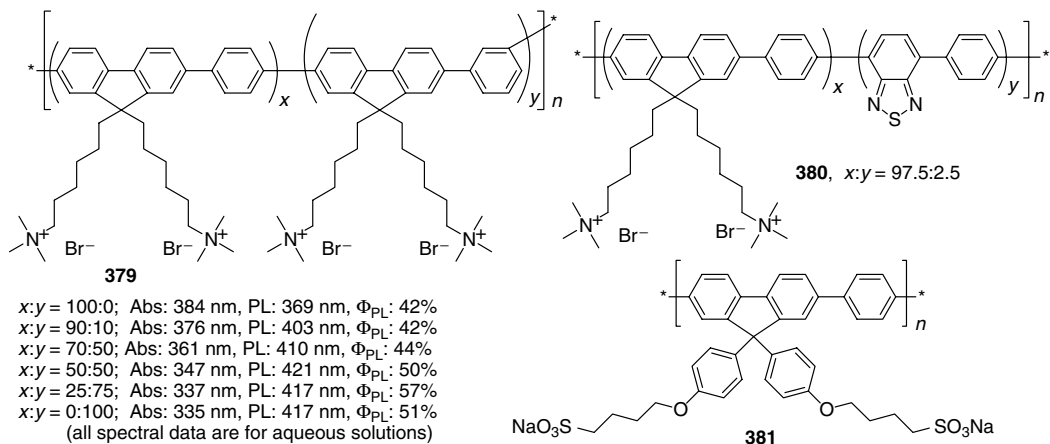


Chart 2.94

Blue emitter 382 [436]: A single-layer PLED ITO/PEDOT/**382**/Ca emits blue light (CIE: $x = 0.15$, $y = 0.16$) with a current efficiency of 3.0 cd/A and an operating voltage of 4.6 V (at 100 cd/m²).

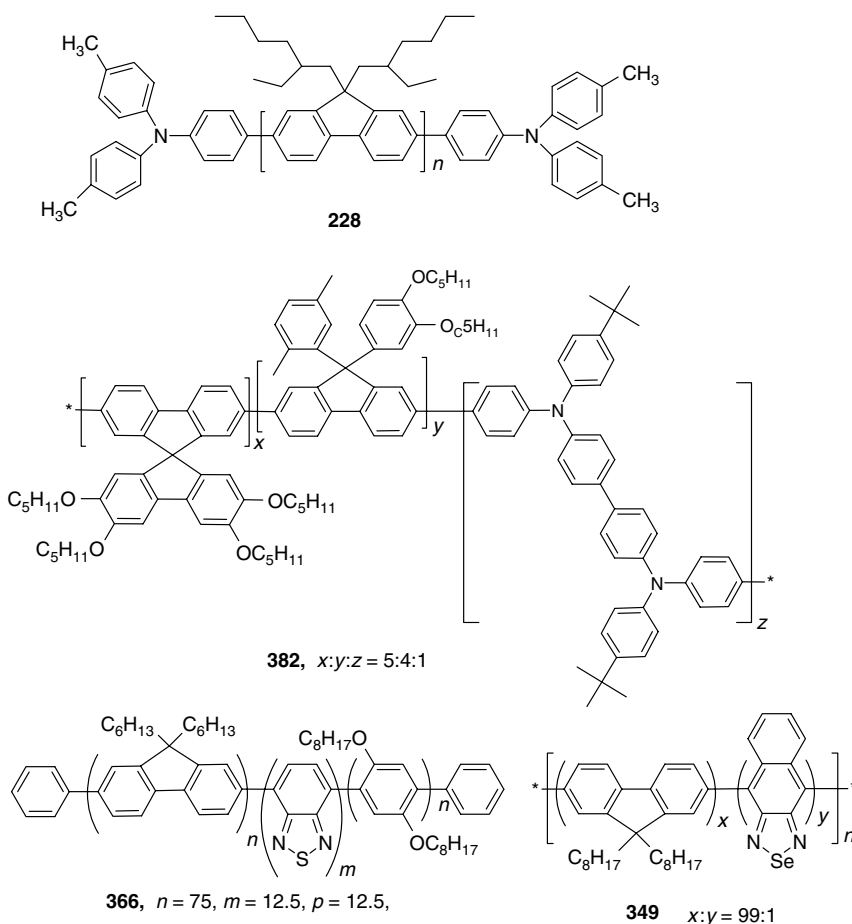


Chart 2.95

Green emitter 366 [435]: The device with the structure ITO/BTPD-PFCB/**366**/Ca/Ag works at the operating voltage of 3.6 V and reaches extremely high $\Phi_{\text{EL}}^{\text{ex}} = 6\%$ (18.5–28.6 cd/A) and a maximum brightness of 59,400 cd/m². These unusually high values are unique and await to be reproduced and surpassed by researchers in the field.

Red emitter 349 [427]: A single-layer PLED ITO/PEDOT/polymer/Ba operates at 8.9 V, emitting saturated red color (CIE: $x = 0.67$, $y = 0.33$) with very high $\Phi_{\text{EL}}^{\text{ex}} = 3.1\%$, corresponding to a photometric current efficiency of 0.9 cd/A. A brightness in excess of 2000 cd/m² was achieved for this device.

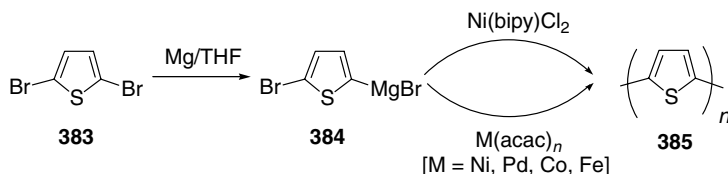
2.4 POLYTHIOPHENES

Polythiophenes (including oligothiophenes) are one of the most studied and important classes of linear conjugated polymers [444,445]. Versatile synthetic approaches to PTs (chemical [446] and electrochemical [447]), easy functionalization and unique, widely tunable electronic properties have been the source of tremendous interest in this class of polymers.

Due to their electron-rich character, the thiophene rings in PTs can be easily and reversibly oxidized by chemical or electrochemical means to form p-doped, usually highly conducting materials. The first electronic transition of undoped PT that strongly depends on structure, lies between 300 and 500 nm ($\epsilon \sim 10,000$ l/(mol cm) [448], and on doping undergoes dramatic bathochromic shifts concomitant with the formation of a so-called “conducting” band that tails from the visible to the deep IR region. In contrast to undoped PTs, known to exhibit reasonably strong luminescence in the visible region of the spectrum, doped PTs are not luminescent, although partially doped PTs have been used in LECs and doped PEDOT is routinely used as an electrode for PLED (mostly as a second layer on ITO-covered glass).

Although in terms of EL materials PTs have not been studied as widely as PPVs or PFs, they present an important class of LEPs. PTs emit orange-to-red light, consistent with their band gap of ca. 2 eV. Often the luminescence efficiency of PTs in the solid state is relatively low [449,450], much lower than that of PPV and PFs. A possible explanation is that it originates from their solid-state structure and has a tendency of strong interchain interactions (especially for low-molecular-weight oligomers). This feature is an advantage of PTs in some electronic applications as, for example, field effect transistors [451]. However, it becomes one of the most critical drawbacks for application as emissive materials in LED. Whereas in solution the PL efficiency (Φ_{PL}) of poly(3-alkylthiophenes) is ~ 30 – 40% , it drastically drops down to 1–4% and lower in the solid state due to increased contribution of nonradiative decay via interchain interactions and intersystem crossing caused by the heavy-atom effect of sulfur [452]. Thiophene-based polymers have stronger spin–orbital coupling than phenylene-based polymers due to the internal heavy atom effect of the sulfur heteroatom and hence triplet state processes play a greater role in their photophysics [453].

Another feature of PTs is the phenomenon of thermochromism [454], which has been shown for poly(3-alkyl)thiophenes in many publications. It is believed that the thermochromism observed in poly(3-alkyl)thiophene films originates from the thermal movement of the side chains, shifting a predominantly planar structure of chains at low temperatures to a random coil conformation when the temperature is increased, thus forcing the polymer backbone out of planarity. This leads to a decreased orbital overlap and effective conjugation length, resulting in band gap increase and blue-shifted polymer absorbance (from red to purple or purple-blue) [455,456]. The process is completely reversible and on cooling, the initial color is restored. Although thermochromism is of theoretical interest for understanding the effect of structural and electronic features of PTs, it is undesirable for LED applications, as it could lead to changes of the emission wavelength and the QE of the device during the operation.



SCHEME 2.59 Synthesis of polythiophene via metal-catalyzed couplings.

2.4.1 GENERAL SYNTHETIC ROUTES TO POLYTHIOPHENES

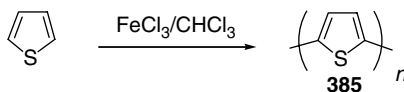
Polymerization of thiophenes can be carried out in different ways and the most used methods can be generalized into three categories: (i) electropolymerization, (ii) metal-catalyzed-coupling reactions, and (iii) chemical oxidative polymerization. Electropolymerization is a widely used method to prepare insoluble films of PTs and represents a simple and efficient way to study optical and electronic properties of PTs [447], although it is rarely used in preparation of EL materials. In 1980, Yamamoto et al. [457] reported the Ni-catalyzed polycondensation of 2,5-dibromothiophene **383**. The latter was allowed to react with Mg in THF, affording 2-magnesiobromo-5-bromothiophene **384** that in the presence of Ni(bipy)Cl₂ produced PT **385** (Scheme 2.59). In the same year, Lin and Dudek [458] described another example of a metal-catalyzed route to unsubstituted PT **385**, exploiting acetylacetonates of Ni, Pd, Co, or Fe as catalysts.

The PT synthesized by these methods is a low-molecular-weight material due to the fact that even at low molecular weights, the material is insoluble and precipitates from THF; moreover, the elemental analysis indicates the presence of 1–3% of Mg [446]. Later a Ni(dppp)Cl₂ catalyst was exploited for polycondensation polymerization of bromo(iodo)-Grignard reagents of type **384** [459]. Another polycondensation approach to PT, also reported by Yamamoto et al. [460], included heating of **383** with Ni(cod)₂ and triphenylphosphine in DMF at 60–80°C. Due to very high yield (near quantitative), this reaction has been applied in the syntheses of a wide range of conjugated polymers.

The FeCl₃-mediated polymerization of thiophene in chloroform was described 20 years before [461] and currently is the most widely exploited oxidative route to 3(3,4)-substituted PTs (Scheme 2.60). It produces rather high molecular-weight polymers (often $M_w = 20,000$ –400,000) with polydispersity from 1.3 to 5 [462,463]. Other oxidative agents (e.g., ammonium persulfate) are of limited use, although oxidative coupling with CuCl₂ is widely used as a dimerization reaction of lithio-thiophenes in the syntheses of oligothiophenes.

As already mentioned, unsubstituted PT is an insoluble and infusible material. Once the polymer is prepared, it is difficult (if not impossible) to further process it as a material for electronic applications. The solubility can be greatly enhanced by the introduction of side chains at position 3 (or at both, 3 and 4). The most widely studied side chains are *n*-alkyl substituents that can be easily introduced into the thiophene core by reaction of 3-bromothiophene with alkyl-Grignard reagents [464].

While 3-substitution efficiently improves the solubility and the processability of the PTs, polymerization of 3-*R*-thiophenes can result in three different types of coupling of the thiophene rings along the polymer main chain, i.e., HT, HH, and TT (Chart 2.96).



SCHEME 2.60 Synthesis of polythiophene via chemical oxidation polymerization.

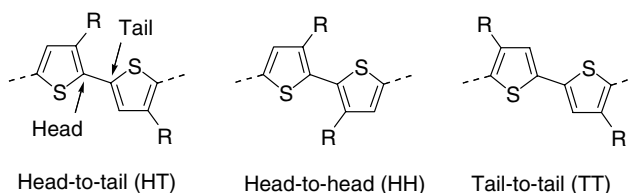
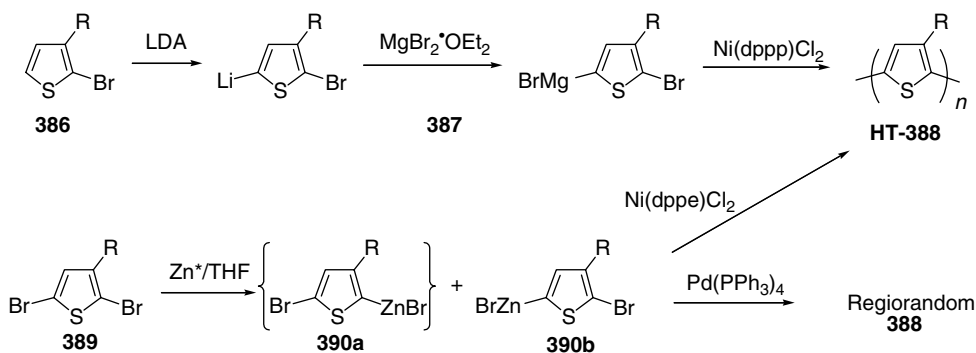


Chart 2.96

Generally, both oxidative polymerization and metal-catalyzed polycondensation afford all three possible types of isomers, although this process is not completely random and electronic and steric factors have an influence on somewhat preferred HT coupling, which could reach more than 80–94% [465,466]. Amou et al. [465] showed that the regioregularity of FeCl_3 -synthesized poly(3-hexylthiophene) (P3HT, **395**) depends on the temperature of the reaction and the concentration, and in diluted solutions at -45°C , the regioregularity of P3HT approaches 90% [465].

Several approaches leading to selective formation of the least sterically hindered HT-regioregular PTs have been developed in the last decade. The McCullough method presents the first synthesis of regioregular HT poly(alkyl)thiophenes (HT-PATs, **HT-388**) (yielding almost 100% HT coupling) (Scheme 2.61) [467,468]. It is based on regiospecific metallation of 2-bromo-3-*R*-thiophene (**386**) with lithium diorganoamide (LDA) at position 5 and its further transformation into Grignard derivative **387**. The latter is polymerized with catalytic amounts of $\text{Ni}(\text{dppp})\text{Cl}_2$ using the Kumada cross-coupling method. The important modification of this synthetic route replaces the lithiation reaction by treatment of the dibromothiophene derivative with methylmagnesium or vinylmagnesium bromide, which affords the Grignard intermediate in one step [469–471]. Other methods for preparing regioregular PTs, exploiting Stille [472] or Suzuki [473] coupling instead of Grignard reagents, have also been developed. Rieke and coworkers [474,475] have used highly reactive “Rieke zinc” (Zn^*) that reacts with 2,5-dibromo-3-*R*-thiophenes (**389**) at low temperature, affording predominantly the 5-metallated compound (**390b**); polymerization with the Kumada catalyst $\text{Ni}(\text{dppp})\text{Cl}_2$ produced HT-regioregular PATs **HT-388** (in contrast, the monodentate $\text{Pd}(\text{PPh}_3)_4$ -ligated catalyst yields regiorandom PATs **388** under the same conditions). The



SCHEME 2.61 McCullough and Rieke methods of synthesis of regioregular HT-poly(3-alkylthiophenes) **HT-388**. (From McCullough, R.D. and Lowe, R.D., *J. Chem. Soc., Chem. Commun.*, 70, 1992; McCullough, R.D., Lowe, R.D., Jayaraman, and Anderson, D.L., *J. Org. Chem.*, 58, 904, 1993.)

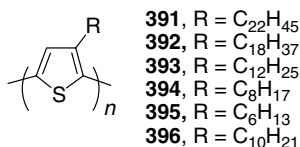


Chart 2.97

detailed aspects of synthesis and characterization of regioregular PTs were reviewed recently by McCullough [446].

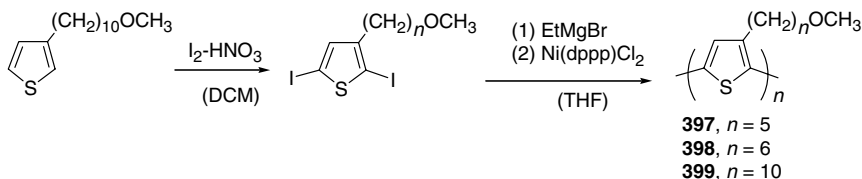
The presence of HH coupling in irregular PTs causes an increased twisting of thiophene units (due to steric repulsion) with concomitant loss of conjugation. This results in an increased band gap (blue shift in an absorption and luminescence), decreased conductivity, and other undesirable changes in electronic properties. As it will be shown below, regioregularity also plays an important role in luminescence properties of PTs and is used as a tool to tune the properties of PT-based LEDs.

2.4.2 LIGHT-EMITTING THIOPHENE HOMOPOLYMERS

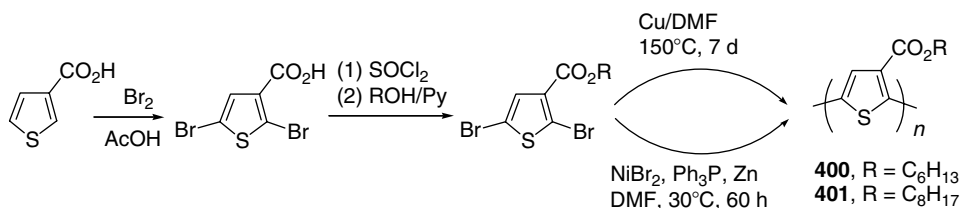
2.4.2.1 Polythiophenes as Red-Light Emitters

PT LEDs were first reported by Ohmori et al. [476,477] in 1991. Poly(3-alkylthiophenes) **391–393** (prepared by oxidation of 3-alkylthiophenes with FeCl₃ in chloroform [461]) as red-orange-emitting material (peak emission at 640 nm for **391**) in single-layer ITO/**391–393**/Mg:In devices were described (Chart 2.97). It was shown that the luminescence efficiency follows a linear dependence on the length of the alkyl chain, showing about a fourfold increased EL efficiency for PT with R = C₂₂H₄₅, compared to R = C₁₂H₂₅ (although no quantum yield values have been given in these reports), possibly owing to the improved confinement of excitons on the main chain with an increase of the side-chain length [478]. The use of a carrier-confining layer (TPD **299**) was shown to markedly increase (by 3–5 times) the device efficiency [477]. Shortly afterwards, Heeger's group [479] reported EL in poly(3-octylthiophene) **394** that showed red-orange luminescence with $\Phi_{\text{EL}}^{\text{ex}}$ at room temperature of 0.025% in ITO/**394**/Ca configuration. Greenham et al. [480], while studying the EL from PTs **393** and **395** (also prepared by oxidation of the monomers with FeCl₃), achieved a significantly higher emission efficiency of 0.2% for **393**, also using Ca as a cathode (**395** gave 0.05% and use of Al cathode gave 0.01 and 0.003% yield, respectively).

Bolognesi and coworkers [481–483] reported the Ni-initiated polymerization of 2,5-diiodothiophenes yielding poly(3-alkylthiophene)s **397–399**, containing a methoxy group at the end of the alkyl chain (Scheme 2.62). Small shifts in EL of polymer **399** to higher energies



SCHEME 2.62 Synthesis of alkylthiophenes **397–399** through oxidative iodination of the thiophene followed by Ni-catalyzed polymerization. (From Bolognesi, A., Botta, C., Geng, Z., Flores, C., and Denti, L., *Synth. Met.*, 71, 2191, 1995; Bolognesi, A., Porzio, W., Bajo, G., Zannoni, G., and Fanning, L., *Acta Polym.*, 50, 151, 1999.)



SCHEME 2.63 Synthesis of alkoxy carbonyl-PTs. (From Pomerantz, M., Yang, H., and Cheng, Y., *Macromolecules*, 28, 5706, 1995.)

compared to polymer **394** (from 1.8 to 1.95 eV) were mentioned [479,481]. The effect could be the result of asymmetry of the rather wide band (comparison with P3DT **396** reveals smaller blue shifts of 0.05 eV [484]). Polymers **397** and **398** showed high (for PTs) PLQYs in solution (38–45% in THF) that, however, decreased in the films [483]. A general explanation of this decrease as a result of the interchain interactions is supported by temperature-dependent PL experiments. On gradual heating of the sample to 140°C, the PL intensity increased by $\times 2$ and $\times 6$ times for **397** and **398**, respectively. $\Phi_{\text{EL}}^{\text{ex}}$ for **397** and **398** in ITO/polymer/Al diodes were relatively low (10^{-5} – 10^{-4} and $5 \times 10^{-3}\%$, respectively, at the same voltages).

A larger blue shift in fluorescence was observed for alkoxy carbonyl-substituted PTs **400** and **401**. The polymers were prepared from 2,5-dibromo-substituted monomers by two methods: (i) Ullmann reaction with Cu powder and (ii) Ni(0)-mediated polymerization (Scheme 2.63) [485]. Both polymers have similar molecular weights ($M_n \sim 3000$), although the Cu-prepared polymers showed higher quality and lower polydispersity. PL emission maxima for the Cu-prepared polymers **400** and **401** were red-shifted, compared to the Ni-prepared polymers (by 13–15 nm (≈ 0.05 – 0.06 eV) in solution and 25–30 nm (≈ 0.08 – 0.10 eV) in films, Table 2.4). This demonstrates that the properties of the polymer depend on the preparation method and, consequently conclusions from small shifts of 0.05–0.1 eV in PL–EL energies of the materials, prepared by different methods, should be made with care.

Another example of the effect of the polymerization method on the optical properties of the resulting polymer is the synthesis of polymer **402** (Scheme 2.64) [486]. Polymers obtained by oxidative polymerization of the corresponding 3-(methoxyphenyl)thiophene with FeCl_3 (CHCl_3 -soluble fraction), and with $\text{Mg}/\text{Ni}(\text{dppp})\text{Cl}_2$ or $\text{Ni}(\text{cod})_2$ polymerizations of the corresponding dibromothiophene derivatives showed somewhat different maxima in absorption (and PL emission) spectra: 405 (520), 433 (555), and 435 (560) nm, respectively.

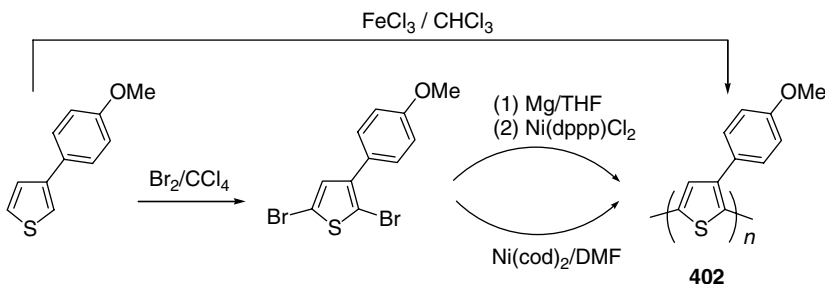
Jin et al. [487] synthesized and studied the PL and EL properties of polymers **403** and **404** that differ by the position of the alkoxy substituent in the phenyl ring, expecting different distortion of the polymer main chain (and consequently conjugation length) due to different steric factors for *para*- and *ortho*-substitution (Chart 2.98). The absorption spectrum of the “*ortho*-polymer” **403** showed a substantial blue shift of 40 nm compared to “*para*” **404** and a decrease in EL turn-on voltage (4.5 and 6.5 V, respectively). Both polymers demonstrated nearly the same PL and EL maxima (Table 2.1).

A series of PT derivatives (**405**–**407**) with electron-transporting benzotriazole moieties in the side chains was prepared (Scheme 2.65) [488]. Polymer **405** was insoluble in common organic solvents (THF, CHCl_3 , or DMF). In contrast, polymers **406** and **407**, endowed with longer tethers, possessed improved solubility as well as high molecular weight and thermal stability ($T_{\text{dec}} > 300^\circ\text{C}$). They showed pronounced blue shifts of 50–70 nm in absorption, PL and EL maxima, compared to P3OT **394** (Table 2.4); somewhat speculatively attributed to steric hindrance [488]. The EL efficiency was not enhanced as dramatically as the authors expected, although they showed 3–7 times higher $\Phi_{\text{EL}}^{\text{ex}}$ values. This was rationalized by considering the energy diagram in Figure 2.25. The HOMO levels found from photoelectron

TABLE 2.4
Properties of Poly(3-*R*)thiophenes, Prepared by the Ulmann (Cu), Yamamoto (Ni), or FeCl₃ Polymerization

Polymer (Method)	<i>M_n</i> (g/mol) (PDI)	$\lambda_{\text{max}}^{\text{abs}}$ (nm) (Solution)	$\lambda_{\text{max}}^{\text{abs}}$ (nm) (Film)	$\lambda_{\text{max}}^{\text{PL}}$ (nm) (Φ_{PL} (%))	$\lambda_{\text{max}}^{\text{PL}}$ (nm) (Φ_{PL} (%))	$\lambda_{\text{max}}^{\text{PL}}$ (nm) (Φ_{PL} (%))	$\lambda_{\text{max}}^{\text{EL}}$ (nm) ($\Phi_{\text{EL}}^{\text{ex}}$ (%))	Ref.
394							1.8 eV	479
394 (FeCl ₃)	16,800 (6.22)		500			655	650 (0.012%) ^a	488
395 (50% HT)	4,000 (1.7)	413 (CHCl ₃)	420	567, 600 (9%)	608 (0.8%)			489
395 (60% HT)	3,000 (1.6)	420 (CHCl ₃)	432	572, 600 (12%)	608, 643 (0.3%)			489
395 (70% HT)			456		650		630 (1.3 × 10 ⁻⁵ %) ^b	450
395 (80% HT)	40,000 (2.3)	440 (CHCl ₃)	518	580, 614 (14%)	670, 714 (0.2%)			489
HT-395 (98% HT)			510		717		662 (3.85 × 10 ⁻⁴ %) ^b	450
396			496					
397 (Ni)	5,900 (1.4)	451 (Toluene)	550					482
398 (Ni)	9,900 (1.5)	450 (Toluene)	535					482
399 (Ni)	9,450 (1.6)	448 (Toluene)	530					482
399 (Ni)	8,000 (2)		470			660	635	481
400 (Cu)	3,030 (2.3)	423 (THF)	447		570 (THF)	620		485
401 (Cu)	4,060 (1.9)	430 (THF)	450		568 (THF)	630		485
400 (Ni)	3,050 (3.2)	408 (THF)	429		555 (THF)	595		485
401 (Ni)	3,510 (2.8)	408 (THF)	430		555 (THF)	600		485
400	6,700 (2.5)	410 (THF)	434			600	600 (0.016%) ^a	493
401	9,400 (3.2)	439 (THF)	460			610	615 (0.018%) ^a	493
HHHT-400	8,100 (1.8)	387 (THF)	377			590	590 (0.0085%) ^a	493
HHHT-401	8,700 (2.0)	389 (THF)	381			600	600 (0.0047%) ^a	493
403 (FeCl ₃)	3,100 (2.8)		400	525 (CHCl ₃)			600 ^c	487
404 (FeCl ₃)	3,400 (1.6)		440	534 (CHCl ₃)			607 ^c	487
406 (FeCl ₃)	17,000 (2.07)		444			580	580 (0.09%) ^a	488
407 (FeCl ₃)	20,000 (1.89)		446			588	600 (0.04%) ^a	488

^aITO/polymer/Al.
^bITO/polymer/Mg/Al.
^cITO/PEDOT/polymer/Al.



SCHEME 2.64 Preparation of methoxyphenyl-PT **402**. (From Yamamoto, T. and Hayashi, H., *J. Polym. Sci., Part A: Polym. Chem.*, 35, 463, 1997.)

spectroscopy were -5.45 , -5.62 , and -4.57 eV for **406**, **407**, and P3OT (**394**), respectively. The LUMO energy levels (estimated as E_{HOMO} plus optical band gap from UV-vis spectra) were at -3.31 , -3.42 , and -2.61 eV. Thus, both HOMO and LUMO levels of **406** and **407** were lowered compared with those of P3OT **394** through introduction of the electron-withdrawing benzotriazole moieties. This strong effect can certainly be attributed to the replacement of the alkoxy substituents with alkyl groups and not due to the triazole moieties, although the latter might have contributed to the reduced LUMO. The authors note that the total barrier to charge injection was not reduced, although $\Phi_{\text{EL}}^{\text{ex}}$ enhancement was observed. The observed enhancement is not surprising, in our opinion, because the hole and electron injection balance (which was improved significantly) rather than total barrier is expected to determine the EL efficiency.

2.4.2.2 The Effect of Regioregularity of Polythiophenes on Electroluminescence

Regioregularity in PTs plays an important role in their band-gap control. The random polymerization of 3-alkylthiophenes leads to a larger degree of HH coupling, which in turn become the sites showing the largest twist distortion between thiophene units, resulting in a decreased effective conjugation length. On the other hand, HT-regioregular PTs show longer conjugation lengths and a red shift of their absorption and PL.

Xu and Holdcroft [489] studied the effect of regioregularity on luminescent properties of P3HT **395**. They found that increasing the percentage of HT coupling in P3HT from 50% HT to 80% HT results in red shifts of both absorption and emission maxima as well as fluorescence efficiency in solution from 9 to 14% (Table 2.4). On the other hand, an increased planarization of regioregular HT PT facilitates aggregation, which results in a decrease of the Φ_{PL} emission efficiency in the solid state (from 0.8% for 50% HT to 0.2% for 80% HT). Later, McCullough and coworkers [450] performed comparative studies on EL performance of HT-regioregular and regiorandom P3HT **395**. Compared to nonregioregular material, the HT-regioregular polymer showed a narrower EL spectrum and an approximate doubling in $\Phi_{\text{EL}}^{\text{ex}}$.

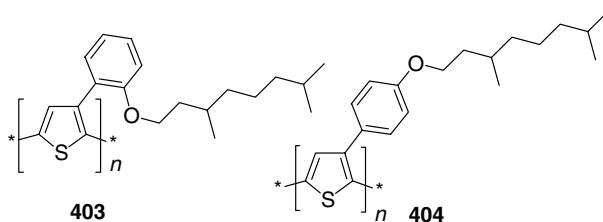
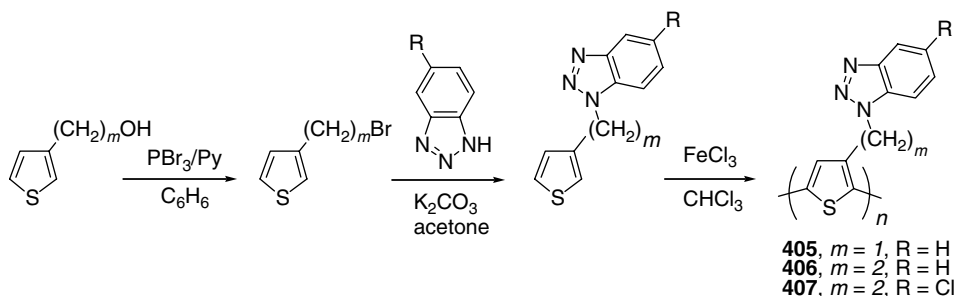


Chart 2.98



SCHEME 2.65 Synthesis of triazole-containing PTs. (From Ahn, S.-H., Czae, M.-Z., Kim, E.-R., Lee, H., Han, S.-H., Noh, J., and Hara, M., *Macromolecules*, 34, 2522, 2001.)

($1.5 \times 10^{-4}\%$ vs. $7 \times 10^{-5}\%$, at 6 mA current, Table 2.4). However, very low QE and preferential degradation of LEDs with irregular P3HT might be responsible for the difference.

Regioregular HT-coupled poly(3-decylthiophene) (**HT-396**, Chart 2.99) is an EL polymer exhibiting a well-defined vibronic structure in its absorption spectrum (Figure 2.26a; 0–0 transition at 2.0 eV), a red emission with good color purity, but a rather low QE in the solid state ($\Phi_{PL}^{film} = 1 \pm 0.1\%$) [490]. Its regioregular HH–TT-coupled isomer **HHTT-396** [491] showed large blue shifts (Figure 2.26b) in absorption, fluorescence, and EL spectra. In addition, **HHTT-396** emits green light with one order of magnitude higher PL ($\Phi_{EL}^{film} = 11 \pm 0.1\%$) and two orders of magnitude higher EL ($\Phi_{EL}^{int} = 0.001$ and 0.25–0.30%, respectively), but requires higher turn-on voltage [490]. The blue shifts and the increased emission efficiency of HHTT-regioregular polymers were explained by pronounced interannular conformational distortion in the HH fragment ($\sim 70^\circ$ in HH and $\sim 0^\circ$ in HT fragments, as suggested by AM1 semiempirical calculations [492]).

Pomerantz et al. [493] prepared regioregular polymers **HHTT-400** and **HHTT-401** (Scheme 2.66) and compared them with previously synthesized irregular polymers **400** and **401** (Scheme 2.63) [485]. Regioregular polymers showed blue shifts in absorption for solution and films (23–30 nm and 57–79 nm, respectively; Table 2.4), interpreted in terms of shorter conjugation length. Blue shifts in PL and EL were much less-pronounced (10–15 nm) and the PLED showed 2–4 times lower Φ_{EL}^{ex} (Table 2.4) [493].

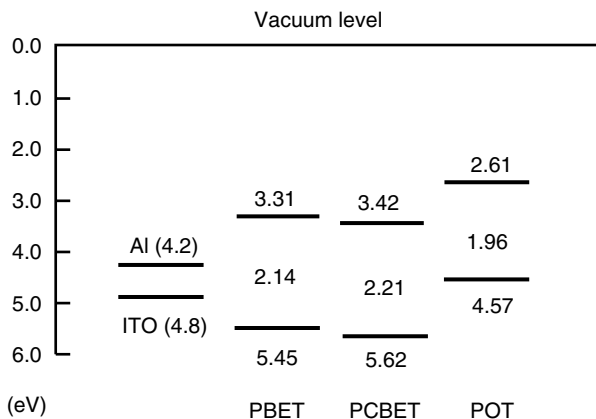


FIGURE 2.25 Energy diagram of substituted PT **406** (PBET), **407** (PCBET), and **394** (POT). (From Ahn, S.-H., Czae, M.-Z., Kim, E.-R., Lee, H., Han, S.-H., Noh, J., and Hara, M., *Macromolecules*, 34, 2522, 2001. With permission.)

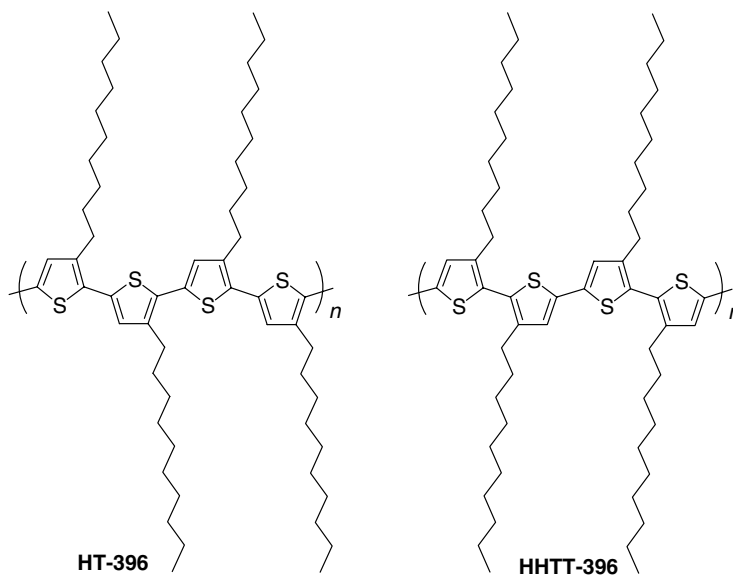


Chart 2.99

Hadziioannou and coworkers [494] synthesized a number of regioregular-alkylated polymers **HHTT-394**, **408–410** (Scheme 2.67) and demonstrated PL and EL color tuning through a variation of the length of the coplanar blocks between the HH links. They also found blue shifts of more than 100 nm in absorption, PL and EL spectra in the sequence **410** \rightarrow **409** \rightarrow **HHTT-394** \rightarrow **408**, i.e., increasing HOMO–LUMO gap with increasing steric hindrance. The energies of absorption and emission maxima were linear functions of the inverse number of thiophene units ($1/n$), between the two consecutive HH links (Figure 2.27), in agreement with theoretical predictions that the band-gap scales linearly with the inverse of the chain length [495]. These results clearly demonstrate that the effective conjugation length is limited by HH links.

2.4.2.3 Emission Color Tuning in Polythiophenes

Although the first publications on EL of poly(3-alkylthiophenes) described materials with red-orange emission (610–640 nm), a large number of PTs with emissions covering the full visible region, i.e., from blue to red and NIR, were later reported. These EL color changes were achieved by structural variations in PT side chains, as well as by controlling the regioregularity.

EL color tuning through introduction of various substituents is widely used in other LEPs but, probably, is not as impressive there. To understand the wide range of colors available from PTs, it is necessary to look at the underlying phenomena. The PT emission color depends directly on the effective conjugation length, determined by the twist angle between the thiophene units. Theory predicts a large change in the band gap of PT, depending on the torsion angle between consecutive thiophene units: the difference in the band gap of fully planar and 90°-twisted PTs is calculated to be 1.7 eV [496].

These observations inspired Inganäs and coworkers [107,497,498] to exploit the principle of steric hindrance to design PTs with emission colors spanning the full visible spectrum. A wide range of 3-substituted and 3,4-disubstituted thiophenes has been synthesized and successfully polymerized by FeCl_3 in chloroform, affording polymers **411–424** [466, 498–501] (Chart 2.100).

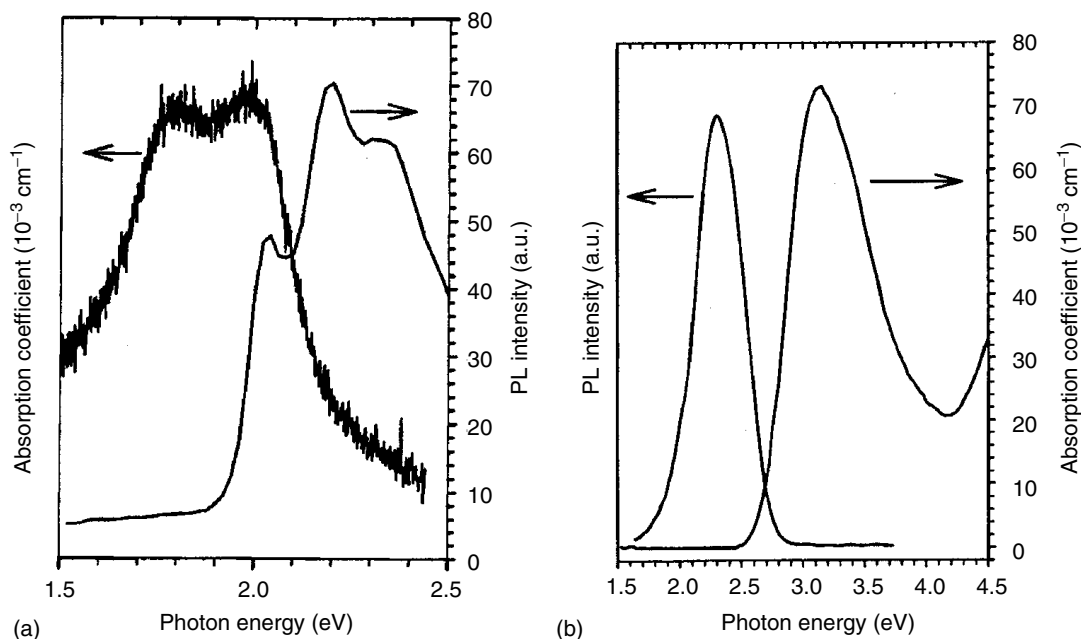
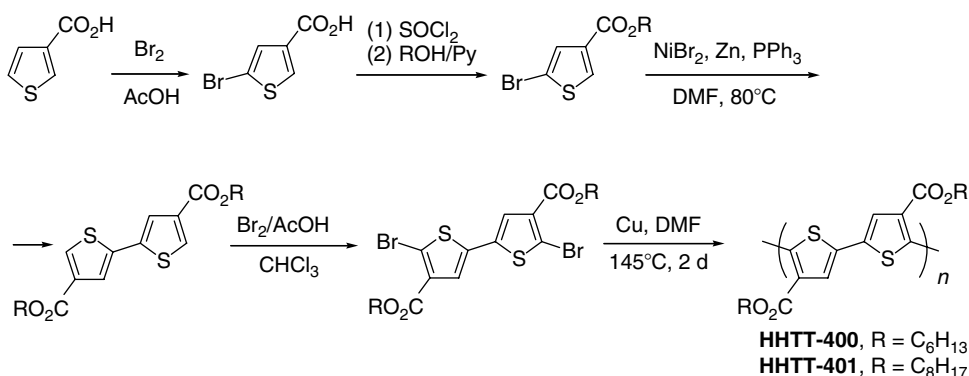
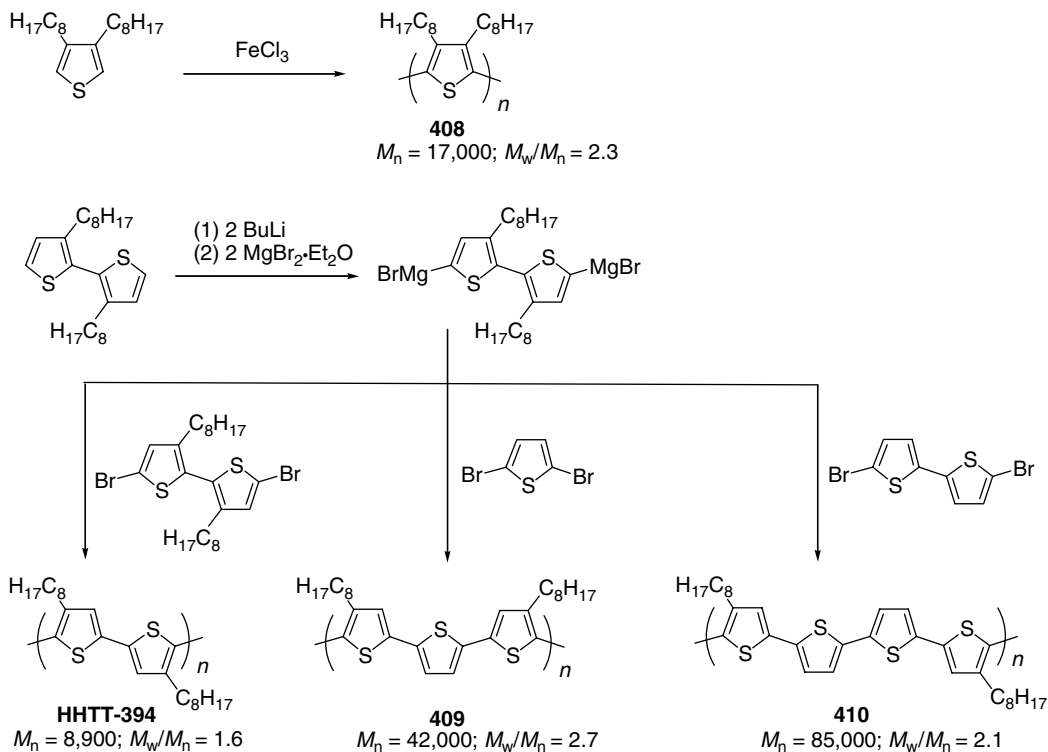


FIGURE 2.26 PL and absorption spectra of thin films of regioregular polythiophenes **HT-396** (a) and **HHTT-396** (b), spin coated on a fused silica substrate. (From Barta, P., Cacialli, F., Friend, R.H., and Zagórska, M., *J. Appl. Phys.*, 84, 6279, 1998. With permission.)

Although the emission of substituted PTs is not very predictable due to the interplay of several factors (steric effects, regioregularity, electronic effects, side-chain crystallization, etc.), the full visible range of PL and EL emissions from red to blue can be covered by variations of the PT substituents in positions 3(,4) (Figure 2.28). A shift in band gap can also be seen through the change of electrochemical oxidation potentials. Additional evidence for the modification of the effective conjugation in these PTs was also found from Raman spectroscopy studies (shift of the symmetrical C=C stretching: from 1442 to 1506 per cm^{-1}) [498]. However, calculation of the chromatic coordinates for these polymers showed that they cover only part of the chromatic space (Figure 2.29): no deep green colors are available in this



SCHEME 2.66 Synthesis of regioregular HHTT alkoxy carbonyl-PTs. (From Pomerantz, M., Cheng, Y., Kasim, R.K., and Elsenbaumer, R.L., *J. Mater. Chem.*, 9, 2155, 1999.)



SCHEME 2.67 Synthesis of regioregular HH TT octyl-PTs. (From Gill, R.E., Malliaras, G.G., Wildeman, J., and Hadziioannou, G., *Adv. Mater.*, 6, 132, 1994.)

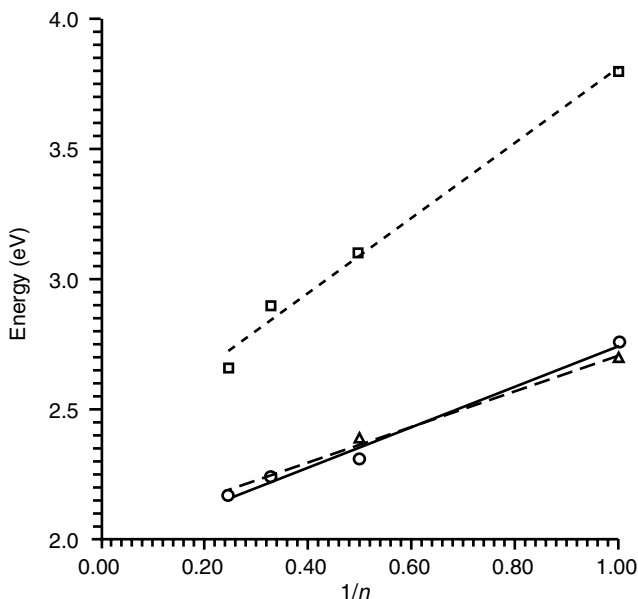


FIGURE 2.27 The absorption (□----), PL (Δ---) and EL (○—) energies of polymers **HH TT-394, 408–410** in thin films vs. an inverse number of thiophene units between the head-to-head links. (From Gill, R.E., Malliaras, G.G., Wildeman, J., and Hadziioannou, G., *Adv. Mater.*, 6, 132, 1994. With permission.)

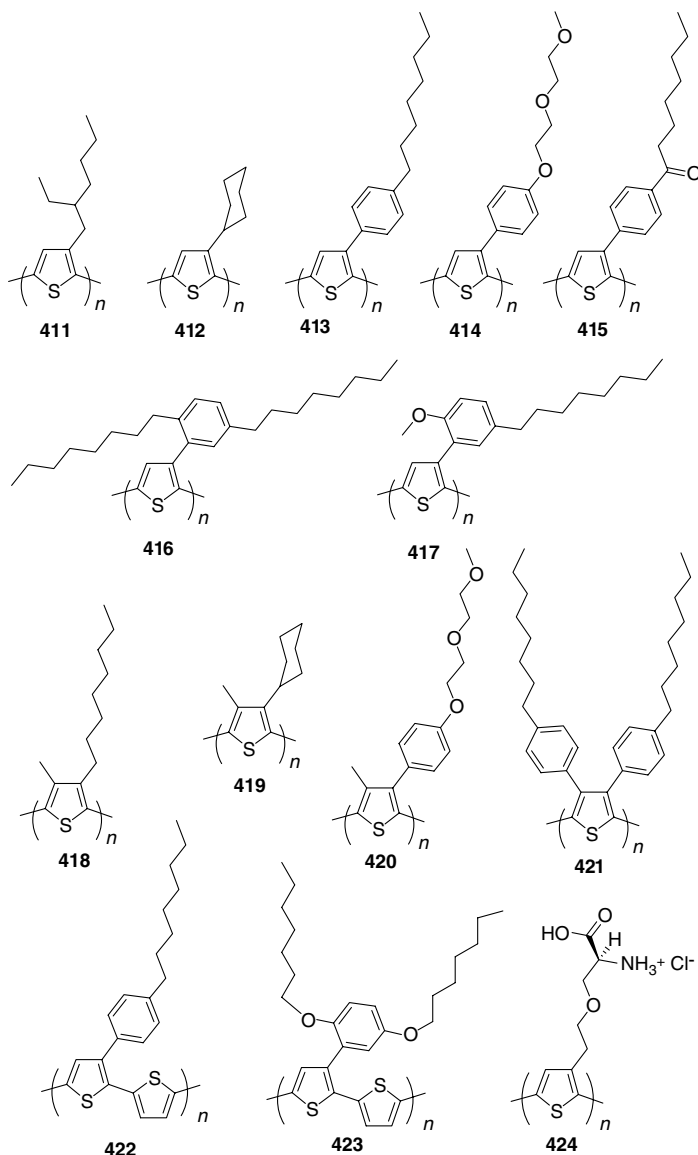


Chart 2.100

family of PTs, mostly due to the broadness of the emission spectra. Some absorption and emission data of these polymers are collected in Table 2.5. The large steric hindrance in **419** allowed a shift of the EL down to 460 nm, with a concomitant drop in QE.

A certain balance should be kept in distortion of the thiophene planarity as a way to prevent the formation of interchain aggregates. Introducing two substituents at positions 3 and 4 of PT allows a shift of the emission through the entire visible range and prevents interchain interactions (resulting in a smaller decrease of the quantum yield in the solid state compared to solution). Highly crowded disubstituted PTs **418–421** show very low luminescence efficiency already in solution (Table 2.5) due to substantial distortion of the backbone [107,498].

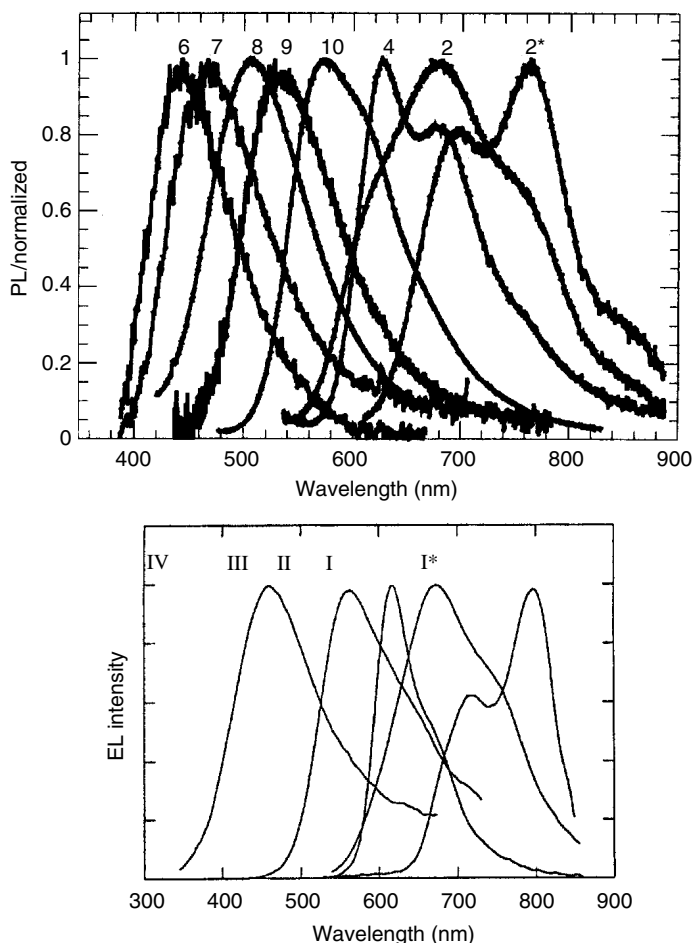


FIGURE 2.28 Top: PL spectra from spin-coated films of PTs: 2 = **413**, 4 = **422**, 6 = **419**, 7 = **418**, 8 = **421**, 9 = **420**, 10 = **412**; 2* = **413** treated with chloroform vapor at room temperature. (From Andersson, M.R., Thomas, O., Mammo, W., Svensson, M., Theander, M., and Inganäs, O., *J. Mater. Chem.*, 9, 1933, 1999. With permission.) Bottom: EL spectra of ITO/Polymer/Ca/Al devices: I = **413**, II = **422**, III = **412**, IV = **418**; I* = **413** upon thermal treatment or by chloroform vapor. (From Andersson, M.R., Berggren, M., Inganäs, O., Gustafsson, G., Gustafsson-Carlberg, J.C., Selse, D., Hjertberg, T., and Wennerström, O., *Macromolecules*, 28, 7525, 1995. With permission.)

In this context, polymer **416** represents a well-balanced material showing high PL efficiency in solution and solid state. The steric factor of the dialkylphenyl substituent is similar to those in **413–415**, as follows from the similarity of their absorption and emission energies. Molecular structure simulation shows that two octyloxy groups in the phenyl ring force its rotation to ca. 90° out of the thiophene plain. In this configuration, the bulky side chains prevent interchain interactions yet allow conjugation within the backbone. Spin-cast films of **416** show clear vibronic features in absorption ($\lambda_{\text{max}} = 532$ nm, $\Delta E = 0.18$ eV) and PL ($\lambda_{\text{max}} = 659$ nm, $\Delta E = 0.16$ eV) that, together with a very small Stokes shift of only 0.10 eV, suggest a highly ordered film (Table 2.5). Several PLEDs prepared with this polymer with structure: ITO/**416**/Ca/Al and ITO/**416**/PBD/Ca/Al configurations showed $\Phi_{\text{EL}}^{\text{ex}} = 0.1$ and 0.7%, respectively [502].

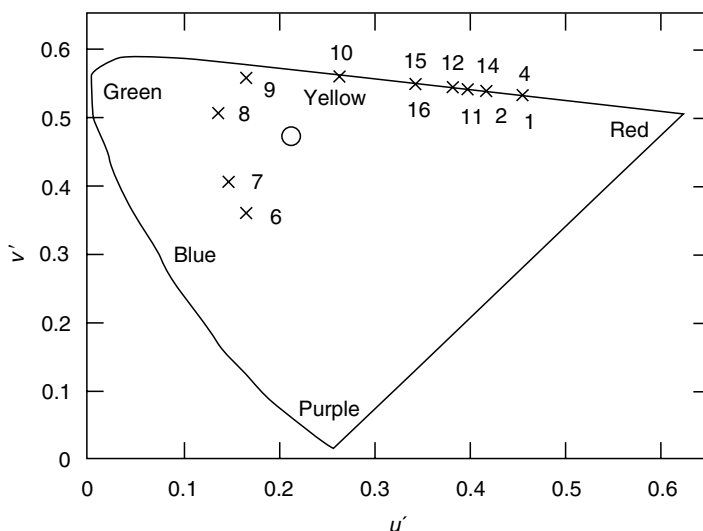


FIGURE 2.29 Chromatic coordinates for PTs: 1 = **394**, 2 = **413**, 4 = **422**, 6 = **419**, 7 = **418**, 8 = **421**, 9 = **420**, 10 = **412**, 11 = **414**, 12 = **415**, 14 = **416**, 15 = **411**, 16 = **417** and the white spot (o) (The u' - v' coordinates are 1976 modification of CIE xy coordinates, the white point $x = y = 0.33$ corresponds to $u' = 0.211$, $v' = 0.474$). (From Andersson, M.R., Thomas, O., Mammo, W., Svensson, M., Theander, M., and Inganäs, O., *J. Mater. Chem.*, 9, 1933, 1999. With permission.)

The highly regioregular polymer **413**, obtained by oxidative polymerization with FeCl_3 ($94 \pm 2\%$ HT) required some special attention because it could exist in two different forms. In its pristine form, the absorption maximum of spin-cast films is at 493 nm (2.68 eV) [466,503]. On treating the films with chloroform vapor, the maximum was shifted to 602 nm (2.06 eV) and the spectrum showed fine vibronic structure with $\Delta E = 0.19$ eV, typical of a more planar ordered conformation (Figure 2.30, top). This conversion could also be achieved by heating the film and, in contrast to the widely observed thermochromism in PTs, is irreversible. The PLEDs prepared with spin-coated **413** show red EL centered at 670 nm (1.85 eV). When the diode is heated, the emission is shifted continuously well into the NIR as a function of heating time and increasing temperature. On prolonged heating, **413** is converted into an ordered film with an EL emission maximum at 800 nm (1.55 eV) (Figure 2.30, bottom) [504]. It is noteworthy that simple exposure to chloroform vapor results in a more pronounced ordering of the polymer than when heating to 200°C.

As an alternative strategy, the high-luminescence efficiency observed in solution can be preserved by incorporating the polymer in an inert-solid matrix. A possible problem of phase segregation can be solved by careful design of the polymer and the matrix. Thus, polymer **424**, when blended with polyacrylic acid (PAA), did not suffer phase segregation probably due to attractive ionic-hydrogen bonding interactions between the PT and the matrix [502,505]. As a result, the PL QE of **424**:PAA (1:100) was 16% (cf. 26% in solution), much higher than in **424** film (4%). Unfortunately, no PLED with the material was reported, and one can suggest that the performance of such a device would be low due to a very low concentration of the emitting (and conducting) component.

Another approach to tuning the optical properties and improving the emission of PT derivatives in the solid state was proposed by Holdcroft and coworkers [506] (Scheme 2.68). They used postfunctionalization of P3HT **395** by electrophilic substitution reaction to afford polymers **425** followed by Pd-catalyzed coupling (Suzuki, Stille, or Heck methodologies) of

TABLE 2.5
Tuning the Properties of Electroluminescent PTs via Conjugation Control

Polymer (Regioregularity, % HT)	<i>M_n</i> (g/mol) (PDI)	λ_{abs} (nm) (Film)	λ_{PL} (nm) (Film)	Φ_{PL} (%) (CHCl ₃)	Φ_{PL} (%) (Film)	λ_{EL} (nm) ^a	$\Phi_{\text{EL}}^{\text{ex}}$ (%) ^a	Turn-On Voltage (V)	Ref.
P3OT 394 (70)	35,000 (3.14)	506		27	4				108
411 (~70)		464	593	26	9				108
412 (77)	6,000 (9.3)	405 [413 ^b]	574	27	9	555	0.01 (7 V)	2.4	108, 498
413 (94)	8,000 (6.25)	482 (555 ^c)	677 (764 ^c)	18	9 (3 ^c)				108
	23,000 (2.26)	485	670			670	0.3 (6 V)	1.4	498
414 (88)	7,800 (3.2)	476 (552 ^c)	616 (783 ^c)	20	8				108
415 (85)	9,400 (2.9)	454 (555 ^c)	638 (795 ^c)	14	10				108
416 (90)	36,000 (1.94)	494, 532, 577	606, 659, 720	37	24		0.1 ^a /0.7 ^d		108, 502
417 (90)	46,000 (3.48)	470	590	29	11				108
418	42,000 (2.17)	326	468	4.6	2.2				108
419	26,000 (2.77)	303 [305 ^b]	442	1.3	0.8	460 ^d	0.6 (25 V) ^d <10 ⁻⁴ (4 V)	7 ^d	108, 498
420	16,000 (3.0)	380	532	3.8	2.8				108
421	21,000 (3.0)	346	504	1.1	1.0				108
422	9,000 (9.1)	513 [518 ^b]	627	27	5	610	0.1 (8 V)	1.6	108, 498
423	24,500 (4.3)	510	598	31	4		(2–16) × 10 ⁻³ (2.8–3.6 V)		108
427			550–580						508
428a	2,300 (2.0)	332	428						509
428b	3,400 (3.4)	342	429, 470, 520			415, 474, 508			509
428	5,000 (5.0)	384	524						509
428d	6,800 (6.8)	389	470, 525						509
429a	4,300 (4.3)	443	605			607			509
429b	5,600 (5.6)	451	620			612			509

^aITO/polymer/Ca/Al.

^bFrom Andersson, M.R., Berggren, M., Inganäs, O., Gustafsson, G., Gustafsson-Carlberg, J.C., Selse, D., Hjertberg, T., and Wennerström, O., *Macromolecules*, 28, 7525, 995.

^cAnnealed film.

^dITO/polymer/PBD/Ca/Al.

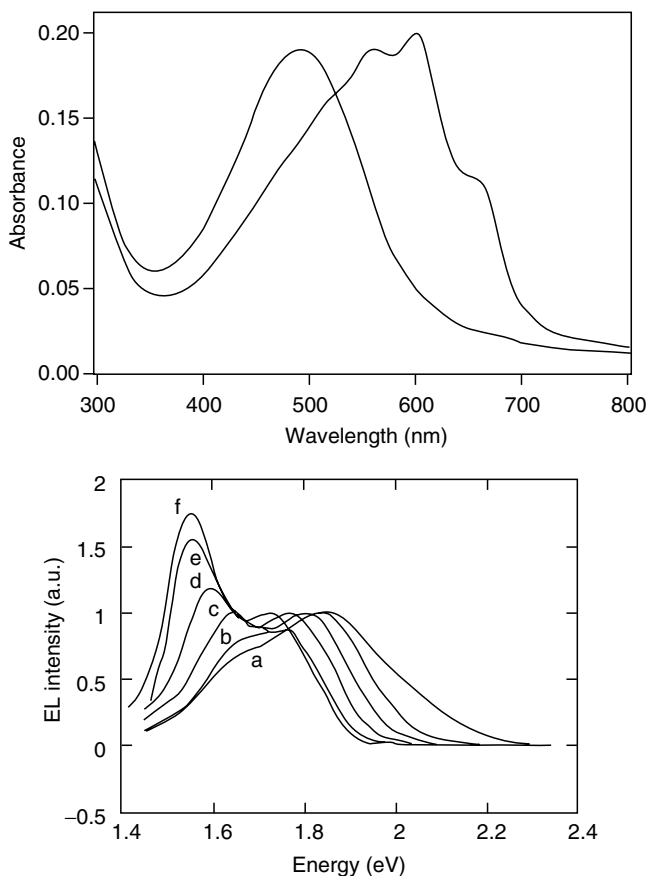


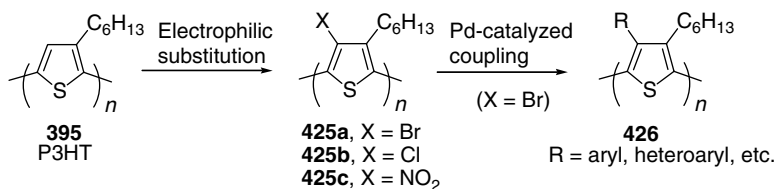
FIGURE 2.30 Top: UV-vis absorption spectra of a spin-coated film of **413** on glass ($\lambda_{\max} = 493$ nm) and the same film treated with chloroform vapor ($\lambda_{\max} = 602$ nm, $\Delta E = 0.19$, 0.15, 0.19 eV). (From Anderson, M.R., Selse, D., Berggren, M., Järvinen, H., Hjertberg, T., Inganäs, O., Wennerström, O., Österholm, J.-E., *Macromolecules*, 27, 6503, 1994. With permission.) Bottom: EL of ITO/**413**/Ca/Al device at different heating temperatures: (a) unheated device; (b) $T = 100^\circ\text{C}$, 6 s; (c) 100°C , +6 s; (d) 200°C , +10 s; (e) 200°C , +20 s; and (f) treated with chloroform before evaporating the contact. (From Berggren, M., Gustaffson, G., Inganäs, O., Anderson, M.R., Wennerström, O., and Hjertberg, T., *Appl. Phys. Lett.*, 65, 1489, 1994. With permission.)

425a to afford polymers **426** [507]. In this case, functionalization with bulky aryl substituents (**426**) allowed a substantial increase of Φ_{PL} in the films from 1.6 to 13–22%.

Saxena and Shirodkar [508] prepared copolymers **427** by oxidative (FeCl_3) polymerization of a mixture of 3-hexyl and 3-cyclohexylthiophenes, varying the monomer ratio from 1:9 to 9:1. The copolymers emitted yellow-green to green light (550–580 nm) and the ITO/**427**/Al devices showed $\Phi_{\text{EL}}^{\text{ex}}$ in the range of 0.002–0.016% [508]. However, even for the best emissive copolymer ($x:y = 2:3$) $\Phi_{\text{EL}}^{\text{ex}}$ was only 0.016% with a charge-carrier mobility of $5.6 \times 10^{-4} \text{ cm}^2/(\text{V s})$ (Chart 2.101).

2.4.3 LIGHT-EMITTING THIOPHENE BLOCK COPOLYMERS WITH CONJUGATION BREAK

The above approaches used the idea of conjugation length control in PTs by distorting the polymer backbone with bulky substituents as side groups. Hadzioannou and coworkers [509,510] demonstrated PL and EL tuning via exciton confinement with block copolymers



SCHEME 2.68 Postfunctionalization of PT **395**. (From Li, Y., Vamvounis, G., and Holdcroft, S., *Macromolecules*, 35, 6900, 2002; Li, Y., Vamvounis, G., Yu, J., and Holdcroft, S., *Macromolecules*, 34, 3130, 2001.)

428a–d and **429a–f**, containing oligothiophene and alkylsilylene units (Chart 2.102). Precise control of the conjugation length of the oligothiophene blocks, interrupted by silylene units, allowed emission tuning from blue to orange-red (Table 2.5). Later, Yoshino et al. [511] reported similar extended block copolymers **428d–h** that showed changes in EL color from green to red with increasing oligothiophene block length.

2.4.4 POLYTHIOPHENES FOR LIGHT-EMITTING ELECTROCHEMICAL CELLS

Two polymers with hydrophilic oligo(ethylene oxide) side chains, **430** and **431**, have been synthesized (Scheme 2.69) and studied in LECs [512]. Under applied bias, p-doping of the EL polymer took place at the anode, whereas at the opposite electrode the cathode material was reduced, although the reported $\Phi_{\text{EL}}^{\text{ex}}$ was relatively low ($\sim 10^{-2}\%$).

2.4.5 BLENDS OF POLYTHIOPHENES

It was demonstrated that blends of 3(3,4)-substituted PT derivatives of different band gaps gave rise to a voltage-controlled variable color light source [513]. Because of different turn-on voltages of high and low band-gap polymers, the emission color can be potentially tuned applying different bias. When a relatively low voltage was applied to the polymer blend PLED, the low band-gap polymer started to emit first, followed by higher band-gap emission as the voltage increased. An effective phase separation, however, is required to minimize the Förster energy transfer onto the low band-gap species. A blend of PTs **419**:**422** (50:50) at 22 V showed EL at ca. 630 nm, originating from the emission of **422**. When the voltage was increased an additional emission at ca. 440 nm (corresponding to the EL of **419**) appeared, reaching a comparable intensity at 27 V [513,514].

Other combinations of PTs in a blend, **418**:**412**:**422**:PMMA (PMMA is poly(methyl methacrylate) (10:4:1:1)) produced EL emission of the ITO/polymer blend/PBD/Ca/Al device at 20 V, very close to the equienergy white point as defined by the CIE, while providing a relatively high $\Phi_{\text{EL}}^{\text{ex}} = 0.4\text{--}0.6\%$ (at 20 V) (Figure 2.31) [515]. PMMA was used in this case to

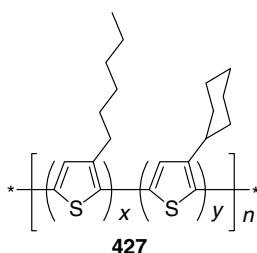


Chart 2.101

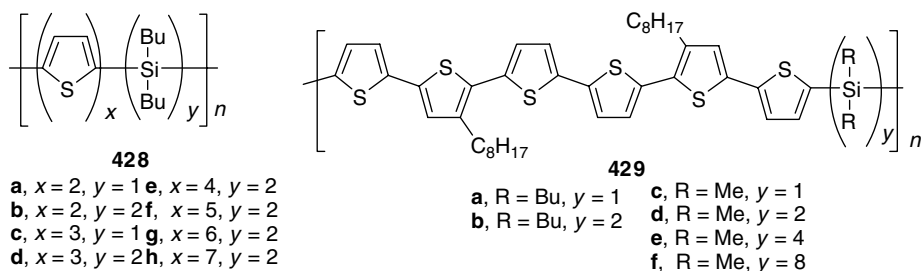
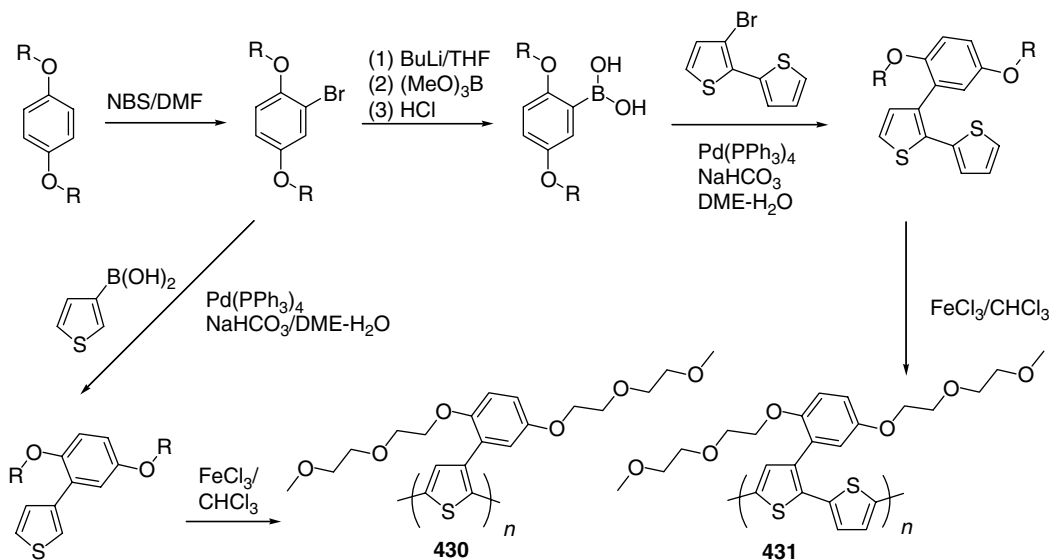


Chart 2.102

diminish energy transfer from the high band-gap to the low band-gap polymers. Several other inert polymer matrices (polystyrene, polycarbonate, polyvinylchloride, poly(2,6-dimethyl-1,4-phenyleneoxide)) showed similar effects [516].

Destri et al. [517] reported the electrochemical synthesis of polymer **432**, which produced a mixture of oligomers up to dodecamer. According to the MALDI-TOF mass spectrum, the maximum peak corresponded to the tetramer (12 thiophene units). The ITO/**432**/Ca/Al device emits red light (580–650 nm) comparable to that for regioregular PATs. Blending **432** with PVK and PBD resulted in a white-emitting diode with 0.03% EL efficiency [517]. Blending with PBD also was an effective way to increase $\Phi_{\text{EL}}^{\text{ex}}$ of highly sterically hindered disubstituted PT **419** from <0.0001 to 0.6% with no change in EL maximum [498] (Chart 2.103).

The emission spectrum of some PT and PBD polymer bilayer devices cannot be explained by a linear combination of emissions of the components. Thus, white emission of the PLEDs ITO/**422**/PBD/Al showed $\Phi_{\text{EL}}^{\text{ex}}$ of 0.3% at 7 V, and consisted of blue (410 nm), green (530 nm), and red-orange (620 nm) bands. Whereas the first and the last EL peaks are due to the EL from the PBD and the PT layers, respectively, the green emission probably originates from a transition between electronic states in the PBD layer and hole states in the polymer



SCHEME 2.69 Synthesis of oligo(ethylene oxide)-containing PTs. (From Johansson, T., Mammo, W., Andersson, M.R., and Inganäs, O., *Chem. Mater.*, 11, 3133, 1999.)

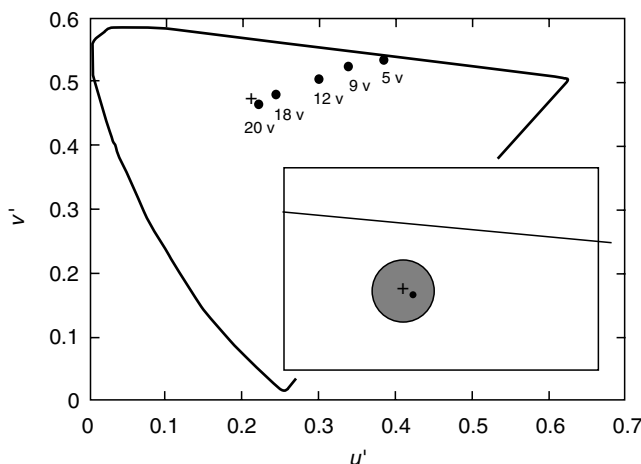


FIGURE 2.31 Chromaticity diagram showing the color of the LED with **418:412:422:PMMA** (10:4:1:1) polymer blend at different voltages. Inset: magnified part of the chromaticity diagram; the shaded circle represents the area, which is defined as white (radius 0.028 and centered at equienergy white point; the u' - v' coordinates are 1976 modification of CIE xy coordinates, the white point $x = y = 0.33$ corresponds to $u' = 0.211$, $v' = 0.474$). (From Granström, M. and Inganäs, O., *Appl. Phys. Lett.*, 68, 147, 1996. With permission.)

layer [518]. Similar results (additional green-blue EL at ~ 495 nm) were demonstrated by PLED ITO/**422**/PBD/Ca/Al [519].

Blending low band-gap PTs with other EL polymers was employed to increase the EL efficiency of a PLED and it was demonstrated that only small additions of PTs can improve the device performance. The $\Phi_{\text{EL}}^{\text{ex}}$ of red-emitting ITO/P3HT(**395**):MEH-PPV/Ca diodes initially increased with P3HT content and went through a maximum at 1 wt% of P3HT with $\Phi_{\text{EL}} = 1.7\%$ [520], which is 2–3 times higher than in the neat ITO/MEH-PPV/Ca diode and three orders of magnitude higher than the ITO/P3HT(**395**)/Ca diode. Later, List and coworkers [521,522] reported a similar observation of efficient yellow-light emission from the blend of blue-emitting ladder-PPP (LPPP **514b**, see below) with small additions (0.5–2%) of orange-emitting **396**. When the concentration of P3DT **396** was as small as 1%, the external EL efficiency of the Al/polymer blend/ITO device was also significantly higher ($\Phi_{\text{EL}}^{\text{ex}} = 4.2\%$) than in pure LPPP **514b** (2%).

2.4.6 POLYTHIOPHENES FOR STRUCTURED AND POLARIZED POLYMER LIGHT-EMITTING DIODES

Apart from the tunable color emission covering the full visible range, there are several other aspects supporting the interest in PTs for PLEDs. PTs are examples of classical conjugated polymers with intrinsic one-dimensionality of the polymer chain. Alignment can induce anisotropy in macroscopic properties such as electron transport or optical properties. Polarized

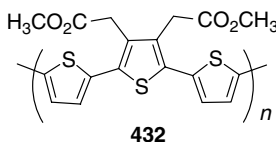


Chart 2.103

EL with $\Phi_{\text{EL}}^{\text{ex}} = 0.05\%$ was observed in multilayer LB-film PLED ITO/**399**/Al, with a ratio in EL between the parallel and perpendicular orientations of 1.3 [523]. An even higher ratio of 2.4 was achieved in ITO/**422**/Ca/Al diode made from a stretch-oriented polymer film [524]. For more information on polarized LEDs, see Chapter 5 in this book.

Among other specific applications of PTs as light-emitting materials, it is necessary to mention microcavity LEDs prepared with PTs **422** and **416** [525,526] and nano-LEDs demonstrated for a device with patterned contact structure, and PT **422** blended in a PMMA matrix that emits from phase-separated nanodomains (50–200 nm) [527,528].

2.4.7 ELECTROLUMINESCENT OLIGOTHIOPHENES

High order and crystallinity of oligothiophenes in the solid state determine their unique optical and electrical properties, i.e., high charge-carrier mobility, anisotropy of electrical and optical properties, etc. In particular, oligothiophenes are widely studied in field-effect transistors (FETs) showing a high level of hole and electron mobilities and high on–off ratios. In this context, one would expect poor suitability of such materials as light-emitting layers in LED. Nevertheless, several publications demonstrate EL from some oligothiophene-based LEDs. For a deeper understanding of the effect of the conjugation length on the electrical properties and emission in PTs, Geiger et al. [529] studied a series of end-capped oligothiophenes **433** (Chart 2.104). The ITO/**433**/Al devices prepared by vacuum sublimation of oligomers showed relatively low turn-on voltages of ca. 2.5 V and moderate current densities (e.g., 7 mA/cm²) with maximum efficiency at ca. 8 V, however the EL efficiency was quite low (estimated internal efficiency $\Phi_{\text{EL}}^{\text{int}} \approx 10^{-2}$ – $10^{-3}\%$). LEDs showed a red shift in the EL peak with increasing number of thiophene units ($n = 3 \rightarrow n = 5$) and a linear dependence of the EL band energy on the inverse number of monomer units. Averaging over EL, PL, and absorbance data, the effective conjugation length was estimated at approximately 9–10 thiophene units.

Several other oligothiophenes were studied in this regard. Variations in the main chain length of phenyl end-capped oligothiophenes **435** also showed red shifts of absorbance (from 375 to 524 nm) and emission (from 470 to 620 nm) with increasing number of thiophene units [530–532]. Sexithiophene end-capped with CH₃ groups (**434**) in ITO/**434**/Al configuration (vacuum sublimed) showed red-orange emission with a very low QE of $\sim 10^{-9}\%$ [533]. Low efficiencies of LEDs, based on crystalline oligothiophenes were somewhat improved by end capping of terthiophene and quaterthiophene with triphenylamino groups (**436**), which led to stable amorphous glasses with luminescence efficiencies of 0.03 and 1.1 lm/W, respectively (at a luminance of 300 cd/m²) [534,535]. A double-layer device with oligomer **436** ($n = 3$) as emitting layer and Alq₃ as ETL showed significantly improved performance, exhibiting a

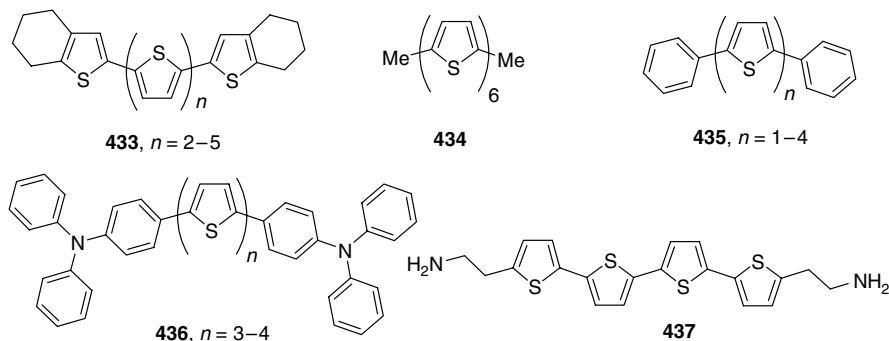


Chart 2.104

maximum luminance of 13,000 cd/m² at driving voltage of 18 V. Undoubtedly, improving the hole-transport properties in these oligomers by end capping with triphenylamino fragments is also an important factor. Terthiophene end capped with 2-aminoethyl groups was also used in hybrid organic–inorganic perovskite materials. When **437** was incorporated within lead halide perovskite layers in an ITO/**437**:PbCl₄/OXD7/Mg/Ag device (OXD7 is 1,3-bis[4-(*tert*-butylphenyl)-1,3,4-oxadiazolyl]phenylene), a bright-green emission (530 nm) from the organic layer was found [536].

A quinquethiophene oligomer unit was used as a core in a light-emitting dendrimer with redox-active triarylamine peripherals (**438**) [537] (Chart 2.105). In this material, an excitation of the peripheral amines at 310 nm results in energy transfer to the highly luminescent fluorophore at the core of the dendrimer with subsequent green emission ($\lambda_{\text{PL}} = 550$ nm) exclusively from the oligothiophene. In an LED containing PBD as the electron-transporting material, the hole transport occurs solely through the peripheral triarylamines, whereas the core oligothiophene plays the role of a light emitter. The EL spectrum was essentially identical to PL ($\lambda_{\text{EL}} = 560$ nm) with no emission from either PBD (390 nm) or peripheral amines (425 nm) and the maximum $\Phi_{\text{EL}}^{\text{ex}}$ was 0.12%.

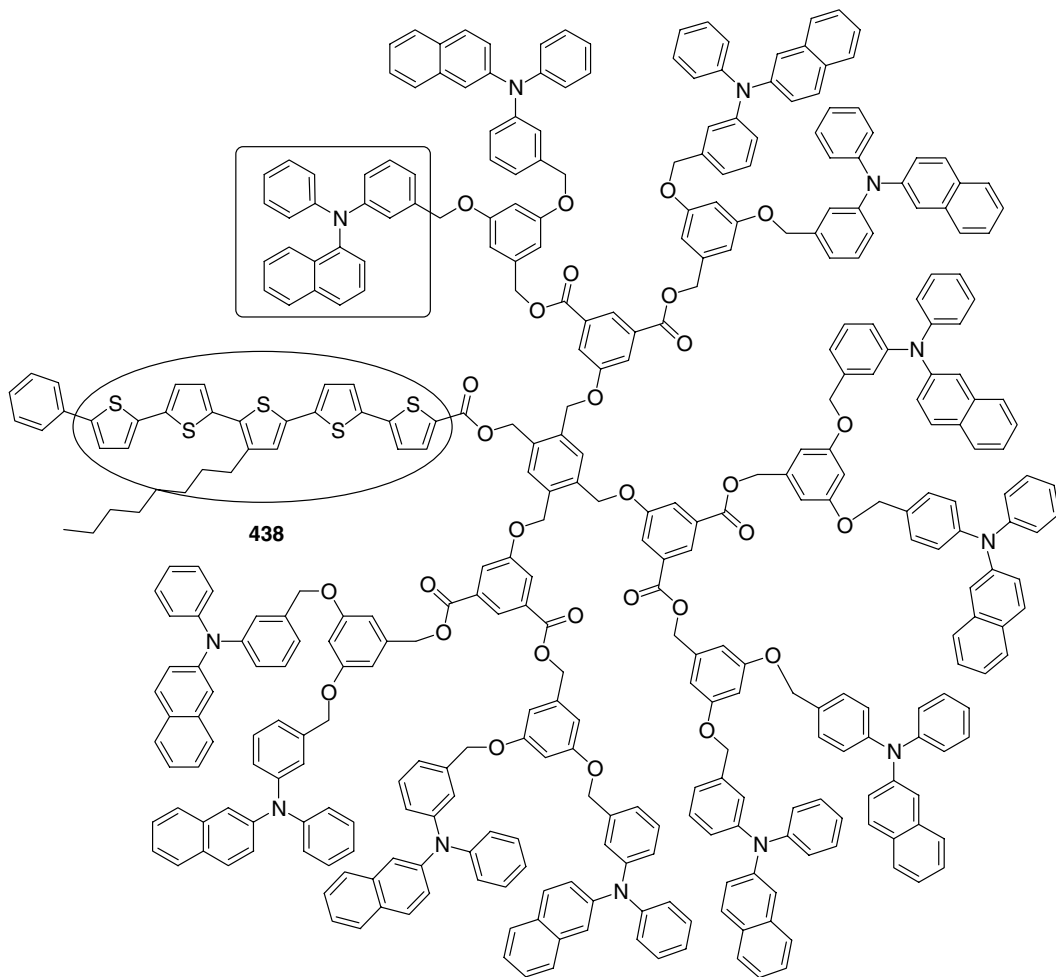


Chart 2.105

2.4.8 THIOPHENE-*S,S*-DIOXIDES AS EMISSIVE AND ELECTRON TRANSPORT MOIETIES

Poly- and oligothiophenes are generally p-type (hole-transporting) semiconducting materials. Recently, Barbarella and coworkers [538,539] reported a novel approach to tailoring the frontier orbitals of thiophene oligomers through a chemical transformation of the thiophene ring into the corresponding thiophene-*S,S*-dioxide (via oxidation with 3-chloroperbenzoic acid). This modification results in “dearomatization” of the thiophene unit and increases the electron deficiency, thus offering an efficient methodology to increase the electron delocalization and the electron transport and injection properties of the material. A comparison of two quaterthiophenes **439** and **440** indicates that a single thiophene-*S,S*-dioxide moiety leads to only a slight increase of the oxidation potential (from 0.95 to 1.04 V vs. Ag/AgCl), whereas the reduction potential is drastically shifted into positive potentials (from -2.12 to -1.28 V) that result in a band-gap contraction by more than 0.7 eV [538] (Chart 2.106). Another feature of this modification is a decreased aggregation tendency, resulting in decreased exciton migration to the nonradiative centers. Consequently, oligomers incorporating thiophene-*S,S*-dioxide units possess good PL properties in solution and the solid state, as well as high (for PTs) EL efficiency. Particularly interesting in this case are the oligomers with a central location of the thiophene-*S,S*-dioxide unit for which the solid-state PLQYs were reported to be as high as 37% (**441** [540]) and 45% (**442** [541]) (and up to 70% for a thiophene-*S,S*-dioxide unit incorporated into oligophenylenes [542]).

Incorporation of thiophene-*S,S*-dioxide units in oligothiophenes allows to vary both absorption and PL energies in a wide range ($\lambda_{\text{max}}^{\text{abs}} \sim 400\text{--}540$ nm, $\lambda_{\text{max}}^{\text{PL}} \sim 525\text{--}725$ nm) [538,542]. Polymers obtained by chemical polymerization of oligomers **441** and **442** with FeCl_3 showed PL in the NIR region (801 and 910 nm, respectively), although the quantum yields were not reported for these materials [542]. A nonoptimized LED with **441** as an active layer (ITO/**441**/Ca/Al) showed a luminance of ~ 100 cd/m² at 7 V and a quite low EL efficiency of 0.03 cd/A at ~ 180 mA/cm² [543]. However, further studies showed that these parameters can be sufficiently improved by blending **441** with PVK and introducing a PEDOT layer: the PLED built as ITO/PEDOT/**441**:PVK, 85:15/Ca/Al configuration showed a maximum luminance of ~ 200 cd/m² at 7 V and an EL efficiency of ~ 0.9 cd/A at 3 mA/cm² [540].

Other thiophene–thiophene-*S,S*-dioxide copolymers were reported by Berlin et al. [544], who synthesized copolymers **443** and **444** with an alternating electron acceptor thiophene-*S,S*-dioxide unit and donor ethylenedioxythiophene (EDOT) units (Chart 2.107). The polymers absorbed at 535 nm ($E_g = 2.3$ eV) in chloroform solution and in films (which is consistent with their electrochemistry: $E_{\text{ox}} \approx 0.40\text{--}0.50$ V, $E_{\text{red}} \approx -1.75\text{--}1.8$ V; $\Delta E \approx 2.2\text{--}2.25$ V) and emitted at 650 nm (Φ_{PL} (film) $\sim 1\%$). Such a high band gap (which exceeds that in PEDOT

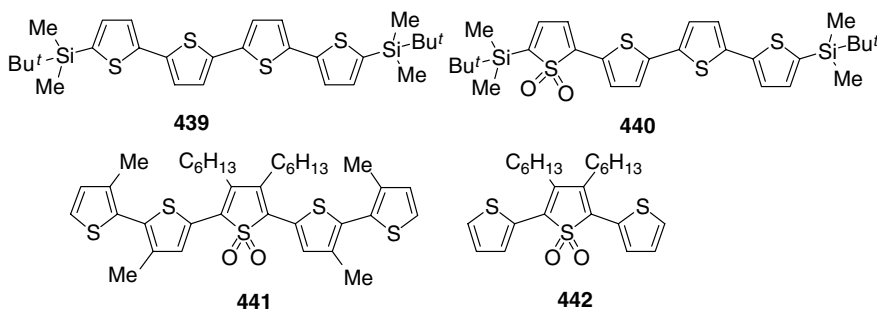


Chart 2.106

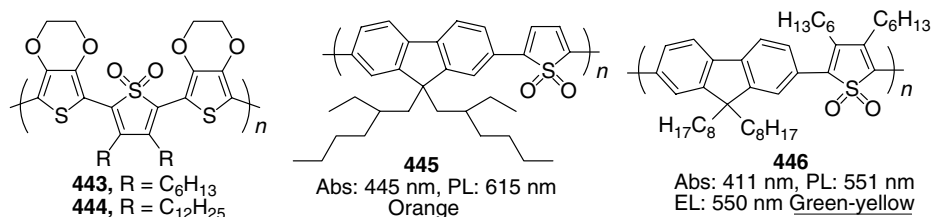


Chart 2.107

homopolymer by ~ 0.6 eV) strongly suggests a disruption of the conjugation (possibly owing to two alkyl substituents in the thiophenedioxide moiety). The EL emission spectrum was entirely the same as PL emission, and $\Phi_{\text{EL}}^{\text{ex}} = 0.01\%$ at 100 cd/m^2 was found for ITO/TPD:**443**: PC (40:40:20)/Ca diode (PC is bisphenol-A-polycarbonate).

These pioneering works stimulated recent research activities in incorporating the thiophene-*S,S*-dioxide unit into various copolymers PLEDs built with such copolymers were reported by several groups. Charas and coworkers studied PLEDs based on copolymer **445** obtained by Suzuki coupling of 2,5-dibromothiophene-*S,S*-dioxide with diboronic ester of 9,9-*bis*(2-ethylhexyl)fluorene [545] and its blends with PFO **196** [546,547]. The copolymer **445** emitted orange light ($\lambda_{\text{PL}}^{\text{film}} = 615 \text{ nm}$), and there was a strong suppression of PLQY going from solution to the solid state ($\Phi_{\text{PL}}^{\text{cyclohexane}} = 19\%$, $\Phi_{\text{PL}}^{\text{film}} = 0.5\%$). A single-layer ITO/**445**/Ca PLED exhibited quite low EL efficiency ($\Phi_{\text{EL}}^{\text{ex}} = 2.2 \times 10^{-4}\%$), which was attributed to a combination of low PL efficiency and charge-transport limitations. Upon inserting a hole injection PEDOT layer, the EL efficiency was increased to $\Phi_{\text{EL}}^{\text{ex}} = 9 \times 10^{-4}\%$ and the maximum luminance increased from 0.2 cd/m^2 to about 5.3 cd/m^2 . The optoelectronic characteristics of the devices were improved by blending **445** with PFO, allowing an increase in $\Phi_{\text{EL}}^{\text{ex}}$ up to 0.21% (for ITO/PEDOT/PFO:**445**(95:5)/PBD/Ca architecture) and a decrease in the turn-on voltage from 16 to 5–5.5 V. Remarkably, the EL of the blend in this case was almost exclusively from the copolymer **445**, in spite of the low ratio of the latter.

The same Suzuki methodology was used to synthesize a similar copolymer **446** [548]. The polymer showed a solvent-dependent green-yellow emission (from 545 nm in THF to 565 nm in chloroform) as often observed for polar chromophores. The PL QE also varied with the solvent (from 11% in THF to 21% in decalin) but, in contrast to copolymer **445**, no strong decrease in emission efficiency was observed in the solid state ($\Phi_{\text{PL}}^{\text{film}} = 13\%$) that could be attributed to the effects of substituents at the thiophene ring. LEDs based on **446** showed, for an ITO/PEDOT/**446**/Ca/Al architecture, a turn-on voltage of ca. 10 V with a maximum brightness of 340 cd/m^2 at 22 V and appreciable $\Phi_{\text{EL}}^{\text{ex}} = 0.14\%$.

Beaupré and Leclerc [407] reported fluorene–thiophene copolymers, in which fluorene and thiophene-*S,S*-dioxide fragments were separated by one or two thiophene units (**447** and **448**, respectively) (Chart 2.108). The electronic effect of an additional thiophene unit (the system can be viewed as an alternating donor–acceptor polymer) and the planarization factor known for longer oligothiophene units, resulted in a pronounced band-gap contraction. These copolymers are p- and n-dopable, as followed from their electrochemistry, with band gaps of 2.0 and 2.2 eV for **447** and **448**, respectively. The PLEDs, fabricated with configurations ITO/LiF/polymer/PBD/LiF/Al/Ag showed rather low turn-on voltages of 4 V, but the maximum brightness (120 cd/m^2 at 7 V and 15 cd/m^2 at 8 V, for **447** and **448**, respectively) was lower than that for copolymer **446**. Although highly efficient ($\Phi_{\text{PL}}^{\text{film}} \approx 40\text{--}70\%$) solid-state PL was demonstrated from some oligothiophenes and oligophenylenes containing thiophene-*S,S*-dioxide units [542]; the efficiency of similar fluorene copolymers is remarkably lower.

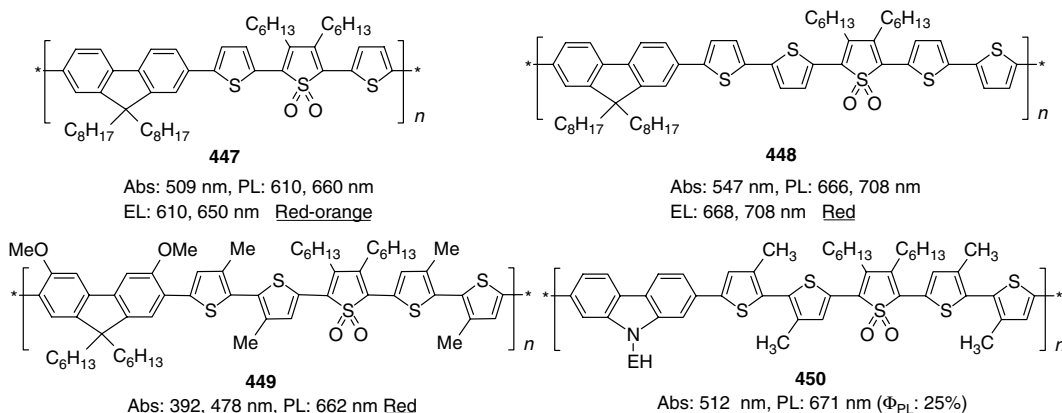


Chart 2.108

The combination of thiophene and thiophene-*S,S*-dioxide units in a copolymer allows tuning the emission color from green to pure red [407,549]. However, the PLEDs fabricated with these materials showed a rather low $\Phi_{\text{EL}}^{\text{ex}} < 0.01\%$ that further decreased with an increasing number of thiophene units. Similar results (significant decrease of the PL QE) were observed for thiophene–thiophene-*S,S*-dioxide copolymers containing 3,6-dimethoxyfluorene (**449** [303]) and carbazole units (**450** [550]) ($\Phi_{\text{PL}} = 20\text{--}25\%$ in solution).

Also, a danger of potential instability toward n-doping of the thiophene-*S,S*-dioxide containing oligomeric and polymeric EL materials can be foreseen, based on the known instability of other classes of heterocyclic systems with SO_2 fragment in the cycle toward reductive cleavage. However, it should be mentioned that such a behavior has not, so far, been reported for the above thiophene-*S,S*-dioxide-containing materials.

2.4.9 COPOLYMERS OF THIOPHENES WITH OTHER CONJUGATED MOIETIES

2.4.9.1 Thiophene Copolymers with Aromatic Moieties

Salaneck and coworkers [551] first reported EL from alternating phenylene–thiophene copolymer **452**. Its band gap, ionization potential, and electron affinity, calculated with the VEH method, are 3.08, 5.29, and 2.22 eV, respectively. These values are between the corresponding values for poly(*p*-phenylene) (PPP) **471** (3.28, 5.43, and 2.15 eV [552]) and PT **385** (1.6, 5.0, and 3.4 eV [553]). The steric hindrance of heptyl side groups in this polymer results in interannular torsion angles of 50° that are substantially larger than that of PPP (23°); nevertheless, their band gaps are smaller than that of PPP. Phenylene–thiophene copolymers **451** and **452** emit blue light at ca. 450–475 nm, with somewhat different reported $\Phi_{\text{EL}}^{\text{ex}}$ of $\sim 0.2\%$ [554] and 0.03% [555], respectively, for ITO/polymer/Ca configurations. It has also been shown that the efficiency of the device can be substantially improved (up to 2%) by blending of **452** with substituted PPP (1:10) (**474e**, see below) [554]. This is among the highest values reported for thiophene-based LEP (Chart 2.109).

An important series of copolymers **453**, containing thiophene–phenylene–thiophene repeating units, have been reported by Huang and coworkers [556–558]. Polymers were obtained via FeCl_3 oxidation of corresponding thiophene–phenylene–thiophene trimers that were synthesized by Pd-catalyzed coupling of 1,4- R^2 , R^3 -2,5-dibromobenzenes with the corresponding 3- R^1 -2-thienylzinc chlorides. By changing the substituents R^1 and R^2 , the polymer emission can be tuned from greenish-yellow to pure green.

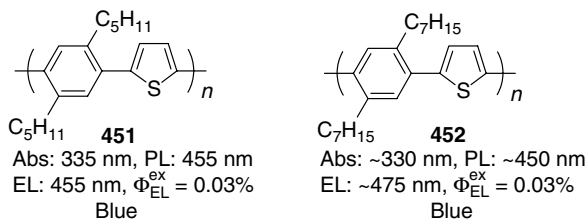


Chart 2.109

While retaining much of the substituted PT character (e.g., good hole-transport properties and stability), these materials exhibit significantly improved fluorescence efficiency in the solid state (Φ_{PL} up to 29%) that leads to $\Phi_{\text{EL}}^{\text{ex}}$ of up to 0.1% for ITO/**453**/Ca PLED (Table 2.6). Other widely studied thiophene copolymers with aromatic 9,9-disubstituted fluorene units were already described above in Section 2.3.

Alternating oligothiophene-containing copolymers **454–458** with 1,1-binaphthyl units, which interrupt the conjugation due to the large torsion angle between the naphthalene rings were reported. The nonplanar structure could prevent the self-quenching processes in the solid state and variation in the length of the oligothiophene segment from one to seven thiophene rings tuned the emission color from yellow-green to red (Table 2.7) [559]. A single-layer device ITO/**455**/Al prepared with copolymer **455** emitted orange light (λ_{EL} at 568 nm with a shoulder at 590 nm) with a turn-on voltage of 5.7 V, luminance 25 cd/m² at 8.0 V, and $\Phi_{\text{EL}}^{\text{ex}} = 0.005\%$ [560] (Chart 2.110).

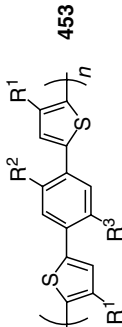
Copolymer **459**, prepared by Stille coupling of dibromophenylene with 2,5-*bis*(tributylstannyl)thiophene, represents another example of a phenylene-*alt*-thiophene backbone, where the substituted phenylene unit forms an oligophenylene-vinylene fragment that is not in the main conjugation chain [561]. A PLED fabricated with this polymer (ITO/**459**/Al) emitted green light (520 nm) with a turn-on voltage of ca. 9.5 V, but no other data on luminance or efficiency of the device were reported (Chart 2.111).

2.4.9.2 Thiophene Copolymers with Heteroaromatic Moieties

Several copolymers (**460–466**) containing electron-rich thiophene and electron-deficient 1,3,4-oxadiazole units have been reported by Huang and coworkers [562–565]. Structural variations, particularly different lengths of oligothiophene fragments, allowed the tuning of the band gap and PL energy of these materials (Table 2.8). An ITO/**460c**/Ca single-layer LED emitted blue light with a turn-on voltage of 8 V at forward bias. Although the polymer showed very high $\Phi_{\text{PL}} = 79\%$, $\Phi_{\text{EL}}^{\text{ex}}$ of the device was only ~0.0001% due to unoptimized device structure and, possibly, a purity problem (Chart 2.112).

Jenekhe and coworkers [566,567] reported the synthesis of other *n*-type conjugated copolymers with alternating bithiophene and *bis*-quinoline units, **467a–f** that showed reversible reduction at –1.65 to –1.80 eV vs. SCE (onsets at ca. –1.4 to –1.52 V) and thus expected to exhibit good electron transport properties (Scheme 2.70). These polymers emit green light ($\lambda_{\text{PL}}^{\text{sol}} = 502\text{--}504$ nm, $\lambda_{\text{PL}}^{\text{film}} = 517\text{--}524$ nm) with moderate efficiency in solution ($\Phi_{\text{PL}} = 22\text{--}28\%$) that, however, dropped down to 1–3% in the solid state. The poor luminescence quantum yield of **467**, compared to other polyquinolines, might be due to charge-transfer quenching in these donor–acceptor copolymers. As an emissive material, **467** exhibits weak green EL (529–538 nm) with $\Phi_{\text{EL}}^{\text{ex}} = 0.004\text{--}0.015\%$ for an ITO/PEDOT/**467**/Al configuration. A red shift in absorption (37 nm), PL (44 nm), and EL (33 nm) was observed for films of HT polymer **467f**, compared to a HH analog **467b** [567]. This had no effect on Φ_{PL}

TABLE 2.6
Tuning the Properties of Substituted Phenylene–Thiophene Copolymers



R ¹	R ²	R ³	M _n (g/mol)	PDI	λ _{max} ^{abs} (nm)	λ _{max} ^{PL} (nm)	Φ _{PL} (%)	Φ _{EL} ^{gx} (%)	Turn-On Voltage (V) ^a	Ref.
<i>n</i> -C ₆ H ₁₃	CH ₃	CH ₃	20,400	2.92	340	477	10	0.004	17	556, 558
<i>n</i> -C ₆ H ₁₃	H	H	12,600	1.48	346	470	15 ± 1			
<i>n</i> -C ₆ H ₁₃	H	H	19,700	2.74	396	524	20	0.02	13	556, 558
<i>n</i> -C ₆ H ₁₃	OC ₁₀ H ₂₁	OC ₁₀ H ₂₁	31,200	2.31	378	505	22 ± 2			
<i>n</i> -C ₆ H ₁₃	OC ₁₀ H ₂₁	OC ₁₀ H ₂₁	14,600	1.92	430	530	29	0.1	8	556, 558
<i>n</i> -C ₆ H ₁₃	OC ₁₀ H ₂₁	OC ₁₀ H ₂₁	26,100	1.27	405	520	27 ± 3			
<i>n</i> -C ₆ H ₁₃	CH ₃	CH ₃			360	466	6			556
<i>n</i> -C ₆ H ₁₃	H	H			376	495	11			556
<i>n</i> -C ₆ H ₁₃	OC ₁₀ H ₂₁	OC ₁₀ H ₂₁			410	505	16	0.05	9	556
<i>p</i> -(<i>n</i> -C ₄ H ₉)Ph	<i>n</i> -C ₁₀ H ₂₁	<i>n</i> -C ₁₀ H ₂₁	82,300	2.19	442	532	11	(~0.1)	(~7)	557
<i>p</i> -(<i>n</i> -C ₄ H ₉)Ph	CH ₃	EH	68,500	1.51	426	538	12	(~0.1)	(~7)	557
<i>p</i> -(<i>n</i> -C ₄ H ₉)Ph	EH	EH	43,600	1.68	429	533	11	0.1	7	557

^aITO/polymer/Ca.

TABLE 2.7
Properties of Binaphthyl-Linked Thiophene Block Copolymers with Different Conjugation Length

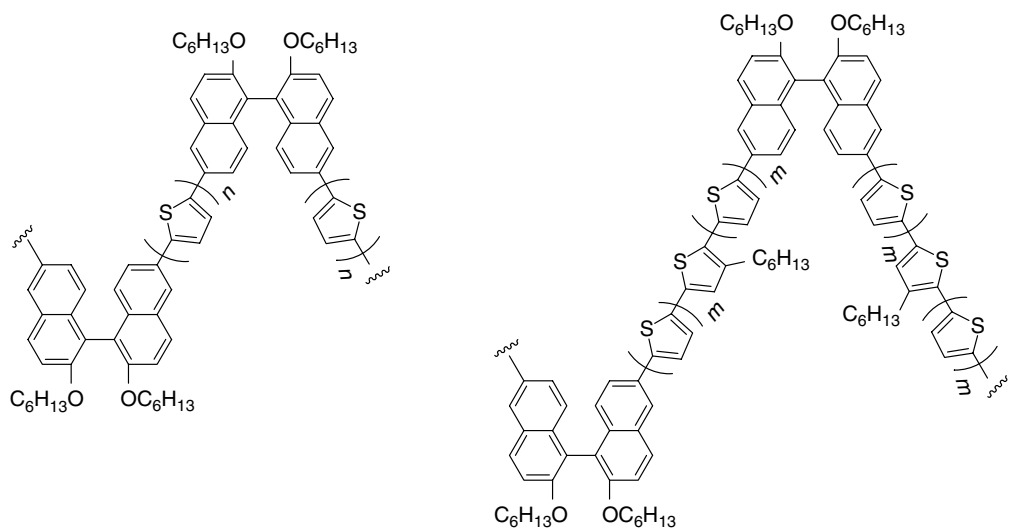
Compound	M_n (g/mol)	PDI	$\lambda_{\max}^{\text{abs}}$ (nm)	$\lambda_{\max}^{\text{PL}}$ (nm) (DCM)	Φ_{PL} (%) (DCM) ^a
454 , $n = 1$	13,900	2.6	368	421, 446, 475sh	54
455 , $n = 2$	18,100	1.7	406	463, 498	26
456 , $n = 4$	5100	1.1	440	515, 549sh	23 (19 ^b)
457 , $m = 2$	17,400	1.6	434	530, 568sh	5.4 (23 ^b)
458 , $m = 3$	2300	2.6	454	545, 583, 631sh	6.5 (7.2 ^b)

^aExcitation at 380 nm.

^bExcitation at the longest wavelength absorption maximum.

of materials and performance of the devices. A large improvement in performance of PLEDs was found for bilayer devices ITO/MEH-PPV/**467**/Al, where polymers **467** act as ETL materials. The diodes showed bright orange-red EL emission of MEH-PPV with turn-on voltages of 8.5–9 V and a luminance in the range of 948 cd/m² for **467a** to 2170 cd/m² for **467b** ($\Phi_{\text{EL}}^{\text{ex}}$ was in the range of 0.86% for **467e** to 1.4% for **467b**) [567]. Similarly, polymer **467c** can be used in polymer blend systems, where a single-layer blend PLED ITO/MEH-PPV:**467c** (72:28)/Al showed a turn-on voltage of 6 V, a luminance of 1480 cd/m² at 14 V, current density of 279 mA/cm², and $\Phi_{\text{EL}}^{\text{ex}} = 0.64\%$ [566].

A low band-gap ($E_g \sim 1.6$ eV) conjugated thiophene copolymer **468** with pyrrole and BT units was synthesized by Stille coupling [568]. They showed emission in the NIR region ($\lambda_{\text{EL}} \sim 800$ nm) with turn-on voltage below 4 V but with very low efficiency (Chart 2.113).



454, $n = 1$; Abs = 368 nm, PL = 421, 446, 475sh nm

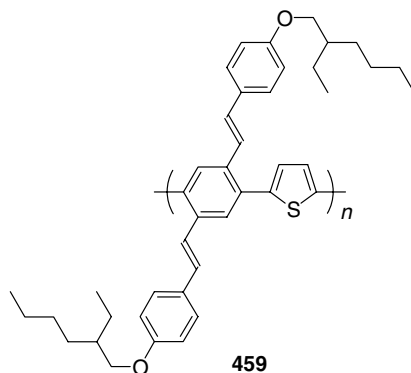
455, $n = 2$; Abs = 406 nm, PL = 463, 498 nm

456, $n = 4$; Abs = 440 nm, PL = 515, 549sh nm

457, $m = 2$; Abs = 434 nm, PL = 530, 568sh nm

458, $m = 3$; Abs = 454 nm, PL = 545, 583, 631sh nm

Chart 2.110



Abs: 362 nm, PL: 530 nm, EL: 520 nm. Green

Chart 2.111

Blending with dialkoxy-PPV **14** in a device (ITO/PEDOT/polymer blend layer/LiF/Ca) substantially improved the EL efficiency (by about two orders of magnitude). A moderately efficient energy transfer from the higher band-gap PPV ($\lambda_{\text{EL}} = 650$ nm) to PT **468** ($\lambda_{\text{EL}} = 830$ nm) allowed fine-tuning of the emission color by changing the component ratio (Figure 2.32) [569].

Oligo-2,5-thienylenevinylens (OTV) have been recognized as a potential class of linear conjugated systems for micro- and nanoelectronics [570]. Comparison of optical data for OTV with other classes of conjugated oligomers (oligothiophenes, oligo-2,5-thiophene ethynylens, oligo-1,4-phenylene vinylens, oligo-1,4-phenylene ethynylens, oligoacetylenes)

TABLE 2.8
Electrochemical and Optical Properties of Oxadiazole–Thiophene Copolymers

Compound	M_n (g/mol) (PDI)	$\lambda_{\text{max}}^{\text{abs}}$ (nm) Film (Solution)	$\lambda_{\text{max}}^{\text{PL}}$ (nm) Film (Solution)	Φ_{PL} (%)	E_g^{opt} (eV) (Film)	E_{red} (V) (Ref. Electrode)
460a		(330)	(425)	7.6 ^a	(2.87)	
460b		395 (364)	475 (433)	68 ^a	2.83 (2.85)	Onset −1.86 (SCE)
460c		396, 440sh (375)	486 (438) ^b 455, 469, 478 ^c	79 ^a	2.79 (2.84)	Onset −1.88 (SCE); onset −1.54 (Ag/Ag ⁺)
462	5419 (1.9)	420, 443	489			pc/pa −1.83/−1.60 (SCE)
461	7574 (2.0)	441, 471	530			pc/pa −1.95/−1.70 (SCE)
463	2814 (1.4)	439sh, 461, 494sh	580			pc/pa −1.79/−1.70 (SCE)
464	3830 (1.8)	358	462		3.04	pc/pa −1.73/−1.53 (SCE); $E_g^{\text{CV}} = 3.02$
465	24,900 (1.41)	376 (342)	498, 526 (444, 462)		2.83	pc/pa −1.86/−1.75 (SCE); $E_g^{\text{CV}} = 2.84$
466	2870 (2.0)	430	568		2.54	pc/pa −1.76/−1.67 (SCE); $E_g^{\text{CV}} = 2.51$

^aRelative quantum yield vs. quinine sulfate.

^bFrom Huang, W., Meng, H., Yu, W.-L., Gao, J., and Heeger, A.J., *Adv. Mater.*, 10, 593, 1998.

^cFrom Huang, W., Yu, W.-L., Meng, H., Pei, J., and Li, S.F.Y., *Chem. Mater.*, 10, 3340, 1998.

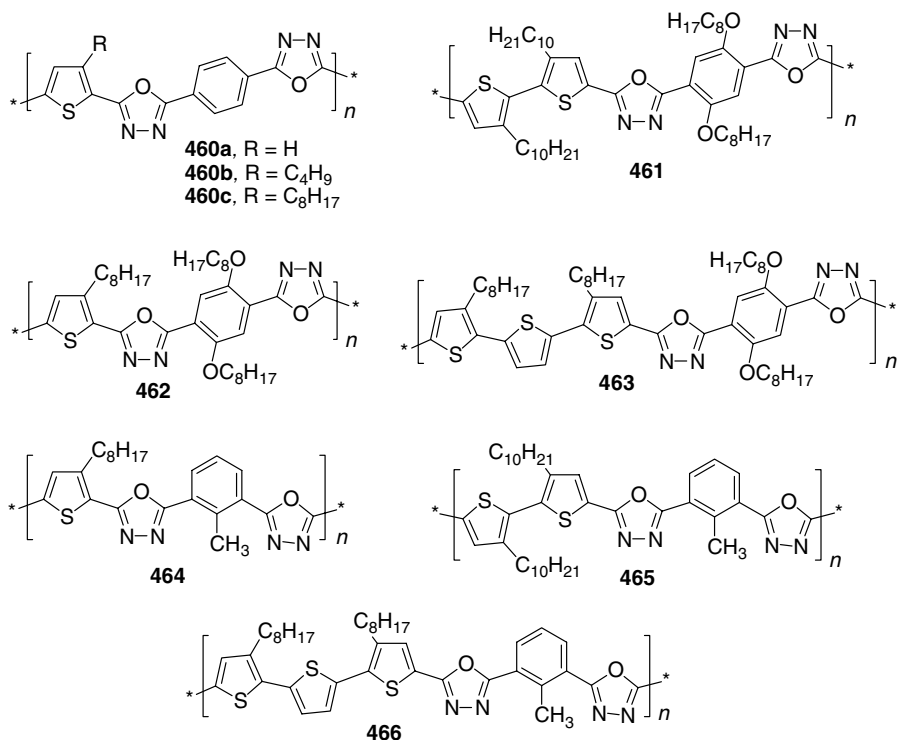
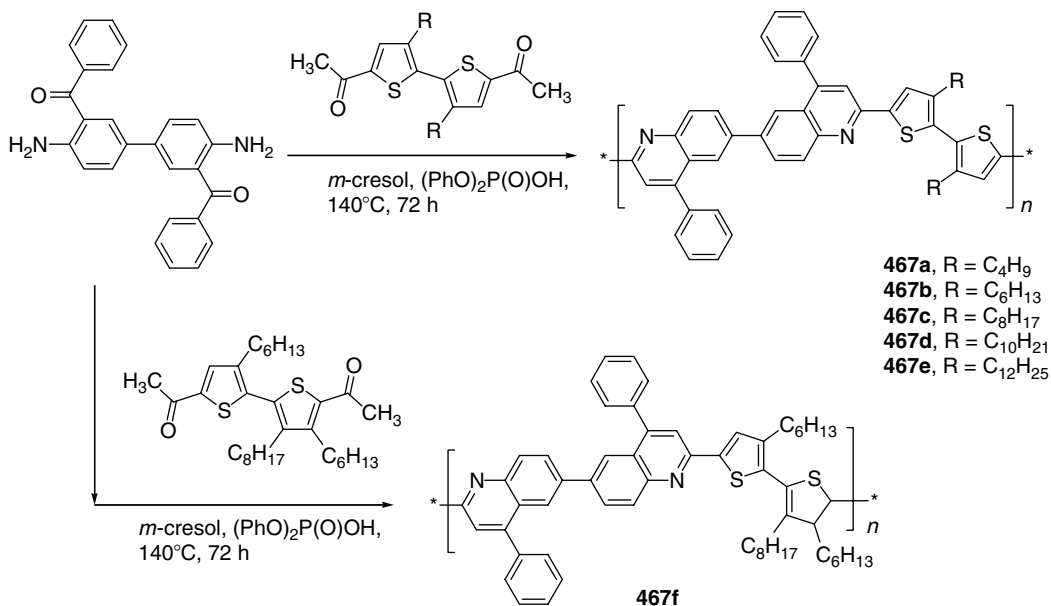


Chart 2.112



SCHEME 2.70 Synthesis of bisquinoline–thiophene copolymers. (From Tonzola, C.J., Alam, M.M., and Jenekhe, S.A., *Adv. Mater.*, 14, 1086, 2002; Tonzola, C.J., Alam, M.M., Bean, B.A., and Jenekhe, S.A., *Macromolecules*, 37, 3554, 2004.).

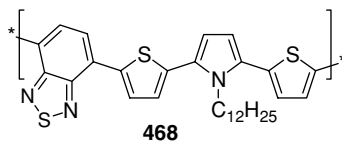


Chart 2.113

showed that OTV exhibit the longest effective conjugation length among the known systems and the smallest $\Delta E_{\text{HOMO-LUMO}}$ values, promising the lowest band gap for the corresponding polymers. We are not aware of any report of poly-2,5-thienylenevinylene (PTV, **469** [26]), a fluorescent material, in spite of strong NIR PL and EL observed in cyano-substituted PTV (**121** [44]). Furthermore, blending 5–25% of PTV **469** into PPV **1** completely quenched the luminescence of the latter and the resulting blend was not emissive (Chart 2.114).

2.4.10 CONCLUSIONS

PTs represent an important class of (generally) low band-gap conjugated polymers for LED applications. Variation in substituents that changes the torsion angle of the thiophene rings allows tuning of the emission over a wide range, from blue-greenish to deep-red and NIR. PTs possess a strong aggregation tendency that decreases the PL and EL emission efficiency but that can be minimized by introducing bulky substituents. Regioregularity in mono-3-substituted PTs offers an additional control over the light-emitting properties of these materials. PATs have higher HOMO energies than PPVs or PFs (e.g., for poly-3-octylthiophene: HOMO = -4.57 eV, $E_g = 1.96$ eV), thus decreasing the hole injection barrier from the ITO electrode.

Relatively efficient blue (polymer **419**, $\Phi_{\text{EL}}^{\text{ex}} = 0.6\%$ [498]), red (polymer **416**, $\Phi_{\text{EL}}^{\text{ex}} = 0.7\%$ [502]), and white (blend of **412**, **418**, and **422**, $\Phi_{\text{EL}}^{\text{ex}} = 0.3\%$ [515]) emitters have been reported for thiophene homopolymers, although their performance is far from the champions of other classes of LEP.

On the other hand, very respectable performances were demonstrated by blends of PT with other emitting polymers, as exemplified by a yellow-emitting blend of LPPP **514b** with **396** ($\Phi_{\text{EL}}^{\text{ex}} = 4.2\%$) [521]. Furthermore, easy functionalization of the thiophene nucleus and its electron-

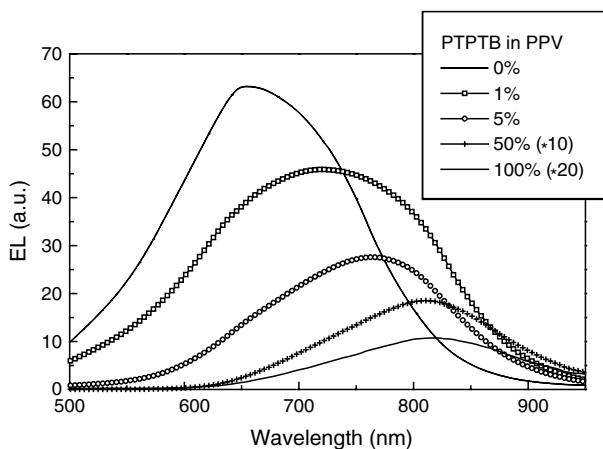


FIGURE 2.32 Electroluminescence spectra of ITO/PEDOT/active layer/LiF/Ca devices with **468** (PTPTB) and **14** (PPV) as an active layer. (From Brabec, C.J., Winder, C., Sariciftci, N.S., Hummelen, J.C., Dhanabalan, A., van Hal, P.A., and Janssen, R.A.J., *Adv. Funct. Mater.*, 12, 709, 2002. With permission.)

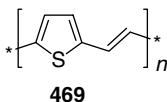


Chart 2.114

rich character make it attractive for the design of various copolymers with other classes of aromatics and heteroaromatic systems, allowing EL color tuning and hole–electron transport properties of the materials. In fact, many of the best performing LEPs contained a certain amount of thiophene comonomer units in the structure (e.g., pure red emitter **341** [418]).

2.5 MISCELLANEOUS CLASSES OF LIGHT-EMITTING POLYMERS

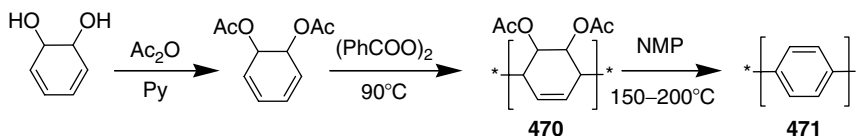
In the previous sections, we described three main classes of LEP: PPV, PF, and PTs, although many other conjugated and nonconjugated polymers have also been used as EL materials for LEDs. Without making an attempt to cover all types of polymers ever used as EL materials, we describe below the most important classes and the most prominent examples of EL polymers, not covered in the previous sections. Some more examples of such systems can be found in recent reviews on blue LEPs [227], polycarbazoles [571], and the general topic of organic EL materials [6,10,20].

2.5.1 POLY-*p*-PHENYLENES

Material instability is one of the major limitations of PLEDs. In this light, a very high thermal stability of polyphenylenes, combined with high PLQY, renders them attractive as materials for device applications. The first PPP-based PLED was described by Leising and coworkers [572,573] in 1992. Polymer **471** was synthesized by aromatization of a soluble precursor **470** (Scheme 2.71). Owing to the relatively high band gap of PPP **471** (2.7–3.0 eV), the PLED ITO/**471**/Al emitted blue light with $\lambda_{\text{EL}} \sim 460$ nm ($\Phi_{\text{EL}}^{\text{ex}} = 0.01\%$, turn-on voltage of 10 V) [573]. High-efficiency EL was never reported for this particular polymer, which might be due to intrinsic defects in the structure ($\sim 15\%$ of *meta*-linkage) associated with the synthetic method.

Considerable interest has been paid to solution-processible PPP materials, prepared by introducing long-solubilizing substituents into the phenylene rings of the backbone (**472–474**) (Chart 2.115). Synthesis of such systems was typically achieved via Ni-catalyzed Yamamoto coupling of 1,4-dihalophenylenes or Pd-catalyzed Suzuki coupling of halides with boronic acids or esters, both of which delivered well-defined polymers with molecular weight of $\sim 10^4$ [574–576]. Numerous substituted PPPs, including dialkyl (**472a,b** [575] and **474** [576]), alkoxy (**472c–e** [577] and **472f–h** [578]), benzoyl (**472i** [579]), as well as dialkoxy (**472j** [580], **472k** [581], **472l** [582], **472m** [63]) PPPs have been synthesized and studied in PLEDs.

Steric hindrance due to alkyl substituents increases the torsion angle between phenylene units, which results in an additional (unwanted) increase of the band gap. The emission band shifts into the violet region of the spectrum ($\lambda_{\text{PL}} \sim 400$ nm) [583]. The hypsochromic shift



SCHEME 2.71 Synthesis of PPP by soluble precursor way.

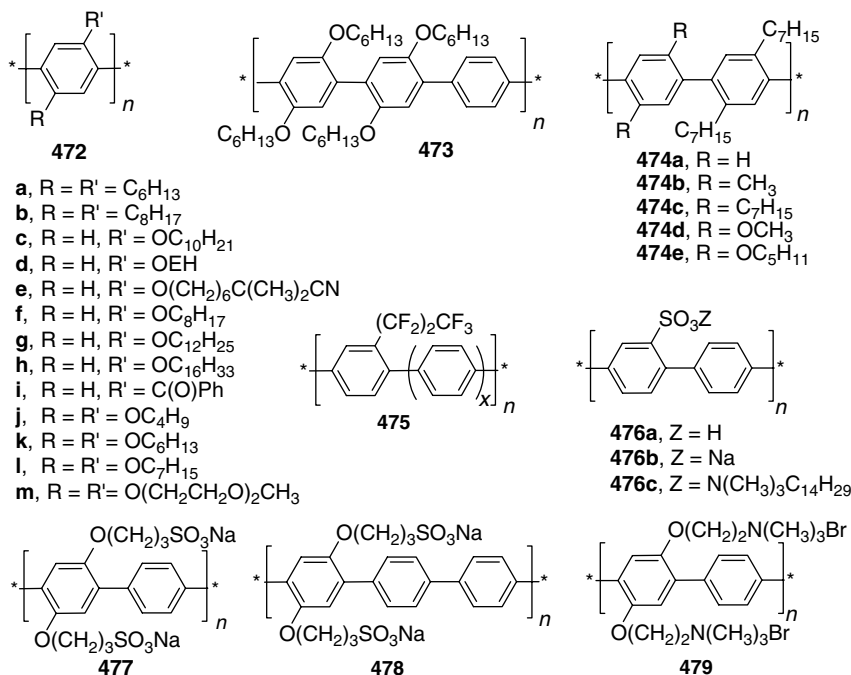


Chart 2.115

due to less sterically demanding alkoxy group is less dramatic ($\lambda_{\text{EL}} = 420$, with much weaker bands at ~ 500 and ~ 600 nm). These polymers show quite high solid-state PLQY (35–45%) [577]. Although a relatively poor EL performance ($\Phi_{\text{EL}}^{\text{ex}} = 0.15\%$, brightness 30 cd/m^2) was reported by Chen and Chao [578] for alkoxy derivatives **472f–h**, Heeger and coworkers [577,584] succeeded in fabrication of the very efficient violet blue-emitting PLEDs with alkoxy-PPPs **472c–e**. The $\Phi_{\text{EL}}^{\text{ex}} = 1.8\%$ was reported for the single-layer device ITO/**472c**/Ca [584]. It can be further increased to 3% using a second HTL (in devices ITO/PPV **1**/**472c**/Ca [584] or ITO/PVK/**472c**/Ca [577]). ~ 5 times lower efficiency was obtained using a high work-function electrode (Al). Somewhat lower but also very respectable efficiencies were demonstrated by PLEDs with two other alkoxy-PPPs: ITO/PVK/**472d**/Ca (2%) and ITO/PVK/**472e**/Ca (1.4%) [577].

A second alkoxy substituent in PPP may increase the chain twisting and further enlarge the band gap. Thus, a band gap of 3.4 eV and PL–EL maxima at ~ 400 and ~ 500 nm have been reported for polymer **472k**, synthesized by oxidative (FeCl_3) polymerization of di(heptyloxy)benzene [581]. On the other hand, this could be a result of defective polymer structure (due to the synthetic method), as a PL maximum of 435 nm was reported for dibutoxy-PPP **472j** [580]. By blending the latter with PVK **535** (10%) and PBD **21** (10%) to improve the charges-transport properties of the material, a very efficient ($\Phi_{\text{EL}}^{\text{ex}} = 1.2\%$) PLED was fabricated with a stable Al cathode but the reported turn-on voltage was high (20 V). In 1995, Heeger and coworkers [63] used the dialkoxy-PPP **472m** to demonstrate the idea of LEC, in which a $\Phi_{\text{EL}}^{\text{ex}} = 2\%$ was achieved with an Al cathode (in the device configuration ITO/**472l**:PEO:LiOTf/Al).

The band gap in substituted PPPs can be tuned to some extent by “diluting” the substituted phenylene rings with unsubstituted phenylenes. A bathochromic shift in absorption was observed for copolymer **473** ($E_g = 2.95 \text{ eV}$) compared to the “all-substituted” homopolymer **472k** ($E_g = 3.1 \text{ eV}$) [581]. Sandwiching this polymer between ITO and Ca electrodes afforded a

blue-emitting PLED with $\Phi_{\text{EL}}^{\text{ex}} = 0.5\%$. Even a higher efficiency PLED ($\Phi_{\text{EL}}^{\text{ex}} = 2\%$) was fabricated from PPP alkoxy and alkyl copolymer **474a**, when blended with 10% of diheptyl-phenylene–thienylene copolymer **452** (device ITO/**474:452**/Ca) [585]. Several other PPP homo- and copolymers **474b–e** based on the diheptylphenylene units have been synthesized [576].

A very different route to soluble PPP derivatives was demonstrated by Yoshino and coworkers [586], who introduced perfluorinated alkyl substituents into PPP **471** by reaction with perfluorobutanoyl peroxide. The resulting modified polymer **475** was soluble in common organic solvents and a solution-fabricated PLED ITO/**475**/Mg:In emitted blue to green light (depending on voltage) with band half-width of over 200 nm.

Some EL devices based on sulfonated copolymer **476** were reported by Neher and coworkers [587]. These polyelectrolyte materials are soluble in DMSO (or in mixed solvents, for **476c**). The solution PL maximum (400 nm) does not depend on the counterion, however, the EL maximum is more sensitive to coulombic interactions and can be shifted from ~ 480 –500 nm (for the sodium salt **476b**) to 454 nm (for the acid **476a**). The $\Phi_{\text{EL}}^{\text{ex}}$ of the devices, fabricated between ITO and Al electrodes, is between 0.5 and 0.8%. Later, Reynolds and coworkers [588] reported related polymers **477** and **478**, where the ionic sulfonate substituents are separated from the PPP backbone by an alkoxy chain. In contrast to **476**, these polymers were soluble in water. A PLED device fabricated by sandwiching the blend of **477** with polyethyleneimine (as a counterion source) between ITO and Al electrode showed very low $\Phi_{\text{EL}}^{\text{ex}} \sim 0.01\%$ [588,589]. An interesting approach to fabrication of multilayer PLEDs via sequential adsorption of PPP cationic (**477**) and anionic (**479**) layers from a water solution was demonstrated by Baur et al. [589]. Although the $\Phi_{\text{EL}}^{\text{ex}}$ of the device ITO/35 bilayers (**477/479**)/Al was very low (0.002%), the importance of this work is in the demonstration of a novel device fabrication method. Another approach taking advantage of the cationic–anionic LEP interaction was reported by Yang and coworkers [181], who prepared dual-color LED matrix by ink-jetting a solution of an anionic PPV derivative **148** on a spin-coated film of **479**.

In the previous sections, we described the effective tuning of EL properties of other classes of LEP (PPV, PF, PT) by introduction of phenylene units into their backbone (e.g., copolymers **125**, **271**, **272**, **291–293**, **451–453**). Likewise, a series of very effective EL materials were designed by separating the oligophenylene ($n = 2$ –5) blocks by ethylene, vinylene, or ethynylene units (copolymers **480–490**) [590] (Chart 2.116). Changing the length of the phenylene block and separating bridges, the polymer absorption (336–406 nm) and PL maxima (401–480 nm) can be varied over a wide range. A solid-state PLQY of up to 60–70% was reported for some of these materials. The EL can be tuned over an even wider range (423–650 nm) in multilayer PLEDs and by varying the polymer composition and the device structure, certain PLEDs with internal QE up to 4% were engineered (Table 2.9).

Aggregation-induced quenching has been a problem for several polymers of this series. Thus, a relatively low solid-state PLQY was observed for rigid polymers with short PPP blocks (9% for **481** and **482**). Quenching can be suppressed by blending the light-emitting PPP **481** with a hole-transporting poly(phenylbiphenylsilylene). The result was a fivefold increase of the PL efficiency [591]. An ITO/polymer blend/Al device exhibited a $\Phi_{\text{EL}}^{\text{ex}} = 0.2\%$ that was up to two orders of magnitude higher than that obtained in a device with a pure polymer **481** layer.

A series of terphenylene–vinylene copolymers **491–493** was recently synthesized by Ahn and coworkers [592] via Suzuki coupling. Interestingly, neither alkoxy groups nor pendant phenyl substituents (attached to the vinylene moiety) have any significant effect on the emission properties. The PLEDs fabricated with each of these copolymers (ITO/polymer/Al) emit blue light with $\lambda_{\text{EL}} \sim 450$ nm (above a turn-on voltage of 8–10 V).

A Diels–Alder cyclization polymerization was recently used by Cho and coworkers [593] for the synthesis of sterically hindered copolymers **494a,b**, in which terphenylene or

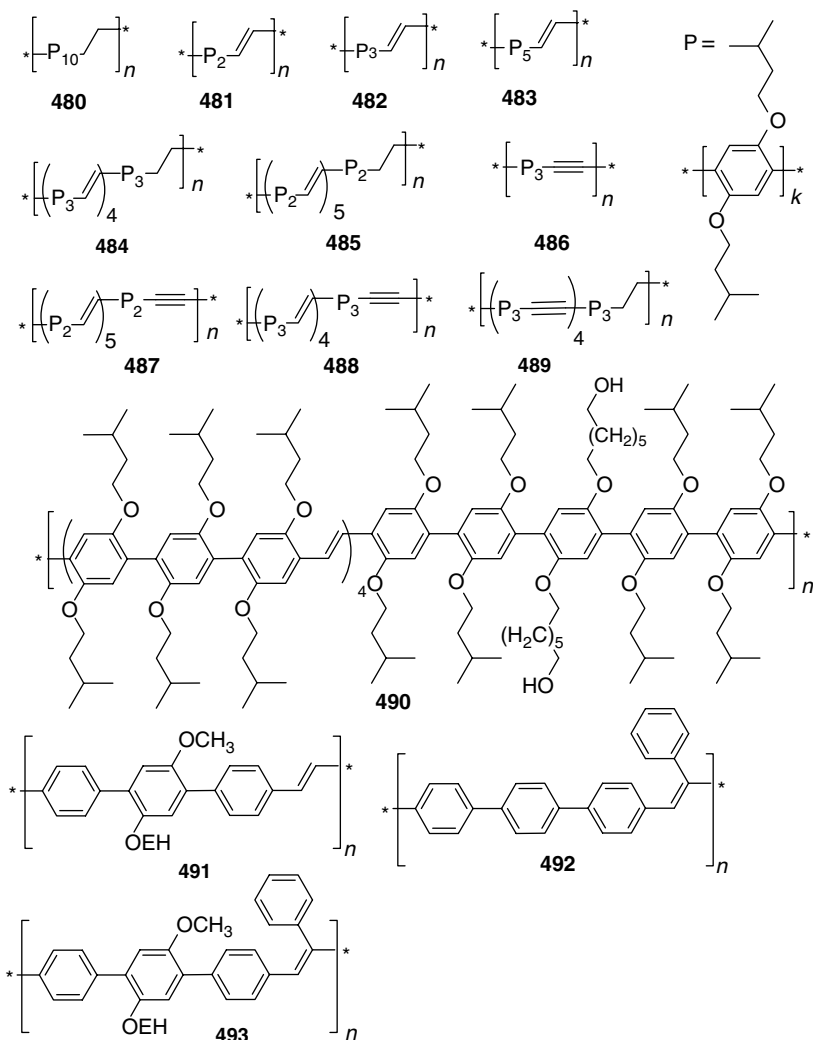


Chart 2.116

quinquephenylene blocks are separated by dihexylfluorene units (Scheme 2.72). Based on the absence of any metal catalyst or initiator in the synthesis, the authors claim this method to be a way to intrinsically high-purity LEPs. However, similar to fluorene homopolymers, the emission of **494** in the solid state suffers from a defect-dependent (see Section 2.3) “green band” at ~ 530 nm that became more pronounced in the EL spectra (the main peak is at ~ 450 – 470 nm).

Scherf and coworkers [594] reported copolymers **495a,b** containing unsubstituted PPP blocks separated by long-chain-substituted aliphatic blocks (Chart 2.117). Compound **495a** showed a liquid crystalline behavior. The PL emission maxima can be tuned by changing the length of the oligophenylene block (396 nm for **495a** and 429 nm for **495b**). A low-efficiency ($\Phi_{\text{EL}}^{\text{ex}} = 0.05\%$) PLED was fabricated by blending a very small amount of **495a** into a PVK matrix (ITO/PVK:**495** (0.045%)/Al).

Later, Kallitsis and coworkers reported similar PPP copolymers, with oligophenylene blocks separated by nonconjugated aliphatic chains. Copolymers **496** [595], **497** and **498** [596] contained the oligophenylene blocks in a main chain or as pendant substituents,

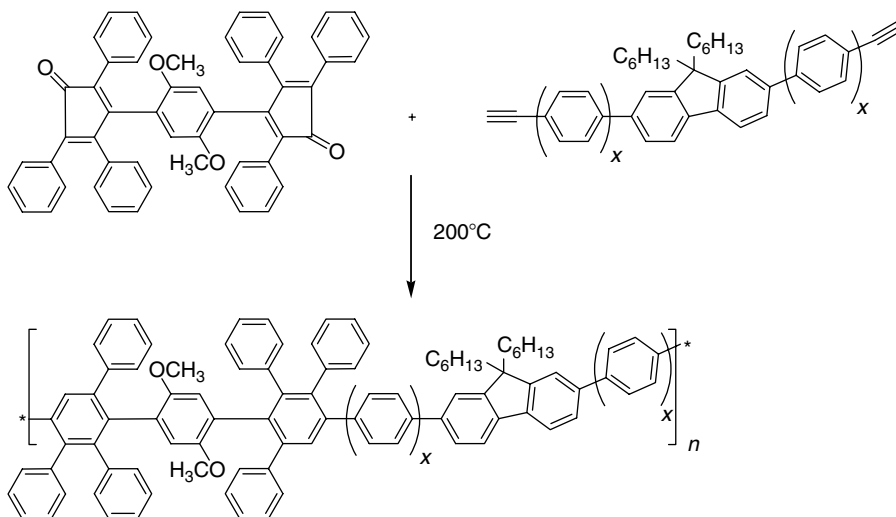
TABLE 2.9
Tuning the Device Performance (EL Maxima, Turn-On Field, and Internal QE) in PPP Copolymers

Polymer	Monolayer (ITO/pol/Ca)			Bilayer (ITO/PVK/pol/Ca)			Triple Layer (ITO/PVK/pol/PBD ^a /Ca)			Monolayer (ITO/pol/Al)		
	λ_{max} (nm)	Onset (MV/cm)	Eff (%)	λ_{max} (nm)	Onset (MV/cm)	Eff (%)	λ_{max} (nm)	Onset (MV/cm)	Eff (%)	λ_{max} (nm)	Onset (MV/cm)	Eff (%)
PPP	450	3.2	0.01		1.3	0.16	423	0.44	0.6		1.5	0.01
P3V		0.94	0.04		0.82	0.10	464	0.83	0.4			
P3/5V		1.2	0.24		0.44	0.13	459	0.69	4.0		2.4	0.02
P2V	483	1.3	0.06				486	0.50	2.0 ^b	482	1.7	0.02
P3A		1.0	0.3		0.5	0.2	650					
P10E	452 (400)	1.4	0.1	450	1.5	0.09	450	0.70	1.0	450	2.1	0.10
P3VE				464	0.75	0.15	463	0.54	1.4			0.12

^a25% in PMMA matrix.
^bNo PVK layer.

PPP, 471; P3V, 482; P3/5V, 490; P2V, 481; P3A, 486; P10E, 480; and P3VE, 484.

Source: From Remmers, M., Neher, D., Grüner, J., Friend, R.H., Gelinck, G.H., Warman, M., Quattrocchi, C., dos Santos, D.A., and Brédas, J.-L., *Macromolecules*, 29, 7432, 1996. With permission.



494a, $x = 0$, Abs: 330 nm, PL: 476 nm, EL: 430, 530 nm

494b, $x = 1$, Abs: 340 nm, PL: 455 nm, EL: 480, 540 nm

SCHEME 2.72 Synthesis of oligophenylene-fluorene copolymers via Diels-Alder cyclization. (From Park, S.J., Jung, S.-H., Kim, J.M., and Cho, H.-N., *Mater. Sci. Eng. C*, 24, 99, 2004.)

respectively. Elongation of the oligophenylene block from terphenylene (**497**, **498a**) to quinquenylphenylene (**498b**) resulted in a small but observable red shift of PL maxima, from ~ 390 to 407 nm. A somewhat longer wavelength emission was demonstrated by polymers **496a,b**,

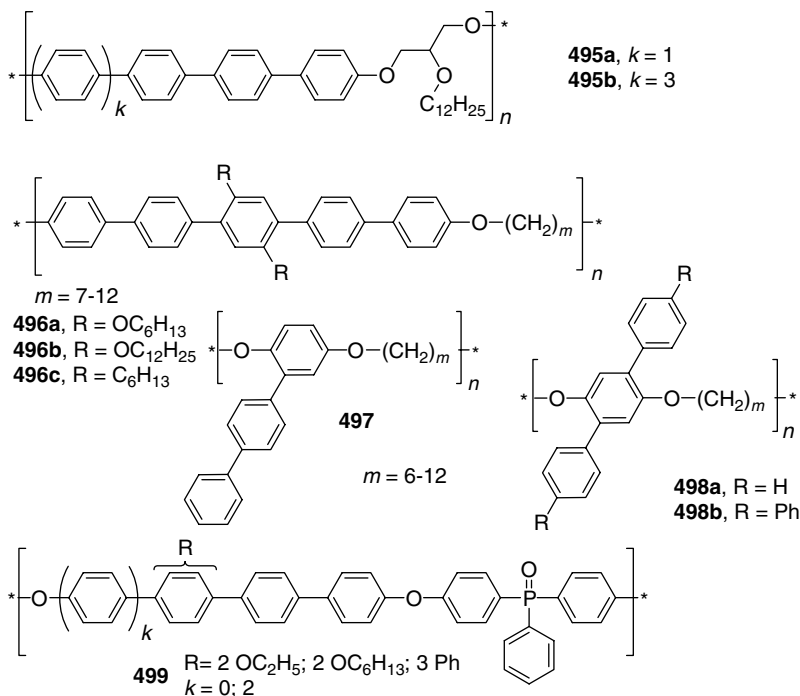


Chart 2.117

having quinquephenylene blocks in the polymer chain but introduction of alkyl groups to the oligophenylene block (**496c**) results in an expected emission blue shift to 372 nm, due to the above-mentioned steric factor. Some related blue-emitting quinquephenylene block copolymers **499** with triphenylphosphine oxide units were reported to have a very high T_g (270°C), but their luminescence efficiency was not investigated in detail [597].

Several blue luminescent PPP-type polymers containing naphthalene and anthracene moieties were synthesized by Suzuki polymerization (**500**, **501** [598]) as well as by a soluble precursor route (**502**, **503** [599]) (Chart 2.118). The anthracene-2,6-diyl polymers **502**, **503** showed the longest wavelength emission (green-yellow), but no data on the EL performance was reported. Later, Jen et al. [600] reported a very efficient PLED based on polynaphthalene **504**. An orthogonal 1,1'-binaphthyl connection confines the conjugation within the 1,1'-binaphthyl-6,6'-diyl unit, enlarging the band gap of the polymer (3.33 eV) and shifting the fluorescence band into the blue. The PL spectrum of **504** is characterized by emission peaks at 390 and 410 nm and a broad shoulder at 500–600 nm. Only the latter is observed in the EL spectrum ($\lambda_{EL} \sim 540$ nm) attributed to an excimer emission. Alternatively, the higher wavelength emission could be due to planarization of the normally twisted 1,1'-binaphthyl unit. A device ITO/**504**/ETL/Al (ETL — perfluorinated copper phthalocyanine) showed $\Phi_{EL}^{ex} = 2\%$ (4.9 lm/W) and a maximum brightness of 9400 cd/m², although the turn-on voltage was rather high (15 V for single-layer device and 20 V for double layer with ETL). Anthracene-containing block copolymers **505** [601] and **506** [602] have been prepared as highly fluorescent blue-emitting materials. The luminous efficiency of 0.4 cd/A was reported for the device ITO/PEDOT/**506b**/Mg:Ag [602].

Other light-emitting polycyclic aromatic hydrocarbons (PAH) have also been introduced as pendant groups in nonconjugated polymers, delivering amorphous EL materials. Thus, blue EL was recently reported from perylene-containing poly(methylacrylamide) **507** [603]. The PLED fabricated from **507** emitted blue light with $\lambda_{EL} = 478$ –491 nm (depending on the polymer ratios) and showed a moderate maximum brightness of 500 cd/m² (at 15 V) but rather low $\Phi_{EL}^{ex} \sim 0.01\%$. A higher efficiency ($\Phi_{EL}^{ex} = 0.34\%$) PLED device was fabricated with nonconjugated polymer **508** containing dialkoxy-substituted anthracene pendant moieties [604] (Chart 2.119).

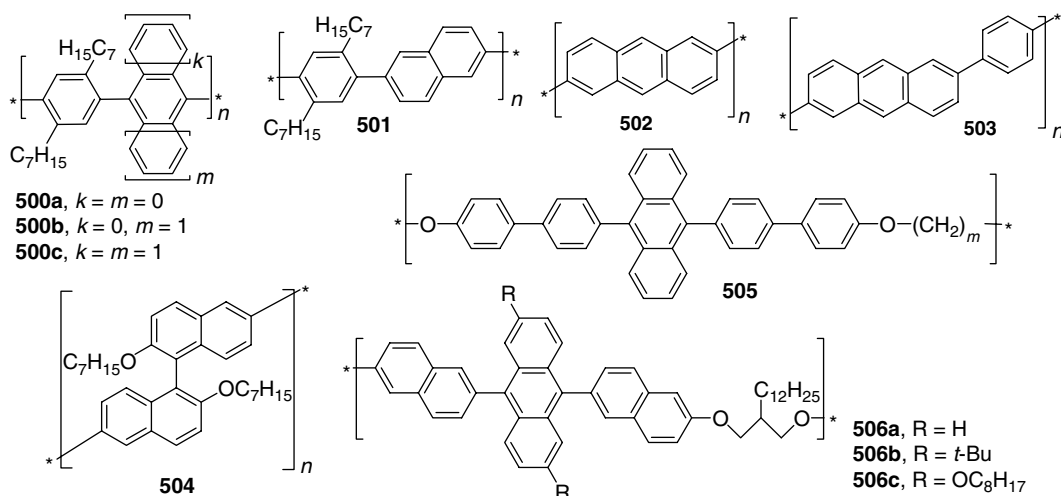


Chart 2.118

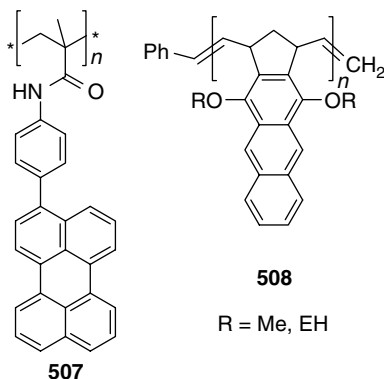


Chart 2.119

Generally, the fluorescence wavelength and quantum yield of PPP polymers are very sensitive to the dihedral angle between the phenylene units in the chain. As the energy barrier of this rotation is low, the PL (and EL) maxima depend on the film fabrication conditions. This ambiguity can be eliminated by designing the polymer, where the phenylene rings are fixed at a certain angle. Prominent examples of such systems, where the phenylene units are bound in fully planar pairs are the PF materials discussed above. In 1995, Müllen and coworkers [605] reported poly(tetrahydropyrene) **509** (Chart 2.120). The six-member unsaturated cyclic bridges fix the biphenylene pairs at a dihedral angle of $15\text{--}20^\circ$, which is higher than that in PFs ($\sim 0^\circ$), but somewhat lower than in other PPP (23° for unsubstituted **471**). In contrast to PPP, the ethylene bridge offers an opportunity to introduce solubilizing substituents into polymer **509** without affecting the dihedral angle and, thus, the emission properties could remain constant ($\lambda_{\text{PL}} = 425\text{ nm}$ in solution, 457 nm in films). In this line, the same group later reported a poly(indenofluorene) **510** with three phenylene units under planarization ($\lambda_{\text{PL}} = 432\text{ nm}$) [606]. This indenofluorene unit was also exploited in the Yamamoto synthesis of random indenofluorene–anthracene copolymer **511**, which emitted a deep-blue color ($\lambda_{\text{PL}} = 435\text{ nm}$; CIE: $x = 0.21$, $y = 0.23$) and demonstrated significantly higher color stability (in solid-state PL and EL experiments) compared to homopolymer **510** [607].

As the next step in this way, Müllen and coworkers [608] have reported PPP-type polymers **512**, containing planar pentaphenylene blocks. As expected, the emission maximum ($\lambda_{\text{PL}} = 445\text{ nm}$) of **512** was found between those of indenofluorene **510** ($432\text{--}434\text{ nm}$) and completely planar ladder-type PPP (450 nm) (see Section 2.5.2) [608]. Single-layer PLEDs ITO/PEDOT/**512b**/Ca/Al showed stable pure-blue emission with brightness in excess of 200 cd/m^2 (at 7 V) (Chart 2.121).

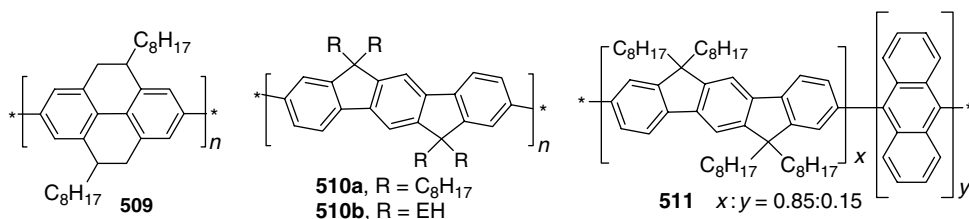


Chart 2.120

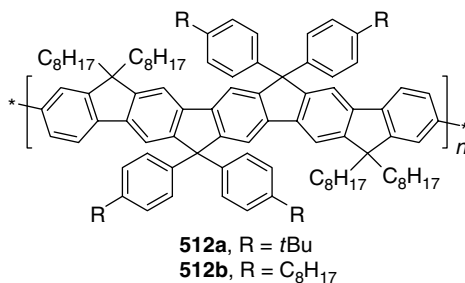


Chart 2.121

2.5.2 LADDER-TYPE POLY-*p*-PHENYLENES

An ultimate correction of the intrachain dihedral angle was achieved in LPPP, first synthesized by Scherf and Müllen (**513**, **514**) [609] (Chart 2.122). The synthesis of these and other types of conjugated ladder-type polymers was reviewed by Scherf and Müllen [610] in 1992, and more recently, by Scherf [611]. Due to planarization of the backbone, the band gap of LPPP is decreased to 2.6 eV, and the solution emission maximum is shifted to ~450 nm. The first LPPP-based EL device was reported by Grem and Leising [583] for polymer **513b** using Al, Ca, and In anodes and ITO as a cathode. The EL spectra confirmed the tendency of the LPPP to aggregate in the solid state, which resulted in yellow-emission color. Considering that blue-light EL was one of the objectives for exploration of PPP-type materials, this tendency of a red shift of the EL maximum stands as a major obstacle. The early studies claimed an excimer formation (rather than ground state aggregates) as an origin of the low-energy emission [612]. On the other hand, in the light of recent findings that ketone (fluorenone) defect quenching is responsible for the red shift of the emission in PF polymers (see

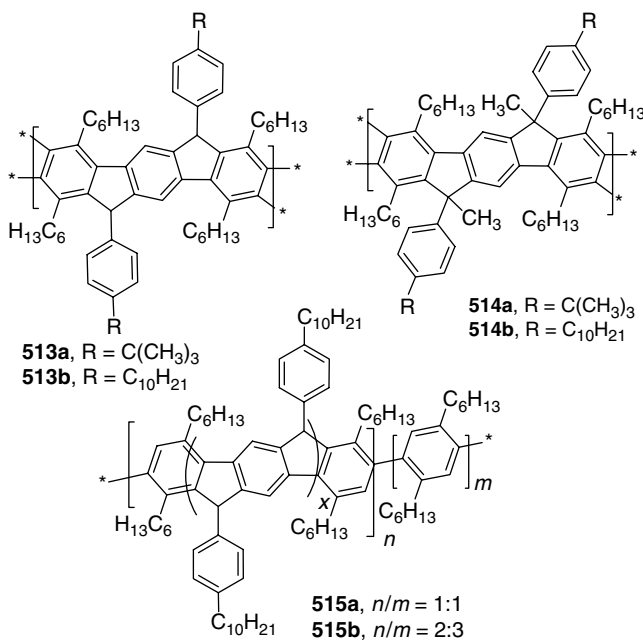


Chart 2.122

also Section 2.3) [293,294], the same mechanism of blue-emission quenching can be anticipated for LPPP materials [294,613]. This is particularly true for polymer **513a** because the hydrogen-terminated methylene bridge in this compound should be more sensitive to oxidation. In fact, it was shown that replacing the hydrogen atom in the methylene bridge with CH_3 reduces the luminescence quenching in the solid state (cf. **513b**: $\Phi_{\text{PL}} = 72\%$ (in solution) and 10% (in films); **514b**: $\Phi_{\text{PL}} = 84\%$ (in solution) and 24% (in films) [612]; Φ_{PL} as high as 40% for **514b** in films was claimed later [611]). The long-wavelength emission in the PL and EL spectra of pure **514b** in films, although not completely eliminated, was dramatically suppressed compared to **513b** [614,618]. The problem of low-energy emission in ladder-type PPP was the subject of recent studies by UV-vis and IR spectroscopic annealing experiments, complemented with quantum chemical calculations. Three types of oxidative defects (ketonic, phenolate, and phenol defects) have been discussed as responsible for the low-energy emission [613].

Whereas the initial measurements of the freshly fabricated PLED ITO/**514b**/Al showed $\Phi_{\text{EL}}^{\text{ex}} = 0.1\%$, maturing the device by passing 1 mA current increases $\Phi_{\text{EL}}^{\text{ex}}$ up to 4% (at 1 μA current). The PLED emitted blue-green light (CIE: $x = 0.23$, $y = 0.33$ [522]) with a turn-on voltage of ~ 10 V and a maximum brightness of 2000 cd/m^2 . This record value QE of 4% (as well as typical values of 1.5–2% [522]) for a simple single-layer PLED using Al cathode is really outstanding and attracted much attention to this class of LEPs. Other related applications such as polymer lasers [616,617], photovoltaics, and semiconductors have been also demonstrated for polymers **514** [611]. Recently, the first nanosphere-based PLED was fabricated by spin coating a water emulsion of **514b** (stabilized with poly(styrene sulfonate) (PSS)) on ITO/PEDOT anode [618]. The device emitted blue-green light with an EL efficiency of 0.5 cd/A (with Al cathode), which compares favorably to the efficiency obtained using traditional organic solution deposition technique (0.3 cd/A in the same device structure).

An efficient white-emitting PLED was fabricated by blending LPPP **514b** with phenylene ethynylene-pyrene copolymer (**525**, see below) [619]. Blends of blue-emitting **514b**, with a very small amount of red-emitting **525**, demonstrated efficient energy transfer, emitting rather pure white light (CIE: $x = 0.31$, $y = 0.33$) at all driving potentials. The $\Phi_{\text{EL}}^{\text{ex}}$ as high as 1.2% (the highest for a white PLED at that time) was reported for the device ITO/**514b:525**:PMMA/Al. An efficient yellow-emitting PLED was fabricated with **514b** by blending in small amounts (1%) of PT **396** [521,522]. The precise emission color of this device can be tuned by adjusting the amount of the PT component and $\Phi_{\text{EL}}^{\text{ex}}$ as high as 4.2% was achieved. The PLED fabricated under the same conditions with neat **514b** showed a QE of 2%.

It is noteworthy that a lower QE was reported for **514b** using a Ca cathode [67]. A $\Phi_{\text{EL}}^{\text{ex}}$ of ITO/**514b**/Ca was only 0.4%, although it can be improved to 1.3% by modifying the ITO anode with PANI or SiO_2 nanoparticle layer. For the latter, a very high brightness of over $40,000 \text{ cd/m}^2$ was demonstrated.

As mentioned above, in spite of the origin of the long-wavelength emission in PF and related materials due to ketone defects, aggregation is responsible for the emission shift in the solid state. This is because strong inter- and intrachain interactions allow an efficient quenching of the excitons in the entire material by a relatively few defect sites. To minimize the formation of the aggregates as observed in fully planar LPPP segmented so-called stepladder copolymers **515**, where the completely flat LPPP blocks are separated by distorted PPP segments has been designed [620,621]. Indeed, whereas the homopolymer **513b** reveals a dramatic red shift of the emission when going from a solution to a film, the emission of segmented copolymer **515** stays almost unaltered (Figure 2.33). Sandwiching **515b** between ITO and Al electrodes affords a pure blue-light emitting PLED with an average QE of 0.2% [620].

A significant suppression of the yellow emission band of LPPP was also achieved by dilution in PVK matrix, resulting in 2–3 times increase in EL efficiency, compared to the device prepared with neat LPPP (ITO/polymer/Al) [622].

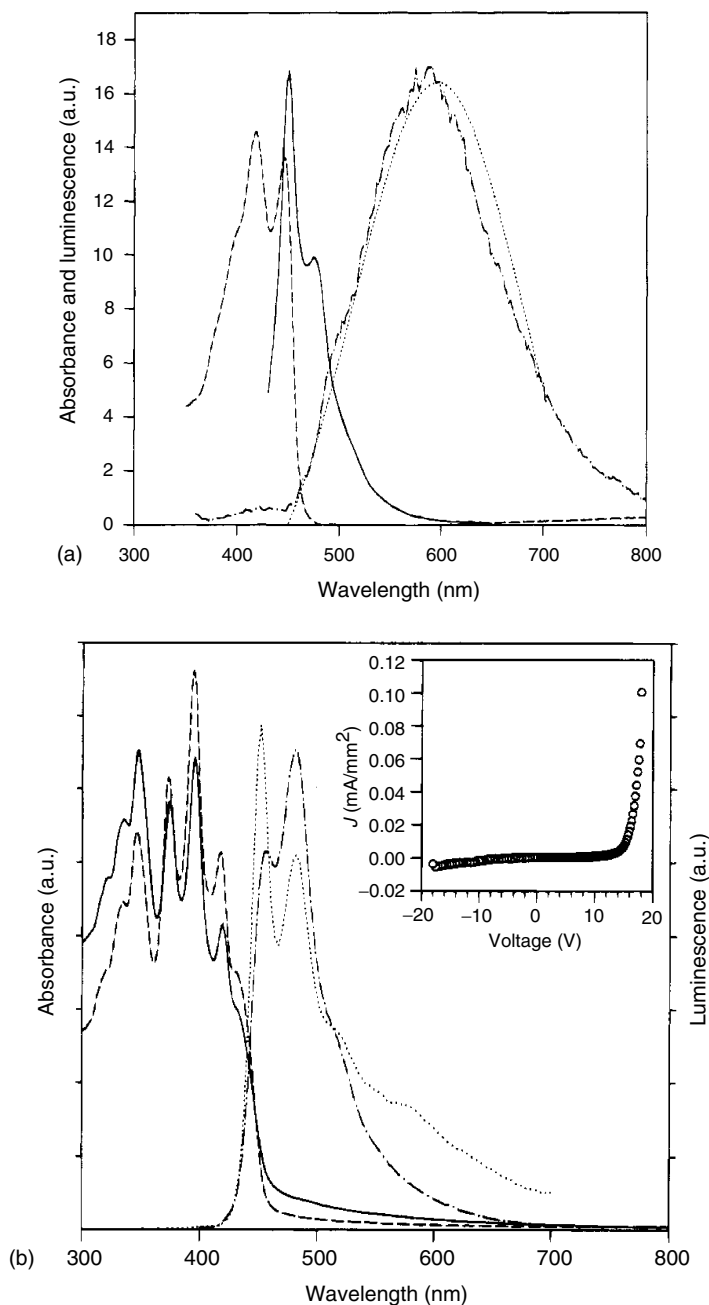


FIGURE 2.33 Top: Absorption (dashed line), solution PL (solid line), PL in films (dotted–dashed line), and EL (dotted line) spectra for **513b**. Bottom: Absorption spectra of **515a** (dashed line), **515b** (solid line), PL (dotted line), and EL (dotted–dashed line) spectra of **515b**. Inset: I–V characteristic of ITO/**515b**/Al device. (From Grem, G., Paar, C., Stampfl, J., Leising, G., Huber, J., and Scherf, U., *Chem. Mater.*, 7, 2, 1995. With permission.)

2.5.3 POLY(PHENYLENE ETHYNYLENE)S

After the first successful synthesis of a soluble poly(phenylene ethynylene) (PPE) derivative by Giesa and coworkers and elaboration of elegant methods for preparation of different derivatives of this polymer, PPE materials have played important roles in many electronic applications, from sensors and molecular wires to polarized displays [623–625]. The first EL from PPE was reported in 1993 by Swanson et al. [626] for dialkoxy-PPE **516** sandwiched between ITO and Ca electrodes [626] (Chart 2.123). The polymer **516** has a low band gap of ~ 2.25 eV and emits orange-red light with $\lambda_{\text{PL}} \sim 585$ nm and $\lambda_{\text{EL}} \sim 605$ nm (with a broad tail at ~ 800 nm). A very detailed study of a series of dialkoxy-PPE polymers and copolymers was conducted by Wrighton and coworkers [627–629]. A PLQY of up to 86 and 36% was demonstrated for polymers **517** in solution and in films, respectively [629]. It was demonstrated that the polymer band gap and the emission maxima are shifted from the solution ($E_{\text{g}} \sim 2.6$ eV, $\lambda_{\text{PL}} = 473$ nm) to the solid state ($E_{\text{g}} \sim 2.25$ – 2.45 eV, $\lambda_{\text{PL}} \sim 530$ – 590 nm). These shifts as well as the observed decrease in the PLQY in films are related to the degree of crystalline order and can be controlled by the substitution pattern. Some PLED devices ITO/polymer/Al were reported for copolymers **517** ($R = \text{C}_{18}\text{H}_{37}$, $R' = \text{EH}$) [630]. The EL performance of the device with neat polymer was rather low ($\Phi_{\text{EL}}^{\text{ex}} = 0.004\%$, maximum brightness 4 cd/m^2), but it can be essentially improved by blending with poly-TPD hole-transporting material ($\Phi_{\text{EL}}^{\text{ex}} = 0.02\%$, maximum brightness 146 cd/m^2).

Wudl and coworkers [631] reported epicholestanoxy PPE **516c**, where the steroid substituents were supposed to suppress crystallization in the solid state and, therefore, to maximize the PL efficiency. PPEs **518**, synthesized by Swager's group [632,633], contained triptycene units, which acted as “insulating cover,” providing a good separation between the PPE chains. Consequently, the PL spectra in solution and in films were almost identical ($\lambda_{\text{PL}} = 455$ nm). Due to the nanoporous structure formed by the triptycene molecular shape, polymers **518** act as efficient sensors for trinitrotoluene (TNT), an explosive. The latter is based on fluorescence quenching by the nitroaromatic electron-accepting TNT molecules [632]. Targeting possible biosensor applications, Schanze and coworkers [634] reported water-soluble PPE polyelectrolyte **519**, similar to the PPV-type material **148**. Aggregation of **519** was observed on changing the solvent from MeOH to water. Significant red shift and broadening of the emission spectrum occurred. Swager's group [635] reported a cyclophane-type PPE **520**, for which an interesting aggregation-related phenomenon was observed. While the PL of **520** in solution and in Langmuir–Blodgett films has a narrow emission band ($\lambda_{\text{PL}} = 470$ – 480 nm, band half-width ~ 30 nm) and very low quantum yield (5–6%); aggregation of the polymer in spin-coated films increases the quantum yield to 21%; and the aggregate emission is seen as a very wide band ($\lambda_{\text{PL}} = 520$ nm, band half-width ~ 140 nm), contrary to expectation.

An interesting example of extremely long monodisperse phenylene ethynylene “wires” **521** insulated (wrapped) by dendritic substituents was recently reported by Jiang and coworkers [636]. For the oligomers with the first-generation dendrimer substituents (G_1), the PLQY decreased with increasing “wire” length (n), from 80–90% to below 60%, whereas steadily high (above 80%) Φ_{PL} was observed for all the oligomers containing bulkier G_3 substituents. Furthermore, in contrast to the G_1 -substituted homologs, increasing the concentration of **521-G₃** (in THF solution) does not decrease the fluorescence yield.

The EL of poly(*o*-phenylene ethynylene) **522** was reported by Onoda and coworkers [637]. As expected, the optical band gap of **522** (3.1 eV) is larger than that of *para*-connected polymer **516**, making the former a blue-purple-emitting material ($\lambda_{\text{PL}} \sim 400$). Interestingly, **522** possess a low LUMO energy and can be n-doped electrochemically (partially reversible wave at $E_{\text{pc}} = -1.2$ V vs. Ag/Ag^+ (~ -0.9 V vs. SCE)). The PLED ITO/**522**/Al emits blue light with two peaks at $\lambda_{\text{EL}} \sim 410$ and 430 nm.

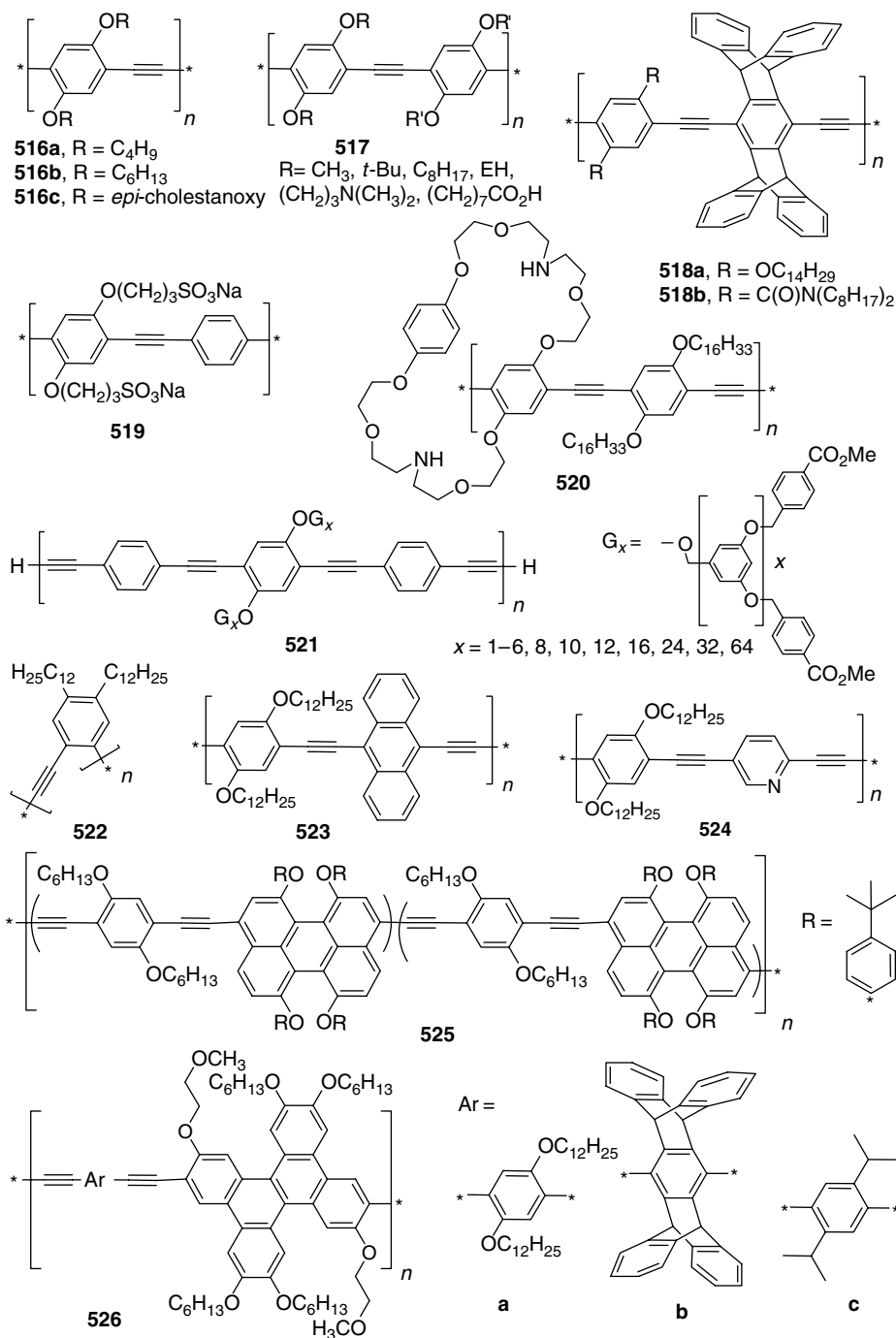


Chart 2.123

Just as with other conjugated polymers, the emission color of PPE can be tuned by introducing different conjugated fragments in the polymer chain (copolymers **523** and **524**) [627,638]. Thus, red-orange EL ($\lambda_{\text{EL}} \sim 590$ nm and a shoulder at 530 nm) was reported for the anthracene-based polymer **523** (in PLED ITO/**523**/Al), whereas

introducing a pyridine moiety into the polymer chain results in a significant blue shift of the emission, and a blue-green-emitting ($\lambda_{\text{EL}} \sim 480$ nm) PLED was fabricated with this material [638].

Higher polycyclic aromatic units such as perylene (**525** [639]) and dibenzocrysene moieties (**526a–c** [640]) were introduced into the PPE backbone. The former are red-emitting materials with $\lambda_{\text{PL}} = 580\text{--}590$ nm, and were used to create a white-emitting PLED with LPPP [619]. Significantly higher energy, blue-color emission was observed from the crysene derivatives ($\lambda_{\text{PL}} = 474\text{--}480$, $\Phi_{\text{PL}} = 25\text{--}34\%$) [640]. The latter were employed as fluorescent sensor materials and demonstrated better sensitivity than other similar iptycene-containing LEPs (e.g., **518**) [640].

2.5.4 SUBSTITUTED POLYACETYLENES

Polyacetylene (PA), the first and the most conducting polymer, was traditionally regarded as a nonemissive material. Although it is certainly true for the unsubstituted PA in the doped and neutral states, strong fluorescence has recently been demonstrated from disubstituted (diphenyl and phenylalkyl) PAs [641–643]. Kobayashi and coworkers [642] fabricated red, green, and blue EL devices by sandwiching monophenyl-PA (**527**), diphenyl-PA (**528**), and phenylalkyl-PA (**529**), respectively, between ITO and Mg:Al electrodes (Chart 2.124). As expected from a low PLQY ($<0.1\%$) of monophenyl-PA, efficiency of the red-emitting PLED based on polymer **527** was negligibly low ($\sim 10^{-4}\%$). Better results were demonstrated by green- (**528**) and blue-emitting (**529**) disubstituted PAs ($\Phi_{\text{EL}}^{\text{ex}} \sim 0.01\%$), in accordance with their high PL efficiency ($>60\%$). The structural variations included biphenyl- and carbazole-PAs **530** [644,648] and **531** [646]. The former is UV- and violet-emitting material ($\lambda_{\text{PL}} = 350\text{--}370$ nm), where the emitting sites (biphenyl chromophores) are separated from the PA backbone by a long alkyl chain. In contrast, strong green fluorescence ($\lambda_{\text{PL}} = 525$ nm) of the carbazole **531** cannot be attributed to the individual carbazolyl substituents. A remarkably efficient PLED ($\Phi_{\text{EL}}^{\text{ex}} = 2\%$, maximum brightness 2700 cd/m^2) was fabricated from **531** as a bilayer device ITO/**531**/Alq₃/Mg/Al, where Alq₃ acts as an ETL and the observed EL is exclusively due to PA [646].

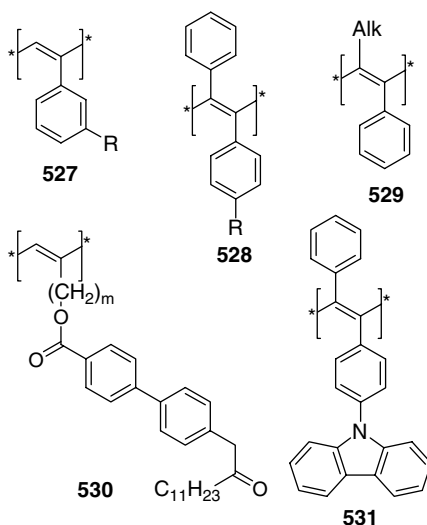


Chart 2.124

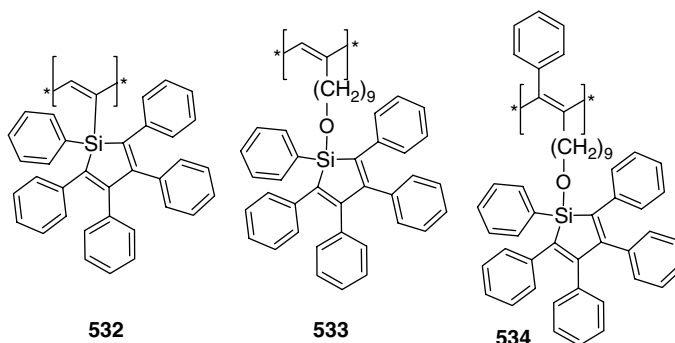


Chart 2.125

Inspired by very high EL efficiency of OLEDs with molecular siloles, Tang and coworkers [647] reported an interesting series of silole-substituted PAs **532–534** (Chart 2.125). Whereas the fluorescence of all three polymers in solution was very low ($\Phi_{\text{PL}} < 0.5\%$), a significant increase of the PLQY (20–50 times) was observed in the solid state of **533** and **534**. The phenomenon was observed earlier in molecular siloles, as well as in cyclophane-PPE **520**. While an efficient energy transfer from silole to the PA backbone renders **532**, a red-emitting material ($\lambda_{\text{EL}} = 664$ nm), the longer backbone-to-silole bridged **533** and **534** exhibited blue-green fluorescence ($\lambda_{\text{EL}} = 512$ nm). The EL efficiency of single-layer devices with all three polymers was similar ($\sim 0.013\%$), in spite of different PL properties, suggesting that the device performance was limited by charge-transport processes. Indeed, a multilayer device ITO/**534**:(PVK **535**)/BCP/Alq₃/Al emitted blue light ($\lambda_{\text{EL}} = 496$ nm) with a relatively high current and quantum efficiencies (1.45 cd/A and 0.55%, respectively) and a maximum brightness of 1118 cd/m² [647].

2.5.5 CARBAZOLE-CONTAINING POLYMERS

A high hole mobility and excellent photoconductive properties of carbazole-containing polymers, such as PVK (**535**) and poly(*N*-epoxypropylcarbazole) (PEPK, **536**), put them among the most studied polymers for optoelectronic application (Chart 2.126). They have been commercialized in a number of devices and processes (photocopiers, laser printers, holographic security stamps, etc.) [571]. The first application of carbazole-containing polymer (PVK, **535**) in an EL device was described in 1983 by Partridge [3], although the reported blue EL was due to molecular fluorescent dyes, incorporated into a PVK matrix. In 1994, Karasz and coworkers [202] reported blue EL from pure PVK material (devices ITO/PVK/Ca and ITO/PVK/Al) as well as from a mixture of PVK with PPV block

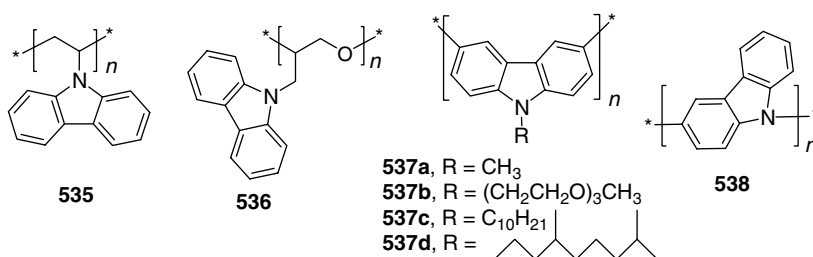


Chart 2.126

copolymer **171b**. Using PBD/PMMA blend as an additional ETL, a brightness of 200 cd/m² was achieved. Generally, the EL properties of nonconjugated carbazoles are quite poor. On the other hand, as an excellent hole-transporting material, PVK has been extensively used as an HTL [102,217,364,384–386] or as a hole-transporting material in blends with other conjugated EL materials in PLEDs [406,517,540]. Chapter 4 of this book gives many examples of PVK as a host material for high-efficiency phosphorescent PLEDs, using organo-metallic phosphorescent dopants.

Several carbazole homopolymers (**537a** [648], **537b** [649], **537c,d** [650], and **538** [651]) have been synthesized as blue-fluorescent materials. The PL maximum of **537c** in solution is ~420 nm and it shifts to ~490 nm in films [650]. A blue-emitting single-layer LEC ($\lambda_{\text{EL}} \sim 440$ and 490 nm) with $\Phi_{\text{EL}}^{\text{ex}} = 0.02\%$ was reported for polymer **537b** [649]. Interestingly, mixing **537b** with polyquinoxaline (**585b**) results in emission of a new color corresponding to an energy difference between the LUMO of polyquinoxaline and the HOMO of polycarbazole. A significantly improved $\Phi_{\text{EL}}^{\text{ex}}$ of an LEC (1%) was demonstrated with this polymer blend material [649].

3,6-Carbazole–diacetylene copolymer **539** was used as a HTL in bilayer devices with macrocyclic carbazole oligomer **540**, which acted as an electron-transporting and light-emitting material [652] (Chart 2.127). Copolymer **539** itself is a blue-emitting material ($\lambda_{\text{PL}} = 400$ nm), whereas the oligomers **540** exhibit green fluorescence with $\lambda_{\text{PL}} = 520$ nm. Quite remarkably, the cyclooctamer **540** could be prepared in 45% yield by simple Knoevenagel coupling of carbazole-3,6-dicarbaldehyde with 3,6-*bis*-(cyanoacetoxymethyl)carbazole. The PLED fabricated as ITO/**539**/**540**/Al demonstrated $\Phi_{\text{EL}}^{\text{ex}} = 0.44\%$, although the device maximum brightness was rather low (60 cd/m²).

A series of carbazole-3,6-diyl polymers, including homopolymer **537c**, alternating carbazole–oxadiazole and carbazole–fluorene copolymers **541–545** and analogous random copolymers containing all three (carbazole, fluorene, and oxadiazole) units were prepared and

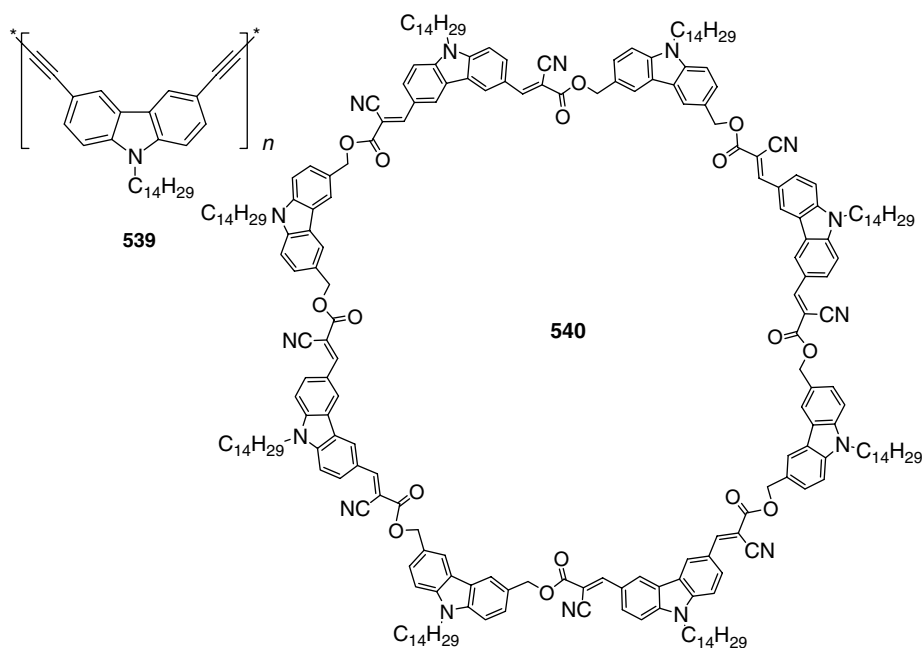


Chart 2.127

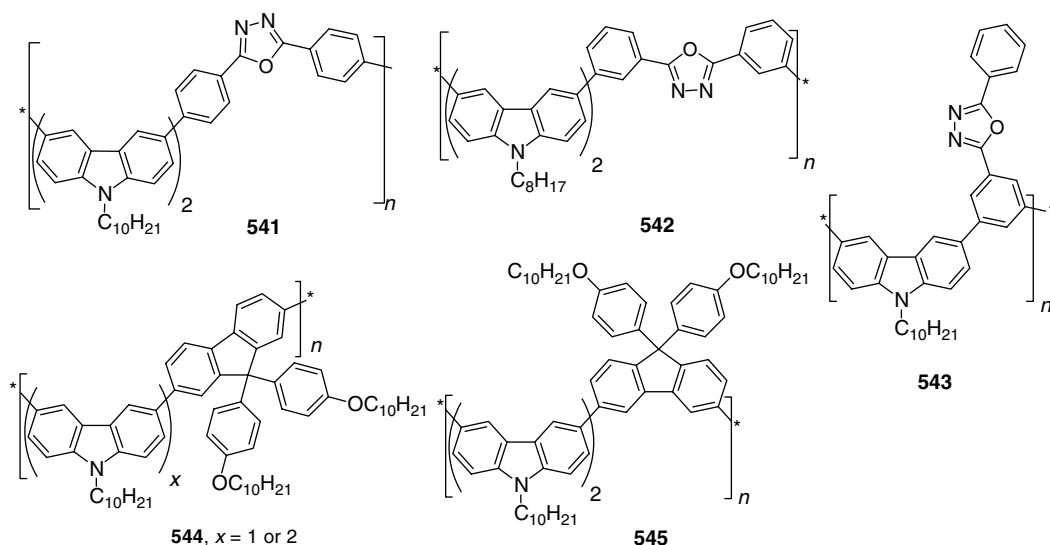


Chart 2.128

studied as host materials for electrophosphorescent LEDs [653] (Chart 2.128). In line with previous observations, the performance of carbazole-3,6-diyl polymers in PLED was quite low (0.2 cd/A for ITO/PEDOT/**537c**/Ba diode), but using a triplet emitter Ir-SC4 (Covion Organic Semiconductors GmbH), very high-efficiency green-phosphorescent PLEDs (up to 23 cd/A) were fabricated. It was shown that small structural variations such as substitution position in the fluorene unit allows control of the triplet energy without disturbing the HOMO–LUMO levels of the polymers.

Cao and coworkers [654,655] prepared random 3,6-carbazole–BT copolymers **546** and **547** by Suzuki coupling (Chart 2.129). PL and EL missions of the carbazole segment were completely quenched for copolymers with BT concentrations as low as 1%, showing an efficient energy transfer on the narrow band-gap BT sites. Copolymers **547** emitted a saturated red light (from 660 to 730 nm, depending on stoichiometry) with a luminance of 70–631 cd/m² and $\Phi_{\text{EL}}^{\text{ex}} = 0.55$ –1.48%. Also, a very high-efficiency red-emitting PLED ($\lambda_{\text{EL}} = 680$ nm; CIE: $x = 0.67$, $y = 0.33$) was fabricated by blending small amounts of **546** ($m:n = 4:1$) into MEH-PPV. The device ITO/PEDOT/MEH-PPV:**547** (240:1)/CsF/Al showed $\Phi_{\text{EL}}^{\text{ex}} = 3.8\%$ [72]. The emission of copolymers **546** was hypsochromically shifted to 570–620 nm and showed a lower $\Phi_{\text{EL}}^{\text{ex}} \sim 0.01$ –0.48%.

It is noteworthy that the polymer involving linking via positions 3 and 6 of the carbazole ring hinders the conjugation due to a “*meta-type*” connection. The poor conjugation might be responsible for low PLQY of polymers **537** (15% for **537b** in THF solution). On the other hand, functionalization of carbazole in positions 2 and 7 is a synthetically challenging task. In contrast

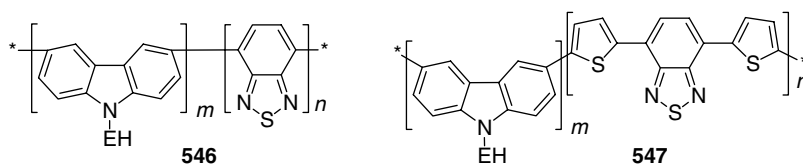
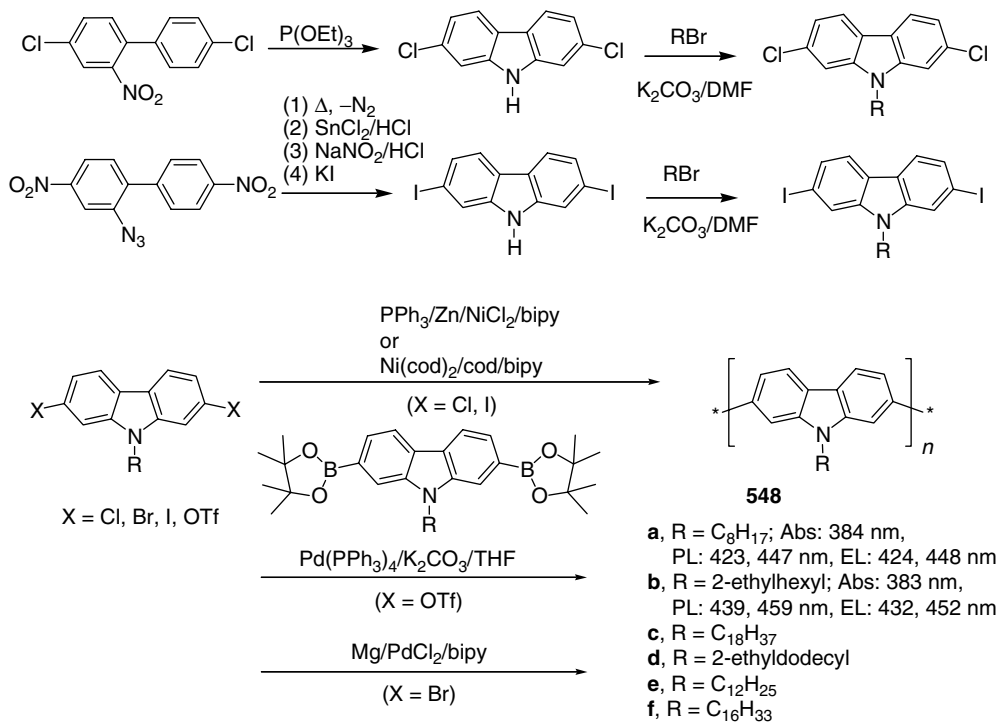


Chart 2.129

to fluorene, electrophilic halogenation of carbazole occurs exclusively at positions 3 and 6 (and then at 1 and 8) due to strong *para*- and *ortho*-directing effect of the nitrogen atom. To prepare fully conjugated polycarbazoles, Leclerc and coworkers synthesized 2,7-dihalogocarbazoles via reductive cyclization of 4,4'-dichloro-2-nitrobiphenyl (in refluxing triethylphosphite) or thermal decomposition of 4,4'-dinitro-2-azidobiphenyl (followed by multistep conversion of the nitrogroups into iodine substituents) (Scheme 2.73). The polymerization was performed by Yamamoto or Suzuki protocols to afford conjugated polymers **548a–c** [345,550,656]. Later, polycarbazoles **548b,d–f** were prepared by Pd-catalyzed cross-coupling of Grignard derivatives of 2,7-dibromocarbazoles [657]. In contrast to 3,6-linked polycarbazoles **537**, polymers **548** showed pure blue emission (λ_{PL} (CHCl_3) = 417–420 nm, λ_{PL} (film) = 439–442 nm) with high PLQY of 76–80% (in solution). For **548**, a blue-emitting PLED was fabricated but an initial test device showed a rather low performance (maximum brightness below 100 cd/m²) [346].

As demonstrated in previous sections, the carbazole unit was introduced as a pendant group or as a chain member in major classes of EL polymers such as PPVs (**95–105**, **141**, **177**, **190**) and PFs (**62**, **63**, **242–245**). A variety of 2,7-carbazole-derived polymers with different conjugated units, such as 2-alkoxy- and 2,5-dialkoxy-1,4-phenylene (**549**) and 1,1'-binaphthalene-6,6'-diyl (**550** [658]), 2,5-pyridine (**551**), 2,7-fluorene (**245** [345,346]), 2,5'-bithiophene (**554** [345]), 5,8-quinoxaline (**552**), quinquethiophene-*S,S*-dioxide (**450** [550]), 2,5-thiophene (**553**), 2,5-furan (**555**), and acetylene (**556** [659]) were reported by Leclerc and coworkers



SCHEME 2.73 Synthesis of 2,7-dihalogocarbazole monomers and their polymerization by Yamamoto and Suzuki protocols. (From Morin, J.-F. and Leclerc, M., *Macromolecules*, 34, 4680, 2001; Morin, J.-F. and Leclerc, M., *Macromolecules*, 35, 8413, 2002; Zotti, G., Schiavon, G., Zecchin, S., Morin, J.-F., and Leclerc, M., *Macromolecules*, 35, 2122, 2002; Iraqi, A. and Wataru, I., *Chem. Mater.*, 16, 442, 2004.)

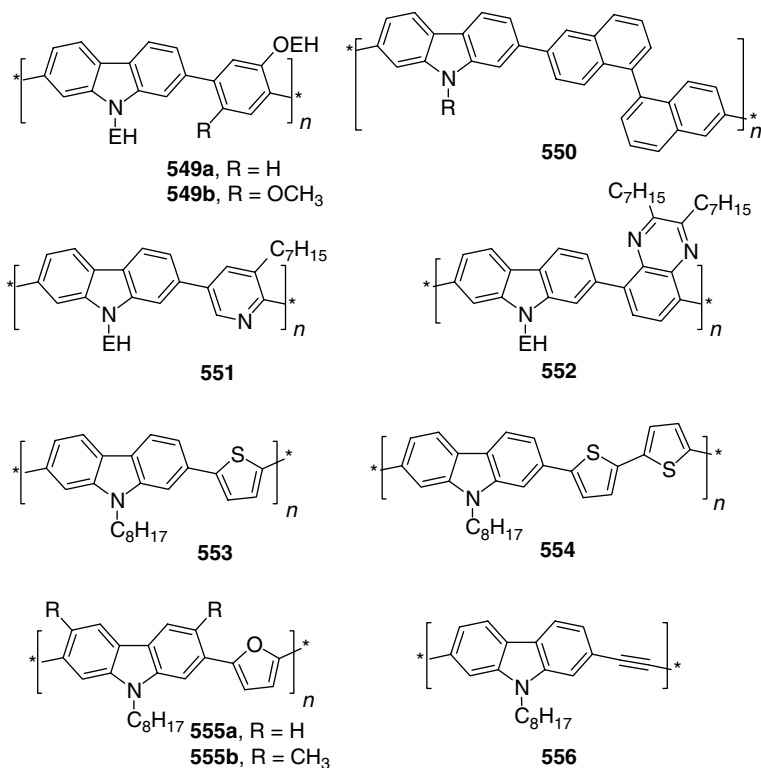
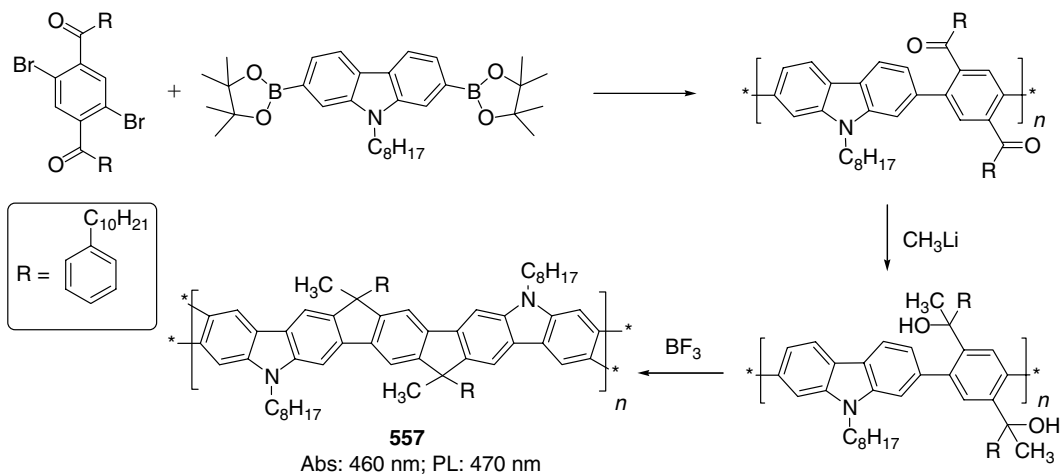


Chart 2.130

(Chart 2.130). Taking advantage of a wide range of electronic properties of the comonomers, an efficient tuning of the HOMO (approximately -5.0 to -5.5 eV) and LUMO (approximately -1.85 to -3.5 eV) energies, and emission color (spanning from blue to red, $\lambda_{\text{PL}} \sim 400$ to 700 nm) was achieved in this series.



SCHEME 2.74 Synthesis of ladder-type polycarbazole **557**. (From Patil, S.A., Scherf, U., and Kadaschuk, A., *Adv. Funct. Mater.*, 13, 609, 2003.)

An interesting hybrid carbazole–fluorene ladder polymer **557** was synthesized recently by Scherf and coworkers [660] via Suzuki coupling of carbazole diboronic ester with dibromodibenzoylbenzene followed by conversion of the ketone into a tertiary alcohol and Lewis-acid catalyzed cyclization (Scheme 2.74). Upon photoexcitation, **557** emits blue light ($\lambda_{\text{PL}} = 470$ nm) with very small Stokes shift (10 nm, 0.057 eV), expected from its rigid geometry. Photophysical studies suggest a nearly defect-free intrachain structure of this material, although practical applications of **557** in LEDs are still to be explored.

Very recently, Leclerc and coworkers [661] synthesized a series of 2,7-carbazolylene–vinylene copolymers **558–561** via Horner–Emmons reaction. Although all the copolymers are fluorescent in solution ($\lambda_{\text{PL}} \sim 460$ –505 nm, $\Phi_{\text{PL}} \sim 16$ –67%), only **559** retains its fluorescence in the solid state ($\lambda_{\text{PL}} = 656$, 701 nm). A device ITO/PEDOT/**559**/LiF/Al/Ag emitted orange-red light ($\lambda_{\text{EL}} = 640$ nm, CIE 1976 coordinates: $u' = 0.40$, $v' = 0.54$) with a low turn-on voltage of 3 V, an efficiency of 0.17 cd/A (at 5 V), and a maximum brightness of 245 cd/m² (at 10 V) (Chart 2.131).

2.5.6 POLY(PYRIDINE)S AND RELATED POLY(N-HETEROCYCLE)S

The first EL from polypyridine was reported by Epstein and coworkers [662] in 1995. The polymer **562**, prepared by Yamamoto Ni-mediated reductive coupling of 2,5-dibromopyridine [663] was soluble in formic acid (due to formation of a protonated form **563**) and could be spin coated on an ITO glass substrate for preparation of PLED (Chart 2.132). It had a rather high PL in the solid state ($37 \pm 3\%$ [664], $30 \pm 3\%$ [665]). The device ITO/**562**/Al emitted green light ($\lambda_{\text{EL}} \sim 500$ nm) at voltages above 8 V. Introduction of an additional HTL (PANI) reduced the turn-on voltage to 4 V [662]. Unfortunately, the efficiency of the device ITO/**562**/Al is very low ($\Phi_{\text{EL}}^{\text{ex}} \sim 0.001\%$ [664] to 0.002% [665]). Also, the issue of deprotonation of the pyridine units (which might occur during vacuum deposition of a second electrode) and the possible influence of residual protonated species has not been addressed.

EL pyridine–phenylene copolymers **564** [666] and **565** [667] have been synthesized and studied by Bryce and coworkers. Although a rather low $\Phi_{\text{EL}}^{\text{ex}} (<0.1\%)$ was reported for the devices, an interesting phenomenon was found for polymers **565**. When the PLED (ITO/PEDOT/**565**/Ca/Al) was fabricated using acidic solutions, a strong red shift in the EL band compared to that obtained with the neutral solution (from 510 to 575 nm) was observed. The authors explained this concept by planarization of the protonated polymer chain as a result of intramolecular hydrogen bonding $\text{N} \cdots \text{H} \cdots \text{O}$. Variation of pyridine linkage in copolymers **565**, **566**, and **567** affects the PL and EL emissions ($\lambda_{\text{EL}} = 444$, 432,

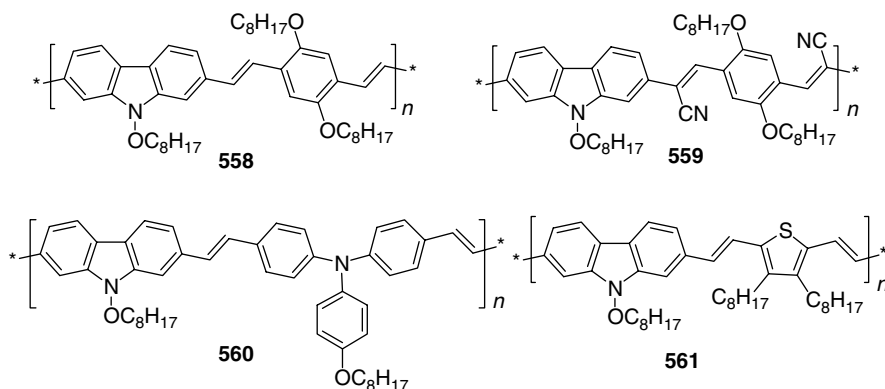


Chart 2.131

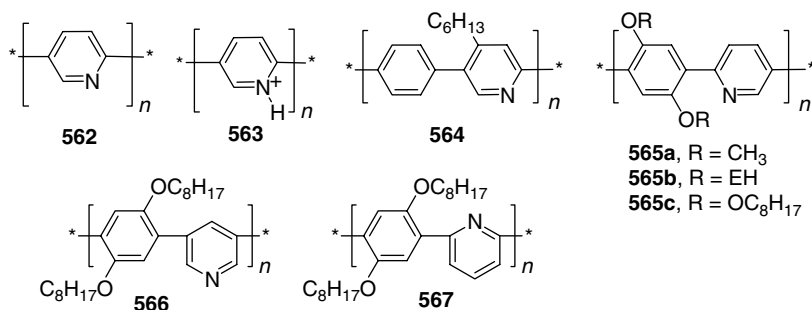


Chart 2.132

and 428 nm, respectively), although the details of the efficiency of LEDs based on these polymers have not been reported [668].

Due to the electronegative atom, polypyridines are good electron acceptors: from UPS and UV-vis absorption spectra, Yamamoto and coworkers [669] estimated $E_A = 3.5$ eV, $I_P = 6.3$ eV. Chen and coworkers [670] reported $E_A = 2.9$ eV, $I_P = 5.7$ eV based on electrochemical measurements. For the double-layer ITO/PPV/**562**/Al device, in which **562** acts as electron transport and hole-blocking layer, Chen and coworkers [670] reported a EL efficiency of 0.12 cd/A that is 17 times higher than for an single-layer PPV-based PLED. The improvement in Φ_{EL}^{ex} by a factor of 60 (from 0.004 to 0.25%) for this device configuration was demonstrated by Monkman and coworkers [665].

Several poly(*p*-pyridine vinylene)s (PPyV, **568**) have been reported as isoelectronic analogs of PPVs (see also PPyV-fluorenevinylene copolymer **310** [403]) (Chart 2.133) [671–673]. The neutral and the protonated (**569**) forms showed strong luminescence from excimeric states that contributed to the observed low PLQYs and red shift in the emission spectra from solution (from 470 to over 600 nm). A device fabricated as ITO/**568**/Al showed an $\Phi_{EL}^{ex} = 0.02\%$, which can be somewhat improved to 0.05% by introduction of PPV **1** as HTL [673]. An efficiency as high as 0.3% was reported for copolymer **570** on a bilayer PLED with a PANI-networked electrode [674]. Several studies of pyridine homo- and copolymers (**562**, **568**, **570**) as light-emitting materials for symmetrically configured ac light-emitting (SCALE) devices [675] and inverted LEDs [674] using high work-function electrodes (Au) have been performed.

Several light-emitting copolymers with pyrazines in the backbone are known. In 1996, a Japanese group reported fluorescent polyimide **571** [676] (Chart 2.134). An LED device based on a Langmuir–Blodgett film of **571** was fabricated as (ITO/**571**/Mg:Al) and showed orange-red emission ($\lambda_{EL} = 560$ nm) with a turn-on voltage of 7 V. Peng and Galvin [158] demonstrated orange emission from the PLED based on pyrazine-containing PPV **572** ($\Phi_{EL}^{ex} = 0.012\%$ and a turn-on voltage of 10 V for ITO/**572**/Al).

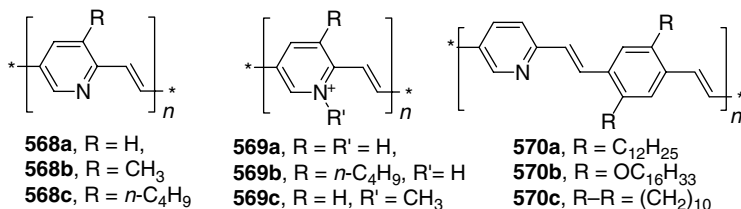


Chart 2.133

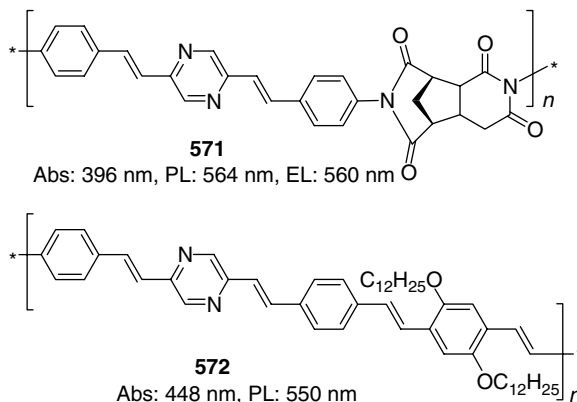


Chart 2.134

A solid study of PL and EL properties of a series of poly(quinoline) homopolymers **573–575** and quinoline and anthrazoline copolymers **576–578** and **467a–e** was reported by Jenekhe and coworkers [566,567,677–679] (Chart 2.135). Changing the substituent R' and a colink R, the emission color was tuned from blue to red ($\lambda_{\text{EL}} = 410\text{--}622\text{ nm}$) (Figure 2.34). The solid-state PLQY of these polymers was usually on the level of 10%, although a higher efficiency (20–30%) was observed for the *tert*-butyl-substituted polymers **574** and **578a** [677]. The PLED devices fabricated with **573–578** in ITO/HTL/polymer/Al configuration showed moderately high $\Phi_{\text{EL}}^{\text{ex}} \sim 0.1\text{--}1\%$, with values repeating the trend of PL efficiencies (the highest $\Phi_{\text{EL}}^{\text{ex}} = 0.92$ and 1.08% were due to polymers **574** and **578a**, respectively). As mentioned before, emissive polymers **467a–e** (Scheme 2.70) showed good electron transport properties and a weak green EL ($\Phi_{\text{EL}}^{\text{ex}} = 0.004\text{--}0.06\%$ in ITO/**467a–e**/Al). A large improvement in the performance of MEH-PPV-based PLEDs was achieved using polymers **467a–e** as the electron transport materials ($\Phi_{\text{EL}}^{\text{ex}}$ was up to 1.4% and brightness up to 2311 cd/m^2) [566,567]. Considering a relatively low EL turn-on voltage of 5–10 V, these polymers present a promising class of polyheterocyclic materials for LED displays.

Jen and coworkers [680,681] reported PLEDs based on variations of the above-mentioned 6,6'-bisquinoline copolymers (**579–582**), containing conjugated and nonconjugated linkers (Chart 2.136). For copolymers with nonconjugated units the EL efficiency was very low (0.002% for ITO/**582**/Al [681]), although a similar value was demonstrated for MEH-PPV in the same device configuration. Introducing conjugated arylamine or phenylene vinylene linkers improves $\Phi_{\text{EL}}^{\text{ex}}$ to 0.018% (for triarylamine copolymer ITO/**579**/Al) and 0.06% (for phenylene vinylene copolymer ITO/**580**/Al) [680]. Also, nonconjugated, relatively more electronegative copolymers **581** and **582**, showed a lower turn-on voltage ($\sim 6\text{ V}$). Many other quinoline-containing polymers have been used in PLEDs as electron-transporting materials in combination with other EL polymers (e.g., quinoline-containing polystyrene **239**, with PFO [336]).

Several other 6,6'-bisquinoline-based copolymers (**583**, **584**) have been reported [682] (Chart 2.137). The absorption and PL spectra of polymers **584a,b** are red-shifted, compared to the analog with *p*-phenylene fragment **583**. The effect is much more pronounced in films than in solution (films: $\lambda_{\text{PL}} \approx 495\text{ nm}$ for **583** and a broad structureless band at $\approx 520\text{--}650\text{ nm}$ for **584a,b**). Single-layer (ITO/PEDOT/polymer/Ca/Ag) devices fabricated with these polymers showed moderate performance with a maximum luminance and a maximum brightness of 0.17–0.58 cd/A and 90–150 cd/m², respectively (Chart 2.137).

In 1996, Yamamoto et al. [683] reported the EL from related poly(quinoxaline)s **585** (Chart 2.138). In contrast to unsubstituted polypyridine, all polymers **585** appeared to be soluble in organic solvents. For all polymers of the series, single-layer (ITO/polymer/Mg(Ag)) and

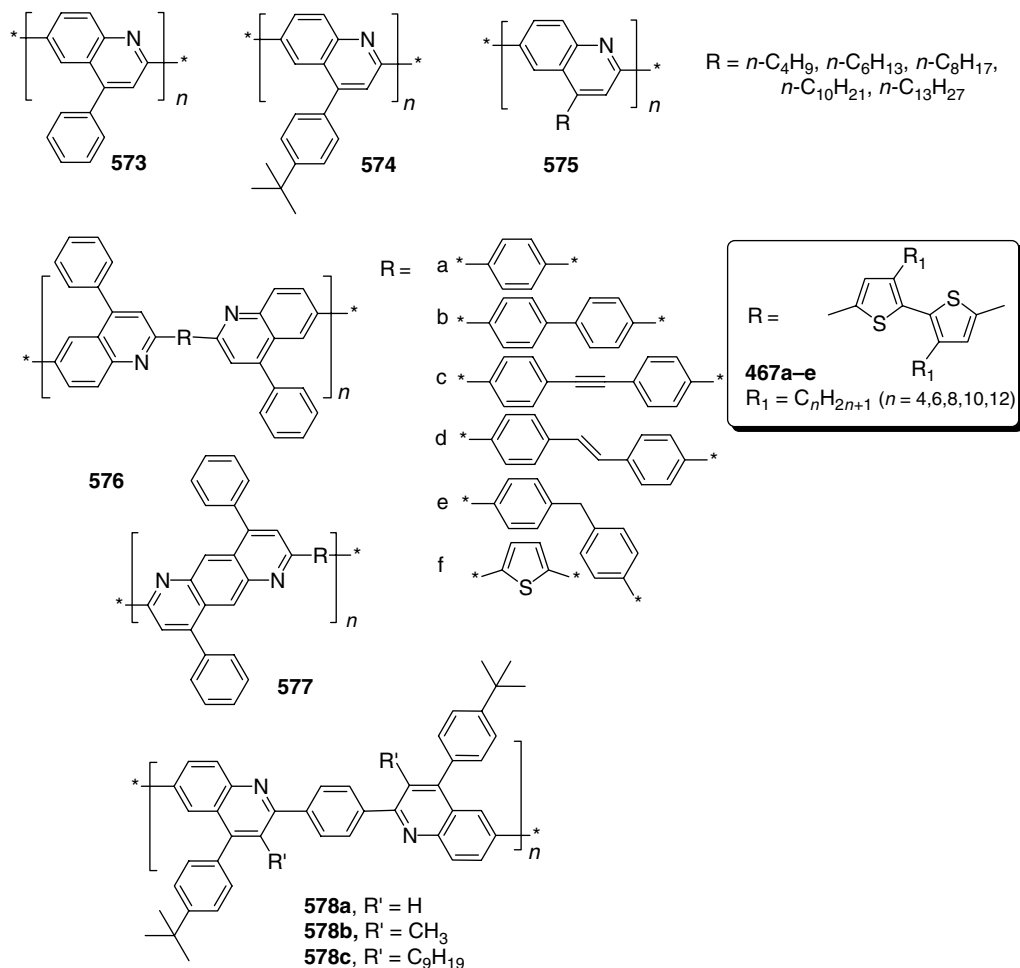


Chart 2.135

double-layer devices with different HTL emitted green-blue light at $\lambda_{\text{max}} = 490 \text{ nm}$, but the device brightness was rather low (on the order of $1\text{--}10 \text{ cd/m}^2$).

A better PLED performance was observed by Jenekhe and coworkers [173] for ITO/PEDOT/polymer/Al devices with quinoxaline-phenylene vinylene copolymers **586** and **587** as emitting layers. The $\Phi_{\text{EL}}^{\text{ex}}$ and maximum brightness were measured as 0.012 and 0.01%, and 120 and 35 cd/m^2 , respectively. The turn-on voltages of these devices were reasonably low, 6.0 and 4.0 V, respectively. The performance of PLEDs with polymer **586** was further improved by blending with 5 wt% of a hole transport material, 1,1-*bis*(di-4-tolylaminophenyl)cyclohexane (TAPC) that enhanced the $\Phi_{\text{EL}}^{\text{ex}}$ to 0.06% and the maximum brightness to 450 cd/m^2 .

Excellent electron-transporting properties of quinoxaline (also demonstrated for nonconjugated quinoxaline-containing polymer **588** [684] and quinoxaline-based polyether **589** [685]) resulted in a substantially decreased turn-on voltage of PPV/**590** PLED (3.6 V), which is much lower than that of pure PPV in the same conditions (7 V). These diodes showed a maximum luminance of 710 cd/m^2 (ca. 40 times brighter than the PPV diode at the same current density and voltage) [686].

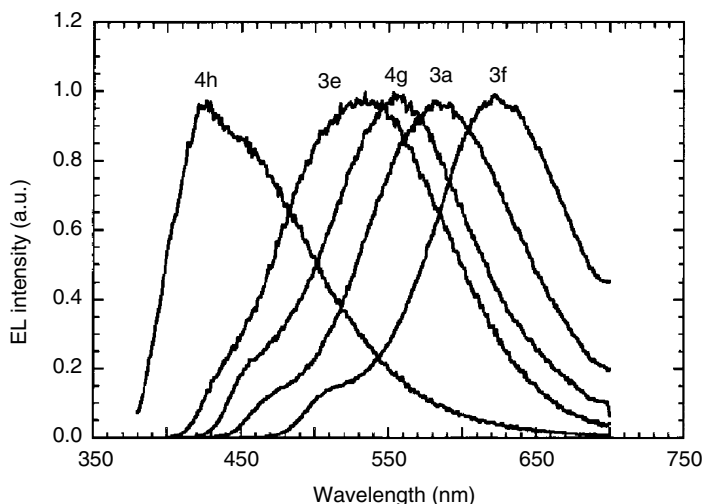


FIGURE 2.34 Tuning the electroluminescence color in polyquinoline derivatives (device structure ITO/HTL/EL polymer/Al, where HTL is triarylamine-based molecular material (for polymers **576**) or PVK **535** (for polymer **578**); EL polymer: **576a** (3a), **576e** (3e), **576f** (3f), **578a** (4g), **578b** (4h). (From Zhang, X., Shetty, A.S., and Jenekhe, S.A., *Macromolecules*, 32, 7422, 1999. With permission.)

Incorporation of phenothiazine was successful in tuning the emission characteristics and LUMO energy level of fluorene-phenothiazine copolymers **352–354**, as discussed earlier [430–432] (Chart 2.139). Phenothiazine homopolymers **591a,b** have also been prepared and characterized [430,431]. Although they emitted blue-greenish light with reasonably high Φ_{PL} in solution (43% for **591a**), the performance of the devices was quite low. Thus, ITO/PEDOT/**591b**/Ca diode showed a maximum brightness of only 9.0 cd/m², and a maximum current efficiency of 0.002 cd/A [431].

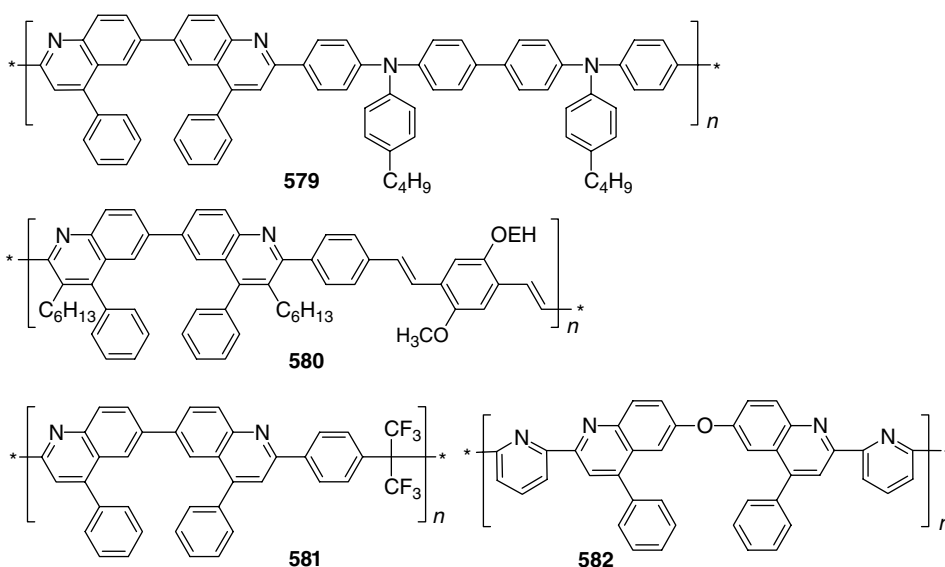


Chart 2.136

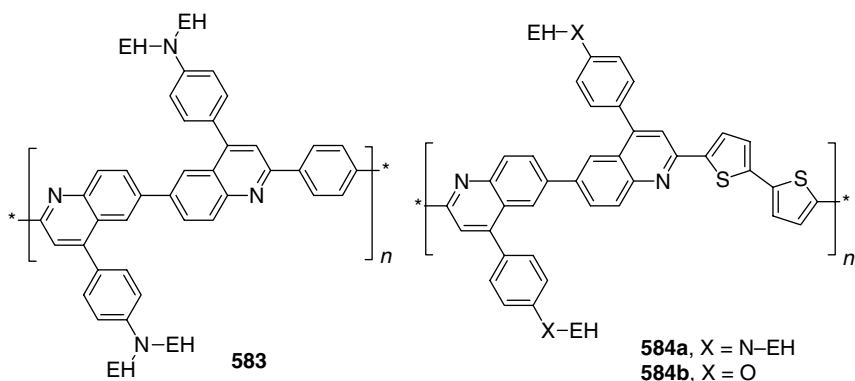


Chart 2.137

2.5.7 OXADIAZOLE, OXAZOLE, AND THIADIAZOLE POLYMERS

Due to relatively high electron affinity and very good PL efficiency, molecular materials based on oxadiazole, particularly, PBD (**21**) are among the most popular electron transport materials for OLEDs. The oxadiazole moieties, including PBD, were introduced as pendant

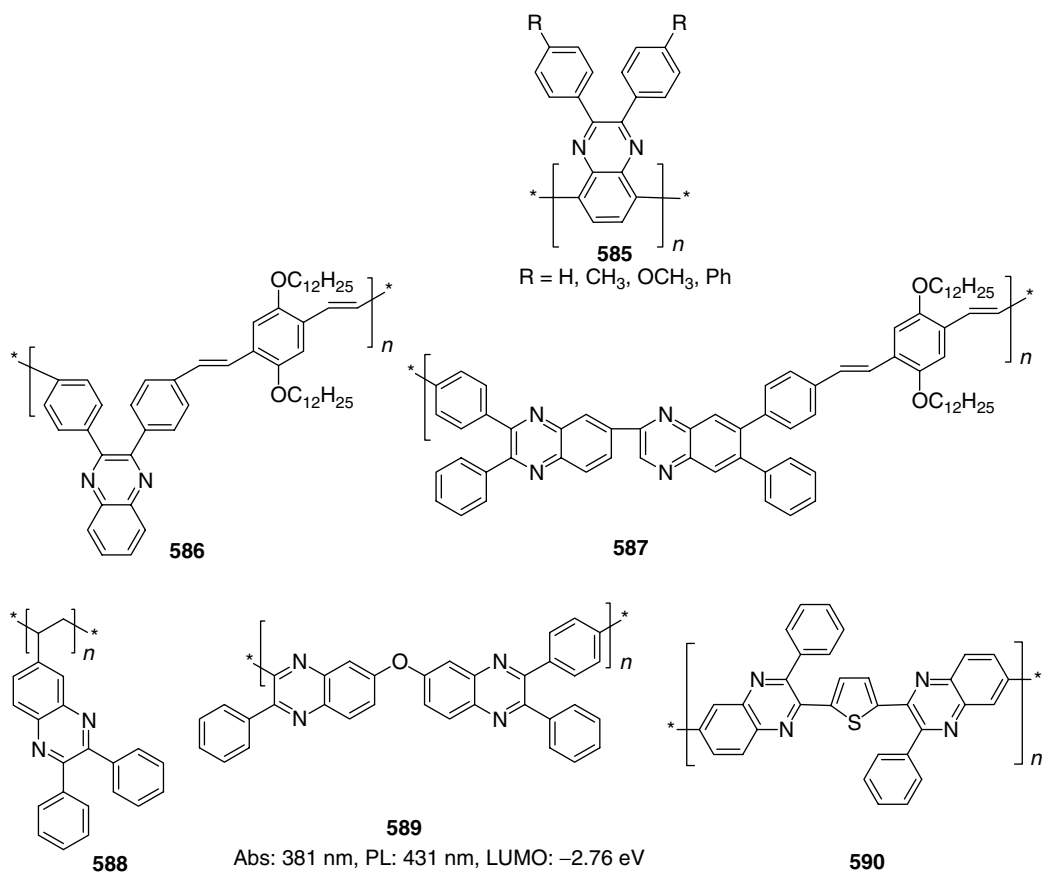
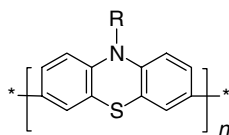


Chart 2.138

**591**

a, R = C₆H₁₃; Abs: 287 nm, PL: 490 nm, EL: 480 nm,
HOMO: -5.0 eV, LUMO: -2.24 eV

b, R = 2-ethylhexyl; Abs: 285 nm, PL: 478 nm, CIE (0.16, 0.32),
HOMO: -5.0 eV, LUMO: -2.23 eV

Chart 2.139

groups in many EL polymers in order to reduce the electron injection barrier and improve the EL efficiency of the device. We have already described oxadiazole-containing PPVs (**61**, **65–68**, **103–104**, **135–142**), PFs (**257–260**, **262–269**), and PTs (**460–466**) in previous parts.

Blends of PBD with EL polymers were employed to balance the charge injection and transport characteristics of PLEDs [68,108,517,580]. To avoid phase separation and molecular PBD crystallization, several groups introduced the PBD moieties as pendant groups in nonconjugated polymethacrylate [687–690] and polyethylene [684] chains. Polymers **592–594** have been studied as materials for PLEDs [687,688], in single-layer devices and in combination with PPV as HTL (Chart 2.140). The authors mentioned that the device instability is a great problem for these systems and that engineering a more robust polymer backbone would be necessary. Later, Register and coworkers [691] synthesized and studied related polymers **595** and **596** based on polystyrene backbones. Having observed the immiscibility of oxadiazole polymer **595** with PVK, the authors designed the copolymer **596** containing electron- and hole-transporting units. The device ITO/**596**/Mg:Al showed improved $\Phi_{\text{EL}}^{\text{ex}}$ of 0.3%, although the turn-on voltage was still high (16 V). Through doping the polymer with different molecular dyes, the emission color was tuned from blue to orange [691]. The use of polymers **597a–c** as electron transport layers in a two-layer LED (ITO/PPV/**597a–c**/Ag) increased the intensity of light emission by a factor of 100, compared with the single-layer ITO/PPV/Ag device; reaching $\Phi_{\text{EL}}^{\text{ex}}$ of up to 0.1% and a maximum brightness of 300 cd/m² at 30 V (turn-on voltage 6.5–8.5 V) [690].

In 1995, Pei and Yang reported polymers **598** [692,693] and **599** [694] with a short conjugation length and wide π – π^* energy gap (Chart 2.141). They were not fluorescent but could be used as an electron injection layer to significantly improve the QE of PLEDs based on PPVs (from 0.002 to 0.08% for MEH-PPV **13** and from 0.03 to 0.30% for BCHA-PPV **23**) [694]. The additional oxadiazole moiety in **599** further enhances the electron transport properties of the polymer and decreases the operation voltage of LEDs. Polymer **600** with a longer conjugation length has an efficient blue fluorescence ($\lambda_{\text{PL}} = 554, 465$ nm, $\Phi_{\text{PL}}(\text{film}) = 35\%$) and the PLED ITO/PANI/**600/598**/Ca emits a bright-blue light with $\Phi_{\text{EL}}^{\text{ex}} = 0.1\%$ (turn-on voltage 4.5 V) [694]. Some other examples of electron-transport and hole-blocking oxadiazole–phenylene copolymers with short conjugation length interrupted by C(CF₃)₂ groups (**601** [695]) or by ether links (**602** [685]) have been reported in the literature.

Holmes and coworkers [695,696] introduced oxadiazole moieties into formally conjugated (although having one *m*-phenylene linkage) polymer **603** (Chart 2.142). The polymerization was performed by condensation of terephthalaldihydrazide with 5-*tert*-butyl-1,3-benzenedicarboxylic acid, followed by dehydration and cyclization of the resulting polyhydrazide. Based on CV studies, the authors concluded that the electron affinity of **603**, although higher than that of MEH-PPV, is below that of, e.g., CN-PPVs and only a moderate PLQY (11%) was found.

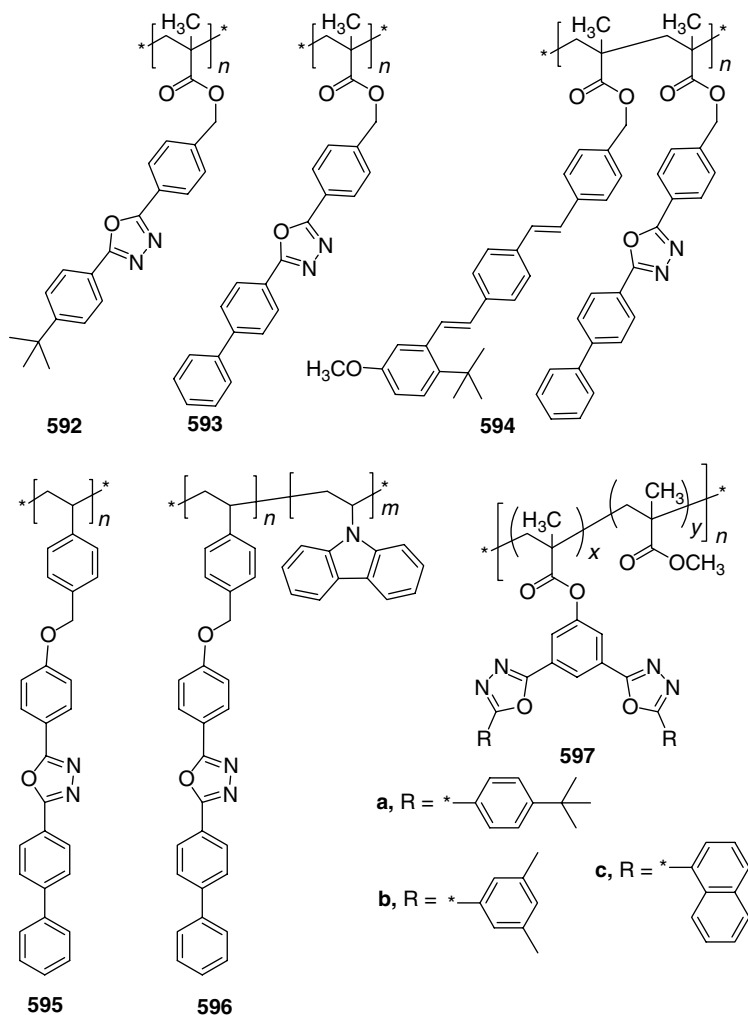


Chart 2.140

Inspired by good electron transport properties and high PL of PBD and, particularly, a claim by Heeger and coworkers [68] of exceptional performance of PBD–MEH–PPV mixtures (EL of up to 50% of the PL yield), Bryce and coworkers [697] reported the first poly(PBD) homopolymer (**604**) and its aza-derivative (**605**). The device ITO/PEDOT/MEH-PPV:**604**/Al showed $\Phi_{\text{EL}}^{\text{ex}}$ of 0.26%, compared to 0.01% obtained with MEH-PPV alone in an identically prepared device.

Janietz and coworkers [698,699] reported blue emission from fully conjugated alternating oxadiazole–phenylene polymers **606a–d** and **607**. Electrochemical estimation of their LUMO energy levels (–2.50 to –2.80 eV) characterizes them as potentially good electron transport materials. A rectification ratio of 10^4 to 10^6 was reported for ITO/**606c**/Al diode in the negative bias region, but no light emission was demonstrated.

Polybenzobisthiazoles **608** and polybenzobisoxazole **609** have been used as efficient electron transport materials in PLEDs [71] (Chart 2.143). Although these polymers show poor fluorescence quantum yields in thin films likely due to excimer formation [700], double-layer devices ITO/PEDOT/polymer/ETL/Al with PPV or MEH-PPV as emissive polymers and

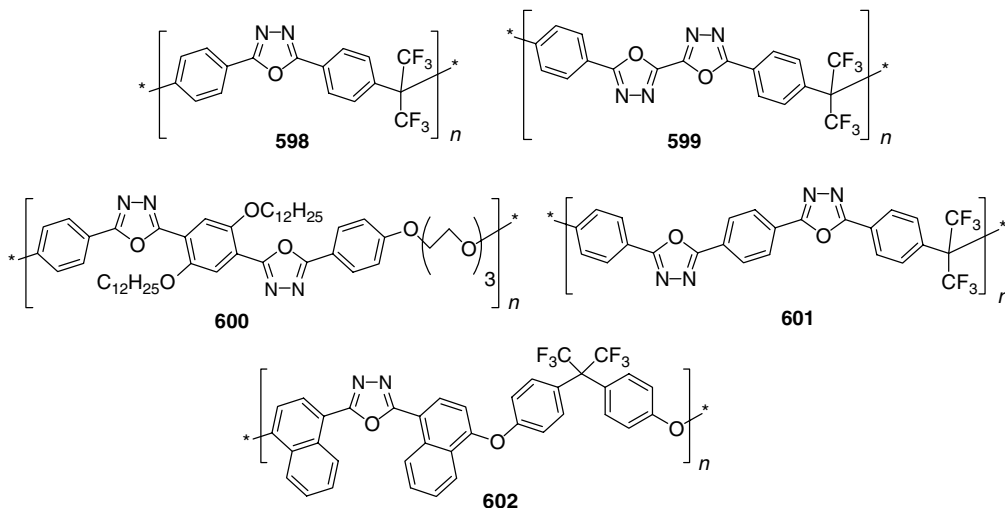
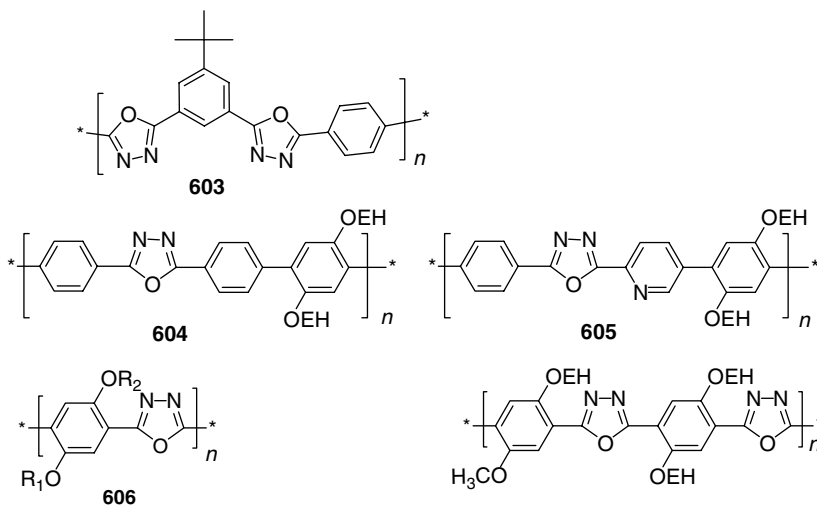


Chart 2.141

608a or **609** as ETL had a turn-on voltage as low as 2.8 V, a luminance of up to 1400 cd/m², and $\Phi_{\text{EL}}^{\text{ex}}$ of up to 2.5%. Very recently benzoxazole-based polymers have been studied as LEP. The fully conjugated polymer **609** was used in oriented fibers to create polarized PLEDs [701]. The resulting device ITO/**609**/Al can be turned on at ~5 V emitting red light ($\lambda_{\text{EL}} = 620$ nm) with polarization ratio of 1.6. The same group reported EL from nonconjugated benzoxazole copolymers **610** [702]. While the ratio $x:y$ decreases from 1:0 to 0:1, the emission band of **610**



- a**, $R_1 = R_2 = n\text{-C}_{12}\text{H}_{25}$; HOMO: -5.92 eV, LUMO: -2.56 eV
- b**, $R_1 = R_2 = n\text{-C}_{16}\text{H}_{33}$; Abs: 415, 445 nm, PL: 484, 515 nm, HOMO: -5.95 eV, LUMO: -2.50 eV
- c**, $R_1 = R_2 = 2\text{-ethylhexyl}$; Abs: 410, 430 nm, PL: 454, 472 nm, HOMO: -5.94 eV, LUMO: -2.80 eV
- d**, $R_1 = \text{CH}_3$, $R_2 = 2\text{-ethylhexyl}$; Abs: 406, 430 nm, PL: 478 nm, HOMO: -5.92 eV, LUMO: -2.78 eV

Chart 2.142

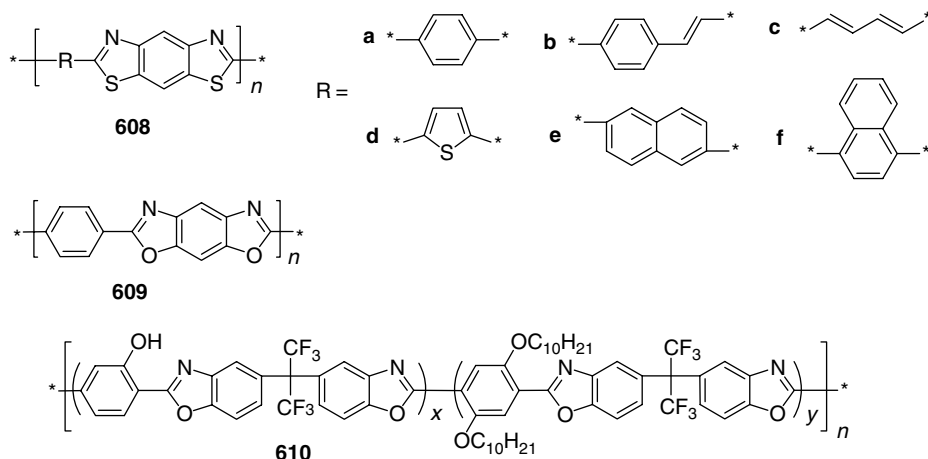


Chart 2.143

broadens significantly (while keeping the maximum at ~ 520 nm), so that at $x:y=0:1$ the emission band covers almost the entire visible region. The emission color of PLED fabricated as ITO/**610**/Al can be tuned from green (CIE: $x=0.25$, $y=0.53$) to the color reported as white, although the reported CIE coordinates ($x=0.24$, $y=0.30$) are relatively far from the definition of white (CIE: $x=0.33$, $y=0.33$).

2.5.8 BORON-, SILICON-, AND PHOSPHORUS-CONTAINING POLYMERS

Introducing heteroatoms such as O, N, S in the backbone of conjugated polymers is routinely used to modify their electronic properties, and particularly, the HOMO–LUMO energies. Other heteroatoms only recently have been studied in this aspect [703].

Several relatively stable boron-containing conjugated polymers have been synthesized by Chujo and coworkers by high-yield hydroboration of C–C bonds (for polymers **611** [704,705]) or C–N (for polymers **613** [706]) triple bonds or by Grignard-type reaction of phenylenedibromide with substituted dimethoxyborane in the presence of Mg (for polymers **612** [707]) (Chart 2.144). The conjugation in these polymers is provided by interaction of the carbon π -system with the vacant p-orbital of boron, which should greatly enhance the electron-transporting properties of the polymers. In solution, **612** and **613** reveal strong blue or blue-green PL with $\lambda_{\text{PL}}=440\text{--}496$ nm, while **611** has three PL maxima of 416 nm (blue), 495 nm (green), and 493 nm (orange-red), thus emitting white light [705]. No EL devices have been reported so far and the stability issue is likely to be a problem for practical applications of these materials [703].

Recently, Tanaka and coworkers [708] prepared phosphorus-containing polymers (2,7-(9-oxo-9-phosphafluorenylene)-*alt-co*-(1,4-arylene))s **614**, which emit blue light in solution (413–433 nm) with quite high Φ_{PL} (68–81%), similar to PFs. In films, however, their emission is red-shifted by 32–44 nm becoming green-blue, which is at a much higher wavelength than that for fluorene-*alt-co*-phenylene analogs [364,365,380,382] (Chart 2.145).

Yamaguchi and coworkers [709] have prepared luminescent silole polymers **615a–e**. The blue emission of the homopolymers **615a,b** can be shifted into the red region by copolymerization with other conjugated units (but for the price of lowered PLQY). Although no device studies have been reported yet, excellent electron-transport properties are expected from such materials [710].

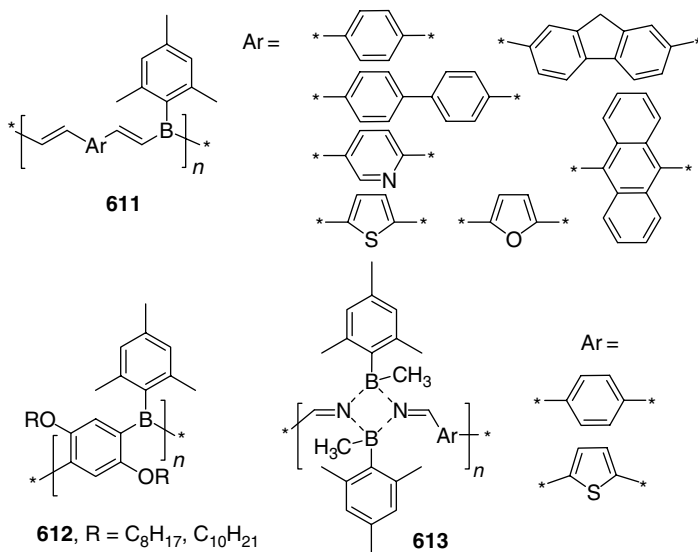


Chart 2.144

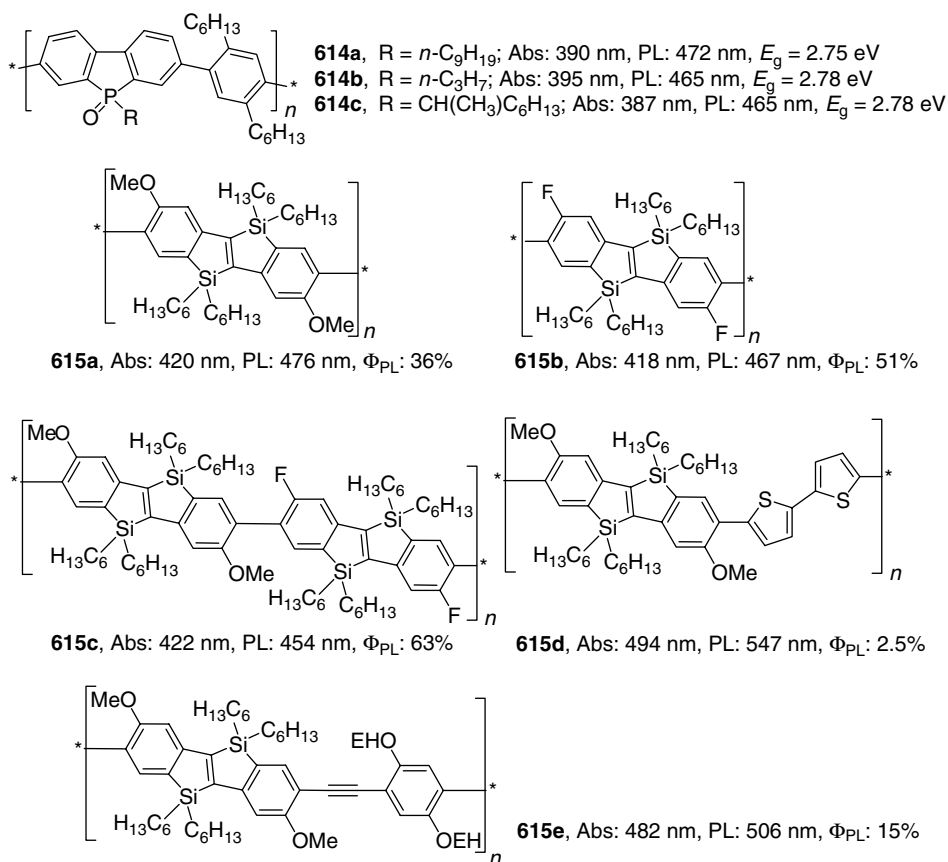


Chart 2.145

2.5.9 CONCLUSIONS

Although the major research activities in PLEDs are now concentrated in three major classes of LEPs — PFs, PPVs and, to a lesser extent, PTs, the study of other classes of conjugated and nonconjugated polymers may give rise to high-performance EL materials with tunable emission color. Importantly, the charge-transport and charge-injection properties can be tuned in a wider region than is accessible by structural modification of PF, PPV, and PT materials. The very high EL performance achieved in PPP-type polymers (including ladder-type PPPs) and very high chemical and thermal stability of the PPP materials render them as very promising candidates for commercial PLEDs. Based on LPPP **514b**, blue-green emitting PLEDs with $\Phi_{\text{EL}}^{\text{ex}}$ up to 4% [614] and the brightness as high as 40,000 cd/m² [67] was achieved by different engineering techniques. An efficient yellow-emitting PLED ($\Phi_{\text{EL}}^{\text{ex}} = 4.2\%$ [522]) and white-emitting PLED ($\Phi_{\text{EL}}^{\text{ex}} = 1.2\%$ [619]) were fabricated by blending LPPP **514b** with PT- and PPE-based polymers, respectively.

Introducing heteroaromatic moieties (mainly with N and, to a lesser extent, with O and S) in the backbone of the polymer or as a pendant group, can substantially modify the LUMO level of the materials, improving their electron-transport properties and facilitating electron injection in PLEDs, but the efficiencies still lag behind the other systems.

2.6 CONCLUSIONS AND OUTLOOK

In the previous four sections, we described the progress in the development of LEPs, from the beginning of the 1990s up to 2004. Practical applications in PLEDs became a field of major research activity throughout the world, in academia and in industrial laboratories. Over 500 different LEPs described in this book (and, most probably, over 1000-reported LEPs) have been developed by efforts of many researchers with different scientific background. At one extreme, this fact is reflected in unsystematic and often illogical approaches the science took in the development of new materials (which was the biggest frustration for the authors, who were trying to integrate all materials in one story). At the other extreme, it allowed an element of serendipity that continues to keep the scientific part of the field alive. Although at the moment the commercial success of PLEDs probably depends more on engineering issues, it would certainly not be possible without several important scientific breakthroughs. Besides the pioneering work of Friend and coworkers [1] on PPV-based PLEDs, the following major discoveries, while certainly not an exhaustive list, should be considered:

- Design of soluble LEPs by introduction of solubilizing substituents
- Prevention of interchain interactions (and resulting luminescence quenching) by sterically hindering substituents
- Fine-tuning the emission of the polymers via copolymerization
- Control of the charge injection and transport by introduction of electron donor–acceptor substituents (or comonomers and end-capping groups)
- Control of the interface at the anode and cathode
- Control of the film morphology as a function of spin-casting solvent.

Following these principles, a number of EL polymers, with an external QE of over 3–4%, have been demonstrated. However, there are still a number of issues to be solved for successful competition with small molecule OLEDs. Since one of the main targets for LEPs is display technology, pure red, green, and blue emitters are of particular importance. Among these, green color is the easiest to achieve. A very high performance of over 6% was demonstrated for a derivative of a traditional class of green-emitting polymers, phenyl-PPV **88** [139], as well as for a PF-based copolymer **366** [435]. A photometric current efficiency of over 20 cd/A was

demonstrated for these materials, which is also due to the higher sensitivity of the human eye to green color. High-efficiency red-emitting polymers are considerably less common, and, in terms of technology, this niche probably belongs to electrophosphorescent PLEDs (which are based on blends of conventional LEPs with phosphorescent metal complexes, or their covalent conjugates; see Chapter 7). With respect to electrofluorescence, the best performing red emitters can be found among the fluorene copolymers with heterocyclic moieties, such as naphthothienodiazole (**349**: EL = 3.1%, 0.9 cd/A [427]). Design of a highly efficient polymer emitter giving a pure blue color is probably one of the major challenges to the LEP field. High-energy excited states (~ 3 eV) generally impose higher reactivity (and lower stability) to blue emitters. Undoubtedly, PFs, as an easily functionalizable polymers, are the most promising materials for blue PLEDs. Although rather efficient ($\Phi_{\text{EL}}^{\text{ex}}$ up to 3%) blue EL was also demonstrated by PPP polymers, the turn-on voltage (over 15–20 V) of the corresponding devices is much too high for display applications. Very pure blue color (CIE: $x = 0.15$, $y = 0.08$) is achieved for triarylamine-terminated dialkyl-PF **228** [253]. A photometric EL efficiency of 1.1 cd/A (turn-on voltage 3.5 V) was demonstrated for a corresponding single-layer PLED and this can be further pushed to 2–3 cd/A in multilayer device configurations [253,326]. Color purity and color stability are the major concerns with blue-emitting polymers. A recent demonstration of the origin of the “parasitic” green band in PFs arising from ketone-defects opens a number of possible (and already partially realized) solutions for this problem.

The next most promising application for EL polymers is general illumination, where high efficiency, stability, and low cost are the major criteria. Although the sufficiently high-efficiency yellow-emitting polymers (e.g., oxadiazole-containing PPV **68**, photometric efficiency of 21.1 cd/A [123]) are already available, the true need is in much less developed white-emitting LEPs. To date, true white color in LEP is available only by blending several types of materials. Thus, a pure white emission (CIE: $x = 0.31$, $y = 0.33$) was demonstrated by a blend of LPPP **514b** with 1% of pyrene-containing PPE **525**, although the achieved efficiency (1.2 cd/A) is still too low for practical applications [619].

Overall, and for each one of the above examples, the stability in terms of color and even more in terms of operation lifetime, is the major issue for PLEDs. The current state-of-the-art operation half-lifetime of PLEDs rarely exceeds 10,000–20,000 h (which, in principle, could be acceptable for many applications) and even that is achievable for only few (mostly, green-emitting) polymers. A very significant role in the device degradation is played by material impurities that are very difficult to control in polymers as in any polydisperse system. Rigorous monomer purification and a careful choice of the polymerization method are just as important for the EL performance as the specific polymer structure. At the same time, the device architecture is also directly responsible for the device efficiency and stability. A careful adjustment of charge-injection barriers can minimize the driving voltage and improve the device efficiency and stability. To conclude, the future progress in PLEDs will depend on a close collaboration between organic and polymer chemists on one side and surface scientists and engineers on the other.

2.7 APPENDIX

2.7.1 SYNTHESIS OF POLY(*p*-PHENYLENE VINYLENE)S

2.7.1.1 The Wessling–Zimmerman (Thermoconversion) Precursor Route to PPV

2.7.1.1.1 Poly(2-fluoro-5-(*n*-hexyloxy)-1,4-phenylene vinylene) (**77**) (Chart 2.146)

From Gurge, R.M., Sarker, A.M., Lahti, P.M., Hu, B., and Karasz, F.E., *Macromolecules*, 30: 8286–8292, 1997. Copyright 1997, American Chemical Society, Washington, D.C. With permission.

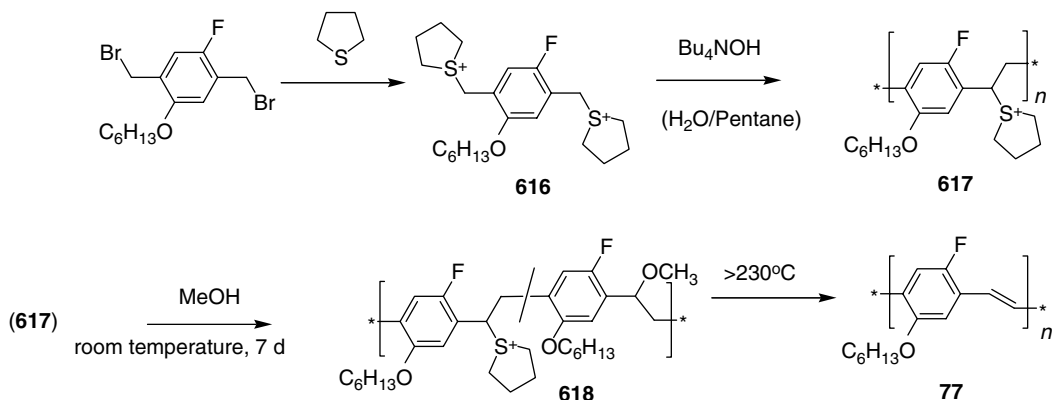


Chart 2.146

Bis(tetrahydrothiophenium) salt 616: 1-Fluoro-4-hexyloxy-2,5-bis(chloromethyl)benzene (1.22 g, 3.19 mmol) was suspended in a solution of tetrahydrothiophene (1.4 g, 15.9 mmol) in 35 ml of dry methanol. The mixture was stirred at 55°C for 24 h. The solvent and excess tetrahydrothiophene were removed by distillation to give an off-white residue, which was dissolved in a minimum amount of methanol and precipitated into 200 ml of dry acetone. After vacuum drying, white powder **616** (1.25 g, 70%) was obtained with melting point 163–166°C (dec). This compound is stable in a freezer under inert atmosphere. An analytical sample was obtained by threefold precipitation from methanol into acetone. Anal. Calcd for $\text{C}_{22}\text{H}_{35}\text{Br}_2\text{FOS}_2$: C, 47.32; H, 6.31; Br, 28.62; F, 3.40; S, 11.48. Found: C, 47.38; H, 6.27; Br, 29.1; F, 3.50; S, 11.52. ^1H NMR (80 MHz, CD_3OD): 7.64 (d, 1H, $J=8.8$ Hz), 7.52 (d, 1H, $J=4.5$ Hz), 4.77 (s, 2H), 4.67 (s, 2H), 4.29 (t, 2H, $J=6.2$ Hz), 3.66 (m, 8H), 2.48 (m, 8H), 1.54 (m, 8H), 1.02 (asym t, 3H, $J=7.5$ Hz).

Polyelectrolyte 617: The *bis*(sulfonium) salt **616** (600 mg, 1.08 mmol) was dissolved in 25 ml of distilled water. The solution was filtered through a glass frit and placed in a 100 ml round-bottom flask. An equal volume of pentane was added to the flask, and the two-phase system was cooled to 0°C under argon. A solution of tetramethylammonium hydroxide was also cooled to 0°C under argon and pentane. Both solutions were thoroughly purged with argon gas for 1 h. Then, the base (0.47 ml, 1.30 mmol) was added swiftly by syringe. The polymerization was allowed to proceed for 1 h at 0°C. The excess base was neutralized with 6 M HCl solution to a phenolphthalein end point. The resulting yellow-green solution was dialyzed against distilled water (Spectropore 1 filters, M_w cutoff 6000–8000) for 3 days to give a uniform green solution. This solution can be used to cast films, which are soluble in methanol but insoluble in THF and CHCl_3 . This material is appropriate for conversion to polyether **618**.

Polyether 618: The sulfonium polyelectrolyte **617** was dissolved in a minimal amount of methanol. The solution was stirred for 1 week under argon, during which pendant polyether **618** precipitated from the solution. The tacky yellow material was completely soluble in CHCl_3 and THF. Polymer **618** can be dissolved in THF and passed through a 0.2-mm filter for GPC or for use in film casting and device fabrication. Cast films can be completely redissolved into CHCl_3 or THF. GPC in THF (polystyrene standards) gave $M_w = 91,500$ and $M_n = 33,800$.

PPV 77: A film of polyether **618** was clamped between two 0.125 in-thick Teflon plates, and then heated at 230°C for 6 h under vacuum (<0.01 mmHg) to give a red film of PPV **77**. The final polymer films are insoluble in CHCl_3 , THF, and MeOH. Anal. Calcd for $\text{C}_{14}\text{H}_{17}\text{OF}$: C, 76.33; H, 7.78; F, 8.62; S, 0.0. Found: C, 72.02; H, 7.44; F, 8.3; S, 0.30. IR

(neat film, cm^{-1}): 962 (*trans* HC=CH). UV-vis (neat film on quartz): $\lambda_{\text{max}} = 455$ nm. PL (neat film on quartz, excitation at 390 nm): $\lambda_{\text{max}} = 630$ nm.

2.7.1.2 Gilch Polymerization Procedure

2.7.1.2.1 Preparation of Poly[2-(3,7-dimethyloctyloxy)-5-methoxy-*p*-phenylene vinylene] (**14**) (Chart 2.147).

From Becker, H., Spreitzer, H., Ibrom, K., and Kreuder, W., *Macromolecules*, 32: 4925–4932, 1999. Copyright 1999, American Chemical Society, Washington, D.C. With permission.

A 4-l, four-neck flask fitted with mechanical (Teflon) stirrer, reflux condenser, thermometer, and dropping funnel was dried (stream of hot air) and flushed with N_2 . The reactor was then charged with 2.3 l of dry 1,4-dioxane, and the solvent was degassed by passing N_2 through it for about 15 min. The solvent was heated to 98°C with an oil bath, and 14.0 g (38.7 mmol) of 2,5-bis(chloromethyl)-1-(3,7-dimethyloctyloxy)-4-methoxybenzene was added as a solid. (The solid was rinsed in with about 10 ml of dry 1,4-dioxane.) A 11.3 g (100 mmol, 2.6 equivalent) sample of potassium *tert*-butoxide, dissolved in 100 ml of 1,4-dioxane, was added dropwise to the reaction solution from the dropping funnel over a period of 5 min. During this addition, the reaction mixture changed color from colorless via greenish to yellow-orange, and the viscosity increased significantly. After the addition was complete, the mixture was stirred further for about 5 min at 98°C ; 8.70 g of potassium *tert*-butoxide (77 mmol, 2 equivalent) in 77 ml of dry 1,4-dioxane was then added over a period of 1 min, and stirring was continued for 2 h at 96 – 98°C . The solution was then cooled to 50°C over a period of about 2 h. The reaction mixture was finally mixed with 15 ml (260 mmol, 1.5 equivalent based on the base) of acetic acid (diluted with the same amount of 1,4-dioxane) and stirred further for 20 min. The solution was then deep orange and the viscosity increased. For the workup, the reaction solution was slowly poured into 2.5 l of intensively stirred water. The resulting mixture was stirred further for 10 min, 200 ml of methanol was added, and the precipitated polymer was filtered off. This was washed with 200 ml of methanol and dried under reduced pressure at room temperature. A 10.04 g (34.8 mmol, 90%) sample of crude polymer was obtained as red fibers. The polymer was purified by dissolving it in 1.1 l of THF (60°C), cooling the solution to 40°C , and precipitating the polymer by dropwise addition of 1.2 l of methanol. After washing with 200 ml of methanol, it was dried at room temperature under reduced pressure. This procedure was repeated once more using 1.0 l of THF and 1.0 l of methanol. A 6.03 g (20.9 mmol, 54%) sample of poly[2-(3,7-dimethyloctyloxy)-5-methoxy-*p*-phenylene vinylene] (**14**) was obtained as a dark-orange, fibrous polymer. ^1H NMR (400 MHz, CDCl_3): 7.7–6.5 (br m, 4H; H_{arom} , olefin-H); 4.5–3.6 (br m, 5H; OCH_3 , OCH_2); 2.1–0.6 (br m, 19H; aliph-H). GPC (THF + 0.25% of oxalic acid; column set SDV500, SDV1000, SDV10000 (from PSS), 35°C , UV detection at 254 nm, polystyrene standard): $M_w = 1.5 \times 10^6$ g/mol,

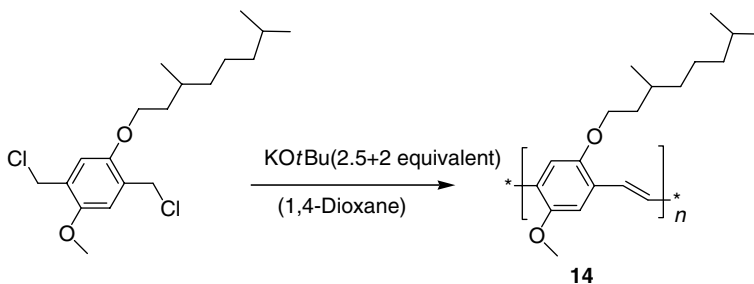


Chart 2.147

$M_n = 3.1 \times 10^5$ g/mol. Elemental analysis: Calcd: C, 79.12%; H, 9.78%; O, 11.09%. Found: C, 78.88%; H, 9.82%; O, 11.00%; Cl, 25 ppm; K, 41 ppm; Na, 23 ppm.

2.7.1.3 Chlorine (Bromine) Precursor Route

2.7.1.3.1 Preparation of Poly{2-[2'-ethylhexyloxy]-5-[4''-methylsulfonyl phenyl]-1,4-phenylenvinylene} (**70**) (Chart 2.148)

From Boardman, F.H., Grice, A.W., Rüther, M.G., Sheldon, T.J., Bradley, D.D.C., and Burn, P.L., *Macromolecules*, 32: 111–117, 1999. Copyright 1999, American Chemical Society, Washington, D.C. With permission.

A solution of potassium *tert*-butoxide dissolved in dry THF (0.3 M, 2.6 ml, 0.8 mmol) was added to a solution of *bis*(bromomethyl)methylsulfonylbiphenyl (0.5 g, 0.9 mmol) in dry THF (3 ml) cooled in an acetone or ice bath under nitrogen. A bright-yellow viscous solution was formed, and dry THF (4 ml) was added. The reaction mixture was allowed to warm to room temperature after 10 min and stirred for 2 h. A small amount of a precipitate was formed. The reaction mixture was filtered through a plug of cotton wool, and the polymer **619** was precipitated by adding the reaction mixture dropwise to ice-cold 2-propanol (50 ml). The mixture was centrifuged for 10 min at 4000 rpm, and the supernatant was removed. The crude polymer **619** was briefly dried under vacuum, dissolved in dry THF, and then precipitated by addition to an excess of 2-propanol. The solid was collected after centrifugation, and the process was repeated a further two times. The residue was finally collected by dissolution in a minimum of THF, and the solvent was removed to leave **619** as an orange-yellow solid (200 mg, 40%). λ_{\max} (thin film)/cm⁻¹ 955 (HC=C), 1154 (SO₂), 1315 (SO₂); λ_{\max} (CH₂Cl₂)/nm 300sh; ¹H NMR (500 MHz; CDCl₃) 0.74–1.00 (br m, CH₃), 1.14–1.90 (br m, CH and CH₂), 2.94–3.25, 3.30–4.10 (br m, CH₃SO₂, OCH₂, and ArCH₂), 5.05–5.23 (br s, CHBr), 6.27–7.63 (br m, Ar H or vinyl H), 7.67–8.05 (br m, ArH); GPC of equilibrated sample, $M_w = 2.7 \times 10^5$ and $M_n = 1.3 \times 10^5$, PDI = 2.1.

Thin films of **619** were heated at 160°C under a dynamic vacuum for 14 h to yield **70**. λ_{\max} (film on KBr disk)/cm⁻¹ 955 (C=CH), 1154 (SO₂), 1315 (SO₂); λ_{\max} (thin film)/nm 285sh, 437.

2.7.1.4 Heck-Coupling Route

2.7.1.4.1 Preparation of Poly[2,5,2,5''-tetraoctyl-*p*-terphenyl-4,4'-ylenevinylene-*p*-phenylene vinylene] (**91**) (Chart 2.149)

From Hilberer, A., Brouwer, H.-J., van der Scheer, B.-J., Wildeman, J., and Hadziioannou, G., *Macromolecules*, 28: 4525–4529, 1995. Copyright 1995, American Chemical Society, Washington, D.C. With permission.

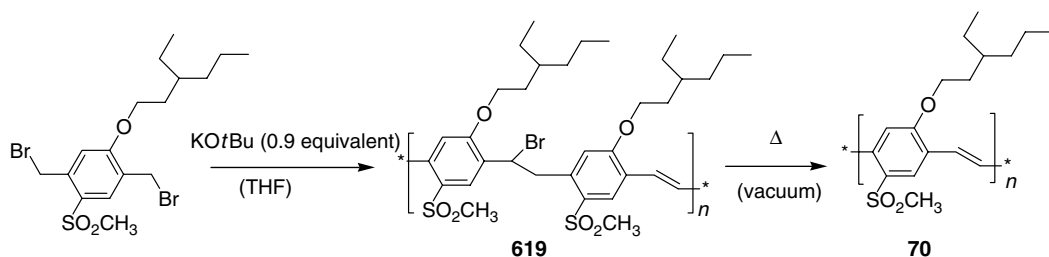


Chart 2.148

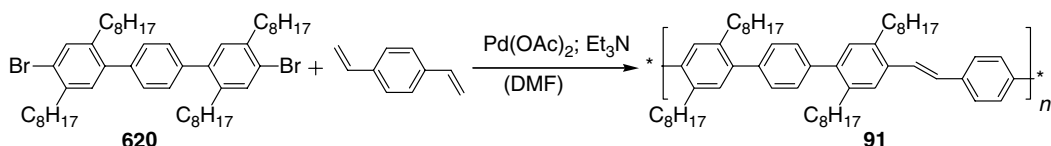


Chart 2.149

A mixture of monomer **620** (1.0 g, 1.2 mmol), *p*-divinylbenzene (0.155 g, 1.2 mmol), $\text{Pd}(\text{OAc})_2$ (0.011 g, 0.05 mmol), tri-*o*-tolylphosphine (0.071 g, 0.23 mmol), triethylamine (2 ml), and DMF (5 ml) was placed in a heavy wall pressure tube. The tube was degassed, closed (Teflon bushing), and heated to 100°C. After 40 h of reaction, thin-layer chromatography showed that the monomers were consumed. The reaction mixture was then poured into methanol (75 ml). The precipitated material was filtered off and dried under vacuum, giving a brown-yellow polymer (0.88 g, conversion = 91%). The crude polymer was dissolved in chloroform and then filtered through a small column of Kiesel gel to remove traces of catalyst. The resulting solution was concentrated and precipitated in methanol (75 ml). The yellow polymer **91** was collected by filtration and thoroughly dried under vacuum. ^1H NMR (broad signals): 0.89 (t, CH_3 , 12H), 1.25/1.29/1.5 (m, CH_2 , 48H), 2.64 (m, CH_2 , 8H), 7.1–7.6 (3 main peaks, arom. CH and vinyl CH, 16H); ^{13}C NMR: 126.8, 128.8, 129.2, 130.1, 131.5 (arom CH), 134.7, 137.2, 137.6, 138.1, 138.2, 140.1 (arom C). Anal. Calcd for $\text{C}_{60}\text{H}_{84}$ (repeating unit): C, 89.49; H, 10.51. Found: C, 88.02; H, 10.51; Br, 0.89.

2.7.1.5 Knoevenagel-Coupling Route

2.7.1.5.1 Preparation of CN-PPV copolymer (**122**) (Chart 2.150)

From Kim, D.-J., Kim, S.-H., Zyung, T., Kim, J.-J., Cho, I., and Choi, S.K., *Macromolecules*, 29: 3657–3660, 1996. Copyright 1996, American Chemical Society, Washington, D.C. With permission.

Under an argon atmosphere, to a stirred solution of equimolar quantities of dialdehyde **621** and 1,4-phenylenediacetonitrile in THF and *tert*-butyl alcohol (1:1) was added dropwise 5 mol% of Bu_4NOH (1 *M* in methanol) at 45°C for 20 min. The resulting paste-like polymeric product that precipitated from the solution during polymerization was collected and thoroughly washed with methanol to remove ionic species and unreacted compounds. The scarlet polymeric product was dried in a vacuum oven at 40°C for 2 days. The polymer yield was 93%. GPC (THF, polystyrene standard): $M_w = 1.5 \times 10^6$ g/mol, $M_n = 3.1 \times 10^5$ g/mol.

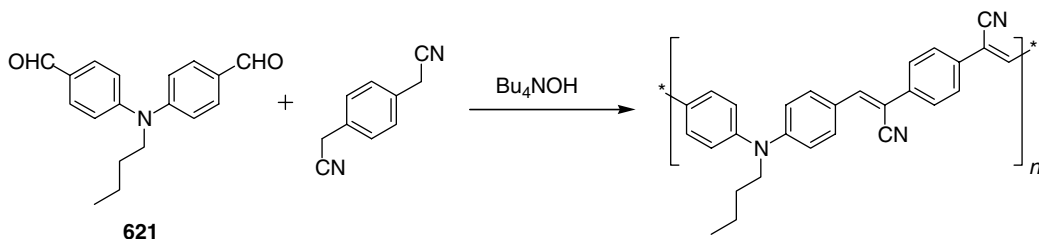


Chart 2.150

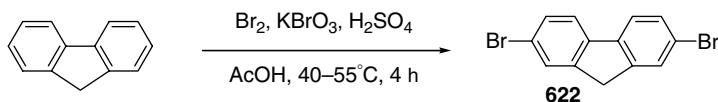


Chart 2.151

2.7.2 SYNTHESIS OF POLYFLUORENES

2.7.2.1 Synthesis of PF Monomers

2.7.2.1.1 2,7-Dibromofluorene (**622**) (Chart 2.151)

From I.I. Perepichka, I.F. Perepichka, M.R. Bryce, and L.O. Pålsson, *Chem. Commun.*, 3397–3399, 2005.

Fluorene (292 g, 1.76 mol) was dissolved in acetic acid (2.6 l) at $\sim 70^\circ\text{C}$ and H_2SO_4 (96%, 25 ml) was added slowly to this solution. The reaction mixture was allowed to cool to $\sim 50^\circ\text{C}$ with stirring, and a solution of bromine (150 ml, 2.92 mol) in acetic acid (200 ml) was added dropwise for 2–3 h, keeping the temperature at $40\text{--}55^\circ\text{C}$ to avoid crystallization of the fluorene. When about 1/3–1/2 of bromine was added, dibromofluorene started to crystallize. Simultaneously, with addition of a second half of bromine, KBrO_3 (100 g, 0.60 mol) was added in small portions (CAUTION: add slowly, exothermic reaction) at $40\text{--}55^\circ\text{C}$ with intense stirring, which promotes intensive precipitation of dibromofluorene. The mixture was stirred for 3–4 h allowing it to cool gradually to room temperature. After cooling the mixture to 10°C , the solid was filtered off, washed with 70% AcOH (0.5 l) and water until pH 7, and dried affording crude product as creme-colored solid (481 g, 85%) of $>95\%$ purity (by ^1H NMR). To further purify the product, it was stirred in AcOH (~ 1 l) at reflux (no full dissolution) for 4 h, cooled, filtered off, washed with AcOH, and dried affording 455 g (80%) of 2,7-dibromofluorene **622**. ^1H NMR (400 MHz, CDCl_3): δ 7.66 (2H, d, $J_{1-3} = 1.8$ Hz, H-1,8), 7.59 (2H, d, $J_{3-4} = 8.0$ Hz, H-4,5), 7.50 (2H, dd, $J_{3-4} = 8.0$ Hz, $J_{1-3} = 1.8$ Hz, H-3,6), 3.89 (2H, s, CH_2). ^{13}C NMR (100 MHz, CDCl_3): δ 144.79, 139.69, 130.15, 128.31, 121.19, 120.94, 36.56.

2.7.2.1.2 2,7-Dibromo-9,9-dihexylfluorene **623** (Chart 2.152)

From I.I. Perepichka, I.F. Perepichka, M.R. Bryce, and L.O. Pålsson, *Chem. Commun.*, 3397–3399, 2005.

Under argon, 3-l, three-neck flask was charged with 2,7-dibromofluorene **622** (130.0 g, 0.40 mol), 1-bromohexane (220 ml, 1.57 mol) and dry THF (1.0 l). After the full dissolution, the mixture was cooled to 0°C and a solution of potassium *tert*-butoxide (100.6 g, 0.90 mol) in dry THF (1.0 l) was added dropwise at 0 to $+5^\circ\text{C}$ with vigorous stirring during 1.5 h. Upon adding the *tert*-butoxide solution, the reaction mixture become orange (generation of fluorene anion) and then the color vanished to light pink (at the end of *tert*-butoxide addition, no orange color is produced). The mixture was stirred at room temperature for 4 h, filtered off from the KBr precipitate, and the solid was washed on a filter with DCM. The filtrate was evaporated on rotavapor, the residue was dissolved in DCM (1.5 l), washed with water, dried over MgSO_4 , and the solvent was evaporated. Excess of 1-bromohexane was removed

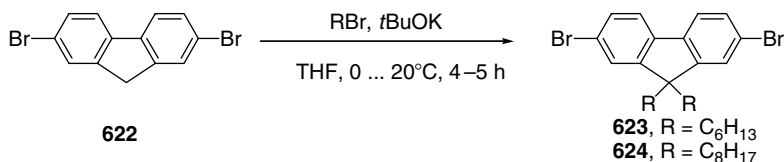


Chart 2.152

in vacuo (80°C, 1 mbar) yielding crude product (196.7 g, 99.6%) as yellow crystals. This was purified by column chromatography (7 × 17 cm column, silica gel, eluent — petroleum ether boiling point of 40–60°C) to afford 2,7-dibromo-9,9-dihexylfluorene **623** (179.5 g, 90.9%) as colorless plates. The material can also be additionally recrystallized from hexane or ethanol. ¹H NMR (500 MHz, CDCl₃): δ 7.51 (2H, d, *J* = 7.8 Hz, H-1,8), 7.45 (2H, dd, *J* = 1.8 Hz and 7.8 Hz, H-3,6), 7.44 (2H, d, *J* = 1.8 Hz, H-4,5), 1.96–1.87 (4H, m, CH₂C₅H₁₁), 1.16–1.08 (4H, m, CH₂CH₂CH₂C₃H₇), 1.08–0.98 (8H, m, [CH₂]₃CH₂CH₂CH₃), 0.78 (6H, t, *J* = 7.4 Hz, CH₃), 0.62–0.53 (4H, m, CH₂CH₂C₄H₉).

2,7-Dibromo-9,9-dioctylfluorene **624** was obtained as described above procedure and after the column chromatography was additionally recrystallized from ethanol yielding pure product in 78% yield. ¹H NMR (400 MHz, CDCl₃): δ 7.52 (2H, dd, *J*_{3–4} = 8.0 Hz, *J*_{1–4} = 0.8 Hz, H-4,5), 7.45 (2H, dd, *J*_{3–4} = 8.0 Hz, *J*_{1–3} = 1.6 Hz, H-3,6), 7.44 (2H, br s, H-1,8), 1.93–1.80 (4H, m, CH₂C₇H₁₅), 1.26–1.00 [20H, m, (CH₂)₂(CH₂)₅CH₃], 0.83 (6H, t, *J* = 7.2 Hz, CH₃), 0.63–0.53 (4H, m, CH₂CH₂C₆H₁₃).

¹³C NMR (100 MHz, CDCl₃): δ 152.57, 139.07, 130.15, 126.18, 121.47, 121.13, 55.69, 40.15, 31.76, 29.86, 29.18, 29.15, 23.62, 22.60, 14.08.

2.7.2.1.3 9,9-Dihexylfluorene-2,7-diboronic acid **625** (Chart 2.153)

From I.I. Perepichka, I.F. Perepichka, M.R. Bryce, and L.O. Pålsson, *Chem. Commun.*, 3397–3399, 2005.

To a stirred solution of 2,7-dibromo-9,9-dihexylfluorene **623** (30.0 g, 60.9 mmol) in dry THF (1.0 l) under argon, solution of BuLi in hexane (2.5 *M*; 54 ml, 135 mmol) was added dropwise at –78°C. The mixture was stirred at this temperature for 6 h to give a white suspension. Triisopropylborate (60 ml, 258 mmol) was added quickly and the mixture was stirred overnight, allowing the temperature to rise gradually to room temperature. Water (300 ml) was added and the mixture was stirred at room temperature for 4 h. Organic solvents were removed on rotavapor (35°C, 40 mbar); water (1.1 l) was added and the mixture was acidified with concentrated HCl. The product was extracted into diethyl ether (7 × 300 ml), organic layer was dried over MgSO₄, and solvent was removed on rotavapor. The residue was dissolved in acetone (110 ml) and reprecipitated into mixture of water (130 ml) and concentrated HCl (70 ml), affording desired product **625** (24.3 g, 94.5%) as white powder. The product can be additionally purified by dissolution in acetone (100 ml) and addition of hexane (200 ml) to this solution. ¹H NMR (400 MHz, acetone-*d*₆): δ 7.99 (2H, dd, H-1,8), 7.90 (2H, dd, *J*_{3–4} = 7.6 Hz, *J*_{1–3} = 1.3 Hz, H-3,6), 7.80 (2H, dd, *J*_{3–4} = 7.6 Hz, *J*_{1–4} = 0.6 Hz, H-4,5), 7.19 (4H, s, OH), 2.12–2.00 (4H, m, CH₂C₅H₁₁), 1.2–0.9 [12H, m, (CH₂)₂(CH₂)₃CH₃], 0.74 (6H, t, *J* = 7.2 Hz, CH₃), 0.64–0.54 (4H, m, CH₂CH₂C₄H₉). ¹³C NMR (100 MHz, acetone-*d*₆): δ 150.87, 144.09, 133.87, 129.39, 119.92, 55.50, 41.09, 32.27, 30.39, 24.57, 23.16, 14.21.

2.7.2.1.4 2,7-Bis(4,4,5,5-tetramethyl-1,3,2-dioxaborolan-2-yl)-9,9-dioctylfluorene (**626**) (Chart 2.154)

From Sonar, P., Zhang, J., Grimsdale, A.C., Müllen, K., Surin, M., Lazzaroni, R., Leclère, P., Tierney, S., Heeney, M., and McCulloch, I., *Macromolecules*, 37: 709–715, 2004. Copyright 2004, American Chemical Society, Washington, D.C. With permission.

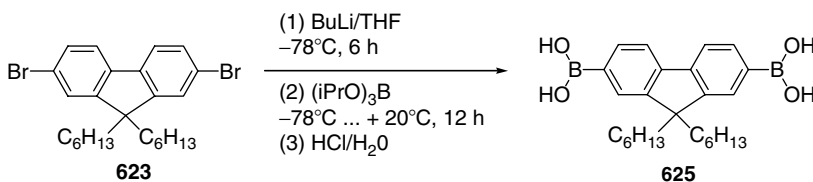


Chart 2.153

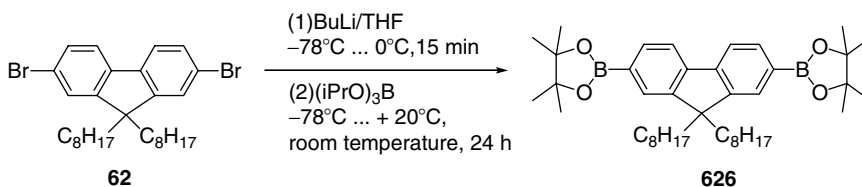


Chart 2.154

To a stirred solution of 2,7 dibromo-9,9-dioctylfluorene **624** (5.0 g, 9.1 mmol) in THF (70 ml) at -78°C was added dropwise *n*-butyllithium in hexanes (7.6 ml, 2.5 *M*, 19 mmol) at -78°C . The mixture was warmed to 0°C for 15 min and then cooled back to -78°C . 2-Isopropoxy-4,4,5,5-tetramethyl-1,3,2-dioxaborolane (4.0 g, 21.5 mmol) was added rapidly to the solution, and the resulting mixture was warmed to room temperature and stirred for 24 h. The mixture was then poured into water and extracted with diethyl ether. The organic extract was washed with brine and dried over magnesium sulfate. The solvent was removed under reduced pressure, and the crude product was purified by column chromatography eluting with 2% ethyl acetate and hexane to give 2,7-*bis*(4,4,5,5-tetramethyl-1,3,2-dioxaborolan-2-yl)-9,9-dioctylfluorene **626** as a pale yellow solid (3.80 g, 65%). HRMS: Calcd for $\text{C}_{41}\text{H}_{64}\text{B}_2\text{O}_4$: 642.59. Found: 642.37. ^1H NMR (250 MHz, CD_2Cl_2): δ 7.83 (d, 2H), 7.76 (s, 2H), 7.73 (d, 2H), 2.05 (m, 4H), 1.44 (s, 24H), 1.25–1.09 (m, 20H), 0.82 (t, 6H), 0.59 (m, 4H). ^{13}C NMR (62.5 MHz, CD_2Cl_2): δ 150.35, 143.82, 133.84, 128.74, 119.23, 83.51, 54.96, 39.36, 31.68, 29.89, 29.08, 29.00, 24.87, 23.50, 22.49, 13.96.

2.7.2.2 Suzuki-Coupling Polymerization (Chart 2.155)

From Ranger, M., Rondeau, D., and Leclerc, M., *Macromolecules*, 30: 7686, 1997. Copyright 1997, American Chemical Society, Washington, D.C. With permission.

Carefully purified 2,7-dibromofluorene derivative (1 equivalent), 2,7-*bis*(4,4,5,5-tetramethyl-1,3,2-dioxaborolan-2-yl)-9,9-dioctylfluorene **626** (1 equivalent), and $\text{Pd}(\text{PPh}_3)_4$ (1.5–0.5 mol%) were dissolved in a mixture of toluene ([monomer] = 0.5 *M*) and aqueous 2 *M* Na_2CO_3 (or K_2CO_3) (1:1.5 toluene). The solution was first put under a nitrogen atmosphere and was refluxed with vigorous stirring for 48 h. The whole mixture was then poured into methanol (150 ml). The precipitated material was recovered by filtration through a Büchner funnel and washed with dilute HCl. The solid material was washed for 24 h in a Soxhlet apparatus using acetone to remove oligomers and catalyst residues. The resulting polymers were soluble in THF and CHCl_3 . Yields: ~65–90%.

Poly[2,7-(9,9-dioctylfluorene)] **196**. ^1H NMR (400 MHz, CDCl_3): δ (ppm) 7.85 (2H, d), 7.68 (4H, m), 2.15 (4H, m), 1.2 (24H, m), 0.8 (6H, t).

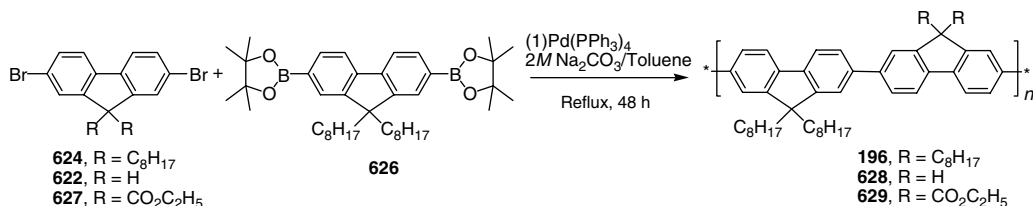


Chart 2.155

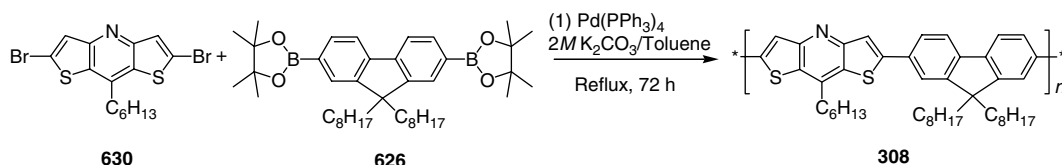


Chart 2.156

Poly[2,7'-(9,9-dioctyl-2',7-bifluorene)] **628**. ^1H NMR (400 MHz, CDCl_3): δ (ppm) 7.1–8.0 (12H, m), 4.0 (2H, s), 2.1 (4H, m), 1.1 (24H, m), 0.8 (6H, t).

Poly-2,7'-(diethyl 9,9-dioctyl-2,7'-bifluorene-9',9'-dicarboxylate)] **629**. ^1H NMR (400 MHz, CDCl_3): δ (ppm) 8.2 (2H, s), 7.75 (5H, m), 7.65 (5H, m), 4.45–4.2 (4H, m), 2.1 (4H, m), 1.7 (1.5H, m), 1.4–1.0 (24H, m), 0.9–0.6 (6H, 2t).

2.7.2.2.1 Fluorene copolymer **308** (Chart 2.156)

From Sonar, P., Zhang, J., Grimsdale, A.C., Müllen, K., Surin, M., Lazzaroni, R., Leclère, P., Tierney, S., Heeney, M., and McCulloch, I., *Macromolecules*, 37: 709, 2004. Copyright 2004, American Chemical Society, Washington, D.C. With permission.

A solution of 2,6-dibromo-4-hexylbithieno [3,2-*b*:2'3'-*e*]pyridine **630** (0.300 g, 0.466 mmol), 9,9-dioctylfluorene-2,7-di(ethyleneboronate) **626** (0.202 g, 0.466 mmol), and $\text{Pd}(\text{PPh}_3)_4$ (0.020 g, 0.5 mol%) in a mixture of toluene (15 ml) and aqueous 2 *M* K_2CO_3 (10 ml) was refluxed with vigorous stirring for 72 h under N_2 . The cooled mixture was poured into methanol (150 ml), and the precipitate was recovered by filtration and washed with dilute HCl. The precipitate was then extracted with acetone in a Soxhlet apparatus for 24 h. The dried residue was dissolved in dichloromethane and stirred with EDTA solution overnight. The residue of crude polymer was twice dissolved in chloroform and reprecipitated from methanol to give the copolymer **308** as a yellow solid (0.2 g, 67%). Elemental analysis: Found: C 79.09, H 3.15, N 2.11, S 5.23%. Calculated: C 79.58, H 8.65, N 2.11, S 9.66%. GPC: $M_n = 10\,577$ g/mol, $M_w = 31\,297$ g/mol, PDI = 2.95. ^1H NMR (250 MHz, CD_2Cl_2): δ 7.88 (s, 2H), 7.82 (m, 2H), 7.59 (m, 2H), 7.24 (d, 2H), 3.10 (t, 2H), 2.1 (m, 6H), 0.9 (m, 40H). ^{13}C NMR (62.5 MHz, CD_2Cl_2): δ 155.54, 152.60, 142.00, 141.86, 138.89, 128.40, 121.17, 120.99, 120.67, 40.58, 34.64, 32.13, 31.93, 30.29, 29.54, 25.11, 22.95, 14.18.

2.7.2.3 Yamamoto Polymerization

2.7.2.3.1 Poly[(9,9-dihexylfluorene-2,7-diyl)-co-(*N*-hexylcarbazole-3,6-diyl)] **242a**

(Chart 2.157)

From Stéphan, O. and Vial, J.-C., *Synth. Met.*, 106: 115, 1999. Copyright 1999, Elsevier, Amsterdam. With permission.

Mixture of 2,7-dibromo-9,9-dihexylfluorene **623** and 3,6-dibromo-*N*-hexylcarbazole **631** (molar ratio 4:1, total 2.5 mmol), triphenylphosphine (65.6 mg, 0.25 mmol), zinc powder 100

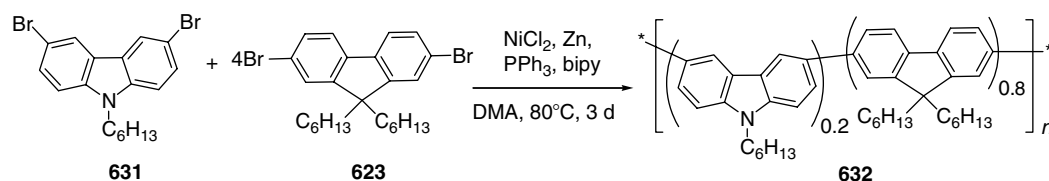


Chart 2.157

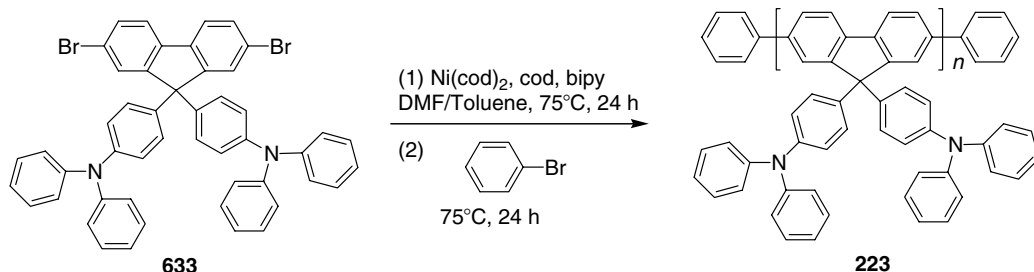


Chart 2.158

mesh, 99.998% (506 mg, 7.75 mmol), 2,2'-dipyridyl (19.5 mg, 0.125 mmol), and nickel chloride (16.2 mg, 0.125 mmol) were charged in a 20 ml flask. *N,N*-Dimethylacetamide (3 ml) was added via syringe and the mixture was stirred at 80°C for 3 days. After cooling, the polymer is precipitated by pouring the solution in a methanol-concentrated HCl mixture. The solid is collected by filtration and purified by subsequent precipitation in methanol–acetone mixture. The number-average molecular weight of the copolymer poly(DHF-*co*-NHH) **632**, evaluated by GPC calibrated with polystyrene standards, has been estimated at 4200 g/mol (polydispersity of about 2.5).

2.7.2.3.2 Poly[9,9-bis(4-diphenylaminophenyl)-2,7-fluorene] **223** (Chart 2.158)

From Ego, C., Grimsdale, A.C., Uckert, F., Yu, G., Srdanov, G., and Müllen, K., *Adv. Mater.*, 14: 809, 2002. Copyright 2002, Wiley-VCH, Weinheim. With permission.

A solution of Ni(cod)₂ (132 mg, 0.48 mmol), 2,2'-bipyridine (75 mg, 0.48 mmol), and 1,5-cyclooctadienyl (52 mg, 0.48 mmol) in dry DMF (3 ml) was heated at 75°C for 30 min under an argon atmosphere. A solution of the monomer **633** (355 mg, 0.44 mmol) in dry toluene (5 ml) was added and the mixture was heated at 75°C for a further 24 h and then poured into a methanol/HCl (2:1) mixture. The crude product was collected, dissolved in CHCl₃, and then precipitated from methanol/acetone (4:1). Residual impurities were removed by extraction with acetone in a Soxhlet apparatus to give polymer **223** (277 mg, 97%). GPC (THF) *M_n*: 12,060 g/mol, *M_w*: 25,240 g/mol, PDI 2.1 (polystyrene standards)/¹H-NMR (300 MHz, C₂D₂Cl₂): 6.60–6.72 (m, 28H, aryl H), 7.40–7.69 (b, 4H, fluorenyl H), 7.70–7.96 (b, 2H, fluorenyl H). ¹³C-NMR (126 MHz, C₂D₂Cl₂): 64.6, 120.6, 123.1, 123.3, 124.7, 125.3, 129.1, 129.4, 139.7, 146.6, 146.9, 148.0, 152.8. λ_{max} (CHCl₃): 308, 384 nm. PL (CHCl₃) 441, 419 nm; (film) 428, 452 nm.

2.7.2.3.3 Poly(dialkylfluorene-*co*-anthracene)s **240a–c** (Chart 2.159)

From Klärner, G., Davey, M.H., Chen, E.-D., Scott, J.C., and Miller, R.D., *Adv. Mater.*, 13: 993–997, 1998. Copyright 1998, Wiley-VCH, Weinheim. With permission.

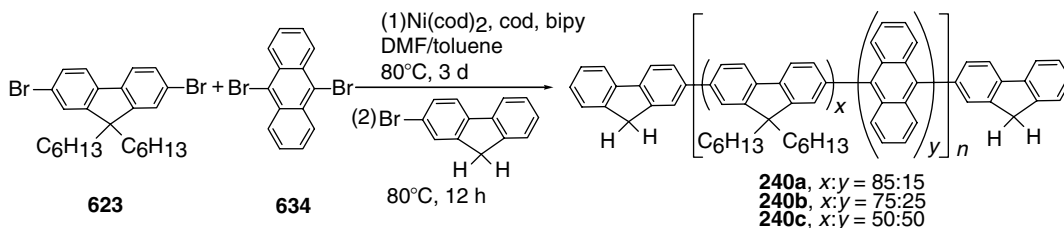


Chart 2.159

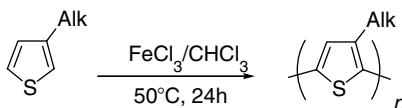


Chart 2.160

Into a Schlenk tube was placed *bis*(1,5-cyclooctadiene)-nickel(0) (2.6 mmol), 2,2'-bipyridyl (2.6 mmol), 1,5-cyclooctadiene (0.2 ml), DMF (4 ml), and toluene (8 ml). The reaction mixture was heated to 80°C for 0.5 h under argon. The dibromide comonomers **623** and **634** dissolved in degassed toluene (8 ml; molar ratio of dibromides to nickel complex: 0.65) were added under argon to the DMF–toluene solution and the polymerization maintained at 80°C for 3 days in the dark. 2-Bromofluorene (molar ratio of dibromides to monobromide: 0.1) dissolved in degassed toluene (1 ml) was added and the reaction continued for 12 h. The polymers were precipitated by addition of the hot solution dropwise to an equivolume mixture of concentrated HCl, methanol, and acetone. The isolated polymers were then dissolved in toluene or dichloromethane and reprecipitated with methanol/acetone (1:1). The copolymers were dried at 80°C *in vacuo*. The isolated yields of copolymers **240a–c** were 79–85%.

2.7.3 SYNTHESIS OF POLYTHIOPHENES

2.7.3.1 Polymerization of Thiophene Monomers with FeCl₃ (Chart 2.160)

From Pomerantz, M., Tseng, J.J., Zhu, H., Sproull, S.J., Reynolds, J.R., Uitz, R., Amott, H.G., and Haider, M.I., *Synth. Met.*, 41–43: 825, 1991. Copyright 1991, Elsevier, Amsterdam. With permission.

Into a 100-ml, three-neck flask equipped with a magnetic stirring bar, condenser, dropping funnel, and an inlet for dry air was put 3-alkylthiophene (7 mmol). A solution of anhydrous FeCl₃ (1.0 g) in chloroform (50 ml) was added to the alkylthiophene over about 20 min and the solution became dark. The mixture was then warmed to 50°C and stirred for 24 h at this temperature, while dry air was bubbled through to remove HCl from the reaction mixture. The black mixture was washed with water to remove excess FeCl₃ to give a dark-green-black mixture. This was stirred with concentrated aqueous ammonia (20 ml) and chloroform for 30 min at room temperature to produce a yellowish-red chloroform solution of dedoped polymer, which was washed several times with water and dried over MgSO₄. Removal of the solvent gave 60–97% yield of the dark-purple poly(3-alkylthiophene). Soxhlet extraction with methanol was used to remove the low-molecular-weight fractions from the bulk polymer.

2.7.3.2 Yamamoto Polymerization (Chart 2.161)

From Yamamoto, T., Morita, A., Miyazaki, Y., Maruyama, T., Wakayama, H., Zhou, Z.H., Nakamura, Y., Kanbara, T., Sasaki, S., and Kubota, K., *Macromolecules*, 25: 1214, 1992. Copyright 1992, American Chemical Society, Washington, D.C. With permission.

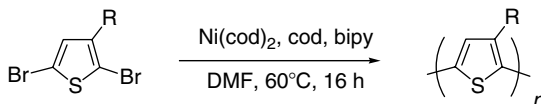


Chart 2.161

$\text{Ni}(\text{cod})_2$ (1.59 g, 6.00 mmol), 1,5-cyclooctadiene (531 mg, 5.00 mmol), and 2,2'-bipyridyl (937 mg, 6.00 mmol) were dissolved in DMF (20 ml), in a Schlenk tube under argon. To the solution was added 2,5-dibromothiophene (1.21 g, 5.00 mmol) at room temperature. The reaction mixture was stirred at 60°C for 16 h to yield a reddish-brown precipitate. The reaction mixture was then poured into HCl-acidic methanol, and the precipitate of PT was separated by filtration. The precipitate was washed with HCl-acidic methanol, ethanol, hot toluene, a hot aqueous solution of EDTA (pH = 3.80), a hot aqueous solution of EDTA (pH = 9), and distilled water in this order and dried under vacuum to yield a reddish-brown powder of PT.

When 3(4)-substituted thiophenes (e.g., 3-hexylthiophene) are used as monomers, the polymers are partly or completely soluble in low polar organic solvents like toluene, chloroform, dichloromethane, THF. Therefore, after washing with ethanol, the polymer is dried, then dissolved in chloroform and reprecipitated into methanol or acetone to remove low-molecular-weight fractions. The solid is collected by filtration, washed with methanol, and dried *in vacuo*.

2.7.3.3 McCullough Method of Preparation of Regioregular HT Poly(3-Alkylthiophenes) (Chart 2.162)

From McCullough, R.D., Lowe, R.D., Jayaraman M., and Anderson, D.L., *J. Org. Chem.*, 58: 904, 1993. Copyright 1993, American Chemical Society, Washington, D.C. With permission.

2.7.3.3.1 Preparation of monomers: 2-bromo-3-*n*-butylthiophene (**386**, $R = n\text{-C}_4\text{H}_9$)

Into a dry round-bottom flask was placed 68.5 ml (0.8 *M*) of acetic acid, which was then sparged with argon (5 min). Then 7.7 g (0.055 mol) of freshly distilled 3-*n*-butylthiophene was added. The mixture was cooled to 10°C, whereupon a 2.5 *M* solution of bromine (2.8 ml, 0.055 mol) in acetic acid was added dropwise from an addition funnel over a period of 30 min, while the temperature was maintained at 10–15°C. The material was then stirred in an ice bath for 30 min and was then poured onto ice. The mixture was then extracted into CHCl_3 , the CHCl_3 layer washed with NaOH until pH = 6 and dried over MgSO_4 , and the solvent removed by rotary evaporation. The product was twice-distilled (80°C/1.8 mmHg) to yield 5.8 g (48%) of **386** ($R = n\text{-C}_4\text{H}_9$). In a similar manner, the monomers with $R = n\text{-C}_6\text{H}_{13}$ (49%), $n\text{-C}_8\text{H}_{17}$ (40%), $n\text{-C}_{12}\text{H}_{25}$ (41%) have been obtained.

2.7.3.3.2 Polymerization of **386** ($R = n\text{-C}_6\text{H}_{13}$) using 0.5 mol% catalyst

Into a dry round-bottom flask was placed dry diisopropylamine (2.11 ml, 15 mmol) and freshly distilled, dry THF (75 ml, 0.2 *M*). To the mixture was added 6.0 ml of 2.5 *M* *n*-BuLi (15 mmol) at room temperature. The mixture was cooled to –40°C and stirred for 40 min. The reaction mixture, containing LDA, was then cooled to –78°C, and 2-bromo-3-hexylthiophene

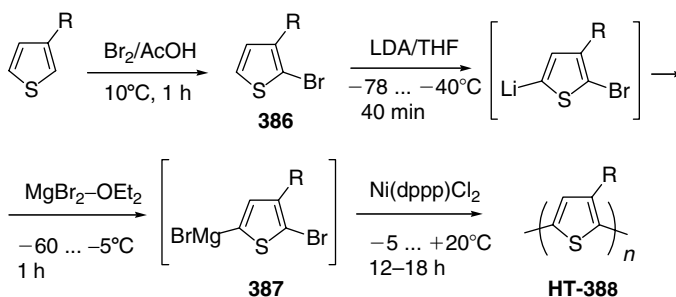


Chart 2.162

(**386**, $R = n\text{-C}_6\text{H}_{13}$) (3.7 g, 15 mmol) was added. The mixture was stirred for 40 min at -40°C . The mixture was then cooled to -60°C , $\text{MgBr}_2\cdot\text{Et}_2\text{O}$ (3.87 g, 15 mmol) was added, and the reaction was stirred at -60°C for 20 min. The reaction was then warmed to -40°C and stirred for 15 min. The reaction was then allowed to slowly warm to -5°C , whereupon all of the $\text{MgBr}_2\cdot\text{Et}_2\text{O}$ had reacted. At -5°C , Ni(dppp)Cl_2 (39 mg, 0.072 mmol, 0.48 mol%) was added. The mixture was allowed to warm to room temperature overnight ($\approx 12\text{--}18$ h). The polymer was then precipitated with MeOH (300 ml), and the resulting red precipitate was then filtered and washed with MeOH, H_2O , and MeOH again. The solid was then dried under vacuum. Removal of oligomers and impurities was achieved by subjecting the solid to Soxhlet extractions with MeOH first followed by hexanes. The polymer was then dissolved in CHCl_3 using a Soxhlet extractor, the CHCl_3 was removed, and the residue was dried under vacuum to yield 760 mg (36% yield) of 95% HT coupled P3HT **HT-388** ($R = n\text{-C}_6\text{H}_{13}$). The most recent preparation (precipitation with hexane) resulted in 98% HT-HT-coupled polymer. GPC analysis (THF-soluble fraction): $M_w \approx 10,000$ and $\text{PDI} = 1.6$.

2.7.3.3.3 Polymerization of **386** ($R = n\text{-C}_8\text{H}_{17}$) using 2×0.5 mol% catalyst

The exact procedure was performed as listed above except on a 18 mmol scale; however, after stirring for 15 h, 0.41 mol% of Ni(dppp)Cl_2 was added (40 mg, 0.074 mmol) at 25°C . The solution was then stirred an additional 18 h. The polymer was then precipitated with MeOH (400 ml) and allowed to remain for 2 days in MeOH, and the red precipitate was allowed to settle. The solution was decanted and the solid filtered and washed with MeOH, H_2O , and MeOH again. The solid was dried under vacuum and Soxhlet extracted with MeOH and hexanes. The polymer was then dissolved in CHCl_3 using a Soxhlet extractor, the CHCl_3 was removed, and the residue was dried and yielded 2.28 g (65% yield) of 96% HT poly(3-octylthiophene). The most recent preparation gave 97% HT-HT coupling. GPC analysis (THF-soluble fraction): $M_w = 24,424$ and $\text{PDI} = 1.98$.

2.7.3.4 Rieke-Zinc (Zn^*)-Mediated Polymerization

2.7.3.4.1 Typical preparation of Rieke zinc (Zn^*)

From Chen, T.-A., Wu, X., and Rieke, R.D., *J. Am. Chem. Soc.*, 117: 233, 1995. Copyright 1995, American Chemical Society. Washington, D.C. With permission.

Procedure A. Finely cut (ca. $5 \times 5 \times 0.75$ mm) lithium (0.15 g, 22.0 mmol) and a catalytic amount (10 mol%) of naphthalene (0.28 g, 2.20 mmol) were weighed into a 100-ml, two-neck, round-bottom flask equipped with an elliptical Teflon stir bar in an argon drybox; the flask was sealed with a septum and a condenser topped with stopcock outlet. Similarly, ZnCl_2 (1.50 g, 11.0 mmol) was weighed into a 50 ml, two-neck, round-bottom flask, equipped with a stir bar; the flask was sealed with a septum and stopcock. The flasks were then transferred to the manifold system and the argon inlet fitted. THF (15 ml) was added to the flask with lithium and naphthalene, while ZnCl_2 was dissolved in THF (25 ml). To the flask with lithium and naphthalene, the THF solution of ZnCl_2 was transferred via cannula dropwise so as addition was completed in ca. 1.5 h under moderate stirring. The reaction mixture was further stirred until the lithium was consumed (ca. 30 min), and the resulting black suspension of active zinc thus prepared was ready for use.

Procedure B. Finely cut (0.15 g, 22.0 mmol) and a stoichiometrical amount of naphthalene (2.80 g, 22.0 mmol) were weighed into a 100-ml flask, and ZnCl_2 (1.5 g, 11.0 mmol) was weighed into a 50-ml flask. The Lithium and naphthalene were dissolved in THF (20 ml) in ca. 2 h. ZnCl_2 was dissolved in THF (20 ml) and the solution was transferred into the flask with lithium naphthalide via cannula over 10 min. The reaction mixture was further stirred for 1 h, and the resulting black suspension of active zinc thus prepared was ready for use.

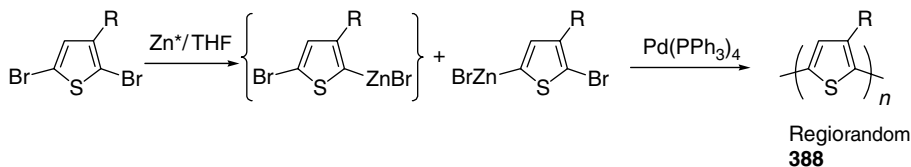


Chart 2.163

2.7.3.4.2 *Pd-Catalyzed preparation of regiorandom poly(3-alkylthiophenes) (HT-388) from 2,5-dibromoalkylthiophenes (389) and Rieke zinc (Zn*)*
(Chart 2.163)

From Chen, T.-A., Wu, X., and Rieke, R.D., *J. Am. Chem. Soc.*, 117: 233, 1995. Copyright 1995, American Chemical Society, Washington, D.C. With permission.

2,5-Dibromo-3-alkylthiophene (alkyl = *n*-C₆H₁₃ or *n*-C₈H₁₇) (10.0 mmol) in THF (20 ml) was added to the flask with newly prepared Zn* (11.0 mmol in 40 ml of THF) via cannula at 0°C, and the mixture was stirred for 1 h at room temperature. A 0.2 mol% amount of Pd(PPh₃)₄ (23.1 mg, 0.02 mmol, in 20 ml of THF) was added via cannula. The mixture was then stirred for 24 h at room temperature (or reflux for 6 h). The polymer was precipitated with a solution of MeOH (100 ml) and 2 N HCl (50 ml), and purified by reprecipitation from the polymer solution of chloroform upon addition of MeOH. After drying under vacuum, red-brown, rubber-like polymers of regiorandom PATs were obtained in 97–99% yields.

2.7.3.4.3 *Ni-Catalyzed preparation of regioregular HT poly(3-alkylthiophenes) (HT-388) from 2,5-dibromoalkylthiophenes (389) and Rieke zinc (Zn*)* (Chart 2.164).

From Chen, T.-A., Wu, X., and Rieke, R.D., *J. Am. Chem. Soc.*, 117: 233, 1995. Copyright 1995, American Chemical Society, Washington, D.C. With permission.

2,5-Dibromo-3-alkylthiophene (**389**, alkyl = *n*-C₄H₉, *n*-C₆H₁₃, *n*-C₈H₁₇, *n*-C₁₀H₂₁, *n*-C₁₂H₂₅, *n*-C₁₄H₂₉) (10.0 mmol, in 20 ml of THF) was added via a cannula to the newly prepared Zn* (11.0 mmol, in 40 ml of THF) at –78°C. The mixture was stirred for 1 h at this temperature and allowed to warm to 0°C naturally in ca. 3 h; 0.2 mol% of Ni(dppe)Cl₂ (11.0 mg, 0.02 mmol, in 20 ml of THF) was added via cannula at 0°C. The mixture was stirred for 24 h at room temperature. A dark-purple precipitate was formed gradually in this period. The mixture was poured into a solution of MeOH (100 ml) and 2 N HCl (50 ml); the resulting dark precipitate was filtered and washed with MeOH and 2 N HCl solution, and then dried. Reprecipitation of polymer from chloroform solution upon addition of MeOH and drying under vacuum gave dark polymer of regioregular HT poly(3-alkylthiophenes). Purification of polymer by Soxhlet extractions with MeOH for 24 h and then with hexane for 24 h afforded of regioregular **HT-388** in 67–82% yields. The regioregularity of the polymers, according to NMR analysis, was from 97 to >98.5% of HT linkage.

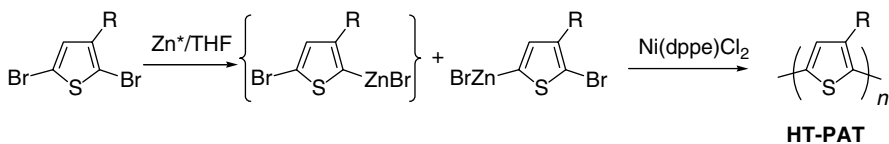


Chart 2.164

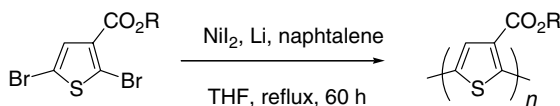


Chart 2.165

2.7.3.5 Rieke-Nickel-Catalyzed Polymerization

2.7.3.5.1 Poly(alkyl thiophene-3-carboxylates) (**400** and **401**) (Chart 2.165)

From Pomerantz, M., Cheng, Y., Kasim, R.K., and Elsenbaumer, R.L., *J. Mater. Chem.*, 9: 2155–2163, 1999. Copyright 1999, The Royal Society of Chemistry, Cambridge. With permission.

A 25-ml one-necked flask was charged with NiI_2 (1.563 g, 4.994 mmol), freshly cut lithium (0.080 g, 11 mmol), naphthalene (0.064 g, 0.50 mmol), and THF (10 ml), and the mixture was stirred vigorously at room temperature for 12 h under argon. To the precipitated black-nickel powder, alkyl 2,5-dibromo-3-carboxylate ($\text{R} = n\text{-C}_6\text{H}_{13}$ or $n\text{-C}_8\text{H}_{17}$) (2.0 mmol) in THF (5 ml) was added directly via a syringe. The mixture was refluxed for 60 h under argon. The reaction mixture was diluted with diethyl ether to 100 ml, and then filtered to remove the metal powder. The dark-red organic phase was washed with water (3×50 ml) and dried over MgSO_4 . The ether was removed with rotary evaporator, and a dark-red solid polymer was obtained. The polymer was extracted with methanol in a Soxhlet extractor for 48 h to remove the low-molecular-weight material and, after drying under vacuum at room temperature, a red solid was obtained. The yields are 32–33%.

2.7.4 COMMERCIAL AVAILABILITY OF LIGHT-EMITTING POLYMERS

To address new researchers entering the field of PLED, especially those, not trained in organic synthesis, we should mention that many LEP are now available commercially from several companies, such as Aldrich (www.sigma-aldrich.com), American Dyes Source (www.adsdyes.com), H.W. Sands (<http://www.hwsands.com/>), and Dow Chemicals (<http://www.dow.com/pled/>).

In Aldrich, the widest collection belongs to PPV derivatives, which includes dialkoxy-PPVs (e.g., MEH-PPV **13**, **14**), phenyl-substituted PPV **43**, *meta-para*-linked PPV copolymer **159**, etc. Many monomer precursors for PPV synthesis by Gilch and Wittig procedure as well as the Wessling–Zimmerman precursor **2** for unsubstituted PPV are also available.

ACKNOWLEDGMENTS

We thank Dr. Weishi Wu at DuPont Display and Dr. Gary A. Johansson at DuPont CRD for proof reading of the manuscript. DFP thanks the National Science and Engineering Research Council for support through the Discovery and AGENO grants.

REFERENCES

1. J.H. Burroughes, D.D.C. Bradley, A.R. Brown, R.N. Marks, K. Mackay, R.H. Friend, P.L. Burn, and A.B. Holmes, Light-emitting diodes based on conjugated polymers, *Nature*, 347: 539–541, 1990.
2. R.H. Partridge, Radiation Sources, U.S. Patent 3,995,299, November 30, 1976.
3. R.H. Partridge, Electroluminescence from polyvinylcarbazole films (parts 1–4), *Polymer*, 24: 733–762, 1983.

4. R.J. Visser, Application of polymer light-emitting materials in light-emitting diodes, backlights and displays, *Philips J. Res.*, 51: 467–477, 1998.
5. R.H. Friend, D.D.C. Bradley, and P.D. Townsend, Photo-excitation in conjugated polymers, *J. Phys. D: Appl. Phys.*, 20: 1367–1384, 1987.
6. D.R. Baigent, N.C. Greenham, J. Gruener, R.N. Marks, R.H. Friend, S.C. Moratti, and A.B. Holmes, Light-emitting diodes fabricated with conjugated polymers — recent progress, *Synth. Met.*, 67: 3–10, 1994.
7. A. Greiner, B. Bolle, P. Hesemann, J.M. Oberski, and R. Sander, Preparation and structure–property relationships of polymeric materials containing arylenevinylene segments — perspectives for new light-emitting materials, *Macromol. Chem. Phys.*, 197: 113–134, 1996.
8. J.L. Segura, The chemistry of electroluminescent organic materials, *Acta Polym.*, 49: 319–344, 1998.
9. R.H. Friend, R.W. Gymer, A.B. Holmes, J.H. Burroughes, R.N. Marks, C. Taliani, D.D.C. Bradley, D.A. Dos Santos, J.L. Brédas, M. Lögdlung, and W.R. Salaneck, Electroluminescence in conjugated polymers, *Nature*, 397: 121–127, 1999.
10. U. Mitschke and P. Bäuerle, The electroluminescence of organic materials, *J. Mater. Chem.*, 10: 1471–1507, 2000.
11. R.E. Martin, F. Geneste, and A.B. Holmes, Synthesis of conjugated polymers for application in light-emitting diodes (PLEDs), *C.R. Acad. Sci. Paris, t. I, Série IV*: 447–470, 2000.
12. A. Greiner, Design and synthesis of polymers for light-emitting diodes, *Polym. Adv. Technol.*, 9: 371–389, 1998.
13. L. Dai, B. Winkler, L. Dong, L. Tong, and A.W.H. Mau, Conjugated polymers for light-emitting applications, *Adv. Mater.*, 13: 915–925, 2001.
14. I.D. Rees, K.L. Robinson, A.B. Holmes, C.R. Towns, and R. O'Deil, Recent Developments in Light-Emitting Polymers, *MRS Bulletin*, June 2002, pp. 451–455.
15. F. Babudri, G.M. Farinola, and F. Naso, Synthesis of conjugated oligomers and polymers: the organometallic way, *J. Mater. Chem.*, 14: 11–34, 2004.
16. L. Akcelrud, Electroluminescent polymers, *Prog. Polym. Sci.*, 28: 875–962, 2003.
17. N. Tessler, G.J. Denton, and R.H. Friend, Lasing from conjugated-polymer microcavities, *Nature*, 382: 695–697, 1996.
18. F. Hide, M. Díaz-García, M.R. Andersson, Q. Pei, and A.J. Heeger, Semiconducting polymers: a new class of solid-state laser materials, *Science*, 273: 1833–1836, 1996.
19. G. Yu, J. Gao, J.C. Hummelen, F. Wudl, and A.J. Heeger, Polymer photovoltaic cells: enhanced efficiencies via a network of internal donor–acceptor heterojunctions, *Science*, 270: 1789–1791, 1995.
20. A. Kraft, A.C. Grimsdale, and A.W. Holmes, Electroluminescent conjugated polymers — seeing polymers in a new light, *Angew. Chem. Int. Ed.*, 37: 402–428, 1998.
21. R.A. Wessling and R.G. Zimmerman, Polyelectrolytes from Bis Sulfonium Salts, U.S. Patent 3,401,152, 1968.
22. (a) A. Beerden, D. Vanderzande, and J. Gelan, The effect of anions on the solution behaviour of poly(xylylene tetrahydrothiophenium chloride) and on the elimination to poly(*p*-phenylene vinylene), *Synth. Met.*, 52: 387–394, 1992; (b) R.O. Garay, U. Baier, C. Bubeck, and K. Müllen, Low-temperature synthesis of poly(*p*-phenylene vinylene) by the sulfonium salt route, *Adv. Mater.*, 5: 561–564, 1993.
23. P.L. Burn, A.B. Holmes, A. Kraft, D.D.C. Bradley, A.R. Brown, R.H. Friend, and R.W. Cymer, Chemical tuning of electroluminescent copolymers to improve emission efficiency and allow patterning, *Nature*, 356: 47–49, 1992.
24. D.A. Halliday, P.L. Burn, D.D.C. Bradley, R.H. Friend, O.M. Gelsen, A.B. Holmes, A. Kraft, J.H.F. Martens, and K. Pichler, Large changes in optical response through chemical pre-ordering of poly(*p*-phenylene vinylene), *Adv. Mater.*, 5: 40–43, 1993.
25. S. Son, A. Dodabalapur, A.J. Lovinger, and M.E. Galvin, Luminescence enhancement by the introduction of disorder into poly(*p*-phenylene vinylene), *Science*, 269: 376–378, 1995.
26. W.J. Mitchell, C. Pena, and P.L. Burn, Thermal routes to low HOMO–LUMO energy gap poly(arylene vinylene)s, *J. Mater. Chem.*, 12: 200–205, 2002.
27. A. Marletta, F.A. Castro, C.A.M. Borges, O.N. Oliveira, Jr., R.M. Faria, and F.E.G. Guimarães, Enhanced optical properties of layer-by-layer films of poly(*p*-phenylene vinylene) alternated

- with a long chain counterion and converted at low temperatures, *Macromolecules*, 35: 9105–9109, 2002.
28. S. Iwatsuki, M. Kubo, and T. Kumeuchi, New method for preparation of poly(phenylene vinylene) film, *Chem. Lett.*, 2: 1971–1974, 1991.
 29. E.G.J. Staring, D. Braun, G.L.J.A. Rikken, R.J.C.E. Demandt, Y.A.R.R. Kessener, M. Bauwmans, and D. Broer, Chemical vapour deposition of poly(1,4-phenylene vinylene) films, *Synth. Met.*, 67: 71–75, 1994.
 30. (a) K.M. Vaeth and K.F. Jenson, Selective growth of poly(*p*-phenylene vinylene) prepared by chemical vapor deposition, *Adv. Mater.*, 11: 814–820, 1999; (b) K.M. Vaeth and K.F. Jenson, Chemical vapor deposition of poly(*p*-phenylene vinylene) based light emitting diodes with low turn on voltage, *Appl. Phys. Lett.*, 71: 2091–2093, 1997.
 31. Y.-J. Miao and G.C. Bazan, Paracyclophene route to poly(*p*-phenylene vinylene), *J. Am. Chem. Soc.*, 116: 9379–9380, 1994.
 32. V.P. Conticello, D.L. Gin, and R.H. Grubbs, Ring-opening metathesis polymerization of substituted bicyclo[2.2.2]octadienes: a new precursor route to poly(*p*-phenylene vinylene), *J. Am. Chem. Soc.*, 114: 9708–9710, 1992.
 33. H.G. Gilch and W.L. Wheelwright, Polymerization of α -halogenated *p*-xylenes with base, *J. Polym. Sci. Part A*, 4: 1337–1349, 1966.
 34. J. Wiesecke and M. Rehahn, [2,2]Paracyclophanes with defined substitution pattern — key compounds for the mechanistic understanding of the Gilch reaction to poly(*p*-phenylene vinylene), *Angew. Chem. Int. Ed.*, 42: 567–570, 2003.
 35. B.R. Hsieh, Y. Yu, A.C. van Laeken, and H. Lee, General methodology toward soluble poly(*p*-phenylene vinylene) derivatives, *Macromolecules*, 30: 8094–8095, 1997.
 36. (a) C.J. Neef and J.P. Ferraris, MEH-PPV: improved synthetic procedure and molecular weight control, *Macromolecules*, 33: 2311–2314, 2000; (b) J.P. Ferraris and C.J. Neef, Methods for the Synthesis and Polymerization of α, α' -Dihalo-*p*-Xylenes, U.S. Patent 6,426,399 B1, July 30, 2002.
 37. A. Issaris, D. Vanderzande, and J. Gelan, Polymerization of a *p*-quinodimethane derivative to a precursor of poly(*p*-phenylene vinylene) — indications for a free radical mechanism, *Polymer*, 38: 2571–2574, 1997.
 38. H. Becker, H. Spreitzer, K. Ibrom, and W. Kreuder, New insights into the microstructure of Gilch-polymerized PPVs, *Macromolecules*, 32: 4925–4932, 1999.
 39. W.J. Swatos and B. Gordon, III, Polymerization of 2,2-di-*n*-hexyloxy- α, α' -dichloro-*p*-xylene with potassium *tert*-butoxide: a novel route to poly(2,5-di-*n*-hexyloxy-*p*-phenylene vinylene), *Polym. Prepr.*, 31(1): 505–506, 1990.
 40. D.M. Johansson, M. Theander, G. Srdanov, G. Yu, O. Inganäs, and M.R. Andersson, Influence of polymerization temperature on molecular weight, photoluminescence, and electroluminescence for a phenyl-substituted poly(*p*-phenylene vinylenes), *Macromolecules*, 34: 3716–3719, 2001.
 41. B.R. Hsieh and W.R. Feld, A dehydrochlorination (DHCL) route to poly(2,3-diphenyl-1,4-phenylene vinylene) (DP-PPV), *Polym. Prepr.*, 34(2): 410–411, 1993.
 42. L. Lutsen, P. Adriaenssens, H. Becker, A.J. Van Breemen, D. Vanderzande, and J. Gelan, New synthesis of a soluble high molecular weight poly(arylene vinylene): poly[2-methoxy-5-(3,7-dimethyloctyloxy)-*p*-phenylene vinylene]. Polymerization and device properties, *Macromolecules*, 32: 6517–6525, 1999.
 43. R.W. Lenz and C.E. Handlovits, Thermally stable hydrocarbon polymers: polyterephthalyldienes, *J. Org. Chem.*, 25: 813–817, 1960.
 44. S.C. Moratti, R. Cervini, A.B. Holmes, D.R. Baigent, R.H. Friend, N.C. Greenham, J. Grüner, and P.J. Hamer, High electron affinity polymers for LEDs, *Synth. Met.*, 71: 2117–2120, 1995.
 45. J. Liao and Q. Wang, Ruthenium-catalyzed Knoevenagel condensation: a new route toward cyano-substituted poly(*p*-phenylene vinylene)s, *Macromolecules*, 37: 7061–7063, 2004.
 46. A. Hilberer, H.-J. Brouwer, B.-J. van der Scheer, J. Wildeman, and G. Hadzioannou, Synthesis and characterization of a new efficient blue-light-emitting copolymer, *Macromolecules*, 28: 4525–4529, 1995.

47. A. Greiner and W. Heitz, New synthetic approach to poly(1,4-phenylene vinylene) and its derivatives by palladium catalyzed arylation of ethylene, *Macromol. Chem. Rapid Commun.*, 9: 581–588, 1988; and references therein.
48. R.N. McDonald and T.W. Campbell, The Wittig reaction as a polymerization method, *J. Am. Chem. Soc.*, 82: 4669–4671, 1960.
49. B. Francois, S. Izzillo, and P. Iratçabal, Substituted PPV block copolymer from anionically prepared precursor, *Synth. Met.*, 102: 1211–1212, 1999.
50. M. Aguiar, M.C. Fugihara, I.A. Hümmelgen, L.O. Péres, J.R. Garcia, J. Gruber, and L. Akcelrud, Interchain luminescence in poly(acetoxy-*p*-phenylene vinylene), *J. Lumin.*, 96: 219–225, 2002.
51. D.D.C. Bradley, Conjugated polymer electroluminescence, *Synth. Met.*, 54: 401–415, 1993.
52. M. Strukelj, F. Papadimitrakopoulos, T.M. Miller, and L.J. Rothberg, Design and application of electron-transporting organic materials, *Science*, 267: 1969–1972, 1995.
53. N. Tessler, N.T. Harroson, and R.H. Friend, High peak brightness polymer light-emitting diodes, *Adv. Mater.*, 10: 64–68, 1998.
54. M. Alvaro, A. Corma, B. Ferrer, M.S. Galletero, H. García, and E. Peris, Increasing the stability of electroluminescent phenylene vinylene polymers by encapsulation in nanoporous inorganic materials, *Chem. Mater.*, 16: 2142–2147, 2004.
55. P. Kumar, A. Mehta, S.M. Mahurin, S. Dai, M.D. Dadmun, B.G. Sumpter, and M.D. Barnes, Formation of oriented nanostructures from single molecules of conjugated polymers in microdroplets of solution: the role of solvent, *Macromolecules*, 37: 6132–6140, 2004.
56. K.-Y. Jen, L.W. Shackletter, and R. Elsenbaumer, Synthesis and conductivity of poly(2,5-dimethoxy-1,4-phenylene vinylene), *Synth. Met.*, 22: 179–183, 1987; and references therein.
57. I. Murase, T. Ohnishi, T. Noguchi, and M. Hirooka, Highly conducting poly(phenylene vinylene) derivatives via soluble precursor process, *Synth. Met.*, 17: 639–644, 1987.
58. S.H. Askari, S.D. Rughooputh, and F. Wudl, Soluble substituted-polyphenylene vinylene (PPV) conducting polymers: spectroscopic studies, *Synth. Met.*, 29: E129–E134, 1989.
59. F. Wudl and G. Srdanov, Conducting Polymer Formed of Poly(2-Methoxy-5- (2'-Ethylhexyloxy)-*p*-Phenylene Vinylene), U.S. Patent 5,189,136, February 23, 1993.
60. D.W.J. McCallien, A.C. Thomas, and P.L. Burn, A study of the molecular weight of the chloro-precursor polymer to MEHPPV, *J. Mater. Chem.*, 9: 847–849, 1999.
61. P.L. Burn, A.W. Grice, A. Tajbakhsh, D.D.C. Bradley, and A.C. Thomas, Insoluble poly [2-(2'-ethylhexyloxy)-5-methoxy-1,4-phenylene vinylene] for use in multiplayer light-emitting diodes, *Adv. Mater.*, 9: 1171–1176, 1997.
62. D. Braun and A.J. Heeger, Visible light emission from semiconducting polymer diodes, *Appl. Phys. Lett.*, 58: 1982–1984, 1991.
63. Q. Pei, G. Yu, C. Zhang, Y. Yang, and A.J. Heeger, Polymer light-emitting electrochemical cells, *Science*, 269: 1086–1088, 1995.
64. Q. Pei, Y. Yang, C. Zhang, and A.J. Heeger, Polymer light-emitting electrochemical cells: *in situ* formation of a light-emitting p–n junction, *J. Am. Chem. Soc.*, 118: 3922–3929, 1996.
65. S.A. Carter, M. Angelopoulos, S. Karg, P.J. Brock, and J.C. Scott, Polymeric anodes for improved polymer light-emitting diode performance, *Appl. Phys. Lett.*, 70: 2067–2069, 1997.
66. Y. Cao, G. Yu, and A.J. Heeger, Efficient, low operating voltage polymer light-emitting diodes with aluminum as the cathode material, *Adv. Mater.*, 10: 917–920, 1998.
67. V. Blyznyiuk, B. Ruhstaller, P.J. Brock, U. Scherf, and S.A. Carter, Self-assembled nanocomposite polymer light-emitting diodes with improved efficiency and luminance, *Adv. Mater.*, 11: 1257–1261, 1999.
68. Y. Cao, I.D. Parker, G. Yu, C. Zhang, and A.J. Heeger, Improved quantum efficiency for electroluminescence in semiconducting polymers, *Nature*, 397: 414–417, 1999.
69. T.-W. Lee, O.O. Park, J.-J. Kim, J.-M. Hong, and Y.C. Kim, Efficient photoluminescence and electroluminescence from environmentally stable polymer/clay nanocomposites, *Chem. Mater.*, 13: 2217–2222, 2001.
70. B.J. Matterson, J.M. Lupton, A.F. Safonov, M.G. Salt, W.L. Barnes, and I.D.W. Samuel, Increased efficiency and controlled light output from a microstructured light-emitting diode, *Adv. Mater.*, 13: 123–127, 2001.

71. M.M. Alam, and S.A. Jenekhe, Polybenzobisazoles as efficient electron-transport materials for improving the performance and stability of polymer light-emitting diodes, *Chem. Mater.*, 14: 4775–4780, 2002.
72. Y.-H. Niu, J. Huang, and Y. Cao, High-efficiency polymer light-emitting diodes with stable saturated red emission: use of carbazole-based copolymer blends in a poly(*p*-phenylene vinylene) derivative, *Adv. Mater.*, 15: 807–811, 2003.
73. X.Y. Deng, W.M. Lau, K.Y. Wong, K.H. Low, H.F. Chow, and Y. Cao, High efficiency low operating voltage polymer light-emitting diodes with aluminum cathode, *Appl. Phys. Lett.*, 84: 3522–3524, 2004.
74. H. Spreitzer, H. Becker, E. Kluge, W. Kreuder, H. Schenk, R. Demandt, and H. Schöo, Soluble phenyl-substituted PPVs — new materials for highly efficient polymer LEDs, *Adv. Mater.*, 10: 1340–1343, 1998.
75. H. Frohne, D.C. Müller, and K. Meerholz, Continuously variable hole injection in organic light emitting diodes, *Chemphyschem.*, 707–711, 2002.
76. I.D. Parker, Y. Cao, and C.Y. Yang, Lifetime and degradation effects in polymer light-emitting diodes, *J. Appl. Phys.*, 85: 2441–2447, 1999.
77. E. Peeters, M.P.T. Christiaans, R.A.J. Janssen, H.F.M. Schöo, H.P.J.M. Dekkers, and E.W. Meijer, Circularly polarized electroluminescence from a polymer light-emitting diode, *J. Am. Chem. Soc.*, 119: 9909–9910, 1997.
78. B.S. Chuah, F. Cacialli, D.A. dos Santos, N. Feeder, J.E. Davies, S.C. Moratti, A.B. Holmes, R.H. Friend, and J.L. Brédas, A highly luminescent polymer for LEDs, *Synth. Met.*, 102: 935–936, 1999.
79. R.E. Martin, F. Geneste, B.S. Chuah, C. Fischmeister, Y. Ma, A.B. Holmes, R. Riehn, F. Cacialli, and R.H. Friend, Versatile synthesis of various conjugated aromatic homo- and copolymers, *Synth. Met.*, 122: 1–5, 2001.
80. S.-C. Lo, A.K. Sheridan, I.D.W. Samuel, and P.L. Burn, Comparison of the electronic properties of poly[2-(2'-ethylhexyloxy)-1,4-phenylene vinylene] prepared by different precursor routes, *J. Mater. Chem.*, 9: 2165–2170, 1999.
81. F. Wudl and H.M. Peters, Highly Soluble, Conductive, Luminescent Polyphenylene Vinylenes, and Products and Uses Thereof, PCT Patent Appl. WO 94/20589, September 15, 1994.
82. P.L. Burn, D.D.C. Bradley, R.H. Friend, D.A. Halliday, A.B. Holmes, R.W. Jackson, and A. Kraft, Precursor route chemistry and electronic properties of poly(*p*-phenylene vinylene), poly[(2,5-dimethyl-*p*-phenylene)vinylene] and poly[(2,5-dimethoxy-*p*-phenylene)vinylene], *J. Chem. Soc. Perkin Trans.*, 1: 3225–3231, 1992.
83. G.J. Sarnecki, P.L. Burn, A. Kraft, R.H. Friend, and A.B. Holmes, The synthesis and characterization of some poly(2,5-dialkoxy-1,4-phenylene vinylenes), *Synth. Met.*, 55: 914–917, 1993.
84. S. Wang, J. Yang, Y. Li, H. Lin, Z. Guo, S. Xiao, Z. Shi, D. Zhu, H.-S. Woo, D.L. Carroll, I.-S. Kee, and J.-H. Lee, Composites of C60 based poly(phenylene vinylene) dyad and conjugated polymer for polymer light-emitting devices, *Appl. Phys. Lett.*, 80: 3847–3849, 2002.
85. F. Wudl, S. Höger, C. Zhang, P. Pakbaz, and A.J. Heeger, Conjugated polymers for organic LEDs: poly[2,5-bis(3a,5b-cholestanoxo)phenylene vinylene] (BCHA-PPV); a processible, yellow light emitter, *Polym. Prepr.*, 34(1): 197–198, 1993.
86. C.L. Gettinger, A.J. Heeger, J.H. Drake, and D.J. Pine, A photoluminescence study of poly (phenylene vinylene) derivatives: the effect of intrinsic persistence length, *J. Chem. Phys.*, 101: 1673–1678, 1994.
87. F. Wudl and S. Høger, Highly Organic Solvent Soluble, Water Insoluble Electroluminescent Polyphenylene Vinylenes having Pendant Steroid Group and Products and Uses Thereof, U.S. Patent 5,679,757, October 21, 1997.
88. M.R. Andersson, G. Yu, and A.J. Heeger, Photoluminescence and electroluminescence of films from soluble PPV-polymers, *Synth. Met.*, 85: 1275–1276, 1997.
89. R.O. Garay, B. Mayer, F.E. Karasz, and R.W. Lenz, Synthesis and characterization of poly[2,5-bis(triethoxy)-1,4-phenylene vinylene], *J. Polym. Sci. A*, 33: 525–531, 1995.
90. B.S. Chuah, D.-H. Hwang, S.T. Kim, S.C. Moratti, A.B. Holmes, J.C. De Mello, and R.H. Friend, New luminescent polymers for LEDs, *Synth. Met.*, 91: 279–282, 1997.

91. M. Fahlman, M. Lögdlund, S. Stafström, W.R. Salaneck, R.H. Friend, P.L. Burn, A.B. Holmes, K. Kaeriyama, Y. Sonoda, O. Lhost, F. Meyers, and J.L. Brédas, Experimental and theoretical studies of the electronic structure of poly(*p*-phenylene vinylene) and some ring-substituted derivatives, *Macromolecules*, 28: 1959–1965, 1995.
92. L.M. Leung and G.L. Chik, Phase-transfer catalysed synthesis of disubstituted poly(phenylene vinylene), *Polymer*, 34: 5174–5179, 1993.
93. Y. Sonoda, Y. Nakao, and K. Kaeriyama, Preparation and properties of poly(1,4-phenylene vinylene) derivatives, *Synth. Met.*, 55–57: 918–923, 1993.
94. A.G.J. Staring and R.J.C.E. Demandt, Light-Emitting Diode Comprising an Active Layer of 2,5-Substituted Poly(*p*-Phenylene Vinylene), PCT Patent Appl. WO 32526, November 30, 1995.
95. B.J. Schwartz, F. Hide, M.R. Andersson, and A.J. Heeger, Ultrafast studies of stimulated emission and gain in solid films of conjugated polymers, *Chem. Phys. Lett.*, 265: 327–333, 1997.
96. S. Höger, J. McNamara, S. Schricker, and F. Wudl, Novel silicon-substituted, soluble poly(phenylene vinylene)s: enlargement of the semiconductor bandgap, *Chem. Mater.*, 6: 171–173, 1994.
97. C. Zhang, S. Hoeger, K. Pakbaz, F. Wudl, and A.J. Heeger, Improved efficiency in green polymer light-emitting diodes with air-stable electrodes, *J. Electron. Mater.*, 23: 453–458, 1994.
98. S.T. Kim, D.-H. Hwang, X.C. Li, J. Grüner, R.H. Friend, A.B. Holmes, and H.K. Shim, Efficient green electroluminescent diodes based on poly(2-dimethyloctylsilyl-1,4-phenylene vinylene), *Adv. Mater.*, 8: 979–982, 1996.
99. D.-H. Hwang, S.T. Kim, H.-K. Shim, A.B. Holmes, S.C. Moratti, and R.H. Friend, Green light-emitting diodes from poly(2-dimethyloctylsilyl-1,4-phenylene vinylene), *J. Chem. Soc., Chem. Commun.*: 2241–2242, 1996.
100. H.Y. Chu, D. Hwang, L. Do, J. Chang, H. Shim, A.B. Holmes, and T. Zyung, Electroluminescence from silyl-disubstituted PPV derivative, *Synth. Met.*, 101: 216–217, 1999.
101. Z. Chen, W. Huang, L. Wang, E. Kang, B.J. Chen, C.S. Lee, and S.T. Lee, A family of electroluminescent silyl-substituted poly(*p*-phenylene vinylene)s: synthesis, characterization, and structure–property relationship, *Macromolecules*, 33: 9015–9025, 2000.
102. T. Ahn, S. Ko, J. Lee, and H. Shim, Novel cyclohexylsilyl — or phenylsilyl-substituted poly(*p*-phenylene vinylene)s via the halogen precursor route and Gilch polymerization, *Macromolecules*, 35: 3495–3505, 2002.
103. D.-H. Hwang, J.-I. Lee, N.-S. Cho, and H.-K. Shim, Light-emitting properties of germlyl-substituted PPV derivative synthesized via soluble precursor, *J. Mater. Chem.*, 14: 1026–1030, 2004.
104. B.R. Hsieh, Y. Yu, E.W. Forsythe, G.M. Schaaf, and W.A. Feld, A new family of highly emissive soluble poly(*p*-phenylene vinylene) derivatives. A step toward fully conjugated blue-emitting poly(*p*-phenylene vinylenes), *J. Am. Chem. Soc.*, 120: 231–232, 1998.
105. H. Spreitzer, W. Kreuder, H. Becker, H. Schoo, and R. Demandt, Aryl-Substituted Poly(*p*-Arylene Vinylenes), Method for the Production and Use Thereof in Electroluminescent Components, PCT Patent Appl. WO 98/27136, June 25, 1998 (in German).
106. H. Becker, H. Spreitzer, W. Kreuder, E. Kluge, H. Schenk, I. Parker, and Y. Cao, Soluble PPVs with enhanced performance — a mechanistic approach, *Adv. Mater.*, 12: 42–48, 2000.
107. H. Becker and P. Stössel, Substituted Poly(Arylene Vinylenes), Method for the Production Thereof and Their Use in Electroluminescent Devices, PCT Patent Appl. WO 01/34722 A1, May 17, 2001 (in German).
108. M.R. Andersson, O. Thomas, W. Mammo, M. Svensson, M. Theander, and O. Inganäs, Substituted polythiophenes designed for optoelectronic devices and conductors, *J. Mater. Chem.*, 9: 1933–1940, 1999.
109. D.M. Johansson, G. Srdanov, G. Yu, M. Theander, O. Inganäs, and M.R. Andersson, Synthesis and characterization of highly soluble phenyl-substituted poly(*p*-phenylene vinylenes), *Macromolecules*, 33: 2525–2529, 2000.
110. D.M. Johansson, X. Wang, T. Johansson, O. Inganäs, G. Yu, G. Srdanov, and M.R. Andersson, Synthesis of soluble phenyl-substituted poly(*p*-phenylene vinylenes) with a low content of structural defects, *Macromolecules*, 35: 4997–5003, 2002.

111. Z. Chen, N.H.S. Lee, W. Huang, Y. Xu, and Y. Cao, New phenyl-substituted PPV derivatives for polymer light-emitting diodes — synthesis, characterization and structure–property relationship study, *Macromolecules*, 36: 1009–1020, 2003.
112. N.H.S. Lee, Z.-K. Chen, W. Huang, Y.-S. Xu, and Y. Cao, Synthesis and characterization of naphthyl-substituted poly(*p*-phenylene vinylene)s with few structural defects for polymer light-emitting diodes, *J. Polym. Sci., Part A: Polym. Chem.*, 42: 1647–1657, 2004.
113. S. Jin, M. Jang, and H. Suh, Synthesis and characterization of highly luminescent asymmetric poly(*p*-phenylene vinylene) derivatives for light-emitting diodes, *Chem. Mater.*, 14: 643–650, 2002.
114. S. Chung, J. Jin, C.H. Lee, and C.E. Lee, Improved-efficiency light-emitting diodes prepared from organic-soluble PPV derivatives with phenylanthracene and branched alkoxy pendants, *Adv. Mater.*, 10: 684–688, 1998.
115. S.H. Lee, B. Jang, and T. Tsutsui, Sterically hindered fluorenyl-substituted poly(*p*-phenylene vinylenes) for light-emitting diodes, *Macromolecules*, 35: 1356–1364, 2002.
116. S.H. Lee, T. Yasuda, and T. Tsutsui, Charge carrier mobility in blue-green emitting fluorenyl-substituted poly(*p*-phenylene vinylene)s, *J. Appl. Phys.*, 95: 3825–3827, 2004.
117. D. Shin, Y. Kim, H. You, and S. Kwon, Sterically hindered and highly thermal stable spirobi-fluorenyl-substituted poly(*p*-phenylene vinylene) for light-emitting diodes, *Macromolecules*, 36: 3222–3227, 2003.
118. S. Chung, K. Kwon, S. Lee, J. Jin, C.H. Lee, C.E. Lee, and Y. Park, Highly efficient light-emitting diodes based on an organic-soluble poly(*p*-phenylene vinylene) derivatives carrying the electron-transporting PBD moiety, *Adv. Mater.*, 10: 1112–1116, 1998.
119. K. Kim, Y. Hong, S. Lee, J. Jin, Y. Park, B. Sohn, W. Kim, and J. Park, Synthesis and luminescence properties of poly(*p*-phenylene vinylene) derivatives carrying directly attached carbazole pendants, *J. Mater. Chem.*, 11: 3023–3030, 2001.
120. J.D. Stenger-Smith, P. Zarras, L.H. Merwin, S.E. Shaheen, B. Kippelen, and N. Peyghambarian, Synthesis and characterization of poly(2,5-bis(*N*-methyl-*N*-hexylamino)phenylene vinylene), a conjugated polymer for light-emitting diodes, *Macromolecules*, 31: 7566–7569, 1998.
121. H. Meng, W. Yu, and W. Huang, Facile synthetic route to a novel electroluminescent polymer — poly(*p*-phenylene vinylene) containing a fully conjugated aromatic oxadiazole side chain, *Macromolecules*, 32: 8841–8847, 1999.
122. Z. Chen, H. Meng, Y. Lai, and W. Huang, Photoluminescent poly(*p*-phenylene vinylene)s with an aromatic oxadiazole moiety as the side chain: synthesis, electrochemistry, and spectroscopy study, *Macromolecules*, 32: 4351–4358, 1999.
123. D.W. Lee, K.-Y. Kwon, J.-I. Jin, Y. Park, Y.-R. Kim, and I.-W. Hwang, Luminescence properties of structurally modified PPVs: PPV derivatives bearing 2-(4-*tert*-butylphenyl)-5-phenyl-1,3,4-oxadiazole pendants, *Chem. Mater.*, 13: 565–574, 2001.
124. S. Jin, M. Kim, J.Y. Kim, K. Lee, and Y. Gal, High-efficiency poly(*p*-phenylene vinylene)-based copolymers containing an oxadiazole pendant group for light-emitting diodes, *J. Am. Chem. Soc.*, 126: 2474–2480, 2004.
125. J. Gordon, T.J. Sheldon, D.D.C. Bradley, and P.L. Burn, The synthesis of an electronically asymmetric substituted poly(arylene vinylene); poly{2-(2'-ethylhexyloxy)-5-[(*E*)-4''-nitrostyryl]-1,4-phenylene vinylene}, *J. Mater. Chem.*, 6: 1253–1258, 1996.
126. F.H. Boardman, A.W. Grice, M.G. Rüther, T.J. Sheldon, D.D.C. Bradley, and P.L. Burn, A new electron-withdrawing group containing poly(1,4-phenylene vinylene), *Macromolecules*, 32: 111–117, 1999.
127. S.W. Ko, B. Jung, T. Ahn, and H. Shim, Novel poly(*p*-phenylene vinylene)s with an electron-withdrawing cyanophenyl group, *Macromolecules*, 35: 6217–6223, 2002.
128. A.C. Grimsdale, F. Cacialli, J. Grüner, X. Li, A.B. Holmes, S.C. Moratti, and R.H. Friend, Novel poly(arylene vinylene)s carrying donor and acceptor substituents, *Synth. Met.*, 76: 165–167, 1996.
129. I. Kang, H. Shim, and T. Zyung, Yellow-light-emitting fluorine-substituted PPV derivative, *Chem. Mater.*, 9: 746–749, 1997.
130. R.M. Gurge, A.M. Sarker, P.M. Lahti, B. Hu, and F.E. Karasz, Light emitting properties of fluorine-substituted poly(1,4-phenylene vinylenes), *Macromolecules*, 30: 8286–8292, 1997.

131. M. Jang, S. Song, and H. Shim, Efficient green light-emitting polymer by balanced injection of electron and holes: new electron accepting perfluorinated substituent, *Polymer*, 41: 5675–5679, 2000.
132. Y. Jin, J. Kim, S. Lee, J.Y. Kim, S.H. Park, K. Lee, and H. Suh, Novel electroluminescent polymers with fluoro groups in vinylene units, *Macromolecules*, 37: 6711–6715, 2004.
133. H. Antoniadis, M.A. Abkowitz, and B.R. Hsieh, Carrier deep-trapping mobility-lifetime products in poly(*p*-phenylene vinylene), *Appl. Phys. Lett.*, 65: 2030–2032, 1994.
134. P.L. Burn, A. Kraft, D.R. Baigent, D.D.C. Bradley, A.R. Brown, R.H. Friend, R.W. Gymer, A.B. Holmes, and R.W. Jackson, Chemical tuning of the electronic properties of poly(*p*-phenylene vinylenes)-based copolymers, *J. Am. Chem. Soc.*, 115: 10117–10124, 1993.
135. Z. Bao, Z. Peng, M.E. Galvin, and E.A. Chandross, Novel oxadiazole side chain conjugated polymers as single-layer light-emitting diodes with improved quantum efficiencies, *Chem. Mater.*, 10: 1201–1204, 1998.
136. Z. Peng and J. Zhang, New oxadiazole-containing conjugated polymer for single-layer light-emitting diodes, *Chem. Mater.*, 11: 1138–1143, 1999.
137. C. Huang, W. Huang, J. Guo, C.-Z. Yang, and E.-T. Kang, A novel rigid-rod alternating poly(*p*-phenylene vinylene) derivative with oligo(ethylene oxide) side chains, *Polymer*, 42: 3929–3938, 2004.
138. B.S. Chuah, F. Geneste, A.B. Holmes, R.E. Martin, H. Rost, F. Cacialli, R.H. Friend, H.-H. Hörhold, S. Pfeiffer, and D.-H. Hwang, The copolymer route to new luminescent materials for LEDs, *Macromol. Symp.*, 154: 177–186, 2000.
139. H. Beck, H. Spreitzer, W. Kreuder, E. Kluge, H. Vestweber, H. Schenk, and K. Treacher, Advances in polymers for PLEDs: from a polymerization mechanism to industrial manufacturing, *Synth. Met.*, 122: 105–110, 2001.
140. P.K.H. Ho, J.-S. Kim, J.H. Burroughes, H. Becker, S.F.Y. Li, T.M. Brown, F. Cacialli, and R.H. Friend, Molecular-scale interface engineering for polymer light-emitting diodes, *Nature*, 404: 481–484, 2000.
141. B. Sohn, K. Kim, D.S. Choi, Y.K. Kim, S.C. Jeoung, and J. Jin, Synthesis and luminescence properties of poly[2-(9,9-dihexylfluorene-2-yl)-1,4-phenylene vinylene] and its copolymers containing 2-(2-ethylhexyloxy)-5-methoxy-1,4-phenylene vinylene units, *Macromolecules*, 35: 2876–2881, 2002.
142. Z. Peng, J. Zhang, and B. Xu, New poly(*p*-phenylene vinylene) derivatives exhibiting high photoluminescence quantum efficiencies, *Macromolecules*, 32: 5162–5164, 1999.
143. J.A. Mikroyannidis, Synthesis by Heck coupling of soluble, blue-light-emitting fully conjugated poly(*p*-phenylene vinylene)s with highly phenylated side groups, *Macromolecules*, 35: 9289–9295, 2002.
144. W.J. Feast, I.S. Millichamp, R.H. Friend, M.E. Horton, D. Phillips, S.D.D.V. Rughooputh, and G. Rumbles, Optical absorption and luminescence in poly(4,4'-diphenylenediphenylvinylene), *Synth. Met.*, 10: 181–191, 1985.
145. F. Cacialli, R.H. Friend, N. Haylett, R. Daik, W.J. Feast, D.A. dos Santos, and J.L. Brédas, Efficient green light-emitting diodes from a phenylated derivative of poly(*p*-phenylene vinylene), *Appl. Phys. Lett.*, 69: 3794–3796, 1996.
146. T. Ahn, S. Song, and H. Shim, Highly photoluminescent and blue-green electroluminescent polymers: new silyl- and alkoxy-substituted poly(*p*-phenylene vinylene) related copolymers containing carbazole or fluorene groups, *Macromolecules*, 33: 6764–6771, 2000.
147. H. Li, Y. Zhang, Y. Hu, D. Ma, L. Wang, X. Jing, and F. Wang, Novel soluble *N*-phenyl-carbazole-containing PPV for light-emitting devices: synthesis, electrochemical, optical and electroluminescent properties, *Macromol. Chem. Phys.*, 205: 247–255, 2004.
148. J.J. Kim, K.-S. Kim, H.C. Kim, and M. Ree, Synthesis and properties of photoluminescent polymers bearing electron-facilitating oxadiazole derivative side groups, *J. Polym. Sci., Part A: Polym. Chem.*, 40: 1173–1183, 2002.
149. S.-H. Jin, J.-E. Jung, D.-K. Park, B.-C. Jeon, S.-K. Kwon, Y.-H. Kim, D.-K. Moon, S.-H. Kim, and Y.-S. Gal, Synthesis and characterization of color tunable electroluminescent polymer by blending oxadiazole containing polymer, *Eur. Polym. J.*, 37: 921–925, 2001.
150. J. Shi and S. Zheng, Conjugated polymer containing arylamine pendants for light-emitting diodes, *Macromolecules*, 34: 6571–6576, 2001.

151. Y.-J. Pu, M. Soma, J. Kido, and H. Nishide, A novel triphenylamine-substituted poly(*p*-phenylene vinylene): improved photo- and electroluminescent properties, *Chem. Mater.*, 13: 3817–3819, 2001.
152. F. Bai, M. Zheng, G. Yu, and D. Zhu, The photo- and electroluminescence of some novel light emitting copolymers, *Thin Solid Films*, 363: 118–121, 2000.
153. A. Kimoto, K. Masachika, J.-S. Cho, M. Higuchi, and K. Yamamoto, Novel poly(*p*-phenylene vinylene)s with a phenylazomethine dendron as a metal-collecting site, *Org. Lett.*, 6: 1179–1182, 2004.
154. Y. Zhang, Y. Hu, H. Li, L. Wang, X. Jing, F. Wang, and D. Ma, Polymer light-emitting diodes based on a bipolar transporting luminescent polymer, *J. Mater. Chem.*, 13: 773–777, 2003.
155. N.C. Greenham, S.C. Moratti, D.D.C. Bradley, R.H. Friend, and A.B. Holmes, Efficient light-emitting diodes based on polymers with high electron affinities, *Nature*, 365: 628–630, 1993.
156. Y. Liu, G. Yu, Q. Li, and D. Zhu, Synthesis and characterization of new poly(cyanoterephthalylidene)s for light-emitting diodes, *Synth. Met.*, 122: 401–408, 2001.
157. D.-J. Kim, S.-H. Kim, T. Zyung, J.-J. Kim, I. Cho, and S.K. Choi, Synthesis of a new class of processible electroluminescent poly(cyanoterephthalidene) derivative with a tertiary amine linkage, *Macromolecules*, 29: 3657–3660, 1996.
158. J.-H. Lee, J.-W. Park, and S.-K. Choi, Synthesis and electroluminescent property of a new conjugated polymer based on carbazole derivative: poly(3,6-*N*-2-ethylhexyl carbazolyl cyanoterephthalidene), *Synth. Met.*, 88: 31–35, 1997.
159. Z. Peng and M.E. Galvin, Polymers with high electron affinities for light-emitting diodes, *Chem. Mater.*, 10: 1785–1788, 1998.
160. X. Wu, Y. Liu, and D. Zhu, Synthesis and characterization of a new conjugated polymer containing cyano substituents for light-emitting diodes, *J. Mater. Chem.*, 11: 1327–1331, 2001.
161. M. Hohloch, J.L. Segura, S.E. Döttinger, D. Honhholz, E. Steinhuber, H. Spreitzer, and M. Hanack, Design, synthesis and study of photoluminescence and electroluminescence of new poly(2,6-naphthylene vinylene) derivatives, *Synth. Met.*, 84: 319–322, 1997.
162. Y. Xiao, W. Yu, S. Chua, and W. Huang, A novel series of copolymers containing 2,5-dicyano-1,4-phenylene vinylene — synthetic tuning of the HOMO and LUMO energy levels of conjugated polymers, *Chem. Eur. J.*, 6: 1318–1321, 2000.
163. Y. Xiao, W.-L. Yu, Z.-K. Chen, N.H.S. Lee, Y.-H. Lai, and W. Huang, Synthesis and characterization of a novel light-emitting copolymer with improved charge-balancing property, *Thin Solid Films*, 363: 102–105, 2000.
164. M.S. Liu, X. Jiang, S. Liu, P. Herguth, and A.K.Y. Jen, Effect of cyano substituents on electron affinity and electron-transporting properties of conjugated polymers, *Macromolecules*, 35: 3532–3538, 2002.
165. I. Benjamin, E.Z. Faraggi, Y. Avny, D. Davydov, and R. Neumann, Fluorinated poly(*p*-phenylene vinylene) copolymers: preparation and use in light-emitting materials, *Chem. Mater.*, 8: 352–355, 1996.
166. R. Riehn, J. Morgado, R. Iqbal, S.C. Moratti, A.B. Holmes, S. Volta, and F. Cacialli, Fluorine substituted poly(*p*-phenylene vinylenes) copolymers, *Synth. Met.*, 124: 67–69, 2001.
167. Z. Peng and J. Zhang, Novel oxadiazole-containing conjugated polymers as efficient single-layer light-emitting diodes, *Synth. Met.*, 105: 73–78, 1999.
168. J.H. Kim, J.H. Park, and H. Lee, Highly efficient novel poly(*p*-phenylene vinylene) derivative with 1,3,4-oxadiazole pendant on a vinylene unit, *Chem. Mater.*, 15: 3414–3416, 2003.
169. Z. Peng, Z. Bao, and M.E. Galvin, Polymers with bipolar carrier transport abilities for light emitting diodes, *Chem. Mater.*, 10: 2086–2090, 1998.
170. J.A. Mikroyannidis, I.K. Spiliopoulos, T.S. Kasimis, A.P. Kulkarni, and S.A. Jenekhe, Synthesis, photophysics, and electroluminescence of conjugated poly(*p*-phenylene vinylene) derivatives with 1,3,4-oxadiazoles in the backbone, *Macromolecules*, 36: 9295–9302, 2003.
171. Z. Peng, Z. Bao, and M.E. Galvin, Oxadiazole-containing conjugated polymers for light-emitting diodes, *Adv. Mater.*, 10: 680–682, 1998.
172. S.-Y. Zhang, F. Kong, R. Sun, R.-K. Yuan, X.-Q. Jiang, and C.-Z. Yang, Synthesis, characterization, and electro-optical properties of a soluble conjugated polymer containing an oxadiazole unit in the main chain, *J. Appl. Polym. Sci.*, 89: 2618–2623, 2003.

173. A.W. Grice, A. Tajbakhsh, P.L. Burn, and D.D.C. Bradley, A blue-emitting triazole-based conjugated polymer, *Adv. Mater.*, 9: 1174–1178, 1997.
174. P. Karastatis, J.A. Mikroyannidis, I.K. Spiliopoulos, A.P. Kulkarni, and S.A. Jenekhe, Synthesis, photophysics and electroluminescence of new quinoxaline-containing poly(*p*-phenylene vinylene)s, *Macromolecules*, 37: 7867–7878, 2004.
175. L.-S. Yu and S.A. Chen, Full-range tunability of electron and hole carrier mobilities and density ratios via incorporation of highly electron-deficient moieties in poly(phenylene vinylene) side chains, *Adv. Mater.*, 16: 744–748, 2004.
176. J.H. Kim and H. Lee, Synthesis, electrochemistry, and electroluminescence of novel red-emitting poly(*p*-phenylene vinylene) derivative with 2-pyran-4-ylidene-malononitrile obtained by the Heck reaction, *Chem. Mater.*, 14: 2270–2275, 2002.
177. B. Jiang, S.-W. Yang, and W.E. Jones, Jr., Conjugated porphyrin polymers: control of chromophore separation by oligophenylene vinylene bridges, *Chem. Mater.*, 9: 2031–2034, 1997.
178. B. Jiang, S.-W. Yang, R. Niver, and W.E. Jones, Jr., Metalloporphyrin polymers bridged with conjugated cyano-substituted stilbene units, *Synth. Met.*, 94: 205–210, 1998.
179. S. Shi and F. Wudl, Synthesis and characterization of a water-soluble poly(*p*-phenylene vinylene) derivative, *Macromolecules*, 23: 2119–2124, 1990.
180. H.-L. Wang, D.W. McBranch, V.I. Klimov, R. Helgeson, and F. Wudl, Controlled unidirectional energy transfer in luminescent self-assembled conjugated polymer superlattices, *Chem. Phys. Lett.*, 315: 173–180, 1999.
181. S.-C. Chang, J. Bharathan, Y. Yang, R. Helgeson, F. Wudl, M.B. Ramey, and J.R. Reynolds, Dual-color polymer light-emitting pixels processed by hybrid inkjet printing, *Appl. Phys. Lett.*, 73: 2561–2563, 1998.
182. L. Chen, D.W. McBranch, H.-L. Wang, R. Helgeson, F. Wudl, and D.G. Whitten, Highly sensitive biological and chemical sensors based on reversible fluorescence quenching in a conjugated polymer, *Proc. Natl. Acad. Sci. USA*, 96: 12287–12292, 1999.
183. F. Cacialli, J.S. Wilson, J.J. Michels, C. Daniel, C. Silva, R.H. Friend, N. Severin, P. Samori, J.P. Rabe, M.J. O'Connell, P.N. Taylor, and H.L. Anderson, Cyclodextrin-threaded conjugated polyrotaxanes, as insulated molecular wires with reduced interstrand interaction, *Nat. Mater.*, 1: 160–164, 2002.
184. J.J. Michels, M.J. O'Connell, P.N. Taylor, J.S. Wilson, F. Cacialli, and H.L. Anderson, Synthesis of conjugated polyrotaxanes, *Chem. Eur. J.*, 9: 6167–6176, 2003.
185. J. Terao, A. Tang, J.J. Michels, A. Krivokapic, and H.L. Anderson, Synthesis of poly(*p*-phenylene vinylene) rotaxanes by aqueous suzuki coupling, *Chem. Commun.*: 56–57, 2004.
186. L. Zheng, R.C. Urian, Y. Liu, A.K. Jen, and L. Pu, A binaphthyl-based conjugated polymer for light-emitting diodes, *Chem. Mater.*, 12: 13–15, 2000.
187. A.M. Sarker, L. Ding, P.M. Lahti, and F.E. Karasz, Synthesis and luminescent studies of poly(*p*-phenylene vinylene)s containing a biphenyl moiety, *Macromolecules*, 35: 223–230, 2002.
188. T. Ahn, M.S. Jang, H.-K. Shim, D.-H. Hwang, and T. Zyung, Blue electroluminescent polymers: control of conjugation length by kink linkages and substituents in the poly(*p*-phenylene vinylene)-related copolymers, *Macromolecules*, 32: 3279–3285, 1999.
189. Y. Pang, J. Li, B. Hu, and F.E. Karasz, A highly luminescent poly[*(m*-phenylene vinylene)-*alt*-(*p*-phenylene vinylene)] with defined conjugation length and improved solubility, *Macromolecules*, 32: 3946–3950, 1999.
190. F. Cacialli, B.S. Chuah, R.H. Friend, S.C. Moratti, and A.B. Holmes, Blue-emitting diodes from a *m*-linked 2,3-substituted alkoxy poly(*p*-phenylene vinylene), *Synth. Met.*, 111: 155–158, 2000.
191. L. Ding, F.E. Karasz, Z. Lin, M. Zheng, L. Liao, and Y. Pang, Effect of Förster energy transfer and hole transport layer on performance of polymer light-emitting diodes, *Macromolecules*, 34: 9183–9188, 2001.
192. H. Schlick, F. Stelzer, F. Meghdadi, and G. Leising, Synthesis and optical characterization of new highly luminescent poly(*m,p*-phenylene vinylene) derivatives, *Synth. Met.*, 119: 529–530, 2001.
193. G. Brizius, N.G. Pschirer, W. Steffen, K. Stitzer, H.-C. zur Loye, and U.H.F. Bunz, Alkyne metathesis with simple catalyst systems: efficient synthesis of conjugated polymers containing vinyl groups in main side chain, *J. Am. Chem. Soc.*, 122: 12435–12440, 2000.

194. D.A.M. Egbe, S. Sell, C. Ulbricht, E. Birckner, and U.-W. Grummt, Mixed alkyl- and alkoxy-substituted poly[(phenylene ethynylene)-*alt*-(phenylene vinylene)] hybrid polymers: synthesis and photophysical properties, *Macromol. Chem. Phys.*, 205: 2105–2115, 2004.
195. L. Ding, D.A.M. Egbe, and F.E. Karasz, Photophysical and optoelectronic properties of green-emitting alkoxy-substituted PE/PV hybrid conjugated polymers, *Macromolecules*, 37: 6124–6131, 2004.
196. D.A.M. Egbe, B. Carbonnier, L. Ding, D. Mühlbacher, E. Birckner, T. Pakula, F.E. Karasz, and U.-W. Grummt, Supramolecular ordering, thermal behaviour, and photophysical, electrochemical, and electroluminescent properties of alkoxy-substituted yne-containing poly(phenylene-vinylene)s, *Macromolecules*, 37: 7451–7463, 2004.
197. Q. Chu, Y. Pang, L. Ding, and F.E. Karasz, Green-emitting PPE–PPV hybrid polymers: efficient energy transfer across the *m*-phenylene bridge, *Macromolecules*, 36: 3848–3853, 2003.
198. H. Liang, J. Yan, and J. Lu, Synthesis and optical characterization of a novel blue luminescent polymer: regioregular poly(1-alkoxy-2,4 -*m*-phenylene vinylene), *Synth. Met.*, 142: 143–145, 2004.
199. P.L. Burn, A.B. Holmes, A. Kraft, D.D.C. Bradley, A.R. Brown, and R.H. Friend, Synthesis of a segmented conjugated polymer-chain giving a blue-shifted electroluminescence and improved efficiency, *J. Chem. Soc., Chem. Commun.*: 32–34, 1992.
200. J.C. Carter, I. Grizzi, S.K. Heeks, D.J. Lacey, S.G. Latham, P.G. May, O. Ruiz de los Paños, K. Pichler, C.R. Towns, and H.F. Wittmann, Operating stability of light-emitting polymer diodes based on poly(*p*-phenylene vinylene), *Appl. Phys. Lett.*, 71: 34–36, 1997.
201. Z. Yang, I. Sokolik, and F.E. Karasz, A soluble blue-light-emitting polymer, *Macromolecules*, 26: 1188–1190, 1993.
202. B. Hu, Z. Yang, and F.E. Karasz, Electroluminescence of pure poly(*N*-vinylcarbazole) and its blends with a multiblock copolymer, *J. Appl. Phys.*, 76: 2419–2422, 1994.
203. R.G. Sun, Y.Z. Wang, D.K. Wang, Q.B. Zheng, E.M. Kylo, T.L. Gustafson, F. Wang, and A.J. Epstein, High PL quantum efficiency of poly(phenylene vinylene) systems through exciton confinement, *Synth. Met.*, 111–112: 595–602, 1999.
204. T. Zyung, D.-H. Hwang, I.-N. Kang, H.-K. Shim, W.-Y. Hwang, and J.-J. Kim, Novel blue electroluminescent polymers with well-defined conjugation length, *Chem. Mater.*, 7: 1499–1503, 1995.
205. N. Benfaremo, D.J. Sandman, S. Tripathy, J. Kumar, K. Yang, M.F. Rubner, and C. Lyons, Synthesis and characterization of luminescent polymers of distyrylbenzenes with oligo(ethylene glycol) spacers, *Macromolecules*, 31: 3595–3599, 1998.
206. F. Cacialli, R.H. Friend, W.J. Feast, and P.W. Lovenich, Poly(distyrylbenzene- *block*-sexi(ethylene oxide)), a highly luminescent processible derivative of PPV, *Chem. Commun.*, 1778–1779, 2001.
207. L. Duan, Y. Qiu, and H. Wang, Blue electroluminescence from a processible derivative of PPV based copolymer with tri(ethylene oxide) segments in the backbone, *Synth. Met.*, 137: 1133–1135, 2003.
208. H. Wang, L. Duan, Y. Qiu, X. Wang, and D. Liu, Synthesis and electroluminescence properties of a novel poly(*p*-phenylene vinylene)-based copolymer with tri(ethylene oxide) segments on the backbone, *J. Appl. Polym. Sci.*, 83: 2195–2200, 2002.
209. E.-N. Chang and S.-A. Chen, Cyano-containing phenylene vinylene-based copolymer as blue luminescent and electron transport material in polymer light-emitting diodes, *J. Appl. Phys.*, 85: 2057–2061, 1999.
210. M. Zheng, L. Ding, E.E. Gürel, P.M. Lahti, and F.E. Karasz, Oxadiazole containing conjugated–nonconjugated blue and blue-green light-emitting copolymers, *Macromolecules*, 34: 4124–4129, 2001.
211. J.A. Mikroyannidis and J.K. Spiliopoulos, Synthesis and optical properties of novel blue-light emitting poly(*p*-phenylene vinylene) derivatives with pendant oxadiazole and cyano groups, *J. Polym. Sci., Part A: Polym. Chem.*, 42: 1768–1778, 2004.
212. A.M. Sarker, E.E. Gürel, M. Zheng, P.M. Lahti, and F.E. Karasz, Synthesis, characterization, and photophysical studies of new blue-emitting segmented copolymers, *Macromolecules*, 34: 5897–5901, 2001.
213. S. Zheng, J. Shi, and R. Mateu, Novel blue light emitting polymer containing an adamantane moiety, *Chem. Mater.*, 12: 1814–1817, 2000.

214. M. Zheng, A.M. Sarker, E.E. Gürel, P.M. Lahti, and F.E. Karasz, Structure–property relationships in light-emitting polymers: optical, electrochemical and thermal studies, *Macromolecules*, 33: 7426–7430, 2000.
215. H.-K. Kim, M.-K. Ryu, K.-D. Kim, S.-M. Lee, S.-W. Cho, and J.-W. Park, Tunable electroluminescence from silicon-containing poly(*p*-phenylene vinylene)-related copolymers with well-defined structures, *Macromolecules*, 31: 1114–1123, 1998.
216. K.-D. Kim, J.-S. Park, H.-K. Kim, T.B. Lee, and K.T. No, Blue electroluminescence from novel silicon-containing poly(cyanoterephthalylidene) copolymers, *Macromolecules*, 31: 7267–7272, 1998.
217. M.R. Robinson, S. Wang, A.J. Heeger, and G.C. Bazan, A tetrahedral oligo(phenylene vinylene) molecule of intermediate dimensions: effect of molecular shape on the morphology and electroluminescence of organic glasses, *Adv. Funct. Mater.*, 11: 413–419, 2001.
218. R. Zhang, G. Zhang, and J. Shen, A new approach for the synthesis of conjugated–non-conjugated poly(phenylene vinylene) — polyacrylamide copolymers, *Chem. Commun.*: 823–824, 2000.
219. J.-K. Lee, R.R. Schrock, D.R. Baigent, and R.H. Friend, A new type of blue-emitting electroluminescent polymer, *Macromolecules*, 28: 1966–1971, 1995.
220. J. Rault-Berthelot, Polyfluorenes, a family of versatile conjugated polymers. Anodic synthesis, physicochemical properties, electrochemical behaviour and application fields, *Recent Res. Dev. Macromol. Res.*, 3: 425–437, 1998.
221. M. Bernius, M. Inbasekaran, E. Woo, W. Wu, and L. Wujkowski, Fluorene-based polymers — preparation and applications, *J. Mater. Sci.: Mater. Electron.*, 11: 111–116, 2000.
222. M.T. Bernius, M. Inbasekaran, J. O'Brien, and W. Wu, Progress in light-emitting polymers, *Adv. Mater.*, 12: 1737–1750, 2000.
223. M. Leclerc, Polyfluorenes: twenty years of progress, *J. Polym. Sci., Part A: Polym. Chem.*, 39: 2867–2873, 2001.
224. D. Neher, Polyfluorene homopolymers: conjugated liquid-crystalline polymers for bright emission and polarized electroluminescence, *Macromol. Rapid Commun.*, 22: 1365–1385, 2001.
225. U. Scherf and E.J.W. List, Semiconducting polyfluorenes — towards reliable structure–property relationships, *Adv. Mater.*, 14: 477–487, 2002.
226. W. Wu, M. Inbasekaran, M. Hudack, D. Welsh, W. Yu, Y. Cheng, C. Wang, S. Kram, M. Tacey, M. Bernius, R. Fletcher, K. Kiszka, S. Munger, and J. O'Brien, Recent development of polyfluorene-based RGB materials for light emitting diodes, *Microelectron. J.*, 35: 343–348, 2004.
227. D.Y. Kim, H.N. Cho, and C.Y. Kim, Blue light emitting polymers, *Prog. Polym. Sci.*, 25: 1089–1139, 2000.
228. M. Grell, D.D.C. Bradley, X. Long, T. Chamberlain, M. Inbasekaran, E.P. Woo, and M. Soliman, Chain geometry, solution aggregation and enhanced dichroism in the liquid-crystalline conjugated polymer poly(9,9-dioctylfluorene), *Acta Polym.*, 49: 439–444, 1998.
229. G. Fytas, H.G. Nothofer, U. Scherf, D. Vlassopoulos, and G. Meier, Structure and dynamics of nondilute polyfluorene solutions, *Macromolecules*, 35: 481–488, 2002.
230. M. Grell, D.D.C. Bradley, M. Inbasekaran, and E.P. Woo, A glass-forming conjugated main-chain liquid crystal polymer for polarized electroluminescence applications, *Adv. Mater.*, 9: 798–802, 1997.
231. B. Scharrel, V. Wachtendorf, M. Grell, D.D.C. Bradley, and M. Hennecke, Polarized fluorescence and orientational order parameters of a liquid-crystalline conjugated polymer, *Phys. Rev. B*, 60: 277–283, 1999.
232. M. Grell, W. Knoll, D. Lupo, A. Miesel, T. Miteva, D. Neher, H.-G. Nothofer, U. Scherf, and A. Yasuda, Blue polarized electroluminescence from a liquid crystalline polyfluorene, *Adv. Mater.*, 11: 671–675, 1999.
233. M. Grell, M. Redecker, K.S. Whitehead, D.D.C. Bradley, M. Inbasekaran, E.P. Woo, and W. Wu, Monodomain alignment of thermotropic fluorene copolymers, *Liq. Cryst.*, 26: 1403–1407, 1999.
234. M. Grell and D.D.C. Bradley, Polarized luminescence from oriented molecular materials, *Adv. Mater.*, 11: 895–905, 1999.
235. K.S. Whitehead, M. Grell, D.D.C. Bradley, M. Jandke, and P. Strohhriegl, Highly polarized blue electroluminescence from homogeneously aligned films of poly(9,9-dioctylfluorene), *Appl. Phys. Lett.*, 76: 2946–2948, 2000.

236. S. Kawana, M. Durrel, J. Lu, J.E. Macdonald, M. Grell, D.D.C. Bradley, P.C. Jules, R.A.L. Jones, and S.L. Bennett, X-ray diffraction study of the structure of thin polyfluorene films, *Polymer*, 43: 1907–1913, 2002.
237. S.H. Chen, H.L. Chou, A.C. Su, and S.A. Chen, Molecular packing in crystalline poly(9,9-di-*n*-octyl-2,7-fluorene), *Macromolecules*, 37: 6833–6838, 2004.
238. M. Grell, D.D.C. Bradley, G. Ungar, J. Hill, and K.S. Whitehead, Interplay of physical structure and photophysics for a liquid crystalline polyfluorene, *Macromolecules*, 32: 5810–5817, 1999.
239. J. Teetsov and M.A. Fox, Photophysical characterization of dilute solution and ordered thin films of alkyl-substituted polyfluorenes, *J. Mater. Chem.*, 9: 2117–2122, 1999.
240. M. Misaki, Y. Ueda, S. Nagamatsu, Y. Yoshida, N. Tanigaki, and K. Yase, Formation of single-crystal-like poly(9,9-dioctylfluorene) thin films by the friction-transfer technique with subsequent thermal treatments, *Macromolecules*, 37: 6926–6931, 2004.
241. M. Oda, H.-G. Nothofer, G. Lieser, U. Scherf, S.C.J. Meskers, and D. Neher, Circularly polarized electroluminescence from liquid-crystalline chiral polyfluorenes, *Adv. Mater.*, 12: 362–365, 2000.
242. H.-Z. Tang, M. Fujiki, and T. Sato, Thermally driven conformational transition of optically active poly[2,7- $\{9,9\text{-bis}[(S)\text{-}2\text{-methyloctyl}]\}$ fluorene] in solution, *Macromolecules*, 35: 6439–6445, 2002.
243. H.-Z. Tang, M. Fujiki, and M. Motonaga, Alkyl side chain effects of optically active polyfluorenes on their chiroptical absorption and emission properties, *Polymer*, 43: 6213–6220, 2002.
244. L. Wu, T. Sato, H.-Z. Tang, and M. Fujiki, Conformation of a polyfluorene derivative in solution, *Macromolecules*, 37: 6183–6188, 2004.
245. M.J. Banach, R.H. Friend, and H. Sirringhaus, Influence of the casting solvent on the thermotropic alignment of thin liquid crystalline polyfluorene copolymer films, *Macromolecules*, 37: 6079–6085, 2004.
246. X. Gong, P.K. Iyer, D. Moses, G.C. Bazan, A.J. Heeger, and S.S. Xiao, Stabilized blue emission from polyfluorene-based light-emitting diodes: elimination of fluorenone defects, *Adv. Funct. Mater.*, 13: 325–329, 2003.
247. M. Fukuda, K. Sawada, and K. Yoshino, Synthesis of fusible and soluble conducting polyfluorene derivatives and their characteristics, *J. Polym. Sci., Part A: Polym. Chem.*, 31: 2465–2471, 1993.
248. M. Ariu, D.G. Lidzey, M. Sims, A.J. Cadby, P.A. Lane, and D.D.C. Bradley, The effect of morphology on the temperature-dependent photoluminescence quantum efficiency of the conjugated polymer poly(9,9-dioctylfluorene), *J. Phys.: Condens. Matter*, 14: 9975–9986, 2002.
249. G. Klaerner and R.D. Miller, Polyfluorene derivatives: effective conjugation lengths from well-defined oligomers, *Macromolecules*, 31: 2007–2009, 1998.
250. Y. Koizumi, S. Seki, A. Acharya, A. Saeki, and S. Tagawa, Delocalization of positive and negative charge carriers on oligo- and poly-fluorenes studied by low-temperature matrix isolation technique, *Chem. Lett.*, 33: 1290–1291, 2004.
251. J. Jo, C. Chi, S. Höger, G. Wegner, and D.Y. Yoon, Synthesis and characterization of mono-disperse oligofluorenes, *Chem. Eur. J.*, 10: 2681–2688, 2004.
252. S. Janietz, D.D.C. Bradley, M. Grell, C. Giebeler, M. Inbasekaran, and E.P. Woo, Electrochemical determination of the ionization potential and electron affinity of poly(9,9-dioctylfluorene), *Appl. Phys. Lett.*, 73: 2453–2455, 1998.
253. T. Miteva, A. Meisel, W. Knoll, H.G. Nothofer, U. Scherf, D.C. Müller, K. Meerholz, A. Yasuda, and D. Neher, Improving the performance of polyfluorene-based organic light-emitting diodes via end-capping, *Adv. Mater.*, 13: 565–570, 2001.
254. L.S. Liao, M.K. Fung, C.S. Lee, S.T. Lee, M. Inbasekaran, E.P. Woo, and W.W. Wu, Electronic structure and energy band gap of poly(9,9-dioctylfluorene) investigated by photoelectron spectroscopy, *Appl. Phys. Lett.*, 76: 3582–3584, 2000.
255. L.S. Liao, L.F. Cheng, M.K. Fung, C.S. Lee, S.T. Lee, M. Inbasekaran, E.P. Woo, and W.W. Wu, Oxygen effect on the interface formation between calcium and a polyfluorene film, *Phys. Rev. B*, 62: 10004–10007, 2000.
256. D. Poplavsky, J. Nelson, and D.D.C. Bradley, Ohmic hole injection in poly(9,9-dioctylfluorene) polymer light-emitting diodes, *Appl. Phys. Lett.*, 83: 707–709, 2003.

257. T. van Woudenberg, J. Wildeman, P.W.M. Blom, J.J.A.M. Bastiaansen, and B.M.W. Langeveld-Voss, Electron-enhanced hole injection in blue polyfluorene-based polymer light-emitting diodes, *Adv. Funct. Mater.*, 14: 677–683, 2004.
258. A.J. Campbell, D.D.C. Bradley, H. Antoniadis, M. Inbasekaran, W.W. Wu, and A.P. Woo, Transient and steady-state space-charge-limited currents in polyfluorene copolymer diode structures with ohmic hole injection contacts, *Appl. Phys. Lett.*, 76: 1734–1736, 2000.
259. M. Redecker, D.D.C. Bradley, M. Inbasekaran, and E.P. Woo, Nondispersive hole transport in an electroluminescent polyfluorene, *Appl. Phys. Lett.*, 73: 1565–1567, 1998.
260. G. Greczynski, M. Fahlman, W.R. Salaneck, N. Johansson, D.A. dos Santos, A. Dkhissi, and J.L. Brédas, Electronic structure of poly(9,9-dioctylfluorene) in the pristine and reduced state, *J. Chem. Phys.*, 116: 1700–1706, 2002.
261. J. Cornil, I. Gueli, A. Dkhissi, J.C. Sancho-Garcia, E. Hennebicq, J.P. Calbert, V. Lemaire, D. Beljonne, and J.L. Brédas, Electronic and optical properties of polyfluorene and fluorene-based copolymers: a quantum-chemical characterization, *J. Chem. Phys.*, 118: 6615–6623, 2003.
262. E. Zojer, A. Pogantsch, E. Hennebicq, D. Beljonne, J. Brédas, and E.J.W. List, Green emission from poly(fluorene)s: the role of oxidation, *J. Chem. Phys.*, 117: 6794–6802, 2002.
263. X.H. Yang, D. Neher, C. Spitz, E. Zojer, J.L. Brédas, R. Günther, and U. Scherf, On the polarization of the green emission of polyfluorenes, *J. Chem. Phys.*, 119: 6832–6839, 2003.
264. I. Franco and S. Tretiak, Electron-vibrational relaxation of photoexcited polyfluorenes in the presence of chemical defects: a theoretical study, *Chem. Phys. Lett.*, 372: 403–408, 2003.
265. I. Franco and S. Tretiak, Electron-vibrational dynamics of photoexcited polyfluorenes, *J. Am. Chem. Soc.*, 126: 12130–12140, 2004.
266. J. Rault-Berthelot and J. Simonet, The anodic oxidation of fluorene and some of its derivatives, *J. Electrochem. Soc.*, 132: 187–192, 1985.
267. J. Rault-Berthelot and J. Simonet, The polyfluorenes: a family of versatile electroactive polymers (I). Electropolymerization of fluorenes, *Nouv. J. Chim.*, 10: 169–177, 1986.
268. M. Fukuda, K. Sawada, and K. Yoshino, Fusible conducting poly(9-alkylfluorene) and poly(9,9-dialkylfluorene) and their characteristics, *Jpn. J. Appl. Phys., Pt. 2—Letters*, 28: L1433–L1435, 1989.
269. M. Fukuda, K. Sawada, S. Morita, and K. Yoshino, Novel characteristics of conducting poly(9-alkylfluorene), poly(9,9-dialkylfluorene) and poly(1,10-bis(9'-alkylfluorenyl)alkane), *Synth. Met.*, 41–43: 855–858, 1991.
270. Y. Ohmori, A. Uchida, K. Muro, and K. Yoshino, Blue electroluminescent diodes utilizing poly(alkylfluorene), *Jpn. J. Appl. Phys.*, 30: L1941–L1943, 1991.
271. Q. Pei and Y. Yang, Efficient photoluminescence and electroluminescence from a soluble polyfluorene, *J. Am. Chem. Soc.*, 118: 7416–7417, 1996.
272. E.P. Woo, W.R. Shiang, M. Inbasekaran, and G.R. Roof, 2,7-Diaryl-9-Substituted Fluorenes and 9-Substituted Fluorene Oligomers and Polymers, U.S. Patent 5,708,130, January 13, 1998.
273. Q. Pei, G. Yu, and Y. Yang, Polyfluorenes as Materials for Photoluminescence and Electroluminescence, PCT Patent WO 97/33323, September 12, 1997.
274. Q. Pei, G. Yu, and Y. Yang, Polyfluorenes as Materials for Photoluminescence and Electroluminescence, U.S. Patent 5,900,327, May 4, 1999.
275. E.P. Woo, W.R. Shiang, M. Inbasekaran, and G.R. Roof, 2,7-Diaryl-9-Substituted Fluorenes and 9-Substituted Fluorene Oligomers and Polymers, U.S. Patent 5,962,631, October 5, 1999.
276. E.P. Woo, M. Inbasekaran, W.R. Shiang, G.R. Roof, M.T. Bernius, and W. Wu, Fluorene-Containing Polymers and Compounds Useful in the Preparation Thereof, U.S. Patent 6,169,163 B1, January 2, 2001.
277. E.P. Woo, W.R. Shiang, M. Inbasekaran, G.R. Roof, M.T. Bernius, and W. Wu, Fluorene-Containing Polymers and Compounds Useful in the Preparation Thereof, U.S. Patent 6,512,083, January 28, 2003.
278. E.P. Woo, W.R. Shiang, M. Inbasekaran, G.R. Roof, M.T. Bernius, and W. Wu, Fluorene-Containing Polymers and Compounds Useful in the Preparation Thereof, U.S. Patent 6,514,632, February 4, 2003.
279. T. Yamamoto, Electrically conducting and thermally stable π -conjugated poly(arylene)s prepared by organometallic processes, *Prog. Polym. Sci.*, 17: 1153–1205, 1992.

280. M. Kreyenschmidt, G. Klaerner, T. Fuhrer, J. Ashenhurst, S. Karg, W.D. Chen, V.Y. Lee, J.C. Scott, and R.D. Miller, Thermally stable blue-light-emitting copolymers of poly(alkylfluorene), *Macromolecules*, 31: 1099–1103, 1998.
281. H.-G. Nothofer, A. Meisel, T. Miteva, D. Neher, M. Forster, M. Oda, G. Liester, D. Sainova, A. Yasude, D. Lupo, W. Knoll, and U. Scherf, Liquid crystalline polyfluorenes for blue polarized electroluminescence, *Macromol. Symp.*, 154: 139–148, 2000.
282. M. Ranger and M. Leclerc, Novel base-dopable poly(2,7-fluorenylene) derivatives, *Chem. Commun.*: 1597–1598, 1997.
283. M. Ranger, D. Rondeau, and M. Leclerc, New well-defined poly(2,7-fluorene) derivatives: photoluminescence and base doping, *Macromolecules*, 30: 7686–7691, 1997.
284. M. Inbasekaran, W. Wu, and E.P. Woo, Process for Preparing Conjugated Polymers, U.S. Patent 5,777,070, July 7, 1998.
285. C.R. Towns and R. O'Dell, Polymer Preparation, PCT Patent WO 00/53656, September 14, 2000.
286. U. Lemmer, S. Heun, R.F. Mahrt, U. Scherf, M. Hopmeier, U. Siegner, E.O. Göbel, K. Müllen, and H. Bässler, Aggregate fluorescence in conjugated polymers, *Chem. Phys. Lett.*, 240: 373–378, 1995.
287. V.N. Bliznyuk, S.A. Carter, J.C. Scott, G. Klärner, R.D. Miller, and D.C. Miller, Electrical and photoinduced degradation of polyfluorene based films and light-emitting devices, *Macromolecules*, 32: 361–369, 1999.
288. J.-I. Lee, G. Klaerner, and R.D. Miller, Oxidative stability and its effect on the photoluminescence of poly(fluorene) derivatives: end group effects, *Chem. Mater.*, 11: 1083–1088, 1999.
289. L.M. Herz and R.T. Phillips, Effects of interchain interactions, polarization anisotropy, and photo-oxidation on the ultrafast photoluminescence decay from a polyfluorene, *Phys. Rev. B*, 61: 13691–13697, 2000.
290. H.-Z. Tang, M. Fujiki, Z.-B. Zhang, K. Torimitsu, and M. Motonaga, Nearly pure blue photoluminescent poly(2,7-[9-{3,5-bis[3,5-bis(benzyloxy)benzyloxy]benzyl} -9-(3,6-dioxaoctyl)]fluorene} in film, *Chem. Commun.*: 2426–2427, 2001.
291. G. Zeng, W.-L. Yu, S.-J. Chua, and W. Huang, Spectral and thermal stability study for fluorene-based conjugated polymers, *Macromolecules*, 35: 6907–6914, 2002.
292. S. Panozzo, J.-C. Vial, Y. Kervela, and O. Stéphan, Fluorene–fluorenone copolymer: stable end efficient yellow-emitting material for electroluminescent devices, *J. Appl. Phys.*, 92: 3495–3502, 2002.
293. E.J.W. List, R. Guentner, P.S. de Freitas, and U. Scherf, The effect of keto defect sites on the emission properties of polyfluorene-type materials, *Adv. Mater.*, 14: 374–378, 2002.
294. M. Gaal, E.J.W. List, and U. Scherf, Excimers or emissive on-chain defects? *Macromolecules*, 36: 4236–4237, 2003.
295. L. Romaner, A. Pogantsch, P.S. de Freitas, U. Scherf, M. Gaal, E. Zojer, and E.J.W. List, The origin of green emission in polyfluorene-based conjugated polymers: on-chain defect fluorescence, *Adv. Funct. Mater.*, 13: 597–601, 2003.
296. S. Gamerith, C. Gadermaier, U. Scherf, and E.J.W. List, Emission properties of pristine and oxidatively degraded polyfluorene type polymers, *Phys. Status Solidi A*, 201: 1132–1151, 2004.
297. P. Scanducci de Freitas, U. Scherf, M. Collon, and E.J.W. List, (9,9-Dialkylfluorene-*co*-fluorenone) Copolymers containing low fluorenone fractions as model systems for degradation-induced changes in polyfluorene-type semiconducting materials, *e-Polymers*, Abstr. No. 009, 2002.
298. W. Zhao, T. Cao, and J.M. White, On the origin of green emission in polyfluorene polymers: the roles of thermal oxidation degradation and crosslinking, *Adv. Funct. Mater.*, 14: 783–790, 2004.
299. M. Sims, D.D.C. Bradley, M. Ariu, M. Koeberg, A. Asimakis, M. Grell, and D.G. Lidzey, Understanding of the origin of the 535 nm emission band in oxidized poly(9,9-dioctylfluorene): the essential role of inter-chain/inter-segment interactions, *Adv. Funct. Mater.*, 14: 765–781, 2004.
300. M. Stoessel, G. Wittmann, J. Staudigel, F. Steuber, J. Blässing, W. Roth, H. Klausmann, W. Rogler, J. Simmerer, A. Winnacker, M. Inbasekaran, and E.P. Woo, Cathode-induced luminescence quenching in polyfluorenes, *J. Appl. Phys.*, 87: 4467–4475, 2000.
301. M.R. Craig, M.M. de Kok, J.W. Hofstraat, A.P.H.J. Schenning, and E.W. Meijer, Improving color purity and stability in a blue emitting polyfluorene by monomer purification, *J. Mater. Chem.*, 13: 2861–2862, 2003.

302. G. Hughes, C. Wang, A.S. Batsanov, M. Fern, S. Frank, M.R. Bryce, I.F. Perepichka, A.P. Monkman, and B.P. Lyons, New pyrimidine- and fluorine-containing oligo(arylene)s: synthesis, crystal structures, optoelectronic properties and a theoretical study, *Org. Biomol. Chem.*, 1: 3069–3077, 2003.
303. S. Beaupré and M. Leclerc, Optical and electrical properties of π -conjugated polymers based on electron-rich 3,6-dimethoxyfluorene unit, *Macromolecules*, 36: 8986–8991, 2003.
304. J.-I. Lee, G. Klaerner, and R.D. Miller, Structure–property relationship for excimer formation in poly(alkylfluorene) derivatives, *Synth. Met.*, 101: 126, 1999.
305. Y.-S. Suh, S.W. Ko, B.-J. Jung, and H.-K. Shim, Synthesis and electroluminescent properties of cyclohexyl-substituted polyfluorenes, *Opt. Mater.*, 21: 109–118, 2002.
306. M. Oda, H.-G. Nothofer, U. Scherf, V. Šunjić, D. Richter, W. Regenstein, and D. Neher, Chiroptical properties of chiral substituted polyfluorenes, *Macromolecules*, 35: 6792–6798, 2002.
307. A. Rieman and W. Ude, Method for Making 9,9-Bis(4-Hydroxyphenyl)-Fluorene, U.S. Patent 4,675,458, June 23, 1987.
308. W. Orth, E. Pastorek, W. Weiss, and H.W. Kleffner, Preparation of 9,9-Bis-(4-Hydroxyphenyl)-Fluorene, U.S. Patent 5,149,886, September 22, 1992.
309. W. Orth, E. Pastorek, W. Weiss, and H.W. Kleffner, Preparation of 9,9-Bis-(4-Hydroxyphenyl)-Fluorene, U.S. Patent 5,169,990, December 8, 1992.
310. M. Yamada, J. Sun, Y. Suda, and T. Nakaya, Synthesis of fluorenebisphenoxy derivatives by acid-sulfur compound catalyzed condensation reaction, *Chem. Lett.*, 28: 1055–1056, 1998.
311. J.-H. Lee and D.-H. Hwang, Alkoxyphenyl-substituted polyfluorene: a stable blue-light-emitting polymer with good solution processability, *Chem. Commun.*: 2836–2837, 2003.
312. D.-H. Hwang, M.-J. Park, and J.-H. Lee, EL properties of stable blue light-emitting polyfluorene copolymers, *Mater. Sci. Eng. C*, 24: 201–204, 2004.
313. S. Setayesh, A.C. Grimsdale, T. Weil, V. Enkelmann, K. Müllen, F. Meghdadi, E.J.W. List, and G. Leising, Polyfluorenes with polyphenylene dendron side chains: toward non-aggregating, light-emitting polymers, *J. Am. Chem. Soc.*, 123: 946–953, 2001.
314. A. Pogantsch, F.P. Wenzl, E.J.W. List, G. Leising, A.C. Grimsdale, and K. Müllen, Polyfluorenes with dendron side chains as the active materials for polymer light-emitting devices, *Adv. Mater.*, 14: 1061–1064, 2002.
315. D. Marsitzky, R. Vestberg, P. Blainey, B.T. Tang, C.J. Hawker, and K.R. Carter, Self-encapsulation of poly-2,7-fluorenes in a dendrimer matrix, *J. Am. Chem. Soc.*, 123: 6965–6972, 2001.
316. C.-H. Chou and C.-F. Shu, Synthesis and characterization of dendronized polyfluorenes, *Macromolecules*, 35: 9673–9677, 2002.
317. Y. Fu, J. Li, S. Yan, and Z. Bo, High molecular weight dendronized poly(fluorene)s with peripheral carbazole groups: synthesis, characterization, and properties, *Macromolecules*, 37: 6395–6400, 2004.
318. D. Vak, C. Chun, C.L. Lee, J.-J. Kim, and D.-Y. Kim, A novel spiro-functionalized polyfluorene derivative with solubilizing side chains, *J. Mater. Chem.*, 14: 1342–1346, 2004.
319. Y. Wu, J. Li, Y. Fu, and Z. Bo, Synthesis and extremely stable blue light emitting poly(spirobi-fluorene)s with suzuki polycondensation, *Org. Lett.*, 6: 3485–3487, 2004.
320. H.-J. Cho, B.-J. Jung, N.S. Cho, J. Lee, and H.-K. Shim, Synthesis and characterization of thermally stable blue light-emitting polyfluorenes containing siloxane bridges, *Macromolecules*, 36: 6704–6710, 2003.
321. D. Sainova, T. Miteva, H.G. Nothofer, U. Scherf, I. Glowacki, J. Ilanski, H. Fujikawa, and D. Neher, Control of color and efficiency of light-emitting diodes based on polyfluorenes blended with hole-transport molecules, *Appl. Phys. Lett.*, 76: 1810–1812, 2000.
322. C. Ego, A.C. Grimsdale, F. Uckert, G. Yu, G. Srdanov, and K. Müllen, Triphenylamine-substituted polyfluorene — a stable blue-emitter with improved charge injection for light-emitting diodes, *Adv. Mater.*, 14: 809–811, 2002.
323. A. Grice, D.D.C. Bradley, M. Grell, M.D. Bradley, M.T. Bernius, M. Inbasekaran, W.W. Wu, and E.P. Woo, High brightness and efficiency blue light-emitting polymer diodes, *Appl. Phys. Lett.*, 73: 629–631, 1998.

324. J. Pei, X.-L. Liu, Z.-K. Chen, X.-H. Zhang, Y.-H. Lai, and W. Huang, First hydrogen-bonding-induced self-assembled aggregates of a polyfluorene derivatives, *Macromolecules*, 36: 323–327, 2003.
325. J.I. Lee, D.-H. Hwang, H. Park, L.-M. Do, H.Y. Chu, T. Zyung, and R.D. Miller, Light-emitting electrochemical cells based on poly(9,9-bis(3,6-dioxaheptyl)-fluorene-2,7-diyl), Vol. 1 *Synth. Met.*, 111–112: 195–197, 2000.
326. D.C. Müller, T. Braig, H.-G. Nothofer, M. Arnoldi, M. Gross, U. Scherf, O. Nuyken, and K. Meerholz, Efficient blue organic light-emitting diodes with graded hole-transport layers, *Chemphyschem.*, 1: 207–211, 2000.
327. S. Xiao, M. Nguyen, X. Gong, Y. Cao, H. Wu, D. Moses, and A.J. Heeger, Stabilization of semiconducting polymers with silsesquioxane, *Adv. Funct. Mater.*, 13: 25–29, 2003.
328. G. Klärner, J.-I. Lee, V.Y. Lee, E. Chan, J.-P. Chen, A. Nelson, D. Markiewicz, R. Siemens, J.C. Scott, and R.D. Miller, Cross-linkable polymers based on dialkyfluorenes, *Chem. Mater.*, 11: 1800–1805, 1999.
329. J.P. Chen, G. Klaerner, J.-I. Lee, D. Markiewicz, V.Y. Lee, R.D. Miller, and J.C. Scott, Efficient, blue light-emitting diodes using cross-linked layers of polymeric arylamine and fluorene, *Synth. Met.*, 107: 129–135, 1999.
330. X. Gong, W. Ma, J.C. Ostrowski, K. Bechgaard, G.C. Bazan, A.J. Heeger, S. Xiao, and D. Moses, End-capping as a method for improving carrier injection in electrophosphorescent light-emitting diodes, *Adv. Funct. Mater.*, 14: 393–397, 2004.
331. H. Frohne, D.C. Müller, and K. Meerholz, Continuously variable hole injection in organic light emitting diodes, *ChemPhysChem.*, 3: 707–711, 2002.
332. Y. Li, J. Ding, M. Day, Y. Tao, J. Lu, and M. D'orio, Novel stable blue-light-emitting oligofluorene networks immobilized by boronic acid anhydride linkages, *Chem. Mater.*, 15: 4936–4943, 2003.
333. W.-J. Lin, W.-C. Chen, W.-C. Wu, Y.-H. Niu, and A.K.-Y. Jen, Synthesis and optoelectronic properties of starlike polyfluorenes with a silsesquioxane core, *Macromolecules*, 37: 2335–2341, 2004.
334. V. Cimrová and D. Vyprachticky, Enhanced electroluminescence from light-emitting devices based on poly(9,9-dihexadecylfluorene- 2,7-diyl) and polysilane blends, *Appl. Phys. Lett.*, 82: 642–644, 2003.
335. T.M. Brown, J.S. Kim, R.H. Friend, F. Cacialli, R. Daik, and W.J. Feast, Built-in electroabsorption spectroscopy of polymer light-emitting diodes incorporating a doped poly(3,4-ethylene diox-ythiophene) hole injection layer, *Appl. Phys. Lett.*, 75: 1679–1681, 1999.
336. A.P. Kulkarni and S.A. Jenekhe, Blue light-emitting diodes with good spectral stability based on blends of poly(9,9-dioctylfluorene): interplay between morphology, photophysics, and device performance, *Macromolecules*, 36: 5285–5296, 2003.
337. J.H. Park, Y.T. Lim, O.O. Park, J.K. Kim, J.-W. Yu, and Y.C. Kim, Polymer/gold nanoparticle nanocomposite light-emitting diodes: enhancement of electroluminescence stability and quantum efficiency of blue-light-emitting polymers, *Chem. Mater.*, 16: 688–692, 2004.
338. G. Klärner, M.H. Davey, E.-D. Chen, J.C. Scott, and R.D. Miller, Colorfast blue-light-emitting random copolymers derived from di-*n*-hexylfluorene and anthracene, *Adv. Mater.*, 13: 993–997, 1998.
339. J.P. Chen, D. Markiewicz, V.Y. Lee, G. Klaerner, R.D. Miller, and J.C. Scott, Improved efficiencies of light-emitting diodes through incorporation of charge transporting components in tri-block polymers, *Synth. Met.*, 107: 203–207, 1999.
340. J.K. Kim, S.I. Hong, H.N. Cho, D.Y. Kim, and C.Y. Kim, An alternating copolymer for a blue light-emitting diode, *Polym. Bull.*, 38: 169–176, 1997.
341. O. Stéphan and J.-C. Vial, Blue light electroluminescent devices based on a copolymer derived from fluorene and carbazole, *Synth. Met.*, 106: 115–119, 1999.
342. C. Xia and R.C. Advincula, Decreased aggregation phenomena in polyfluorenes by introducing carbazole copolymer units, *Macromolecules*, 34: 5854–5859, 2001.
343. Y. Li, J. Ding, M. Day, Y. Tao, J. Lu, and M. D'orio, Synthesis and properties of random and alternating fluorene/carbazole copolymers for use in blue light-emitting devices, *Chem. Mater.*, 16: 2165–2173, 2004.

344. J. Lu, Y. Tao, M. D'orio, Y. Li, J. Ding, and M. Day, Pure deep blue light-emitting diodes from alternating fluorene/carbazole copolymers by using suitable hole-blocking materials, *Macromolecules*, 37: 2442–2449, 2004.
345. J.-F. Morin and M. Leclerc, Synthesis of conjugated polymers derived from *N*-alkyl-2,7-carbazoles, *Macromolecules*, 34: 4680–4682, 2001.
346. J.-F. Morin, S. Beaupré, M. Leclerc, I. Lévesque, and M. D'orio, Blue light-emitting devices from new conjugated poly(*N*-substituted-2,7-carbazole) derivatives, *Appl. Phys. Lett.*, 80: 341–343, 2002.
347. M. Redecker, D.D.C. Bradley, M. Inbasekaran, W.W. Wu, and E.P. Woo, High mobility hole transport fluorene–triarylamine copolymers, *Adv. Mater.*, 11: 241–246, 1999.
348. M. Redecker, D.D.C. Bradley, K.J. Baldwin, D.A. Smith, M. Inbasekaran, W.W. Wu, and E.P. Woo, An investigation of the emission solvatochromism of a fluorene–triarylamine copolymer studied by time resolved spectroscopy, *J. Mater. Chem.*, 9: 2151–2154, 1999.
349. E.P. Woo, M.T. Bernius, M. Inbasekaran, and W. Wu, Fluorene-Containing Polymers and Electroluminescent Devices Therefrom, U.S. Patent 6,309,763, October 30, 2001.
350. M. Inbasekaran, E. Woo, W. Wu, M. Bernius, and L. Wujkowski, Fluorene homopolymers and copolymers, *Synth. Met.*, 111–112: 397–401, 2000.
351. Q. Fang and T. Yamamoto, New alternative copolymer constituted of fluorene and triphenylamine units with a tunable –CHO group in the side chain. Quantitative transformation of the –CHO group to –CH=CHAr groups and optical and electrochemical properties of the polymers, *Macromolecules*, 37: 5894–5899, 2004.
352. B.-J. Jung, J.-I. Lee, H.Y. Chu, L.-M. Do, and H.-K. Shim, Synthesis of novel fluorene-based poly(iminoarylene)s and their application to buffer layer in organic light-emitting diodes, *Macromolecules*, 35: 2282–2287, 2002.
353. W. Yang, J. Huang, C. Liu, Y. Niu, Q. Hou, R. Yang, and Y. Cao, Enhancement of color purity in blue-emitting fluorene–pyridine-based copolymers by controlling the chain rigidity and effective conjugation length, *Polymer*, 45: 865–872, 2004.
354. F.-I. Wu, S. Reddy, and C.-F. Shu, Novel oxadiazole-containing polyfluorene with efficient blue electroluminescence, *Chem. Mater.*, 15: 269–274, 2003.
355. S. Hamai and F. Hirayama, Actinometric determination of absolute fluorescence quantum yields, *J. Phys. Chem.*, 87: 83–89, 1983.
356. C. Shu, R. Dodda, F. Wu, M.S. Liu, and A.K. Jen, Highly efficient blue-light-emitting diodes from polyfluorene containing bipolar pendant groups, *Macromolecules*, 36: 6698–6703, 2003.
357. H.-H. Sung and H.-C. Lin, Novel alternating fluorene-based conjugated polymers containing oxadiazole pendants with various terminal groups, *Macromolecules*, 37: 7945–7954, 2004.
358. J. Ding, M. Day, G. Robertson, and J. Roovers, Synthesis and characterization of alternating copolymers of fluorene and oxadiazole, *Macromolecules*, 35: 3474–3483, 2002.
359. S. Janietz, J. Barche, A. Wedel, and D. Sainova, *n*-Type copolymers with fluorene and 1,3,4-heterodiazole moieties, *Macromol. Chem. Phys.*, 205: 187–198, 2004.
360. X. Zhan, Y. Liu, X. Wu, S. Wang, and D. Zhu, New series of blue-emitting and electron-transporting copolymers based on fluorene, *Macromolecules*, 35: 2529–2537, 2002.
361. N.C. Yang, Y.H. Park, and D.H. Suh, Synthesis and properties of new ultraviolet-blue-emissive fluorene-based aromatic polyoxadiazoles with confinement moieties, *J. Polym. Sci., Part A: Polym. Chem.*, 41: 674–683, 2003.
362. X.-H. Zhou, J.-C. Yan, and J. Pei, Exploiting an imidazole-functionalized polyfluorene derivative as a chemosensory material, *Macromolecules*, 37: 7078–7080, 2004.
363. M.S. Liu, Z. Jiang, P. Herguth, and A.K.-Y. Jen, Efficient cyano-containing electron-transporting polymers for light-emitting diodes, *Chem. Mater.*, 13: 3820–3822, 2001.
364. W.-L. Yu, J. Pei, Y. Cao, W. Huang, and A.J. Heeger, New efficient blue light emitting polymer for light emitting diodes, *Chem. Commun.*: 1837–1838, 1999.
365. W.-L. Yu, Y. Cao, J. Pei, W. Huang, and A.J. Heeger, Blue polymer light-emitting diodes from poly(9,9-dihexylfluorene-*alt-co*-2,5-dicycloxy-*p*-phenylene), *Appl. Phys. Lett.*, 75: 3270–3272, 1999.
366. W.-L. Yu, J. Pei, W. Huang, and A.J. Heeger, Spiro-functionalized polyfluorene derivatives as blue light-emitting materials, *Adv. Mater.*, 12: 828–831, 2000.

367. D. Marsitzky, J. Murray, J.C. Scott, and K.R. Carter, Amorphous poly-2,7-fluorene networks, *Chem. Mater.*, 13: 4285–4289, 2001.
368. X.-M. Liu, C. He, X.-T. Hao, L.-W. Tan, Y. Li, and K.S. Ong, Hyperbranched blue-light-emitting alternating copolymers of tetrabromoarylmethane/silane and 9,9-dihexylfluorene-2,7-diboronic acid, *Macromolecules*, 37: 5965–5970, 2004.
369. Q. Peng, M. Xie, Y. Huang, Z. Lu, and D. Xiao, New series of highly phenyl-substituted polyfluorene derivatives for polymer light-emitting diodes, *J. Polym. Sci., Part A: Polym. Chem.*, 42: 2985–2993, 2004.
370. N.G. Pschirer and U.H.F. Bunz, Poly(fluorenylene ethynylene)s by alkyne metathesis: optical properties and aggregation behavior, *Macromolecules*, 33: 3961–3963, 2000.
371. X. Jiang, S. Liu, H. Ma, and A.K. Jen, High-performance blue light-emitting diode based on a binaphthyl-containing polyfluorene, *Appl. Phys. Lett.*, 76: 1813–1815, 2000.
372. S. Liu, X. Jiang, H. Ma, M.S. Liu, and A.K.-Y. Jen, Triarylamine-containing poly(perfluorocyclobutane) as hole-transporting materials for polymer light-emitting diodes, *Macromolecules*, 33: 3514–3517, 2000.
373. W. Wang, J. Xu, and Y.-H. Lai, Alternating conjugated and transannular chromophores: tunable property of fluorene–paracyclophane copolymers via transannular π – π interaction, *Org. Lett.*, 5: 2765–2768, 2003.
374. W. Wang, J. Xu, Y.-H. Lai, and F. Wang, Alternating aromatic and transannular chromophores with and without linker: effect of transannular π – π interaction on the optical property of dithia-paracyclophane-based copolymers, *Macromolecules*, 37: 3546–3553, 2004.
375. B. Liu, W.-L. Yu, J. Pei, S.-Y. Liu, Y.-H. Lai, and W. Huang, Design and synthesis of bipyridyl-containing conjugated polymers: effects of polymer rigidity on metal ion sensing, *Macromolecules*, 34: 7932–7940, 2001.
376. X. Kong and S.A. Jenekhe, Block copolymers containing conjugated polymer and polypeptide sequences: synthesis and self-assembly of electroactive and photoactive nanostructures, *Macromolecules*, 37: 8180–8183, 2004.
377. T. Virgili, D. Lidzey, and D.D.C. Bradley, Efficient energy transfer from blue to red in tetraporphyrin-doped poly(9,9-dioctylfluorene) light-emitting diodes, *Adv. Mater.*, 12: 58–62, 2000.
378. F.-I. Wu, R. Dodda, D.S. Reddy, and C.-F. Shu, Synthesis and characterization of spiro-linked poly(terfluorene): a blue-emitting polymer with controlled conjugated length, *J. Mater. Chem.*, 12: 2893–2897, 2002.
379. B. Liu, W.-L. Yu, Y.-H. Lai, and W. Huang, Blue-light-emitting fluorene-based polymers with tunable electronic properties, *Chem. Mater.*, 13: 1984–1991, 2001.
380. A. Donat-Bouillud, I. Lévesque, Y. Tao, M. D'Iorio, S. Beaupré, P. Blondin, M. Ranger, J. Bouchard, and M. Leclerc, Light-emitting diodes from fluorene-based π -conjugated polymers, *Chem. Mater.*, 12: 1931–1936, 2000.
381. I. Lévesque, A. Donat-Bouillud, Y. Tao, M. D'Iorio, S. Beaupré, P. Blondin, M. Ranger, J. Bouchard, and M. Leclerc, Organic tunable diodes from polyfluorene derivatives, *Synth. Met.*, 122: 79–81, 2001.
382. M. Ranger and M. Leclerc, Optical and electrical properties of fluorene-based π -conjugated polymers, *Can. J. Chem.*, 76: 1571–1577, 1998.
383. P. Blondin, J. Bouchard, S. Beaupré, M. Belletête, G. Duroche, and M. Leclerc, Molecular design and characterization of chromic polyfluorene derivatives, *Macromolecules*, 33: 5874–5879, 2000.
384. J. Pei, W.-L. Yu, W. Huang, and A.J. Heeger, The synthesis and characterization of an efficient green electroluminescent conjugated polymer: poly[2,7-bis(4-hexylthienyl)-9,9-dihexylfluorene], *Chem. Commun.*: 1631–1632, 2000.
385. B. Liu, W.-L. Yu, Y.-H. Lai, and W. Huang, Synthesis, characterization, and structure–property relationship of novel fluorene–thiophene-based conjugated copolymers, *Macromolecules*, 33: 8945–8952, 2000.
386. J. Pei, W.-L. Yu, J. Ni, Y.-H. Lai, W. Huang, and A.J. Heeger, Thiophene-based conjugated polymers for light-emitting diodes: effect of aryl groups on photoluminescence efficiency and redox behavior, *Macromolecules*, 34: 7241–7248, 2001.

387. B. Liu, W.-L. Yu, J. Pei, Y.-H. Lai, W. Huang, Y.-H. Niu, and Y. Cao, Synthesis and characterization of novel fluorene–thiophene-based conjugated copolymers, *Mater. Sci. Eng. B*, 85: 232–235, 2001.
388. B. Liu, Y.-H. Niu, W.-L. Yu, Y. Cao, and W. Huang, Application of alternating fluorene and thiophene copolymers in polymer light-emitting diodes, *Synth. Met.*, 129: 129–134, 2002.
389. G. Vamvounis and S. Holdcroft, Enhancing solid-state emission from conjugated polymers via self-forming host–guest systems, *Adv. Mater.*, 16: 716–719, 2004.
390. E. Lim, B. Jung, and H. Shim, Synthesis and characterization of a new light-emitting fluorene–thienof[3,2-*b*]thiophene-based conjugated copolymer, *Macromolecules*, 36: 4288–4293, 2003.
391. M. Inbasekaran, W. Wu, and E.P. Woo, Process for Preparing Conjugated Polymers, U.S. Patent 5,777,070, July 7, 1998.
392. Y. He, S. Gong, R. Hottori, and J. Kanicki, High performance organic polymer light-emitting heterostructure devices, *Appl. Phys. Lett.*, 74: 2265–2267, 1999.
393. C.I. Wilkinson, D.G. Lidzey, L.C. Palilis, R.B. Fletcher, S.J. Martin, X.H. Wang, and D.D.C. Bradley, Enhanced performance of pulse driven small area polyfluorene light emitting diodes, *Appl. Phys. Lett.*, 79: 171–173, 2001.
394. A.J. Campbell, D.D.C. Bradley, and H. Antoniadis, Dispersive electron transport in an electroluminescent polyfluorene copolymer measured by the current integration time-of-flight method, *Appl. Phys. Lett.*, 79: 2133–2135, 2001.
395. I.S. Millard, High-efficiency polyfluorene polymers suitable for RGB applications, *Synth. Met.*, 111–112: 119–123, 2000.
396. A.R. Buckley, M.D. Rahn, J. Hill, J. Cabanillas-Gonzalez, A.M. Fox, and D.D.C. Bradley, Energy transfer dynamics in polyfluorene-based polymer blends, *Chem. Phys. Lett.*, 339: 331–336, 2001.
397. Q. Peng, Z.-Y. Lu, Y. Huang, M.-G. Xie, D. Xiao, S.-H. Han, J.-B. Peng, and Y. Cao, Novel efficient green electroluminescent conjugated polymers based on fluorene and triarylpyrazoline for light-emitting diodes, *J. Mater. Chem.*, 14: 396–401, 2004.
398. P. Sonar, J. Zhang, A.C. Grimsdale, K. Müllen, M. Surin, R. Lazzaroni, P. Leclère, S. Tierney, M. Heeney, and I. McCulloch, 4-Hexylbithieno[3,2-*b*:2',3'-*e*]pyridine: an efficient electron-accepting unit in fluorene and indenofluorene copolymers for light-emitting devices, *Macromolecules*, 37: 709–715, 2004.
399. K. Nomura, H. Morimoto, Y. Imanishi, Z. Ramhani, and Y. Geerts, Synthesis of high molecular weight *trans*-poly(9,9-di-*n*-octylfluorene-2,7-vinylene) by the acyclic diene metathesis polymerization using molybdenum catalysts, *J. Polym. Sci., Part A: Polym. Chem.*, 39: 2463–2470, 2001.
400. S.-H. Jin, H.-J. Park, J.Y. Kim, K. Lee, S.-P. Lee, D.-K. Moon, H.-J. Lee, and Y.-S. Gal, Polyfluorenevinylene derivative by Gilch polymerization for light emitting diode applications, *Macromolecules*, 35: 7532–7534, 2002.
401. D.-H. Hwang, J.-D. Lee, J.-M. Kang, S. Lee, C.-H. Lee, and S.-H. Jin, Synthesis and light-emitting properties of poly(9,9-di-*n*-octylfluorenyl-2,7-vinylene) and PPV copolymers, *J. Mater. Chem.*, 13: 1540–1545, 2003.
402. Y. Jin, J. Ju, J. Kim, S. Lee, J.Y. Kim, S.H. Park, S.-M. Son, S.-H. Jin, K. Lee, and H. Suh, Design, synthesis, and electroluminescent property of CN-poly(dihexylfluorenevinylene) for LEDs, *Macromolecules*, 36: 6970–6975, 2003.
403. J.K. Kim, J.W. Yu, J.M. Hong, H.N. Cho, D.Y. Kim, and C.Y. Kim, An alternating copolymer consisting of light emitting and electron transporting units, *J. Mater. Chem.*, 9: 2171–2176, 1999.
404. Commercially available from American Dye Source, Inc (see at www.adsdyes.com).
405. Q. Peng, Z. Lu, Y. Huang, M. Xie, D. Xiao, and D. Zou, Novel light-emitting polymers derived from fluorene and maleimide, *J. Mater. Chem.*, 13: 1570–1574, 2003.
406. X. Zhan, S. Wang, Y. Liu, X. Wu, and D. Zhu, New series of blue-emitting and electron-transporting copolymers based on cyanostilbene, *Chem. Mater.*, 15: 1963–1969, 2003.
407. S. Beaupré and M. Leclerc, Fluorene-based copolymers for red-emitting diodes, *Adv. Funct. Mater.*, 12: 192–196, 2002.
408. N.S. Cho, D.-H. Hwang, B.-J. Jung, E. Lim, J. Lee, and H.-K. Shim, Synthesis, characterization, and electroluminescence of new conjugated polyfluorene derivatives containing various dyes as comonomers, *Macromolecules*, 37: 5265–5273, 2004.

409. S.-H. Jin, M.-Y. Kim, D.-S. Koo, and Y.-I. Kim, Synthesis and properties of poly(fluorene-*alt*-cyanophenylene vinylene)-based alternating copolymers for light-emitting diodes, *Chem. Mater.*, 16: 3299–3307, 2004.
410. Q. Peng, Z.-Y. Lu, Y. Huang, M.-G. Xie, S.-H. Han, J.-B. Peng, and Y. Cao, Synthesis and characterization of new red-emitting polyfluorene derivatives containing electron-deficient 2-pyran-4-ylidene-malononitrile moieties, *Macromolecules*, 37: 260–266, 2004.
411. M. Chen, E. Perzon, M.R. Andersson, S.K.M. Jönsson, M. Fahlman, and M. Berggren, 1 Micron wavelength photo- and electroluminescence from π -conjugated polymer, *Appl. Phys. Lett.*, 84: 3570–3572, 2004.
412. J. Pei, X.-L. Liu, W.-L. Yu, Y.-H. Lai, Y.-H. Niu, and Y. Cao, Efficient energy transfer to achieve narrow bandwidth red emission from Eu^{3+} -grafting conjugated polymers, *Macromolecules*, 35: 7274–7280, 2002.
413. P. Lu, H. Zhang, F. Shen, B. Yang, D. Li, Y. Ma, X. Chen, and J. Li, A wide-bandgap semiconducting polymer for ultraviolet and blue light emitting diodes, *Macromol. Chem. Phys.*, 204: 2274–2280, 2003.
414. Q.D. Ling, E.T. Kang, K.G. Neoh, and W. Huang, Synthesis and nearly monochromatic photoluminescence properties of conjugated copolymers containing fluorene and rare earth complexes, *Macromolecules*, 36: 6995–7003, 2003.
415. G. Klärner, J.-I. Lee, M.H. Davey, and R.D. Miller, Exciton migration and trapping in copolymers based on dialkylfluorenes, *Adv. Mater.*, 11: 115–119, 1999.
416. J.-I. Lee, T. Zyung, R.D. Miller, Y.H. Kim, S.C. Jeoung, and D. Kim, Photoluminescence study on exciton migration and trapping in a copolymer based on poly(fluorene), *J. Mater. Chem.*, 10: 1547–1550, 2000.
417. J.-I. Lee, G. Klaerner, M.H. Davey, and R.D. Miller, Color tuning in polyfluorenes by copolymerization with low band gap comonomers, *Synth. Met.*, 107: 1087–1088, 1999.
418. D.-H. Hwang, N.S. Cho, B.-J. Jung, H.-K. Shim, J.-I. Lee, L.-M. Do, and T. Zyung, Band gap tuning of new light emitting conjugated polymers, *Opt. Mater.*, 21: 199–203, 2002.
419. N.S. Cho, D.-H. Hwang, J.-I. Lee, B.-J. Jung, and H.-K. Shim, Synthesis and color tuning of new fluorene-based copolymers, *Macromolecules*, 35: 1224–1228, 2002.
420. H.N. Cho, J.K. Kim, D.Y. Kim, C.Y. Kim, N.W. Song, and D. Kim, Statistical copolymers for blue-light-emitting diodes, *Macromolecules*, 32: 1476–1481, 1999.
421. S. Jin, S.Y. Kang, M. Kim, Y.U. Chan, J. Young, K. Lee, and Y. Gal, Synthesis and electroluminescence properties of poly(9,9-di-*n*-octylfluorenyl-2,7-vinylene) derivatives for light-emitting display, *Macromolecules*, 36: 3841–3847, 2003.
422. W. Yang, Q. Hou, C. Liu, Y. Niu, J. Huang, R. Yang, and Y. Cao, Improvement of color purity in blue-emitting polyfluorene by copolymerization with dibenzothiophene, *J. Mater. Chem.*, 13: 1351–1355, 2003.
423. N. Nemoto, H. Kameshima, Y. Okano, and T. Endo, Synthesis of novel π -conjugating polymers based on dibenzothiophene, *J. Polym. Sci., Part A: Polym. Chem.*, 41: 1521–1526, 2003.
424. Y. Niu, Q. Hou, and Y. Cao, Thermal annealing below the glass transition temperature: a general way to increase performance of light-emitting diodes based on copolyfluorenes, *Appl. Phys. Lett.*, 81: 634–636, 2002.
425. O. Stéphan, F. Tran-Van, and C. Chevrot, New organic materials for light emitting devices based on dihexylfluorene-*co*-ethylenedioxythiophene copolymers exhibiting improved hole-injecting properties, *Synth. Met.*, 131: 31–40, 2002.
426. R. Yang, R. Tian, Q. Hou, W. Yang, and Y. Cao, Synthesis and optical and electroluminescent properties of novel conjugated copolymers derived from fluorene and benzoselenadiazole, *Macromolecules*, 36: 7453–7460, 2003.
427. J. Yang, C. Jiang, Y. Zhang, R. Yang, W. Yang, Q. Hou, and Y. Cao, High-efficiency saturated red emitting polymers derived from fluorene and naphthoselenadiazole, *Macromolecules*, 37: 1211–1218, 2004.
428. Q. Hou, Y. Xu, W. Yang, M. Yuan, J. Peng, and Y. Cao, Novel red-emitting fluorene-based copolymers, *J. Mater. Chem.*, 12: 2887–2892, 2002.

429. Q. Hou, Q. Zhou, Y. Zhang, W. Yang, R. Yang, and Y. Cao, Synthesis and electroluminescent properties of high-efficiency saturated red emitter based on copolymers from fluorene and 4,7-di(4-hexylthien-2-yl)-2,1,3-benzothiadiazole, *Macromolecules*, 37: 6299–6305, 2004.
430. X. Kong, A.P. Kulkarni, and S.A. Jenekhe, Phenothiazine-based conjugated polymers: synthesis, electrochemistry, and light-emitting properties, *Macromolecules*, 36: 8992–8999, 2003.
431. D.-H. Hwang, S.-K. Kim, M.-J. Park, J.-H. Lee, B.-W. Koo, I.-N. Kang, S.-H. Kim, and T. Zyung, Conjugated polymers based on phenothiazine and fluorene in light-emitting diodes and field effect transistors, *Chem. Mater.*, 16: 1298–1303, 2004.
432. D.-H. Hwang, M.-J. Park, S.-K. Kim, N.-H. Lee, C. Lee, Y.-B. Kim, and H.-K. Shim, Characterization of white electroluminescent devices fabricated using conjugated polymer blends, *J. Mater. Res.*, 19: 2081–2086, 2004.
433. For recent review on white-emitting OLEDs see: B.W. D'Andrade and S.R. Forrest, White organic light-emitting devices for solid-state lighting, *Adv. Mater.*, 16: 1585–1595, 2004.
434. C. Ego, D. Marsitzky, S. Becker, J. Zhang, A.C. Grimsdale, K. Müllen, J.D. MacKenzie, C. Silva, and R.H. Friend, Attaching perylene dyes to polyfluorene: three simple, efficient methods for facile color tuning of light-emitting polymers, *J. Am. Chem. Soc.*, 125: 437–443, 2003.
435. P. Herguth, X. Jiang, M.S. Liu, and A.K.-Y. Jen, Highly efficient fluorene and benzothiadiazole-based conjugated copolymers for polymer light-emitting diodes, *Macromolecules*, 35: 6094–6100, 2002.
436. C.D. Müller, A. Falcou, N. Reckefuss, M. Rojahn, V. Widerhirn, P. Rudati, H. Frohne, O. Nuyken, H. Becker, and K. Meerholz, Multicolour organic light-emitting displays by solution processing, *Nature*, 421: 829–833, 2003.
437. B. Liu, W.-L. Yu, Y.-H. Lai, and W. Huang, Synthesis of a novel cationic water-soluble efficient blue photoluminescent conjugated polymer, *Chem. Commun.*: 551–552, 2000.
438. B. Liu, W.-L. Yu, Y.-H. Lai, and W. Huang, Blue-light-emitting cationic water-soluble polyfluorene derivatives with tunable quaternization degree, *Macromolecules*, 35: 4975–4982, 2002.
439. F. Huang, H. Wu, D. Wang, W. Yang, and Y. Cao, Novel electroluminescent polyelectrolytes based on polyfluorene, *Chem. Mater.*, 16: 708–716, 2004.
440. F. Huang, L. Hou, H. Wu, X. Wang, H. Shen, W. Cao, W. Yang, and Y. Cao, High-efficiency, environment-friendly electroluminescent polymers with stable high work function metal as a cathode: green- and yellow-emitting conjugated polyfluorene polyelectrolytes and their neutral precursors, *J. Am. Chem. Soc.*, 126: 9845–9853, 2004.
441. B. Liu, S. Wang, G.C. Bazan, and A. Mikhailovsky, Shape-adaptable water-soluble conjugated polymers, *J. Am. Chem. Soc.*, 125: 13306–13307, 2003.
442. B. Liu and G.C. Bazan, Interpolyelectrolyte complexes of conjugated copolymers and DNA: platforms for multicolor biosensors, *J. Am. Chem. Soc.*, 126: 1942–1943, 2004.
443. H.D. Burrows, V.M.M. Lobo, J. Pina, M.L. Ramos, J.S. de Melo, A.J.M. Velente, M.J. Tapia, S. Pradhan, and U. Scherf, Fluorescence enhancement of the water-soluble poly{1,4-phenylene-[9,9-bis(4-phenoxybutyl)sulfonate]fluorene-2,7-diyl}copolymer in *n*-dodecylpentaoxyethylene glycol ether micelles, *Macromolecules*, 37: 7425–7427, 2004.
444. J. Roncali, Conjugated poly(thiophenes): synthesis, functionalization, and applications, *Chem. Rev.*, 92: 711–738, 1992.
445. D. Fichou, Ed., *Handbook of Oligo- and Polythiophenes*, Wiley, Weinheim, 1999, p. 534.
446. R.D. McCullough, The chemistry of conducting polythiophenes, *Adv. Mater.*, 10: 93–116, 1998.
447. J. Roncali, Electrogenerated functional conjugated polymers as advanced electrode materials, *J. Mater. Chem.*, 9: 1875–1893, 1999.
448. M. Theander, O. Inganäs, W. Mammo, T. Olinga, M. Svensson, and M. Andersson, Photophysics of substituted polythiophenes, *J. Phys. Chem. B*, 103: 7771–7780, 1999.
449. N.C. Greenham, I.D.W. Samuel, G.R. Hayes, R.T. Phillips, Y.A.R.R. Kessener, S.C. Moratti, A.B. Holmes, and R.H. Friend, Measurements of absolute photoluminescence quantum efficiencies in conjugated polymers, *Chem. Phys. Lett.*, 241: 89–96, 1995.
450. F. Chen, P.G. Mehta, L. Takiff, and R.D. McCullough, Improved electroluminescence performance of poly(3-alkylthiophenes) having a high head-to-tail (HT) ratio, *J. Mater. Chem.*, 6: 1763–1766, 1996.
451. F. Garnier, Organic-based electronics *à la Carte*, *Acc. Chem. Res.*, 32: 209–215, 1999.

452. H. Saadeh, T. Goodson, III, and L. Yu, Synthesis of a polyphenylene-*co*-furan and polyphenylene-*co*-thiophene and comparison of their electroluminescent properties, *Macromolecules*, 30: 4608–4612, 1997.
453. B. Kraabel, D. Moses, and A.J. Heeger, Direct observation of the intersystem crossing in poly(3-octylthiophene), *J. Chem. Phys.*, 103: 5102–5108, 1995.
454. M. Leclerc and K. Fäid, Conformation-induced chromism in conjugated polymers, in: *Handbook of Conducting Polymers*, T.A. Skotheim, R.L. Elsenbaumer, and J.R. Reynolds, Eds., Marcel Dekker, New York, 1998, pp. 695–706.
455. G. Zerbi, B. Chierichetti, and O. Ingänas, Vibrational spectra of oligothiophenes as model of polythiophenes, *J. Chem. Phys.*, 94: 4637–4645, 1991.
456. G. Zerbi, B. Chierichetti, and O. Ingänas, Thermochromism in polyalkylthiophenes: molecular aspects from vibrational spectroscopy, *J. Chem. Phys.*, 94: 4646–4658, 1991.
457. Y. Yamamoto, K. Sanechika, and A. Yamamoto, Preparation of thermostable and electric-conducting poly(2,5-thienylene), *J. Polym. Sci., Polym. Lett. Ed.*, 18: 9–12, 1980.
458. J.W.-P. Lin and L.P. Dudek, Synthesis and properties of poly(2,5-thienylene), *J. Polym. Sci., Polym. Chem. Ed.*, 18: 2869–2873, 1980.
459. M. Kobayashi, J. Chen, T.-C. Chung, F. Moraes, A.J. Heeger, and F. Wudl, Synthesis and properties of chemically coupled poly(thiophene), *Synth. Met.*, 9: 77–86, 1984.
460. T. Yamamoto, A. Morita, Y. Miyazaki, T. Maruyama, H. Wakayama, Z.H. Zhou, Y. Nakamura, T. Kanbara, S. Sasaki, and K. Kubota, Preparation of π -conjugated poly(thiophene-2,5-diyl), poly(*p*-phenylene), and related polymers using zerovalent nickel complexes. Linear structure and properties of the π -conjugated polymers, *Macromolecules*, 25: 1214–1223, 1992.
461. K. Yoshino, S. Hayashi, and R. Sugimoto, Preparation and properties of conducting heterocyclic polymer films by chemical method, *Jpn. J. Appl. Phys., Part 2*, 23: L899–L900, 1984.
462. M. Leclerc, F.M. Diaz, and G. Wegner, Structural analysis of poly(3-alkylthiophenes), *Makromol. Chem.*, 190: 3105–3116, 1989.
463. M. Pomerantz, J.J. Tseng, H. Zhu, S.J. Sproull, J.R. Reynolds, R. Uitz, H.G. Amott, and M.I. Haider, Processable polymers and copolymers of 3-alkylthiophenes and their blends, *Synth. Met.*, 41–43: 825–833, 1991.
464. K. Tamao, S. Kodama, I. Nakajima, M. Kumada, A. Minato, and K. Suzuki, Nickel-phosphine complex-catalyzed Grignard coupling — II: Grignard coupling of heterocyclic compounds, *Tetrahedron*, 38: 3347–3354, 1982.
465. S. Amou, O. Haba, K. Shirato, T. Hayakawa, M. Ueda, K. Takeuchi, and M. Asai, Head-to-tail regioregularity of poly(3-hexylthiophene) in oxidative coupling polymerization with FeCl_3 , *J. Polym. Sci., Part A: Polym. Chem.*, 37: 1943–1948, 1999.
466. M.R. Andersson, D. Selse, M. Berggren, H. Järvinen, T. Hjertberg, O. Inganäs, O. Wennerström, and J.-E. Österholm, Regioselective polymerization of 3-(4-octylphenyl)thiophene with FeCl_3 , *Macromolecules*, 27: 6503–6506, 1994.
467. R.D. McCullough and R.D. Lowe, Enhanced electrical conductivity in regioselectively synthesized poly(3-alkylthiophenes), *J. Chem. Soc., Chem. Commun.*: 70–72, 1992.
468. R.D. McCullough, R.D. Lowe, M. Jayaraman, and D.L. Anderson, Design, synthesis, and control of conducting polymer architectures: structurally homogeneous poly(3-alkylthiophenes), *J. Org. Chem.*, 58: 904–912, 1993.
469. R.S. Loewe, S.M. Khersonsky, and R.D. McCullough, A simple method to prepare head-to-tail coupled, regioregular poly(3-alkylthiophenes) using Grignard metathesis, *Adv. Mater.*, 11: 250–253, 1999.
470. R.S. Loewe, P.C. Ewbank, J. Liu, L. Zhai, and R.D. McCullough, Regioregular, head-to-tail coupled poly(3-alkylthiophenes) made easy but the GRIM method: investigation of the reaction and the origin of regioselectivity, *Macromolecules*, 34: 4324–4333, 2001.
471. R.D. McCullough and R.S. Loewe, Method of Forming Poly-(3-Substituted) Thiophenes, U.S. Patent 6,166,172, December 26, 2000.
472. R.D. McCullough, P.C. Ewbank, and R.S. Loewe, Self-assembly and disassembly of regioregular, water soluble polythiophenes: chemoselective ionchromatic sensing in water, *J. Am. Chem. Soc.*, 119: 633–634, 1997.

473. S. Guillerez and G. Bidan, New convenient synthesis of highly regioregular poly(3-octylthiophene) based on the Suzuki coupling reaction, *Synth. Met.*, 93: 123–126, 1998.
474. T.A. Chen and R.D. Rieke, The first regioregular head-to-tail poly(3-hexylthiophene-2,5-diyl) and a regiorandom isopolymer: nickel versus palladium catalysis of 2(5)-bromo-5(2)- (bromozincio)-3-hexylthiophene polymerization, *J. Am. Chem. Soc.*, 114: 10087–10088, 1992.
475. T.-A. Chen, X. Wu, and R.D. Rieke, Regiocontrolled synthesis of poly(3-alkylthiophenes) mediated by Rieke zinc: their characterization and solid-state properties, *J. Am. Chem. Soc.*, 117: 233–244, 1995.
476. Y. Ohmori, M. Uchida, K. Muro, and K. Yoshino, Visible-light electroluminescent diodes utilizing poly(3-alkylthiophenes), *Jpn. J. Appl. Phys., Part 2*, 30: L1938–L1940, 1991.
477. Y. Ohmori, M. Uchida, K. Muro, and K. Yoshino, Effects of alkyl chain lengths and carrier confinement layer on characteristics of poly(3-alkylthiophene) electroluminescent diodes, *Solid State Commun.*, 80: 605–608, 1991.
478. M. Uchida, Y. Ohmori, C. Morishima, and K. Yoshino, Visible and blue electroluminescent diodes utilizing poly(3-alkylthiophene)s and poly(alkylfluorene)s, *Synth. Met.*, 55–57: 4168–4173, 1993.
479. D. Braun, G. Gustafsson, D. McBranch, and A.J. Heeger, Electroluminescence and electrical transport in poly(3-octylthiophene) diodes, *J. Appl. Phys.*, 72: 564–568, 1992.
480. N.C. Greenham, A.R. Brown, D.D.C. Bradley, and R.H. Friend, Electroluminescence in poly(3-alkylthienylene)s, *Synth. Met.*, 57: 4134–4138, 1993.
481. A. Bolognesi, C. Botta, Z. Geng, C. Flores, and L. Denti, Modified poly(3-alkylthiophene) for LED preparation, *Synth. Met.*, 71: 2191–2192, 1995.
482. A. Bolognesi, W. Porzio, G. Bajo, G. Zannoni, and L. Fanning, Highly regioregular poly(3-alkylthiophenes): a new synthetic route and characterization of the resulting polymers, *Acta Polym.*, 50: 151–155, 1999.
483. A. Bolognesi, C. Botta, and L. Cecchinato, Optical properties and electroluminescence of poly(3-alkylmethoxy-thiophene) single- and double-layer structures, *Synth. Met.*, 111–112: 187–189, 2000.
484. A. Bolognesi, W. Porzio, F. Provasoli, and T. Ezquerra, The thermal behavior of low-molecular-weight poly(3-decylthiophene), *Makromol. Chem.*, 194: 817–827, 1993.
485. M. Pomerantz, H. Yang, and Y. Cheng, Poly(alkyl thiophene-3-carboxylates). Synthesis and characterization of polythiophenes with a carbonyl group directly attached to the ring, *Macromolecules*, 28: 5706–5708, 1995.
486. T. Yamamoto and H. Hayashi, π -Conjugated soluble and fluorescent poly(thiophene-2,5-diyl)s with phenolic, hindered phenolic and *p*-C₆H₄OCH₃ substituents. Preparation, optical properties, and redox reaction, *J. Polym. Sci., Part A: Polym. Chem.*, 35: 463–474, 1997.
487. S.H. Jin, B.U. Yoo, S.Y. Kang, Y.S. Gal, and D.K. Moon, Synthesis and electro-optical properties of polythiophene derivatives for electroluminescence display, *Opt. Mater.*, 21: 153–157, 2002.
488. S.-H. Ahn, M.-Z. Czae, E.-R. Kim, H. Lee, S.-H. Han, J. Noh, and M. Hara, Synthesis and characterization of soluble polythiophene derivatives containing electron-transporting moiety, *Macromolecules*, 34: 2522–2527, 2001.
489. B. Xu and S. Holdcroft, Molecular control of luminescence from poly(3-hexylthiophenes), *Macromolecules*, 26: 4457–4460, 1993.
490. P. Barta, F. Cacialli, R.H. Friend, and M. Zagórska, Efficient photo- and electroluminescence of regioregular poly(alkylthiophene)s, *J. Appl. Phys.*, 84: 6279–6284, 1998.
491. M. Zagórska and B. Krische, Chemical synthesis and characterization of soluble poly(4,4'-dialkyl-2,2'-bithiophenes), *Polymer*, 31: 1379–1383, 1990.
492. P. Barta, P. Dannetun, S. Stafström, M. Zagórska, and A. Proñ, Temperature evolution of the electronic band structure of the undoped and doped regioregular analog of poly(3-alkylthiophenes): a spectroscopic and theoretical study, *J. Chem. Phys.*, 100: 1731–1741, 1994.
493. M. Pomerantz, Y. Cheng, R.K. Kasim, and R.L. Elsenbaumer, Poly(alkylthiophene-3-carboxylates). Synthesis, properties and electroluminescence studies of polythiophenes containing carbonyl group directly attached to the ring, *J. Mater. Chem.*, 9: 2155–2163, 1999.

494. R.E. Gill, G.G. Malliaras, J. Wildeman, and G. Hadziioannou, Tuning of photo- and electroluminescence in alkylated polythiophenes with well-defined regioregularity, *Adv. Mater.*, 6: 132–135, 1994.
495. J.L. Brédas, R. Silbey, D.S. Boudreaux, and R.R. Chance, Chain-length dependence of electronic and electrochemical properties of conjugated systems: polyacetylene, polyphenylene, polythiophene, and polypyrrole, *J. Am. Chem. Soc.*, 105: 6555–6559, 1983.
496. M. Boman and S. Stafström, Interpretation of anomalous absorption spectra. A theoretical study of the geometric, electronic and optical properties of poly[3-(4-octylphenyl)thiophene], *Mol. Cryst. Liq. Cryst. Sci. Technol.*, 256: 705–710, 1994.
497. O. Inganäs, Making polymer light emitting diodes with polythiophenes, in: *Organic Electroluminescent Materials and Devices*, S. Miyata and H.S. Nalwa, Eds., Gordon & Breach, Langhorne, 1997, pp. 147–175.
498. M.R. Andersson, M. Berggren, O. Inganäs, G. Gustafsson, J.C. Gustafsson-Carlberg, D. Selse, T. Hjertberg, and O. Wennerström, Electroluminescence from substituted poly(thiophenes): from blue to near-infrared, *Macromolecules*, 28: 7525–7529, 1995.
499. M.R. Andersson, W. Mammo, T. Olinga, M. Svensson, M. Theander, and O. Inganäs, Synthesis of regioregular phenyl substituted polythiophenes with FeCl₃, *Synth. Met.*, 101: 11–12, 1999.
500. Q. Pei, H. Järvinen, J.E. Österholm, O. Inganäs, and J. Laakso, Poly[3-(4-octylphenyl)thiophene], a new processible conducting polymer, *Macromolecules*, 25: 4297–4301, 1992.
501. M. Berggren, G. Gustafsson, O. Inganäs, M.R. Andersson, O. Wennerström, and T. Hjertberg, Green electroluminescence in poly-(3-cyclohexylthiophene) light-emitting diodes, *Adv. Mater.*, 6: 488–490, 1994.
502. M.R. Andersson, M. Berggren, T. Olinga, T. Hjertberg, O. Inganäs, and O. Wennerström, Improved photoluminescence efficiency of films from conjugated polymers, *Synth. Met.*, 85: 1383–1384, 1997.
503. A. Ruseckas, E.B. Namadas, T. Ganguly, M. Theander, M. Svensson, M.R. Andersson, O. Inganäs, and V. Sundström, Intra- and interchain luminescence in amorphous and semicrystalline films of phenyl-substituted polythiophene, *J. Phys. Chem. B*, 105: 7624–7631, 2001.
504. M. Berggren, G. Gustafsson, O. Inganäs, M.R. Andersson, O. Wennerström, and T. Hjertberg, Thermal control of near-infrared and visible electroluminescence in alkyl-phenyl substituted polythiophenes, *Appl. Phys. Lett.*, 65: 1489–1491, 1994.
505. M. Berggren, P. Bergman, J. Fagerström, O. Inganäs, M.R. Andersson, H. Weman, M. Granström, S. Stafström, O. Wennerström, and T. Hjertberg, Controlling inter-chain and intra-chain excitations of a poly(thiophene) derivative in thin films, *Chem. Phys. Lett.*, 304: 84–90, 1999.
506. Y. Li, G. Vamvounis, and S. Holdcroft, Tuning optical properties and enhancing solid-state emission of poly(thiophene)s by molecular control: a postfunctionalization approach, *Macromolecules*, 35: 6900–6906, 2002.
507. Y. Li, G. Vamvounis, J. Yu, and S. Holdcroft, A novel and versatile methodology for functionalization of conjugated polymers. Transformation of poly(3-bromo-4-hexylthiophene) via palladium-catalyzed coupling chemistry, *Macromolecules*, 34: 3130–3132, 2001.
508. V. Saxena and V.S. Shirodkar, A study of light-emitting diodes constructed with copolymers having cyclohexyl thiophene and hexyl thiophene units, *J. Appl. Polym. Sci.*, 77: 1051–1055, 2000.
509. G.G. Malliaras, J.K. Herrema, J. Wildeman, R.H. Wieringa, R.E. Gill, S.S. Lampoura, and G. Hadziioannou, Tuning of the photo- and electroluminescence in multi-block copolymers of poly[(silanylene)-thiophene]s via exciton confinement, *Adv. Mater.*, 5: 721–723, 1993.
510. J.K. Herrema, P.F. van Hutten, R.E. Gill, J. Wildeman, R.H. Wieringa, and G. Hadziioannou, Tuning of the luminescence in multiblock alternating copolymers. 1. Synthesis and spectroscopy of poly[(silanylene)thiophene]s, *Macromolecules*, 28: 8102–8116, 1995.
511. K. Yoshino, M. Hirohata, T. Sonoda, R. Hidayat, A. Fujii, A. Naka, and M. Ishikawa, Electroluminescence and photoluminescence characteristics of poly(disilanylene oligophenylene)s and poly(disilanylene oligothiophenylene)s, *Synth. Met.*, 102: 1158, 1999.
512. T. Johansson, W. Mammo, M.R. Andersson, and O. Inganäs, Light-emitting electrochemical cells from oligo(ethylene oxide)-substituted polythiophenes: evidence for *in situ* doping, *Chem. Mater.*, 11: 3133–3139, 1999.

513. M. Berggren, O. Inganäs, G. Gustafsson, J. Rasmussen, M.R. Andersson, T. Hjertberg, and O. Wennerström, Light-emitting diodes with variable colours from polymer blends, *Nature*, 372: 444–446, 1994.
514. O. Inganäs, M. Berggren, M.R. Andersson, G. Gustafsson, T. Hjertberg, O. Wennerström, P. Dyreklev, and M. Granström, Thiophene polymers in light emitting diodes: making multicolor devices, *Synth. Met.*, 71: 2121–2124, 1995.
515. M. Granström and O. Inganäs, White light emission from a polymer blend light emitting diode, *Appl. Phys. Lett.*, 68: 147–149, 1996.
516. M. Granström, M. Berggren, D. Pede, O. Inganäs, M.R. Andersson, T. Hjertberg, and O. Wennerström, Self-organizing polymer films — a route to novel electronic devices based on conjugated polymers, *Supramol. Sci.*, 4: 27–34, 1997.
517. S. Destri, U. Giovanella, A. Fazio, W. Porzio, B. Gabriele, and G. Zotti, A new soluble poly(bithiophene)-co-3,4-di(methoxycarbonyl)methylthiophene for LED, *Org. Electron.*, 3: 149–156, 2002.
518. M. Berggren, G. Gustafsson, O. Inganäs, M.R. Andersson, T. Hjertberg, and O. Wennerström, White light from an electroluminescent diode made from poly[3(4-octylphenyl)-2,2'-bithiophene] and an oxadiazole derivative, *Appl. Phys. Lett.*, 76: 7530–7534, 1994.
519. T. Granlund, L.A.A. Pettersson, M.R. Andersson, and O. Inganäs, Interference phenomenon determines the color in an organic light emitting diode, *J. Appl. Phys.*, 81: 8097–8103, 1997.
520. G. Yu, H. Nishino, A.J. Heeger, T.-A. Chen, and R.D. Rieke, Enhanced electroluminescence from semiconducting polymer blends, *Synth. Met.*, 72: 249–252, 1995.
521. E.J.W. List, L. Holzer, S. Tasch, G. Leising, M. Catellani, and S. Luzzati, Efficient, single layer yellow light emitting diodes made of a blend of a ladder-type poly(*p*-phenylene) and polyalkylthiophene, *Opt. Mater.*, 12: 311–314, 1999.
522. E.J.W. List, L. Holzer, S. Tasch, G. Leising, U. Scherf, K. Müllen, M. Catellani, and S. Luzzati, Efficient single-layer yellow-light emitting-diodes with ladder-type poly(*p*-phenylene/poly(decylthiophene) blends, *Solid State Commun.*, 109: 455–459, 1999.
523. A. Bolognesi, G. Bajo, J. Paloheimo, T. Östergård, and H. Stubb, Polarized electroluminescence from an oriented poly(3-alkylthiophene) Langmuir–Blodgett structure, *Adv. Mater.*, 9: 121–124, 1997.
524. P. Dyreklev, M. Berggren, O. Inganäs, M.R. Andersson, O. Wennerström, and T. Hjertberg, Polarized electroluminescence from an oriented substituted polythiophene in a light emitting diode, *Adv. Mater.*, 7: 43–45, 1995.
525. M. Berggren, O. Inganäs, T. Granlund, S. Guo, G. Gustafsson, and M.R. Andersson, Polymer light-emitting diodes placed in microcavities, *Synth. Met.*, 76: 121–123, 1996.
526. M. Granström, Novel polymer light-emitting diode designs using poly(thiophenes), *Polym. Adv. Technol.*, 8: 424–430, 1997.
527. M. Granström, M. Berggren, and O. Inganäs, Micrometer- and nanometer-sized polymeric light emitting diodes, *Science*, 267: 1479–1481, 1995.
528. M. Granström and O. Inganäs, Flexible arrays of sub-micron sized polymeric light-emitting diodes, *Adv. Mater.*, 7: 1012–1015, 1995.
529. F. Geiger, M. Stoldt, H. Schweizer, P. Bäuerle, and E. Umbach, Electroluminescence from oligothiophene-based light-emitting devices, *Adv. Mater.*, 5: 922–925, 1993.
530. S.A. Lee, Y. Yoshida, M. Fukuyama, and S. Hotta, Phenyl-capped oligothiophenes: novel light-emitting materials with different molecular alignments in thin films, *Synth. Met.*, 106: 39–43, 1999.
531. S. Hotta, Y. Ichino, Y. Yoshida, and M. Yoshida, Spectroscopic features of thin films of thiophene/phenylene co-oligomers with vertical molecular alignment, *J. Phys. Chem. B*, 104: 10316–10320, 2000.
532. S.A. Lee, S. Hotta, and F. Nakanishi, Spectroscopic characteristics and intermolecular interactions of thiophene/phenylene co-oligomers in solutions, *J. Phys. Chem. A*, 104: 1827–1833, 2000.
533. K. Uchiyama, H. Akimichi, S. Hotta, H. Noge, and H. Sakaki, Electroluminescence from thin film of a semiconducting oligothiophene deposited in ultrahigh vacuum, *Synth. Met.*, 63: 57–59, 1994.
534. T. Noda, H. Ogawa, N. Noma, and Y. Shirota, A novel yellow-emitting material, 5,5''-bis{4-[bis(4-methylphenyl)amino]phenyl}-2,2': 5',2''-terthiophene, for organic electroluminescent devices, *Appl. Phys. Lett.*, 70: 699–701, 1997.

535. T. Noda, H. Ogawa, N. Noma, and Y. Shirota, A novel family of amorphous molecular materials containing an oligothiophene moiety as color-tunable emitting materials for organic electroluminescent devices, *Adv. Mater.*, 9: 720–722, 1997.
536. K. Chondroudis and D.B. Mitzi, Electroluminescence from an organic–inorganic perovskite incorporating a quaterthiophene dye within lead halide perovskite layer, *Chem. Mater.*, 11: 3028–3030, 1999.
537. A.W. Freeman, S.C. Koene, P.R.L. Malenfant, M.E. Thompson, and J.M.J. Fréchet, Dendrimer-containing light-emitting diodes: toward site-isolation of chromophores, *J. Am. Chem. Soc.*, 122: 12385–12386, 2000.
538. G. Barbarella, L. Favaretto, M. Zambianchi, O. Pudova, C. Arbizzani, A. Bongini, and M. Mastragostino, From easily oxidized to easily reduced thiophene-based materials, *Adv. Mater.*, 10: 551–554, 1998.
539. G. Barbarella, L. Favaretto, G. Sotgiu, M. Zambianchi, L. Antolini, O. Pudova, and A. Bongini, Oligothiophene *S,S*-dioxides. Synthesis and electronic properties in relation to the parent oligothiophenes, *J. Org. Chem.*, 63: 5497–5506, 1998.
540. G. Gigli, M. Ani, G. Barbarella, L. Favaretto, F. Cacialli, and R. Cingolani, High photo and electroluminescence efficiency oligothiophenes, *Physica E*, 7: 612–615, 2000.
541. L. Antolini, E. Tadesco, G. Barbarella, L. Favaretto, G. Sotgiu, M. Zambianchi, D. Casarini, G. Gigli, and R. Cingolani, Molecular packing and photoluminescence efficiency in odd-membered oligothiophene *S,S*-dioxides, *J. Am. Chem. Soc.*, 122: 9006–9013, 2000.
542. G. Barbarella, L. Favaretto, G. Sotgiu, M. Zambianchi, A. Bongini, C. Arbizzani, M. Mastragostino, M. Anni, G. Gigli, and R. Cingolani, Tuning solid-state photoluminescence frequencies and efficiencies of oligomers containing one central thiophene-*S,S*-dioxide unit, *J. Am. Chem. Soc.*, 122: 11971–11978, 2000.
543. G. Gigli, G. Barbarella, L. Favaretto, F. Cacialli, and R. Cingolani, High-efficiency oligothiophene-based light-emitting diodes, *Appl. Phys. Lett.*, 75: 439–441, 1999.
544. A. Berlin, G. Zotti, S. Zecchin, G. Schiavon, M. Cocchi, D. Virgili, and C. Sabatini, 3,4-Ethylenedioxy-substituted bithiophene-*alt*-thiophene-*S,S*-dioxide regular copolymers. Synthesis and conductive, magnetic and luminescence properties, *J. Mater. Chem.*, 13: 27–33, 2003.
545. A. Charas, J. Morgado, J.M.G. Martinho, L. Alcácer, S.F. Lim, R.H. Friend, and F. Cacialli, Synthesis and luminescence properties of three novel polyfluorene copolymers, *Polymer*, 44: 1843–1850, 2003.
546. A. Charas, J. Morgado, J.M.G. Martinho, L. Alcácer, and F. Cacialli, Electrochemical and luminescent properties of poly(fluorene) derivatives for optoelectronic applications, *Chem. Commun.*: 1216–1217, 2001.
547. A. Charas, J. Morgado, J.M.G. Martinho, A. Fedorov, L. Alcácer, and F. Cacialli, Excitation energy transfer and spatial exciton confinement in polyfluorene blends for application in light-emitting diodes, *J. Mater. Chem.*, 12: 3523–3527, 2002.
548. M. Passini, S. Destri, W. Porzio, C. Botta, and U. Giovanella, Electroluminescent poly(fluorene-*co*-thiophene-*S,S*-dioxide): synthesis, characterisation and structure–property relationships, *J. Mater. Chem.*, 13: 807–813, 2003.
549. S. Destri, M. Pasini, W. Porzio, G. Gigi, D. Pisignano, and C. Capolupo, Emission properties and solid-state aggregation in poly(fluorene–thiophene-*S,S*-dioxide) and in its model oligomer, *Synth. Met.*, 138: 289–293, 2003.
550. J.-F. Morin and M. Leclerc, 2,7-Carbazole-based conjugated polymers for blue, green, and red light emission, *Macromolecules*, 35: 8413–8417, 2002.
551. M. Fahlman, J. Birgersson, K. Kaeriyama, and W.R. Salaneck, Poly(2,5-diheptyl-1,4-phenylene-*alt*-2,5-thienylene): a new material for blue-light-emitting diodes, *Synth. Met.*, 75: 223–228, 1995.
552. J.-L. Brédas and A.J. Heeger, Influence of donor and acceptor substituents on the electronic characteristics of poly(*p*-phenylene vinylene) and poly(*p*-phenylene), *Chem. Phys. Lett.*, 217: 507–512, 1994.
553. J.-L. Brédas, R.L. Elsenbaumer, R.R. Chance, and R. Silbey, Electronic properties of sulfur containing conjugated polymers, *J. Chem. Phys.*, 78: 5656–5662, 1983.
554. J. Birgersson, K. Kaeriyama, P. Barta, P. Bröms, M. Fahlman, T. Granlund, and W.R. Salaneck, Efficient blue-light emitting devices from conjugated polymer blends, *Adv. Mater.*, 8: 982–985, 1996.

555. H. Saadeh, T. Goodson, III, and L. Yu, Synthesis of a poly(phenylene-*co*-furan and poly(phenylene-*co*-thiophene) and comparison of their electroluminescent properties, *Macromolecules*, 30: 4608–4612, 1997.
556. J. Pei, W.-L. Yu, W. Huang, and A.J. Heeger, A novel series of efficient thiophene-based light-emitting conjugated polymers and application in polymer light-emitting diodes, *Macromolecules*, 33: 2462–2471, 2000.
557. A.-L. Ding, J. Pei, Y.-H. Lai, and W. Huang, Phenylene-functionalized polythiophene derivatives for light-emitting diodes: their synthesis, characterization and properties, *J. Mater. Chem.*, 11: 3082–3086, 2001.
558. J. Pei, W.-L. Yu, J. Ni, Y.-H. Lai, W. Huang, and A.J. Heeger, Thiophene-based conjugated polymers for light-emitting diodes: effect of aryl groups on photoluminescence efficiency and redox behavior, *Macromolecules*, 34: 7241–7248, 2001.
559. K.Y. Musick, Q.-S. Hu, and L. Pu, Synthesis of binaphthyl-oligothiophene copolymers with emissions of different colors: systematically tuning the photoluminescence of conjugated polymers, *Macromolecules*, 31: 2933–2942, 1998.
560. Y. Liu, G. Yu, A.K.-Y. Jen, Q.-S. Hu, and L. Pu, A binaphthyl-bithiophene copolymer for light-emitting devices, *Macromol. Chem. Phys.*, 203: 37–40, 2002.
561. S.-Y. Song and H.-K. Shim, Synthesis of poly(phenylene-*alt*-thiophene) polymer and characterization of its emitting properties, *Synth. Met.*, 111–112: 437–439, 2000.
562. W. Huang, H. Meng, W.-L. Yu, J. Gao, and A.J. Heeger, A new blue light-emitting polymer containing substituted thiophene and an arylene-1,3,4-oxadiazole moiety, *Adv. Mater.*, 10: 593–596, 1998.
563. W. Huang, W.-L. Yu, H. Meng, J. Pei, and S.F.Y. Li, New series of blue-light-emitting polymers constituted of 3-alkylthiophenes and 1,4-di(1,3,4-oxadiazolyl)phenylene, *Chem. Mater.*, 10: 3340–3345, 1998.
564. W. Huang, H. Meng, W.-L. Yu, J. Pei, Z.-K. Chen, and Y.-H. Lai, A novel series of *p*-*n* diblock light-emitting copolymers based on oligothiophenes and 1,4-bis(oxadiazolyl)-2,5-dialkyloxybenzenes, *Macromolecules*, 32: 118–126, 1999.
565. H. Meng and W. Huang, Novel photoluminescent polymers containing oligothiophene and *m*-phenylene-1,3,4-oxadiazole moieties: synthesis and spectroscopic and electrochemical studies, *J. Org. Chem.*, 65: 3894–3901, 2000.
566. C.J. Tonzola, M.M. Alam, and S.A. Jenekhe, New soluble *n*-type conjugated copolymer for lightemitting diodes, *Adv. Mater.*, 14: 1086–1090, 2002.
567. C.J. Tonzola, M.M. Alam, B.A. Bean, and S.A. Jenekhe, New soluble *n*-type conjugated polymers for use as electron transport materials in light-emitting diodes, *Macromolecules*, 37: 3554–3563, 2004.
568. A. Dhanabalan, J.K.J. van Duren, P.A. van Hal, J.L.J. van Dongen, and R.A.J. Janssen, Synthesis and characterization of a low bandgap conjugated polymer for bulk heterojunction photovoltaic cells, *Adv. Funct. Mater.*, 11: 255–262, 2001.
569. C.J. Brabec, C. Winder, N.S. Sariciftci, J.C. Hummelen, A. Dhanabalan, P.A. van Hal, and R.A.J. Janssen, A low-bandgap semiconducting polymer for photovoltaic devices and infrared emitting diodes, *Adv. Funct. Mater.*, 12: 709–721, 2002.
570. J. Roncali, Oligothiénylenevinylenes as a new class of multianometer linear π -conjugated systems for micro- and nanoelectronics, *Acc. Chem. Res.*, 33: 147–156, 2000.
571. J.V. Grazulevicius, P. Strohriegel, J. Pielichowski, and K. Pielichowski, Carbazole-containing polymers: synthesis, properties and applications, *Prog. Polym. Sci.*, 29: 1297–1353, 2003.
572. G. Grem, G. Leditzky, B. Ullrich, and G. Leising, Realization of a blue-light emitting device using poly(*p*-phenylene), *Adv. Mater.*, 4: 36–37, 1992.
573. G. Grem, G. Leditzky, and G. Leising, Blue electroluminescent device based on conjugated polymer, *Synth. Met.*, 51: 383–389, 1992.
574. A.-D. Schlüter and G. Wegner, Palladium and nickel catalyzed polycondensation — the key to structurally defined polyarene and other aromatic polymers, *Acta Polym.*, 44: 59–69, 1993.
575. M. Rahahn, A.-D. Schlüter, G. Wegner, and W.J. Feast, Soluble poly(*p*-phenylene)s. 1. Extension of the Yamamoto synthesis to dibromobenzenes substituted with flexible side chains, *Polymer*, 30: 1054–1059, 1989.

576. N. Tanigaki, H. Masude, and K. Kaeriyama, Substituted poly(*p*-phenylene)s prepared from 2,5-diheptylbenzene-1,4-bis(trimethylene boronate), *Polymer*, 38: 1221–1226, 1997.
577. Y. Yang, Q. Pei, and A.J. Heeger, Efficient blue polymer light-emitting diodes from a series of soluble poly(*p*-phenylene)s, *J. Appl. Phys.*, 79: 934–936, 1996.
578. S.-A. Chen and C.-I. Chao, Poly(2-alkoxy-*p*-phenylene)s as deep-blue light-emitting polymers, *Synth. Met.*, 79: 93–96, 1996.
579. A. Edwards, S. Blumstengel, I. Sokolik, R. Dorsinville, H. Yun, T.K. Kwei, and Y. Okamoto, Blue photo- and electroluminescence from poly(benzoyl-1,4-phenylene), *Appl. Phys. Lett.*, 70: 298–300, 1997.
580. J. Huang, H. Zhang, W. Tian, J. Hou, Y. Ma, J. Shen, and S. Liu, Violet-blue electroluminescent diodes utilizing conjugated polymer blends, *Synth. Met.*, 87: 105–108, 1997.
581. W.-X. Jing, A. Kraft, S.C. Moratti, J. Grüner, F. Cacialli, P.J. Hamer, A.B. Holmes, and R.H. Friend, Synthesis of a polyphenylene light-emitting copolymer, *Synth. Met.*, 67: 161–163, 1994.
582. M. Hamaguchi and K. Yoshino, Blue electroluminescence from poly(2,5-diheptyloxy-1,4-phenylene), *Jpn. J. Appl. Phys.*, 34: L587–L589, 1995.
583. G. Grem and G. Leising, Electroluminescence of “wide-bandgap” chemically tunable cyclic conjugated polymers, *Synth. Met.*, 57: 4105–4110, 1993.
584. Y. Yang, Q. Pei, and A.J. Heeger, Efficient blue light-emitting diodes from a soluble poly(*p*-phenylene): internal field emission measurement of the energy gap in semiconducting polymers, *Synth. Met.*, 78: 263–267, 1996.
585. J. Birgerson, M. Fahlman, P. Bröm, and W.R. Salneck, Conjugated polymer surfaces and interfaces: a mini-review and some new results, *Synth. Met.*, 80: 125–130, 1996.
586. M. Hamaguchi, H. Sawada, J. Kyokane, and K. Yoshino, Blue electroluminescence from poly(*p*-phenylene) solubilized by perfluoropropylation, *Chem. Lett.*, 25: 527–528, 1996.
587. V. Cimrová, W. Schmidt, R. Rulkens, M. Schulze, W. Meyer, and D. Neher, Efficient blue light-emitting devices based on rigid-rod polyelectrolytes, Vol. 25 *Adv. Mater.*, 8: 585–588, 1996.
588. S. Kim, J. Jackiw, E. Robinson, K.S. Schanze, J.R. Reynolds, J. Baur, M.F. Rubner, and D. Boils, Water soluble photo- and electroluminescent alkoxy-sulfonated poly(*p*-phenylenes) synthesized via palladium catalysis, *Macromolecules*, 31: 964–974, 1998.
589. J.W. Baur, S. Kim, P.B. Balanda, J.R. Reynolds, and M.F. Rubner, Thin-film light-emitting devices based on sequentially adsorbed multilayers of water-soluble poly(*p*-phenylene)s, *Adv. Mater.*, 10: 1452–1455, 1998.
590. M. Remmers, D. Neher, J. Grüner, R.H. Friend, G.H. Gelinck, J.M. Warman, C. Quattrocchi, D.A. dos Santos, and J.-L. Brédas, The optical, electronic, and electroluminescent properties of novel poly(*p*-phenylene)-related polymers, *Macromolecules*, 29: 7432–7445, 1996.
591. V. Cimrová, D. Neher, M. Remmers, and I. Kšínek, Blue light-emitting devices based on novel polymer blends, *Adv. Mater.*, 10: 676–680, 1998.
592. Y.-H. Kim, J.-H. Ahn, D.-C. Shin, and S.-K. Kwon, Synthesis and characterization of poly(terphenylenevinylene) derivatives containing alkoxy substituents and (or) phenyl pendant group, *Polymer*, 45: 2525–2532, 2004.
593. S.J. Park, S.-H. Jung, J.M. Kim, and H.-N. Cho, Highly phenyl-substituted fluorene copolymers for light-emitting diode, *Mater. Sci. Eng. C*, 24: 99–102, 2004.
594. M.A. Keegstra, V. Cimrová, D. Neher, and U. Scherf, Synthesis and electroluminescent properties of quaterphenyl and sexiphenyl containing copolymers, *Macromol. Chem. Phys.*, 197: 2511–2519, 1996.
595. F.D. Konstandakopoulou, K.G. Gravalos, and J.K. Kallitsis, Synthesis and characterization of processible aromatic–aliphatic polyethers with quinquephenyl segments in the main chain for light-emitting applications, *Macromolecules*, 31: 5264–5271, 1998.
596. J.K. Kallitsis, K.G. Gravalos, A. Hilberer, and G. Hadzioannou, Soluble polymers with laterally attached oligophenyl units for potential use as blue luminescent materials, *Macromolecules*, 30: 2989–2996, 1997.

597. V. Deimede, J.K. Kallitsis, and T. Pakula, Synthesis and properties of amorphous blue-light-emitting polymers with high glass-transition temperatures, *J. Polym. Sci., Part A: Polym. Chem.*, 39: 3168–3179, 2001.
598. K. Kaeriyama, Y. Tsukahara, S. Negoro, N. Tanigaki, and H. Masuda, Preparation and properties of soluble polyphenylenes, *Synth. Met.*, 84: 263–264, 1997.
599. P. Hodge, G.A. Power, and M.A. Rabjohns, Synthesis of poly(2,6-anthracene-2,6-diyl) and a copolymer containing alternately anthracene-2,6-diyl and *p*-phenylene units, *Chem. Commun.*: 73–74, 1996.
600. A.K.-Y. Jen, Y. Liu, Q.-S. Hu, and L. Pu, Efficient light-emitting diodes based on a binaphthalene-containing polymer, *Appl. Phys. Lett.*, 75: 3745–3747, 1999.
601. F.D. Konstandakopoyloy and J.K. Kallitsis, Soluble rigid–flexible polyethers containing bis(biphenyl)anthracene or bis(styryl)anthracene units in the main chain for light-emitting applications, *J. Polym. Sci., Part A: Polym. Chem.*, 37: 3826–3837, 1999.
602. S. Zheng and J. Shi, Novel blue-emitting polymers containing dinaphthylanthracene moiety, *Chem. Mater.*, 13: 4405–4407, 2001.
603. C.H. Lee, S.H. Ryu, and S.Y. Oh, Characteristics of a single-layered organic electroluminescent device using a carrier-transporting copolymer and a non-conjugated light-emitting polymer, *J. Polym. Sci., Part B: Polym. Phys.*, 41: 2733–2743, 2003.
604. M.-L. Tsai, C.-Y. Liu, Y.-Y. Wang, J.-Y. Chen, T.-C. Chou, H.-M. Lin, S.-H. Tsai, and T.J. Chow, Preparation and luminescent properties of polymer containing dialkoxyacenes, *Chem. Mater.*, 16: 3373–3380, 2004.
605. M. Kreyenschmidt, F. Uckert, and K. Müllen, A new soluble poly(*p*-phenylene) with tetrahydropyrene repeating units, *Macromolecules*, 28: 4577–4582, 1995.
606. S. Setayesh, D. Marsitzky, and K. Müllen, Bridging the gap between polyfluorene and ladder-poly-*p*-phenylene: synthesis and characterization of poly-2,8-indenofluorene, *Macromolecules*, 33: 2016–2020, 2000.
607. D. Marsitzky, J.C. Scott, J.-P. Chen, V.Y. Lee, R.D. Miller, S. Setayesh, and K. Müllen, Poly-2,8-(indenofluorene-*co*-anthracene) — a colorfast blue-light-emitting random copolymer, *Adv. Mater.*, 13: 1096–1099, 2001.
608. J. Jacob, S. Sax, T. Piok, E.J.W. List, A.C. Grimsdale, and K. Müllen, Ladder-type pentaphenylenes and their polymers: efficient blue-light emitters and electron-accepting materials via a common intermediate, *J. Am. Chem. Soc.*, 126: 6987–6995, 2004.
609. U. Scherf and K. Müllen, Polyarylenes and poly(arylene vinylenes), 7. A soluble ladder polymer via bridging of functionalized poly(*p*-phenylene)-precursors, *Makromol. Chem., Rapid Commun.*, 12: 489–497, 1991.
610. U. Scherf and K. Müllen, Design and synthesis of extended π -systems: monomer, oligomers, polymers, *Synthesis*: 23–38, 1992.
611. U. Scherf, Ladder-type materials, *J. Mater. Chem.*, 9: 1853–1864, 1999.
612. J. Stampfl, S. Tasch, G. Leising, and U. Scherf, Quantum efficiencies of electroluminescent poly(*p*-phenylenes), *Synth. Met.*, 71: 2125–2128, 1995.
613. L. Romaner, G. Heimel, H. Weisenhofer, P.S. de Freitas, U. Scherf, J.-L. Brédas, E. Zojer, and E.J.W. List, Ketonic defects in ladder-type poly(*p*-phenylenes), *Chem. Mater.*, 16: 4667–4674, 2004.
614. S. Tasch, A. Niko, G. Leising, and U. Scherf, Highly efficient electroluminescence of new wide band gap ladder-type poly(*p*-phenylenes), *Appl. Phys. Lett.*, 68: 1090–1092, 1996.
615. G. Leising, S. Tasch, F. Meghdadi, L. Athouel, G. Froyer, and U. Scherf, Blue electroluminescence with ladder-type poly(*p*-phenylene) and *p*-hexaphenyl, *Synth. Met.*, 81: 185–189, 1996.
616. C. Kallinger, M. Hilmer, A. Haugeneder, M. Perner, W. Spirk, U. Lemmer, J. Feldmann, U. Scherf, K. Müllen, A. Gombert, and V. Wittwer, A flexible conjugated polymer laser, *Adv. Mater.*, 10: 920–923, 1998.
617. C. Bauer, H. Giessen, B. Schnabel, E.-B. Kley, C. Schmitt, U. Scherf, and R.F. Mahrt, A surface-emitting circular grating polymer laser, *Adv. Mater.*, 13: 1161–1164, 2001.
618. T. Piok, S. Gamerith, C. Gadermaier, H. Plank, F.P. Wenzl, S. Patil, R. Montenegro, T. Tietzke, D. Neher, U. Scherf, K. Landfester, and E.J.W. List, Organic light-emitting devices fabricated from semiconducting nanospheres, *Adv. Mater.*, 15: 800–803, 2003.

619. S. Tasch, E.J.W. List, O. Ekström, W. Graupner, G. Leising, P. Schlichting, U. Rohr, Y. Geerts, U. Scherf, and K. Müllen, Efficient white light-emitting diodes realized with new processible blends of conjugated polymers, *Appl. Phys. Lett.*, 71: 2883–2885, 1997.
620. G. Grem, C. Paar, J. Stampfl, G. Leising, J. Huber, and U. Scherf, Soluble segmented stepladder poly(*p*-phenylenes) for blue-light-emitting diodes, *Chem. Mater.*, 7: 2–4, 1995.
621. J. Grüner, P.J. Hamer, R.H. Friend, H.-J. Huber, U. Scherf, and A.B. Holmes, A high efficiency blue-light-emitting diode based on novel ladder poly(*p*-phenylene)s, *Adv. Mater.*, 6: 748–752, 1994.
622. Y. Xiaohui, H. Yanbing, W. Zhenjia, C. Xiaohong, X. Zheng, and X. Xurong, Blue polymer light emitting diode based on ladder poly(*p*-phenylene), *Thin Solid Films*, 363: 211–213, 2000.
623. R. Giesa, Synthesis and properties of conjugated poly(arylene ethynylene)s, *J. Macromol. Sci., C, Rev. Macromol. Chem. Phys.*, 36: 631–670, 1996.
624. U.H.F. Bunz, Poly(arylene ethynylene)s: syntheses, properties, structures, and applications, *Chem. Rev.*, 100: 1605–1644, 2000.
625. C. Weder, S. Sarwa, A. Montali, C. Bastiaansen, and P. Smith, Incorporation of photoluminescent polarizers into liquid crystal displays, *Science*, 279: 835–837, 1998.
626. L.S. Swanson, J. Shinar, Y.W. Ding, and T.J. Barton, Photoluminescence, electroluminescence, and optically detected magnetic resonance study of 2,5-dialkoxy derivatives of poly(*p*-phenylene acetylene) (PPA) and PPA-based light-emitting diodes, *Synth. Met.*, 55: 1–6, 1993.
627. T.M. Swager, C.J. Gil, and M.S. Wrighton, Fluorescence studies of poly(*p*-phenylene)s: the effect of anthracene substitution, *J. Phys. Chem.*, 99: 4886–4893, 1995.
628. D. Ofer, T.M. Swager, and M.S. Wrighton, Solid-state ordering and potential dependence of conductivity in poly(2,5-dialkoxy-*p*-phenylene ethylene), *Chem. Mater.*, 7: 418–425, 1995.
629. C. Weder and M.S. Wrighton, Efficient solid-state photoluminescence in new poly(2,5-dialkoxy-*p*-phenylene ethynylene)s, *Macromolecules*, 29: 5157–5165, 1996.
630. C. Schmitz, P. Pösch, M. Thelekkat, H.-W. Schmidt, A. Montali, K. Feldman, P. Smith, and C. Weder, Polymeric light-emitting diodes based on poly(*p*-phenylene ethynylene), poly(triphenyldiamine), and spiroquinoxaline, *Adv. Funct. Mater.*, 11: 41–46, 2001.
631. R.A.J. Hanssen, N.S. Sariciftci, K. Pakbaz, J.J. McNamara, S. Schricker, A.J. Heeger, and F. Wudl, Photoinduced absorption of π -conjugated polymers in solution, *Synth. Met.*, 69: 441–442, 1995.
632. J.-S. Yang and T.M. Swager, Fluorescent porous polymer films as TNT chemosensors: electronic and structural effects, *J. Am. Chem. Soc.*, 120: 11864–11873, 1998.
633. V.E. Williams and T.M. Swager, Iptycene-containing poly(arylene ethynylene)s, *Macromolecules*, 33: 4069–4073, 2000.
634. C. Tan, M.R. Pinto, and K.S. Schanze, Photophysics, aggregation and amplified quenching of a water-soluble poly(phenylene ethynylene), *Chem. Commun.*: 446–447, 2002.
635. R. Deans, J. Kim, M.R. Machacek, and T.M. Swager, A poly(*p*-phenylene ethynylene) with a highly emissive aggregated phase, *J. Am. Chem. Soc.*, 122: 8565–8566, 2000.
636. W.-S. Li, D.-L. Jiang, and T. Aida, Photoluminescence properties of discrete conjugated wires wrapped within dendrimeric envelopes: “dendrimer effects” on π -electronic conjugation, *Angew. Chem. Int. Ed.*, 43: 2943–2947, 2004.
637. K. Yoshino, K. Tada, and M. Onoda, Optical properties of poly(3,4-dialkyl-1,6-phenylene ethynylene), *Jpn. J. Appl. Phys.*, 33: L1785–L1788, 1994.
638. K. Tada, M. Onoda, M. Hirohata, T. Kawai, and K. Yoshino, Blue-green electroluminescence in copolymer based on poly(1,4-phenylene ethynylene), *Jpn. J. Appl. Chem.*, 35: L251–L253, 1996.
639. H. Quante, P. Schlichting, U. Rohl, Y. Geerts, and K. Müllen, Novel perylene-containing polymers, *Macromol. Chem. Phys.*, 197: 4029–4044, 1996.
640. S. Yamaguchi and T.M. Swager, Oxidative cyclization of bis(biaryl)acetylenes: synthesis and photophysics of dibenzo[*g,p*]chrysene-based fluorescent polymers, *J. Am. Chem. Soc.*, 123: 12087–12088, 2001.
641. S.V. Frolov, A. Fujii, D. Chinn, M. Hirohata, R. Hidayat, M. Taraguchi, T. Masuda, K. Yoshino, and Z.V. Vardeny, Microlasers and micro-LEDs from disubstituted polyacetylene, *Adv. Mater.*, 10: 869–872, 1998; and references therein.

642. R. Sun, Q. Zheng, X. Zhang, T. Masuda, and T. Kobayashi, Light-emitting substituted polyacetylenes, *Jpn. J. Appl. Phys.*, 38: 2017–2023, 1999; and references therein.
643. R. Hidayat, S. Tatsuhara, D.W. Kim, M. Ozaki, K. Yoshino, M. Teraguchi, and T. Masuda, Time-resolved study of luminescence in highly luminescent disubstituted polyacetylene and its blend with poorly luminescent monosubstituted polyacetylene, *Phys. Rev. B*, 61: 10167–10173, 2000; and references therein.
644. Y.M. Huang, J.W.Y. Lam, K.K.L. Cheuk, W. Ge, and B.Z. Tang, Strong luminescence from poly(1-alkynes), *Macromolecules*, 32: 5976–5978, 1999.
645. J.W.Y. Lam, Y. Dong, K.K.L. Cheuk, J. Luo, Z. Xie, H.S. Kwok, Z. Mo, and B.Z. Tang, Liquid crystalline and light-emitting polyacetylenes: synthesis and properties of biphenyl-containing poly(1-alkynes) with different functional bridges and spacer length, *Macromolecules*, 35: 1229–1240, 2002.
646. Q. Zheng, R. Sun, X. Zhang, T. Masuda, and T. Kobayashi, Electroluminescent devices based on poly(diphenylacetylene) with carbazolyl side groups, *Jpn. J. Appl. Phys.*, 36: L1508–L1510, 1997.
647. J. Chen, Z. Xie, J.W.Y. Chen, C.C.W. Law, and B.Z. Tang, Silole-containing polyacetylenes. Synthesis, thermal stability, light-emission, nanodimensional aggregation and restricted intramolecular rotation, *Macromolecules*, 36: 1108–1117, 2003.
648. S.T. Wellinghoff, D. Zhi, T.J. Kedrowski, S.A. Dick, S.A. Jenekhe, and H. Ishida, Electronic conduction mechanism in polycarbazole iodine complexes, *Mol. Cryst. Liq. Cryst.*, 106: 289–304, 1984.
649. Y. Yang and Q. Pei, Light-emitting electrochemical cells from a blend of *p*- and *n*-type luminescent conjugated polymers, *Appl. Phys. Lett.*, 70: 1926–1928, 1997.
650. Z.-B. Zhang, M. Fujiki, H.-Z. Tang, M. Motonaga, and K. Torimitsu, The first high molecular weight poly(*N*-alkyl-3,6-carbazole)s, *Macromolecules*, 35: 1988–1990, 2002.
651. S. Grigalevicius, J.V. Grazulevicius, V. Gaidelis, and V. Jankauskas, Synthesis and properties of poly(3,9-carbazole) and low-molecular-mass glass-forming carbazole compounds, *Polymer*, 43: 2603–2608, 2002.
652. S. Maruyama, X.-T. Tao, H. Hokari, T. Noh, Y. Zhang, T. Wada, H. Sasabe, H. Suzuki, T. Watanabe, and S. Miyata, Electroluminescent applications of a cyclic carbazole oligomers, *J. Mater. Chem.*, 8: 893–898, 1999.
653. A. van Dijken, J.J.A.M. Bastiaansen, N.M.M. Kikken, B.M.W. Langeveld, C. Rothe, A. Monkman, I. Bach, P. Stössel, and K. Brunner, Carbazole compounds as host materials in light-emitting diodes: polymer hosts for high-efficiency light-emitting diodes, *J. Am. Chem. Soc.*, 126: 7718–7727, 2004.
654. J. Huang, Y. Niu, W. Yang, Y. Mo, M. Yuan, and Y. Cao, Novel electroluminescent polymers derived from carbazole and benzothiadiazole, *Macromolecules*, 35: 6080–6082, 2002.
655. J. Huang, Y. Xu, Q. Hou, W. Yang, M. Yuan, and Y. Cao, Novel red electroluminescent polymers derived from carbazole and 4,7-bis(2-thienyl)-2,1,3-benzothiadiazole, *Macromol. Rapid Commun.*, 23: 709–712, 2002.
656. G. Zotti, G. Schiavon, S. Zecchin, J.-F. Morin, and M. Leclerc, Electrochemical, conductive, and magnetic properties of 2,7-carbazole-based conjugated polymers, *Macromolecules*, 35: 2122–2128, 2002.
657. A. Iraqi and I. Wataru, Preparation and properties of 2,7-linked *N*-alkyl-9*H*-carbazole main-chain polymers, *Chem. Mater.*, 16: 442–448, 2004.
658. J.-F. Morin, P.-L. Boudreault, and M. Leclerc, Blue-light-emitting conjugated polymers derived from 2,7-carbazoles, *Macromol. Rapid Commun.*, 23: 1032–1036, 2002.
659. J.-F. Morin and M. Leclerc, Solvatochromic properties of 2,7-carbazole-based conjugated polymers, *Macromolecules*, 36: 4624–4630, 2003.
660. S.A. Patil, U. Scherf, and A. Kadaschuk, New conjugated ladder polymer containing carbazole moieties, *Adv. Funct. Mater.*, 13: 609–614, 2003.
661. J.-F. Morin, N. Drolet, Y. Tao, and M. Leclerc, Syntheses and characterization of electroactive and photoactive 2,7-carbazolenevinylene-based conjugated oligomers and polymers, *Chem. Mater.*, 16: 4619–4626, 2004.

662. D.D. Gebler, Y.Z. Wang, J.W. Blatchford, S.W. Jessen, L.-B. Lin, T.L. Gustafson, H.L. Wang, T.M. Swager, A.G. MacDiarmid, and A.J. Epstein, Blue electroluminescent devices based on soluble poly(*p*-pyridine), *J. Appl. Phys.*, 78: 4264–4266, 1995.
663. T. Yamamoto, T. Murayama, Z.-H. Zhou, T. Ito, T. Fukuda, Y. Yoneda, F. Begum, T. Ikeda, S. Sasaki, H. Takezoe, A. Fukuda, and K. Kubota, π -Conjugated poly(pyridine-2,5-diyl), poly(2,2'-bipyridine-5,5'-diyl), and their alkyl derivatives. Preparation, linear structure, function as a ligand to form their transition metal complexes, catalytic reactions, *n*-type electrically conducting properties, optical properties, and alignment on substrates, *J. Am. Chem. Soc.*, 116: 4832–4845, 1994.
664. M. Halim, I.D.W. Samuel, J.N.G. Pillow, A.P. Monkman, and P.L. Burn, Control of colour and charge injection in conjugated dendrimer/polypyridine bilayer LEDs, *Synth. Met.*, 102: 1571–1574, 1999.
665. S. Dailey, M. Halim, E. Rebourt, L.E. Horsburgh, I.D.W. Samuel, and A.P. Monkman, An efficient electron-transporting polymer for light-emitting diodes, *J. Phys.: Condens. Matter*, 10: 5171–5178, 1998.
666. C. Wang, M. Kilitziraki, J.A.H. MacBride, M.R. Bryce, L.E. Horsburgh, A.K. Sheridan, A.P. Monkman, and I.D.W. Samuel, Tuning the optoelectronic properties of pyridine-containing polymers for light-emitting devices, *Adv. Mater.*, 12: 217–222, 2000.
667. A.P. Monkman, L.-O. Pålsson, R.W.T. Higgins, C. Wang, M.R. Bryce, A.S. Batsanov, and J.A.K. Howard, Protonation and subsequent intramolecular hydrogen bonding as a method to control chain structure and tune luminescence in heteroatomic conjugated polymers, *J. Am. Chem. Soc.*, 124: 6049–6055, 2002.
668. S.-C. Ng, H.-F. Lu, H.S.O. Chan, A. Fujii, T. Laga, and K. Yoshino, Blue electroluminescence from a novel donor/acceptor polymer structure, *Adv. Mater.*, 12: 1122–1125, 2000.
669. T. Miyamae, D. Yoshimura, H. Ishii, Y. Ouchi, K. Seki, T. Miyazaki, T. Koike, and T. Yamamoto, Ultraviolet photoelectron spectroscopy of poly(pyridine-2,5-diyl), poly(2,2'-bipyridine-5,5'-diyl), and their K-doped states, *J. Chem. Phys.*, 103: 2738–2744, 1995.
670. M.-Y. Hwang, M.-Y. Hua, and S.-A. Chen, Poly(pyridine-2,5-diyl) as electron-transport/hole blocking layer in poly(phenylene vinylene) light-emitting diode, *Polymer*, 40: 3233–3235, 1999.
671. M.J. Marsella, D.-K. Fu, and T.M. Swager, Synthesis of regioregular poly(methyl pyridinium vinylene): an isoelectric analogue to poly(phenylene vinylene), *Adv. Mater.*, 7: 145–147, 1995.
672. J. Tian, C.-C. Wu, W.E. Thompson, J.C. Sturm, R.A. Register, M.J. Marsella, and T.M. Swager, Electroluminescent properties of self-assembled polymer thin films, *Adv. Mater.*, 7: 395–398, 1995.
673. J. Tian, C.-C. Wu, M.E. Thompson, J.C. Sturm, and R.A. Register, Photophysical properties, self-assembled films, and light-emitting diodes of poly(*p*-pyridylvinylene)s and poly(*p*-pyridinium vinylene)s, *Chem. Mater.*, 7: 2190–2198, 1995.
674. Y.Z. Wang, D.D. Gebler, D.K. Fu, T.M. Swager, A.G. MacDiarmid, and A.J. Epstein, Light-emitting devices based on pyridine-containing conjugated polymers, *Synth. Met.*, 85: 1179–1182, 1995.
675. A.J. Epstein, J.W. Blatchford, Y.Z. Wang, S.W. Jessen, D.D. Gebler, L.B. Lin, T.L. Gustafson, H.-L. Wang, Y.W. Park, T.M. Swager, and A.G. MacDiarmid, Poly(*p*-pyridine)- and poly(*p*-pyridyl vinylene)-based polymers: their photophysics and application to SCALE devices, *Synth. Met.*, 78: 253–261, 1996; and references therein.
676. A. Wu, T. Akagi, M. Jikei, M. Kakimoto, Y. Imai, S. Ukishima, and Y. Takahashi, New fluorescent polyimides for electroluminescent devices based on 2,5-distyrylpyrazine, *Thin Solid Films*, 273: 214–217, 1996.
677. X. Zhang, A.S. Shetty, and S.A. Jenekhe, Electroluminescence and photophysical properties of polyquinolines, *Macromolecules*, 32: 7422–7429, 1999.
678. Y. Zhu, M.M. Alam, and S.A. Jenekhe, Regioregular head-to-tail poly(4-alkylquinoline)s: synthesis, characterization, self-organization, photophysics, and electroluminescence of new *n*-type conjugated polymers, *Macromolecules*, 36: 8958–8968, 2003.
679. X. Zhang and S.A. Jenekhe, Electroluminescence of multicomponent conjugated polymers. 1. Roles of polymer/polymer interfaces in emission enhancement and voltage-tunable multicolor emission in semiconducting polymer/polymer heterojunction, *Macromolecules*, 33: 2069–2082, 2000.

680. M.S. Liu, Y. Liu, R.C. Urian, H. Ma, and A.K.-Y. Jen, Synthesis and characterization of polyquinolines for light-emitting diodes, *J. Mater. Chem.*, 9: 2201–2204, 1999.
681. Y. Liu, H. Ma, and A.K.-Y. Jen, Synthesis and characterization of quinoline-based copolymers for light-emitting diodes, *J. Mater. Chem.*, 11: 1800–1804, 2001.
682. H. Krüger, S. Janietz, D. Sainova, and A. Wedel, New organo-soluble conjugated polyquinolines, *Macromol. Chem. Phys.*, 204: 1607–1615, 2003.
683. T. Yamamoto, K. Sugiyama, T. Kushida, T. Inoue, and T. Kanbara, Preparation of new electron-accepting π -conjugated polyquinoxalines. Chemical and electrochemical reduction, electrically conducting properties, and use in light-emitting diodes, *J. Am. Chem. Soc.*, 118: 3930–3937, 1996.
684. S. Dailey, W.J. Feast, R.J. Peace, I.C. Sage, S. Till, and E.L. Wood, Synthesis and device characterization of side-chain polymer electron transport materials for organic semiconducting applications, *J. Mater. Chem.*, 11: 2238–2243, 2001.
685. P. Pösch, R. Fink, M. Thelakktat, and H.-W. Schmidt, A comparison of hole blocking/electron transport polymers in organic LEDs, *Acta Polym.*, 47: 487–494, 1998.
686. Y. Cui, X. Zhang, and S.A. Jenekhe, Thiophene-linked polyphenylquinoxaline: a new electron transport conjugated polymer for electroluminescent devices, *Macromolecules*, 32: 3824–3826, 1999.
687. F. Cacialli, X.-C. Li, R.H. Friend, S.C. Moratti, and A.B. Holmes, Light-emitting diodes based on poly(methacrylates) with distyrylbenzene and oxadiazole side chains, *Synth. Met.*, 75: 161–168, 1995.
688. X.-C. Li, F. Cacialli, M. Giles, J. Grüner, R.H. Friend, A.B. Holmes, S.C. Moratti, and T.M. Yong, Charge transport polymers for light emitting diodes, *Adv. Mater.*, 7: 898–900, 1995.
689. M. Strukelj, T.M. Miller, F. Papadimitrakopoulos, and S. Son, Effects of polymeric electron transporters and the structure of poly(*p*-phenylene vinylene) on the performance of light-emitting diodes, *J. Am. Chem. Soc.*, 117: 11976–11983, 1995.
690. M. Greczmiel, P. Stroehriegl, M. Meier, and W. Brütting, Polymethacrylates with pendant oxadiazole units synthesis and application in organic LEDs, *Macromolecules*, 30: 6042–6046, 1997.
691. X. Jiang, R.A. Register, K.A. Killeen, M.E. Thompson, F. Pschenitzka, and J.C. Sturm, Statistical copolymers with side-chain hole and electron transport groups for single-layer electroluminescent device applications, *Chem. Mater.*, 12: 2542–2549, 2000.
692. Q. Pei and Y. Yang, Bright blue electroluminescence from an oxadiazole-containing copolymer, *Adv. Mater.*, 7: 559–561, 1995.
693. Y. Yang and Q. Pei, Electron injection polymer for polymer light-emitting diodes, *J. Appl. Phys.*, 77: 4807–4809, 1995.
694. Q. Pei and Y. Yang, 1,3,4-Oxadiazole-containing polymers as electron-injection and blue electroluminescent materials in polymer light-emitting diodes, *Chem. Mater.*, 7: 1568–1575, 1995.
695. R. Cervini, X.-C. Li, G.W.C. Spencer, A.B. Holmes, S.C. Morath, and R.H. Friend, Electrochemical and optical studies of PPV derivatives and poly(aromatic oxadiazoles), *Synth. Met.*, 84: 359–360, 1997.
696. X.-C. Li, G.C.W. Spencer, A.B. Holmes, S.C. Moratti, F. Cacialli, and R.H. Friend, The synthesis, optical and charge-transport properties of poly(aromatic oxadiazoles), *Synth. Met.*, 76: 153–156, 1996.
697. C. Wang, M. Kilitziraki, L.-O. Pålsson, M.R. Bryce, A.P. Monkman, and I.D.W. Samuel, Polymeric alkoxy PBD [2-(4-biphenyl)-5-phenyl-1,3,4-oxadiazole] for light-emitting diodes, *Adv. Funct. Mater.*, 11: 47–50, 2001.
698. S. Janietz and S. Anlauf, A new class of organosoluble rigid-rod fully aromatic poly(1,3,4-oxadiazole)s and their solid-state properties, 1., *Macromol. Chem. Phys.*, 203: 427–432, 2002.
699. S. Janietz, S. Anlauf, and A. Wedel, A new class of organosoluble rigid-rod, fully aromatic poly(1,3,4-oxadiazole)s and their solid-state properties, 2., *Macromol. Chem. Phys.*, 203: 433–538, 2002.
700. S.A. Jenekhe and J.A. Osaheni, Excimers and exciplexes of conjugated polymers, *Science*, 265: 765–768, 1994.
701. C.C. Wu, P.Y. Tsay, H.Y. Cheng, and S.J. Bai, Polarized luminescence and absorption of highly oriented, fully conjugated, heterocyclic aromatic rigid-rod polymer poly-*p*-phenylenebenzoxazole, *J. Appl. Phys.*, 95: 417–423, 2004.

702. S.J. Bai, C.C. Wu, T.D. Dang, F.E. Arnold, and B. Sakaran, Tunable and white light-emitting diodes of monolayer fluorinated benzoxazole graft copolymer, *Appl. Phys. Lett.*, 84: 1656–1658, 2004.
703. C.D. Entwistle and T.B. Marder, Application of three-coordinate organoboron compounds and polymers in optoelectronics, *Chem. Mater.*, 16: 4574–4585, 2004.
704. M. Matsumi, K. Naka, and Y. Chujo, Extension of π -conjugation length via the vacant p-orbital of the boron atom. Synthesis of novel electron deficient π -conjugated systems by hydroboration polymerization and their blue light emitting, *J. Am. Chem. Soc.*, 120: 5112–5113, 1998.
705. N. Matsumi, M. Miyata, and Y. Chujo, Synthesis of organoboron π -conjugated polymers by hydroboration polymerization between heteroaromatic diynes and mesitylborane and their light emitting properties, *Macromolecules*, 32: 4467–4469, 1999.
706. M. Matsumi, K. Naka, and Y. Chujo, π -Conjugated poly(cyclodiborazane)s with intramolecular charge transferred structure, *Macromolecules*, 33: 3956–3957, 2000.
707. M. Matsumi, K. Naka, and Y. Chujo, Poly(*p*-phenylene-borane)s, novel organoboron π -conjugated polymers via Grignard reagent, *J. Am. Chem. Soc.*, 120: 10776–10777, 1998.
708. Y. Makioka, T. Hayashi, and M. Tanaka, Poly[2,7-(9-oxo-9 -phosphafluorenylene)-*alt-co*-(1,4-arylene)]s: phosphours-containing π -conjugated polymers, *Chem. Lett.*, 33: 44–45, 2004.
709. C. Xu, H. Yamada, A. Wakamiya, S. Yamaguchi, and K. Tamao, Ladder bis-silicon-bridged stilbenes as a new building unit for fluorescent π -conjugated polymers, *Macromolecules*, 37: 8978–8983, 2004.
710. S. Yamaguchi and K. Tamao, A key role of orbital interaction in the main group element-containing π -electron systems, *Chem. Lett.*, 34: 2–7, 2005.

3 Organic Small Molecule Materials for Organic Light-Emitting Diodes

Hong Meng and Norman Herron

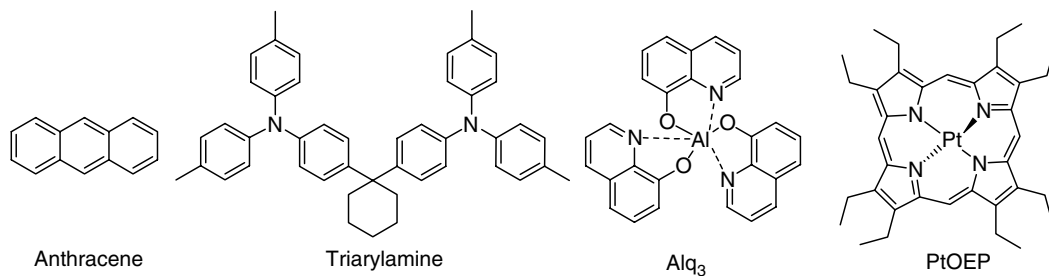
CONTENTS

3.1	Introduction	296
3.1.1	Organic Light-Emitting Diode Device Structure.....	297
3.1.2	Organic Light-Emitting Diode Operating Mechanism.....	300
3.2	Anode and Cathode Materials.....	301
3.2.1	Anode Materials.....	301
3.2.2	Cathode Materials.....	302
3.3	Hole Injection Materials and Cathode Interfacial Materials	303
3.3.1	Hole Injection Materials	303
3.3.1.1	Organic–Inorganic Interface	304
3.3.1.2	Porphyrinic Metal Complexes	305
3.3.1.3	Conducting Polymers, PEDOT–PSS, Doped Polyaniline and Polypyrrole	305
3.3.1.4	SAM-TPD	307
3.3.1.5	Fluorocarbon Polymers	307
3.3.1.6	Inorganic Hole Injection Materials.....	308
3.3.1.7	Doping the Hole Transport Materials	308
3.3.2	Cathode Interfacial Materials	309
3.3.2.1	LiF, CsF	310
3.3.2.2	M ₂ O: Al (M: Li, Na, K, Rb)	310
3.3.2.3	Li/Cs Dopant with BCP and Li–Quinolate Complexes	311
3.3.2.4	Organic Polymer Surfactants	311
3.4	Hole Transport Materials	312
3.4.1	Triarylaminers	312
3.4.2	Triphenylmethanzenes	320
3.4.3	Phenylazomethines and Their Metal Complexes.....	321
3.5	Electron Transport Materials.....	322
3.5.1	Metal Chelate Electron Transport Materials	323
3.5.2	TPBI and N-Containing Aromatic Transport Materials	326
3.5.3	Oxadiazole and Triazole Transport Materials	328
3.5.4	Fluorine-Substituted Electron Transport Materials	328
3.5.5	Silole (Silacyclopentadiene)	329
3.5.6	4 <i>n</i> - π and Boron-Based Electron Transport Materials.....	330

3.6	Light-Emitting Materials	330
3.6.1	Host–Guest Molecules	332
3.6.2	Host Materials	333
3.6.2.1	Electron Transport Hosts	333
3.6.2.2	Hole Transport Hosts	334
3.6.2.3	Silane Compound Host Materials for Blue and White Phosphorescent Organic Light-Emitting Diodes.....	336
3.6.2.4	Fluorescent Blue Host Materials	337
3.6.2.5	Polymer Hosts	338
3.6.3	Fluorescent Dopants	338
3.6.3.1	Green Fluorescent Dopants	339
3.6.3.2	Red Fluorescent Dopants	343
3.6.3.3	Blue Fluorescent Emitters.....	349
3.6.3.4	White Fluorescent Organic Light-Emitting Diodes	365
3.6.4	Phosphorescent Dopants	369
3.6.4.1	Synthesis of Iridium Complexes	370
3.6.4.2	Green Phosphorescent Dopants	372
3.6.4.3	Red Phosphorescent Dopants.....	375
3.6.4.4	Blue Phosphorescent Dopants	377
3.6.4.5	White Phosphorescent Organic Light-Emitting Diodes.....	379
3.7	Stabilizers and Hole- and Electron-Blocking Materials.....	382
3.7.1	Stabilizers	382
3.7.2	Sensitizers	385
3.7.3	Hole-Blocking Materials	386
3.7.4	Electron-Blocking Materials.....	389
3.8	Current Best Performance of the Three Primary Color Materials and Device Structures	390
3.8.1	Red Emitters and Device Structures	391
3.8.2	Green Emitters and Device Structures	392
3.8.3	Blue Emitters and Device Structures.....	393
3.9	Conclusion and Remarks.....	394
	Acknowledgments	395
	References	395

3.1 INTRODUCTION

Small-molecule organic light-emitting diodes (SMOLEDs), inspired by the search for blue light-emitting devices based on organic crystals such as anthracene, can be traced back to the early work of Pope et al. in the 1960s [1]. The development of thin-film organic electroluminescent devices with relatively low driving voltages (below 30 V DC) by Vincett et al. at Xerox Canada in 1982 was a major step forward in this field [2]. A significant breakthrough in achieving high electrical efficiency OLEDs using small-molecule-based organic materials was the discovery of the organic light-emitting diodes (OLEDs) reported by Kodak scientists in 1987 [3]. In that publication, a double layer consisting of thin films of a hole transport triarylamine and a light emitting and electron transporting Alq₃ layer, sandwiched between a transparent indium tin oxide (ITO) electrode and an Al/Mg electrode, emitted green light under applied DC voltage. Although the quantum efficiency (QE) of such fluorescent



SCHEME 3.1 Chemical structures of anthracene, a hole transport triarylamine, an electron transport and a green emitter Alq₃, and a phosphorescent dopant PtOEP.

material based SMOLEDs is limited by spin statistics to only ~25%, the recently developed phosphorescent SMOLEDs from the Princeton and USC groups achieved quantum efficiencies approaching 100% [4,5]. These efficiencies far exceed those of any previously described devices. Such a fundamental breakthrough in device engineering and materials selection has ignited progress in the OLED field (Scheme 3.1 shows the chemical structures of organic materials used in the early studies). Undoubtedly, device construction, device engineering and, particularly, new materials design continue to drive advances in this field.

Numerous review articles have covered research in the SMOLED field and many have focused on various aspects of the design, synthesis, and applications of many classes of materials (Table 3.1). Several major companies such as Kodak, Sony, Samsung, DuPont, as well as newly born R&D companies such as Universal Display Corporation (UDC), Novaled GmnH, e-Ray optoelectronics Technology Co. Ltd., America Organic Semiconductor, LLC, etc., have targeted the development of high efficiency, long lifetime small-molecule-based OLED materials and devices.

Like Chapter 2 that reviews polymeric light-emitting materials, this chapter will attempt to review all of the important small molecule materials used in OLEDs. In many cases, where such data is available, we will also describe the related device structures and electroluminescence (EL) performance associated with those materials. One of the difficulties in evaluating the relative merits of any given set of materials in OLEDs is the strong interplay of the materials stack and the device architecture chosen for the test device. This is further complicated by the diverse measures of device performance, which are often used to describe the test devices — combinations of luminance and power efficiencies, brightness and voltage stability expressed as lifetimes under diverse luminance and current conditions, defect and black spot appearance and growth, etc. In such an undertaking, it is often tempting to make value judgments and critical assessments of the various data under review, however, we have attempted to refrain from such analysis, fraught with controversy as it is, and have tried to simply present an unbiased selection of representative data from the original authors' works. It is left to the reader to evaluate the merits and conclusions of this work by a careful reading of the primary publications.

3.1.1 ORGANIC LIGHT-EMITTING DIODE DEVICE STRUCTURE

OLED devices are fabricated on a glass, plastic, metal, or ceramic substrate as a multilayer-stacked structure represented in Figure 3.1.

The simplest manifestation of an OLED is a sandwich structure consisting of an emission layer (EML) between an anode and a cathode. More typical is an increased complexity OLED structure consisting of an anode, an anode buffer or hole injection layer (HIL), a hole transport layer (HTL), a light-emitting layer, an electron transport layer (ETL), a cathode

TABLE 3.1
The Most Important Reviews Covering SMOLEDs

Year	Title	Authors	Publication
1997	Growth and characterization of electroluminescent display devices using vacuum-deposited organic materials	S.R. Forrest, P.E. Burrows, M.E. Thompson	<i>Organic Electroluminescent Materials and Devices</i> , pp. 415–458
1997	Organic light-emitting materials and devices, vol. 314	Z.H. Kafafi (Ed.)	SPIE Proceeding series, 424 pp. ISBN: 0819425702
1997	<i>Organic Electroluminescent Materials and Devices</i>	S. Miyata, H.S. Nalwa (Eds.)	CRC Press, 496 pp. ISBN: 2919875108
1998	The chemistry of electroluminescent organic materials	J.L. Segura	<i>Acta Polymerica</i> , 49: 319–344
1998	Metal chelates as emitting materials for organic electroluminescence	C.H. Chen, J. Shi	<i>Coordination Chemistry Reviews</i> , 171: 161–174
1998	Low molecular weight and polymeric heterocyclics as electron transport/hole-blocking materials in organic light-emitting diodes	M. Thelakkat, H. Schmidt	<i>Polymers for Advanced Technologies</i> , 9: 429–442
1998	Organic light-emitting materials and devices, vol. 347	Z.H. Kafafi (Ed.)	SPIE Proceeding series, 360 pp. ISBN: 0819429317
1999	Phosphorescent materials for application to organic light emitting devices	M.A. Baldo, M.E. Thompson, S.R. Forrest	<i>Pure and Applied Chemistry</i> , 71: 2095–2106
2000	Organic materials for electronic and optoelectronic devices	Y. Shirota	<i>Journal of Materials Chemistry</i> , 10: 1–25
2000	The electroluminescence of organic materials	U. Mitschke, P. Bäuerle	<i>Journal of Materials Chemistry</i> , 10: 1471–1507
2000	Organic light-emitting materials and devices III, vol. 379	Z.H. Kafafi (Ed.)	SPIE Proceeding series, 444 pp. ISBN: 0819432830
2001	<i>Organic Electronic Materials: Conjugated Polymers and Low Molecular Weight Organic Solids</i>	R. Farchioni, G. Grosso (Eds.)	Springer, 448 pp. ISBN: 3540667210
2001	Organic light-emitting materials and devices, vol. IV	Z.H. Kafafi (Ed.)	SPIE Proceeding series, 510 pp. ISBN: 0819437506
2002	Organic light emitting diodes (OLEDs) for general illumination update 2002	M. Stolka (Ed.)	Publisher Optoelectronics Industry Development Association (OIDA), Washington DC, 2002
2002	Charge-transporting molecular glasses	P. Stroehriegel, J.V. Grazulevicius	<i>Advanced Materials</i> , 14: 1439–1452
2002	Organo lanthanide metal complexes for electroluminescent materials	J. Kido, Y. Okamoto	<i>Chemical Reviews</i> , 102: 2357–2368
2002	Recent progress of molecular organic electroluminescent materials and devices	L.S. Hung, C.H. Chen	<i>Materials Science and Engineering</i> , R39: 143–222
2002	Organic light-emitting materials and devices, vol. 314	Z.H. Kafafi (Ed.)	SPIE Proceeding series, 400 pp. ISBN: 0819441783
2003	Organic light-emitting diode materials	S.K. Schrader	Proceedings of SPIE — The International Society for Optical Engineering, 4991: 45–63
2003	Organic light emitting devices	M. Pfeiffer, S.R. Forrest	<i>Nanoelectronics and Information Technology Advanced Electronic Materials and Novel Devices</i> , pp. 915–931

TABLE 3.1
The Most Important Reviews Covering SMOLEDs

Year	Title	Authors	Publication
2003	Thin-film permeation-barrier technology for flexible organic light-emitting devices	J.S. Lewis, M.S. Weaver	<i>IEEE Journal of Selected Topics in Quantum Electronics</i> , 10: 45–57
2003	Amorphous silicon back-plane electronics for OLED displays	A. Nathan, A. Kumar, K. Sakariya, P. Servati, K.S. Karim, D. Striakhilev, A. Sazonov	<i>IEEE Journal of Selected Topics in Quantum Electronics</i> , 10: 58–69
2003	Phosphorescence as a probe of exciton formation and energy transfer in organic light emitting diodes	M. Baldo, M. Segal	<i>Physica Status Solidi A: Applied Research</i> , 201: 1205–1214
2003	Combinatorial and spread techniques in the fabrication of organic-based photonic and optoelectronic devices	G.E. Jabbour, Y. Yoshioka	<i>High-Throughput Analysis</i> , pp. 377–393
2003	<i>Conjugated Polymer Surfaces and Interfaces: Electronic and Chemical Structure of Interfaces for Polymer Light Emitting Devices</i>	W.R. Salaneck, S. Stafstrom, J.L. Brédas	Cambridge University Press, 169 pp. ISBN: 0521544106
2003	<i>Handbook of Luminescence, Display Materials And Devices Organic Light-Emitting Diodes, vol. 1</i>	H.S. Nalwa, L.S. Rohwer	American Scientific Publishers, 1374 pp. ISBN: 1-58883-010-1
2003	Organic light-emitting materials and devices VI	H. Antoniadis, Z.H. Kafafi (Eds.)	SPIE Proceeding series, 276 pp. ISBN: 0819445681
2003	<i>Light-Emitting Diodes</i>	E.F. Schubert (Ed.)	Cambridge University Press, 326 pp. ISBN: B0007M01WS
2003	<i>Organic Light Emitting Devices</i>	J. Shinar (Ed.)	Springer, 384 pp. ISBN: 0387953434
2004	Transparent flexible plastic substrates for organic light-emitting devices	Y. Hong, Z. He, N.S. Lennhoff, D.A. Banach, J. Kanicki	<i>Journal of Electronic Materials</i> , 33: 312–320
2004	Evolution of red organic light-emitting diodes: materials and devices	C.T. Chen	<i>Chemistry of Materials</i> , 16: 4389–4400
2004	Manufacturing and commercialization issues in organic electronics	J.R. Sheats	<i>Journal of Materials Research</i> , 19: 1974–1989
2004	Degradation phenomena in small-molecule organic light-emitting devices	H. Aziz, Z.D. Popovic	<i>Chemistry of Materials</i> , 16: 4522–4532
2004	OLEDs: a new technology for lighting and displays	P. Destruel, J. Farenc, P. Jolinat, I. Seguy, S. Archambeau, M. Mabiala, G. Ablart	<i>Institute of Physics Conference Series</i> , 182: 135–141
2004	Electron transport materials for organic light-emitting diodes	A.P. Kulkarni, C.J. Tonzola, A. Babel, S.A. Jenekhe	<i>Chemistry of Materials</i> , 16: 4556–4573
2004	Recent progress in phosphorescent materials for organic light emitting diodes	S. Tokito	<i>Journal of Photopolymer Science and Technology</i> , 17: 307–314
2004	<i>Organic Light-Emitting Diodes: Principle, Characteristics, and Processes</i>	J. Kolinowski (Ed.)	Marcel Dekker, 466 pp. ISBN: 0824759478

continued

TABLE 3.1 (continued)
The Most Important Reviews Covering SMOLEDs

Year	Title	Authors	Publication
2004	Organic light-emitting materials and devices VII	Z.H. Kafafi (Ed.)	SPIE Proceeding series, 382 pp. ISBN: 08194250871
2004	<i>Organic Light-Emitting Devices: A Survey</i>	J. Shinar (Ed.)	Springer, 309 pp. ISBN: 0387-95343-4
2005	Electrochemiluminescence from organic emitters	D. Dini	<i>Chemistry of Materials</i> , 17: 1933–1945
2005	The rise of organophosphorus derivatives in π -conjugated materials chemistry	M. Hissler, P.W. Dyer, R. Reau	<i>Topics in Current Chemistry</i> , 250: 127–163
2005	<i>Organic Electroluminescence</i>	Z. Kafafi, B.J. Thomson (Eds.)	Taylor & Francis, 512 pp. ISBN: 0824759060
2006	<i>Organic Light Emitting Devices: Synthesis, Properties and Applications</i>	K. Muller, U. Scherf (Eds.)	Wiley, 400 pp. ISBN: 3-527-31218-8

interfacial layer, and a cathode. In some devices, hole blocking layer (HBL), electron blocking layer (EBL), and a stabilizer layer are also applied to achieve the desired performance. Although the structure of a typical OLED (shown in Figure 3.1) can contain many layers, not all of these layers are necessarily present in all OLED architectures. Indeed, much of the current research on OLEDs focuses on the development of the simplest possible and most easily processed architecture that can deliver the optimal combination of device properties.

3.1.2 ORGANIC LIGHT-EMITTING DIODE OPERATING MECHANISM

The light generating mechanism of OLEDs can be summarized by the following processes and is illustrated in Figure 3.2.

The function of each layer can be summarized as follows.

1. Electron and hole injection from the cathode and the anode

When an electric field is applied between the anode and the cathode, electrons and holes are injected from the cathode and the anode, respectively, into the organic layers. With a matched energy barrier between the electron and the hole injection layers (EILs and HILs) and the cathode and the anode, electrons and holes are efficiently injected into the ETL and HTL.

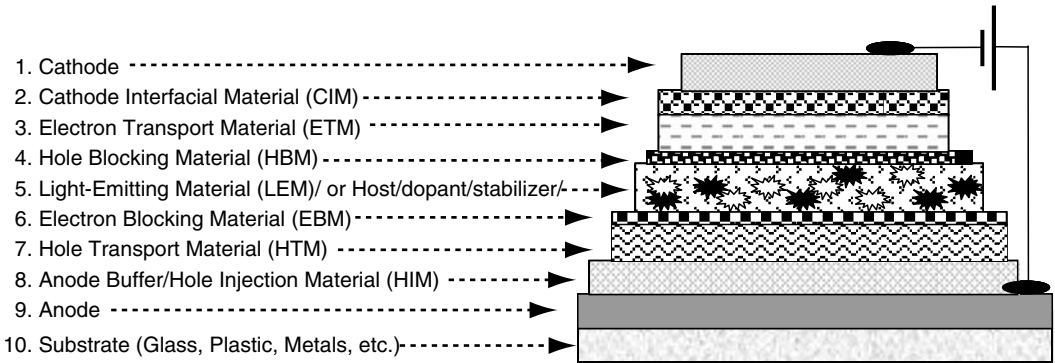


FIGURE 3.1 Schematic of a multilayer OLED device structure.

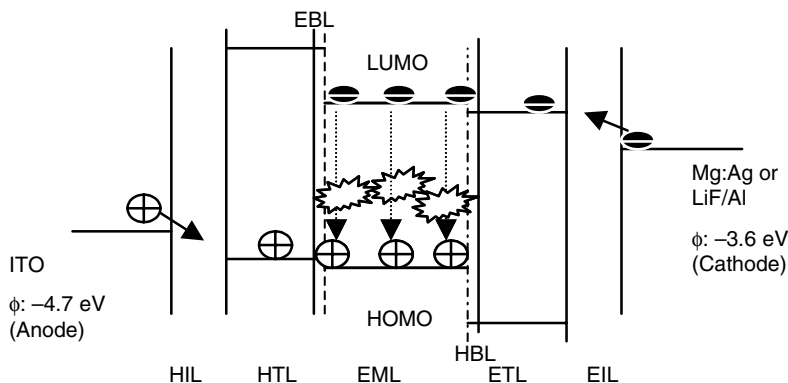


FIGURE 3.2 The function of each layer in an OLED.

2. Electron and hole migration through the electron and hole transport layers

Once the electrons and holes have been injected, they migrate into ETL and HTL to form excited states referred to as polarons by physicists or radical ions by chemists. These polarons or radical ions move, by means of a so-called “charge-hopping mechanism,” through the electron and hole transport materials (ETMs and HTMs), which typically possess good charge mobility properties, and eventually into the EML.

3. Charge recombination

The charges then meet at the organic EML and the device is optimized by fine-tuning so as to match the number of electrons and holes coming through the EBL or HBL. Once the opposite charges recombine, an exciton is formed and depending upon the nature of the emission materials (EMs) and according to appropriate selection rules, singlet fluorescence or triplet phosphorescence is emitted.

3.2 ANODE AND CATHODE MATERIALS

In the following sections, materials appropriate for inclusion into all of the layers shown will be described, but creative device physicists and material chemists continue to manipulate these materials into ever more intricate and elegant architectures. This includes the addition of new layers of new materials with new functions such that, as is usually the case, any review of this type that attempts to cover such a rapidly developing area will be outdated even before it is published.

3.2.1 ANODE MATERIALS

The anode material is, most typically, transparent ITO coated onto a glass or plastic substrate. Chapter 5 describes the details of such transparent anode materials. The general requirements for an anode material are as follows:

1. Highly conductive so as to reduce contact resistance
2. High work function (WF) ($\phi > 4.1 \text{ eV}$) to promote efficient hole injection
3. Good film-forming and wetting properties of applied organic materials so as to ensure good contact with these adjacent organic layers

4. Good stability, both thermal and chemical
5. Transparent, or else highly reflective if used in top emitting OLEDs

Clearly, in any light-emitting device, the light must escape from the device, and in OLEDs the window through which this occurs is typically provided by the anode ITO. ITO is a highly degenerate n-type semiconductor with high conductivity. It is transparent in the visible range owing to its large band gap of over 4.0 eV [6]. Although other transparent and conductive electrode materials certainly exist (e.g., fluorine doped tin oxide (FTO) [7], aluminum-doped zinc oxide (AZO) [8]), the ready availability of glass substrates, pre-coated and (as needed) pre-patterned with ITO as an item of commerce (due to its extensive use in liquid crystal display (LCD) screens) make ITO the most common material of choice. Although ITO has many desirable properties, it does suffer from several shortcomings. Most notably, ITO has a relatively high resistivity ($\sim 2 \times 10^{-4} \Omega \text{ cm}$), moderate surface roughness (typically $\sim 2 \text{ nm}$), a chemically reactive surface (which may result in ion migration into the device), and a low and variable WF (4.5–4.8 eV), leading to hole injection difficulties with some materials. The WF of ITO is quite sensitive to cleaning procedures (ozone or plasma treatments) used during device fabrication. Deposition techniques used for generating thin ($\sim 100 \text{ nm}$) coatings of ITO typically require sputtering (e-beam, pulsed laser [9], etc.) from an ITO target (typically 0–14% SnO_2 in In_2O_3) or from an In/Sn alloy in a reactive oxygen (Ar-O_2) atmosphere. In many instances, such deposition must be followed by annealing of the film at quite high temperature ($>200^\circ\text{C}$) to reduce the resistivity to acceptable levels. Such high-temperature annealing processes are precluded for plastic substrates leading to even poorer resistivity in such systems. Attempts have been made to develop solution-coating approaches to generate ITO anodes but still require high-temperature annealing to reduce the resistance [10]. It is most often the poor conductivity of ITO that limits the size of passive matrix OLED displays. Nevertheless, recently, new techniques have been developed to deposit ITO at low temperature to produce ITO-coated plastic substrate such as PET or PEN, and commercial ITO-coated plastic substrates are now available [11].

Other materials such as gold ($\phi = 4.9 \text{ eV}$), aluminum ($\phi = 4.2 \text{ eV}$), indium-doped zinc oxide, magnesium indium oxide, nickel tungsten oxide, or other transparent conductive oxide materials, have been studied as anodes in OLEDs. Furthermore, the WF of ITO can be varied by surface treatments such as application of a very thin layer of Au, Pt, Pd, or C, acid or base treatments, self-assembly of active surface molecules, or plasma treatment.

Anode materials are most typically deposited by evaporation, sputtering, or chemical vapor deposition methods. Other methods such as screen printing, laser ablation, electrochemical deposition, etc., have also been used.

3.2.2 CATHODE MATERIALS

Unlike the constraints on anode material, the constraints on cathode materials are usually lower because typically they do not need to constitute the transparent electrode material. In certain instances, where a completely transparent OLED is needed (windshield and heads-up displays), ITO may also be used as the cathode with suitable modification [12]. In general, cathode materials are pure metals or metal alloys. The requirements for cathode materials are as follows:

1. High conductivity
2. Low WF to promote electron injection
3. Good film-forming and wetting properties to ensure good contact with adjacent organic layers

4. Good stability
5. Highly reflective or transparent if used in top-emitting OLEDs

Typically, the cathode is a low WF metal or alloy system, such as Mg, Ca, Ba, Al. Clearly, a low WF facilitates electron injection into the lowest unoccupied molecular orbital (LUMO) level of the ETL material. However, low WF also implies high chemical reactivity and problems can occur with direct chemical reduction of organic materials in contact with such low WF metals. Although production of such species may be detrimental to device performance, it may, in favorable instances, actually assist in charge injection. Ease of oxidation of low WF metals and alloys can also lead to difficulties in processing devices that become very sensitive to moisture and oxygen contaminants. A very popular solution to the problem of low WF, yet readily processible cathodes, is the two-layer cathode comprising a thin (<5 nm) layer of LiF vapor deposited onto Al. This cathode owes its discovery to work from Kodak, which showed that this combination, especially in contact with reducible species in the ETL, such as aluminum tris-8-hydroxyquinoline (Alq_3), leads to the production of anionic species (e.g., Alq_3^- at the electrode surface, possibly with a Li^+ counter-cation and with cogeneration of AlF_3) [13]. This selective doping at the electrode and ETL interface then leads to improved charge injection similar to when lower WF cathode metals are used. This same principle has been used to generate other hybrid cathode systems although all typically use an alkali metal, alkali earth or rare-earth salt or oxide in conjunction with Al [14]. It is often the reactivity of the cathode metals which demands the high-quality hermetic seals used in OLED devices and, in many cases of device failure due to inadequate sealing, black spot defects show up in the device due to attack of air and moisture on the cathode metal. A common approach to controlling this problem is to include a sacrificial getter material inside the encapsulated device to scavenge water and oxygen before they can corrode the cathode. The most popular cathode materials are Al ($\phi = 4.2$ eV), LiF/Al ($\phi = 3.6\text{--}3.8$ eV), Ca/Al, Mg/Ag ($\phi = 2.90$ eV), and Ba/Al (2.60 eV). Although even lower WF can be achieved with, e.g., Yb ($\phi = 2.4$ eV), the low reflectivity index of the latter makes it less suitable for OLED applications. The active metal Ca ($\phi = 2.60$ eV) often has to be accompanied with other metals such as Al to increase the device lifetime. It is worth noting that the WF of the metals can be affected by their purity, their deposition method, and the surface structure, and the crystal orientation of the deposited films.

Research on cathode materials focuses on reduction of the high chemical activity of the lower WF metals (e.g., Ca/Al), the increase of the chemical stability, and improvement of the sticking coefficient of the interlayer materials (e.g., LiF/Al).

3.3 HOLE INJECTION MATERIALS AND CATHODE INTERFACIAL MATERIALS

3.3.1 HOLE INJECTION MATERIALS

Closely related to the anode modifications described above, the use of a HIL material to improve charge injection into the OLED device has spawned a number of materials, which have been shown to provide benefits, particularly in terms of lower operating voltages and extended lifetimes of devices.

The HIL acts as an interface connection layer between the anode and the HTL so as to improve the film forming property of the subsequent organic layer and to facilitate efficient hole injection. Hole injection materials (HIMs) should have good adhesion to the anode and should serve to smooth the anode surface. The most common HIMs are

1. Porphyrinic metal complexes
2. Self-assembled silane compounds

3. Plasma-deposited fluorocarbon polymers or vacuum-deposited Teflon, polyimide, or parylene
4. Electron donors doped with Lewis acids such as FeCl_3 , SbCl_5 , and π -electron acceptor F4-TCNQ to form so-called p-i-n structures
5. Conducting polymers such as PEDOT-PSS, doped polyaniline or polypyrrole, and
6. Inorganic insulators such as SiO_2 , Si_3N_4

3.3.1.1 Organic-Inorganic Interface

Since an OLED is a multilayer device structure, the interfacial electronic structure at the organic-metal and organic-organic interfaces plays an important role in the devices. The interface structure and energy level alignment of organic-inorganic and organic-organic has been investigated by Kahn and Seki [15,16]. These studies are very helpful in elucidating the role of the HIM as well as the electron injection material (EIM), although much work is still needed to fully understand this field. A recent book, edited by Salaneck et al., emphasizes the interface issues, ubiquitous in organic electronics, and interested readers may find additional detailed information there [17,18]. Hung et al. combined organic-metal interface energy diagrams and ultraviolet photo electron spectroscopy (UPS) results as shown in Figure 3.3 [19].

By careful examination of the various work dealing with organic-metal interfaces, they concluded the following:

1. In general, the dipolar difference between the metal and organic is negative (vacuum level lowered) with the exception that when electron withdrawing groups such as fluorine atoms are attached to the metal surface this value is positive.
2. The higher the WF of the metal, the larger the shift of the dipolar energy.
3. The interface dipole in organic-organic junctions is negligible with the exception of strong donor-acceptor interfaces where a barrier of 0.2–0.3 eV may exist due to the charge transfer process.
4. The dipolar difference is very complex in organic-metal interfaces (metal may deposit into the organic layer).

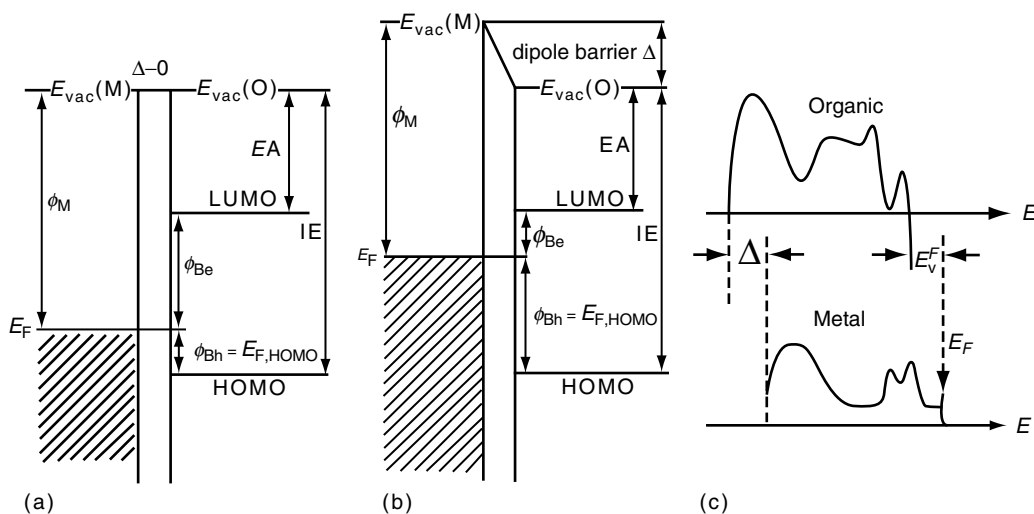
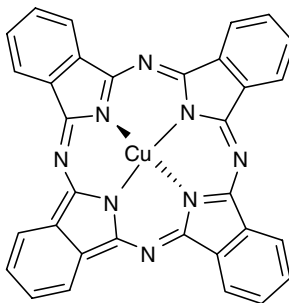


FIGURE 3.3 Schematic of an organic-metal interface energy diagram (a) without and (b) with an interface dipole and (c) UPS spectra of metal and organic. (From Hung, L.S. and Chen, C.H., *Mater. Sci. Eng.*, R39, 143, 2002. With permission.)



CuPc 1

SCHEME 3.2 Chemical structure of CuPc.

3.3.1.2 Porphyrinic Metal Complexes

In 1996, the Kodak group achieved a highly stable OLED by introducing a thin layer (~15 nm) of copper phthalocyanine (CuPc) (Scheme 3.2) between the anode (ITO) layer and the hole transport (α -NPD) layer [20]. The function of the CuPc as a HIM has two possible controversial mechanisms: One study showed that an optimized thin layer of CuPc actually lowers the driving voltage by reducing the hole injection barrier compared to a α -NPD–ITO interface as was explained by the Kodak group. Another study, however, showed that inserting the CuPc helps to balance the hole and electron currents (by way of sacrificing the hole injection efficiency), but results in an increased operating voltage [21]. Norton et al., using UPS, studied the interfacial band energies of CuPc inserted between ITO and α -NPD and concluded that the good wetting of CuPc on ITO may also partially contribute to the enhancement of the device stability, in addition to balancing the hole and electron injection [22]. Kahn et al. also studied the interface of ITO–CuPc–NPD by UPS as well as the characteristics of related hole-only devices and concluded that the effects of the CuPc layer depend on the WF of the underlying ITO [23]. These researchers measured the offset between their ITO and CuPc at about 0.70 eV. α -NPD and CuPc are offset by about 0.5 eV (see Figure 3.4). In this case the CuPc layer improves the hole injection.

CuPc (**1**) is a readily available pigment material that has very high thermal stability and is a modest semiconductor. When applied to ITO as a thin overlayer (usually by high-vacuum evaporation), the highest occupied molecular orbital (HOMO) level of the CuPc effectively pins the ITO WF at ~5.1 eV, which can lead to improved charge injection at lower voltages and much less sensitivity of performance upon ITO cleaning protocols [24]. Although CuPc has found widespread use, other phthalocyanines, including the metal-free version, have also been used for HIL applications [25]. The structurally similar porphyrin materials have also found applicability for this purpose. Further improvement of the device efficiency was achieved by adapting so-called quantum well layers. In the report by Qiu's group, an OLED device with an optimum quadriquantum-well structure of four alternating layers of CuPc and NPB gives three times the efficiency compared with the conventional structure [26]. The authors explained that this observation is due to the improved balance between holes and electrons.

3.3.1.3 Conducting Polymers, PEDOT–PSS, Doped Polyaniline and Polypyrrole

The performance of OLED devices employing CuPc as a HIL is unstable due to thermally induced HTM crystallization on the CuPc surface [27]. One approach to improve the hole injection and enhance the device stability is to overcoat the CuPc or else to directly deposit

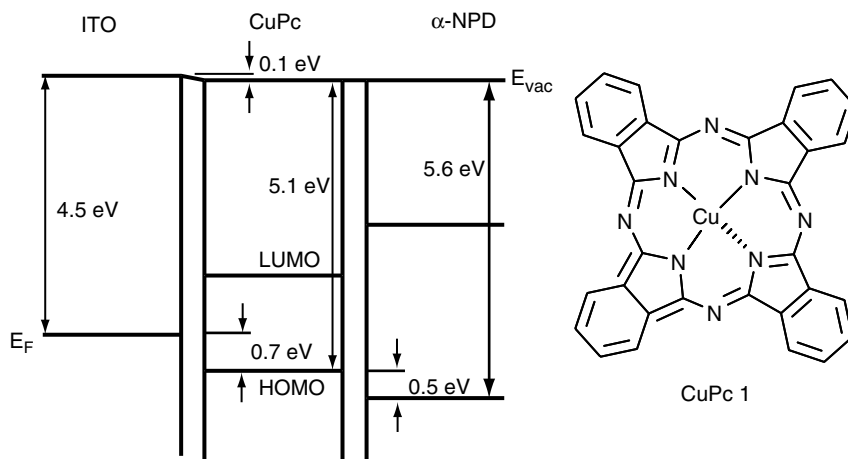
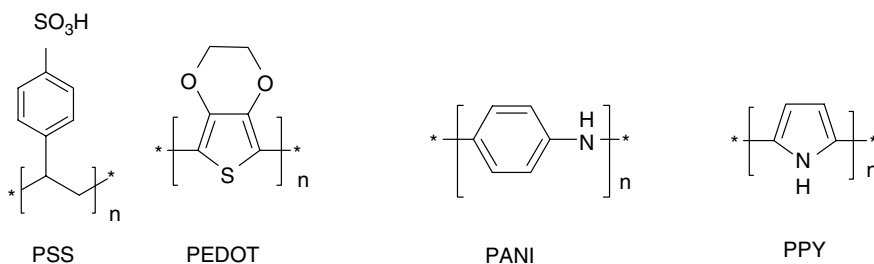


FIGURE 3.4 Molecular level alignment diagrams constructed using the HOMO and vacuum levels measured using UPS. The lowest unoccupied molecular orbital LUMO positions are inferred assuming a HOMO/LUMO gap equal to the onset of optical absorption. The chemical structure of CuPc is shown. (From Hill, I.G. and Kahn, A., *J. Appl. Phys.*, 86, 2116, 1991. With permission.)

onto the ITO itself with a buffer layer of a conductive polymer such as acid-doped (typically using polystyrene sulfonic acid, PSS) PEDOT (poly-3,4-ethylenedioxythiophene) [28], PANI (polyaniline) [29], or (polypyrrole) (Scheme 3.3) [30]. Such coatings can typically be deposited from water solutions and suspensions of the polymer by spin coating, ink-jet printing, etc. Such layers can result in improved surface smoothness and compatibility with subsequent organic layers, a somewhat higher WF (>5.0 eV) for better hole injection, as well as improved barrier properties by protecting the EMLs of the device from the reactive ITO surface. The smoothing effect of a conductive polymer layer should not be underestimated as conductive spikes on a native ITO surface are often large enough to contribute to serious electrical shorting to the cathode (given that the typical organic layers used in OLEDs are very thin). On the negative side, however, most of the available conductive polymer materials used for this application are strongly acidic due to the doping necessary to induce conductivity. The acidity can, in many instances, lead to corrosion problems (the ITO surface may actually partially dissolve during coating) and also problems with EMLs, which may be acid-sensitive (e.g., many are based on amine-containing host or guest materials that can react with acid functionality). This effect of the material acidity can manifest itself as a short device lifetime, including poor shelf life.



SCHEME 3.3 Chemical structures of conducting polymers.

SCHEME 3.4 Chemical structures of TPD-Si₂ HIMs.

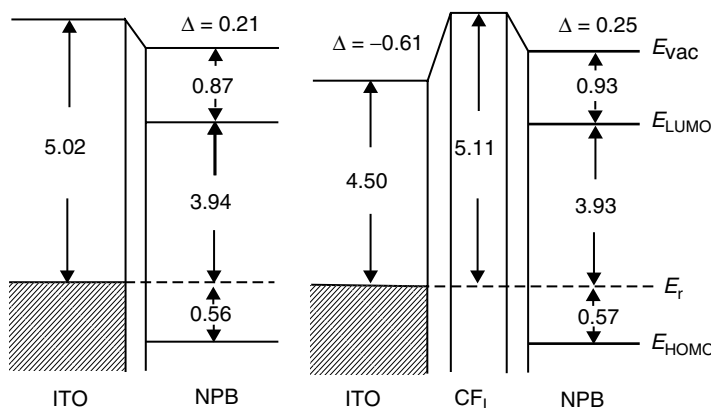


FIGURE 3.5 UPS spectra of NPB on an UV-ozone-treated ITO substrate (left) and NPB on an untreated ITO substrate overlaid by a 0.3-nm thick CF_x film (right), and the schematic energy level diagrams of and for the corresponding interfaces. The positions of E_{HOMO} and vacuum level (E_{VAC}) are derived from UPS measurements, and the position of the lowest unoccupied molecular orbital of NPB (E_{LUMO}). (From Tang, J.X., Li, Y.Q., Zheng, L.R., and Hung, L.S., *J. Appl. Phys.*, 95, 4397, 2004. With permission.)

and hole injection is attributed to the dipolar layer formed by the negatively charged fluorine [37]. The WF of ITO is strongly influenced by the electrostatic conditions at the surface. The introduction of the plasma-treated polyfluorocarbon creates a dipolar interface between ITO and the polymer layer, which leads to a lower barrier between the ITO and the HTL as depicted in Figure 3.5.

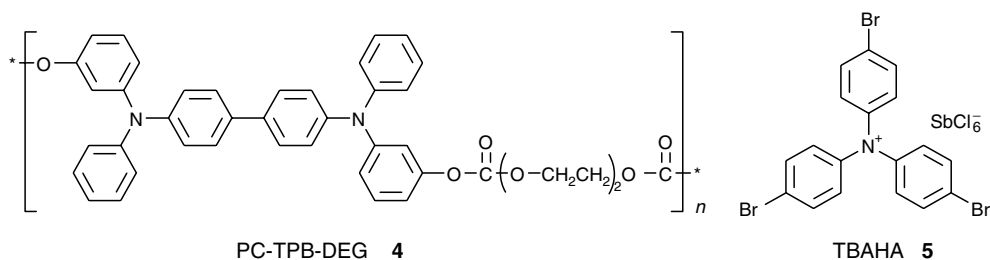
Instead of using plasma-polymerized polyfluorocarbon as HIL, Qiu et al. utilized a thermally deposited Teflon (polytetrafluoroethylene) thin layer as a HIL, which results in the same effect [38].

3.3.1.6 Inorganic Hole Injection Materials

It has been reported that a thin interfacial oxide layer such as SiO_2 , SiO_xN_y , or TiO_2 can improve device performance [39–41]. Although the exact mechanism of such thin buffer layers is not clear, the enhanced performance may arise from the improved smoothness of the surface of ITO, which leads to more homogeneous adhesion of the HTL. In addition, the optimized thickness of the buffer layer also helps balance the device charges due to reduced hole injection.

3.3.1.7 Doping the Hole Transport Materials

A doping strategy was first explored using PLEDs where a hole injecting conducting polymer such as polythiophene was doped with an oxidizing agent, such as FeCl_3 [42] or MEH-PPV, was doped with iodine [43]. In SMOLEDs, a HTL doped with a strong electron acceptor compound has been used as a HTL, for example, vanadyl-phthalocyanine (VOPc) HTL has been doped with tetrafluorotetracyanoquinodimethane ($\text{F}_4\text{-TCNQ}$ (**7**)) and a hole-transporting polycarbonate polymer PC-TPB-DEG (**4**) has been doped with tris(4-bromophenyl)aminium hexachloroantimonate (TBAHA, **5**) (Scheme 3.5) [44,45]. These HTLs dramatically lower the driving voltage and improve the device efficiency.



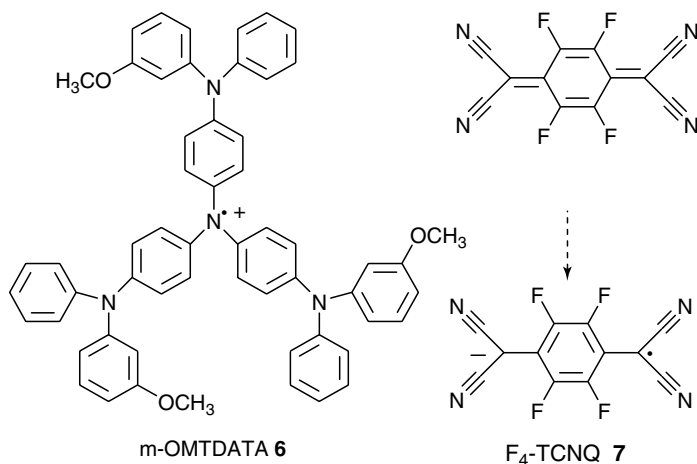
SCHEME 3.5 Chemical structures of the p-n injection materials.

Recently, a series of p-doped aromatic diamines have been reported by Pfeiffer et al. as excellent HIMs, e.g., 4,4',4''-tris(*N,N*-diphenylamino)triphenylamine (TDATA) or 1,4-benzenediamine, *N*-(3-methoxyphenyl)-*N'*,*N'*-bis[4-[(3-methoxyphenyl)phenylamino]phenyl]-*N*-phenyl (*m*-OMTDATA, **6**) doped with a very strong acceptor F_4 -TCNQ (**7**) by controlled coevaporation (Scheme 3.6) [46,47]. Multilayered OLEDs consisting of [ITO/ F_4 -TCNQ (2%):TDATA (100 nm)/TPD (10 nm)/Alq₃ (65 nm)/LiF (1 nm)/Al] achieved a very low operating voltage of 3.4 V, giving 100 cd/m² at 9.1 mA/cm².

Often the choice of HIL material is dictated by a combination of electronic and processing constraints, and additional materials of this type will undoubtedly be developed as perceived needs for OLED manufacturing arise.

3.3.2 CATHODE INTERFACIAL MATERIALS

Due to the relatively high mobility of holes compared with the mobility of electrons in organic materials, holes are often the major charge carriers in OLED devices. To better balance holes and electrons, one approach is to use low WF metals, such as Ca or Ba, protected by a stable metal, such as Al or Ag, overcoated to increase the electron injection efficiency. The problem with such an approach is that the long-term stability of the device is poor due to its tendency to create detrimental quenching sites at areas near the EML–cathode interface. Another approach is to lower the electron injection barrier by introducing a cathode interfacial material (CIM) layer between the cathode material and the organic layer. The optimized thickness of the CIM layer is usually about 0.3–1.0 nm. The function of the CIM is to lower



SCHEME 3.6 Chemical structures of the p-n injection materials.

the WF of the cathode and to enhance the electron injection by reducing the high chemical reactivity of the low WF metals, thereby increasing the chemical stability and improving the sticking coefficient of the interlayer materials. The typical CIM materials are

1. LiF, CsF
2. M_2O : Al (M: Li, Na, K, Rb)
3. CH_3COOM : Al
4. Li/Cs dopant with BCP, etc.
5. Organic polymer surfactants

3.3.2.1 LiF, CsF

One typical example of CIM is the introduction of a very thin layer of LiF between the cathode Al and ETL such as Alq_3 [48]. It has been demonstrated that such a thin layer of LiF dramatically improves the device performance and efficiency. In addition, this LiF/Al bilayer is also stable relative to $Mg_{0.9}Ag_{0.1}$ and should be compatible with Si device processing [49].

Figure 3.6 (left) shows the interfacial energy diagrams before and after LiF is introduced between an Al cathode and the ETM (Alq_3). The barrier heights for electron injection were 0.1 eV for the Alq_3 –LiF–Al interface and 0.5 eV for the Alq_3 –Al interface. The thin LiF layer reduces the barrier height by about 0.4 eV. As a consequence, it is expected that the current–voltage characteristics of the EL device can be greatly improved by interposing one to two monolayers of LiF between Alq_3 and Al as presented in Figure 3.6 (right).

Not only is the CIM layer widely used in SMOLED but is also applied in PLED. The CDT group has exploited LiF and CsF thin films in combination with Ca and Al cathodes and has achieved high efficiency and long lifetime PLED devices [50].

3.3.2.2 M_2O : Al (M: Li, Na, K, Rb)

Other insulator materials such as CsF [51,52], CsCl [53], CaF_2 [54], MgF_2 [55], NaCl [56] followed by deposition of a normal Al cathode have shown similar beneficial effects.

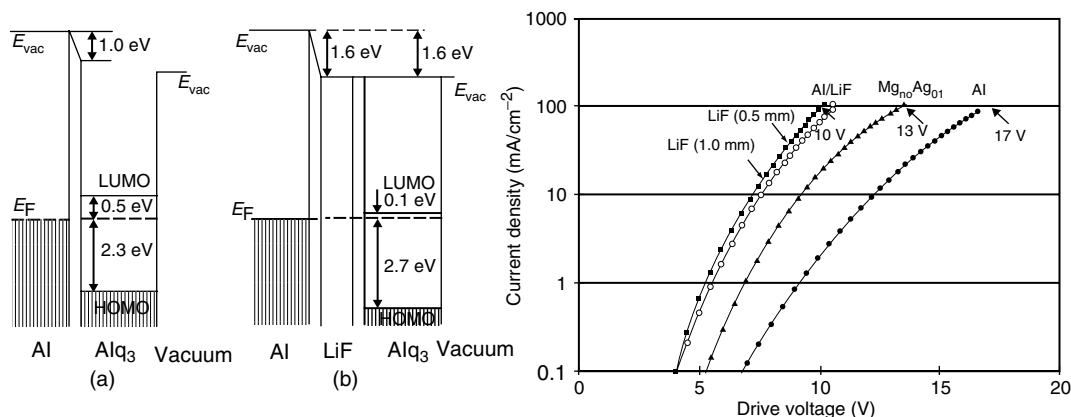


FIGURE 3.6 Energy diagrams of (a) the Alq_3 –Al interface and (b) the Alq_3 –LiF–Al interface (left). (From Mori, T., *Appl. Phys. Lett.*, 73, 2763, 1998. With permission.) Current–voltage characteristics of three EL devices using an Al, a $Mg_{0.9}Ag_{0.1}$, and an Al/LiF electrode, respectively (right). (From Hung, L.S., Tang, C.W., and Mason, M.G., *Appl. Phys. Lett.*, 70, 152, 1997. With permission.)

However, using alkaline earth metal fluorides gives a less pronounced improvement. The use of CsF and LiF as CIM layer has the same effect. However, unlike LiF, CsF reacts directly with Al and releases Cs metal, whereas the dissociation of LiF in the presence of Al is thermodynamically disallowed and proceeds only in the presence of suitable reducible organic materials such as Alq₃. Thus CsF is more generally applicable to many organic materials.

3.3.2.3 Li/Cs Dopant with BCP and Li–Quinolate Complexes

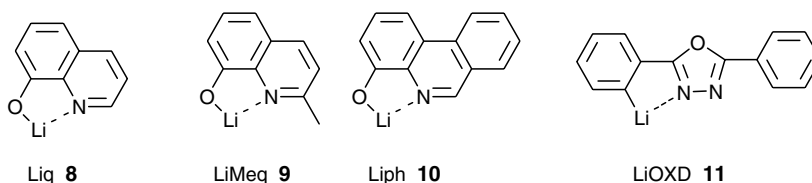
Kido et al. reported using a Li-doped Alq₃ layer as a CIM, which generates the radical anions of Alq₃ that, in turn, serve as intrinsic electron carriers and lead to improved device performance [57]. Lithium salts such as acetate or benzoate can also enhance the electron injection by a similar mechanism [58].

The use of inorganic alkali metal salts, such as LiF, CsF, NaF, as interfacial materials has been demonstrated to improve electron injection and to enhance the EL efficiency of OLEDs. The fact that using Li or Cs metal as the interface between aluminum and the organic layer (such as Alq₃) lowers the driving voltage indicates that modification of the Alq₃–Al interface with either elemental lithium or lithium compounds causes doping, which results in the creation of quinolate radical anions that then favor electron injection. This leads to the question of whether the properties of improved electron injection and good EL efficiency can be realized together in a simple lithium–quinolate complex. Lithium–quinolate complexes, 8-hydroxyquinolinolitolithium (Liq, **8**), 2-methyl-8-hydroxyquinolinolitolithium (LiMeq, **9**), 4-phenanthridinolitolithium (Liph, **10**), and 2-(5-phenyl-1,3,4-oxadiazolyl)phenolitolithium (LiOXD, **11**), have all been synthesized and investigated as EIMs used between the cathode Al and Alq₃ (Scheme 3.7) [59–63]. The results confirm that the function of these Lithium–quinolate complexes is the same as that of LiF. A very thin layer (0.5–5.0 nm) of the complex deposited on the Alq₃ layer enhances the QE of the devices and reduces the driving voltage. In addition, the advantage of using Liq over LiF as an injection layer is that the efficiency is less sensitive to the Liq thickness.

Just as p-doping HIMs have been exploited, n-doping EIMs have also been explored by Pfeiffer et al. With a p-doped HIL and 4,7-diphenyl-1,10-phenanthroline (BPhen) doped via coevaporation of Cs metal as an EIM in a phosphorescent organic light-emitting diode (PHOLED) device, they have achieved a power efficiency of ca. 77 lm/W and an EQE of 19.3% at 100 cd/m² with an operating voltage of only 2.65 V. More importantly, the efficiency decays weakly with increasing brightness, and a power efficiency of 50 lm/W is obtained even at 4000 cd/m² [64]. Such a p–i–n device features efficient carrier injection from both contacts into the doped transport layers and low ohmic losses in these highly conductive layers, and low operating voltages are obtained compared to conventional undoped OLEDs.

3.3.2.4 Organic Polymer Surfactants

Zyung et al., using ionomers such as sodium-sulfonated polystyrene as a CIM, have achieved an improved device performance [65,66]. Yang's group has used 0.2 wt% calcium acetylac-



SCHEME 3.7 Chemical structures of Li-quinolate complexes.

tonate ($\text{Ca}(\text{acac})_2$) solution in ethoxyethanol solvent with polyoxyethylene tridecyl ether $\text{C}_{13}\text{H}_{27}(\text{OCH}_2\text{CH}_2)_n\text{OH}$ as a surfactant CIM in a green PLED and has achieved device efficiency as high as 28 cd/A at 2650 cd/m² brightness, more than a factor of 3 higher than devices using calcium or aluminum as the cathode [67]. Recently, Jen's group, using a layer of neutral surfactant with a general chemical formula $\text{C}_m\text{H}_{2m+1}(\text{OC}_k\text{H}_{2k})_n\text{OH}$, reported it as a CIM in PLEDs to facilitate the electron injection through the high WF metal Al cathode. The external luminous efficiency of the device can reach 3.59 cd/A, which is higher than the control device (1.89 cd/A) using calcium as the cathode [68].

3.4 HOLE TRANSPORT MATERIALS

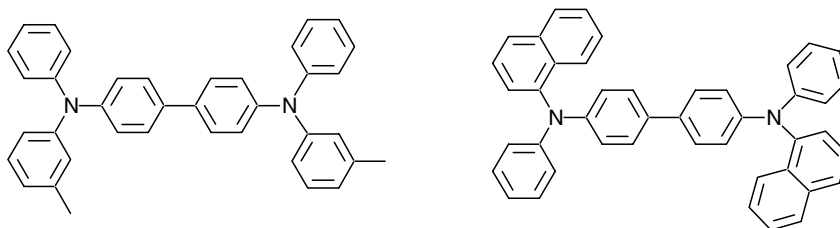
The HTL materials are very common in small-molecule-based OLED devices but are less common in polymer-based devices because conjugated polymers are usually good hole conductors themselves. They serve to provide a hole-conductive (via charge hopping) pathway for positive charge carriers to migrate from the anode into the EML. On the basis of this requirement, HTMs are usually easily oxidized and are fairly stable in the one-electron oxidized (radical-cation) form. This further translates into the materials having a fairly shallow HOMO energy level — preferably isoenergetic with the anode/HIL WF and somewhat lower in energy than the HOMO energy level of the EML. This latter property improves the chances of charge flow into the EML with minimal charge trapping. As the main function of the HTL is to conduct the positive charge carrier holes, hole-traps (higher energy HOMO materials) should be avoided either in the bulk of the material (i.e., hole-trapping impurity levels $\ll 0.1\%$ are typically required) or at interfaces. Another, perhaps less commonly appreciated, function of the HTL is that it should act as an EBL to prevent the flow of electrons from the EML and ultimately to the anode. For this purpose, a very shallow LUMO level is desirable. With these properties in mind, the commonly used HTL materials fall into several simple chemical classes:

1. Triarylamines
2. Triphenylmethanes
3. Phenylazomethines

3.4.1 TRIARYLAMINES

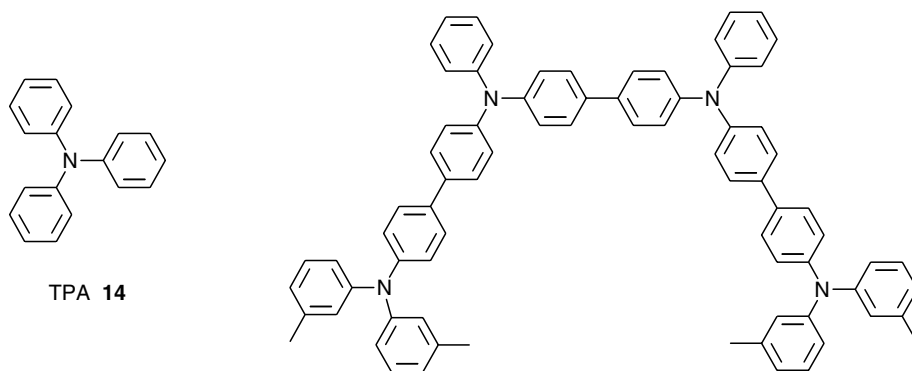
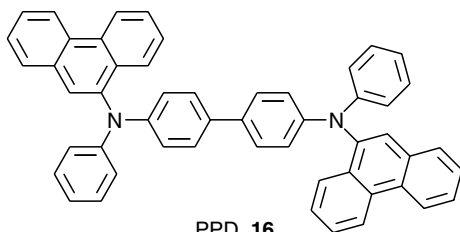
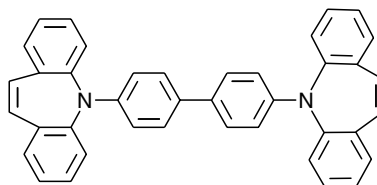
The most commonly used HTL materials are triarylamine compounds. These compounds were developed as HTMs for photoconductive applications such as xerography [69]. They naturally have been selected as HTMs for OLED applications largely because of their ready availability and their good electrochemical and thermal stabilities. The hole mobilities of these materials are also adequate for OLED applications. In addition, high purity, so as to ensure low hole-trap contamination, is believed necessary for long-lived OLED performance and such materials may often be train sublimed to very high purity.

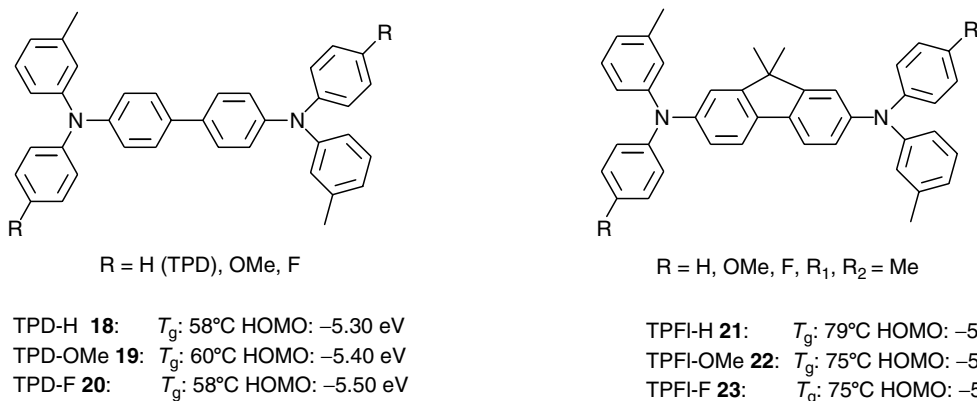
Two of the most widely used HTMs of the triarylamine family in OLEDs are *N,N'*-(3-methylphenyl)-1,1'-biphenyl-4,4'-diamine (TPD, **12**) and 4,4'-bis[*N*-(1-naphthyl-1)-*N*-phenyl-amino]-biphenyl (α -NPD, **13**) (Scheme 3.8). TPD and α -NPD have modestly high hole drift mobility, and were initially developed as charge transport layers in xerography. However, TPD and α -NPD, which have low glass transition temperature (T_g) of 65°C and 95°C, respectively, tend to crystallize or expand during device operation. For comparison, the T_g of Alq_3 is $>170^\circ\text{C}$. It is commonly believed that a good HTM should have both a low-energy barrier from the anode and a relatively high T_g . These properties will improve the hole injection efficiency, reduce the crystallization, and thus increase the lifetime of the device.

TPD **12** T_g : 65°C HOMO: -5.50 eV; LUMO: -2.30 eV α -NPD **13** T_g : 95°C HOMO: -5.70 eV; LUMO: -2.60 eV**SCHEME 3.8** Chemical structures of typical hole transport materials of TPD and NPD or α -NPD.

Adachi et al. showed that the ionization potential (IP) of HTLs was found to be the dominant factor for obtaining high durability in organic EL devices [70]. The formation of the small energy barrier at the interface of a HTL and anode was required for high durability. However, their results showed that there are no straightforward relationships between melting point, T_g of the HTMs, and durability of the EL devices.

Fujikawa et al. studied a series of triphenylamine (TPA, **14**) oligomers from the dimer TPD up to the related pentamer and used them as HTMs [71]. Their results indicated that the thermal stability of the OLEDs was dramatically improved using a HTM TPTE (**15**) (Scheme 3.9), a tetramer of TPA. The resulting OLED devices show uniform light emission in continuous operation up to 140°C without breakdown [72].

TPA **14**TPTE **15** T_g : 130°C HOMO:PPD **16** T_g : 152°C HOMO: -XXX eV; LUMO: -XXX eVISB **17** T_g : 115°C HOMO: -5.45 eV; LUMO: -2.06 eV**SCHEME 3.9** Chemical structures of high glass transition temperature HTMs.



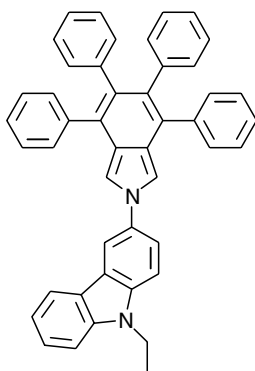
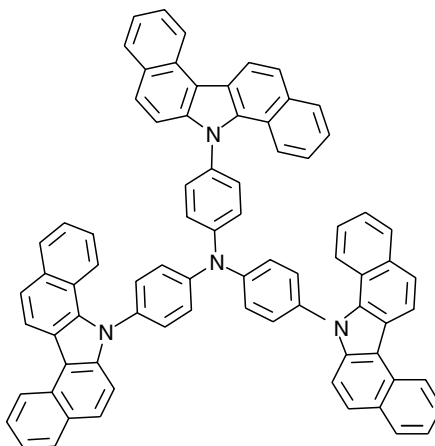
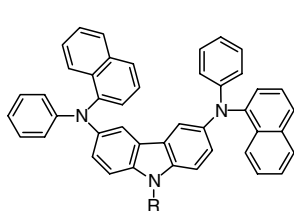
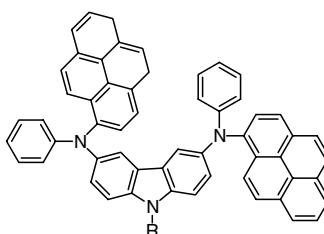
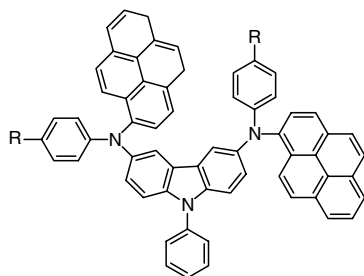
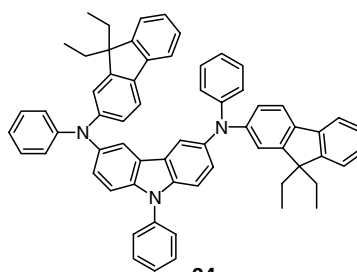
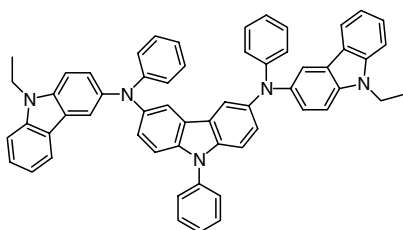
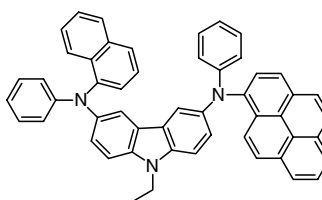
SCHEME 3.10 Chemical structures of HTMs.

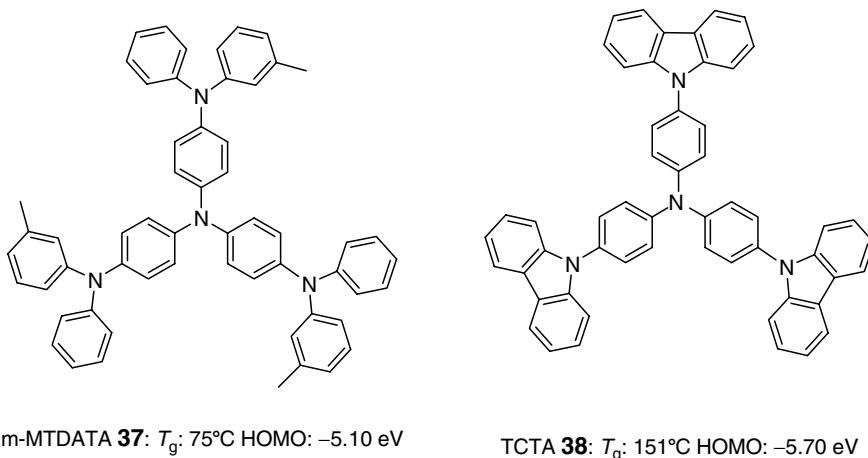
Using the same biphenyl backbone as TPD and α -NPD, Thompson's group synthesized a series of triarylamines with high T_g s ranging from 85 to 155°C as HTMs [73]. The OLED devices fabricated by using PPD (**16**) or ISB (**17**) showed comparable device performance to the TPD or NPD devices, while maintaining the high T_g . The HTL can be composed of one compound or a mixture of several HTMs (Scheme 3.9). Interestingly, in contrast to the reports of Shirota and coworkers, who reported that the energetics between ITO and HTL interface was critical to the operating voltage and the QE of an OLED [74], Thompson's group found that there is no relationship between the HOMO energy and the device QE or turn-on voltage. Instead, they have shown that an asymmetrical substitution of the amine group hinders charge transport, thereby raising the turn-on and operating voltages.

Replacement of the biphenyl bridge with a fluorene unit (Scheme 3.10) can moderately change the T_g (15–20°C higher in fluorene containing species) and electronic absorption spectra (red-shift of about 30 nm for fluorene species). The fluorene-unit-based and biphenyl compounds-based triarylamine compounds have the same range of hole mobilities. Brédas et al. studied the details of these changes related to their optical and electronic properties, and related these to the device performance [75]. Their results showed that the fluorene series has similar OLED performance as the biphenyl species. Introducing electron-withdrawing fluorine atoms or electron-donating methoxy groups can tune the electron IP, with little effect on the T_g . Later studies by Wong et al. showed that bulky 9,9-diarylfuorene-substituted triarylamine increased T_g up to 134°C [76].

A highly phenylated isoindole HTM 1,3,4,5,6,7-hexaphenyl-2-{3'-(9-ethylcarbazolyl)}-isoindole (HPCzI, **24**) was designed and synthesized by Lee's group (Scheme 3.11) [77]. The hole mobility of a HPCzI thin film was $4.3\text{--}6.0 \times 10^{-5} \text{ cm}^2/(\text{V s})$ (studied by using transient EL with an applied electric field in the range of 7.6×10^5 to $1.4 \times 10^6 \text{ V/cm}$), which is of the same order of magnitude as that of NPD ($7.8\text{--}9.9 \times 10^{-5} \text{ cm}^2/(\text{V s})$). The performance of a bilayer device ITO/HPCzI/Alq₃/MgAg showed comparable luminescent efficiency to the same device structure where NPD was used as the HTL. The benefit of HPCzI as a HTM is that the current efficiency is quite stable when the device is operated under higher current density. Chen synthesized a star-shaped triarylamine with a very high T_g as a HTM, 4,4',4''-tri(*N*-dibenzo[*a,g*]carbazoyl)triphenylamine (TDCTA, **25**) [78]. The device fabricated using TDCTA as a HTL showed good hole-transporting properties, although the hole barrier is higher due to the deeper HOMO energy level of TDCTA (−5.72 eV).

Tao et al. reported a series of light-emitting peripheral diarylamine derivatives containing carbazole units, which possess dual functions, as both active emitting materials and HTMs (Scheme 3.12) [79]. These luminescent materials are amorphous, with high T_g (120–194°C),

**HPCzI 24** T_g : 150°C HOMO: -5.10 eV; LUMO: -2.20 eV**TDCTA 25** T_g : 212°C HOMO: -5.72 eV**SCHEME 3.11** Chemical structures of HTMs.**R = Et 26, R = Ph 27****R = Et 28, R = Ph 29, *p*-CNPh 30,
R = 9,9'-diethylfluorene 31****R = Me 32, R = OMe 33****34****35****36****SCHEME 3.12** Chemical structures of some hole transport materials based on carbazole units.

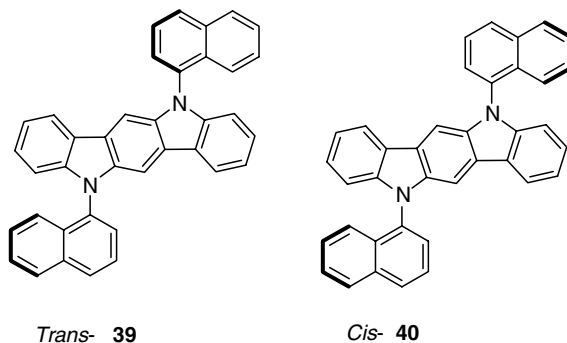


SCHEME 3.13 Chemical structures of start-burst HTMs.

high thermal stability ($T_d > 450^\circ\text{C}$), and with HOMO energy levels of 4.86–5.04 eV are also suitable for HTMs. OLED devices fabricated using these materials appear to be very stable. Using high T_g ($>150^\circ\text{C}$) tri- and tetra-substituted carbazole derivatives as HTMs, Wang et al. achieved high-performance OLEDs, comparable with the same device structure using NPD as the HTL [80].

Earlier work by Shirota et al. focused on the investigation of starburst triarylamine amorphous glasses with high T_g as HTMs. Scheme 3.13 shows the chemical structures of two representative star-burst HTMs 4,4',4''-tris(3-methylphenylphenylamino)-triphenylamine (m-MTDATA, **37**) ($T_g = 75^\circ\text{C}$) and 4,4',4''-tri(*N*-carbazolyl)triphenylamine (TCTA, **38**) ($T_g = 150^\circ\text{C}$) [81,82]. OLEDs fabricated using such materials showed dramatically improved thermal stability and high efficiency. Recently, Tao's group also reported a series of star-like hole transport and emitting materials based on carbazole or diphenylthienylamine units [83,84].

An interesting series of high T_g HTMs based on novel indolo[3,2-*b*]carbazoles has been discovered by the Xerox group [85]. These compounds not only showed the desired hole transport properties and high T_g of 164°C but also display an unusual atropisomerism with two discrete *trans*- and *cis*-rotational isomers (Scheme 3.14), which greatly improves their tendency to form stable amorphous glasses.



SCHEME 3.14 Chemical structures of atropisomers of HTMs.

A new branched carbazole derivative with phenyl ethylene moieties attached, 1,3,5-tris(2-(9-ethylcarbazyl-3)ethylene)benzene (TECEB, **41**) (Scheme 3.15), was prepared as a HTM for OLEDs [86]. TECEB has a HOMO energy level of -5.2 eV and hole-drift mobility of 10^{-4} $\text{cm}^2/(\text{V s})$, comparable to NPD. The device performance (maximum luminance of about $10,000$ cd/m^2 and current efficiency of 3.27 cd/A) in a standard HTL/tris-(8-hydroxyquinoline) aluminum double-layer device is also comparable to NPD, but TECEB has a higher T_g (130°C) and its ease of synthesis is superior to NPD. Distyryl units linked to a TPD derivative, *N,N'*-bis(4-(2,2-diphenylethenyl)-phenyl)-*N,N'*-di(*p*-tolyl)-bendidine (DPS, **42**) (Scheme 3.15), reported by Yamashita and coworkers, showed good hole transport properties and improved thermal stability compared with the parent TPD [87].

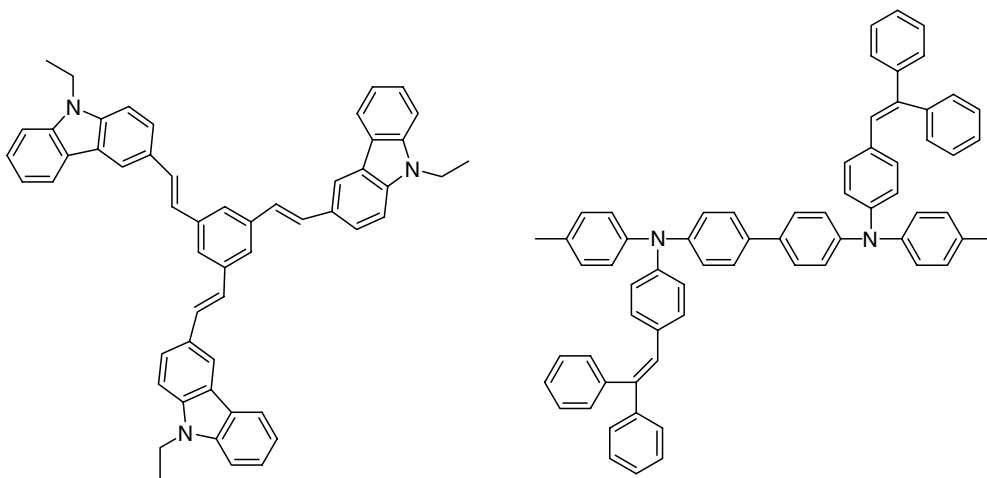
Spiro-shaped HTMs have been studied extensively (Scheme 3.16) [88,89]. The introduction of a spiro center improves the thermal stability of the amorphous state without significantly changing charge-transport properties. Compared with using NPD, TPD HTMs, using **43** in ITO/HTM/ $\text{Alq}_3/\text{LiF}/\text{Al}$ devices showed very high luminescent efficiency [90].

Ha et al. demonstrated that dispersed TPD in a fluorine-containing polyimide matrix as a HTM has significantly improved device performance (Scheme 3.17) [91]. Flexible and fluorinated polyimide as a matrix exhibits the lowest turn-on voltage and a high EL efficiency [92].

Recently, Liao et al. reported a highly efficient blue LED using a composite hole transport material (c-HTM) having a CuPc (**1**) doped in α -NPD (**13**) (Scheme 3.18) [93]. This c-HTL reduces the hole current and thus balances the hole-electron charge recombination, although a slight increase of the driving voltage has been observed for such c-HTM-based device.

Grubbs' group reported a series of cross-linkable triarylamine-containing poly(norbornenes) (**51**) and investigated them as the HTMs in a bilayer OLED (Scheme 3.19) [94]. However, cross-linking was found to decrease the device performance due to the low T_g of the polymers and the poor film quality after UV irradiation.

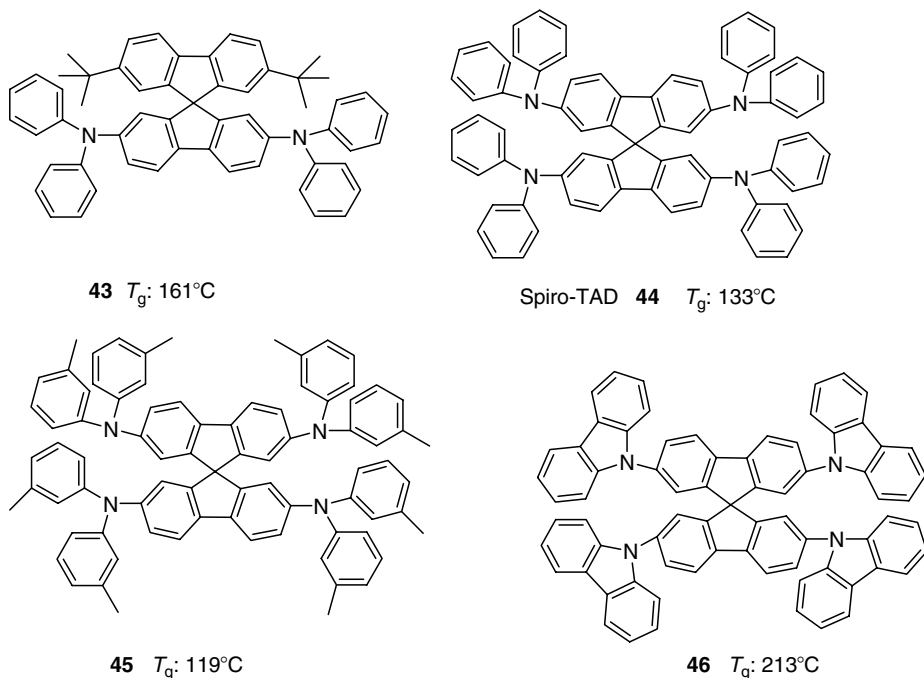
Improved cross-linkable HTMs have been investigated. These include photo-cross-linkable and thermo-cross-linkable polymers. A new type of low molecular weight HTM based on



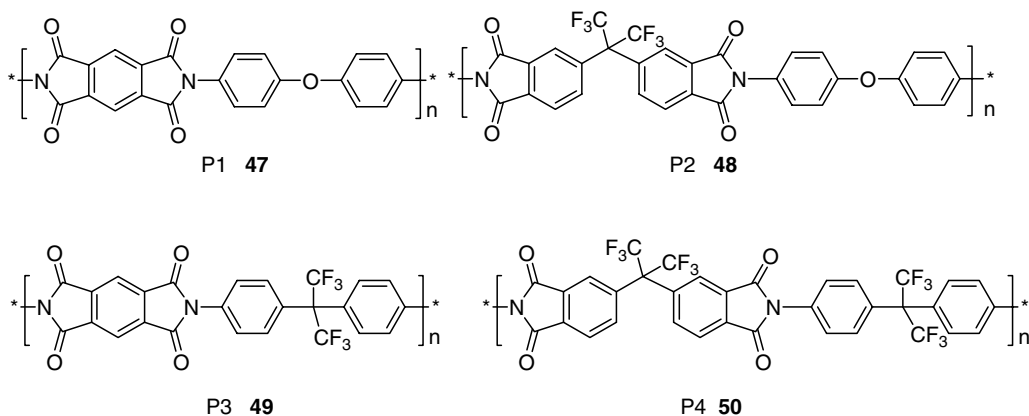
TECEB **41**: T_g : 130°C HOMO: -5.20 eV

DPS **42**: T_g : 90°C HOMO: -5.10 eV

SCHEME 3.15 Chemical structures of HTMs.



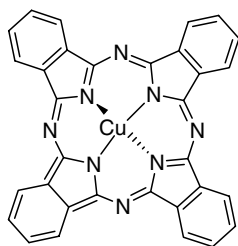
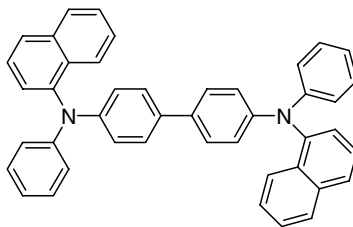
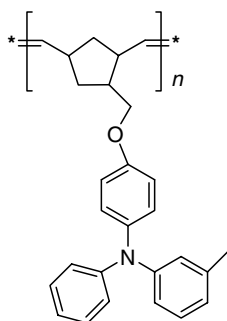
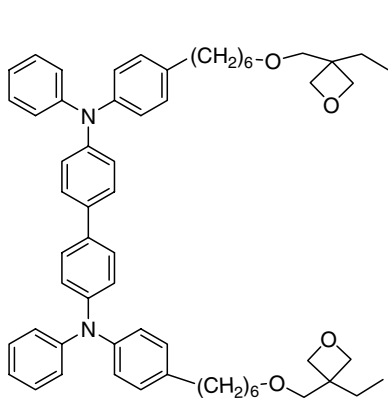
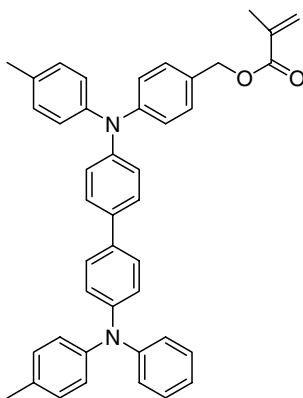
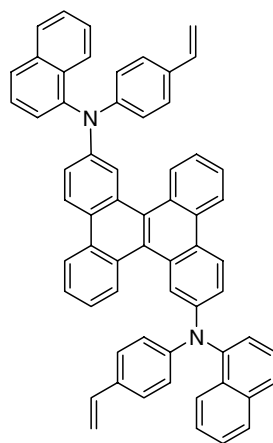
SCHEME 3.16 Chemical structures of HTMs.



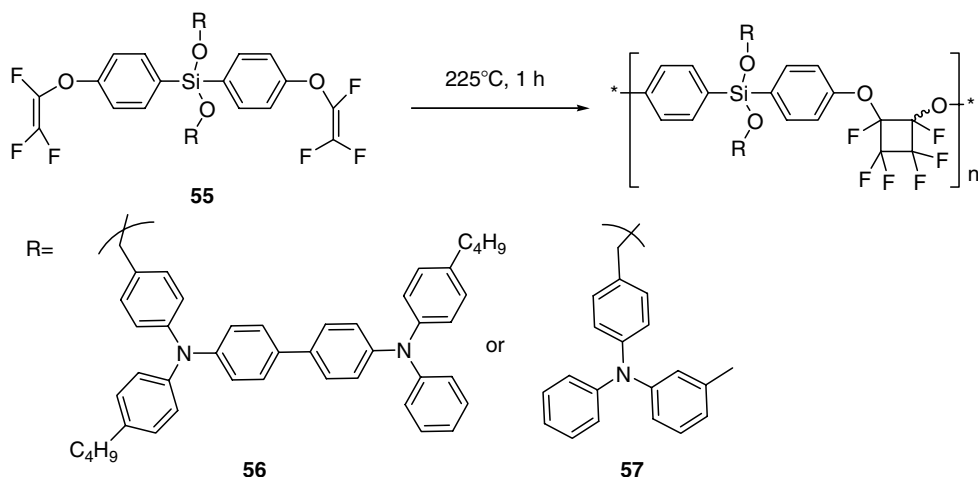
SCHEME 3.17 Chemical structures of polyimide materials used as hosts for NPD doping.

TPAs bearing cross-linkable oxetane functionalities (**52**) (Scheme 3.20) has been developed [95,96]. This material can be easily photo-patterned by exposure to a very short wavelength UV light source to form a patterned and insoluble HTL. Similar photo-cross-linkable HTMs based on side-chain acrylate or styryl functional groups have been synthesized (**53**, **54**) [97]. A series of spiro-linked and photo-cross-linkable HTMs have been patented by the Canon group [98].

Recently, Jen's group synthesized a series of high T_g fluorinated polymers with a hole transporting TPA group covalently attached as side chains (**55**) (Scheme 3.21) [99]. This type of polymer can be processed into thin films by simple thermal cyclopolymerization without introducing any by-products [100]. The polymers (**56**, **57**) are insoluble in most organic solvents and can be conveniently streamlined into a multilayer device fabrication process [101,102]. The

CuPc **1** α -NPD **13****SCHEME 3.18** Composite hole transport material (c-HTM): CuPc (**1**) and α -NPD (**13**).**51****SCHEME 3.19** Chemical structure of cross-linkable hole transport polymer.**52****53****54****SCHEME 3.20** Chemical structures of photo-cross-linkable HTMs.

HOMO energy level of the polymer is -5.32 eV. It was demonstrated that the EL performance of super yellow PPV and blue polyfluorene derivatives using this hole transport polymer is comparable to or better than that using PEDOT-PSS as a HTL [102].

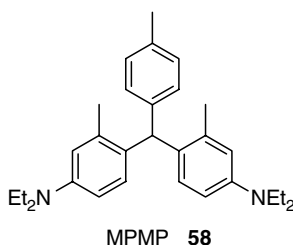


SCHEME 3.21 Chemical structures of HTMs.

3.4.2 TRIPHENYLMETHANES

As with the triarylamines, the triphenylmethanes were first developed for xerographic and photoconductor applications [103]. The prototypical example of a material of this type is MPMP (**58**) shown in Scheme 3.22.

This compound has one of the highest hole mobilities known for amorphous organic materials but is prone to crystallization and has a low T_g , making it less useful for long-lived OLED architectures. The HOMO and LUMO energy levels of MPMP are -5.53 and -1.88 eV, respectively, and the hole mobility of MPMP is in the range of 10^{-3} to 10^{-4} $\text{cm}^2/(\text{V s})$ as measured by time-of-flight (TOF) method [104]. This value is comparable with the best TPA compounds. Experimental results confirmed that there is little difference in the energetics and the mobility between the MPMP and NPD HTMs. However, when using MPMP as a HTM with a green iridium complex phosphorescent-emitter-based OLED, the device showed improved QE compared with the equivalent NPD-based device, especially when using neat films of the iridium complex as the emitter [105]. The authors explained that this difference in device performance is due to the high triplet energy level of MPMP (>3 eV) compared with NPD, which is 2.55 eV. The lower triplet energy level of NPD contributes to the energy transfer quenching processes from the excited state of the iridium emitter to the triplet state of the HTM [105].

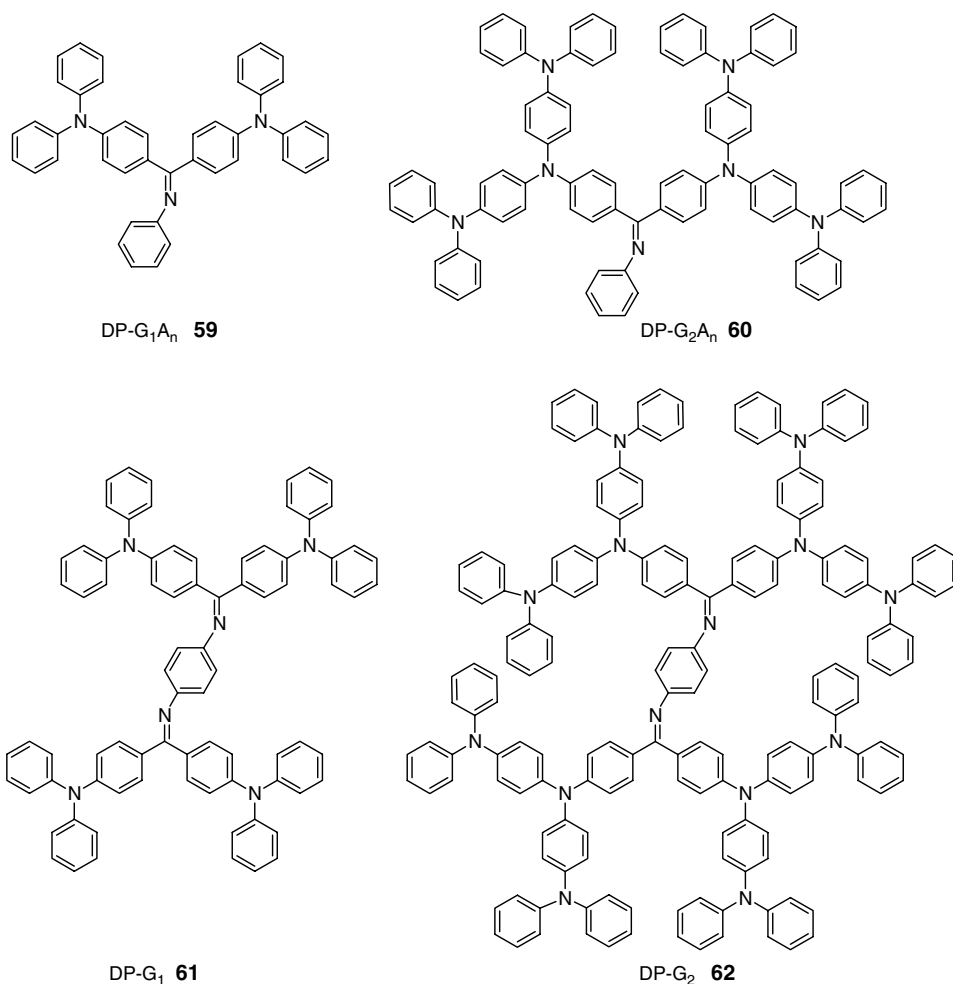


SCHEME 3.22 Chemical structures of HTMs.

3.4.3 PHENYLAZOMETHINES AND THEIR METAL COMPLEXES

Yamamoto et al. have designed and synthesized a series of novel diphenylamine-substituted phenylazomethine dendrimers (DP- G_n , **59–62**) (Scheme 3.23) as HTMs [106–109]. These dendrimers showed a relatively high thermal stability, a multiredox system due to the terminal amine moiety, and a stepwise metal complexation with metal ions. The EL performance of the double-layer devices utilizing these dendrimers as HTMs (HOMO: -5.2 to -5.4 eV) and Alq₃ as the emitting and ETMs increased with higher dendrimer generations. Using the metal ion-complexed (0.5 equiv. SnCl₂) DP- G_2 dendrimers, the luminance and EL efficiency of the devices were increased by more than double and over 30%, respectively. These phenylazomethine dendrimers, capable of forming metal complexes, are novel and promising materials for highly efficient OLEDs [110,111].

Other classes of organic compounds have been proposed and tested as HTL materials but have yet to gain wide acceptance. A few of the more interesting examples include isoindoles [112], bisphenol–acetophenone–polycarbonate [113], and polysilanes [114].



SCHEME 3.23 Diphenylamine-substituted phenylazomethine dendrimers (DP- G_n , $n = 1, 2$).

3.5 ELECTRON TRANSPORT MATERIALS

Perhaps the most widely investigated layer in an OLED device is the ETL. This layer functions as a conducting material to help transport electrons from the cathode and into the organic layers of the device — ideally transporting the electrons via a hopping mechanism involving transitory production of anion radicals of the molecules involved. As such, the material needs to have a LUMO level close in energy to the WF of the cathode material used so as to aid charge injection. It also needs to be comprised of a material that is relatively stable in its one-electron reduced form. As with all organic layers, it should form good amorphous films and have a high T_g to favor stable operation over extended periods.

Since most of the high-efficiency organic emitters have p-type character and mainly hole-transporting behavior to achieve high efficiency device performance, an electron transport material is necessary to balance the charge injection and transport. In fact, it is documented that introducing an ETM into OLEDs results in orders of magnitude improvement in the device performance. The functions of the ETMs are to reduce the energy barrier between the cathode and the emitter and to help the electrons be easily transported to the emitter. Two good recent reviews of ETMs have been published [115,116]. Figure 3.7 shows the energy level diagrams of a single-layer OLED and a double-layer OLED after the introduction of the ETM layer. The electron injection energy barrier (ΔE_e) is determined by the electron affinity (EA) or the LUMO level and the WF of the cathode (Φ_c), while the hole injection energy barrier (ΔE_h) is determined by the IP or the HOMO level and the WF of the anode (Φ_a). Introducing an ETM lowers the energy barrier for electron injection ($\Delta E_{e2} < \Delta E_{e1}$). Meanwhile, most ETMs also serve as a HBL to efficiently confine the exciton formation in the EML and thus balance charge injection.

A good ETM should have the following properties:

1. High EA (< 3.2 eV). This will match the WF of the cathode and reduce the energy barrier difference between the cathode and the emitter.
2. Reasonably good electron transport mobility ($\mu_e > 10^{-5}$ cm²/(V s)). This aids transporting electrons to the emitter layer and efficiently confines the exciton in the EML.
3. High thermal stability ($T_g > 120^\circ\text{C}$). The materials should not easily crystallize and should withstand Joule heating during device operation.

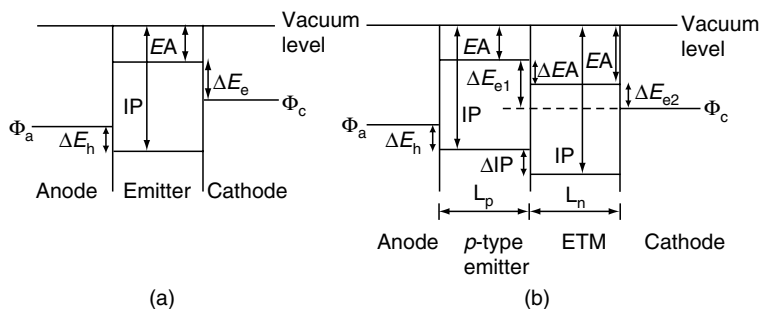


FIGURE 3.7 Energy-level diagrams of (a) a single-layer OLED and (b) a two-layer OLED based on a p-type emitter and an ETM. (From Kulkarni, A.P., Tonzola, C.J., Babel, A., and Jenekhe, S.A., *Chem. Mater.*, 16, 4556, 2004. With permission.)

4. Stable electrochemistry and electric field stability (reversible one-electron reduction). Withstanding a high electric field is a key issue for the lifetime of the device.
5. Match the optical band gap of the emitters. The materials should avoid light absorption and scattering to maximize light output and increase the efficiency.
6. Phase compatibility and processibility. The materials should be processible and compatible with neighboring materials to get pin-hole-free and uniform films.

On the basis of these criteria, the chemical structures of useable ETMs include:

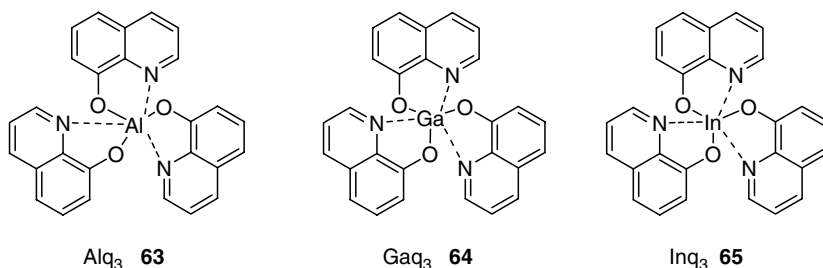
1. Metal chelates
2. Oxadiazole compounds
3. N=C (imine) containing quinoline, anthrazoline, phenanthraline, and pyridine compounds
4. Cyano and F-substituted compounds
5. Others

Methods to determine or justify the utility of the electron transport properties of ETM are TOF electron mobility and electron-only diode device measurement as well as the overall OLED performance.

3.5.1 METAL CHELATE ELECTRON TRANSPORT MATERIALS

The most commonly used material of this type is certainly Alq₃ (**63**) (Scheme 3.24) and almost all long-lived OLED devices include Alq₃ as the ETL. Interestingly, Alq₃ was the first emission and electron transport material explored by the Kodak group in their pioneering papers, and, so far, it is still one of the best electron transport materials, emission materials, and host materials. It is worthwhile mentioning here that, in addition to the use of metal chelates as electron transport materials, most of them can also be used as emission materials. In other words, many are electron transporting and emission materials.

Alq₃ has risen to a prominent position among OLED materials and remains the most widely studied metal chelate material. In the Alq₃ crystal structure, the distorted octahedral geometry of the 8-hydroxyquinoline ligands surrounding the Al³⁺ ion center makes it less prone to photoluminescence (PL) quenching in the solid state. It is thermally stable, has a *T_g* of 172°C [117], and can easily be thermally deposited to form pin-hole free amorphous thin films due to its intrinsic polymorphic phase behavior [118]. The electron mobility of Alq₃ is $1.4 \times 10^{-6} \text{ cm}^2/(\text{V s})$, far higher than its hole mobility $2.0 \times 10^{-8} \text{ cm}^2/(\text{V s})$ as estimated by TOF measurements [119]. The HOMO energy level is -5.95 eV and its LUMO energy level is -3.00 eV [120]. These optical and electronic data indicate that Alq₃ is an electron acceptor, consistent with its use as an efficient ETM. For example, using Alq₃ as an ETM has enabled



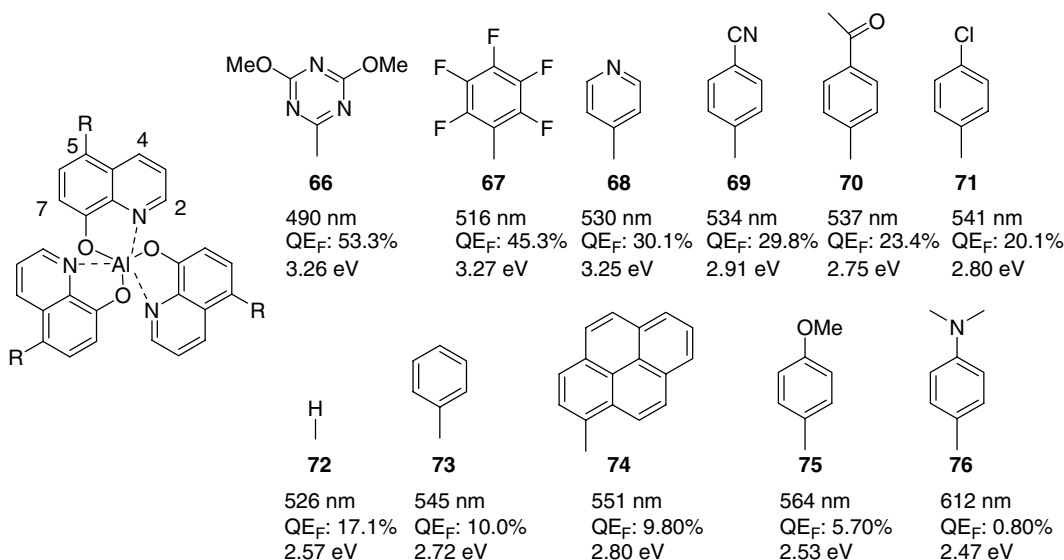
SCHEME 3.24 Chemical structures of Alq₃, Gaq₃, and Inq₃.

an over 100 times improvement in EQE of MEH-PPV bilayer OLEDs compared to the MEH-PPV single-layer OLEDs [121].

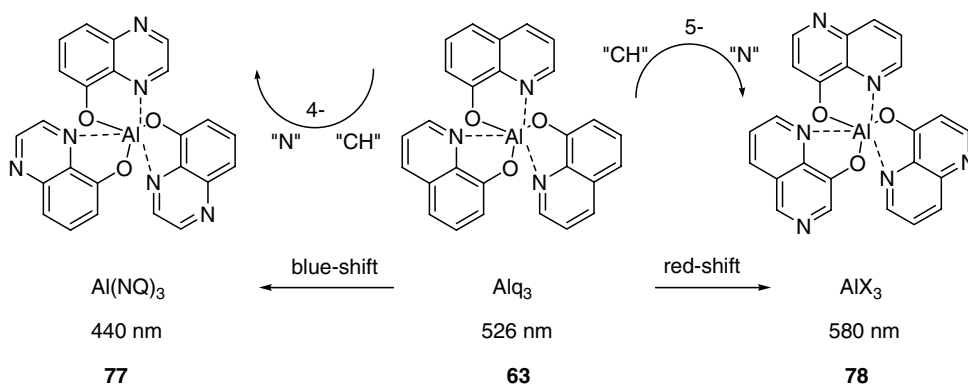
In addition to Alq_3 , the same group metal chelates GaQ_3 (**64**) and InQ_3 (**65**) have also been investigated as ETMs as well as EMs (Scheme 3.24). Chen et al. studied the OLED performance using these metal chelates and found that as the size of the metal ion increased, the luminescent efficiency decreased and the electron mobility increased [122]. The observed performance has been confirmed by PL QE measurements, UPS, and ultraviolet-visible (UV-vis) spectral data. Alq_3 has a solid-state fluorescence QE of 25–32% [123], which is four times higher than the fluorescence efficiency of GaQ_3 and InQ_3 . The emission spectrum shifts from 528 nm (Alq_3) to 548 nm (GaQ_3) and 556 nm (InQ_3) when the size of the central metal ion increases. The electron affinities of Alq_3 , GaQ_3 , and InQ_3 are -3.1 , -2.9 , and -3.4 eV, respectively.

By varying the substituents at the 5-position of aluminum tris-8-hydroxyquinoline (Alq_3) chelates using electron-withdrawing or electron-donating groups attached to aryl moieties, a new class of electroluminescent compounds with tunable emission colors ranging from bluish-green to orange-red have been synthesized. Their OLED performances have been investigated, but the luminescence and QE of the devices were lower than that of the parent Alq_3 -based device (**66–76**) (Scheme 3.25) [124,125]. The results indicate that the emission color shifts from blue to red when the substituents change from strong electron-withdrawing to strong electron-donating groups. At the same time the QE decreases accordingly. The electron mobility of this class of materials has not been reported. Kido et al. studied the OLED performance using tris(4-methyl-8-quinolinolate) Al(III) chelates (Almq_3) as EML, host material, and ETM, and found that the OLED EQE of Almq_3 is twice that of the Alq_3 -based device [126].

Theoretical modeling work predicting the emission color of Alq_3 derivatives has shown that the emission properties of the ligand dominate the fluorescence of the complexes [127,128]. The electronic $\pi-\pi^*$ transitions in Alq_3 are localized on the quinolate ligands with the filled π orbitals (HOMOs) located on the phenoxide side of the quinolate ligand, and the



SCHEME 3.25 Chemical structures and optical properties of Alq_3 derivatives (maximum emission wavelength, photoluminescent quantum efficiency in CH_2Cl_2 and the band gap are listed).

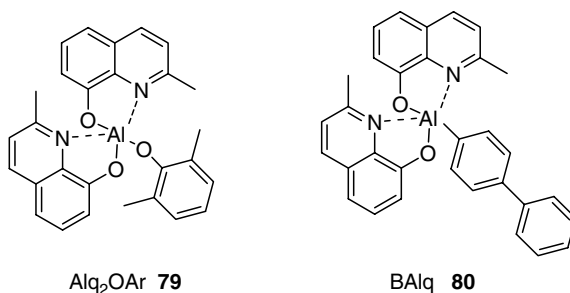


SCHEME 3.26 Chemical structures of Alq_3 derivatives with blue- and red-shifted emission.

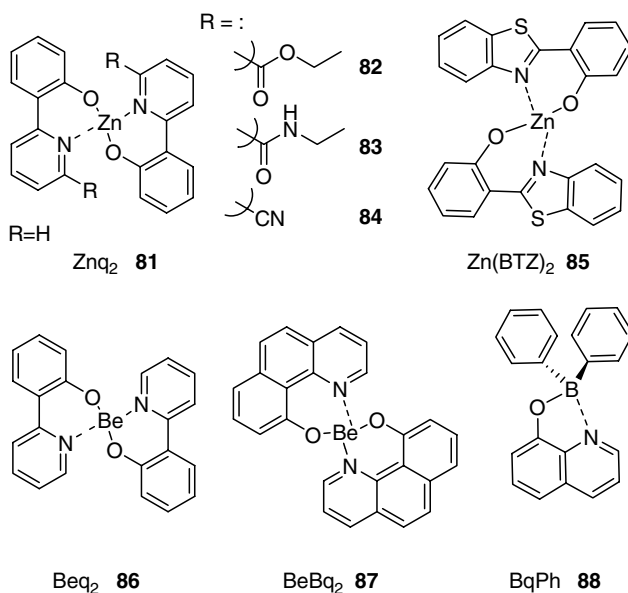
unfilled π^* orbitals (LUMOs) are on the pyridyl side. Substitution of an electron-withdrawing substituent at the C-5 or C-7 position of the phenoxide side of the quinolate ligand will cause a blue-shift of the absorption spectrum relative to the parent unsubstituted Alq_3 . An electron-withdrawing substituent at the C-4 or C-2 position of the pyridyl side will, conversely, cause a red-shift. This trend will be reversed when using electron-donating substituents. This general rule helps the rational design of any desired emission color in the Alq_3 series and is the basis of the effects shown in Scheme 3.26.

Another example is where the Kodak group claim in a patent that replacing CH at the 5-position of the quinolate ligand with a N atom results in a compound Al(NQ)_3 (**77**) with a hypsochromically shifted Alq_3 emission at 440 nm, a 90 nm blue-shift from the parent Alq_3 emission (Scheme 3.26) [129]. A red-shifted emission compound AlX_3 (**78**) is attributed to the reverse effect, when a nitrogen atom replaces the CH at the 4-position of the quinolate ligand.

Interestingly, methyl substitution at the C-2 position of the quinoline ligand hinders the formation of stable tris-chelates of aluminum. However, a phenolic ligand bearing bulky substituents, such as 2,5-dimethylphenol or 4-phenylphenol, used as an ancillary ligand can effectively shield the Al^{3+} from nucleophilic attack and has been found to improve stability (Scheme 3.27) [130]. Alq_2OAr (**79**) compounds show greenish-blue emission with a peak of ~490 nm. BALq (**80**) has an emission wavelength peak of 476 nm. The blue-shifts of C-2 methyl-substituted Al complexes are due to the steric hindrance enforced by the 2-methyl group with the bulky ligands, which reduces the conjugation overlap. OLEDs made using such materials show poor efficiency however. Alternately, these materials are suitable as HBLs due to their large band gap coupled with their high EA.



SCHEME 3.27 Chemical structures of stable Alq_3 derivatives.



SCHEME 3.28 Chemical structures of Zn₂, Be₂ chelates.

Despite the ubiquity of aluminum hydroxyquinolate chelates as ETMs, other metal chelates of substituted 8-hydroxyquinoline, such as Group II metal ions of Zn²⁺ and Be²⁺ have also been used as the ETM in OLEDs (Scheme 3.28) [131–133].

Zuppiroli et al. studied a series of electron-withdrawing-group substituted bis-(8-hydroxyquinoline)zinc(II) (Znq₂, **81**) derivatives as ETMs [134]. They found that these Znq₂ derivatives showed excellent electron transport properties compared to Alq₃. This is due to the better π – π overlap of molecular orbitals of the Znq₂ derivatives and the extended electronic states in its tetrameric form with respect to Alq₃ [135]. Higher electron mobilities compared to Alq₃ may also contribute to better electron transport properties of such Zn complexes, when used as ETMs in OLEDs.

Bis(2-(2-hydroxyphenyl)benzothiazolate)zinc(II) (Zn(BTZ)₂, **85**) is an excellent white emitter. The HOMO and LUMO energy levels of Zn(BTZ)₂ are –5.41 eV and –2.65 eV, respectively. Just as was found by Zuppiroli et al. for Znq₂ derivatives, Zhu et al., found that the electron transport of Zn(BTZ)₂ is better than Alq₃, though the electron injection barrier is higher for Zn(BTZ)₂ [136]. This has been explained by the strong intermolecular interaction of Zn(BTZ)₂ molecules. This same group has examined the use of Zn(BTZ)₂ as an ETM in PLEDs and the results are consistent with those with SMOLEDs [137].

Beryllium chelates bis(2-(2-hydroxyphenyl)-pyridine)beryllium (Beq₂, **86**) and bis(10-hydroxybenzo-quinolinato) beryllium (BeBq₂, **87**) have also been investigated as electron transport emitters having blue or white emission. In some cases, when using BeBq₂ as an ETM, it shows higher electron transport properties compared with Alq₃. The improved performance may be explained by the matched energy level of the ETM and the EM [138–140].

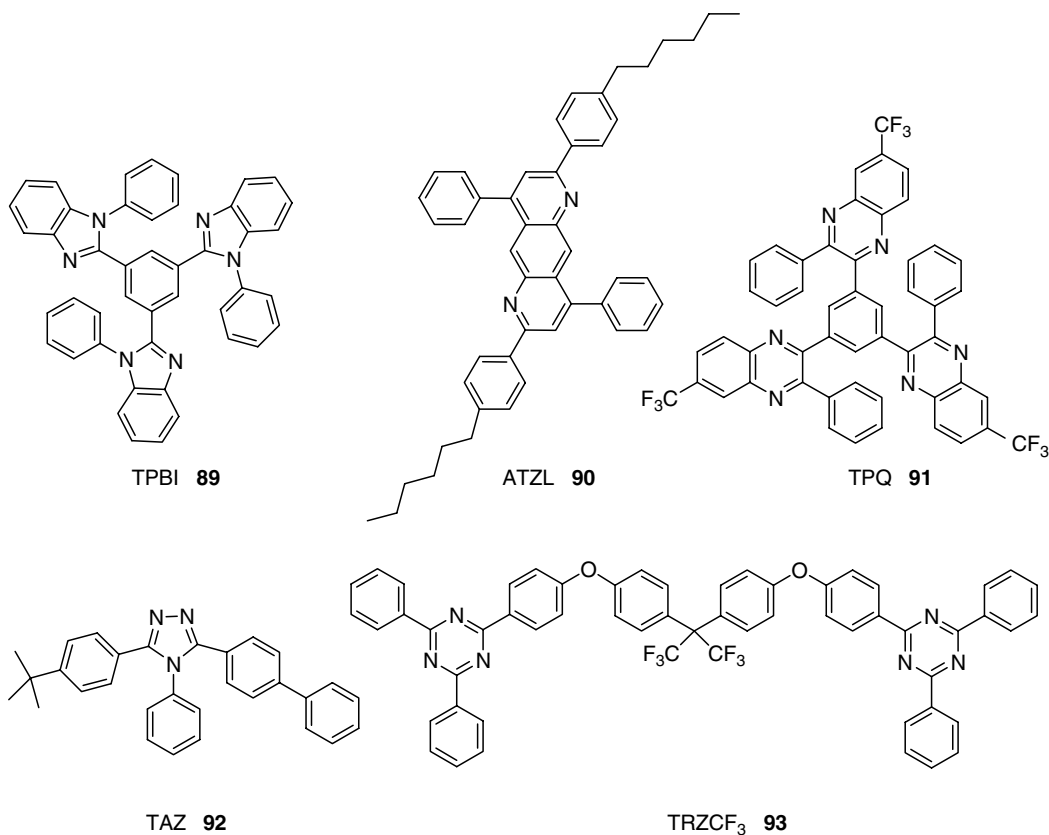
3.5.2 TPBI AND N-CONTAINING AROMATIC TRANSPORT MATERIALS

A dendritic molecular species 1,3,5-tris(*N*-phenylbenzimidazol-2-yl)benzene (TPBI, **89**) and its derivatives were patented by Kodak as blue emitters and ETMs [141,142]. The reason to add TPBI as a key ETM is because this material has received much attention recently and

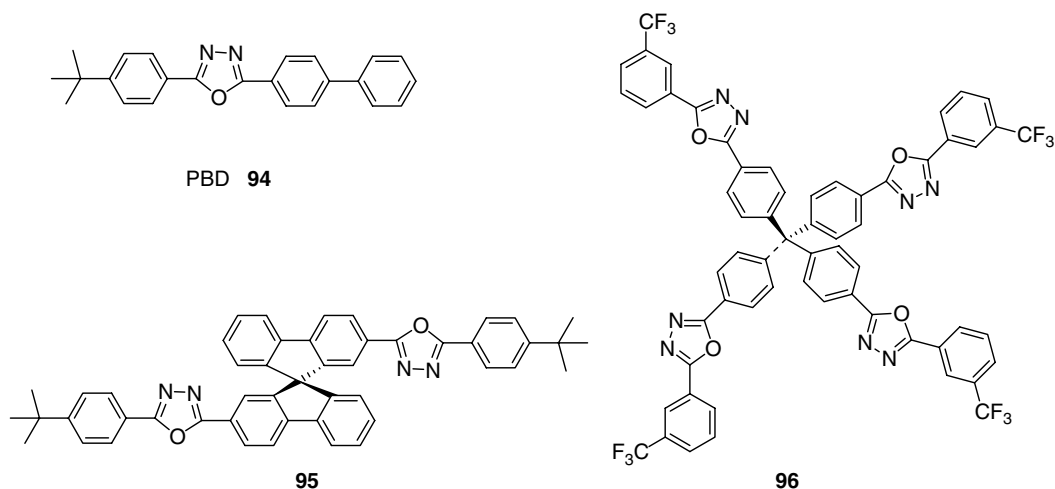
there are more than 100 papers that use TPBI as the ETM or host material in the literature. TPBI's structure is shown in Scheme 3.29. It can be easily synthesized by heating a mixture of *N*-phenyl-1,2-phenylenediamine (3 equiv.) and 1,3,5-benzenetricarbonyl chloride (1 equiv.). The electron mobility of TPBI is of the order of 10^{-6} – 10^{-5} $\text{cm}^2/(\text{V s})$, which is slightly higher than Alq_3 and its mobility is also electric field dependent as measured by transient EL spectroscopy [143,144]. Compared with Alq_3 , TPBI has a large band gap and its LUMO level is -2.7 eV while its HOMO level is in the range of -6.2 to -6.7 eV, making it also function as a hole blocking and possible host material [145,146]. Using TPBI as an ETL and HBL, high-efficiency (55 cd/A) devices based on a solution processible phosphorescent green emitter have been demonstrated [147].

Jenekhe's group has recently explored a series of anthrazoline compounds as n-type semiconductors [148]. These polycyclic anthrazolines have a relatively high EA (2.9–3.1 eV) and high electron mobility owing to their rigid and planar structure. In addition, these compounds are thermally stable with T_g s over 300°C . They can also form amorphous thin films by either spin-coating or vapor deposition. MEH-PPV-based OLEDs, fabricated using ATZL (**90**) as the ETM, show up to a 50-fold improvement in brightness with EQE as high as 3.1%, when compared with single-layer PLEDs.

Tris(phenylquinoxaline) compounds containing two imine nitrogens on a phenyl ring, possess high EA (2.6–2.8 eV), high mobility (10^{-4} $\text{cm}^2/(\text{V s})$ at 10^6 V/cm), and good thermal stability. Star-shaped TPQ (**91**) was investigated for application as an ETM in a PPV-based



SCHEME 3.29 Chemical structure of TPBI and other N-containing ETMs.



SCHEME 3.30 Chemical structures of oxadiazole-based ETMs.

PLED, which resulted in a fivefold enhancement in brightness compared to single-layer devices, with EQEs of -0.01 to 0.11% [149].

1,3,5-Triazines are well-known compounds with high thermal stability and higher EA than 1,3,4-oxadiazoles (PBD) and 1,2,4-triazoles (TAZ, **92**). Schmidt et al. studied a series of dimeric 1,3,5-triazine ethers for application as ETMs for OLEDs [150]. However, despite their high EA, the efficiency of the OLEDs improved only modestly. One possible explanation is due to their rather poor electron mobilities.

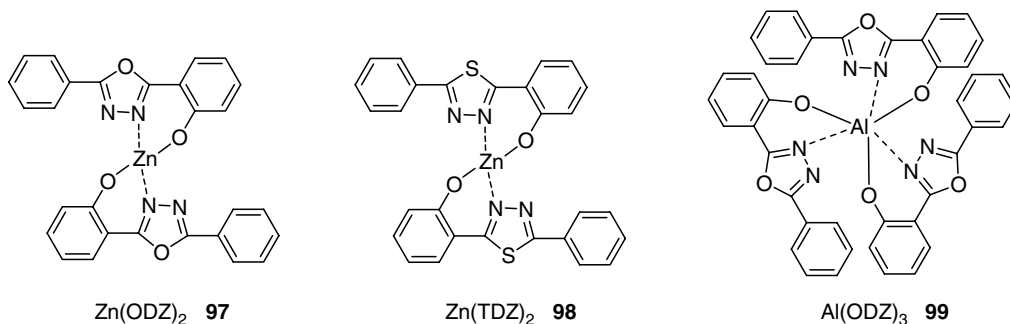
3.5.3 OXADIAZOLE AND TRIAZOLE TRANSPORT MATERIALS

Oxadiazole-based ETMs are perhaps the most widely investigated organic ETMs. The initial work studying 5(4-biphenyl)-2-(4-*tert*-buty-phenyl)-1,3,4-oxadiazole (PBD, **94**) (Scheme 3.30) as an ETM in OLEDs is a result of its high EA and its excellent thermal stability [151]. The EA value of PBD is 2.16 eV and IP is 6.06 eV [152]. While the device efficiency is improved by introducing the PBD layer, the thin film of vacuum evaporated PBD, owing to its low T_g (60°C), tends to crystallize during device operation due to Joule heating. Later work focused on the design of amorphous oxadiazole compounds for OLED applications. Spiro-linked oxadiazole compounds (e.g., **95**) and star-shaped tetraphenylmethane-based oxadiazole (e.g., **96**) were developed to reduce crystallinity and yet maintain solubility and stability. By introducing CF_3 groups, it can be tailored to have an even higher EA (2.26 eV) compared with PBD. However, no long-lived stable OLEDs based on this class of ETMs has yet been demonstrated.

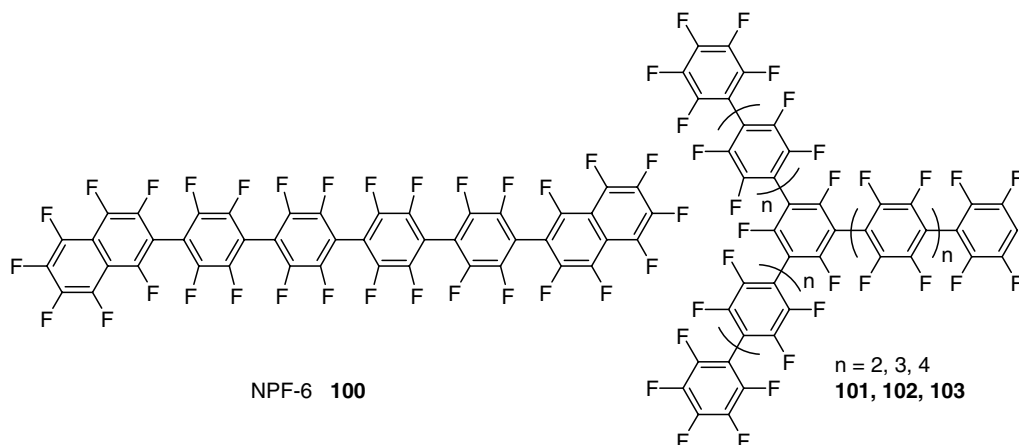
Tanaka et al. reported a series of oxadiazole metal chelate materials (**97–99**) (Scheme 3.31). However, these complexes suffer stability issues due to the intrinsic instability of the excited state of the molecules. Therefore the lifetimes of OLEDs fabricated using these compounds are fairly short [153,154].

3.5.4 FLUORINE-SUBSTITUTED ELECTRON TRANSPORT MATERIALS

A perfluorinated, para-conjugated oligophenylene with high EA exhibited improved electron transport properties and was investigated as an ETM (**100–103**) (Scheme 3.32) [155]. The electron mobility of NPF-6 (**100**), determined by the TOF technique, is much higher than that



SCHEME 3.31 Chemical structures of oxadiazole metal chelates.



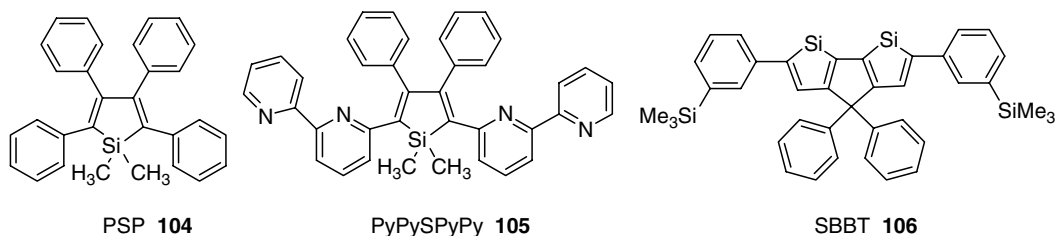
SCHEME 3.32 Chemical structures of fluorinated ETMs.

of Alq_3 under the same conditions. In fact, an OLED fabricated using NPF-6 as the ETL showed higher QE than an equivalent Alq_3 -based device.

3.5.5 SILOLE (SILACYCLOPENTADIENE)

In contrast to the lowering of the LUMO energy levels via introduction of electron-withdrawing groups (such as $\text{C}=\text{N}$ double-bond containing aromatic heterocycles, metal-quinolinol complexes, and CN- or F-substituted conjugated systems) to achieve high EA compounds for ETMs, the high electron accepting ability of the silole ring ascribed to the $\sigma^*-\sigma^*$ conjugation between the σ^* orbital of the exocyclic σ bonds on silicon and the σ^* orbital of the butadiene moiety in the ring makes silole compounds with a low LUMO energy level particularly suitable for use as ETMs. Scheme 3.33 shows some examples of silole ETMs (**104–106**) recently investigated by several groups [156–160]. 2,5-Bis-(2',2''-bipyridin-6-yl)-1,1-dimethyl-3,4-diphenylsilacyclopentadiene (PyPySPyPy, **105**) showed an electron mobility of $2 \times 10^{-4} \text{ cm}^2/(\text{V s})$ at 0.64 MV/cm measured by the TOF technique, higher than that of Alq_3 [161]. Compared to Alq_3 , the EAs of these compounds are slightly higher (3.3 eV), which in part explains their superior electron transport properties.

Improved EL efficiencies were obtained when using these compounds as the ETM layer [162]. Besides their use as ETMs, some siloles are also being explored as emissive materials or host materials for OLEDs [163]. However, it was also reported that the stability of devices



SCHEME 3.33 Chemical structures of silole compounds as ETMs.

using silole compounds is lower compared with equivalent Alq₃-based devices [164]. Further improvement in such device performance by designing new silole compounds is necessary.

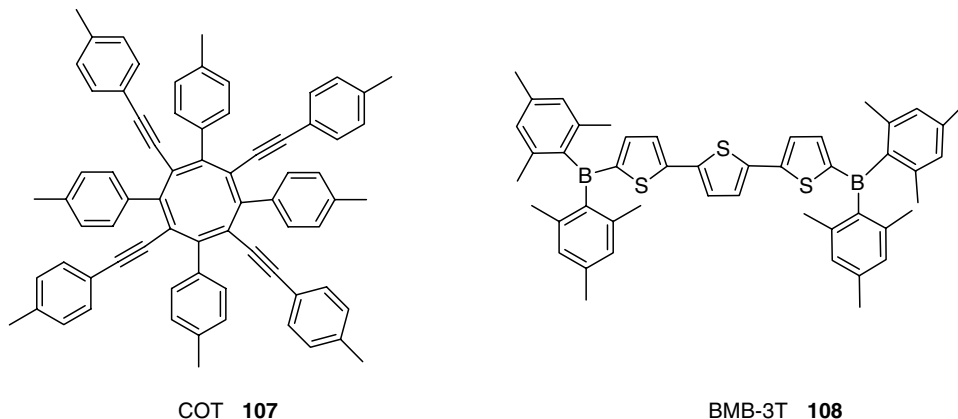
3.5.6 4*n*- π AND BORON-BASED ELECTRON TRANSPORT MATERIALS

The Thompson group proposed the use of 4*n*- π octasubstituted cyclooctatetraenes (e.g., COTs, **107**) (Scheme 3.34) as the ETM in blue OLEDs [165]. They are thermally stable and may be vapor deposited while possessing high T_g of $\sim 214^\circ\text{C}$. Cyclic voltammetry indicates that these COTs are reduced in sequential one-electron steps and have reversible reductions with EA > 2.45 eV and large optical band gaps (> 3.2 eV), indicating high IPs and good hole-blocking properties. These octasubstituted COTs have been used as ETLs in blue OLEDs, i.e., ITO/NPD 400 Å/octasubstituted COT 400 Å/Mg-Ag ITO, NPD) *N,N'*-diphenyl-*N,N'*-dinaphthylbenzidine). EQEs of 0.1–0.2% (ph/el) were observed, with turn-on voltages of ca. 6 V.

The electron-withdrawing dimesitylboryl substituted compound 5,5''-bis-(dimesitylboryl)-2,2':5',2''-terthiophene (BMB-3T, **108**) was recently reported as an ETM [166]. The molecule showed reversible two-peak reductions with high EA (3.05 eV) and can form amorphous films by vacuum evaporation. Using BMB-3T as the ETM for Alq₃ OLEDs, a brightness of 21,400 cd/m² and an EQE of 1.1% were obtained, compared to 13,000 cd/m² and 0.9% for OLEDs without BMB-3T.

3.6 LIGHT-EMITTING MATERIALS

The material that gets most of the glory in OLED devices is naturally that which generates the light output. In many cases, however, the so-called EML is actually a mixture of two or more



SCHEME 3.34 Chemical structures of COT and BMB-3T.

materials wherein there is at least one electroluminescent emissive material in conjunction with a charge transporting host material. Such guest–host systems are extremely common in SMOLED devices whereas in polymeric LED devices the EML is usually composed of a single polymer comprised of multiple distinct monomer units, which combine to produce the necessary emissive and charge transporting properties into a single-phase material. This is a broad generalization, of course, and there are certainly examples of SMOLEDs, which use a single material as the EML, and of polymer OLEDs, which use multiple phases (e.g., polymer blends or doped polymers) as the EML.

Considering the roles that must be fulfilled by the EML, many properties must be effectively combined. The layer must be able to transport charge — both holes and electrons — in order that the charge carriers are able to move through the layer and find each other. The recombined charges must then create an excited state in the material, which can collapse from this exciton state back to its ground state and in doing so emit a photon of light. All of this must occur efficiently with little to none of the input energy being dissipated as heat or electrochemical transformations of the materials themselves. Furthermore, mixtures of materials, if used for long-lived devices, must remain uniformly dispersed (a high T_g and have good film forming properties as a solid solution) and not be subject to materials migration under an applied electric field (no electrophoresis). This latter requirement tends to exclude ionic materials from this application.

The chemical and photo-physical characteristics of the emissive material itself lead to categorization of OLEDs containing them into two main types:

1. SMOLEDs contain small-molecule emissive materials that can be processed by either vacuum deposition (evaporative) techniques or solution coating. The emissive small molecule may be a fluorescent (singlet excited state) or a phosphorescent (triplet excited state) emitter.
2. PLEDs contain polymeric emissive materials that are almost exclusively processed by solution coating (spin coating or inkjetting). This has been discussed in Chapter 2. While most polymer work uses fluorescent emissive materials, there are a few examples of phosphorescent materials being incorporated into a polymer chain and being used as phosphorescent emitters. This part of the materials discussion will be covered in Chapter 4.

The phenomenon of organic EL was first demonstrated using a small-molecule fluorescent emitter in a vapor-deposited OLED device. The Kodak group first used metal oxinoid materials such as the octahedral complex aluminum tris-8-hydroxyquinoline (Alq_3) (discussed above as an ETM) as the fluorescent green emitter in their pioneering work on OLED architectures [167].

To this day, Alq_3 is a stable emitter material in SMOLED devices and metallic complexes of this type have many of the desired stability and film-forming properties necessary to provide useful performance. The complex can exist as both *fac* and *mer* isomers and little attention is usually given to which isomer is present in the thin films of devices, although the starting material for the evaporation is usually predominantly *mer*. A large body of work using other oxinoid complexes, particularly with zinc and magnesium, has shown similar performances. These materials have good electron transporting abilities in addition to their luminescent properties and consequently also find great utility in the ETL (*vide supra*). At this stage the oxinoid materials, especially Alq_3 and BAIq , are also, more typically, used as host materials for other more efficient dopant materials of lower emission energy.

A bewildering array of materials has been used as emitters in SMOLEDs since this early work on Alq_3 . In the following sections, we will present a brief review of host–guest emitter materials and give a perspective description of all the current state-of-the-art small molecule materials for emission at the three primary colors needed for full-color display applications.

3.6.1 HOST-GUEST MOLECULES

The principle of the electronic processes in molecules can be schematically illustrated with the classical Jablonski diagram, which was first proposed by Prof. A. Jablonski in 1935 to describe absorption and emission of light. Figure 3.8 illustrates the electronic processes of the host-guest molecules.

When a host molecule is excited from the ground state by either absorbing light energy or being driven by electric energy to a higher vibrational energy level, it is subjected to collisions with the surrounding molecules. It can directly release its energy through radiative decay or nonradiative decay processes to the ground state, or in the presence of a suitable guest molecule, energy transfer processes will occur. The latter event, depicted in the left side of the diagram as an energy transfer transition from the host molecule to the guest molecule, occurs through Förster, Dexter, or radiative energy transfer processes. At this point, the radiative decay processes will occur from the luminescent guest molecules. It may be noted that the emission spectrum observed is sometimes the emission from only the guest molecules due to complete energy transfer processes, but sometimes it combines the guest and host molecule emission due to incomplete energy transfer.

Because molecular excited states may also transfer from molecule to molecule while conserving their spin and energy, one can treat them as quasiparticles named excitons. The highly localized excited states are known as Frenkel excitons, having radii of a few angstroms. One can treat the Frenkel exciton as the hop of charge carriers (electron, hole) to a neighboring molecule. Due to the fact that the rate of exciton hopping is given by the multiplication between the rate of electron transfer and the rate of hole transfer, the theory of electron transfer can shed light on the understanding of exciton hopping.

During OLED operation, singlet and, in some cases, triplet excitations may first be created in the host material. Then through charge or energy transfer from the host to the guest, singlet or triplet excited states are formed in the guest. For an effective guest-host system, several factors have to be considered, such as the phase compatibility of the host and guest, the aggregation of the molecules, and the host-guest energy level and orbital alignment.

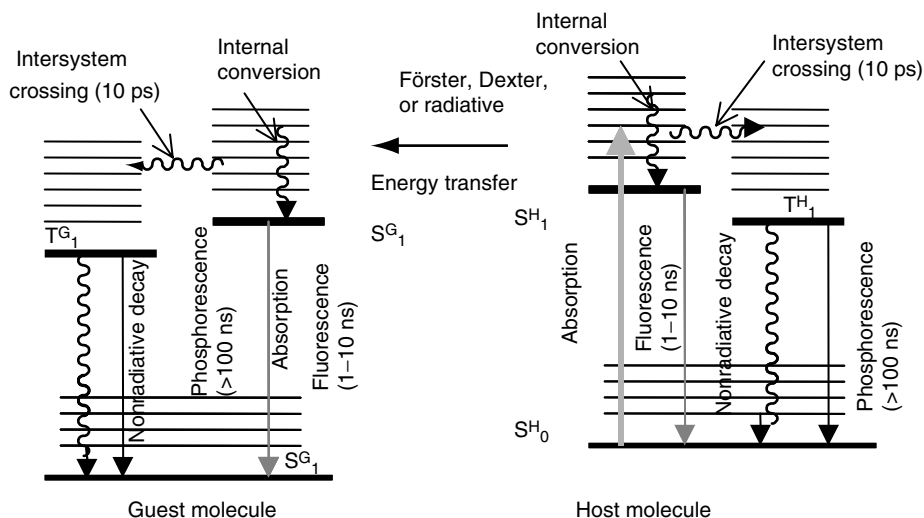


FIGURE 3.8 Electronic processes of host-guest molecules, in which the guest molecules can emit light through both singlet and triplet states. S^H_0 , S^G_0 : a singlet ground state of the host and guest molecules, respectively. S^H_1 , S^G_1 : a first excited singlet state of the host and guest molecules, respectively. T^H_1 , T^G_1 : a first excited triplet state of the host and guest molecules, respectively.

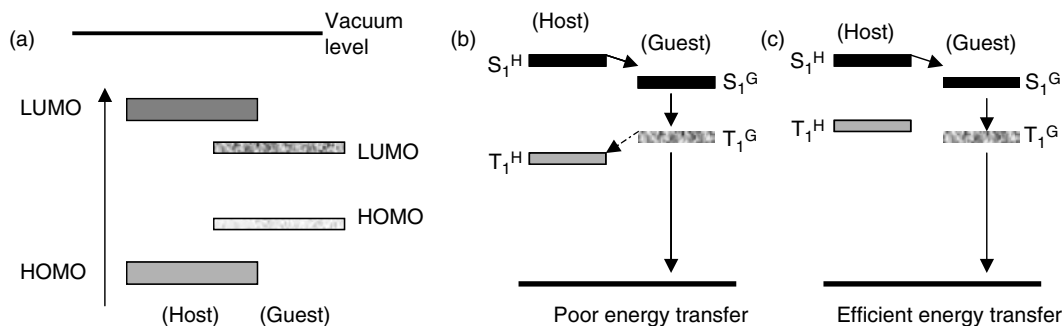


FIGURE 3.9 Energy level relationship in a phosphorescent guest–host system.

Thomas and coworkers have studied efficient EL in a host–guest system and, using computation methods, predicted suitable host carbazole molecules for phosphorescent Ir guest complexes [168]. In this charge transfer process, the band gap of the guest should fall within the band gap of the host to favor transport of electrons and holes from the host to the guest, where they should then recombine (see Figure 3.9). If such energy transfer processes dominate, efficient energy transfer requires that the energy of the excited state of the host should be higher than that of the emissive excited state of the guest. This applies to both singlet excited states and triplet excited states of the host and the guest as shown in Figure 3.9.

The efficiency of charge or energy transfer for the singlet excited (fluorescent) state is easy to verify if there is an overlap between the emission spectrum of the host and the absorption spectrum of the guest. Beyond this requirement, for an efficient energy transfer from the host to the guest of the triplet state (phosphorescent), the excited triplet state of the host should be higher than that of the guest. In the following section, we will discuss some widely used host materials and appropriate guest or dopant materials.

3.6.2 HOST MATERIALS

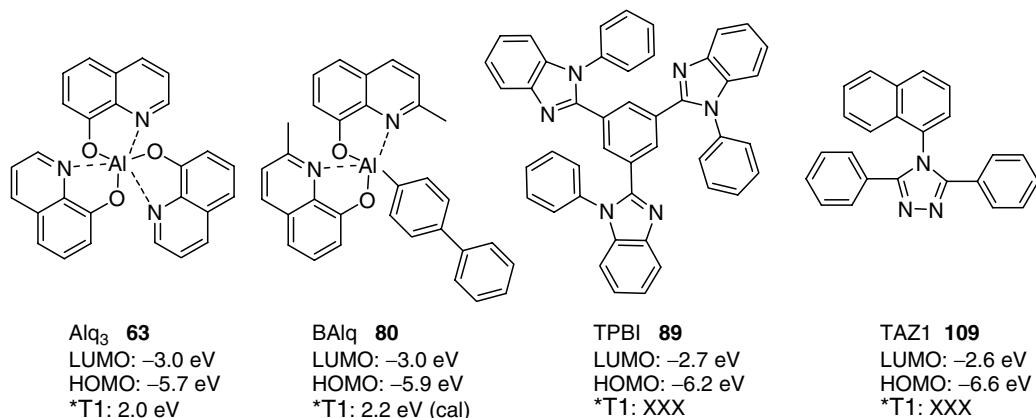
The basic requirements for the host materials dictate that they should have the following properties:

1. Good electron and hole conduction with thermal, chemical, and electrochemical stabilities.
2. Matching HOMO and LUMO energy levels with the guest materials. For efficient energy transfer processes, the LUMO energy level of the host normally should be shallower than the corresponding LUMO energy level of the guest. Likewise, the HOMO energy level of the host should be deeper than that of the guest.
3. For a triplet emissive guest (phosphorescent) dopant, the triplet energy level of the host normally should be higher than that of the guest.
4. Fast energy transfer processes.
5. Phase compatibility with the guest materials.

Typical host materials can be summarized as electron transport hosts, hole transport hosts, bipolar hosts, large band-gap hosts for blue or white emission, or polymer hosts.

3.6.2.1 Electron Transport Hosts

Scheme 3.35 shows the chemical structure of electron transport host materials. One of the most widely studied electron transport-based hosts is Alq₃ (**63**). It was also the first OLED



SCHEME 3.35 Chemical structures of electron transport hosts.

host material reported by Tang et al., and has a HOMO energy level of -5.7 eV and a LUMO energy level of -3.0 eV with a band gap of 2.7 eV. The triplet energy level of Alq₃ was determined to be 2.0 eV. Singlet emission peaks centered at 560 nm make it suitable as a host for green and red emission.

BAlq (**80**), aluminum (III) bis(2-methyl-8-quinolinato)-4-phenylphenolate, one of the recently explored very good hole blocking materials (HBMs), has recently been used as a host material for phosphorescent OLEDs [169]. BAlq has HOMO and LUMO energy levels of -5.90 and -3.0 eV, respectively [170]. Its triplet energy level has not been reported. A recent theory modeling study of this molecule predicted the triplet energy is about 2.2 eV, which is 0.2 eV higher than that of Alq₃ [171]. This property of BAlq makes it suitable as a host material for red phosphorescent dopants, such as bis(2-(2'-benzo[4,5-a]thienyl)pyridinato-N,C3') iridium (acetylacetonate) ((Btp)₂Ir(acac)), which has a triplet energy level of 2.02 eV [172]. In fact, long lifetime and high efficiency of red phosphorescent OLEDs in such an architecture have been reported.

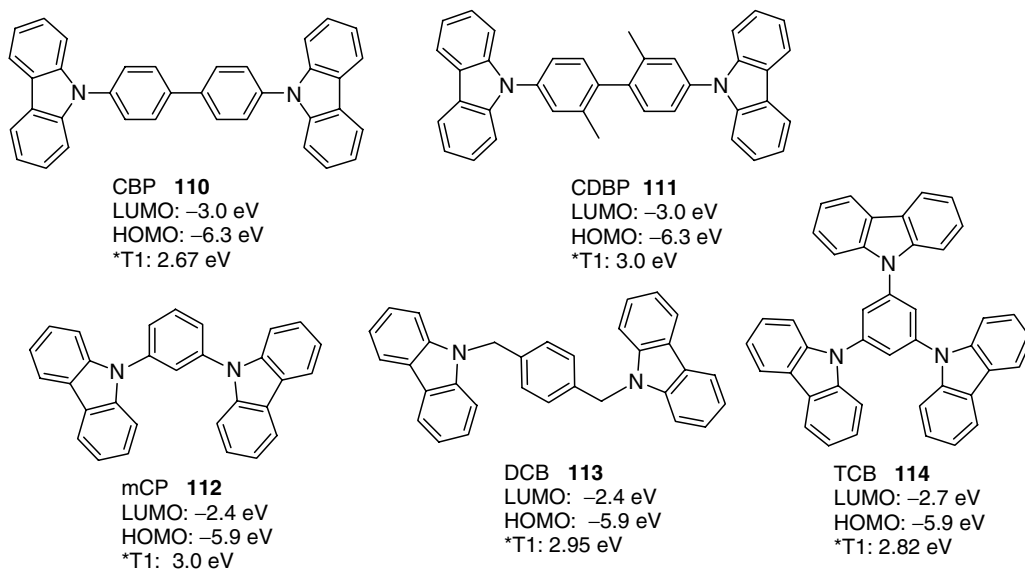
TPBI (**89**), 1,3,5-tris(*N*-phenylbenzimidazole-2-yl)benzene is another electron transport host material for both fluorescent and phosphorescent dopants. It has a large band gap of 3.5 – 4.0 eV with HOMO (-6.2 to -6.7 eV) and LUMO (-2.7 eV), making it suitable for singlet green and red emission and in some case for blue dopants [145]. TPBI also possesses good hole-blocking properties owing to its deep HOMO energy level.

Another large band-gap electron transport host is 3-phenyl-4-(1'-naphthyl)-5-phenyl-1,2,4-triazole (TAZ), which has a HOMO (-6.6 eV) and LUMO (-2.6 eV). Using TAZ1 (**109**) as the host, a maximum EQE (Φ_{ext}) of 15.5% and a luminous power efficiency of 40 lm/W can be achieved in a phosphorescent OLED; the value of Φ_{ext} is almost double compared with that using a CBP host device [173]. The authors explain that this is because the phosphorescent decay lifetime of 7% Ir(ppy)₃ in the TAZ (τ -650 ns) is longer than that in CBP (τ -380 ns) and the phosphorescence efficiency is approximately proportional to the excited state lifetime [174].

Normally an electron transport host is suitable for hosting emitters that have a dominant hole transport nature so as to balance the charge transport in the devices.

3.6.2.2 Hole Transport Hosts

In contrast to electron transport hosts, hole transport hosts are suitable for electron-dominated emitters. Scheme 3.36 shows the chemical structures of some typical hole transport host materials. A widely used hole transport host material for triplet emitters is



SCHEME 3.36 Chemical structures of hole transport hosts.

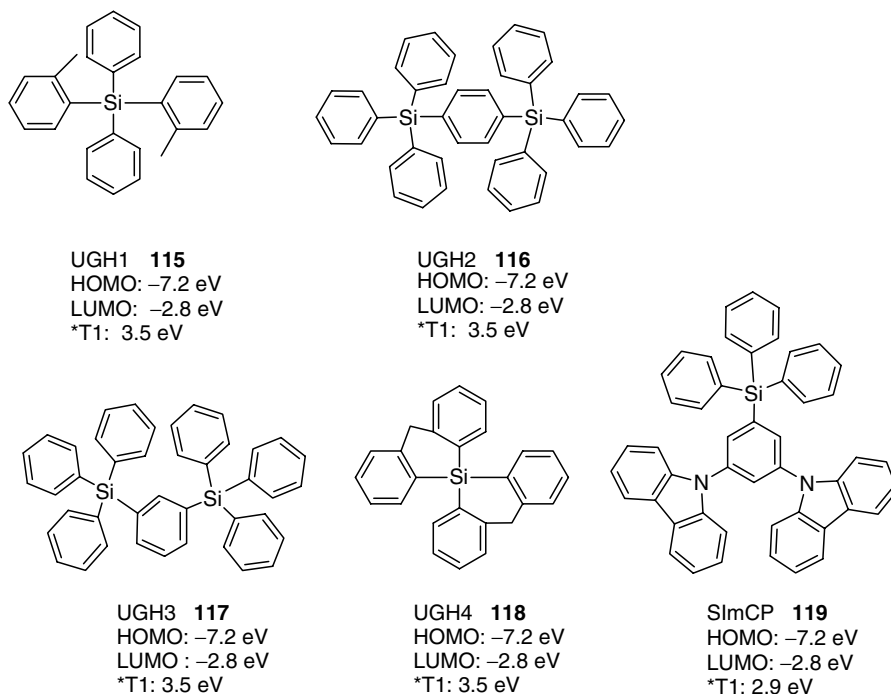
4,4'-bis(9-carbazolyl)-biphenyl (CBP, **110**). The HOMO and LUMO energy levels of CBP are -6.30 and -3.0 eV, respectively. The triplet energy level of CBP is 2.67 eV. Interestingly, CBP was reported to have a bipolar transport character [175]. These properties enable CBP to act as a good host material for green, yellow, and red triplet emitters. The triplet energy level is too low to yield highly efficient devices with blue triplet emitters, although a blue phosphorescent device has been fabricated using CBP as a host and a turquoise blue triplet emitter iridium(III)bis[(4,6-difluorophenyl)-pyridinato-*N,C2'*]picolinate (Firpic) as a guest. Firpic has a higher triplet energy level (2.75 eV) compared with CBP and therefore this endothermic host–guest energy transfer produces a low-efficiency device [176]. To improve this, Tokito et al. reported a CBP derivative, 4,4'-bis(9-carbazolyl)-2,2'-dimethylbiphenyl (CDBP, **111**), in which two methyl groups are grafted onto the biphenyl unit, which enforces a nonplanar structure and generates a significant blue-shift of the triplet state (from 2.67 to 3.0 eV) [177]. A dramatically improved external efficiency of blue phosphorescent and white phosphorescent devices has been achieved employing CDBP as a host, indicating an efficient triplet energy confinement on the phosphorescent guests [177–179].

In the search for effective guest–host systems employing triplet emitters, carbazole compounds have most often been selected as the host materials. Besides the above mentioned CBP and its derivatives, various carbazole compounds have been screened as hosts (Scheme 3.36) [168,180]. One example of a large band-gap host material reported by the Forrest group is *N,N'*-dicarbazolyl-3,5-benzene (mCP, **112**) [181]. mCP and CBP have similar charge injection and transport properties, but mCP has a triplet energy of 3.0 eV. This large triplet energy allows efficient energy transfer to the triplet emitter guest. In fact, using mCP as a host and Firpic as the blue phosphorescent dopant, the EQE of the resulting PHOLED is 7.5% . This value is 50% higher than the equivalent CBP containing device ($\eta_{\text{ext}} = 5\%$), clearly demonstrating the beneficial effect of a higher triplet energy level for mCP. Another carbazole compound is *N,N'*-dicarbazolyl-1,4-dimethene-benzene (DCB, **113**), which has two carbazoles linked with a phenyl moiety decoupled by two methylene groups [182]. DCB is a large

band-gap molecule with a band gap of 3.5 eV while its triplet energy is 2.95 eV. The expected exothermic charge transfer process is observed in blue and white devices, where (Firpic) is used as the blue phosphorescent dopant [183].

3.6.2.3 Silane Compound Host Materials for Blue and White Phosphorescent Organic Light-Emitting Diodes

The challenge for achieving exothermic energy transfer in blue electrophosphorescence is in selecting a higher triplet energy host. The carbazole-based host materials typically have triplet energies below 3 eV, and this value is close to the band gap of deep blue dopants. Obviously, to achieve a deep blue phosphorescent OLED, host materials need to have much larger triplet energies, so as to maintain efficient exothermic energy transfer from host to guest. This is a difficult task, not only because of the limited availability of such large band-gap materials but also the difficulty of charge injection from charge transport materials to such large band-gap host materials, which normally have deeper HOMO and shallower LUMO energy levels. To circumvent these limitations, the Forrest group proposed an idea to employ a host molecule that has a large band gap and higher triplet energy levels as an inert matrix, leaving the guest molecules to both conduct and trap charges, allowing for direct exciton formation on the guest phosphor [184]. This process allows exciton formation, and recombination at the guest molecular sites while eliminating the need for an electrically active host. Bear in mind that an exothermic path from host to guest must be maintained for an efficient charge transfer. This also requires large triplet energy level host materials so as to avoid back flow of the transferred excitons formed on guest molecules to the lower energy host molecules. Arysilane compounds have been found suitable for such applications. Scheme 3.37 shows the chemical structures of several arysilane compounds: diphenyldi(*o*-tolyl)silane (UGH1, **115**), *p*-bis(triphenylsilyl)benzene (UGH2, **116**), *m*-bis(triphenylsilyl)benzene (UGH3, **117**), and 9,9'-spirobisanthracene (UGH4, **118**) [185]. These host materials have large band gaps in the range



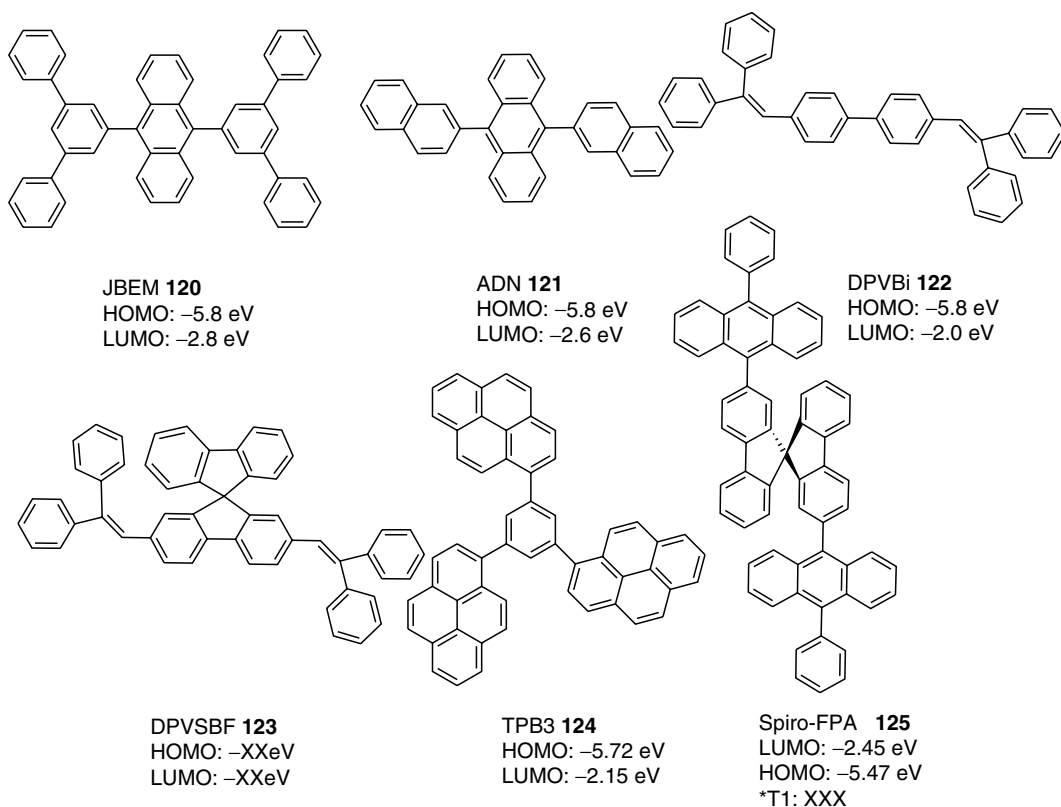
SCHEME 3.37 Chemical structures of silane transport hosts.

of 4.5–5.0 eV, and their triplet energies are all greater than 3 eV. The large energy gaps of these materials may be attributed to the isolation of phenyl groups by Si atoms, which preclude direct conjugation between aromatic phenyl–phenyl rings.

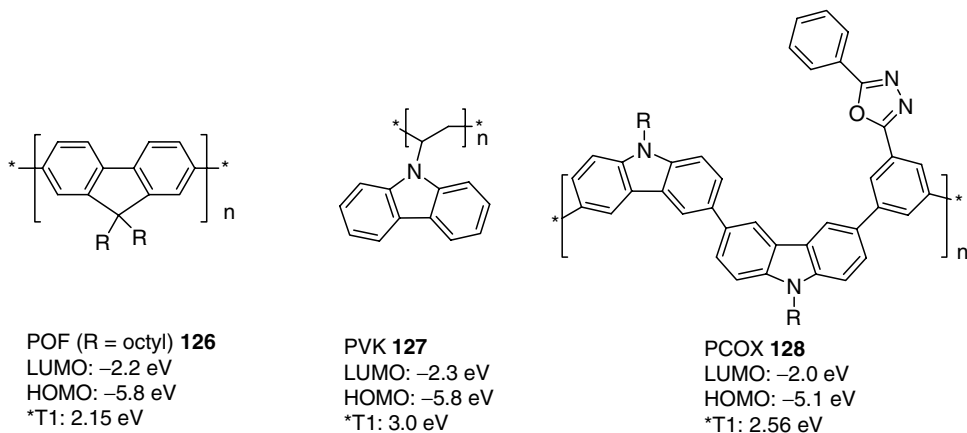
These UGH series materials have electronic structures that are similar in their ground and excited states, indicating that there is little or no conjugation between the arylsilicon groups. The singlet energy band gap and triplet energies of all these molecules are ~4.4 and ~3.5 eV, respectively. They do, however, have different glass transition temperatures and melting points associated with their differing structural configurations. The morphology of the thin films prepared using UGH1 is crystalline and very rough, which limits its application as a host material. UGH2, UGH3 and UGH4 give smooth, pinhole-free thin films. However, UGH4 solutions and thin films are not air-stable and thus have not been considered practical. High EQE PHOLED devices using UGH2 and UGH3 as host materials and the turquoise phosphorescent dopant Firpic ($E_t = 2.72$ eV) as a guest have been achieved. Recently, a new host material, 3,5-bis(9-carbazoyl)tetraphenylsilane (SimCP, **119**), a hybrid material of mCP and UGH1 host has been developed. When using SimCP in place of mCP, an improved device performance has been obtained. This is probably due to the high T_g of SimCP host with the more branched structure of SimCP, preventing molecular aggregation and thus diminishing triplet–triplet annihilation.

3.6.2.4 Fluorescent Blue Host Materials

The most widely used fluorescent blue host materials are anthracene and distyryl-based compounds as shown in Scheme 3.38. These materials have good phase-compatibility with



SCHEME 3.38 Chemical structures of anthracene and distyryl hosts.



SCHEME 3.39 Chemical structures of some polymer hosts.

their guest blue emitters, which in turn also belong to the anthracene, distyryl amine compounds, perylene, and fluorene derivatives.

These materials have large band gaps and are thermally stable with high T_g . Details describing the use of these materials will be presented in the section on fluorescent blue dopants.

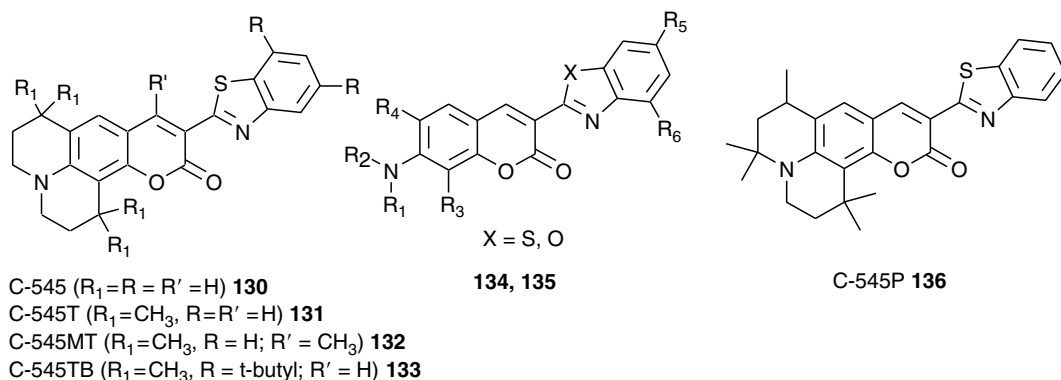
3.6.2.5 Polymer Hosts

Solution-processible polymers with large band gaps and relatively high triplet energies may also be suitable for use as host materials. Examples of these include polyalkylfluorene (POF, **126**), polyvinylene carbazole (PVK, **127**), and rigid polycarbazoles (e.g., PCOX, **128**) (Scheme 3.39). They can be used as host materials for a wide range of colors. Details will be described in Chapter 4.

3.6.3 FLUORESCENT DOPANTS

To match up with host materials, the basic requirements for the guest or dopant materials are:

1. Highly fluorescent.
2. For green pixel color, the standard of Commission Internationale de l'Eclairage (CIE) 1931 color chromaticity coordinates are (0.30, 0.60). For red color, the standard of CIE 1931 color chromaticity coordinates are (≥ 0.62 , ≤ 0.37), the standard red CRT Phosphors of the Society of Motion Picture and Television Engineers (SMPTE-C) is (0.64, 0.34), and the European Broadcasting Union (EBU) is (0.64, 0.33). For blue pixel color, the standard of CIE 1931 color chromaticity coordinates are (0.14–0.16, 0.11–0.15). For white pixel color, the standard of CIE 1931 color chromaticity coordinates are (0.313, 0.329).
3. Matched HOMO and LUMO energy level with host materials.
4. For a triplet emissive guest (phosphorescent) dopant, the triplet energy level of the dopant normally should be lower than that of the host.
5. Fast energy transfer processes.
6. The dopant materials should have phase compatibility with the host materials.



SCHEME 3.40 Chemical structures of green dopants of Coumarin dyes.

3.6.3.1 Green Fluorescent Dopants

3.6.3.1.1 Coumarin Dyes

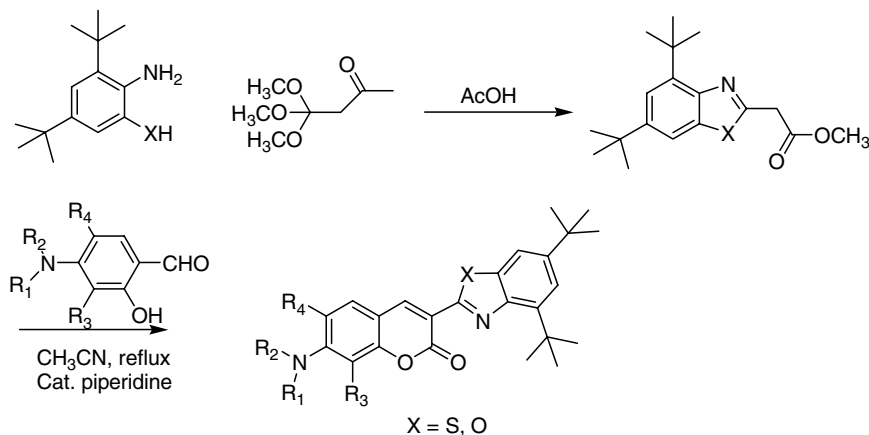
The first class of green dopants is the Coumarin dyes (**130–136**) (Scheme 3.40). Coumarin laser dyes such as (10-(2-benzothiazolyl)-1,1,7,7-tetramethyl-2,3,6,7-tetrahydro-1H,5H,11H-[1]benzo-pyrano[6,7,8-ij]quinolizin-11-one) (C-545T, **131**), its bulky *t*-butyl group substituted derivative C-545TB (**133**) and the methyl group substituted C-545MT (**132**) have been widely investigated as green fluorescent dopants.

These green coumarin dopants generally have a high fluorescent QE in their dilute solutions (up to 90%). When these green dyes are doped in electroluminescent devices, the quantum efficiencies of the devices are similarly high. To match the requirements of high color purity, stability, and high QE, substituted coumarins have been designed and synthesized. Chen et al. of Kodak patented a series of green dopants (**134, 135**) based on versions of the coumarin molecule [186]. For example, C-545 (**130**) shows a high fluorescent QE, however it tends to aggregate in the solid state due to its nearly planar chemical structure. As a result, even 1% doping in an OLED device can cause an undesirable shift in the hue attributed to an emission shoulder at long wavelength [187]. The design of green dopant C-545T judiciously introduces the sterically hindered tetra-methyl groups at the julolidyl ring and, in doing so, dramatically reduces the dye quenching and keeps the desirable green color and high luminescent properties [188]. Further improvement of the coumarin dyes has led to the discovery of the thermally stable green dopants C-545MT and C-545TB [189]. Devices fabricated using C-545TB in the structure ITO/CHF₃plasma/NPB/Alq₃:1% C-545TB/Alq₃/Mg:Ag gave a saturated green emission CIE (0.30, 0.64) with an output of 2585 cd/m², luminescent efficiency of 12.9 cd/A with a power efficiency of 3.5 lm/W at driving current density of 20 mA/cm². The syntheses of these coumarin compounds is described in the patent literature and is outlined in Scheme 3.41.

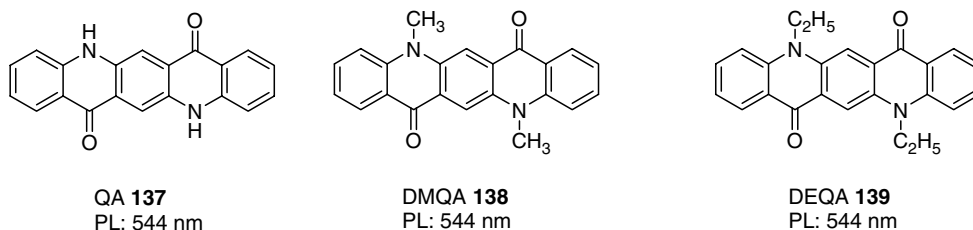
Chen's group has synthesized a new green dopant C-545P (**136**) (Scheme 3.40) by introducing asymmetric tetra-methyl steric spacers on the julolidyl ring [190]. C-545P has good thermal and photo stabilities, and when used as a dopant in an Alq₃-hosted OLED, it shows better device performance than that of C-545T. This is attributed to the asymmetric substituents, which minimize aggregation. The authors, however, did not compare the performance with C-545TB.

3.6.3.1.2 Quinacridones

The second class of green dopants is the family of quinacridone (**137–139**) (Scheme 3.42) fluorescent dyes. Patents on derivatives of these compounds have been filed by Kodak for use in OLEDs [191].



SCHEME 3.41 Synthetic steps to Green-Kodak.



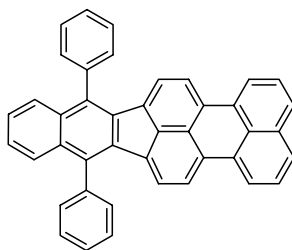
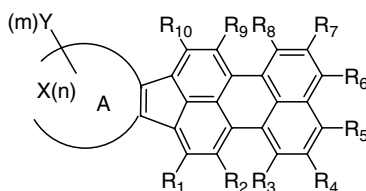
SCHEME 3.42 Chemical structures of quinacridone derivatives DMQA and DEQA.

Using DMQA as a green dopant, Shi et al. of the Kodak group fabricated a green OLED with a device structure of ITO/CuPc/NPD/Alq₃:0.8%DMQA/Alq₃/Mg:Ag. An EL efficiency of 7.3 cd/A and a maximum light output of 1462 cd/m² have been achieved with a half-life time of 7500 h [192]. They found that using QA as a dopant, the device is very unstable. This is presumably due to the intermolecular hydrogen bonding in the unsubstituted QA. The N=H moiety contributes to hydrogen bonding of neighboring QA molecules, which favors quenching of the fluorescence. Wakimoto et al. also studied the stability of the OLED devices based on quinacridone compounds as dopants [193]. Their study supports that the steric hindrance invoked by the bulky substituents of quinacridone prevent excimer formation and prolong the lifetime of the devices. For example, using DEQA as a green dopant in Alq₃, Murata et al. demonstrated efficient and thermally stable OLED performance [194]. In a paper published in the proceedings of a recent SID conference, Qiu et al. demonstrated a very high efficiency OLED using DMQA as a green dopant. Surprisingly, in their simple OLED structure, ITO/Teflon/Alq₃:0.7%DMQA/BAIq/Alq₃/Mg:Ag, they achieved a luminance of over 88,000 cd/m² with an EQE of 5.4% (21.1 cd/A) at a voltage of 19.8 V and current density of 418 mA/cm² [195]. In a recently published patent, Kodak disclosed a highly stable and longer lifetime OLED using DMQA as the green dopant in a double host material (aminoanthracene and Alq₃) in the device structure [196].

3.6.3.1.3 Indeno[1,2,3-cd]Perylenes

The third class of green dopants is indeno[1,2,3-cd]perylene compounds (Scheme 3.43).

Kodak recently applied for a patent on a series of green dopants based on the [1,2,3-cd]perylene skeleton (**140**) [197,198,199]. They claim using the [1,2,3-cd]perylene dopant improves the luminescent efficiency (7.4 cd/A) and stability (lifetime >2200 h at 70°C)

Indeno[1,2,3-*cd*]perylene **140**Kodak-[1,2,3-*cd*]perylenes

X: a chain of a combined total of "n" carbon or heteroatoms to serve to complete a 5, 6, 7 member ring

Y: an independently selected substituent, two of which may join to form fused rings

R₁---R₁₀: independently selected as hydrogen or substituents; provided that any of the indicated substituents may join to form further fused rings.

SCHEME 3.43 Chemical structures of indeno[1,2,3-*cd*]perylene and its derivatives.

compared with pure Alq₃ or Alq₃ doped with quinacridone-green dopant devices. However the color purity (λ_{max} 500–550 nm) is still an issue. Their device structure is ITO/CHF₃ plasma(1 nm)/NPD(75 nm)/TBADN(38 nm):0–2.5%-[1,2,3-*cd*]perylene/BAlq(10 nm)Alq₃(28 nm)/Mg:Ag(220 nm).

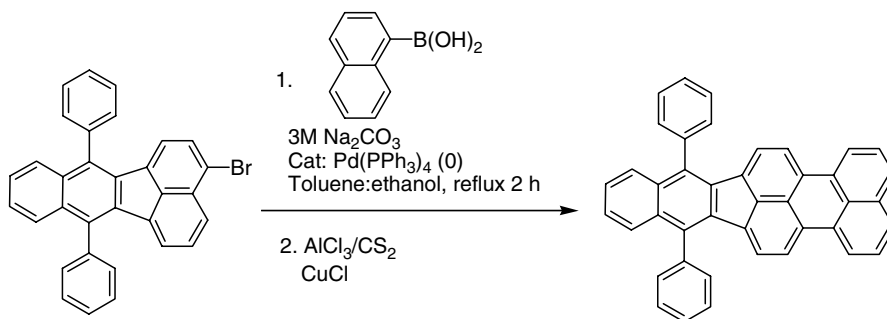
The synthesis of this compound is a two-step procedure as outlined in Scheme 3.44.

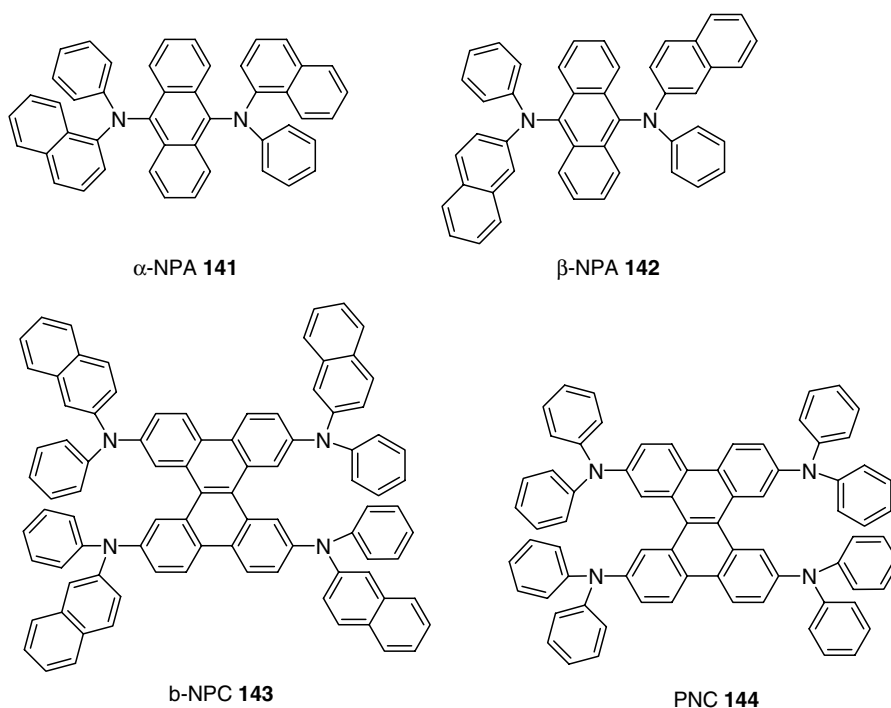
3.6.3.1.4 Diaminoanthracene Compounds

The fourth class of green emitters is the diaminoanthracene compounds (**141–144**) (Scheme 3.45). Very high efficiency and bright green OLEDs have been fabricated with diaminoanthracene derivatives as either HTMs or both hole transport and emitting materials [200]. The optimized devices emit narrow (full width at half maximum (FWHM) of 52 nm) green light with a remarkable maximum EQE of 3.68%, a current efficiency of 14.79 cd/A, a power efficiency of 7.76 lm/W, and a maximum brightness of 64,991 cd/m². Tokito et al. also reported blue-green hole transport emitting materials using related dibenzochrysene derivatives [201].

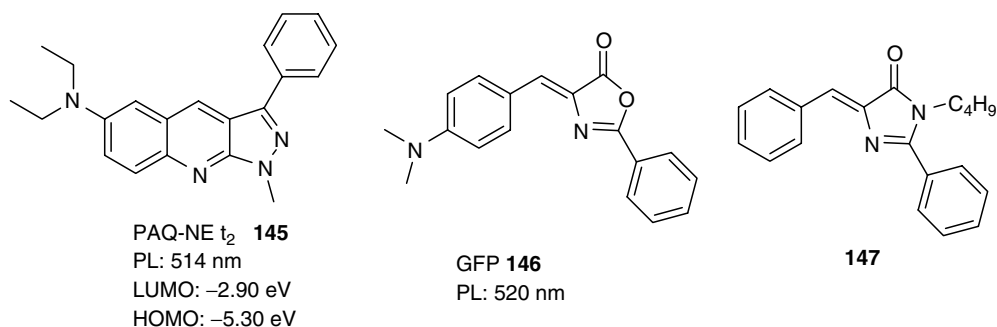
3.6.3.1.5 Other Heterocyclic Green Dopants

Other green dopants as shown in Scheme 3.46 (**145–147**) have been investigated, though the efficiency is not high.

**SCHEME 3.44** Synthesis of [1,2,3-*cd*]perylene. (From Debad, J.D., Morris, C.J., Lynch, V., Magnus, P., and Bard, A.J., *J. Am. Chem. Soc.*, 118, 2374, 1996; Adams R. and Gold, M.H., *J. Am. Chem. Soc.*, 62, 56, 1940.)

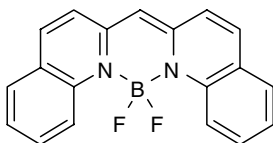


SCHEME 3.45 Chemical structures of green dopants of diaminaoanthracene and diaminodibenzochry-sene materials.



SCHEME 3.46 Chemical structures of green dopants.

Using a high doping level of ca. 16% of heterocyclic nitrogen-containing compound PAQ-NEt₂ as a dopant in the device ITO/NPD/NPD:16%PAQ-NEt₂/TPBI/Mg:Ag, Tao et al. fabricated a device which gave a sharp, bright, and efficient green EL peaked at 530 nm with an FWHM of 60 nm [202]. The maximum luminance is 37,000 cd/m² at 10.0 V with a maximum power efficiency of 4.2 lm/W, a luminescent efficiency of 6.0 cd/A, and an EQE of 1.6%. Interestingly, whereas the PL of the doped film showed emission of the host NPD material even at the high doping concentration of 20%, the host emission was not observed in the EL spectrum. This is presumed to be due to charge-trapping processes, which occur in competition with the energy transfer process. The biologically active oxazolone compound GFP has also been investigated as a green dopant in OLEDs, however the efficiency is very low [203].

**148**

PL: 520 nm

SCHEME 3.47 Chemical structure of a boron chelate-based green dopant.

3.6.3.1.6 Metal Chelates

The sixth class of green emitters is metal organic complexes. Alq₃ was the first green emitter. Alq₃ emission exhibits relatively saturated green color (CIE 1931 coordinates (0.32, 0.55)) and so far, it is still one of the best green emitters available.

Other metal complexes such as those of Boron shown in Scheme 3.47 (**148**) have also been reported to be viable green emitters.

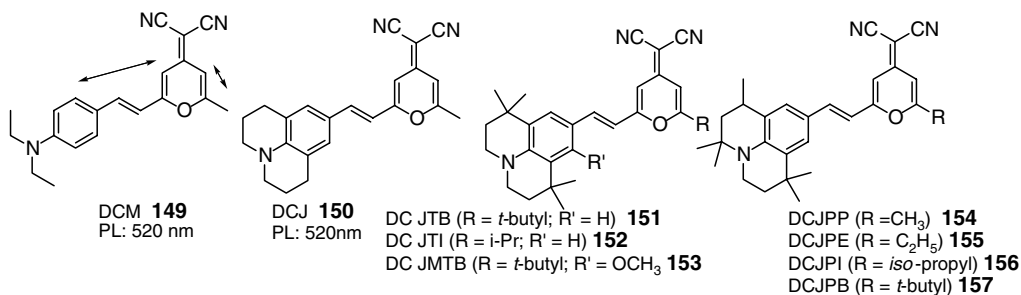
3.6.3.2 Red Fluorescent Dopants

A series of red fluorescent dyes has been recently reviewed by Chen [204]. The red fluorescent dopants, according to their structural characteristics, are summarized as:

1. Pyran-containing compounds or DCM type
2. Push-pull red emitters
3. Polyacenes red emitters
4. Metal chelates

3.6.3.2.1 DCM Series

4-(Dicyanomethylene)-2-methyl-6-*p*-(dimethylamino)styryl]-4*H*-pyran (DCM, **149**) (Scheme 3.48), is a bright and efficient red arylidene laser dye invented in 1974 [205], and was the first dopant in host-guest system OLEDs introduced by Kodak researchers in 1989. The device ITO/HTL/Alq:DCM/Mg:Ag showed an EQE of 2.3%. The emission is orange-red with peak emission in the range of 570–620 nm for DCM and 610–650 nm for DCJ (**150**) depending on the concentration of the dopants. High concentration doping results in more saturated red emission, however, low efficiency due to concentration quenching becomes a factor at these high dopant levels.

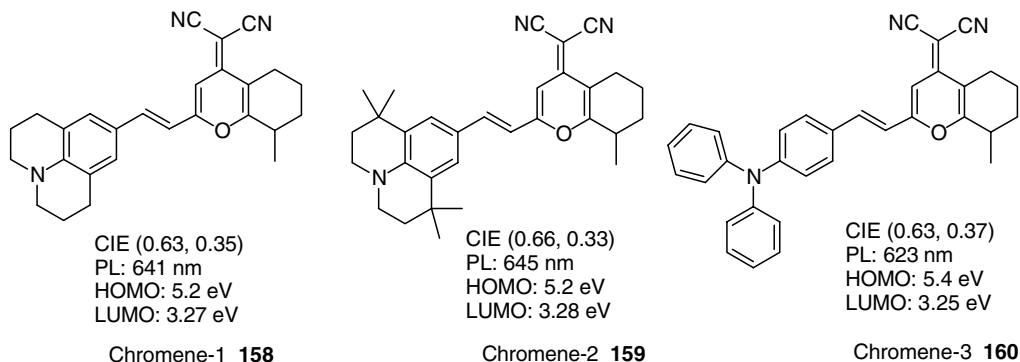
**SCHEME 3.48** Chemical structures of the DCM series.

The DCM molecule has an electron-donor π -acceptor (so-called push-pull) structure. By introducing a more rigid julolidine ring into the donor moiety, the Kodak group prepared a DCJ molecule, which has about a 10 nm red-shift of the emission spectrum. The molecule shows high QE and a more saturated red emission compared with DCM [206,207]. However, both the DCM and DCJ series have an active methyl group, which can suffer further condensation reactions to form undesired bis-condensation by-products. This by-product shows a broad, very weak fluorescence. Consequently, during the synthesis of materials in the DCM or DCJ series, careful control of the reaction condition and repeated purification of the product is needed to get high-performance devices. The drawbacks of such a complex, synthetic protocol and tedious purification processes make for difficulties in large-scale manufacturing. This problem can be solved by substituting bulky and sterically demanding substituents such as *iso*-propyl and *tert*-butyl group for the parent methyl group. This leads to the DCJTB series (**151–153**), which exhibit improved high QE while suppressing the concentration quenching. More importantly, the bulky *tert*-butyl or *iso*-propyl substituent at the pyran ring avoids further condensation with aldehyde groups and improves the purity of the materials [206,208]. However, the red OLEDs using the DCJTB series have the drawback of requiring higher doping concentrations, of the order of 2–4%, to tune the CIE to a standard red. Unlike the symmetric DCJTB series, the unsymmetrically substituted DCJPR series (**154–157**) has five methyl groups instead of four and offers an excellent red emission with comparable performance, yet with relatively lower required doping level of 0.5–2.5% [209].

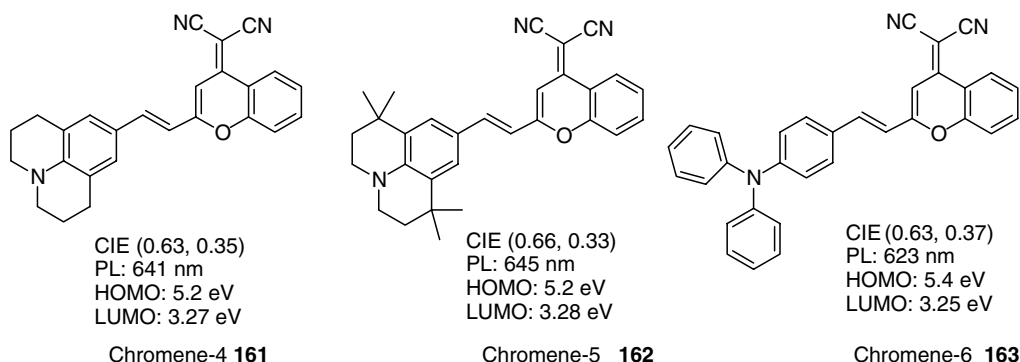
While the DCJTB series replaced the active methyl group with *tert*-butyl or *iso*-propyl substituents to avoid bis-Knoevenagel condensation reactions during the synthesis of DCM or DCJ series, Zhang et al. came up with the idea of using substituted cyclohexane rings to block the reactive site of the pyran ring. They then synthesized a series of 4H-benzopyran-based red emitters (**158–160**) as shown in Scheme 3.49 [210].

Yet another strategy was developed by Lee et al. using a bis-condensation inactive chromene ring instead of the pyran ring so as to generate a series of chromene-based red dopants (**161–163**) as shown in Scheme 3.50 [211].

The merit of these chromene dopants is their relatively long emission wavelength peaks compared to DCM or DCJTB materials due to the more conjugated chromene moiety, and this contributes to the more saturated red emission. In fact the EL spectra of OLED devices of ITO/TPD/Alq₃:chromene-dopants/Alq₃/Mg:Ag exhibited satisfactory red emission color, especially for Chromene-1 and Chromene-2 dopants. However, these chromene-based red emitters showed lower fluorescent quantum yield (18%, 15%, and 54% for Chro-



SCHEME 3.49 Chemical structures of 4H-benzopyran-based red emitters.

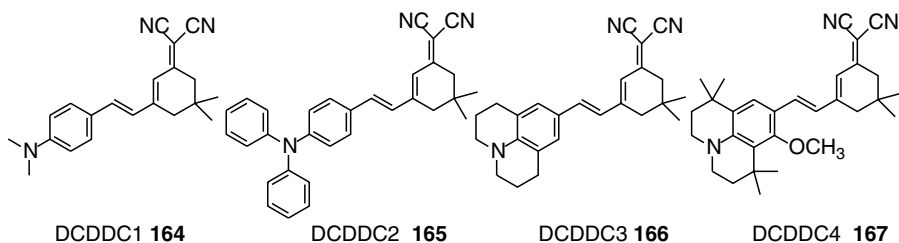


SCHEME 3.50 Chemical structures of chromene-based red emitters.

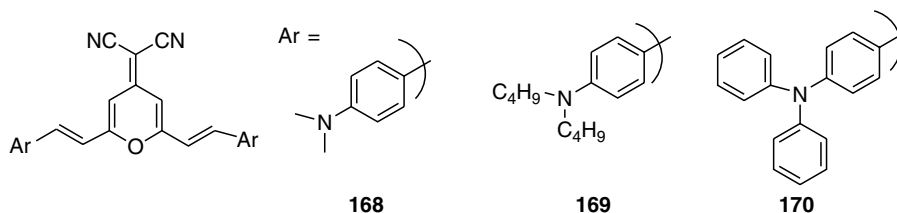
Chromene-1, Chromene-2, and Chromene-3, respectively) compared with the DCM (>70%) or DCJTb series (78%). As a result, the efficiency of the OLEDs of these compounds is in general not competitive with that of devices made from DCM or DCJTb. Nevertheless, the convenient synthetic procedures and the possibility of further chemical modification of the chromene series provide the possibility to yet prepare high-efficiency red dopants.

The impurity issues of DCM materials have been solved by the above mentioned methods through the elimination of the active methyl group by introducing unsymmetrical pyran moieties. Another issue for the DCM series is color purity. The emission spectra of the DCM red emitters demonstrate poor red color saturation having a broad emission band centered at 590–620 nm and a large FWHM (100 nm). Tao et al. reported a DCDDC dopant which shows a bright red emission with a peak wavelength of 650 nm and an FWHM of only 70 nm (Scheme 3.51) [212]. The DCDDC molecules (**164–167**) can be easily synthesized in high yield and purity [213].

The main backbone of DCDDC is the same as that of DCM except that the former lacks a double bond at the pyrene ring but rather has an additional methyl substituent on the 6-position of the ring. This minor difference leads to DCDDC having a narrow emission band due to the simple one donor–acceptor system, while in the DCM series, the mixture of two donor–acceptor effects produces broad emission bands. OLEDs fabricated with the architecture ITO/PVK:TPD/Alq₃:1%DCDDC/Alq₃/Mg:Ag have a turn-on voltage of 5 V, and the peak luminance of 5600 cd/m² at 15 V and a highest EL power efficiency of 1.6 lm/W. The device exhibits red emission with a peak maximum at 630 nm and an additional shoulder emission of 530 nm from Alq₃, which disappears at 2% doping but at the price of a lower power efficiency. This is common to the red emission OLEDs due to inefficient energy transfer processes, and this can be improved when using additional assistant dopants, as will



SCHEME 3.51 Chemical structures of isophorone-based red emitters.



SCHEME 3.52 Chemical structures of red emitter of bis-condensed DCMs.

be discussed for the DCM series. The authors also pointed out that by further modification of the chemical structure of DCDCC, it is possible to achieve even better red dopants. Following DCDCC, Lee et al. reported a series of isophorone-based red emitters [214]. However, the QE of these red emitters is in the range of 10–20%, significantly lower than the DCM or DCJTb series. The OLED devices using these materials as dopants showed saturated red emission along with stable current efficiency at high driving voltages.

Instead of eliminating the bis-condensed byproducts by the above strategy, Shim et al. have found that some bis-condensation products themselves show high fluorescence, if properly designed. A series of bis-condensed DCM derivatives has been synthesized (**168**–**170**) (Scheme 3.52) [215].

Knoevenagel condensation of 1:2.1 stoichiometric ratio of the pyran and aldehyde generates a pure bis-condensation product. Due to the extended π -conjugated system, these bis-condensed red emitters are about 40–50 nm red-shifted compared with their respective mono-substituted DCM analogues.

Using a 5.2% doping level of compound **169**, EL with color close to the NTSC red standard with CIE (0.658, 0.337) was achieved. Due to the inefficiency of the low-energy transfer processes, emission from the host or the electron transporter is often observed. To overcome this, Hamada et al. reported improved red emission by using a codopant such as rubrene as a sensitizer to assist the energy transfer processes between the host and the red dopant; however, this process involves complex deposition control. To simplify the device fabrication processes while keeping the high efficiency of the device, several strategies have been applied. Qiu's group used a new host and an ETM composed of the binuclear complex bis(salicylidene-*o*-aminophenolato)-bis(8-quinolinoato)-bisgallium(III) ($\text{Ga}_2(\text{saph})_2\text{Q}_2$), which replaced Alq_3 and achieved a pure red emission based on a DCJTb red emitter with CIE (0.67, 0.33), and an efficiency of 2.04 cd/A, which is double that of the Alq_3 -based device [216]. Lee et al. proposed a double layer structure with introduction of a HBL between the dopant and the ETL. The luminescent efficiency is doubled compared with the equivalent no-HBL device. A detailed discussion of these strategies will be presented in later sections.

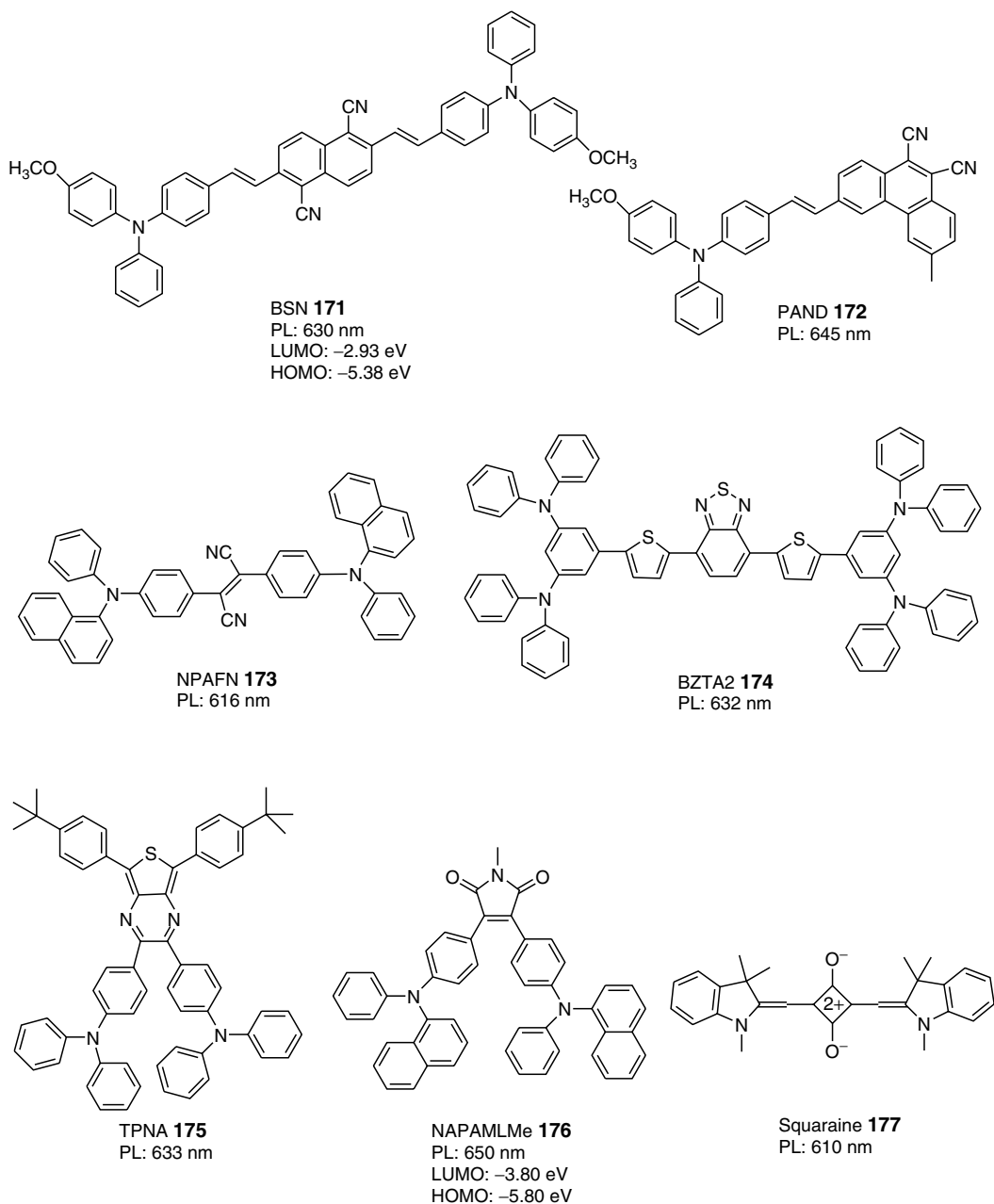
By optimization of device structures and by using different hole and electron injection or transport materials, Chen et al. achieved an excellent red OLED with a very high efficiency based on the DCJTb molecule. The OLED structure is glass (0.7 mm)/ SiO_2 (20 nm)/ITO/ CF_x /NPD(110 nm)/ Alq_3 :5% rubrene:2%DCJTb(30 nm)/ Alq_3 (55 nm)/LiF(0.1 nm)/Al (200 nm). A luminescent efficiency of 3.24 cd/A with CIE (0.643, 0.354) and a power efficiency of 1.19 lm/W at a drive current density of 20 mA/cm² at 8.53 V is reported [217].

3.6.3.2.2 Other Push–Pull Red Emitters

Red emission chromophores having a long wavelength emission band are usually polar, such as the above DCM series. The push–pull red emitters are normally prone to aggregation in the solid state owing to dipole–dipole interactions or through intermolecular π – π stacking, especially when the molecules are flat as is the case for DCM. As a consequence, the push–pull red

emitter is used mainly as the dopant in guest–host systems. However, there are some push–pull molecules that have a twisted molecular structure and can be used as undoped red emitters. This class of red emitters demonstrates better performance as compared with the arylamine-substituted PAH series (**171–177**). The molecular structures are shown in Scheme 3.53.

All of these molecules have an electron withdrawing group in the center and two electron-donating arylamine groups attached at each end. They all demonstrate strong red fluorescence



SCHEME 3.53 Chemical structures of push–pull red emitters.

in the solid state and they can also be used as nondoped OLED materials. Undoped OLEDs avoid reproducibility problems of reliably achieving the optimum doping concentration during processing and are easily adapted to a mass production line.

The 1,10-dicyano-substituted bis-styrylnaphthalene derivative (BSN) reported by Sony has a very high photoluminescent QE up to 80% with emission wavelength of 630 nm. In a device of [ITO/2-TNATA/NPD/BSN/Alq₃/Li₂O/Al], BSN as a red emitter without dopants displays an impressive high-color stability with luminous efficiency of 2.8 cd/A at 500 cd/m² with CIE (0.63, 0.37) [218]. In a recent patent, Sony disclosed another high-efficiency, stable, and bright red emitter 3-(2-{4-[(4-methoxy-phenyl)-phenyl-amino]-phenyl}-vinyl)-6-methyl-phenanthrene-9,10-dicarbonitrile (PAND) [219]. This compound emits bright red emission with maximum wavelength emission at 645 nm.

The nondoped red emitter (bis(4-(*N*-(1-naphthyl)phenylamino)phenyl)fumaronitrile) (NPAFN), reported by Chen's group, showed very interesting photoluminescent properties: in solution, the compound barely emits red emission, however, in the solid state, it exhibits strong orange-red emission at the maximum wavelength of 616 nm, and in the OLED ITO/NPAFN/BCP/TPBI/Mg:Ag, an EL had a pure red emission with a maxima wavelength at 636 nm, corresponding to CIE (0.64, 0.35).

BTZA2 containing a benzo[1,2,5]thiadiazole core and peripheral diarylamines groups exhibits strong red fluorescence in the solid state. Single-layer OLEDs fabricated using this compound demonstrated a maximum brightness of over 5000 cd/m² [220].

Compound NAPAMLMc is an amorphous glass material reported by Chen et al. in a nondoped OLED [221]. An optimized OLED device, with a structure of ITO/NPD/NAPAMLMc/BCP/Alq₃/Mg:Ag, emits pure red light with CIE (0.66, 0.33), a brightness of 4600 cd/m², and an EQE as high as 1.6%. In addition, the color of the red emission is quite stable and is also voltage-independent, which has been attributed to the very well-confined excitonic zone. A saturated red emission with CIE (0.64, 0.33) has been observed using a star-shaped thieno-[3,4-*b*]-pyrazine (TPNA) red emitter in a simple double layer OLED: ITO/TPNA/TPBI/Mg:Ag, in which the TPNA compound functions as a hole-transporting red emitter [222].

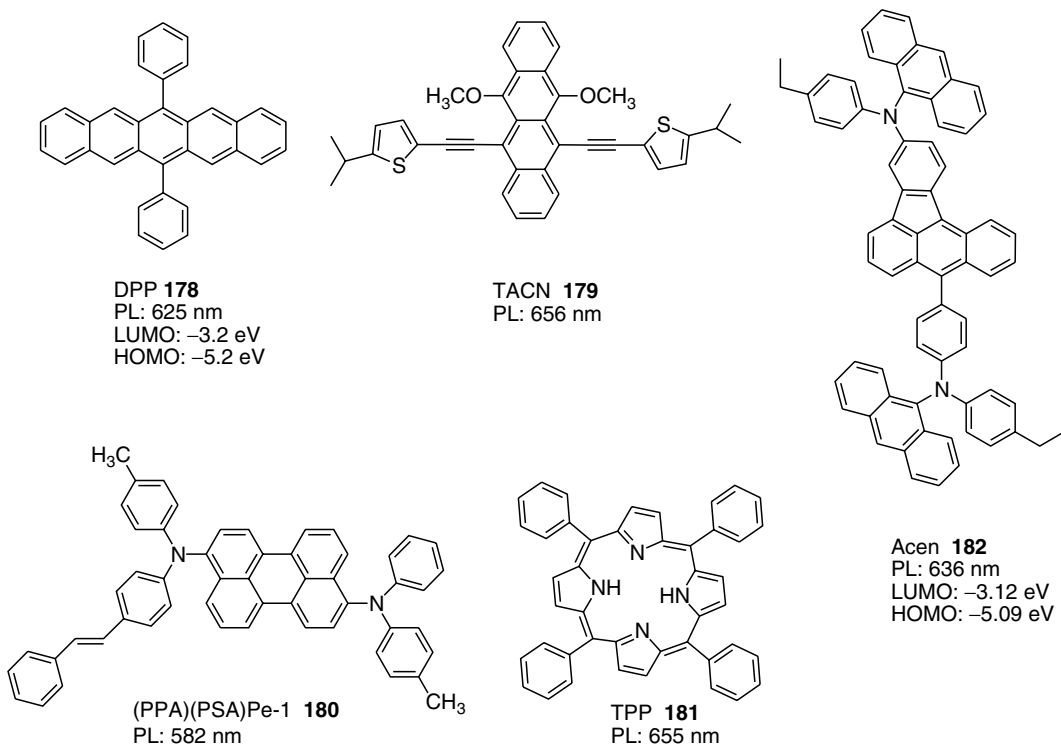
Squaraine dyes, widely applied in the fields of organic solar cells, electrophotography, optical storage systems, imaging materials, and laser dyes, emit sharp red emission with a rather small Stokes shift. Using Alq₃ as the host, red emissive OLEDs with an architecture of ITO/NPD/Alq₃:Sq/Mg:Ag can be prepared. However, green emission from the Alq₃ host cannot be avoided due to the inefficient energy transfer process [223]. Using NPD as the host material can, however, lead to pure red emission [224].

3.6.3.2.3 Polyacenes Red Emitters

Scheme 3.54 lists some examples of polyacene-based red emitters (**178–182**). 6,13-Diphenylpentacene (DPP) doped in an Alq₃ host, emits pure red light centered at 625 nm with CIE (0.63, 0.34) and with an external EL QE of 1.3% at 100 A/m² [225]. Benzo[*a*]aceanthrylene- and perylene-substituted arylamine compounds (Acen, (PPA)(PSA)Pe-1) have also been investigated as red dopants [226]. In an OLED device of ITO/NPD/Acen/BCP/Alq₃/Mg:Ag, red emission with CIE (0.64, 0.34) has been observed. Porphyrin-macrocyclic compound 5,10,15,20 tetraphenyl-21H, 23H porphine (TPP, **181**) shows a very narrow red emission along with a longer wavelength emission shoulder, this red color is too red for display application. None of these red emitters demonstrated high efficiency in red LEDs, therefore they are not good candidates for display applications.

3.6.3.2.4 Metal Chelates

It is well-known that rare-earth complexes such as europium complexes emit sharp spectral bands due to electronic transitions between inner d and f orbitals of the central rare-earth



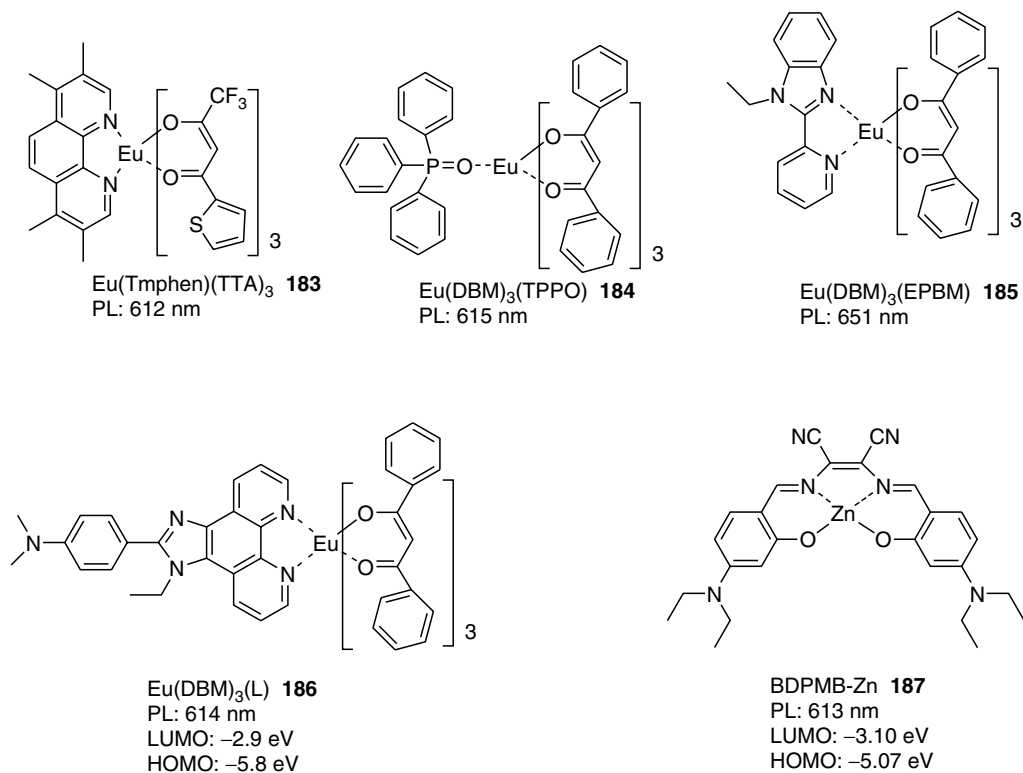
SCHEME 3.54 Chemical structures of polyacene red emitters.

metal ions and are expected to show high luminescent efficiency since both singlet and triplet excitons are involved in the luminescence process. A pure red light with a peak of 612 nm and a half bandwidth of 3 nm, was observed in the OLED employing Eu(Tmphen)(TTA)₃ (**183**) complex as a red dopant [227] (Scheme 3.55). The devices show a maximum luminance up to 800 cd/m², an EQE of 4.3%, a current efficiency of 4.7 cd/A, and a power efficiency of 1.6 lm/W. However, the EL QE decreases markedly with increasing current due to the triplet-triplet annihilation in the device. Other europium complexes such as Eu(DBM)₃(TPPO) (**184**), Eu(DBM)₃(EPBM) (**185**), and Eu(DBM)₃(L) (**186**) were also investigated as red dopants in OLEDs [228]. Although rare-earth complexes have good color purity, their efficiency and chemical stability, so far, fall short of the requirements for commercial applications.

Schiff bases with intramolecular charge transfer complexes such as 2,3-bis[(4-diethylamino-2-hydroxybenzylidene)amino]but-2-enedinitrile zinc (II) (BDPMB-Zn, **187**) emit red fluorescence with fluorescent quantum yields up to 67%. OLEDs with a structure of ITO/TPD/TPD:BDPMB-Zn/Alq₃:BDPMB-Zn/Alq₃/Mg-Ag showed very bright saturated red emission with CIE (0.67, 0.32) with a luminance of 2260 cd/m² at 20 V and a current efficiency of 0.46 cd/A (at 20 mA/cm²). In addition, the EL spectra do not change with the doping concentration in the range of 0.5–3% [229].

3.6.3.3 Blue Fluorescent Emitters

For the blue pixel, the standard CIE 1931 color chromaticity coordinates are (0.14–0.16, 0.11–0.15). Since a relatively large band gap is required for blue emitters, the appropriate blue host materials with even larger band gap are needed to optimize the energy transfer requirements. The main challenge in designing the blue emitter or its host is the device stability.

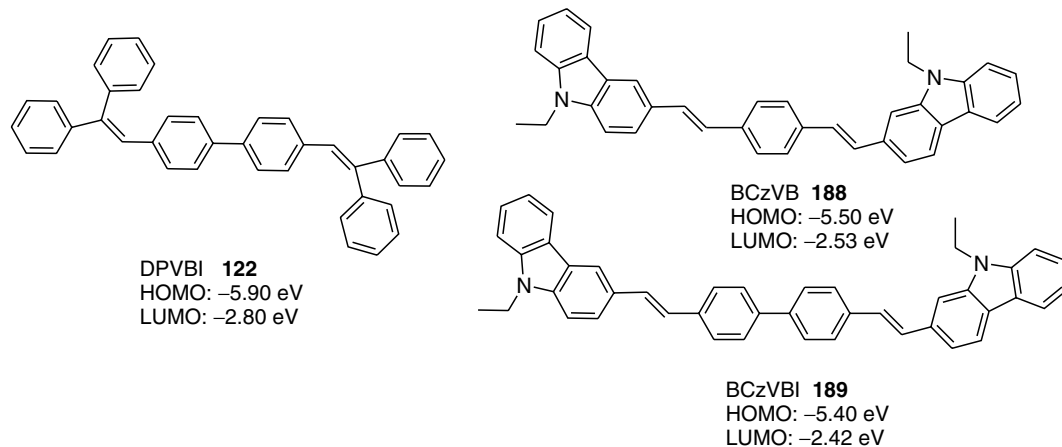


SCHEME 3.55 Chemical structures of red emitters of metal chelates.

Many large band-gap organic materials have been explored for blue emission. To summarize, they are the distyrylarylene series, anthracenes, perylenes, fluorenes, heterocyclic compounds, and metal complexes.

3.6.3.3.1 Distyrylarylene Series

The most efficient fluorescent blue emitters yet reported belong to the distyrylarylene (DSA) series (Scheme 3.56) and it is likely that the first generation of commercial blue OLEDs will use these materials as emitters or hosts.

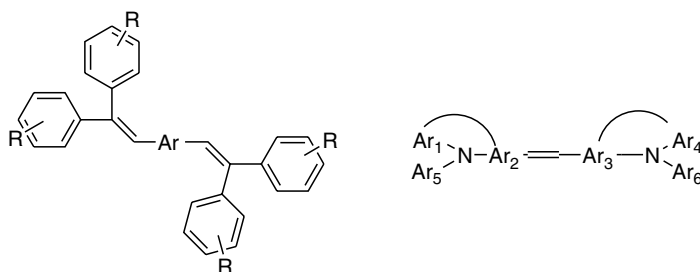


SCHEME 3.56 Chemical structures of DSA-host DPVBI and dopants BCzVB and BCzVBI.

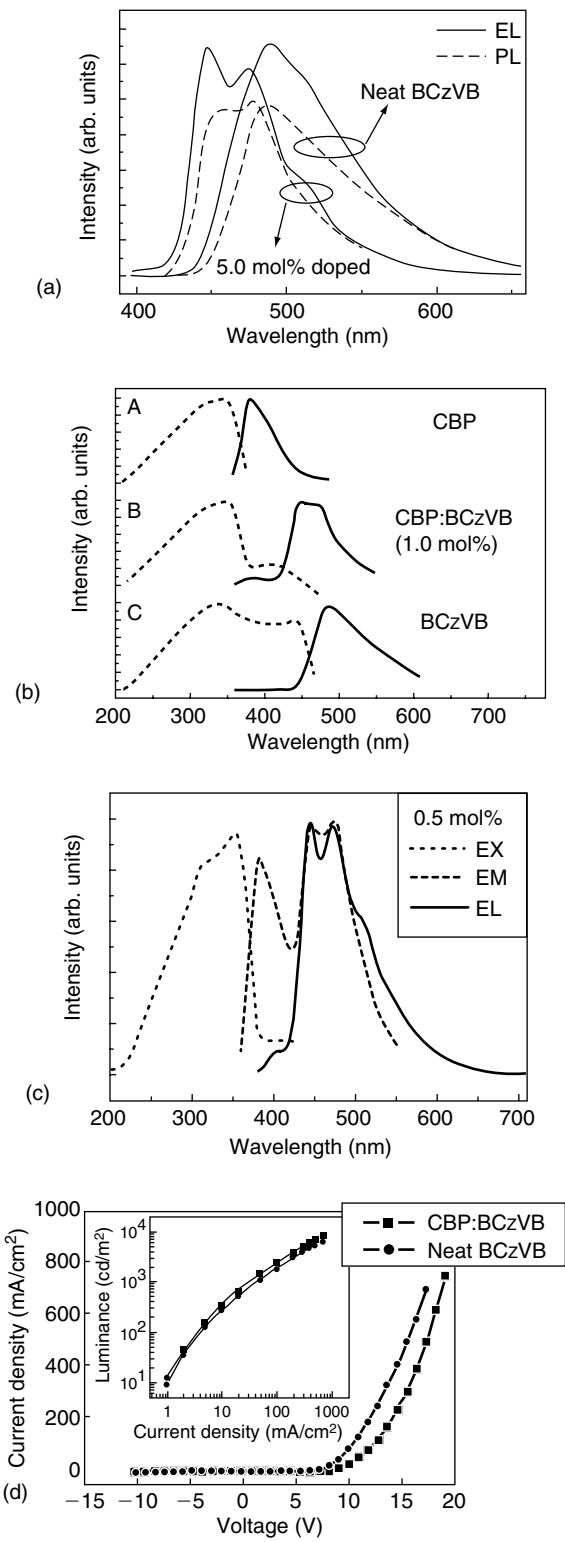
Hosokawa et al. first reported the use of a distyrylarylene (DSA) host DPVBI and amino-substituted DSA such as BCzVB (**188**) and BCzVBI (**189**) as dopants in a blue OLED with an OLED structure of ITO/CuPc/TPD/DPVBI:BCzVB or BCzVBI/Alq₃/Mg:Ag [230]. Both amino-substituted DSAs gave almost identical EL emission with a peak maximum centered at 468 nm with two shoulders at 445 and 510 nm. The highest luminous efficiency was observed in a BCzVBI doped device that gave luminous efficiency of 1.5 lm/W with an EQE of 2.4%. The highest luminance, over 10,000 cd/m², in the blue region was obtained at 14 V. The efficiency is twice that of the undoped device, which gives luminous efficiency of 0.7–0.8 lm/W. The molecular structures of the host and dopants are shown in Scheme 3.56. The nonplanar host DPVBI has a blue emission with a band gap of 3.08 eV. The authors also pointed out that the EL characteristics are attributable to the dopant owing to the efficient energy transfer mechanism and not to a charge trapping mechanism. This material also has nice film-forming properties. The initial half-life time of the above device was measured to be 500 h at an initial luminance of 100 cd/m². Later, the same group used an improved HTL with a DSA host and a DSA–amine dopant that gave a half-life time over 5000 h.

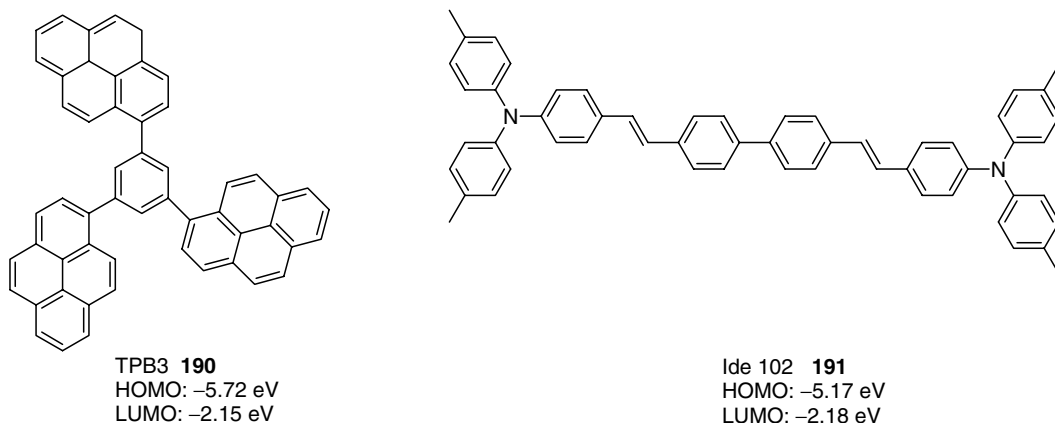
These DSA hosts and DSA–amine blue emitter dopants were patented by Idemitsu Kosan Co. Ltd., Japan (Scheme 3.57), and are likely to become a commercial blue emitter candidate [231].

Using the familiar dicarbazole material CBP as a host material and introducing BAq as a HBM and LiQ as an EIL in the BCzVB doped OLED device with a structure of ITO/TPD/CBP:BCzVB/BAq/Alq₃/LiQ/Al, Wu et al. achieved a maximum luminance of 11,000 cd/m² with a QE of 3.3% [232]. It is interesting to note that the emission spectra of CBP doped with BCzVB either in PL or in EL are quite different from the neat BCzVB- or DPVBI-doped BCzVB in PL or EL, with the former blue-shifted and having better color purity. The EL emission of the CBP doped with BCzVB exhibits a dominant peak at 448 nm with an additional peak at 476 nm of FWHM of 60 nm while the emission color corresponds to CIE (0.15, 0.16), where the neat BCzVB or DPVBI doped with BCzVB has CIE (0.16, 0.21). The authors explain such color differences between the CBP-doped and neat BCzVB or DPVBI-doped BCzVB devices are due to the different excitation mechanisms of the two different guest–host doped systems. The excitation mechanism of the CBP-doped-with-BCzVB device is attributed to both Förster energy transfer and carrier trapping whereas the DPVBI-doped-with-BCzVB device is only a Förster energy transfer dominated process as mentioned by Hosokawa et al. This conclusion has been deduced from the HOMO and LUMO energy levels of the hosts and the dopant and confirmed by an experimental study (Figure 3.10).



SCHEME 3.57 Chemical structures of DSA series patented by Idemitsu Kosan Co. Ltd.





SCHEME 3.58 Chemical structure of triarylbenzene host and DSA-amine guest.

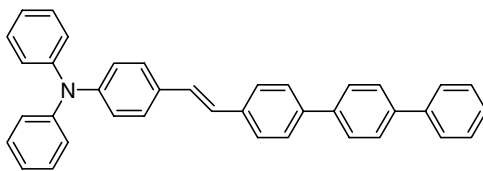
It can be seen from Figure 3.10a and d that the emission spectra of the neat BCzVB and DPVBi doped with BCzVB are essentially the same and can be attributed to an energy transfer process. The emission spectrum of CBP doped with BCzVB is quite different; it comes from emission contributed from both CBP and BCzVB molecules owing to both charge trapping as well as a partial energy transfer process.

The emitter DPVBI (**122**) has a low T_g of $\sim 64^\circ\text{C}$. This can be increased to a higher T_g by introducing more robust substituents. Tao's group designed a DPVBI analogue using a spirobifluorene unit instead of a biphenyl [233]. This rigid and orthogonally shaped spirobifluorene DPVSBF (**123**) exhibits a T_g of $\sim 115^\circ\text{C}$. Improved performance has been observed both in blue OLEDs and in doped white OLEDs. In addition, the lifetime of DPVSBF-doped devices has been improved, which is also attributed to the higher morphological stability of the spirobifluorene DPVSBF host.

Ueno studied a series of different triaryl- or tetraaryl-benzene host materials and found that using triarylbenzene (TPB3, **190**) (Scheme 3.58) as a host material with a DSA-amine (Ide 102, **191**) doped OLED showed a peak luminance of $142,000\text{ cd/m}^2$ at 12 V. This device also showed a luminescent efficiency of 6.0 lm/W at 5 V and 820 cd/m^2 and an external efficiency of 2.4%. The lifetime of the device is also better than that of a device with DPVBI as the host.

Recently, Chen's group reported a deep blue OLED based on an asymmetric mono(styryl) amine derivative DB1 (**192**) as shown in Scheme 3.59. PL spectra of this deep blue dopant in toluene solution showed a peak emission of 438 nm, which is about 20 nm hypsochromic shift compared with DSA-amine symmetric dopant, due to the shorter chromophoric conjugated length of the mono(styryl) amine. OLED device based on this blue dopant achieved a very high efficiency of 5.4 cd/A , with CIE coordinates of (0.14, 0.13) [234].

FIGURE 3.10 (a) EL (solid line) spectra of ITO/TPD/CBP:BCzVB (5.0 mol%)/Alq₃/Liq/Al and ITO/TPD/BCzVB/Alq₃/Liq/Al devices at 20 mA/cm^2 , along with the corresponding PL (dashed line) spectra of the CBP:BCzVB (5.0 mol%) and BCzVB film. (b) PL EX (dotted line) and EM (solid line) spectra of deposited films of CBP (A), CBP:BCzVB (1.0 mol%) (B), and BCzVB (C), respectively. (c) EX and EM spectra of CBP:BCzVB (0.5 mol%) film and EL spectrum of ITO/TPD/CBP:BCzVB (0.5 mol%)/Alq₃/Liq/Al device. (d) EL spectra for multilayer devices. For devices with the BCzVBi doped layer, the BCzVB doped layer and the nondoped layer, EL spectra are shown by open circles, closed circles, and a solid curve, respectively. (From Wu, Y.Z., Zheng, X.Y., Zhu, W.Q., Sun, R.G., Jiang, X.Y., Zhang, Z.L., and Xu, S.H., *Appl. Phys. Lett.*, 83, 5077, 2003. With permission.)



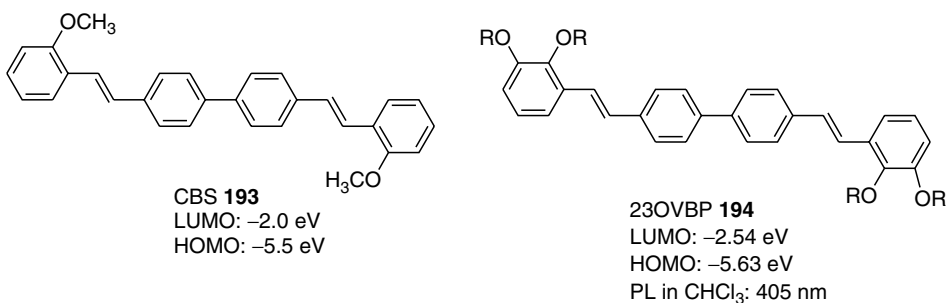
DB1 **192**
HOMO: -5.2 eV

SCHEME 3.59 An asymmetric mono(styryl) amine as a deep blue dopant material.

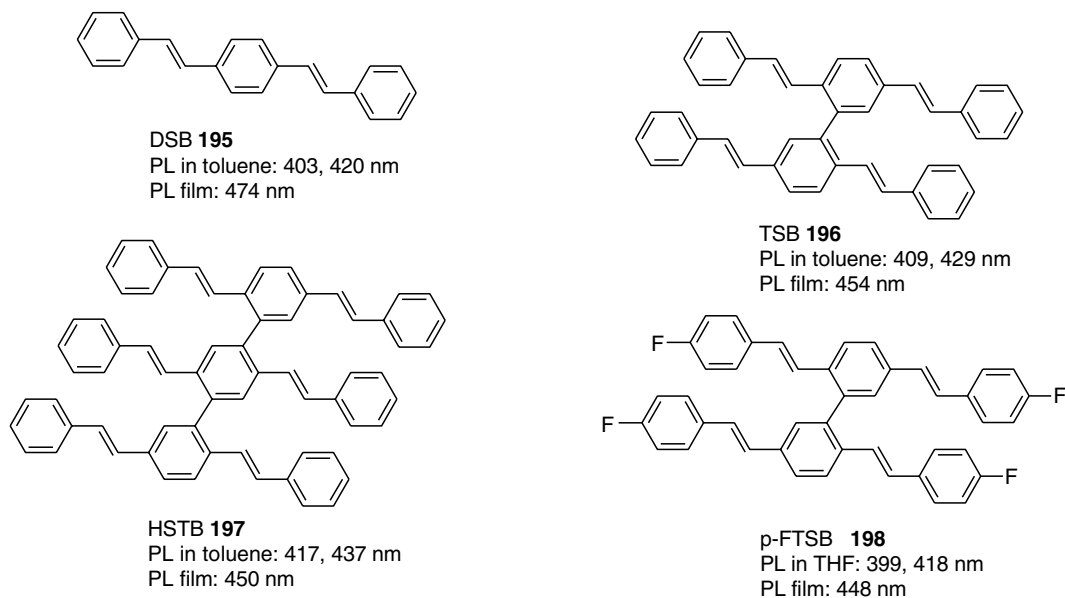
By introducing methoxy groups, Huang et al. designed the more soluble DSA derivative CBS (**193**, **194**) (Scheme 3.60) [235] and this compound is easy to purify. In the triple layer devices ITO/TPD/CBS/Alq₃ or Tb complex/Al, the multipeak emission with band peaks centered at 505 nm was observed when Alq₃ was used as the ETM due to emission from the Alq itself in the ETL. However, a blue emission was observed when the ETM was changed to a Tb complex.

Same as arylamine DSA derivatives used as guest materials in blue OLEDs, Geise et al. synthesized a series of alkoxy-substituted biphenyl vinyl compounds as dopant materials [236]. These authors studied OLEDs fabricated using PVK as a host polymer and hole-transporting PBD as a codopant with a PLED structure of ITO/PEDOT-PSS/PVK:23OVBP:PBD/LiF/Al, which gave an optimized QE of 0.7% and brightness of 1600 cd/m² at 100 mA/cm² with emission peak at 450 nm.

A notable design of oligo-phenyl vinyl blue emitters by Ma et al. is shown in Scheme 3.61 (**195–198**) [237,238]. By linking two or three distyrylbenzene molecule units through phenyl-phenyl bond, the dimers **196** and trimer **197** exhibit very interesting optical properties. In dilute toluene solution, distyrylbenzene molecule **195** shows deep blue emission with maximum emission peaks at 403 and 420 nm, and its dimer and trimer show a slight red-shift emission (10–20 nm) compared with **195**. However, in the solid state, the emission spectrum properties are quite different with both dimer and trimer blue-shifted compare with **195**. The trimer emits a pure blue color with a maximum emission peak at 450 nm; the dimer emits at a maximum peak emission of 454 nm; and **195** red-shifts itself about 54 nm from its dilute solution with a peak emission at 474 nm. Besides, the trimer also exhibits the highest solid-state photoluminescent efficiency. The authors explained that these are due to the weak intermolecular interactions of **197** in the solid states. The fluorine dimer **198** shows a slight blue-shift emission in the solid state compared with **195**. OLED fabricated using trimer as



SCHEME 3.60 Chemical structures of oligo-phenyl vinyl compounds.



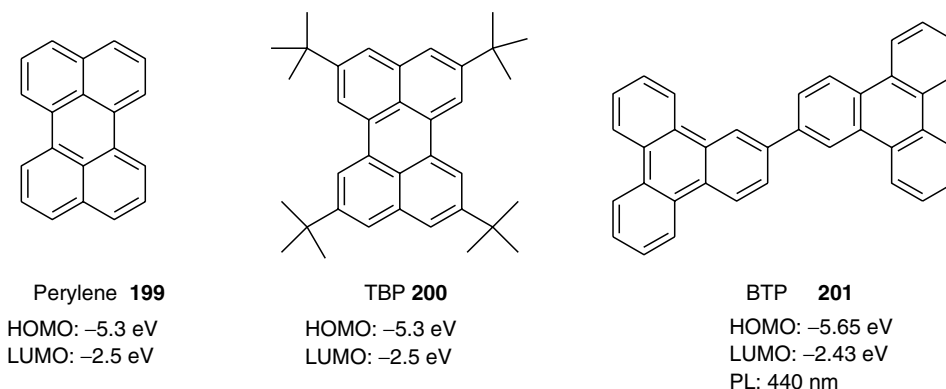
SCHEME 3.61 Chemical structures of oligo-phenyl vinyl blue emitters.

emitter emitted a blue light with CIE (0.19, 0.22) with a highest luminescent efficiency of 3.5 cd/A (1.6 lm/W) and a brightness of about 3837 cd/m².

3.6.3.3.2 Anthracene Series

Besides distyrylarylene as a blue host or dopant in blue OLED application, anthracene materials with high QE and emission color in the blue range make them attractive materials.

In realizing the poor film-forming property of 9,10-(diphenyl)anthracene, the Kodak group improved this property by designing a series of blue emitters based on further substituted anthracene derivatives. The chemical structures of these materials were patented in a U.S. Patent in 1999 [239]. In their patent, Kodak also reported the EL data using one of these compounds as a host material and using TBP as a blue dopant (Scheme 3.62). The device structures is ITO/CuPc/NPD/anthracene compound:0.5%TBP/Alq₃/Mg:Ag. The EL of the device showed blue emission with CIE color coordinates of (0.144, 0.196). Without the



SCHEME 3.62 Chemical structures of blue perylene-based and biaryl-based emitters.

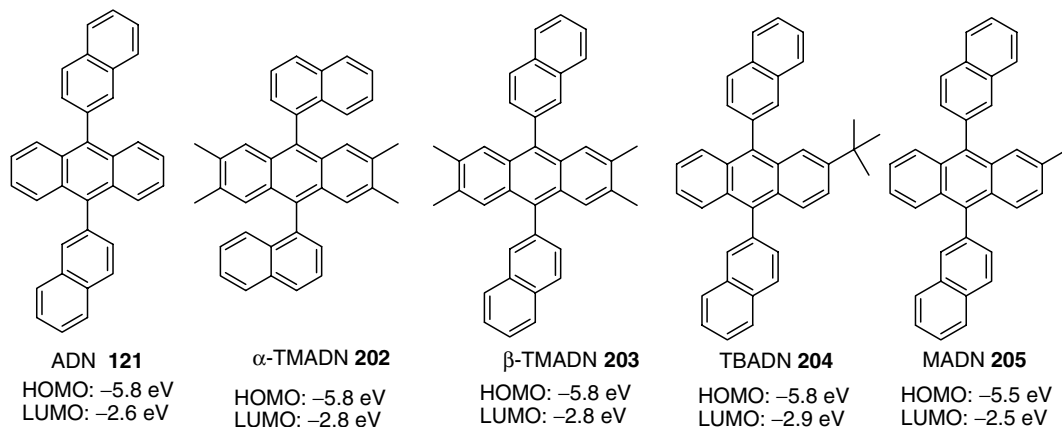
dopant the EL emission with CIE color coordinates are (0.162, 0.107). No efficiency data or device lifetime data are reported.

Perylene (**199**) and its derivative (TBP, **200**) have been widely used as blue dopant materials owing to their excellent color purity and stability. Efficient blue emitters with excellent CIE coordinates are found in biaryl compound 2,2'-bistriphenylenyl (BTP, **201**) as shown in Scheme 3.62 [145]. A device of structure ITO/TPD/BTP/TPBI/Mg:Ag emits bright blue emission with CIE (0.14, 0.11). A maximum brightness of 21,200 cd/m² at 13.5 V with a maximum EQE of 4.2% (4.0 cd/A) and a power efficiency of 2.5 lm/W have been achieved.

Jiang et al. were the first to report a relatively stable blue OLED based on anthracene derivative JBEM (**120**) [240]. With the similar OLED structure as that used above by Kodak of ITO/CuPc/NPD/JBEM:perylene/Alq/Mg:Ag and using JBEM as a blue host material, the device shows a maximum luminance of 7526 cd/m² and a luminance of 408 cd/m² at a current density of 20 mA/cm². The maximum efficiency is 1.45 lm/W with CIE (0.14, 0.21). A half-life of over 1000 h at initial luminance of 100 cd/m² has been achieved. The authors also compared the device performance using DPVBI as a host, which gave them a less stable device.

Several groups have studied naphthalene substituted anthracene derivatives as hosts or emitter materials in blue OLEDs (**121**, **202–205**) (Scheme 3.63). The Kodak group used ADN as a host and TBP as a dopant in ITO/CuPc/NPD/ADN:TBP/Alq₃/Mg:Ag [241]. They achieved a narrow vibronic emission centered at 465 nm with CIE (0.154, 0.232) and a luminescent efficiency as high as 3.5 cd/A. In comparison, the undoped device shows a broad and featureless bluish-green emission centered at 460 nm with CIE (0.197, 0.257) and an EL efficiency below 2.0 cd/A. The operational lifetimes of the doped device and the undoped device were 4000 and 2000 h at an initial luminance of 636 cd/m² and 384 cd/m², respectively.

Normally, using ADN as an EML inserted between the HTL and ETL in the multilayer device results in broad emission as was observed in the above Kodak device. This is due to emission from the ETL material Alq₃. Increasing the thickness of the ADN layer cannot completely avoid this undesired emission, and, in addition, the operating voltage is high and the device is not stable. Hung et al., by introducing an additional HBL and confining the exciton emission in the ADN layer, achieved a pure blue emission color with CIE (0.1566, 0.1076). The device structure is ITO/NPD/ADN/BCP/Alq₃/Mg:Ag. However, the drawback with this device is the operating voltage that is high due to the high energy barrier between the BCP and the Alq₃ layers. By replacing both BCP and Alq₃ with a combined high



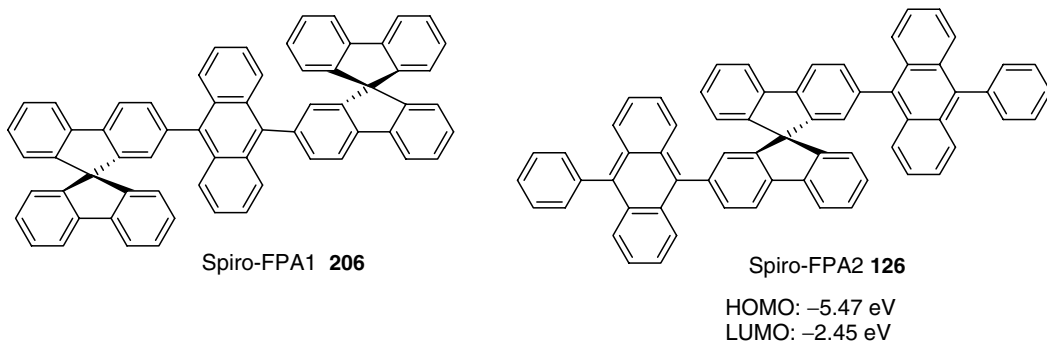
SCHEME 3.63 Chemical structures of naphthalene substituted anthracenes.

electron mobility ETM and HBM TPBI, and by using a doped perylene device structure ITO/NPD/ADN:0.5%perylene/TPBI/LiF/Mg:Ag, a low driving voltage and a pure blue emission device is achieved. The device exhibits a luminescent efficiency of 3.6 cd/A with CIE (0.1451, 0.1446). It is envisioned that, if a HIL is incorporated into such a device, the efficiency will be improved further. Using this device structure but employing an unsymmetric anthracene derivative TBADN as the blue emitter in a nondoped device, Lee et al. achieved a blue device with excellent color purity with CIE (0.14, 0.10) and a maximum current efficiency of 2.6 cd/A [242]. The EL emission of the device is also stable compared with ADN devices when operated at high current. The authors attributed the color purity of the TNADN device to the bulky *tert*-butyl group on ADN, which prevents charged complex formation at the interface.

Very recently, Qiu's group modified the ADN structure and synthesized α -TMADN and (β -TMADN that contain substituted tetra-methyl anthracene [243]. This sterically congested nonplanar structure hinders the close spacing of the molecules and improves the film-forming properties. The OLED device structure is ITO/NPD/TMADN/Bphen/Mg:Ag. The device with β -TMADN as the EM exhibits blue emission with CIE (0.163, 0.221). A high EQE of 2.8% and a brightness up to 10,000 cd/m² at 12 V with the maximum efficiency of 4.5 cd/A (2.51 lm/W) have been achieved. The performance of the device using a blend of the two molecules α -TMADN and β -TMADN (9:1) demonstrates even better results with a brightness over 12,000 cd/m² at 15 V and a maximum efficiency of 5.2 cd/A (2.72 lm/W) and color coordinates of (0.152, 0.229) with emission color centered at 466 nm.

Chen's group designed MADN through introduction of one methyl substituent at the C-2 position of the anthracene ring. This material can form nice films without the problem of crystallization while keeping the HOMO and LUMO energy of ADN. The efficiency (1.4 cd/A) of MADN-based blue OLEDs with CIE (0.15, 0.10) is slightly lower than the equivalent ADN device. Later, using a styrylamine as a dopant, and an optimized device structure (ITO/CF_x/NPD/MADN:DSA-Ph/Alq₃/LiF/Al, Chen et al. achieved a very high efficiency OLED with EL efficiency of 9.7 cd/A at 20 mA/cm² and 5.7 V while the lifetime of such a device is projected to have a half-decay lifetime of 46,000 h at an initial brightness of 100 cd/m², although the color purity is sacrificed with an emission peak shift from 452 nm with CIE (0.15, 0.10) to a major peak at 464 nm with a shoulder centered at 490 nm with CIE (0.16, 0.32) [244].

Other derivatives have been reported such as the spiro-linked fluorene-anthracenes (**126**, **206**), which preserve the optical and electrochemical properties of anthracene while reducing the tendency for crystallization and enhancing the solubility and T_g (Scheme 3.64). Highly efficient deep blue OLEDs have been demonstrated by using Spiro-FPA1 (**206**) as an emitter material in a p-i-n type OLED structure: ITO/MeO-TPD:2%F4-TCNQ/Spiro-TAD(**44**)/



SCHEME 3.64 Chemical structures of spirofluorene substituted anthracenes.

Spiro-FPA1/TPBI/Bphen:Cs/Al. A very low operating voltage of 3.4 V at luminance of 1000 cd/m² was obtained, which is the lowest value reported for either small-molecule or polymer blue electroluminescent devices. Pure blue color with CIE coordinates (0.14, 0.14) have been measured with very high current (4.5 cd/A) and quantum efficiencies (3.0% at 100 cd/m² at 3.15 V) [245]. In another paper, Spiro-FPA2 (**126**) was used as a host material with an OLED device structure of ITO/CuPc/NPD/spiro-FPA2:1%TBP/Alq₃/LiF that produces a high luminescent efficiency of 4.9 cd/A [246].

By introducing the hole transport arylamine as an end cap for an anthracene backbone, Lin et al. designed a series of novel materials (**207–212**) (Scheme 3.65) [247]. The aim of these dual function materials is to combine the emitting property of the blue anthracene lumino-phore with the hole transport property of the triarylamine to simplify the device fabrication steps. Though the introduction of the arylamino moieties produces moderate QE ($\Phi_f \sim 20\%$) for these materials, the OLEDs using them as emitters as well as HTMs demonstrate only moderate EL performance with a maximum luminance of 12,922 cd/m² and 1.8 lm/W with CIE (0.15, 0.15).

3.6.3.3.3 Other Heterocyclic Compounds

Pyrazole-containing compounds are useful blue dyes. Tao's group studied a series of pyrazolo [3,4-*b*]quinoline derivatives as blue emitters (**217**) (Scheme 3.66) [248]. An EQE about 3.5% using one of the dopants 4-(*p*-methoxyphenyl)-3-methyl-1-phenyl-1*H*-pyrazolo[3,4-*b*]quinoline (MeOPAQ-H) in an OLED with a configuration of ITO/NPD/CBP/TPBI:MeOPAQ-H/TPBI/Mg:Ag was achieved. A brightness of 13,000 cd/m² with a blue emission CIE (0.19, 0.16) was demonstrated. Other pyrazole derivatives such as Pyzo-1 (**218**) and Pyzo-2 (**219**) also emitted blue light, but the EL performance is rather poor [249]. Heterocyclic compounds such as tri(*p*-terphenyl-4-yl)amine (*p*-TTA, **213**), were investigated as blue emitters, however, their performance is also very poor [250]. Phenanthrolines (**214–216**), e.g., BCP (**216**), widely used as HBMs, were used as blue emitting materials in the late 1990s [251,252]. The pure blue emission in this case may come from the HTM NPD emission.

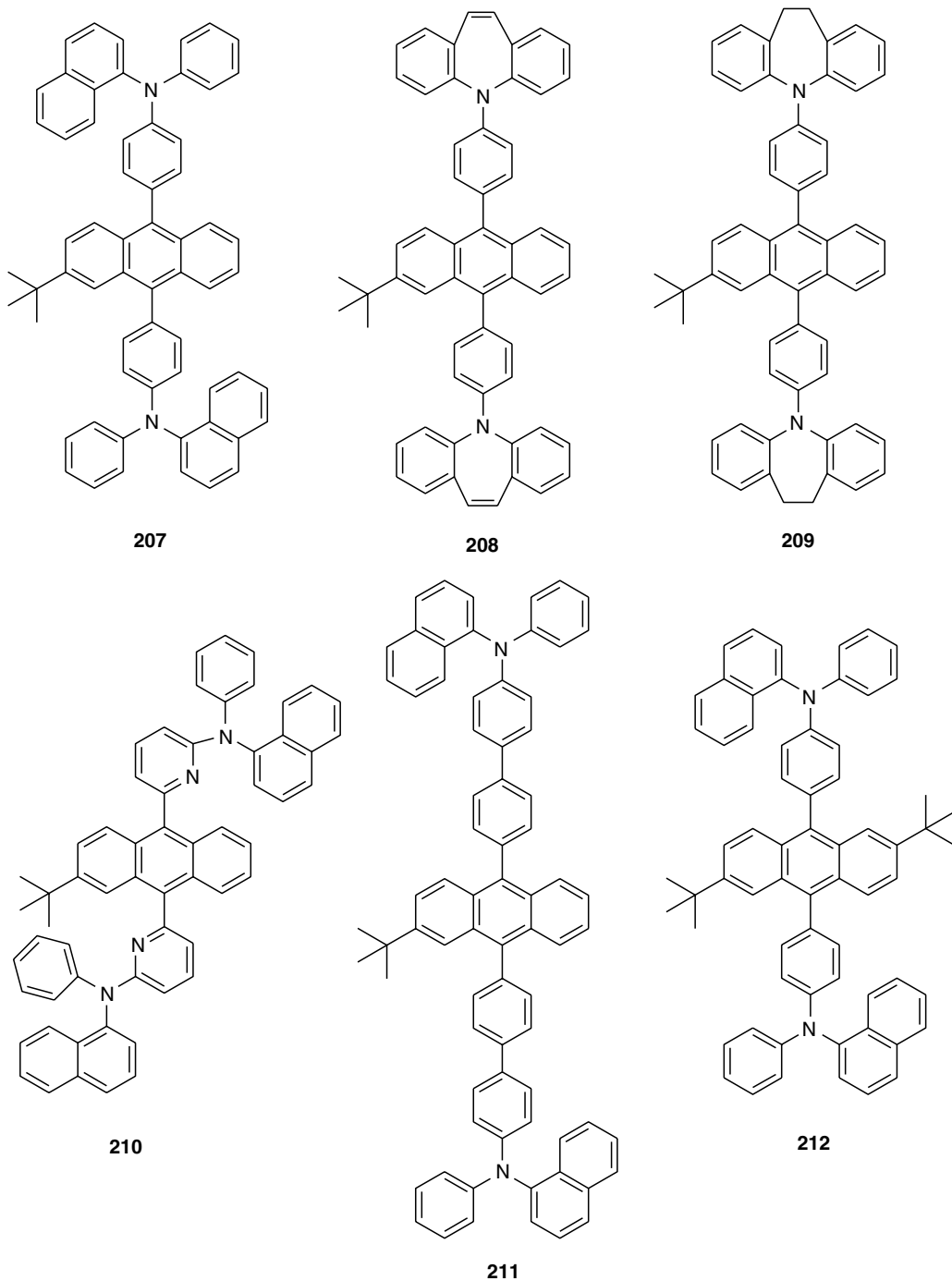
Recently Wudl's group synthesized a new indolizino[3,4,5-*ab*]isoindole derivative INI Blue as a blue guest material for OLEDs (**220**) [253]. An OLED with structure of ITO/CuPc/CBP/INI Blue/Salq/Alq₃/MgF₂ generates a very bright blue emission with a CIE (0.165, 0.188). The maximum luminance is 5674 cd/m² with a power efficiency of 0.94 lm/W and current efficiency of 2.7 cd/A. The device was claimed to be quite stable, although the lifetime has not been reported.

Wang's group systematically studied a series of blue emitters based on 7-azaindole compounds (**221**, **222**) (Scheme 3.67) [254]. Interestingly, blue emitters such as 1,3,5-tri(*N*-7-azaindolyl)-benzene (AZAIN-1) and 4,4'-di(*N*-7-azaindolyl)-biphenyl (AZAIN-2), when used as the emitting layers in OLEDs, can function as both hole transporters and emitter materials. The presence of a HTL such as NPD or TPD in these OLED devices decreases the luminescent efficiency. Devices fabricated with structure ITO/CuPc/AZAIN-1 or 2/PBD/LiF/Al emitted deep blue emission.

3.6.3.3.4 Spiro-Linked Blue Emitters

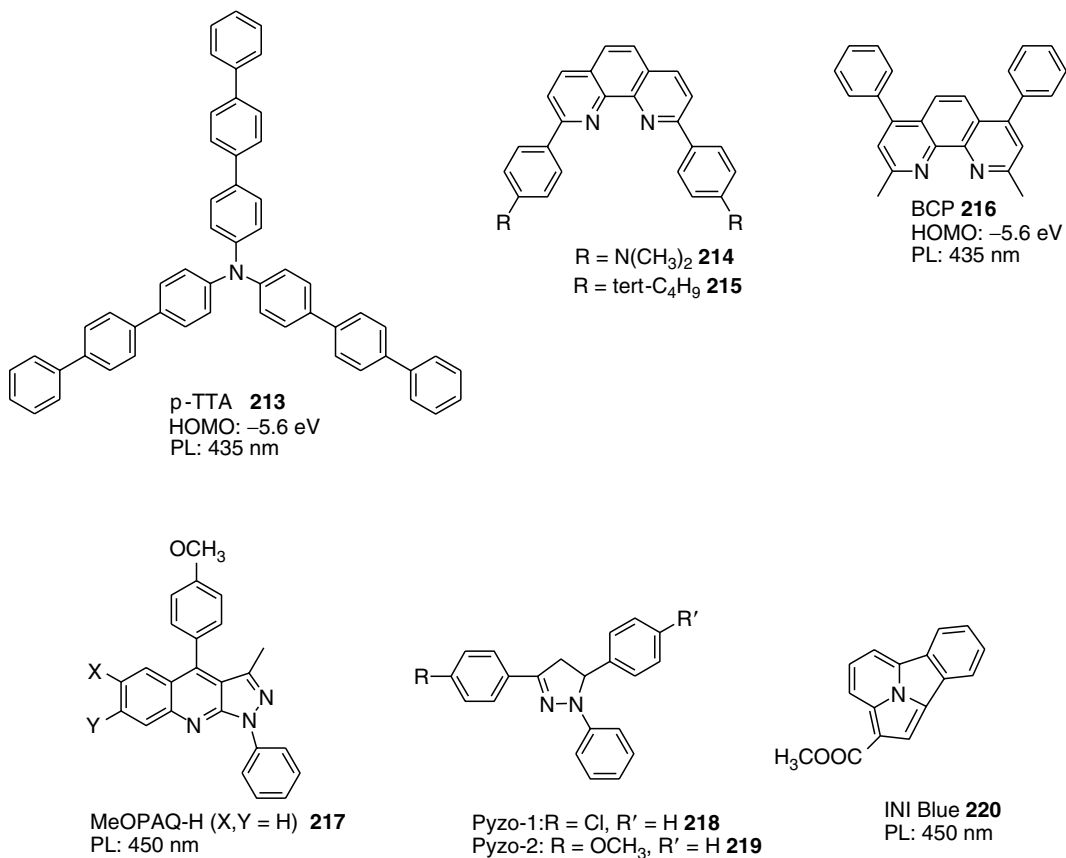
Spiro-linked organic glasses, which improve the processibility and morphology of the films at the same time keeping the electronic properties intact, are very interesting materials for OLEDs. Salbeck et al. designed a series of spiro-linkage fluorene compounds with electron-donating and electron-withdrawing groups (**223–228**) (Scheme 3.68) [255,256].

A blue OLED with a very low turn-on voltage of 2.7 V and a luminance of 500 cd/m² at 5 V with structure ITO/Spiro-TAD/Spiro-PBD/Al:Mg has been reported. The robust and morphologically stable spirobifluorene-cored pyrimidine oligoaryl blue emitter

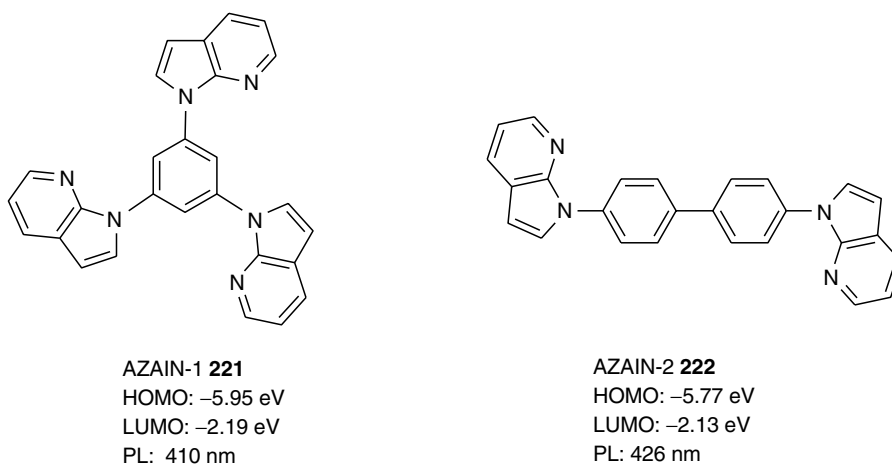


SCHEME 3.65 Chemical structures of substituted anthracene arylamine.

2,7-bis[2-(4-*tert*-butylphenyl)pyrimidine-5-yl]-9,9'-spirobifluorene (TBPSF) with very high PL QE (80%) has been recently reported by Wu et al. [257]. When using this material as an emitter or a host layer in ITO/PEDOT-PSS/NCB/TBPSF:0–1%Perylene/Alq₃/LiF/Al, the nondoped

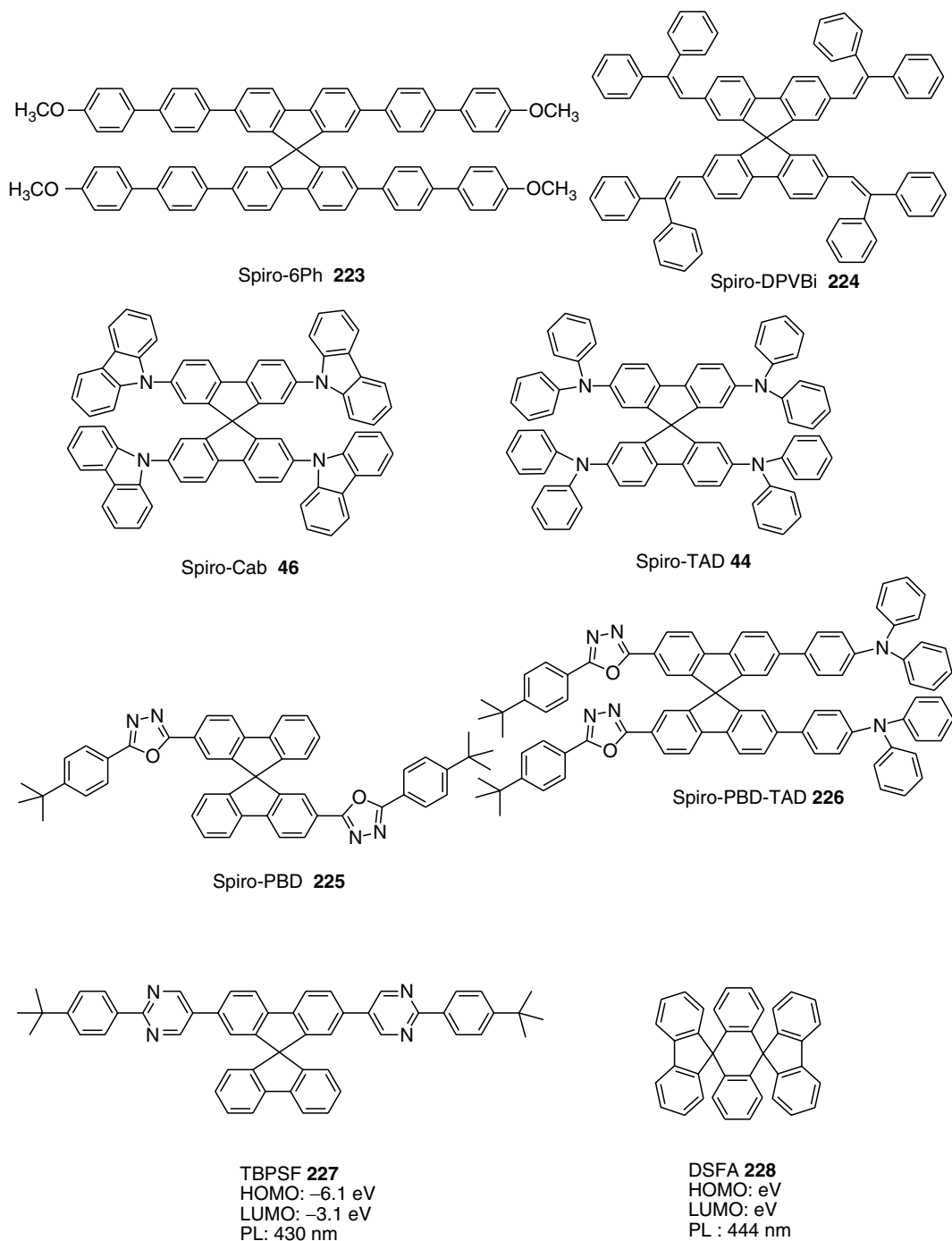


SCHEME 3.66 Chemical structures of blue emitting heterocyclic compounds.



SCHEME 3.67 Chemical structures of deep blue 7-azaindole derivatives.

and doped devices exhibit unusual longevity even to currents up to 5000 mA/cm², with maximal brightness over 30,000 and 80,000 cd/m² for nondoped and doped devices, respectively. The EL efficiencies of nondoped and doped devices are 2.3% (1.6 cd/A) and 4% (5.2 cd/A), respectively.



SCHEME 3.68 Chemical structures of spiro-linked blue emitters and transporters.

Qiu's group investigated the spirofluorene linked dihydroanthracene compound di-spiro-9,9'-di-fluorene-9'',9'''-(9,10-dihydro-anthracene) (DSFA), originally developed in the 1930s, as a blue emitter in ITO/m-MTDATA/NPD/DSFA/Mg:Ag [258]. The device exhibited a

pure blue emission CIE (0.17, 0.15) at a low turn-on voltage of 6 V with a maximum luminescent efficiency of 4.73 lm/W (15.1 cd/A).

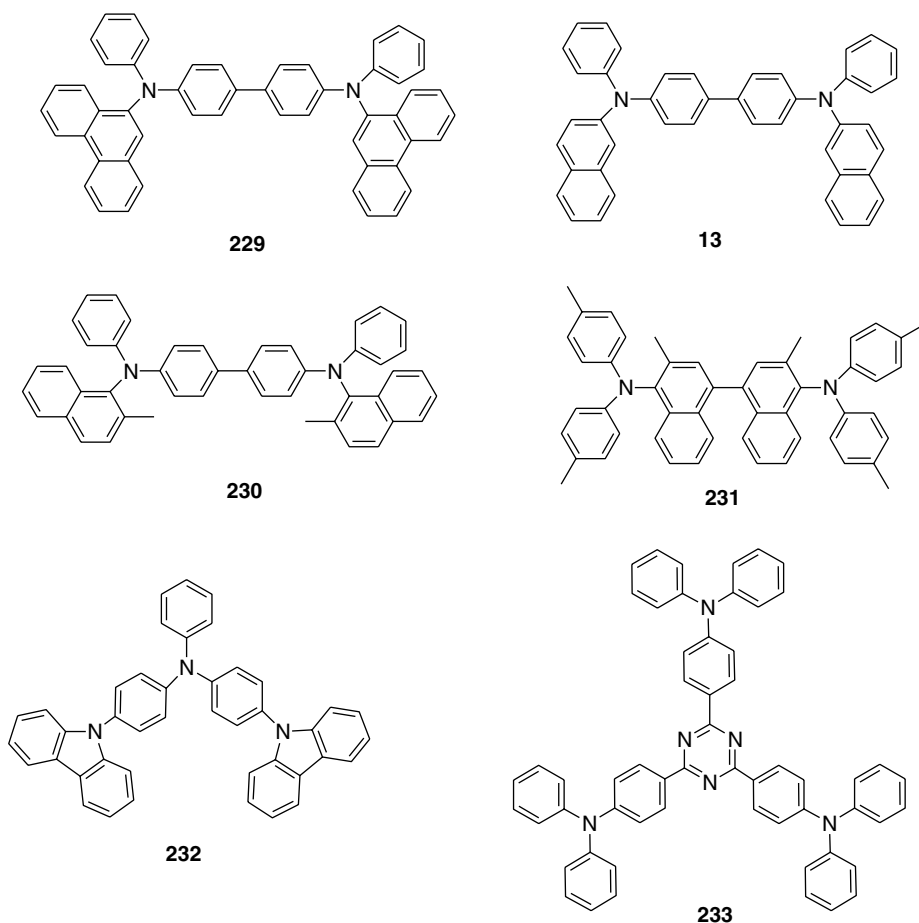
3.6.3.3.5 Aromatic Amine Blue Emitters

Some HTMs such as the aromatic amines (**229–233**) can emit efficient blue light if used with an appropriate HBL (Scheme 3.69) [259].

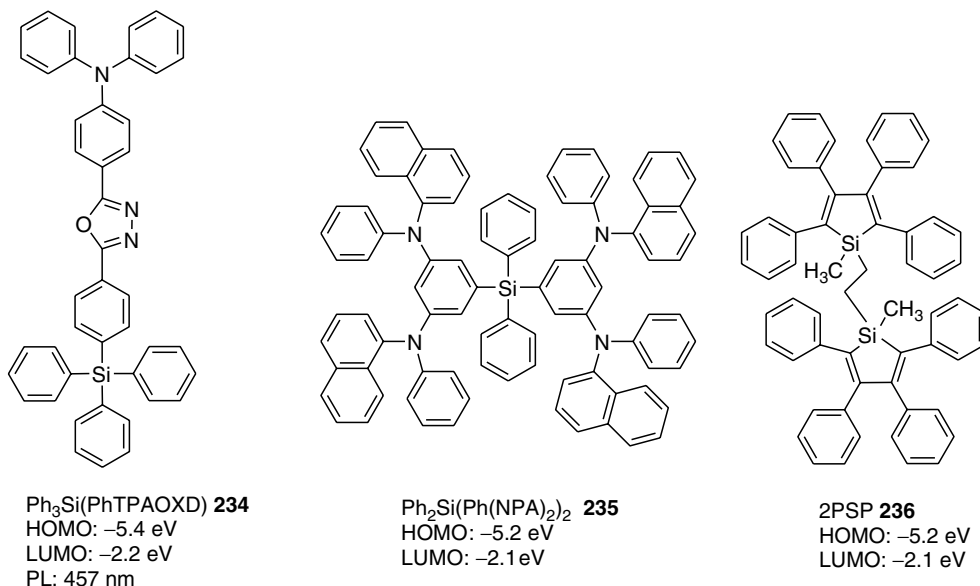
3.6.3.3.6 Organosilicon Blue Emitters

Aromatic chromophores consisting of linked organosilicon compounds possess excellent charge transport properties due to the interaction between the Si 3d orbitals and the ligands. These organosilicon compounds have been proven to be good EMs due to their excellent film-forming properties and their high T_g . Chen et al. reported an efficient blue emitter based on the tetraphenylsilane compound (**234–236**) shown in Scheme 3.70 [260].

OLED ITO/NPD/ $\text{Ph}_3\text{Si}(\text{PhTPAOXD})/\text{Alq}_3/\text{Mg:Ag}$ emits pure blue light with an EL emission band centered at 460 nm (FWHM: 75 nm) and a CIE (0.17, 0.17). The maximum luminance exceeds 20,000 cd/m² at 15 V, with an EQE of 1.7% and a power efficiency of 0.9 lm/W. Later, the same group optimized the device structures by introducing a HTL of an organosilicon compound and achieved a much higher performance [261]. An optimized OLED



SCHEME 3.69 Chemical structures of aromatic amines: blue emitters as well as hosts.



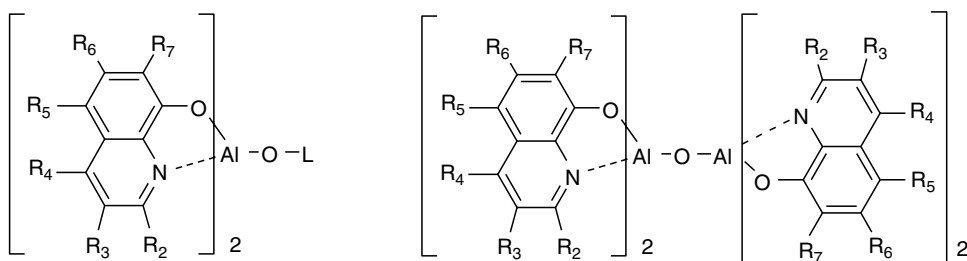
SCHEME 3.70 Chemical structures of organosilicon blue emitter and HTMs.

with a structure of ITO/Ph₂Si(Ph(NPA)₂)₂/NPD/Ph₃Si(PhTPAOXD)/Alq₃/Mg:Ag possesses good stability and color purity with EL emission maximum at 460 nm, corresponding to CIE (0.16, 0.18). The device shows a maximum EL efficiency of 19,000 cd/m² and an EQE of 2.4% (3.1 cd/A) with a power efficiency of 1.1 lm/W.

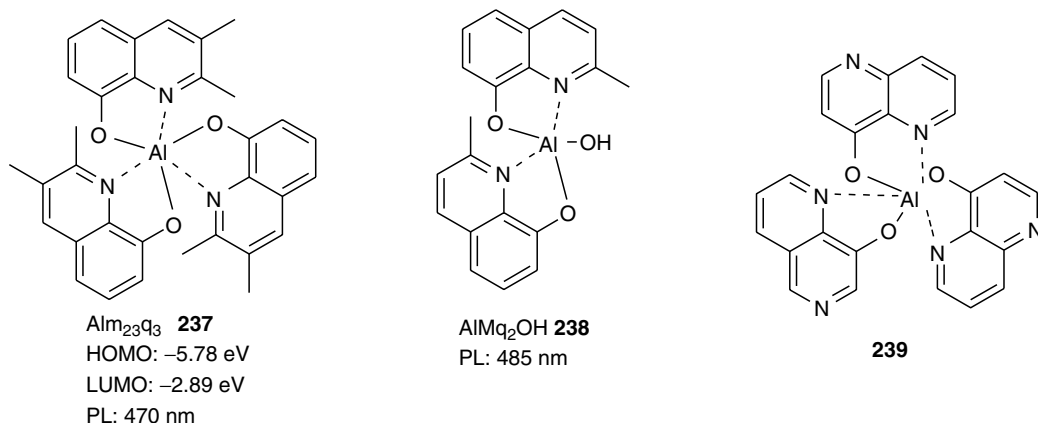
Compound 2PSP (**236**) exhibits a bright blue-greenish emission with a solid-state photoluminescent QE of 97%. OLED devices using 2PSP as the EML showed a very low operating voltage, an external EL QE of 4.8%, and luminous power efficiency of 9 lm/W at a brightness of 100 cd/m². This value is the best efficiency achieved for SMOLED using undoped emissive and carrier transport layers and is close to the theoretical limit for a device using a fluorescent emitter [262].

3.6.3.3.7 Metal Chelates

Owing to its outstanding stability and luminescent efficiency, Alq₃ is the most widely used and studied emitting material. By structural modifications of Alq₃, several blue emitters based on Alq₃ structures have been investigated and Kodak has patented the basic structures of several possible blue emitters based on Alq₃ (Scheme 3.71) [129,263]. The first blue aluminum chelate structure contains a phenolato ligand and two R₂-8-quinolinolato ligands. The second



SCHEME 3.71 Chemical structures of blue Alq₃ derivatives patented by Kodak.



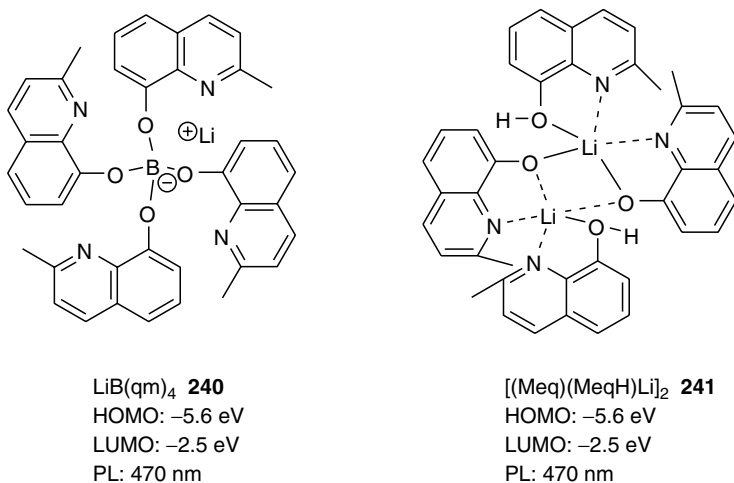
SCHEME 3.72 Chemical structures of blue Alq₃ derivatives.

blue aluminum chelate structure comprises a bis(R₂-8-quinolinolato) aluminum (III)-μ-oxo-bis(R₂-8-quinolinolato)-aluminum (III).

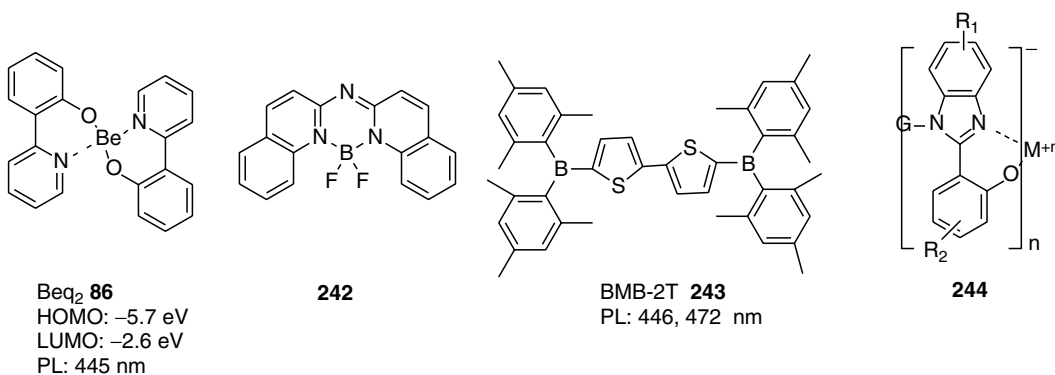
Yu et al. synthesized two methyl-substituted Alq₃, named tris(2,3-dimethyl-8-hydroxyquinoline) aluminum complex (Alm₂₃q₃, **237**) (Scheme 3.72) [264]. This compound emits blue color with an emission peak centered at 470 nm and FWHM of 90 nm. OLEDs with a structure of ITO/TPD/Alm₂₃q₃/Mg:Ag emit blue light and the luminous efficiency is 0.62 lm/W with a maximum luminance of 5400 cd/m² at 19 V.

Bis(2-methyl-8-quinolinolato)aluminum hydroxide with only two quinolate ligands emits blue color with the maximum peak emission at 485 nm and FWHM of 80 nm [265]. Devices fabricated with a structure of ITO/CuPc/NPD/Almq₂OH/LiF/Al give a maximum brightness of 14,000 cd/m² at 480 mA/cm².

Replacing the metal Al by a boron atom as the metal chelate center, Tao et al. reported lithium tetra-(2-methyl-8-hydroxy-quinolino) boron (LiB(qm)₄, **240**) (Scheme 3.73) quantitatively prepared by reaction of lithium borohydride (LiBH₄) with four equivalents of 2-methyl-8-hydroxy-quinoline in ethanol at room temperature [266]. LiB(qm)₄ is a pure blue emitter with a maximum peak emission at 470 nm with FWHM of 75 nm. Devices of



SCHEME 3.73 Chemical structures of blue boron chelates.



SCHEME 3.74 Chemical structures of metal chelates as blue emitters.

ITO/TPD:PVK/LiB(qm)4/Mg:Ag show a turn-on voltage of 5 V with luminescent efficiency of 1.3 lm/W and a maximum luminance of 6900 cd/cm². By inserting an additional electron transport Alq₃ layer, the device efficiency decreased to 0.8 lm/W [267]. The blue-shift of this boron compound was attributed to the lack of interaction between the boron center and the nitrogen atoms of the ligand. However, this assumption was found to be erroneous since the reported structure of LiB(qm)4 is incorrect based on the structure elucidated by Radu et al. at DuPont Displays [268]. The correct structure of the product is [(Meq)(MeqH)Li]₂, which contains the identical percent of C, H, N as reported for LiB(qm)4, but with only trace amounts of boron. This lithium complex, during thermal evaporation, loses the nonluminescent ligand Meq.

Beryllium chelates such as bis[2-(2-hydroxyphenyl)pyridine]beryllium (Beq₂, **86**) (Scheme 3.74) emit pure blue light with an emission peak centered at 465 nm [269]. ITO/NPD/Bepp2/LiF/Al exhibited a maximum luminance of 15,000 cd/m² and a maximum luminescent efficiency of 3.43 lm/W (3.8 cd/A). The emission color may have contributions from both NPD and Bepp2 as stated by the authors.

5,5'-Bis(dimesitylboryl)-2,2'-bithiophene (BMB-2T, **242**) forms a stable amorphous glass and emits pure blue color with a high fluorescence QE of 86% in THF solution [270]. However, an OLED with ITO/m-MTDATA/TPD/BMB-2T/Mg:Ag emits with a broad emission due to an exciplex with TPD. The exciplex can be prevented by insertion of a thin layer of 1,3,5-tris(biphenyl-4-yl)benzene (TBB) between TPD and BMB-2T, leading to a pure blue emission. It seems that the boron complex or boron-containing compounds easily form an exciplex with common HTMs. Other similar blue emitter materials also demonstrate such behavior.

Other metal chelate materials of ligands such as benzimidazole have been disclosed in a Kodak patent as their beryllium or aluminum complexes (**244**) [271]. These materials generate very pure blue color within CIE range of (0.15–0.16, 0.12–0.17) [154,272].

3.6.3.4 White Fluorescent Organic Light-Emitting Diodes

White LEDs have many applications including as backlights in liquid crystal displays (LCDs), serving as light sources in fabricating full-color OLED displays using color filtering techniques and as general lighting sources.

The simplest method yet most complex structure for white OLEDs consists of three primary emission colors: blue, green, and red. Kido et al. reported using three emitter layers with different carrier transport properties to produce a white emission [273]. The multilayer structure of such an OLED is ITO/TPD/*p*-EtTAZ/Alq₃/Alq₃:Nile Red/Alq₃/Mg:Ag, in which a blue emission from the TPD layer, a green emission from the Alq₃ layer, and a red

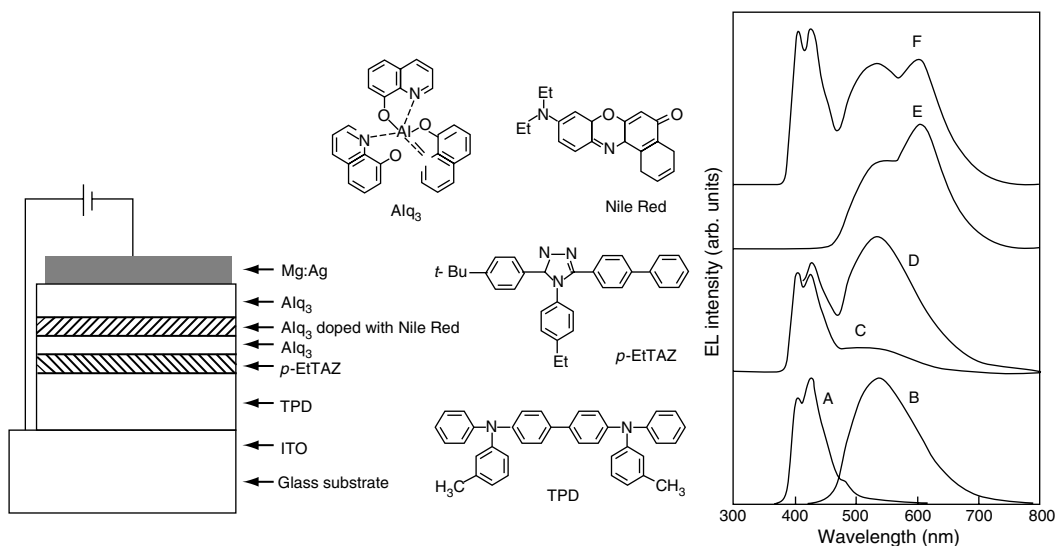


FIGURE 3.11 Configuration of the white OLED structure and the chemical structures of the materials (left). EL spectra of (A) ITO/TPD/p-EtTAZ/Mg:Ag; (B) ITO/TPD/Alq/Mg:Ag; (C) ITO/TPD/p-EtTAZ(5 nm)/Alq/Mg:Ag; (D) ITO/TPD/p-EtTAZ(3 nm)/Alq/Mg:Ag; (E) ITO/TPD/Alq/Alq:1% Nile Red/Alq/Mg:Ag; and (F) ITO/TPD/p-EtTAZ(3 nm)/Alq/Alq:1%Nile Red/Alq/Mg:Ag (right). (From Kido, J., Kimura, M., and Nagai, K., *Science*, 267, 1332, 1995. With permission.)

emission from the Nile red dye are produced (see Figure 3.11). These three primary color emissions produce the white light by carefully controlling the recombination zone and modulation of the doping level. A maximum luminance over 2200 cd/m² is achieved at 16 V.

This strategy, although it can be used to achieve white emission, leads to a device fabrication process, which is tedious and where the emission color is sensitive to the operating voltage and device structure parameters such as active layer thickness and doping concentration.

White emission can also be achieved by directly combining a blue emitter and an orange-red emitter as codopants. The combination of blue and orange-red emission generates white emission.

Cheon and Shinar demonstrated that by deposition of a thin layer of the blue emitter DPVBI on the DCM-2-doped NPD device (Figure 3.12), an efficient white OLED with a brightness of over 50,000 cd/m² and a power efficiency of 4.1 lm/W (external efficiency of 3.0%) could be achieved [274].

Tao et al. reported a very bright white OLED with much extended lifetime using 2,7-bis(2,2-diphenylvinyl)-9,9'-spirobifluorene (DPVSBF) doped with DCJTb as the EML. The device ITO/NPD/DPVSBF:0.2%DCJTb/Alq₃/LiF/Al showed a brightness of 1575 cd/m² with an EQE of 3.31%, a luminous efficiency of 8 cd/A, and a power efficiency of 5.35 lm/W at current density of 20 mA/cm² at 4.7 V. The CIE stayed constant at (0.32–0.35, 0.34–0.36) when driving voltages changed from 6 to 12 V.

More recently, a highly efficient and chromatically stable white OLED based on an anthracene derivative blue emitter doped with yellow-orange 5,6,11,12-tetraphenylnaphthacene (rubrene) was reported by Qiu's group [275]. By simple deposition of the mixture of the predoped rubrene and two anthracene derivatives in the host material NPD, a maximum brightness of 20,100 cd/m² with a peak EQE of 2.4% (5.6 cd/A) at 9 V and luminance independent CIE coordinates of (0.32, 0.34) has been achieved in an OLED with the device structure of ITO/NPD/ADN:2.5%TBADN:0.025%rubrene/Alq₃/Mg:Ag. The results also indicate that using two anthracene derivatives improves the morphology of the doped films

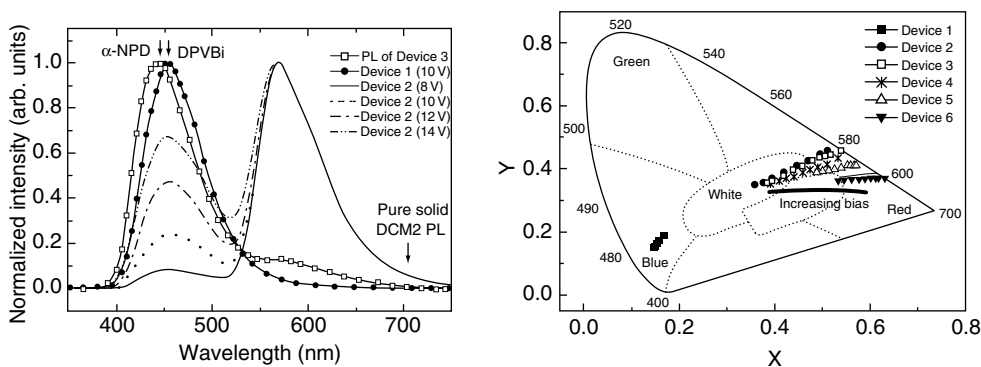


FIGURE 3.12 Normalized PL spectrum of Device 3 (open squares), EL spectrum of Device 1 at 10 V (solid circles), and the EL spectra of Device 2 biased at 8, 10, 12, and 14 V (solid and dashed lines) (left). Color coordinates of the EL vs. applied voltage. The EL of all of the devices blue-shifted with increasing voltage (right). (From Cheon, K.O. and Shinar, J., *Appl. Phys.*, 81, 1738, 2002. With permission.)

and depresses the crystallization of the dopant, which in turn contributes to the high performance and stability of the device. This strategy has also been applied to achieve a high-efficiency blue OLED by the same group.

A further strategy to achieve white emission uses rare-earth complexes. For example, a dysprosium complex (**245**) emits two band emissions: a yellow band (580 nm) corresponding to the $^4F_{9/2} \rightarrow ^6H_{13/2}$ transition and a blue band (480 nm) corresponding to $^4F_{9/2} \rightarrow ^6H_{15/2}$ transition of Dy^{3+} ion in the complex. Li et al. reported Dy-complex white emission OLEDs of a structure of ITO/PVK:Dy complex/Mg:Ag device [276]. Figure 3.13 shows the PL and EL emission spectra of such a complex and its device, respectively.

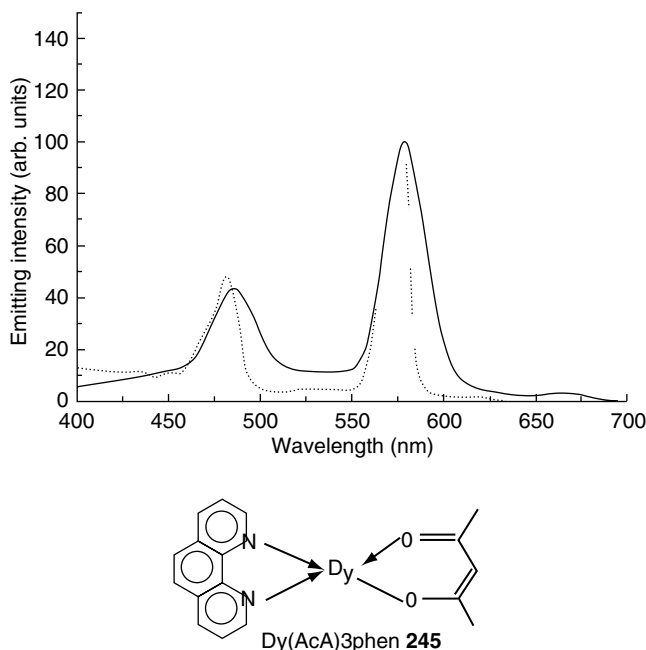
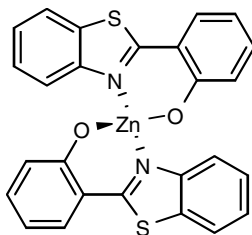
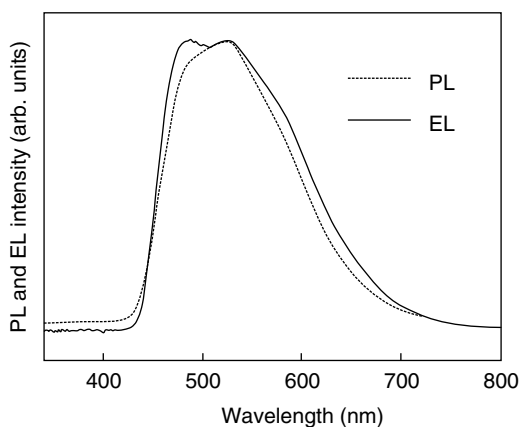


FIGURE 3.13 PL spectrum of thin film of $Dy(AcA)3phen$ and EL spectrum of the device ITO/PVK: $Dy(AcA)3phen$ /Mg:Ag. (From Hong, Z., Li, W.L., Zhao, D., Liang, C., Liu, X., and Peng, J., *Synth. Met.*, 111–112, 43, 2000. With permission.) The chemical structure of compound **245** was not correct in the original paper.

Stable white emission with CIE coordinates of (0.3519, 0.3785) was obtained in such a rare-earth-based OLED device. The authors mentioned that the QE of the device was not good, possibly due to the inefficient energy transfer process between the ligand and the rare-earth metal. A suitable choice of the ligand may improve this type of device performance.

The broad PL emission spectra of some metal chelates match the requirements for white emission. Hamada et al. investigated a series of Zn complexes and found bis(2-(2-hydroxyphenyl)benzothiazolate)zinc ($\text{Zn}(\text{BTZ})_2$, **246**) is the best white emission candidate. An OLED with a structure of ITO/TPD/ $\text{Zn}(\text{BTZ})_2$ /OXD-7/Mg:In showed greenish-white emission with CIE (0.246, 0.363) with a broad emission spectrum (FWHM 157 nm) consisting of two emission peaks centered at 486 and 524 nm (Figure 3.14) [277]. A maximum luminance of 10,190 cd/m^2 at 8 V was achieved. The electronic and molecular structure of $\text{Zn}(\text{BTZ})_2$ have been elucidated by Liu et al. [278]. There is evidence that the dimeric structure $[\text{Zn}(\text{BTZ})_2]_2$ in the solid state is more stable than its monomer $\text{Zn}(\text{BTZ})_2$. They also found that the electron transport property of $\text{Zn}(\text{BTZ})_2$ is better than that of Alq_3 .

Another interesting white emitting diode based on a boron hydroxyphenylpyridine complex (**247**) was reported by Wang et al. [279]. The PL emission of such a material in fluid solution as well as in the solid state is blue (450 nm). However, the EL spectrum of ITO/NPD/(mdppy)BF/LiF/Al gives a broad emission band with a stable CIE coordinate



$\text{Zn}(\text{BTZ})_2$
HOMO: -5.41 eV
LUMO: -2.65 eV

246

FIGURE 3.14 Chemical structure of $\text{Zn}(\text{BTZ})_2$ and its PL spectrum and EL spectrum of the device. (From Hamada, Y., Sano, T., Fujii, H., Nishio, Y., Takahashi, H., and Shibata, K., *Jpn. J. Appl. Phys.*, 35, L1339, 1996. With permission.)

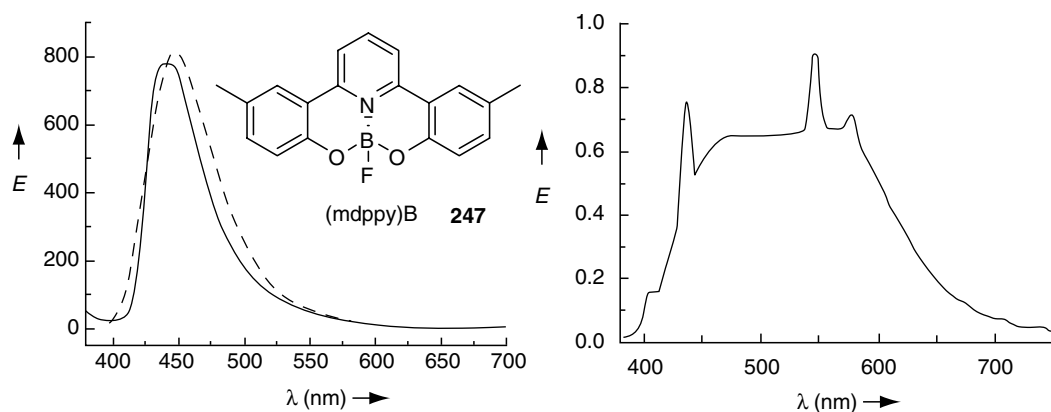


FIGURE 3.15 PL spectra of solid thin film of (mdppy)BF and NPD (dotted line) (left) and EL spectrum of ITO/NPD/(mdppy)BF/Al (right). (From Liu, Y., Guo, J., Zhang, H., and Wang, Y., *Angew. Chem. Int. Ed.*, 41, 182, 2002. With permission.)

of (0.30, 0.36) (Figure 3.15). The authors explained that this white emission is due to the formation of the exciplex between NPD and (mdppy)BF. A maximum efficiency of 3.6 lm/W (6.5 cd/A) with a luminance of 110 cd/m² at 5.5 V was achieved.

Very recently, a white emitting diode fabricated from a single-emitting component has been reported by Lee et al. [280]. An OLED with a structure of three layers ITO/TECEB/BCP/Alq₃/Mg:Ag emits a broad emission band from blue to red-orange with CIE coordinates of (0.298–0.304, 0.31–0.327). Interestingly, the long-wavelength emissions do not come from the interface exciplex nor from the Alq₃. They are produced by electronic excitation of TECEB (**41**) as evidenced by a single-layer device with an OLED structure of ITO/TECEB/Mg:Ag, which emits a similar spectrum as the three-layer device (see Figure 3.16). This identical EL spectrum implies that TECEB is the exclusive component responsible for the white emission. The authors propose that the longer wavelength emissions come from the singlet electromer (TECEB⁺/TECEB[−])* rather than the excimer as supported by its PL spectra in solution and in the solid state. In addition, and more likely, phosphorescence of TECEB may contribute to the longer wavelength emission as well, as confirmed by the transient luminescence lifetime decay test.

3.6.4 PHOSPHORESCENT DOPANTS

Some of the highest efficiency phosphorescent dopant materials are the iridium organometallic complexes — particularly when compared with lanthanide complexes, organic phosphorescents [281], and platinum complexes. The triplet lifetime of this class of materials is short, normally around 1–100 μs. The phosphorescent QE (ϕ_p) is high at room temperature and the color of the dopants can be easily tuned simply by modification of the ligand chemical structures. In addition, in contrast to platinum complex-based devices, the iridium complex-based PHOLEDs can exhibit only a slow drop-off in QE when operated at high current — in large part because of the reduced triplet–triplet quenching that results from the short excited state lifetimes.

The first iridium complex used in PHOLED devices was *fac* tris(2-phenylpyridine) iridium Ir(ppy)₃ complex [282]. It has a short triplet lifetime (~1 μs) and high phosphorescent efficiency (ϕ_p = 40% at room temperature in solution) [283]. However, in the solid state, most iridium complexes showed very low phosphorescent QE due to aggregate quenching. In most cases, the complexes have to be diluted in host materials to avoid reducing the

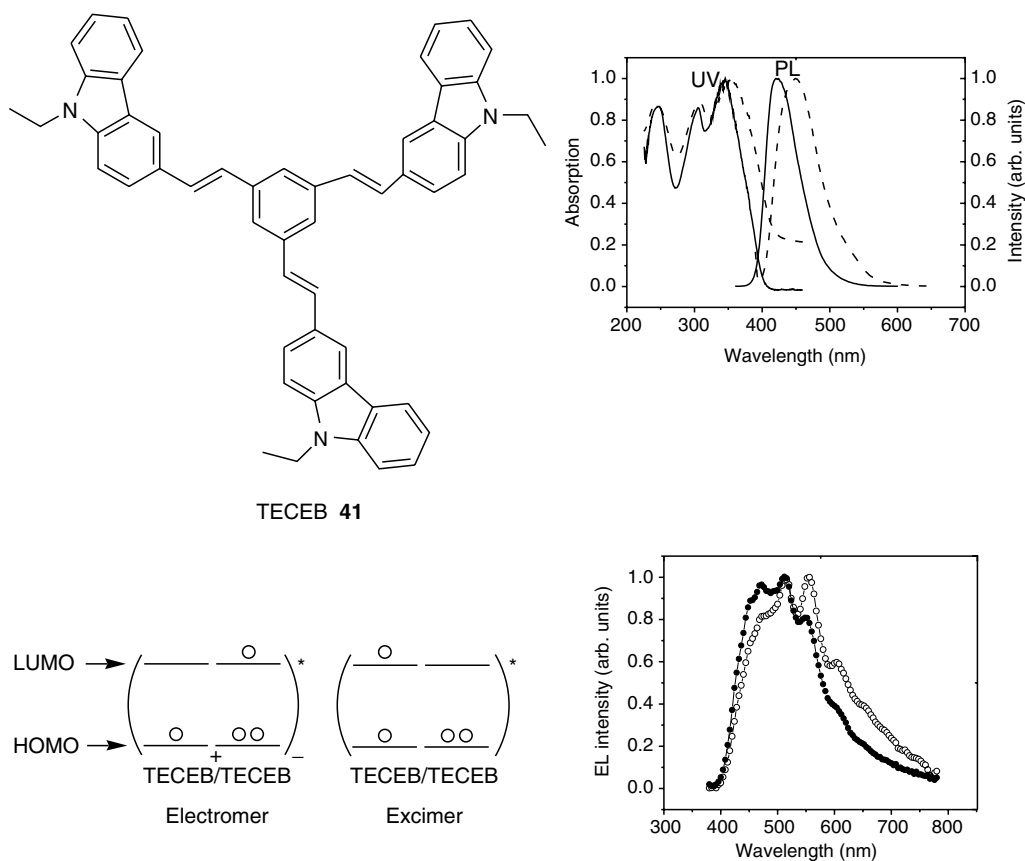
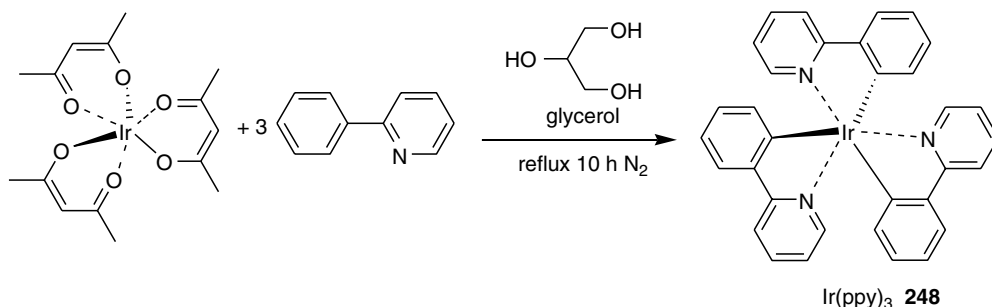


FIGURE 3.16 Chemical structure of TECEB and its UV/PL spectra in solution (solid lines) and in solid films (dotted lines) (up); The electromer and excimer of TECEB and EL spectra of ITO/TECEB/BCP/Alq₃/Mg:Ag (solid circles) and ITO/TECEB/Mg:Ag (open circles) (down). (From Li, J.Y., Liu, D., Ma, C., Lengyel, O., Lee, C., Tung, C., and Lee, S., *Adv. Mater.*, 16, 1538, 2004. With permission.)

phosphorescence efficiency. For example, Ir(ppy)₃ suffers aggregate quenching when the doping level is above 8 wt% in a CBP host [282]. In neat thin films, ϕ_p decreases below 1%, while in the doped film of 7.9% CBP host, ϕ_p reaches over 60% and can become as high as 90% when it is doped at 1% in polystyrene films [284]. Recent studies have demonstrated that ϕ_p of 2% Ir(ppy)₃ doped into CBP gave 100% phosphorescence QE [285]. PHOLEDs fabricated with the structure ITO/NPD/CBP:Ir(ppy)₃/BCP/Alq₃/Mg:Ag showed a QE and a power efficiency of 8% (28 cd/A) and 31 lm/W, respectively. Later, using the same device configuration but with a slightly higher dopant concentration of 6.5% Ir(ppy)₃ in CBP and Al/Li₂O as the cathode instead of Mg:Ag, a Japanese group reproduced the device performance with 1.8 times higher QE compared with the original Princeton group data [286].

3.6.4.1 Synthesis of Iridium Complexes

The facial isomer of Ir(ppy)₃ (**248**) was isolated as a by-product (10%) when reacting IrCl₃H₂O with excess of the ligand 2-phenylpyridine (PPY), which gives a major component of dichloro-bridged dimer [Ir(ppy)₂Cl]₂ (72%) [287]. An improved method to synthesize *fac* tris-ortho-metalated iridium complexes in high yield involves utilizing the commercially available starting material Ir(acac)₃ (acac = 2,4-pentanedionate or acetylacetonate) [288]. Scheme 3.75 shows the reaction.



SCHEME 3.75 Schematic reaction to synthesis *fac*-Ir(ppy)₃ via bidentate acac ligand exchange.

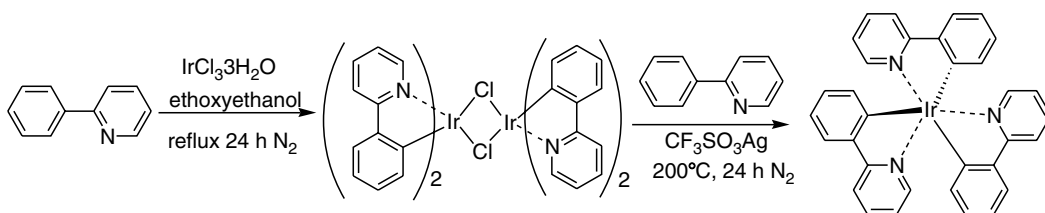
Due to the *trans* effect of Ir–C bonds in the ligand exchange, the product is largely the *fac* isomer. Compared with the direct ligand reaction with IrCl₃·H₂O, this method gives relatively high yields (~50%) of the desired *fac*-Ir(ppy)₃ or its derivatives.

Almost 10 years later, Güdel et al. proposed a general synthetic method for facial tris cyclometalated Ir³⁺ and Rh³⁺ complexes by reaction of dichloro-bridged dimers of Ir(ppy)₂ with excess ppy ligand using AgCF₃SO₃ as a halide scavenger and promoter (Scheme 3.76) [289].

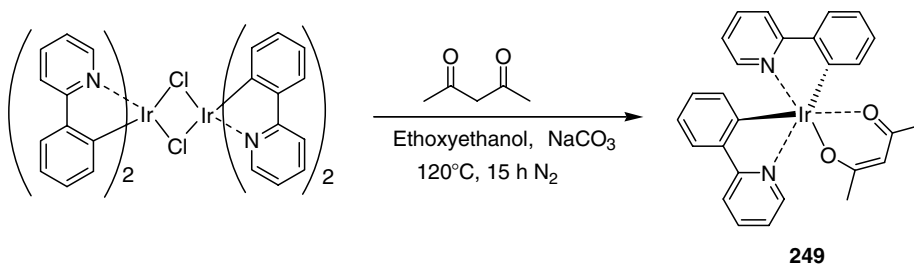
The first step is the synthesis of chloro-bridged dimer by reaction of IrCl₃·H₂O with excess of the C[^]N ligand. This dimer can be converted to either its tris-ligand complex or other monomeric complexes by replacing the chloride bridges with a third C[^]N ligand or some other bidentate anionic ligand.

This two-step synthetic method can thus be extended to the synthesis of bis-cyclometalated Ir(III) complexes (C[^]N)₂Ir(LX) (**249**) (Scheme 3.77) [290].

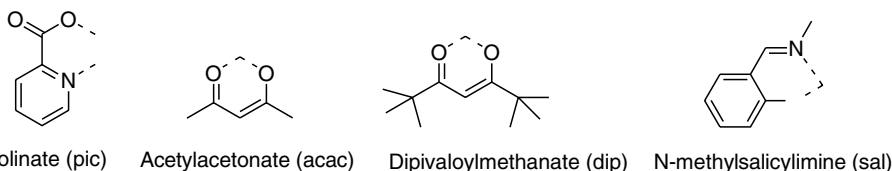
The photoactive ligands can be phenylpyridines, quinoline derivatives, or benzimidazoles and the ancillary ligand can be selected from the following structures in addition to the photoactive ligand itself (Scheme 3.78) [291].



SCHEME 3.76 Schematic reaction to synthesis *fac*-Ir(ppy)₃ via dichloro-bridged dimers of Ir(ppy)₂.



SCHEME 3.77 Schematic reaction to synthesis *fac*-Ir(ppy)₂(acac) via dichloro-bridged dimers of Ir(ppy)₂.



SCHEME 3.78 Chemical structures of some bidentate and monoanionic ancillary ligands.

By using different ligands (Scheme 3.79), Thompson's group has successfully designed a series of highly phosphorescent iridium complexes with the emission color tuned from green to red [292]. Their results indicate that there can be dramatic phosphorescent color emission changes when the C[^]N ligand changes, while changes in the ancillary ligand lead to only minor shifts of the emission colors.

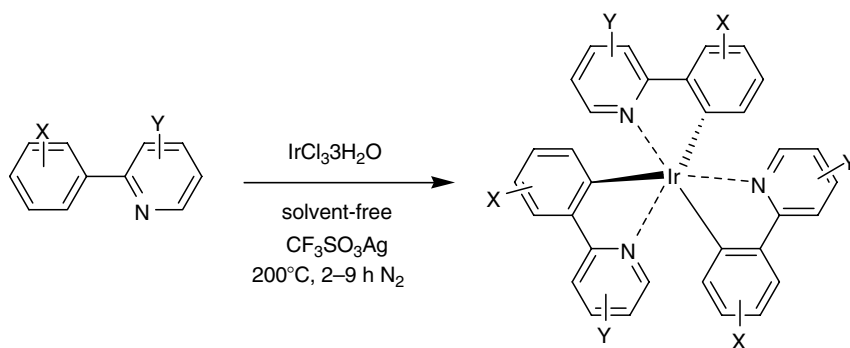
Recently, a facile synthesis of substituted 2-aryl pyridine ligands was reported by Lohse et al. [293]. DuPont researchers have also successfully synthesized a series of fluorine-substituted Ir complexes based on these same families of ligands using a simplified synthetic approach (Scheme 3.79) [294].

In the following sections, different phosphorescent iridium complexes will be discussed.

3.6.4.2 Green Phosphorescent Dopants

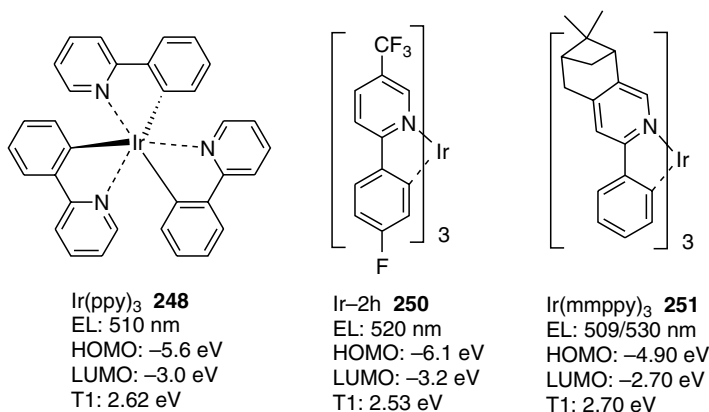
3.6.4.2.1 Phenyl Pyridine Iridium Complexes

Scheme 3.80 lists some iridium complexes used in green PHOLEDs. Ir(ppy)₃ is the original green dopant as mentioned earlier. The peak wavelength of Ir(ppy)₃ thin films is 510 nm with an FWHM of 70 nm. The color of the Ir(ppy)₃-based device corresponds to CIE coordinates of (0.27, 0.63). The doped device of 6% Ir(ppy)₃ in a CBP host exhibited high QE performance (~8%), however, the neat thin film of Ir(ppy)₃ only gave ~0.8% QE, almost ten times lower than the doped device. By introducing electron-withdrawing fluorine groups, the DuPont team was able to demonstrate that the thin neat film of Ir-2h (**250**) could give high-efficiency device performance [295]. The result is in accordance with the photoluminescent QE measurement. In the thin film the QE of Ir-2h is ten times higher than that of Ir(ppy)₃. This, in part, is due to less pronounced self-quenching processes in the bulky substituted Ir-2h complex. The bulky substituent effect to suppress the self-quenching of the iridium dopant



X, Y selected from H, F, CF_3 , OCF_3 , OCH_3 , Cl, CN, etc.

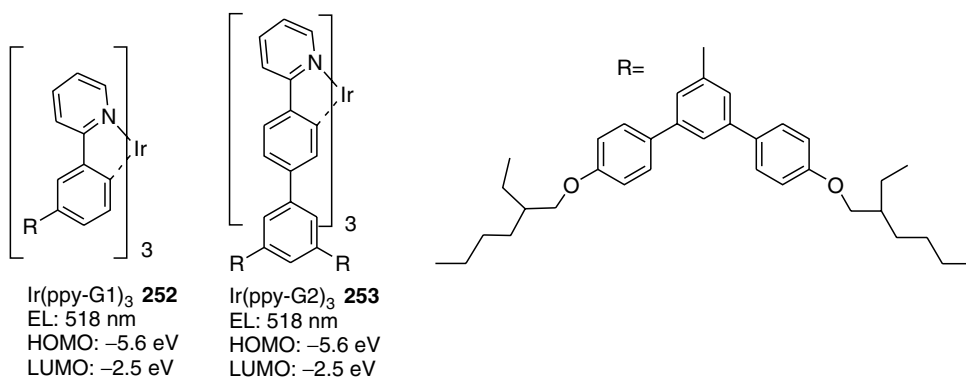
SCHEME 3.79 A new synthetic method to Ir(ppy)₃.



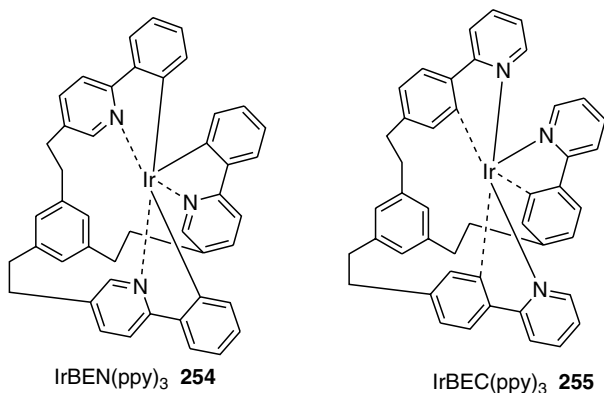
SCHEME 3.80 Green iridium complexes of Ir(ppy)₃ derivatives.

was clearly demonstrated by introducing even more bulky substituents such as in the iridium complex Ir(mpppy)₃ (**251**). This iridium complex also showed higher solid state QE.

Another way to increase the QE of iridium complexes is by elaboration into dendrimeric structures, which usually consist of surface groups, dendrons, and cores (**252**, **253**) (Scheme 3.81). Dendrimers have some advantages such as a convergent synthesis that allows for a modular approach to different generations of the dendrimers, the fine tuning of the electronic properties and processibility, the flexibility to control the intermolecular interactions, and the ease of the purification process. Burn et al. reported a series of iridium dendrimer complexes and have successfully fabricated solution processible PHOLEDs by spin coating of the host and guest mixture solution to the ITO substrate followed by cathode deposition [296]. The dendrimer complexes also exhibit high photoluminescent QE compared with nondendrimeric iridium complexes. It is interesting to note that the higher the generation number of the dendrimers, the higher the QE it has [297]. Spin coating 20% Ir(ppy-G2)₃ in CBP as an active layer, a maximum EQE and power efficiency were 8.1% (28 Cd/A) and 6.9 lm/W, respectively. Similar devices made using Ir(ppy)₃ demonstrated ten times lower QE. High-efficiency PHOLEDs have been achieved in double-layer devices with the device configuration of ITO/Ir(ppy-G1)₃:TCTA/TPBI/LiF/Al by selecting 4,4',4''-tris(*N*-carbazolyl)triphenylamine (TCTA) as the host material and using TPBI as the ETL or HBL. The best devices have a maximum efficiency of 40 lm/W (55 cd/A) at 4.5 V and 400 cd/m². The low turn-on voltage of 3.0 V and a maximum brightness of 12,000



SCHEME 3.81 Solution processible iridium dendrimer complex.



SCHEME 3.82 Iridium complex based on star-linked ligands.

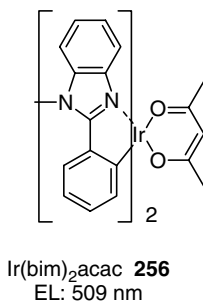
cd/m² at 7 V have been observed. The devices are modestly stable but not yet comparable with the more complex vacuum-evaporated Ir(ppy)₃-based devices containing both HTL and ETL [298]. The high efficiency is attributed to the excellent uniform film-forming properties of the dendrimer Ir complex in the host layer, and the balanced charge injection.

Color tuning the green emission of Ir(ppy)₃ has been achieved by substitution of donor or acceptor groups either on the phenyl or on the pyridine ring. Another method to tune the color of emission is through ligand changes. While the phosphorescent QE of Ir(ppy)₃ in solution at room temperature is about 40–50%, a Swiss group could increase the QE close to 100% by changing the ligand configuration [299]. By introducing ligands such as CN-, NCS-, and NCO-, which have strong ligand field stabilization energy, a large gap between the E_g and LUMO of the ligand is created. This approach may allow for tuning the emission color to the blue range. The QE is also increased. Unfortunately, such materials are unstable for vacuum deposition due to the nonvolatile nature of these iridium complex salts. Though the materials may be solution-processible, their ionic charge makes it unlikely that long-lived devices can be achieved.

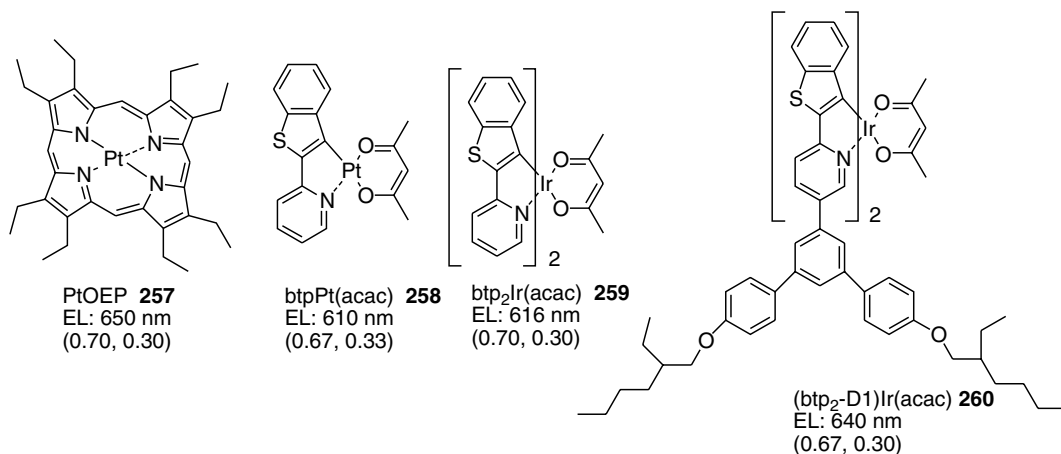
Ma et al. at PPG recently applied for patents on a series of iridium star-like bidentate complexes [300]. Examples of two such green dopants are shown in Scheme 3.82 (**254**, **255**). OLEDs fabricated using the dopants showed green emission with higher EQE and enhanced stability compared with a similar Ir(ppy)₃-based device.

3.6.4.2.2 Benzoimidazole Iridium Complexes

Another high-efficiency series of iridium complexes is based on benzoimidazole ligands complex such as in Ir(bim)₂acac (**256**) (Scheme 3.83) [301]. Ir(bim)₂acac exhibits green



SCHEME 3.83 Chemical structure of green Ir complex based on benzoimidazole ligands.



SCHEME 3.84 Chemical structure of red-phosphorescent dopants.

phosphorescence in dilute CH₂Cl₂ solution with a maximum peak emission at 509 nm and a QE of about 40%. It can be doped as high as 12% without losing its QE. Disclosed by PPG and the UDC companies, this green dopant also showed improved EL performance as compared with an equivalent Ir(ppy)₃ device [302].

3.6.4.3 Red Phosphorescent Dopants

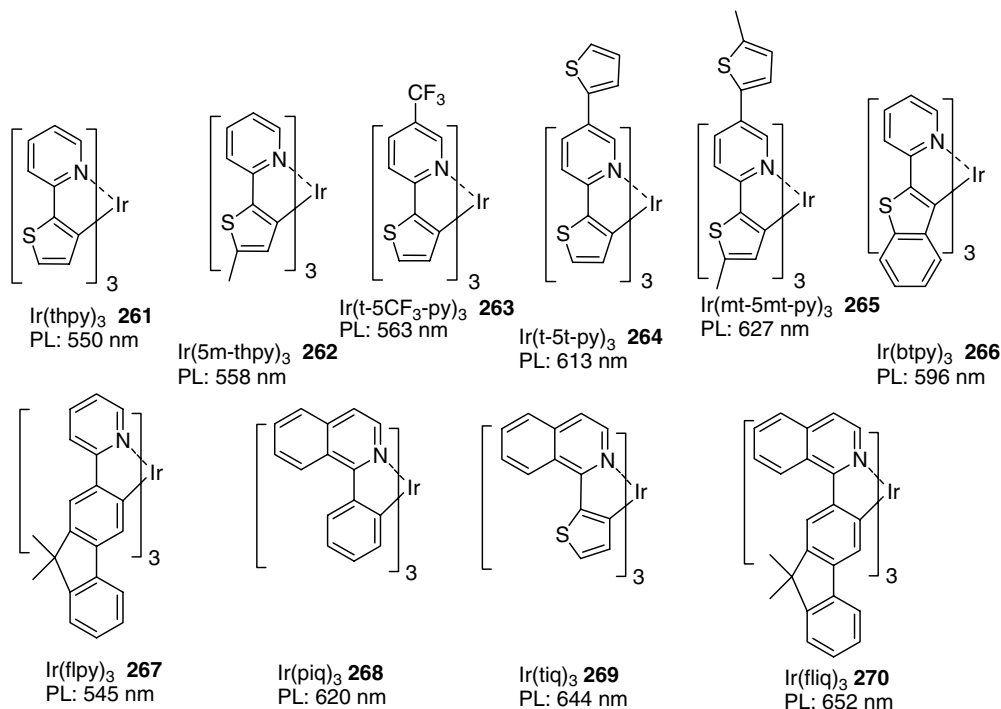
3.6.4.3.1 2-Benzo[b]thiophen-2-yl-Pyridine Iridium Complexes

Pt(II) octaethylporphine (PtOEP) was one of the first nonlanthanide phosphorescent organo-metallic complexes used in OLED devices [303]. It showed a very nice narrow red emission band centered at 650 nm. The drawback of such platinum complexes is their long triplet lifetime, which leads to low QE especially in high-current conditions, rendering them poor candidates for phosphorescent OLED applications. The iridium chelate complex, btp₂Ir(acac) (Scheme 3.84), however, showed high QE device performance. Introducing dendrimer substituents, a solution-processible iridium red complex (btp₂-D1)Ir(acac) gave pure red emission.

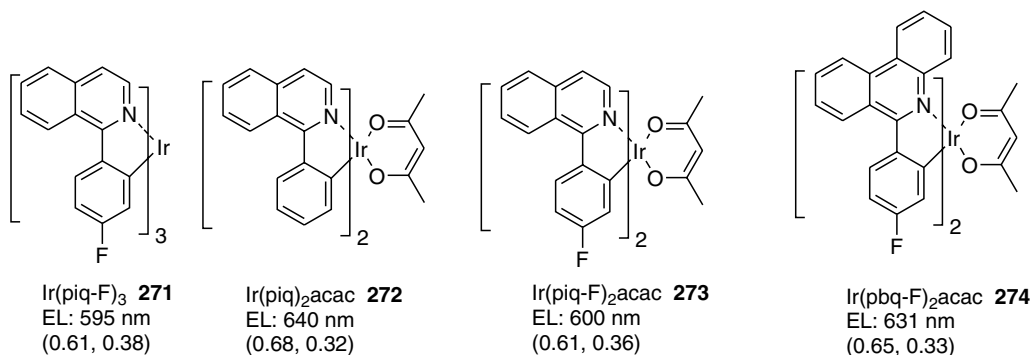
3.6.4.3.2 Phenylisoquinoline Iridium Complexes

To create pure red phosphorescent emission, a systematic study of the ligand structure and the emission properties was carried out by Tsuboyama et al. (Scheme 3.85) [304]. It was found that the red-shift of the phosphorescence is attributable to introduction of more conjugated ligands.

Recently, Tao and Liu's group reported a series of highly efficient red-emissive phenylisoquinoline iridium complexes (Scheme 3.86) [305]. These iridium complexes showed triplet lifetimes (1.2–2.5 μs in CH₂Cl₂ and 0.15–0.56 μs in solid-film states) considerably shorter than that of Ir(btp)₂(acac) (6 μs in THF). The phosphorescent QEs of these complexes are also higher. Devices fabricated using the configuration of ITO/NPD/6%Ircomplex:CBP/BCP/Alq₃/Mg:Ag exhibited bright orange-red or orange color emission. It is interesting to note that the emission color is independent of the applied voltage. The EQE decreased very slowly with increasing current, in contrast with the Ir(btp)₂(acac)-based device, ranking this class of materials as attractive candidates for red emission display applications.



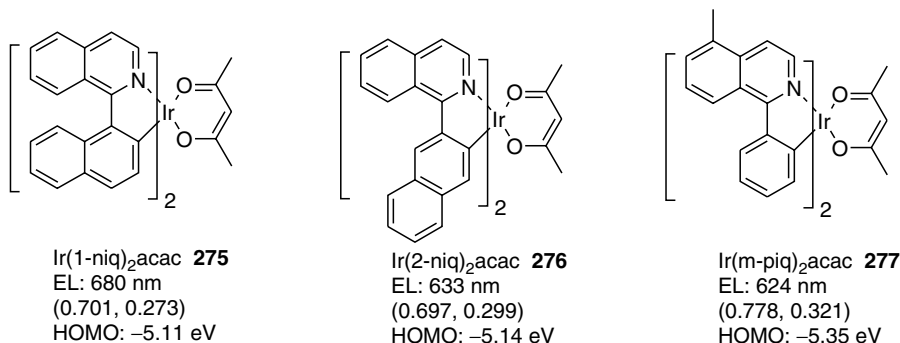
SCHEME 3.85 Chemical structure of some orange to red phosphorescent dopants.



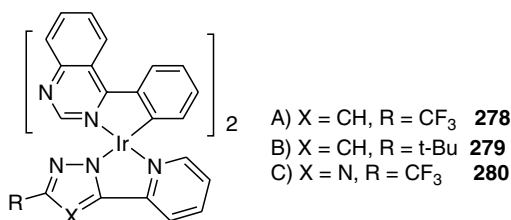
SCHEME 3.86 Chemical structures of some phenylisoquinoline iridium complexes.

Following on from the isoquinoline iridium complexes, various modifications of the ligands on iridium have been designed in order to achieve high efficiency as well as highly stable devices. Yang et al. report a series of phenyl and naphthalene ligand red iridium complexes (Scheme 3.87) [306]. Red phosphorescent iridium dendrimers have been prepared by the Burn group [307].

Just as with nondoped red fluorescent dyes, nondoped phosphorescent iridium complexes consisting of two chelating phenyl-substituted quinazoline and one (2-pyridyl) pyrazolate or triazolate have recently been reported by Chen et al. (**278–280**) (Scheme 3.88) [308]. All of these complexes exhibited bright red phosphorescence with relatively short excited state lifetimes of 0.4–1.05 μ s. PHOLEDs fabricated using the compounds A and B with relatively



SCHEME 3.87 Chemical structure of red-phosphorescent dopants.



SCHEME 3.88 Chemical structure of red iridium complexes.

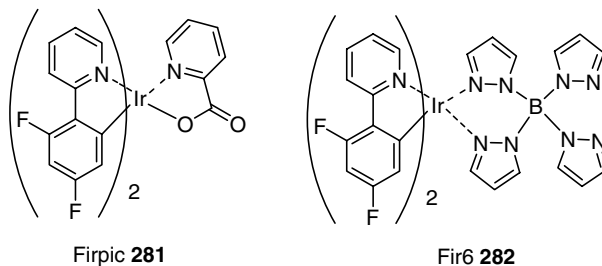
higher doping level up to 21% gave saturated red emission 626 nm, and 652 nm corresponding to CIE (0.66, 0.34), (0.69, 0.31), respectively. The EQE of a doped device is ~6.3%. The nondoped device fabricated by using complex A showed an EQE of 5.5% at 8 V, and a current density of 20 mA/cm² with luminance as high as 5780 cd/m². The high efficiency of phosphorescence under high doping level is attributed to the relatively very short emission lifetime.

3.6.4.4 Blue Phosphorescent Dopants

3.6.4.4.1 Phenylpyridine Complexes

In the case of blue emitters, phosphorescent materials still lag behind their fluorescent counterparts. One particular problem is finding a material with a high-enough triplet state to correspond to a blue emission wavelength. Furthermore, finding a host into which this material may be doped without quenching the emissive state is a major challenge since the triplet state of the host must be even higher in energy than the emitter triplet state. The high-energy triplet state of a blue phosphorescent emitter appears to be difficult to maintain without degradation, therefore lifetimes of phosphorescent blues are a problem. Most work reported in this area has focused on a material dubbed Firpic and developed by the USC and Princeton groups (**281**, **282**) (Scheme 3.89) [309,310].

Heteroleptic iridium(III)bis[(4,6-di-fluorophenyl)-pyridinato-*N*,*C*2'-picolinate] (Firpic) and bis(4',6'-difluorophenylpyridinato)tetrakis-1-pyrazolyl)borate (Fir6) use fluoro-substituted phenylpyridine ligands and an anionic 2-picolinic acid or poly(pyrazolyl)borate as an auxiliary ligand, respectively [311]. Devices fabricated by using ITO/CuPc/NPD/CBP or mCP:6%Firpic/BAIq/LiF/Al exhibited a maximum QE of 6.1% and a luminous power efficiency of 7.7 lm/W with a peak luminance of 6400 cd/m². The EL performance has been improved by using a graded doped EML in a host DCB, which shows a peak power efficiency of 15.4 cd/A and a maximum brightness of 35,000 cd/m², a sharp increase



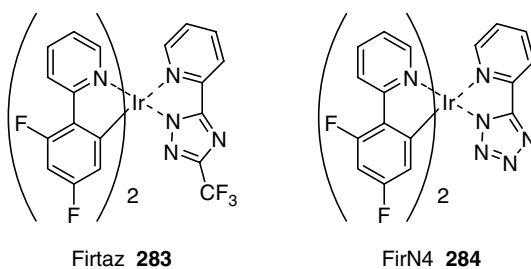
SCHEME 3.89 Chemical structures of some blue-phosphorescent dopants.

compared to the conventional PHOLED, which has a peak power efficiency of 8.7 cd/A and a maximum brightness of 17,000 cd/m² [312]. This material, in a suitably high energy carbazole host, has given up to 20 cd/A but with poor blue chromaticity CIE (0.17, 0.34), which is a common problem with such materials resulting from the long wavelength emission tail that seems to arise from vibronic structure. Improvement of color purity and QE using Fir6 as blue dopant and Si-based large band-gap material as a host gave peak quantum and power efficiencies of 12% and 14 lm/W in UGH2, with a CIE (0.16, 0.26) [313]. Again, lifetimes of such systems are still problematic with only hundreds of hours of operation being claimed.

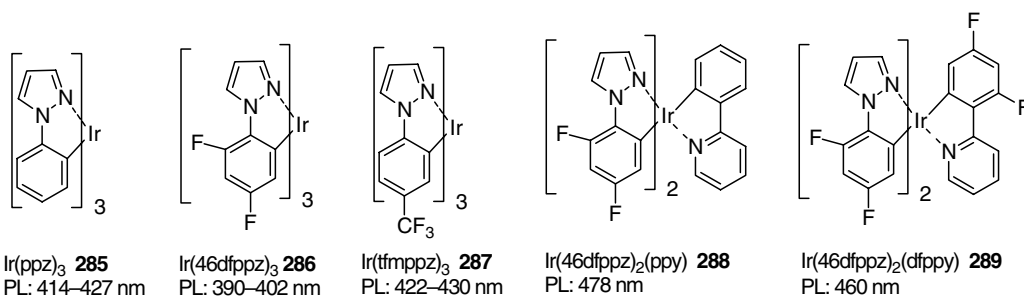
Chen and coworkers have developed two new phosphorescent blue emitters, which have two identical 2-(2,4-difluorophenyl)pyridine ligands and are derivatives of the Firpic compound, iridium(III) bis(4,6-difluorophenylpyridinato)-3-(trifluoromethyl)-5-(pyridin-2-yl)-1,2,4-triazolate (Firtaz) and iridium(III) bis(4,6-difluorophenylpyridinato)-5-(pyridin-2-yl)-1*H*-tetrazolate (FirN4) (Scheme 3.90) [314]. Both these two blue emitters show a 10-nm blue-shift of the emission compared with Firpic. Unfortunately, the efficiency of such blue emitters is inferior to those of Firpic and Fir6. There is no lifetime data reported for such devices.

3.6.4.4.2 Phenylpyrazole Complexes

In addition to using pyrazole as the auxiliary ligand to blue-shift the emission of phenylpyridine homoleptic iridium complexes, replacing the pyridine ring of phenylpyridine ligands with a pyrazole ring can also widen the HOMO and LUMO band gap of the complexes as a consequence of lowering the HOMO and raising the LUMO energy levels of the complexes, respectively. Thompson's group synthesized a series of blue homoleptic phenylpyrazolyl iridium complexes (**285–289**) (Scheme 3.91) [315]. However, these homoleptic complexes showed strong ultrapure blue to blue emission (390–440 nm) only at very low temperature (77 K) but, unfortunately, they all showed very weak emission at room temperature, rendering them unsuitable for PHOLED applications. Although heteroleptic phenylpyrazolyl–phenylpyridine complexes showed moderate emission at room temperature, the emission color is bluish-green, and there is no device data reported for these complexes [316].



SCHEME 3.90 Chemical structure of blue-phosphorescent dopants.



SCHEME 3.91 Chemical structure of blue-phosphorescent dopants.

Very recently, UDC claimed that they have successfully achieved a luminescent efficiency of 22 cd/A for a sky blue PHOLED with CIE (0.16, 0.37) with over 15,000 h operating lifetime at 200 cd/m² [317]. The possible chemical structure of this sky blue emitter probably involves replacing the phenyl ring of phenylpyrazolyl with an extended fluorenyl unit, which has effective emission at room temperature, as presented at a recent ACS meeting by Forrest [318].

The progress with phosphorescent blue emitters suggests that it may be quite possible to achieve high-efficiency blue phosphorescent candidates by carefully designing the proper ligands coupled with appropriate selection of auxiliary ligands.

3.6.4.5 White Phosphorescent Organic Light-Emitting Diodes

As an alternative backlight source, with their potential for high efficiency, low cost, and large area fabrication, white organic phosphorescent LEDs have been paid great attention for lighting applications. White emission can be achieved either through multilayer OLED structures, which combine different EMLs to cover the entire visible spectrum, or through blue or bluish-green emitters in combination with its excimer emission to achieve the desired white light emission. An ideal white light source has a CIE (0.33, 0.33).

As with fluorescent white OLEDs, the first attempt to achieve white PHOLEDs was described by the Forrest group using multilayer device structures intergrating blue (Firpic), yellow ($\text{bt}_2\text{Ir}(\text{acac})$), and orange-red ($\text{btp}_2\text{Ir}(\text{acac})$) phosphorescent dopants (Figure 3.17) [319]. Through control of the dopant concentration and thickness, white emission with desired color can be achieved.

By using a large band-gap host material UGH2, selecting different phosphorescent dopants, and controlling the doping concentration and thickness, a very high-efficiency white PHOLED was presented by the Forrest group. The devices have various white emission colors with CIE coordinates varying from (0.43, 0.45) at 0.1 mA/cm² to (0.38, 0.45) at 10 mA/cm², with a color rendering index (CRI) of 80 and a maximum EQE up to 46 lm/W [320].

A very high-efficiency white emitting OLED fabricated by the combination of a fluorescent blue emitter and a phosphorescent red emitter was reported by Qin and Tao [321]. The device structure is ITO/NPD30 nm/TCTA:2%TPP20 nm/BCP:0.4%Ir(piq)₃20 nm/Alq₃40 nm/Mg:Ag. The white emission contributed from both fluorescent blue light and phosphorescent red light was observed between 10 and 15 V and a maximum white light luminance of 1076 cd/m² with CIE (0.27, 0.24) with an efficiency of 1.35 cd/A was achieved. This practical approach to white light emitting is a clever strategy considering the currently available, relatively stable, and high-efficiency blue fluorescent, and very high-efficiency red phosphorescent materials, though further work still needs to be done to optimize the device performance.

The above strategy, using three primary colors as phosphorescent dopants, has a big problem in controlling the efficiency of the energy transfer, which eventually will result in

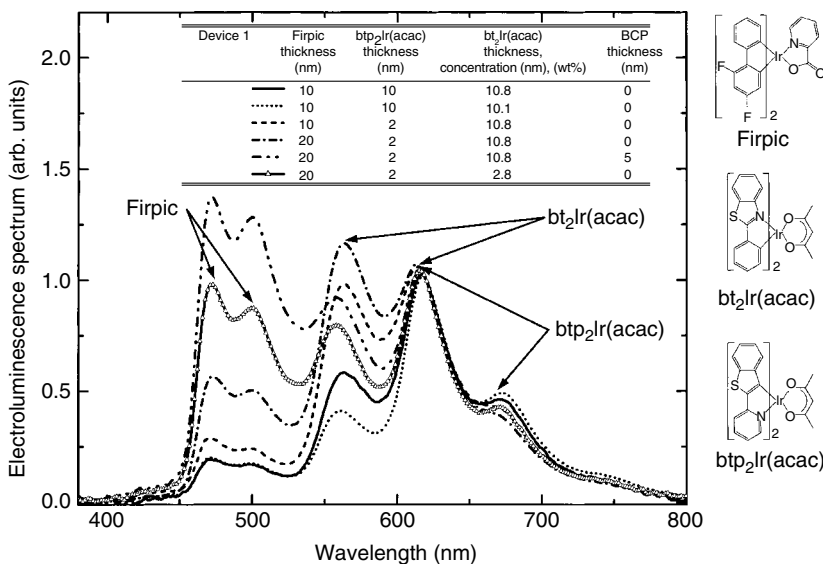


FIGURE 3.17 Variation, at 10 mA/cm², in the electroluminescence spectra with layer thickness, dopant concentration, and the insertion of an exciton or hole blocking layer between the Firpic and btp₂Ir(acac) doped layers for the Device 1. The molecular structural formulae of btp₂Ir(acac), Firpic, and bt₂Ir(acac) (right). (From D'Andrade, B.W., Thompson, M.E., and Forrest, S.R., *Adv. Mater.*, 14, 147, 2002. With permission.)

unbalanced brightness of the colors. In addition, the difficult manufacturing processes of such an approach will be difficult to render the approach to be cost-effective. One alternative approach to achieve white emission is by using a phosphorescent excimer (similarly to what was described in white fluorescent OLEDs). The excimer dopant can emit a broad spectrum and high-quality white emission may simultaneously arise from its monomer and aggregate states.

By a careful study of the optical and electronic properties of phosphorescent dopants with host material CBP, the Forrest group selected two blue phosphorescent dopants Firpic and platinum(II) [2-(4,6-difluorophenyl)pyridinato-N,C2'] (2,4-pentanedionato) (FPt1) as excimers in their white PHOLED structure (Figure 3.18) [322]. Although the planar structure of the dopant FPt1 forms a broad excimer emission, the codopant of a blue dopant of Firpic (Firpic does not form excimer emission) with FPt1 balances the emission color and produces the desired white emission with CIE (0.33, 0.44). Both of these blue dopants have a similar triplet energy and overlapped emission spectra, which is good for energy transfer when using CBP as a host. Since the triplet energy level of CBP is above the triplet levels of the two dopants, an endothermal triplet energy transfer process is expected between the host and the dopants. Nevertheless, a white PHOLED fabricated using two dopants where each doping concentrations is 6% in CBP produces a bright white emission with a maximum EQE of 4.4% (10.1 cd/A), and a luminance of 34,000 cd/m² at 16.6 V with a power efficiency of 4.8 lm/W and a CRI of 78.

As described by the same group, efficient white electrophosphorescence has been achieved with a single emissive dopant by screening a series of dopant molecules based on platinum(II) [2-(4,6-difluorophenyl)pyridinato-N,C2'] β-diketonates, which have a blue monomer emission (λ_{max}: 468, 500, 540 nm) and a broad orange aggregate emission (λ_{max}: 580 nm) in the doped host system. Since the intensity of the orange band increases relative to the blue monomer emission as the doping level increases, by judicious control of the ratio of monomer to

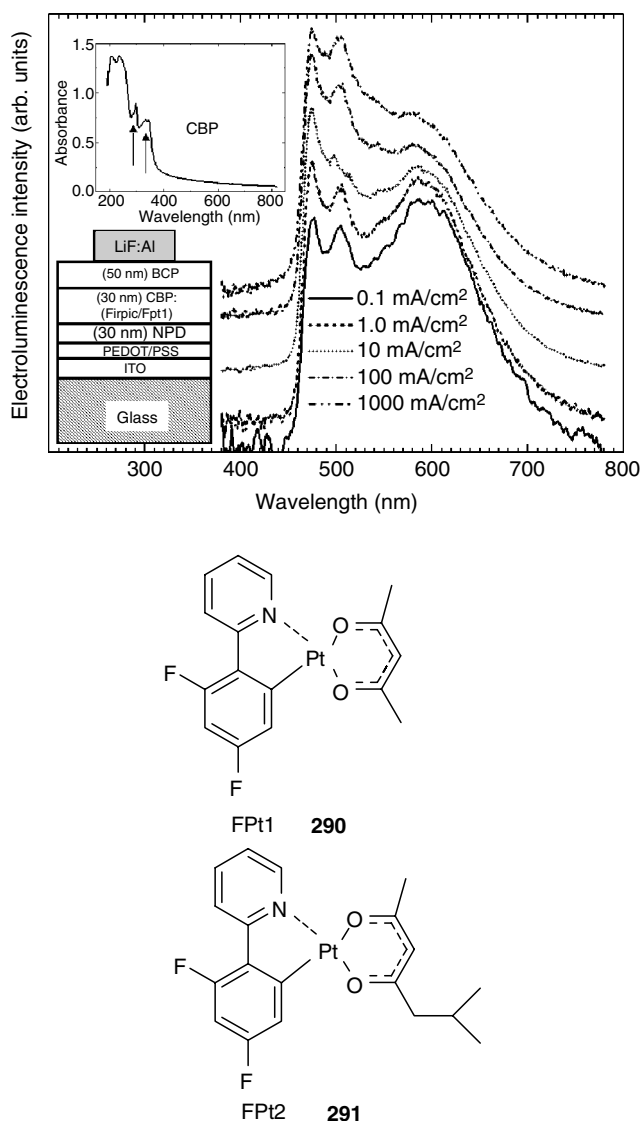


FIGURE 3.18 Normalized EL spectra of the white PHOLED at several current densities; upper insert: Absorption of neat CBP films (100 nm) and lower insert: A White PHOLED structure (left) and the chemical structures of phosphorescent dopants (right). (From D'Andrade, B.W., Brooks, J., Adamovich, V., Thompson, M.E., and Forrest, S.R., *Adv. Mater.*, 14, 1032, 2002. With permission.)

aggregate emission, the doping concentration, the degree of steric bulk on the dopant, and the choice of the host material, a pure white emission spectrum close to standard white illumination has been achieved in a white PHOLED using a single phosphorescent excimer dopant platinum(II) [2-(4,6-difluorophenyl)pyridinato-N,C2'] (6-methyl-2,4-heptandionato-O,O) (FPt2). A high-efficiency white PHOLED with a structure of ITO/NPD/Irppz/mCBP: 10–20% FPt2/BCP/Alq₃/LiF/Al emits white emission with CIE (0.36, 0.44) and CRI value above 67 at both low (1 cd/m²) and high luminescence (500 cd/m²) levels. The devices gave a peak EQE of 6.4% (12.2 lm/W, 17.0 cd/A) [323].

The triplet phosphorescent excimer approach to a white PHOLED requires only energy transfer from the host to the monomer dopant or charge trapping on the dopant but lacks energy transfer to the excimer owing to the zero ground state of the excimer. This strategy avoids the cascade energy transfer processes in different color dopants and allows simple optimization of doping levels to achieve the desired white color.

While the above methods have been widely used in white OLED research, other strategies can be envisioned such as (1) using stacked OLED structures, where blue, green, and red OLEDs operate independently to achieve the combined white color emission [324] (2) using one blue OLED coupled with green and red emitters resulting in white emission [325], and (3) employing multimode optical cavities to capture white emission, which has been investigated in Alq₃-based OLED [326]. However, there are pros and cons to using all of these methods.

White PHOLEDs may become the most effective light source of the future due to their 100% internal emission efficiency, which raises the possibility to approach the upper limit of the maximum external power efficiency of 80 lm/W with CRI >80 [327]. Currently, the major challenge facing such white PHOLEDs are their lifetime and color stability under operating conditions.

3.7 STABILIZERS AND HOLE- AND ELECTRON-BLOCKING MATERIALS

3.7.1 STABILIZERS

High-efficiency fluorescent red OLEDs usually use a doping system, i.e., by doping a red dopant into a suitable host material. The problem of such a system is that the resultant emission color is not pure red due to the poor energy transfer processes from the host to the guest. Hamada et al. proposed a new doping method using a second dopant as a sensitizer to assist the energy transfer from the host to the first red dopant [328]. Two OLED devices were fabricated in the device structures of a conventional red OLED (cell [2,0]): ITO/CuPc 20 nm (HIL)/NPD 50 nm (HTL)/Alq₃:DCM (2%)40 nm (EML)/MgIn, and new OLED (cell [2,5]): ITO/CuPc 20 nm (HIL)/NPD 50 nm (HTL)/Alq₃:DCM2 (2%):rubrene (5%)40 nm (EML)/MgIn. In this case, DCM2 was used as the red dopant, rubrene was used as the second dopant or sensitizer, and Alq₃ was used as the host material. Comparing the electroluminescent spectra of cell [2,0] and cell [2,5] as shown in Figure 3.19, it is clear to see that the cell [2,5] with 5% rubrene emits pure red color whereas cell [2,0] has additional emission from the host Alq₃ which causes an orange

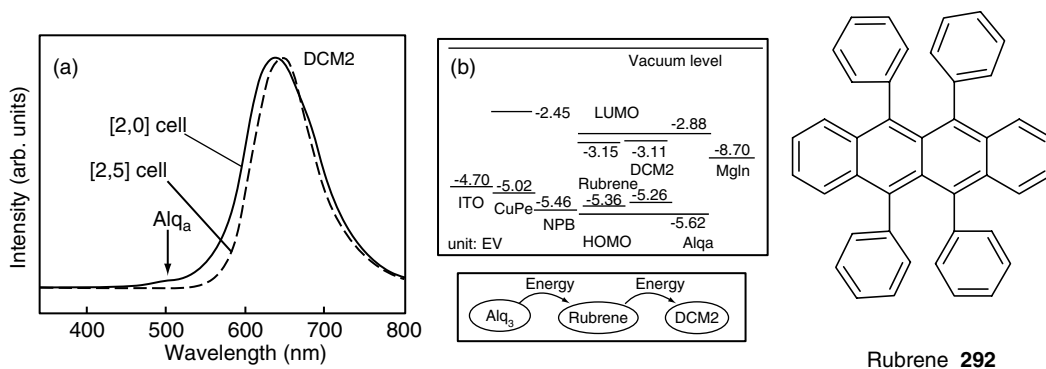


FIGURE 3.19 (a) EL spectra of cell [2,0] and cell [2,5]. (b) the energy diagram of cell [2,5]. (From Hamada, Y., Kanno, H., Tsujioka, T., Takahashi, H., and Usuki, T., *Appl. Phys. Lett.*, 75, 1682, 1999. With permission.)

color. Since the HOMO and LUMO energy levels of rubrene are between those of the dopant DCM2 and the host Alq₃, the energy transfer process between Alq₃ and DCM2 has dramatically improved by the mediation of the rubrene which acts as the energy transfer aid (Figure 3.19). Besides achieving pure red emission in the cell [2,5], lower turn-on voltages and higher luminance efficiencies compared with cell [2,0] have also been observed.

This new doping method has been widely used by several groups for red emissive OLEDs. Ohmori et al. reported two red emissive dopants doped into Alq₃ and reported high-efficiency OLEDs compared with the single red dopant [329]. Li et al. used rubrene as the sensitizer in the red DCJTb dopant system and achieved a high-efficiency and pure red OLED. The energy transfer rates have been studied by fitting the fluorescence decay curves [330]. The EL efficiency of such DCJTb-doped in Alq₃ with 5% of rubrene as a codopant has been dramatically improved by Chen et al. using CF_x as the HIL [331]. Mori et al. applied a photosensitizer dye such as DCM as a second codopant in the Alq₃ doped with red squarylium dye. The EL efficiency and luminance of this system are — two to three times higher than that of the simple squarylium-doped Alq₃ device [332]. Figure 3.20 shows the EL spectra and the energy levels of the various materials. Obviously, the DCM doping in the Sq-dye doped Alq₃ device enhances the energy transfer and improves the device performance. Again, the HOMO and LUMO energy levels of DCM are between the host Alq₃ and Sq, respectively.

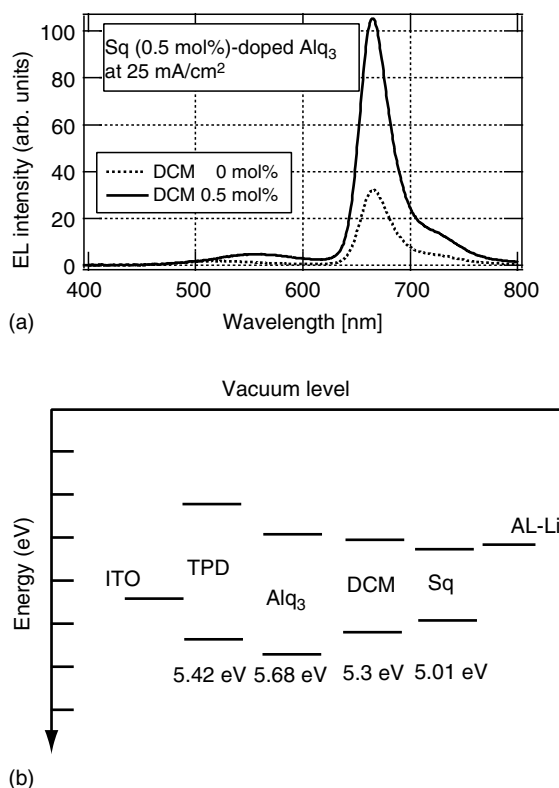


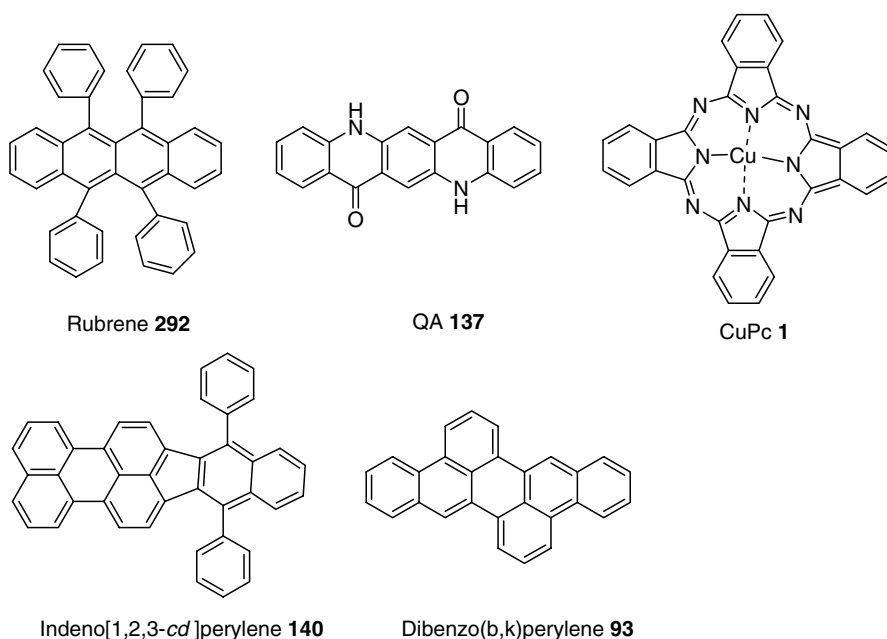
FIGURE 3.20 (a) EL spectra of the ITO/TPD/Alq₃:DCM(0% or 0.5%)/Sq(0.5%)/Al:Li and (b) energy level of ITO, TPD, Alq₃, DCM, Sq and Al-Li. (From Mori, T., Kim, H., Mizutani, T., and Lee, D., *Jpn. J. Appl. Phys.*, 40, 5346, 2001. With permission.)

Feng et al. used 5,12-dihydro-quin[2,3-*b*]acridine-7,14-dione or quinacridone (QAD) as an assistant dopant in the red dye DCJTB doped in Alq₃ system. The emission efficiency and the purity of the red color are greatly improved in addition to lowering the driving voltage [333]. Instead of using rubrene as a codopant (normally 5%), Chen et al. used 60% of rubrene and 40% of Alq₃ as the cohost materials doped with 2% DCJTB with a device structure of ITO/CFX/NPD/40%Alq₃-60%Rubrene:2%DCJTB/Alq₃/LiF/Al [334]. The EL efficiency was boosted to 4.4 cd/A with a power efficiency of 2.1 lm/W at 20 mA/cm² and 6.8 V, and the red color CIE coordinates are [0.65, 0.35]. The half-life time (L_0 : 100 cd/m²) of such a device is projected to be 33,810 h.

Further improvements of the device luminescent efficiency, stability, power efficiency, and driving voltage have been reported in a Kodak patent [335]. In their claim, high-efficiency and stable OLEDs can be achieved by codoping a hole trapping agent such as 5% NPD along with 5% of a rubrene stabilizer as an exciton trap into the 2% DCJTB-doped Alq₃ devices. Kodak's patent also claims that 0.1–1.0% phthalocyanine (Pc) or its metal complex such as CuPc, indenoperylene compounds, or mixtures of benzenoid compounds can be used as stabilizers [336,337].

The chemical structures of the widely used stabilizers are listed in Scheme 3.92.

It is worth mentioning here that introducing the dopant stabilizer may also prevent HTL recrystallization and extend the lifetime of the device via this morphological mechanism as proposed by Popovic et al. [338]. In their work, they investigated the effect of a series of aromatic hydrocarbon dopants in the HTL on the lifetime devices. The addition of selected dopants such as rubrene (which has a relatively higher HOMO level than the HTM) to NPD led to an increase in device lifetime by more than an order of magnitude. They explained that this is due to the stabilization of morphology of the HTL and the charge trapping at the HTL, which reduced the hole mobility and helped balance the charge injection [339]. An example of this approach has been recently applied to increase the lifetime and efficiency of fluorescent deep blue OLEDs [340]. Meanwhile, life extension by use of dopants is consistent with the



SCHEME 3.92 Chemical structures of common stabilizers.

recently proposed mechanism that OLED degradation is primarily caused by excess holes traversing the EML and ultimately being injected into the Alq₃ ETL [341].

3.7.2 SENSITIZERS

As an extension of the fluorescent sensitizer concept, Forrest et al. have applied this approach to phosphorescent OLEDs, in which the sensitizer is a phosphorescent molecule such as Ir(ppy)₃ [342]. In their system, CBP was used as the host, the green phosphor Ir(ppy)₃ as the sensitizer, and the red fluorescent dye DCM2 as the acceptor. Due to the triplet and the singlet state energy transfer processes, the efficiency of such devices is three times higher than that of fluorescent sensitizer-only doped device. The energy transfer processes are shown in Figure 3.21.

In their follow-up paper, they also demonstrated 100% efficient energy transfer of both singlet and triplet excited states. The device exhibits peak external efficiency and power efficiency of 25 cd/A and 17 lm/W at 0.01 mA/cm², respectively [343]. Liu demonstrated a high-efficiency red OLED employing DCJTb as a fluorescent dye doped in TPBI with a green phosphorescent Ir(ppy)₃ as a sensitizer. A maximum brightness and luminescent efficiency of

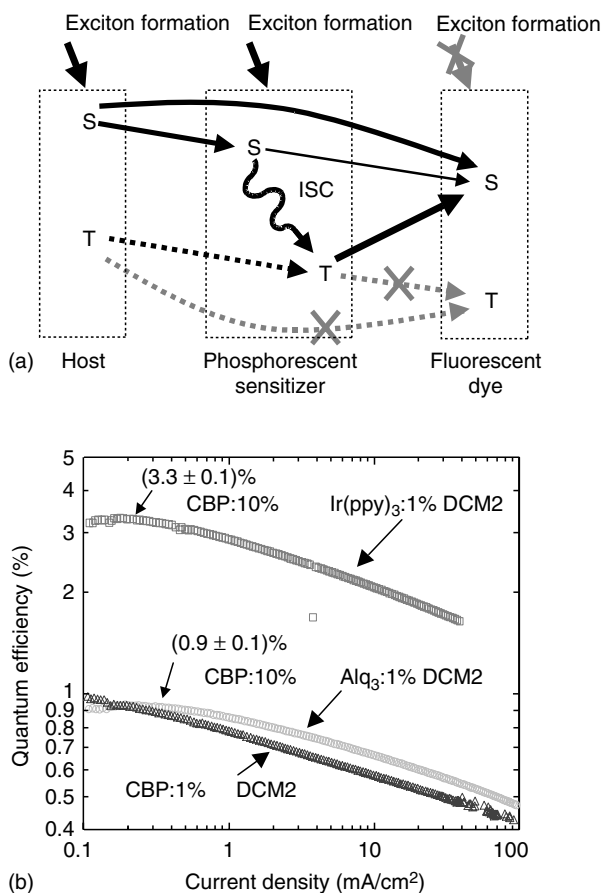


FIGURE 3.21 (a) Energy transfer mechanisms of phosphorescent dye as a sensitizer and (b) the EL external efficiency of the DCM2 doped devices. (From Baldo, M.A., Thompson, M.E., and Forrest, S.R., *Nature*, 403, 750, 2000. With permission.)

10,000 cd/m² at 19 V and 3.6 cd/A at 5 V, respectively, have been achieved [344]. Kodak recently disclosed that by using perylene derivatives as stabilizers, white OLEDs with improved color purity, very high efficiency, and longer lifetimes are possible [345].

3.7.3 HOLE-BLOCKING MATERIALS

It has been noted above that the observation of host emission is often due to inefficient energy transfer processes. It is also found that emission from the host, ETL and HTL can sometimes be observed. This is due to unbalanced charge injection, which ultimately limits the EL efficiency. One of the layers which has become key to the rise of phosphorescent emitter systems and their very high efficiencies is the HBL. Used to prevent leakage of positive charge carriers through to the cathode, this layer helps confine the charge carriers to the EML. It further serves to confine the excitons created in the EML to permit their efficient emission of photons (and hence is sometimes also referred to as an exciton-blocking layer or anti-quenching layer). The key properties of a material used for this layer are that it has electron transport capability (deep LUMO level) coupled with a deep HOMO level to limit hole transport capacity. In some cases, a single material can act as both the ETL and the HBL but it has become more common to decouple these two functions. For phosphorescent emitter systems, the relatively long-lived nature of the excitons (microseconds) means that their confinement to the EML is especially crucial. Without a HBL, such emissive states can migrate through the EML and into adjacent layers, causing them to lose much of their efficiency via quenching of the excitons by the ETL material or the cathode itself.

The concept of using HBMs in OLEDs started with the pioneering work of Kijima et al. when they were trying to get pure blue emission from an EL device with Alq₃ as ETM and NPD as an EML [346]. An undesired green emission color from Alq₃ was suppressed when a thin layer of BCP was added between the NPD and Alq₃ layers.

Without using Alq₃ as the ETM, BCP has been used as an ETL and was demonstrated in DPVBI-based blue OLEDs [347]. BCP has superior electron transport properties and its electron mobility is around 5.2×10^{-4} cm²/(V s) (5.5×10^5 V/cm) as measured by the TOF method [348]. The concept of using BCP has been extended into doped OLEDs.

BCP as a HBM in the device ITO/NPD/DNA/BCP/Alq₃/MgAg can reduce the emission color from Alq₃, however, it also increases the operating voltage. Hung et al. demonstrated that by replacing BCP with TPBI, a widely used ETM, it can dramatically reduce the operating voltage [144]. Their results are based on the systematic study of the electron mobility, as well as the HOMO and LUMO energy levels of TPBI, Alq₃, and BCP. Compared with BCP, TPBI showed much better electron mobility and less of a charge injection barrier with Alq₃. Figure 3.22 shows DNA/TPBI/Alq₃ energy level diagrams with consideration of the dipole interface effects.

It is clear from Figure 3.22 that the hole transport from DNA to Alq₃ is quite easy due to the barrier difference which is only ~0.2 eV. However, when an additional layer of TPBI is used between DNA and Alq₃, the hole barrier difference between DNA and TPBI is 0.8 eV. While the electron barrier between DNA and TPBI is 0.3 eV, and TPBI and Alq₃ is 0.5 eV, respectively. Similar measurements using BCP instead of TPBI predict a higher electron barrier than that of TPBI. The device structure was optimized by combination of an EIL using LiF and TPBI used as both ETL and HBL and achieved a high-efficiency EL emission with much lower operating voltage. In the blue OLED device, with a device configuration of ITO/NPD/DNA/TPBI/Alq₃/LiF/MgAg, blue emission of CIE (0.1451, 0.1446) with a current density of 20 mA/cm² at 5.5 V and a luminance of 680 cd/m² was achieved.

The first study using HBMs in PHOLEDs was conducted by O'Brien et al. when they studied the energy transfer efficiency in a PtOEP-doped PHOLED [349]. They observed that

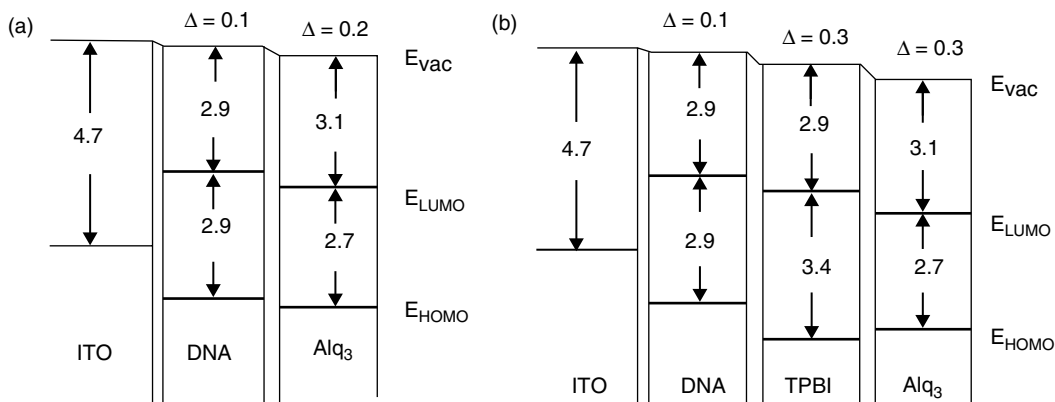


FIGURE 3.22 (a) Energy diagrams of DNA–Alq₃ bilayer and (b) DNA–TPBI–Alq₃ multilayer, the value Δ gives the interface dipoles between the adjacent layers. (From Li, Y., Fung, M.K., Xie, Z., Lee, S., Hung, L., and Shi, J., *Adv. Mater.*, 14, 1317, 2000. With permission.)

when a guest material PtOEP was doped in a thin layer of host material such as CBP or Alq₃, the device gave much lower EL efficiency compared with when doped in a thick host material. But, if the thicker host material is used in the device then a higher turn-on voltage is needed to drive the device. They found that inserting an additional very thin layer of a HBM such as BCP between the ETL and the doped thin host layer can improve the EL efficiency while keeping the driving voltage low. This HBL blocks the holes from being injected to the ETL and confines the exciton in the EML. Figure 3.23 shows the effect of using a HBL in this device.

Obviously, in a thin layer host material doped device, the EL efficiency is quite low and additional Alq₃ emission is observed, however, when a HBL of BCP was used, the EL efficiency dramatically increased and there was no Alq₃ emission in the spectra.

As the EL efficiency is limited by the poor phosphorescent dopant PtOEP, by using a good red phosphorescent iridium complex, Liu et al. demonstrated a very highly efficient PHOLED by applying a HBM [350]. The device structure is ITO/NPD/CBP:6% Ir(ppy)₃/BCP/Alq₃/Mg:Ag.

Ikai et al. used a new HBM of a starburst perfluorinated phenylene that showed even better performance compared with BCP [351]. Probably the most commonly used material in this application is Balq, which was initially developed as a blue emissive material (*vide supra*). Closely related to the green emitter material Alq₃ mentioned above, this material is widely used because it has been shown to have very favorable lifetime performance (>10,000 h at 500 cd/m²) in green Ir(ppy)₃ phosphorescent devices [352]. This is often attributed to the high T_g of this material coupled with its good film-forming properties when vapor deposited. Other HBL materials of this type include further aluminum hydroxyquinolate phenolates mentioned in the same publication, as well as benzimidazoles such as TPBI and bipyridines or phenanthrolines such as bathocuproine BCP. All of these serve as good HBLs in an electronic sense, but typically give shorter device lifetimes, especially for BCP, which tends to crystallize rapidly in devices [353]. Boron compounds were also investigated as HBMs. One example of these compounds is TTPhPhB used as a HBM in blue or violet blue OLEDs and which showed improved device performance [354].

The chemical structures of various HBMs are listed in Scheme 3.93. Good HBMs must have a wide energy band gap (both singlet and triplet states), a high ionization energy (a deep HOMO) and the LUMO energy level should be closely aligned with that of the ETL.

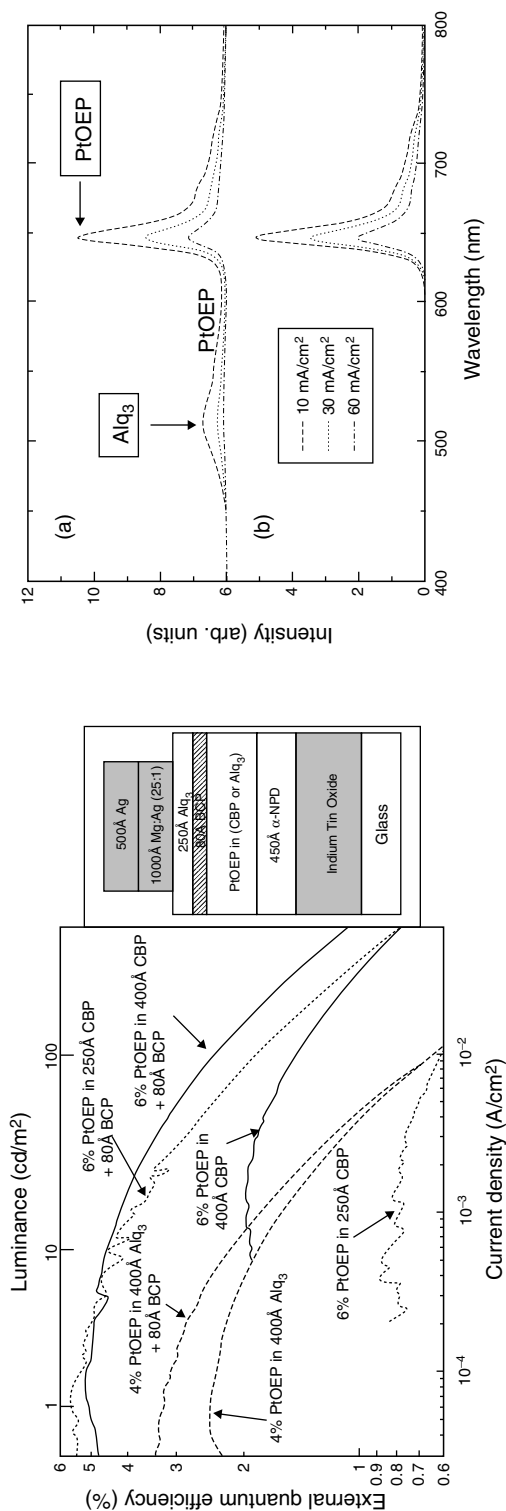
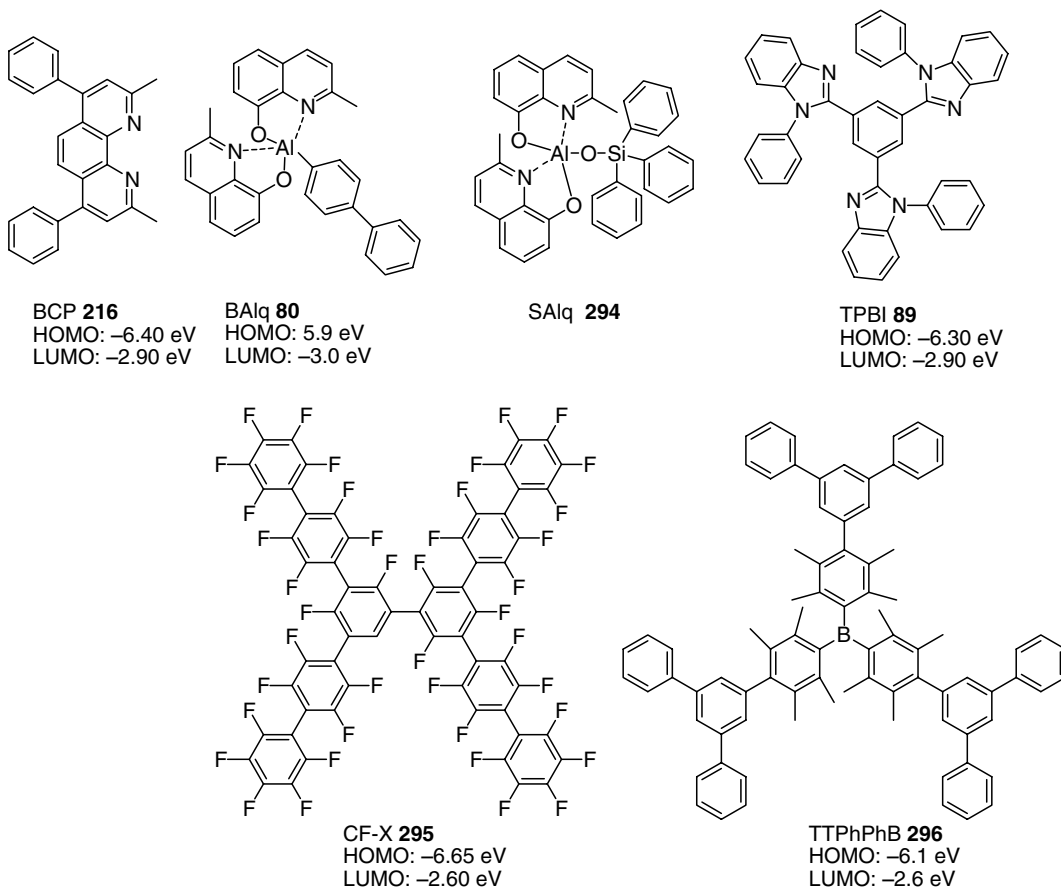


FIGURE 3.23 External quantum efficiencies of PtOEP/CBP and PtOEP/Alq₃ devices as a function of current with and without a BCP blocking layer (left). Emission spectra of CBP-based electroluminescent devices with and without a BCP exciton blocking layer (right). (From O'Brien, D.F., Baldo, M.A., Thompson, M.E., and Forrest, S.R., *Appl. Phys. Lett.*, 74, 442, 1999. With permission.)



SCHEME 3.93 Chemical structure of some common HBMs.

Furthermore, it should be thermally stable, should be phase compatible, and should readily form uniform amorphous thin films [355].

3.7.4 ELECTRON-BLOCKING MATERIALS

Serving a similar function as the HBMs, electron-blocking materials (EBMs) block electrons from passing through the EML to the HTM or anode electrode to improve the device efficiency and achieve color purity. The concept of using EBMs was first presented by the Forrest group in the study of white PHOLEDs [356]. In their white PHOLED structure ITO/NPD/CBP:IrPtcec/BCP/Alq₃/LiF/Al, an undesired blue emission from NPD was observed when the operation voltage was increased. This is due to the electron or exciton leaking from the EML into the NPD layer, which will lead to poor charge confinement in the EML. To prevent this leakage, they designed the compound *fac*-tris(1-phenylpyrazolato-*N*, *C*2') iridium(III) (Irppz, **297**) which has a relatively shallower LUMO energy compared with the HTM NPD, while the hole barrier between the NPD and Irppz is sufficiently low to allow ready transport of holes from NPD. Figure 3.24 depicts the energy diagram of the materials and Scheme 3.94 lists the chemical structures of the EBMs [357].

The PHOLED with an EBL added and with a device structure ITO/NPD/Irppz/CBP:IrPtcec/BCP/Alq₃/LiF/Al, gave stable white emission without NPD emission even when

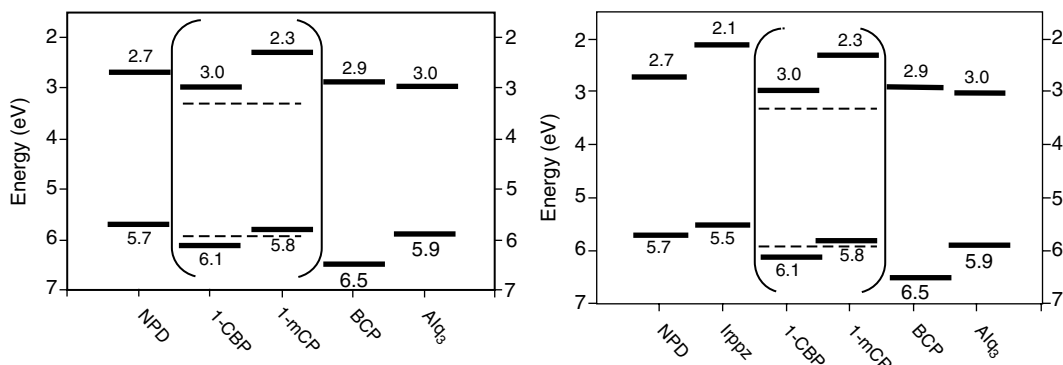
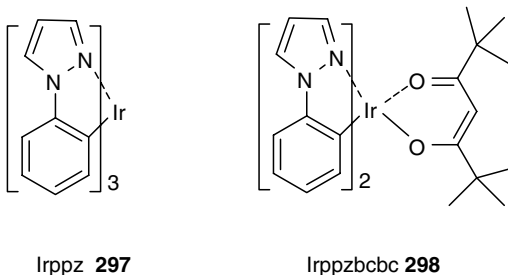


FIGURE 3.24 Energy level diagrams of the HOMO/LUMO levels of the OLED materials. (From Adamovich, V., Brooks, J., Tamayo, A., Alexander, A.M., Djurovich, P.I., D'Andrade, B.W., Adachi, C., Forrest, S.R., and Thompson, M.E., *New J. Chem.*, 26, 1171, 2002. With permission.)



SCHEME 3.94 Chemical structures of EBMs.

operated at a high voltage. The QE of the electron blocking added device is double that of a no-EBM device.

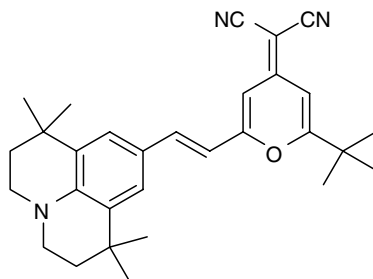
It is worth mentioning here that simple HTMs may also function as EBLs. This has been discussed recently by Hou et al. in a study of the current and efficiency related with the HTL (NPD) thickness in Alq₃-based OLEDs [358]. The results showed that a thickness of ~5 nm of the HTL is sufficient for hole injection and transport while ~20 nm of the HTL will give high luminescent efficiency and this is attributed to the electron-blocking effect of the thicker NPB.

The requirements for EBMs are as follows:

1. Wide band gap to prevent exciton leakage into the HTL
2. Shallow LUMO energy level to block electrons
3. HOMO energy level matching the HTL to facilitate hole transport
4. Thermal stability and good film-forming properties

3.8 CURRENT BEST PERFORMANCE OF THE THREE PRIMARY COLOR MATERIALS AND DEVICE STRUCTURES

The following section is our attempt to cull the best performance materials for each of the three primary colors, red, green, and blue, from the published literature. As noted above, we base these selections on the reported data and make no attempt to critically evaluate the quality of the experimental study, taking it at face value. Although this may be less than ideal,



DCJTBT 151

ITO/CFx/NPB(120 nm)/40%Alq₃:60%rubrene:2%DCJTBT (30 nm)/Alq₃(50 nm)/LiF(1 nm)/Al(200 nm)

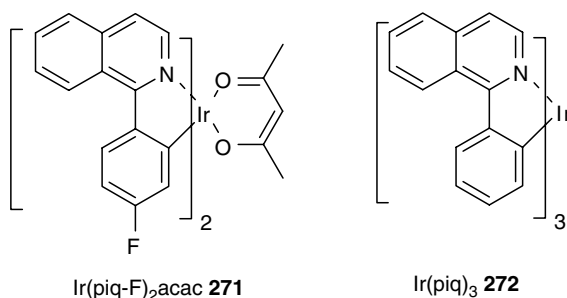
SCHEME 3.95 Highly efficient red fluorescent emitting materials and the device configuration structure.

it is necessary given the complex interplay of performance characteristics and the evaluations of those characteristics used by differing authors. It is ultimately left to the reader to do a critical appraisal to the original data itself.

3.8.1 RED EMITTERS AND DEVICE STRUCTURES

A leading material reported as a red emitter is the fluorescent dye material typified by 4-(dicyanomethylene)-2-*tert*-butyl-6-(1,1,7,7-tetramethyljulolidyl-9-enyl)-4*H*-pyran (DCJTBT) [359]. This material is typically doped into an electron transporting host matrix such as Alq₃ and delivers good chromaticity with CIE (0.646, 0.351) and a reasonable EL efficiency up to 4.4 cd/A and a power efficiency of 2.09 lm/W at 20 mA/cm² and 6.8 V. The operational stability of the DCJTBT-doped EL device has a projected half-life of over 33,800 h driven at an initial brightness of 100 cd/m² (Scheme 3.95) [360].

The highest efficiency red emitters belong to the class of phosphorescent materials and are based on iridium organometallic complexes. The best performance achieved in guest–host systems, for example using a carbazole host and an Ir emitter Ir(piq-F)₂acac, has a maximum power efficiency and luminescent efficiency up to 4.73 lm/W and 13.7 cd/A, respectively. An EQE of 6.7% at 20 mA/cm² with CIE (0.61, 0.36) has been demonstrated (Scheme 3.96) [361].



ITO/NPB(40 nm)/CBP:6%Ir(piq-F)₂acac(30 nm)/BCP(10 nm)/Alq₃(30 nm)/Mg:Ag

SCHEME 3.96 Highly efficient red phosphorescent emitting materials and the device configuration structure.

Other work by Tsuboyama et al. reported a very highly efficient red PHOLED with power efficiency of 8.0 lm/W at 100 cd/m² using Ir(piq)₃ as a dopant [362]. Most exciting, however, is the relatively recent demonstration of exceptional lifetimes for these materials in OLED devices where work from UDC has claimed a 14 cd/A red CIE (0.65, 0.35) with a lifetime of 25,000 h at 500 nit. Such performance promises much for phosphorescent red emitters in commercial devices and even higher efficiencies have been realized in systems that compromise the chromaticity toward the deep red with CIE (0.67, 0.33) and lifetimes >100,000 h at 500 cd/m² [363].

3.8.2 GREEN EMITTERS AND DEVICE STRUCTURES

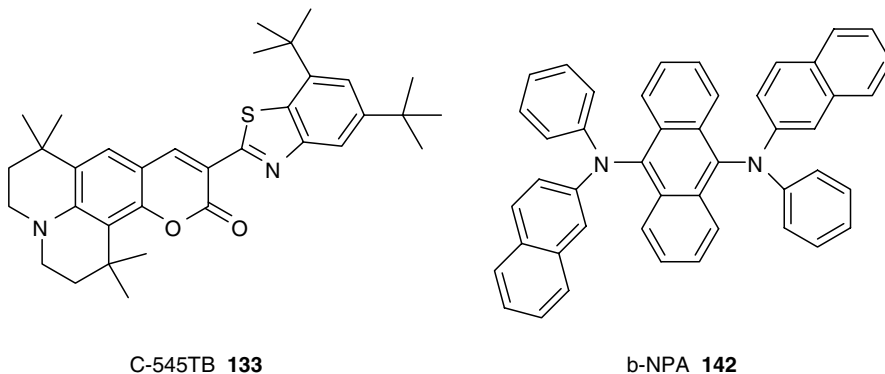
As noted above, the whole field of OLEDs began with the green SMOLED emitter Alq₃. At this time the leading candidate emitters that have emerged from an enormous number of experiments fall, once again, into two camps — fluorescent and phosphorescent.

In the fluorescent world, Kodak's coumarin compound 9-(5,7-di-*tert*-butyl-benzothiazol-2-yl)-1,1,6,6-tetramethyl-2,3,5,6-tetrahydro-1*H*,4*H*-11-oxa-3a-aza-benzo[de]anthracen-10-one (545TB) doped into an Alq₃ host produces a highly efficient device in the configuration structure of ITO/CHF₃plasma/NPD(75 nm)/Alq₃:1%C-545TB(38 nm)/Alq₃(38 nm)/Mg:Ag(10:1)(200 nm), which gave a saturated green emission CIE (0.30, 0.64) with an output of 2585 cd/m², a luminescent efficiency of 12.9 cd/A with a power efficiency of 3.5 lm/W at a driving current density of 20 mA/cm² (Scheme 3.97) [189].

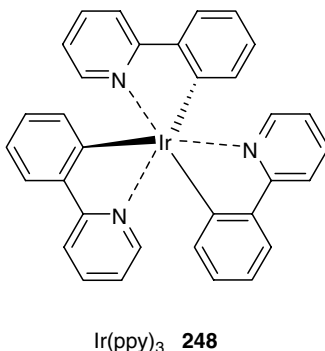
Another high efficiency, high brightness, green OLED with CIE (0.33, 0.63) was fabricated using 9,10-bis(2-naphthylphenylamino)anthracene(β-NPA) as a neat film in a device configuration of ITO/m-MTDATA(920 nm)/β-NPA(40 nm)/TPBI(50 nm)/Mg:Ag [364]. The optimized devices emit narrow green light (FWHM: 52 nm) with a remarkable maximum EQE of 3.68%, a current efficiency of 14.79 cd/A, a power efficiency of 7.76 lm/W, and a maximum brightness of 64,991 cd/m².

Once again, the most recent developments have been in the area of green phosphorescent materials where phenomenal efficiencies are now beginning to be coupled with good device lifetimes. The prototypical emitter of this type is iridium-tris-2-phenylpyridine (Ir(ppy)₃) used as a dopant (Scheme 3.98), usually diluted into a carbazole type host, because it is prone to serious self-quenching problems.

This simple material has CIE (0.30; 0.63) and has demonstrated power efficiencies as high as 77 lm/W. The very high efficiency and low-voltage p-i-n structure with a double-EML has



SCHEME 3.97 Highly efficient green fluorescent emitting materials.



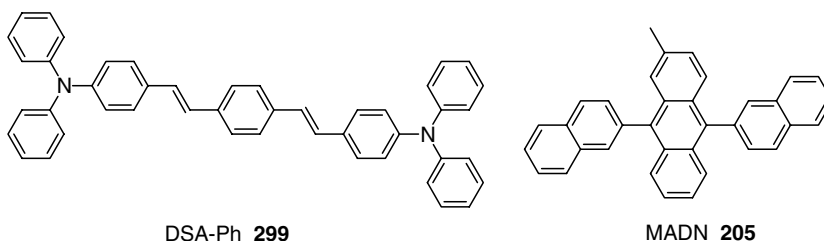
SCHEME 3.98 Highly efficient green phosphorescent emitting material.

been recently presented by Leo et al.: ITO/MeO-TPD:2%F4-TCNQ(100 nm)/TAD(10 nm)/TCTA:8%Ir(ppy)₃(10 nm)/TAZ:8%Ir(ppy)₃(10 nm)/BCP(10 nm)/BCP:Cs(50 nm)/Al(100 nm). This device gave a power efficiency of 77 lm/W and an EQE of 19.3% at 100 - cd/m² with an operating voltage of 2.65 V. Once again, work from UDC has demonstrated related Ir-based green emitters with CIE (0.32, 0.63), an external quantum yield of 23%, and an EL efficiency of 80 cd/A, and lifetimes in excess of 15,000 h at 1000 nit [363].

3.8.3 BLUE EMITTERS AND DEVICE STRUCTURES

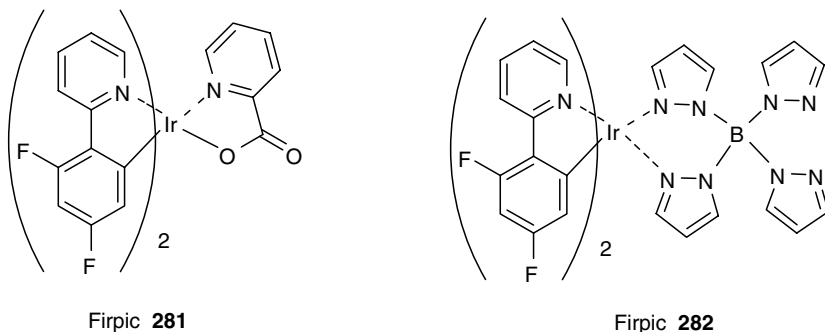
If there is one clear need in the field of OLED materials it continues to be in the area of blue emitters. A blue emissive material with good color coordinates CIE (0.10, <0.10) coupled with long device lifetime (>10,000 h) and high electrical efficiency (>5 cd/A) is the holy grail of materials chemists in this field. A major effort to find such materials continues in many laboratories including our own and the current sets of available materials may be supplanted at any time. However, the current best candidate blue emitters in the SMOLED area compromise many desirable properties — the most troublesome being long lifetime.

Blue fluorescent emitters based on fused polyaromatic ring systems have long been known and systematic work has steadily improved the efficiencies and colors, while pushing the limits of stability in an operational device. A sky blue based on styrylamine doped 2-methyl-9,10-di(2-naphthyl)anthracene OLED was reported to provide the highest efficiency device (Scheme 3.99) [365].



ITO/CF_x/NPD(70 nm)/MADN(40 nm):3%DSA-Ph/Alq₃(10 nm)/LiF(1 nm)/Al(200 nm)

SCHEME 3.99 Highly efficient blue fluorescent emitting materials and the device configuration structure.



SCHEME 3.100 Highly efficient blue phosphorescent emitting materials and the device configuration structure.

This system has shown moderate chromaticity (0.16, 0.32) while achieving an EL efficiency of 9.7 cd/A and 5.5 lm/W at 20 mA/cm² and 5.7 V and the half-decay lifetime of 46,000 h at an initial brightness of 100 nit. During the recent SID (2005) conference, the same group presented a very deep blue OLED with a CIE (0.14, 0.13) after modification of the chemical structure of the dopant and introducing an additional layer of cohost material (NPD:CuPc). The EL efficiency of 5.4 cd/A and an EQE of 5.1% at 20 mA/cm² and 6.8 V with a projected half-decay lifetime of 9700 h at an initial brightness of 100 nit has been achieved [340].

In the case of blue emitters, phosphorescent materials still lag behind their fluorescent counterparts. One particular problem is finding a material with a high enough triplet state to correspond to a blue emission wavelength. Furthermore, finding a host into which this material may be doped without quenching the emissive state is a major challenge since the triplet state of the host must be higher in energy than the emitter triplet state. The high energy triplet state of a blue phosphorescent emitter appears to be difficult to maintain without degradation and so lifetimes of phosphorescent blues are a problem. Most work reported in this area has focused on a material dubbed Firpic and developed by the USC and Princeton groups (Scheme 3.100) [366].

This material, in a suitably high-energy carbazole host, has given up to 20 cd/A but with poor blue chromaticity, CIE (0.17, 0.34), which is a common problem with such materials, resulting from the long wavelength emission tail that seems to arise from vibronic structure. Lifetimes of such systems are still problematic with only hundreds of hours of operation being claimed. Clearly, more work and significant inventions are needed in this area.

3.9 CONCLUSION AND REMARKS

While the individual materials described in the preceding sections are all valuable and in many cases essential for the realization of good, long-lived performance in OLED devices, it is equally true that the materials themselves are only a small part of the OLED story. As frequently alluded to above, the precise architecture into which the materials are placed is crucially important to device performance. Furthermore, while the bulk materials properties themselves, and especially their purities, are important, the interfaces formed between different materials are equally critical. Both chemical and morphological effects at any of the materials' interfaces in a device can have profound effects on the overall device performance. It is the precise interplay of materials design, processing, and ultimate device architecture that must be controlled if the remarkable phenomenon of efficient EL in organic materials is ever to be transformed into the display technology of the future.

ACKNOWLEDGMENTS

We would like to thank our colleagues at DuPont CR&D and DuPont Displays for their many valuable insights, discussions, and encouragement, as well as helpful suggestions regarding the contents of this review. Special thanks to Dr. Marc B. Goldfinger for proof-reading the manuscript.

REFERENCES

1. M. Pope, H.P. Kallmann, and P. Magnante, "Electroluminescence in organic crystals," *J. Chem. Phys.*, 38: 2042–2043 (1963).
2. R.S. Vincett, W.A. Barlow, R.A. Hann, and G.G. Roberts, "Electron conduction and low voltage blue electroluminescence in vacuum-deposited organ films," *Thin Solid Films*, 94: 171–183 (1982).
3. C.W. Tang and S.A. Vanslyke, "Organic electroluminescent diodes," *Appl. Phys. Lett.*, 51: 913–915 (1987).
4. M.A. Baldo, D.F. O'Brien, Y. You, A. Shoustikov, S. Sibley, M.E. Thompson, and S.R. Forrest, "Highly efficient phosphorescent emission from organic electroluminescent devices," *Nature*, 395: 151–154 (1998).
5. Y. Kawamura, K. Goushi, J. Brooks, J.J. Brown, H. Sasabe, and C. Adachi, "100% phosphorescence quantum efficiency of Ir (III) complexes in organic semiconductor films," *Appl. Phys. Lett.*, 86: 71104–71106 (2005).
6. T. Nagamoto, Y. Maruta, and O. Omoto, "Electrical and optical properties of vacuum-evaporated indium–tin oxide films with high electron mobility," *Thin Solid Films*, 192: 17–25 (1990).
7. T. Kawashima, H. Matsui, and N. Tanabe, "New transparent conductive films: FTO coated ITO," *Thin Solid Films*, 445: 241–244 (2003).
8. N.W. Schmidt, T.S. Totushek, W.A. Kimes, D.R. Callender, and J.R. Doyle, "Effects of substrate temperature and near-substrate plasma density on the properties of d.c. magnetron sputtered aluminum-doped zinc oxide," *J. Appl. Phys.*, 94: 5514–5521 (2003).
9. Y. Wu, C.H.M. Maree, R.F. Haglund Jr., J.D. Hamilton, M.A. Morales Paliza, M.B. Huang, L.C. Feldman, and R.A. Weller, "Resistivity and oxygen content of indium–tin oxide films deposited at room temperature by pulsed-laser ablation," *J. Appl. Phys.*, 86: 991–994 (1999).
10. H. Tomonaga and T. Morimoto, "Indium–tin oxide coatings via chemical solution deposition," *Thin Solid Films*, 392: 243–248 (2001).
11. O. Marcovitch, Z. Klein, and I. Lubezky, "Transparent conductive indium oxide films deposited on low temperature substrates by activated reactive evaporation," *Appl. Opt.*, 28: 2792–2795 (1989).
12. J.K. Mahon, T.X. Zhou, P.E. Burrows, S.R. Forrest, and M.E. Thompson, "Small-molecule organic light emitting devices in flat panel display applications," *Light-Emitting Diodes: Research, Manufacturing, and Applications*, Second *SPIE Proceedings*, vol. 3279, pp. 87–92 (1998).
13. M.G. Mason, C.W. Tang, L.S. Hung, P. Raychaudhuri, J. Madathil, D.J. Giesen, L. Yan, Q.T. Le, Y. Gao, S.T. Lee, L.S. Liao, L.F. Cheng, W.R. Salaneck, D.A. dos Santos, and J.L. Bredas, "Interfacial chemistry of Alq₃ and LiF with reactive metals," *J. Appl. Phys.*, 89: 2756–2765 (2001).
14. Y. Cao, "Thin metal-oxide layer as stable electron-injecting electrode for light emitting diodes," *PCT Int. Appl.*, WO 2000022683, pp. 37, (2000).
15. I.G. Hill, A. Rajagopal, A. Kahn, and Y. Hu, "Molecular level alignment at organic semiconductor–metal interfaces" *Appl. Phys. Lett.*, 73: 662–664 (1998).
16. H. Ishii, K. Sugiyama, E. Ito, and K. Seki, "Energy level alignment and interfacial electronic structures at organic–metal and organic–organic interfaces," *Adv. Mater.*, 11: 605–625 (1999).
17. W.R. Salaneck, S. Stafstrom, and J.L. Bredas, *Conjugated Polymer Surfaces and Interfaces: Electronic and Chemical Structure of Interfaces for Polymer Light Emitting Devices*, Cambridge University Press, London (2003).
18. W.R. Salaneck, K. Seki, A. Kahn, and J. Pireaux, *Conjugated Polymer and Molecular Interfaces*, 1st ed., Marcel Dekker, New York (2001).

19. L.S. Hung and C.H. Chen, "Recent progress of molecular organic electroluminescent materials and devices," *Mater. Sci. Eng.*, R39: 143–222 (2002).
20. S.A. Vanslyke, C.H. Chen, and C.W. Tang, "Organic electroluminescent devices with improved stability," *Appl. Phys. Lett.*, 69: 2160–2162 (1996).
21. E.W. Forsythe, M.A. Abkowitz, and Y. Gao, "Tuning the carrier injection efficiency for organic light-emitting diodes," *J. Phys. Chem. B*, 104: 3948–3952 (2000).
22. S.M. Tadayyon, H.M. Grandin, K. Griffiths, P.R. Norton, H. Aziz, and Z.D. Popovic, "CuPc buffer layer role in OLED performance: a study of the interfacial band energies," *Organ. Electron.*, 5: 157–166 (2004).
23. I.G. Hill and A. Kahn, "Combined photoemission in vacuotransport study of the indium tin oxide/copper phthalocyanine/*N*, *N*8-diphenyl- *N*, *N*8-bis. 1-naphthyl.-1,18biphenyl-4,49diamine molecular organic semiconductor system," *J. Appl. Phys.*, 86: 2116–2122 (1991).
24. F. Nuesch, M. Carrara, M. Schaer, D.B. Romero, and L. Zuppiroli, "The role of copper phthalocyanine for charge injection into organic light-emitting devices," *Chem. Phys. Lett.*, 347: 311–317 (2001).
25. S.H. Jung, J.H. Choi, S.M. Yang, W.J. Cho, and C.S. Ha, "Syntheses and characterization of soluble phthalocyanine derivatives for organic electroluminescent devices," *Mater. Sci. Eng. B: Solid-State Mater. Adv. Technol.*, 85: 160–164 (2001).
26. Y. Qiu, Y. Gao, P. Wei, and L. Wang, "Organic light-emitting diodes with improved hole-electron balance by using copper phthalocyanine aromatic diamine multiple quantum wells," *Appl. Phys. Lett.*, 80: 2628–2630 (2002).
27. J. Cui, Q. Huang, J.G.C. Veinot, H. Yan, and T.J. Marks, "Interfacial microstructure function in organic light-emitting diodes: assembled tetraaryldiamine and copper phthalocyanine interlayers," *Adv. Mater.*, 14: 565–569 (2002).
28. W.H. Kim, A.J. Makinen, N. Nikolov, R. Shashidhar, H. Kim, and Z.H. Kafafi, "Molecular organic light-emitting diodes using highly conducting polymers as anodes," *Appl. Phys. Lett.*, 80: 3844–3846 (2002).
29. Y. Yang and A.J. Heeger, "Polyaniline as a transparent electrode for polymer light-emitting diodes: lower operating voltage and higher efficiency," *Appl. Phys. Lett.*, 64: 1245–1247 (1994).
30. J. Gao, A.J. Heeger, J.Y. Lee, and C.Y. Kim, "Soluble polypyrrole as the transparent anode in polymer light-emitting diodes," *Synth. Met.*, 80: 221–223.
31. J. Schwartz, E.L. Bruner, N. Koch, A.R. Span, S.L. Bernasek, and A. Kahn, "Controlling the work function of indium–tin oxide: differentiating dipolar from local surface effects," *Synth. Met.*, 138: 223–227 (2003).
32. J. Lee, B. Jung, J. Lee, H.Y. Chu, L. Do, and H. Shim, "Modification of an ITO anode with a hole-transporting SAM for improved OLED device characteristics," *J. Mater. Chem.*, 12: 3494–3498 (2002).
33. Q. Huang, J. Cui, H. He, J.G.C. Veinot, and T.J. Marks, "Small molecule organic light-emitting diodes can exhibit high performance without conventional hole transport layers," *Appl. Phys. Lett.*, 81: 3528–3530 (2002).
34. Q. Huang, J. Cui, J.G.C. Veinot, H. He, and T.J. Marks, "Realization of high-efficiency/high-luminance small-molecule organic light-emitting diodes: synergistic effects of siloxane anode functionalization hole-injection layers, and hole exciton-blocking electron-transport layers," *Appl. Phys. Lett.*, 82: 331–333 (2003).
35. H. Yan, P. Lee, N.R. Armstrong, A. Graham, G.A. Evmenenko, P. Dutta, and T.J. Marks, "High-performance hole-transport layers for polymer light-emitting diodes. Implementation of organo-siloxane cross-linking chemistry in polymeric electroluminescent devices," *J. Am. Chem. Soc.*, 127: 3172–3183 (2005).
36. L.S. Hung, L.R. Zheng, and M.G. Mason, "Anode modification in organic light-emitting diodes by low-frequency plasma polymerization of CHF₃," *Appl. Phys. Lett.*, 78: 673–675 (2001).
37. J.X. Tang, Y.Q. Li, L.R. Zheng, and L.S. Hung, "Anode–organic interface modification by plasma polymerized fluorocarbon films," *J. Appl. Phys.*, 95: 4397–4403 (2004).
38. Y. Qiu, U. Gao, L. Wang, and D. Zhang, "Efficient light emitting diodes with Teflon buffer layer," *Synth. Met.*, 130: 235–237 (2002).

39. Z.B. Deng, X.M. Ding, S.T. Lee, and W.A. Gambling, "Enhanced brightness and efficiency in organic electroluminescent devices using SiO₂ buffer layer," *Appl. Phys. Lett.*, 74: 2227–2229 (1999).
40. C.O. Poon, F.L. Wong, S.W. Tong, R.Q. Zhang, C.S. Lee, and S.T. Lee, "Improved performance and stability of organic light-emitting devices with silicon oxy-nitride buffer layer," *Appl. Phys. Lett.*, 83: 1038–1040 (2003).
41. Z. Zhang, Z. Deng, C. Liang, M. Zhang, and D. Xu, "Organic light-emitting diodes with a nanostructured TiO₂ layer at the interface between ITO and NPB layers," *Displays*, 24: 231–234 (2003).
42. D.B. Romero, M.Z. Schaer, B. Cesar, and B. Francois, "Effects of doping in polymer light-emitting diodes," *Appl. Phys. Lett.*, 67: 1659–1661 (1995).
43. F. Huang, A.G. MacDiarmid, and B.R. Hsieh, "An iodine-doped polymer light-emitting diode," *Appl. Phys. Lett.*, 71: 2415–2417 (1997).
44. J. Blochwitz, M. Pfeiffer, T. Fritz, and K. Leo, "Low voltage organic light emitting diodes featuring doped phthalocyanine as hole transport material," *Appl. Phys. Lett.*, 73: 729–731 (1998).
45. A. Yamamori, C. Adachi, T. Koyama, and Y. Taniguchi, "Doped organic light emitting diodes having a 650-nm-thick hole transport layer," *Appl. Phys. Lett.*, 72: 2147–2149 (1998).
46. X. Zhou, M. Pfeiffer, J. Blochwitz, A. Werner, A. Nollau, T. Fritz, and K. Leo, "Very-low-operating-voltage organic light-emitting diodes using a *p*-doped amorphous hole injection layer," *Appl. Phys. Lett.*, 78: 410–412 (2001).
47. G. He, O. Schneider, D. Qin, X. Zhou, M. Pfeiffer, and K. Leo, "Very high-efficiency and low voltage phosphorescent organic light-emitting diodes based on a *p*-*i*-*n* junction," *J. Appl. Phys.*, 95: 5773–5777 (2004).
48. T. Mori, H. Fujikawa, S. Tokito, and Y. Taga, "Electronic structure of 8-hydroxyquinoline Aluminium/LiF/Al interface for organic electroluminescent device studied by ultraviolet photoelectron spectroscopy," *Appl. Phys. Lett.*, 73: 2763–2765 (1998).
49. L.S. Hung, C.W. Tang, and M.G. Mason, "Enhanced electron injection in organic electroluminescence devices using an Al/LiF electrode," *Appl. Phys. Lett.*, 70: 152–154 (1997).
50. T.M. Brown, R.H. Friend, I.S. Millard, D.J. Lacey, T. Butler, J.H. Burroughes, and F. Cacialli, "Electronic line-up in light-emitting diodes with alkali-halide/metal cathodes," *J. Appl. Phys.*, 93: 6159–6172 (2003).
51. P. Piromreun, H. Oh, Y. Shen, G.G. Malliaras, J.C. Scott, and P.J. Brock, "Role of CsF on electron injection into a conjugated polymer," *Appl. Phys. Lett.*, 77: 2403–2405 (2000).
52. M.Y. Chan, S.L. Lai, M.K. Fung, S.W. Tong, C.S. Lee, and S.T. Lee, "Efficient CsF/Yb/Ag cathodes for organic light-emitting devices," *Appl. Phys. Lett.*, 82: 1784–1786 (2003).
53. Y. Yi, S.J. Kang, K. Cho, J.M. Koo, K. Han, K. Park, M. Noh, C.N. Whang, and K. Jeong, "Origin of the improved luminance–voltage characteristics and stability in organic light-emitting device using CsCl electron injection layer," *Appl. Phys. Lett.*, 86: 213502–213504 (2005).
54. J. Lee, Y. Park, S.K. Lee, E.J. Cho, D.Y. Kim, H.Y. Chu, H. Lee, L.M. Do, and T. Zyung, "Tris-(8-hydroxyquinoline)aluminum-based organic light-emitting devices with Al/CaF₂ cathode: performance enhancement and interface electronic structures," *Appl. Phys. Lett.*, 80: 3123–3125 (2002).
55. C.H. Lee, "Enhanced efficiency and durability of organic electroluminescent devices by inserting a thin insulating layer at the Alq₃/cathode interface," *Synth. Met.*, 91: 125–127 (1997).
56. S.J. Kang, D.S. Park, S.Y. Kim, C.N. Whang, K. Jeong, and S. Im, "Enhancing the electroluminescent properties of organic light-emitting devices using a thin NaCl layer," *Appl. Phys. Lett.*, 81: 2581–2583 (2002).
57. J. Kido and T. Matsumoto, "Bright organic electroluminescent devices having a metal doped electron injection layer," *Appl. Phys. Lett.*, 73: 2866–2868 (1998).
58. G. Chimed and F. Masamichi, "A lithium carboxylate ultrathin film on an aluminum cathode for enhanced electron injection in organic electroluminescent devices," *Jpn. J. Appl. Phys., Part 2*, 38: L1348–L1350 (1999).
59. C. Schmitz, H. Schmidt, and M. Thelakkat, "Lithium-Quinolate complexes as emitter and interface materials in organic light-emitting diodes," *Chem. Mater.*, 12: 3012–3019 (2000).

60. Z. Liu, O.V. Salata, and N. Male, "Improved electron injection in organic LED with lithium quinolate/aluminium cathode," *Synth. Met.*, 128: 211–214 (2002).
61. A. Fukase and J. Kido, "Organic electroluminescent devices having self-doped cathode interface layer," *Jpn. J. Appl. Phys.*, 41: L334–L336 (2002).
62. F. Liang, J. Chen, L. Wang, D. Ma, X. Jing, and F. Wang, "A hydroxyphenyloxadiazole lithium complex as a highly efficient blue emitter and interface material in organic light-emitting diodes," *J. Mater. Chem.*, 13: 2922–2926 (2003).
63. X. Zheng, Y. Wu, R. Sun, W. Zhu, X. Jiang, Z. Zhang, and S. Xu, "Efficiency improvement of organic light emitting diodes using 8-hydroxy quinolino lithium as an electron injection layer," *Thin Solid Films*, 478: 252–255 (2005).
64. G. He, M. Pfeiffer, K. Leo, M. Hofmann, J. Birnstock, R. Pudzich, and J. Salbeck, "High-efficiency and low-voltage p-i-n electrophosphorescent organic light-emitting diodes with double-emission layers," *Appl. Phys. Lett.*, 85: 3911–3913 (2004).
65. H. Lee, K. Choi, D. Hwang, L. Do, T. Zyung, J. Lee, and J. Park, "Using ionomer as an electron injecting and hole blocking material for polymer light emitting diodes," *Appl. Phys. Lett.*, 72: 2382–2384 (1998).
66. T. Lee, O.O. Park, L. Do, T. Zyung, T. Ahn, and H. Shim, "Polymer light emitting devices using ionomers as an electron injecting and hole blocking layer," *J. Appl. Phys.*, 90: 2128–2134 (2001).
67. Q. Xu, J. Quyang, Y. Yang, T. Ito, and J. Kido, "Ultrahigh efficiency green polymer light emitting diodes by nanoscale interface modification," *Appl. Phys. Lett.*, 83: 4695–4697 (2003).
68. Y. Niu, H. Ma, Q. Xu, and A.K.-Y. Jen, "High efficiency light emitting diodes using neutral surfactants and aluminium cathode," *Appl. Phys. Lett.*, 86: i.d. 083504, 3 pages (2005).
69. Horgan and M. Anthony, Composite Layered Imaging Member for Electrophotography, U.S. Patent 4047948, pp. 14, (1977).
70. C. Adachi, K. Nagai, and N. Tamoto, "Molecular design of hole transport materials for obtaining high durability in organic electroluminescent diodes," *Appl. Phys. Lett.*, 66: 2679–2681 (1995).
71. H. Fujikawa, S. Tokito, and Y. Taga, "Energy structures of triphenylamine oligomers," *Synth. Met.*, 91: 161–162 (1997).
72. S. Tokito, H. Tanaka, A. Okada, and Y. Taga, "High-temperature operation of an electroluminescent device fabricated using a novel triphenylamine derivative," *Appl. Phys. Lett.*, 69: 878–880 (1996).
73. D.F. O'Brien, P.E. Burrows, S.R. Forrest, B.E. Koene, D.E. Loy, and M.E. Thompson, "Hole transporting materials with high glass transition temperatures for use in organic light-emitting devices," *Adv. Mater.*, 10: 1108–1112 (1998).
74. C. Giebeler, H. Antoniadis, D.D.C. Bradley, and Y. Shirota, "Influence of the hole transport layer on the performance of organic light-emitting diodes," *J. Appl. Phys.*, 85: 608–615 (1999).
75. R.D. Hrehha, C.P. George, A. Haldi, B. Domercq, M. Malagoli, S. Barlow, J. Brédas, B. Kippelen, and S.R. Marder, "2,7-bis(diarylamino)-9,9-dimethylfluorenes as hole-transport materials for organic light-emitting diodes," *Adv. Func. Mater.*, 13: 967–973 (2003).
76. K. Wong, Z. Wang, Y. Chien, and C. Wang, "Synthesis and properties of 9,9-diarylfuorene-based triaryldiamines," *Org. Lett.*, 3: 2285–2288 (2001).
77. B. Mi, P. Wang, M. Liu, H. Kwong, N. Wong, C. Lee, and S. Lee, "Thermally stable hole-transporting material for organic light-emitting diode: an isoindole derivative," *Chem. Mater.*, 15: 3148–3151 (2003).
78. J.P. Chen, H. Tanabe, X. Li, T. Thoms, Y. Okamura, and K. Ueno, "Novel organic hole transport material with very high T_g for light-emitting diodes," *Synth. Met.*, 132: 173–176 (2003).
79. K.R.J. Thomas, J.T. Lin, Y. Tao, and C. Ko, "Light-emitting carbazole derivatives: potential electroluminescent materials," *J. Am. Chem. Soc.*, 123: 9404–9411 (2001).
80. Q. Zhang, J. Chen, Y. Cheng, L. Wang, D. Ma, X. Jing, and F. Wang, "Novel hole-transporting materials based on 1,4-bis(carbazoly)benzene for organic light-emitting devices," *J. Mater. Chem.*, 14: 895–900 (2004).
81. Y. Kuwabara, H. Ogawa, H. Inada, N. Noma, and Y. Shirota, "Thermally stable multilayered organic electroluminescent devices using novel starburst molecules, 4,4',4''-tri(*N*-carbazolyl)

- triphenylamine (TCTA) and 4,4',4''-tris(3-methylphenylphenylamino)triphenylamine (m-MTDATA), as hole-transport materials,” *Adv. Mater.*, 6: 677–679 (1994).
82. Y. Shirota, “Organic materials for electronic and optoelectronic devices,” *J. Mater. Chem.*, 10: 1–25 (2000).
 83. K.R.J. Thomas, J.T. Lin, Y. Tao, and C. Ko, “New star-shaped luminescent triarylamines: synthesis, thermal, photophysical, and electroluminescent characteristics,” *Chem. Mater.*, 14: 1354–1361 (2002).
 84. I. Wu, J.T. Lin, Y. Tao, E. Balasubramaniam, Y.Z. Su, and C. Ko, “Diphenylthienylamine-based star-shaped molecules for electroluminescence applications,” *Chem. Mater.*, 13: 2626–2631 (2001).
 85. N. Hu, S. Xie, Z. Popovic, B. Ong, and A. Hor, “5,11-Dihydro-5,11-di-1-naphthlindolo[3,2-b]carbazole: atropisomerism in a novel hole-transport molecule for organic light-emitting diodes,” *J. Am. Chem. Soc.*, 121: 5097–5098 (1999).
 86. J. Li, D. Liu, Y. Li, C. Lee, H. Kwong, and S. Lee, “A high T_g carbazole-based hole-transporting material for organic light-emitting devices,” *Chem. Mater.*, 17: 1208–1212 (2005).
 87. K. Yamashita, T. Mori, T. Mizutani, H. Miyazaki, and T. Takeda, “EL properties of organic light-emitting-diode using TPD derivatives with diphenylstyryl groups as hole transport layer,” *Thin Solid Films*, 363: 33–36 (2000).
 88. T. Spehr, R. Pudzich, T. Fuhrmann, and J. Salbeck, “Highly efficient light emitters based on the spiro concept,” *Org. Electron.*, 4: 61–69 (2003).
 89. U. Bach, C. De Cloedt, H. Spreitzer, and M. Gratzel, “Characterization of hole transport in a new class of spiro-linked oligotriphenylamine compounds,” *Adv. Mater.*, 12: 1060–1063 (2000).
 90. S. Tokito, K. Noda, K. Shimada, S. Inoue, M. Kimura, Y. Sawaki, and Y. Taga, “Influence of hole transporting material on device performance in organic light-emitting diode,” *Thin Solid Films*, 363: 290–293 (2000).
 91. C.S. Ha, J.H. Shin, H. Lim, and W.J. Cho, “Characterization of organic electroluminescent devices introducing fluorine-containing polyimide to hole-transporting layer,” *Mater. Sci. Eng., B*, 85: 195 (2001).
 92. J.H. Shin, J. Park, W. Lee, N. Jo, W. Cho, and C. Ha, “Organic electroluminescent devices using fluorine-containing polyimides as a hole transporting layer,” *Synth. Met.*, 137: 1017–1018 (2003).
 93. C. Liao, M. Lee, C. Tsai, and C.H. Chen, “Highly efficient blue organic light-emitting devices incorporating a composite hole transport layer,” *Appl. Phys. Lett.*, 86: i.d. 203507, 3 pages (2005).
 94. E. Bellmann, S.E. Shaheen, S. Thayumanavan, S. Barlow, R.H. Grubbs, S.R. Marder, B. Kippelen, and N. Peyghambarian, “New triarylamine-containing polymers as hole transport materials in organic light-emitting diodes: effect of polymer structure and cross-linking on device characteristics,” *Chem. Mater.*, 10: 1668–1676 (1998).
 95. M.S. Bayerl, T. Braig, O. Nuyken, D.C. Muller, M. Gross, and K. Meerholz, “Crosslinkable hole-transport materials for preparation of multilayer organic light emitting devices by spin-coating,” *Macro Rapid Commun.*, 20: 224–228 (1999).
 96. E. Bacher, S. Jungermann, M. Rojahn, V. Wiederhorn, and O. Nuyken, “Photopatterning of crosslinkable hole-conducting materials for application in organic light-emitting devices,” *Macromol. Rapid Commun.*, 25: 1191–1196 (2004).
 97. Y. Zhang, R. Hreha, G. Jabbour, B. Kippelen, N. Peyghambarian, and S.R. Marder, “Photocrosslinkable polymers as hole-transport materials for organic light-emitting diodes,” *J. Mater. Chem.*, 12: 1703–1708 (2002).
 98. X.C. Li, “Organic light-emitting device based on crosslinkable spiro-type conjugated compounds,” *U.S. Patent Appl. Publ.* (2004) pp. 13.
 99. S. Liu, X. Jiang, H. Ma, M.S. Liu, and A.K.-Y. Jen, “Triarylamine-containing poly(penfluorocyclobutane) as hole-transporting material for polymer light-emitting diodes,” *Macromolecules*, 33: 3514–3517 (2000).
 100. J. Ji, S. Narayan-Sarathy, R.H. Neilson, J.D. Oxley, D.A. Babb, N.G. Rondon, and W.S. Jr. Smith, “[p-(Trifluorovinyl)oxy]phenyl]lithium: formation, synthetic utility, and theoretical support for a versatile new reagent in fluoropolymer chemistry,” *Organometallics*, 17: 783–785 (1998).

101. X. Jiang, M.S. Liu, and A.K.-Y. Jen, "Bright and efficient exciplex emission from light-emitting diodes based on hole-transporting amine derivatives and electron-transporting polyfluorenes," *J. Appl. Phys.*, 91: 10147–10152 (2002).
102. X. Gong, D. Moses, A.J. Heeger, S. Liu, and A.K.-Y. Jen, "High-performance polymer light-emitting diodes fabricated with a polymer hole injection layer," *Appl. Phys. Lett.*, 83: 183–185 (2003).
103. P.M. Borsenberger, "Hole transport in *bis*(4-*N,N*-diethylamino-2-methylphenyl)-4-methylphenylmethane doped polymers," *Phys. Status Solidi B: Basic Res.*, 173: 671–680 (1992).
104. P.M. Borsenberger, W.T. Gruenbaum, and E.H. Magin, "Hole transport in vapor-deposited triphenylmethane glasses," *Jpn. J. Appl. Phys.*, 35: 2698–2703 (1996).
105. Y. Wang, "Dramatic effects of hole transport layer on the efficiency of iridium-based organic light-emitting diodes," *Appl. Phys. Lett.*, 85: 4848–4850 (2004).
106. M. Higuchi, S. Shiki, K. Ariga, and K. Yamamoto, "First synthesis of phenylazomethine dendrimer ligands and structural studies," *J. Am. Chem. Soc.*, 123: 4414–4420 (2001).
107. M. Higuchi, M. Tsuruta, H. Chiba, S. Shiki, and K. Yamamoto, "Control of stepwise radial complexation in dendritic polyphenylazomethines," *J. Am. Chem. Soc.*, 125: 9988–9997 (2003).
108. A. Kimoto, J. Cho, M. Higuchi, and K. Yamamoto, "Novel carbazole dendrimers having a metal coordination site as a unique hole-transport material," *Macromolecular Symposia 209 (Organometallic and Coordination Clusters and Polymers)*: pp. 51–65 (2004).
109. K. Yamamoto, M. Higuchi, S. Shiki, M. Tsuruta, and H. Chiba, "Stepwise radial complexation of imine groups in phenylazomethine dendrimers," *Nature*, 415: 509–511 (2002).
110. A. Kimoto, J. Cho, M. Higuchi, and K. Yamamoto, "Synthesis of asymmetrically arranged dendrimers with a carbazole dendron and a phenylazomethine dendron," *Macromolecules*, 37: 5531–5537 (2004).
111. J. Cho, A. Kimoto, M. Higuchi, and K. Yamamoto, "Synthesis of diphenylamine-substituted phenylazomethine dendrimers and the performance of organic light-emitting diodes," *Macro Chem. Phys.*, 206: 635–641 (2005).
112. B. Mi, P. Wang, M. Liu, H. Kwong, N. Wong, C. Lee, and S.T. Lee, "Thermally stable hole-transporting material for organic light-emitting diode: an isoindole derivative," *Chem. Mater.*, 15: 3148–3151 (2003).
113. H. Sugimura, Y. Kojima, S. Nishigaki, and K. Emoto, "High mobility hole transport materials having enamine structure," *Ninth International Congress on Advances in Non-Impact Printing Technologies*, Japan Hardcopy, October 4–8, 1993, Yokohama, pp. 627–630 (1993).
114. H. Suzuki, H. Meyer, J. Simmerer, J. Yang, and D. Haarer, "Electroluminescent devices based on poly(methylphenylsilane)," *Adv. Mater.*, 5: 743–746 (1993).
115. P. Kulkarni, C.J. Tonzola, A. Babel, and S.A. Jenekhe, "Electron transport materials for organic light-emitting diodes," *Chem. Mater.*, 16: 4556–4573 (2004).
116. G. Hughes and M.R. Bryce, "Electron-transporting materials for organic electroluminescent and electronphosphorescent devices," *J. Mater. Chem.*, 15: 94–107 (2005).
117. K.A. Higginson, X. Zhang, and F. Papadimitrakopoulos, "Thermal and morphological effects on the hydrolytic stability of Aluminum Tris(8-hydroxyquinoline) (Alq_3)," *Chem. Mater.*, 10: 1017–1020 (1998).
118. M. Brinkmann, G. Gadret, M. Muccini, C. Taliani, N. Masciocchi, and A. Sironi, "Correlation between molecular packing and optical properties in different crystalline polymorphs and amorphous thin films of *mer*-Tris(8-hydroxyquinoline)Aluminum(III)," *J. Am. Chem. Soc.*, 122: 5147–5157 (2000).
119. R.G. Kepler, P.M. Beeson, S.J. Jacobs, R.A. Anderson, M.B. Sinclair, V.S. Valencia, and P.A. Cahill, "Electron and hole mobility in tris(8-hydroxyquinolinolato- N_1, O_8) Aluminum," *Appl. Phys. Lett.*, 66: 3618–3620 (1995).
120. J.D. Anderson, E.M. McDonald, P.A. Lee, M.L. Anderson, E.L. Ritchie, H.K. Hall, T. Hopkins, E.A. Mash, J. Wang, A. Padias, S. Thayumanavan, S. Barlow, S.R. Marder, G.E. Jabbour, S. Shaheen, B. Kippelen, N. Peyghambarian, R.M. Wightman, and N.R. Armstrong, "Electrochemistry and

- electrogenerated chemiluminescence processes of the components of aluminum quinolate/triarylamine, and related organic light-emitting diodes,” *J. Am. Chem. Soc.*, 120: 9646–9655 (1998).
121. K. Kim, D.W. Lee, and J. Jin, “Electroluminescence properties of poly [2- (2'-ethylhexyloxy)-5-methoxy-1, 4-phenylenevinylene]/tris 8-hydroxyquinoline aluminum two-layer devices,” *Synth. Met.*, 114: 49–56 (2000).
 122. B.J. Chen, X.W. Sun, and Y.K. Li, “Influences of central metal ions on the electroluminescence and transport properties of tris-8-hydroxyquinoline metal chelates,” *Appl. Phys. Lett.*, 82: 3017–3019 (2003).
 123. D.Z. Garbuzov, V. Bulović, P.E. Burrows, and S.R. Forrest, “Photoluminescence efficiency and absorption of aluminum-tris-quinolate (Alq_3) thin films,” *Chem. Phys. Lett.*, 249: 433–437 (1996).
 124. R. Pohl, V.A. Montes, J. Shinar, and P. Anzenbacher Jr., “Red-green-blue emission from tris(5-aryl-8-quinolinolate)Al(III) complexes,” *J. Organ. Chem.*, 69: 1723–1725 (2004).
 125. V.A. Montes, C. Li, R. Pohl, J. Shinar, and P. Anzenbacher Jr., “Effective color tuning in organic light-emitting diodes based on Aluminium tris(5-aryl-8-hydroxyquinoline) complexes,” *Adv. Mater.*, 16: 2001–2003 (2004).
 126. J. Kido and Y. Iizumi, “Fabrication of highly efficient organic electroluminescent devices,” *Appl. Phys. Lett.*, 73: 2721–2723 (1998).
 127. M. Sugimoto, M. Anzai, K. Sakanoue, and S. Sakaki, “Modulating fluorescence of 8-quinolinolato compounds by functional groups: a theoretical study,” *Appl. Phys. Lett.*, 79: 2348–2350 (2001).
 128. M. Sugimoto, S. Sakaki, K. Sakanoue, and M.D. Newton, “Theory of emission state of tris-8-quinolinolato.aluminum and its related compounds,” *J. Appl. Phys.*, 90: 6092–6097 (2001).
 129. S.A. Vanslyke, P.S. Bryan, and F.V. Lovecchio, U.S. Patent 5,150,006 (1992).
 130. P.S. Bryan, F.V. Lovecchio, and S.A. Vanslyke, U.S. Patent 5,141,671 (1992).
 131. L.S. Sapochak,, F.E. Benincasa, R.S. Schofield, J.L. Baker, K.K.C. Riccio, D. Fogarty, H. Kohlmann, K.F. Ferris, and P.E. Burrows, “Electroluminescent Zinc(II) Bis(8-hydroxyquinoline): structural effects on electronic states and device performance,” *J. Am. Chem. Soc.*, 124: 6119–6125 (2002).
 132. C.H. Chen and J. Shi, “Metal chelates as emitting materials for organic electroluminescence,” *Coord. Chem. Rev.*, 171: 161–174 (1998).
 133. Y. Hamada, T. Sano, H. Fujii, Y. Nishio, H. Takahashi, and K. Shibata, “Organic light-emitting diodes using 3- or 5-hydroxyflavone–metal complexes,” *Appl. Phys. Lett.*, 71: 3338–3340 (1997).
 134. N. Donze, P. Pechy, M. Gratzel, M. Schaer, and L. Zuppiroli, “Quinolate zinc complexes as electron transporting layers in organic light-emitting diodes,” *Chem. Phys. Lett.*, 315: 405–410 (1999).
 135. Y. Kai, M. Morita, N. Yasuoka, and N. Kasai, “The crystal and molecular structure of anhydrous zinc 8-quinolinolate complex, $[\text{Zn}(\text{C}_9\text{H}_6\text{NO})_2]_n$,” *Bull. Chem. Soc. Jpn.*, 58: 1631–1635 (1985).
 136. G. Yu, S. Yin, Y. Liu, Z. Shuai, and D. Zhu, “Structures, electronic states, and electroluminescent properties of a Zinc(II) 2-(2-hydroxyphenyl)benzothiazolate complex,” *J. Am. Chem. Soc.*, 125: 14816–14824 (2003).
 137. X. Xu, G. Yu, Y. Liu, R. Tang, F. Xi, and D. Zhu, “Effect of metal chelate layer on electroluminescent and current–voltage characteristics,” *Appl. Phys. Lett.*, 86: id 202109, 3 pages (2005).
 138. S.W. Pyoa, S.P. Lee, H.S. Lee, O.K. Kwon, H.S. Hoe, S.H. Lee, Y. Ha, Y.K. Kim, and J.S. Kim, “White-light-emitting organic electroluminescent devices using new chelate metal complexes,” *Thin Solid Films*, 363: 232–235 (2000).
 139. T. Sano, Y. Nishio, Y. Hamada, H. Takahashi, T. Usuki, and K. Shibata, “Design of conjugated molecular materials for optoelectronics,” *J. Mater. Chem.*, 10: 157–161 (2000).
 140. Y. Li, Y. Liu, J. Guo, F. Wu, W. Tian, B. Li, and Y. Wang, “Photoluminescent and electroluminescent properties of phenol–pyridine beryllium and carbonyl polypyridyl Re(I) complexes codeposited films,” *Synth. Met.*, 118: 175–179 (2001).
 141. J. Shi, C.W. Tang, and C.H. Chen, “Blue Organic Electroluminescent Devices,” U.S. Patent 5,645,948, pp. 22 (1997).
 142. J. Shi, C.W. Tang, and C.H. Chen, “Electron Transporting Materials for Organic Electroluminescent Devices,” *Eur. Pat. Appl.*, pp. 36 (1998).

143. T.C. Wong, J. Kovac, C.S. Lee, L.S. Hung, and S.T. Lee, "Transient electroluminescence measurements on electron-mobility of *N*-arylbenzimidazoles," *Chem. Phys. Lett.*, 334: 61–64 (2001).
144. Y. Li, M.K. Fung, Z. Xie, S. Lee, L. Hung, and J. Shi, "An efficient pure blue organic light-emitting device with low driving voltages," *Adv. Mater.*, 14: 1317–1321 (2000).
145. H.T. Shih, C.H. Lin, H.H. Shih, and C.H. Vheng, "High-performance blue electroluminescent devices based on a biaryl," *Adv. Mater.*, 14: 1409–1412 (2002).
146. C. Adachi, M.A. Baldo, S.R. Forrest, S. Lamansky, M.E. Thompson, and R.C. Kwong, "High-efficiency red electrophosphorescent devices," *Appl. Phys. Lett.*, 78: 1622–1624 (2001).
147. S. Lo, N.A.H. Male, J.P.J. Markham, S.W. Magennis, P.L. Burn, O.V. Salata, and I.D.W. Samuel, "Green phosphorescent dendrimer for light-emitting diodes," *Adv. Mater.*, 14: 975–979 (2002).
148. C.J. Tonzola, M.M. Alam, W. Kaminsky, and S.A. Jenekhe, "New *n*-type organic semiconductors: synthesis, single crystal structures, cyclic voltammetry, photophysics, electron transport, and electroluminescence of a series of diphenylanthrazolines," *J. Am. Chem. Soc.*, 125: 13548–13558 (2003).
149. M. Redecker, D.D.C. Bradley, M. Jandke, and P. Strohriegel, "Electron transport in starburst phenylquinoxalines," *Appl. Phys. Lett.*, 75: 109–111 (1999).
150. R. Fink, Y. Heischkel, M. Thelakkat, and H.-W. Schmidt, "Synthesis and application of dimeric 1,3,5-triazine ethers as hole-blocking materials in electroluminescent devices," *Chem. Mater.*, 10: 3620–3625 (1998).
151. C. Adachi, T. Tsutsui, and S. Saito, "Organic electroluminescent device having a hole conductor as an emitting layer," *Appl. Phys. Lett.*, 55: 1489–1491 (1989).
152. J. Pommerehne, H. Vestweber, W. Guss, R.F. Mahrt, H. Bassler, M. Porsch, and J. Daub, "Efficient two layer LEDs on polymer blend basis," *Adv. Mater.*, 7: 551–554 (1995).
153. H. Tanaka, S. Tokito, Y. Taga, and A. Okada, "Novel metal–chelate emitting materials based on polycyclic aromatic ligands for electroluminescent devices," *J. Mater. Chem.*, 8: 1999–2003 (1998).
154. S. Tokito, K. Noda, H. Tanaka, Y. Taga, and T. Tsutsui, "Organic light-emitting diodes using novel metal–chelate complexes," *Synth. Met.*, 111–112: 393–396 (2000).
155. Y. Sakamoto, T. Suzuki, A. Miura, H. Fujikawa, S. Tokito, and Y. Taga, "Synthesis, characterization, and electron-transport property of perfluorinated phenylene dendrimers," *J. Am. Chem. Soc.*, 122: 1832–1833 (2000).
156. K. Tamao, M. Uchida, T. Izumizawa, K. Furukawa, and S. Yamaguchi, "Silole derivatives as efficient electron transporting materials," *J. Am. Chem. Soc.*, 118: 11974–11975 (1996).
157. G. Yu, S. Yin, Y. Liu, J. Chen, X. Xu, X. Sun, D. Ma, X. Zhan, Q. Peng, Z. Shuai, B. Tang, D. Zhu, W. Fang, and Y. Luo, "Structures, electronic states, photoluminescence, and carrier transport properties of 1,1-disubstituted 2,3,4,5-tetraphenylsiloles," *J. Am. Chem. Soc.*, 127: 6335–6346 (2005).
158. X. Zhan, C. Risko, F. Amy, C. Chan, W. Zhao, S. Barlow, A. Kahn, J. Brédas, and S.R. Marder, "Electron affinities of 1,1-diaryl-2,3,4,5-tetraphenylsiloles: direct measurements and comparison with experimental and theoretical estimates," *J. Am. Chem. Soc.*, 127: 9021–9029 (2005).
159. S.H. Lee, B. Jang, and Z.H. Kafafi, "Highly fluorescent solid-state asymmetric spiro-silabifluorene derivatives," *J. Am. Chem. Soc.*, 127: 9071–9078 (2005).
160. H. Murata, G.G. Malliaras, M. Uchida, Y. Shen, and Z.H. Kafafi, "Non-dispersive and air stable electron transport in an amorphous organic semiconductor," *Chem. Phys. Lett.*, 339: 161–166 (2001).
161. H. Murata, Z.H. Kafafi, and M. Uchida, "Efficient organic light-emitting diodes with undoped active layers based on silole derivatives," *Appl. Phys. Lett.*, 80: 189–191 (2002).
162. M. Uchida, T. Izumizawa, T. Nakano, S. Yamaguchi, K. Tamao, and K. Furukawa, "Structural optimization of 2,5-diarylsiloles as excellent electron-transporting materials for organic electroluminescent devices," *Chem. Mater.*, 13: 2680–2683 (2001).
163. B.Z. Tang, X. Zhan, G. Yu, P.P.S. Lee, Y. Liu, and D. Zhu, "Efficient blue emission from siloles," *J. Mater. Chem.*, 11: 2974–2978 (2001).
164. J. Ohshita, M. Nodono, H. Kai, T. Watanabe, A. Kunai, K. Komaguchi, M. Shiotani, A. Adachi, K. Okita, Y. Harima, K. Yamashita, and M. Ishikawa, "Synthesis and optical, electrochemical, and electron-transporting properties of silicon-bridged bithiophenes," *Organometallics*, 18: 1453–1459 (1999).

165. P. Lu, H. Hong, G. Cai, P. Djurovich, W.P. Weber, and M.E. Thompson, "Synthesis of octasubstituted cyclooctatetraenes and their use as electron transporters in organic light emitting diodes," *J. Am. Chem. Soc.*, 122: 7480–7486. (2000).
166. T. Noda and Y. Shirota, "5,5'-Bis(dimesitylboryl)-2,2'-bithiophene and 5,5'-Bis(dimesitylboryl)-2,2':5,2''-terthiophene as a novel family of electron-transporting amorphous molecular materials," *J. Am. Chem. Soc.*, 120: 9714–9715 (1998).
167. S.A. Vanslyke, C.W. Tang, and L.C. Roberts, "Electroluminescent Device with Organic Luminescent Medium," U.S. Patent 4,720,432A, pp. 16 (1988).
168. T. Thoms, S. Okada, J. Chen, and M. Furugori, "Improved host material design for phosphorescent guest–host systems," *Thin Solid Films*, 436: 264–268 (2003).
169. T. Tsuji, S. Kawami, S. Miyaguchi, T. Naijo, T. Yuki, S. Matsuo, and H. Miyazaki, SID Symposium Digest of Technical Papers, Vol. 35, Issue 1, May 2004, pp. 900 (2004).
170. *IEEE J. Sel. Top. Quantum Electron.*, 10: 101 (2004).
171. T. Chu, Y. Wu, J. Chen, and C.H. Chen, "Characterization of electronic structure of Aluminum (III) bis(2-methyl-8-quinolinato)-4-phenylphenolate (BALq) for phosphorescent organic light emitting devices," *Chem. Phys. Lett.*, 404: 121–125 (2005).
172. F. Chen, G. He, Y. Yang, "Triplet exciton confinement in phosphorescent polymer light-emitting diodes," *Appl. Phys. Lett.*, 82: 1006–1008 (2003).
173. C. Adachi, M.A. Baldo, S.R. Forrest, and M.E. Thompson, "High-efficiency organic electrophosphorescent devices with tris(2-phenylpyridine)iridium doped into electron-transporting materials," *Appl. Phys. Lett.*, 77: 904–906 (2000).
174. M. Klessinger and J. Michl, *Excited States and Photochemistry of Organic Molecules*, VCH Publishers, New York (1995).
175. H. Kanai, S. Ichinosawa, and Y. Sato, "Effect of aromatic diamines as a cathode interface layer," *Synth. Met.*, 91: 195–196 (1997).
176. C. Adachi, R.C. Kwong, P. Djurovich, V. Adamovich, M.A. Baldo, M.E. Thompson, and S.R. Forrest, "Endothermic energy transfer: a mechanism for generating very efficient high-energy phosphorescent emission in organic materials," *Appl. Phys. Lett.*, 79: 2062–2064 (2001).
177. S. Tokito, T. Iijima, Y. Suzuri, H. Kita, T. Tsuzuki, and F. Sato, "Confinement of triplet energy on phosphorescent molecules for highly-efficient organic blue-light-emitting devices," *Appl. Phys. Lett.*, 83: 569–571 (2003).
178. S. Tokito, T. Iijima, T. Tsuzuki, and F. Sato, "High-efficiency white phosphorescent organic light-emitting devices with greenish-blue and red-emitting layers," *Appl. Phys. Lett.*, 83: 2459–2461 (2003).
179. I. Tanaka, Y. Tabata, and S. Tokito, "Energy-transfer and light-emission mechanism of blue phosphorescent molecules in guest–host systems," *Chem. Phys. Lett.*, 400: 86–89 (2004).
180. K. Brunner, A. van Dijken, H. Borner, J.J.A.M. Bastiaansen, N.M.M. Kikken, and B.M.W. Langeveld, "Carbazole compounds as host materials for triplet emitters in organic light-emitting diodes: tuning the HOMO level without influencing the triplet energy in small molecules," *J. Am. Chem. Soc.*, 126: 6035–6042 (2004).
181. R.J. Holmes, S.R. Forrest, Y.J. Tung, R.C. Kwong, J.J. Brown, S. Garon, and M.E. Thompson, "Blue organic electrophosphorescence using exothermic host–guest energy transfer," *Appl. Phys. Lett.*, 82: 2422–2424 (2003).
182. G.T. Lei, L.D. Wang, L. Duan, J.H. Wang, and Y. Qiu, "Highly efficient blue electrophosphorescent devices with a novel host material," *Synth. Met.*, 144: 249–252 (2004).
183. G. Lei, L. Wang, and Y. Qiu, "Blue phosphorescent dye as sensitizer and emitter for white organic light-emitting diodes," *Appl. Phys. Lett.*, 85: 5403–5405 (2004).
184. R.J. Holmes, B.W. D'Andrade, S.R. Forrest, X. Ren, J. Li, and M.E. Thompson, "Efficient, deep-blue organic electrophosphorescence by guest charge trapping," *Appl. Phys. Lett.*, 83: 3818–3820 (2003).
185. X. Ren, J. Li, R.J. Holmes, P.I. Djurovich, S.R. Forrest, and M.E. Thompson, "Ultrahigh energy gap hosts in deep blue organic electrophosphorescent devices," *Chem. Mater.*, 16: 4743–4747 (2004).

186. C.H. Chen, C.W. Tang, J. Shi, and K.P. Klubek, "Green Organic Electroluminescent Devices," U.S. Patent 6,020,078 (2000).
187. T. Wakimoto and Y. Yonemoto, Japan Patent 6,240,243 (1994).
188. J.L. Fox and C.H. Chen, U.S. Patent 4,736,032 (1988).
189. C.H. Chen and C.W. Tang, "Efficient green organic light-emitting diodes with sterically hindered coumarin dopants," *Appl. Phys. Lett.*, 79: 3711–3713 (2001).
190. M. Lee, C. Yen, W. Yang, H. Chen, C. Liao, C. Tsai, and C.H. Chen, "Efficient green coumarin dopants for organic light-emitting devices," *Org. Lett.*, 6: 1241–1244 (2004).
191. J. Shi and C.W. Tang, "Organic electroluminescent devices with high operational stability," U.S. Patent 5,593,788, pp. 13 (1997).
192. J. Shi and C.W. Tang, "Doped organic electroluminescent devices with improved stability," *Appl. Phys. Lett.*, 70: 1665–1667 (1997).
193. T. Wakimoto, Y. Yonemoto, J. Funaki, M. Tsuchida, R. Murayama, H. Nakada, H. Matsumoto, S. Yamamura, and M. Nomura, "Stability characteristics of quinacridone and coumarin molecules as guest dopants in the organic LEDs," *Synth. Met.*, 91: 15–19 (1997).
194. H. Murata, C.D. Merritt, H. Inada, Y. Shiota, and Z.H. Kafafi, "Molecular organic light-emitting diodes with temperature-independent quantum efficiency and improved thermal durability," *Appl. Phys. Lett.*, 75: 3252–3254 (1999).
195. L. Wang, Y. Gao, P. Wei, and Y. Qiu, "Novel structure organic light-emitting diodes with high performance," *SID Digest Tech. Pap.*, 35: 703–705 (2004).
196. K.P. Klubek and C.W. Tang, "Stable Organic Light Emitting Devices Using Aminoanthracenes," U.S. Patent 0,153,163 (2005).
197. C.T. Brown and D.Y. Kondakov, "Efficient electroluminescent device," *Eur. Pat. Appl.*, EPI357613A2 (2003).
198. J.D. Debad, C.J. Morris, V. Lynch, P. Magnus, and A.J. Bard, "Dibenzotetraphenylperiflanthene: synthesis, photophysical properties, and electrogenerated chemiluminescence," *J. Am. Chem. Soc.*, 118: 2374–2379 (1996).
199. R. Adams and M.H. Gold, "Synthesis of 1,3-diphenyldihydroisobenzofurans, 1,3-diphenylisobenzofurans and *o*-dibenzoylbenzenes from the diene addition products to dibenzoylethylene," *J. Am. Chem. Soc.*, 62: 56–61 (1940).
200. M. Yu, J. Duan, C. Lin, C. Cheng, and Y. Tao, "Diaminoanthracene derivatives as high-performance green host electroluminescent materials," *Chem. Mater.*, 14: 3958–3963 (2002).
201. S. Tokito, K. Noda, H. Fujikawa, and Y. Taga, "Highly efficient blue-green emission from organic light-emitting diodes using dibenzochrysene derivatives," *Appl. Phys. Lett.*, 77: 160–162 (2000).
202. Y.T. Tao, E. Balasubramaniam, A. Danel, B. Jarosz, and P. Tomasik, "Sharp green electroluminescence from 1*H*-pyrazolo[3,4-*b*]quinoline-based light-emitting diodes," *Appl. Phys. Lett.*, 77: 1575–1577 (2000).
203. Y. You, Y. He, P.E. Burrows, S.R. Forrest, N.A. Petasis, and M.E. Thompson, "Fluorophores related to the green fluorescent protein and their use in optoelectronic devices," *Adv. Mater.*, 12: 1678–1681 (2000).
204. C. Chen, "Evolution of red organic light-emitting diodes: materials and devices," *Chem. Mater.*, 16: 4389–4400 (2004).
205. F.G. Webster and W.C. McColgin, U.S. Patent 3,852,683 (1974).
206. C.H. Chen, K.P. Klubek, and J. Shi, "Red Organic Electroluminescent Materials," U.S. Patent 5,908,581 (1999).
207. C.H. Chen, C.W. Tang, and J. Shi, "Red Organic Electroluminescent Devices," U.S. Patent 5,935,720 (1999).
208. C.H. Chen, C.W. Tang, J. Shi, and K.P. Klubek, "Recent developments in the synthesis of red dopants for Alq₃ hosted electroluminescence," *Thin Solid Films*, 363: 327–331 (2000).
209. M. Chang, W. Huang, and W. Huang, "Red Organic Electroluminescent Materials," U.S. Patent 6,649,089 (2003).
210. C. Ma, Z. Liang, X. Wang, B. Zhang, Y. Cao, L. Wang, and Y. Qiu, "A novel family of red fluorescent materials for organic light-emitting diodes," *Synth. Met.*, 138: 537–542 (2003).

211. X.H. Zhang, B.J. Chen, X.Q. Lin, O.Y. Wong, C.S. Lee, H.L. Kwong, S.T. Lee, and S.K. Wu, "A new family of red dopants based on chromene-containing compounds for organic electroluminescent devices," *Chem. Mater.*, 13: 1565–1569 (2001).
212. X.T. Tao, S. Miyata, H. Sasabe, G.J. Zhang, T. Wada, and M.H. Jiang, "Efficient organic red electroluminescent device with narrow emission peak," *Appl. Phys. Lett.*, 78: 279–281 (2001).
213. R. Lemke, "Knoevenagel condensation in dimethylformamide," *Synthesis*, 5: 359–361 (1974).
214. J. Li, D. Liu, Z. Jong, S. Tong, P. Wang, C. Ma, O. Lengyel, C. Lee, H. Kwong, and S. Lee, "A new family of isophorone-based dopants for red organic electroluminescent devices," *Chem. Mater.*, 15: 1486–1490 (2003).
215. B. Jung, C. Yoon, H. Shim, L. Do, and T. Zyung, "Pure-red dye for organic electroluminescent devices: *bis*-condensed DCM derivatives," *Adv. Func. Mater.*, 11: 430–434 (2001).
216. J. Qiao, Y. Qiu, L. Wang, L. Duan, Y. Li, and D. Zhang, "Pure red electroluminescence from a host material of binuclear gallium complex," *Appl. Phys. Lett.*, 81: 4913–4915 (2002).
217. T. Liu, C. Iou, S. Wen, and C.H. Chen, "4-(Dicyanomethylene)-2-*t*-butyl-6-(1,1,7,7-tetramethyljulolidyl-9enyl)-4H-pyran doped red emitters in organic light-emitting devices," *Thin Solid Films*, 441: 223–227 (2003).
218. K. Takada, M. Ichimura, T. Ishibashi, and S. Tamura, "*Bis*(aminostyryl)stilbene-type compound, synthetic intermediate for the compound, manufacture of the intermediate and the compound, and organic electroluminescent device," *Jpn. Kokai Tokkyo Koho*, JP2001131128, pp. 44 (2001).
219. T. Ishibashi, M. Ichimura, S. Tamura, and N. Ueda, "Organic electroluminescent device or display using styryl compound," *PCT Int. Appl.*, WO 2004003104, pp. 142 (2004).
220. K.R.J. Thomas, J.T. Lin, M. Velusamy, Y. Tao, and C. Chuen, "Color tuning in benzo[1,2,5]thiadiazole-based small molecules by amino conjugation/deconjugation: bright red light emitting diodes," *Adv. Func. Mater.*, 14: 83–90 (2004).
221. H. Yeh, L. Chan, W. Wua, and C. Chen, "Non-doped red organic light-emitting diodes," *J. Mater. Chem.*, 14: 1293–1298 (2004).
222. K.R.J. Thomas, J.T. Lin, Y. Tao, and C. Chuen, "Star-shaped thieno-[3,4-*b*]-pyrazines: a new class of red-emitting electroluminescent materials," *Adv. Mater.*, 114: 822–826 (2002).
223. T. Mori, K. Miyachi, T. Kichimi, and T. Mizutani, "Electrical and luminescent properties of color-changeable organic electroluminescent diode using squarylium dyes," *Jpn. J. Appl. Phys.*, 33: 6594–6598 (1994).
224. B. Zhang, W. Zhao, Y. Cao, X. Wang, Z. Zhang, and X. Jiang, "Photoluminescence and electroluminescence of squarylium cyanine dyes," *Synth. Met.*, 91: 237–241 (1997).
225. L.C. Picciolo, H. Murata, and Z.H. Kafafi, "Organic light-emitting devices with saturated red emission using 6,13-diphenylpentacene," *Appl. Phys. Lett.*, 78: 2378–2380 (2001).
226. T. Huang, J.T. Lin, Y. Tao, and C. Chuen, "Benzo[*a*]aceanthrylene derivatives for red-emitting electroluminescent materials," *Chem. Mater.*, 15: 4854–4862 (2003).
227. J. Fang and D. Ma, "Efficient red organic light-emitting devices based on a europium complex," *Appl. Phys. Lett.*, 83: 4041–4043 (2003).
228. L. Huang, K. Wang, C. Huang, F. Lia, and Y. Huang, "Bright red electroluminescent devices using novel second-ligand contained europium complexes as emitting layers," *J. Mater. Chem.*, 11: 790–793 (2001).
229. P. Wang, Z. Hong, Z. Xie, S. Tong, O. Wong, C. Lee, N. Wong, L. Hung, and S. Lee, "A *bis*-salicylaldiminato Schiff base and its zinc complex as new highly fluorescent red dopants for high performance organic electroluminescence devices," *Chem. Commun.*, 1664–1665 (2003).
230. C. Hosokawa, H. Higashi, H. Nakamura, and T. Kusumoto, "Highly efficient blue electroluminescence from a distyrylarylene emitting layer with a new dopant," *Appl. Phys. Lett.*, 67: 3853–3855 (1995).
231. C. Hosokawa, H. Higashi, H. Nakamura, and T. Kusumoto, U.S. Patent 5,389,444 (1995).
232. Y.Z. Wu, X.Y. Zheng, W.Q. Zhu, R.G. Sun, X.Y. Jiang, Z.L. Zhang, and S.H. Xu, "Highly efficient pure blue electroluminescence from 1,4-*bis*[2-(3-*N*-ethylcarbazoryl)vinyl]benzene," *Appl. Phys. Lett.*, 83: 5077–5079 (2003).
233. C.H. Chuen, Y.T. Tao, F.I. Wu, and C.F. Shu "White organic light emitting diodes based on 2,7-*bis*(2,2-diphenylvinyl)-9-9'-spirobifluorene: improvement in operational lifetime," *Appl. Phys. Lett.*, 85: 4609–4611 (2004).

234. M. Lee, S. Liao, C. Tsai, and C.H. Chen, "Highly efficient, deep-blue doped organic light-emitting devices," *Adv. Mater.*, 17: 2493–2497 (2005).
235. L. Huang, H. Tian, F. Li, D. Gao, Y. Huang, and C. Huang, "Blue organic electroluminescent devices based on a distyrylarylene derivatives as emitting layer and a terbium complex as electron-transporting layer," *J. Luminescence*, 97: 55–59 (2002).
236. X.B. Ding, J.G. Zheng, Y.D. Jin, G. Aerts, B.X. Peng, P.L. Heremans, G. Borghs, and H.J. Geise, "Development and characterization of alkyloxy-substituted biphenyl compounds as guest in blue OLEDs," *Synth. Met.*, 142: 267–273 (2004).
237. F. He, H. Xu, B. Yang, Y. Duan, L. Tian, K. Huang, Y. Ma, S. Liu, S. Feng, and J. Shen, "Oligomeric phenylenevinylene with cross dipole arrangement and amorphous morphology: enhanced solid-state luminescence efficiency and electroluminescence performance," *Adv. Mater.*, 17: 2710–2714 (2005).
238. Y. Duan, F. He, G. Cheng, J. Li, Y. Ma, and S. Liu, "Blue electroluminescent devices based on a trimeric phenylenevinylene derivative as emitting layer," *Thin Solid Films*, 492: 275–278 (2005).
239. J. Shi, C.H. Chen, and K.P. Klubek, "Organic Electroluminescent Elements for Stable Blue Electroluminescent Devices," U.S. Patent 5,972,247 (1999).
240. X. Jiang, Z. Zhang, X. Zheng, Y. Wu, and S. Xu, "A blue organic emitting diode from anthracene derivative," *Thin Solid Films*, 401: 251–254 (2001).
241. J. Shi and C.W. Tang, "Anthracene derivatives for stable blue-emitting organic electroluminescence devices," *Appl. Phys. Lett.*, 80: 3201–3203 (2002).
242. S. Tao, Z. Hong, Z. Peng, W. Ju, X. Zhang, P. Wang, S. Wu, and S. Lee, "Anthracene derivative for a non-doped blue emitting organic electroluminescence device with both excellent color purity and high efficiency," *Chem. Phys. Lett.*, 397: 1–4 (2004).
243. Y. Kan, L. Wang, L. Duan, Y. Hu, G. Wu, and Y. Qiu, "Highly-efficient blue electroluminescence based on two emitter isomers," *Appl. Phys. Lett.*, 84: 1513–1515 (2004).
244. M. Lee, H. Chen, C. Liao, C. Tsai, and C.H. Chen, "Stable styrylamine-doped blue organic electroluminescent device based on 2-methyl-9,10-di(2-naphthyl)anthracene," *Appl. Phys. Lett.*, 85: 3301–3303 (2004).
245. D. Gebeyehu, K. Walzer, G. He, M. Pfeiffer, K. Leo, J. Brandt, A. Gerhard, and H. Vestweber, "Highly efficient deep-blue organic light-emitting diodes with doped transport layers," *Synth. Met.*, 148: 205–211 (2005).
246. W. Shen, R. Dodda, C. Wu, F. Wu, T. Liu, H. Chen, C.H. Chen, and C. Shu, "Spirobifluorene-linked bis-anthracene: an efficient blue emitter with pronounced thermal stability," *Chem. Mater.*, 16: 930–934 (2004).
247. K. Danel, T. Huang, J.T. Lin, Y. Tao, and C. Chuen, "Blue-emitting anthracenes with end-capping diarylamines," *Chem. Mater.*, 14: 3860–3865 (2002).
248. Y.T. Tao, E. Balasubramaniam, A. Danel, A. Wisla, and P. Tomasik, "Pyrazoloquinoline derivatives as efficient blue electroluminescent materials," *J. Mater. Chem.*, 11: 768–772 (2001).
249. Z. Lu, Q. Jiang, W. Zhu, M. Xie, Y. Hou, X. Chen, Z. Wang, D. Zou, and T. Tsutsui, "Efficient blue emission from pyrazoline organic light emitting diodes," *Synth. Met.*, 111–112: 425–427 (2000).
250. H. Ogawa, K. Ohnishi, and Y. Shirota, "Tri(*p*-terphenyl-4-yl)amine as a novel blue-emitting material for organic electroluminescent devices," *Synth. Met.*, 91: 243–245 (1997).
251. Y. Kijima, N. Asai, and S. Tamura, "A blue organic light emitting diode," *Jpn. J. Appl. Phys.*, 38: 5274–5277 (1999).
252. T. Tachikawa, S. Terazono, and S. Tokita, "Blue light-emitting electroluminescent devices with 2,9-disubstituted 1,10-phenanthrolines," *Synth. Met.*, 91: 247–248 (1997).
253. T. Mitsumori, M. Bendikov, O. Dautel, F. Wudl, T. Shioya, H. Sato, and Y. Sato, "Synthesis and properties of highly fluorescent indolizino[3,4,5-*ab*]isoindoles," *J. Am. Chem. Soc.*, 126: 16793–16803 (2004).
254. Q. Wu, J.A. Lavigne, Y. Tao, M. D'Iorio, and S. Wang, "Novel blue luminescent/electroluminescent 7-azaindole derivatives: 1,3-di(*N*-7-azaindoly)benzene, 1-bromo-3,5-di(*N*-7-azaindoly)benzene, 1,3,5-tri(*N*-7-azaindoly)benzene, and 4,4'-di(*N*-7-azaindoly)biphenyl," *Chem. Mater.*, 13: 71–77 (2001).

255. J. Salbeck, N. Yu, J. Bauer, F. Weissörtel, and H. Bestgen, "Low molecular organic glasses for blue electroluminescence," *Synth. Met.*, 91: 209–215 (1997).
256. T. Spehr, R. Pudzich, T. Fuhrmann, and J. Salbeck, "Highly efficient light emitters based on the spiro concept," *Org. Electron.*, 4: 61–69 (2003).
257. C.C. Wu, Y.T. Lin, H.H. Chiang, T.Y. Cho, C.W. Chen, K.T. Wong, Y.L. Liao, G.H. Lee, and S.M. Peng, "Highly bright blue organic light-emitting devices using spirobifluorene-cored conjugated compounds," *Appl. Phys. Lett.*, 81: 577–579 (2002).
258. B. Li, Y. Qiu, L. Wang, and Y. Gao, "Spiro-annulated compound as stable and high efficiency blue host light emitter," *Jpn. J. Appl. Phys.*, 9: 5599–5601 (2002).
259. Y. Sato, S. Ichinosawa, T. Ogata, M. Fugono, and Y. Murata, "Blue-emitting organic EL devices with a hole blocking layer," *Synth. Met.*, 111–112: 25–29 (2000).
260. L. Chan, H. Yeh, and C. Chen, "Blue light-emitting devices based on molecular glass materials of tetraphenylsilane compounds," *Adv. Mater.*, 13: 1637–1641 (2001).
261. L. Chan, R. Lee, C. Hsieh, H. Yeh, and C. Chen, "Optimization of high-performance blue organic light-emitting diodes containing tetraphenylsilane molecular glass materials," *J. Am. Chem. Soc.*, 124: 6469–6479 (2002).
262. H. Murata, Z.H. Kafafi, and M. Uchida, "Efficient organic light-emitting diodes with undoped active layers based on silole derivatives," *Appl. Phys. Lett.*, 80: 189–191 (2002).
263. S.A. Vanslyke, "Blue Emitting Internal Junction Organic Electroluminescent Device(I)," U.S. Patent 5,151,629 (1992).
264. J. Yu, Z. Chen, Y. Sakuratani, H. Suzuki, M. Tokita, and S. Miyata, "A novel blue light emitting diode using tris(2,3-dimethyl-8-hydroxyquinoline) Aluminum(III) as emitter," *Jpn. J. Appl. Phys.*, 38: 6762–6763 (1999).
265. L.M. Leung, W.Y. Lo, K.M. Lee, and W.K. Choi, "A high-efficiency blue emitter for small molecule-based organic light-emitting diode," *J. Am. Chem. Soc.*, 122: 5640–5641 (2000).
266. X.T. Tao, H. Suzuki, T. Wada, S. Miyata, and H. Sasabe, "Highly efficient blue electroluminescence of lithium tetra-(2-methyl-8-hydroxy-quinolinato) boron," *J. Am. Chem. Soc.*, 121: 9447–9448 (1999).
267. X.T. Tao, H. Suzuki, T. Wada, H. Sasabe, and S. Miyata, "Lithium tetra-(8-hydroxy-quinolinato) boron for blue electroluminescent applications," *Appl. Phys. Lett.*, 75: 1655–1657 (1999).
268. A.J. Middleton, W.J. Marshall, and N.S. Radu, "Elucidation of the structure of a highly efficient blue electroluminescent materials," *J. Am. Chem. Soc.*, 125: 880–881 (2003).
269. Y. Liu, J. Guo, J. Feng, H. Zhang, Y. Li, and Y. Wang, "High-performance blue electroluminescent devices based on hydroxyphenyl-pyridine beryllium complex," *Appl. Phys. Lett.*, 78: 2300–2302 (2001).
270. T. Noda, H. Ogawa, and Y. Shirota, "A blue-emitting organic electroluminescent device using a novel emitting amorphous molecular material, 5,5'-bis(dimesitylboryl)-2,2'-bithiophene," *Adv. Mater.*, 11: 283–285 (1999).
271. J. Shi, C.H. Chen, and K.P. Klubek, "Blue Luminescent Materials for Organic Electroluminescent Devices," U.S. Patent 5,755,999 (1998).
272. J. Shi and C.H. Chen, "Efficient Blue Organic Electroluminescent Devices," U.S. Patent 5,928,802 (1999).
273. J. Kido, M. Kimura, and K. Nagai, "Multilayer white light emitting organic electroluminescent device," *Science*, 267: 1332–1334 (1995).
274. K.O. Cheon and J. Shinar, "Bright white small molecular organic light-emitting devices based on a red-emitting guest–host layer and blue-emitting 4,4'-bis(2,2'-diphenylvinyl)-1,1'-biphenyl," *Appl. Phys.*, 81: 1738–1740 (2002).
275. L. Wang, L. Duan, G. Lei, and Y. Qiu, "Bright white organic light-emitting diodes based on anthracene derivatives and rubrene," *Jpn. J. Appl. Phys.*, 43: L560–L562 (2004).
276. Z. Hong, W.L. Li, D. Zhao, C. Liang, X. Liu, and J. Peng, "White light emission from OEL devices based on organic dysprosium complex," *Synth. Met.*, 111–112: 43–45 (2000).
277. Y. Hamada, T. Sano, H. Fujii, Y. Nishio, H. Takahashi, and K. Shibata, "White light emitting materials for organic electroluminescent devices," *Jpn. J. Appl. Phys.*, 35: L1339–L1341 (1996).

278. G. Yu, S. Yin, Y. Liu, Z. Shuai, and D. Zhu, "Structures, electronic states, and electroluminescent properties of a zinc(II) 2-(2-hydroxyphenyl)benzothiazolate complex," *J. Am. Chem. Soc.*, 125: 14816–14824 (2003).
279. Y. Liu, J. Guo, H. Zhang, and Y. Wang, "Highly efficient white organic electroluminescence from a double-layer device based on a boron hydroxyphenylpyridine complex," *Angew. Chem. Int. Ed.*, 41: 182–184 (2002).
280. J.Y. Li, D. Liu, C. Ma, O. Lengyel, C. Lee, C. Tung, and S. Lee, "White light emission from a single emitting component organic electroluminescent device," *Adv. Mater.*, 16: 1538–1541 (2004).
281. F. Liang, L. Wang, D. Ma, X. Jing, and F. Wang, "Oxadiazole-containing material with intense blue phosphorescence emission for organic light-emitting diodes," *Appl. Phys. Lett.*, 81: 4–6 (2002).
282. M.A. Baldo, S. Lamansky, P.E. Burrows, M.E. Thompson, and S.R. Forrest, "Very high-efficiency green organic light-emitting devices based on electrophosphorescence," *Appl. Phys. Lett.*, 75: 4–6 (1999).
283. K.A. King, P.J. Spellane, and R.J. Watts, "Excited-state properties of a triply ortho-metalated Iridium(III) complex," *J. Am. Chem. Soc.*, 107: 1431–1432 (1985).
284. W. Holzer, A. Penzkofer, and T. Tsuboi, "Absorption and emission spectroscopic characterization of Ir(ppy)₃," *Chem. Phys.*, 308: 93–102 (2005).
285. Y. Kawamura, K. Goushi, J. Brooks, and J.J. Brown, "100% Phosphorescence quantum efficiency of Ir(III) complexes in organic semiconductor films," *Appl. Phys. Lett.*, 86: i.d. 071104, 3 pages (2005).
286. T. Tsutsui, M. Yang, M. Yahiro, K. Nakamura, T. Watanabe, T. Tsuji, Y. Fukuda, T. Wakimoto, and S. Miyaguchi, "High quantum efficiency in organic light-emitting devices with iridium-complex as a triplet emissive center," *Jpn. J. Appl. Phys.*, 38: L1502–L1504 (1999).
287. S. Sprouse, K.A. King, P.J. Spellane, and R.J. Watts, "Photophysical effects of metal-carbon σ bonds in ortho-metalated complexes of Ir(III) and Rh(III)," *J. Am. Chem. Soc.*, 106: 6647–6653 (1984).
288. K. Dedeian, P.I. Djurovich, F.O. Garces, G. Carlson, and R.J. Watts, "A new synthetic route to the preparation of a series of strong photoreducing agents: *fac* tris-ortho-metalated complexes of Iridium (III) with substituted 2-phenylpyridines," *Inorg. Chem.*, 30: 1685–1687 (1991).
289. M.G. Colombo, T.C. Brunold, T. Riedener, H.U. Güdel, M. Fortsch, and H. Biirgi, "Facial tris cyclometalated Rh³⁺ and Ir³⁺ complexes: their synthesis, structure, and optical spectroscopic properties," *Inorg. Chem.*, 33: 545–550 (1991).
290. S. Lamansky, P. Djurovich, D. Murphy, F. Abdel-Razzaq, H.-E. Lee, C. Adachi, P.E. Burrows, S.R. Forrest, and M.E. Thompson, "Highly phosphorescent *bis*-cyclometalated iridium complexes: synthesis, photophysical characterization, and use in organic light emitting diodes," *J. Am. Chem. Soc.*, 123: 4304–4312 (2001).
291. B. Ma, R.W. Walters, D.B. Knowles, R. Kwong, Y. Tung, P.I. Djurovich, and M.E. Thompson, "Organic Light Emitting Materials and Devices," U.S. Patent 0,086,742A1 (2004).
292. S. Lamansky, P. Djurovich, D. Murphy, F. Abdel-Razzaq, R. Kwong, I. Tsyba, M. Bortz, B. Mui, R. Bau, and M.E. Thompson, "Synthesis and characterization of phosphorescent cyclometalated iridium complexes," *Inorg. Chem.*, 40: 1704–1711 (2001).
293. O. Lohse, P. Thevenin, and E. Waldvogel, "The Palladium catalysed suzuki coupling of 2- and 4-chloropyridines," *Synlett*, 45–48 (1999).
294. V.V. Grushin, N. Herron, D.D. LeCloux, W.J. Marshall, V.A. Petrov, and Y. Wang, "New, efficient electroluminescent materials based on organometallic Ir complexes," *Chem. Commun.*, 16: 1494–1495 (2001).
295. Y. Wang, N. Herron, V.V. Grushin, D. LeCloux, and V. Petrov, "Highly efficient electroluminescent materials based on fluorinated organometallic iridium compounds," *Appl. Phys. Lett.*, 79: 449–451 (2001).
296. J.P. Markham, S.C. Lo, S.W. Magennis, P.L. Burn, and I.D.W. Samuel, "High-efficiency green phosphorescence from spin-coated single-layer dendrimer light emitting diodes," *Appl. Phys. Lett.*, 80: 2645–2647 (2002).

297. S.C. Lo, E.B. Namdas, P.L. Burn, and I.D.W. Samuel, "Synthesis and properties of highly efficient electroluminescent green phosphorescent Iridium cored dendrimers," *Macromolecules*, 36: 9721–9730 (2003).
298. S.C. Lo, N.A.H. Male, J.P.J. Markham, S.W. Magennis, P.L. Burn, O.V. Salata, and I.D.W. Samuel, "Green phosphorescent dendrimer for light-emitting diodes," *Adv. Mater.*, 14: 975–979 (2002).
299. Md.K. Nazeeruddin, R. Humphry-Baker, D. Berner, S. Rivier, L. Zuppiroli, and M. Graetzel, "Highly phosphorescence iridium complexes and their application in organic light-emitting devices," *J. Am. Chem. Soc.*, 125: 8790–8797 (2003).
300. B. Ma, R. Walters, and R. Kwong, "OLEDs Utilizing Multidentate Ligand Systems," U.S. Patent 200,5170,206, pp. 35 (2005).
301. B. Ma, D.B. Knowles, C.S. Brown, D. Murphy, and M.E. Thompson, "Organic Light Emitting Materials and Devices," *PCT Int. Appl.*, WO 045002 A1 (2004).
302. B. Ma, D.B. Knowles, C.S. Brown, D. Murphy, and M.E. Thompson, "Organic Light Emitting Materials and Devices," U.S. Patent 6,687,266 B1, pp. 17 (2004).
303. M.A. Baldo, D.F. O'Brien, Y. You, A. Shoustikov, S. Sibley, M.E. Thompson, and S.R. Forrest, "Highly efficient phosphorescent emission from organic electroluminescent devices," *Nature*, 395: 151–154 (1998).
304. A. Tsuboyama, H. Iwawaki, M. Furugori, T. Mukaide, J. Kamatani, S. Igawa, T. Moriyama, S. Miura, T. Takiguchi, S. Okada, M. Hoshino, and K. Ueno, "Homoleptic cyclometalated iridium complexes with highly efficient red phosphorescence and application to organic light-emitting diodes," *J. Am. Chem. Soc.*, 125: 12971–12979 (2003).
305. Y. Su, H. Huang, C. Li, C. Chien, Y. Tao, P. Chou, S. Datta, and R. Liu, "Highly efficient red electrophosphorescent devices based on iridium isoquinoline complexes: remarkable external quantum efficiency over a wide range of current," *Adv. Mater.*, 15: 884–888 (2003).
306. C. Yang, C. Tai, and I. Sun, "Synthesis of a high-efficiency red phosphorescent emitter for organic light emitting diodes," *J. Mater. Chem.*, 14: 947–950 (2004).
307. M.J. Frampton, E.B. Namdas, S. Lo, P.L. Burn, and I.D.W. Samuel, "The synthesis and properties of solution processible red-emitting phosphorescent dendrimers," *J. Mater. Chem.*, 14: 2881–2888 (2004).
308. Y. Song, S. Yeh, C. Chen, Y. Chi, C. Liu, J. Yu, Y. Hu, P. Chou, S. Peng, and G. Lee "Bright and efficient, non-doped, phosphorescent organic red-light-emitting diodes," *Adv. Func. Mater.*, 14: 1221–1226 (2004).
309. C. Adachi, R.C. Kwong, P. Djurovich, V. Adamovich, M.A. Baldo, M.E. Thompson, and S.R. Forrest, "Endothermic energy transfer: a mechanism for generating very efficient high-energy phosphorescent emission in organic materials," *Appl. Phys. Lett.*, 79: 2082–2084 (2001).
310. R.J. Holmes, S.R. Forrest, Y.-J. Tung, R.C. Kwong, J.J. Brown, S. Garon, and M.E. Thompson, "Blue organic electrophosphorescence using exothermic host-guest energy transfer," *Appl. Phys. Lett.*, 82: 2422–2424 (2003).
311. J. Li, P.I. Djurovich, B.D. Alleyne, I. Tsyba, N.N. Ho, R. Bau, and M.E. Thompson, "Synthesis and characterization of cyclometalated Ir(III) complexes with pyrazolyl ancillary ligands," *Polyhedron*, 23: 419–428 (2004).
312. G. Lei, L. Wang, and Y. Qiu, "Improved performance of electrophosphorescent organic light-emitting diode by graded doped emissive layer," *Jpn. J. Appl. Phys., Part 2: Lett. Express Lett.*, 43: L1226–L1228 (2004).
313. R.J. Holmes, B.W. D'Andrade, S.R. Forrest, X. Ren, J. Li, and M.E. Thompson, "Efficient, deep-blue organic electrophosphorescence by guest charge trapping," *Appl. Phys. Lett.*, 83: 3818–3820 (2003).
314. S. Yeh, M. Wu, C. Chen, Y. Song, Y. Chi, M. Ho, S. Hsu, and C.H. Chen, "New dopant and host materials for blue-light-emitting phosphorescent organic electroluminescent devices," *Adv. Mater.*, 17: 285–289 (2005).
315. A.B. Tamayo, B.D. Alleyne, P.I. Djurovich, S. Lamansky, I. Tsyba, N.N. Ho, R. Bau, and M.E. Thompson, "Synthesis and characterization of facial and meridional tris-cyclometalated Iridium(III) complexes," *J. Am. Chem. Soc.*, 125: 7377–7387 (2003).

316. K. Dedeian, J. Shi, N. Shepherd, E. Forsythe, and D.C. Morton, "Photophysical and electrochemical properties of heteroleptic tris-cyclometalated Iridium(III) complexes," *Inorgan. Chem.*, 44: 4445–4447 (2005).
317. <http://www.universaldisplay.com>.
318. T. Sajoto, A.B. Tamayo, P.I. Djurovich, M. Yousufuddin, R. Bau, M.E. Thompson, R.J. Holmes, and S.R. Forrest, "Recent Progress in Blue Phosphorescent Iridium(III) Complexes and Their Application to Organic Light Emitting Devices (OLEDs)," Abstracts of Papers, 229th ACS National Meeting, March 13–17, 2005, San Diego, CA, United States (2005).
319. B.W. D'Andrade, M.E. Thompson, and S.R. Forrest, "Controlling exciton diffusion in multilayer white phosphorescent organic light emitting devices," *Adv. Mater.*, 14: 147–151 (2002).
320. B.W. D'Andrade, R.J. Holmes, and S.R. Forrest, "Efficient organic electrophosphorescent white-light-emitting device with a triple doped emissive layer," *Adv. Mater.*, 16: 624–628 (2004).
321. D. Qin and Y. Tao, "White organic light emitting diodes comprising of blue fluorescence and red phosphorescence," *Appl. Phys. Lett.*, 86: 113507–113509 (2005).
322. B.W. D'Andrade, J. Brooks, V. Adamovich, M.E. Thompson, and S.R. Forrest, "White light emission using triplet excimers in electrophosphorescent organic light-emitting devices," *Adv. Mater.*, 14: 1032–1036 (2002).
323. V. Adamovich, J. Brooks, A. Tamayo, A.M. Alexander, P.I. Djurovich, B.W. D'Andrade, C. Adachi, S.R. Forrest, and M.E. Thompson, "High efficiency single dopant white electrophosphorescent light emitting diodes," *New J. Chem.*, 26: 1171–1178 (2002).
324. L.S. Liao, K.P. Klubek, and C.W. Tang, "High-efficiency tandem organic light-emitting diodes," *Appl. Phys. Lett.*, 84: 167–169 (2004).
325. A.R. Duggal, J.J. Shiang, C.M. Heller, and D.F. Foust, "Organic light-emitting devices for illumination quality white light," *Appl. Phys. Lett.*, 80: 3470–3472 (2002).
326. A. Dodabalapur, L.J. Rothberg, and T.M. Miller, "Color variation with electroluminescent organic semiconductors in multimode resonant cavities," *Appl. Phys. Lett.*, 65: 2308–2310 (1994).
327. B.W. D'Andrade and S.R. Forrest, "White organic light-emitting devices for solid-state lighting," *Adv. Mater.*, 16: 1585–1595 (2004).
328. Y. Hamada, H. Kanno, T. Tsujioka, H. Takahashi, and T. Usuki, "Red organic light-emitting diodes using an emitting assist dopant," *Appl. Phys. Lett.*, 75: 1682–1684 (1999).
329. Y. Ohmori, H. Kajii, T. Sawatani, H. Ueta, and K. Yoshino, "Enhancement of electroluminescence utilizing confined energy transfer for red light emission," *Thin Solid Films*, 393: 407–411 (2001).
330. F. Li, J. Lin, J. Feng, G. Cheng, H. Liu, S. Liu, L. Zhang, X. Zhang, and S.T. Lee, "Electrical and optical characteristics of red organic light-emitting diodes doped with two guest dyes," *Synth. Met.*, 139: 341–346 (2003).
331. T. Liu, C. Iou, S. Wen, and C.H. Chen, "4-(Dicyanomethylene)-2-*t*-butyl-6-(1,1,7,7-tetramethyljulolidyl-9-enyl)-4H-pyran doped red emitters in organic light emitting devices," *Thin Solid Films*, 441: 223–227 (2003).
332. T. Mori, H. Kim, T. Mizutani, and D. Lee, "Electroluminescent properties in organic light-emitting diode doped with two guest dyes," *Jpn. J. Appl. Phys.*, 40: 5346–5349 (2001).
333. J. Feng, F. Li, W. Gao, G. Cheng, W. Xie, and S. Liu, "Improvement of efficiency and color purity utilizing two-step energy transfer for red organic light-emitting devices," *Appl. Phys. Lett.*, 81: 2935–2937 (2002).
334. T. Liu, C. Iou, and C.H. Chen, "Doped red organic electroluminescent devices based on a cohost emitter system," *Appl. Phys. Lett.*, 83: 5241–5243 (2003).
335. T.K. Hatwar, G. Rajeswaran, C.W. Tang, and J. Shi, "Organic Electroluminescent Devices with Improved Stability and Efficiency," *Eur. Pat. Appl.*, EP1162674B1 (2004).
336. D.Y. Kondakov, C.T. Brown, and V. Jarikov, "Stable Electroluminescent Device," *Eur. Pat. Appl.*, EP1359629A2 (2003).
337. V.J. Viktor, "Organic Light-Emitting Diode Devices with Improved Operational Stability," U.S. Patent 0,076,853 A1 (2004).
338. Z.D. Popovic, S. Xie, N. Hu, A. Hor, D. Fork, G. Anderson, and C. Tripp, "Life extension of organic LEDs by doping of a hole transport layer," *Thin Solid Films*, 363: 6–8 (2000).

339. N. von Malm, J. Steiger, R. Schmechel, and H. von Seggern "Trap engineering in organic hole transport materials," *J. Am. Phys.*, 89: 5559–5563 (2001).
340. M. Lee, C. Liao, C. Tsai, and C.H. Chen, "Highly Efficient Deep Blue Organic Light-emitting Device," Proceedings of the 2005 Society for Information Display, Boston, 2005, pp. 810–813 (2005).
341. H. Aziz, Z.D. Popovic, N. Hu, A. Hor, G. Xu, and X. Gu "Degradation mechanism of small molecule-based organic light-emitting devices," *Science*, 283: 1900–1902 (1999).
342. M.A. Baldo, M.E. Thompson, and S.R. Forrest, "High-efficiency fluorescent organic light-emitting devices using a phosphorescent sensitizer," *Nature*, 403: 750–753 (2000).
343. B.W. D'Andrade, M.A. Baldo, C. Adachi, J. Brooks, M.E. Thompson, and S.R. Forrest, "High-efficiency yellow double-doped organic light-emitting devices based on phosphor-sensitized fluorescence," *Appl. Phys. Lett.*, 79: 1045–1047 (2001).
344. S. Liu, J. Feng, and Y. Zhao, "Enhanced red emission from fluorescent organic light-emitting devices utilizing a phosphorescent sensitizer," *Jpn. J. Appl. Phys.*, 43: 2320–2322 (2004).
345. T.K. Hatwar, J.R. Vargas, and V.V. Jarikov, "Stabilized white-light-emitting OLED devices employing a stabilizing substituted perylene material," U.S. Patent 2,005,089,714, pp. 21 (2005).
346. Y. Kijima, N. Asai, and S. Tamura, "A blue organic light emitting diode," *Jpn. J. Appl. Phys.*, 38: 5274–5277 (1999).
347. Y. Sakon, T. Ohnuma, M. Hashimoto, S. Saito, T. Tsutsui, and C. Adachi, "Electroluminescent Devices," U.S. Patent US 5077142 (1991).
348. S. Naka, H. Okada, H. Onnagawa, and T. Tsutsui, "High electron mobility in bathophenanthroline," *Appl. Phys. Lett.*, 76: 197–199 (2000).
349. D.F. O'Brien, M.A. Baldo, M.E. Thompson, and S.R. Forrest, "Improved energy transfer in electrophosphorescent devices," *Appl. Phys. Lett.*, 74: 442–444 (1999).
350. Y. Su, H. Huang, C. Li, C. Chien, Y. Tao, P. Chou, S. Datta, and R. Liu, "High efficient red electrophosphorescent devices based on iridium isoquinoline complexes: remarkable external quantum efficiency over a wide range of current," *Adv. Mater.*, 15: 884–888 (2003).
351. M. Ikai, S. Tokito, Y. Sakamoto, T. Suzuki, and Y. Taga, "Highly efficient phosphorescence from organic light-emitting devices with an exciton-block layer," *Appl. Phys. Lett.*, 79: 156–158 (2001).
352. R.C. Kwong, M.R. Nugent, L. Michalski, T. Ngo, K. Rajan, Y. Tung, M.S. Weaver, T.X. Zhou, M. Hack, M.E. Thompson, S.R. Forrest, and J.J. Brown, "High operational stability of electrophosphorescent devices," *Appl. Phys. Lett.*, 81: 162–164 (2002).
353. T. Watanabe, K. Nakamura, S. Kawami, Y. Fukuda, T. Tsuji, T. Wakimoto, and S. Miyaguchi, "Optimization of Driving Lifetime Durability in Organic LED Devices Using Ir Complex," Proceedings of SPIE (The International Society for Optical Engineering), 4105 (Organic Light-Emitting Materials and Devices IV), pp. 175–182 (2001).
354. M. Kinoshita, H. Kita, and Y. Shirota, "A novel family of boron-containing hole-blocking amorphous molecular materials for blue- and blue-violet-emitting organic electroluminescent devices," *Adv. Func. Mater.*, 12: 780–786 (2002).
355. V.I. Adamovich, S.R. Cordero, P.I. Djurovich, A. Tamayo, M.E. Thompson, B.W. D'Andrade, and S.R. Forrest, "New charge-carrier blocking materials for high efficiency OLEDs," *Org. Electron.*, 4: 77–87 (2003).
356. V. Adamovich, J. Brooks, A. Tamayo, A.M. Alexander, P.I. Djurovich, B.W. D'Andrade, C. Adachi, S.R. Forrest, and M.E. Thompson, "High efficiency single dopant white electrophorescent light emitting diodes," *New J. Chem.*, 26: 1171–1178 (2002).
357. M.E. Thompson, V. Adamovich, X. Ren, A. Tamayo, and P.I. Djurovich, "Organic Light Emitting Devices with Electron Blocking Layers," U.S. Patent 0,048,101, pp. 30 (2004).
358. S.T. Zhang, Z.J. Wang, J.M. Zhao, Y.Q. Zhan, Y. Wu, Y.C. Zhou, X.M. Ding, and X.Y. Hou, "Electron blocking and hole injection: the role of *N*, *N'*-Bis(naphthalene-1-yl)-*N'*, *N'*-bis(phenyl)-benzidine in organic light-emitting devices," *Appl. Phys. Lett.*, 84: 2916–2918 (2004).
359. V.V. Jarikov, "Organic Light-Emitting Diode Devices with Improved Operational Stability," *Eur. Pat. Appl.*, EP1359790, pp. 33 (2003).
360. T. Liu, C. Lou and C.H. Chen, "Doped red organic electroluminescent devices based on a cohost emitter system," *Appl. Phys. Lett.*, 83: 5241–5243 (2003).

361. Y. Su, H. Huang, C. Li, C. Chien, Y. Tao, P. Chou, S. Datta, and R. Liu, "Highly efficient red electrophosphorescent devices based on iridium isoquinoline complexes: remarkable external quantum efficiency over a wide range of current," *Adv. Mater.*, 15: 884–888 (2003).
362. A. Tsuboyama, H. Iwawaki, M. Furugori, T. Mukaide, J. Kamatani, S. Igawa, T. Moriyama, S. Miura, T. Takiguchi, S. Okada, M. Hoshino, and K. Ueno, "Homoleptic cyclometalated iridium complexes with highly efficient red phosphorescence and application to organic light-emitting diode," *J. Am. Chem. Soc.*, 125: 12971–12979 (2003).
363. <http://www.universaldisplay.com/PHOLED.htm>. Accessed on November 2, 2005.
364. M. Yu, J. Duan, C. Lin, C. Cheng, and Y. Tao, "Diaminoanthracene derivatives as high-performance green host electroluminescent materials," *Chem. Mater.*, 14: 3958–3963 (2002).
365. M. Lee, H. Chen, C. Liao, C. Tsai, and C.H. Chen, "Stable styrylamine-doped blue organic electroluminescent device based on 2-methyl-9,10-di(2-naphthyl)anthracene," *Appl. Phys. Lett.*, 85: 3301–3303 (2004).
366. R.J. Holmes, S.R. Forrest, Y.J. Tung, R.C. Kwong, J.J. Brown, S. Garon, and M.E. Thompson, "Blue organic electrophosphorescence using exothermic host–guest energy transfer," *Appl. Phys. Lett.*, 82: 2422–2424 (2003).

4 Phosphorescent Polymer Light-Emitting Diodes

Dmitrii F. Perepichka, Hong Meng, and Mang-Mang Ling

CONTENTS

4.1	Introduction	413
4.2	Photophysical Aspects of Electrophosphorescence	414
4.2.1	Singlet–Triplet Excitons Ratio	414
4.2.2	Exciton Transfer Processes	415
4.3	Nonconjugated Polymers as Host Materials	417
4.4	Conjugated Polymers as Host Materials	428
4.4.1	Polyfluorenes	428
4.4.2	Poly(<i>p</i> -Phenylenes)	432
4.4.3	Polycarbazoles	436
4.4.4	Polythiophenes	438
4.5	Metallorganic Electrophosphorescent Polymers	438
4.6	Electrophosphorescent Dendrimers	443
4.7	Conclusions and Remarks	444
	Acknowledgment	445
	References	445

4.1 INTRODUCTION

Light-emitting diodes (LEDs) based on luminescent small organic molecules (OLEDs) and polymers (PLEDs) have become one of the major areas in the science of organic materials. A number of commercial OLED-based displays are already in the market for several years, and commercialization has already been initiated for PLED displays. In spite of technological problems of efficiency and stability of PLEDs as compared to OLEDs (which is, first of all, a material purity issue), the former promises to revolutionize the display-manufacturing technology as it provides the possibility of inexpensive solution fabrication (see also Chapter 2). Indeed, ambient temperature and pressure fabrication conditions (spin coating, bar coating, ink-jet printing, etc., of PLED-based large-area screens), enabled by good film-forming properties of polymers, are particularly attractive for the industrial application. However, even the best PLEDs show the external quantum efficiency (EQE) of not more than 5–6%, which limits the achieved power efficiency below ~20 lm/W (compared to ~90 lm/W for the best inorganic light-emitting devices) [1]. Besides the energy consumption issue, low efficiency also poses a problem of heat dissipation, which affects the device stability. Tailoring the efficiency of OLEDs and PLEDs is a very complex material and device-engineering task; however, one of the major improvement potentials follows from a simple consideration of the basic photophysics.

The principle of operation of all LEDs is based on radiative decay of excited states (excitons) created in the molecule (polymer, inorganic material) by injecting electrons and holes in the lowest unoccupied molecular orbital (LUMO) and highest occupied molecular orbital (HOMO), respectively. As these electrons and holes are generally injected with random spins, their recombination would give both symmetric (triplet) and antisymmetric (singlet) states in the ratio of 3:1 (based on statistics consideration). Only one of these, a singlet, has an allowed transition to the ground state, which means that only 25% of the created excitons can produce light in typical fluorescent materials. Therefore, to increase the efficiency of an LED, one would need either to control the spin of the injected electrons and holes or to find a way to harvest the formed triplet excitons. There is a limited understanding on how the spin control can be achieved (but see the recent progress in this direction in Ref. [2,3]). Radiative decay of triplet states, known as phosphorescence, is known to be an efficient process in many heavy-metal complexes with efficient spin-orbital coupling.

At the same time, the early reports on OLED devices fabricated with phosphorescent Eu^{3+} complexes did not discuss the triplet-harvesting issue and also showed rather low quantum efficiency, due to low solid state photoluminescence (PL) quantum yield of these emitters [4,5]. Only in 1998, Forrest and coworkers [6] reported phosphorescent OLEDs with very high efficiency using energy transfer from the fluorescent organic host material (Alq_3) to the triplet-emitting dopant (Pt-porphine complex), which breaks the 25% theoretical efficiency limit of the electrophosphorescent emission. Since then, a number of high-efficiency electrophosphorescent OLEDs have been fabricated (and already been commercialized), where a nearly 100% internal quantum efficiency has been achieved [7].

There is no reason why the same principle cannot be applied for light-emitting polymers as host materials to pave a way to high-efficiency solution-processible LEDs. In fact, polymer-based electrophosphorescent LEDs (PPLEDs) based on polymer fluorescent hosts and lanthanide organic complexes have been reported only a year after the phosphorescent OLED was reported [8]. In spite of a relatively limited research activity in PPLEDs, as compared with phosphorescent OLEDs, it is hoped that 100% internal quantum efficiency can also be achieved for polymer LEDs. In this chapter, we will give a brief description of the photophysics beyond the operation of electrophosphorescent devices, followed by the examples of the materials, devices, and processes, experimentally studied in the field till the beginning of 2005.

4.2 PHOTOPHYSICAL ASPECTS OF ELECTROPHOSPHORESCENCE

4.2.1 SINGLET-TRIPLET EXCITONS RATIO

Before describing the phosphorescent light emission in PLEDs, we will briefly review the relevant basic photophysical principles. Pauli exclusion principle states that no two electrons in an atom can have identical quantum numbers. A simple quantum mechanical calculation can show that the total spin of two electrons has a value of either 0, where the spin state is antisymmetric (called a singlet) under electron exchange, or 1, where there are three possible symmetric spin states under electron exchange (called triplets) [9]. The optical transitions are allowed only from singlet to singlet and from triplet to triplet, but not between singlet and triplet states.

During photoexcitation, all the formed excitons are singlets. The radiative decay back to a singlet ground state is allowed and the PL quantum yield of 100% is observed in many molecules. In an electroluminescent process, however, the injection of electrons from cathode and holes from anode in the device is generally spin-independent and random. Their recombination results in the formation of four possible spin states (usually with equal cross section), one singlet and three triplets. As the radiative transition from the triplet excited state to the singlet ground state is prohibited, the theoretical maximum quantum yield of electrophosphorescence is limited to 25%. Having said this, we should mention that in the last few years,

an increasing number of theoretical [10,11] and experimental [12–16] studies suggest that the singlet excitons yield (η_S) in some materials such as conjugated polymers can be significantly higher than 25% due to spin-dependent exciton formation process [17]. Vardeny and coworkers [13] demonstrated a nonmonotonic dependence between the ratio of singlet–triplet exciton formation cross sections (σ_S/σ_T) and the band gap of conjugated polymers. The minimum value of σ_S/σ_T (~ 2) was reported for the polymer with the band gap around 2.5 eV, and this can be increased to as high as 5 for the polymers with either higher or lower band gap.

There is a certain amount of controversy in some of these reports, for example, η_S from $20 \pm 4\%$ [18] to $\sim 45\%$ [13] was reported for thin films of poly(2-methoxy-5-(2'-ethylhexyloxy)-1,4-phenylene vinylene) (MEH-PPV). For small molecules, however, the η_S close to 25% is invariantly observed [13,19]. Whatever is the case, a significant amount of triplets is formed in PLEDs, and harvesting these can result in a tremendous growth of the device efficiency. The triplet emission in organic polymers (as well as small molecules) is prohibited and usually cannot be observed at room temperature. However, many transition metals show high-yield triplet emission (phosphorescence) due to effective intersystem crossing enabled by strong spin–orbital interaction. Therefore, transferring the formed triplets to triplet-emitting dopants can potentially increase the internal quantum efficiency of the electroluminescent devices to 100%. A practical realization of this goal for PLEDs is given in the following sections, but before that we would like to describe briefly the basic principles of the exciton transfer processes relevant to the operation of phosphorescent LEDs.

4.2.2 EXCITON TRANSFER PROCESSES

The electronic processes in the host–guest molecular system are best illustrated by a classical Jablonski diagram [20], which was first proposed in 1933 to describe absorption and emission of light (Figure 4.1).

When a host molecule in its ground state (S_0^H) absorbs light, it is excited to a higher energy singlet state (S_1^H). At this point, it can directly release the absorbed energy via radiative decay, generating a photon with energy equal to $S_1^H - S_0^H$ or, the molecule could be subject to

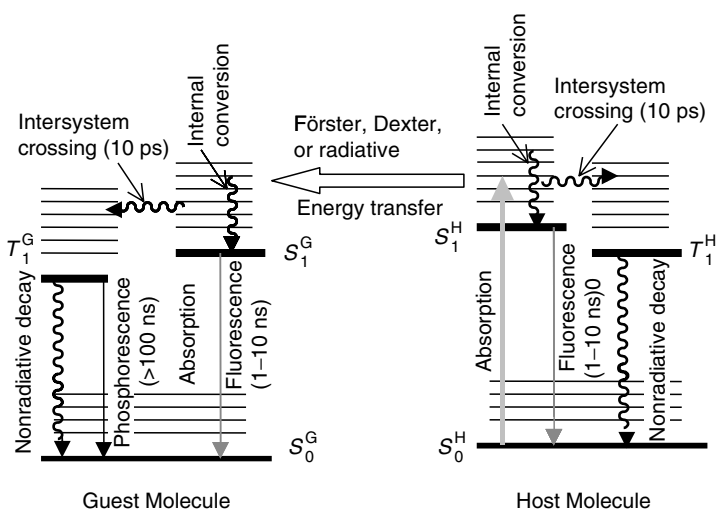


FIGURE 4.1 Electronic processes in fluorescent host–phosphorescent guest molecular systems. S_0^H , S_0^G : A singlet ground state of the host and guest molecules, respectively. S_1^H , S_1^G : A first excited singlet state of the host and guest molecules, respectively. T_1^H , T_1^G : The first excited triplet state of the host and guest molecules, respectively.

collisions with the surrounding molecules, and undergo nonradiative decay processes to the ground state (or even decompose). In the presence of the guest molecules, the energy transfer processes may occur, which brings the guest molecule to its first excited state and returns the host to the ground state. This energy transfer may occur via Förster, Dexter, or radiative energy transfer mechanisms, as will be described later. Then radiative decay processes will occur in the guest molecules. In the real host–guest systems, one can observe the emission of the host molecule, the guest molecule, or a combination of both, depending on the efficiency of the energy transfer processes.

As these excited states may transfer from molecule to molecule while conserving their spin, one can treat them as quasiparticles called excitons. The highly localized excited states with radius of few angstroms are known as Frenkel excitons. The rate of exciton transfer (hopping) relates to the electron transfer rate. According to Marcus equation, the rate of electron transfer is in exponential relation with the change in free energy (driving force) [21,22]:

$$k = k_{\max} \exp\left(-\frac{(\Delta G_0 + \lambda)^2}{4\lambda k_B T}\right) \quad (4.1)$$

where k_{\max} is an electronic coupling coefficient, ΔG_0 is the change in free energy, λ is the reorganization energy depending on the distance between molecules, k_B is the Boltzmann constant, and T is the temperature.

In most cases, when the driving force is lower than the reorganization energy, the electron transfer rate increases when the driving force $|\Delta G_0|$ is increased. There is, however, the so-called “Marcus inversion region” ($-\Delta G_0 > \lambda$), such that the larger the driving force, the lower the electron transfer rate.

The principles of Marcus theory are most directly related to Dexter energy transfer process, which is based on direct electron exchange between the host and the guest (Figure 4.2) [23]. Both the HOMO and the LUMO of the guest must be within the HOMO–LUMO gap of the host molecule to allow such electron transfer processes, and its efficiency depends on the driving force (determined by the difference in HOMO and LUMO energies of the host and the guest). The rate constant of the Dexter energy transfer decreases exponentially with the distance between the host and the guest molecules:

$$k = K \cdot J \cdot \exp(-2r/L) \quad (4.2)$$

where r is the distance, L is the characteristic length on the order of 1–5 Å at which the transfer is effective, K is a prefactor related to electron exchange, and J is the spectral overlap integral.

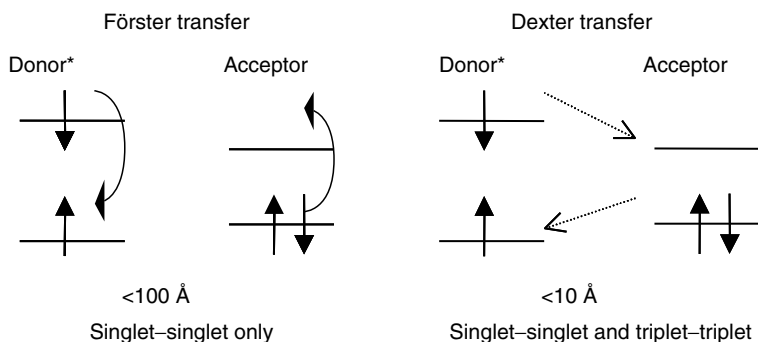


FIGURE 4.2 Comparison of Förster and Dexter energy transfer processes.

Therefore, Dexter energy transfer is a short-range process, which is significant only at distances $<10 \text{ \AA}$. As this can be logically concluded from the Figure 4.2, Dexter mechanism allows both singlet–singlet and triplet–triplet energy transfers.

Another major energy transfer process, the so-called Förster transfer mechanism is based on a dipole–dipole interaction between the host excited state and the guest ground state (Figure 4.2) [24]. It does not include the transfer of electrons and may occur over significantly larger distances. The rate constant of the Förster energy transfer is inversely proportional to the sixth power of the distance R between the molecules:

$$k = \left(\frac{R_0}{R}\right)^6 \frac{1}{\tau_D} \quad (4.3)$$

where τ_D is the lifetime of the donor excited state and the constant R_0 is the critical quenching radius (usually between 50 and 100 \AA).

Under this mechanism, a long-range (up to 100 \AA) energy transfer can occur without the emission of a photon, but it requires the emission spectrum of the host to overlap with the absorption spectrum of the guest molecule. Naturally, the excited state of the guest (S_1^G) should be lower in energy than the excited state of the host (S_1^H), but otherwise the relative position of HOMO and LUMO orbitals of the host and the guest is not important. Considering that the ground state of the guest is (always) a singlet, the Förster mechanism allows for energy transfer only from singlet to singlet. As shown later, the Förster and Dexter transfer processes often coexist in the real host–guest system and both of them play a role in phosphorescent LEDs.

In real phosphorescent LED devices, high yield of excitons localized on the guest molecule (usually present in low concentration) is determined not only by energy transfer from the host matrix, but also by a charge trapping on these molecules, which then leads to preferential exciton formation on these species. If the HOMO (LUMO) of the guest lies above (below) that of the host material, a hole (electron) generated in the host during LED operation may be trapped on the guest energy well, until meeting its counterparticle and forming an exciton. The higher the difference between the HOMO (LUMO) orbitals of the host and the guest, the higher is the efficiency of hole (electron) trapping, and sometimes direct charge trapping could be the prime mechanism of the exciton generation on the guest molecules. However, the charge trapping also creates a barrier for charge transport across the device, resulting in significant increase of the operating voltage.

Once the excitons have been generated and transferred onto guest the molecule, the emissive properties of the latter determine the luminescence quantum yield. For phosphorescent guests, a major nonradiative process responsible for decreased quantum efficiency is the so-called triplet–triplet annihilation, which results in the formation of one singlet ground state and one excited state (i.e., one exciton is lost) (Equation 4.4). This annihilation is particularly pronounced for the molecules with long phosphorescence lifetime and it is held responsible for a strong decrease of the efficiency in PPLED at high current densities [25]:



4.3 NONCONJUGATED POLYMERS AS HOST MATERIALS

Following the encouraging results demonstrated by metal complex-based phosphorescent OLEDs [5,6,26], several groups started investigating a possibility to attain electrophosphorescence in solution-processible polymer-based LEDs. The first report on using

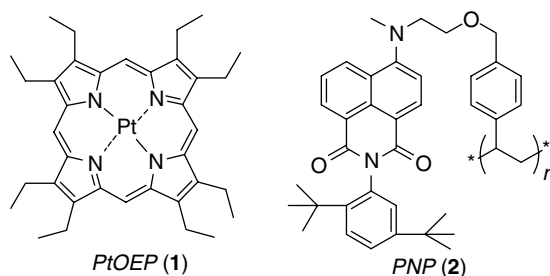


CHART 4.1 Chemical structure of PtOEP and PNP.

triplet-emitting metal complexes blended in semiconducting polymers, acting as a host, appeared in 1999 [8,27,28]. Thus, Tessler and coworkers [8] used *N*-arylnaphthalimide-containing polystyrene (PNP **2**) as a host material and platinum octaethylporphyrin (PtOEP **1**) as a triplet-emissive dopant (phosphor) (Chart 4.1) [8]. An overlap between the host emission and the guest absorption allows an efficient Förster energy transfer from the host to the guest (Figure 4.3). Based on time-resolved photo- and electroluminescent experiments, the authors suggest that the transfer of both singlet and triplet states of the PNP polymer onto platinum complex is taking place, although the direct charge trapping and recombination on PtOEP may also be responsible for the increased red emission.

To date, the most widely investigated host polymer material for PPLEDs is poly(9-vinylcarbazole) (PVK **4**, Chart 4.2), which is due to its high-energy blue-emissive excited state, excellent film-forming properties, high thermal stability, and reasonable hole mobility ($\sim 10^{-5} \text{ cm}^2/(\text{V s})$) [29,34]. The first report mentioning the energy transfer from the PVK onto a triplet-emitting dye (Eu–phenanthroline complex) appeared in 1999, although the authors have chosen another polymer, poly(*p*-phenylene) to fabricate a PPLED (see below) [30]. Lee et al. [33] reported a PLED device using the PVK host material and a green-emitting tris(2-phenylpyridine)iridium complex Ir(ppy)₃ (**3**) (for the synthesis and

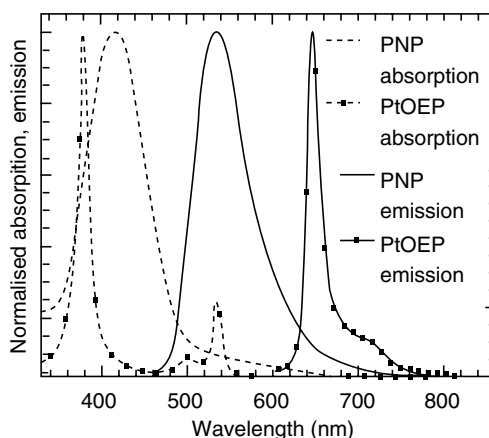


FIGURE 4.3 Absorption and emission spectra of the host PNP (**2**) and the guest PtOEP (**1**) (5% in poly(methylmethacrylate) excited at 514.5 nm). (From Cleave, V., Yahioğlu, G., Barny, P.L., Friend, R.H., and Tessler, N., *Adv. Mater.*, 11, 285, 1999. With permission.)

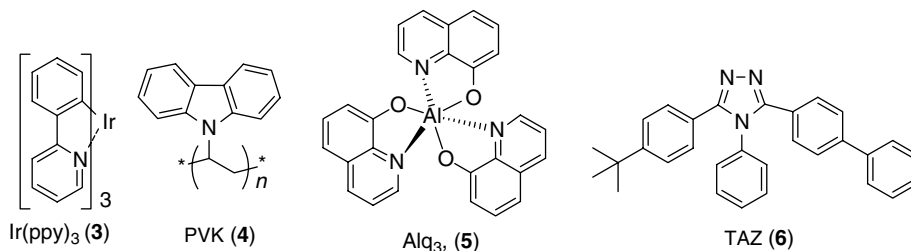


CHART 4.2 Chemical structure of Ir(ppy)₃, PVK, Alq₃, and TAZ.

photophysics of a large series of Ir complexes, see Refs. [31,32]) as a phosphorescent dopant. The multilayer device built with 8% Ir(ppy)₃ and PVK emissive layer showed the maximum EQE of 1.9% (with only little decrease upon 100 times increase of the operating current) and light output in excess of 2500 cd/m² (Figure 4.4). Although the efficiency was lower than that of the best small molecules-based electrophosphorescent LED, it was significantly higher than that of similar structure device without phosphorescent dopant [34].

A higher efficiency, yet simpler structure PPLED device fabricated with the same dopant and host materials was almost simultaneously reported by Yang and Tsutsui [35]. The highest EQE of their device ITO/PVK:5%Ir(ppy)₃/OXD-7/Mg:Ag (where ITO is indium tin oxide) (using OXD-7 (7) as an electron-transporting layer (ETL), Chart 4.3) reached the value of 7.5%, which was the first reported PLED with external efficiency above 5%, an upper limit of the fluorescent PLEDs. The power efficiency was 5.8 lm/W at the luminance of 106 cd/m².

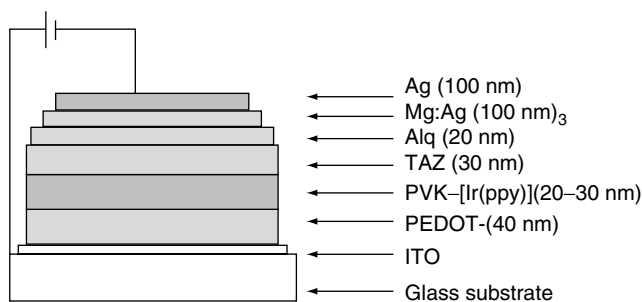


FIGURE 4.4 Multilayer PPLED configuration. (From Lee, C., Lee, K.B., and Kim, J., *Appl. Phys. Lett.*, 77, 2280, 2000. With permission.)

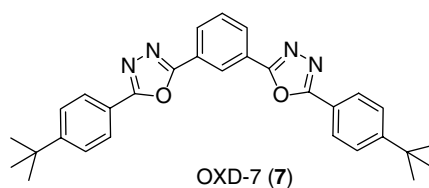


CHART 4.3 Chemical structure of OXD-7.

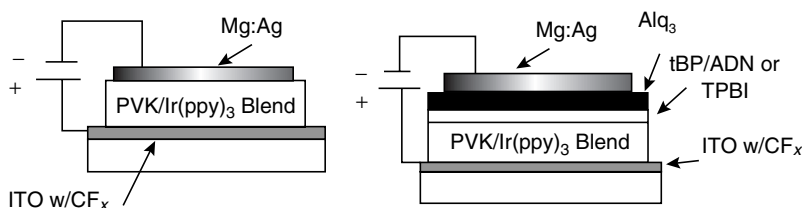


FIGURE 4.5 PPLED structure for a single layer (left) and multilayered (right) devices. (From Vaeth, K.M. and Tang, C.W., *J. Appl. Phys.*, 92, 3447, 2002. With permission.)

A detailed study of the influence of film morphology, guest concentration, and device structure on the performance of $\text{Ir(ppy)}_3/\text{PVK}$ -based PPLEDs has been undertaken by Vaeth and Tang [36] at Kodak. They evaluated different solvents for spin-coating deposition of polymer films and found that only relatively low-volatile solvents such as toluene or chlorobenzene can reproducibly form the high-quality pinhole-free films. The efficiency of a single layer device [$(\text{C}_n\text{F}_{2n}\text{-modified ITO})/\text{PVK}:\text{Ir(ppy)}_3/\text{Mg/Ag}$] measured at 20 mA/cm^2 was 5 cd/A at 1.5% concentration of Ir(ppy)_3 and reached the value of 8.7 cd/A when the dopant concentration was increased to 3.5% (limited by the solubility in chlorobenzene) (Figure 4.5). Balancing the charge transport and injection via blending with electron-transporting material, 2-(4-biphenyl)-5-(4-*tert*-butylphenyl)-1,3,4-oxadiazole (PBD) (**8**) and introducing additional hole blocking and electron injection layers (TPBI **9**, ADN **10**, tBP **11**, and Alq_3 **5**) significantly improve the device efficiency; the very high current efficiency of 30 cd/A and the EQE of 8.5% were reported for the multilayer device ($\text{C}_n\text{F}_{2n}\text{-modified ITO})/\text{PVK}:\text{PBD}:\text{3.5\% Ir(ppy)}_3/\text{TPBI}/\text{Alq}_3/\text{Mg/Ag}$ (Chart 4.4, Figure 4.5).

A further optimization of the performance of the $\text{PVK}-\text{Ir(ppy)}_3$ -based LEDs was reported in 2003 [37]. The authors undertook a systematic variation of a number of factors affecting the charge injection and recombination, cf. concentration of the dopant and thickness of the electroluminescent layer, electron- and hole-transporting layers, hole-blocking layer, and cathode material. Small changes (ca. 50%) in the thickness of electroluminescent layer can increase the EQE of the device by more than a factor of 3 (Figure 4.6), although, very likely, in lieu of a reduced lifetime. The best performance was achieved for a simple device with poly(3,4-ethylenedioxythiophene) (PEDOT)-modified anode ($\text{ITO}/\text{PEDOT}/\text{PVK}:\text{3\% Ir(ppy)}_3/\text{CsF}/\text{Mg:Ag}$). An unprecedented maximum current efficiency of 37.3 cd/A (10.5%) for PLED devices was achieved at the high brightness of 2240 cd/A (at 10 V). The

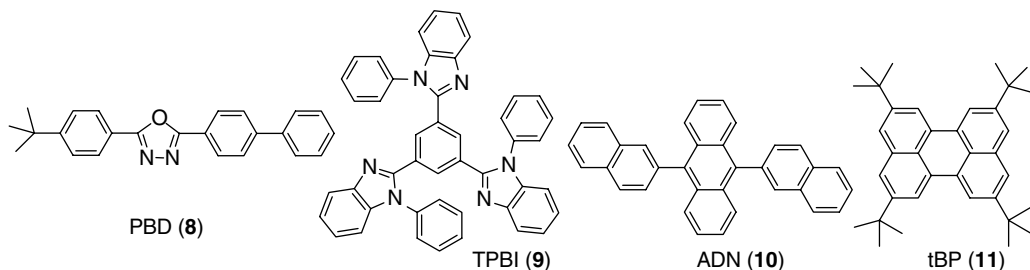


CHART 4.4 Chemical structure of PBD, TPBI, ADN, and tBP.

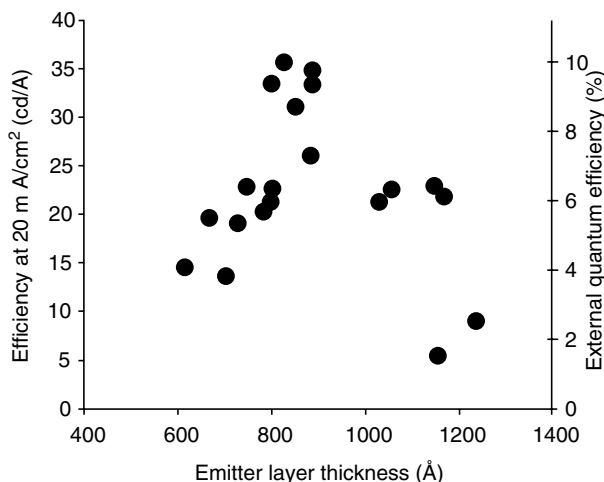
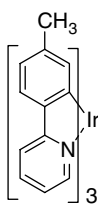


FIGURE 4.6 The dependence of the current efficiency on the thickness of the electroluminescent layer for PPLED ITO/PEDOT/PVK (**4**):3% Ir(ppy)₃ (**3**)/CsF/Mg:Ag. (From Vaeth, K.M. and Dicillo, J., *J. Polym. Sci.: Part B: Polym. Phys.*, 41, 2715, 2003. With permission.)

efficiency changes very little even at higher brightness, showing 36 cd/A (10.1%) at 7200 cd/A (at 12 V).

Using a methylated analog of Ir(ppy)₃ (Ir(mppy)₃ **12**, Chart 4.5), Neher and coworkers [38] have recently prepared another highly efficient PPLED operating at very low voltage (5.5 V); a single layer device ITO/PEDOT/Ir(mppy)₃-PBD-PVK/CsF/Al showed peak power efficiency of 14.1 lm/W (27 cd/A, 7.6%).

Yang and coworkers [39] suggested that the long lifetime of the triplet excitons may cause the concentration quenching (due to triplet-triplet annihilation) and thus account for the observed decrease of the quantum efficiency at high current densities. On the other hand, the long lifetime of the triplet state of the host materials would facilitate the energy transfer [40]. To compare the mutual influence of these factors, the authors studied the PPLEDs fabricated with PVK (**4**) and poly(dioctylfluorene) PDOF (**13**) host materials (the triplet exciton lifetime of 100 and 2.5 ms, respectively), and the platinum (PtOX **14**) or iridium (Btp₂Ir **15**) complexes as guest phosphorescent materials (the triplet lifetime of 80 and 5 μs, respectively) (Chart 4.6, Table 4.1) [39]. To balance the charge transport and injection for the polymers with different HOMO and LUMO levels, an electron transport material PBD (**8**) was blended in PVK-based PPLEDs, whereas a hole-transporting PVK layer was introduced into polyfluorene-based devices (Table 4.2). As expected from the triplet state lifetimes, PVK-based devices



Ir(mppy)₃ (**12**)

CHART 4.5 Chemical structure of Ir(mppy)₃.

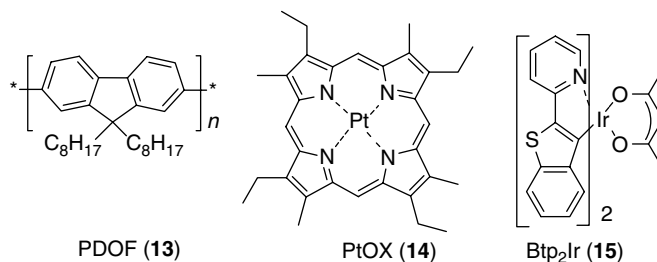


CHART 4.6 Chemical structure of PDOF, PtOX, and Btp₂Ir.

showed better performance than polyfluorene-based devices. The Btp₂Ir dopant appeared to be more efficient than PtOX, and also showed a higher stability. The PVK–Btp₂Ir device emitted very pure saturated red light ($\lambda_{\max} = 614$ nm, CIE: 0.66, 0.33), revealing the maximum EQE of 3.3% and a brightness of 1400 cd/m².

The same group investigated the degradation mechanism of PVK–PtOX-based PPLED [41]. The results suggest that electron trapping with the formation of anionic PtOX (14) species is responsible for the device instability and thus blending the electron transport material PBD (8), which competes with the triplet emitter in electron-trapping processes, and improves the device half-lifetime by approximately 40 times (to 45 h), although it is still very far from a technologically acceptable level.

Kawamura et al. [42] used PVK host polymer doped with a series of phosphorescent iridium complexes Flrpic (16), Ir(ppy)₃ (3), Bt₂Ir (17), Btp₂Ir (15) to achieve full color spectrum, from blue to red, and their mixture for white color emission (Figure 4.7). The multilayer PPLED device ITO/PEDOT/PVK:complex/BCP/Alq₃/Mg:Ag was built with bathocuproine (BCP 18) as a hole- or exciton-blocking layer to confine long-living triplet

TABLE 4.1
Photophysical Parameters of Some Polymer Hosts and Phosphorescent Dopants

Compound	HOMO (eV)	LUMO (eV)	E_g (eV)	E_T (eV) ^a	λ_{PL} (nm)	Φ_{PL} (%)	T_1 (lifetime)	Ref.
PVK 4	−5.54	−2.04	3.5	2.50	410	5	(100 ms)	56 (55)
PDOF 13	−5.77	−2.08	3.69	2.15	420	50	2.5 ms	56
PF3CNP1 32	−5.74	−2.89	3.15		475			59
PtOX 14	−5.3	−2.9	2.4	1.91	650		80 μ s	41,55
Ir(ppy) ₃ 3	−5.12	−2.11	3.01	2.41	516	(40)	(2 μ s)	56 (31)
PPIr 19	−5.20	−2.19	3.01	2.41	516	(34)	(1.5 μ s)	56 (32)
Ir(Ocppy) ₃ 33	−5.04	−2.20	2.84	2.41	518			56
Bt ₂ Ir 17	−5.36	−2.65	2.69	2.23	560	(26)	(1.8 μ s)	56 (32)
Btp ₂ Ir 15	−5.16	−2.38	2.78	2.02	614	(21)	(5.8 μ s)	56 (32)
Bzq ₂ Ir 20				2.26	548	27	4.5 μ s	32
Bsn ₂ Ir 21				2.05	606	22	1.8 μ s	32
Ir(DPF) ₃ 22	−4.69	−2.10	2.59	2.27	546			50
Ir(HFP) ₃ 24	−4.73	−2.25	2.48	2.07	600			50
Ir(DPPF) ₃ 23	−4.80	−2.21	2.59	2.25	550			50

^aAbove HOMO.

TABLE 4.2
Performance of ITO/PEDOT/PVK (4):PBD (8):Dopant/Ca/Al (I) and ITO/PEDOT/PVK/PDOF (13):Dopant/Ca/Al (II) PPLEDs, Doped with Btp₂Ir (15) and with PtOX (14) Complexes

Host	Dopant (wt%)	Maximum QE at mA/cm ² Brightness (cd/m ²)	QE at High-Current Density at mA/cm ² QE/Maximum QE	Maximum Brightness (cd/m ²)
PVK	BtpIr (4%)	3.3%	2.2%	1400
		5.7	80	
		147	65%	
	PtOX (4%)	2.5%	0.79%	270
		3.1	60	
		28	32%	
PF	BtpIr (5%)	2.4%	1.0%	800
		1.3	80	
		25	43%	
	PtOX (5%)	1.2%	0.26%	125
		1.7	80	
		12	21%	

Source: From Chen, F., Yang, Y., Thompson, M.E., and Kido, J., *Appl. Phys. Lett.*, 80, 2308, 2002. With permission.

states in the luminescent region [43]. The electroluminescence (EL) characteristics of the prepared PPLEDs containing 5 wt% of iridium complexes are listed in Table 4.3. All single component PPLEDs exhibited pure color emission originating from the guest molecules, suggesting very efficient energy transfer from the host. The highest EQE (5.1%) was demonstrated by green PPLED using Ir(ppy)₃ as a dopant, whereas essentially lower efficiencies

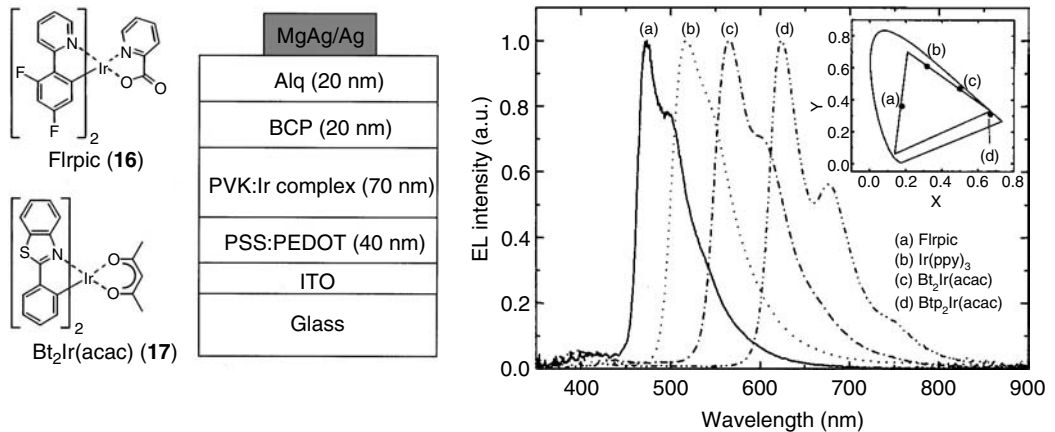


FIGURE 4.7 (Left) Chemical structures of PPLED materials. (Right) The device structure and the electroluminescence spectra of the PPLEDs prepared with PVK (4) host polymer and the above dopants (5 wt%). (From Kawamura, Y., Yanagida, S., and Forrest, S.R., *J. Appl. Phys.*, 92, 87, 2002. With permission.)

TABLE 4.3

Characteristics of PPLEDs with PVK (4)–Ir Complex (5 wt%) Blends: External QE (η_{ext}) and Power Efficiency (η_p) Are Given as Functions of Current Density; λ_{max} Is the EL Emission Peak; the J_0 Is the Current at Which the η_{ext} Falls to 50% of Its Peak Value and Is Characteristic of a Triplet–Triplet Annihilation Rate)

	Flrpic ^a	Ir (ppy) ₃	Bt ₂ Ir (acac)	Btp ₂ Ir (acac)
λ_{max} (nm)	474	517	565	623
CIE (<i>x</i> , <i>y</i>)	(0.18, 0.36)	(0.32, 0.61)	(0.50, 0.47)	(0.67, 0.31)
η_{ext} (%) [η_p (lm/W)] at 0.1 mA/cm ²	0.96 (0.69)	4.9 (6.3)	1.5 (1.1)	2.2 (0.60)
1	1.2 (0.70)	5.1 (5.2)	2.0 (1.3)	2.1 (0.44)
10	1.2 (0.60)	4.8 (3.8)	1.8 (1.0)	1.8 (0.32)
100	0.96 (0.39)	3.5 (2.2)	1.2 (0.59)	1.3 (0.18)
J (mA/cm ²) for 100 cd/m ²	3.4	0.55	1.7	6.1
J_0 (mA/cm ²)	410	260	190	190

^a10 wt% doped device.

Source: From Kawamura, Y., Yanagida, S., and Forrest, S.R., *J. Appl. Phys.*, 92, 87, 2002. With permission.

were observed for blue Flrpic-, yellow Bt₂Ir-, and red Btp₂Ir-based PPLEDs. This can be due to poor energy overlap between the PVK host and those dopants. Interestingly, for the red PPLED, the efficiency can be increased from 2.2 to 3.3% by employing a sensitizer. Adding an additional green dopant Ir(ppy)₃ as a sensitizer allows for the energy transfer from PVK, through Ir(ppy)₃, to Btp₂Ir. Blending several dopants with different emission color into PVK host matrix leads to white-emitting devices, although the ratio of dopants must be carefully controlled to avoid a complete energy transfer to the lowest energy (most red) emitter. For example, PPLED in configuration ITO/PEDOT/PVK:10% Flrpic (**16**):0.25% Bt₂Ir (**17**):0.25% Btp₂Ir (**15**)/BCP (**18**)/Alq₃/Mg:Ag emitted white color (CIE: 0.33, 0.41) with the maximum $\eta_{\text{ext}} = 2.1\%$ and $\eta_p = 1.4$ lm/W at 10 V.

These (Bt₂Ir **17**, Btp₂Ir **15**) and other (PPIr **19**, Bzq₂Ir **20**, Bsn₂Ir **21**) (Chart 4.7) Ir-based dopants have been simultaneously studied by Thompson and coworkers [44], revealing similar good efficiencies in PVK-based PPLEDs.

Even higher efficiency red, blue, and green PPLEDs have been fabricated with the above complexes and PVK using Cs as a cathode (device ITO/PEDOT/PVK:OXD-7 (**7**):Ir

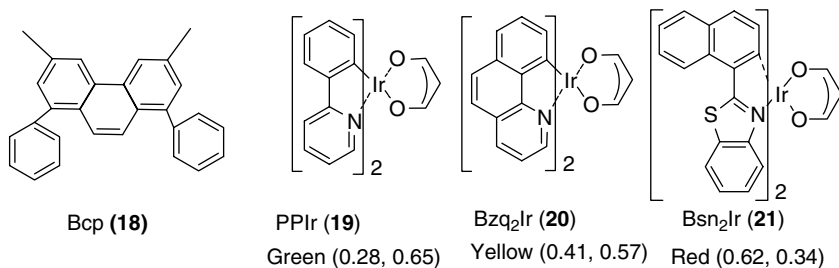


CHART 4.7 Chemical structure of BCP, PPIr, Bzq₂Ir, and Bsn₂Ir.

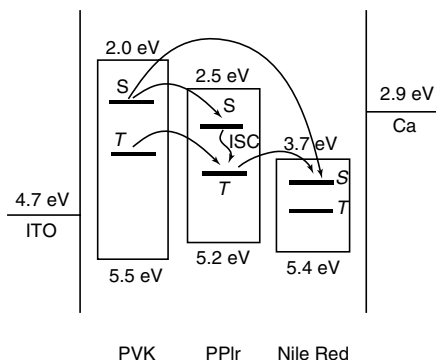
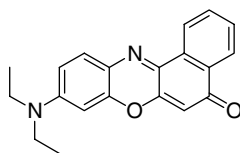


FIGURE 4.8 Energy diagram and proposed energy transfer mechanism in the blend system. (From He, G., Chang, S., Chen, F., Li, Y., and Yang, Y., *Appl. Phys. Lett.*, 81, 1509, 2002. With permission.)

complex/Cs/Al) [45]. Using Btp₂Ir (**15**), Ir(ppy)₃ (**3**), and Flrpic (**16**) phosphorescent dopants, red (CIE: 0.66, 0.33), green (CIE: 0.31, 0.60), and blue (CIE: 0.17, 0.30) emission with efficiency as high as 4.3, 31, and 14 cd/A, respectively, was achieved.

Yang and coworkers [46] tried to improve the efficiency of PLEDs using the phosphorescent sensitizer to transfer all singlet and triplet excitons from the host polymer (PVK) to the singlet fluorescent dye as illustrated in Figure 4.8. They used PPIr (**19**) (Chart 4.7) as the phosphorescent dopant and Nile Red (**21**) (Chart 4.8) as a fluorescent dye. Because of the very low concentration of PPIr and Nile Red, their absorption could hardly be observed. However, when the blend film was excited at 300 nm, the main emission came from PPIr and Nile Red, indicating a complete energy transfer from the host to the dye materials. Furthermore, the EL spectrum of PPLED built as ITO/PEDOT/PVK:PBD:PPIr:Nile Red (100:100:1:1)/Ca/Al showed a single band at 600 nm corresponding to emission of Nile Red. The authors suggest that the energy transfer proceeds through a combination of singlet-singlet (PVK → Nile Red) and triplet-singlet (PPIr → Nile Red) transitions (Figure 4.8). The Förster mechanism was claimed for both processes on the basis of a very low concentration (and thus, a large separation) of the dye molecules, although it should be prohibited for the later process (triplet-singlet transfer). Nevertheless, comparing the prepared PPLED with those of control devices fabricated without PPIr (**19**) sensitizer or with a fluorescent green sensitizer Alq₃ (**5**) showed approximately threefold higher EL efficiency for the former (6.4 cd/A). This fact strongly supports the authors' claim that the triplets formed or transferred on PPIr phosphor undergo further transfer onto Nile Red dopant.

Heeger and coworkers [47] at University of California, Santa Barbara (UCSB) reported high-efficiency PPLEDs based on PVK polymer doped with a new π -extended iridium



Nile Red (**21**)

CHART 4.8 Chemical structure of Nile Red.

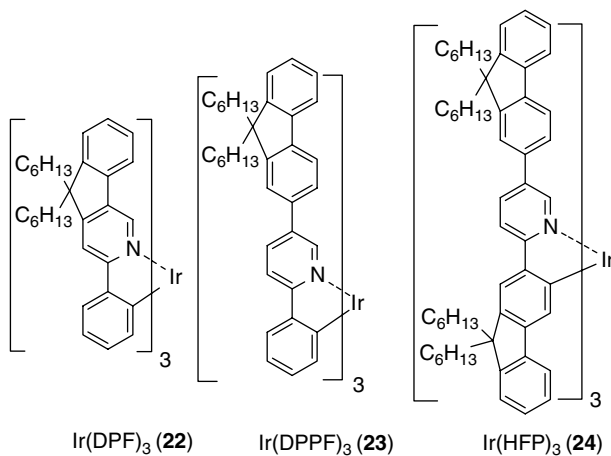


CHART 4.9 Chemical structure of $\text{Ir}(\text{DPF})_3$, $\text{Ir}(\text{DPPF})_3$, and $\text{Ir}(\text{HFP})_3$.

complex $\text{Ir}(\text{DPF})_3$ (**22**) (blended with PBD (**8**) as electron transporter) (Chart 4.9). The good overlap of the emission of the host polymer with absorption of the dopant $\text{Ir}(\text{DPF})_3$ allows an efficient Förster energy transfer between the host and the guest materials (Figure 4.9). Indeed, studying the concentration dependence of the PL spectra reveals an almost complete transfer of the PVK short-wavelength emission into the red emission of the Ir complex at concentrations above ~1% (although total suppression of the PVK–PBD PL emission was achieved only at 8% dopant concentration). In EL devices, there was no short-wavelength emission even at extremely low concentration of $\text{Ir}(\text{DPF})_3$ (0.001 mol% per repeat unit of PVK), which suggests that the charge trapping on the metal complex rather than just Förster energy transfer, is responsible for the EL of this PPLED. The device built as ITO/PEDOT/PVK–PBD (40%): $\text{Ir}(\text{DPF})_3$ /Ca/Ag emits yellowish-green light at $\lambda_{\text{max}} = 550 \text{ nm}$ (shoulder at

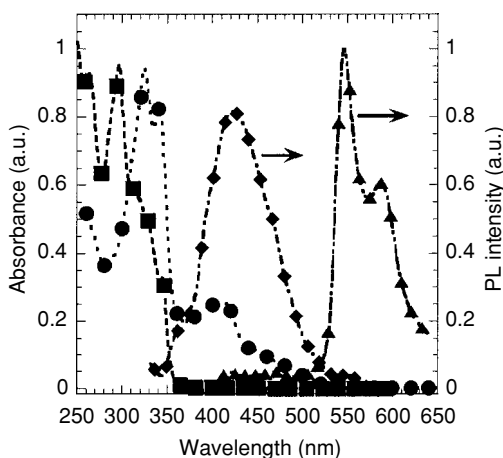


FIGURE 4.9 The normalized absorption or emission spectra of the neat films of $\text{Ir}(\text{DPF})_3$ (**22**) (absorption: ●, emission: ▲) and the blend films of PVK (**4**)–PBD (**8**) (40 wt%) (absorption: ■, emission: ◆). (From Gong, X., Robinson, M.R., Ostrowski, J.C., Moses, D., Bazan, G.C., and Heeger, A.J., *Adv. Mater.*, 14, 581, 2002. With permission.)

590 nm) with an EQE of 10%, luminous efficiencies as high as 36 cd/A, and the brightness in excess of 8000 cd/m² at 75 mA/cm² (55 V). Although the operating voltage was very high, the device efficiency for the first time approached that of small molecule-based phosphorescent LEDs, yet at a very low doping level.

A somewhat lower operating voltage was reported by the same group for a related guest dopant Ir(DPPF)₃ (**23**) [48]. A green-yellow-emitting ($\lambda_{\text{max}} = 550$ nm, 590 sh nm) single-layer device ITO/PEDOT/PVK:PBD:Ir(DPPF)₃/Ca/Ag achieved the maximum brightness of 3500 cd/m² at 30 V (cf. 47 V for a Ir(DPF)₃ [47]). A high EQE of 8% (29 cd/A) was achieved in this device, although the high operating voltage resulted in relatively low power efficiency of ~3.3 lm/W.

As already demonstrated, the efficient color tuning in the PVK–Ir complex systems can be achieved by the modification of the organic ligands. An extended conjugation in another member of the fluorene–pyridine complexes, Ir(HFP)₃ (**24**), shifts the emission maximum into the red by ca. 30 nm. A bright-red electrophosphorescent device was fabricated with Ir(HFP)₃ as a guest material in the configuration ITO/PEDOT/PVK:PBD: Ir(HFP)₃/Ca/Ag ($\lambda_{\text{max}} \sim 580$ nm) [49]. The maximum EQE of 5% (7.2 cd/A) was achieved at a brightness of 170 cd/m².

The same group later published an account comparing the performance of the three fluorene-containing dopants described above with PVK host polymer (as well as with several polyfluorene hosts, see below) [50]. Analyzing the PL and EL properties of different host–guest combinations, they have reached the conclusion that the Förster energy transfer plays only a minor role in the operation of such PPLEDs and that the direct charge trapping by dopants is the major mechanism of the electrophosphorescent process.

Although platinum and, particularly, iridium complexes are the two most frequently used classes of dopants for PPLEDs, the other metals such as gold, copper, rhenium, ruthenium, and europium have also been studied as dopants. Ma et al. [27] have studied two phosphorescent complexes, Au2MDP (**25**) and Cu4MDP (**26**) (Chart 4.10) as dopants in PVK host polymer. The solution PL quantum yields for these two phosphors (23 and 42%, respectively) are rather high comparing to the other gold and copper complexes. The PPLEDs fabricated in configuration ITO/PVK:Au2MDP/Al and ITO/PVK:Cu4MDP/Al can be turned on at 10 and 12 V, respectively. However, the EQE of these devices appeared to be very low (0.1% for Cu4MDP), which can be partially attributed to unoptimized device structure, with very high charge injection barriers. Comparison of the PL and EL spectra of the device suggests a significant increase in the ratio of triplet–singlet emission in the EL process, suggesting that the charge trapping mechanism occurs also for these dopants.

Ma et al. also studied PVK-based PPLEDs using rhenium complex in [28,51]. They have prepared the PPLED in configuration ITO/PVK:bpyRe (**27**):DCM (**28**)/Al (DCM is 4-(dicyanomethylene)-2-methyl-6-[*p*-(dimethylamino)styryl]-4*H*-pyran), where the bpyRe

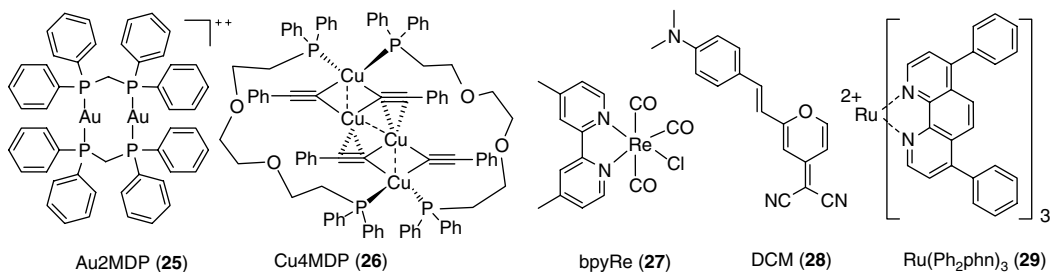


CHART 4.10 Chemical structure of Au2MDP, Cu4MDP, bpyRe, DCM, and Ru(Ph₂phn)₃.

complex (Chart 4.10) acts as a coupler of energy transfer between the PVK host and DCM-fluorescent emitter, which allows to harvest both singlet and triplet excitons [51]. The device emitted red light with $\lambda_{\max} \sim 570$ nm (CIE: 0.45, 0.53). The highest electroluminescent efficiency (0.42 cd/A) was shown by the devices containing 10 wt% of bpyRe complex and 1 wt% of DCM dye, which is a reasonably good value for the unoptimized single-layer device. This efficiency is ten times higher than that of the similar device without the phosphorescent bpyRe dopant, and is twice higher than that of the PVK-based device containing the bpyRe (27) but not the DCM dye (0.2 cd/A) [28]. Recently, a detailed study of PL and EL of PVK films doubly doped with green-emitting Ir(ppy)₃ (3) and a red-emitting ruthenium dye Ru(Ph₂phn)₃ (29) was reported [52].

4.4 CONJUGATED POLYMERS AS HOST MATERIALS

4.4.1 POLYFLUORENES

Yang and coworkers [53] were the first to use polyfluorene as a host material in PPLED application. They demonstrated an electrophosphorescent device using conjugated polyfluorene PDOF (13) as the host material and PtOX (14) as a dopant. The emission spectrum of PDOF overlaps well with the absorption of the PtOX dopant suggesting an efficient energy transfer from PDOF to PtOX. The device in configuration ITO/PEDOT/PVK/PDOF:PtOX/Ca:Al, having only 1% of the dopant, showed deep-red emission at $\lambda_{\max} = 656$ nm with an EQE of 2.3% at 11 cd/m², which is twice higher than that of the fluorescent PDOF-based PLED.

O'Brien et al. [54] employed a similar Pt complex (PtOEP 1) in PDOF-based PPLEDs. The light-emitting device was built with *N,N*-diphenyl-*N',N'*-di(3-carboxyphenyl)-4,4'-diaminobiphenyl (BFA) as hole-transporting or injecting layer (ITO/BFA/PDOF:4% PtOEP/Ca), which allowed to reach the maximal EQE of 3.5% and a peak brightness >200 cd/m². The operating voltage (~25 V), however, is much higher than that of polyfluorene-based fluorescent PLEDs and is certainly above the technologically acceptable level. Absorption and PL spectra of PtOEP/PDOF blends suggest an efficient Förster energy transfer (Figure 4.10), but measurements of triplet state dynamics in PDOF (by photoinduced absorption spectroscopy) show that virtually no Dexter energy transfer takes place in this system [55]. Accordingly, the PDOF triplets cannot be transferred onto the dopant and are

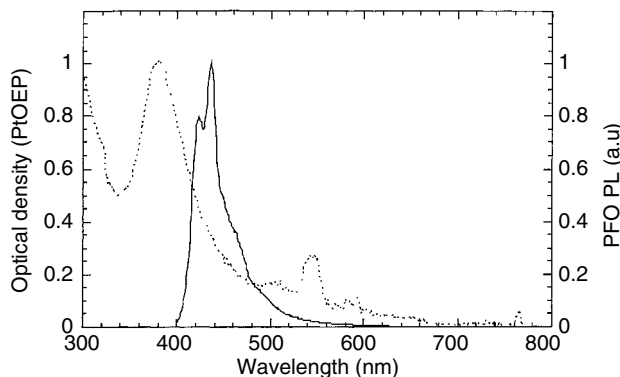


FIGURE 4.10 The emission spectra of the host PDOF (13) (solid line) and the absorption of the guest PtOEP (1) (broken line). (From O'Brien, D.F., Gieblerb, C., Fletcherb, R.B., Cadbyb, A.J., Palilisb, L.C., Lidzeyb, D.G., Laneb, P.A., Bradley, D.D.C., and Blau, W., *Synth. Met.*, 116, 379, 2001. With permission.)

not expected to contribute to the emission, and there must be some other mechanism responsible for high-observed electroluminescent efficiency. Indeed, increase of the driving voltage with increasing concentration of PtOEP (**1**), and the fact that the ionization potential of PtOEP is 0.5 eV lower than that of PDOF suggest that a direct trapping of holes (followed by electron trapping and recombination) occurs on PtOEP. As a result, higher electric field (i.e., higher operating voltage) is needed to transport the required amount of charge through the device.

As in conventional, electrofluorescent devices, the turn-on voltage of electrophosphorescent devices can be essentially decreased in liquid electroluminescent cells (LEC). Yang and coworkers [56] have prepared red-emitting LEC using hydrophilic polyfluorene BDOH-PF (**30**) host (Chart 4.11) together with triplet emitter Btp₂Ir (**15**) [56]. The turn-on voltage was as low as ~3 V, and a power efficiency of 1.0 lm/W was achieved, whereas the corresponding conventional PPLED device (without electrolyte) showed six times lower power efficiency and higher turn-on voltage.

A very detailed study of the energy transfer processes in PPLEDs have been recently reported by Kim and coworkers [57]. They compared the behavior of the nonconjugated PVK and conjugated fluorene–phenylene host copolymer poly[9,9'-di-*n*-hexyl-2,7-fluorene-alt-1,4-(2,5-di-*n*-hexyloxy)phenylene] (PFHP **31**) (Chart 4.11), while using Ir(ppy)₃ (**3**) and PtOEP (**1**) as the guest dopants. The emission of both polymers is in good overlap with the absorption spectra of the dopants, suggesting efficient Förster energy transfer. The experimental results indicated efficient singlet and triplet energy transfers in PVK (**4**)/Ir(ppy)₃ and PVK/PtOEP systems due to large Förster radius, high energy (2.46 eV), and long lifetime of the host triplet state. In the case of the conjugated PFHP, similar criteria do not result in efficient energy transfer, which authors explain by the formation of the aggregates in the conjugated polymer. However, the actual triplet energy of PFHP (**31**) (2.3 eV) is lower than that of Ir(ppy)₃ (2.4 eV), which might well explain the observed behavior (Table 4.1). The PPLED fabricated as ITO/PEDOT/PVK–Ir(ppy)₃/TAZ (**6**)/Alq₃ (**5**)/LiF/Al showed the maximum EQE up to 6%, which is 15 times higher than that of a corresponding device using PFHP as a host polymer. Lower efficiency of conjugated PDOF-based PPLED as compared to nonconjugated PVK in PPLEDs was also mentioned by Yang and coworkers [39,58], who ascribed this fact to quenching the phosphorescence of Ir complexes by low-energy triplet state of the polymer.

Bazan and coworkers [50,59] have studied fluorene copolymer PF3CNP1 (**32**) containing electron-deficient dicyanophenylene fragment as a host material for PPLEDs (Chart 4.12). They used π -extended fluorene-containing dopants Ir(DPF)₃ (**22**), Ir(DPPF)₃ (**23**), and Ir(HFP)₃ (**24**), which have previously shown excellent results in PVK-based devices. The spectral overlap of the guest absorption and host emission suggests an efficient Förster energy transfer (Figure 4.11). The PPLED ITO/PEDOT/PF3CNP1:Ir(HFP)₃/Ca/Ag with only 1 wt% of the dopant exhibited a maximum luminescence of 2200 cd/m² and a maximum EQE of 1.5% and electroluminescent efficiency of 3 cd/A (achieved at 15 V) [59]. These values

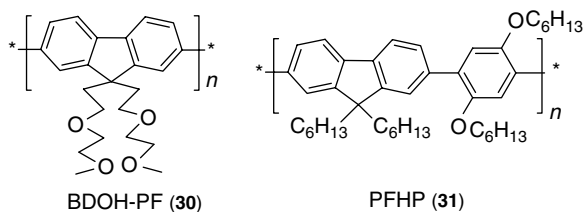


CHART 4.11 Chemical structure of BDOH-PF and PFHP.

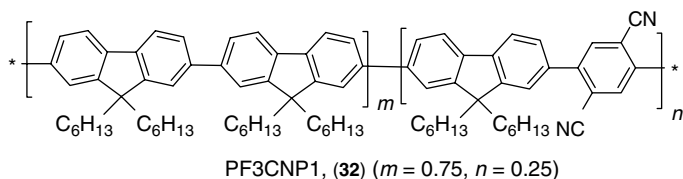


CHART 4.12 Chemical structure of PF3CNP1.

are essentially lower than those for the similar PVK-based device, although the turn-on voltage was brought down to 4.5 V, as compared to 10 V for a similar PVK-based device [49]. In addition, the stability of polyfluorene-based device was also higher. Recently, even higher efficiency red-emitting device made from Ir(HFP)₃ (**24**) and PDOF (**13**) was reported by the same group: PPLED ITO/PEDOT/PDOF:Ir(HFP)₃/Ca/Ag showed an EQE of 4.5%, a current efficiency of 6.2 cd/A, a maximum brightness >1000 cd/A, and a turn-on voltage ~5 V [50].

Yang and coworkers [60] studied the energy transfer from the PDOF host polymer onto a series of iridium complexes (Ir(ppy)₃ **3**, PPIr **19**, Bt₂Ir **17**, Btp₂Ir **15**) with triplet energy levels positioned below and above that of the host polymer (Table 4.1). They found a relationship between the triplet energy of the dopants and the photoluminescent emission. When the triplet exciton (T_1) of the dopant (PPIr **19**) is higher in energy than that of the host polymer, it can be quenched via back energy transfer from dopant onto the polymer, and only the emission of the latter is observed (Figure 4.12). This is not the case if the triplet energy of the dopant (Btp₂Ir **15**) is lower than that of the host polymer, and the triplet excitons, thus confined on the dopant, can decay radiatively with high quantum yield. When the triplet energy levels of the dopant (Bt₂Ir **17**) and the host polymer are close, the competition between the energy transfer processes from the host to the dopant and from the dopant back to the host polymer will take place. However, in the PPLED devices, the charge trapping process often results in domination of the dopant EL, regardless of the energy level difference.

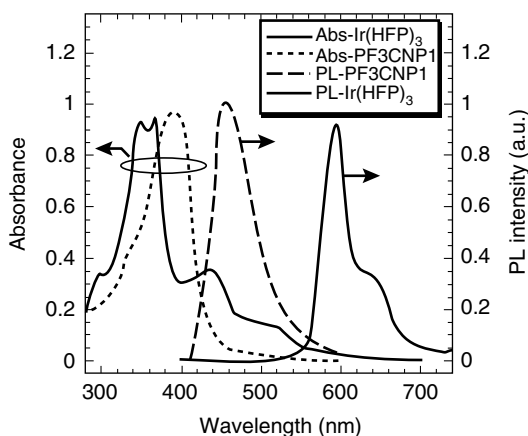


FIGURE 4.11 The absorption or emission spectra of the guest Ir(HFP)₃ (**24**) and host PF3CNP1 (**32**) materials. (From Gong, X., Ostrowski, J.C., Bazan, G.C., Moses, D., Heeger, A.J., Liu, M.S., and Jen, A.K.Y., *Adv. Mater.*, 15, 45, 2003. With permission.)

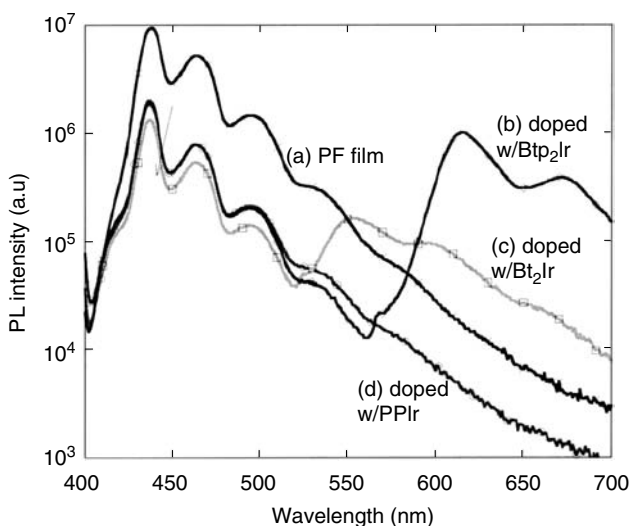


FIGURE 4.12 The PL spectra of the (a) undoped PDOF (**13**) film, PDOF doped with (b) 11 wt% Btp₂Ir (**15**), (c) 10 wt% Bt₂Ir (**17**), and (d) 10 wt% PPIr (**19**), pumping at 382 nm. (From Chen, F., He, G., and Yang, Y., *Appl. Phys. Lett.*, 82, 1006, 2003. With permission.)

Nevertheless, the device efficiency correlates with the above-mentioned charge transfer processes: the dopant Btp₂Ir with the lowest triplet energy showed the highest EQE (2%).

Yang and coworkers also compared the electroluminescent performance of these phosphorescent dopants as well as the alkyl-substituted Ir(Ocppy)₃ (**33**) (Chart 4.13) blended in PDOF (**13**) and PVK (**4**) [58]. The study once again confirmed a relatively poor performance (in terms of brightness and efficiency) of the PDOF host as compared to nonconjugated PVK (Table 4.4). Interestingly, the “plasticizing” alkyl substituents in the complex Ir(Ocppy)₃ (**33**) improve the film morphology (as demonstrated by atomic force microscopy) and give the best current efficiency, although the turn-on voltage of the PPLED with this dopant also tends to be the highest (which is explained by more efficient hole trapping on this complex) [58].

Thus, to achieve high EL efficiency, the triplet energy of a host material should be above that of the dopant. For this reason, conjugated polyfluorenes are not expected to perform well with green dopants due to their low triplet energy, although it can be used as an efficient host material for red-emitting PPLEDs. Very recently, the red-emitting PLED having highest efficiency based on polyfluorene was reported by Cao and coworkers [61]. Blending

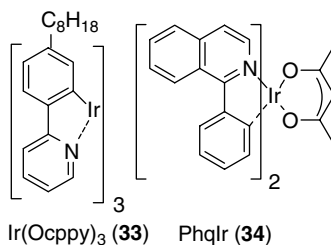


CHART 4.13 Chemical structure of Ir(Ocppy)₃ and PhqIr.

TABLE 4.4

Comparison of the Performance of PVK (4) (ITO/PEDOT/PVK:PBD:Dopant/Ca/Al) and PDOF (13) (ITO/PEDOT/PVK/PDOF: Dopant/Ca/Al)-Based PPLED with Different Dopants

Host	Dopant (wt% in Host)	Turn-On Voltage (V)	Efficiency (cd/A)	λ_{\max} (nm)
PVK	Ir(ppy) ₃ (3%)	5.5	12.7	516
	PPIr (3%)	5.2	13.0	516
	Ir(Ocppy) ₃ (3%)	9.6	16.0	518
	BtIr (3%)	5.5	8.0	560
	BtpIt (4%)	6.5	2.6	614
	Ir(ppy) ₃ (3%)	4.5	3.9	520
	PPIr (3%)	4.5	4.1	526
PF	Ir(Ocppy) ₃ (2%)	11.0	6.2	518
	BtIr (5%)	5.2	3.0	560
	BtpIr (5%)	5.0	1.9	614

Source: From Chen, F.C., Yang, Y., and Pei, Q., *Appl. Phys. Lett.*, 81, 4278, 2002. With permission.

silsesquioxane end-capped PDOF and triplet emitter PhqIr (**34**), they have produced saturated red light with CIE-coordinated values of 0.67, 0.33. The device ITO/PEDOT/PVK/PDOF:PBD(30%): PhqIr(2%)/Ba/Al showed an EQE as high as 12% and current efficiency of 5.2 cd/A (at 15 V).

An interesting approach to white-emitting polyfluorene-based PPLEDs was reported by Moses and coworkers [62,63]. As described in detail in Chapter 2, fluorenone defects in the polyfluorene ring result in efficient quenching of the blue fluorene emission producing green color. The group at UCSB deliberately introduced low concentration (1%) of fluorenone units into PDOF (**13**) chain and blended this green-emitting material with blue-emitting pristine PDOF and small amount (~1%) of the red-emitting phosphorescent dopant Ir(HFP)₃ (**24**) to produce pure white light with current efficiency of up to 3 cd/A (turn-on voltage 5 V, maximal brightness 6100 cd/m²) (Figure 4.13, device II). The color of such device (CIE: 0.32, 0.33) is almost independent of the current density.

Recently, Shu and coworkers [64] used the Os(fppz) triplet emitter to improve the EL of the fluorene copolymer PF-Q (**35**) (Chart 4.14) [64]. A red-emitting PPLED ITO/PEDOT/2.4%Os(fppz):PF-Q (**35**)/TPBI (**9**)/Mg:Ag showed an EQE of 6.6% and a maximum brightness of 10,400 cd/m², which is almost ten times higher than that in a similar device without a triplet emitter.

4.4.2 POLY(*p*-PHENYLENES)

The first report on increasing efficiency of a conjugated PLED via doping with a phosphorescent dye was described in 1999 by Heeger and coworkers [30], who added triplet-emitting europium complexes to substituted poly(*p*-phenylene) CN-PPP (**36**). Comparing the absorption spectra of a series of Eu-phenanthroline complexes (**37**) with the emission of the CN-PPP, they have shown that only phenyl- or naphthyl-substituted dopants can efficiently accept the energy transfer from the host polymer (Figure 4.14). As expected from the overlap of the polymer emission and the dyes absorption spectra, the most efficient energy transfer was observed for naphthyl-substituted Eu (dnm) (**37d**), as manifested in complete replacement

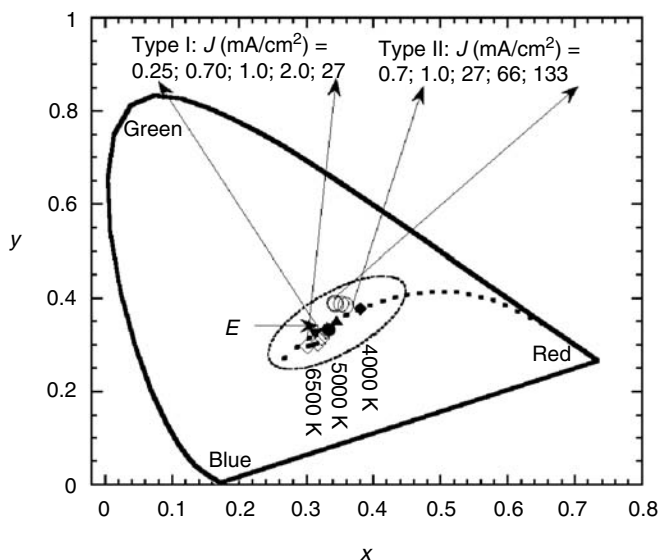


FIGURE 4.13 CIE chromaticity diagram of white PLEDs on the base of PDOF (**13**) and Ir(HFP)₃ (**24**). (From Chen, F., He, G., and Yang, Y., *Appl. Phys. Lett.*, 82, 1006, 2003. With permission.)

of the CN-PPP (**36**) PL by the dopant emission ($\lambda_{\text{PL}} \sim 610$ nm) at 5 wt% concentration. The PLED device fabricated with PVK (**4**) as a hole-transporting layer (ITO/PVK/CN-PPP:5% Eu (dnm) (**37d**)/Ca) showed an EQE of 1.1%. Although this is not a great value even for fluorescent PLEDs, the paper presented an important demonstration that adding a triplet-emitting dye increases the efficiency of the device (cf. 0.3% for PLED without the Eu complex). The authors also mention achieving a very narrow emission spectral width (<4 nm) as a route to improved color purity. It is noteworthy that the increase of the device efficiency occurs in spite of a very low Φ_{PL} of the Eu complex (2% cf. 80% for CN-PPP polymer), which is due to a very long phosphorescent lifetime of ca. 0.5 ms. The role of harvesting the triplets was mentioned in the paper, though, at that time, only as one of the hypotheses.

Clearly, using a triplet emitter with shorter excited state lifetime should improve the device efficiency. In 2002, Cao and coworkers [65] used iridium complexes Ir(ppy)₃ (**3**) and its

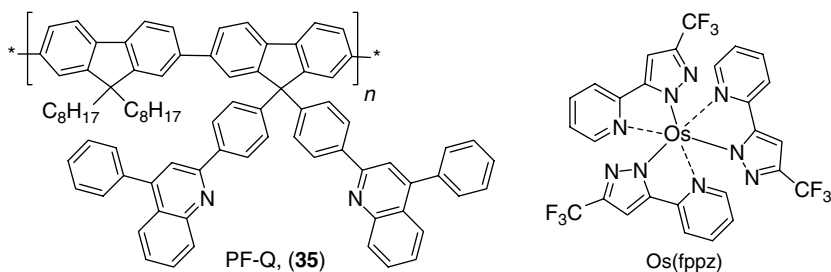


CHART 4.14 Chemical structure of PF-Q and Os(fppz).

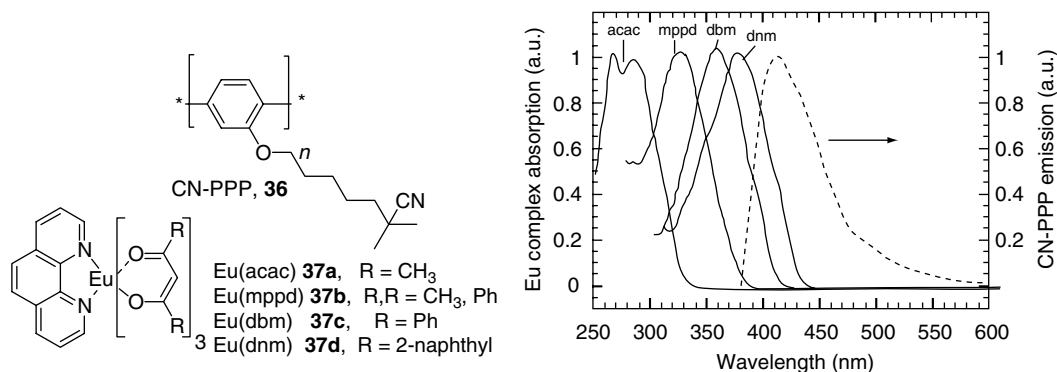


FIGURE 4.14 (Left) The molecular structure of Eu triplet emitters (**37**) and CN-PPP (**36**) host polymer. (Right) Emission spectrum of CN-PPP (broken line) and absorption of the Eu complexes with different ligands (solid lines). (From McGehee, M.D., Bergstedt, T., Zhang, C., Saab, A.P., O'Regan, M.B., Bazan, G.C., Srdanov, V.I., and Heeger, A.J., *Adv. Mater.*, 11, 1349, 1999. With permission.)

derivatives with shorter decay time to dope poly(*p*-phenylene)s EHO-PPP (**38**) (Chart 4.15) and CN-PPP (**36**) and demonstrated significantly improved device efficiency. The good overlap between the absorption band of the dopant Ir(ppy)₃ (**3**) and the emission of the host EHO-PPP and CN-PPP polymers meets the requirement for the Förster energy transfer. PPLEDs were fabricated using PVK (**4**) as a hole-transporting layer as ITO/PVK/host polymer:iridium complex/Ba/Al. The best device was made with 4 wt% Ir(Bu-ppy)₃ (**40**)-doped CN-PPP. The maximum EQE and EL efficiencies were 5.1% and 12 cd/A, respectively, observed at a brightness of 800 cd/m² and current density of 6.8 mA/cm². It changes only scarcely in the brightness range of 120–2500 cd/m², in contrast to many small-molecule phosphorescent LEDs [26]. The authors compared the quantum efficiency of EL devices made with different host materials (PVK **4**, PDHF **39**, CN-PPP **36**, and EHO-PPP **38**) using 2% of the iridium dopants, at current density of 13.3 mA/cm² (Table 4.5) [65].

All the devices emitted green light with a peak at 515 nm (CIE: 0.33, 0.58). The EQE of CN-PPP (**36**) and EHO-PPP (**38**) were close, with the former a little bit higher. However, very low quantum efficiency was found in devices made with host polymers PDHF (**39**) (Chart 4.15) and PVK (**4**) in spite of good overlap of the emission spectra of these two polymers with

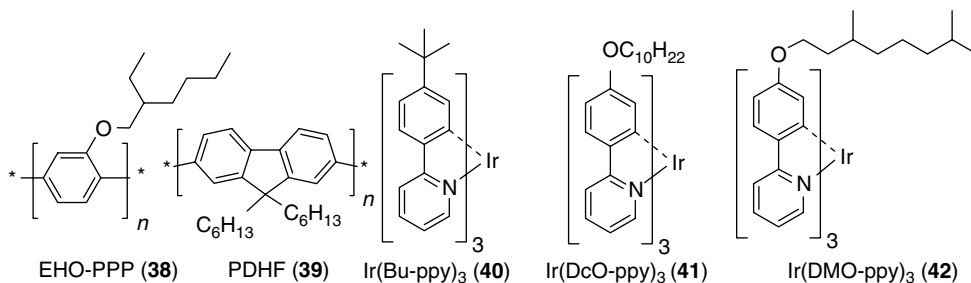


CHART 4.15 Chemical structure of EHO-PPP, PDHF, Ir(Bu-ppy)₃, Ir(DcO-ppy)₃, and Ir(DMO-ppy)₃.

TABLE 4.5
Device Performance of PPLEDs with Ir(ppy)₃ (3) and Ir(Bu-ppy)₃ (40) Dopants and Different Host Polymers

Host Polymer			Device Parameter of 2% Ir Complex-Doping Conc.					
Polymer	λ_{\max}	QE (%) ^a	IrR ₃	V	I (mA/cm ²)	cd/m ²	cd/A	QE (%)
PDHF	420	0.50	Ir(ppy) ₃	14.5	13.3	9	0.07	0.04
PVK	410	0.005	Ir(ppy) ₃	16.0	13.3	5	0.02	0.01
EHO-PPP	415	0.20	Ir(ppy) ₃	22.0	13.3	334	2.51	1.06
EHO-PPP	415	0.20	Ir(Bu-ppy) ₃	22.7	13.3	521	3.91	1.65
PPP	430	0.22	Ir(ppy) ₃	33.0	13.3	597	4.48	2.15
PPP	430	0.22	Ir(Bu-ppy) ₃	28.3	13.3	942	7.07	2.99

^aExternal QE of device with pure host blue polymer in same device configuration as doped polymer ITO/PVK/host polymer/Ba/Al.

Source: From Zhu, W., Mo, Y., Yuan, M., Yang, W., and Cao, Y., *Appl. Phys. Lett.*, 80, 2045, 2002. With permission.

the guest materials. Interestingly, the iridium complex with *t*-butyl group Ir(Bu-ppy)₃ (**40**) as the guest material showed higher quantum efficiency than Ir(ppy)₃ (**3**). The authors attribute this improvement to the more homogeneous distribution of the guest molecules in the host polymer matrix, owing to the alkyl substituent. However, the same group later has demonstrated that using longer alkyl chains in the ligand (complexes Ir(DcO-ppy)₃ (**41**) and Ir(DMO-ppy)₃ (**42**)), on the contrary, decreases the efficiency of the device (with CN-PPP host) [66]. The *t*-butyl-substituted complex still remains the most efficient in the series, providing a high EQE even at a very high brightness (4.2%, 10 cd/A at 2500 cd/m²). At the same time, extending the conjugation in the ligand can be used to tune the emission color, and a red-emitting PPLED ($\lambda_{\text{EL}} \sim 600$ nm, CIE: 0.59, 0.38) was fabricated with CN-PPP host and isoquinoline-Ir complex (PhqIr **34**) [67]. The two-layer device ITO/PVK/CN-PPP: 4%PhqIr/Ba/Al showed the external efficiency of 1.3% (0.47 cd/A).

Neher and coworkers [68] suggested that replacing PDOF (**13**) with a similar host polymer, ladder poly(*p*-phenylene) (LPPP) (**43**) (Chart 4.16), may reduce the hole-trapping process in PtOEP (**1**)-doped PPLEDs due to lower hole trap depth (i.e., the difference of host–guest HOMO levels), which is only 0.2 eV, compared with 0.5 eV for PDOF/PtOEP. Indeed, a single-layer PPLED fabricated as ITO/PEDOT/LPPP+PtOEP/Ca/Al had the switch-on voltage of only 4V, which, in contrast to polyfluorene PPLEDs, was independent of the dopant concentration. The maximum efficiency (achieved at ~ 7 V) was quite low (0.06 cd/A), although it was significantly improved in double layer devices using PBD (**8**) or Alq₃ (**5**) electron-injecting layers (0.5 cd/A at 8 V) and triple-layer devices using both electron- and hole (PVK)-injecting layers (1.2 cd/A, 2.5%). For the latter, the brightness of 100 cd/m² is achieved at a voltage of ~ 13 V, which is significantly lower than that for other PtOEP (**1**)-based LEDs. The relatively low efficiency of the devices was explained by inefficient Förster energy transfer (due to a poor host–guest spectral overlap), while the offset between the HOMOs of the polymer and the Pt complex is still too high for the Dexter energy transfer. The authors conclude that an alternative concept of reducing the operating voltage must be developed.

Lupton et al. [69] studied delayed PL and EL of another ladder polyphenylene, PhLPPP (**44**). A pronounced phosphorescence at ca. 600 nm was observed at room temperature. Elemental analysis revealed the presence of ~ 80 ppm of Pd (that is one Pd atom per 1700 polymer units), as an unintentional impurity originating from the polymerization catalyst,

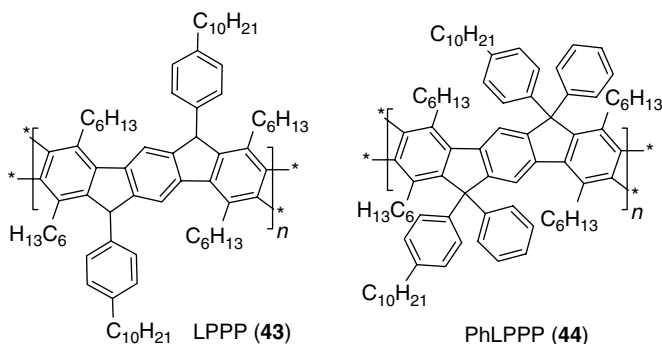


CHART 4.16 Chemical structure of LPPP and PhLPPP.

presumably covalently bound to the polymer backbone. This finding adds an additional scrutiny for the purification of electroluminescent-conjugated polymers, most of which are prepared with the help of transition metal catalysis.

Recently, Harrison et al. [89] demonstrated a near-infrared PPLED based on polyphenylene PPP-OR11 (45) and lanthanide complex Yb(TPP)Tp (46) (Chart 4.17). Complete quenching of the polymer emission was observed at the dye concentration of 5%, producing near-IR emission of the dopant at $\lambda_{\text{EL}} = 977$ nm. The PPLED device can be turned on at 4 V (cf. 8 V for corresponding PPLEDs with nonconjugated polymers), although the EQE is very low ($\sim 0.01\%$).

4.4.3 POLYCARBAZOLES

As we already mentioned, the efficiency of PPLEDs based on conjugated polymers is usually lower than of those based on nonconjugated polymers (as PVK). Although high-efficiency red PPLED based on polyfluorene as the host material has been recently demonstrated [61], the use of the conjugated polymers to achieve green electrophosphorescence is very difficult and it is practically impossible for blue color emission. This is due to quenching of the triplet emission of the transition metal complex by lower energy triplet state of the conjugated polymers [70]. At the same time, high triplet energy polymers usually also possess high band gap, which increases the charge injection barriers and the operating voltage of the device and reduces the power efficiency. The polymers with the singlet–triplet gap ($E_{\text{S}\rightarrow\text{T}}$) less than ~ 0.5 eV are rare [71]; $E_{\text{S}\rightarrow\text{T}}$ of 0.62 eV (between zero phonon fluorescence and phosphorescence peaks) was recently reported, and in most electroluminescent polymers it is

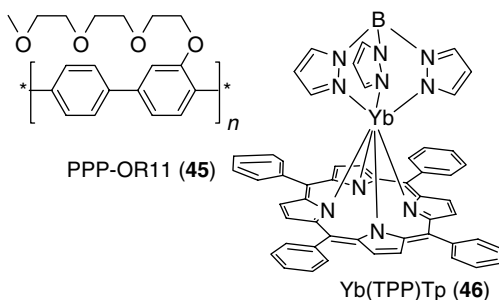


CHART 4.17 Chemical structure of PPP-OR11 and Yb(TPP)Tp.

higher [72,73]. Therefore, high triplet energy (at least ≥ 2.5 eV) results from high band gap (>3 eV).

To address this problem, a series of carbazole-3,6-diyl conjugated homo- and copolymers **47–56** with fluorene and oxadiazole units have been studied as host materials for triplet emitter Ir-SC4 (**57**) (Figure 4.15) [74]. Controlling the conjugation in the polymer by changing the linkage position of the fluorene and oxadiazole units, the authors could tune the triplet energy from 2.3 to 2.6 eV without affecting the polymer band gap. Conjugation in the

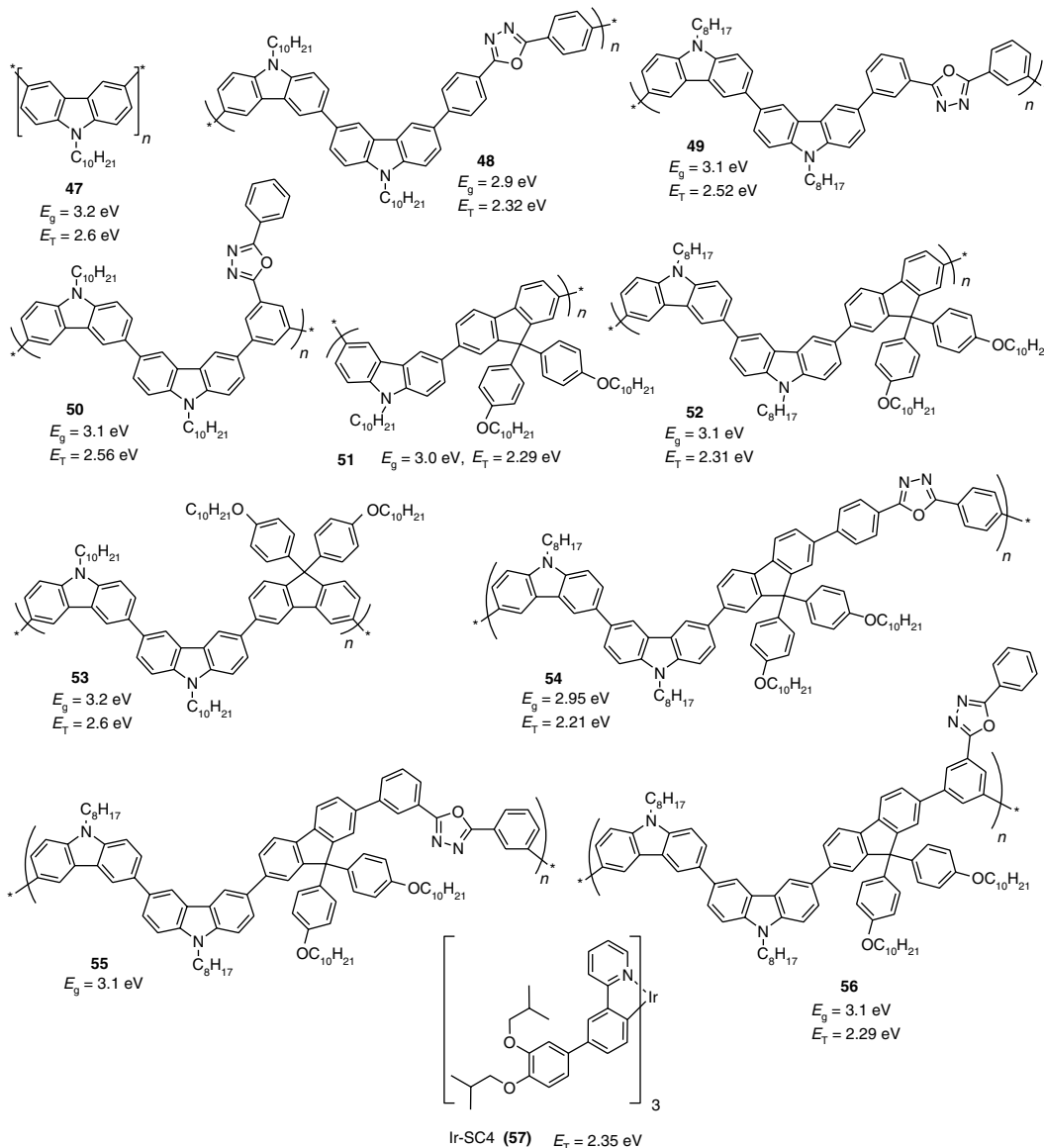


FIGURE 4.15 Structure, band gap (E_g) and triplet energy (E_T) of carbazole-3,6-diyl polymers (**47–56**) used as guest materials for triplet emitter Ir-SC4 (**57**). (van Dijken, A., Bastiaansen, J.J.A.M., Kikken, N.M.M., Langeveld, B.M.W., Rothe, C., Monkman, A., Bach, I., Stössel, P., and Brunner, K., *J. Am. Chem. Soc.*, 126, 7718, 2004.)

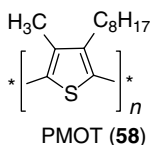


CHART 4.18 Chemical structure of PMOT.

homopolymer **47** is reduced by a “meta” (3,6-) connection, and introducing highly conjugated fluorene or oxadiazole units with “para” connection decreases the energy of the triplet by ca. 0.3 eV. Only polymers **47**, **49**, **50**, and **53** with all “meta” connections have the sufficiently high triplet energy to offset the green triplet emitter Ir-SC4 ($E_T = 2.35$ eV). Accordingly, the current efficiency of PPLEDs fabricated with these materials was significantly higher compared to other polymers in the series, cf. 23 cd/A for **50** versus 0.45 cd/A for **48** (in device ITO/PEDOT/polymer:Ir-SC4/Ba/Al).

4.4.4 POLYTHIOPHENES

Polythiophene, due to its low band gap and low triplet energy, is not expected to be a good host material for PPLEDs. Nevertheless, recently Wang et al. [90] demonstrated an efficient energy transfer from poly(dialkylthiophene) (PMOT **58**) (Chart 4.18) to PtOX (**14**) (Chart 4.6) dopant. Two alkyl substituents on thiophene ring result in significant twist of the polymer increasing the band gap to ~3.2 eV (S_1 at 3.77 eV), which becomes essentially high for energy transfer to red-emitting phosphors. Indeed, while PMOT itself shows blue emission at $\lambda_{PL} \sim 480$ nm, its blend with 5% of PtOX emits a single band at 650 nm. The PPLED ITO/PEDOT/8%PtOX:PMOT/Al showed EL efficiency of 0.7 cd/A, which is a significant improvement from a similar device without phosphorescent dye (0.05 cd/A). It is worth mentioning that the triplet energy of polymer **58** is extremely low (2.2 eV) for so wide band-gap polymer. Therefore, only few phosphors, possessing lower triplet energy (cf. PtOX: $T_1 = 1.9$ eV) may perform well with this host material.

4.5 METALLORGANIC ELECTROPHOSPHORESCENT POLYMERS

Most reported PPLEDs were fabricated by doping a polymer with a phosphorescent dye. However, aggregation and phase separation effects may cause serious problems for device performance and aging. In this section, we describe the very recent progress in intrinsically electrophosphorescent polymers containing triplet-emitting complexes either as pendant substituents or as a part of a backbone.

The EL from a metallorganic polymer PPEP (**59**) (Chart 4.19) containing transition metal (Pt) as a part of the polymer backbone has been studied by Friend and coworkers [14]. Both

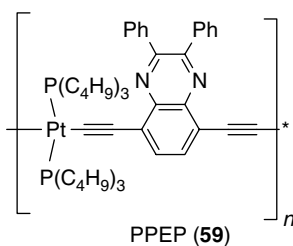


CHART 4.19 Chemical structure of PPEP.

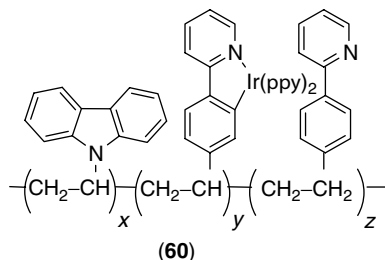


CHART 4.20 Chemical structure of a comonomer.

triplet (at ~750 nm) and singlet (at ~560 nm) emissions have been observed in PL and EL spectra. Although no performance data for the PPLEDs have been reported, the key conclusion of the work was that there is a spin-dependent exciton formation in the conjugated polymers. The singlet–triplet ratio for PPEP determined from the ratio of the singlet and triplet emission in PL and EL spectra was 57%, whereas the usual 1:4 ratio (22%) was found for an analog monomer. The authors suggest that do not always the phosphorescent materials have to be used in order to achieve the quantum efficiency above 25%.

Nevertheless, in practice, the presence of a triplet-emitting dopant does significantly improve the PLED performance, often giving the EQE well above 5%, which could not be achieved in fluorescent LEDs. The Korean group was the first to publish nonconjugated PVK copolymers **60** containing iridium-complex as a comonomer (Chart 4.20) [75]. The polymer was prepared by copolymerization of vinylcarbazole with vinylphenylpyridine followed by metallization to afford ~8 wt% concentration of the Ir complex. Green PL and EL was demonstrated for the films of **60** ($\lambda_{\text{PL/EL}} \sim 520$ nm). The multilayer PPLED ITO/PEDOT/**60**/TAZ (**6**)/Alq₃ (**5**)/LiF/Al showed a relatively low (as for phosphorescent LEDs) turn-on voltage of 8 V, a high efficiency of 4.4% (5.0 lm/W), and a maximum brightness of 12,900 cd/m² at 24 V. Interestingly, PVK triplet harvesting occurs by intramolecular rather than intermolecular energy transfer: the emission of diluted (10^{-4} M) solutions of **60** occurs solely from the carbazole units ($\lambda_{\text{PL}} \sim 375$ nm), whereas at higher concentrations (10^{-2} M) strong Ir complex emission ($\lambda_{\text{PL}} \sim 520$ nm) is observed.

The Japanese group reported a series of similar iridium-containing polymers **61**, **62**, **63** [76,77]; **64**, **65** [78] (Chart 4.21). Employing complexing ligands with different electron-donating abilities, pure green (**61**, $\lambda_{\text{PL/EL}} \sim 523$ nm), blue (**62**, $\lambda_{\text{PL/EL}} \sim 475$ nm), and red (**63**, $\lambda_{\text{PL/EL}} \sim 620$ nm) phosphorescent polymers were obtained. The role of different electron transport materials (blended with the polymer at 30 wt%) as well as the iridium complex ratio was investigated and the best performance was achieved for device ITO/PEDOT/polymer:OXD-7/Ca/Al (OXD-7 (**7**) used as an electron-transporting material) and 0.2 mol% (EQE 5.5%, current efficiency 7.1 cd/A), 0.6 mol% (9%, 30 cd/A), and 1.0 mol% (3.5%, 4.1 cd/A) of Ir for the red-, green-, and blue-emitting polymers, respectively [76]. The performance was further increased in multilayer device, containing additional ETLs (BALq, Chart 4.21), even with aluminum cathode. The devices ITO/PEDOT/polymer blend:OXD-7/BALq/LiF/Al showed an extraordinarily high EQE of 6.6% (**63**: red, current efficiency 14.5 cd/A, maximum brightness 1600 cd/m²), 11% (**61**: green, 40.3 cd/A, 15,000 cd/m²), and 6.9% (**62**: blue, 5.5 cd/A, 3000 cd/m²) [77].

Furthermore, efficient (4.5%) pure white-emitting PPLED (CIE: 0.34, 0.36) was fabricated from a 10:1 blend of a blue-emitting **62** with red-emitting **63** polymers [76]. Recently, even higher efficiency white-emitting PPLED was fabricated in a similar manner by blending

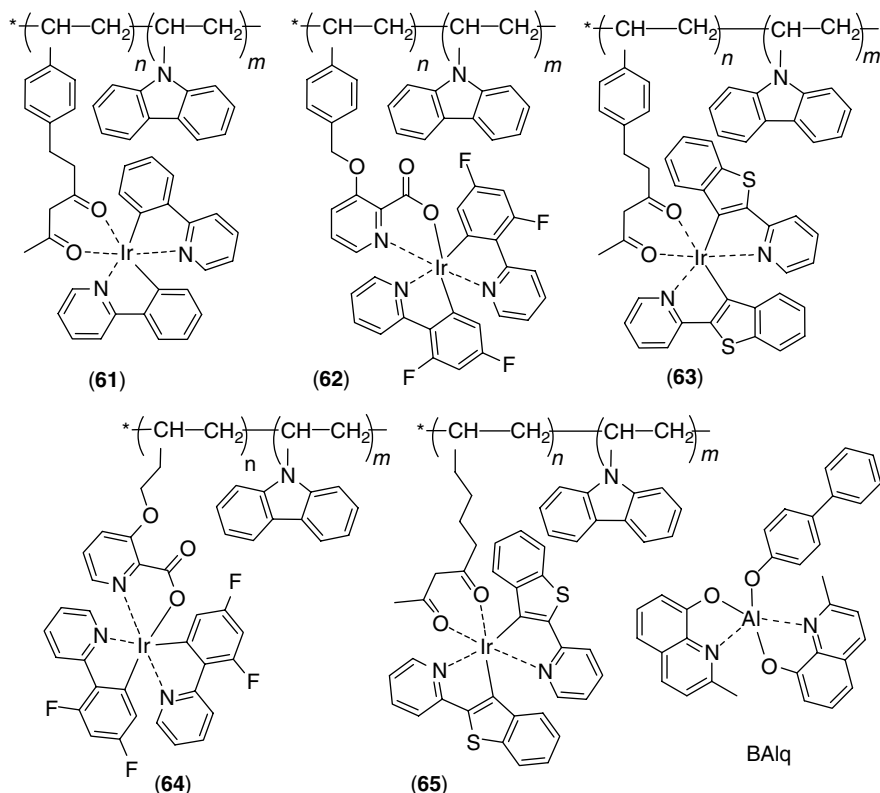


CHART 4.21 Chemical structure of iridium-containing polymers.

a blue-emitting **64** with red-emitting **65** polymers [78]. The device ITO/PEDOT/polymer blend:OXD-7/BAIq/LiF/Al can be turned on at ~5 V to emit pure white light (CIE: 0.34, 0.36) with the EQE as high as 6.0% (5.2 lm/W at 100 cd/m²) and a maximum brightness of 2000 cd/m².

An interesting new approach to phosphorescent polymers has been reported by Thompson and coworkers [79]. Using a living polymerization reaction (with alkoxyamine catalyst), they have prepared the polymer **66** (Chart 4.22), which contains the electron transport oxadiazole

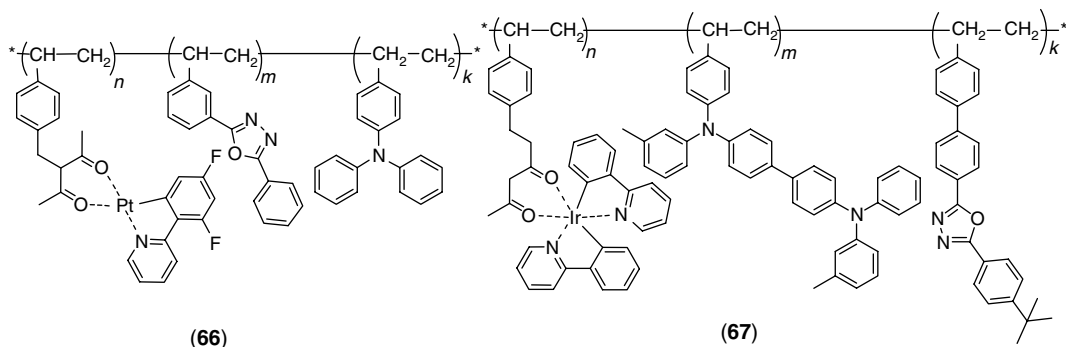


CHART 4.22 Chemical structure of the polymer that contains the electron transport oxadiazole units, hole-transporting triphenylamine units, and triplet-emitting Pt complex.

units, hole-transporting triphenylamine units, and triplet-emitting Pt complex, all grafted on polystyrene chain. Based on the known wide emission spectrum of Pt complex (which consists of blue emission of isolated complex and red emission of the aggregate), near-white-emitting PPLED ($x = 0.30 - 0.38$, $y = 0.43 - 0.50$, depending on the ratio between comonomers) was fabricated and the EQE of 4.6% was reported.

Very recently, the highest efficiency PPLED device has been fabricated with polymer **67** [80]. The authors mentioned that relatively low HOMO of the carbazole (lower than the anode work function, -4.5 eV for ITO) in previously studied polymers **61–65** results in high operating voltage. Furthermore, the device efficiency is compromised by low electron mobility of PVK. Therefore, they prepared polymer **67** with triarylamine hole-transporting and oxadiazole electron-transporting units, together with Ir emitter. Tuning the first two components, a good balance between the electron and the hole injection in the device has been achieved, which resulted in external efficiency of 11.8% and the record (for polymer PLED) power efficiency of 38.6 lm/W in the device ITO/PEDOT/**67**/Cs (green emitter).

The first example of triplet-emitting complexes grafted onto polyfluorene backbone was reported in 2002 by Pei et al. [81]. Copolymers **68a–c** containing a chelating 2,2'-bipyridyl moiety in a side chain can be prepared with different Eu content (Chart 4.23). Their emission is governed by a moderately efficient energy transfer from polyfluorene onto the Eu center, and can be tuned by changing the complex ligands and the content of Eu [81]. The most effective energy transfer manifested in a single red emission band at 612 nm was observed for the complex **68a** and required the Eu content as high as ~ 25 mol%. However, the PLED fabricated with PVK hole-transporting layer (ITO/PVK/**68a**/Ba/Al) showed a very low EQE of 0.07%, which is a reflection of a very long phosphorescence lifetime and a low quantum yield generally observed in Eu complexes [30]. A related polyfluorene–Eu complex **69c** with carboxylic-chelating moiety of the polymer ligand was reported by Huang and coworkers [82]. Again, the efficiency of the energy transfer was relatively low, confirming poor performance of Eu complexes as triplet-emitting dopants.

The first efficient phosphorescent fluorene polymer was reported by Chen et al. [83], who synthesized a series of polyfluorenes containing both the triplet-emitting iridium complex and

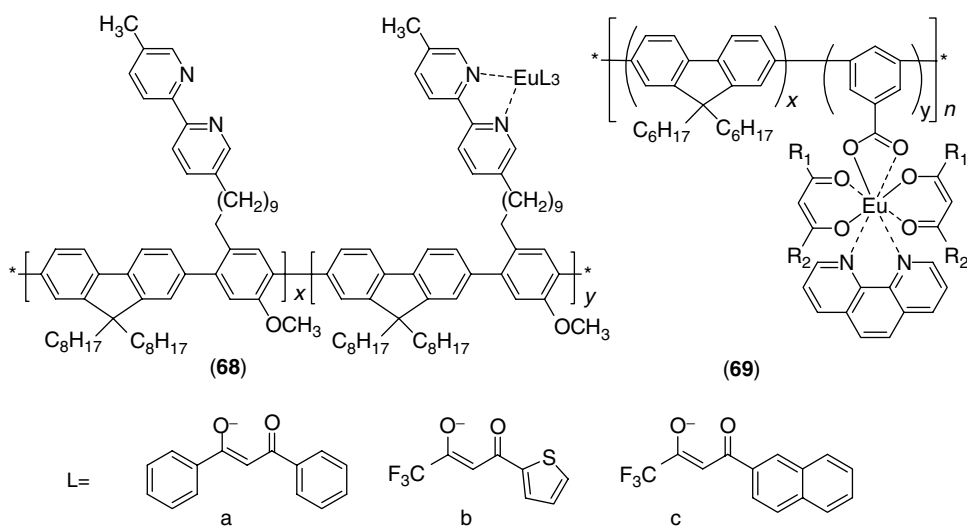


CHART 4.23 Chemical structure of copolymers prepared with different Eu content to contain a chelating 2,2'-bipyridyl moiety in a side chain.

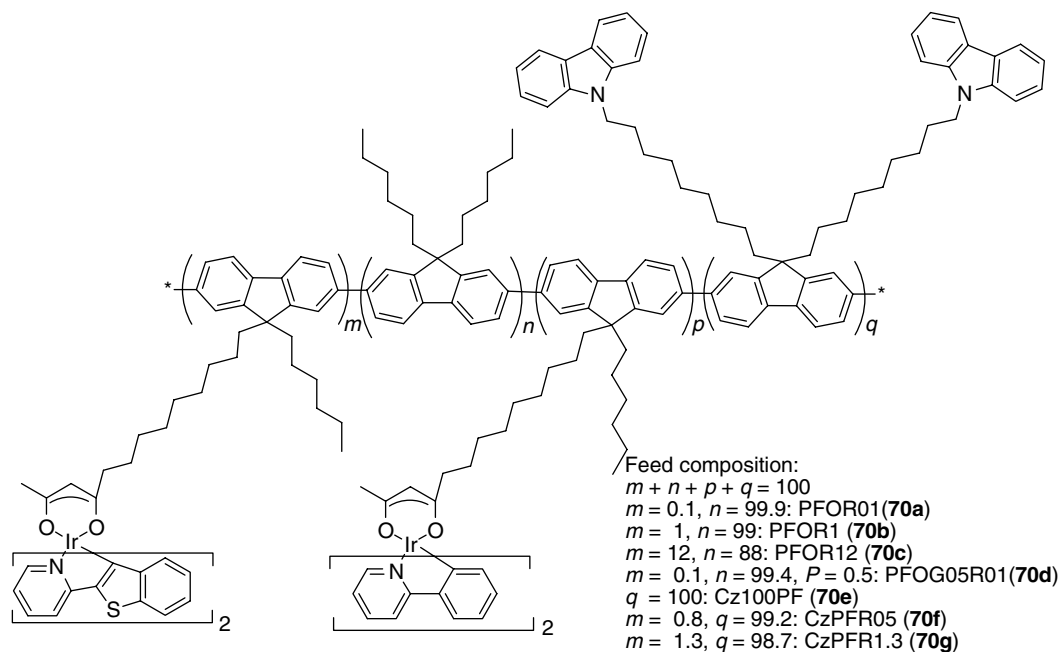


CHART 4.24 Chemical structure of copolymers with different content of phosphorescent and hole-transporting units.

the charge-transporting carbazole moieties as pendant groups on the polymer chain. By simply changing the comonomers feeding ratio in Suzuki or Yamamoto polymerization reactions, the copolymers **70** with different content of phosphorescent and hole-transporting units have been prepared (Chart 4.24). The performance of the PPLEDs fabricated with these materials in configuration ITO/PEDOT/polymer/Ca/Al is given in Table 4.6. The charge

TABLE 4.6
The Characteristics of PLEDs Fabricated with Polymers Containing Phosphorescent Moieties as Pendant Groups (PFO Stands for PDOF 13)

Polymer	Turn-On Voltage ^a (V/100 nm)	Maximum Efficiency (cd/A) (η_{\max} , %) (V)	Maximum Brightness (cd/m ²) (V)
PFO	5.7	0.049 (0.05) (9)	258 (11)
PFOR01	6.9	0.037 (0.017) (8)	57 (11)
PFOR1	6.9	0.88 (0.57) (10)	1479 (13)
PFOR12	8.0	1.0 (0.43) (17.5)	508 (23)
PFOG05R01	6.7	0.23 (0.16) (15)	335 (18)
Cz100PF	3.3	1.28 (0.74) (5)	5029 (7)
CzPFR08	4.3	2.16 (1.32) (9)	3735 (10)
CzPER1.3	4.9	2.8 (1.59) (7)	4321 (15)

^aBrightness over 0.2 cd/m².

Source: From Chen, X., Liao, J., Liang, Y., Ahmed, M.O., Tseng, H., and Chen, S., *J. Am. Chem. Soc.*, 125, 636, 2003. With permission.

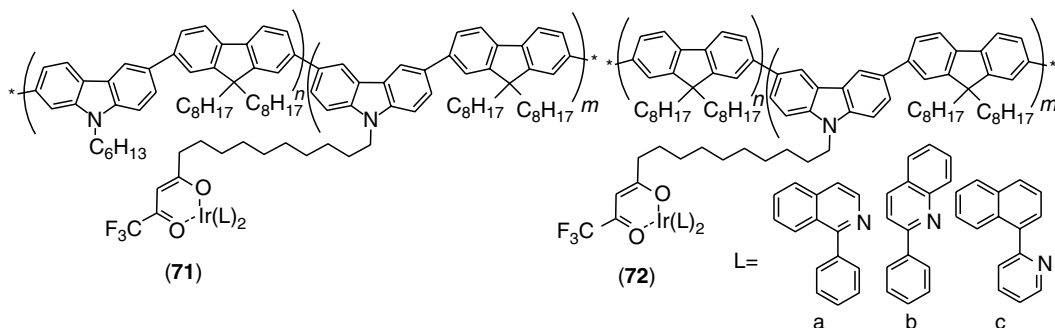


CHART 4.25 Chemical structure of electrophosphorescent fluorene copolymers where the hole-transporting carbazole units have been introduced in the polymer backbone.

mobility of the copolymers containing iridium complex moieties was up to two orders of magnitude lower than that of PDOF (**13**) homopolymers, which indicates a strong charge trapping on the phosphorescent moieties. However, the efficiency of the Ir-containing copolymers was substantially higher than those without the Ir moieties, and in the case of copolymer CzPFR13 (**70 g**), the maximum EQE of 1.59% (electroluminescent efficiency 2.8 cd/A) was achieved at a low voltage of 7 V (and brightness 65 cd/m²). Moreover, the efficiency stays relatively high (1.6 cd/A) at a high brightness of 4320 cd/m² (achieved at 15 V).

Later, Yang and coworkers [84] reported similar electrophosphorescent fluorene copolymers **71** and **72**, where the hole-transporting carbazole units have been introduced in the polymer backbone (Chart 4.25). Optimizing the polymer structure (comonomer ratio) and the device structure (blending with electron-transporting material PBD **8**), the EQE of 4.9% has been achieved.

A different type of phosphorescent polyfluorenes (green-emitting **73** and red-emitting **74**) (Chart 4.26) was recently prepared by Holmes and coworkers [85]. The triplet-emitting iridium complex was made a part of a conjugated polymer backbone, which should provide more efficient energy transfer. The dopant concentration was adjusted by controlling the length of the polymer ($n \sim 5, 10, 20, 30$, and 40). The triplet-state emission was observed in all polymers, and the energy transfer was more efficient than that in corresponding blends. The PPLED devices, fabricated as ITO/PEDOT/polymer/Ca/Al, showed moderately high EL efficiency of 1.5% (for red-emitting **74**, $n = 40$).

4.6 ELECTROPHOSPHORESCENT DENDRIMERS

The triplet-emitting metals can be also used as multidentate sites to synthesize solution-processible phosphorescent dendrimers. Samuel and coworkers [86] reported an extremely high efficiency single layer LED fabricated from a first-generation dendrimer **75** (Chart 4.27) blended with electron-transporting (TPBI **9**) and hole-transporting (4,4'-bis(9-carbazolyl)diphenyl (CBP)) materials [86]. The green-emitting ($\lambda_{EL} = 518$ nm) device with ITO and LiF/Al electrodes showed the EQE of 10.4% and very high power efficiency of 12.8 lm/W (at 8 V), whereas the operating voltage (at 100 cd/m²) was as low as 6 V. Later, the same group has reported red-emitting phosphorescent dendrimers **76** and **77** [87]. The resulting multilayer OLEDs, fabricated by spin-coating, showed a high EQE (4.6%, 4.5 lm/W) and saturated red-color emission (CIE: 0.67, 0.33). Furthermore, the precise color of the device can be conveniently adjusted by blending green-emitting dendrimer **75** with red-emitting **76** to afford very high-efficiency devices (current efficiency of up to 31 cd/A) [88].

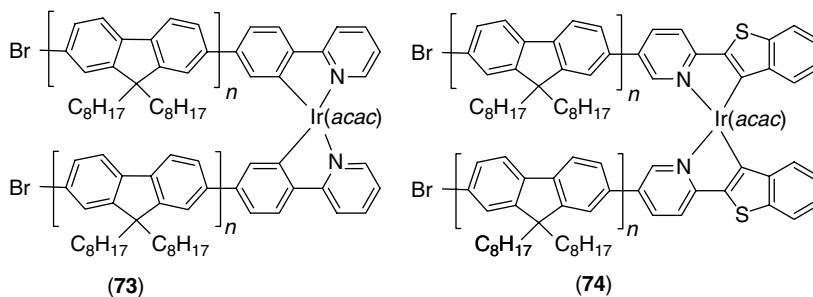


CHART 4.26 Chemical structure of green-emitting and red-emitting phosphorescent polyfluorenes.

4.7 CONCLUSIONS AND REMARKS

Polymer-based electrophosphorescent LEDs are a very new research area explored only since 1999. Nevertheless, the practical achievements reported for the last 5 years suggest a strong potential of this technology to pioneer the manufacturing of large-area low-cost displays in the future by solution techniques. The electroluminescent efficiency demonstrated by PPLEDs, although still a little lower than that of the best phosphorescent small molecules OLEDs, overrides conventional, fluorescent polymer LEDs by approximately a factor of 2 (EQE up to 12%, current efficiency up to 40 cd/A). Most of the phosphorescent polymeric materials studied consist of a fluorescent host polymer doped by a low-molecular phosphorescent dye, although several prominent examples of metallorganic phosphorescent polymers have been recently demonstrated.

Although the empirical search was a major contributor toward new host materials and guest dopants, the rational design based on consideration of energy levels and energy transfer criteria is playing a very important role in the creation of specific host–guest systems. The well-developed theory of electron and exciton transfer allows work to out the basic material requirements. Thus, the spectral overlap between the host emission and the guest absorption is needed for effective Förster transfer of singlet exciton, and the HOMO and LUMO levels of the dopant should preferably be within the band gap of the host materials (to facilitate the Dexter transfer of triplets). Thus, one needs a wide band-gap polymer (yet highly fluorescent and possessing substantial charge mobility) and a smaller gap efficient phosphor dopant. At the same time, the triplet energy of the polymer should be above the triplet of the dopant to preclude back transfer of the triplet excitons on the polymer. This latter condition is difficult to fulfill [71] and the structure–property relationships are not well established in this area. Probably, high-level computational study should be implemented to help in design of such novel host materials.

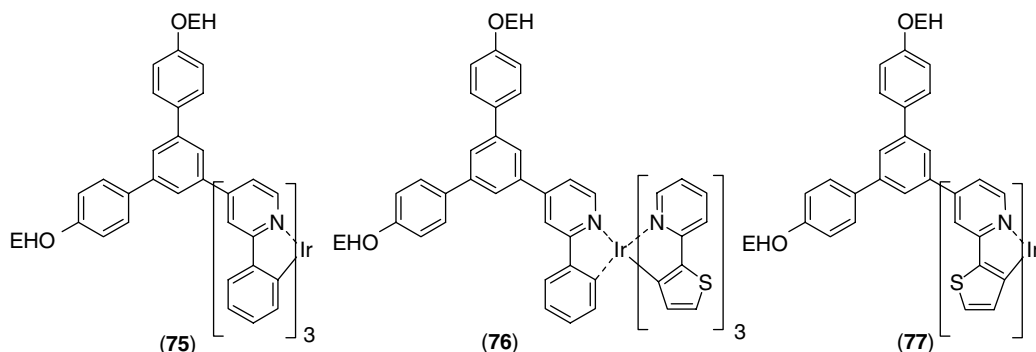


CHART 4.27 Chemical structure of a first-generation dendrimer.

So far poly(*N*-vinylcarbazole) PVK has been shown as the most efficient host polymer for PPLEDs. In combination with green-emitting tris(2-phenylpyridine) iridium complex Ir(ppy)₃ (**3**) or with its fluorinated analog blue-emitting Flrpic (**16**), the champion efficiencies of 37.3 cd/A (10.5%) [37] and 14 cd/A [45] have been achieved for green- and blue-emitting PPLEDs, respectively. The conjugated polymers are usually poor hosts for high-energy blue and green emitters, but can perform rather well with red-emitting phosphors. Thus, an EQE of 12% (5.2 cd/A) was reported for a red-emitting PPLED built with poly(dioctylfluorene) PDOF (**13**) and bis(1-phenylisoquinoline) iridium acetonylacetate PhqIr (**34**) [61].

At the same time, a rather high operating voltage, as compared to fluorescent PLEDs results in a relatively low power conversion efficiency (particularly for nonconjugated hosts). There was so far only one report on PPLED device with high power efficiency (highest efficiency 38.6 lm/W [80]), while for the majority of PPLEDs it does not exceed 20 lm/W, a value already achieved in fluorescent PLEDs. This is caused by direct charge trapping on the phosphor dopants, which also might be responsible for the device degradation.

The most important problem for commercialization of PPLEDs is their short operation lifetime. The lower operation stability of phosphorescent LEDs as compared to fluorescent devices might be expected from longer lifetime of emitting states (triplet excitons), which facilitates by-side chemical processes. Surprisingly, there are only scarce studies of this issue in the literature [41], and, unfortunately, the device stability has rarely been the main objective in the synthesis of new host and guest materials. Clearly, systematic studies of the device degradation and accompanying chemical processes are needed for rational design of new phosphors and polymer hosts with practically acceptable stability.

ACKNOWLEDGMENT

We thank Dr. Charles J DuBois at DuPont CRD for proof reading of the manuscript. DFP thanks the National Science and Engineering Research Council for support through the Discovery and AGENO grants.

REFERENCES

1. SR Forrest, The road to high efficiency organic light emitting devices, *Org. Electron.*, 4: 45–48, 2003.
2. CH Li, G Kioseoglou, OMJ van't Erve, AT Hanbicki, BT Jonker, R Mallory, M Yasar, and A Petrou, Spin injection across (110) interfaces: Fe/GaAs(110) spin-light-emitting diodes, *Appl. Phys. Lett.*, 85: 1544–1546, 2004.
3. E Arisi, I Bergneti, V Dediu, MA Loi, M Muccini, M Murgia, G Ruani, C Taliani, and R Zamboni, Organic light-emitting diodes with spin-polarized electrodes, *J. Appl. Phys.*, 93: 7682–7683, 2003.
4. J Kido, H Haromichi, K Hongawa, K Nagai, and K Okuyama, Bright red light-emitting organic electroluminescent devices having a europium complex as an emitter, *Appl. Phys. Lett.*, 65: 2124–2126, 1994.
5. T Sano, M Fujita, T Fujii, Y Hamada, K Shibata, and K Kuroki, Novel europium complex for electroluminescent devices with sharp red emission, *Jpn. J. Appl. Phys.*, 34(Part 1): 1883–1887, 1995.
6. MA Baldo, DF O'Brien, Y You, A Shoustikov, S Sibley, ME Thompson, and SR Forrest, Highly efficient phosphorescent emission from organic electroluminescent devices, *Nature*, 395: 151–154, 1998.
7. C Adachi, MA Baldo, ME Thompson, and SR Forrest, Nearly 100% internal phosphorescence efficiency in an organic light emitting device, *J. Appl. Phys.*, 90: 5048–5051, 2001.
8. V Cleave, G Yahiloglu, PL Barny, RH Friend, and N Tessler, Harvesting singlet and triplet energy in polymer LEDs, *Adv. Mater.*, 11: 285–288, 1999.
9. PW Atkins and RS Friedman, *Molecular Quantum Mechanics*, 3rd ed., Oxford University Press, Oxford, 1997, pp. 109–119.
10. Z Shuai, D Beljonne, RJ Silbey, and JL Bredas, Singlet and triplet exciton formation rates in conjugated polymer light-emitting diodes, *Phys. Rev. Lett.*, 24: 131–134, 2000.

11. S Ramasesha, S Mazumdar, K Tandon, and M Das, Electron correlation effects in electron–hole recombination and triplet–triplet scattering in organic light emitting diodes, *Synth. Met.*, 139: 917–920, 2003.
12. Y Cao, ID Parker, G Yu, C Zhang, and AJ Heeger, Improved quantum efficiency for electroluminescence in semiconducting polymers, *Nature*, 397: 414–417, 1999.
13. M Wohlgenannt, K Tandon, S Mazumdar, S Ramasesha, and ZV Vardeny, Formation cross-sections of singlet and triplet excitons in π -conjugated polymers, *Nature*, 409: 494–497, 2001.
14. JS Wilson, AS Dhoot, AJAB Seeley, MS Khan, A Köhler, and RH Friend, Spin-dependent exciton, formation in π -conjugated compounds, *Nature*, 413: 828–831, 2001.
15. AS Dhoot and NC Greenham, Triplet formation in polyfluorene derivatives, *Adv. Mater.*, 24: 1834–1837, 2002.
16. W Wohlgenannt, XM Jiang, C Yang, OJ Korovyanko, and ZV Vardeny, Spin-dependent polaron pair recombination in π -conjugated polymers: enhanced singlet exciton densities, *Synth. Met.*, 139: 921–924, 2003.
17. A Köhler and J Wilson, Phosphorescence and spin-dependent exciton formation in conjugated polymers, *Org. Electron.*, 4: 179–189, 2003.
18. M Segal, MA Baldo, RJ Holmes, SR Forrest, and ZG Soos, Excitonic singlet–triplet ratios in molecular and polymeric organic materials, *Phys. Rev. B*, 68: 075211, 2003.
19. MA Baldo, DF O’Brien, ME Thompson, and SR Forrest, Excitonic singlet–triplet ratio in a semiconducting organic thin film, *Phys. Rev. B*, 60: 14422, 1999.
20. A Jablonski, Efficiency of anti-stokes fluorescence in dyes, *Nature*, 131: 839–841, 1933.
21. RA Marcus, On the theory of oxidation–reduction reactions involving electron transfer. I, *J. Chem. Phys.*, 24: 966–979, 1956.
22. GL Closs and JR Miller, Intramolecular long-distance electron transfer in organic materials, *Science*, 240: 440–447, 1988.
23. DL Dexter, A theory of sensitized luminescence in solids, *J. Chem. Phys.*, 21: 836–850, 1953.
24. T Förster, Transfer mechanisms of electronic excitation, *Discussions Faraday Soc.*, 27: 7–17, 1959.
25. MA Baldo, C Adachi, and SR Forrest, Transient analysis of electrophosphorescence II. Transient analysis of triplet–triplet annihilation, *Phys. Rev. B*, 62: 10967–10977, 2000.
26. C Adachi, MA Baldo, SR Forrest, and ME Thompson, High-efficiency organic electrophosphorescent devices with tris(2-phenylpyridine)iridium doped into electron-transporting materials, *Appl. Phys. Lett.*, 77: 904–906, 2000.
27. Y Ma, CM Che, HY Chao, X Zhou, WH Chan, and J Shen, High luminescence gold(I) and copper(I) complexes with a triplet excited state for use in light-emitting diodes, *Adv. Mater.*, 11: 852–857, 1999.
28. Y Li, Y Wang, Y Wu, and J Shen, Carbonyl polypyridyl Re(I) complexes as organic electroluminescent materials, *Synth. Met.*, 99: 257–260, 1999.
29. WD Gill, Drift mobilities in amorphous charge-transfer complexes of trinitrofluorenone and poly-*n*-vinylcarbazole, *J. Appl. Phys.*, 43: 5033–5040, 1972.
30. MD McGehee, T Bergstedt, C Zhang, AP Saab, MB O’Regan, GC Bazan, VI Srdanov, and AJ Heeger, Narrow bandwidth luminescence from blends with energy transfer from semiconducting conjugated polymers to europium complexes, *Adv. Mater.*, 11: 1349–1354, 1999.
31. A Tsuboyama, H Iwawaki, M Furugori, T Mukaide, J Kamatani, S Igawa, T Moriyama, S Muira, T Takiguchi, S Oakada, M Hoshino, and K Ueno, Homoleptic cyclometalated iridium complexes with highly efficient red phosphorescence and application to organic light-emitting diode, *J. Am. Chem. Soc.*, 125: 12971–12979, 2003.
32. S Lamansky, P Djurovich, D Murphy, F Abdel-Razzaq, HE Lee, C Adachi, PE Burrows, SR Forrest, and ME Thompson, Highly phosphorescent bis-cyclometalated iridium complexes: synthesis, photophysical characterization, and use in organic light-emitting diodes, *J. Am. Chem. Soc.*, 123: 4304–4312, 2001.
33. C Lee, KB Lee, and J Kim, Polymer phosphorescent light-emitting devices doped with tris (2-phenylpyridine) iridium as a triplet emitter, *Appl. Phys. Lett.*, 77: 2280–2282, 2000.
34. J Kido, K Hongawa, K Okuyama, and K Nagai, Bright blue electroluminescence from poly (N-vinylcarbazole), *Appl. Phys. Lett.*, 63: 2627–2629, 1993.

35. M Yang and T Tsutsui, Use of poly(9-vinylcarbazole) as host material for iridium complexes in high-efficiency organic light-emitting devices, *Jpn. J. Appl. Phys.*, 39: L828–L829, 2000.
36. KM Vaeth and CW Tang, Light-emitting diodes based on phosphorescent guest/polymeric host systems, *J. Appl. Phys.*, 92: 3447–3453, 2002.
37. KM Vaeth and J Dicillo, High-efficiency doped polymeric organic light-emitting diodes, *J. Polym. Sci.: Part B: Polym. Phys.*, 41: 2715–2725, 2003.
38. X Yang, D Neher, D Hertel, and TK Däubler, Highly efficient single-layer polymer electrophosphorescent devices, *Adv. Mater.*, 16: 161–166, 2004.
39. F Chen, Y Yang, ME Thompson, and J Kido, High-performance polymer light-emitting diodes doped with a red phosphorescent iridium complex, *Appl. Phys. Lett.*, 80: 2308–2310, 2002.
40. MA Baldo, S Lamansky, PE Burrows, ME Thompson, and SR Forrest, Very high-efficiency green organic light-emitting devices based on electrophosphorescence, *Appl. Phys. Lett.*, 75: 4–6, 1999.
41. SC Chang, G He, FC Chen, TF Guo, and Y Yang, Degradation mechanism of phosphorescent-dye-doped polymer light-emitting diodes, *Appl. Phys. Lett.*, 79: 2088–2090, 2001.
42. Y Kawamura, S Yanagida, and SR Forrest, Energy transfer in polymer electrophosphorescent light emitting devices with single and multiple doped luminescent layers, *J. Appl. Phys.*, 92: 87–93, 2002.
43. DF O'Brien, MA Baldo, ME Thompson, and SR Forrest, Improved energy transfer in electrophosphorescent devices, *Appl. Phys. Lett.*, 74: 442–444, 1999.
44. S Lamansky, PI Djurovich, F Abdel-Razzaq, S Garon, DL Murphy, and ME Thompson, Cyclometalated Ir complexes in polymer organic light-emitting diodes, *J. Appl. Phys.*, 92: 1570–1572, 2002.
45. A Nakamura, T Tada, M Mizukami, and S Yagyu, Efficient electrophosphorescent polymer light-emitting devices using a Cs/Al cathode, *Appl. Phys. Lett.*, 84: 130–132, 2004.
46. G He, S Chang, F Chen, Y Li, and Y Yang, Highly efficient polymer light-emitting devices using a phosphorescent sensitizer, *Appl. Phys. Lett.*, 81: 1509–1511, 2002.
47. X Gong, MR Robinson, JC Ostrowski, D Moses, GC Bazan, and AJ Heeger, High-efficiency polymer-based electrophosphorescent devices, *Adv. Mater.*, 14: 581–585, 2002.
48. X Gong, JC Ostrowski, D Moses, GC Bazan, and AJ Heeger, Electrophosphorescence from a polymer guest–host system with an iridium complex as guest: Förster energy transfer and charge trapping, *Adv. Funct. Mater.*, 13: 439–444, 2003.
49. X Gong, JC Ostrowski, GC Bazan, D Moses, and AJ Heeger, Red electrophosphorescent from polymer doped with iridium complex, *Appl. Phys. Lett.*, 81: 3711–3713, 2002.
50. X Gong, JC Ostrowski, D Moses, GC Bazan, and AJ Heeger, High-performance polymer-based electrophosphorescent light-emitting diodes, *J. Polym. Sci. B: Polym. Phys.*, 41: 2691–2705, 2003.
51. S Kan, X Liu, F Shen, J Zhang, Y Ma, Y Wang, and J Shen, Improved efficiency of single-layer polymer light-emitting devices with poly(vinylcarbazole) doubly doped with phosphorescent and fluorescent dyes as the emitting layer, *Adv. Funct. Mater.*, 13: 603–608, 2003.
52. F Shen, H Xia, C Zhang, D Lin, X Liu, and Y Ma, Spectral investigation for phosphorescent polymer light-emitting devices with doubly doped phosphorescent dyes, *Appl. Phys. Lett.*, 84: 55–57, 2004.
53. TF Guo, SC Chang, Y Yang, RC Kwong, and ME Thompson, Highly efficient electrophosphorescent polymer light-emitting devices, *Org. Electron.*, 1: 15–20, 2000.
54. DF O'Brien, C Giebelerb, RB Fletcherb, AJ Cadbyb, LC Palilisb, DG Lidzeyb, PA Laneb, DDC Bradley, and W Blau, Electrophosphorescence from a doped polymer light emitting diode, *Synth. Met.*, 116: 379–383, 2001.
55. PA Lane, LC Palilis, DF O'Brien, C Giebeler, AJ Cadby, DG Lidzey, AJ Campbell, W Blau, and DDC Bradley, Origin of electrophosphorescence from a doped polymer light emitting diode, *Phys. Rev. B*, 63: 235206, 2001.
56. FC Chen, Y Yang, and Q Pei, Phosphorescent light-emitting electrochemical cell, *Appl. Phys. Lett.*, 81: 4278–4280, 2002.
57. Y Noh, C Lee, J Kim, and K Yase, Energy transfer and device performance in phosphorescent dye doped polymer light emitting diodes, *J. Chem. Phys.*, 118: 2853–2864, 2003.

58. FC Chen, SC Chang, G He, S Pyo, Y Yang, M Kurotaki, and J Kido, Energy transfer and triplet exciton confinement in polymeric electrophosphorescence devices, *J. Polym. Sci. B: Polym. Phys.*, 41: 2681–2690, 2003.
59. X Gong, JC Ostrowski, GC Bazan, D Moses, AJ Heeger, MS Liu, and AKY Jen, Electrophorescence from a conjugated copolymer doped with an iridium complex: high brightness and improved operational stability, *Adv. Mater.*, 15: 45–49, 2003.
60. F Chen, G He, and Y Yang, Triplet exciton confinement in phosphorescent polymer light-emitting diodes, *Appl. Phys. Lett.*, 82: 1006–1008, 2003.
61. C Jiang, W Yang, J Peng, S Xiao, and Y Cao, High-efficiency, saturated red-phosphorescent polymer light-emitting diodes based on conjugated polymers doped with an Ir complex, *Adv. Mater.*, 16: 537–541, 2004.
62. X Gong, W Ma, JC Ostrowski, GC Bazan, D Moses, and AJ Heeger, White electrophosphorescence from semiconducting polymer blends, *Adv. Mater.*, 16: 615–619, 2004.
63. X Gong, D Moses, AJ Heeger, and S Xiao, White light electrophosphorescence from polyfluorene-based light-emitting diodes: utilization of fluorenone defects, *J. Phys. Chem. B*, 108: 8601–8605, 2004.
64. HJ Su, FI Wu, CF Shu, YL Tung, Y Chi, and GH Lee, Polyfluorene containing diphenylquinoline pendants and their applications in organic light emitting diodes, *J. Polym. Sci. A: Polym. Chem.*, 43: 859–869, 2005.
65. W Zhu, Y Mo, M Yuan, W Yang, and Y Cao, Highly efficient electrophorescent devices based on conjugated polymers doped with iridium complexes, *Appl. Phys. Lett.*, 80: 2045–2047, 2002.
66. W Zhu, C Liu, L Su, W Yang, M Yuan, and Y Cao, Synthesis of new iridium complexes and their electrophosphorescent properties in polymer light-emitting diodes, *J. Mater. Chem.*, 13: 50–55, 2003.
67. W Zhu, M Zhu, Y Ke, L Su, M Yuan, and Y Cao, Synthesis and red electrophosphorescence of a novel cyclometalated iridium complex in polymer light-emitting diodes, *Thin Solid Films*, 446: 128–131, 2004.
68. XH Yang, D Neher, U Scherf, SA Bagnich, and H Bässler, Polymer electrophorescent devices utilizing a ladder-type poly(para-phenylene) host, *J. Appl. Phys.*, 93: 4413–4419, 2003.
69. JM Lupton, A Pogantsch, T Piok, EJW List, S Patil, and U Scherf, Intrinsic room-temperature electrophosphorescence from a π -conjugated polymer, *Phys. Rev. Lett.*, 89: 167401, 2002.
70. M Sudhakar, PI Djurovich, TE Hogen-Esch, and ME Thompson, Phosphorescence quenching by conjugated polymers, *J. Am. Chem. Soc.*, 125: 7796–7797, 2003.
71. A Köhler and D Beljonne, The singlet–triplet exchange energy in conjugated polymers, *Adv. Funct. Mater.*, 14: 11–18, 2004.
72. YV Romanovskii, A Gerhard, B Schweitzer, U Scherf, RI Personov, and H Bässler, Phosphorescence of π -conjugated oligomers and polymers, *Phys. Rev. Lett.*, 84: 1027–1030, 2000.
73. D Hertel, S Setayesh, HG Nothofer, U Scherf, K Müllen, and H Bässler, Phosphorescence in conjugated poly(para-phenylene-derivatives), *Adv. Mater.*, 13: 65–70, 2001.
74. A van Dijken, JJAM Bastiaansen, NMM Kiggen, BMW Langeveld, C Rothe, A Monkman, I Bach, P Stössel, and K Brunner, Carbazole compounds as host materials in light-emitting diodes: polymer hosts for high-efficiency light-emitting diodes, *J. Am. Chem. Soc.*, 126: 7718–7727, 2004.
75. CL Lee, NG Kang, YS Cho, JS Lee, and JJ Kim, Polymer electrophosphorescent device: comparison of phosphorescent dye doped and coordinated systems, *Opt. Mater.*, 21: 119–123, 2002.
76. S Tokito, M Suzuki, F Sato, M Kamachi, and K Shirane, High-efficiency phosphorescent polymer light-emitting devices, *Org. Electron.*, 4: 105–111, 2003.
77. S Tokito, M Suzuki, and F Sato, Improvement of emission efficiency in polymer light-emitting devices based on phosphorescent polymers, *Thin Solid Films*, 445: 353–357, 2003.
78. M Suzuki, T Hatekayama, S Tokito, and F Sato, High-efficiency white phosphorescent polymer light-emitting devices, *IEEE J. Selected Top. Quantum Electron.*, 10: 115–120, 2004.
79. PT Furuta, L Deng, S Garon, ME Thompson, and JMJ Fréchet, Platinum-functionalized random copolymers for use in solution-processible, efficient, near-white organic light-emitting diodes, *J. Am. Chem. Soc.*, 126: 15388–15389, 2004.
80. M Suzuki, S Tokito, F Sato, T Igarashi, K Kondo, T Koyama, and T Yamaguchi, Highly efficient polymer light-emitting devices using ambipolar phosphorescent polymers, *Appl. Phys. Lett.*, 86: 103507, 2005.

81. J Pei, XL Liu, WL Yu, YH Lai, YH Niu, and Y Cao, Efficient energy transfer to achieve narrow bandwidth red emission from Eu^{3+} -grafting conjugated polymers, *Macromolecules*, 35: 7274–7280, 2002.
82. QD Ling, ET Kang, KG Neoh, and W Huang, Synthesis and nearly monochromatic photoluminescence properties of conjugated copolymers containing fluorene and rare earth complexes, *Macromolecules*, 36: 6995–7003, 2003.
83. X Chen, J Liao, Y Liang, MO Ahmed, H Tseng, and S Chen, High-efficiency red-light emission from polyfluorenes grafted with cyclometalated iridium complexes and charge transport moiety, *J. Am. Chem. Soc.*, 125: 636–637, 2003.
84. J Jiang, C Jiang, W Yang, H Zhen, F Huang, and Y Cao, High-efficiency electrophosphorescent fluorene-alt-carbazole copolymers *N*-grafted with cyclometalated Ir complexes, *Macromolecules*, 38: 4072–4080, 2005.
85. AJ Sandee, CK Williams, NR Evans, JE Davies, CE Boothby, A Köhler, RH Friend, and AB Holmes, Solution-processible conjugated electrophosphorescent polymers, *J. Am. Chem. Soc.*, 126: 7041–7048, 2004.
86. TD Anthopoulos, JPJ. Markham, EB Namdas, IDW Samuel, SC Lo, and PL Burn, Highly efficient single-layer dendrimer light-emitting diodes with balanced charge transport, *Appl. Phys. Lett.*, 82: 4824–4826, 2003.
87. TD Anthopoulos, MJ Frampton, EB Namdas, PL Burn, and IDW Samuel, Solution-processable red phosphorescent dendrimers for light-emitting device applications, *Adv. Mater.*, 16: 557–560, 2004.
88. EB Namdas, TD Anthopoulos, IDW Samuel, MJ Frampton, SC Lo, and PL Burn, Simple color tuning of phosphorescent light-emitting diodes, *Appl. Phys. Lett.*, 86: 161104–161106, 2005.
89. BS Harrison, TJ Foley, AS Knefely, JK Mwaura, GB Cunningham, TS Kang, M. Boug Lettaya, JM Boncella, JR Reynolds, and KS Schanze, Near-infrared photo- and electroluminescence of alkoxy-substituted poly(p-phenylene) and nonconjugated polymer/lanthanide tetraphenylporphyrin blends, *Chem. Mater.*, 16: 2938–2947, 2004.
90. X Wang, MR Andersson, ME Thompson, and O Inganäs, Electrophosphorescence from substituted poly(thiophene) doped with iridium or platinum complex, *Thin Solid Films*, 468: 226–233, 2004.

5 Polarized Light Emission from Organic Light-Emitting Diodes

Daniel Steiger and Christoph Weder

CONTENTS

5.1	Introduction	451
5.2	Representation of Linearly and Circularly Polarized Photoluminescence	454
5.3	Linearly Polarized Photo- and Electroluminescence from Uniaxially Oriented Molecules	457
5.3.1	Tensile Deformation.....	457
5.3.2	Rubbing and Friction Deposition	461
5.3.3	Orientation of Nonliquid-Crystalline Materials on Orienting Substrates	462
5.3.4	Langmuir–Blodgett Technique.....	464
5.3.5	Orientation of Liquid-Crystalline Light-Emitting Materials.....	464
5.3.6	Overview of LEDs Emitting Linearly Polarized Light.....	469
5.4	Circularly Polarized Luminescence	469
5.4.1	Circularly Polarized Luminescence from Achiral Dyes Doped in Chiral Matrices	471
5.4.2	Circularly Polarized Luminescence from Conjugated Polymers	472
5.4.3	Other Systems for Circularly Polarized Luminescence.....	474
5.5	Conclusions.....	474
	Acknowledgment.....	474
	References	474

5.1 INTRODUCTION

Uniaxially oriented, form-anisotropic photoluminescent (PL) molecules usually exhibit anisotropic optical characteristics, i.e., linearly polarized absorption and emission. The phenomenon of linearly polarized PL from inorganic crystals has been known for more than a century [1] and was reported for oriented blends of ductile polymers and low-molecular-weight organic PL molecules as early as the 1930s [2]. The emission of linearly polarized light has since been observed for a plethora of materials, which were oriented by a broad variety of orientation methods [3]. A similar effect is the emission of circularly polarized (CP) light, which can be observed in the case of chiral PL molecules [4] and also in the case of nonchiral PL molecules that are embedded in a chiral matrix [5]. The emission of linearly or circularly polarized light from photoluminescent matter has recently attracted a great deal of interest, and photoluminescent polarizers [6–10] may be useful for a variety of applications that range from security features [11] to liquid-crystal displays (LCDs) [12].

Polarized chromatic light, which is essential for a variety of devices and applications, is usually generated by the use of an isotropic light source in combination with a polarizer [13].

Probably the technologically most important application of this combination is in LCDs, which currently represent the dominating flat-panel display technology [14]. In the case of backlit LCDs, a white light source is employed, and the three primary colors red, green, and blue are generated by means of absorbing color filters. However, dichroic sheet polarizers and conventional color filters rely on the principle of light absorption and are extremely energy-inefficient elements [15]. As a matter of fact, in conventional LCDs about 90% of the light generated by the backlight is absorbed by the back polarizers and the color filters, and consequently these devices exhibit severe limitations in brightness and energy efficiency [15]. One approach of improving the yield of polarized light is the replacement of dichroic polarizers with elements that reflect or scatter light [16–19]. By using appropriate supplementary elements to recycle reflected or scattered energy, the ultimate efficiency of these systems can, in principle, approach unity (twice that of dichroic polarizers). In practice, efficiencies up to 80% are achieved [15]. Rather than recycling wrongly polarized light, an alternative way to improve the overall efficiency of the system is to directly generate polarized light. In this context, the combination of PL polarizers with a monochromatic, an ultraviolet (UV), or a blue light source [7, 12] has been proposed. This approach is attractive as it not only eliminates an absorbing polarizer but also makes the terribly inefficient color filters obsolete. The PL materials act as active color filters, and in principle, isotropic-to-polarized conversion efficiencies that approach the PL quantum efficiency of the emitting species could be attainable by this concept. Taking this approach one step further, one arrives at light sources that directly emit polarized chromatic light, a feature that had, hitherto, been unique to lasers. Although the general idea had already been proposed in the patent literature [20], Dyreklev et al. [21] were the first to demonstrate that the concept of polarized light emission can also be exploited in the case of polymer light-emitting diodes (PLEDs). Most conventional PLEDs and also light-emitting diodes (LEDs) based on low-molecular-weight organic emitters (OLEDs) comprise an isotropic (i.e., unoriented, nonchiral) emitting layer, and concomitantly their emission is essentially unpolarized [22–24]. However, as the singlet excited states generated through the recombination of electrons and holes are identical with those generated through photoexcitation [25], light-emitting devices comprising a uniaxially oriented emitting layer and an otherwise conventional architecture emit linearly polarized light (Figure 5.1a). In their pioneering study, Dyreklev et al. employed a modestly oriented conjugated polymer, and as a result, the emission of the device was only moderately polarized, as evidenced by the reported ratio of 2.4 of the electroluminescence (EL) intensities observed through a linear polarizer oriented parallel and perpendicular to the direction of uniaxial alignment (Figure 5.1b) [21].

Beyond their potential application as a backlight in LCDs, light sources that generate polarized chromatic light are technologically important for a variety of applications and devices that range from optical data storage, to communications systems, to LCD projectors, to medical applications. CP LEDs allow display configurations in which the reflection of ambient light is reduced and which therefore exhibit significantly improved contrast. Thus, the concept of polarized LEDs generated much excitement, and considerable research and development activities focused on this subject have evolved around the globe [26–28]. The general architecture of an LED emitting linearly polarized light (and similarly CP light, *vide infra*) is rather straightforward and only differs from conventional LEDs in that a uniaxially oriented emitting layer is used (cf. Figure 5.1a). However, as will become apparent later in this chapter, the implementation of the concept is a nontrivial exercise. The fabrication of highly oriented emitting layers requires special materials and processing steps, which are often not compatible with the stringent demands of OLED and PLED technologies (cf. Refs. [22–25] and Chapter 5 and Chapter 6).

In view of the large number of publications on polarized light-emitting materials and polarized LEDs that have appeared to date, and with reference to the excellent reviews by

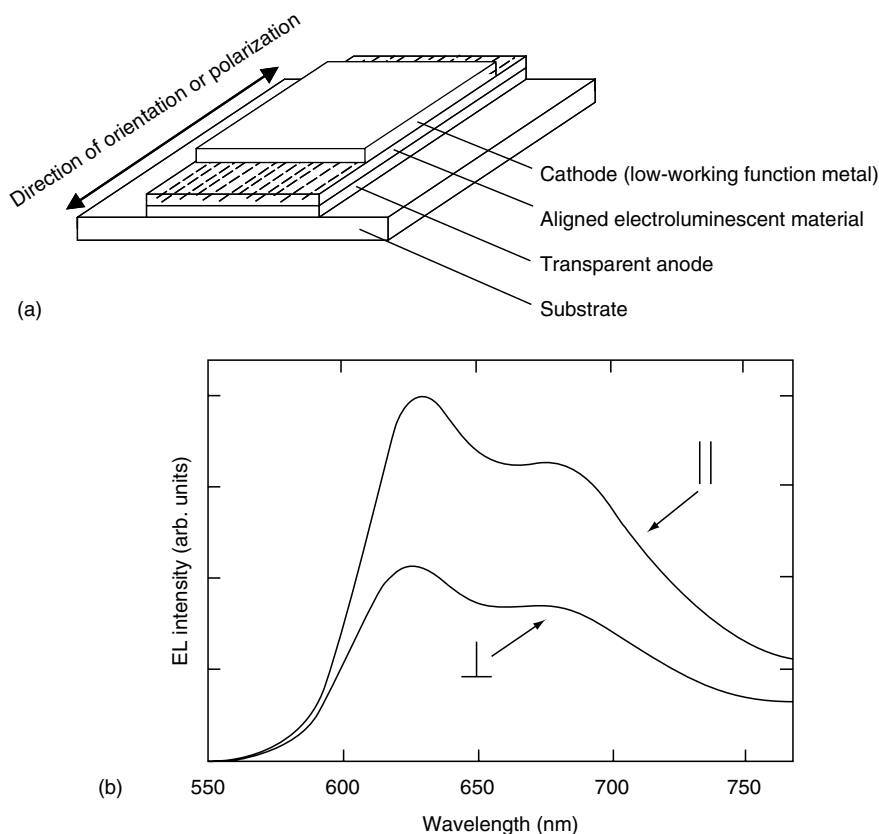


FIGURE 5.1 (a) Simplified schematic representation of the architecture of a single-layer LED emitting polarized light. The electroluminescent polymer is uniaxially oriented in the plane of the device, causing the emitted light to be linearly polarized. (b) Spectral distribution of the polarized EL displayed by the first polarized LED reported by Dyreklev et al. The two curves reflect the EL intensities detected through a linear polarizer oriented parallel (||) and perpendicular (⊥) to the orientation direction of the light-emitting polymer. (From Dyreklev, P., Berggren, M., Inganäs, O., Andersson, M.R., Wennerström, O., and Hjertberg, T., *Adv. Mater.*, 7, 43, 1995. With permission.)

Grell and Bradley [26], Neher [27], and O'Neill and Kelly [28], which summarize many activities, it is clearly outside the scope of this chapter to review in detail the exciting progress that the field has seen during the past nine years. Rather, we have attempted to give a concise overview on the general aspects of emission of linearly polarized light from uniaxially oriented organic matter. The method employed to process the oriented emitting layer usually has a most significant influence on many important device parameters, and thus, the different orientation methodologies were used as a guideline for the organization of this text. We discuss illustrative examples of various devices from the viewpoint of aspects that are particularly relevant for a specific application. We have not made an organizational separation between low-molecular-weight and PLEDs, because many concepts equally apply to both materials' platforms. As will become evident from the examples discussed herein, the most promising material candidates for linearly polarized LEDs appear to be oligomers that are situated at the border between low-molecular-weight and polymeric species. The materials systems and architectures that may be used for LEDs that emit CP light are quite different from those used in linearly polarized LEDs, and thus, a separate section is devoted to the subject of CP emission.

5.2. REPRESENTATION OF LINEARLY AND CIRCULARLY POLARIZED PHOTOLUMINESCENCE

A rigorous and complete mathematical treatment of the polarization of light and the interaction of light with oriented matter is outside the scope of this chapter. These subjects have been thoroughly dealt with before and can be found in a number of comprehensive texts [29–32]; the reader is referred to the excellent book by Michl and Thulstrup [3] for a more detailed treatment of optical spectroscopy with polarized light. Here, a conventional, qualitative representation is given to establish the nomenclature and conventions to be used and to facilitate the understanding of the concepts presented.

Using Maxwell's framework of light as an electromagnetic wave, the wavelike behavior of light is represented by an oscillating electric field. The latter is always accompanied by an orthogonal magnetic field of similar frequency. However, as the organic materials discussed here are generally nonmagnetic, the following description of the polarization of light is reduced to the electric field component. For monochromatic light propagating as a plane wave along an optical axis (defined here as the z -axis, cf. Figure 5.2a) the electric field vector $E(r, t)$ as a function of time, t , is given by:

$$E(z, t) = E_x^{(0)} \sin(\omega t - kz + \phi_x) + E_y^{(0)} \sin(\omega t - kz + \phi_y) \quad (5.1)$$

where $E_x^{(0)}$, $E_y^{(0)}$, ϕ_x , and ϕ_y describe the amplitude and phase of the wave along the x - and y -axes, respectively, ω is the circular frequency, which is related to the wavelength (λ) and speed of light (c) by $\omega = 2\pi c/\lambda$, and $k = \omega c$ is the propagation vector. The polarization of light is determined by the time course of the electric field vector, as illustrated in Figure 5.2. For monochromatic light propagating along an optical axis (z -axis), $E(r, t)$ lies in the transverse plane (xy -plane). If the propagating electric field vector describes an ellipse (Figure 5.2c), the light is said to be elliptically polarized. One can consider elliptically polarized light as a general form of polarization and linear and circular polarizations as special cases of this more general form. The polarization is characterized by the orientation and eccentricity of the ellipse and determined by both the magnitudes of $E_x^{(0)}$ and $E_y^{(0)}$ and the relative phases ϕ_x and ϕ_y of these components. The polarization is said to be right-handed when $(\phi_y - \phi_x) < 180^\circ$, and left-handed when $-180^\circ < (\phi_y - \phi_x) < 0^\circ$. Thus, at a fixed position z , the tip of the electric field vector rotates periodically in the xy -plane, tracing out the ellipse. At a fixed time t , the locus of the tip of the electric field vector follows a helical trajectory in space, lying on the surface of an elliptical cylinder (Figure 5.2c). When the ellipse degenerates into a circle, the wave is said to be circularly polarized. This is the case when the phase difference $(\phi_y - \phi_x)$ is $\pm \pi/2$ and $E_x^{(0)} = E_y^{(0)}$ and when the elliptical cylinder depicted in Figure 5.2c becomes circular. When the ellipse degenerates into a straight line, the wave is said to be linearly polarized. This is the case if one of the amplitude components vanishes (the light is then said to be polarized in the direction of the remaining amplitude component) or if the phase difference $(\phi_y - \phi_x)$ is 0 or π .

In the process of absorption by a molecule, the electric field vector of linearly polarized light interacts with the electric dipole transition moment of the molecule. The probability of an absorption process is given by the square of the scalar product of the electric dipole transition moment vector and the electric field vector of the light, and is thus proportional to the square of the cosine of the angle between them. This leads to an orientational dependence of the absorption of linearly polarized light and, similarly, of the light emission from photo- and electroluminescent molecules. It allows one to use spectroscopy with linearly polarized light to investigate the nature of molecular transitions as well as the nature of the orientation of molecular assemblies [3]. Alternatively, as described in this contribution, this orientational

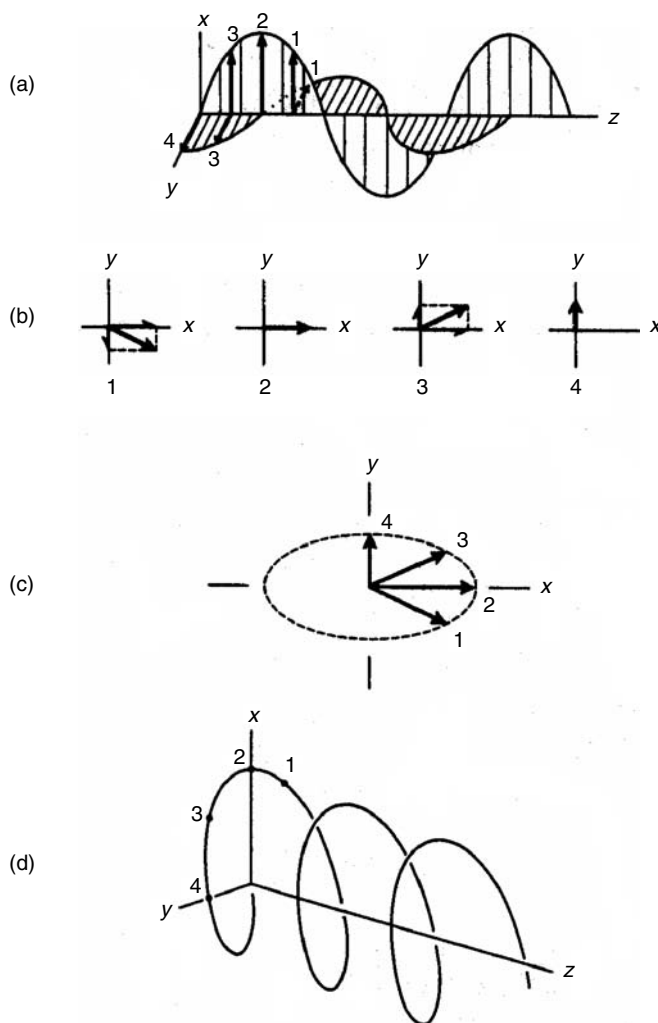


FIGURE 5.2 Wave representation of elliptically polarized light. (a) Orthogonal linear components with unequal amplitudes and 90° relative phase shift; (b) vector sums of the two components shown in (a) at positions labeled 1 through 4; (c) illustration of the fact that the tip of the electric field vector traces an ellipse when viewed along the propagation direction; (d) spatial dependence of the electric field vector represented in (a) to (c) at some point in time. (From Kliger, D.S., Lewis, J.W., and Randall, C.E., *Polarized Light in Optics and Spectroscopy*, San Diego, Academic, 1990. With permission.)

dependence can be employed to create optical elements, which absorb or emit highly polarized light. The direction of the electric dipole transition moment vector in the molecular framework is frequently referred to as the absolute polarization direction of the transition or its absolute polarization. However, it is noteworthy to state that the latter not necessarily (but often) coincides with the molecule's main geometric axis. A sample is said to be dichroic or to exhibit linear dichroism if it absorbs or emits light to different degrees depending on its linear polarization. In general, all materials that are at least partially oriented will exhibit linear dichroism in one or another region of the electromagnetic spectrum. The degree of

polarization is frequently represented by the optical anisotropy r_A , and is defined for optical absorption as:

$$r_A = \frac{A_p - A_s}{A_p + 2A_s} \quad (5.2)$$

where A_p and A_s are the absorptions observed parallel (p) and perpendicular (s) to the direction of uniaxial alignment, respectively. The degree of emission polarization is defined in analogy to Equation 5.2 as:

$$r_E = \frac{E_p - E_s}{E_p + 2E_s} \quad (5.3)$$

where E_p and E_s are the emission intensities observed parallel and perpendicular to the direction of uniaxial alignment, respectively. Ignoring the simplifications that have been made to arrive at Equation 5.2 and Equation 5.3 (cf. Refs. [3,33,34]), many authors employ Equation 5.2 and Equation 5.3 to extract a value for the order parameter S of the system, which is frequently used as a geometric term to describe the orientation of form-anisotropic molecules in a two-dimensional framework ($0 < S < 1$ where a value of $S = 1$ indicates perfect uniaxial orientation). An alternative representation of optical anisotropy that is used by many authors is the linear dichroic ratio or polarization ratio, DR , defined for absorption as:

$$DR_A = \frac{A_p}{A_s} \quad (5.4)$$

and for emission as:

$$DR_E = \frac{E_p}{E_s} \quad (5.5)$$

Dichroic ratios are very useful to describe the PL emission from a physiological point of view (e.g., brightness of a device as perceived by the human eye), and we have attempted to consistently employ this representation throughout this text. Most authors express DR_E as a ratio of intensities at a given wavelength, usually at a maximum of the emission spectrum, and, unless otherwise stated, we here follow this convention. However, quite frequently the emission spectra of p- and s-polarized are not identical, so that it would be more appropriate to compare the integrated emission spectra in order to allow for an apple-to-apple comparison.

The degree of CP absorption is usually expressed by the difference in absorption of left- and right-handed CP light (circular dichroism, ΔA) or by the so-called anisotropy factor g :

$$\Delta A = A_L - A_R \quad (5.6)$$

$$g = \Delta A / A \quad (5.7)$$

where A_L and A_R are absorbance for left and right CP light, respectively, and A is the normal absorbance of the material. Similarly, the degree of circularly polarized photo- and electroluminescence (CPPL and CPEL) is usually expressed by the difference in emission of left- and right-handed CP light (ΔI) or by the so-called dissymmetry factor g_{em} :

$$\Delta I = I_L - I_R \quad (5.8)$$

$$g_{\text{em}} = 2(I_{\text{L}} - I_{\text{R}})/(I_{\text{L}} + I_{\text{R}}) \quad (5.9)$$

where I_{R} and I_{L} are the right- and left-handed emission intensities, respectively. Consequently, the maximum value of g_{em} is ± 2 , corresponding to purely right- or left-handed CP light. A more detailed and comprehensive discussion elaboration of the theory behind the generation of circularly polarized luminescence (CPL) can be found in the illustrative article of Chen et al. [35] and the literature cited therein.

5.3 LINEARLY POLARIZED PHOTO- AND ELECTROLUMINESCENCE FROM UNIAXIALLY ORIENTED MOLECULES

As mentioned before, the architectural key feature for highly linearly polarized absorption, photo- and electroluminescence is a high degree of uniaxial orientation of form-anisotropic emitting molecules. Light-emitting semiconducting conjugated polymers are preferable because of their high aspect ratios and high chain rigidities. Thus, many of the examples relate to this class of materials. However, high degrees of uniaxial orientation can also be achieved in rigid-rod, low-molecular-weight molecules. Typical structural elements of rodlike, conjugated, luminescent moieties that are frequently employed for the design of low-molecular-weight, as well as polymeric light-emitting materials are shown in Figure 5.3. It should be noted that the solubility of these species is rather limited and therefore solubilizing side-chains (not shown) are usually employed. In the following sections, we have discussed different approaches to induce order and alignment of these chromophores. These approaches can be subdivided into mechanical alignment (tensile deformation, rubbing and friction deposition) and self-assembly-type techniques (orientation on orienting substrates, Langmuir–Blodgett films, liquid-crystalline materials).

5.3.1 TENSILE DEFORMATION

The tensile deformation of ductile, semicrystalline polymers has long been known as an extremely versatile method to introduce high degrees of uniaxial order in polymeric materials [36]. Orientation of the macromolecules is introduced by solid-state drawing at temperatures close to, but below the melting temperature of the polymer. While this method is not applicable to neat low-molecular-weight organic emitters, guest–host systems can easily be

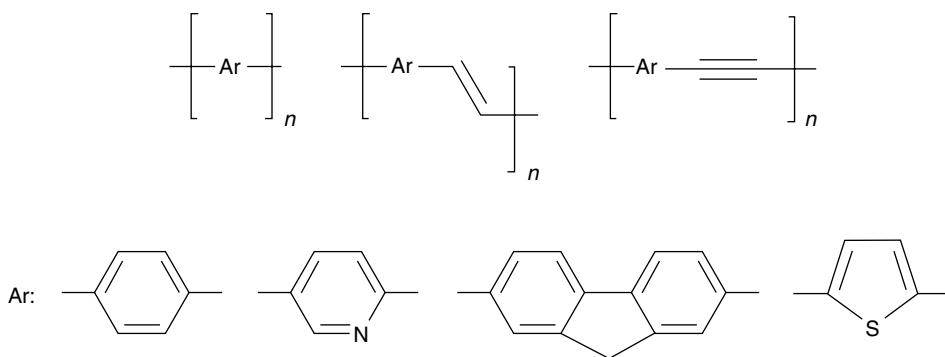


FIGURE 5.3 Typical rod-like conjugated moieties with high aspect ratios, employed in the design of orientable light-emitting chromophores.

produced, in which the form-anisotropic guest molecules adopt the orientation of the polymeric host [37]. Different possibilities exist to incorporate the guest molecules into the polymeric host; the most common procedures are (i) the production of films by casting a solution comprising both components and by evaporating the solvent; (ii) melt-mixing of the two components and subsequent melt-processing of the resulting blend into a desired shape; (iii) swelling of the polymer with a solution comprising the guest and subsequent evaporation of the solvent; and (iv) diffusion of the guest from the vapor phase into the polymer. The tensile deformation step can always be performed after the incorporation of the guest, but for techniques (iii) and (iv) that rely on diffusion it can, in principle, also be done beforehand. Uniaxially oriented guest–host systems, comprising dichroic absorbing dyes have been investigated extensively in the past by many research groups, mainly to monitor the orientation process of polymers as a result of mechanical deformation [3,33,34,38]. This concept is also the method of choice to manufacture dichroic sheet polarizers based on semicrystalline polymers and dichroic dyes [39–41]. Similarly, a number of groups have undertaken to study the properties of such uniaxially oriented polymer systems comprising PL guest molecules. Investigations have, for example, been made on films based on blends of form-anisotropic low-molecular-weight [8,9,42], oligomeric [43], as well as conjugated polymeric PL species [6,7,12,44], and different matrix polymers including polystyrene, polyethylene (PE), polyvinylchloride, polyvinylalcohol, or polycarbonate were employed. The extent of polarization, which is usually similar for absorption and emission, observed in these systems depends primarily on the geometric shape of the PL molecules and, in line with the concept of pseudoaffine deformation [45], the draw ratio λ is applied to the films during deformation. The draw ratio is defined as $\lambda = (l - l_0)/l_0$, where l_0 and l are the lengths of a sample before and after deformation, respectively; for high degrees of deformation, λ is often approximated by $\lambda = l/l_0$. Extremely high dichroic ratios of up to 70 were reported in independent studies for gel-processed blends of conjugated polymers such as poly(2-methoxy-5-(2'-ethyl-hexyloxy)-*p*-phenylene vinylene) (MEH-PPV) [44] and poly[2,5-dioctyloxy-1,4-diethynyl-phenylene-*alt*-2,5-bis(2'-ethylhexyloxy)-1,4-phenylene] (EHO-OPPE) [6,7,12] and ultrahigh molecular weight polyethylene (UHMW-PE) (cf. Figure 5.4 and Figure 5.5).

Similarly large anisotropies were later reported for highly emissive blends of alkoxy-substituted bis(phenylethynyl)benzene derivatives and polyolefins such as linear low-density polyethylene (LLDPE) and isotactic polypropylene (*i*-PP) [8,9]. The latter systems reach high levels of anisotropy at very low draw ratios, which is advantageous from a processing point of view.

The guest–host systems discussed above are extremely appealing because unparalleled degrees of optical anisotropy can readily be achieved. However, while many of the emitting materials employed in these blends have, in their neat form, been demonstrated to be useful emitters in actual LEDs [46,47], these blends could hitherto not be successfully employed in a diode configuration. One practical limitation arises from the fact that the thickness of mechanically drawn blend films is at best as low as a few micrometers, thus about one order of magnitude higher than the typical emitting layer in OLEDs [22–24]. However, the main problem is clearly related to the fact that the light-emitting molecules are embedded in an electrically insulating host polymer, which stifles the necessary charge transport through the material.

As demonstrated in the above-mentioned early work by Dyreklev et al. [21], both problems can be circumvented by stretch-orienting a film of the neat light-emitting material. This can, for example, be achieved by depositing the light-emitting polymer on top of a deformable substrate, e.g., a ductile polymer film. After alignment of this bilayer structure, the oriented light-emitting layer is separated from the substrate and applied to the LED device. Dyreklev's study made use of poly(3-(4-octylphenyl)-2,2'-bithiophene) (PTOPT, cf. Figure 5.4) as the light-emitting material, which was deposited and oriented on a ductile PE

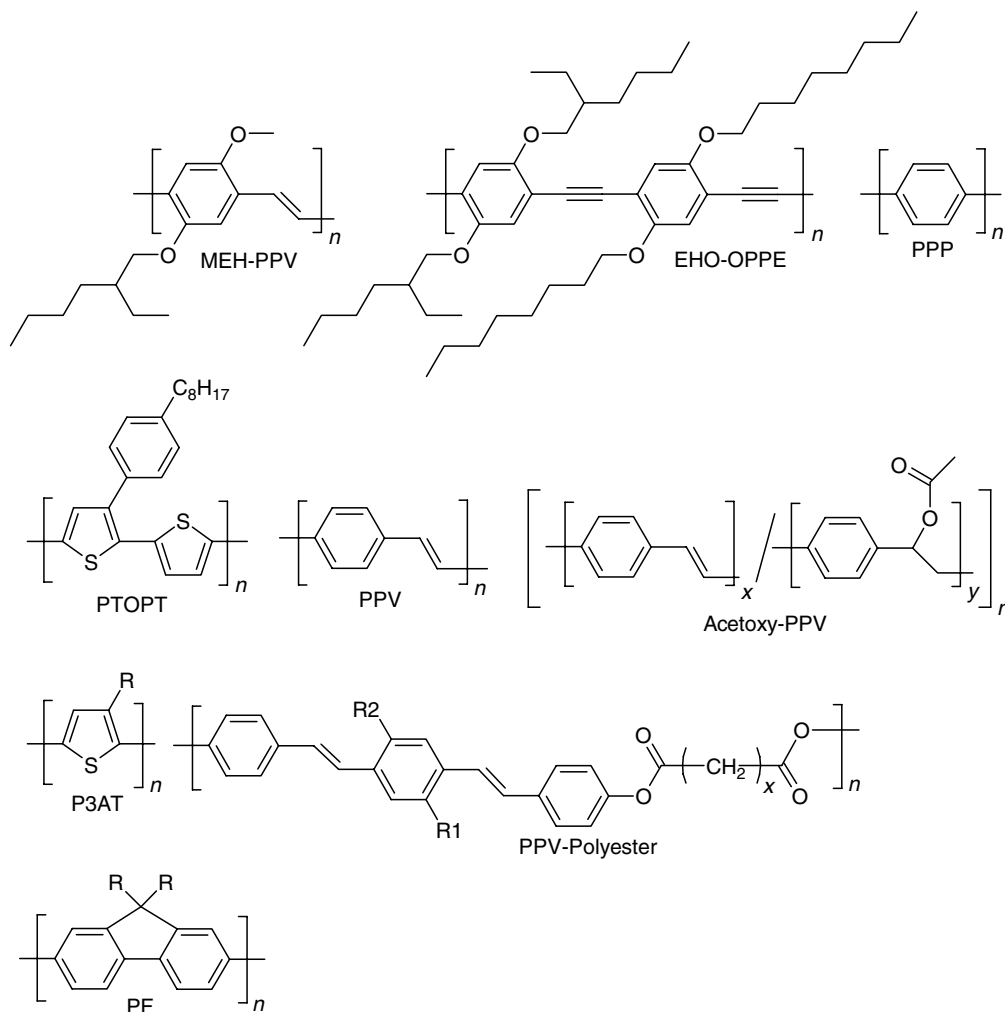


FIGURE 5.4 Chemical structures of photo- and electroluminescent polymers employed for polarized LEDs: poly(2-methoxy-5-(2'-ethyl-hexyloxy)-*p*-phenylene vinylene) (MEH-PPV); poly[2,5-dioctyloxy-1,4-diethynyl-phenylene-*alt*-2,5-bis(2'-ethylhexyloxy)-1,4-phenylene] (EHO-OPPE); poly(*p*-phenylene), PPP; poly(3-(4-octylphenyl)-2,2'-bithiophene), PTOPT; poly(*p*-phenylene vinylene), PPV; poly(3-alkylthiophene vinylene), P3AT; Acetoxy-PPV; PPV-polyester, poly(9,9-dialkyl fluorene), PF.

film. The PE–PTOPT bilayer film was stretched, apparently under ambient conditions, to a draw ratio l/l_0 of 2. The oriented PTOPT was subsequently transferred to the LED device by applying a thermal transfer process, which involved pressing the oriented PTOPT–LLDPE film at elevated temperature to an appropriate substrate, i.e., an indium tin oxide (ITO) coated glass. The latter was, however, first covered with an isotropic film of PTOPT to facilitate adequate adhesion of the oriented PTOPT layer on the substrate. A calcium electrode was vacuum-deposited on top of the PTOPT, and the resulting LED displayed an emission dichroic ratio, DR_E , of 2.4, with an onset voltage of 2 V and an external efficiency, η_{ext} , of up to 0.1%. Apart from the polarized nature of the emitted light, the device parameters were reported to be similar to nonoriented LEDs, but the DR_E achieved with this first polarized LED was rather low. The low anisotropy of the device may first of all be related to

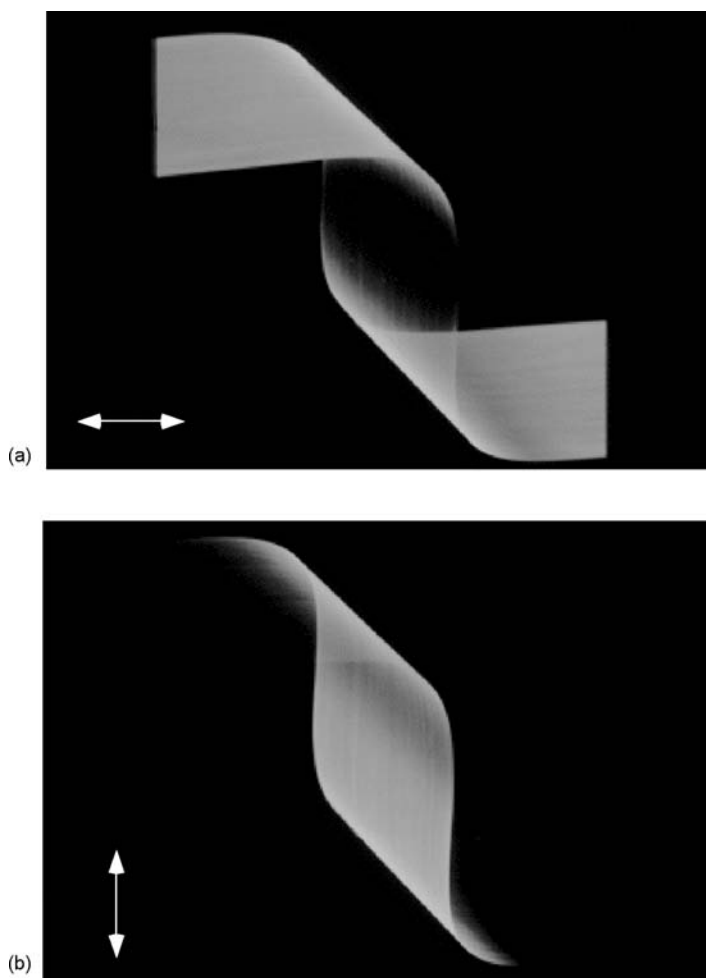


FIGURE 5.5 Polarized PL from a gel-processed, uniaxially drawn film of EHO-OPPE (cf. Figure 5.4) in UHMW-PE. Twisted tapes (drawn to a draw ratio $\lambda = 80$) are shown under excitation with UV light (365 nm) and the pictures were taken through a linear polarizer with its polarization axis oriented horizontally (a) and vertically (b). (After Weder, C., Sarwa, C., Bastiaansen, C., and Smith, P., *Adv. Mater.*, 9, 1035, 1997.)

the presence of an isotropic PTOPT adhesion layer. The latter had a similar thickness as the oriented PTOPT layer and presumably emitted unpolarized light, thereby limiting the anisotropy of the device. The low draw ratio further severely limits the attainable optical dichroism. Unfortunately, deformation to higher draw ratios led to the formation of cracks in the light-emitting materials, which of course are intolerable, as they would lead to shortening of the final device. This problem appears to be inherent for many conjugated polymers, as these materials often display poor mechanical characteristics and high thermal transition temperatures, which translate into low ductility at ambient temperature. However, plasticization of the conjugated polymer or deformation at temperatures close to its glass transition temperature (T_g) would solve this problem. Indeed, an intriguing protocol of tensile deformation of an inherently intractable conjugated polymer — poly(*p*-phenylene vinylene) (PPV, cf. Figure 5.4) — was reported by Bradley et al. [48]. One way of synthesizing PPV is via the so-called precursor route, where in a first step a nonconjugated sulfonium salt precursor polymer is synthesized.

This polyelectrolytic precursor is highly soluble and can be processed into thin films by solution casting or spin coating. The precursor polymer is subsequently converted into the conjugated PPV by thermally induced elimination of a thioalkyl hydrochloride salt. To achieve chain orientation, Bradley et al. applied a constant tensile force on a precursor PPV film during this elimination process, which allowed to deform films up to a draw ratio of 6. Lemmer et al. took this approach a step further by demonstrating that polarized LEDs can be achieved by evaporating gold electrodes onto a stretch-oriented, freestanding PPV film [49]. The resulting EL devices emitted polarized light with a DR_E of up to about 8; however, the thickness of the PPV film prevented a conventional sandwich architecture and an in-plane arrangement of two gold electrodes, which were separated by a distance of 20 μm or more, was used instead. As a result, the onset voltage of these devices was of the order of 500 V.

Thus, in summary, tensile alignment is a very efficient way of achieving high degrees of optical anisotropy. In addition, stretch alignment could be very interesting from a manufacturing standpoint as it potentially allows the use of a roll-to-roll process, where several process steps, e.g., film formation, alignment, and cathode coating could be done on the same manufacturing line. However, broad exploitation of the approach has hitherto been stifled by the difficulty to produce sufficiently thin layers of the light-emitting material, which exhibit good charge transport characteristics and can adequately be transferred into an LED device.

5.3.2 RUBBING AND FRICTION DEPOSITION

Two alternative procedures to achieve mechanically induced alignment are based on rubbing [50–54] or friction deposition of conjugated light-emitting polymers [55]. It has long been known that rigid-rod polymers can be mechanically aligned by rubbing a film of the polymer with, for example, a cotton or nylon cloth attached to a rotating drum. An important technological application of this process is in LCDs, where rubbed polyimide (PI) films are used as liquid-crystalline (LC) alignment layers [15]. Detailed optical phase retardation and infrared dichroism studies about the effect of the rubbing process on the molecular orientation have been described by van Aarle et al. [56]. The mechanism leading to the orientation of LCs on rubbing-induced alignment layers has been the subject of intensive debate for decades. The speculations ranged from rubbing-induced microgrooves or scratches on the polymer surface [57] to near-surface alignment of polymer chains upon rubbing, which then acts as an alignment layer for LC molecules [58]. Today, the latter seems to be the commonly accepted mechanism. Rubbing alignment is also possible in case of conjugated polymers [59], and in principle the approach allows to exploit the advantages of mechanical orientation in thin-film architectures suitable for LEDs. Hamaguchi and Yoshino were the first to report polarized EL based on rubbing-aligned conjugated polymer films [50]. Polarized EL was observed in LEDs comprising rubbing-aligned poly(2,5-dinonyloxy-1,4-phenylene vinylene) as the emissive layer and additional layers of PPV and oxadiazol-doped polystyrene for balanced charge injection and transport. An onset voltage of 10 V and DR_E of up to 4.0 were reported for these multilayer devices; interestingly, the authors observed different DR_E values for photo- and electroluminescence, as well as a current dependence of the DR_E in the LEDs, which suggests that unoriented molecules significantly contribute to the EL emission, particularly at low fields. Much higher degrees of optical anisotropy were subsequently described by Jandke et al. [51]. With the notions that PPV is too rigid to be effectively oriented by rubbing and that PPV precursor polymers are too soft for a rubbing process, these authors have designed and employed a synthetic compromise, featuring conjugated PPV segments and plasticizing, non-conjugated moieties (Acetoxy-PPV, Figure 5.4). Rubbed films of this copolymer display excitingly high PL dichroism, characterized by DR_E values of up to 18, corresponding to an order parameter, S , of 0.90. Polarized EL of appreciable brightness (up to 200 cd/m^2) was

demonstrated in multilayer devices that comprised ITO, an unoriented 120-nm-thick acetoxy-PPV layer, a 30-nm-thick layer of rubbed acetoxy-PPV, a 30-nm-thick poly(phenylquinoxaline) electron transport layer, and an Al top electrode. Interestingly, the EL of these devices was strongly polarized, as reflected by the DR_E of 12, despite the presence of a comparably thick layer of unoriented acetoxy-PPV. This demonstrates that charge-recombination predominantly occurred within the acetoxy-PPV. A potential drawback of the rubbing alignment approach is the mechanical scratches, which were detected by atomic force microscopy (AFM). These scratches can lead to leakage currents, which limit the functionality and lifetime of the device [51]. The devices reported by Jandke et al. suggest, however, that this problem can, at least in part, be overcome by an additional transport layer. Another limitation of rubbing or friction deposition for applications in LEDs is the relatively thin layers, in which orientation can efficiently be induced. The available data suggest that by rubbing not only the surface of the films are aligned but also the depth of the alignment layer can reach 5 to 60 nm depending on the rubbing density or rubbing pressure. This might be sufficient to efficiently align the emitting layer used in EL devices.

A related approach is the uniaxial orientation of electroluminescent polymers through friction deposition. In contrast to rubbing, where the polymer is first deposited on a substrate in isotropic fashion and is oriented in a second (the rubbing) step, friction deposition is a one-step procedure in which the solid polymer, for example in the shape of a block or cylinder, is dragged at elevated temperatures and with a certain pressure over a smooth, rigid (optionally heated) substrate such as glass or metal [60]. This process can result in the deposition of a thin layer of the polymer on the substrate, in which the individual molecules are uniaxially aligned along the drawing direction. With this method, Tanigaki et al. prepared oriented films of PPP (Figure 5.4), which displayed good optical anisotropy in absorption but suffered from discontinuities [55]. In a recent paper, Nagamatsu et al. described similar attempts to apply this technique to poly(3-alkylthiophene)s (P3AT, Figure 5.4) [61]. UV-vis and x-ray diffraction data demonstrated that the polythiophene backbones were indeed uniaxially aligned along the friction-drawing direction. The authors report DR_A between 10 and 100, but it is somewhat unclear whether these values are inflated by the fact that the absorption peaks of the two polarization components display maxima at quite different wavelengths [61]. Although this method may lead to very high degrees of optical anisotropy, discontinuities and mechanical defects may represent a major obstacle for the exploitation of this framework in connection with LEDs.

5.3.3 ORIENTATION OF NONLIQUID-CRYSTALLINE MATERIALS ON ORIENTING SUBSTRATES

Polarized PL can also be observed from low-molecular-weight or polymeric PL materials that are epitaxially grown on orienting substrates, such as friction-deposited poly(tetrafluoroethylene) [54,60], rubbed PI [62], or photoaligned orientation layers [63]. Epitaxial processes have also been used by a number of groups for the preparation of polarized LEDs [64,65]. It should be noted, however, that most conventional orientation layers (*vide supra*) are based on materials that are electrical insulators [66]. This represents a problem for their use as an orientation layer in LEDs, as the injection of charges (usually holes) has to also occur through this layer. Approaches to solve this problem include the incorporation of a hole-transporting (HT) compound into the polymer used for the alignment layer (usually by blending, *vide infra*) or the fabrication of alignment layers from inherently (semi)conducting polymers. For example, Era et al. demonstrated polarized EL by epitaxial vapor deposition of *p*-sexiphenyl (PPP, $n = 6$, cf. Figure 5.4) on a rubbed orientation layer of the same material [62]. The dichroic ratio reported for LEDs produced using this architecture (with ITO and Mg:Ag

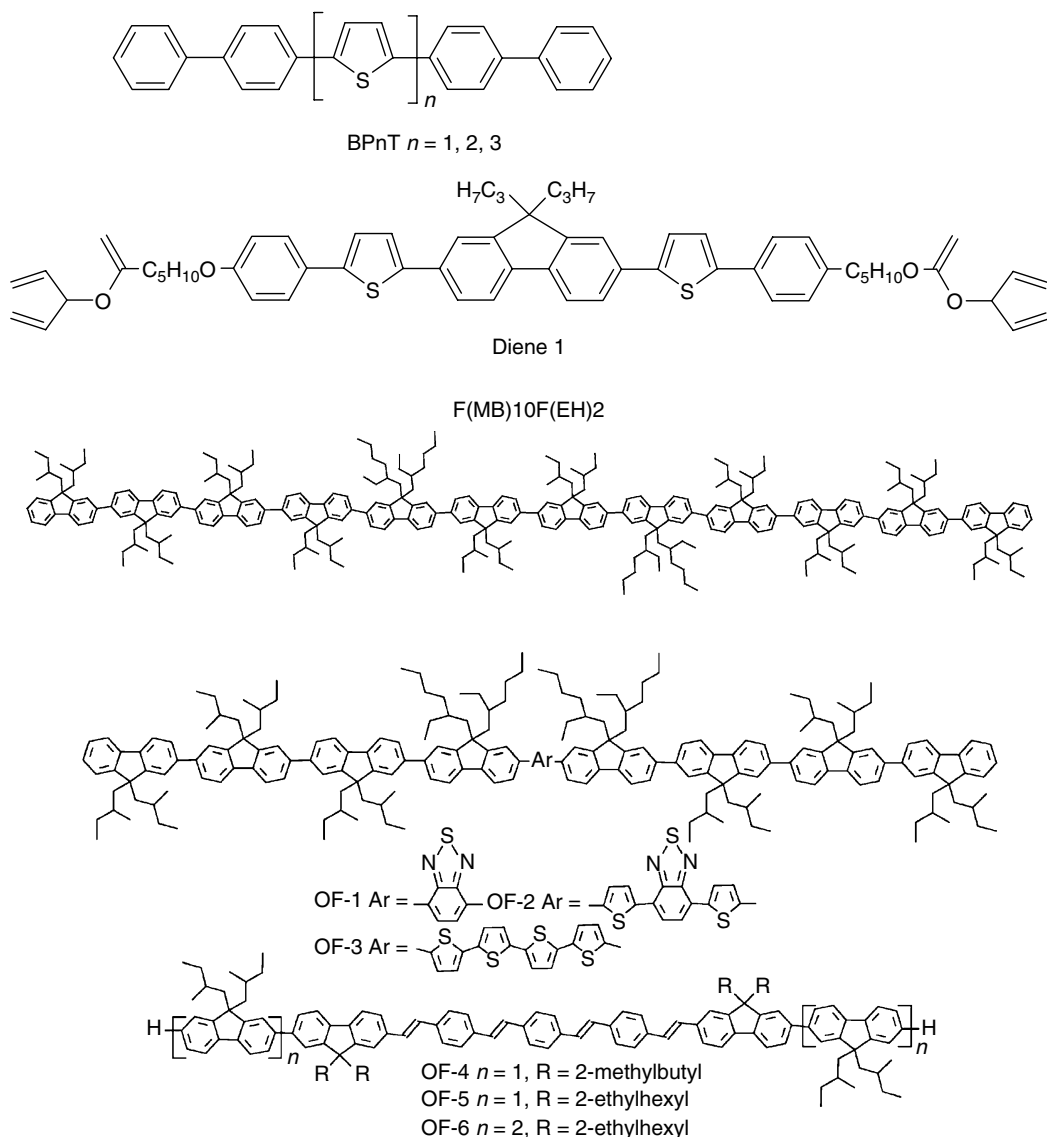


FIGURE 5.6 Chemical structures of low-molecular and oligomeric photo- and electroluminescent materials suitable for polarized LEDs: BPnT, Diene 1, F(MB)10F(EH)2, OF-1, OF-2, OF-3, OF-4, OF-5, OF-6. (From Culligan, S.W., Geng, Y., Chen, S.H., Klubek, K., Vaeth, K.M., Tang, C.W., *Adv. Mater.*, 15, 1176, 2003; Geng, Y., Chen, A.C.A., Ou, J.J., Chen, S.H., Klubek, K., Vaeth, K.M., Tang, C.W., *Chem Mater.*, 15, 4352, 2003. With permission.)

electrodes and an additional oxadiazol derivative-based electron transport layer) was around 5, and the external device efficiency was estimated to be 0.14%. Highly polarized emission from oligo(biphenylthiophenes) (BPnT, Figure 5.6) that were vapor-deposited and epitaxially grown on an orientation layer was reported by Yoshida et al. [67]. Building on earlier studies [68] and to solve the problem that traditional orientation layers are nonconducting, the authors made use of a uniaxially aligned semiconducting alignment layer based on rubbed PPP (Figure 5.4). Very high polarization ratios were observed for PL emission ($DR_E = 93.5$) but it is unclear why the absorption dichroism was substantially lower ($DR_E = 14.7$).

5.3.4 LANGMUIR–BLODGETT TECHNIQUE

The formation of monomolecular layers at the air–water interface and their deposition onto solid substrates as ordered thin organic films was achieved as far as the early 1930s [69] when GE Research Laboratories' Katharine Blodgett and Irving Langmuir discovered a general method that allows the deposition of successive monomolecular layers of amphiphilic molecules on a variety of substrates. Since these initial studies, the method, now known as Langmuir–Blodgett (LB) technique, has become the most versatile tool for the production of ultrathin films with controllable thickness, molecular ordering, and few defects [70]. More recently, deposition by the LB technique has been demonstrated to yield layers or films that exhibit anisotropic optical properties [71–73].

The fundamentals of the main-chain orientation behavior of so-called hairy-rod type polymers — macromolecules with rigid backbone and very often flexible side-chains — obtained by the LB technique have been described by Wegner et al. [74]. Using the LB technique a number of side-chain-substituted, rigid-rod-conjugated polymers, including PT [72], PPP [71], PPV [75–77], and poly(*p*-phenylene ethynylene) (PPE) [78] derivatives, were processed into multilayer thin films, in which the conjugated chain molecules were predominantly oriented with their backbones parallel to the dipping direction. In an effort to have chemically and thermally more robust devices these LB-induced long-range orders were stabilized by cross-linking the material in a photochemical reaction [79]. Carefully deposited LB multilayers display anisotropic properties and can be used as emissive layers for LEDs that emit polarized light. However, the degree of optical anisotropy is usually very modest, with DR_E usually between 2 and 5.

5.3.5 ORIENTATION OF LIQUID-CRYSTALLINE LIGHT-EMITTING MATERIALS

So far the most important and the most successful approach for linearly polarized EL is probably the exploitation of the orientational long-range order of LC materials. Low-molecular-weight molecules, oligomers, and polymeric materials can exhibit intrinsic liquid crystallinity, and the organization of light-emitting LC molecules, typically on orienting substrates such as rubbed PI films, are an attractive way to generate polarized emission of light. Excellent review articles on this subject have appeared in the recent past [26–28]. Early LC systems investigated for polarized light-emission include low-molecular-weight [80] oligomeric [81] and polymeric PL liquid crystals, vitrified LCs [82], cross-linked LC materials [83], and guest–host systems [84]. The latter are known since the late 1960s and typically consist of an LC (very often nematic) host matrix into which high-aspect-ratio dye molecules are incorporated. Neat low-molecular-weight liquid crystals used for polarized emission of light encompass a variety of molecules including benzothiazoles [85] and oxadiazoles [86]. The use of emissive layers that remain liquid crystalline after processing is, however, problematic because liquid flow and intermixing of layers limit the long-term device stability in an LED. Quenching the LC into an ordered glass or fixation of the ordered state through chemical reaction are possibilities that solve this problem. Anisotropic networks formed by the photopolymerization of LC dienes that combine fluorene, thiophene, and phenylene segments (e.g., Diene 1, Figure 5.6) were, for example, investigated by O'Neill and Kelly and others [87]. These materials were typically aligned in the nematic LC phase and quenched into a glassy state before cross-linking into a polymer network by exposure to UV light. Alignment was achieved on a photoalignment layer based on a polymeric coumarin derivative, which had been doped with a rather high fraction (30%) of a hole-conducting triphenylene derivative [87]. This elegant approach combines two intriguing concepts. First of all, it adopts the contact-free photoalignment scheme — a protocol originally developed for LCDs [63b], in

which illumination with polarized light generates surface anisotropy in a photoreactive alignment layer — to OLEDs. Secondly, the problem of limited charge transport through the orientation layer was, at least in part, solved by incorporation of a hole conductor, causing the latter to display almost adequate charge-transport characteristics. LEDs based on this system and ITO and Al electrodes displayed a DR_E of 10 and a maximum brightness of 60 cd/m^2 at a driving voltage of 11 V. Higher brightness was observed when the doping level of the hole conductor in the orientation layer was increased, but with a reduction in DR_E . Conversely a polarized LED with a DR_E of 11 was produced from a 20% doped device, but in this case the brightness was reduced. While these data suggest that there is some room for improvement of the orientation layer, the dichroic ratios achieved in this work appear to be maximized, and limited by the order parameter, S , which can be achieved with low-molecular-weight liquid crystals.

Aspect ratios in and achievable order parameters are usually higher in LC polymers, particularly in hairy-rod conjugated polymers, derivatized with solubilizing side-chains [88]. These materials are further advantageous because they display usually relatively high nematic to glass transition temperatures and good film-forming properties. Thus, most LC polymers employed for polarized LEDs are representatives of this class of materials (*vide infra*). However, a number of other LC polymer architectures has also been investigated [88], including polymers with LC side-chains and semiflexible or segmented chains in which flexible spacer units are incorporated between nematic or discotic mesogenic moieties (cf. Figure 5.7).

Wendorff and Greiner and others were the first to report polarized EL created with LC polymers [89–92]. The LC polymers employed in their initial studies were PPV derivatives that were segmented with flexible alkyl spacers (PPV-Polyester, Figure 5.4). LEDs comprising these polymers on rubbed PI displayed emission dichroic ratios of up to about 7. However, the macroscopic order parameter was found to strongly depend on the processing parameters. The key step for a high degree of orientation is an annealing process, in which the polymer (originally deposited in essentially isotropic fashion by spin coating onto the alignment layer) is brought into a thermotropic nematic state for an extended period of time. Under these conditions the material slowly adopts the orientation of the alignment layer, and the orientation can be maintained by finally quenching the polymer to temperatures below the T_g . The need for high-temperature annealing, related to the comparably high viscosity of the system, represents a main disadvantage of this general approach (*vide infra*). Another disadvantage of the segmented polymers used in these initial studies are the possible limitations in charge transport caused by the flexible segments, which are not conjugated and interrupt the charge transport along the polymer chain. This problem is, of course, readily solved by employing fully conjugated, preferably thermotropic LC polymers, such as side-chain-substituted PPPs [93], PPVs [94], PPEs [95], and poly(9,9-dialkyl fluorene) (PF) [96]. Grell et al. have conducted an extensive study of PFs including poly(9,9-dioctyl fluorene) and poly(9,9-di(2-ethylhexyl) fluorene) (PF, $R = n$ -octyl, 2-ethylhexyl, Figure 5.4) [97]. The former polymer forms a nematic LC phase when heated to about 170°C . By using a PI alignment layer and employing an annealing or a quenching scheme, the LC polyfluorenes could be processed into stable, oriented emitting layers, which displayed a DR_E of 6.5. Polarized EL of copolyfluorenes with benzodithiazole ($DR_E \sim 5$) and dithiophenes ($DR_E \sim 5$) was also reported, but the devices could not quite reach the dichroic ratios of ethylhexyl-substituted polyfluorenes [98]. Poly(9,9-di(2-ethylhexyl) fluorene) displayed LC behavior with a higher degree of molecular order than poly(9,9-dioctyl fluorene), presumably due to its lower effective diameter, which is concomitant with a higher aspect ratio. Poly(9,9-dioctyl fluorene) was shown to orient well ($DR_E = 15$) on a rubbed film of PI doped with a starburst-amine hole conductor [99]. This orientation layer exhibits HT properties that are comparable to those of films of the neat hole

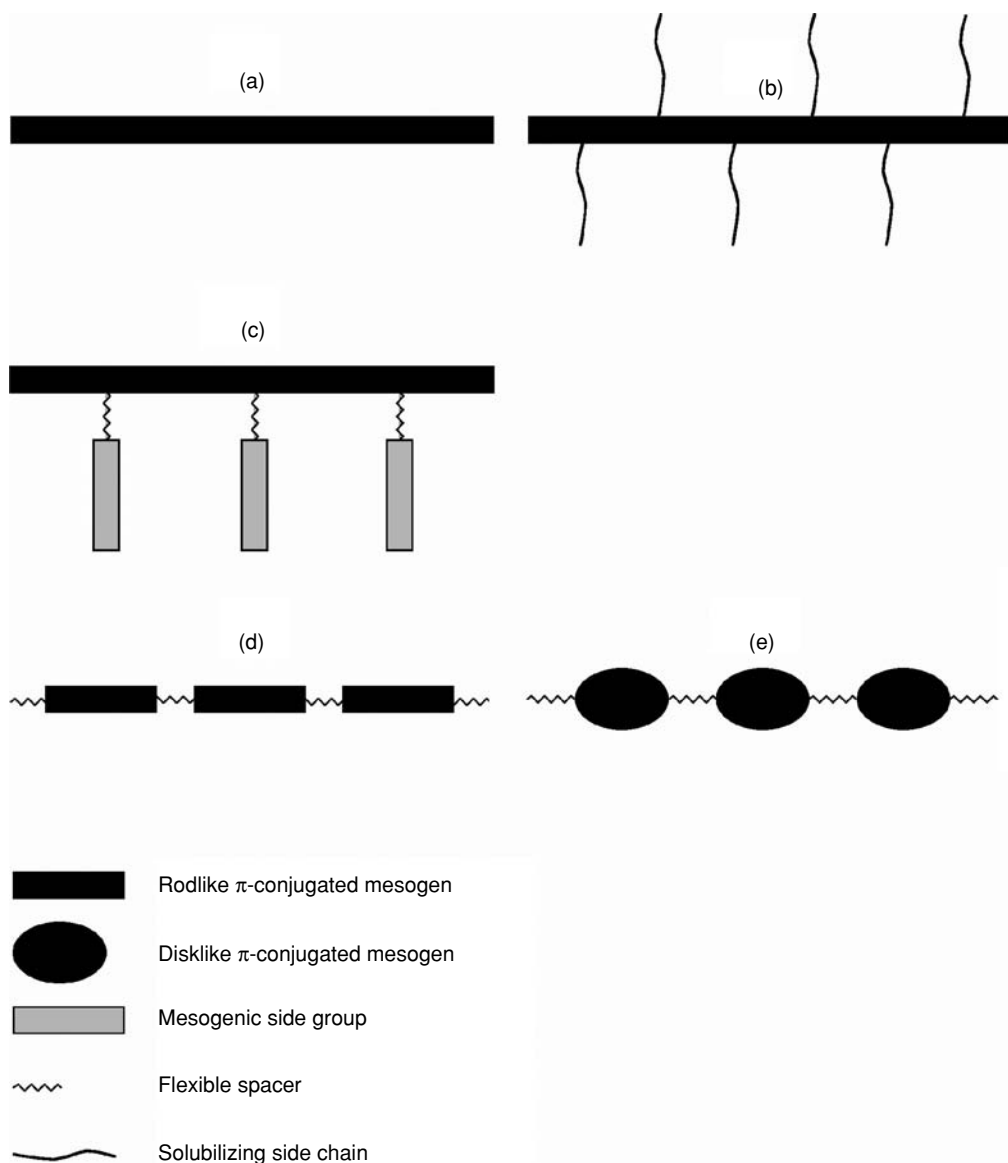


FIGURE 5.7 Schematic Representation of typical, (partially) electroluminescent LC polymer architectures. (a) Rodlike structure. (b) Hairy-rod structure. (c) Combined main-chain-side-chain system. (d) Semiflexible segmented structure. (e) Semiflexible segmented structure with disklike mesogen. (After Weder, C. and Smith, P., Main-chain liquid-crystalline polymers for optical and electronic devices, in *Encyclopedia of Materials: Science and Technology*, Buschow, K.H., Cahn, R.W., Flemings, M.C., Ilchner, B., Kramer, E.J., and Mahajan, S., Eds., Elsevier Science, New York, 2001.)

conductors, and as a result, EL devices which combine good polarization ($DR_E = 15$) with appreciable brightness (45 cd/m^2) could be realized [99]. Device optimization of the ethylhexyl polyfluorene system increased the polarization ratio in blue emission to $DR_E = 21$ and the brightness to 100 cd/m^2 [100,101], and in devices based on poly(9,9-di(2-ethylhexyl) fluorene) end capped with bis(4-methylphenyl)phenylamine, DR_E s of up to 26 could be achieved [102].

Unfortunately, most of the above-referred studies limit the characterization of LEDs to dichroic ratio, emission maximum, and sometimes brightness, but no device efficiencies are quoted. Expanding on earlier work by Grell et al. [97], Whitehead et al. revisited LEDs based on poly(9,9-dioctyl fluorene) [103]. Following work by Jandke et al. [51] and using a rubbed PPV film as the alignment layer, the dichroic ratio of LEDs comprising this polymer could be improved up to a DR_E of 25 (Figure 5.8). This value is based on a comparison of peak maxima; the dichroism was slightly lower ($DR_E=19$) when the integrals of the p- and s-polarized spectra were compared. The devices reached a brightness of up to 327 cd/m^2 with an efficiency of 0.12 cd/A .

Even higher efficiencies were reported by Miteva et al. who, building on earlier work [102], employed a PF that was end capped with hole-trapping moieties [104]. In contrast to their earlier studies, the number-average molecular weight, M_n , of the polymer was reduced to 12,000 and optimized multilayer LEDs were based on a thin layer of a hole conductor, a PI alignment layer comprising 10% of the hole conductor, the oriented PF, and a Ca/Al top electrode. The integrated DR_E of their best devices was 21, with a brightness of 200 cd/m^2 (at 19 V) and a luminance efficiency of 0.25 cd/A . The brightness could be further increased to 800 cd/m^2 (at 19 V) by increasing the concentration of the hole conductor in the PI orientation layer to 20%, but at the same time the DR_E was reduced to 15. An exciting further development is the use of these materials in devices that rely on noncontact alignment of a fluorescent LC polymer by a photoinduced alignment of polyfluorenes on photoaddressable alignment layers. Sainova et al. demonstrated that DR s of 10–14 at a luminance of 200 cd/m^2 and an efficiency of 0.3 cd/A can be achieved if polyfluorenes are deposited on a photoaddressable polymer (PAP), based on a hydroxyethyl methyl methacrylate (HEMA) backbone that was substituted with an azobenzene chromophore and comprising various amounts of a hole-conducting amine [105]. In a subsequent paper, it was shown that the device performance can be improved by decreasing the thickness of the alignment layer and devices with an external

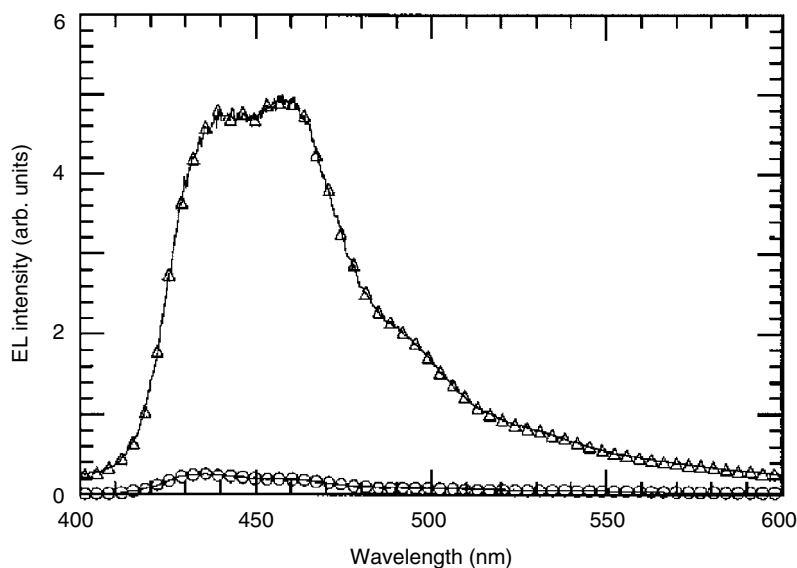


FIGURE 5.8 Electroluminescence from an LED based on ITO-rubbed PPV-aligned poly(9,9-dioctyl fluorene)/Ca recorded through a polarizer oriented parallel (triangles) and perpendicular (circles) to the orientation direction. (From Whitehead, K.S., Grell, M., Bradley, D.D.C., Jandke, M., and Strohriegel, P., *Appl. Phys. Lett.*, 76, 2946, 2000. With permission.)

efficiency of 0.66 cd/A with a DR_E of about 10 were reported [106]. Of course, one advantage of PAPs is that they allow the formation of patterned or pixilated structures with very high resolution that are able to emit polarized light (Figure 5.9).

Most of the LC polymer systems discussed so far contain the LC moiety incorporated in the polymer main chain. One of the few examples of polarized emission of light using a side-chain LC system was reported by Chang et al. [107]. A polyacrylate was used as the polymer backbone. The nematic LC side-chains consisted of ethyl- and propyl-substituted bis-tolan units. When deposited on a rubbed PEDOT film, polarized EL dichroic ratios were reported to be around 6.

Monodisperse LC oligomers represent an interesting compromise between low-molecular-weight and polymeric LCs, as they seem to combine high aspect ratio, which may translate into high dichroic ratios, with a comparably low viscosity, which allows for rapid orientation. Moreover, the well-defined molecular architecture may allow for efficient purification, which is important for the electronic devices at hand. A systematic structure–property study of monodisperse oligomeric fluorenes with varying lengths and different pendant side-chains has been presented by Geng et al. [108]. The T_g and LC behavior were found to be strongly

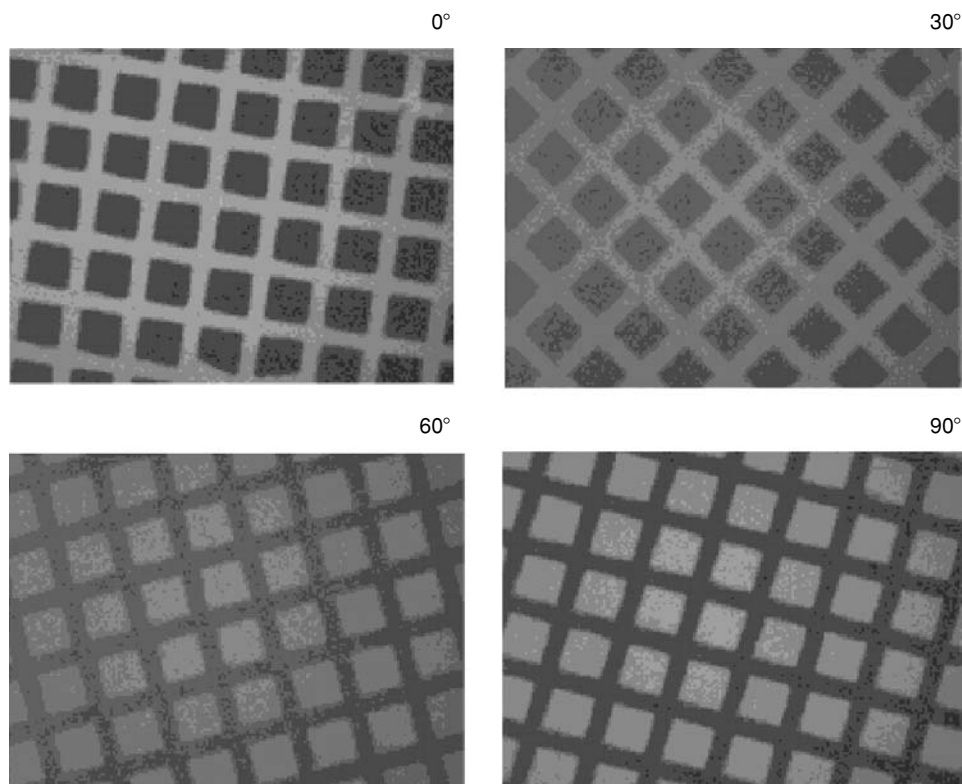


FIGURE 5.9 Polarized fluorescence microscopy images of the fluorescence patterns of a poly(fluorene) deposited on a photoaddressable polymer (PAP) alignment layer. The patterns were obtained by selective alignment of the PAP, followed by deposition of the light-emitting polymer on top of the PAP layer, and annealing of the multilayer structure. On each picture, the rotation angle of the sample is noted, where 0 means that the analyzer of the polarization microscope is parallel to the molecular orientation after the first photoalignment step. (From Sainova, D., Zen, A., Nothofer, H.G., Asawa-pirom, U., Scherf, U., Hagen, R., Bieringer, T., Kostromine, S., and Neher, D., *Adv. Funct. Mater.*, 12, 49, 2002. With permission.)

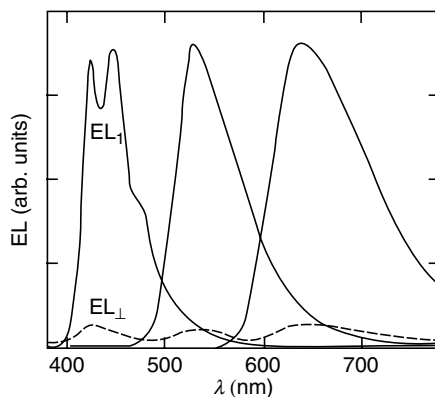


FIGURE 5.10 Polarized EL spectra of LEDs based on a rubbed PEDOT–PSS conductive orientation layer, an oligo(9,9-dialkyl fluorene) emissive layer, a 1,3,5-tri(phenyl-2-benzimidazolyl)benzene electron transport or hole blocking layer, a lithium fluoride electron injection layer, and a Mg/Ag cathode layer. The oligomers used as emitters were F(MB)10F(EH)2 (blue emission), OF-1 (green emission), and OF-2 (red emission), and the spectra recorded through a polarizer oriented parallel (solid lines) and perpendicular (dashed lines) to the orientation direction. (From Geng, Y., Chen, A.C.A., Ou, J.J., Chen, S.H., Klubek, K., Vaeth, K.M., and Tang, C.W., *Chem. Mater.*, 15, 4352, 2003. With permission.)

dependent on the structure of these oligofluorenes. Co-oligomeric fluorenes with different branched side-chains were shown to exhibit superior stable glassy nematic films when compared to homo-oligomeric or unbranched fluorenes (Figure 5.6, F(MB)10F(EH)2) [109]. Color control was achieved by introducing a variety of band gap reducing aromatic groups at the center of these molecules (Figure 5.6, OF-1, OF-2, OF-3) [110]. LEDs were based on a rubbed PEDOT–PSS conductive orientation layer, an oligo(9,9-dialkyl fluorene) emissive layer, a 1,3,5-tri(phenyl-2-benzimidazolyl)benzene electron transport or hole blocking layer, a lithium fluoride electron injection layer, and a Mg/Ag cathode layer. The devices exhibit combinations of characteristics that may represent the best overall performances of polarized LEDs reported to date. With F(MB)10F(EH)2 as an emitter (cf. Figure 5.6) the emission is deep blue and is characterized by an integrated DR_E of 25, a luminance yield of up to 1.10 cd/A, and a brightness of up to 900 cd/m² [109]. With OF-1 and OF-2, green and red emissions are achieved and the devices display an integrated DR_E of 16 and 14, a luminance yield of up to 5.9 and 0.51 cd/A, and a brightness of up to 1180 and 100 cd/m², respectively (Figure 5.10) [110].

5.3.6 OVERVIEW OF LEDs EMITTING LINEARLY POLARIZED LIGHT

The key data of the various example devices emitting linearly polarized light discussed in this chapter are compiled in Table 5.1. It can be seen that significant progress has been made over the last few years, as far as the combination of high DR_E , high luminance, and high quantum yield are concerned. Indeed, devices have become available that cover the entire visible spectral range and combine reasonable luminance and quantum efficiencies. The values of DR_E are also substantial, although for many applications a cleanup polarizer will have to be employed.

5.4 CIRCULARLY POLARIZED LUMINESCENCE

Polarized luminescence has attracted widespread attention due to potential applications in optical information displays, processing, and storage. The state of the art of materials and

TABLE 5.1
Performance of Polarized LEDs Produced by Different Alignment Techniques and with Different EL Materials

Alignment Technique	Device Structure ^a	DR_E^b	Luminance ^c (cd/m ²)	η_{ext}^d (cd/A)	λ_{max} (nm) color	Ref.
Conjugated polymer stretched on ductile substrate	ITO/isotropic PTOPT/stretched PTOPT/Ca/Al	2.4	n.a.	0.1	630, 680	21
Conjugated polymer stretched as precursor	Stretched PPV/gold-gold; in-plane electrode arrangement	8	n.a.	n.a.	n.a.	48
Rubbing of plasticized conjugated copolymer	ITO/isotropic Acetox-PPV/rubbed Acetox-PPV/ET/Al	12	200 (max)	n.a.	511 green-yellow	51
Epitaxial growth of oligomer on rubbed oligomer alignment layer	ITO/rubbed sexiphenyl/vacuum-deposited sexiphenyl/ET/Mg:Ag	5	n.a.	(0.14%)	~430	62
LB-deposition of conjugated polymer	ITO/Cr/Au/dialkoxo-PPP/Al	3–4	n.a.	(0.05%)	536/524	71
Cross-linked LC on noncontact alignment layer	ITO/photoalignment layer:HT/cross-linked LC/Al	10	60 (11 V)	n.a.	~500, 530	87
LC polyfluorene on rubbed PPV	ITO/rubbed PPV/LC	25/19 (I)	200 327 (max)	0.12	433, 458 blue	103
LC polyfluorene on rubbed PI:HT	poly(9,9-dioctyl fluorene)/Ca ITO/HT/rubbed PI:HT/LC	21 (I)	200 (19 V)	0.25	425, 450, 475 blue	104
LC polyfluorene on photoalignment layer	poly(9,9-dioctyl fluorene)/Ca/Al ITO/PEDOT/PAP:HT/LC	15 (I) 14	800 (19 V) 200	n.a. 0.3	~425, ~450, ~475	105
LC oligofluorene on rubbed PEDOT:HT	poly(9,9-dioctyl fluorene)/Ca/Al ITO/PEDOT:HT/F(MB)10F(EH)2/ET/LiF/Mg:Ag	27–32/25 (I)	214 (6.2 V) ~1000 (max)	1.10	424, 448 blue	109
LC oligofluorene on rubbed PEDOT:HT	ITO/PEDOT:HT/OF-1/ET/LiF/Mg:Ag	18/16 (I)	1180 (7.9 V) ~6000 (max)	5.91	533 green	110
LC oligofluorene on rubbed PEDOT:HT	ITO/PEDOT:HT/OF-2/ET/LiF/Mg:Ag	14/14 (I)	101 (7.5 V)	0.51	643 red	110

^aITO, indium tin oxide, HT, hole-transporting agent, ET, electron-transporting agent. For chemical structures see Figure 5.4 and Figure 5.6.
^bBased on ratio of peak maxima unless an (I) indicates that integrated spectra were compared.
^cAt voltage indicated. Values refer to driving conditions under which DR_E and η_{ext} were measured except where (max) indicates maximum luminance reported.
^dExternal device efficiency in cd/A, except where (%) indicates that the efficiency was expressed by the fraction of photons extracted per charge injected.

devices that rely on uniaxially oriented emitting species and generate linearly polarised light is, as discussed in the previous sections, quite advanced, and technological exploitation may be seen in the near future. On the other hand, CP emission of light is more challenging to generate and comparably little research efforts have been devoted to this subject to date. CPL is typically achieved with helically arranged luminophores [4,111]. This helical arrangement of the chromophores is very difficult to influence or promote by an external force field and, consequently, has to be achieved by self-assembly or self-orientation of the optically active materials. The technological challenges and the limited number of technologically relevant applications where CP light might be of benefit are probably the main reasons why there has not been as much progress as in the case of linearly polarized light. CP light has been proposed to be of potential interest in several areas. One important potential use are back-lights for LCDs, as CP light can be converted very efficiently into linearly polarized light by means of a quarter-wave ($\lambda/4$) plate [112,113]. Another example is the use of CP-emitting layers in LEDs. Together with a linear polarizer, the reflection of ambient light at the back metal contact can be efficiently suppressed and the contrast of the device is significantly enhanced [113]. Other applications include optical data storage and photochemical switches [114–117], stereoscopic displays [118], and color image projection systems [119]. As mentioned heretofore, two fundamentally different concepts are employed to design materials that display CPL, namely the incorporation of nonchiral dyes into a chiral matrix and the use of conjugated polymers with chiral side-chains. Examples of both platforms are discussed in the following subsections.

5.4.1 CIRCULARLY POLARIZED LUMINESCENCE FROM ACHIRAL DYES DOPED IN CHIRAL MATRICES

In particular most of the early studies on CPL were based on the incorporation of a luminescent achiral chromophore in a chiral nematic or cholesteric liquid crystal. Chiral nematic liquid crystals (CNLC) are intrinsically birefringent and exhibit a helical supramolecular architecture, which is characterized by the pitch length p (Figure 5.11).

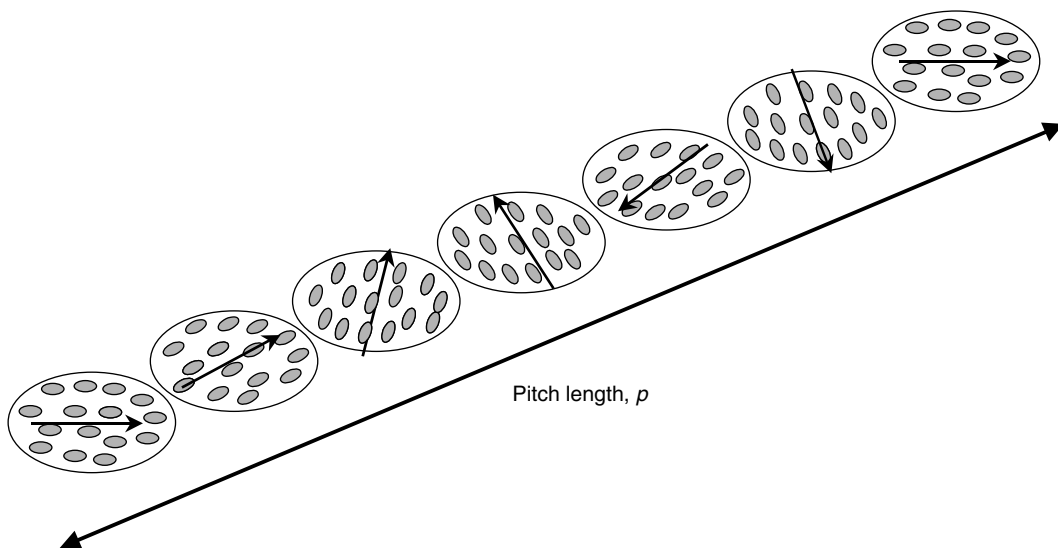


FIGURE 5.11 Supramolecular, helical architecture and definition of pitch length p of chiral nematic liquid crystals.

Films of pure CNLCs have a unique transmission behavior as CP light with the same sense of circular polarization as the CNLC is filtered out by reflection, while CP light of the opposite handedness as the CNLC film is transmitted. This selective optical transmission characteristic is referred to as a one-dimensional photonic stop-band or a selective reflection band. The stop-band is centered at a certain wavelength λ_c , which is dependent on the pitch length p and the average refractive index \bar{n} of the CNLC:

$$\lambda_c = \bar{n} \cdot p \quad (5.10)$$

The doping of CNLCs with dyes that emit light with a maximum wavelength λ_E has been of interest for many years, mainly triggered by applications in lasers [120] or twisted nematic LCDs [28]. In recent years several studies [5,10,121] of these systems have shown the importance of the choice of the pitch length p versus λ_E . Commonly, researchers distinguish three different regimes, the Mauguin regime ($\lambda_E \ll \bar{n} \cdot p$), the resonance regime ($\lambda_E \sim \bar{n} \cdot p$), and the regime where $\lambda_E \gg \bar{n} \cdot p$. One of the critical findings for the generation of pure and efficient CP light with CNLC and dye systems is that an overlap of the emission band of the dye (λ_E) and the stop-band of the CNLC should be avoided [10,121], because a sharp reversal of the handedness of the circular polarization occurs at the edges of the photonic stop-band. This leads to a reduction of the overall CP efficiency. This problem can, for example, be overcome by choosing organolanthanide dyes with narrow emission bandwidths that fall perfectly within the photonic stop-band [10]. Modulation of the degree of circular polarization by UV irradiation has been shown by Wendorff et al. using cholesteric mixtures with photochemically controllable, CP fluorescence [117]. The pitch of the helix could be modified upon irradiation of UV light that caused an *E*–*Z* photoisomerization of a chiral photochromic dopant. Because of the relative stability of the images created by this technique, these novel photopatternable materials could open up new platforms in advanced data storage systems.

In summary, one can say that LC and dye systems can give very pure CP light with dissymmetry factors of up to 1.8, but this excellent performance is limited to very narrow bandwidths and films of a minimum thickness of 15 to 35 μm [5]. A more important drawback, as far as LEDs are concerned, is the fact that most CNLC and dye systems display electrical insulating behavior. Conjugated polymers on the other hand have the potential to combine adequate charge transport characteristics and suitable optical properties. The combination of an LC and a conjugated polymer has been reported by Katsis et al. [122]. A chiral nematic PPP was reported to display a dissymmetry factor of -1.3 within the spectral region and between 0.3 and 0.9 outside the selective reflection band. It should also be noted here that the film thickness (2 μm) of the chiral nematic PPP-film was much thinner than the films of the glass-forming liquid crystals in previous work (35 μm) [5] of the same group. Although the required film thickness is still about one order of magnitude higher than typically employed in LEDs, this promising result suggests that further work with conjugated polymers may be valuable.

5.4.2 CIRCULARLY POLARIZED LUMINESCENCE FROM CONJUGATED POLYMERS

Another approach to CPL is the synthesis of conjugated polymers with intrinsic chiro-optical properties. A variety of polymers with CPPL have been synthesized so far. Most of them are based upon well-known conjugated polymers such as poly(thiophene)s [4,111], poly(phenylene vinylene)s [123], poly(thienylene vinylene)s [124], ladder polymers [125], PPPs [126], poly(phenylene ethynylene)s, [127] and poly(fluorenes) [128]. All of them have been modified with chiral side-chains, which induce the chiro-optical properties.

The highest dissymmetry factor (g_{em}) obtained to date by means of an optically active polymeric emission layer is as high as 0.38 [127]. In this case the emissive layer was a poly(phenylene ethynylene) derivatized with chiral dimethyloctyl (DMO) side-chains. Interestingly, the polymer with the highest g -value was not the homopolymer in which all of the repeat units were derivatized with chiral side-chains, but a copolymer comprising 50% DMO and 50% racemic 2-ethylhexyl side-chains. Although the high dissymmetry factors have not been fully explained, the authors assume that they originate from strand formation during annealing. In other words, the authors believe that the large anisotropy factors are probably caused by helical supramolecular assembly of the PPE chains rather than intramolecular interactions.

Somewhat different conclusions regarding the origin of the chiro-optical properties were drawn by Oda et al. This group also reported a rather high dissymmetry factor (0.28) for LEDs based on a chiral conjugated polymer. The respective emissive layer consisted of a polyfluorene substituted with chiral (*R*)-2-ethylhexyl side-chains [128,129]. The values for CPPL (0.28) and CPEL (0.25) were considerably higher than the value reported for the first CP light-emitting device (CPEL = -0.0013) [123], which was based on a chirally substituted PPV derivative. An interesting aspect of this work is the observation that the further away is the chiral center from the backbone the weaker is the chiro-optical response. This suggested that intrachain effects are more likely to be responsible for chiro-optical properties rather than interchain exciton couplings [129]. Another finding is the detection of an odd–even effect regarding the sign of the anisotropy factor g and the number of carbon atoms along the alkyl side-chain between the backbone and the chiral center.

Not many publications about chiral conjugated polymers investigate the detailed origin of the chiro-optical properties. The induction of the overall helical architecture by the chiral side-chains can be accomplished in different ways. The detailed helical organization has been investigated in the case of polythiophenes by Langeveld-Voss et al. [111]. It is concluded in this work that the chiro-optical properties stem from “a helical packing of predominantly planar chains” (Figure 5.12c).

Very recently, an exciting approach to control the chiral ordering in optically active polythiophenes by a doping process has been reported [130]. It was found that the addition of $\text{Fe}(\text{ClO}_4)_3$, NaSO_3CF_3 , or AgSO_3CF_3 to chiral polythiophenes had a dramatic effect on the chiral arrangement of the polymer chains. No detailed description of the nature of the helical

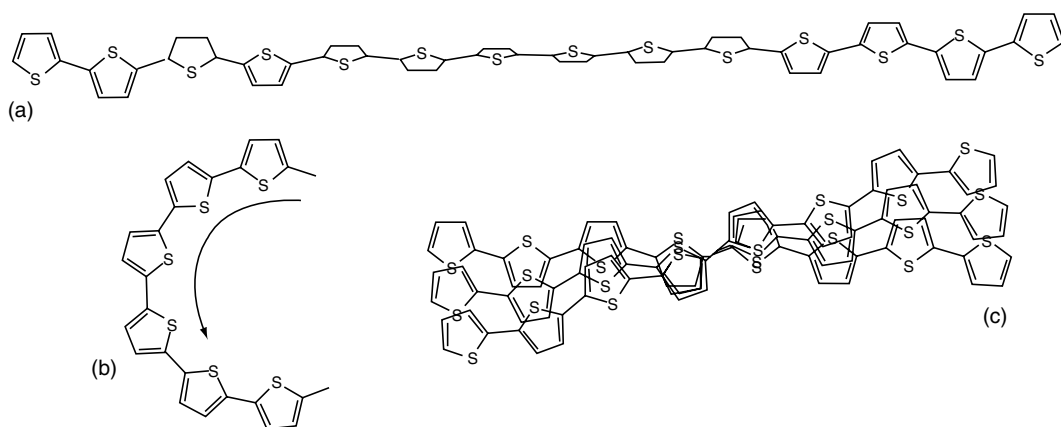


FIGURE 5.12 Three different helical organizations of polythiophenes: (a) helical transoid, (b) helical cisoid, and (c) helical packing of predominantly planar chains. (From Langeveld-Voss, B.M.W., Janssen, R.A.J., and Meijer, E.W., *J. Mol. Struct.*, 21, 285, 2000. With permission.)

arrangement of the chains is reported. Nevertheless, this work represents an elegant new tool to control the chiral morphology that was previously only possible with time-consuming chemical modification of the conductive polymers.

5.4.3 OTHER SYSTEMS FOR CIRCULARLY POLARIZED LUMINESCENCE

Very recently there has been a report about bridged triarylamine helicenes exhibiting CPL [131]. These molecules preferentially emit and absorb CP light without the help of an LC matrix. Currently, there seems to be ongoing work to further increase the efficiency of these types of CPL materials and to develop first devices of polarized OLEDs.

The most exciting piece of work for CPL is using a combination of a classical PLED and a CNLC film on top [113]. Simply by using the Al cathode in the back of the device as a “recycling mirror” the researchers produced a very efficient device that created CP light with an outstanding dissymmetry factor of 1.6. This device consists of an emission layer based on an achiral polyfluorene derivative, which, consequently, emits isotropic light. The CP fraction of the latter that has the matching handedness subsequently passes through the CNLC. The fraction with the opposite sense of chirality is reflected at the CNLC. Upon reflection at the Al cathode (recycling mirror) this light changes its handedness and, then, is able to pass the CNLC. In such a way each photon should in principle be able to leave the system with the same circular polarization, thus creating a very efficient and highly CP emission device. Although the authors did not disclose any data on brightness, efficiency, or turn-on voltage, this photon-recycling device is an important milestone toward highly circularly or linearly polarized EL for LEDs especially because it does not require an emissive layer with chiro-optical properties.

5.5 CONCLUSIONS

In just about a decade of research and development, the area of polarized light emission from OLEDs has come a long way. Many exciting proofs-of-concept have been accomplished, and much improvements and breakthroughs have followed up. However, in order to be successful and competitive with existing technologies in the market place, new systems must be kept simple and cost-effective. At the same time they have to be able to clearly outperform current technology. Although this is a very challenging task, it is likely that some of the approaches discussed in this chapter are very promising and appear to be sufficiently mature for technological exploitation in the near future.

ACKNOWLEDGMENT

C.W. acknowledges support from the National Science Foundation under Grant No. DMR-0215342.

REFERENCES

1. E Lommel, Ueber die dichrotische Fluoreszenz des Magnesiumplatincyanürs. Experimenteller Beweis der Perpendicularität der Lichtschwingungen zur Polarisationssebene, *Ann der Physik und Chemie*, 8:634–640, 1879.
2. A Jablonski, Über die Polarisation der Photolumineszenz der doppelbrechenden Kautsky-Phosphore, *Acta Phys Polon*, A14:421–434, 1934.
3. J Michl and EW Thulstrup, *Spectroscopy with Polarized Light*, 1st ed., VCH Publishers, New York, 1986.

4. BMW Langeveld-Voss, R Janssen, MPT Christiaans, SCJ Meskers, HPJM Dekkers, and EW Meijer, Circular dichroism and circular polarization of photoluminescence of highly ordered poly{3,4-di[(S)-2-methylbutoxy]thiophene}, *J. Am. Chem. Soc.*, 118:4908–4909, 1996.
5. SH Chen, D Katsis, AW Schmid, JC Mastrangelo, T Tsutsui, and TN Blanton, Circularly polarized light generated by photoexcitation of luminophores in glassy liquid-crystal films, *Nature*, 397:506–508, 1999.
6. C Weder, C Sarwa, C Bastiaansen, and P Smith, Highly polarized luminescence from oriented conjugated polymer/polyethylene blend films, *Adv. Mater.*, 9:1035–1039, 1997.
7. A Montali, C Bastiaansen, P Smith, and C Weder, Polarizing energy transfer in photoluminescent materials for display applications, *Nature*, 392:261–264, 1998.
8. M Eglin, A Montali, ARA Palmans, T Tervoort, P Smith, and C Weder, Ultra-high performance photoluminescent polarizers based on melt-processed polymer blends, *J. Mater. Chem.*, 9:2221–2226, 1999.
9. ARA Palmans, M Eglin, A Montali, C Weder, and P Smith, Tensile orientation behavior of alkoxy-substituted *Bis*(phenylethynyl)benzene derivatives in polyolefin blend films, *Chem. Mater.*, 12:472–480, 2000.
10. M Voigt, M Chambers, and M Grell, Circularly polarized emission from a narrow bandwidth dye doped into a chiral nematic liquid crystal, *Liq. Cryst.*, 29:653–656, 2002.
11. P Smith and C Weder, Antifalsification Paper and other Antifalsification Items, Swiss Patent Application 1958/98, 1998.
12. C Weder, C Sarwa, A Montali, C Bastiaansen, and P Smith, Incorporation of photoluminescent polarizers into liquid crystal displays, *Science*, 279:835–837, 1998.
13. DS Kliger, JW Lewis, and CE Randall, *Polarized Light in Optics and Spectroscopy*, Academic Press, San Diego, 1990.
14. TJ Nelson and JR Wullert III, *Electronic Information Display Technologies*, World Scientific Publishing Company, Singapore, 1997.
15. DJ Broer, JAMM van Haaren, P Van de Witte, and C Bastiaansen, New functional polymers for liquid crystal displays review of some recent developments, *Macromol. Symp.*, 154:1–13, 2000.
16. DJ Broer, J Lub, and GN Mol, Wide-band reflective polarizers from cholesteric polymer networks with a pitch gradient, *Nature*, 378:467–469, 1995.
17. DL Wortman, A Recent Advance in Reflective Polarizer Technology, Proceedings of the 1997 International Display Research Conference (Society for Information Display), p. M-98-M-106, 1997.
18. H Jagt, Y Dirix, R Hikmet, and C Bastiaansen, Linear polarizers based on oriented polymer blends, *Adv. Mater.*, 10:934–938, 1998.
19. H Jagt, Y Dirix, R Hikmet, and C Bastiaansen, Linear polarizers based on polymer blends: oriented blends of poly(ethylene-2,6-naphthalenedicarboxylate) and a poly(styrene/methylmethacrylate) copolymer, *Jpn. J. Appl. Phys.*, 37:4389–4392, 1998.
20. AJ Heeger and D Braun, U.S. Patent 5,408,109, 1995 (filed February 27, 1991) to The Regents of the University of California.
21. P Dyreklev, M Berggren, O Inganäs, MR Andersson, O Wennerström, and T Hjertberg, Polarized electroluminescence from an oriented substituted polythiophene in a light emitting diode, *Adv. Mater.*, 7:43–45, 1995.
22. A Kraft, AC Grimsdale, and AB Holmes, Electroluminescent conjugated polymers — seeing polymers in a new light, *Angew. Chem. Int. Ed.*, 37:402–428, 1998.
23. U Mitschke and P Bäuerle, The electroluminescence of organic materials, *J. Mater. Chem.*, 10:1471–1507, 2000.
24. A Greiner and C Weder, Light-emitting diodes, in *Encyclopedia of Polymer Science and Technology*, Vol. 3, JI Kroschwitz, Ed., Wiley-Interscience, New York, 2003, pp. 87–100.
25. DDC Bradley, Electroluminescent polymers: materials, physics and device engineering, *Curr. Opin. Solid State Mater. Sci.*, 1:789–797, 1996.
26. M Grell and DDC Bradley, Polarized luminescence from oriented molecular materials, *Adv. Mater.*, 11:895–905, 1999.
27. D Neher, Polyfluorene homopolymers: conjugated liquid-crystalline polymers for bright blue emission and polarized electroluminescence, *Macromol. Rapid Commun.*, 22:1365–1385, 2001.

28. M O'Neill and SM Kelly, Liquid crystals for charge transport, luminescence, and photonics, *Adv. Mater.*, 15:1135–1146, 2003.
29. P Gay, *An Introduction to Crystal Optics*, Longman, London, 1967.
30. D Clarke and JF Grainger, *Polarized Light and Optical Measurement*, Pergamon Press, Oxford, 1974.
31. W Swindell, *Polarized Light*, Dowden, Hutchinson & Ross, Stroudsburg, PA, 1975.
32. JF Nye, *Physical Properties of Crystals: Their Representation by Tensors and Matrices*, Oxford University Press, New York, 1984.
33. EW Thulstrup and J Michl, A critical comparison of methods for analysis of linear dichroism of solutes in stretched polymers, *J. Phys. Chem.*, 84:82–93, 1980.
34. T Damerou and M Hennecke, Determination of orientational order parameters of uniaxial films with a commercial 90°C-angle fluorescence spectrometer, *J. Chem. Phys.*, 103:6232–6240, 1995.
35. H Shi, BM Conger, D Katsis, and SH Chen, Circularly polarized fluorescence from chiral nematic liquid crystalline films: theory and experiment, *Liq. Cryst.*, 24:163–172, 1998.
36. IM Ward, *Structure and Properties of Oriented Polymers*, Applied Science, London, 1975.
37. IM Ward, The measurement of molecular orientation in polymers by spectroscopic techniques, *J. Polym. Sci., Polym. Symp.*, 58: 1–21, 1977.
38. EW Thulstrup and J Michl, Orientation and linear dichroism of symmetrical aromatic molecules imbedded in stretched polyethylene, *J. Am. Chem. Soc.*, 104:5594–5604, 1982.
39. EH Land, Some aspects of the development of sheet polarizers, *J. Opt. Soc. Am.*, 41: 957–963, 1951.
40. (a) Y Dirix, TA Tervoort, and C Bastiaansen, Optical properties of oriented polymer/dye polarizers, *Macromolecules*, 28:486–491, 1994; (b) Y Dirix, TA Tervoort, C Bastiaansen, Optical properties of oriented polymer/dye polarizers. 2. Ultimate properties, *Macromolecules*, 30:2175–2177, 1997.
41. C Bastiaansen, HW Schmidt, T Nishino, and P Smith, Transparency and dichroism of ultra-drawn UHMW-PE films in the visible wavelength range, *Polymer*, 34:3951–3954, 1993.
42. (a) JV Brestkin, ES Ediljan, NG Bel'niekevic, G Mann, and SJ Frenkel, Untersuchung der Orientierung bei der Deformation von Polyvinylalkohol mit der Methode der polarisierten Lumineszenz, *Acta Polym.*, 31:646–653, 1980; (b) M van Gurp, G van Ginkel, and YK Levine, On the distribution of dye molecules in stretched poly(vinyl alcohol), *J. Polym. Sci., Part B: Polym. Phys.*, 26:1613–1625, 1988; (c) JJ Dekkers, GP Hoornweg, C Maclean, and NH Velthorst, Fluorescence and phosphorescence polarization of molecules oriented in stretched polymers general description, *Chem. Phys. Lett.*, 19:517–523, 1973; (d) H Springer, R Neuert, D Müller, and G Hinrichsen, Orientation analysis of uniaxially drawn polycarbonate films, doped with fluorescent molecules, by UV-dichroism, fluorescence polarization and birefringence, *Colloid Polym. Sci.*, 262:46–50, 1984; (e) H Springer, J Kussi, HJ Richter, and G Hinrichsen, Dichroism of polyvinylchloride films doped with fluorescent molecules, *Colloid Polym. Sci.*, 259:911–916, 1981.
43. (a) LV Natarajan, FM Stein, and RE Blankenship, Linear dichroism and fluorescence polarization of diphenyl polyenes in stretched polyethylene films, *Chem. Phys. Lett.*, 95:525–528, 1983; (b) M Hennecke, T Damerou, and K Müllen, Fluorescence depolarization in poly(*p*-phenylenevinylene) and related oligomers, *Macromolecules*, 26:3411–3418, 1993; (c) T Damerou and MJ Hennecke, Determination of orientational order parameters of uniaxial films with a commercial 90°-angle fluorescence spectrometer, *J. Chem. Phys.*, 103:6232–6240, 1995.
44. (a) TW Hagler, K Pakbaz, J Moulton, F Wudl, P Smith, and AJ Heeger, Highly ordered conjugated polymers in polyethylene: orientation by mesoepitaxy, *Polym. Commun.*, 32:339–342, 1991; (b) TW Hagler, K Pakbaz, and AJ Heeger, Enhanced order and electronic delocalization in conjugated polymers oriented by gel processing in polyethylene, *Phys. Rev. B*, 44:8652–8666, 1991; (c) TW Hagler, K Pakbaz, and AJ Heeger, Polarized-electroabsorption spectroscopy of a soluble derivative of poly(*p*-phenylenevinylene) oriented by gel processing in polyethylene: polarization anisotropy, the off-axis dipole moment, and excited-state delocalization, *Phys. Rev. B*, 49:10968–10975, 1994.
45. PH Hermans and D Heikens, Orientation in cellulose fibers as derived from measurements of dichroism of dyed fibers, *Recl. Trav. Chim. Pays-Bas*, 71:49–55, 1952.

46. (a) F Wudl, PM Allemand, G Srdanov, Z Ni, and D McBranch, Polymers and an unusual molecular crystal with nonlinear optical properties, in *Materials for Nonlinear Optics: Chemical Perspectives*, ACS, Washington, 1991, pp. 683–692; (b) D Braun and AJ Heeger, Visible light emission from semiconducting polymer diodes, *Appl. Phys. Lett.*, 58:1982–1984, 1991.
47. (a) A Montali, P Smith, and C Weder, Poly(*p*-phenylene ethynylene)-based light emitting devices, *Synth. Met.*, 97:123–126, 1998; (b) C Schmitz, P Pösch, M Thelakkat, HW Schmidt, A Montali, K Feldman, P Smith, and C Weder, Polymeric light-emitting diodes based on poly(*p*-phenylene ethynylene), poly(triphenyldiamine), and spiroquinoxaline, *Adv. Funct. Mater.*, 11:41–46, 2001.
48. DDC Bradley, RH Friend, H Lindenberg, and S Roth, Infra-red characterization of oriented poly(phenylene vinylene), *Polymer*, 27:1709–1713, 1986.
49. U Lemmer, D Vacar, D Moses, AJ Heeger, T Ohnishi, and T Noguchi, Electroluminescence from poly(phenylene vinylene) in a planar metal–polymer–metal structure, *Appl. Phys. Lett.*, 68:3007–3009, 1996.
50. M Hamaguchi and K Yoshino, Polarized electroluminescence from rubbing-aligned poly(2,5-dinonyloxy-1,4-phenylenevinylene) films, *Appl. Phys. Lett.*, 67:3381–3383, 1995.
51. M Jandke, P Stroehriegl, J Gmeiner, W Brutting, and M Schwoerer, Polarized electroluminescence from rubbing-aligned poly(phenylenevinylene), *Adv. Mater.*, 11:1518–1521, 1999.
52. A Bolognesi, C Botta, and M Martinelli, Oriented poly(3-alkylthiophene) films: absorption, photoluminescence and electroluminescence behaviour, *Synth. Met.*, 121: 1279–1280, 2001.
53. A Bolognesi, C Botta, D Facchinetti, M Jandke, K Kreger, P Stroehriegl, A Relini, R Rolandi, and S Blumstengel, Polarized electroluminescence in double-layer light-emitting diodes with perpendicularly oriented polymers, *Adv. Mater.*, 13:1072–1075, 2001.
54. I Moggio, J Le Moigne, E Arias-Marin, D Issautier, A Thierry, D Comoretto, G Dellepiane, and C Cuniberti, Orientation of polydiacetylene and poly(*p*-phenylene ethynylene) films by epitaxy and rubbing, *Macromolecules*, 34:7091–7099, 2001.
55. N Tanigaki, K Yase, and A Kaito, Oriented films of poly(*p*-phenylene) by friction-deposition and oriented growth in polymerization, *Mol. Cryst. Liq. Cryst.*, 267:335–340, 1995.
56. NAJM Van Aerle, M Barmantlo, and RWJ Hollering, Effect of rubbing on the molecular orientation within polyimide orienting layers of liquid-crystal displays, *J. Appl. Phys.*, 74:3111–3120, 1993.
57. DW Berreman, Solid surface shape and the alignment of an adjacent nematic liquid crystal, *Phys. Rev. Lett.*, 28:1683–1686, 1972.
58. (a) MB Feller, W Chen, and YR Shen, Investigation of surface-induced alignment of liquid-crystal molecules by optical second-harmonic generation, *Phys. Rev. A: At., Mol., Opt. Phys.*, 43:6778–6792, 1991; (b) MF Toney, TP Russell, JA Logan, H Kikuchi, JM Sands, and SK Kumar, Near-surface alignment of polymers in rubbed films, *Nature*, 374:709–711, 1995.
59. (a) SA Casalnuovo, KC Lim, and AJ Heeger, Reversible optical anisotropy and induced rigidity in polydiacetylene films, *Macromol. Chem., Rapid Commun.*, 5:77–81, 1984; (b) T Kanetake, K Ishikawa, T Koda, Y Tokura, and K Takeda, Highly oriented polydiacetylene films by vacuum deposition, *Appl. Phys. Lett.*, 51:1957–1959, 1987.
60. JC Wittmann and P Smith, Highly oriented thin films of poly(tetrafluoroethylene) as a substrate for oriented growth of materials, *Nature*, 352:414–418, 1991.
61. S Nagamatsu, W Takashima, K Kaneto, Y Yoshida, N Tanigaki, K Yase, and K Omote, Backbone arrangement in friction-transferred regioregular poly(3-alkylthiophene)s, *Macromolecules*, 36:5252–5257, 2003.
62. M Era, T Tsutsui, and S Saito, Polarized electroluminescence from oriented *p*-sexiphenyl vacuum-deposited film, *Appl. Phys. Lett.*, 67:2436–2438, 1995.
63. (a) K Ichimura, M Momose, K Kudo, and H Akiyama, Surface-assisted photolithography to form anisotropic dye layers as a new horizon of command surfaces, *Langmuir*, 11:2341–2343, 1995; (b) M Schadt, H Seiberle, and A Schuster, Optical patterning of multi-domain liquid-crystal displays with wide viewing angles, *Nature*, 381:212–215, 1996.
64. RE Gill, G Hadzioannou, P Lang, F Garnier, and JC Wittmann, Highly oriented thin films of a substituted oligo(*para*-phenylenevinylene) on friction-transferred PTFE substrates, *Adv. Mater.*, 9:331–338, 1997.

65. Y Yoshida, JP Ni, N Tanigaki, and K Yase, Polarized electroluminescence of oligophenyl thin films prepared on friction transferred poly(*p*-phenylenes), *Mol. Cryst. Liq. Cryst.*, 370:69–72, 2001.
66. (a) D Fenwick, P Smith, and JC Wittmann, Epitaxial and graphoeptitaxial growth of materials on highly oriented PTFE substrates, *J. Mater. Sci.*, 31:128–131, 1996; (b) D Fenwick, K Pakbaz, and P Smith, Alignment of fluorescent molecules vapour-deposited on to highly oriented PTFE substrates, *J. Mater. Sci.*, 31:915–920, 1996; (c) K Pichler, RH Friend, PL Burn, and AB Holmes, Chain alignment in poly(*p*-phenylene vinylene) on oriented substrates, *Synth. Met.*, 55:454–459, 1993.
67. Y Yoshida, N Tanigaki, K Yase, and S Hotta, Color-tunable highly polarized emissions from uniaxially aligned thin films of thiophene/phenylene co-oligomers, *Adv. Mater.*, 12:1587–1591, 2000.
68. N Tanigaki, H Kyotani, M Wada, A Kaito, Y Yoshida, EM Han, K Abe, and K Yase, Oriented thin films of conjugated polymers: polysilanes and polyphenylenes, *Thin Solid Films*, 331:229–238, 1998.
69. (a) KB Blodgett, Monomolecular films of fatty acids on glass, *J. Am. Chem. Soc.*, 56:495–495, 1934; (b) KB Blodgett, Films built by depositing successive monomolecular layers on a solid surface, *J. Am. Chem. Soc.*, 57:1007–1022, 1935.
70. G Roberts, *Langmuir–Blodgett Films*, Plenum Press, New York, 1990.
71. V Cimrova, M Remmers, D Neher, and G Wegner, Polarized light emission from LEDs prepared by the Langmuir–Blodgett technique, *Adv. Mater.*, 8:146–149, 1996.
72. A Bolognesi, G Bajo, J Paloheimo, T Östergård, and H Stubb, Polarized electroluminescence from an oriented poly(3-alkylthiophene) Langmuir–Blodgett structure, *Adv. Mater.*, 9:121–124, 1997.
73. Z Ali-Adib, K Davidson, H Nooshin, and RH Tredgold, Magnetic orientation of phthalocyaninato–polysiloxanes, *Thin Solid Films*, 201:187–195, 1991.
74. (a) S Schwegk, T Vahlenkamp, G Wegner, and Y Xu, On the origin of main chain orientation of rigid-rod macromolecules during the Langmuir–Blodgett process, *Thin Solid Films*, 210/211:6–8, 1992; (b) S Schwegk, T Vahlenkamp, Y Xu, and G Wegner, Origin of orientation phenomena observed in layered Langmuir–Blodgett structures of hairy-rod polymers, *Macromolecules*, 25:2513–2525, 1992.
75. M Era, J Koganemaru, T Tsutsui, A Watakabe, and T Kunitake, Spacial distribution of electroluminescence from oriented phenylenevinylene oligomer Langmuir–Blodgett film, *Synth. Met.*, 91:83–85, 1997.
76. A Marletta, D Gonçalves, ON Oliveira Jr., RM Faria, and FEG Guimarães, Highly oriented Langmuir–Blodgett films of poly(*p*-phenylenevinylene) using a long chain sulfonic counterion, *Macromolecules*, 33:5886–5890, 2000.
77. A Marletta, D Gonçalves, ON Oliveira Jr., RM Faria, and FEG Guimarães, Circular dichroism and circularly polarized luminescence of highly oriented Langmuir–Blodgett films of poly(*p*-phenylene vinylene), *Synth. Met.*, 119:207–208, 2001.
78. E Arias, T Maillou, I Moggio, D Guillon, J Le Moigne, and B Geffroy, Amphiphilic phenylene–ethynylene polymers and oligomers for polarized electroluminescence, *Synth. Met.*, 127:229–231, 2002.
79. M Remmers, D Neher, and G Wegner, Photo-cross-linkable poly(*p*-phenylene)s. Synthesis, Langmuir–Blodgett multilayer film properties and pattern formation, *Macromol. Chem. Phys.*, 198:2551–2561, 1997.
80. HJ Coles, GA Lester, and H Owen, Fluorescent dye guest–host effects in advanced ferroelectric liquid crystals, *Liq. Cryst.*, 14:1039–1045, 1993.
81. NS Sariciftci, U Lemmer, D Vacar, AJ Heeger, and RAJ Janssen, Polarized photoluminescence of oligothiophenes in nematic liquid crystalline matrices, *Adv. Mater.*, 8:651–653, 1996.
82. (a) BM Conger, JC Mastrangelo, and SH Chen, Fluorescence behavior of low molar mass and polymer liquid crystals in ordered solid films, *Macromolecules*, 30:4049–4055, 1997; (b) M Grell, DDC Bradley, M Inbasekaran, and EP Woo, A glass-forming conjugated main-chain liquid crystal polymer for polarized electroluminescence applications, *Adv. Mater.*, 9:798–802, 1997.
83. AP Davey, RG Howard, and W Blau, Polarised photoluminescence from oriented polymer liquid crystals, *J. Mater. Chem.*, 7:417–420, 1997.

84. GH Heilmeier and LA Zanoni, Guest–host interactions in nematic liquid crystals: a new electro-optic effect, *Appl. Phys. Lett.*, 13:91–92, 1968.
85. M Funahashi and JI Hanna, Fast hole transport in a new calamitic liquid crystal of 2-(4'-Heptyloxyphenyl)-6-dodecylthiobenzothiazole, *Phys. Rev. Lett.*, 78:2184–2187, 1997.
86. (a) H Tokuhisa, M Era, and T Tsutsui, Polarized electroluminescence from smectic mesophase, *Appl. Phys. Lett.*, 72:2639–2641, 1998; (b) H Mochizuki, T Hasui, T Shiono, T Ikeda, C Adachi, Y Taniguchi, and Y Shirota, Emission behavior of molecularly doped electroluminescent device using liquid-crystalline matrix, *Appl. Phys. Lett.*, 77:1587–1589, 2000.
87. (a) AEA Contoret, SR Farrar, PO Jackson, SM Khan, L May, M O'Neill, JE Nicholls, SM Kelly, and GJ Richards, Polarized electroluminescence from an anisotropic nematic network on a non-contact photoalignment layer, *Adv. Mater.*, 12:971–974, 2000; (b) AEA Contoret, SR Farrar, M O'Neill, JE Nicholls, GJ Richards, SM Kelly, and AW Hall, The photopolymerization and cross-linking of electroluminescent liquid crystals containing methacrylate and diene photopolymerizable end groups for multilayer organic light-emitting diodes, *Chem. Mater.*, 14:1477–1487, 2002.
88. C Weder and P Smith, Main-chain liquid-crystalline polymers for optical and electronic devices, in *Encyclopedia of Materials: Science and Technology*, KH Buschow, RW Cahn, MC Flemings, B Ilschner, EJ Kramer, and S Mahajan, Eds., Elsevier Science, New York, 2001, pp. 5148–5155.
89. G Lüssem, R Festag, A Greiner, C Schmidt, C Unterlechner, W Heitz, JH Wendorff, M Hopmeier, and J Feldmann, Polarized photoluminescence of liquid-crystalline polymers with isolated arylenevinylene segments in the main-chain, *Adv. Mater.*, 7:923–928, 1995.
90. G Lüssem, F Geffarth, A Greiner, W Heitz, M Hopmeier, JM Oberski, C Unterlechner, and JH Wendorff, Polarized electroluminescence of light emitting liquid crystalline polymers, *Liq. Cryst.*, 21:903–907, 1996.
91. G Lüssem and JH Wendorff, Liquid crystalline materials for light-emitting diodes, *Polym. Adv. Technol.*, 9:443–460, 1998.
92. JM Oberski, KU Clauswitz, G Lüssem, F Geffarth, JH Wendorff, and A Greiner, Emission of polarized light from liquid crystalline segmented poly(arylenevinylene)s, *Macromol. Symp.*, 154:235–244, 2000.
93. J Oguma, K Akagi, and H Shirakawa, Synthesis and properties of liquid crystalline poly(*p*-phenylene) and poly(*p*-phenylene vinylene) derivatives, *Synth. Met.*, 101:86–87, 1999.
94. (a) H Martelock, A Greiner, and W Heitz, Structural modifications of poly(1,4-phenylenevinylene) to soluble, fusible, liquid-crystalline products, *Macromol. Chem.*, 192:967–979, 1991; (b) Z Bao, Y Chen, R Cai, and L Yu, Conjugated liquid crystalline polymers-soluble and fusible poly(phenylenevinylene) by the Heck coupling reaction, *Macromolecules*, 26:5281–5286, 1993; (c) RE Gill, A Meetsma, G Hadzioannou, Two novel thermotropic liquid crystalline substituted oligo(*p*-phenylene-vinylene)s: single crystal x-ray determination of an all-trans oligomeric PPV, *Adv. Mater.*, 8:212–216, 1996.
95. (a) D Steiger, P Smith, and C Weder, Liquid-crystalline, highly luminescent poly(2,5-dialkoxy-*p*-phenylene ethynylene), *Macromol. Rapid. Commun.*, 18:643–649, 1997; (b) L Kloppenburg, D Jones, JB Claridge, HC zur Loye, and UHF Bunz, Poly(*p*-phenylene ethynylene)s are thermotropic liquid crystalline, *Macromolecules*, 32:4460–4463, 1999.
96. M Grell, DDC Bradley, G Ungar, J Hill, and KS Whitehead, Interplay of physical structure and photophysics for a liquid crystalline polyfluorene, *Macromolecules*, 32:5810–5817, 1999.
97. M Grell, DDC Bradley, M Inbasekaran, and EP Woo, A glass-forming conjugated main-chain liquid crystal polymer for polarized electroluminescence applications, *Adv. Mater.*, 9:798–802, 1997.
98. KS Whitehead, M Grell, DDC Bradley, M Inbasekaran, and EP Woo, Polarized emission from liquid crystal polymers, *Synth. Met.*, 111:181–185, 2000.
99. M Grell, W Knoll, D Lupo, A Meisel, T Miteva, D Neher, HG Nothofer, U Scherf, and A Yasuda, Blue polarized electroluminescence from a liquid crystalline polyfluorene, *Adv. Mater.*, 11:671–675, 1999.
100. M Grell, DDC Bradley, and KS Whitehead, Materials and devices for polarized electroluminescence, *J. Kor. Phys. Soc.*, 36:331–336, 2000.

101. T Miteva, A Meisel, M Grell, HG Nothofer, D Lupo, A Yasuda, W Knoll, L Kloppenburg, UHF Bunz, U Scherf, and D Neher, Polarized electroluminescence from highly aligned liquid crystalline polymers, *Synth. Met.*, 111:173–176, 2000.
102. HG Nothofer, A Meisel, T Miteva, D Neher, M Forster, M Oda, G Lieser, D Sainova, A Yasuda, D Lupo, W Knoll, and U Scherf, Liquid crystalline polyfluorenes for blue polarized electroluminescence, *Macromol. Symp.*, 154:139–148, 2000.
103. KS Whitehead, M Grell, DDC Bradley, M Jandke, and P Strohriegel, Highly polarized blue electroluminescence from homogeneously aligned films of poly(9,9-dioctylfluorene), *Appl. Phys. Lett.*, 76:2946–2948, 2000.
104. T Miteva, A Meisel, W Knoll, HG Nothofer, U Scherf, DC Müller, K Meerholz, A Yasuda, and D Neher, Improving the performance of polyfluorene-based organic light-emitting diodes via end-capping, *Adv. Mater.*, 13:565–570, 2001.
105. D Sainova, A Zen, HG Nothofer, U Asawapirom, U Scherf, R Hagen, T Bieringer, S Kostromine, and D Neher, Photoaddressable alignment layers for fluorescent polymers in polarized electroluminescence devices, *Adv. Funct. Mater.*, 12:49–57, 2002.
106. XH Yang, D Neher, S Lucht, HG Nothofer, R Guntner, U Scherf, R Hagen, and S Kostromine, Efficient polarized light-emitting diodes utilizing ultrathin photoaddressable alignment layers, *Appl. Phys. Lett.*, 81:2319–2321, 2002.
107. SW Chang, AK Li, CW Liao, and CS Hsu, Polarized blue emission based on a side chain liquid crystalline polyacrylate containing *bis*-tolane side groups, *Jpn. J. Appl. Phys.*, 41:1374–1378, 2002.
108. YH Geng, SW Culligan, A Trajkovska, JU Wallace, and SH Chen, Monodisperse oligofluorenes forming glassy-nematic films for polarized blue emission, *Chem. Mater.*, 15:542–549, 2003.
109. SW Culligan, Y Geng, SH Chen, K Klubek, KM Vaeth, and CW Tang, Strongly polarized and efficient blue organic light-emitting diodes using monodisperse glassy nematic oligo(fluorene)s, *Adv. Mater.*, 15:1176–1180, 2003.
110. Y Geng, ACA Chen, JJ Ou, SH Chen, K Klubek, KM Vaeth, and CW Tang, Monodisperse glassy-nematic conjugated oligomers with chemically tunable polarized light emission, *Chem. Mater.*, 15:4352–4360, 2003.
111. BMW Langeveld-Voss, RAJ Janssen, and EW Meijer, On the origin of optical activity in polythiophenes, *J. Mol. Struct.*, 21:285–301, 2000.
112. M Schadt, Liquid crystal materials and liquid crystal displays, *Annu. Rev. Mater. Sci.*, 27:305–379, 1997.
113. M Grell, M Oda, KS Whitehead, A Asimakis, D Neher, and DDC Bradley, A compact device for the efficient, electrically driven generation of highly circularly polarized light, *Adv. Mater.*, 13:577–580, 2001.
114. NPM Huck, WF Jager, B de Lange, and BL Feringa, Dynamic control and amplification of molecular chirality by circular polarized light, *Science*, 273:1686–1691, 1996.
115. M Suarez and GB Schuster, Photoresolution of an axially chiral bicyclo[3.3.0]octan-3-one: photo-triggers for a liquid-crystal-based optical switch, *J. Am. Chem. Soc.*, 117:6732–6738, 1995.
116. C Wang, H Fei, Y Qiu, Y Yang, Z Wei, Y Tian, Y Chen, and Y Zhao, Photoinduced birefringence and reversible optical storage in liquid-crystalline azobenzene side-chain polymers, *Appl. Phys. Lett.*, 74:19–21, 1999.
117. AY Bobrovski, NI Boiko, VP Shibaev, and JH Wendorff, Cholesteric mixtures with photochemically tunable, circularly polarized fluorescence, *Adv. Mater.*, 15:282–287, 2003.
118. DR Hall, Use of Stereoscopic Systems Using Chiral Liquid Crystals, U.S. Patent 5,699,184, 1997.
119. IEJR Heynderickx and DJ Broer, Illumination System for a Color Projection Device and Circular Polarizer Suitable for Use in Such an Illumination System, and Color Image Projection Device Comprising Such an Illumination System and Circular Polarizer, U.S. Patent 5,626,408, 1997.
120. VI Kopp, B Fan, HKM Vithana, and AZ Genack, Low-threshold lasing at the edge of a photonic stop band in cholesteric liquid crystals, *Opt. Lett.*, 23:1707–1709, 1998.
121. M Voigt, M Chambers, and M Grell, On the circular polarization of fluorescence from dyes dissolved in chiral nematic liquid crystals, *Chem. Phys. Lett.*, 347:173–177, 2001.

122. D Katsis, HP Chen, SH Chen, LJ Rothberg, and T Tsutsui, Polarized photoluminescence from solid films of nematic and chiral-nematic poly(*p*-phenylene)s, *Appl. Phys. Lett.*, 77:2982–2984, 2000.
123. E Peeters, MPT Christiaans, RAJ Janssen, HFM Schoo, HPJM Dekkers, and EW Meijer, Circularly polarized electroluminescence from a polymer light-emitting diode, *J. Am. Chem. Soc.*, 119:9909–9910, 1997.
124. JJLM Cornelissen, E Peeters, RAJ Janssen, and EW Meijer, Chiroptical properties of a chiral-substituted poly(thienylene vinylene), *Acta Polym.*, 49:471–476, 1998.
125. (a) R Fiesel, J Huber, and U Scherf, Synthesis of an optically active poly(*para*-phenylene) ladder polymer, *Angew. Chem. Int. Ed. Engl.*, 35:2111–2113, 1996; (b) R Fiesel, J Huber, U Apel, V Enkelmann, R Hentschke, U Scherf, and K Kabrera, Novel chiral poly(*para*-phenylene) derivatives containing cyclophane-type moieties, *Macromol. Chem. Phys.*, 198:2623–2650, 1997.
126. R Fiesel and U Scherf, A chiral poly(*para*-phenyleneethynylene) (PPE) derivative, *Macromol. Rapid Commun.*, 19:427–431, 1998.
127. JN Wilson, W Steffen, TG McKenzie, G Lieser, M Oda, D Neher, and UHF Bunz, Chiroptical properties of poly(*p*-phenyleneethynylene) copolymers in thin films: large *g*-values, *J. Am. Chem. Soc.*, 124:6830–6831, 2002.
128. M Oda, HG Nothofer, G Lieser, U Scherf, SCJ Meskers, and D Neher, Circularly polarized electroluminescence from liquid-crystalline chiral polyfluorenes, *Adv. Mater.*, 12:362–365, 2000.
129. M Oda, HG Nothofer, U Scherf, V Šunjić, D Richter, W Regenstein, and D Neher, Chiroptical properties of chiral substituted polyfluorenes, *Macromolecules*, 35:6792–6798, 2002.
130. ZB Zhang, M Fujiki, M Motonaga, and CE McKenna, Control of chiral ordering in aggregated poly{3-(*S*)-[2-methylbutyl]thiophene} by a doping-dedoping process, *J. Am. Chem. Soc.*, 125:7878–7881, 2003.
131. JE Field, G Muller, JP Riehl, and D Venkataraman, Circularly polarized luminescence from bridged triarylamine helicenes, *J. Am. Chem. Soc.*, 125:11808–11809, 2003.

6 Transparent Electrode for OLEDs

Furong Zhu

CONTENTS

6.1	Transparent Conducting Thin Films	483
6.1.1	Transparent Conducting Oxides	483
6.1.2	Fundamental Properties of Indium Tin Oxide	484
6.1.2.1	Preparation of Indium Tin Oxide	484
6.1.2.2	Structural Properties of Indium Tin Oxide	485
6.1.2.3	Electrical Properties of Indium Tin Oxide	487
6.1.2.4	Optical Properties of Indium Tin Oxide	489
6.1.2.5	Indium Tin Oxide Composition and Surface Electronic Properties	492
6.2	Anode Modification for Enhancing OLED Performance	494
6.2.1	Indium Tin Oxide Surface Treatment and Modification	494
6.2.2	Color Tuning with Graded Indium Tin Oxide Thickness	502
6.2.3	Non-Indium Tin Oxide Anode for OLEDs	504
6.3	Electrode for Flexible OLEDs	507
6.3.1	Indium Tin Oxide Anode on Flexible Substrates	507
6.3.2	OLEDs on Polymer-Reinforced Ultrathin Glass Sheets	510
6.3.3	Top-Emitting OLEDs on Al-Laminated Plastic Foils	510
6.4	Optical Destructive Electrode for High Contrast OLEDs	516
6.4.1	Black Cathode for High Contrast OLEDs	516
6.4.2	Gradient Refractive Index Anode for High Contrast OLEDs	517
	References	522

6.1 TRANSPARENT CONDUCTING THIN FILMS

6.1.1 TRANSPARENT CONDUCTING OXIDES

The thin films of transparent conducting oxides (TCOs) have widespread applications due to their unique properties of good electrical conductivity and high optical transparency in the visible spectrum range. There have been a great deal of activities in the development of TCOs for a variety of applications. In general, properly doped oxide materials, e.g., ZnO, SnO₂, and In₂O₃, are used individually or in separate layers or as mixtures such as indium tin oxide (ITO) and indium zinc oxide (IZO) for making TCO thin films. ITO, aluminum-doped zinc oxide (AZO), and fluorine-doped tin oxide (FTO) are commonly used TCO materials for different applications. The distinctive characteristics of these TCOs have been widely used in antistatic coatings, heat mirrors, solar cells [1,2], flat panel displays [3], sensors [4], and

organic light-emitting diodes (OLEDs) [5–7]. The properties of TCO films are often optimized accordingly to meet the requirements in the various applications that involve TCO. The light scattering effect due to the usage of textured TCO substrates helps to enhance the light absorbance in thin-film amorphous silicon solar cells [8,9]. However, a rough TCO surface is detrimental for OLED applications. The localized high electric fields induced by the rough TCO surface can cause a nonuniform current flow leading to the dark spot formation or a short device operation lifetime.

The conductivity of ZnO, ITO, and SnO₂ can be controlled across an extremely wide range such that they can behave as insulators, semiconductors, or metal-like materials. However, these materials are all n-type electrical conductors in nature. Their applications for optoelectronics are rather restricted. The lack of p-type conducting TCOs prevent fabrication of p–n junction composed from transparent oxide semiconductors [2]. The fabrication of highly conducting p-type TCOs is, indeed, still a challenge.

In comparison to the research in n-type oxide semiconductors, little work has been done on the development of p-type TCOs. The effective p-type doping in TCOs is often compensated due to their intrinsic oxide structural tolerance to oxygen vacancies and metal interstitials. Recently, significant developments have been reported about ZnO, CuAlO₂, and Cu₂SrO₂ as true p-type oxide semiconductors. The ZnO exhibits unipolarity or asymmetry in its ability to be doped n-type or p-type. ZnO is naturally an n-type oxide semiconductor because of a deviation from stoichiometry due to the presence of intrinsic defects such as Zn interstitials and oxygen vacancies. A p-type ZnO, doped with As or N as a shallow acceptor and codoped with Ga or Zn as a donor, has been recently reported. However, the origin of the p-type conductivity and the effect of structural defects on n-type to p-type conversion in ZnO films are not completely understood.

The advances in TCO materials development are still in a growth stage. The great potential for p-type TCOs and the innovative technologies are predicted to lead to developments beyond anything one can imagine today. These include novel heterostructure applications as part of the rapid emergence of all-oxide electronics. Initial results on ZnO show that a small amount of nitrogen can be incorporated to form a p-type TCO [10]. Theoretical results for III–V and II–VI materials subsequently indicated that codoping of these materials might allow not only type conversion but also high doping levels [11]. Although the conductivity of the p-type oxide semiconductors is still lower than their n-type counterparts, the p-type oxide semiconductors offer the potential for a variety of new devices. The new approaches to p-type doping of oxides and integration of these new materials have led to the hope for oxide semiconductor-based p–n junction for novel transparent electronics.

6.1.2 FUNDAMENTAL PROPERTIES OF INDIUM TIN OXIDE

Among the existing TCOs, ITO is one of the most frequently used TCO materials in practical applications. ITO film has attracted much attention because of its unique characteristics, such as good electrical conductivity, high optical transparency over the visible wavelength region, excellent adhesion to the substrates, stable chemical property, and easy patterning ability. One of the most common uses of the ITO coatings has been as transparent electrodes in photovoltaic cells and flat panel displays including plasma televisions, liquid crystal displays (LCDs), and OLEDs. In some of these, it is important to ensure as low a resistivity and as high an optical transparency as possible. The optical, electrical, structural, and morphological properties of TCO films have direct implications for determining and improving the device performance.

6.1.2.1 Preparation of Indium Tin Oxide

The deposition techniques that are suitable for the preparation of reproducible thin films of ITO include thermal evaporation deposition [12], magnetron sputtering [13,14], electron

beam evaporation [15], spray pyrolysis [16], chemical vapor deposition [17], dip-coating [18,19], and pulsed laser deposition methods [20,21]. Among these available techniques for fabricating ITO films, the direct current (dc) or radio frequency (RF) magnetron sputtering method is most often used to prepare ITO thin films for a wide range of applications. ITO films fabricated using the RF or dc magnetron sputtering method usually require a low oxygen partial pressure in the sputtering gas when both alloy and oxidized targets are used [22,23]. The ITO film quality is determined by a number of factors such as thickness uniformity, surface morphology, optical transparency, and electrical conductivity. This aside, the deposition technologies, the process conditions, and the postdeposition treatments also affect the overall optical and electrical properties of ITO.

In addition to the usage of reactive oxygen gas during dc or RF magnetron sputtering processes, introducing water vapor or hydrogen gas into the gas mixture during the sputtering processes have also been reported. Harding and Window [24] found that good quality ITO films can be obtained using an argon–oxygen–hydrogen mixture during deposition. Ishibashi et al. [25] reported that the carrier concentration of the ITO films increased when water vapor or hydrogen gas was used in the dc magnetron sputtering experiments. However, the mechanism for increased carrier concentration in ITO films was not discussed. Baía et al. [26] reported that conductivity of the ITO films sputtered at room temperature increased significantly followed by reannealing the films in vacuum with hydrogen base pressure. The improvement of the film conductivity with regard to the annealing treatment under hydrogen atmosphere is explained as due to the removal of excess oxygen incorporated and the passivation of the defects in the films. These results indicate clearly that the presence of hydrogen species during the preparation or the postdeposition treatment of ITO films can affect the overall optical and electrical properties of ITO films significantly. A better understanding of process conditions on the overall properties of ITO films is of considerable interest.

The following discussion describes the structural, electrical, and optical properties of the ITO films prepared using an oxidized target with In_2O_3 and SnO_2 in a weight proportion of 9:1. The ITO films are deposited on glass substrates using the RF magnetron sputtering method. The base pressure in the system is about 5.0×10^{-8} torr. A sputtering gas mixture of argon–hydrogen is used for the growth of ITO films. The effect of hydrogen partial pressure on the structural and optoelectronic properties of the ITO films is studied over the hydrogen partial pressure in the range of 0 to 1.6×10^{-5} torr. The ITO films are prepared at a constant substrate temperature of 300°C.

6.1.2.2 Structural Properties of Indium Tin Oxide

The structural properties of the ITO films deposited on glass substrates at various hydrogen partial pressures are characterized by x-ray diffraction (XRD) measurements. Figure 6.1 shows a series of XRD patterns of ITO films deposited over a hydrogen partial pressure in the range of 0 to 1.6×10^{-5} torr. The figure illustrates that ITO films prepared on glass substrates have polycrystalline structures with diffraction peaks corresponding to (221), (222), (400), (440), and (622) reflections. In particular, (222) and (400) are the prominent planes for films prepared by this method, indicating that the ITO films have (111) and (100) preferentially orientated textures. The relative intensity of the (222) reflection increases gradually with increasing hydrogen partial pressure.

The crystallinity of the ITO film depends on the fabrication technique and deposition conditions. ITO films prepared by sputtering usually have preferred orientation in (100) direction and those prepared by reactive thermal evaporation have preferred orientation along (111) plane [27]. Some studies have shown that the dominant crystal orientations in ITO films can be changed under certain conditions. Thilakan and Kumar [28] reported that

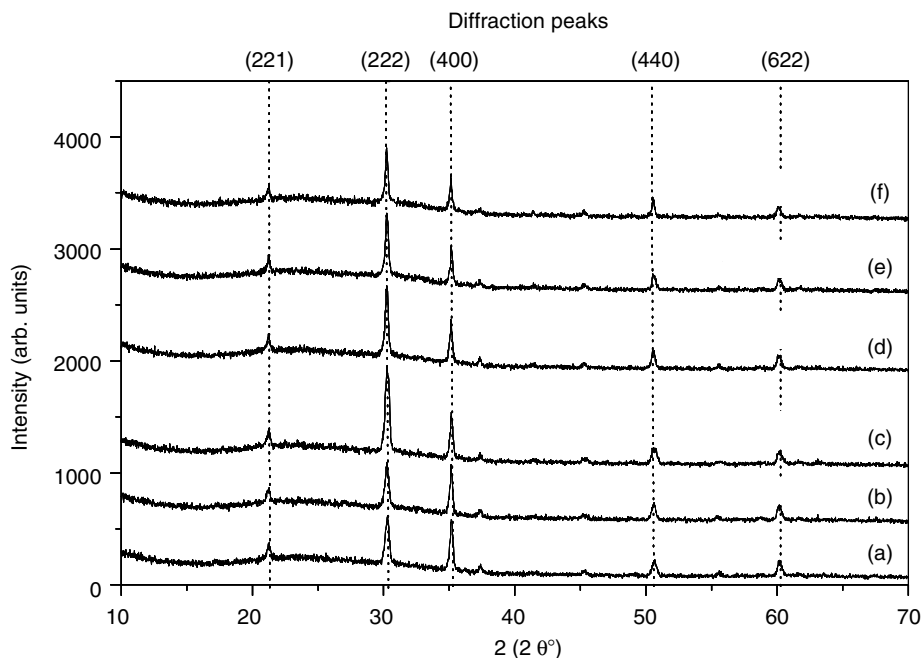


FIGURE 6.1 XRD spectra measured for ITO films grown on glass substrates at different hydrogen pressures of (a) 0 torr, (b) 5.4×10^{-6} torr, (c) 7.9×10^{-6} torr, (d) 1.0×10^{-5} torr, (e) 1.3×10^{-5} torr, and (f) 1.6×10^{-5} torr.

the preferred orientation of ITO can be changed from (222) to (400) when the film deposition rate increased. Meng and Santos [27] also observed a similar orientation transition from (222) to (400) when the substrate temperature increased from room temperature to about 500°C . From Figure 6.1, it appears that the presence of hydrogen in the sputtering gas mixture enhances (222) orientation preferentially. This structural change in ITO films may affect the overall optical and electrical properties of the films.

The interplanar distances for (222), (400), and (440) crystal planes can be obtained by fitting the XRD peaks shown in Figure 6.1. When hydrogen is added to the gas mixture, interplanar separations of ITO films along the orientations of major XRD peaks are generally less than that of the film prepared without hydrogen in sputtering gas mixture. The deviation of interplanar distances along these crystal directions in the ITO films indicates structural or compressive stress in the film. Adding hydrogen to the sputtering gas mixture has been shown to reduce the structural stress in ITO films prepared by RF magnetron sputtering method. The interplanar distances obtained from the major XRD peaks change with hydrogen partial pressure and attain minimum values at a hydrogen partial pressure of 7.9×10^{-6} torr. At this hydrogen partial pressure, minimum value of the plane distance calculated from prominent (222) planes is 2.9369 \AA . This value is less than that of 2.9500 \AA for $\text{In}_2\text{SnO}_{7-x}$, and it is slightly bigger than the value of 2.9210 \AA for In_2O_3 [29]. The decrease in interplanar distance in ITO films is probably related to a reduced lattice constant of the ITO films. This suggests that a possible stress relaxation occurs in the ITO films [29], which can be optimized at the hydrogen partial pressure of about 7.9×10^{-6} torr.

It was suggested that the decrease in the lattice constants of the ITO film is attributed to the presence of the oxygen vacancies [30]. Similar results are also reported by Honda et al. [31], indicating that the lattice constants of oxygen-deficient ITO films are smaller than the

films without the oxygen deficiency. By fitting XRD peaks, it can be found (Figure 6.1) that ITO film prepared at hydrogen partial pressure of 7.9×10^{-6} torr has a maximum diffraction angle that is related to minimum lattice constant. This indicates that the presence of hydrogen species in the sputtering gas mixture during the deposition increases the oxygen deficiency in the ITO films. From this analysis, it appears that adding hydrogen in gas mixture helps to reduce the structural stress in films and possibly increases the number of oxygen vacancies in the film. In the practical device applications, ITO films are often used in thin-film devices and coated subsequently on semiconductor films or dielectric films; as such from device point of view, ITO films with less stress in a device with multilayer configuration is more preferable.

6.1.2.3 Electrical Properties of Indium Tin Oxide

Using experimentally measured film thicknesses, the corresponding film resistivity can be calculated. The sheet resistance and resistivity of the ITO films as a function of processing condition are plotted in Figure 6.2. The figure shows that both sheet resistance and resistivity of the films increased considerably when the hydrogen partial pressure is over 1.3×10^{-5} torr. The relative minimum values of sheet resistance ($10 \text{ } \Omega/\text{square}$) and resistivity ($2.7 \times 10^{-4} \text{ } \Omega \text{ cm}$) can be obtained at the optimal hydrogen partial pressure of 7.9×10^{-6} torr.

Figure 6.3 shows the variation of Hall mobility (μ) and the number of charged electron carriers (carrier concentration, N) in the ITO films determined by Hall effect measurements. The solid square symbols represent the carrier concentration N and the circle marks correspond to the Hall mobility μ of the films prepared at different ITO depositions. The results, shown in Figure 6.3, reveal that N and μ profiles of the ITO films are quite different as a function of hydrogen partial pressure. The carrier concentration of the film increases initially with the hydrogen partial pressure, it reaches to the maximum value of 1.45×10^{21} per cm^3 at the optimal hydrogen partial pressure of 7.9×10^{-6} torr. The number of carriers in ITO film reduces when the hydrogen partial pressure increases over 7.9×10^{-6} torr. Hall

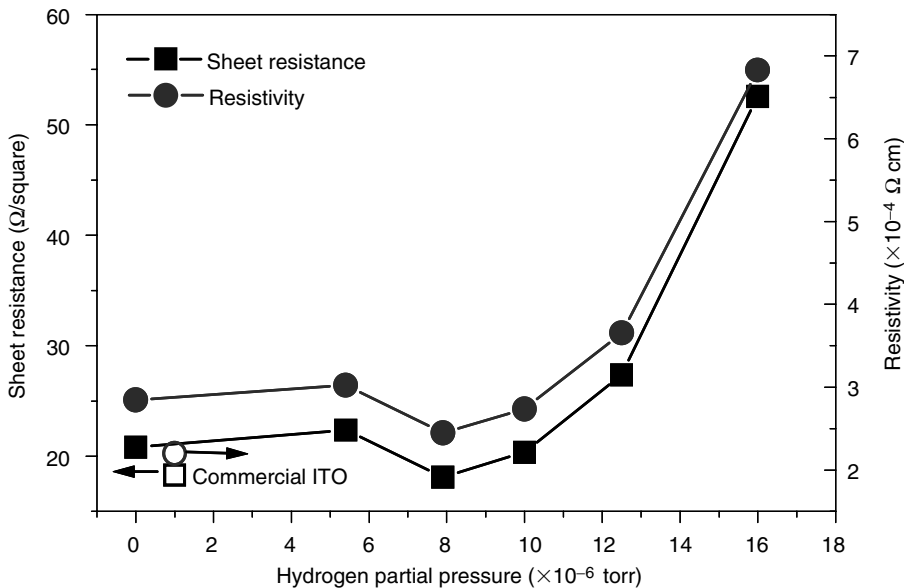


FIGURE 6.2 Sheet resistance and resistivity of ITO films as functions of hydrogen partial pressure.

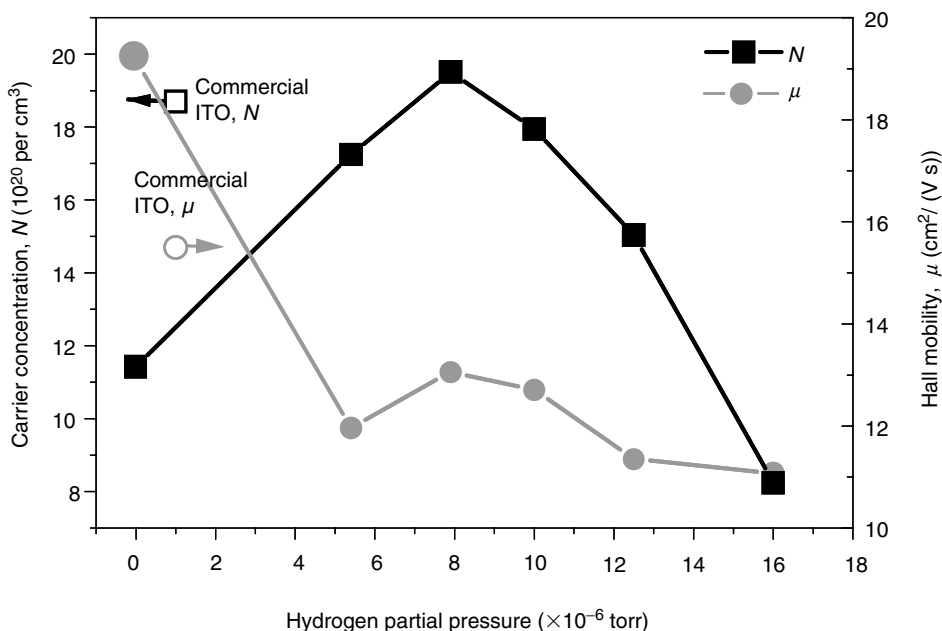


FIGURE 6.3 Carrier concentration and Hall mobility of ITO films as functions of hydrogen partial pressure.

effect measurements reveal that ITO films prepared with hydrogen–argon mixture have higher carrier concentration than that of films prepared with only Ar gas. In contrast with the variation of N at different hydrogen partial pressures, however, the carrier mobility does not change significantly. Although μ also has a relative maximum value at the hydrogen partial pressure of 7.9×10^{-6} torr, Hall effect measurements show that ITO films prepared in the presence of hydrogen generally have lower μ value than that of films fabricated with pure argon gas.

To understand better the mechanism of the carrier concentration variations in films due to the addition of hydrogen into the gas mixture of argon during sputtering processes, a secondary ion mass spectroscopy (SIMS) is used to measure the changes of relative oxygen concentrations in films prepared under different conditions. Figure 6.4 shows the typical oxygen depth profiles of an ITO film prepared with only Ar gas, and an ITO film prepared at the hydrogen partial pressure of 7.9×10^{-6} torr. To compare the relative oxygen contents in different films, the intensities of negatively charged oxygen ions in SIMS are normalized to the corresponding intensities of indium ones acquired in the same measurements. The depth of the films can be converted using sputtering time at a sputtering rate of about 0.22 nm/s. From the SIMS results, it reveals that the relative oxygen content in a film prepared with pure argon gas is higher than that of a film prepared using hydrogen–argon mixture. It indicates that the presence of hydrogen in the sputtering gas mixture of argon makes up for the oxygen lost in films. When hydrogen is added in the sputtering gas mixture, the grow flux during the magnetron sputtering includes a significant amount of energetic hydrogen species with energies over the range of 10–250 eV [32]. These active hydrogen species can remove weakly bound oxygen in the depositing films. As a consequence, the addition of hydrogen in the sputtering gas mixture shows a reducing effect on

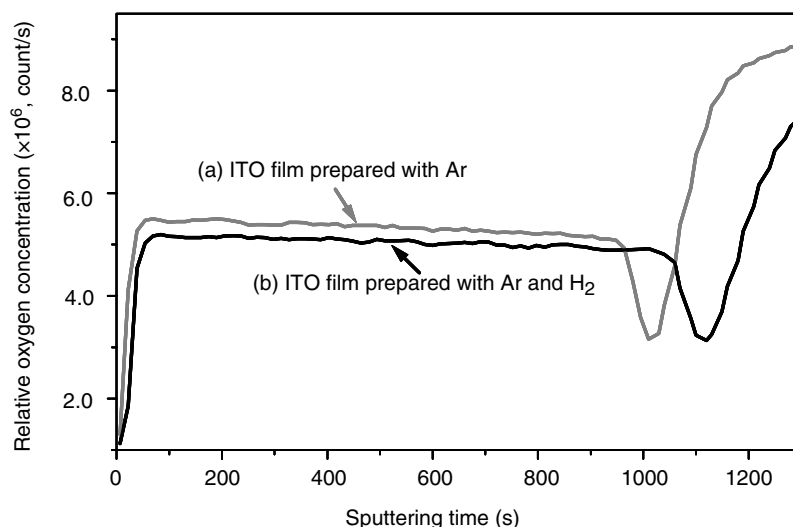


FIGURE 6.4 SIMS depth profiles of (a) an ITO film prepared with pure argon gas and (b) an ITO film prepared at hydrogen partial pressure of 7.9×10^{-6} torr.

oxide and leads to an increase in the number of oxygen vacancies in the films and hence an increase in the number of charged carriers. As the electrical conductivity is proportional to the product of charge carrier concentration and the mobility, the decrease of film resistivity is mainly due to the increase of carrier concentration in ITO films. The above analysis based on SIMS results is consistent with the previous discussions made with the XRD measurements.

6.1.2.4 Optical Properties of Indium Tin Oxide

The optical properties of ITO films prepared on glass at different hydrogen partial pressures are also characterized. The experimentally measured transmittance of the film is obtained by a double beam spectrophotometer over the wavelength ranging from 0.3 to 1.5 μm . Measured wavelength-dependent transmittance over the visible wavelength range is also used to estimate the optical energy band gap of the films. To study the effect of hydrogen partial pressure on the optical properties of the ITO films, the transmittance of the ITO films prepared at several oxygen partial pressures in oxygen–argon mixture over the same wavelength region is presented. Figure 6.5 shows the average transmittance of ITO films of 200-nm thickness measured over the visible light wavelength range of 0.4–0.8 μm , as functions of hydrogen and oxygen partial pressures. The average transmittance of ITO films prepared in oxygen–argon does not change considerably at different oxygen partial pressures. However, the average transmittance of ITO films prepared using hydrogen–argon mixture varies with the hydrogen partial pressure. ITO films with average transmittance of 89% are obtained at the optimal hydrogen partial pressure of 7.9×10^{-6} torr. The hydrogen partial pressure that produces the most transparent ITO film is almost the same as that which gives the most conducting film as shown in Figure 6.2. Optical transmittance results in Figure 6.5 together with electrical measurements suggest that 7.9×10^{-6} torr is a suitable hydrogen partial pressure for ITO film preparation under these conditions.

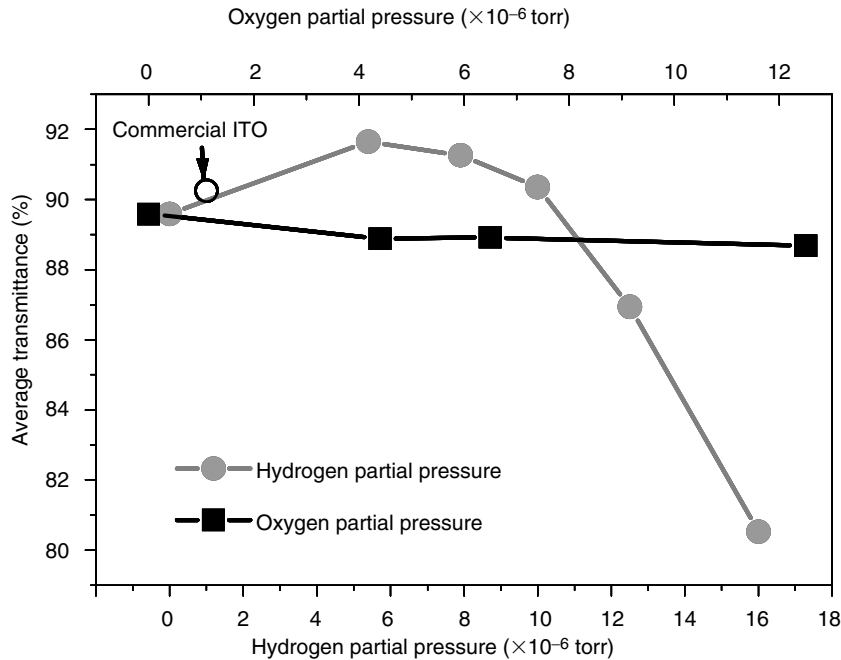


FIGURE 6.5 Average transmittance of ITO films as functions of hydrogen partial pressure, λ , and oxygen partial pressure, ν .

Figure 6.6 shows the optical band gap of ITO films prepared at different hydrogen partial pressures. In the figure both direct and indirect optical band gaps of the films are calculated. Their maximum values of 4.21 and 3.35 eV are obtained for films prepared at the hydrogen partial pressure of 7.9×10^{-6} torr. The variation of both direct and indirect optical band gaps

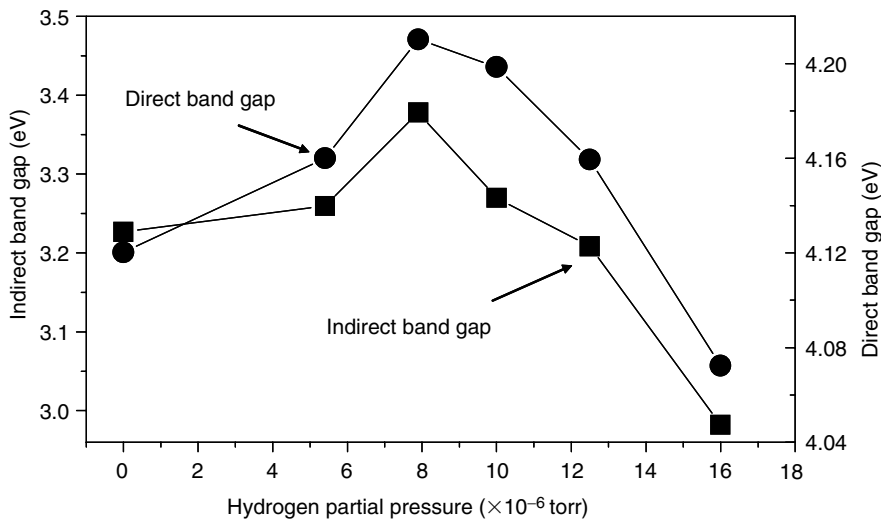


FIGURE 6.6 Calculated direct and indirect optical band gaps of ITO films prepared at different hydrogen partial pressures.

shows a similar behavior. The change in the optical band gap shown in Figure 6.6 is mainly due to the absorption edge shift in the transmittance spectrum near ultraviolet (UV) and visible wavelength regions. It is related to the change in carrier concentration in ITO films that are prepared at different hydrogen partial pressures. This is also known as Moss–Burstein shift and can be expressed as:

$$E_g - E_{g0} = \frac{(\pi\hbar)^2}{2m_r^*} \left(\frac{3N}{\pi} \right)^{2/3} \quad (6.1)$$

where E_{g0} is the intrinsic optical band gap and m_r^* is the reduced effective mass. Figure 6.7 shows a linear dependence of optical band gap on $N^{2/3}$. From the figure, the value of direct intrinsic absorption edge of about 3.75 eV is obtained by extrapolation of N to zero. Different experimental values of 2.98, 3.52, 3.55, and 3.67 eV for intrinsic absorption edges of ITO films have been reported [23,33–35]. The variation of these E_{g0} values is probably due to different deposition conditions used in the film preparations. In these previous experiments, oxidized ITO targets with different weight proportions of In_2O_3 to SnO_2 were employed. However, hydrogen was not introduced in the experiments. The intrinsic absorption edge of ITO films thus obtained is comparable with the published experimental results. The slightly higher E_{g0} value obtained from the ITO films is probably due to the usage of hydrogen–argon mixture during the film preparation. When the hydrogen partial pressure in the gas mixture is over the optimal value, the carrier concentration decreases, and the optical band gap shown in Figure 6.6 is also reduced; these observations are consistent with the variation indicated by Equation 6.1.

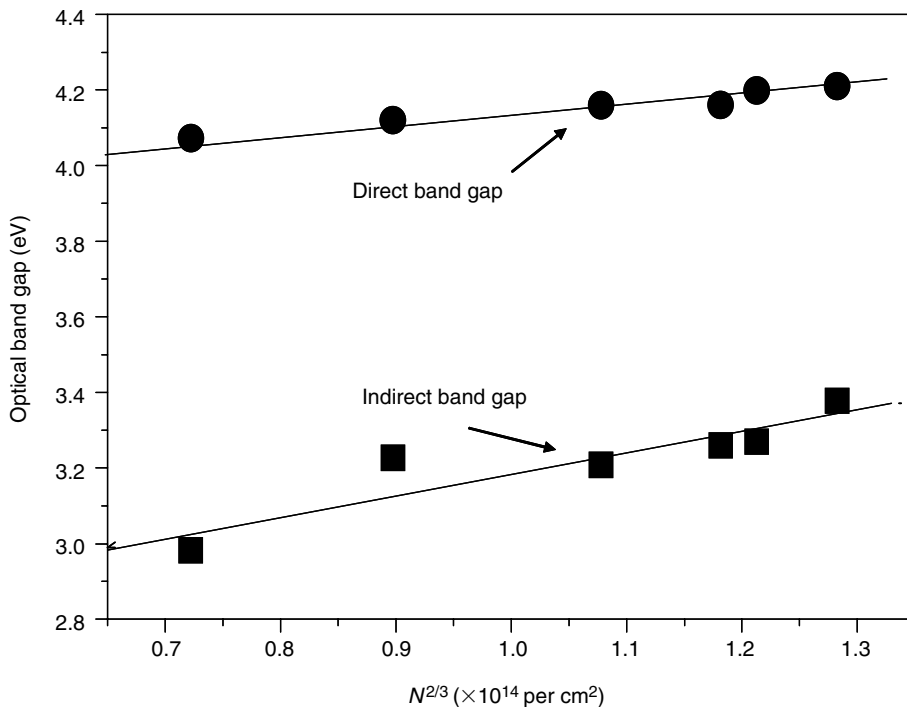


FIGURE 6.7 Optical band gaps as functions of charged carrier concentration in ITO films.

The slope of the straight line for direct band gap, shown in Figure 6.7, yields $m_r^* = 0.61 m_0$. This is in good agreement with values between 0.46 and $0.65m_0$ by previous groups [23,34,35]. The optical properties of ITO films, such as the optical band gap and the effective carrier mass, are affected mainly by the charged carrier density of the films rather than the nature of the dopant itself. Results in Figure 6.3 reveal that the primary effect of using hydrogen–argon mixture during the film deposition seems to increase the number of charge carriers in ITO film. As a consequence, the fundamental absorption edge shifts toward shorter wavelength range and the corresponding increase in the optical band gap is attributed to an increase in carrier concentration.

6.1.2.5 Indium Tin Oxide Composition and Surface Electronic Properties

Ultraviolet photoelectron spectroscopy (UPS) and x-ray photoelectron spectroscopy (XPS) are commonly used to measure the material properties and to understand the technical aspects related to the ITO surface, ITO band structure, electronic structures at ITO–organic interface, anode modification in the OLEDs. XPS peaks of $\text{In}3d_{5/2}$ and $\text{Sn}3d_{5/2}$ measured for ITO films obtained at different hydrogen partial pressures are given in Figure 6.8a and b, respectively. Typical XPS measurements show that ITO films prepared over the hydrogen partial pressure in the range of 0 to 1.6×10^{-5} torr have almost identical atomic compositions. A closer examination of the curves in Figure 6.8a and b shows that the binding energies of $\text{In}3d_{5/2}$ and $\text{Sn}3d_{5/2}$ peaks for films deposited at different hydrogen partial pressures are all at 445.2 and 487.2 eV, respectively. There are no evident shoulders observed at the high binding energy side of $\text{In}3d$ peaks, as illustrated in Figure 6.8, which could relate to the formation of $\text{In}-\text{OH}$ -like bonds in the ITO films [36]. The possible reaction between H^+ and weakly and strongly absorbed oxygen may have taken place during film growth. However, the almost identical binding energies of $\text{In}3d$ and $\text{Sn}3d$ peaks suggest that indium atoms are in the form of In_2O_3 .

XPS peaks of $\text{In}3d$ and $\text{Sn}3d$ obtained from ITO films prepared at different hydrogen partial pressures show typical ITO characteristics. However, the carrier concentration of the ITO films prepared at different hydrogen partial pressures varies considerably over the hydrogen partial pressure in the range of 0 to 5.0×10^{-5} torr. The maximum carrier concentration of 1.45×10^{21} per cm^3 is obtained at an optimal hydrogen partial pressure of 7.9×10^{-6} torr. The difference in the carrier concentration of the films is probably due to the variations of the number of oxygen vacancies in the films prepared at different hydrogen partial pressures. Meng et al. [37] suggested that the increase in the carrier concentration was not attributed to tin dopants, for instance the transition of SnO to SnO_2 , in their annealing experiments. There is no considerable change of chemical bonding energy for $\text{In}3d$ and $\text{Sn}3d$ peaks observed in the XPS measurements (Figure 6.8). This illustrates that there is no reduction of ITO to form the interstitial metallic atoms. Introduction of hydrogen in the gas mixture during RF magnetron sputtering seems only to vary the oxygen deficiency in ITO films. ITO films prepared are therefore nonstoichiometric due to the formation of oxygen vacancies in the films. At the optimal experimental conditions, ITO with a minimum resistivity of $2.7 \times 10^{-4} \Omega \text{ cm}$ and 89% of transmittance over the visible wavelength region can be achieved.

ITO is an ionically bound semiconducting oxide. Oxygen vacancies are formed relatively easily compared with covalently bound materials. ITO films prepared by RF magnetron sputtering are usually nonstoichiometric. The number of the oxygen vacancies is affected by deposition conditions such as sputtering power, substrate temperature, sputtering gas pressure, $\text{Sn}-\text{In}$ composition in target, and the gases in the mixture. Free electrons provided by tin dopants and ionized oxygen vacancy donors comprise the charge carriers for conduction.

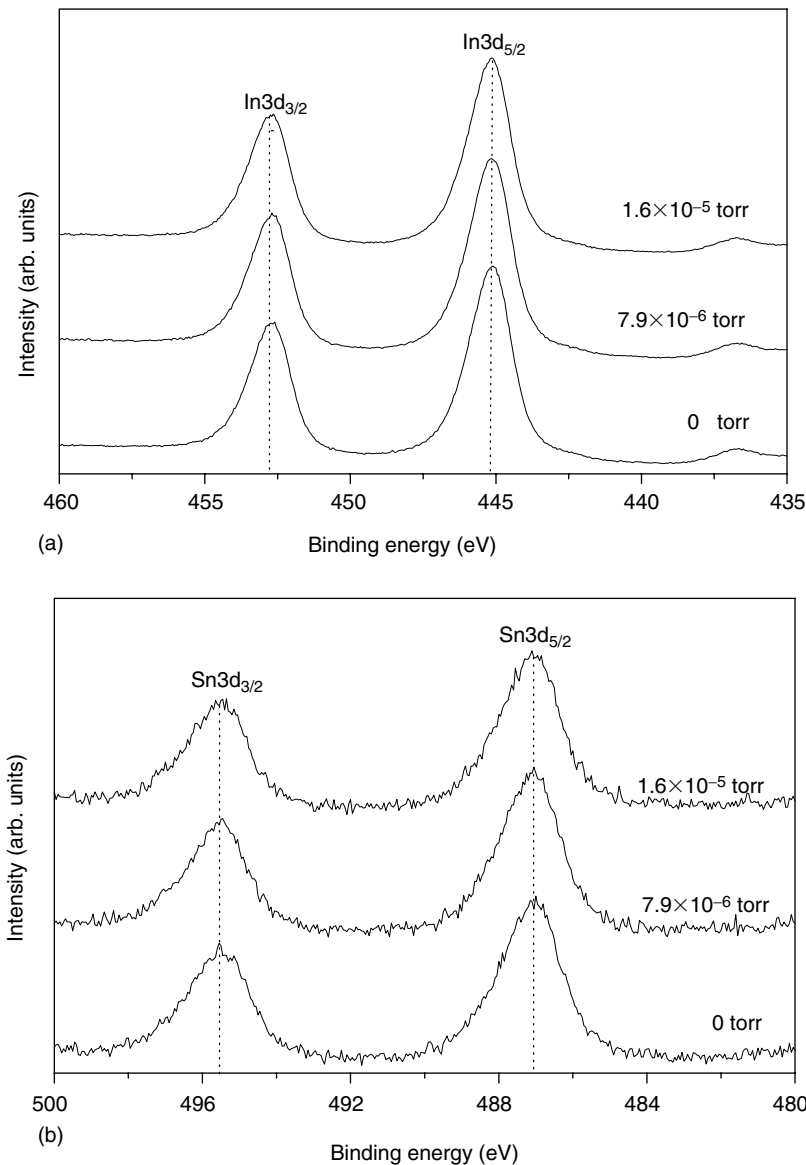


FIGURE 6.8 Comparison of typical (a) In3d and (b) Sn3d XPS peaks measured for ITO films prepared at different hydrogen partial pressures of 0, 7.9×10^{-6} , and 1.6×10^{-5} torr.

Therefore, this material has an n-type character. Banerjee and Das [38] investigated the effect of oxygen partial pressure prepared by electron beam evaporation from a hot-pressed powder of In_2O_3 , SnO_2 mixture in weight by 9:1. They found that the increase in film conductivity was due to an enhancement in Hall mobility, but the carrier concentration decreased with the oxygen partial pressure. Similar correlation between oxygen partial pressure and carrier density also was observed by Honda et al. [23]. Experimental results suggest that the improved electrical properties of ITO films made at the optimal oxygen partial pressure are due to increased carrier mobility in the film. The decrease in carrier concentration is attributed

to the dissipation of oxygen vacancies when oxygen is used in the gas mixture during the preparation. However, from the analyses made for the ITO films in the previous sections of this chapter, the Hall mobility of the films do not increase considerably at different hydrogen partial pressures. The improvement of the film conductivity can be attributed to the increase of the carrier concentration in comparison with that of ITO made without hydrogen in the gas mixture. The above analyses are consistent with the results obtained from the structural, electrical, optical, and compositional measurements made on the ITO films.

The surface electronic properties and work functions of ITO also show strong dependence on the manufacturing process and the method used to clean its surface. In many applications, such as OLEDs and solar cells, the surface electronic properties also play an important role in determining the device performance. The electronic properties at ITO-organic interfaces control the carrier injection of organic devices. In OLEDs, ITO acts as hole-injection electrode that requires a large work function to match the highest occupied molecular orbital (HOMO) of the adjacent organic material for efficient carrier injection.

The electronic properties at the ITO-organic interface are expected to affect directly the characteristics of the devices. As-grown ITO anodes have been found to be less efficient for use as a hole injector than oxygen-plasma-treated ITOs. Wu et al. [7] reported that oxygen, hydrogen, and Ar plasma treatments on the surface of ITO do not have a significant effect on the bulk properties of the ITO film. Results show that reduction in transmittance, increase in sheet resistance, and substantial changes in ITO surface morphology are due to the formation of indium-rich hillocks, and large nonuniformity of surface compositions. The improvement of OLED performance suggests that the surface electronic and morphological properties of ITO have great influence on the device performance than that of the bulk properties.

6.2 ANODE MODIFICATION FOR ENHANCING OLED PERFORMANCE

6.2.1 INDIUM TIN OXIDE SURFACE TREATMENT AND MODIFICATION

Among the many surface treatments of ITO, oxygen plasma treatment is one of the most common technique [7,39–41]. Irrespective of the complexities of various cleaning processes, which may involve ultrasonic cleaning of the ITO substrate in aqueous and organic solutions, the final and the most effective step often invokes the exposure of the precleaned ITO to either UV irradiation or oxygen plasma treatment. It has been reported that oxygen plasma treatment can effectively remove the surface carbon contamination and cause an increase in the work function of ITO [5,42]. This may then lead to a lower energetic barrier at an ITO-hole-transporting layer (HTL) interface and thereby help to enhance hole injection [43,44]. UPS and Kelvin probes are often employed to investigate the changes in the ITO work function due to different surface treatments [45,46]. It shows that an increase in the ITO work function is closely related to the increase in surface oxygen content due to oxygen plasma treatment [5,7,47,48].

ITO is a heavily doped and degenerate n-type oxide semiconductor with both Sn dopants and oxygen vacancies contributing to its conduction. The appropriate ITO surface treatments prior to the deposition of the organic layers, e.g., oxygen plasma or treatment or UV ozone irradiation, enhance the emission efficiency of OLED and improve its operating lifetime. Although the oxygen plasma treatment helps to clean the ITO surface, the removal of hydroxyl functionalities or contaminants on ITO surface does not account fully for the improvement of the OLED performance. Mason et al. [47] reported that oxidative treatments incorporated more oxygen onto the surface, and the work function correlates well with the oxygen addition. The increase in the work function is attributed to the presence of an interfacial dipole resulting from a surface rich in negatively charged oxygen. The

enhancement in OLED performance can be attributed to the presence of an interfacial dipole at ITO–HTL favoring the hole injection. Milliron et al. [43] proposed that an increase in the ITO surface dipole layer can be attributed to the oxidation of SnO_x species, which are induced by the oxygen plasma. The oxidation process only occurs near the surface region of the ITO and has less effect on the bulk of the ITO.

In parallel to a surface dipole model, a surface band bending of ITO is proposed. Yu et al. [49] reported that O_2 or NH_3 plasma results in a shift of the ITO surface Fermi level, E_F , toward the middle of the band gap, while the E_F remained unchanged in the bulk. This leads to an upward bending in the core levels near the ITO surface region. Thus the ITO work function increases, leading to a low energy barrier at the ITO–HTL interface. An oxygen plasma-induced electron-transfer process in ITO films was also proposed. Popovich et al. [50] suggested that the oxygen plasma treatment reduces the number of active electron-transfer sites at the electrode surface, possibly oxygen vacancies, resulting in slower electron-transfer kinetics.

Apart from the existing understanding of the increase in work function of ITO or the presence of an interfacial dipole layer at ITO–HTL interface due to oxygen plasma, it seems that oxygen plasma also modifies an ITO surface effectively by reducing the oxygen deficiency to produce a low-conductivity region. The improvement in OLED performance also correlates directly with a layer of low conductivity, several nanometers thick. Figure 6.9a and b shows the current density–voltage (J – V) and luminance–current density (L – J) curves for a set of identical polymer OLEDs made on ITO substrates treated by oxygen plasma at different oxygen flow rates of 0, 40, 60, and 100 sccm. At a given constant current density of 20 mA/cm^2 , the luminance and efficiency of identical devices made with oxygen plasma treatments fall within a range of 610 – 1220 cd/m^2 and 5.4 – 11.0 cd/A , respectively. These values are 560 cd/m^2 and 5.2 cd/A for the same devices fabricated on nontreated ITO anodes. In this example, the best electroluminescence (EL) performance is found in OLEDs made on an ITO anode treated with plasma using an oxygen flow rate of 60 sccm.

Figure 6.10 shows SIMS depth profiles comparing normalized relative oxygen concentration from the surfaces of a nontreated ITO surface and an ITO surface treated by oxygen plasma using an oxygen flow rate of 60 sccm. Both nontreated and treated ITO samples are covered with a 5-nm-thick lithium fluoride (LiF) capping layer before they are analyzed by a SIMS. This is to prevent any possible contamination on the ITO surfaces when the specimens are exposed to air. The LiF layer is removed by argon ion sputtering during the SIMS measurements. The changes in sheet resistance due to oxygen plasma treatments are measured using an *in situ* four-point probe. The variations in surface content are measured by *ex situ* spectroscopic analyses on the ITO surfaces. It shows clearly that the relative oxygen concentration of treated ITO surface is higher than that of untreated ITO (middle portion of Figure 6.10). Based on the sputter rate used in the measurements, it appears that oxygen plasma treatment can induce an oxygen-rich layer, a few nanometers thick, near the ITO surface. However, the precise thickness of this region is difficult to determine directly by SIMS due to the influence of the interfacial effects that occurred during argon ion sputtering. Using a four-point probe, all treated ITO films are found to have higher sheet resistance than those of nontreated ones. The increase in sheet resistance between the treated and nontreated ITO surfaces are 19, 30, and $85 \text{ } \Omega/\text{square}$ when the ITO is subjected to the plasma treatment with different oxygen flows of 40, 60, and 100 sccm, respectively. This implies that the change in sheet resistance corresponds closely with the increase in oxygen content on the treated ITO surface.

ITO is a ternary ionic-bound degenerate oxide semiconductor. Ionized oxygen vacancy donors and tin dopants govern its conductivity. In an ideal situation, free electrons can be generated from either the oxygen vacancies acting as doubly charged donors (providing two

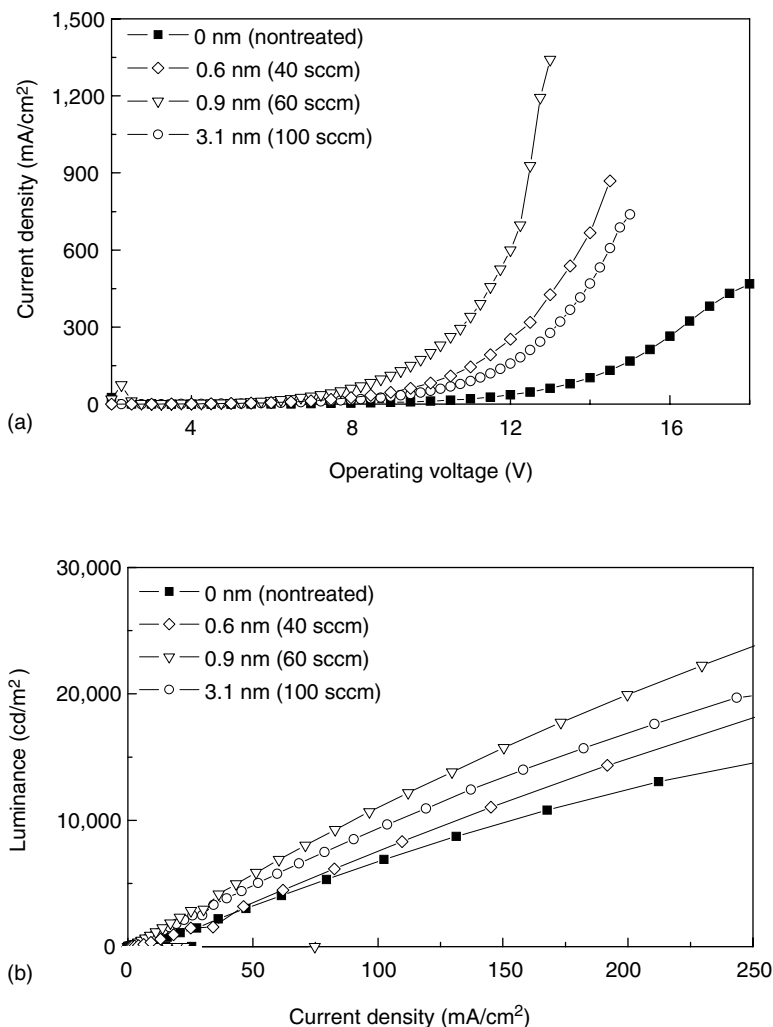


FIGURE 6.9 Current density vs. bias voltage (a) and luminance vs. current density (b) characteristics of identical devices made on ITO anodes treated under different oxygen plasma conditions.

electrons each) or the electrically active tin ionized donor on an indium site [51,52]. Excess oxidation on an ITO surface by oxygen plasma may cause dissipation of oxygen vacancies. Therefore, oxygen plasma treatment results in a decrease in the electrically active ionized donors in a region near the ITO surface leading to an overall increase in the sheet resistance as observed from the *in situ* four-point probe measurements.

By comparing the specimens with highly conducting bulk ITO, it can be proposed that the treated ITO anodes form oxygen plasma-induced low-conductivity layer near the surface. It can be portrayed using a dual-layer model. The cross-sectional views of a nontreated ITO film and an oxygen plasma-induced dual-layer anode are illustrated schematically in Figure 6.11a and b, respectively. Assuming a constant film thickness value, d , for both nontreated and treated ITOs, there is no observable thickness change found in ITO films treated under different conditions. R_0 and R_t are denoted as the sheet resistance measured for nontreated and treated ITO samples. According to the dual-layer parallel resistor model,

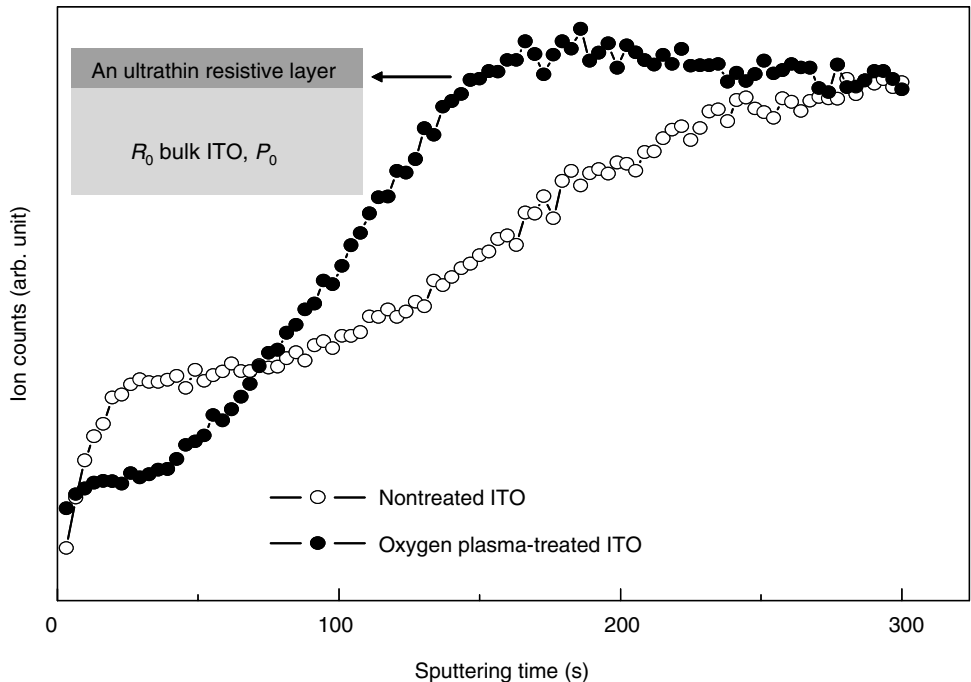


FIGURE 6.10 Comparison of SIMS depth profiles of relative oxygen concentration on the nontreated and oxygen plasma-treated ITO surfaces.

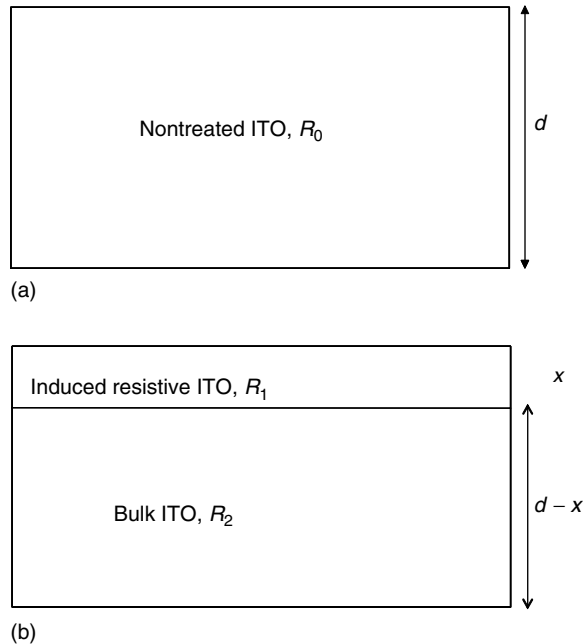


FIGURE 6.11 Schematic diagram of a nontreated ITO anode (a) and an oxygen plasma-induced dual-layer ITO anode consisting of a low-conductivity layer, x , and bulk ITO layer, $d - x$ (b).

$R_t = R_1 R_2 / (R_1 + R_2)$, where R_1 and R_2 are defined as the sheet resistances for a low-conductivity surface layer of thickness x and a conductive bulk ITO layer of thickness $d - x$ as shown in Figure 6.11b.

The sheet resistance of this oxygen-rich ITO layer can be considered to be much larger than that of the bulk ITO, i.e., $R_1 \gg R_2$. Thus, $R_t = R_1 R_2 / (R_1 + R_2)$ can be simplified as $R_t \approx R_2$. As the bulk ITO has the same electrical properties of nontreated ITO, it gives $R_0 = (1 - x/d)R_2$ or $R_0 = (1 - x/d)R_t$. For the four-point probe measurements, the ITO films with a layer thickness of approximately 15 nm are deposited on glass substrates. The nontreated thin ITO film has a sheet resistance of about 400 Ω /square. Substituting for R_0 , R_t , and d , the thickness of the oxygen plasma-induced layer, x , is estimated to be 0.6, 0.9, and 3.1 nm corresponding to increasing flow rates of oxygen. It is interesting to note that with the formation of this thin low-conductivity layer, the EL efficiencies of all OLEDs are greatly enhanced. As a consequence, oxygen plasma-treated ITO behaves somewhat similar to specimens where there is an ultrathin insulating interlayer serving as an efficient hole-injection anode in OLEDs.

Engineering electrode–organic interfaces can substantially enhance the performance of OLEDs. It is understood that the modification of the anode in OLEDs alters the internal electric field distribution resulting in changes in both hole and electron injections. The feasibility of employing surface modification to improve OLED efficiency has also been demonstrated. A variety of stable and densely ordered self-assembled monolayer (SAM) films have been deposited onto ITO surfaces [53,54]. OLEDs incorporating a SAM layer between the ITO electrode surface and HTL have been shown to have good stability and enhanced efficiencies [55,56]. These studies indicate that the surface modification is promising for the improvement of OLED devices. An ITO anode modified with a few nanometers thick interlayer for efficient operation of the OLEDs is reported [57–60]. Zhu et al. demonstrated that the presence of an ultrathin insulating interlayer at the ITO–HTL interface favors the efficient operation of the OLEDs [57].

A method of tailoring the hole–electron current balance in OLEDs by inserting an ultrathin organic tris-(8-hydroxyquinoline) aluminum (Alq_3) interlayer between the anode and the HTL has been demonstrated recently [61]. Figure 6.12a and b, respectively, shows J – V and L – J characteristics for a set of devices made on a bare ITO (shown as 0 nm in Figure 6.12), 1.0-, 2.0-, 3.0-, 4.0-, and 5.0-nm-thick Alq_3 -interlayer-modified ITOs. As is apparent from the results, there are obvious differences in J – V and L – J characteristics in devices made with different Alq_3 interlayer thicknesses. As the thickness of the Alq_3 interlayer increases, the probability of hole transport from ITO to HTL of N,N' -di(naphthalene-1-yl)- N,N' -diphenylbenzidine (NPB) decreases, leading to a weaker hole-injection process. Therefore, to achieve the same current density in the OLEDs, the applied voltage can be increased with increasing Alq_3 thickness. The results in Figure 6.12a illustrate clearly that the increase in operating voltage is not significant when the Alq_3 interlayer thickness is less than 2.0 nm. However, the required voltage increases quite substantially when a thicker Alq_3 interlayer of 3.0–5.0 nm is inserted between ITO and NPB. For instance, the voltages at a current density of 100 mA/cm^2 are 8.32, 9.10, and 9.36 V for devices made with 3.0-, 4.0-, and 5.0-nm-thick Alq_3 interlayers. This voltage is 7.52 V for the device made with a bare ITO anode. In contrast, the current density to obtain a luminance of 2000 cd/m^2 for the devices with 0-, 1.0-, 2.0-, 3.0-, 4.0-, and 5.0-nm-thick Alq_3 interlayer is 97.4, 83.4, 71.4, 68.2, 60.2, and 56.8 mA/cm^2 , respectively. It is clear that the current density decreases with an increase in the interlayer thickness. Table 6.1 is a summary of the luminous efficiency and the corresponding voltage at a current density of 100 mA/cm^2 . As the cathode contact for electron injection in all these devices is the same, the results given in Table 6.1 indicate that an organic

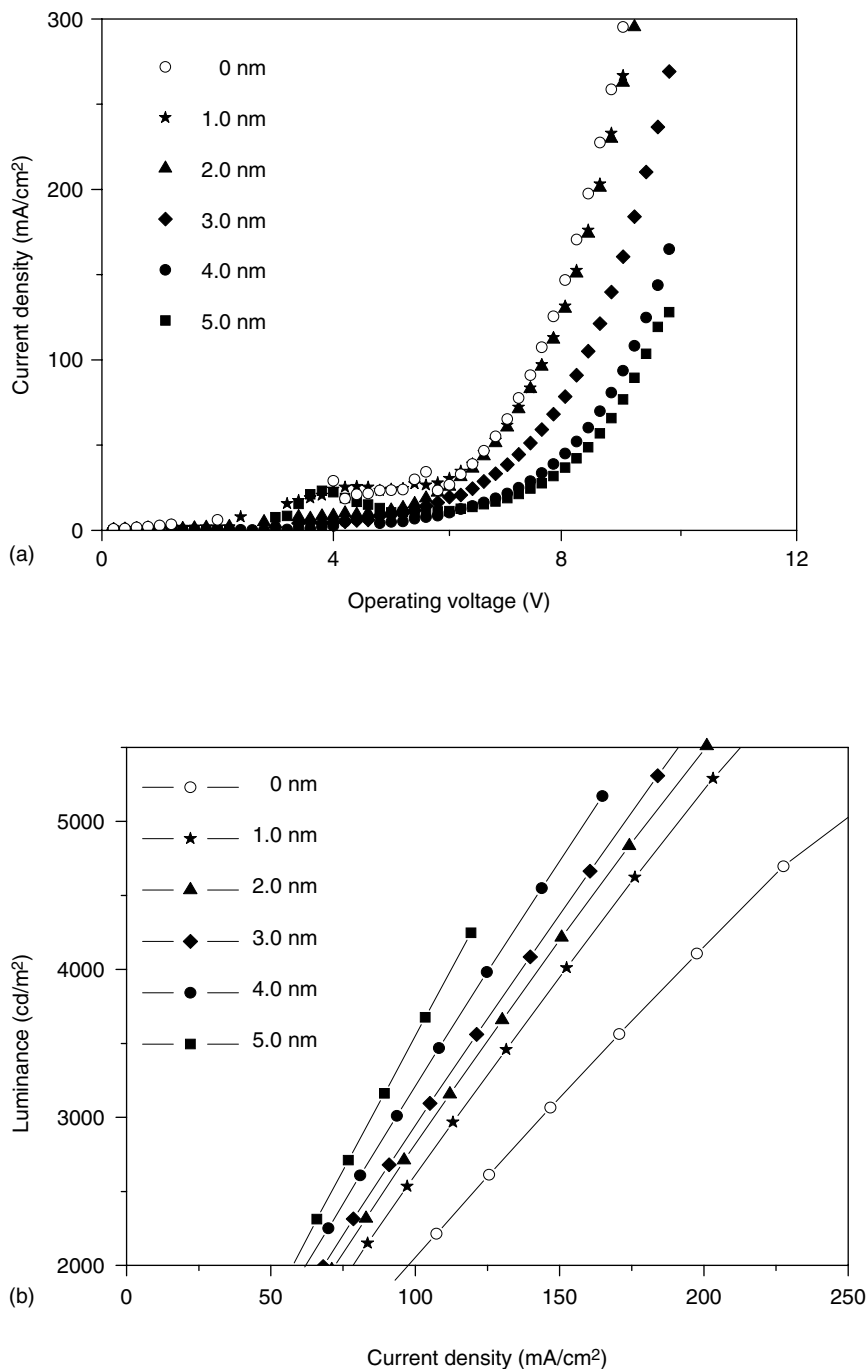


FIGURE 6.12 (a) Current density–voltage and (b) luminance–current density characteristics of OLEDs with a configuration of ITO/Alq₃ interlayer/NPB/Alq₃/Ca/Ag. The thickness of the Alq₃ interlayer was varied over a range of 0–5.0 nm.

TABLE 6.1
Operating Voltage and Corresponding Luminous Efficiency of Identical
OLEDs Made on ITO Anode with Different Alq₃ Modification Layer
Thicknesses, Measured at a Current Density of 100 mA/cm²

ITO Surface Modification Layer Thickness (nm)	Luminous Efficiency (cd/A)	Operating Voltage (V)
0	2.08	7.52
1.0	2.62	7.64
2.0	2.82	7.66
3.0	2.94	8.32
4.0	3.21	9.10
5.0	3.55	9.36

interlayer plays a role in improving the balance of electron and hole currents and hence enhancing the luminous efficiency. The improvement in current balance, which is set by the size of the barrier at the two electrodes, reveals that Alq₃ can alter the barrier height at ITO–HTL interface for carrier injection from ITO to the HTL of NPB.

The enhancement in luminous efficiency achieved by inserting an ultrathin interlayer between the ITO and NPB is mainly due to the reduction of hole injection from ITO to NPB in OLEDs. For a simple approximation, luminous efficiency (η) can be related directly to a ratio of the recombination current (J_r) to the total current density of OLEDs (J_{tot}). If one denotes the current contributions from holes and electrons in OLEDs as J_h and J_e , respectively, then the sum of hole and electron currents, $J_{\text{tot}} = J_h + J_e$, and η can be expressed as

$$\eta \approx \frac{J_r}{J_{\text{tot}}} \quad (6.2)$$

The holes are the majority charge carriers in OLEDs and the hole current is much larger than the electron current in OLEDs, that is, $J_h \gg J_e$. Thus, the total current $J_{\text{tot}} = J_h + J_e$ can be simplified as $J_{\text{tot}} \cong J_h$. Therefore, Equation 6.2 can be written as

$$\eta \approx \frac{J_r}{J_h} \quad (6.3)$$

J_r depends on the number of generated electron–hole pairs, and it is limited by the minority charge carriers in the device, in this case, the electrons. Under this simplified assumption, J_r can be regarded as a constant if every electron–hole pair decayed by emitting light. When the thickness of Alq₃ interlayer increases, fewer holes are injected into the NPB and thus J_h decreases, leading to an increase in η , as can be seen in Equation 6.3.

The values of the highest occupied molecular orbital (E_{HOMO}) for NPB and Alq₃, E_F for ITO, and the vacuum level (E_{VAC}) for each material can be deduced from the UPS measurement and are presented in Figure 6.13a and b. From Figure 6.13a, a barrier of 0.6 eV to hole injection exists at the bare ITO–NPB interface. In comparison, the barrier between the NPB and a 5.0-nm Alq₃-modified ITO increases to about 1.08 eV, as shown in Figure 6.13b. The electronic structure shown in Figure 6.13b suggests that holes are less easily transported from the anode to the NPB with the presence of an Alq₃ interlayer because the barrier to hole injection is increased. The results in Figure 6.13 explain well the differences in the J – V and L – J characteristics of OLEDs shown in Figure 6.12.

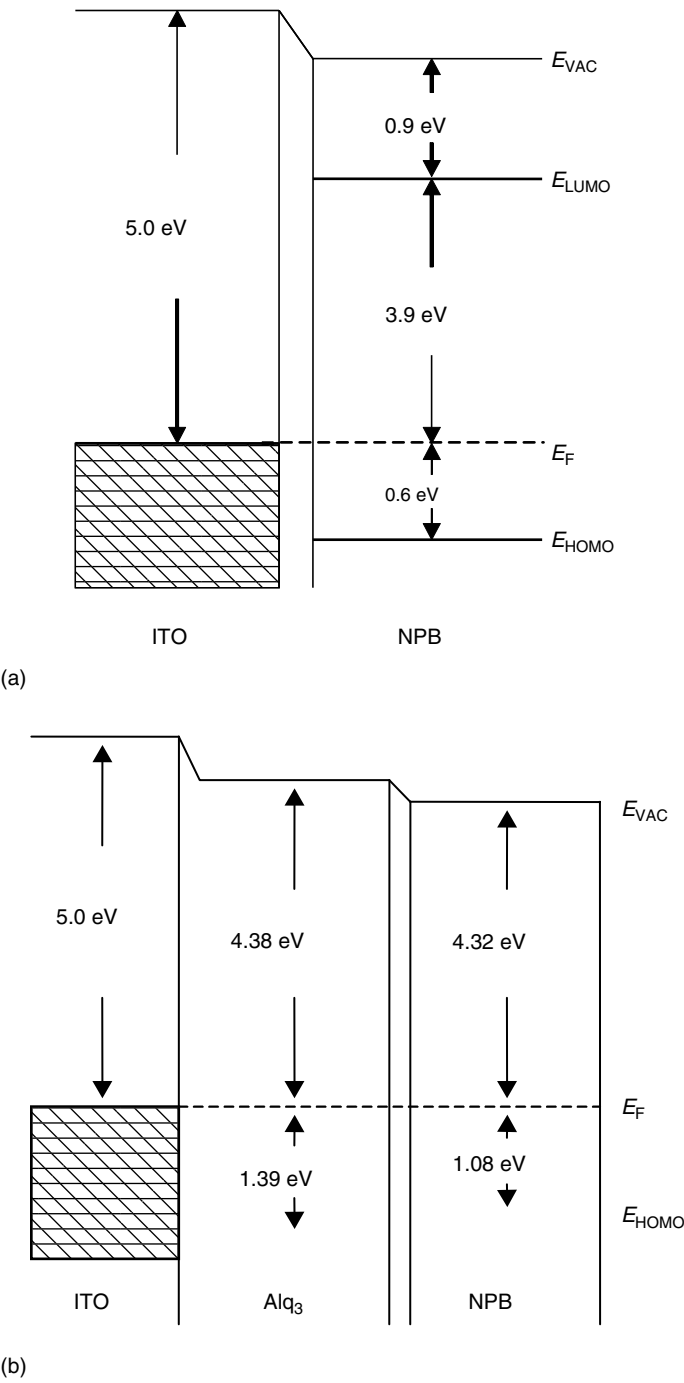


FIGURE 6.13 Interfacial electronic structures of (a) NPB on ITO and (b) NPB on an ultrathin Alq_3 -modified ITO.

The primary effect of the anode modification on the enhancement in luminous efficiency and the increased stability of OLEDs can be attributed to an improved hole–electron current balance. By choosing an interlayer with a suitable thickness of a few nanometers, anode modification enables engineering of the interface electronic properties. The above results indicate that conventional dual-layer OLEDs of ITO/NPB/Alq₃/cathode have an inherent weakness of instability that can be improved by the insertion of an ultrathin interlayer between ITO and HTL. The improvements are attributed to an improved ITO–HTL interfacial quality and a more balanced hole–electron current that enhances the OLED performance.

6.2.2 COLOR TUNING WITH GRADED INDIUM TIN OXIDE THICKNESS

OLED arrays have been used in multicolor and full color image display devices. An image display includes an array of light-emitting pixels. To achieve full color OLED arrays, it is conventional to deposit three subpixels that are capable of emitting light in the red (R), green (G), and blue (B) regions of the visible spectrum, containing specific organic emissive materials for each color to form a pixel. Each subpixel is defined by an OLED. The available techniques for depositing different color layers include inkjet printing, screen printing, spin-coating, thermal evaporation, etc. The organic emissive materials for producing different colors have different life spans. Thus, to ensure proper color mixtures and tones, complicated thin-film transistor arrays are required for the display devices to compensate for the variations in intensity and hue emitted from the subpixels.

The variable or multicolor OLEDs can also be formed using an organic microcavity structure, in which single emissive materials can be used to generate multicolor images, including full color images. The microcavity OLED architecture comprises a stack of organic layers confined between a top electrode and a bottom electrode. The top and the bottom electrodes can be either metallic reflectors or distributed Bragg reflectors. The top and bottom electrodes can be relatively transparent or opaque depending on whether the OLED structure is a top-emitting OLED or a bottom-emitting OLED. By this arrangement, the color can be tuned by varying the thickness of the microcavity length. A multicolor or even full color pixelated OLED display can also be fabricated using the same concept, e.g., a multicolor or full color pixelated display can be produced by forming an array of OLED structures having microcavities on a substrate. The thickness of the transparent conducting or emissive organic layers in the OLED structures can be varied across the substrate surface so as to achieve color tuning.

Figure 6.14 illustrates an OLED microcavity structure that comprises a stack of organic layers for providing EL, an upper electrode, and a bottom bilayer electrode of metal–transparent conductive layer. The thickness of the transparent conductive layer (e.g., ITO) in the OLED structures can be varied across the substrate surface so as to achieve color tuning. One typical structure of the devices is: glass/Ag/ITO (with a graded film

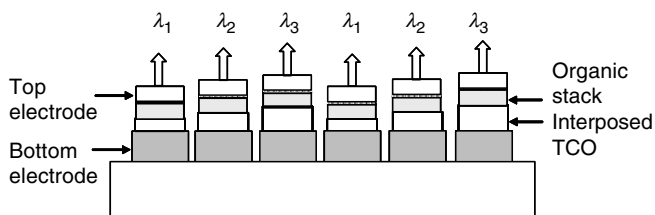


FIGURE 6.14 A cross-sectional view of a multicolor or full color pixelated display produced by forming an array of OLED structures having microcavities on a substrate. The thickness of the interposed transparent conducting layer in the OLED structures is varied across the substrate surface so as to achieve color tuning, e.g., emitting light with different wavelengths of λ_1 , λ_2 , and λ_3 , respectively.

thickness)/HTL/EL/semitransparent cathode. If a top-emitting OLED architecture is used, as shown in Figure 6.14, the upper electrode is a semitransparent cathode and the bottom anode can be formed using a metal–TCO bilayer. In this example, the microcavity structure is defined by the upper semitransparent cathode and the metal–TCO bilayer anode formed on the substrate. The shape of the EL spectra of the devices and efficiency enhancement can be achieved by adjusting the thickness of interposed-ITO layer. An array of the microcavity OLEDs illustrated in Figure 6.14 enables achieving multicolor or full color pixelated display using single organic electroluminescent materials.

Color tuning with graded ITO thickness for achieving multicolor OLED array is developed. To further improve the performance of the top-emitting OLED, a bilayer reflective anode of a metal–ITO is used for hole injection in the top-emitting OLEDs. In the bilayer anode, the metal layer serves as a mirror to reflect the light to the upper semitransparent cathode. Different anode reflectors of Ag/ITO, Cr/ITO, and Ag:Cr/ITO for top-emitting OLEDs are applied. The results show that the identical top-emitting OLEDs made with different reflective anodes have very similar current density–voltage characteristics. This implies that the mirror does not influence the current density–voltage characteristic of the top-emitting OLEDs, as the hole-injection properties at anode–HTL are essentially the same. In the actual device application, however, the top-emitting OLEDs using Ag:Cr/ITO reflective anode have better device durability in comparison with those made with Ag/ITO and Cr/ITO reflective anodes. An improved performance for top-emitting OLEDs having Ag:Cr/ITO is probably attributed to a preferred combination of high reflectance of Ag and a good adhesion at the glass and metal interface.

The emission color of above top-emitting OLEDs can be tuned by varying the thickness of either organic layers or TCO. To achieve a desired microcavity length using uniform organic layer arrangement and an easy fabrication route for pixelated OLEDs, the thickness of ITO can be varied by controlling the film deposition time or dry etching condition. One typical structure of a polymer top-emitting OLED microcavity is [61]: glass/metal (300 nm)/ITO (50 nm)/PEDOT (80 nm)/ph-PPV (80 nm)/semitransparent cathode.

In this example, a layer of Cr:Ag is used as a metal reflector. EL peaks measured for the above top-emitting OLEDs exhibit a wide wavelength shift from 547 to 655 nm as the ITO thickness is varied from 20 to 175 nm. Figure 6.15a shows the normalized EL spectra measured for a set of devices with an identical organic layer structure except for a variation in ITO thicknesses. The photographs of the emitting devices, illustrated on the top of the curves in Figure 6.15a, show EL output with different colors. The variation in color is attributed to the formation of an optical microcavity when embedding an organic stack between a bilayer anode of metal–ITO anode and a semitransparent cathode. Figure 6.15b is a photograph of an array of top-emitting OLEDs emitting variable colors using single emissive material of phenyl substituted poly(*p*-phenylene vinylene) (Ph-PPV).

Figure 6.16 illustrates the correlation between the graded ITO thickness and the EL peak position. The EL peak of the device shows a clear blue shift from 586 to 547 nm as the thickness of the interposed ITO increases from 20 to 65 nm. Likewise, there is a blue shift in EL spectra from 547 to 655 nm when the ITO layer thickness increases from 65 to 175 nm. It demonstrates an easier device fabrication route for multicolor OLED displays using an anode template with a graded ITO thickness.

The electroluminescent devices with optical microcavity structures offer a promising means to achieve the higher performance organic EL diodes that exhibit very high luminance and can be driven with low dc voltages. The OLED devices with optical microcavity structure offer the possibility to control the spectral properties of emission. By replacing the ITO electrode with highly reflective mirrors, a Fabry–Perot microcavity can be introduced into usual thin-film electroluminescent diodes. In recent years, planar microcavity structures have been used to improve the performance of OLEDs. The emitting layer in organic microcavity

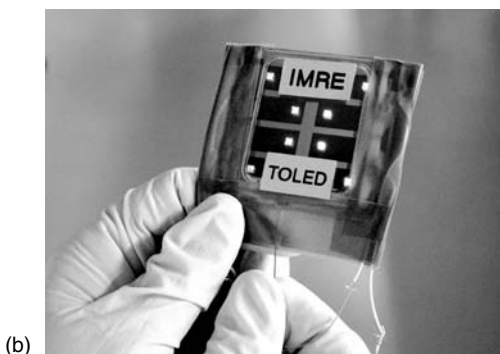
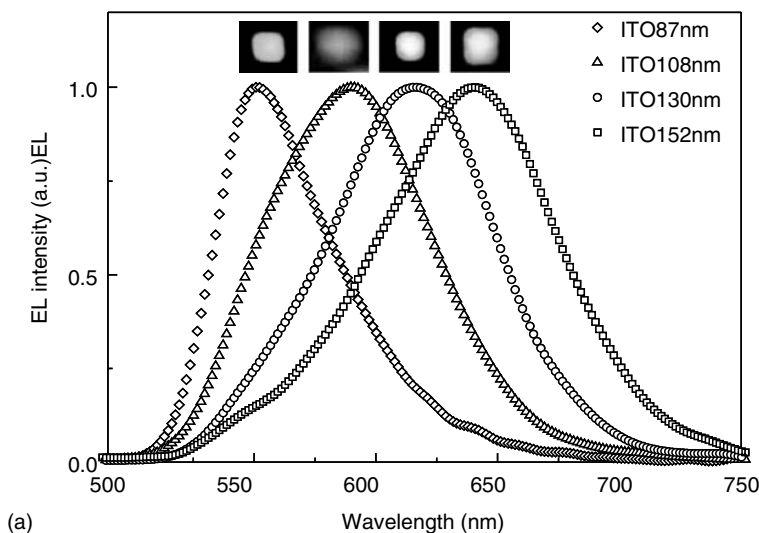


FIGURE 6.15 (a) EL spectra of a set of structurally identical OLEDs having a bilayer anode of metal/ITO. The inset pictures are the actual photographs taken for the microcavity OLEDs demonstrating the color tuning with graded ITO thickness. (b) Top-emitting OLEDs with microcavity architectures to emit variable color and to enhance the light output using single emissive material.

devices is embedded between a transparent electrode and a highly reflective distributed Bragg reflector or a quarter wavelength stack leading to strong modulation of the emission spectrum and angular dependence [61,62]. In some applications, the microcavity effects are desired to achieve directionality and color saturation.

6.2.3 NON-INDIUM TIN OXIDE ANODE FOR OLEDs

ITO has been widely used in flat panel displays including LCDs, plasma displays, and OLEDs. The growth in production of flat screen televisions has led to a doubling in demand for ITO materials. The shortage in indium resources worries the fast growing display industry and creates a need for the development of an efficient solution for low-cost ITO alternatives. AZO is a possible ITO alternative due to its unique optical and electrical characteristics. AZO thin films also are much cheaper compared to ITO and have good potential for application in flat panel displays. The optically transparent and electrically conducting AZO films can be prepared by RF or dc magnetron sputtering technique. Figure 6.17 is a typical atomic

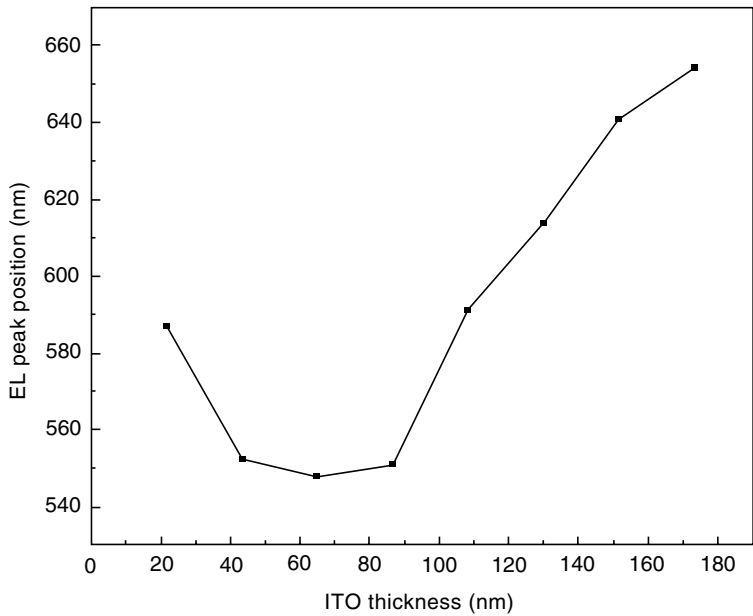


FIGURE 6.16 The measured EL peak position as a function of the ITO thickness.

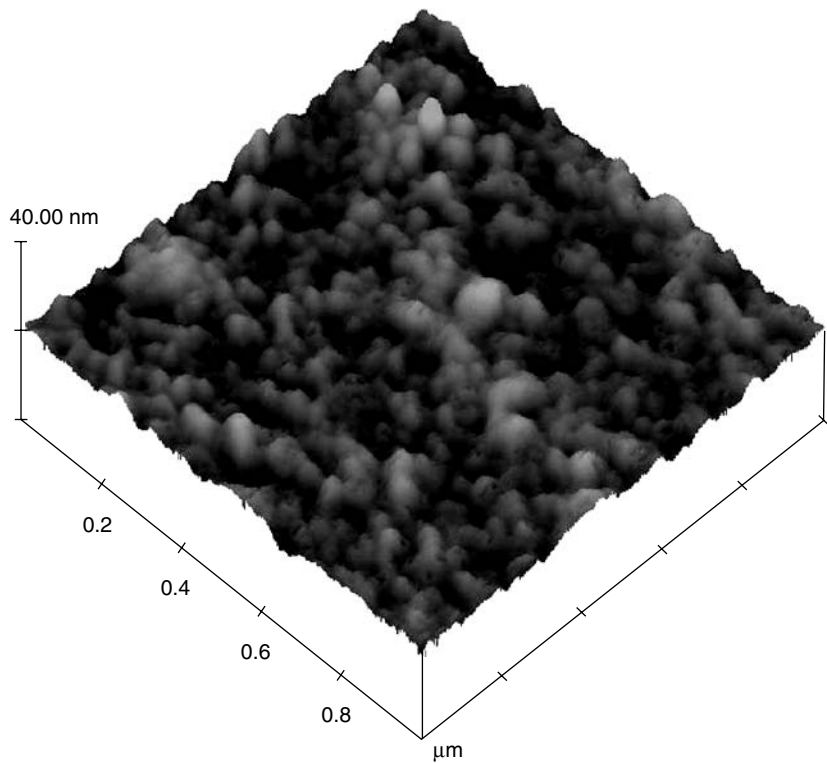


FIGURE 6.17 AFM image of an AZO film prepared for OLEDs.

force microscopic (AFM) image taken for an AZO film prepared for OLEDs. A 200-nm thick AZO film with a root mean square roughness of ~ 2 nm, an average transmittance of 83% in the visible wavelength region, and a sheet resistance of $\sim 30 \Omega/\text{square}$ can be obtained at a low processing temperature. The feasibility of using other doped ZnO thin films and highly conducting polymers as anodes for OLEDs have also been demonstrated recently [63–65].

The J – V , L – V , and E – V characteristics, measured for the OLEDs made with a commercial ITO anode and an AZO anode are plotted in Figure 6.18a and b, respectively. The current density measured for an OLED with an AZO anode is lower than that obtained for a device made with an ITO anode at the same operating voltage. A slight high turn-on voltage observed in the OLED using an AZO anode is attributed to its lower work function compared

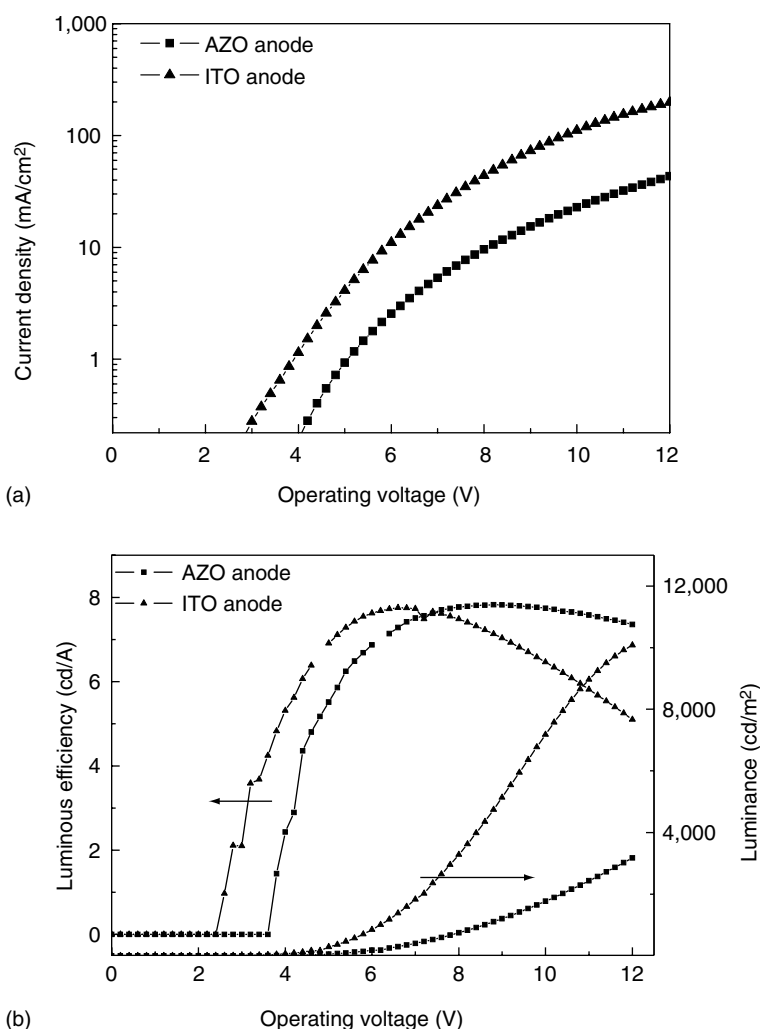


FIGURE 6.18 Current density–voltage, luminance–voltage, and luminous efficiency–voltage characteristics measured for the OLEDs made with an AZO anode and an ITO anode.

to that of the ITO material. This suggests that an anode modification for AZO is required to improve its function as an efficient anode for OLEDs. The electroluminescent efficiency of the OLEDs made with AZO anode is comparable to that of identical devices made with the commercial ITO anode. Although AZO is not treated specially in this case, the initial results demonstrate its potential OLED applications.

Other possible ITO alternatives that can be made relatively transparent for bottom-emitting OLED or nontransparent for top-emitting OLED are thin films of high-work function metals and alloys. The metallic materials including gold, silver, nickel, and their oxides have been explored to replace ITO for OLEDs. Some high-work function metals or their oxides (e.g., silver or nickel oxide) may have a work function value comparable or greater than that of ITO, however they are not satisfied for the requirements of the anode due to the presence of a large dipole barrier at the metal–organic interface. Such a contact usually induces an increase in the hole-injection barrier and thereby decreases the hole-injection efficiency. It has been demonstrated that a silver layer modified with an ultrathin plasma-polymerized hydrocarbon film (CF_x) can be used as an effective anode to enhance hole injection. The top-emitting OLEDs made with Ag/CF_x anode show a maximum EL efficiency of 4.4 cd/A, which is greater than that of a conventional bottom-emitting OLED on glass [61,66].

6.3 ELECTRODE FOR FLEXIBLE OLEDs

6.3.1 INDIUM TIN OXIDE ANODE ON FLEXIBLE SUBSTRATES

The demand for more user-friendly displays is propelling efforts to produce head-worn and hand-held devices that are flexible, lighter, more cost-effective, and more environmentally benign than those presently available. Flexible thin-film displays enable the production of a wide range of entertainment-related, wireless, wearable computing, and network-enabled devices. The display of the future requires that it should be thin in physical dimension, small and large formats, flexible, and full color at a low cost. These demands are sorely lacking in today's display products and technologies such as the plasma display and LCD technologies. OLEDs have the potential to replace LCDs as the dominant flat panel displays. This is because OLEDs have high visibility by self-luminescence, do not require backlighting, and can be fabricated into lightweight, thin, and flexible displays. The OLED stands out as a promising technology that can deliver the above challenging requirements.

Next generation flexible displays are commercially competitive due to their low power consumption, high contrast, lightweight, and flexibility. The use of thin, flexible substrates in OLEDs will significantly reduce the weight of flat panel displays and provide the ability to bend or roll a display into any desired shape. To date, much effort has been focused on fabricating OLEDs on various flexible substrates [67–71]. However, the polymeric flexible substrates, such as polyester, polyethylene terephthalate (PET) are not compatible with high-temperature plasma process. Usually, a processing temperature of above 200°C is required for preparing ITO films with low electrical resistivity and high optical transparency in the visible wavelength region. ITO films formed at a processing temperature below 200°C often have relatively higher resistivity and lower optical transparency than the films prepared at a high substrate temperature. In the application of organic electronics, however, it is often required to coat a layer of TCO on the plastic substrates or the active organic electroluminescent materials that are not compatible with a high processing temperature. The emerging of flexible OLEDs creates a need for the development of low-temperature processing

high-performance ITO film on plastic or other flexible substrates. Therefore, the development of high optical transparency and electrical conductivity ITO at a low processing temperature is of practical importance.

An argon–hydrogen gas mixture has been employed for the deposition of high-quality ITO on an aluminum-laminated PET substrate (Al-PET) and polymer-reinforced ultrathin flexible glass sheet at a low processing temperature using RF magnetron sputtering. The substrates are not heated during or after the film deposition. The actual substrate temperature, which can be raised due to the plasma process during the film deposition, is less than $60 \pm 5^\circ\text{C}$. Sputtering power is kept constant at 100 W. The base pressure in the sputtering system is approximately 2.0×10^{-4} Pa. The hydrogen partial pressure is varied from 1.0 to 4.0×10^{-3} Pa to modulate and optimize the properties of the ITO films. The use of a hydrogen–argon gas mixture enables a broader process window for preparation of the ITO films having high optical transparency and high conductivity [13,72], e.g., a 130-nm-thick ITO film with a sheet resistance of $\sim 25 \pm 2 \Omega/\text{square}$ and an optical transparency of 80% in the visible light range can be fabricated at a substrate temperature of 60°C . The transmittance spectra as a function of wavelength over the range of 300–800 nm measured for a bare PET substrate and a 130-nm-thick ITO-coated PET are shown in Figure 6.19. The ITO film on polymer-reinforced ultrathin flexible glass sheet also has similar optical and electrical properties.

The typical AFM images generated for bare PET, PET with an acrylic layer, and a 130-nm-thick ITO film on an acrylic-layer-coated PET are shown in Figure 6.20a through c, respectively. The surface of bare PET has root mean square (rms) roughness of $\sim 6.0 \pm 0.1$ nm. PET with an acrylic layer has a much lower rms roughness of $\sim 0.35 \pm 0.1$ nm. It shows clearly that the ITO-coated PET foil thus prepared has a very smooth surface with an rms roughness of $\sim 0.37 \pm 0.1$ nm, which is suitable for OLED fabrication. It reveals that the presence of an acrylic layer improves the adhesion between the anode contact and the substrate when subjected to bending as a function of number of cycles from flat to a fixed radius of curvature 12.5 mm. The response of 10,000 cycles of Al-PET/anode to bending shows that there are more than 5% of anode layer delaminated from the substrate, but no

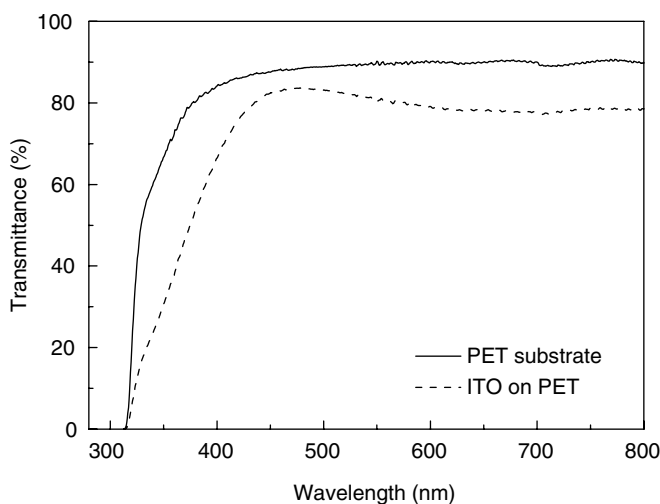


FIGURE 6.19 Wavelength-dependent transmittance of a 130-nm-thick ITO film on an acrylic-layer-coated PET substrate.

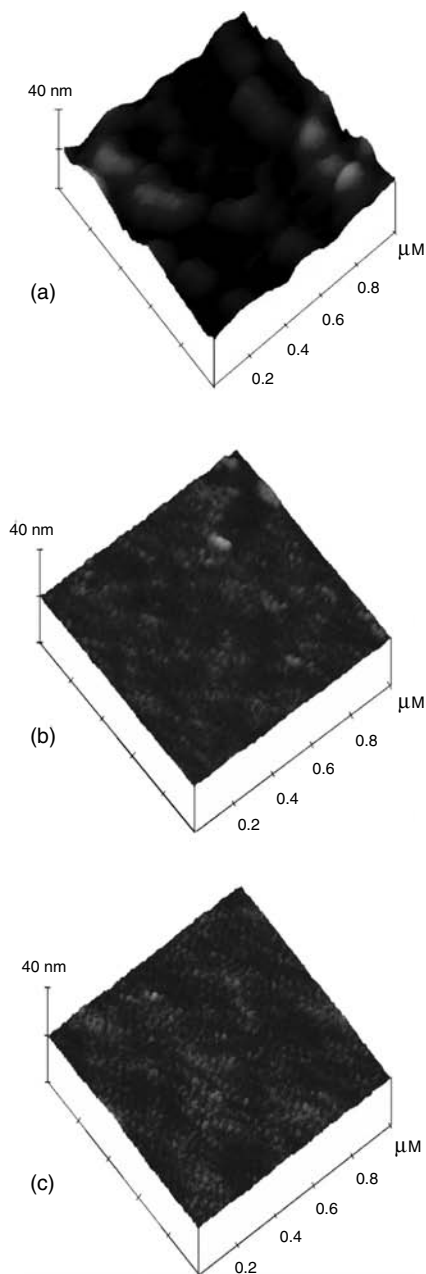


FIGURE 6.20 AFM images of bare PET (a), PET with an acrylic layer (b), and a 130-nm-thick ITO film on an acrylic-layer-coated PET (c).

anode delamination can be observed for Al-PET/acrylic layer/anode after the same bending test. This is consistent with the adhesion analyses made for ITO–polymer substrate, which shows an enhancement of the adhesion between the oxide layer and the polymer substrate through an interfacial modification [61].

6.3.2 OLEDs ON POLYMER-REINFORCED ULTRATHIN GLASS SHEETS

The ultrathin glass sheets with reinforced polymer coatings are suitable for OLED displays with preformed, curved, or conformed shapes. In comparison to the bare ultrathin glass substrate, the robustness of polymer-reinforced ultrathin flexible glass sheets is improved significantly. The response of 1000 cycles of reinforced ultrathin glass to bending shows that there is more than 95% of flexible glass sheet passing 30 mm or higher compression; this is equivalent to a minimum radius of curvature of 28 mm or smaller. The reinforcement of polymer layer helps to distribute evenly the stress that is applied to the ultrathin glass. Further observation shows that the reinforcement polymer layer helps to repair some of the imperfections along the edges and corners of the glass sheet that may be induced or formed during the substrate cutting or preparation. The cracks originated and propagated from the imperfection from the edges and the corners of the flexible glass sheets are the main reasons that cause substrate breakage. In addition to the top reinforcement coating, the edges of the substrates can also be reinforced using the same technique. This is done by applying the reinforcement polymer at the glass edges and the corners after the top reinforcement polymer is coated. The reinforcement polymer layer covers the imperfections so that the cracks are not able to propagate further during the OLED fabrication process.

Figure 6.21a through c shows the J - V , L - V , and E - V characteristics of the OLEDs. The solid triangle and open circle symbols represent device characteristics measured from a typical OLED made with the low-temperature ITO on polymer-reinforced ultrathin flexible glass sheet and a control device made with a commercial ITO-coated 1.1-mm glass substrate, respectively. A maximum EL efficiency of ~ 4.1 cd/A at an operating voltage of 4 V is obtained. The experimentally measured OLED characteristics, as shown in Figure 6.21, indicate that the EL performance of the OLEDs made with low-temperature ITO-coated flexible glass sheets is comparable to that of an identical device made with the commercial ITO-coated rigid glass substrate.

6.3.3 TOP-EMITTING OLEDs ON AL-LAMINATED PLASTIC FOILS

The present OLED technologies employ rigid substrates, such as glass, but flexible device structures are extremely promising for future applications. Substrate materials are essential and a prerequisite for meeting cost, performance, reliability, and manufacturing goals for flexible displays. Over the past few years, stainless steel foil [66], ultrathin glass sheet [68], and a variety of plastic films [69,70] have been considered as possible substrate choices for flexible OLED displays. Stainless steel foil has very good barrier properties but is hard to handle multiple bends. Ultrathin glass sheet with reinforced polymer coating [73] can be suitable for OLED displays with preformed, curved, or conformed shapes, but it has limited flexibility in use. Highly flexible plastic substrates, e.g., PET and polyethylene naphthalate, have also been used for flexible OLEDs. The flexible OLEDs made on ITO-coated PET substrate have been tested under different mechanical stresses and no significant deterioration in the device performance is observed when they are flexed at various bending radii [71]. However, these flexible OLEDs have very short lifetimes because plastics exhibit low resistance to moisture and oxygen. The development of plastic substrates with an effective barrier against the oxygen and moisture has to be achieved before this simple vision of flexible OLEDs can become a reality [74].

It is known that most metals possess lower gas permeability than plastics by 6–8 orders of magnitude. An unbreakable and lightweight thin stainless steel foil substrate has been used for flexible OLEDs [75]. Therefore, a several micrometers thick metal layer can serve as a highly effective barrier to minimize the permeation of oxygen and moisture. Hence, the

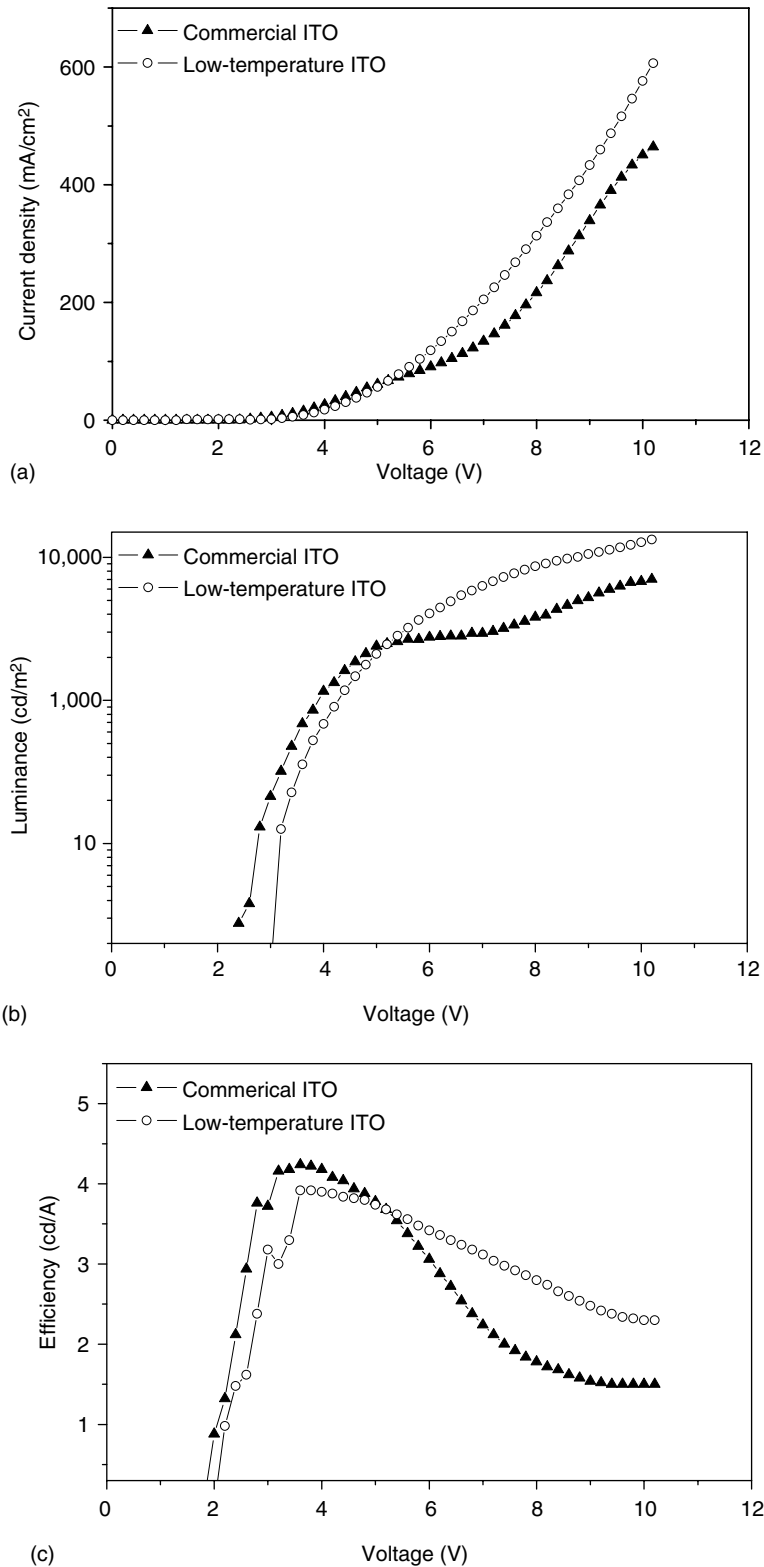


FIGURE 6.21 $J-V$ (a), $L-V$ (b), and $E-V$ (c) characteristics measured for OLEDs made with a commercial ITO-coated 1.1-mm rigid glass substrate and a low-temperature ITO-coated reinforced ultrathin glass sheet.

combination of plastic-metal materials is extremely promising for flexible OLED applications. The flexible substrate consists of a plastic layer laminated onto or coated with a metal layer could be one of the possible solutions for flexible OLEDs. For example, Al-PET foil has very good mechanical flexibility and superior barrier properties. This substrate has the potential to meet permeability standards in excess of the most demanding display requirements of $\sim 10^{-6}$ g/m² day [71]. The robustness of this substrate is also very high. A flexible OLED using Al-PET substrate may provide a cost-effective approach for mass production, such as roll-to-roll processing, which is a widely used industrial process.

A flexible polymer OLED using top-emitting OLED architecture has been developed recently. The concept of the flexible OLED design is based on an integration of top-emitting OLED on an Al-PET foil. Bilayer anode of Ag/ITO or Ag/CF_x and an upper semitransparent cathode are used in the top-emitting polymer OLEDs. Poly(styrene sulfonate)-doped poly(3,4-ethylene dioxythiophene) (PEDOT) is used as a HTL. The light-emitting polymer used is Ph-PPV. The resulting flexible polymer OLEDs exhibit a luminous efficiency of 4.56 cd/A at an operating voltage of 7.5 V.

The surface of a 0.1-mm-thick Al-PET film is precoated with a UV-curable acrylic layer to improve the smoothness of the Al-PET surface and the adhesion between the anode and the substrate. A 200-nm-thick Ag electrode is deposited on the flexible substrate through a shadow mask with an array of 2×2 mm openings by thermal evaporation. The silver contact is then covered by a 130-nm-thick ITO film or modified by a 0.3-nm-thick plasma-polymerized CF_x film to form a bilayer anode of Ag/ITO or Ag/CF_x for improving the carrier injection properties in OLEDs. High-performance low-temperature ITO with a sheet resistance of 25 Ω/square and an rms roughness of ~ 1 nm is deposited on Ag surface. Cross-sectional views of a control device on glass and top-emitting OLEDs formed on an Al-PET substrate with bilayer anodes of Ag/ITO and Ag/CF_x are shown in Figure 6.22a through c. The control device has a similar layer structure of glass/Ag/ITO (130 nm)/PEDOT (80 nm)/PPV (80 nm)/semitransparent cathode.

The experimental J - V and L - V characteristics measured for two top-emitting OLEDs with a configuration of Ag (200 nm)/ITO (130 nm)/PEDOT (80 nm)/ph-PPV (80 nm)/semitransparent cathode on an Al-PET foil (open circles) and on a glass substrate (closed circles) are plotted in Figure 6.23. The top-emitting OLEDs with the same architecture but made on flexible Al-PET foil and a rigid glass have almost identical device performance, which indicates the validity of the bilayer anode for the top-emitting OLEDs. For instance, the current density at 10 V is 236.4 and 243.4 mA/cm² for top-emitting polymer OLEDs on an Al-PET foil and a glass substrate, respectively.

It is believed that the escape possibility of the light trapped by ITO is quite low as the output coupling efficiency of the OLEDs is about $\sim 20\%$ due to the critical angle of total reflection within device [76]. However, this is evitable by replacing ITO with a metallic anode so that the light emitted in the direction toward the anode can be fully reflected back to the upper semitransparent cathode. In contrast to the success in forming a semitransparent cathode on an active layer [66,77], the use of Ag anode in an OLED usually results in a poor device performance due to the existence of a large barrier for the hole injection. Recently, Li et al. [78] demonstrated that the hole injection can be significantly enhanced by inserting a CF_x film between Ag and the organic film, which provides the feasibility to form an ITO-free OLED using bilayer anode of Ag/CF_x. The electrical and optical characteristics of the corresponding device with a configuration of Ag (200 nm)/CF_x (0.3 nm)/Ph-PPV (110 nm)/semitransparent cathode on an Al-PET substrate (Figure 6.22c) are also plotted in Figure 6.23 (open diamonds). In comparison with the top-emitting OLED made with a bilayer anode of Ag/ITO, the top-emitting OLED made with a Ph-PPV layer on CF_x-modified Ag anode requires a slightly higher operating voltage to achieve a similar current

Upper semitransparent cathode
Emissive layer (Ph-PPV)
Hole-transporting layer (PEDOT)
Bottom ITO anode
Mirror
Glass

(a)

Upper semitransparent cathode
Emissive layer (Ph-PPV)
Hole-transporting layer (PEDOT)
Bottom ITO anode
Mirror
Acrylic interlayer
Al-laminated plastic foil

(b)

Upper semitransparent cathode
Emissive layer (Ph-PPV)
Bottom anode (CF _x /Ag)
Mirror
Acrylic interlayer
Al-laminated plastic foil

(c)

FIGURE 6.22 Schematic diagrams of top-emitting polymer OLED with a configuration of: (a) glass/ metallic mirror/ITO/PEDOT/Ph-PPV/semitransparent cathode, (b) Al-PET/acrylic layer/metallic mirror/ITO/PEDOT/Ph-PPV/semitransparent cathode, and (c) Al-PET/acrylic layer/metallic mirror/anode/Ph-PPV/semitransparent cathode.

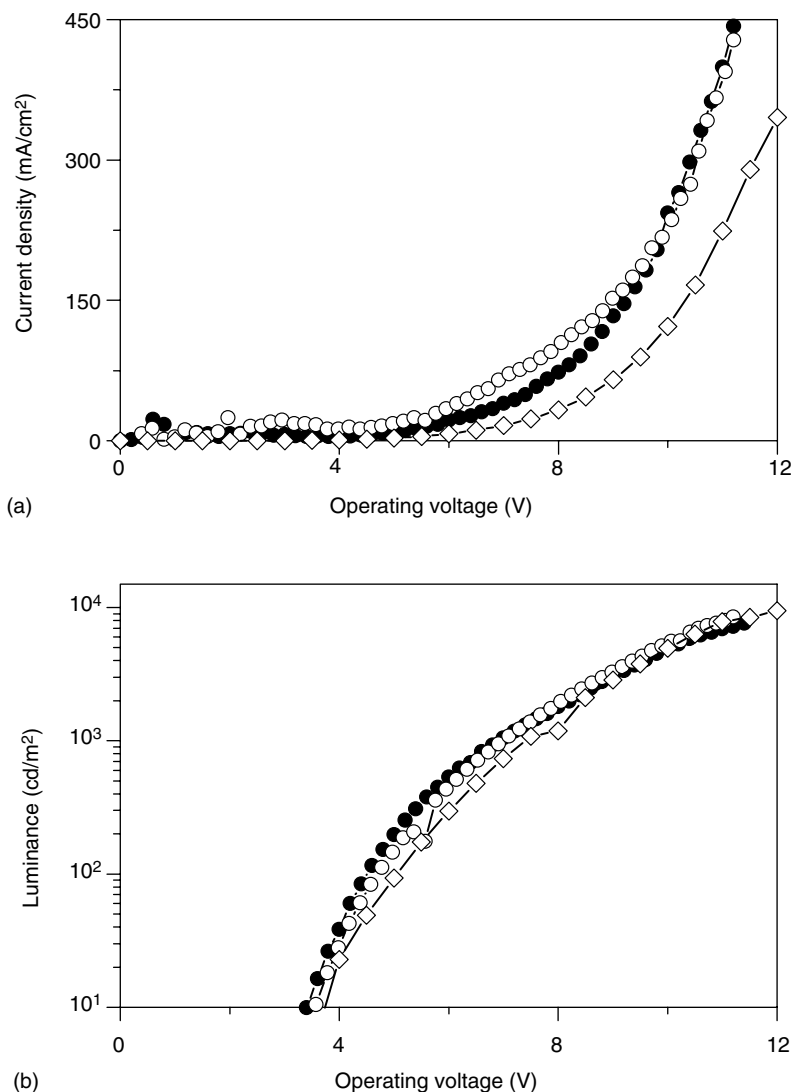


FIGURE 6.23 (a) J - V and (b) L - V characteristics of three devices with a configuration of glass/Ag (200 nm)/ITO (130 nm)/PEDOT (80 nm)/Ph-PPV (80 nm)/semitransparent cathode (closed circles), Al-PET/acrylic layer/Ag (200 nm)/ITO (130 nm)/PEDOT (80 nm)/Ph-PPV (80 nm)/semitransparent cathode (open circles), and Al-PET/acrylic layer/Ag (200 nm)/CF_x (0.3 nm)/Ph-PPV (110 nm)/semi-semitransparent cathode (open diamonds).

density. This is attributed to a thicker Ph-PPV layer of 110 nm used in the device, but results indicate that both Ag/ITO and Ag/CF_x exhibit similar hole-injection behavior in OLEDs [79].

The top-emitting OLED with a bilayer anode of Ag/CF_x and an ultrathin Ag layer used in the upper semitransparent cathode forms an optical microcavity, which can tailor the spectral characteristics of the emitters therein by allowing maximum light emission near the resonance wavelengths of an organic microcavity [80,81]. When the mode wavelength of the cavity is fixed at 550 nm, the thickness of the Ph-PPV layer is determined to be about 110 nm [81].

Therefore, a top-emitting OLED with a Ph-PPV layer of 110 nm would provide a higher luminous efficiency.

The results of luminous efficiency as a function of current density measured for a control device with a structure of glass/Ag (200 nm)/ITO (130 nm)/PEDOT (80 nm)/Ph-PPV (80 nm)/semitransparent cathode (Figure 6.22a) and flexible polymer OLED with a configuration of Al-PET/acrylic layer/Ag (200 nm)/CF_x (0.3 nm)/ph-PPV (110 nm)/semitransparent cathode (Figure 6.22c) are shown in Figure 6.24a. The control device has a maximum luminous efficiency of 2.70 cd/A, while the top-emitting OLED made with a Ph-PPV layer on a bilayer Ag/CF_x anode has a luminous efficiency of 4.56 cd/A. The enhancement of the efficiency in the top-emitting OLED with a CF_x coating is attributed to two factors: (1) Partial light emission in a direction toward the anode, which is trapped by ITO in a control device, is almost completely reflected back to the semitransparent cathode by the Ag/CF_x anode, leading to an increased luminous efficiency. (2) The optical microcavity effect redirects the trapped light outside the device. Figure 6.24b is a photo image of a flexible top-emitting

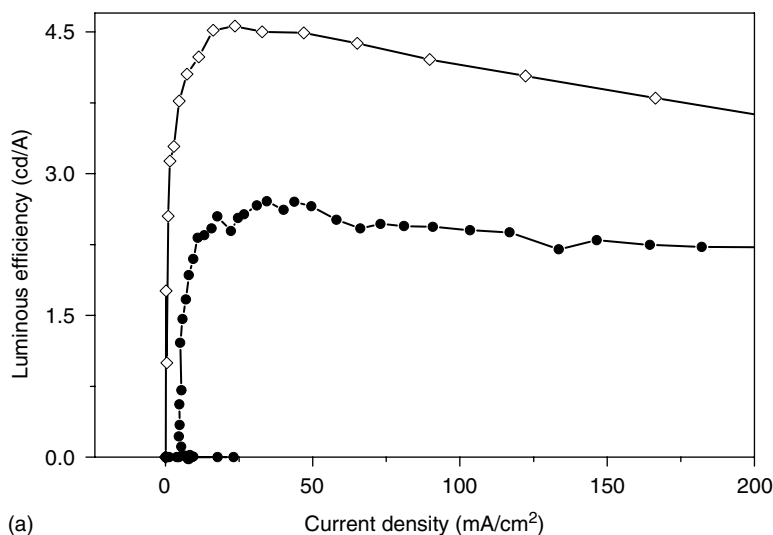


FIGURE 6.24 (a) Luminous efficiency of two top-emitting OLEDs with a configuration of glass/Ag (200 nm)/ITO (130 nm)/PEDOT (80 nm)/Ph-PPV (80 nm)/semitransparent cathode (closed circles), and Al-PET/acrylic layer/Ag (200 nm)/CF_x (0.3 nm)/Ph-PPV (110 nm)/semitransparent cathode (open diamonds). (b) A photo image showing a flexible top-emitting electroluminescent device on an Al-PET substrate.

OLED on an Al-PET substrate. The device performance does not deteriorate after repeated bending, suggesting that there is no significant stress-induced change in the characteristics of the OLEDs fabricated on PET foil [71,82]. The results demonstrate the feasibility of fabricating flexible displays using a variety of plastic substrates including metal-laminated plastic foils, or a metal film sandwiched between two plastic foils. The flexible device structures enable a display to conform, bend, or roll into any shape and thus make possible other product concepts.

6.4 OPTICAL DESTRUCTIVE ELECTRODE FOR HIGH CONTRAST OLEDs

6.4.1 BLACK CATHODE FOR HIGH CONTRAST OLEDs

There have been a great deal of activities in the development of OLEDs. In a conventional structure of the organic or polymeric OLEDs, the devices have a layer (or layers) of organic sandwiched between a transparent anode and the cathode. The metallic cathode is typically used and has a high reflection to the ambient light. If the devices are made on transparent substrates, including rigid glass or clear flexible plastic foils, OLEDs with this configuration are usually very reflective. As such, the contrast of the devices is very low and the visual image of the OLEDs is poorly legible. In many practical applications, especially in bright ambient condition, the visual contrast is more important than the brightness of image. Therefore, a sufficient reduction in the reflection of ambient light from the OLEDs is a prerequisite for high contrast OLED displays.

Much effort has been focused on developing OLEDs with low reflectivity under the ambient light. For example, a circular polarizer film can be bonded to the outside of the glass substrate to improve the visual contrast. This is a very simple solution for improving the contrast of OLEDs. In fact, the polarizer films have been used to enhance LCDs to good effect and can be similarly applied for OLEDs. However, the adding of the polarizer film constitutes an additional bonding step to the production of the OLED displays. This aside, polarizer films are subjective to humidity and temperature environments, as such, the operating condition of the OLED displays is constrained to a limited range of humidity and temperature of the polarizer films. This also results in the inclusion of a material not inherently part of the manufacturing process of the OLEDs. This eventually results in higher costs. This aside, a polarizer also increases the thickness of OLED displays. When using such a circular polarizer in flexible OLED displays, this becomes a genuine concern.

In addition to the straightforward polarizer approach, the feasibility of employing low reflectivity cathode to reduce ambient reflection for achieving low reflectivity OLEDs has been reported. Figure 6.25 is a cross-sectional view of a high contrast OLED with a black cathode. A conducting and light-absorbing contact is used to form an optical destructive interference for reducing the ambient reflection. Hung and Madathil [83] have demonstrated that calcium hexaboride (CaB_6) can be used as ambient light reduction cathode. CaB_6 is highly conductive with a low work function and is substantially black in bulk form. Although the alternative electron injection layer of CaB_6 has an advantage of low reflectivity, the uniform CaB_6 film with stable optical and electrical properties is not very easy to control in the deposition process. A variety of black cathode structures have also been developed to minimize the light reflection at the organic-cathode interface. For example, a reflectionless OLED with a multilayer black cathode structure of $\text{LiF}/\text{Al}/\text{ZnO}/\text{Al}$ was reported [84]. In this multilayer black cathode, the zinc oxide film was deposited by thermal evaporation. It acts as an optical absorbing layer to reduce the ambient light reflection from the metallic cathode. The use of a high conductive black carbon film in multilayer cathode system also was demonstrated by Renault et al. [85]. This black cathode consists of a thin electron injection

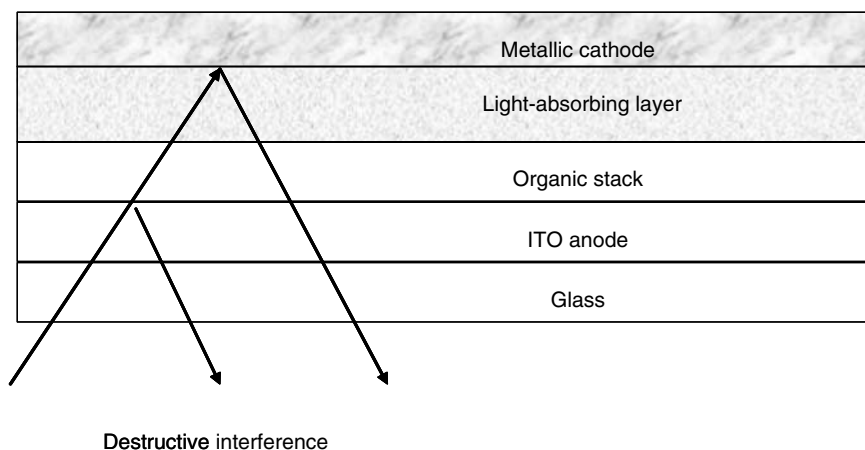


FIGURE 6.25 Schematic diagram showing an OLED with a black cathode, the presence of an optical absorbing layer causes a destructive interference leading to a low reflection.

layer of magnesium, an optically absorbing and electrically conductive carbon layer, and a thick aluminum layer. This multilayer black cathode has a similar charge injection property compared to a conventional cathode of Mg/Al, but it has a much lower reflectivity. The results show that the reflection reduces from nearly 100% for devices using conventional cathode to ~60% for multilayer cathode. The black cathodes using conductive light-absorbing layers with mixtures of organic materials and metals have also been reported. It was demonstrated that the presence of an electrically conductive light-absorbing layer at the cathode of an OLED reduced significantly the total reflectance of an OLED [86]. This electrically conductive light-absorbing layer serves to absorb reflected ambient light from the cathode and improves the overall contrast and legibility. The light-absorbing layer is typically made of a mixture of organic and metal and is placed between the cathode and the organic layer.

Black Layer, which uses an interference destructive layer in low reflectivity cathode for OLEDs, is another example of black cathode developed by Luxell Technologies [87,88]. The Black Layer consists of a layer of thin absorbing material, a layer of transparent materials, and a thick metal layer. The light reflected from the first and second metal layers is equal in amplitude but differs in phase. As such the destructive interference occurs and significant reduction in reflectance can be achieved if appropriate thickness of each layer is used. There are also other methods that use additional light-absorbing layers of a variety of different materials. These methods essentially address the reduction of reflected ambient light by incorporating a low reflectivity composite cathode [68,89–91].

6.4.2 GRADIENT REFRACTIVE INDEX ANODE FOR HIGH CONTRAST OLEDs

A high contrast OLED can also be fabricated using a bilayer or multilayer optical destructive anode to reduce the reflectance of the ambient light from the device. The concept is based on using an anode with a gradient or graded refractive index to minimize the ambient light reflection from OLEDs and hence to enhance the visual contrast. The schematic diagram of the device is shown in Figure 6.26. A bilayer anode consisting of a thin film of semi-transparent metal oxide (e.g., highly oxygen-deficient ITO) and a normal high-work function ITO can be used in OLEDs for reducing ambient reflection. The highly oxygen-deficient ITO film is electrically conducting and optically absorbing. The oxygen-deficient ITO layer is inserted between the anode contact (e.g., ITO) and the rigid or flexible

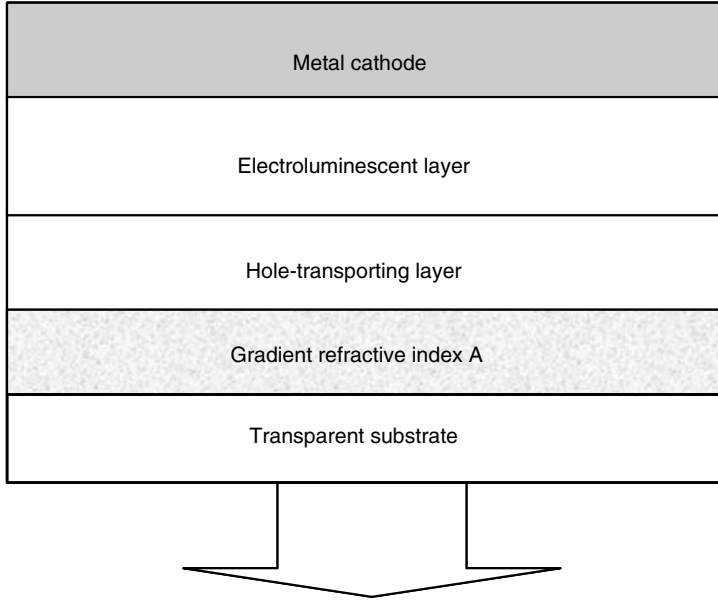


FIGURE 6.26 Schematic diagram of a high contrast OLED using a gradient refractive index anode.

transparent substrate to serve as an optical destructive layer for reducing the ambient light reflection from the OLEDs. A typical structure of a high contrast OLED consists in order of a rigid or flexible substrate, an oxygen-deficient conducting oxide layer, an anode, an organic stack of the hole-transporting and emissive layers, and a high reflectivity metallic cathode. The semitransparent and transparent conducting metal oxide bilayer anode, both layers may be made of ITO, enables to reduce significantly the ambient light reflection from mirror-like surface of the metallic cathode in OLEDs through light-absorbing and optical destructive interference.

From optical point of view, an OLED structure can be considered as a multilayer thin-film system composed of absorbing and nonabsorbing materials, as shown in Figure 6.27. Therefore, the optical properties and optimal structure of such a multilayer device can be investigated by applying thin-film optical analysis techniques. Based on the theory of optical admittance analysis for analyzing the optical properties of a thin-film system [92], the optical properties of an OLED thin-film system can be simulated to reduce the ambient reflection.

Defining $F(\lambda)$ as the flux of the ambient light incident on the display, the reflectance of the device, R_L , can be calculated as [93]

$$R_L = \frac{\int R(\lambda)F(\lambda) d\lambda}{\int F(\lambda) d\lambda} \quad (6.4)$$

where $R(\lambda)$ is the spectral reflectance of the thin-film system. If wavelength-dependent refractive indices of each layer in the OLED system are known, it becomes possible to optimize the thickness of the composite anode structure through minimizing the reflectance. An optimal structure can thus be designed to sufficiently diminish the reflectance of an OLED, while maintains the comparable device performance.

Contrast ratio (CR) of an OLED display is very much dependent on the ambient and the lighting conditions. The actual CR for an OLED display is based on the applications and is different depending on the products such as in-car audio, hand phone, etc. Usually for indoor

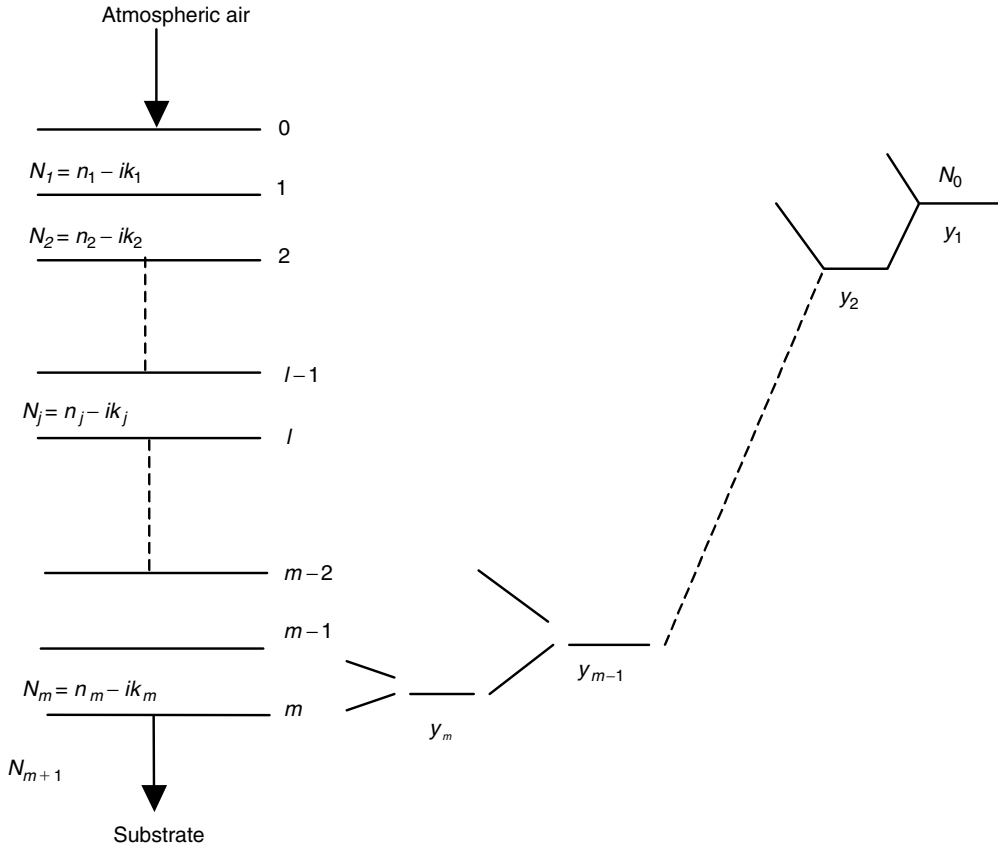


FIGURE 6.27 Schematic representation of an arbitrary multilayer thin-film system.

applications, $CR > 10\text{--}20:1$ is sufficient. According to UDC OLED Technology Roadmap 2001–2010, the targeted CR for OLED displays (300 cd/m^2 , under 500 lx) is expected to be $50:1$, $100:1$, and $200:1$ for 2004, 2007, and 2010, respectively. In a pixelated device, CR can be defined as [91]:

$$CR = \frac{L_{\text{on}} + R_L \times L_{\text{ambient}}}{L_{\text{off}} + R_L \times L_{\text{ambient}}} \quad (6.5)$$

where L_{on} and L_{off} are emitted luminance of active (on) and inactive (off) pixels, L_{ambient} is the ambient luminance or the ambient light incident on the display. The corresponding optical parameters, the real part of refractive index, $n(\lambda)$, and the extinction coefficient, $k(\lambda)$ of each layer will be measured by variable angle spectroscopic ellipsometry. The luminous reflectance R_L and CR of the OLED displays can be then simulated using the Equation 6.4 and Equation 6.5. The optical simulation enables to provide in advance the leading design information of an OLED system with an optimal optical destructive anode structure for a desired high CR .

Figure 6.28 shows the wavelength-dependent reflectance measured for a control device (shown as control device in Figure 6.28) and the OLEDs made with the bilayer ITO electrodes (anode 1 and anode 2 in Figure 6.28) consisting of 170- and 400-nm-thick highly oxygen-deficient semitransparent ITOs, respectively. The thickness of upper ITO (anode contact) is

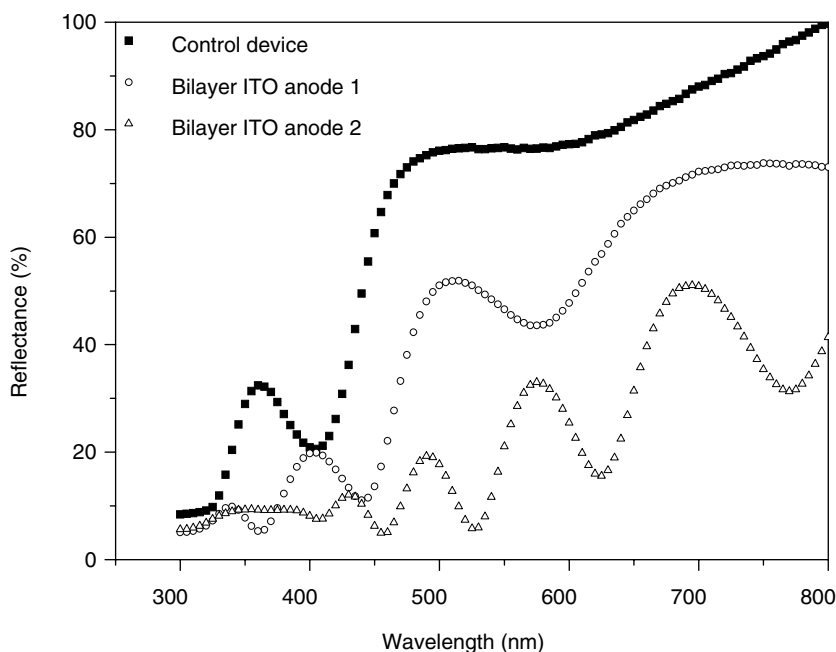


FIGURE 6.28 The ambient light reflection as a function of the wavelength measured for a control device and structurally identical OLEDs made with two different bilayer ITO anodes.

kept constant at 130 nm. In this example, the highly oxygen-deficient semitransparent ITO film is used as an absorbing layer. The stack of a semitransparent ITO film and an optimal transparent ITO anode can be deposited subsequently on glass substrate using RF magnetron sputtering. As is apparent from the results, there are obvious differences on the overall reflectance of OLEDs made with different light-absorbing ITO layer thicknesses. As the thickness of the optical destructive layer increased, the total reflectance of the devices is reduced substantially over the visible wavelength region. The reduction in ambient light reflection from the devices with a bilayer ITO anode structure enables enhancing the visual legibility of OLED displays. The oxygen-deficient ITO also is electrically conductive and the sheet resistance of a bilayer ITO can be lower than that of a bare ITO anode, as it also has an optimal high-work function ITO; both bilayer ITO anode and single layer ITO anode have the similar hole-injection properties. The identical OLEDs made with either bilayer or single layer ITO anode have similar J - V characteristics. However, the luminous efficiency of the device with a bilayer anode with 170-nm-thick oxygen-deficient ITO is approximately 60% of that of a control device operated at the same current density. Such a reduction in luminous efficiency can be attributed to the use of an oxygen-deficient ITO layer as some of the emitted light from the OLED is absorbed by the bilayer anode.

Figure 6.29 shows the photographs taken for a control device with a bare ITO anode, the OLEDs made with the bilayer optical destructive anodes having 170- and 400-nm-thick highly oxygen-deficient ITOs and a top ITO anode, respectively. High reflective cathodes in a control device are evidently seen in Figure 6.29a, and the “black” electrodes shown in Figure 6.29b and c clearly demonstrate the effect of ambient light deduction in devices. It is obvious from Figure 6.29 that the presence of an optical destructive layer, in this case a highly oxygen-deficient ITO layer, between the anode and the substrate reduces the reflection of the OLEDs. It is demonstrated that a conventional OLED with an inherent weakness of high

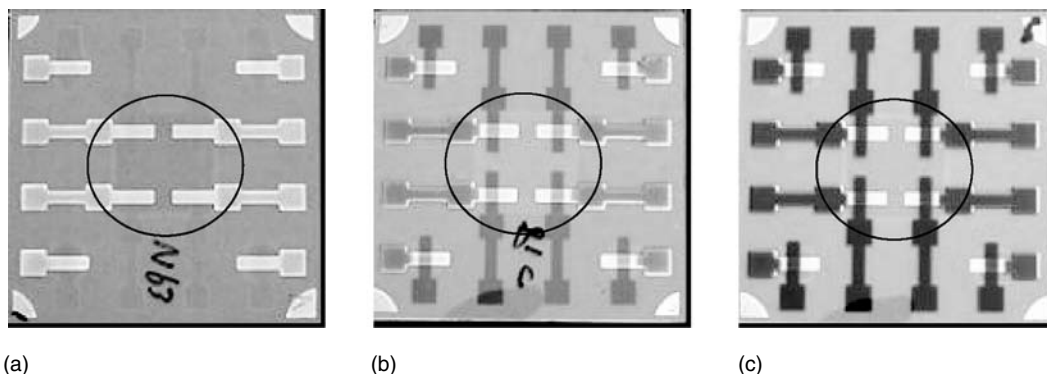


FIGURE 6.29 The photographs taken for the OLEDs with different optical destructive ITO layer thicknesses of (a) a bare ITO, (b) 170 nm, and (c) 400 nm under sunlight environment.

reflectivity from mirror-like cathode (Figure 6.29a) can be overcome by employing a bilayer anode with a gradient or graded refractive index. The results indicate that the OLEDs with a bilayer anode can provide a substantial enhancement in visual legibility and the contrast under the ambient light environment.

The use of an optical destructive anode shows promise for contrast improvements in OLEDs. The multilayer semitransparent anode is capable of reducing the ambient light reflection from the reflective cathode to enhance the contrast of the devices. A multilayer anode may also be made using a stack of layers with graded refractive indices to minimize the total reflection of the ambient light from the conventional OLEDs. If only one type of material is used, e.g., ITO in the above example, the thickness and the refractive index of the anode can be varied with a desired gradient to form an optically absorbing and electronically conducting anode for high contrast OLEDs. The ITO with different refractive indices can be easily engineered by varying the hydrogen partial pressure in the argon–hydrogen gas mixture during the film deposition. As the deposition of an ITO with gradient refractive index is regarded as a part of the anode deposition, there is no additional request for new equipment, materials, and even processing gases. This technique provides a cost-effective approach for achieving high contrast OLEDs.

The fabrication of ITO anode with a gradient refractive index for high contrast OLEDs can be integrated easily to the existing mass production process for device fabrication. It has stable chemical characteristics and can also be easily patterned using well developed lithographic techniques for device fabrications. This aside, reproducible ITO films with different optical and electrical properties can be prepared by different techniques, including reactive thermal evaporation deposition, magnetron sputtering, electron beam evaporation, spray pyrolysis, and chemical vapor deposition. The OLEDs with a bilayer optical absorbing or transparent ITO anode show sufficient reduction of 10–50% in ambient light reflection compared to a control OLED with a bare ITO. As a bilayer has a normal ITO-anode-finished surface, the various surface treatments and the anode modification developed for enhancing OLED performance can be applied to the new anode structure without any change. The multilayer anode provides a feasible and a cost-effective approach for fabrication of visual legible OLED displays.

Although ITO is still one of the most widely used anode materials for OLEDs, other alternatives suited for OLEDs may also be used for making optical destructive anode for high contrast OLED displays using this technique. For example, a multilayer optical destructive anode may be fabricated using other oxide materials, including SnO_2 , FTO, AZO, IZO,

Ga-In-Sn-O, Zn-In-Sn-O, Ga-In-O, and other TCOs suitable for anode in an OLED. These materials can be used individually or with a combination of different materials.

REFERENCES

1. K.L. Chopra, S. Major, and D.K. Pandya, Transparent conductors — a status review, *Thin Solid Films*, 102: 1–46, 1983.
2. I. Hamburg and C.G. Granvist, Evaporated Sn-doped In_2O_3 films: basic optical properties and applications to energy-efficient windows, *J. Appl. Phys.*, 60: R123–R159, 1986.
3. B.H. Lee, I.G. Kim, S.W. Cho, and S.H. Lee, Effect of process parameters on the characteristics of indium tin oxide thin film for flat panel display application, *Thin Solid Films*, 302: 25–30, 1997.
4. J.Q. Hu, F.R. Zhu, J. Zhang, and H. Gong, A room temperature indium tin oxide/quartz crystal microbalance gas sensor for nitric oxide, *Sens. Actuators B*, 93: 175–180, 2003.
5. J.S. Kim, M. Granström, R.H. Friend, N. Johansson, W.R. Salaneck, R. Daik, W.J. Feast, and F. Cacialli, Indium–tin oxide treatments for single- and double-layer polymeric light-emitting diodes: the relation between the anode physical, chemical, and morphological properties and the device performance, *J. Appl. Phys.*, 84: 6859–6870, 1998.
6. I.D. Parker, Carrier tunneling and device characteristics in polymer light-emitting diodes, *J. Appl. Phys.*, 75: 1656–1666, 1994.
7. C.C. Wu, C.I. Wu, J.C. Sturm, and A. Kahn, Surface modification of indium tin oxide by plasma treatment: an effective method to improve the efficiency, brightness, and reliability of organic light emitting devices, *Appl. Phys. Lett.*, 70: 1348–1350, 1997.
8. B. Schröder, Thin-film technology based on hydrogenated amorphous-silicon, *Mater. Sci. Eng., A*, 139: 319–333, 1991.
9. F.R. Zhu, T. Fuyuki, H. Matsunami, and J. Singh, Assessment of combined TCO/metal rare contact for thin film amorphous silicon solar cells, *Sol. Energy Mater. Sol. Cells*, 39: 1–9, 1995.
10. Y.F. Yan, S.B. Zhang, and S.T. Pantelides, Control of doping by impurity chemical potentials: predictions for p-type ZnO, *Phys. Rev. Lett.*, 86: 5723–5726, 2001.
11. G. Xiong, J. Wilkinson, B. Mischuck, S. Tüzemen, K.B. Ucer, and R.T. Williams, Control of p- and n-type conductivity in sputter deposition of undoped ZnO, *Appl. Phys. Lett.*, 80: 1195–1197, 2002.
12. A. Salehi, The effects of deposition rate and substrate temperature of ITO thin films on electrical and optical properties, *Thin Solid Films*, 324: 214–218, 1998.
13. K.R. Zhang, F.R. Zhu, C.H.A. Huan, and A.T.S. Wee, Effect of hydrogen partial pressure on optoelectronic properties of indium tin oxide thin films deposited by radio frequency magnetron sputtering method, *J. Appl. Phys.*, 86: 974–980, 1999.
14. K.R. Zhang, F.R. Zhu, C.H.A. Huan, A.T.S. Wee, and T. Osipowicz, Indium-doped zinc oxide films prepared by simultaneous rf and dc magnetron sputtering, *Surf. Interface Anal.*, 28: 271–274, 1999.
15. J.K. Sheu, Y.K. Su, G.C. Chi, M.J. Jou, and C.M. Chang, Effects of thermal annealing on the indium tin oxide Schottky contacts of n-GaN, *Appl. Phys. Lett.*, 72: 3317–3319, 1999.
16. S. Major and K.L. Chopra, Indium-doped zinc-oxide films as transparent electrodes for solar-cells, *Sol. Energy Mater.*, 17: 319–327, 1988.
17. J. Hu and R.G. Gordon, Atmospheric pressure chemical vapor deposition of gallium doped zinc oxide thin films from diethyl zinc, water, and triethyl gallium, *J. Appl. Phys.*, 72: 5381–5392, 1992.
18. Y. Takahashi, S. Okada, R.B.H. Tahar, K. Nakano, T. Ban, and Y. Ohya, Dip-coating of ITO films, *J. Non-Cryst. Solids*, 218: 129–134, 1997.
19. K. Nishio, T. Sei, and T. Tsuchiya, Preparation and electrical properties of ITO thin films by dip-coating process, *J. Mater. Sci.*, 31: 1761–1766, 1996.
20. H.S. Kwok, X.W. Sun, and D.H. Kim, Pulsed laser deposited crystalline ultrathin indium tin oxide films and their conduction mechanisms, *Thin Solid Films*, 335: 299–302, 1998.
21. H. Kim, A. Piqué, J.S. Horwitz, H. Mattoussi, H. Murata, Z.H. Kafafi, and D.B. Chrisey, Indium tin oxide thin films for organic light-emitting devices, *Appl. Phys. Lett.*, 74: 3444–3446, 1999.
22. C. May and J. Strümpfel, ITO coating by reactive magnetron sputtering — comparison of properties from DC and MF processing, *Thin Solid Films*, 351: 48–52, 1999.

23. S. Honda, M. Watamori, and K. Oura, The effects of oxygen content on electrical and optical properties of indium tin oxide films fabricated by reactive sputtering, *Thin Solid Films*, 281–282: 206–208, 1996.
24. G.L. Harding and B. Window, DC magnetron reactively sputtered indium–tin-oxide films produced using argon–oxygen–hydrogen mixtures, *Sol. Energy Mater.*, 20: 367–379, 1990.
25. S. Ishibashi, Y. Higuchi, Y. Ota, and K. Nakamura, *J. Vac. Sci. Technol., A*, 8: 1399–1402, 1990.
26. I. Baia, M. Quintela, L. Mendes, P. Nunes, and R. Martins, Performances exhibited by large area ITO layers produced by rf magnetron sputtering, *Thin Solid Films*, 337: 171–175, 1999.
27. L.J. Meng and M.P. dos Santos, Properties of indium tin oxide films prepared by rf reactive magnetron sputtering at different substrate temperature, *Thin Solid Films*, 322: 56–62, 1998.
28. P. Thilakan and J. Kumar, Studies on the preferred orientation changes and its influenced properties on ITO thin films, *Vacuum*, 48: 463–466, 1997.
29. L.J. Meng and M.P. dos Santos, Properties of indium tin oxide (ITO) films prepared by r.f. reactive magnetron sputtering at different pressures, *Thin Solid Films*, 303: 151–155, 1997.
30. M. Buchanan, J.B. Webb, and D.F. Williams, Preparation of conducting and transparent thin films of tin-doped indium oxide by magnetron sputtering, *Appl. Phys. Lett.*, 37: 213–215, 1980.
31. S. Honda, A. Tsujimoto, M. Watamori, and K. Oura, Depth profiling of oxygen concentration of indium tin oxide films fabricated by reactive sputtering, *Jpn. J. Appl. Phys.*, 33: L1257–L1260, 1994.
32. M. Katiyar, Y.H. Yang, and J.R. Ableson, Hydrogen-surface reactions during the growth of hydrogenated amorphous silicon by reactive magnetron sputtering: a real time kinetic study by *in situ* infrared absorption, *J. Appl. Phys.*, 77: 6247–6256, 1995.
33. W.G. Haines and H.R. Bube, Effects of heat treatment on the optical and electrical properties of indium–tin oxide films, *J. Appl. Phys.*, 49: 304–307, 1978.
34. S. Ray, R. Banerjee, N. Basu, A.K. Batabyal, and A.K. Barua, Properties of tin doped indium tin oxide thin films prepared by magnetron sputtering, *J. Appl. Phys.*, 54: 3497–3501, 1983.
35. Y. Ohhata, F. Shinoki, and S. Yoshida, Optical properties of r.f. reactive sputtered tin-doped In_2O_3 films, *Thin Solid Films*, 59: 255–261, 1979.
36. Y. Shigesato, Y. Hayashi, A. Masui, and T. Haranou, The structural changes of indium–tin oxide and $\alpha\text{-WO}_3$ films by introducing water to the deposition processes, *Jpn. J. Appl. Phys.*, 30: 814–819, 1991.
37. L.J. Meng, A. Macarico, and R. Martins, Study of annealed indium tin oxide-films prepared by rf reactive magnetron sputtering, *Vacuum*, 46: 673–680, 1995.
38. R. Banerjee and D. Das, Properties of tin oxide films prepared by reactive electron beam evaporation, *Thin Solid Films*, 149: 291–301, 1987.
39. S.A. Van Slyke, C.H. Chen, and C.W. Tang, Organic electroluminescent devices with improved stability, *Appl. Phys. Lett.*, 69: 2160–2162, 1996.
40. J.S. Kim, R.H. Friend, and F. Cacialli, Improved operational stability of polyfluorene-based organic light-emitting diodes with plasma-treated indium–tin-oxide anodes, *Appl. Phys. Lett.*, 74: 3084–3086, 1999.
41. Y. Kurosaka, N. Tada, Y. Ohmori, and K. Yoshino, Improvement of electrode/organic layer interfaces by the insertion of monolayer-like aluminum oxide film, *Jpn. J. Appl. Phys.*, 37: L872–L875, 1998.
42. K. Sugiyama, H. Ishii, Y. Ouchi, and K. Seki, Dependence of indium–tin-oxide work function on surface cleaning method as studied by ultraviolet and x-ray photoemission spectroscopies, *J. Appl. Phys.*, 87: 295–298, 2000.
43. D.J. Milliron, I.G. Hill, C. Shen, A. Kahn, and J. Schwartz, Surface oxidation activates indium tin oxide for hole injection, *J. Appl. Phys.*, 87: 572–576, 2000.
44. F. Steuber, J. Staudigel, M. Stössel, J. Simmerer, and A. Winnacker, Reduced operating voltage of organic electroluminescent devices by plasma treatment of the indium tin oxide anode, *Appl. Phys. Lett.*, 74: 3558–3560, 1999.
45. Y. Park, V. Choong, Y. Gao, B.R. Hsieh, and C.W. Tang, Work function of indium tin oxide transparent conductor measured by photoelectron spectroscopy, *Appl. Phys. Lett.*, 68: 2699–2701, 1996.
46. I.H. Campbell, J.D. Kress, R.L. Martin, D.L. Smith, N.N. Barashkov, and J.P. Ferraris, Controlling charge injection in organic electronic devices using self-assembled monolayers, *Appl. Phys. Lett.*, 71: 3528–3530, 1997.

47. M.G. Mason, L.S. Hung, C.W. Tang, S.T. Lee, K.W. Wong, and M. Wang, Characterization of treated indium–tin-oxide surfaces used in electroluminescent devices, *J. Appl. Phys.*, 86: 1688–1692, 1999.
48. J.A. Chaney and P.E. Pehrsson, Work function changes and surface chemistry of oxygen, hydrogen, and carbon on indium tin oxide, *Appl. Surf. Sci.*, 180: 214–226, 2001.
49. H.Y. Yu, X.D. Feng, D. Grozea, Z.H. Lu, R.N.S. Sodhi, A-M. Hor, and H. Aziz, Surface electronic structure of plasma-treated indium tin oxides, *Appl. Phys. Lett.*, 78: 2595–2597, 2001.
50. N.D. Popovich, S.S. Wong, S. Ufer, V. Sakhrani, and D. Paine, Electron-transfer kinetics at ITO films — influence of oxygen plasma, *J. Electrochem. Soc.*, 150: H255–H259, 2003.
51. F.R. Zhu, C.H.A. Huan, K.R. Zhang, and A.T.S. Wee, Investigation of annealing effects on indium tin oxide thin films by electron energy loss spectroscopy, *Thin Solid Films*, 359: 244–250, 2000.
52. R.B.H. Tahar, T. Ban, Y. Ohya, and Y. Takahashi, Tin doped indium oxide thin films: electrical properties, *J. Appl. Phys.*, 83: 2631–2645, 1998.
53. P.K.H. Ho, M. Granstrom, R.H. Friend, and N.C. Greenham, Ultrathin self-assembled layers at the ITO interface to control charge injection and electroluminescence efficiency in polymer light-emitting diodes, *Adv. Mater.*, 10: 769–774, 1998.
54. C. Yan, M. Zharnikov, A. Golzhauser, and M. Grunze, Preparation and characterization of self-assembled monolayers on indium tin oxide, *Langmuir*, 16: 6208–6215, 2000.
55. S.F.J. Appleyard and M.R. Willis, Electroluminescence: enhanced injection using ITO electrodes coated with a self assembled monolayer, *Opt. Mater.*, 9: 120–124, 1998.
56. J.E. Malinsky, G.E. Jabbour, S.E. Shaheen, J.D. Anderson, A.G. Richter, T.J. Marks, N.R. Armstrong, B.K. Pulak Dutta, and N. Peyghambarian, Self-assembly processes for organic LED electrode passivation and charge injection balance, *Adv. Mater.*, 11: 227–231, 1999.
57. F.R. Zhu, B.L. Low, K.R. Zhang, and S.J. Chua, Lithium-fluoride-modified indium tin oxide anode for enhanced carrier injection in phenyl-substituted polymer electroluminescent devices, *Appl. Phys. Lett.*, 79: 1205–1207, 2001.
58. H. Tang, F. Li, and J. Shinar, Bright high efficiency blue organic light-emitting diodes with $\text{Al}_2\text{O}_3/\text{Al}$ cathodes, *Appl. Phys. Lett.*, 71: 2560–2562, 1997.
59. Z.B. Deng, X.M. Ding, S.T. Lee, and W.A. Gambling, Enhanced brightness and efficiency in organic electroluminescent devices using SiO_2 buffer layers, *Appl. Phys. Lett.*, 74: 2227–2229, 1999.
60. X.M. Ding, L.M. Hung, L.F. Cheng, Z.B. Deng, X.Y. Hou, C.S. Lee, and S.T. Lee, Modification of the hole injection barrier in organic light-emitting devices studied by ultraviolet photoelectron spectroscopy, *Appl. Phys. Lett.*, 76: 2704–2706, 2000.
61. Y.Q. Li, L.W. Tan, X.T. Hao, K.S. Ong, F.R. Zhu, and L.S. Hung, Flexible top-emitting electroluminescent devices on polyethylene terephthalate substrates, *Appl. Phys. Lett.*, 86: i.d. 153508, 3 pages, 2005.
62. R.H. Jordan, A. Dodabalapur, and R.E. Slusher, Efficiency enhancement of microcavity organic light emitting diodes, *Appl. Phys. Lett.*, 69: 1997–1999, 1996.
63. H. Kim, J.S. Horwitz, W.H. Kim, S.B. Qadri, and Z.H. Kafafi, Anode material based on Zr-doped ZnO thin films for organic light-emitting diodes, *Appl. Phys. Lett.*, 83: 3809–3811, 2003.
64. X. Jiang, F.L. Wong, M.K. Fung, and S.T. Lee, Aluminum-doped zinc oxide films as transparent conductive electrode for organic light-emitting devices, *Appl. Phys. Lett.*, 83: 1875–1877, 2003.
65. W.H. Kim, A.J. Mäkinen, N. Nikolov, R. Shashidhar, H. Kim, and Z.H. Kafafi, Molecular organic light-emitting diodes using highly conducting polymers as anodes, *Appl. Phys. Lett.*, 80: 3844–3846, 2002.
66. Z.Y. Xie, L.S. Hung, and F.R. Zhu, A flexible top-emitting organic light-emitting diode on steel foil, *Chem. Phys. Lett.*, 38: 691–696, 2003.
67. C. Fou, O. Onitsuka, M. Ferreira, M.F. Rubner, and B.R. Hsieh, Fabrication and properties of light-emitting diodes based on self-assembled multilayers of poly(phenylene vinylene), *J. Appl. Phys.*, 79: 7501–7509, 1996.
68. A.N. Krasnov, High-contrast organic light-emitting diodes on flexible substrates, *Appl. Phys. Lett.*, 80: 3853–3855, 2002.

69. G. Gustafsson, G.M. Treacy, Y. Cao, F. Klavetter, N. Colaneri, and A.J. Heeger, The plastic LED: a flexible light-emitting device using a polyaniline transparent electrode, *Synth. Met.*, 57: 4123–4127, 1993.
70. G. Gu, P.E. Burrows, S. Venkatesh, and S.R. Forrest, Vacuum-deposited, nonpolymeric flexible organic light-emitting devices, *Opt. Lett.*, 22: 172–174, 1997.
71. R. Paetzold, K. Heuster, D. Henseler, S. Roeger, G. Weittmann, and A. Winnacker, Performance of flexible polymeric light-emitting diodes under bending conditions, *Appl. Phys. Lett.*, 82: 3342–3344, 2003.
72. K.R. Zhang, F.R. Zhu, C.H.A. Huan, and A.T.S. Wee, Indium tin oxide films prepared by radio frequency magnetron sputtering method at a low processing temperature, *Thin Solid Films*, 376: 255–263, 2000.
73. A. Plichta, A. Weber, and A. Habeck, Ultra thin flexible glass substrates, *Mater. Res. Soc. Symp. Proc.*, 769: H9.1.1–H9.1.9, 2003.
74. A.B. Chwang, M.R. Rothman, S.Y. Mao, R.H. Hewitt, M.S. Weaver, J.A. Silvermail, K. Rajan, M. Hack, J.J. Brown, X. Chu, L. Moro, T. Krajewski, and N. Rutherford, Thin film encapsulated flexible organic electroluminescent displays, *Appl. Phys. Lett.*, 83: 413–415, 2003.
75. C.C. Wu, S.D. Theiss, G. Gu, M.H. Lu, J.C. Sturm, S. Wagner, and S.R. Forrest, Integration of organic LEDs and amorphous Si TFTs onto flexible and lightweight metal foil substrates, *IEEE Electron. Device Lett.*, 18: 609–612, 1997.
76. C.F. Madigan, M.H. Lu, and J.C. Sturm, Improvement of output coupling efficiency of organic light-emitting diodes by backside substrate modification, *Appl. Phys. Lett.*, 76: 1650–1652, 2000.
77. L.S. Hung, C.W. Tang, and M.G. Mason, Enhanced electron injection in organic electroluminescence devices using an Al/LiF electrode, *Appl. Phys. Lett.*, 70: 152–154, 1997.
78. Y.Q. Li, J.X. Tang, Z.Y. Xie, L.S. Hung, and S.S. Lau, An efficient organic light-emitting diode with silver electrodes, *Chem. Phys. Lett.*, 386: 128–131, 2004.
79. J.X. Tang, Y.Q. Li, L.S. Hung, and C.S. Lee, Photoemission study of hole-injection enhancement in organic electroluminescent devices with Au/CF_x anode, *Appl. Phys. Lett.*, 84: 73–75, 2004.
80. H. Riel, S. Karg, T. Beielein, B. Ruhstaller, and W. Riess, Phosphorescent top-emitting organic light-emitting devices with improved light outcoupling, *Appl. Phys. Lett.*, 82: 466–469, 2003.
81. H. Becker, S.E. Burns, N. Tessler, and R.H. Friend, Role of optical properties of metallic mirrors in microcavity structures, *J. Appl. Phys.*, 81: 2825–2829, 1997.
82. J. Lewis, S. Grego, B. Chalamala, E. Vrik, and D. Temple, Highly flexible transparent electrodes for organic light-emitting diode-based displays, *Appl. Phys. Lett.*, 85: 3450–3452, 2004.
83. L.S. Hung and J.K. Madathil, Reduction of Ambient-Light-Reflection in Organic Light-Emitting Devices, U.S. Patent 6,429,451 B1, 2002.
84. L.S. Hung and J. Madathil, Reduction of ambient light reflection in organic light-emitting diodes, *Adv. Mater.*, 13: 1787–1790, 2001.
85. O. Renault, O.V. Salata, M. Etchells, P.J. Dobson, and V. Christou, A low reflectivity multilayer cathode for organic light-emitting diodes, *Thin Solid Films*, 379: 195–198, 2000.
86. H. Aziz, Y.F. Liew, H.M. Grandin, and Z.D. Popovic, Reduced reflectance cathode for organic light-emitting devices using metal organic mixtures, *Appl. Phys. Lett.*, 83: 186–188, 2003.
87. A.N. Krasnov, ELDs rise on organic wings electroluminescent-display technology is being rescued from its industrial niche by implementations using organic materials, *Inf. Display*, 18: 18–21, 2002.
88. P.G. Hofstra and A. Krasnov, Organic Electroluminescent Devices, U.S. Patent 6,411,019 B1, 2002.
89. Z.Y. Xie and L.S. Hung, High-contrast organic light-emitting diodes, *Appl. Phys. Lett.*, 84: 1207–1209, 2004.
90. X.D. Feng, R. Khangura, and Z.H. Lu, Metal–organic–metal cathode for high-contrast organic light-emitting diodes, *Appl. Phys. Lett.*, 85: 497–499, 2004.
91. J. Heikenfeld and A.J. Steckl, Contrast enhancement in black dielectric electroluminescent devices, *IEEE Trans. Electron. Devices*, 49: 1348–1352, 2002.
92. F.R. Zhu and J. Singh, On the optical design of thin film amorphous silicon solar cells, *Sol. Energy Mater. Sol. Cells*, 31: 119–131, 1993.
93. F.R. Zhu, P. Jennings, J. Cornish, G. Hefter, and K. Luczak, Optimal and optical design of thin-film photovoltaic devices, *Sol. Energy Mater. Sol. Cells*, 49: 163–169, 1997.

7 Vapor-Deposited Organic Light-Emitting Devices

Michael S. Weaver

CONTENTS

7.1	Vapor-Deposited Organic Light-Emitting Devices	527
7.2	Vapor-Deposited Organic Light-Emitting Device Architectures	529
7.2.1	Anode.....	530
7.2.2	Organic Materials.....	530
7.2.3	Cathode.....	531
7.2.4	Alternative Device Architectures.....	531
7.3	Device Fabrication.....	532
7.3.1	Anode Preparation.....	532
7.3.2	Deposition of Organic Layers	533
7.3.3	Alternative Organic Deposition Techniques	536
7.3.4	Deposition of Cathode	536
7.3.5	Encapsulation of Organic Light-Emitting Device	537
7.4	Device Operation	537
7.4.1	Improving Device Efficiency	540
7.4.2	Improving Internal Quantum Efficiency	541
7.4.3	Improved Efficiency through Doping	542
7.4.4	Improving Power Efficiency	543
7.4.5	Outcoupling.....	543
7.4.6	Lifetime	545
7.5	Vapor-Deposited Organic Light-Emitting Device Displays.....	545
7.5.1	Passive Addressing Schemes.....	545
7.5.2	Active Addressing Schemes	548
7.5.3	Full-Color Displays.....	550
7.6	Future Generation Vapor-Deposited Organic Devices	553
7.6.1	Flexible Displays	553
7.6.2	Lighting	555
7.6.3	Displays and Beyond	557
	References	557

7.1 VAPOR-DEPOSITED ORGANIC LIGHT-EMITTING DEVICES

The first observations of electroluminescence from organic materials were made in the 1950s [1]. Interest in this phenomenon was fueled by the work of Pope et al. [2], who observed electroluminescence from single crystals of anthracene. A voltage was applied between silver paste electrodes that were placed on the opposite sides of an anthracene

crystal. Bright blue emission was observed. However, these devices were impractical for commercial applications because of the high voltages required for their operation and the need for exceptionally pure crystals. Due to innovations in the fields of vacuum and thin-film coating technologies in 1982, Vincett et al. [3] fabricated light-emitting devices based on evaporated thin films of anthracene. These were an order of magnitude thinner than the single crystals used by Pope et al. By using very thin vapor-deposited films, high fields are generated across the devices at much lower voltages, thereby substantially improving the device efficiency.

By taking advantage of modern thin-film organic vapor deposition techniques, the field of organic electroluminescence or organic light-emitting devices (OLEDs) gained new impetus in the 1980s. In 1987, Tang and VanSlyke [4,5] reported a key breakthrough in terms of improved device performance. They separated the functions of charge transport and emission in a device by introducing monopolar charge transport layers. This device, along with the chemical structures of the materials used, is shown in Figure 7.1. OLED architectures are now far more complicated compared to the early devices. The idea of using multilayer [6] structures to separate the functions of charge injection, charge transport, and emission can be extended to three layers or more by using an emitter layer sandwiched between a hole injection layer (HIL) or hole transport layer (HTL) and an electron transport layer (ETL).

Another important early advance made by Tang et al. [7] is the use of fluorescent doping, i.e., the addition of a small percentage of an emissive fluorescent material into a host matrix. This can be used to alter the color of emission, in addition to improving the efficiency and the lifetime of devices. The technique of simultaneously vapor depositing the host and the fluorescent dopant material is now widely used in the field of OLEDs.

Over the last 50 years, remarkable improvements in the performance of vapor-deposited OLEDs have been made. Operating voltages have been decreased from a few kilovolts to a few volts, at the same time efficiencies are now approaching 100 lm/W. These improvements in device performance have made commercial displays based on vapor-deposited OLEDs viable. This technology is now poised to compete with liquid crystal displays (LCDs) in an expanding flat panel display marketplace.

Early displays [8] based on vapor-deposited OLEDs were simple alphanumeric devices. More recently, there have been rapid increases in the complexity of these devices. In 1996, Pioneer Corporation demonstrated a monochrome 64×256 pixel OLED display [9] that was subsequently developed into a product and was incorporated into automobile stereos (see Figure 7.2). Today full-color, high-resolution vapor-deposited OLED displays as large as 24" have been developed [10].

In addition to display applications, researchers are also exploring the use of vapor-deposited organic materials in devices such as photovoltaics [11], organic lasers [12], and organic thin-film transistors (TFTs) [13].

The aim of this chapter is to give the reader a broad overview of the field of vapor-deposited small-molecule OLEDs. It is beyond the scope of this chapter to cover every aspect of these devices, however key references are given throughout the text for those readers who are interested in delving more deeply into this topic. Section 7.2 describes the key elements of a typical OLED. Alternative device architectures are also briefly described. Section 7.3 describes the typical fabrication methods and materials used in the construction of vapor-deposited OLEDs. Section 7.4 describes the physics of an OLED in addition to the improvement of the performance over time made through advances in device architectures and materials. Section 7.5 discusses OLED displays and Section 7.6 looks at the future exciting possibilities for the field of vapor-deposited organic devices.

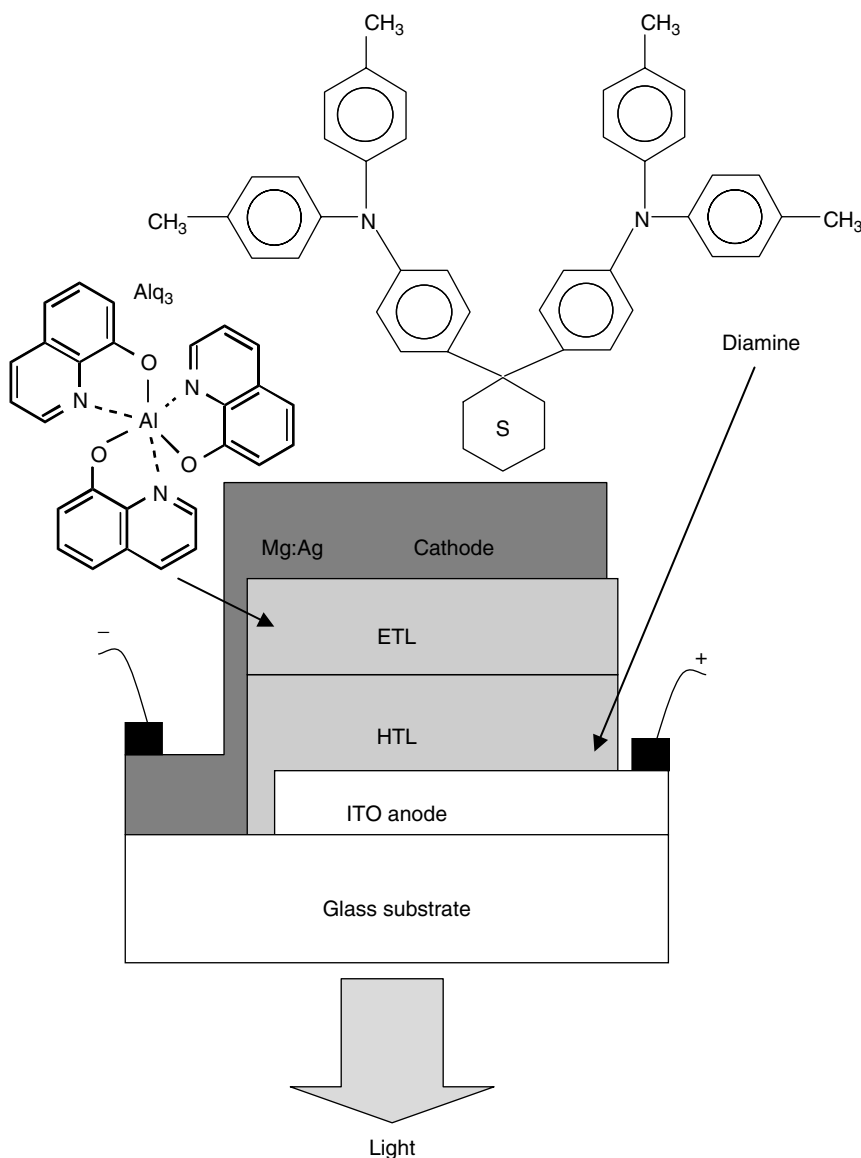


FIGURE 7.1 A two-layer vapor-deposited OLED first demonstrated by Tang et al. [4]. The diamine acts as the hole transporting layer, Alq₃ acts as the electron transporting or emitting layer. The external quantum efficiency was ~1%.

7.2 VAPOR-DEPOSITED ORGANIC LIGHT-EMITTING DEVICE ARCHITECTURES

Figure 7.1 shows one of the simplest possible OLED architectures. It consists of two organic layers sandwiched between a transparent anode and a metal cathode. When a voltage is applied across the device, electrons and holes are injected into the organic layers at the electrodes and move through the device under the influence of a high-applied electrical field (of the order of 10^6 V/cm). These charges can then combine via a Coulombic interaction, forming excited molecular species, some of which may then emit light as they decay to their ground state. This process is described in more detail in Section 7.4.



FIGURE 7.2 The world's first commercially available OLED display (1999). The display is manufactured by Pioneer Corporation and is incorporated into automotive stereos.

The following sections will first describe the major components of a typical bottom-emitting OLED: the transparent anode, the organic layers, and the metal cathode. Alternative device architectures are also briefly described.

7.2.1 ANODE

The anode in OLED devices is typically indium–tin-oxide (ITO), because it is a stable, transparent, and highly conductive material. It is also easily patterned using standard lithographic techniques to define different emitting regions or pixels on a substrate. A thin inorganic barrier layer (e.g., SiO_2) is often used between the polished glass substrate and the ITO film to prevent the migration of ions from the glass into the subsequently deposited device. Various groups have looked at different types of ITO (e-beam and sputtered) and the effects of annealing in O_2 and other surface treatments [14–17]. In the case of transparent conductive metal oxides (e.g., ITO) the stoichiometry and thickness of the oxide is controlled to realize a specific transparency, outcoupling constant, and conductivity of the film. Typically in OLED displays, the film is 50- to 200-nm thick. Additionally as OLEDs are field-dependent devices, and the organic films are of the same order of magnitude in thickness as the anode, the surface roughness of the anode must be low. This is to prevent shorting of the OLEDs and nonuniform light emission. Typically a surface roughness of <2 nm root mean square (rms) is required. In the case of flexible substrates, achieving this uniformity can be problematic. For example, commercially available heat-stabilized polyethylene terephthalate (PET) substrates have surface asperities up to 150 nm [18]. Here, additional planarizing layers must be employed prior to deposition of the anode. See Section 7.6 for more discussion of flexible substrates and devices.

Semitransparent layers of various polymers [19], metals [20], and metal oxides [21] have been used as alternatives to ITO, however ITO is the present industry standard due to its favorable properties and its widespread use in the more mature and widespread LCD industry.

7.2.2 ORGANIC MATERIALS

A wide range of small-molecule organic materials have been used in vapor-deposited OLEDs. Some of the requisite properties of the materials used in vapor deposition are listed below:

- The organic materials must evaporate without decomposing during the fabrication process. The typical deposition temperature range is between 150 and 450°C. Factors that contribute to the ultimate temperature used in addition to the physical properties of the material include the vacuum pressure, source to substrate geometry, and required deposition rate.

- The organic material, once deposited, must form high-quality, defect-free films with precisely controlled thicknesses, typically in the region of 5–200 nm.
- The films must be stable for long periods. Some materials, particularly those with a low glass transition temperature (T_g) may crystallize over time [22,23]. Crystallization may be accelerated when the temperature of the thin film is raised during device operation [24–26]. Therefore, a high T_g is often desirable for the long-term durability of the OLED, e.g., $T_g > 85^\circ\text{C}$.

The morphology of the organic films can be assessed using optical microscopy (in particular techniques such as Nomarski microscopy, atomic force microscopy, and surface profiling techniques). It should also be noted that the purity of the organic materials used is of crucial importance for efficient charge transport and emission in addition to the lifetime of the OLED.

As described earlier, the multiple organic layers in OLED devices must collectively fulfill three main functions: charge injection, charge transport through the device, and light emission. Although these functions may be separated and materials optimized for each property independently, choosing an appropriate combination of emitting and charge transporting films to avoid exciplex formation [27], for example, is essential for building efficient devices [28].

7.2.3 CATHODE

The cathode is typically a low work function metal or metal alloy that facilitates the injection of electrons into the organic material adjacent to it. A low work function metal is necessary to minimize the barrier to electron injection into the adjacent organic material that typically has lowest unoccupied molecular orbital (LUMO) levels of ~ 3 eV. Low work function metals that have been used include In, Mg, Ca, and Ba. However, all of these are reactive under ambient conditions and require careful encapsulation after completion of the device. Tang et al. found that, while Mg is a difficult material to deposit reproducibly onto many organic materials, evaporating a small amount of Ag from a second source during the Mg evaporation (coevaporation is typically in a 10:1 ratio) resulted in more reproducible results and much improved film formation [4]. Murayama et al. [29] found that aluminum cathodes with a codeposited 0.1% Li concentration resulted in increased device efficiencies and reduced drive voltages. Recent work has increased our understanding of these systems, particularly with respect to the way lithium diffuses. The result has been that the use of multilayer Al:Li:Al cathodes [30] and the use of lithium-doped organic electron injecting layers [31] each provide for good injection characteristics. More recently, researchers reported that the presence of a thin insulating layer such as LiF [32] between the cathode and the organic layers leads to improved device performance. LiF/Al or $\text{Li}_2\text{O}/\text{Al}$ [33] cathodes are now widely used in the vapor-deposited OLED community.

7.2.4 ALTERNATIVE DEVICE ARCHITECTURES

Described above are examples of typical materials used in traditional bottom-emitting OLEDs, i.e., in a device architecture where light exits through a transparent anode that is in intimate contact with a transparent substrate. Alternative device architectures are also possible, for example top-emitting OLEDs (TOLEDs). Here the cathode is transparent, thereby allowing light to exit through the top of the device. Cathodes in such a device architecture can be formed by using a thin metal contact [34], a thin metal (e.g., ~ 10 nm of Mg/Ag) in conjunction with a conductive metal oxide (e.g., ITO) [35], or a metal-free electrode [36]. In a top-emitting configuration, the anode is usually a high reflectance high work function material or composite of materials (e.g., Pt, Ag/ITO, or Al/Ni).

Transparent OLEDs can also be made if the anode itself is also transparent [37]. For further discussion of top-emitting devices, see Section 7.5.

Other device architectures include inverted OLEDs. Here the cathode is in intimate contact with the substrate. The organic layers are then deposited onto the cathode in reverse order, i.e., starting with the electron transport material and ending with the HIL. The device is completed with an anode contact. In this case, as above, one of the electrodes is transparent, and light exits from the device through that contact. For example, Bulovic et al. [38], fabricated a device in which Mg/Ag was the bottom contact and ITO the top electrode. The advantage of this type of architecture is that it allows for easier integration with n-type TFTs (see Section 7.5 for a discussion of active-matrix drive OLED displays).

7.3 DEVICE FABRICATION

Figure 7.3 shows a simple schematic example of the basic steps required to fabricate a bottom emitting vapor-deposited OLED test pixel similar to the device shown in Figure 7.1.

7.3.1 ANODE PREPARATION

All substrate preparations prior to the deposition of the organic materials are carried out in a clean room environment to minimize particulates on the anode surface. OLEDs are typically

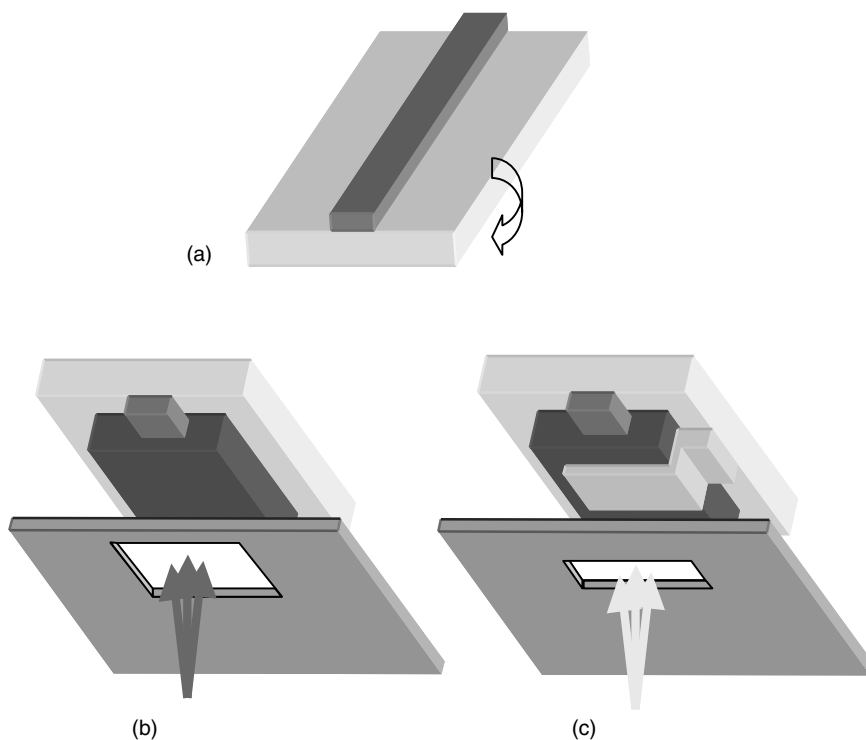


FIGURE 7.3 Schematic representation of the basic steps required in fabricating a vapor-deposited OLED test pixel. (a) anode patterning via lithography, (b) deposition of the organic, and (c) metal cathode layers through shadow masks.

of the order of 80–200-nm thick, and therefore any particles on the surface may lead to breaks in the continuity of the film, resulting in electrical shorts or visible defects. In the case of simple test devices, the clean ITO substrate is first patterned using standard photolithographic techniques to form transparent anodes as shown in Figure 7.3a. For a display, the substrate topography is more complicated and may include transistors or bus lines, etc. This situation is discussed in detail in Section 7.5. Even in the case of these more complicated structures, as for example in a 150 dots per inch (dpi) full-color display where the anode pitch is 56 μm , patterned anodes are easily realized using conventional lithographic techniques. Once the anode is patterned, the substrate is then transferred to a vacuum deposition chamber. Prior to the growth of the organic layers, the ITO surface is usually subjected to some additional pretreatment step, e.g., oxygen plasma [39] or UV ozone exposure [7]. This pretreatment, prior to device fabrication, leads to an enhanced device performance that is believed to be due, in part, to a resultant increase in the work function of the ITO surface [15].

The typical thickness of the ITO layer is 80–200 nm, which is of the same order of thickness as the total organic layer. Therefore, devices risk the possibility of nonuniform emission or shorts developing due to the presence of a thinner organic film and higher electrical fields at the sides of the patterned ITO electrodes (substrate to ITO step). This is especially true when fabricating displays, where high yields are necessary. To counter this problem, some manufacturers add additional complexity to the pixel by adding a grid material. Here, again using lithography, a nonconductive material is deposited over the pixel and patterned so as to leave an opening to the ITO that will eventually define the active area of the pixel. This method is used to limit the possibility of shorting at the edges of the ITO to substrate step. Photoresist materials or inorganic oxides, e.g., SiO_2 , are often used as the grid material. The fabrication conditions are chosen so as to give the grid edge a tapered profile so that when the organic and metal films are deposited into the opening, shadowing effects do not occur at the edges of the film, leaving nonuniform thinner films in these regions that may be prone to electrical shorts.

7.3.2 DEPOSITION OF ORGANIC LAYERS

The organic layers are deposited sequentially onto the anode through a shadow mask (see Figure 7.3b) by thermal evaporation [40] from resistively heated source boats in a high-vacuum environment. In research tools, a given evaporation chamber will often contain several different materials. In manufacturing tools, multiple evaporation chambers are often used with a limit of only one or two types of material per chamber to minimize the risk of cross contamination between evaporation sources. The shadow mask defines the area on the substrate over which the organic layers are deposited. If the final device is a full-color display, at least three shadow masks are typically needed to independently define the red, green, and blue pixels. For high-resolution displays, high accuracy is required in positioning the shadow mask and depositing the three colors. For example, a 150 dpi display has a subpixel pitch of 56 μm . Therefore, to prevent an overlap of one organic layer color over to the next pixel and to maximize the fill factor or active area of the display, a mask alignment accuracy of 5 μm is stated as a requirement by most manufacturers. This alignment process is typically achieved through the aid of (a) a moving stage, (b) cameras to locate the correct relative position of mask to substrate, and (c) an electromagnet to fix the mask in position. Masking accuracy, in addition to reduced feathering, i.e., poor definition of the edges of the organic film, is improved by using contact alignment. The alignment procedure usually takes place in a chamber that is remote from the organic deposition chambers. Often additional

masks are used to define the deposition area for the organic layers common to all the three colors, e.g., the charge injection and transport layers. In this case and when monochrome devices are fabricated, the alignment tolerances are not as stringent.

The organic deposition sources are made of a variety of materials including ceramics (e.g., boron nitride, aluminum oxide, and quartz) or metallic boats (e.g., tantalum or molybdenum). Deposition is carried out in high vacuum at a base pressure of around 10^{-7} torr. The vacuum conditions under which OLEDs are fabricated are extremely important [41] and evaporation rates, monitored using quartz oscillators, are typically in the range 0.01–0.5 nm/s in research and development tools. In manufacturing, higher rates or multiple sources may be used to reduce tact times.

Depending upon the organic material in question, evaporation takes place from either the liquid or the solid state. In general, this occurs from the liquid state if at the melting point the material does not reach a vapor pressure $>10^{-3}$ torr. For example, 4,4'-bis[*N*-(1-naphthyl)-*N*-phenyl-amino] biphenyl (NPB), a hole transport material used in OLEDs, melts before evaporating under typical growth rates. Most of the other organic materials achieve a higher vapor pressure well before their melting point and therefore evaporation is achieved via sublimation of the material.

The deposition geometry, i.e., the relative position of the substrate and sources, is of paramount importance when fabricating OLEDs (see Figure 7.4). For a substrate on a plane at right angles to a point evaporation source, the deposited film thickness d can be expressed by the following relationship:

$$d = \frac{M_e \cos \varphi}{4\pi\rho r^2} \quad (7.1)$$

where M_e is the total evaporated mass, r is the source-to-substrate distance, ρ is the deposited film density, and φ is the angle subtended by the line joining source and substrate measurement points and the normal from the substrate plane to source position.

OLEDs typically operate under applied fields of 10^6 V/cm and are of the order of 100 nm in thickness. The current through the device and the light emitted from the device, above the threshold voltage, increase with a power law dependence on the applied field. Therefore, any significant variations in film thickness across a display will lead to visible nonuniformities in emission. In commercial evaporators, to reduce production costs, manufacturers maximize the number of displays per substrate and the size of the substrate. They typically require a uniformity tolerance of ~ 3 to 5% for the organic films across a substrate. A complete discussion of the relationship between film uniformity and deposition geometry is beyond the scope of this chapter. For an excellent discussion of this and the various methods used to maximize film uniformities, see Milton Ohring's discussion [42]. In brief, the relationship between the film thickness d (see Figure 7.4) at a given point on a substrate located parallel to a surface source can be expressed as

$$\frac{d}{d_0} = \frac{1}{[1 + (L/h)^2]^{3/2}} \quad (7.2)$$

where d_0 is the thickest point of the film and h is the substrate to source distance at this point (i.e., the shortest distance between the source and the substrate). L is the distance between the source and the point on the substrate at which d is measured. As is apparent from this

*For an ideal point source, the factorial is 3/2.

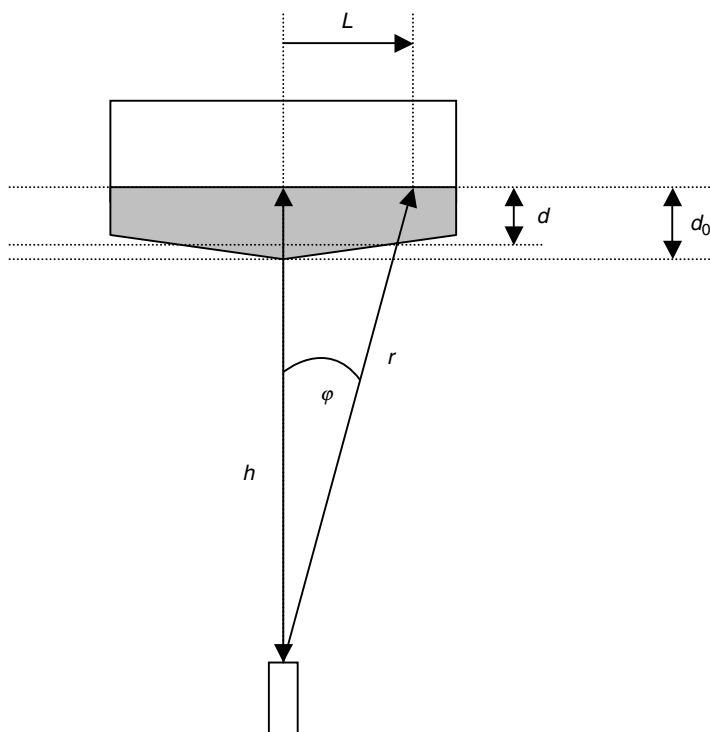


FIGURE 7.4 Schematic diagram of the deposition geometry for a substrate on a plane at right angles to a point evaporation source. d is the deposited film thickness; d_0 is the thickest point of the film and h is the substrate-to-source distance at this point (i.e., the shortest distance between the source and substrate); r is the source-to-substrate distance, φ is the angle subtended by the line joining source and substrate measurement points and the normal from the substrate plane to source position; L is the distance between the source and the point on the substrate at which d is being measured.

relationship, as the substrate size increases, to minimize the difference between d and d_0 , i.e., to obtain a uniform film within acceptable tolerances, the source-to-substrate distance (h) must be increased. Using this simple relationship to achieve a uniformity tolerance of 5% across a 300-mm substrate, a throw distance from a point source of 80 cm is needed. As a result of the larger throw distances used in manufacturing, consequently in order to achieve reasonable deposition rates, the deposition source temperatures are often significantly higher perhaps by as much as 50°C. This places additional stability requirements on the materials that are used in manufacturing. Typically, a manufacturer expects to continuously deposit from a source for at least 24 h at this elevated temperature. Therefore, the materials used must be able to withstand this environment without degradation that may reduce the quality of the deposited material or impact the ability to adequately access stable deposition conditions, i.e., the material's purity must be high and its decomposition temperature significantly above the evaporation temperature.

Other manufacturers are developing linear sources [43]. Here the deposition source is a long linear evaporation source that stretches beyond the width of the substrate. Depending upon the design, either the source or the substrate is translated relative to each other in one direction. The advantage of this geometry is that the substrates no longer need to be at such a great distance from the source to achieve the requisite film uniformity. In addition, substrate rotation is no longer necessary. Materials usage and deposition rates are envisaged to be higher by using

this technique, and, to date, organic thin-film nonuniformities of $<5\%$ over 300×400 mm substrates at a throw distance of 100 mm have been demonstrated [43].

7.3.3 ALTERNATIVE ORGANIC DEPOSITION TECHNIQUES

Various other techniques can also be used to deposit small-molecule materials as thin films. Organic molecular beam deposition [44], spin coating [45–47], doctor blade, ink-jet printing [48,49], thermal transfer [50], Langmuir–Blodgett films [51,52], chemical vapor deposition [53], and self-assembled films [54] have also been used to deposit thin organic layers. Organic vapor phase deposition (OVPD), in particular, looks to be a very exciting new technique to deposit small-molecule materials [55]. Vapor-phase epitaxy is used extensively in the inorganic semiconductor industry, and the analogous technique OVPD is now being developed for organic materials.

To deposit materials using OVPD, the organic material is vaporized and then an inert carrier gas such as nitrogen is used to dilute and carry the material to the cooled substrate. The walls of the deposition chamber are kept hot, thus preventing the organic material from condensing on anything but the substrate surface. Two regimes of growth can occur. The first is the mass transport, where the growth rate is determined by the arrival rate of the source materials at the substrate. The second is the kinetic regime, where, due to viscous flow effects, a boundary layer forms at the substrate due to the slower moving gas. The material must diffuse through this region and so the growth rate in this regime is dependent on the concentration of the material and the depth and shape of the boundary layer.

OVPD has a potentially significant advantage over vapor deposition in manufacturing OLEDs as OVPD is far less wasteful in terms of materials usage. In addition to the obvious advantage that OVPD has in terms of manufacturing compatibility, it also has the potential to be a more accurate deposition tool. This is due to the fact that the deposition rate is controlled by the mass flow controllers rather than by the temperature of a thermal source. When thermally evaporating organic materials, small changes in temperature have significant effects on the deposition rate due to the rapid changes in vapor pressure at the material's sublimation point. OVPD avoids this problem by controlling the flow of the carrier gas.

7.3.4 DEPOSITION OF CATHODE

Metals and metal oxides used in the cathode are typically deposited at higher deposition rates than the organic layers. Layer thicknesses vary depending upon the device architecture, e.g., 10 nm to 1 μm . Aluminum is often the first choice as a cathode material (see Section 7.2 for other cathode materials). Aluminum evaporates from a liquid phase. In many research tools, the primary method of deposition is via thermal evaporation from resistively heated sources. For aluminum deposition, boron nitride crucibles or tungsten wires are often used as sources. An e-beam evaporation source can also be used. This has the advantage of having a reduced risk of source contamination due to the amount of material in contact with the source boat in the liquid phase, in addition to the reduced contaminant level, e.g., oxygen content, of the deposited film as a consequence of the higher evaporation rates that can be realized. However, care must be taken to avoid the possibility of secondary electrons causing damage to the organic layers. Sputtering deposition techniques can also be used to deposit the cathode, depending on the material [56]. However, care has to be taken when employing this technique to avoid damage from radiation, charging, and heating.

The metal cathode is deposited onto the organic layers through a shadow mask (see Figure 7.3c). For active-matrix OLED (AMOLED) displays, a single unbroken cathode is often used over the entire display area.

7.3.5 ENCAPSULATION OF ORGANIC LIGHT-EMITTING DEVICE

The final step in the OLED fabrication process is encapsulation. This step is necessary to ensure a long device lifetime. OLEDs [4,57,58] built on glass substrates have been shown to have lifetimes (generally defined as the time taken to decay to half the initial luminance at constant current) of tens of thousands of hours [59,60]. There have been many proposed mechanisms for the decay in luminance, but most theories agree that one of the dominant degradation mechanisms in unencapsulated OLEDs, which have far shorter lifetimes than encapsulated devices, is exposure of the organic–cathode interface to atmospheric oxygen and water. This leads to oxidation and delamination of the metal cathode [61,62] as well as potential chemical reactions within the organic layers. As most of the OLED work, to date, has been focused on the development and manufacture of glass-based displays, the degradation problem is ameliorated by sealing the display in an inert atmosphere, e.g., a nitrogen or argon glove box (<1 ppm water and oxygen), using a glass or metal lid attached by a bead of UV-cured epoxy resin [63]. A desiccant such as CaO or BaO is often located in the package to react with any residual water incorporated in the package or diffusing through the epoxy seal. In addition to encapsulation techniques using a lid, thin-film encapsulation techniques are also possible. For a more detailed description of these, see Section 7.6 of this chapter or, for example, Lewis et al. [64].

7.4 DEVICE OPERATION

Figure 7.5 shows a schematic example of the electroluminescent process in a typical two-layer OLED device architecture. When a voltage is applied to the device, five key processes must take place for light emission to occur from the device.

1. *Charge injection*: Holes must be injected from the anode into the HTL while electrons are injected from the cathode into the ETL.
2. *Charge transport*: The holes and electrons must move through the device under the influence of the applied electrical field. The mobility of holes in typical hole transport organic materials is approximately $10^{-3} \text{ cm}^2/(\text{V s})$ [65]. For electrons the mobility is usually one or more orders of magnitude lower [66].
3. *Exciton formation*: The holes and electrons must combine in the emitter region of the device via a Coulombic interaction to form excitons [67] (neutral excited species); other excited states are also possible such as excimer [68] or exciplex excited states [69,70].
4. *Exciton decay*: When an exciton decays radiatively a photon is emitted. When the excitons form in fluorescent materials radiative decay is limited to singlet excitons and emission occurs close to the recombination region [7] of the OLED due to the relatively short lifetime of the excited state (of the order of 10 ns). For phosphorescent materials, emission can occur from triplet excitons. Due to the longer excited state lifetime (of the order of hundreds of nanoseconds), triplet excitons can diffuse further before decaying.
5. *Light emission*: Light is observed from photons that exit the OLED structure. Typically many photons are lost due to processes such as total internal reflection and self-absorption of the internal layers [71]. In typical bottom-emitting device architectures, only 20–30% of the photons created exit the device through the front of the substrate.

Figure 7.6 shows typical current density–voltage–luminance (J – V – L) and emission characteristics of an OLED device. OLEDs have a similar electrical characteristic to that of a rectifying diode. In forward bias, the device starts with a small current at low voltages. In this region, charge carriers are injected into the device but little exciton formation, hence light

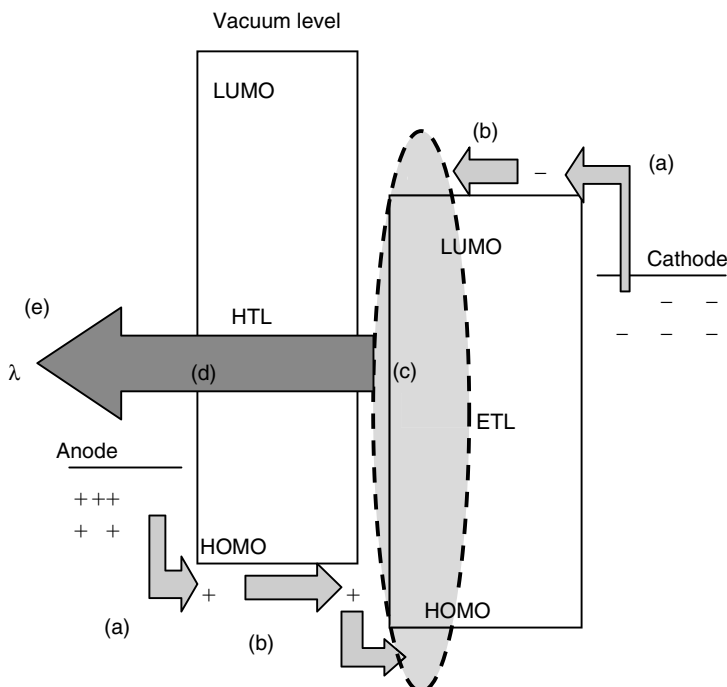


FIGURE 7.5 A schematic diagram of the light emission process in a typical two-layer OLED device architecture. For light emission to exit from the device five key processes must take place: (a) charge injection of holes and electrons at the anode and cathode, (b) charge transport through the device, (c) exciton formation, (d) exciton decay, and (e) light emission.

emission, occurs. As the voltage is raised, the current quickly increases obeying a power law dependence on the voltage. Here, many charges are injected into the device, moving through the charge transport layers and then forming excited species that radiatively decay to produce light. The electroluminescence spectra from OLEDs are generally broad with full width half maxima usually greater than 50 nm. The light emitted from the OLED is directly proportional to the current passing through it. Under reverse bias, there is a small leakage current and in most cases no light emission. Many groups have attempted to model the electrical and light-emitting behavior of OLEDs [72].

In general, a two-layer device structure is more efficient than single-layer architectures. There are two key reasons for this. First, each layer can be separately optimized for the injection and transport of one carrier type. Second, exciton formation and radiative decay take place close to the HTL–ETL interface away from the quenching sites at the organic–metal contacts.

To facilitate good charge transport in an OLED, the organic materials must satisfy three key requirements; they must have a high mobility for either electrons or holes, a good injection efficiency from the contact electrode, and suitable band offsets with other organic layers within the device. These processes are discussed in detail by, for example, Kalinowski [73] and Greenham and Friend [74].

For hole transport, many of the first materials used in OLEDs were originally developed for use in xerography. Various models have been proposed to describe charge transport in such materials [75,76]. One of the most common classes of material used is the arylamines,

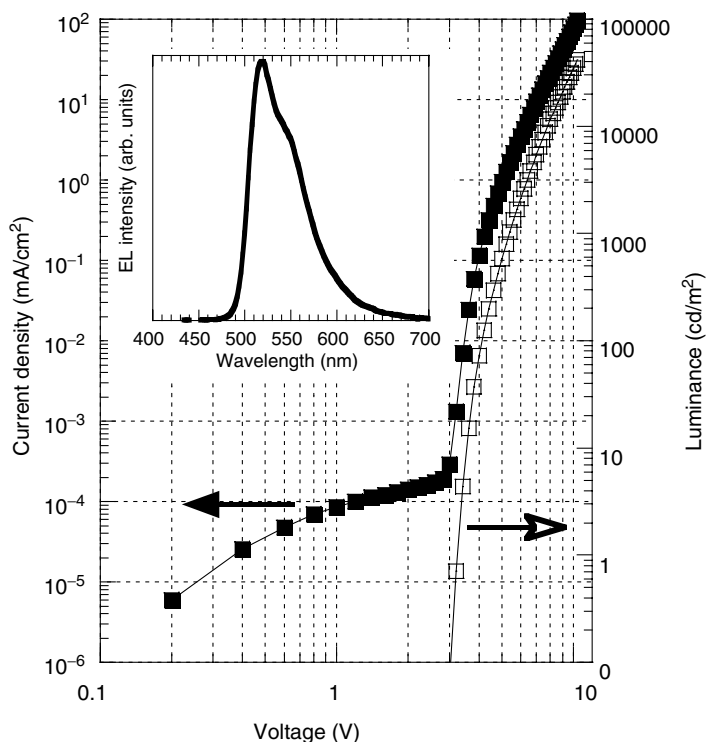


FIGURE 7.6 Typical current density (filled squares)–voltage–luminance (open squares) (J – V – L) and emission characteristics (inset figure) of an OLED device. This J – V – L data is from the device discussed later in Figure 7.10.

one common example of which is NPB (see Figure 7.7). This family of materials exhibits high hole mobilities [77] and a reasonable energy level (ionization potential) that is lined up with the work function of ITO (>4.7 eV), thus giving a relatively small barrier to hole injection. NPB, for example, has a hole mobility of 10^{-3} to 10^{-4} $\text{cm}^2/(\text{V s})$ and an ionization potential that defines the highest occupied molecular orbital (HOMO) level of 5.4 eV [65]. Often in small-molecule OLEDs, an additional hole injection layer is added between the hole transport material and the anode. This is designed to facilitate a smaller energy barrier to hole injection and to counter issues at this interface such as recrystallization and delamination of the organic layer at the anode, which can occur when thin films are deposited by vapor deposition onto the anode surface. For example, copper phthalocyanine (CuPc), shown in Figure 7.7, has been frequently used on ITO anodes to increase the adhesion of subsequent organic layers and to increase device lifetime [78,79]. Thin layers of carbon [80] between the ITO and the HTL have also been shown to decrease the operating voltage and improve the device characteristics. In addition, thin fluorocarbon films on ITO have been used to enhance the stability of the anode interface [80].

The criteria for good electron transport materials are that they should transport electrons, block holes, and have a small barrier to electron injection from the metal cathode. The most commonly used ETL in vacuum-deposited OLEDs is tris-(8-hydroxyquinoline) aluminum (Alq_3), as shown in Figure 7.7. Alq_3 , for example, has a LUMO energy level of 3 eV [65] and an electron mobility of $\sim 5 \times 10^{-5}$ $\text{cm}^2/(\text{V s})$ [66].

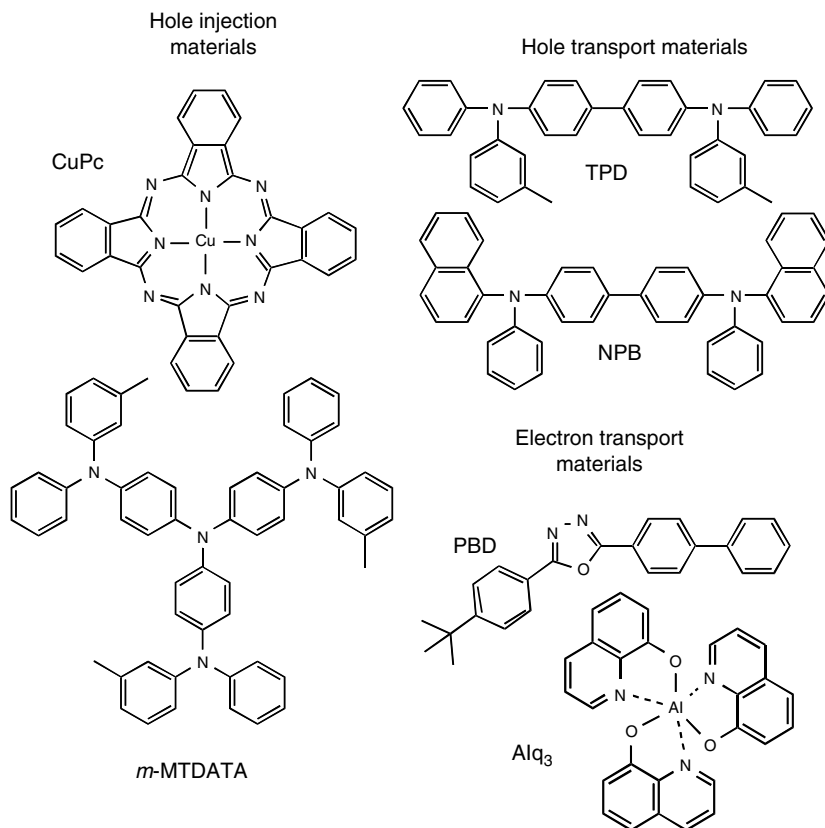


FIGURE 7.7 Examples of hole injecting, hole transporting, and electron transporting materials.

7.4.1 IMPROVING DEVICE EFFICIENCY

For a Lambertian emitting OLED source, where V is the operating voltage, η_{le} is the luminance efficiency (in cd/A), the power efficiency (η) is given by

$$\eta = \eta_{\text{le}} \pi / V \quad (7.3)$$

$$\eta_{\text{le}} = k \eta_{\text{Int}} \cdot \eta_{\text{Out}} \quad (7.4)$$

where η_{Int} is the internal quantum efficiency (% excitons to photons), η_{Out} is the outcoupling efficiency (a measure of how many generated photons are emitted from the device), and k is a constant depending on the photopic response of the human eye. Hence

$$\eta = k \eta_{\text{Int}} \cdot \eta_{\text{Out}} \pi / V \quad (7.5)$$

As a result, power efficiency is a function of the internal quantum efficiency, η_{Int} , the light extraction, η_{Out} , and the voltage, V . Thus, to improve device performance, advances in these three key areas are required. Examples of strategies used to maximize power efficiency are described below.

7.4.2 IMPROVING INTERNAL QUANTUM EFFICIENCY

A wide range of dyes, many of which were originally developed as laser dyes, have been used as emitter materials in OLEDs. One criterion for emitter materials is a high photoluminescence (PL) efficiency with a specific desired color of emission depending upon the application. However, high PL quantum efficiencies in dilute solutions do not always translate to high electroluminescence quantum efficiencies when incorporated into devices. This may be due to quenching via interactions with different molecules [82], oxygen, or the electrodes [83], or due to concentration quenching in the solid state (generally through the formation of aggregate states). One solution to this latter problem is to add substituent groups to the molecule so as to prevent aggregation by increasing the steric hindrance and hence limit the formation of aggregate states [84,85]. Unfortunately, this can lead to poor charge transport through the material, which in turn would lead to an increased device operating voltage and a poor power efficiency.

An elegant solution to this problem is to dope the emissive dye into an organic matrix or host. This effectively dilutes the concentration of the emissive dye (the dopant) and thus prevents aggregation. As long as the dopant is red-shifted compared to the host, i.e., there is adequate overlap of the host emission and dopant absorption spectra to facilitate Förster transfer of the excitons (in fluorescent materials), excitons formed in the host material will tend to migrate to the dopant prior to relaxation. This results in emission that is predominantly from the dopant. Tang et al. [7] found that adding a small percentage of 4-(dicyanomethylene)-2-methyl-6-(4-dimethylaminostyryl)-4*H*-pyran (DCM1), (see Figure 7.8), to an Alq₃ layer, shifted the emission from green to orange-red. Doped devices are therefore fabricated by vapor depositing the host and dopant material at the same time. The ratio of host to dopant is determined by controlling the relative rate of evaporation of the two

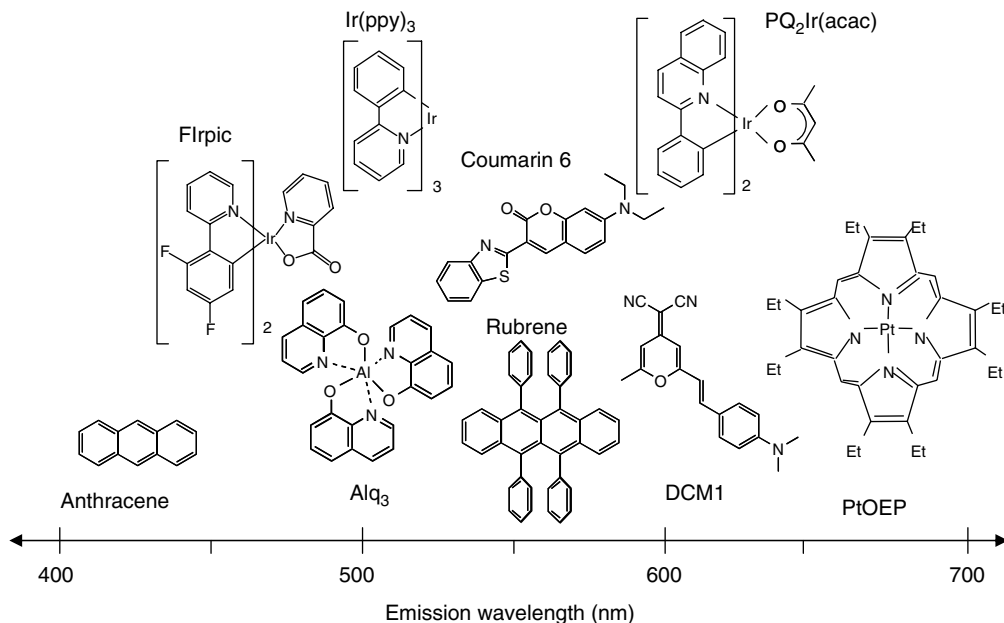


FIGURE 7.8 Molecular structures of several organic emitter materials. Their positions on the diagram are arranged as a function of their emission color with blue emitters on the left, green in the center, and red on the right hand side.

materials to form a doped layer within the device. The key benefit of this approach, which is now widely used within the industry [86], is that it allows the processes of charge transport, exciton formation, and emission to be optimized separately within the host and dopant materials. This also allows emitters to be used that would not otherwise form good films.

7.4.3 IMPROVED EFFICIENCY THROUGH DOPING

The doping of the emissive layer in an OLED has been used extensively as a way of improving efficiency and lifetime, in addition to being used to modify the emission color. Tang et al. [7] first introduced fluorescent dyes, 3-(2-benzothiazolyl)-7-diethylaminocoumarin (coumarin 540 or coumarin 6 and DCMs, as dopants in Alq₃ to improve the efficiency and color purity of devices (see Figure 7.8). Since then, a wide range of fluorescent dopants have been used in OLEDs [87,88]. The ground state of most materials has a singlet spin state $S=0$. Emission of a photon in fluorescent materials conserves spin, therefore only singlet $S=0$ excited states typically emit light. Decay from the triplet $S=1$ excited states is typically a nonradiative process for most organic materials and so these triplet excitons are lost from the perspective of light emission. The maximum possible internal quantum efficiency that can be obtained in an OLED using fluorescent materials is limited by the ratio of these excited states $S=0$ and $S=1$ or the so-called exciton singlet-to-triplet ratio, which is approximately 1:3 [89]. This limits fluorescent OLEDs to a maximum internal quantum efficiency of approximately 25%. Recently, phosphorescent OLEDs (PHOLEDs) [90], which incorporate heavy metal organometallic compounds as dopants, have surpassed this efficiency [91].

In a PHOLED system, all the singlet excited state excitons may be converted into the triplet excited state through intersystem crossing (S_1 to T_1) via the presence of a heavy metal atom. In these devices, the triplet states can emit radiatively (T_1 to S_0), enabling record high conversion efficiencies. The first generation of PHOLEDs contained platinum 2,3,7,8,12,13,17,18-octaethyl-12*H*,23*H*-porphyrin (PtOEP) as the phosphor [90] (see Figure 7.8). Porphine complexes possess long-lived triplet states that have been used in oxygen detection. This lifetime is reduced by addition of a platinum atom to the porphine ring due to the increased spin-orbit coupling. The result is an enhancement in efficiency due to the combined effect of forming 75% of the excitons directly as triplets in addition to the 25% that intersystem cross from the singlet excited state to the triplet excited state. The first published PtOEP devices had an external quantum efficiency of 4%. This was subsequently increased to 6% with the introduction of a blocking layer within the device structure [92]. Although this is an impressive device efficiency it could only be realized at low drive currents and luminance levels. At high luminance levels due to the long-lived nature of the triplet excitons in PtOEP ($>10\ \mu\text{s}$) the available dopant sites in the device at low dopant concentrations become saturated, which results in a roll-off in efficiency with increased current.

Later generations of PHOLEDs have improved considerably upon the early promise of PtOEP. In organometallic complexes the presence of a heavy metal atom in addition to allowing intersystem crossing from the singlet S_1 to the triplet T_1 excited state on the organic ligands can also participate in the transfer of an electron to an organic ligand. This is known as metal-ligand charge transfer (MLCT). The resultant excitons have a larger overlap with the metal atom than is the case with ligand excitons. The spin-orbit coupling is therefore enhanced, resulting in a mixing between the MLCT triplet and the singlet. To ensure high efficiency, particularly at high luminance levels, it is essential to minimize the triplet excited state lifetime. To achieve this, the MLCT triplet energy should be lower than that of the ligand. The $5d^6$ complexes that use Ir^{3+} provide for this possibility. PHOLEDs incorporating phosphorescent organometallic iridium compounds have exhibited green electroluminescence

with maximum external quantum efficiencies of 19% [93,94]. Allowing for effects such as outcoupling, the internal quantum efficiency of such devices has been estimated to be close to 100%. Figure 7.8 contains examples of Ir^{3+} organometallic complexes that exhibit light emission spanning the visible spectrum from blue [95] through green [91] to red [96].

PHOLEDs also show excellent stability under display drive conditions. First generation phosphorescent dopants such as PtOEP, *fac* tris(2-phenylpyridine)iridium ($\text{Ir}(\text{ppy})_3$), and iridium(III)*bis*(2-phenylquinolyl-*N,C*2)acetylacetonate ($\text{PQ}_2\text{Ir}(\text{acac})$) have demonstrated lifetimes of several thousands of hours [60,96]. Recent PHOLEDs have shown lifetimes in excess of 30,000 h at display brightnesses [97].

7.4.4 IMPROVING POWER EFFICIENCY

In typical OLEDs, the applied voltage V is usually 5–8 V, when illuminated at 500–1000 cd/m^2 , i.e., greater than twice the voltage of the emitted photon V_λ . The voltage drop across the emission layer itself is usually 2 to 3 V, depending upon the emission wavelength. The remaining voltage is dropped predominantly across the ETL, across the HTL, and at the heterojunction interfaces. Current transport in low-mobility organic films is space-charge limited [98] and high electric fields are required to inject the necessary charge to generate the desired photon flux. Band misalignments at the heterojunction interfaces also result in voltage loss. However, the drive voltage can be significantly reduced by conductivity doping of the transport layers [99]. Recently, conductivity doping was demonstrated using green $\text{Ir}(\text{ppy})_3$ -doped PHOLEDs [100]. It was observed that the drive voltage necessary to produce 100 cd/m^2 was 2.65 V, i.e., only slightly higher than V_λ . This device used p-type (tetrafluoro-tetracyanoquinodimethane ($\text{F}_4\text{-TCNQ}$)) and n-type (Li) doping of the HTL and ETL, respectively.

7.4.5 OUTCOUPLING

Once photons are created within conventional bottom-emitting OLEDs, the external quantum efficiency, i.e., the number of photons emitted from the viewing side (or glass substrate) per injected charge, is limited by a number of loss mechanisms. Photons can be lost through self-absorption of the organic layers, waveguiding within the device, and absorption of the photons in the cathode. For typical bottom-emitting OLEDs fabricated on glass substrates, approximately 20% of the photons generated exit the glass through the front surface. This is a very approximate, but often quoted, estimate. To a first approximation the outcoupling efficiency, i.e., the fraction of light emitted by the device, χ is given by

$$\chi = 1 - \left(- (1/n_i^2) \right)^{1/2} \quad (7.6)$$

where n_i is the refractive index of the emissive layer [101]. For typical materials used in an OLED with $n_i = 1.7$, Equation 7.6 produces an estimated outcoupling efficiency of 19%. Most of the remaining light is waveguided in the substrate and the organic layers.

Hence, we find that today, the most significant limitation to the efficiency of OLEDs is the internal reflection of about 80% of the emitting light in the glass substrate. In this case, without light extraction enhancement outcoupling, $\eta_{\text{ext}} \sim 20\%$ presents a fundamental limit for devices with 100% internal efficiency.

The relationship given above is only a first-order approximation and the actual amount of light emitted is color-, material-, and thickness-dependent. Methods employed to overcome efficiency limitations due to light trapping have primarily concentrated on expanding the escape cone of the substrate and suppressing the waveguide modes. These methods

include introducing rough or textured surfaces [102], mesa structures [103], and lenses [104], and the use of reflecting surfaces or distributed Bragg reflectors [105,106]. Consequently, many of the methods used to improve LED outcoupling [107] have also been applied to OLEDs. For polymer LEDs (PLEDs) [108], it was shown that a corrugated substrate increased the light output by a factor close to two by Bragg-scattering in the forward direction. A similar improvement was achieved by placing a single millimeter-sized hemispherical lens [109,110] on the substrate aligned with the OLED on its opposite surface. Also, shaping of the device into a mesa structure showed an increase of η_{ext} by a factor of two [111]. The incorporation of monolayers of silica spheres with diameters of 550 nm as a scattering medium in a device, or the positioning of these monolayers on the substrate, also showed enhanced light output [112]. Recently, Tsutsui et al. showed that the external quantum efficiency can be doubled by incorporating a thin layer of a very low refractive index silica aerogel ($n_i \sim 1.03$) in the device [113].

Another method of enhancing the outcoupling efficiency has been the use of an ordered array of microlenses [114]. In a conventional planar structure, the light generated in the OLED is either emitted externally or waveguided in the substrate or the ITO–organic layer and lost (Figure 7.9). Substrate patterning destroys the substrate waveguide, redirecting the waveguiding modes externally, thus increasing the outcoupling efficiency. The lenses are produced using a simple fabrication process, and require no alignment with the OLEDs. Furthermore, the emission spectrum of the lensed OLEDs exhibits no angular dependence. In particular, the light output for high angles of observation with respect to the surface normal is

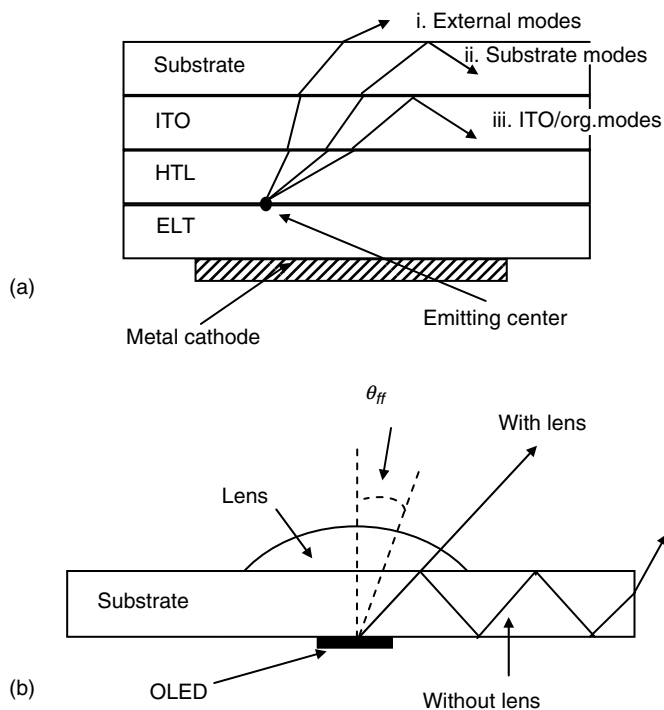


FIGURE 7.9 Outcoupling in an OLED. (a) Three radiative modes in an OLED: (i) external modes, (ii) substrate modes, and (iii) ITO–organic modes. (b) Attaching a lens to the backside of an OLED converts some of the light from substrate to external modes.

considerably increased. Experimentally, the external quantum efficiency of an electrophosphorescent device is found to increase from 9.5% using a flat glass substrate to 14.5% using a substrate with a micromolded lens array.

Although a significant increase of η_{ext} was observed for the reported methods above, they are often accompanied by changes in the radiation pattern. This can lead to undesirable angular-dependent emission spectra or, in the case of displays, a blurring of the display as light emitted from neighboring pixels exits the display distant to the originating pixel. Therefore, a manufacturable increase in the outcoupling scheme for OLED displays has to date not been realized.

7.4.6 LIFETIME

One issue that limited the early adoption of OLEDs in commercial products was device stability both during storage and in operation. Suggested causes of degradation include indium migration from the ITO anode [115], morphological instability of the organic materials [116], fixed charge accumulation within the device [117], damage to the electrodes, and the formation of nonemissive dark spots [63,118,119]. Water and oxygen are known to cause problems in OLEDs. Therefore, a great deal of effort has been directed toward the encapsulation of devices. Encapsulation is typically carried out under a nitrogen atmosphere inside a glove box.

In addition to extrinsic environmental causes of degradation in OLEDs some groups have explored the limitations of the individual device materials to transport charge and emit light. For example, Aziz et al. have proposed that in simple Alq_3 devices hole transport through the Alq_3 layer is the dominant cause of device degradation due to the instability of the Alq_3^+ cationic species [120]. A useful overview of the factors affecting device reliability is given by Forrest et al. [121] and Popovic and Aziz [122].

The minimum target set by many manufacturers for test pixel architectures prior to adoption in a commercial display is a lifetime of 10,000 h at display brightness. However, the lifetime of a similar pixel obtained in a display is often less than this value due to additional complications such as pixel yield and added heat load [26] to the pixel from the display. However, great strides in lifetime have been made within the OLED community, with several manufacturers claiming lifetimes at display brightness of >100,000 h.

7.5 VAPOR-DEPOSITED ORGANIC LIGHT-EMITTING DEVICE DISPLAYS

One of the most obvious markets for thin-film vapor-deposited organic materials is in flat panel displays [123], a market currently dominated by LCDs. Over the last two decades, a great improvement in the lifetime and efficiency of OLEDs have been achieved. OLED displays can already be found in simple applications such as automobile stereos, mobile phones, and digital cameras. However, to exploit the advantages of the technology fully, it is necessary to pattern the OLEDs to form monochrome, or more preferentially, full-color displays. This section will consider the difficulties involved in addressing such displays (either passively or actively) and the variety of patterning methods that can be used to produce full-color displays.

7.5.1 PASSIVE ADDRESSING SCHEMES

Displays based on OLEDs may be addressed either passively or actively [124], and the drive requirements are quite different in each case. In passive-matrix addressing, the display is addressed one line at a time, so if a display has 480 lines then a pixel can only be emitting for

1/480th of the time. This has important implications for the materials and device structure chosen, because it means that to achieve an average luminance of 200 cd/m^2 the instantaneous luminance on the pixel must be $(200 \times 480) 96,000 \text{ cd/m}^2$. This leads to high current densities in the metal tracks, requiring expensive driver integrated circuits (ICs) capable of handling high currents and generating significant heating problems. It is therefore necessary to design materials and device structures capable of operating under pulsed operation. By successfully operating their displays at a duty ratio of 0.002, researchers at Idemitsu Kosan were able to conclude that it is possible to operate passively addressed panels with less than 500 lines at video-rate [125].

Previously, there had been a perception in the OLED research field that PHOLEDs, although highly desirable for use in active-matrix applications because of their high efficiency, were unsuitable for passive-matrix applications. The first generation of PHOLEDs contained PtOEP as the phosphorescent dopant. However, these devices had a spectral dependence on applied current. This was a result of the long radiative lifetime of PtOEP ($>10 \mu\text{s}$). As the applied current was increased, dopant sites within the device became saturated, resulting in the inability of excitons to transfer from the host material. Some of these excitons then decayed, emitting light characteristic of the host material. The devices also exhibit a steep roll-off in efficiency that has been mainly interpreted as the result of triplet-triplet annihilation. However, the latest generations of PHOLEDs have efficiency roll-offs at high drives that are comparable to or better than the conventional fluorescent OLED or PLED devices [126], and they show higher efficiency at the high luminance values needed in a passively addressed display. For example, a red PHOLED, designed for long lifetime ($>20,000 \text{ h}$), has been demonstrated with Commission Internationale d'Éclairage (CIE) coordinates of (0.65, 0.35) with an efficiency of 8.5 cd/A at $10,000 \text{ cd/m}^2$. Figure 7.10 shows the efficiency characteristics of a new green PHOLED. This particular dopant has improved efficiency characteristics (82 cd/A at 1000 cd/m^2 and 45 cd/A at $50,000 \text{ cd/m}^2$) and is therefore even more suitable for passive-matrix (as well as active-matrix) display applications [97].

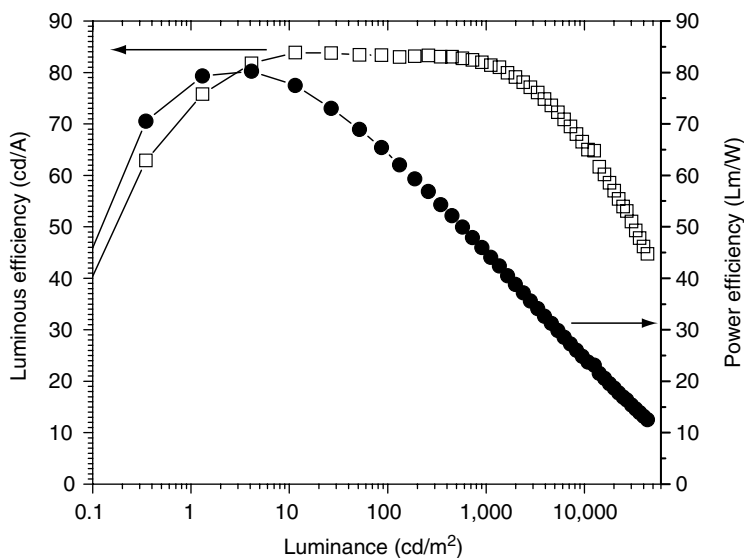


FIGURE 7.10 Luminous efficiency (open squares) and power efficiency (filled circles) versus luminance for a PHOLED incorporating an improved green phosphorescent dopant.

The main advantages of passive addressing are that it is relatively inexpensive and that, in principle, it is possible to drive small-to-medium-sized displays. However, large-area, high-resolution displays ($>5''$) are problematic due to the high current densities and hence increased power consumption (I^2R) described above. For a more detailed discussion of these issues see, for example, Gu and Forrest [127].

For passive-matrix OLED (PMOLED) displays the individual pixels have to be addressed via addressable row and column electrodes hence the necessity to pattern the metal cathode into rows. The thickness of these rows is dependent on the display resolution. If we again consider a 150-dpi display, a cathode row pitch of $169\text{ }\mu\text{m}$ is required. It is possible on a small scale to pattern these features using a string cathode mask, i.e., where very thin parallel metal strings are used to break the deposited film into patterned cathode rows. However, for high-resolution displays, or indeed any display of appreciable size, this technique is problematic due to the low fill factor that can be realized. This is due to the width of the strings that is necessitated by the need for mechanical integrity and the issue of a poorly defined deposition footprint due to feathering at the edges of the deposited metal film.

An alternative method to define the cathode rows is by an integrated shadow mask (ISM) as shown in Figure 7.11. This shows a cross section of one individual element of the ISM. This mushroom feature is patterned on the substrate orthogonal to the anode columns. These features are placed at intervals equal to the required display pitch. After deposition of the organic layers, the subsequently deposited metal is then broken into regularly patterned electrically isolated rows. The ISM is usually constructed from photoresist material that can be patterned with high precision using lithography, thus enabling a higher fill factor and consequently higher resolution PMOLED displays to be realized. Other proposed schemes for patterning the metal cathode on OLED displays include stamping [128], laser ablation [129], and lithography [130].

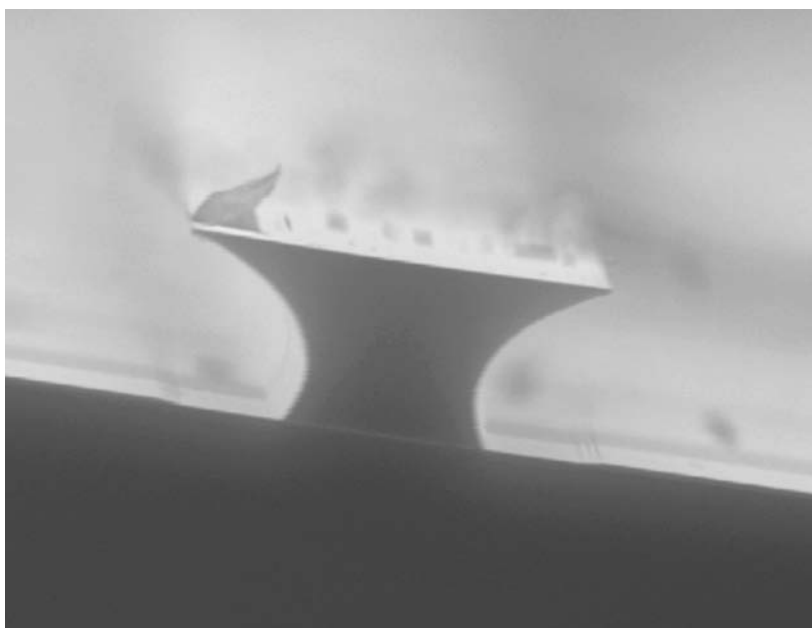


FIGURE 7.11 A scanning electron micrograph image of an ISM cross section.

7.5.2 ACTIVE ADDRESSING SCHEMES

Many LCDs are based on active-matrix addressing, in which an active device circuit containing one or more TFTs is connected to each pixel. The TFT circuit at each pixel effectively acts as an individual electrical switch that provides the means to store display information on a storage capacitor for the entire frame time, such that the pixel can remain emitting during this entire time rather than for a small fraction of time, as is the case in passive addressing.

A remaining challenge in manufacturing AMOLED displays is the requirement for a backplane that provides a constant uniform drive current. Presently, the pixel and driver circuitry must compensate for the initial nonuniformities of the low-temperature polysilicon TFTs or the threshold voltage shift of the amorphous silicon (α -Si) TFTs [131,132]. Most pixel designs incorporate more than two transistors along with a conventional bottom-emitting OLED [131,133]. This can significantly diminish the aperture ratio, forcing the OLED to operate at a high luminance level, reducing lifetime. One solution is to build TOLEDs over a planarized backplane [35,134]. Figure 7.12 shows a 24" OLED display by Sony that uses a TOLED device architecture [10].

However, until recently, it was a commonly held belief that TOLEDs are less efficient than their bottom-emitting counterparts, such that any gain in aperture ratio must be large to offset the efficiency loss. However, this assumption has recently been disproved. Lu et al. [135] compared the characteristics of equivalent green (Ir(ppy)_3) top-emitting PHOLEDs, bottom-emitting PHOLEDs, and transparent PHOLEDs. They observed that the TOLED had a 15% higher luminous efficiency than the bottom-emitting PHOLED in an equivalent device architecture. This was despite the fact that the reflectivity of the TOLED anodes was more than 3% lower than the Al cathodes of the bottom-emitting structure, and the transmissivity of the TOLED cathode was more than 30% lower than the transmissivity of the ITO-coated glass substrate of the bottom-emitting architecture. The enhanced luminance of the TOLEDs was attributed to a more favorable microcavity structure. The microcavity effect does shift the



FIGURE 7.12 A 24" AMOLED display fabricated by Sony using top-emission pixel architectures.

1931 CIE coordinates of the TOLED (-0.06 , -0.01) more than that of the bottom-emitting device (-0.03 , $+0.01$) when one considers a viewing angle of 60° . However, this is of minor concern for green emission but care must be taken when applying this design to blue and red pixels.

Also, it has been observed that top-emission OLEDs can be fabricated with lifetimes equivalent to conventional bottom-emitting devices [136]. In a display where top-emitting architectures have a larger fill factor, less current density is required per pixel to produce the same amount of light as compared to an equivalent bottom-emitting design. Therefore, top-emitting displays may enable longer lifetimes in addition to any potential power savings. Figure 7.13 shows an example of a transparent 2.2" display shown at the 2003 SID conference by Samsung SDI.

OLEDs appear ideally suited to active-matrix addressing as they are a low-voltage technology. Active addressing offers several advantages over passive addressing. Active addressing (a) eliminates the problem of cross talk due to reverse bias leakage currents, (b) extends display lifetimes, and (c) improves efficiency due to the lower operating voltages and currents that are necessary. In addition, it reduces power losses and heating problems due to resistive heating in the ITO tracks (I^2R losses). There has, therefore, been considerable interest in combining vapor-deposited small-molecule materials with poly-Si TFTs [131,137,138], and in 1995 TDK announced the first full-color (240×320 pixel) actively addressed OLED display [139]. Polycrystalline silicon (p-Si) TFTs, until recently, were preferred as it was widely believed that conventional α -Si TFTs could not accommodate the high currents required. However, in 2002, AU Optronics successfully demonstrated a 4" full-color AMOLED display based on an α -Si TFT backplane and incorporating a high-efficiency red phosphorescent material. The use of the red phosphorescent subpixel reduced display power consumption by 42%, compared to a comparable display based on only

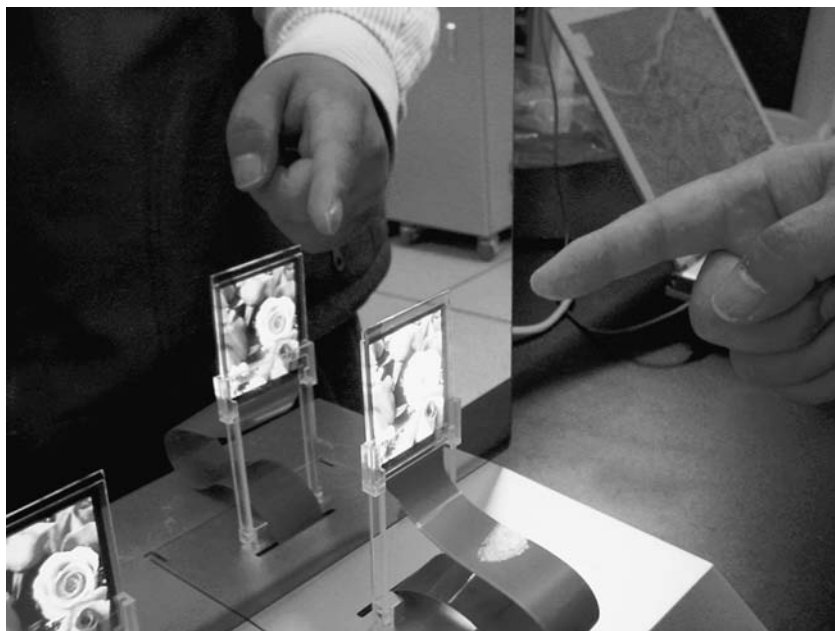


FIGURE 7.13 A 2.2" full-color transparent AMOLED display fabricated by Samsung SDI incorporating phosphorescent dopants.

fluorescent materials [140]. This display not only illustrates the benefits of PHOLEDs, but also demonstrates the possibility of using α -Si TFT backplanes in full-color AMOLEDs. More recently, Miwa et al. demonstrated a 20" AMOLED using an α -Si TFT backplane [141]. If the stability, issues of α -Si TFTs can be addressed, then the potential cost savings to AMOLED displays are significant due to the maturity of the α -Si backplane industry.

The next step in the development of actively addressed OLED displays may be an all organic TV. At present, poly-Si TFTs are expensive (particularly for larger area displays) and therefore detract from cheap production costs, which is one of the widely perceived main advantages of OLED technology. However, if organic materials can be used to make the TFT, as well as the OLED, using similar fabrication processes, then the cost of production can be substantially reduced. Field effect transistors have been fabricated using organic materials [142] and in 1998 Sirringhaus et al. [143] constructed the first all-plastic polymer TFT and PLED. In the same year, a vapor-deposited OLED was fabricated for the first time in combination with an organic thin-film field effect transistor [144]. These types of ICs open up the possibility of producing low-cost, flexible plastic displays.

7.5.3 FULL-COLOR DISPLAYS

Various ways of making full-color displays have been proposed. These are summarized in Figure 7.14. Perhaps the most obvious method is simply to fabricate red, green, and blue subpixels side by side on the same substrate (Figure 7.14a). Many companies have adopted this approach, e.g., Pioneer demonstrated a full-color QVGA (320×240 pixels) display at the Japan Electronics Show in 1998. Figure 7.15 is an example of a full-color display patterned using a side-by-side approach.

In conventional LCDs, emission from a white backlight is filtered using absorption filters to produce red, green, and blue emission. The same technique can also be used with OLEDs (Figure 7.14b). This approach has one advantage over the side-by-side approach (Figure 7.14a) in that for high-resolution displays precision shadow masking is unnecessary as the pixels (color filters) are patterned via lithography. However, for each pixel color, approximately two thirds of the light is wasted due to the need to absorb the unwanted elements of the white emission to render a saturated color from each pixel element. White emission is generally produced by combining the emission from two or more dyes [145]. For example, TDK combined the emission from two separate dopants, coumarin 6 and rubrene (see Figure 7.8), to approximate white emission. Conventional color filters were then used to produce red, yellow, and green emission [146]. The white emitter or the color filter approach was used in a commercial AMOLED display by Sanyo-Eastman Kodak. Figure 7.16 shows this display.

Another technique for fabricating full-color displays is based on the fact that blue light can be converted into green or red light by using dyes that absorb blue light and then emit green or red light via PL. Researchers at Idemitsu Kosan [147] have demonstrated color displays based on blue emitters and color-change filters (Figure 7.14c). They have developed a range of distyrylarylene derivatives that give high efficiencies (up to 6 lm/W) with lifetimes of over 20,000 h. More recently they demonstrated a (0.15, 0.15) blue with an efficiency of 5.9 cd/A and a lifetime of 7000 h at display luminance [148]. In 1998, they showed a 10" VGA (640×480 pixels) color display [149].

When a relatively broad emitter is confined in a microcavity, the dimensions of the microcavity influence the emission spectrum and peak wavelength (Figure 7.14d) [150]. This idea has been developed by researchers at several companies to produce red, green, and blue emission [151,152]. The main advantage of the technique is that red, green, and blue emission can be obtained from one broad organic emitter. However, one disadvantage of this approach is that the emission from such devices is strongly directional, leading to a narrow viewing

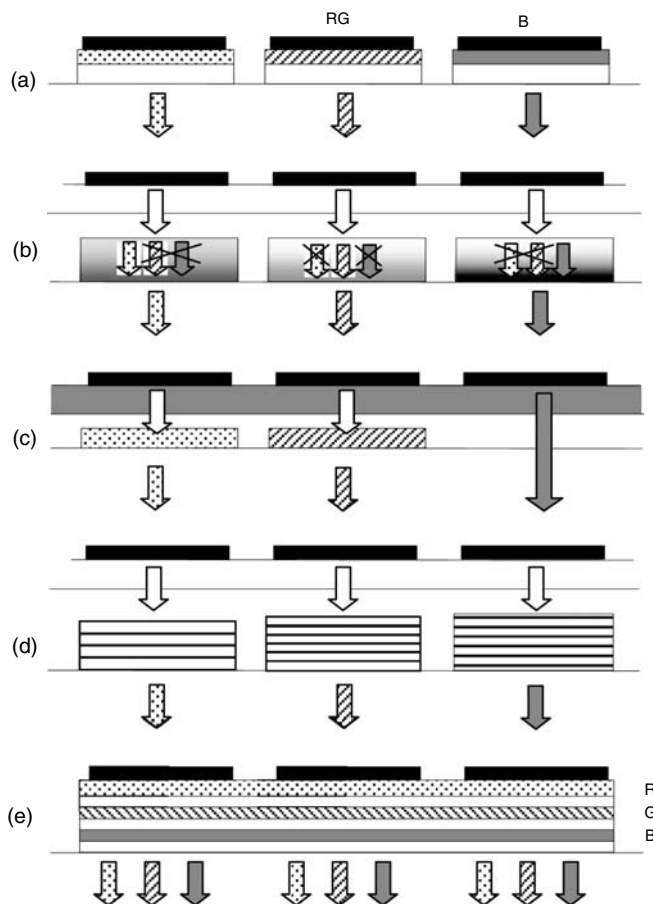


FIGURE 7.14 Various methods of pixel design to achieve full-color displays: (a) red, green, and blue subpixels side by side on the same substrate; (b) white OLED backlight is filtered using absorption filters to produce red, green, and blue emission; (c) blue OLEDs and down conversion PL red or green color-change filters; (d) a relatively broad emitter (e.g., white) in combination with microcavities to selectively emit red, green, and blue light; and (e) red, green, and blue pixels stacked on top of each other.

angle, i.e., the emission intensity is usually at a peak orthogonal to the display surface and decreases with a distortion of the color (blue spectral shift) as the viewing angle is increased.

An elegant way of achieving full-color displays is to stack the red, green, and blue pixels on top of each other [153] (Figure 7.14e). As there are no subpixels, this has the advantage of increasing the resolution of the display by a factor of three. However, it requires semitransparent electrodes that are also compatible with high current densities. A similar approach that would avoid this problem might be to develop structures in which the emission color can be varied simply by varying the applied voltage [154,155].

Another intriguing possibility for patterning the pixels in an OLED display without the use of high-precision shadow masking is the technique of laser-induced thermal imaging (LITI) [50,156,157]. This approach to patterning makes use of a donor film coated with a light-to-heat conversion layer, which in turn is coated with the organic layer (or multiple layers) that are the intended components of the OLED. The organic layer is placed in contact with the OLED substrate and the donor film is scanned with the intended deposition pattern



FIGURE 7.15 A commercially available Fujitsu cell phone incorporating a Pioneer manufactured OLED subdisplay that contains both phosphorescent (red) and fluorescent (green and blue) pixels.



FIGURE 7.16 A commercially available digital camera containing a full-color AMOLED display from Sanyo–Eastman Kodak.

using a laser. The donor film is typically a transparent flexible material, e.g., a polyester, and the conversion film is chosen to absorb the laser light in the IR region of the spectrum and convert this light to heat. Typical coatings include carbon. As the film is scanned, the light is converted to heat and the OLED material is transferred from the conversion film to the substrate. To achieve a high-quality OLED, the deposited materials must be chosen to have the requisite mechanical properties, e.g., weak cohesion and the correct balance of donor film or deposited film adhesive forces. The use of this technique is still in the early stages of development for OLEDs but holds great promise.

Patterning small-molecule organic displays via ink-jet printing is also explored within the OLED industry. Ink-jet printing has been researched extensively within the PLED community as a means of patterning full-color PLED displays culminating in a demonstration of a 40" display in 2004 by Seiko Epson [158]. The application of this technique to small-molecule OLED displays is now under investigation by a number of groups.

Each of the techniques described above has unique strengths and weaknesses, and the optimum device structure for commercial full-color displays will also be heavily influenced by the ease with which it can be mass-produced. Currently full-color OLED displays have been manufactured commercially by using two of the above described techniques only, i.e., (a) side-by-side pixels deposited by high-precision shadow masking and (b) using white OLEDs and color absorption filters.

7.6 FUTURE GENERATION VAPOR-DEPOSITED ORGANIC DEVICES

7.6.1 FLEXIBLE DISPLAYS

OLED displays can also be fabricated on flexible substrates [159–161] such as metal foils or plastic. This enables entirely new display features such as conformability, ruggedness, flexibility, and reduced weight.

To build an OLED display on a flexible substrate, a number of important issues have to be investigated in addition to those encountered when processing rigid glass or silicon substrates. Issues such as chemical stability, temperature limits, and mechanical stability all have to be addressed. Nevertheless, Figure 7.17 shows a 128×64 (60 dpi) monochrome passive-matrix vapor-deposited OLED display on a flexible substrate. It was fabricated by Universal Display Corporation and was exhibited in May 2000. It is believed to be the first report of such a display built on a plastic substrate. The plastic is 175- μm thick and the pixels are $500 \times 400 \mu\text{m}$ in size. Figure 7.18 shows a close-up view of a typical pixel. In this particular architecture, a metal bus line has also been added to lower the column resistivity of the display. This significantly reduces the power losses incurred by the ITO electrodes and should enable scale up to larger area passive-matrix displays.

To realize the enormous potential of this flexible display technology, however, a number of important issues still require solutions. In particular, fabrication technologies, suitable for plastic substrates and extended device operating-lifetimes, must be demonstrated. The problem incurred when using a flexible plastic substrate material is that polymers are very poor barriers to the diffusion of water and oxygen due to their low density. To realize the long lifetimes needed for displays, the OLED package must have an estimated permeability of less than $10^{-6} \text{ g}/(\text{m}^2 \text{ day})$ at 25°C [18]. Typical plastic substrate materials have permeabilities of $0.1\text{--}1.0 \text{ g}/(\text{m}^2 \text{ day})$ at 25°C , and are unsuitable for a commercial OLED product. One approach to overcome this issue is to use thin-film coatings of dense dielectric materials to inhibit diffusive processes. Here a barrier film is deposited directly onto the completed OLED, e.g., a thick Si_xN_y film [162]. However, such a film has to be almost defect-free in terms of pinholes and grain boundaries within the inorganic layer.



FIGURE 7.17 A 128×64 monochrome PMOLED display on a $175\text{-}\mu\text{m}$ thick flexible PET substrate. The image is displayed at a luminance of 200 cd/m^2 .

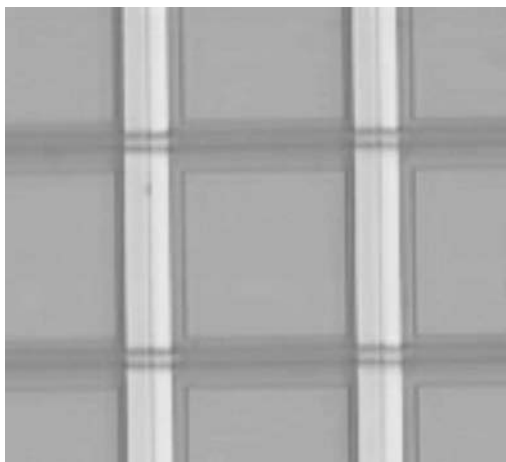


FIGURE 7.18 A magnified view of a flexible PMOLED on a PET substrate. The pixel pitch is $317\text{ }\mu\text{m}$ and the active pixel area is defined by each square.

One solution being explored is the use of a multilayer barrier coating [18,163] on the plastic substrate and the OLED. This consists of a hybrid organic–inorganic multilayer barrier coating [18,164]. The composite barrier consists of alternating layers of polyacrylate films and an inorganic oxide. Acrylic monomer is deposited by flash evaporation in vacuum onto the OLED surface [164]. The condensed monomer is cured using UV light to form a nonconformal highly cross-linked polyacrylate film that acts to planarize the substrate (or

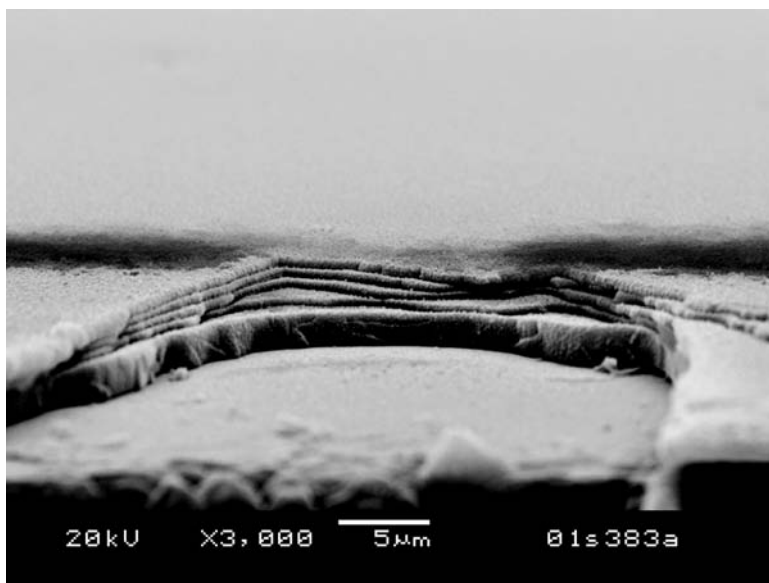


FIGURE 7.19 A scanning electron micrograph image of the cross section of a multilayer PET–Al₂O₃ barrier film.

OLED) surface. The surface roughness of the coated sample is <1 nm rms [18]. A 10–30-nm thick Al₂O₃ film is subsequently deposited onto the polymer layer as a barrier to the diffusion of water and oxygen. By repeating the alternating process to deposit multiple layers, the polymer layers decouple any defects in the oxide layers, thereby preventing propagation of defects through the multilayer structure. Both the optical and barrier properties of the composite layer can be tailored by varying the total number and thickness of the polymer and inorganic layers in the thin-film coating, yielding an engineered barrier [165]. Figure 7.19 shows a scanning electron micrograph of a fracture cross section of a generic multilayer barrier structure. In this particular configuration, ten layers are used. For a more thorough review of thin-film encapsulation of OLEDs, see, for example, Lewis and Weaver [64].

OLEDs grown and encapsulated using these techniques are beginning to show significant promise. Recently, Chwang et al. demonstrated the effects of flexing a 64×64 (180 dpi) passive-matrix flexible OLED (FOLED) display fabricated on a PET substrate with thin film encapsulation [166]. In addition, lifetimes of thin-film-encapsulated OLED test pixels on flexible substrates have now been demonstrated to be thousands of hours [162,167].

7.6.2 LIGHTING

In 2001 in the United States alone, lighting was estimated to consume 8.2 quad (approximately 762 TWh), or about 22% of the total electricity generated. Incandescent lighting is the leading energy consumer at 321 TWh, followed by fluorescent lighting with about 313 TWh. Efficacy for incandescent lights is in the range 10–20 lm/W, and for fluorescent lamps in the range 30–90 lm/W. Within the past 30 to 50 years little progress has been made in the energy efficiency of conventional sources of light — incandescent, fluorescent, and halogen. At present, approximately 70% of the energy used by these sources is wasted as heat, so significant savings can be made by the introduction of new, higher performance illumination sources. The introduction of solid-state lighting technologies such as OLEDs could

significantly reduce the energy usage in lighting applications, in addition to opening up new lighting possibilities, large-area light walls, or architectural lighting features. However, to achieve the price (such as \$3 per 1000 lm) and performance (>90 lm/W) required to enable the wholesale OLEDs to compete in general illumination applications, large improvements in device performance are needed, particularly in terms of lifetime under high drive conditions.

In the vapor-deposited OLED community, a number of approaches have been employed to produce white light emission. White OLEDs have been demonstrated based on multilayer structures, e.g., stacked backlights [153,168], multidoping of single-layer structures [145], phosphorescent monomer–excimer emission layers [169] and on doping of phosphorescent materials into separate bands within the emission zone, called a tri-junction [170]. The tri-junction device has produced the highest white OLED efficiency of 16% external quantum efficiency demonstrated thus far [171].

All of these approaches have varying degrees of merit but each deals with the emission of white light conceptually at a pixel level. For lighting, the emission can be generated using a white-producing system as opposed to using individual pixels. For example, white light for illumination purposes can be generated in a similar way to many displays, i.e., using two or three individual color elements that, when combined, produce white emission, e.g., yellow and blue or red, green, and blue striped arrays [172–174]. The advantage of this approach is that the individual elements can be separately driven and optimized. This has the potential benefits of improved efficiency and lifetime, and allowing for the ability to compensate for differential aging of the white emission as a function of time.

Although the power efficiency and lifetime requirements are difficult targets, OLED device lighting architectures have fewer constraints in certain areas than when used in displays. For example, lighting application allows for much greater flexibility in improving outcoupling from an OLED because the factors such as blurring between pixels are no longer an issue. As discussed earlier, 70 to 80% of the photons produced in an OLED are usually lost within the device. Table 7.1 shows examples of the current status of OLEDs in terms of luminous efficiency and voltage.

Assuming that the Hero luminous efficiency and voltage data in Table 7.1 can be combined, a speculative power efficiency for white emission of approximately 60 lm/W can be derived, assuming a color balance of 3:6:1 of red (0.65, 0.35), green (0.31, 0.64), and blue (0.15, 0.15) components. This efficiency is obtained without any outcoupling enhancements. Ignoring fill-factor issues, by applying an outcoupling factor of ~ 2 [101,175] would allow OLEDs to realize a power efficiency of 120 lm/W. This would be a very competitive efficiency for lighting applications. However, the challenge for OLEDs will be to realize large lighting

TABLE 7.1
Examples of the Current Status of OLEDs in Terms of Luminous Efficiency and Voltage

Parameter	Status of Stable Devices ^a	Hero Devices Demonstrated ^b
Red luminance efficiency (cd/A)	15 [180]	18 [181]
Green luminance efficiency (cd/A)	62 [182]	83 [97]
Blue luminance efficiency (cd/A)	5.9 [148]	10 [183]
Device voltage (V)	6–8	2.9 (R); 2.9 (G); 3.4 (B) [184]

^aDevices with $\sim 10,000$ h or more lifetime with parameters measured at luminance levels of 500 cd/m² for red and 1000 cd/m² for blue and green.

^bData shown at 300 cd/m² for red, 600 cd/m² for green, and 100 cd/m² for blue.

elements with a similar efficiency at high brightness with long lifetimes and manufactured at low cost. For complete discussion of white OLEDs, see D'Andrade and Forrest [176].

7.6.3 DISPLAYS AND BEYOND

The field of vapor-deposited OLEDs has grown markedly over the last two decades to the point where virtually every large display manufacturer has a research program or is in the process of commercializing its OLED displays. Issues of course still remain to be resolved. For television applications, lifetimes need to be improved still further. As a disruptive flat panel display technology, OLEDs on glass-based substrates need to be cost competitive with LCDs. One issue facing vapor-deposited OLED display manufacturers is employing very large-area shadow masks that are necessary as the mother glass size is increased to reduced display unit costs. Issues such as the shadow mask integrity, alignment, and thermal expansion all need to be addressed. However, great progress is rapidly made in solving these problems.

Now that organic materials have been developed that have the requisite qualities for commercialization and that the manufacturing infrastructure is being put into place, what is next for vapor-deposited organic materials? Already a number of research groups throughout the world are attempting to use similar materials for electrically pumped lasers. Optical pumping has already been demonstrated [12]. The realization of this goal is a formidable challenge as the estimated threshold current densities required, for amorphous organic materials, are of the order of $<1000 \text{ A/cm}^2$ [177]. However, research is in progress.

In photovoltaics, organic solar cells with conversion efficiencies of $>4\%$ have been demonstrated [178]. The challenge here is not only to improve efficiencies and lifetimes but also to compete on cost with silicon solar cells. Another intriguing possibility is the idea of fabricating organic computers. Organic TFTs are under development that at present have mobilities of the order of $1 \text{ cm}^2/(\text{V s})$ [179]. However, improvements are still necessary for the commercialization of organic TFTs, but it could be argued that the demands on the organic materials incorporated into these devices are less severe than those placed on their OLED counterparts.

The field of vapor-deposited OLEDs has seen amazing progress over the last two decades, from Tang's first efficient device, to OLED cell phone displays in every day use, and 24" displays have been demonstrated. However, progress is being made in solving these problem.

REFERENCES

1. A Bernanose, Electroluminescence of organic compounds, *Br. J. Appl. Phys.*, (Suppl. 4):S54–S55, 1955.
2. M Pope, HP Kallmann, and PJ Magnante, Electroluminescence in organic crystals, *J. Chem. Phys.*, 38:2042–2043, 1963.
3. PS Vincett, WA Barlow, RH Hann, and GG Roberts, Electrical conduction and low voltage blue electroluminescence in vacuum-deposited organic films, *Thin Solid Films*, 94:171–183, 1982.
4. CW Tang and SA VanSlyke, Organic electroluminescent diodes, *Appl. Phys. Lett.*, 51:913–915, 1987.
5. SA VanSlyke and CW Tang, Organic Electroluminescent Devices Having Improved Power Conversion Efficiencies, U.S. Patent 4,539,507, September 3, 1985.
6. C Adachi, S Tokito, T Tsutsui, and S Saito, Electroluminescence in organic films with three-layer structure, *Jpn. J. Appl. Phys.*, 27(Part 2):L269–L271, 1988.
7. CW Tang, SA VanSlyke, and CH Chen, Electroluminescence of doped organic thin films, *J. Appl. Phys.*, 65(9):3610–3616, 1989.
8. H Tokailin, M Matsuura, H Higashi, C Hosokawa, and T Kusumoto, Characteristics of Blue Organic Electroluminescent Devices with Distyryl Arylene Derivatives, Proceedings of the International Society for Optical Engineering, Vol. 1910, San Jose, 1993, pp. 38–47.

9. T Wakimoto, R Murayama, K Nagayama, Y Okuda, H Nakada, and T Tohma, Organic LED Dot-Matrix Display, Proceedings of the Society for Information Displays, Technical Digest 27, San Diego, 1996, pp. 849–852.
10. S Terada, G Izumi, Y Sato, M Takahashi, M Tada, K Kawase, K Shimotoku, H Tamashiro, N Ozawa, T Shibasaki, C Sato, T Nakadaira, Y Iwase, T Sasaoka, and T Urabe, A 24 Inch AM-OLED Display with XGA Resolution by Novel Seamless Tiling Technology, Proceedings of the Society for Information Displays International Symposium Digest of Technical Papers, Vol. 34(Book 2), Baltimore, 2003, pp. 1463–1465.
11. CW Tang, Two-layer organic photovoltaic cell, *Appl. Phys. Lett.*, 48:183–185, 1986.
12. VG Kozlov, V Bulovic, PE Burrows, and SR Forrest, Laser action in organic semiconductor waveguide and double-heterostructure devices, *Nature*, 389:362–364, 1997.
13. K Kudo, M Yamashina, and T Morizumi, Field effect measurement of organic dye films, *Jpn. J. Appl. Phys.*, 23:130, 1984.
14. K Furukawa, Y Terasaka, H Ueda, and M Matsumura, Effect of a plasma treatment of ITO on the performance of organic electroluminescent devices, *Synth. Met.*, 91:99–101, 1997.
15. MG Mason, LS Hung, CW Tang, ST Lee, KW Wong, and M Wang, Characterization of treated indium–tin-oxide surfaces used in electroluminescent devices, *J. Appl. Phys.*, 86:1688–1692, 1999.
16. ZB Deng, XM Ding, ST Lee, and WA Gambling, Enhanced brightness and efficiency in organic electroluminescent devices using SiO₂ buffer layers, *Appl. Phys. Lett.*, 74:2227–2229, 1999.
17. I-M Chan, T-Y Hsu, and FC Hong, Enhanced hole injections in organic light emitting devices by depositing nickel oxide on indium tin oxide anode, *Appl. Phys. Lett.*, 81:1899–1901, 2002.
18. PE Burrows, GL Graff, ME Gross, PM Martin, M Hall, E Mast, C Bonham, W Bennet, L Michalski, MS Weaver, JJ Brown, D Fogarty, and LS Sapochak, Gas Permeation and Lifetime Tests on Polymer-Based Barrier Coatings, Proceedings of the International Society for Optical Engineering, Vol. 4105, San Diego, 2000, pp. 75–83.
19. Y Yang and AJ Heeger, Polyaniline as a transparent electrode for polymer light-emitting diodes: lower operating voltage and higher efficiency, *Appl. Phys. Lett.*, 64:1245–1247, 1994.
20. H Riel, S Karg, T Beierlein, B Ruhstaller, and W Riess, Phosphorescent top-emitting organic light-emitting devices with improved light outcoupling, *Appl. Phys. Lett.*, 82:466–468, 2002.
21. S Tokito, K Nada, and Y Taga, Metal oxides as a hole-injecting layer for an organic electroluminescent device, *J. Phys. D: Appl. Phys.*, 29:2750–2753, 1996.
22. SW Yin, Z Shuai, and Y Wang, A quantitative structure–property relationship study of the glass transition temperature of OLED materials, *J. Chem. Inf. Comput. Sci.*, 43:970–977, 2003.
23. DF O'Brien, PE Burrows, SR Forrest, BE Koene, DE Loy, and ME Thompson, Hole transporting materials with high glass transition temperatures for use in organic light-emitting devices, *Adv. Mater.*, 10:1108–1112, 1998.
24. X Zhou, J He, LS Liao, M Lu, XM Ding, XY Hou, M Zhang, XQ He, and ST Lee, Real-time observation of temperature rise and thermal breakdown processes in organic LEDs using an IR imaging and analysis system, *Adv. Mater.*, 12:265–269, 2000.
25. M Ishii and Y Taga, Influence of temperature and drive current on degradation mechanisms in organic light-emitting diodes, *Appl. Phys. Lett.*, 80:3430–3432, 2002.
26. JC Sturm, W Wilson, and M Iodice, Thermal effects and scaling in organic light emitting flat panel displays, *IEEE J. Sel. Top. Quant. Electron.*, 4(1):75–82, 1998.
27. K Itano, H Ogawa, and Y Shirota, Exciplex formation at the organic solid-state interface: yellow emission in organic light-emitting diodes using green fluorescent tris(8-quinolinolato)aluminum and hole-transporting molecular materials with low ionization potentials, *Appl. Phys. Lett.*, 72:636–638, 1998.
28. C Adachi, T Tsutsui, and S Saito, Blue light-emitting organic electroluminescent devices, *Appl. Phys. Lett.*, 56:799–801, 1989.
29. R Murayama, S Kawami, T Wakimoto, H Sato, H Nakada, T Namiki, K Imai, and M. Nomura, Organic EL devices doped with a quinacridone derivative showing higher brightness and luminescent efficiency, *Jpn. Soc. Appl. Phys., Extended Abstracts (54th Autumn Meeting, 1993)*, 3:1127, 1993.
30. EI Haskal, A Curioni, PF Seidler, and W Andreoni, Lithium–aluminum contacts for organic light-emitting devices, *Appl. Phys. Lett.*, 71:1151–1153, 1997.

31. J Kido and T Matsumoto, Bright organic electroluminescent devices having a metal-doped electron-injecting layer, *Appl. Phys. Lett.*, 73:2866–2868, 1998.
32. LS Hung, CW Tang, and MG Mason, Enhanced electron injection in organic electroluminescent devices using an Al/LiF electrode, *Appl. Phys. Lett.*, 70:152–155, 1997.
33. T Wakimoto, Organic Electroluminescent Device, U.S. Patent 5,739,635, April 14, 1998.
34. LS Hung, CW Tang, MG Mason, P Raychaudhuri, and J Madathil, Application of an ultrathin LiF/Al bilayer in organic surface-emitting diodes, *Appl. Phys. Lett.*, 78:544–546, 2001.
35. V Bulovic, G Gu, PE Burrows, SR Forrest, and ME Thompson, Transparent light-emitting devices, *Nature*, 380:29, 1996.
36. G Parthasarathy, PE Burrows, V Khalfin, VG Kozlov, and SR Forrest, A metal-free cathode for organic semiconductor devices, *Appl. Phys. Lett.*, 72:2138–2140, 1998.
37. G Gu, V Bulovic, PE Burrows, and SR Forrest, Transparent organic light emitting devices, *Appl. Phys. Lett.*, 68:2606–2608, 1996.
38. V Bulovic, P Tian, PE Burrows, MR Gokhale, SR Forrest, and ME Thompson, A surface-emitting vacuum-deposited organic light emitting device, *Appl. Phys. Lett.*, 70:2954–2956, 1997.
39. CC Wu, CI Wu, JC Sturm, and A Kahn, Surface modification of indium tin oxide by plasma treatment: an effective method to improve the efficiency, brightness, and reliability of organic light emitting devices, *Appl. Phys. Lett.*, 70:1348–1350, 1997.
40. EB Grapper, in *Handbook of Thin Film Process Technology*, 1st ed., DA Glocker and SI Shah, Eds., IOP Publishing, Bristol, 1995, pp. A1.0:1–A1.1:7.
41. A Böhler, S Dirr, H-H Johannes, D Ammermann, and W Kowalsky, Influence of the process vacuum on the device performance of organic light-emitting diodes, *Synth. Met.*, 91:95–97, 1997.
42. M Ohring, *The Materials Science of Thin Films*, 1st ed., Academic Press, London, 1992, pp. 79–145.
43. SA VanSlyke, A Pignato, D Freeman, N Redden, D Waters, H Kikuchi, T Negishi, H Kanno, Y Nishio, and M Nakai, Linear Source Deposition of Organic Layers for Full-Color OLED, Proceedings of the Society for Information Display, Digest of Technical Papers, Vol. 33(Suppl. 2), Boston, 2002, pp. 886–889.
44. SR Forrest, Ultrathin organic films grown by organic molecular beam deposition and related techniques, *Chem. Rev.*, 97:1793–1896, 1997.
45. C-L Lee, KB Lee, and J-J Kim, Polymer phosphorescent light-emitting devices doped with tris(2-phenylpyridine) iridium as a triplet emitter, *Appl. Phys. Lett.*, 77:2280–2282, 2000.
46. DF O'Brien, C Giebler, RB Fletcher, AJ Cadby, LC Palilis, DG Lidzey, PA Lane, DDC Bradley, and W Blau, Electrophosphorescence from a doped polymer light emitting diode, *Synth. Met.*, 116:379–383, 2001.
47. JPJ Markham, S-C Lo, SW Magennis, PL Burn, and IDW Samuel, High-efficiency green phosphorescence from spin-coated single-layer dendrimer light-emitting diodes, *Appl. Phys. Lett.*, 80:2645–2647, 2002.
48. TR Hebner, CC Wu, D Marcy, MH Lu, and JC Sturm, Ink-jet printing of doped polymers for organic light emitting devices, *Appl. Phys. Lett.*, 72:519–521, 1998.
49. TR Hebner and JC Sturm, Local tuning of organic light-emitting diode by dye droplet application, *Appl. Phys. Lett.*, 73:1775–1777, 1998.
50. TA Isberg, CA Jalbert, JS Staral, WA Tolbert, and MB Wolk, Process for Preparing High Resolution Emissive Arrays and Corresponding Articles, U.S. Patent 5,998,085, December 7, 1999.
51. GG Roberts, M McGinnity, WA Barlow, and PS Vincett, Electroluminescence, photoluminescence and electroabsorption of a lightly substituted anthracene Langmuir film, *Solid State Commun.*, 32:683–686, 1979.
52. M Era, C Adachi, T Tsutsui, and S Saito, Organic electroluminescent device with cyanine dye Langmuir–Blodgett film as an emitter, *Thin Solid Films*, 210/211:468–470, 1992.
53. MS Weaver and DDC Bradley, Organic electroluminescence devices fabricated with chemical vapour deposited films, *Synth. Met.*, 83:61–66, 1996.
54. F Papadimitrakopoulos, DL Thomsen, and KA Higginson, Quinoline-Based Polymeric Metal Chelate Light-Emitting Diodes, Proceedings of the International Society for Optical Engineering, Vol. 3148, San Diego, 1997, pp. 170–177.

55. MA Baldo, M Deutsch, PE Burrows, H Gossenberger, M Gerstenberg, V Ban, and SR Forrest, Organic vapor phase deposition, *Adv. Mater.*, 10:1505–1514, 1998.
56. LS Hung, LS Liao, CS Lee, and ST Lee, Sputter deposition of cathodes in organic light emitting diodes, *J. Appl. Phys.*, 86:4607–4612, 1999.
57. C Adachi, MA Baldo, SR Forrest, and ME Thompson, High-efficiency organic electrophosphorescent devices with tris(2-phenylpyridine)iridium doped into electron-transporting materials, *Appl. Phys. Lett.*, 77:904–906, 2000.
58. JH Burroughs, DDC Bradley, AR Brown, RN Marks, K MacKay, RH Friend, PL Burn, and AB Holmes, Light-emitting diodes based on conjugated polymers, *Nature*, 347:539–541, 1990.
59. J Shi and CW Tang, Doped organic electroluminescent devices with improved stability, *Appl. Phys. Lett.*, 70:1665–1667, 1997.
60. PE Burrows, SR Forrest, TX Zhou, and L Michalski, Operating lifetime of phosphorescent organic light emitting devices, *Appl. Phys. Lett.*, 76:2493–2495, 2000.
61. YF Liew, H Aziz, N-X Hu, HSO Chan, G Xu, and Z Popovic, Investigation of the sites of dark spots in organic light-emitting devices, *Appl. Phys. Lett.*, 77:2650–2652, 2000.
62. D Kolosov, DS English, V Bulovic, PF Barbara, SR Forrest, and ME Thompson, Direct observation of structural changes in organic light emitting devices during degradation, *J. Appl. Phys.*, 90:3242–3247, 2001.
63. PE Burrows, V Bulovic, SR Forrest, LS Sapochak, DM McCarty, and ME Thompson, Reliability and degradation of organic light emitting devices, *Appl. Phys. Lett.*, 65:2922–2924, 1994.
64. JS Lewis and MS Weaver, Thin film permeation barrier technology for flexible organic light emitting devices, *IEEE J. Sel. Top. Quant. Electron.*, 10:47–57, 2004.
65. W Brutting, S Berleb, and AG Muckl, Device physics of organic light-emitting diodes based on molecular materials, *Org. Electron.*, 2:1–36, 2001.
66. C Hosokawa, H Tokailin, H Higashi, and T Kusumoto, Transient behaviour of thin film electroluminescence, *Appl. Phys. Lett.*, 60:1220–1222, 1992.
67. M Pope and CE Swenberg, *Electronic Processes in Organic Crystals*, 1st ed., Clarendon Press, Oxford, 1982.
68. J Kalinowski, G Giro, M Cocchi, V Fattori, and P DiMarco, Unusual disparity in electroluminescence and photoluminescence spectra of vacuum-evaporated films of 1,1-bis ((di-4-tolylamino) phenyl) cyclohexane, *Appl. Phys. Lett.*, 76:2352–2354, 2000.
69. K Itano, H Ogawa, and Y Shirota, Exciplex formation at the solid state interface: yellow emission in organic light-emitting diodes using green-fluorescent tris(8-quinolinoato)aluminium and hole-transporting molecular materials with low ionization potentials, *Appl. Phys. Lett.*, 72:636–638, 1998.
70. LC Palilis, AJ Makinen, M Uchida, and ZH Kafafi, Highly efficient molecular organic light-emitting diodes based on exciplex emission, *Appl. Phys. Lett.*, 82:2209–2211, 2003.
71. MH Lu and JC Sturm, Optimization of external coupling and light emission in organic light-emitting devices: modelling and experiment, *J. Appl. Phys.*, 91:595–604, 2002.
72. DDC Bradley, Electroluminescent polymers: materials, physics and device engineering, *Curr. Opin. Solid State Mater. Sci.*, 1:789–797, 1996.
73. J Kalinowski, in *Organic Electroluminescent Materials and Devices*, S Miyata and HS Nalwa, Eds., Gordon & Breach, Amsterdam, 1997, pp. 1–72.
74. NC Greenham and RH Friend, Semiconductor device physics of conjugated polymers, *Solid State Phys.*, 49:2–149, 1995.
75. PM Borsenberger and DS Weiss, *Organic Photoreceptors for Imaging Systems*, Marcel Dekker, New York, 1993.
76. PE Burrows, Z Shen, V Bulovic, DM McCarty, SR Forrest, JA Cronin, and ME Thompson, Relation between electroluminescence and current transport in organic heterojunction light-emitting devices, *J. Appl. Phys.*, 79:7991–8006, 1996.
77. M Stolka, JF Yanus, and DM Pai, Hole transport in solid solutions of a diamine in polycarbonate, *J. Phys. Chem.*, 88:4707–4714, 1984.
78. CW Tang, Organic Electroluminescent Cell, U.S. Patent 4,356,429, October 26, 1982.
79. SA VanSlyke, CH Chen, and CW Tang, Organic electroluminescent devices with improved stability, *Appl. Phys. Lett.*, 69:2160–2162, 1996.

80. A Gyoutoku, S Hara, T Komatsu, M Shirinashihama, H Iwanaga, and K Sakanoue, An organic electroluminescent dot-matrix display using carbon underlayer, *Synth. Met.*, 91:73–75, 1997.
81. JX Tang, YQ Li, LR Zheng, and LS Hung, Anode/organic interface modification by plasma fluorocarbon films, *J. Appl. Phys.*, 95:4397–4403, 2004.
82. Y Kawamura, J Brooks, JJ Brown, H Sasabe, and C Adachi, Intermolecular interaction and a concentration-quenching mechanism of phosphorescent Ir(III) complexes in a solid film, *Phys. Rev. Lett.*, 96:017404-1-017404-4, 2006.
83. VE Choong, Y Park, N Shivaparan, CW Tang, and Y Gao, Deposition-induced photoluminescence quenching of tris-(8-hydroxyquinoline) aluminum, *Appl. Phys. Lett.*, 71:1005–1007, 1997.
84. V Adamovich, J Brooks, A Tamayo, AM Alexander, PI Djurovich, BW D'Andrade, C Adachi, SR Forrest, and ME Thompson, High efficiency single dopant white electrophosphorescent light emitting diodes, *New J. Chem.*, 26:1171–1178, 2002.
85. Y Wang, N Herron, VV Grushin, D LeCloux, and V Petrov, Highly efficient electroluminescent materials based on fluorinated organometallic iridium compounds, *Appl. Phys. Lett.*, 79:449–451, 2001.
86. Y Sato, T Ogata, S Ichinosawa, and Y Murata, Characteristics of organic electroluminescent devices with new dopants, *Synth. Met.*, 91:103–107, 1997.
87. T Sano, H Fijii, Y Nishio, Y Hamada, H Takahashi, and K Shibata, Organic electroluminescent devices doped with condensed polycyclic aromatic compounds, *Synth. Met.*, 91:27–30, 1997.
88. Y Hamada, T Sano, K Shibata, and K Kuroki, Influence of the emission site on the running durability of organic electroluminescent devices, *Jpn. J. Appl. Phys.*, 34:L824–L826, 1995.
89. MA Baldo, DF O'Brien, ME Thompson, and SF Forrest, The excitonic singlet–triplet ratio in a semiconducting organic thin film, *Phys. Rev. B*, 60:14422–14428, 1999.
90. MA Baldo, DF O'Brien, Y You, A Shoustikov, S Sibley, ME Thompson, and SR Forrest, Highly efficient phosphorescent emission from organic electroluminescent devices, *Nature*, 395:151–154, 1998.
91. MA Baldo, S Lamansky, PE Burrows, ME Thompson, and SR Forrest, Very high-efficiency green organic light-emitting devices based on electrophosphorescence, *Appl. Phys. Lett.*, 75:4–6, 1999.
92. DF O'Brien, MA Baldo, ME Thompson, and SR Forrest, Improved energy transfer in electrophosphorescent devices, *Appl. Phys. Lett.*, 74:442–444, 1999.
93. C Adachi, MA Baldo, ME Thompson, and SR Forrest, Nearly 100% internal phosphorescence efficiency in an organic light emitting device, *J. Appl. Phys.*, 90:5048–5051, 2001.
94. M Ikai, S Tokito, Y Sakamoto, T Suzuki, and Y Taga, Highly efficient phosphorescence from organic light-emitting devices with an exciton-block layer, *Appl. Phys. Lett.*, 79:156–158, 2001.
95. C Adachi, RC Kwong, P Djurovich, V Adamovich, MA Baldo, ME Thompson, and SR Forrest, Endothermic energy transfer: a mechanism for generating high-energy phosphorescent emission in organic materials, *Appl. Phys. Lett.*, 79:2082–2084, 2001.
96. RC Kwong, MR Nugent, L Michalski, T Ngo, K Rajan, Y-J Tung, MS Weaver, TX Zhou, M Hack, ME Thompson, SR Forrest, and JJ Brown, High operational stability of electrophosphorescent devices, *Appl. Phys. Lett.*, 81:162–164, 2002.
97. V Adamovich, RC Kwong, MS Weaver, M Hack, and JJ Brown, Maximizing the Efficiency Lifetime Product for Phosphorescent OLEDs, Proceedings of the International Display Research Conference, Daegu, 2004, pp. 272–276.
98. RN Marks, The Optical and Electronic Response of Poly(*p*-Phenylene Vinylene) Thin Film Devices. Ph.D. thesis, University of Cambridge, Cambridge, UK, 1993.
99. J Blochwitz, M Pfeiffer, M Hofman, and K Leo, Non-polymeric OLEDs with a doped amorphous hole transporting layer and operating voltages down to 3.2 V to achieve 100 cd/m², *Synth. Met.*, 127:169–173, 2002.
100. M Pfeiffer, SR Forrest, K Leo, and ME Thompson, Electrophosphorescent p-i-n organic light-emitting devices for very-high-efficiency flat-panel displays, *Adv. Mater.*, 14:1633–1636, 2002.
101. T Tsutsui, M Yahiro, H Yokogawa, K Kawano, and M Yokoyama, Doubling coupling-out efficiency in organic light-emitting devices using a thin silica aerogel layer, *Adv. Mater.*, 13:1149–1152, 2001.

102. V Bulovic, VB Khalfin, G Gu, PE Burrows, DZ Garbuzov, and SR Forrest, Weak microcavity effects in organic light-emitting devices, *Phys. Rev. B*, 58:3730–3740, 1998.
103. SR Forrest, PE Burrows, and DZ Garbuzov, Displays Having Mesa Pixel Configuration, U.S. Patent 6,091,195, July 18, 2000.
104. RJ Nelson and RG Sobers, Minority-carrier lifetime and internal quantum efficiency of surface-free GaAs, *J. Appl. Phys.*, 49:6103–6108, 1978.
105. I Schnitzer, E Yablonovitch, C Caneau, TJ Gmitter, and A Scherer, 30% External quantum efficiency from surface textured, thin-film light-emitting diodes, *Appl. Phys. Lett.*, 63:2174–2176, 1993.
106. RH Haitz, Light-Emitting Diode with Diagonal Faces, U.S. Patent 5,087,949, February 11, 1992.
107. TH Gessmann and EF Schubert, High efficiency AlGaInP light-emitting diodes for solid state lighting applications, *J. Appl. Phys.*, 95:2203–2216, 2004.
108. FA Kish Jr. and SA Stockman, Transparent Substrate Light Emitting Diodes with Directed Light Output, U.S. Patent 6,015,719, January 18, 2000.
109. SH Fan, PR Villeneuve, JD Joannopoulos, and EF Schubert, High extraction efficiency of spontaneous emission from slabs of photonic crystals, *Phys. Rev. Lett.*, 78:3294–3297, 1997.
110. M Boroditsky, R Vrijen, TF Krauss, R Coccioli, R Bhat, and E Yablonovitch, Spontaneous emission extraction and Purcell enhancement from thin-film 2-D photonic crystals, *J. Lightwave Technol.*, 17:2096–2112, 1999.
111. BJ Matterson, JM Lupton, AF Safonov, MG Salt, WL Barnes, and IDW Samuel, Increased efficiency and controlled light output from a microstructured light-emitting diode, *Adv. Mater.*, 13:123–127, 2001.
112. CF Madigan, MH Lu, and JC Sturm, Improvement of output coupling efficiency of organic light-emitting diodes by backside substrate modification, *Appl. Phys. Lett.*, 76:1650–1652, 2000.
113. T Yamasaki, K Sumioka, and T Tsutsui, Organic light-emitting device with an ordered monolayer of silica microspheres as a scattering medium, *Appl. Phys. Lett.*, 76:1243–1245, 2000.
114. S Möller and SR Forrest, Improved light out-coupling in organic light emitting diodes employing ordered microlens arrays, *J. Appl. Phys.*, 91:3324–3327, 2001.
115. ST Lee, ZQ Gao, and LS Hung, Metal diffusion from electrodes in organic light-emitting diodes, *Appl. Phys. Lett.*, 75:1404–1406, 1999.
116. KA Higginson, X-M Zhang, and F Papadimitrakopoulos, Thermal and morphological effects on the hydrolytic stability of aluminum tris(8-hydroxyquinoline) (Alq_3), *Chem. Mater.*, 10:1017–1020, 1998.
117. DY Kondakov, JR Sandifer, CW Tang, and RH Young, Nonradiative recombination centers and electrical aging of organic light-emitting diodes: direct connection between accumulation of trapped charge and luminance loss, *J. Appl. Phys.*, 93:1108–1119, 2003.
118. H Aziz, Z Popovic, S Xie, A-M Hor, N-X Hu, C Tripp, and G Xu, Humidity-induced crystallization of tris(8-hydroxyquinoline) aluminum layers in organic light-emitting devices, *Appl. Phys. Lett.*, 72:756–758, 1998.
119. BH Cumpston and KF Jensen, Electromigration of aluminum cathodes in polymer-based electroluminescent devices, *Appl. Phys. Lett.*, 69:3941–3943, 1996.
120. H Aziz, ZD Popovic, N-X Hu, A-M Hor, and G Xu, Degradation mechanism of small molecule based organic light emitting diodes, *Science*, 283:1900–1902, 1999.
121. SR Forrest, PE Burrows, and ME Thompson, in *Organic Electroluminescent Materials and Devices*, S Miyata and HS Nalwa, Eds., Gordon & Breach, Amsterdam, 1997, pp. 447–453.
122. ZD Popovic and H Aziz, Reliability and degradation of small molecule-based organic light-emitting devices (OLEDs), *IEEE J. Sel. Top. Quant. Electron.*, 8:362–371, 2002.
123. J Kido, Organic displays, *Phys. World*, 12(Suppl. 3):27–30, 1999.
124. YA Ono, *Electroluminescent Displays*, World Scientific, Singapore, 1995, pp. 98–117.
125. C Hosokawa, M Eida, M Matsuura, K Fukuoka, H Nakamura, and T Kusumoto, Organic multi-color electroluminescence display with fine pixels, *Synth. Met.*, 91:3–7, 1997.
126. RC Kwong, MR Nugent, L Michalski, T Ngo, K Rajan, YJ Tung, AB Chwang, MS Weaver, TX Zhou, M Hack, and JJ Brown, Display Properties of High-Efficiency Electrophosphorescent Diodes, Proceedings of the Society for Information Display, Digest of Technical Papers, Vol. 33(Suppl. 2), Boston, 2002, pp. 1365–1367.

127. G Gu and SR Forrest, Design of flat-panel displays based on organic light-emitting devices, *IEEE J. Sel. Top. Quant. Electron.*, 4:83–99, 1998.
128. C Kim, PE Burrows, and SR Forrest, Micropatterning of organic electronic devices by cold-welding, *Science*, 288:831–833, 2000.
129. S Noach, EZ Faraggi, G Cohen, Y Avny, R Neumann, D Davidov, and A Lewis, Microfabrication of an electroluminescent polymer light emitting diode pixel array, *Appl. Phys. Lett.*, 69:3650–3652, 1996.
130. DG Lidzey, MS Weaver, MA Pate, TA Fisher, DDC Bradley, and MS Skolnick, Photoprocessed and micropatterned conjugated polymer LEDs, *Synth. Met.*, 82:141–148, 1996.
131. RMA Dawson, Z Shen, DA Furst, S Connor, J Hsu, MG Kane, RG Stewart, A Ipri, CN King, PJ Green, RT Flegal, S Pearson, WA Barrow, E Dickey, K Ping, CW Tang, S VanSlyke, F Chen, and J Shi, Design of an Improved Pixel for a Polysilicon Active-Matrix Organic LED Display, Proceedings of the Society for Information Display, Digest of Technical Papers, Vol. 29, Anaheim, 1998, pp. 11–14.
132. MJ Powell, C van Berkel, and JR Hughes, Time and temperature dependence of instability mechanisms in amorphous silicon thin-film transistors, *Appl. Phys. Lett.*, 54:1323–1325, 1989.
133. Y He, R Hattori, and J Kanicki, Four-thin film transistor pixel electrode circuits for active-matrix organic light-emitting displays, *Jpn. J. Appl. Phys.*, 40:(Part 1):1199–1208, 2001.
134. P Burrows, G Gu, SR Forrest, PE Vicenzi, and TX Zhou, Semitransparent cathodes for organic light emitting devices, *J. Appl. Phys.*, 87:3080–3085, 2000.
135. MH Lu, MS Weaver, TX Zhou, M Rothman, RC Kwong, M Hack, and JJ Brown, High efficiency top-emitting organic light-emitting devices, *Appl. Phys. Lett.*, 81:3921–3923, 2002.
136. MH Lu, MS Weaver, TX Zhou, M Rothman, RC Kwong, M Hack, and JJ Brown, Highly Efficient Top-Emitting Electrophosphorescent Organic Light-Emitting Devices, Proceedings of the 2nd International Meeting on Information Displays, Daegu, 2002, pp. 90–93.
137. CW Tang and BC Hsieh, Method of Fabricating a TFT-EL Pixel, U.S. Patent 5,550,066, August 27, 1996.
138. LK Lam, P Fleming, and DG Ast, Asia Display '98 225–228, 1998.
139. *Nikkei Sangyo Shinbun*, October 27, 1995 (in Japanese).
140. JJ Lih, CF Sung, MS Weaver, M Hack, and JJ Brown, A Phosphorescent Active-Matrix OLED Display Driven by Amorphous Silicon Backplane, Proceedings of the Society for Information Displays International Symposium Digest of Technical Papers, Vol. 34(Book 1), Baltimore, 2003, pp. 14–17.
141. T Tsujimura, Y Kobayashi, K Murayama, A Tanaka, M Morooka, E Fukumoto, H Fujimoto, J Sekine, K Kanoh, K Takeda, K Miwa, M Asano, N Ikeda, S Kohara, S Ono, C-T Chung, R-M Chen, J-W Chung, C-W Huang, H-R Guo, C-C Yang, C-C Hsu, H-J Huang, W Riess, H Riel, S Karg, T Beierlein, D Gundlach, S Alvarado, C Rost, P Mueller, F Libsch, M Maestro, R Polastre, A Lien, J Sanford, and R Kaufman, A 20-inch OLED Display Driven by Super-Amorphous-Silicon Technology, Proceedings of the Society for Information Displays International Symposium Digest of Technical Papers, Vol. 34(Book 1), Baltimore, 2003, pp. 6–9.
142. JH Burroughes, CA Jones, and RH Friend, New semiconductor device physics in polymer diodes and transistors, *Nature*, 335:137–141, 1988.
143. H Sirringhaus, N Tessler, and RH Friend, Integrated optoelectronic devices based on conjugated polymers, *Science*, 280:1741–1744, 1998.
144. A Dodabalapur, Z Bao, A Makhija, JG Laquindanum, VR Raju, Y Feng, HE Katz, and J Rogers, Organic smart pixels, *Appl. Phys. Lett.*, 73:142–144, 1998.
145. J Kido, K Hongawa, K Okuyama, and K Nagai, White light-emitting organic electroluminescent devices using the poly(*N*-vinylcarbazole) emitter layer doped with three fluorescent dyes, *Appl. Phys. Lett.*, 64:815–817, 1994.
146. M Arai, K Nakaya, O Onitsuka, T Inoue, M Codama, M Tanaka, and H Tanabe, Passive matrix display of organic LEDs, *Synth. Met.*, 91:21–25, 1997.
147. C Hosokawa, M Eida, M Matsuura, K Fukuoka, H Nakamura, and T Kusumoto, Organic Multicolor EL Display with Fine Pixels, Proceedings of the Society for Information Displays International Symposium Digest of Technical Papers, Vol. 28, Boston, 1997, pp. 1073–1076.

148. C Hosokawa, K Fukuoka, H Kawamura, T Sakai, M Kubota, M Funahashi, F Moriwaki, and H Ikeda, Improvement of Lifetime in Organic Electroluminescence, Proceedings of the Society for Information Displays International Symposium Digest of Technical Papers, Vol. 35(Book 2), Seattle, 2004, pp. 780–783.
149. C Hosokawa, M Matsuura, M Eida, K Fukuoka, H Tokailin, and T Kusumoto, Full Color Organic EL Display, Proceedings of the 1998 Society for Information Displays International Symposium Digest of Technical Papers, Vol. 29, Anaheim, 1998, pp. 7–10.
150. S Tokito, Y Taga, and T Tsutsui, Strongly modified emission from organic electroluminescent device with a microcavity, *Synth. Met.*, 91:49–52, 1997.
151. T Nakayama, Y Itoh, and A Kakuta, Organic photo- and electroluminescent devices with double mirrors, *Appl. Phys. Lett.*, 63:594–595, 1993.
152. A Dodabalapur, LJ Rothberg, TM Miller, and EW Kwock, Microcavity effects in organic semiconductors, *Appl. Phys. Lett.*, 64:2486–2488, 1994.
153. PE Burrows, SR Forrest, SP Sibley, and ME Thompson, Color-tunable organic light-emitting devices, *Appl. Phys. Lett.*, 69:2959–2961, 1996.
154. M Uchida, Y Ohmori, T Noguchi, T Ohnishi, and K Yoshino, Color-variable light-emitting diode utilizing conducting polymer containing fluorescent dye, *Jpn. J. Appl. Phys.*, 32:L921–L924, 1993.
155. T Mori, K Obata, K Imaizumi, and T Mizutani, Preparation and properties of an organic light emitting diode with two emission colors dependent on the voltage polarity, *Appl. Phys. Lett.*, 69:3309–3311, 1996.
156. ST Lee, JY Lee, MH Kim, MC Suh, TM Kang, YJ Choi, JY Park, JH Kwon, and HK Chung, A New Patterning Method for Full-Color Polymer Light-Emitting Devices: Laser Induced Thermal Imaging (LITI), Proceedings of the Society for Information Display, Digest of Technical Papers, Vol. 33(Suppl. 2), Boston, 2002, pp. 784–787.
157. ST Lee, BD Chin, MH Kim, TM Kang, MW Song, JH Lee, HD Kim, HK Chung, MB Wolk, E Bellman, JP Baetzold, S Lamansky, V Savvateev, TR Hoffend, JS Staral, RR Roberts, and Y Li, A Novel Patterning Method for Full-Color Organic Light-Emitting Devices: Laser Induced Thermal Imaging (LITI), Proceedings of the Society for Information Display, Digest of Technical Papers, Vol. 35(Suppl. 2), Seattle, 2004, pp. 1008–1011.
158. www.epson.co.jp, 2004.
159. G Gu, PE Burrows, S Venkatesh, and SR Forrest, Vacuum-deposited, non-polymeric flexible organic light-emitting devices, *Opt. Lett.*, 22:172–174, 1997.
160. G Gu, PE Burrows, and SR Forrest, Vacuum-Deposited, Non-Polymeric Flexible Organic Light Emitting Devices, U.S. Patent 5,844,363, December 1, 1998.
161. MS Weaver, WD Bennet, C Bonham, PE Burrows, GL Graff, ME Gross, M Hall, RH Hewitt, SY Mao, E Mast, PM Martin, LA Michalski, T Ngo, K Rajan, MA Rothman, and JA Silvernail, Flexible Organic LEDs, Proceedings of the Society for Information Display, Electronic Information Displays Conference, London, 2000, pp. 191–222.
162. A Yoshida, S Fujimura, T Miyake, T Yoshizawa, H Ochi, A Sugimoto, H Kubota, T Miyadera, S Ishizuka, M Tsuchida, and H Nakada, 3-Inch Full-Color OLED Display Using a Plastic Substrate, Proceedings of the 2003 Society for Information Displays International Symposium Digest of Technical Papers, Vol. 34(Book 2), Baltimore, 2003, pp. 856–859.
163. PM Martin, Barrier coatings from potato chips to display chips, *Vac. Technol. Coating*, 10:20–24, 2000.
164. JD Affinito, ME Gross, PA Mournier, MK Shi, and GL Graff, Ultrahigh rate, wide area, plasma polymerized films from high molecular weight/low vapour pressure liquid or solid monomer precursors, *J. Vac. Sci. Technol.*, A, 17:1974–1981, 1999.
165. Barix[®], Vitex Systems Inc., 3047 Orchard Parkway, San Jose, CA 95134.
166. AB Chwang, MA Rothman, SY Mao, RH Hewitt, MS Weaver, JA Silvernail, K Rajan, M Hack, JJ Brown, X Chu, L Moro, T Krajewski, and N Rutherford, Thin Film Encapsulated Flexible Organic Electroluminescent Displays, Proceedings of the Society for Information Display, Digest of Technical Papers, Vol. 34(2), Baltimore, 2003, pp. 868–871.

167. AC Chwang, MA Rothman, SY Mao, RH Hewitt, MS Weaver, JA Silvernail, K Rajan, M Hack, JJ Brown, X Chu, M Lorenza, T Krajewski, and N Rutherford, Thin film encapsulated flexible OLED displays, *Appl. Phys. Lett.*, 83:413–415, 2003.
168. Z Shen, PE Burrows, V Bulovic, SR Forrest, and ME Thompson, Three-color, tunable, organic light-emitting devices, *Science*, 276:2009–2011, 1997.
169. BW D'Andrade, J Brooks, V Adamovich, ME Thompson, and SR Forrest, White emission using triplet excimers in electrophosphorescent organic light-emitting devices, *Adv. Mater.*, 14:1032–1036, 2002.
170. BW D'Andrade, ME Thompson, and SR Forrest, Controlling exciton diffusion in multilayer white phosphorescent organic light emitting devices, *Adv. Mater.*, 14:147–151, 2002.
171. Y Tung, T Ngo, M Hack, J Brown, N Koide, Y Nagara, Y Kato, and H Ito, High Efficiency Phosphorescent White OLED for LCD Backlight and Display Applications, Proceedings of the Society for Information Display, Digest of Technical Papers, Vol. 35, Seattle, 2004, pp. 48–51.
172. AR Duggal, Color Tunable Organic Electroluminescent Light Source, U.S. Patent 6,661,029, December 9, 2003.
173. H Antoniadis and K Pichler, Organic Light Emitting Diode Light Source, U.S. Patent 6,680,578, January 20, 2004.
174. M Hack, MH Lu, and MS Weaver, Organic Light Emitting Devices for Illumination, U.S. Patent Application 20,040,032,205, February 19, 2004.
175. G Gu, DZ Garbuzov, PE Burrows, S Venkatesh, and SR Forrest, High-external-quantum-efficiency organic light-emitting devices, *Opt. Lett.*, 22:396–398, 1997.
176. B D'Andrade and SR Forrest, White organic light-emitting devices for solid state lighting, *Adv. Mater.*, 16:1585–1595, 2004.
177. MA Baldo, RJ Holmes, and SR Forrest, Prospects for electrically pumped organic lasers, *Phys. Rev. B*, 66:035320.1–035321.16, 2002.
178. J Xue, S Uchida, BP Rand, and SR Forrest, 4.2% efficient organic photovoltaic cells with low series resistances, *Appl. Phys. Lett.*, 84:3013–3015, 2004.
179. DJ Gundlach, H Klauk, CD Sheraw, CC Kuo, JR Huang, and TN Jackson, High-Mobility, Low Voltage Organic Thin Film Transistors, Proceedings of the International Electron Devices Meeting Technical Digest, December 1999, pp. 111–114.
180. VI Adamovich, MS Weaver, RC Kwong, and JJ Brown, High temperature operation and stability of phosphorescent OLEDs, *Curr. Appl. Phys.*, 5:15–18, 2005.
181. Universal Display Corporation, Unpublished result, 2004.
182. MS Weaver, Phosphorescent OLEDs: Commercial Readiness and Recent Developments, Presentation at the International Display Research Conference, Daegu, August 25, 2004.
183. MS Weaver, Phosphorescent OLEDs, Presentation at the SID Delaware Valley Chapter Meeting, Ewing, September 29, 2004.
184. J Blochwitz, J Brandt, M Hofmann, J Birnstock, M Pfeiffer, G He, P Wellmann, and K Leo, Full Color Active Matrix OLED Displays with High Aperture Ratio, Proceedings of the Society for Information Display, Digest of Technical Papers, Vol. 35, Seattle, 2004, pp. 1000–1003.

8 Print-Based Manufacturing Technologies for Organic Light-Emitting Displays

Sue A. Carter

CONTENTS

8.1	Introduction	567
8.2	Device Architectures	568
8.3	Materials for Print-Based Manufacturing.....	569
8.3.1	Hole-Injecting and Transporting Materials.....	569
8.3.2	Materials for Light-Emitting Organic Layer.....	570
8.3.3	Electron Injecting and Transporting Materials.....	572
8.4	Print-Based Manufacturing Technologies.....	573
8.4.1	Ink-Jet Printing	573
8.4.2	Screen Printing	574
8.4.3	Roll-to-Roll Printing Processes: Gravure, Flexographic, and Offset Printing.....	577
8.5	Encapsulation of Light-Emitting Polymer Semiconductor Devices.....	577
8.6	Potential Competition and Markets Available to Print-Based Organic Displays.....	579
	Acknowledgments	580
	References	580

8.1 INTRODUCTION

The discovery of efficient electroluminescence in thin films of conjugated polymers in 1990 initiated a large international effort by academics, industries, and national laboratories to understand and develop a new technology based on polymer light emitters. From the scientific point of view, such a large effort opened new avenue for research in the area of charge transport in disordered, highly correlated, and low-dimension materials, as well as in the novel synthesis of semiconducting polymers and small-molecule organics with unprecedented purity. From the technology point of view, such materials promised a complete paradigm shift in the manufacture of semiconducting devices, enabling inexpensive liquid-based processing under atmospheric conditions rather than expensive high-temperature and vacuum-based processing. This promise motivated significant progress in polymer material development, purity, and stability, and helped to revitalize the promise for two other related fields, namely organic photovoltaics and transistors. Organic-based light-emitting devices are now competitive to many inorganic-based devices in efficiency and stability. Nonetheless, the initial promise of inexpensive liquid-based or print-based manufacturing has yet to be fully realized.

The remaining challenges in developing liquid-based, organic light-emitting displays are threefold. The first challenge is to develop an organic electroluminescent (EL) ink, which is suitable for patterning in a uniform and repetitive manner, by using a printing process that is scalable to high-volume manufacturing. The second challenge is to develop a method for patterning every layer in the device using a print-based process. The third challenge involves developing an encapsulation process, which is cost-effective and mechanically flexible, while maintaining sufficient device lifetime. In this chapter, we consider recent and future technological developments that will offer solutions to these challenges. We will consider device architectures that favor printing technologies as well as the materials that are optimal for manufacturing fully printed displays. We will focus our discussion on three basic printing technologies, namely ink-jet printing, screen printing, and roll-to-roll printing and discuss the advantages and disadvantages of each technology. Finally, we address potential competitive technologies to printed organic displays and the potential new markets that are enabled by the development of inexpensive print-based manufacturing of organic light-emitting displays.

8.2 DEVICE ARCHITECTURES

Most light-emitting organic displays are based on the light-emitting diode (LED) device architecture, shown in Figure 8.1b. Currently, the organic light-emitting diode (OLED) device architecture results in the longest lifetimes and the best overall display performance. The LED device architecture relies on matching the work function of the electrodes to the conduction band, i.e., lowest unoccupied molecular orbital (LUMO), and the valence band, i.e., highest occupied molecular orbital (HOMO), of the polymer to obtain efficient charge injection. The starting material is a substrate, glass or plastic, with a transparent bottom electrode, normally indium tin oxide (ITO) that has been blanket deposited using a sputtering process. These substrates are readily commercially available, although improvements in the plastic substrate are needed to achieve sufficient encapsulation while maintaining flexibility and minimizing shorting. A hole transporting layer is needed in cases where there exists a significant barrier to hole injection between the bottom electrode and the semiconducting polymer layer. Such materials are typically a conducting polymer, such as polyethylenedioxythiophene doped with polystyrenesulfonic acid (PEDOT-PSS) or polyaniline (PAni), or a semiconducting polymer, such as the polyarylamines or polyvinylcarbazol (PVK). These materials are printable with proper surface preparation, such as an UV or a plasma-based treatment. The third layer, the EL polymer layer, is also printable, although, as discussed in more detail below, considerable effort must be made to optimize the EL polymer ink and substrate surface for the different print processes. The fourth layer is typically an electron

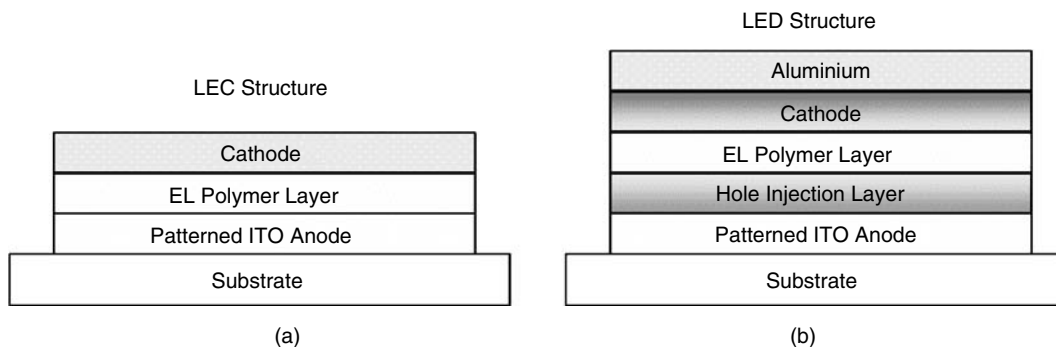


FIGURE 8.1 Comparison of (a) LEC and (b) LED assembly.

transporting layer, but, likewise, the layer is not needed if the barrier to electron injection is small as is normally the case for low work function electrodes, such as calcium or barium.

Finding a suitable electron transporting layer that is printable has proven to be one of the main challenges for fully printing the OLED structure; however, the greatest related challenge is the printing of the last top electrode layer, namely the electron injecting metal. This material is typically not printable because it is not stable in air and oxidizes upon exposure, thus air-stable printable inks that are also conducting cannot be formulated. Materials such as aluminum that are often considered air-stable when evaporated are not stable when incorporated into printable pastes because of the formation of a thin insulating oxide layer on the particle surface. Because of these challenges, the top electrode is normally deposited by vacuum-based processing and this can greatly increase the cost of the print-based manufacturing, making OLED displays uncompetitive with related fully printable display technologies for many applications. Finally, we note that the LED architecture typically involves several very thin layers (<100 nm) that are difficult to inexpensively integrate with high yield and uniformity in a full print-based manufacturing line.

An alternative architecture, namely the light-emitting electrochemical cell (LEC) or p-i-n architecture, shown in Figure 8.1a, solves many of the disadvantages of the LED structure, while introducing new challenges for display performance. The LEC structure achieves efficient charge injection through ionic dopants, either salts or surfactants, which can be introduced in the polymer or electrode inks and pastes. These ionic dopants can dope the polymer to form a p- or n-type conducting polymer at the electrode interface and can also introduce dipole layers at the electrodes; in both cases, the barrier to charge injection is greatly lowered. The number of layers in an active LEC, or p-i-n, device structure can therefore be as few as three layers, compared to as many as six layers for an LED device. Fewer layers are clearly more beneficial for inexpensive manufacturing and integration.

The LEC device architecture typically consists of an ITO-coated polyethylene terephthalate (PET), a doped EL polymer ink, and an air-stable top electrode such as silver. Because the LEC structure is relatively insensitive to the work function of the electrodes, many choices exist for printing both the bottom transparent electrode and the top electrode. The top electrode can also be transparent so that fully printed heads-up displays can be fabricated. Finally, because the dopants render much of the active polymer layer conducting, the LEC structure can operate with high efficiency at much greater active layer thicknesses than the LED structure. This makes the device much more forgiving to nonuniformities in the print process, enables the printing of multiple layers onto one another without shorting, and allows for the use of lower grade substrates that may be rougher or have lower barrier properties. Moreover, the greater thickness devices are less sensitive to exposure to airborne particles, enabling a nonclean room manufacturing process. Such advantages, however, currently come at a sacrifice in display performance, mainly in lifetime and to a lesser extent device efficiency. Significantly, more research would be needed into stabilizing the electrochemical reactions that occur inside an LEC to enable lifetimes approaching that of LED displays.

8.3 MATERIALS FOR PRINT-BASED MANUFACTURING

8.3.1 HOLE-INJECTING AND TRANSPORTING MATERIALS

A substantial amount of research and development work has been done in formulating the inks needed for print-based processing. Let us first consider the printing and patterning of the transparent anode. The transparent anode can be patterned using either a subtractive or an additive process. The starting material is a substrate, glass or plastic, with a transparent bottom electrode, normally ITO, that has been blanket deposited using a RF sputtering process. For plastic substrates, the patterning process can be done with a printable weak etch material, and a water spray with salt additives is used to neutralize the etch and

rinse it off the substrate. This process is inexpensive and rapid and has been fully integrated into print-based manufacturing lines for some time. For glass substrates, the etch procedure is more difficult due to the strong bond between the transparent oxide and SiO_2 , and a much stronger chemical etch or photolithographic process is used for patterning the ITO. Such processes can be relatively expensive when incorporated into a print-based manufacturing line. In both cases, the chemical etch process can result in uneven edges, due to cracking and flaking, which limit the ultimate resolution of the display. Moreover, a substantial amount of ITO is wasted in a subtractive process. Highly conductive anodes with transparency only slightly less than ITO can also be made from very thin metal films, such as silver or gold; however, they suffer from the same edge problems as the ITO under a wet chemical etch process. A possible advantage to transparent metal film is that they do not form strong bonds with glass, suggesting that commercially available weak etch can be used for patterning films deposited on glass, as well as plastic.

An alternative approach is to directly print the transparent electrode using a suitable transparent conducting ink. Such a process is additive and can lead to a much higher edge uniformity and less material waste. Examples of such materials include transparent oxide particles made from doped SnO_2 , ZnO:Al or ITO suspended in a polymer binder, metal oxide solgel solutions, polythiophene- and polyaniline-based transparent conducting polymer inks, and carbon nanorod or polymer composite pastes. Unfortunately, printable transparent inks typically have resistivities that are orders of magnitude greater than ITO, resulting in resistive loss and heating across the display. Consequently, the use of these printable transparent electrodes limits displays to small sizes and low brightness. The development of a printable transparent material with a conductivity comparable to sputtered films (i.e., $10 \text{ } \Omega/\text{square}$) would revolutionize the printable display industry.

While the printable transparent conductive inks cannot normally be used as electrodes on their own, they can serve as a hole transport layer when printed on top of transparent anode. In this case, lower conductivities may be desirably to limit crosstalk between adjacent pixels. The material largely used is PEDOT-PSS, but several other materials based on polyarylamines, PVKs, and PANis can be used. When the device architecture requires a hole injection layer, such as in the case of LEDs, consideration must be made into the effect that the printing of light-emitting organic layer will have on the transparent hole transport layer and vice versa. Many of the printable hole transport layers are either soluble in similar organic solvents as the EL organic material or in an aqueous solution, such as water. In the former case, the subsequent deposition of the EL material results in detrimental blending between the two layers, resulting in electroluminescence quenching and possible shorting. In the latter case, polymers that are soluble in aqueous solutions will absorb water during the print process after they are dried, leading to degradation of the polymer device. In either case, substantial surface treatment is typically needed to enable adhesion between the transparent metal oxide and the printed hole transporting layer.

8.3.2 MATERIALS FOR LIGHT-EMITTING ORGANIC LAYER

Most of the research and development of the materials for printing has been focused on the light-emitting organic layer with the emphasis on developing inks where a semiconducting polymer serves as the light-emitting material. Several companies, such as Sumation and Marck, are currently manufacturing EL polymers that can be made into inks suitable for a print-based manufacturing line. Spin-cast devices made from such inks have achieved lifetimes greater than 200,000 h, sufficient for commercial passive-matrix display applications, although such devices patterned via printing typically have substantially lower lifetimes. More recently, a movement toward developing materials other than conjugated polymers as

the printable light-emitting chromophore has occurred due to a belief that the efficiency of light-emitting polymers (LEPs) is limited because only the singlet fluorescent states are emissive and that these singlet states are populated at lower densities than the nonemitting triplet states. Small-molecule organic phosphor emitters with efficiencies exceeding those of the EL polymers have been developed; however, these materials are not printable on their own. However, recent results have shown that the organic phosphor materials can be embedded in a printable polymer matrix, such as PVK, resulting in very high efficiencies for idealized electrodes. If sufficient charge injection and transport can be obtained for such a composite systems using printable electrodes, higher efficiency, printable organic EL inks can also be developed.

The printability of the light-emitting organic layer depends mainly on the ink viscosity, solvent evaporation rate, and interactions between the ink and the deposition surface. Each printing technology requires substantially different ink viscosities and most of the effort to date has been on developing the relatively low-viscosity inks needed for spin-casting and ink-jet printing. As can be seen in Table 8.1, a majority of the higher-throughput print-based manufacturing processes will require substantially higher viscosities. The viscosity of the ink is controlled by a number of factors such as solution concentration, polymer solubility, polymer molecular weight, and other solution additives. Several companies manufacturing materials have developed processes that allow them to synthesize EL polymer materials with a wide range of molecular weights so that most of viscosities shown in Table 8.1 can be achieved at solution concentrations on the order of 1% polymer to solution by weight.

The solvent evaporation rate is also critically important to minimize clogging and achieve good film uniformity. In general, a solvent with a boiling point above 130°C is chosen so that the patterning mechanism, such as the screen or printhead, is not clogged by the EL polymer due to premature solvent evaporation. Much higher boiling point solvents are available, but these can be difficult to remove in the rapid drying times required by the full print-based manufacturing process, and insufficient solvent removal leads to a dramatic reduction in display lifetime. Addition of a retarder to the polymer ink can also be used to decrease solvent evaporation and extend the working lifetime of the EL polymer inks. Gel-type retarders are typically chosen to be chemically inert in the EL polymer solution and are removed with the solvent from the EL polymer by heating and applying a vacuum to the film. Another approach to rapid solvent evaporation is to use an enclosed system for holding the LEP ink prior to printing.

If a p-i-n (i.e., LEC) device architecture is used, the choice of the ionic dopant and surfactant additives to the light-emitting organic ink are critical to the print uniformity and resulting device performance and stability. The ionic dopants have limited solubility and can prematurely fall out of solution during the printing process. Most of the previous works in

TABLE 8.1
Typical Properties for Major Printing Technologies

	Standard Si-processing	Ink-Jet	Screen Printing	Offset, Gravure, and Flexography
Substrate or wafer diameter (m)	~0.3	<1	>1	>3
Production speed (m/s)	<0.001	<0.1	>1	>5
Laternal resolution (μm)	<0.1	>30	>100	>30
Layer thickness (μm)	0.002 to 2	0.02 to 20	0.1 to 40	0.1 to 10
Production line costs	>\$5000 million	>\$20 million	<\$1 million	>\$20 million
Ink viscosity (cP)	NA	1 to 50	5 to 10000	5 to 10000

this area have been on lithium salts, primarily because the mobility of lithium ion is sufficiently fast and a reasonable switching time, 100 ms or less, can be obtained. However, many display markets do not require millisecond switching times. Additionally, lithium-based compounds used in other LEP devices are often too unstable for the atmospheric deposition and the ensuing encapsulation process. Salts with large organic cations are even less mobile but tend to be more soluble and stable to standard atmospheric processing. Another consideration is the anion. Frequently, salts with organic anions are used due to greater solubility in the organic solvents; however, inorganic anions have also been used with some success and can result in greater stability. In addition, solubility issues with the salt can be mitigated through the use of surfactants.

8.3.3 ELECTRON INJECTING AND TRANSPORTING MATERIALS

The major hurdle in developing a cost-effective, print-based technique for manufacturing organic light-emitting displays is encountered in the deposition method for the top electrode, normally the cathode. The LED device architecture requires a material that can inject electrons into the conduction band of the organic semiconductor and due to relatively high LUMO level in the organics, low work function metals that oxidize readily in air are required. Since printing is a process done under atmospheric conditions, all the electrodes must be completely stable in the presence of water and oxygen. None of the cathodes currently used in OLED manufacturing, such as Mg, Ca, Ba, LiF, or even Al are printable. In theory, an electron injection layer could be printed onto the EL polymer to decrease the barrier to electron injection from the printable electrodes; however, because the barrier to injection is greater than 1 eV between the organic LUMO level and the work function of printable electrodes, several layers would be required. Moreover, suitable electron transporting layers that are also printable are not readily available.

An alternative approach to this challenge is to reverse the device architecture and use a metal foil or aluminized mylar as the substrate. Unlike aluminum paste that suffers from insulating oxide layers forming around each particle, aluminized mylar is sufficiently conducting for display applications. Moreover, aluminized mylar can be readily patterned using the same printable weak etch used for ITO-coated plastic. Aluminum is not a sufficient electron injector on its own so at least one electron transporting layer needs to be printed onto aluminum before the deposition of the LEP layer, which requires the development of a printable electron transporting material. However, the biggest hurdle to this approach is that the printed top electrode, namely the anode, would have to be transparent. Although several printable materials exist that can efficiently inject holes into EL organic materials, as mentioned above, none of these materials are sufficiently conducting for display applications of any reasonable size or brightness. Only very small and low-brightness fully printed organic displays could be made using this reverse architecture approach without the development of higher conductivity transparent inks. Consequently, print-based fabrication of OLED displays currently requires the addition of a nonprintable vacuum processing step for deposition of the top electrode, greatly reducing the processing speed and increasing the cost of manufacturing.

The LEC structure that involves the addition of ionic dopants and surfactants to the printable inks enables the ability to print a top electrode without restriction by the work function of the metal. Silver, nickel, or carbon particle-based pastes are generally the preferred printable electron injecting electrodes; however, the shape and size of the particles combined with the softening properties of the solvent can create electrical shorts throughout the device when printed over a thin polymer layer that is only several hundred nanometers thick. For optimal performance, the commercially available pastes must be optimized for printing onto soluble thin films to make a fully screen-printed polymer EL display.

As mentioned previously, a common material used in making LEP devices is the conducting polymer called PEDOT–PSS. Although this material is typically used as a hole injector or transporter deposited over ITO, PEDOT–PSS can also be used as a printable top electrode because it is dispersed in an aqueous solvent in which the EL polymer is insoluble and because it is soft enough to punch through the thin EL polymer layer and short out the film. PEDOT–PSS is available in printable versions that have reasonably high conductivity to enable efficient device operation over small distances, which in certain display geometries may be sufficient for making contact with the conducting traces.

For the silver-based inks, standard silver pastes as well as binderless silver inks and nanoparticle-based inks are available. In these systems, the choice of the binder, the solvent, the particle morphology, and the particle surface characteristics are critical to device performance. Detrimental interactions and outgassing from the polymer binder into the light-emitting film can completely quench the electroluminescence. In addition, ions involved in the electrochemical doping can migrate into the binder from the light-emitting film or react with surfactants on the metal particle surfaces so that they are ineffective in doping LEP and improving injection. The silver particles can also penetrate into the polymer and create shorts over time due to electromigration effects. Binderless silver inks as well as silver nanoparticle inks may provide possible pathways to mitigate these effects. Several other printable electrode materials, such as nickel-based and carbon-based systems, are known to have few electromigration issues than the silver inks, although they tend to suffer from low conductivity and high absorption. Because of their relatively high transparency and high surface area, carbon-based inks made from conductive nanorods may provide new possibilities as electrodes for electrochemical displays.

8.4 PRINT-BASED MANUFACTURING TECHNOLOGIES

The print-based manufacturing technologies offer substantially higher productivity than more traditional, high-temperature, and vacuum technologies used to process silicon and related materials. High-volume print-based production offers over a 1000 times improvement in speed (see Table 8.1) and typically requires much lower capital equipment costs and lower skill labor to operate, resulting in substantial cost savings. This cost savings comes at a penalty of resolution and material purity; however, these penalties tend to be considerably less important for many electronic applications, such as displays.

We consider several printing technologies in this chapter, namely ink-jet, screen printing, and gravure, flexography, and offset printing (Figure 8.2). Ink-jet and screen printing use selective permeable surfaces where the printing ink passes distinguished openings in a surface, a printhead, or a screen. Gravure and flexography printing use the topology of the surface so that the print fluid remains in the lower or the upper elevated parts. For offset printing, a change in the surface conditions, for example, between hydrophobic and hydrophilic, determines the patterning mechanism. We do not consider electrophotography or toner printing in this chapter because it is a difficult method for depositing the polymer film, although it may work quite well for depositing the electrodes. Table 8.1 compares typical properties of the manufacturing technique.

8.4.1 INK-JET PRINTING

Most of the companies working on OLED displays are focusing on ink-jet printing as the method for depositing the light-emitting organic ink. Although, in theory, ink-jet printing does not offer significant advantage over gravure or offset printing in terms of speed or resolution, it is significantly easier to implement for printing the thinner films and dot-like

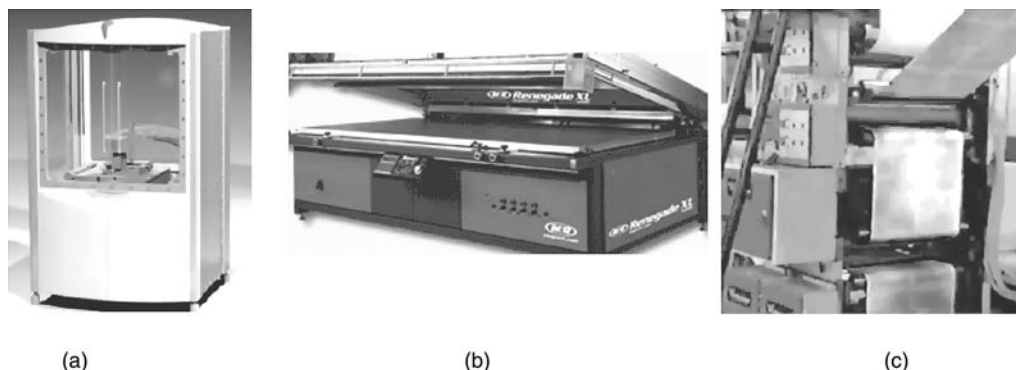


FIGURE 8.2 Typical manufacturing tools used for (a) ink-jet printing, (b) screen printing, and (c) roll-to-roll processing.

features needed for full-color organic-matrix displays. In full-color OLED displays, the RGB light is typically generated by different organic emitting materials that emit the appropriate red, green, and blue components. The polyfluorene class of materials can meet the color specs and viscosities required for the ink-jet printing of RGB displays.

The ink-jet process relies on using a piezoelectric printhead that can create deformation on a closed cavity through the application of an electric field. This causes the fluid in the cavity to be ejected through the nozzle whose volume is determined by the applied voltage, nozzle diameter, and ink viscosity. The final width of the drop of the substrate is a result of the volume of fluid expelled and the thickness of the droplet on the surface. In addition, the drop placement is critical to the ultimate resolution of the display. Typical volumes expelled from a printhead are 10 to 40 pl, resulting in a subpixel width between 65 and 100 μm . Drop accuracies of $\pm 15 \mu\text{m}$ have been reported such that resolutions better than 130 ppi are achievable; however, because the solvent to polymer ratio is so high, the drops must be contained during the evaporation process to obtain the desired resolution and film thickness. This containment can be a patterned photoresist layer that has been chemically modified so that the EL polymer ink does not stick to it.

Ink-jet printing through a single nozzle head is inherently very slow. To obtain reasonable print speed, hundreds of printheads are necessary. Drop volume uniformity between pixels becomes a concern with such multihead systems and can be further complicated by the drying of the solid polymer material in the nozzles due to solvent evaporation. The control over ink viscosity and solvent boiling point is consequently critical to the ultimate display uniformity and resolution. Printhead reliability may be a concern for high-speed, large-scale manufacturing of OLED displays due to the varying solvent evaporation rates and clogging.

Several companies, including Seiko, Epson, Phillips, Dupont, and Toshiba, have reported manufacturing full-color OLED displays up to 17" diagonal where the polymer-based EL ink was deposited using ink-jet printing. The ink-jet process offers significant promise for the development of active-matrix OLED displays. Nonetheless, none of these displays are manufactured using a full print-based manufacturing process so that the ultimate costs of the displays remain relatively high.

8.4.2 SCREEN PRINTING

At the time of writing, only one technique, namely screen printing, has been used to fully print an organic light-emitting display. Screen printing does not offer the resolution of ink-jet printing nor the speed of offset or gravure printing; however, it does offer the least expensive

capitol equipment cost of all the printing technologies, making it very cost-effective for production volumes of less than 100,000 units. Additionally, screen printing is versatile in that it can be used in sheet mode to print on a wide range of rigid and flexible substrates, including glass, plastic, metal, cloth, and paper. For higher volume productions, a sheet-fed screen-printing process can be combined with roll-to-roll processing. For these reasons, screen printing appears to be the strongest deposition technology for inexpensively fabricating light-emitting organic displays in both low- and medium-resolutions at moderate volumes. Moreover, with well over 10,000 screen-printing companies in the United States, a strong pool of available screen-printing know-how and capacity already exists, making a fully printable, EL display technology highly transferable to other firms in the industry.

The screen-printing process itself involves pushing the polymer ink through threads (normally made from polymer) of a screen which form a cross-mesh pattern defined by the screen mesh (number of threads per inch) and the thickness of the thread, as shown in Figure 8.3. The pattern is created by blocking off some of the holes in the cross-mesh pattern with a photo-curable polymer emulsion that is defined using a crude optical lithography process. The polymer ink is poured onto this screen and pushed through the remaining open holes using a rubber blade. The solvent is then evaporated from the polymer using a belt oven. Once dried, the next layer, such as the top electrode, is then deposited. The ink consistency, the substrate preparation, the synthetic screen fabric, the squeegee material and angle, the print speed, the positioning between the screen and the substrate, and the emulsion responsible for patterning, all affect the resulting film uniformity and thickness.

Screen printing has been used by the printed circuit industry to resolutions down to 50 μm ; however, the practical limitations are above 100 μm due to the edge and alignment effects in printing organic light-emitting displays. Film thicknesses for screen printing are usually determined by the theoretical ink-volume that varies with the screen mesh and thread thickness; however, these relations may not be accurate for LEP inks. Typical mesh sizes between 240 and 400 mesh and thread thicknesses on the order of 40 μm can result in film thicknesses well below 50 nm in a single pass; however, multiple passes are usually needed to improve the uniformity of the LEP film over large areas. LEP thicknesses for fully printable displays typically need to be over a few hundred nanometers to reduce shorting and to increase uniformity of emission over the entire display.

The printability of the LEP ink is determined by a number of factors, including the viscosity of the ink, the solvent evaporation rate, and the interactions between the ink and the screen, emulsion, and substrate. Screen-printable solutions normally require considerably

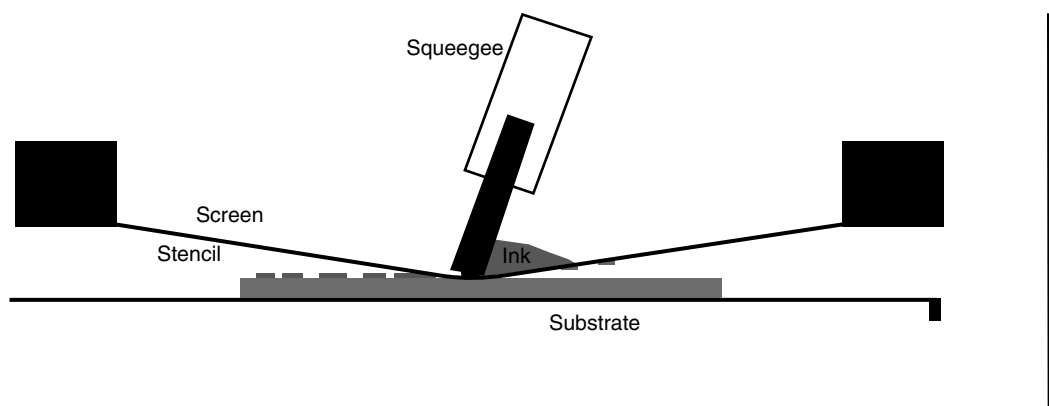


FIGURE 8.3 Typical process for screen printing. The screen is patterned using a photoemulsion.

higher viscosity than what is used for ink-jet printing, as can be seen in Table 8.1. The higher viscosity prevents the polymer solution from running or bleeding through the holes in the screen prior to printing, which can lead to blurred edges, loss of patterning, and sticking between the screen and the substrate. The need for a polymer solution with a relatively high viscosity normally requires higher concentrations of polymer in solution than those used for spin-casting or ink-jet printing. A solution's viscosity and printability also depend on the molecular weight of the semiconducting polymer, which can vary by as much as one order of magnitude between different material suppliers. To overcome variability in batch quality and to better control solution viscosity, high molecular weight polymer additives or viscous solvents can be added to the ink in small concentration to help ink consistency.

The solvent evaporation rate is also very important to screen printing. Screen-printable solutions normally require solvents with significantly slower evaporation rates (or higher boiling temperatures) than what are used for spin casting. The slower evaporation rate provides sufficient time for the polymer beads, which are formed when the polymer solution is pushed through the holes in the screen, to join together into a continuous film. An evaporation rate that is too fast can also cause the polymer to prematurely dry in the screen or cause the screen cross-hatch pattern to be left in the printed film. Careful selection of the solvent is therefore crucial to the screen-printing process. Complicating the selection process, polymer semiconductors often have varying solvent dependence, necessitating changes in the solvent for each material. These challenges normally overcome in screen printing by adding retarders in small concentration to reduce the solvent evaporation rate and improve the polymer ink workability; however, such retarders have to be added with care as they may cause premature degradation of the light-emitting polymer or electroluminescence quenching. One of the key challenges to high-volume manufacturing of fully screen-printed displays will be in controlling changes in the ink viscosity and solvent evaporation during the manufacturing process.

Several organizations, including Add-Vision, Siemens, and the University of Arizona, have demonstrated polymer-based, light-emitting devices where the polymer semiconductor layer was deposited using a screen-printing process. Add-Vision has produced full-color, fully screen-printed displays that can meet the cost points expected for a print-based manufacturing process (see Figure 8.4).

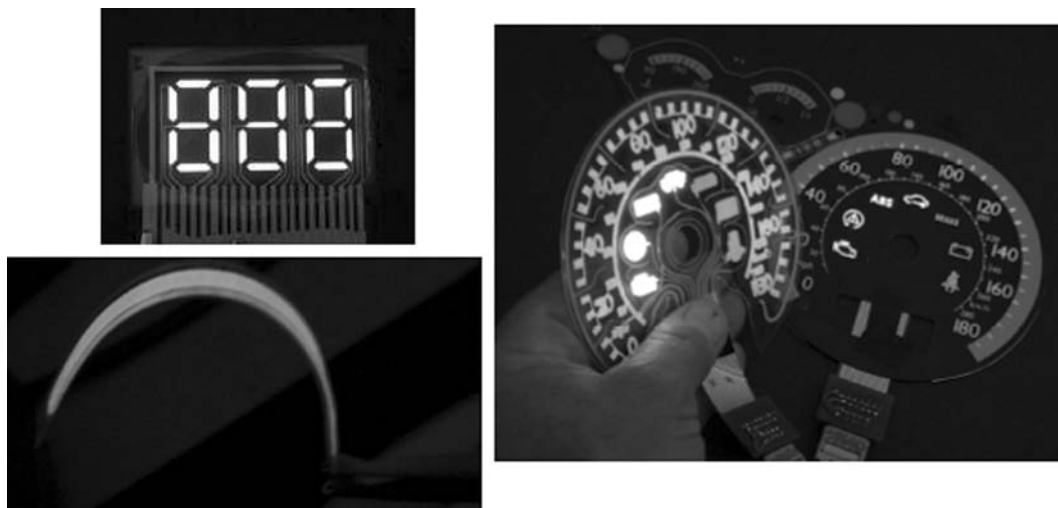


FIGURE 8.4 Examples of Add-Vision's fully screen-printed, light-emitting displays.

8.4.3 ROLL-TO-ROLL PRINTING PROCESSES: GRAVURE, FLEXOGRAPHIC, AND OFFSET PRINTING

Although a sheet-fed process, such as screen printing or ink-jet printing, can be fed into a reel-to-reel or a web-based manufacturing line to increase speed, greater cost savings can be found by going directly to a roll-to-roll process. Roll-to-roll processing obtains its patterning through modifications of the rolls used to deposit the ink. The two processes that are actively considered for OLED fabrication include chemical modifications, namely offset printing, and a topology modifications, namely gravure and flexographic printing. In some cases, it is advantageous to combine these methods. Limited progress has been made on using these techniques for OLED fabrication, although web-based processing is generally considered as the path to achieve lowest cost product in high volumes. Moreover, these manufacturing processes may offer the only solution for competitive cost-effective OLED lighting.

Gravure and flexographic printing are grouped here because they use the same basic process. A print cylinder consisting of lowered parts (gravure) or elevated parts (flexography) is rotated in an ink trough that deposits ink onto the print cylinder. This ink is then pressed on a substrate that is rotated using an impression cylinder. A few successful attempts have been made by companies, such as DNP, to deposit an LEP layer using a gravure process. This method is attractive because it mitigates problems due to clogging of the screen or printhead, and it does not involve chemical surface modifications inherent to offset printing.

In the offset process, a printing plate cylinder is used to offset the image onto a compressible blanket cylinder, which then transfers the patterned ink onto a substrate contained on the impression cylinder, as shown in Figure 8.5. The offset process takes advantage of changes in chemical or physical functionality of the surface of the cylinders to obtain patterning. These changes normally involve a change in hydrophobicity, oleophobicity, or surface charge. The effect of these surface conditions on the performance of the light-emitting organic display has not been systematically studied. Such studies are needed because OLED devices are very sensitive to the presence of residual charges as well as water.

Both impression and offset printing processes can use rigid or flexible substrates, although the high-speed presses use mainly flexible substrates. The requirement for flexibility has been one of the main obstacles in the implementation of roll-to-roll technology because the flexible plastic substrates currently do not have sufficient barrier properties to enable fabrication of OLEDs with long lifetimes. An alternative would be to use very thin flexible glass; however, the use of such fragile glass poses its own challenges in terms of tooling, cutting, and handling. In addition, roll-to-roll manufacturing processes typically require very high volumes over relatively large areas to be cost-effective compared with other techniques, such as screen printing. Although many of the initial commercial applications of OLEDs may require lower production volumes, the development of roll-to-roll process for manufacturing organic displays will be needed for cost reduction and long-term growth.

A clear intermediate step in roll-to-roll manufacturing is to use screen printing. Screen printing shares several commonalities with web printing, including similar ink viscosities and similar requirements for processing under atmospheric conditions. Polymer ink and electrode paste formulations developed for screen printing should be transferable to the higher volume manufacturing, enabling a more rapid adaptation of these manufacturing technologies.

8.5 ENCAPSULATION OF LIGHT-EMITTING POLYMER SEMICONDUCTOR DEVICES

The final step in making a fully printed polymer-based light-emitting display is the encapsulation step. Encapsulation is perhaps the most critical step in the process as unencapsulated devices fail within a few days of fabrication. For devices using evaporated cathodes that are

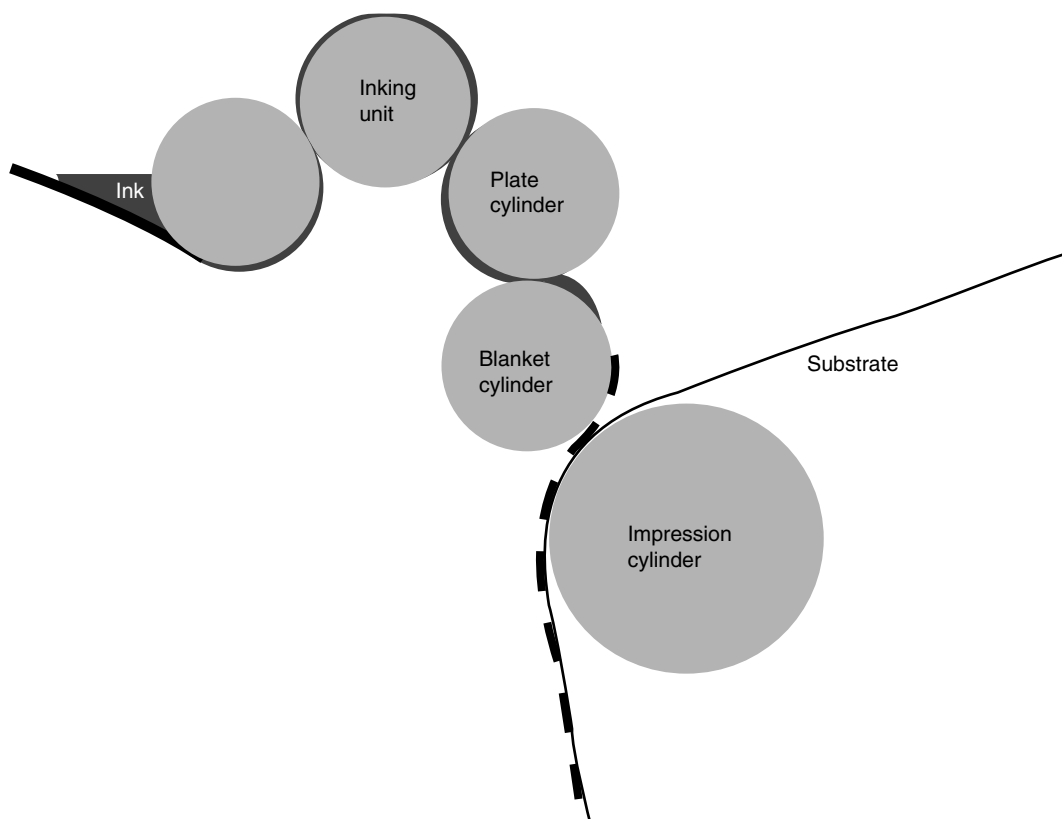


FIGURE 8.5 Typical print process for roll-to-roll printing. The blanket cylinder is used for offset printing.

not stable in air, encapsulation failure mainly causes degradation of the cathode. Also, electrically induced hot-spot formation and reactions with water can cause delamination between the EL polymer and the electrodes. Over longer term operation, the semiconducting polymer photobleaches and undergoes other irreversible reactions in the presence of oxygen, light, or electrical bias. For fully printed devices that use air-stable electrodes and electrochemical dopants (i.e., the p-i-n architecture), the dopants can react with water and oxygen under electrical bias, causing numerous detrimental affects, not the least of which is black-spot formation. A manufacturing tool compatible with a high-volume manufacturing line must be able to remove residual solvents and water from the organic light-emitting devices and encapsulate the device with an oxygen and water-impermeable barrier in time frames of a few seconds to a few minutes.

Currently, there are no commercially available manufacturing tools that are optimized for encapsulating LEP displays in a high-volume print-based manufacturing line. An encapsulation tool capable of these speeds will probably have to be modified from the advanced food and biomedical packaging systems where sheet-fed or roll-to-roll controlled atmosphere packaging (CAP) and modified atmosphere packaging (MAP) are frequently used. Several different adhesive systems could be used, but would have to be compatible with the speed of the printing process. Such adhesive systems include low-temperature lamination, printable epoxies, and printable UV and thermally curable sealants. Oxygen getters and printable desiccants can be further used to reduce water and oxygen contamination. The encapsulation sheet can be thin glass or one of the several barrier plastics currently under development. For

some low-lifetime applications, particularly involving the LEC architecture, metallized plastics, such as aluminized mylar, may prove adequate.

8.6 POTENTIAL COMPETITION AND MARKETS AVAILABLE TO PRINT-BASED ORGANIC DISPLAYS

Other printable display technologies exist that could compete with organic light-emitting displays. Some of these technologies include light-emitting quantum dots, fully printed field-emissive phosphor displays, and alternating current phosphor electroluminescent (ACPEL) devices. We discuss here only the later technology, namely ACPEL or EL displays, as the others are still years away from commercialization. Advancements in particle encapsulation technology allowed ACPEL displays to be manufactured using printing technologies over a decade ago. These displays are fabricated from a phosphorescent particle, namely ZnS and its alloys. They can emit over most of the visible spectrum, but they only do it efficiently in a characteristic blue-green emission. At over a \$100 million dollar market, these displays have enjoyed some commercial success as inexpensive backlights (i.e., DayGlo watches), electronic signage, and even pixilated displays. Nonetheless, the wide scale commercialization of this technology has been limited by its inherent technological weaknesses, which include high operating voltage (120 V), expensive AC driver electronics, limited operating lifetimes, limited color range, and relatively low brightness ($<200 \text{ cd/m}^2$) that prevents daylight viewing. Moreover, capacitive coupling effects can inhibit effective passive addressing, a key requirement of low-cost, high information content messaging applications.

Organic light-emitting display technology (see Table 8.2) overcomes these inherent weaknesses with its low operating voltage requirements (2 to 10 V), inexpensive DC driver

TABLE 8.2
Fully Printed ACPEL Displays vs. Light-Emitting Organic Displays

Characteristic	ACPEL Display	Light-Emitting Organic Display ^a
Substrate	Glass or plastic	Glass or plastic
Electrical behavior	Capacitor	Diode-like
Voltage (V)	High voltage: 50 to 150	Low voltage: 2 to 10
Current drawn (mA/in. ²)	$<2 \text{ AC}$	$>10 \text{ DC}$
Addressing	Direct drive	Direct drive, matrix addressing
Luminous efficiency	High	High
Pixel luminance (cd/m ²)	<300	$>10,000$
Smallest pixel size	Limited by particle size ($\sim 50 \text{ }\mu\text{m}$)	Limited only by print resolution
Colors	Blue, green, orange, white	Red–blue–green (RGB)
Viewing angle	Wide: 160 degree viewing angle	Wide: 160 degree viewing angle
Patternability	High: printable ink-like characteristics	High: printable ink-like characteristics
Switching times	High, microseconds. However, lack of addressing limits video capability	High, microseconds. Video enabling. Slower switching speeds (100 μs) for LEC architectures
Expected lifetime (h)	<5000	$>10,000$
Cost of manufacturing	Low: $<\$0.20/\text{in.}^2$	Low: $<\$0.20/\text{in.}^2$ if fully printed; moderate: if not fully printed
Mechanical flexibility	Moderate: plastic substrates	High: plastic substrates

^aThese statistics are comparing fully printed ACPEL displays with spin-cast OLED displays with evaporated top electrode.

electronics, moderate lifetimes ($>10,000$ h), full RGB color range, and potential for very high brightness (>2000 cds/m²) that enables passive addressing and viewing under daylight conditions. These benefits open up the door to a wide range of technologies and applications that are not feasible using the ACPEL technology. Nonetheless, the demonstration and commercial viability of screen-printable, phosphor-based EL displays point to the promise of an entirely printable manufacturing technology for organic-based EL displays.

The development of inexpensive print-based manufacturing of organic light-emitting displays with the properties similar to those discussed in Table 8.2 enables numerous new market opportunities. These markets include electronic displays used in high-resolution displays, such as those found in laptops and PDAs, as well as displays found in the low-resolution display market (defined as displays having less than 100,000 pixels), such as alphanumeric displays. In the market for emerging display technologies, *Display Search* projects that the worldwide market for OLEDs will grow to \$4.2 billion; however, being able to operate in both the printing and electronic display industries, significant untapped target markets exist for organic displays that have not been included in this analyst's projection of the OLED market.

For example, most high-resolution display manufacturers are unable to meet the needs of the in-store media market because the market requires electronic displays that are of low cost and have peel-and-stick qualities, such as practically disposable alphanumeric displays that could be integrated into temporary and semipermanent signage. Additionally, inexpensive display technology could quickly impact the industrial and electronic market with a myriad of printed alphanumeric, segmented, and pixilated displays. In time, fully printed organic light-emitting displays may penetrate the billion-dollar market for large format LED displays, as well as the multibillion dollar market for print-on-vinyl displays used throughout the outdoor advertising world, by delivering dynamic content to public spaces. General diffuse lighting is another very large potential application of OLED technology, but it will likely require a fully print-based manufacturing process to meet cost points. Finally, there are untapped markets for organic displays for toys, vending machines, gaming, clothing, paper products, packaging, indicator lights, flat backlights, and instrument panels that, combined with the above applications, far exceed the market for active- and passive-matrix displays considered in OLED projections. In theory, all of these markets could be available to organic light-emitting displays if a cost-effective print-based manufacturing process was developed.

ACKNOWLEDGMENTS

We would like to thank Matt Wilkinson, Rob Roeloffs, and Jim Sheets for very helpful conversations.

REFERENCES

At the time of this writing, few comprehensive publications exist on high-volume print technologies for organic light-emitting polymer displays. We list some of these few below as well as other places where you can get more information on the chapter topics:

Transparent Polymer Electrodes:

S.A. Carter, M. Angelopoulos, S. Karg, P.J. Brock, and J.C. Scott, Polymeric anodes for improved polymer light-emitting diode performance, *Appl. Phys. Lett.*, 70: 2067–2069, 1997.

LEC Architecture:

Q.B. Pei, G. Yu, C. Zhang, Y. Yang, and A.J. Heeger, Polymer light-emitting electrochemical cells, *Science*, 268: 1086–1088, 1995.

U.S. Patent 5895717 and U.S. Patent 6284435.

Screen Printing:

D.A. Pardo, G.E. Jabbour, and N. Peyghambarian, Applications of screen printing in the fabrication of organic light-emitting devices, *Adv. Mater.*, 17: 1249–1252, 2000.

J. Birnstock, J. Blässing, A. Hunze, M. Stöel, K. Heuser, J. Wörle, A. Winnacker, and G. Wittmann, Screen-printed passive matrix displays based on light-emitting polymers, *Appl. Phys. Lett.*, 78: 3905–3907, 2001.

U.S. Patent 6,605,483.

Ink-Jet Printing:

T.R. Hebner, C.C. Wu, D. Marcy, M.H. Lu, and J.C. Strum, Ink-jet printing of doped polymers for organic light emitting devices, *Appl. Phys. Lett.*, 72: 519–521, 1998.

S.C. Chang, J. Liu, J. Bharathan, Y. Yang, J. Onohara, and J. Kido, Multicolor organic light-emitting diodes processed by hybrid inkjet printing, *Adv. Mater.*, 11: 734–737, 1999.

Y. Yang, S.C. Chang, J. Bharathan, and J. Liu, Organic/polymeric electroluminescent devices processed by hybrid ink-jet printing, *J. Mater. Sci.-Mater. Electron.*, 11: 89–97, 2000.

Other Printing Technologies:

Z. Bao, J. Rogers, and H. Katz, Printable organic and polymeric semiconducting materials and devices, *J. Mater. Chem.*, 9: 1895–1904, 1999.

Huebler, U. Hahn, W. Beier, N. Lasch, and T. Fischer, High Volume Printing Technologies for the Production of Polymer Electronic Structures, Proceedings of POLYTRONIC 2002, Zalagerszeg, Hungary, June 23–26, 2002.

9 Amorphous Silicon Thin-Film Transistor Active-Matrix Organic Light-Emitting Displays

Jerzy Kanicki and Yongtaek Hong

CONTENTS

9.1	Introduction	583
9.2	a-Si:H TFT Pixel Electrode Circuits for AM-OLEDs	584
9.2.1	Voltage-Driven 1- or 2-a-Si:H TFTs Pixel Electrode Circuits	584
9.2.2	Voltage-Driven 3-a-Si:H TFTs Pixel Electrode Circuits	588
9.2.3	Current-Driven 4-a-Si:H TFTs Pixel Electrode Circuits	592
9.3	3- and 4-a-Si:H TFTs AM-PLEDs Fabrication Steps	595
9.4	Electrical Properties and Stabilities of the a-Si:H TFTs	596
9.5	Electrical Properties of the a-Si:H TFT Pixel Electrode Circuits.....	601
9.5.1	Voltage-Driven 3-a-Si:H TFTs Pixel Electrode Circuit.....	601
9.5.2	Current-Driven 4-a-Si:H TFTs Pixel Electrode Circuit	603
9.5.3	Optoelectronic Characteristics of Current-Driven 4-a-Si:H TFTs Pixel Electrode Circuit	605
9.6	a-Si:H TFT AM-PLEDs	606
9.6.1	100 dpi Current-Driven 4-a-Si:H TFTs AM-PLED.....	606
9.6.2	200 dpi Current-Driven 4-a-Si:H TFTs AM-PLED.....	611
9.6.3	200 dpi Voltage-Driven 3-a-Si:H TFTs AM-PLED.....	611
9.7	Conclusions.....	614
	Acknowledgments	615
	References	615

9.1 INTRODUCTION

Today's flat-panel display (FPD) industry is dominated by the combination of passive-matrix liquid-crystal displays (LCDs) and active-matrix liquid-crystal displays (AM-LCDs). Several other FPD technologies (for example, field-emission or electroluminescent (EL) displays), which trace their origins at least as far back as LCDs, have either fallen by the wayside or, at best, penetrated only limited display market segments. Will passive-matrix organic light-emitting displays or active-matrix organic light-emitting displays (AM-OLEDs) fare any better against AM-LCDs, which today have become an entrenched FPD technology with a large installed manufacturing base and well-developed infrastructure for parts supply and integration?

It is generally accepted that the device geometry of organic light-emitting devices (OLEDs) and organic polymer light-emitting devices (PLEDs) are virtually ideal for FPD applications: a layer of luminescent material (small molecule or organic polymer) is placed

between two electrodes in a sandwich geometry; light is emitted on the passage of electrical current supplied by either passive- or active-matrix pixel electrode circuits, with a color that, in general, depends on the choice of organic materials. It is difficult to imagine anything simpler, flatter, or lighter.

More specifically, the following OLEDs or PLEDs characteristics are very attractive for FPD applications: Lambertian self-emission [1], which produces a wide viewing angle; fast response time (below microseconds), which is suitable for moving images; high luminous efficiency and low operation voltage, which guarantee low power consumption; lightweight, very thin structure, and robustness to the external impact as well as good daylight visibility through high brightness and contrast, which are desirable for portable displays; broad color gamut, which is suitable for full-color displays; simple, low-temperature fabrication processes, and low-cost organic materials, which make manufacturing cost-effective; and thin-film conformability on plastic substrates. All of these properties render OLEDs or PLEDs a promising candidate for flexible display applications [2,3]. However, many other obstacles must be overcome before the potential of this new technology can be realized. These include operating and storage lifetime; environment sensitivity to water and oxygen; drive schemes (passive- versus active-matrix approach); power efficiency and consumption; integration with the drive electronics; fine patterns control with vivid colors; high light output extraction; and the full cost analysis of manufacturing.

To solve some of these important issues, tremendous research efforts from academia and industry have been underway since the first appearance in 1997 of the OLED-based monochromatic car stereo displays in the market [4]. AM-OLEDs based on thin-film transistor (TFT) technology, in particular, have attracted considerable attentions for high-resolution, large-size FPD applications, such as laptop and TV screens. Recently, several FPD companies (such as Toshiba and Matsushita [5], Kodak and Sanyo [6], Sony [7], Samsung SDI [8], Chi Mei Optoelectronics, and IBM Japan [9]) have reported 15- to 24-in. TFT AM-OLED prototypes with wide extended graphics array (WXGA, 1200×768) or XGA (1024×768) resolution (Figure 9.1). The specifications of these prototypes are summarized in Table 9.1. It is noted that most of the AM-OLEDs are based on the polycrystalline silicon (poly-Si) TFTs technology [5–8] due to their better electrical performance and operational stability in comparison to the hydrogenated amorphous silicon (a-Si:H) TFTs. However, in 2003, Chi Mei Optoelectronics and IBM Japan [9] showed that the a-Si:H TFTs can also be used for large area high information AM-OLEDs when a proper and stable a-Si:H TFT process is developed. Since a much matured a-Si:H TFT technology is already available at low cost from the AM-LCD industry, it is expected that the a-Si:H TFT technology might challenge the poly-Si TFT technology in the near future for AM-OLEDs.

In this chapter, we describe mainly a-Si:H TFTs AM-OLEDs technology, developed at the University of Michigan within Kanicki's group since 1999, that one day may be able to compete not only with the poly-Si TFT AM-OLEDs but also with the a-Si:H TFT AM-LCDs. The a-Si:H TFT AM-OLEDs developed by others are only briefly described in this chapter.

9.2 A-SI:H TFT PIXEL ELECTRODE CIRCUITS FOR AM-OLEDs

9.2.1 VOLTAGE-DRIVEN 1- OR 2-A-SI:H TFTs PIXEL ELECTRODE CIRCUITS

In 1996, Wu et al. [10] reported that a-Si:H TFT can be used as a constant-current-providing (or driving) device in combination with the OLEDs. They integrated a top-light-emitting OLED and one driving a-Si:H TFT (T1) on thin stainless steel foil substrates. A schematic representation of the equivalent pixel circuit is shown in Figure 9.2a. When data voltage,



FIGURE 9.1 Images of AM-OLED prototypes reported by (a) Toshiba and Matsushita, (b) Kodak and Sanyo, and (c) Sony.

V_{data} is applied to the gate electrode of the TFT (T1), a corresponding drain current will flow through T1 and subsequently through the OLED for a given supply voltage V_{DD} . This current induces light emission from the OLED once a critical value is reached at a given voltage. However, this one-TFT pixel electrode circuit cannot be used in practical AM-OLEDs because OLEDs exhibit no memory effect and need to continuously convert electrical power into optical power to sustain the light emission. Hence to maintain OLED luminance, electrical power needs to be continuously supplied to the OLED during the whole

TABLE 9.1
Specifications of AM-OLED Prototypes

	Toshiba and Matsushita [5]	Kodak and Sanyo [6]	Sony [7]	Samsung SDI [8]	Chi Mei Opto electronics and IBM Japan [9]
Size (in.)	17 WXGA,	15 WXGA,	24.2 XGA,	15.5 WXGA,	20 WXGA,
Resolution	1280 × 768	1280 × 720	1024 × 768	1280 × 768	1280 × 768
TFT technology	Polysilicon	Polysilicon	Polysilicon	Polysilicon	Amorphous silicon
Peak brightness	300 cd/m ²	N/A	>200 cd/m ²	N/A	500 cd/m ²
Emissive material	Polymer	Small molecule	Small molecule	Small molecule	Small molecule
Year	2002	2002	2003	2003	2003

Note: N/A, not available.

frame period. In this pixel circuit, each select line will remain high only for a period of $1/N$ of the frame rate, where N is number of lines, and the a-Si:H TFT associated with the pixel will only be ON during that time. The electric power supplied by the data line during this period will be quickly consumed and dissipated by the OLED. Therefore, in such a scheme the OLED will be OFF during the remaining $(N-1)/N$ of the frame period, similar to the case of the passive-matrix display. To achieve a continuous pixel electrode excitation during the whole frame period, one pixel needs at least two TFTs with an appropriate storage capacitor as shown in Figure 9.2b. One TFT (T1) is used as the switching element (data-selecting device) as in the one-TFT driving scheme. The second TFT (T2, driving device) will provide a continuous power supply to the OLED throughout the entire frame time. T1 and T2 operate in the linear and saturation regime, respectively. The size of T2 should be larger than the size of T1 and the OFF-current of T1 should be very low to prevent any charge leakage from storage capacitor. With the combination of the two TFTs, electric power can therefore be continuously provided to the OLED to sustain the light emission. The control and data signal waveforms are also included in Figure 9.2b.

Specifically, when V_{select} is high (select time), T1 is ON and data voltage (column electrode) is written onto (stored in) the storage capacitor, C_{st} , through T1 until the T2 gate voltage equals the data line voltage. Then, T2 will be ON to allow corresponding current ($I_{\text{pixel_OLED}}$) to flow from the source line (V_{DD}) through T2 to the common cathode (ground) of pixel_OLED. The OLED pixel will then emit light, e.g., OLED is turn on. The current level is controlled by the gate voltage of T2 and the current source is programmed by setting the gate voltage of T2. This is achieved during a short addressing time of about 25 μs when T1 is turn on. When V_{select} is low (deselect time), T1 is OFF and the stored (programmed) voltage (charge stored in C_{st}) will determine the amount of current flow through the pixel_OLED. Therefore, if there is no change in the stored or programmed voltage, the same amount of current should flow from V_{DD} (high voltage or power or source line) through T2 to the pixel_OLED (cathode or ground), producing a continuous pixel light emission with the same luminance level. The storage capacitor prevents appreciable charge discharge via leakage through T1, thus allowing continuous OLED current, while the other rows are selected sequentially. It is important that the T1 off-current (leakage current) is less than 10^{-12} A to prevent any spurious signals to other pixels in the same column, which can be responsible for display cross talks.

A single pixel 2-a-Si:H TFTs AM-OLED was demonstrated in 1998 by Lu et al. [11], where a spin-coated organic polymer was used as the light-emitting material. They showed the single pixel circuit operation using the video graphics array (VGA) timing sequence. A fully

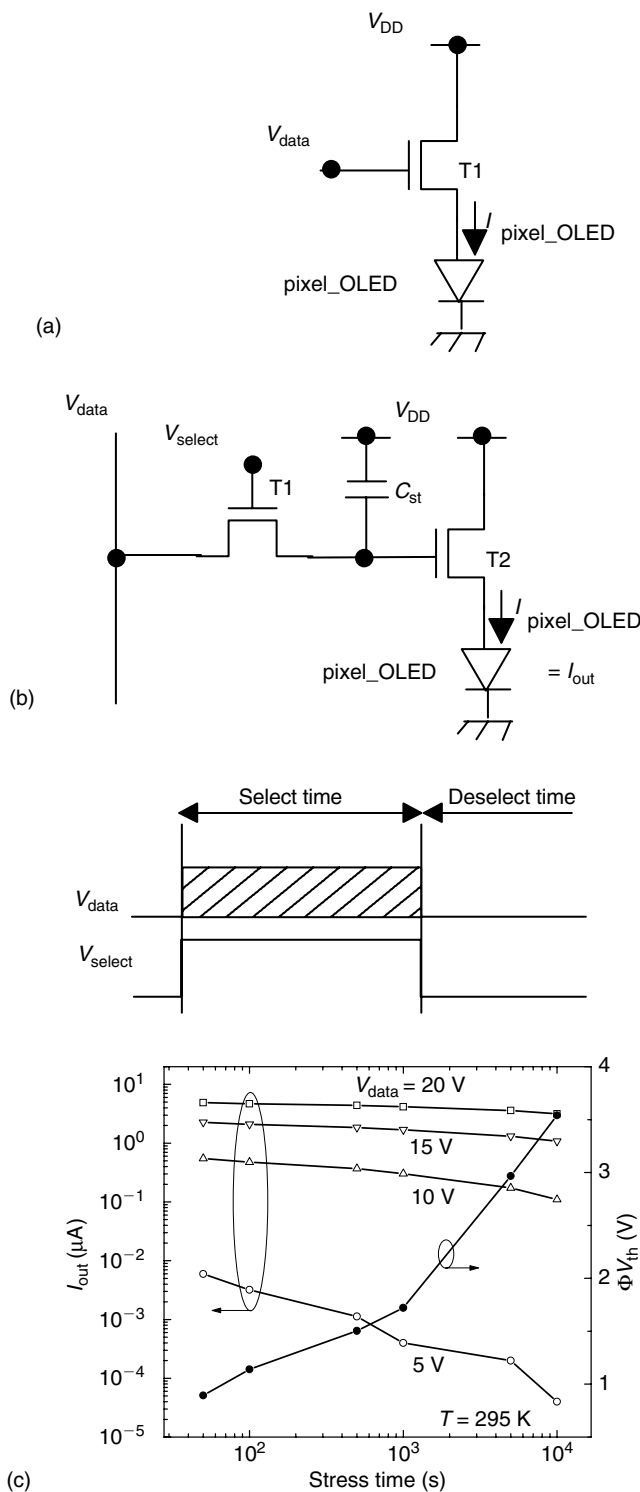


FIGURE 9.2 Schematic diagram of (a) 1- and (b) 2-a-Si:H TFTs pixel electrode circuits, and (c) bias stress result for circuit (b). Control signal waveforms for 2-a-Si:H TFTs pixel electrode circuits are also included in (b).

functional, full-color 2-a-Si:H TFTs AM-OLED prototype was only demonstrated in 2003 by AU Optronics Co. and Universal Display Corp. [12]. They reported 4 in. display, with $160 (\times \text{RGB}) \times 234$ resolution, 300 cd/m^2 peak brightness, 262,000 colors (6 bits for each color), $>300:1$ contrast ratio, and 670 mW power consumption for the video images. By using the phosphorescent R, G, and B light-emitting materials, they reduced power consumption of the AM-OLED by 42% in comparison with the fluorescent organic materials-based AM-OLED. Also a high external power efficient phosphorescent pixel_OLED with low drive voltage can significantly decrease the a-Si:H TFT AM-OLED operational voltage, which directly affects the operational stability of T2 a-Si:H TFT. Higher T2 TFT electrical stability is expected when gate voltage is reduced during display operation.

It is well known that the threshold voltage of a-Si:H TFTs can change with the device operation time and under influence of the gate voltage [13]. Any increase in a-Si:H TFT threshold voltage will introduce a change (reduction) in luminance of the AM-OLEDs, since display luminance is directly proportional to the output current flow. From Figure 9.2b, we can observe that data voltage (V_{data}) is a sum of V_{GS_T2} and voltage across the pixel_OLED. Therefore, shifts in the a-Si:H TFT (T2) threshold voltage during the display operation or any threshold voltage variations from pixel-to-pixel will lead to $I_{\text{pixel_OLED}}$ variations at a given V_{data} , leading to a reduced pixel luminance over time and a nonuniform light emission across the entire AM-OLED screen [14]. Figure 9.2c illustrates the variation of the output current characteristics for the 2-a-Si:H TFTs pixel electrode circuit as a function of the bias stress time [15]. From Figure 9.2c, for a bias stress time of 10^4 s the threshold voltage of T2 shifted $\sim 3.54 \text{ V}$, while the output current levels dropped by 40 and 85% for the data voltages of 20 and 10 V, respectively. These experimental results indicate that this type of pixel electrode circuit has a poor electrical reliability, and it will be very difficult (if not impossible) to achieve uniform luminance across the whole display panel over time.

In general, therefore, this pixel electrode structure is too simple to guarantee stable display electrical performance over time. Overall the anticipated problems with this pixel circuit include variation in the threshold voltage and field-effect mobility (mentioned above) of T2, leading to poor light emission uniformity and differential aging of the TFTs and OLEDs, leading to color shifts and additional nonuniformity of display luminance. Finally, finite line resistance can lead to voltage drops along the power and data lines by amounts dependent on the current requirements of pixel circuits.

To obtain a stable a-Si:H TFTs AM-OLED, a compensation method for the a-Si:H TFT threshold voltage and field-effect mobility shifts must be included in the pixel electrode circuits to maintain constant current through the OLED. Voltage- or current-driven schemes, which are described below, have been proposed to address these important issues. Voltage and current signals are used as a data signal in each driving scheme. In the voltage-driven scheme, the threshold voltage shift of a-Si:H TFTs is compensated by using complex threshold voltage memory and then employing data voltage writing steps during the select time. In current-driven scheme, the data current directly writes the shifted threshold voltage information and data signal onto the pixel [16]. It should be noted that the current-driven scheme needs a data current driver that is not standardized yet, while for the voltage-driven scheme, a data voltage driver is commercially available for AM-LCDs. Other specifications for each driving scheme are summarized in Table 9.2 and more details about these pixel electrode circuits are provided below.

9.2.2 VOLTAGE-DRIVEN 3-A-Si:H TFTs PIXEL ELECTRODE CIRCUITS

The effect of a-Si:H TFT threshold voltage variation on pixel electrode stability can be somewhat reduced by introducing an additional n-channel a-Si:H TFT into the 2-a-Si:H TFT pixel electrode circuit. Several such possible 3-TFTs pixel circuits are discussed below.

TABLE 9.2
Comparison between Voltage- and Current-Driven AM-OLED Schemes

	Voltage-Driven	Current-Driven
Data signal	Voltage	Current
Data signal driver	Commercially available (AM-LCD driver can be used)	Under development (standardization may be required)
Slow charging time issue at low display brightness levels	No	Yes (can be solved by current-mirror or current-sink type scheme)
TFT threshold voltage compensation	Yes (complicated threshold voltage member steps needed)	Yes (direct current writing)
TFT field-effect mobility compensation	No	Yes (direct current writing)
OLED threshold voltage compensation	Yes (by driving TFT)	Yes (by driving TFT and direct current writing)

A voltage-driven 3-a-Si:H TFTs pixel electrode circuit was reported by Kim and Kanicki in 2002 [17] and is shown in Figure 9.3a. The pixel electrode circuit has five components: C_{st} , a storage capacitor; T1, a switching TFT; T2, an active resistor; T3, a constant current driver TFT; and an organic PLED.

The pixel is selected through the switching transistor (T1) while the scan voltage (V_{scan}) is “high.” The driver TFT (T3) is used to provide constant current to the PLED. The active resistor (T2) partially compensates for the current drifts associated with the a-Si:H TFT (T3) driver and PLED characteristics shifts. While V_{scan} stays high, the switching TFT turns ON, and the data voltage, V_{data} , is transferred and stored in the storage capacitor, providing the turn-on signal to the gate electrode of the driver TFT T3. This selecting operation of each pixel occurs during a very short period of time, called the scan period, which is usually defined by the number of rows of the display.

To fully charge the storage capacitor to the data voltage level, the switching speed of TFT T1 is important. The storage voltage in C_{st} can be reduced by channel injection, hold-mode feed-through, parasitic capacitances, and leakage current. Depending on the data voltage level, which is now applied to the gate electrode of T3, the driver TFT provides the corresponding output current (I_{out}) to the PLED. The PLED luminance is linear function of this output current. Hence, the PLED’s maximum luminance depends on the current capacity of the driver TFT, storage capacity of C_{st} , and the power luminance efficiency of the PLED. After the scan period, the pixel has a long retention period. During this period, V_{scan} stays low and the switching TFT T1 turns off, disconnecting the data line from the T3. Nonetheless, the output current level needs to be maintained at the same level in order to keep the PLED luminance level unchanged. To accomplish this, the charge in the storage capacitor needs to be maintained for the entire retention period since C_{st} keeps the image data (V_{data}); any decrease of stored voltage will result in decrease of driving current and the luminance of the PLED. Hence a very low OFF-current ($\sim 10^{-12}$ A) of the switching TFT is critical in this circuit. In other words, a high ON/OFF current ratio for the switching TFT is required.

Since in this circuit the active resistor shares a high voltage drop (V_{DD}) with the driving TFT and PLED, any reduction in I_{out} will be reflected by a voltage increase at node A ($V_A = V_{DD} - V_{AR}$, where V_{AR} is the voltage drop across the active resistor) (Figure 9.3a). As V_A increases, V_{DS} of T3 increases, resulting in an increase of I_{out} . This represents partial compensation for an initial I_{out} decrease that can be optimized for a given pixel electrode circuit. For T3 threshold voltage shifts discussed later on in this chapter, it was established through simulation and

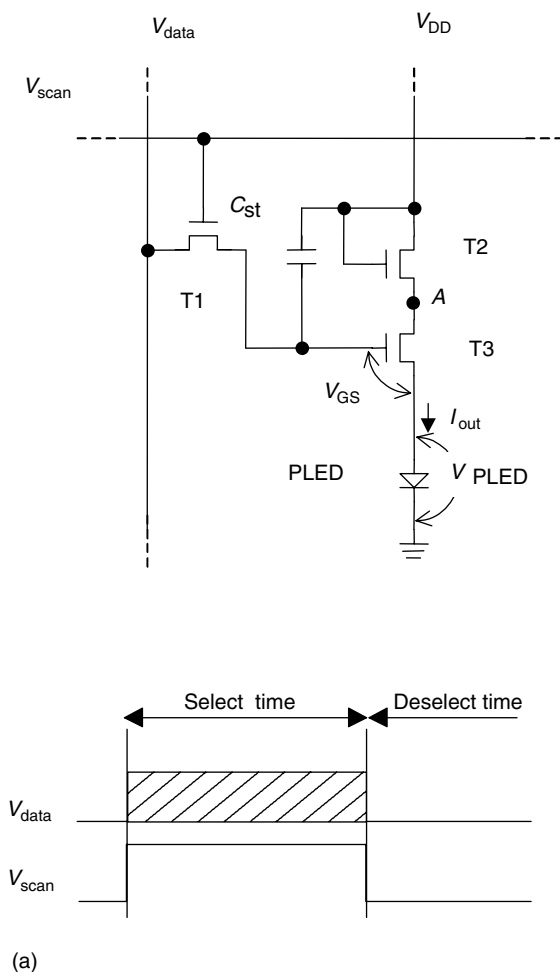


FIGURE 9.3 Schematic diagram of 3-a-Si:H TFT pixel electrode circuits: (a) University of Michigan. (From Kim, J.H., Hong, Y., and Kanicki, J., *IEEE Electron Device Lett.*, 24, 451, 2003. With permission.) (b) IBM. (From Sanford, J.L. and Libsch, F.R., *SID Tech. Dig.*, 34, 10, 2003. With permission.) Control signal waveforms for 3-a-Si:H TFTs pixel electrode circuit are also included.

experiments that the reductions of output current were 6, 14, and 28% for V_{data} of 5, 10, and 15 V, respectively. These reductions are too large for any practical display applications.

It should be noted that the operating point (output current level) and the linearity of the pixel electrode circuit can be optimized through better design of the active resistor dimensions (W/L) [17,18]. For example, it is expected that this pixel circuit will have better linearity with increasing W/L ratio of T2 for the same W/L ratio of T3. Since large W/L ratio of T2 corresponds to lower resistance value, the voltage drop across T2 is lower (see node A equation above). But, at the same time, the driving current I_{out} tends to saturate when T3 enters triode region, which is preferred when partial compensation of the driving current drift (due to the increase of threshold voltage of T3) is desirable. Since the higher data voltage V_{data} corresponds to higher driving current, a higher voltage drop is produced at active resistor T2, and therefore, T3 is pushed into triode region.

Hence, in this 3-a-Si:H TFT pixel circuit, the linearity and threshold voltage compensation are both limited by the properties of driving TFT T3. To acquire better linearity, T3

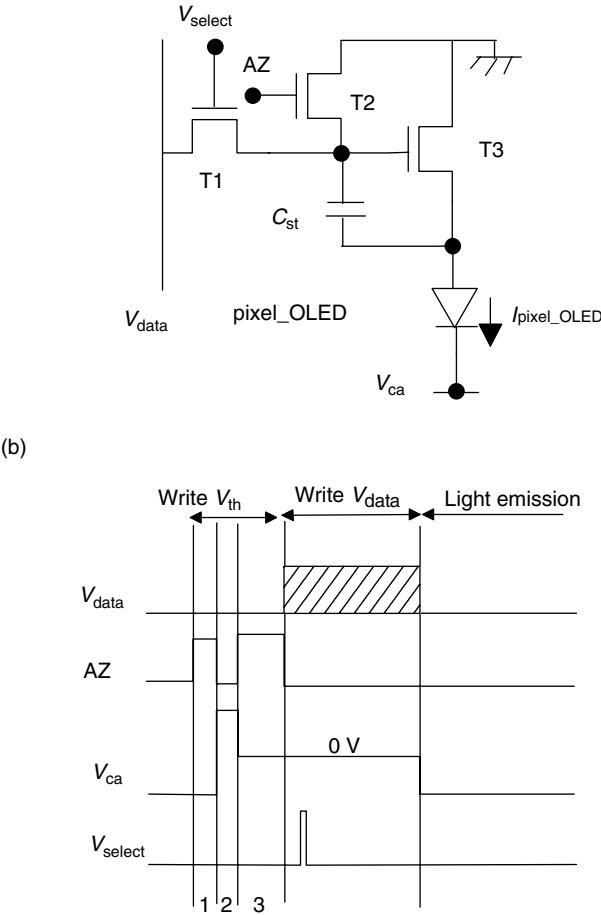


FIGURE 9.3 (continued)

needs to operate in the saturation region. To gain better compensation of threshold voltage shift, T3 needs to operate in the triode region. A more complex circuit design or driving scheme is needed to achieve better performance in both linearity and threshold voltage compensation.

A higher performance voltage-driven pixel electrode circuit has been reported in 2003 by Sanford and Libsch [14], which consists of three n-type a-Si:H TFTs, one select (V_{select}), one control line (AZ), and one programmable cathode line (V_{ca}) as shown in Figure 9.3b. T1 and T2 are switching TFTs, and T3 is a driving TFT. This pixel electrode circuit can compensate for T3 threshold voltage variations with the proper signals and timing as shown in Figure 9.3b. During Write V_{th} (threshold voltage) period, V_{select} is low (T1 is OFF), isolating the V_{data} line. The threshold voltage writing (Write V_{th} period) involves three steps. During the first step, the OLED cathode voltage, V_{ca} , is negative and the AZ input is high, turning ON T2. The current will flow from ground electrode through T2 to charge up C_{st} up to desirable voltage level, providing the turn-on signal to the gate electrode of T3. In this case, $V_{GS} = V_{DS}$ of T3 and it can be said that T3 operates in saturation regime. Next current (I_{pixel_OLED}) flows from ground through T3 to the pixel_OLED and the pixel_OLED will emit light. At the same time, C_{st} is charged to desirable value. Similar to

the previous pixel electrode circuit, the light emission during this short period is not related to the actual data signal and will not affect the display image. During this short period, V_{GS_T3} is larger than V_{th_T3} and is stored across a storage capacitor (C_{st}). During the second step, V_{ca} is brought to positive voltage and AZ input is low, turning off T2. A reverse bias is applied across the pixel_OLED via the reverse conduction of T3. In addition, the gate-to-drain and drain-to-source voltages of T3 are reversed to remove any residual charge induced to insure normal pixel operation. During the third step, V_{ca} is set at 0 V and the AZ input is high. T3 will be ON and the current will flow until the V_{GS_T3} approximately equal to the V_{th_T3} is established across the C_{st} . After this initial threshold voltage establishment, data signals for all the pixels are written into each C_{st} during Write V_{data} period. When V_{select} is high and T1 is ON, data voltage is written into each pixel circuit of the selected row. The voltage across the C_{st} is $V_{data} + V_{th_T3}$, which is maintained during the rest of the Write V_{data} period (V_{select} is low and T1 is OFF). During Write V_{data} period, V_{ca} is set to 0 V and the AZ input is low. After the data voltage has been written to all the rows in the display, V_{ca} is brought to a negative voltage. Current flows from ground through T3 to the pixel_OLED and the pixel_OLED emits light. $I_{pixel_OLED} \propto (V_{GS_T3} - V_{th_T3})^2 \propto (V_{data} + V_{th_T3} - V_{th_T3})^2 \propto (V_{data})^2$ flows through the pixel_OLED since T3 operates in saturation regime. Therefore, I_{pixel_OLED} is independent of V_{th_T3} and proportional to $(V_{data})^2$. In this pixel electrode circuit, AZ and V_{ca} are connected to all the pixels in the display and the pixel_OLED emits light only after the data voltage writing is finished. They also reported several variations of this pixel electrode circuit in Ref. [19], which showed similar threshold voltage compensation.

This voltage-driven pixel electrode circuit can successfully compensate for the a-Si:H TFT threshold voltage variation. The pixel_OLED turn-on voltage shift can also be compensated by operating the driving TFT in the saturation regime, in which the current flowing through the driving TFT (thus through the pixel_OLED) depends on V_{GS} and not V_{DS} , of the driving TFT T3. Therefore, any voltage shift in the pixel_OLED will be automatically compensated by changing V_{DS} of T3. However, the voltage-driven driving scheme can have only limited compensation capability for the a-Si:H TFT field-effect mobility variations across the whole display.

Therefore, if active-matrix a-Si:H TFT array shows variations in both threshold voltage and field-effect mobility, which is often the case, a current-driven pixel electrode circuits described below can have an advantage over voltage-driven pixel circuit in fully compensating for all TFT electrical parameter changes. In addition, since OLED brightness is directly related to the current flow through the driving TFT, the current-driven active-matrix driving method can produce a very uniform AM-OLED luminance by directly writing data current onto each pixel electrode.

9.2.3 CURRENT-DRIVEN 4-A-Si:H TFTs PIXEL ELECTRODE CIRCUITS

A schematic diagram of 4-a-Si:H TFTs pixel electrode circuit and the signal waveforms are shown in Figure 9.4. The organic PLED symbol is also included in Figure 9.4 to show the PLED connection with the pixel electrode circuit, which is denoted as pixel_PLED. The anode and cathode of pixel_PLED are connected to the source of T3 and ground, respectively, to complete the entire pixel circuit, which is called AM-PLED pixel in this chapter to differentiate it from the pixel electrode circuit. In active-matrix displays, all the pixels in a single row are selected for a certain period of the frame time (select time) and are deselected while other rows are selected during the rest of the frame time (deselect time). In this AM-PLED pixel, two control signals ($V_{select1}$ and $V_{select2}$) with opposite polarity define the select and deselect times (Figure 9.4) and also determine the current flow path, leading to the driving TFT T3 and pixel_PLED by turning ON and OFF the switching TFTs, T1/T2 and

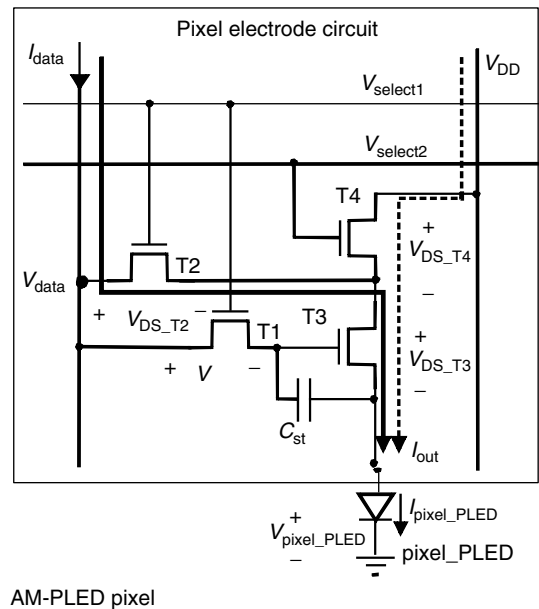


FIGURE 9.4 Schematic diagram of 4-a-Si:H TFTs pixel electrode circuit and control signal waveforms are shown. (From Hong, Y., Nahm, J.-Y., and Kanicki, J., *IEEE J. Selected Top. Quantum Electron. Org. Light-Emitting Diodes*, 10, 1, 2004. With permission.)

T4, respectively. It is also noted that the current (I_{data}) is supplied to the AM-PLED pixel as a data signal during select time, whose value varies according to the display gray-scale levels.

During select time ($V_{select1}$ is high, $V_{select2}$ is low), T1 and T2 are ON, and T4 is OFF (Figure 9.4). The data current flows from the data line (I_{data}) to pixel_PLED through T2 and T3 (solid line in Figure 9.4), triggering pixel_PLED light emission and commencing charging of the storage capacitor (C_{st}). The C_{st} charging process continues until V_{GS_T3} and V_{DS_T3} reach specific values corresponding to I_{DS_T3} ($= I_{data} = I_{out} = I_{pixel_PLED}$). Since I_{data} determines V_{GS_T3} and V_{DS_T3} values during select time, they can change from pixel-to-pixel if there is variation in the pixel_PLED turn-on voltage, and pixel circuit TFTs threshold voltage and field-effect mobility. These device parameter variations can be

caused by the manufacturing and material variations, as well as AM-PLED pixel circuit aging. When the charging process ends, a specific V_{GS_T3} value is stored in C_{st} . The charging process should be completed during select time for all I_{data} gray-scale levels. The charged V_{GS_T3} value is maintained and pixel_PLED continuously emits light until select time ends.

The gate potential of T3 equals the potential (V_{data}) of the I_{data} line, i.e., V_{DS_T1} is negligible, after the charging time, while V_{DS_T2} is not negligible due to the continuous I_{data} flow through T2 during select time; V_{DS_T2} directly depends on I_{data} . The AM-PLED pixel configuration and driving conditions, however, do impose the requirement on V_{DS_T2} that, during select time, T1 operates in linear regime, T2 operates from linear to on set of saturation regime, and T3 operates in the saturation regime. To ensure that T3 operates in the saturation regime, V_{DS_T2} should be smaller than V_{th_T3} (threshold voltage of T3) for all I_{data} gray-scale levels during select time ($V_{GS_T3} - V_{th_T3} \leq V_{DS_T3} \rightarrow V_{GD_T3} \leq V_{th_T3}$, $V_{GD_T3} = V_{DS_T2}$). Therefore, the I_{data} value that corresponds $V_{DS_T2} = V_{th_T3}$ will be the I_{data} operational limit that can be applied to AM-PLED pixel during select time for normal display operation condition.

During deselect time ($V_{select1}$ is low, $V_{select2}$ is high), T1 and T2 are OFF, and T4 is ON. The V_{DD} provides current flow to T3 and pixel_PLED through T4. The AM-PLED pixel is designed for T3 to operate in the saturation regime during deselect time. In addition, V_{GS_T3} does not change during deselect time if the charge variation in C_{st} is negligible. Therefore, for the same V_{GS_T3} value, I_{DS_T3} ($= I_{out} = I_{pixel_PLED}$) will be very close to I_{data} , resulting in continuous pixel_PLED light emission that corresponds to I_{data} . It is noted that, during deselect time, the V_{DS_T3} value is different from the V_{DS_T3} established during select time due to the current flow path change during deselect time (dotted line in Figure 9.4). Since the pixel_PLED luminance is proportional to I_{pixel_PLED} , its value will remain unchanged during both select and deselect times. However, if the driving TFT T3 shows nonideal characteristics in the saturation regime, I_{pixel_PLED} will be affected by V_{DS_T3} variation during deselect time, leading to variable pixel_PLED luminance. Additionally, if there is significant leakage current through T1 during deselect time, I_{pixel_PLED} is affected by the change of the stored charge in C_{st} , resulting in inconsistent pixel_PLED luminance.

As I_{data} increases, the operating point of T3 will move from saturation into linear regime for a given V_{DD} value, leading to I_{pixel_PLED} deviation downwards from I_{data} and corresponding decrease of pixel_PLED luminance during deselect time. Hence, the I_{data} operational limit to ensure operation of T3 in the saturation regime ($V_{GS_T3} - V_{th_T3} \leq V_{DS_T3}$) during deselect time must be established.

Knowing I_{data} operational limits during select and deselect times, it is important that the pixel electrode circuit parameters are carefully designed to balance those two limits and to achieve largest possible I_{data} operational range.

In our initial pixel electrode circuit with one V_{select} line, a diode-connected TFT was used for T4 [15]. In addition, for the AM-PLED pixel simulation, the simulation conditions were unintentionally selected for T4 to operate in deep saturation regime ($V_{DS_T4} = V_{GS_T4}$) [20]. Both publications may mislead readers by indicating that the AM-PLED is designed for T4 to operate in saturation regime [21]. T4 should, however, operate in linear to onset of saturation ($V_{DS_T4} \leq V_{GS_T4} - V_{th_T3}$) regime to obtain a small voltage drop across T4 for a given I_{data} . This will allow for T3 to operate in saturation regime with a large operational range of V_{DS_T3} for a given V_{DD} value.

Cadence Spectre was used to simulate the pixel electrode circuit. The a-Si:H TFT model used in the simulation is described in Ref. [22]. In the initial simulation, the following parameters were used: TFT field-effect mobility (μ) = 0.49 cm²/(V s) in linear region, TFT threshold voltage (V_{th}) = 2.55 V, $V_{select1}$ (high) = $V_{select2}$ (high) = 30 V, $V_{select1}$ (low) = $V_{select2}$ (low) = 0 V, V_{DD} = 30 V, C_{ST} = 5 pF, C_{OLED} = 1.5 pF, TFT parasitic capacitance

model parameter: C_{gso} (gate-to-source) = C_{dso} (gate-to-drain) = 5 nF/m. Based on the pixel circuit simulation results [23], AM-PLED prototypes with resolutions of 100 dpi (50×50 arrays) and 200 dpi (100×100 arrays) were designed and fabricated, and are described in this chapter. It is noted that the V_{th} and μ values used in the initial design are different from the experimental data described in this chapter since an improved a-Si TFT process was used to fabricate the a-Si:H TFT AM-PLEDs.

9.3 3- AND 4-a-Si:H TFTS AM-PLEDs FABRICATION STEPS

To demonstrate an application of 3- and 4-a-Si:H TFTs pixel electrode circuits in 100 and 200 dpi AM-PLEDs, we have fabricated a small size (0.5×0.5 in.²) engineering demonstration displays for both voltage- and current-driving pixel electrode methods, described above [24]. The processing steps of such units are described below.

First a chromium (Cr, 2000 Å) layer was deposited on the Corning 1737 glass substrates by a DC sputtering method. The Cr gates and selection lines were then patterned by wet-etching (Mask #1). Following gate line definition, hydrogenated amorphous silicon nitride (a-SiN_x:H) (3000 Å)/a-Si:H (1000 Å)/p-doped a-Si:H (n+a-Si:H) (300 Å) trilayer was deposited by plasma-enhanced chemical vapor deposition (PECVD) method without breaking vacuum at a substrate temperature of 300°C. Using reactive ion etching (RIE) with a gas mixture of O₂ and CCl₂F₂, the device active islands were defined (Mask #2). The gate via contact was then patterned through the a-SiN_x:H layer by wet-etching in buffered hydrofluoric acid (BHF) (Mask #3). After the gate via formation, a molybdenum (Mo, 2000 Å) layer was deposited by a DC sputtering method and source/drain (S/D) electrodes, row and column lines were patterned by wet-etching (Mask #4). Using S/D metal and photoresist as masks, back-channel-etching of the n+a-Si:H was performed by RIE with a gas mixture of O₂ and CCl₂F₂. This is a critical step in TFT fabrication and needs to be carefully optimized for the control of a-Si:H TFT OFF-current. To reduce the S/D contact resistances the MoSi₂ was formed at the contacts through thermal annealing for 2 h at 230°C in nitrogen. Then, benzocyclobutene (BCB, $0.3 \sim 2$ μm) was spun coated and thermally cured at carefully controlled temperature steps (up to 250°C) in nitrogen on top of the fabricated pixel electrode circuits to provide a planarized, flat surface for the deposition of the indium tin oxide (ITO) and PLED layers. To fabricate interconnects between Mo and ITO electrodes that will be deposited on the top of BCB, a contact was formed through the cured BCB planarization layer by using RIE with a gas mixture of O₂ and CF₄ (Mask #5). After contact via definition, *in situ* argon (Ar) back sputtering was performed over the BCB layer surface to improve the adhesion between ITO and BCB layer. ITO (1000 Å) was deposited by a DC sputtering method, then thermally annealed (described below), and finally patterned by wet-etching in a solution of nitric acid (HNO₃), hydrochloric acid (HCl), and deionized water (Mask #6) to form the PLED ITO anode electrode. The ITO was cured in a furnace at 250°C in nitrogen ambient to reduce its sheet resistance and to increase its transmittance.

In 3-a-Si:H TFTs 200 dpi AM-PLED the active-resistor had a channel width of 15 μm, and the driving and switching TFTs had channel widths of 105 and 30 μm, respectively, with the same channel length of 10 μm. The storage capacitance was 0.4 pF. The top and cross-section views of the AM-PLED backplane are shown in Figure 9.5. The inset shows a blow up of single pixel electrode circuit and its cross-section view.

In 4-a-Si:H TFT AM-PLEDs, the size (W/L) of TFT was 50 μm/6 μm, 143 μm/6 μm, 172 μm/6 μm, and 189 μm/6 μm for T1, T2, T3, and T4, respectively. The size of the storage capacitor was 100×172 μm², which corresponds to about 3.5 pF. The top and cross-section view of the fabricated pixel electrode circuit is shown in Figure 9.6.

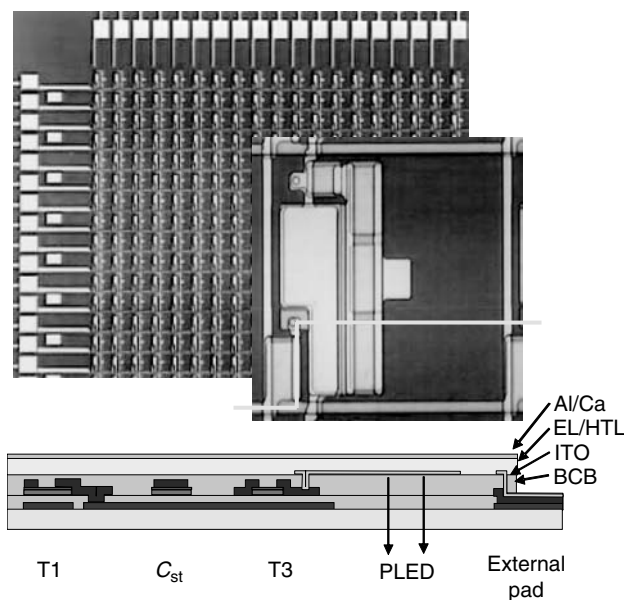


FIGURE 9.5 Top view of 3-a-Si:H TFTs 200 dpi AM-PLED back plane. Inset shows single pixel circuit and the top-view and cross-section schematics. (From Kim, J.H., Hong, Y., and Kanicki, J., *IEEE Electron Device Lett.*, 24, 451, 2003. With permission.)

Once the active-matrix arrays were fabricated, the ITO surface was treated with UV-ozone treated for 10 min before a hole injection layer (HIL) (poly(3,4-ethylene dioxythiophene) (PEDOT) doped with poly(styrenesulfonate) (PSS)) was deposited from a water-based solution by spin-coating method and was thermally cured. Next, the red- or green-light-emissive polyfluorene layer (LEL) is deposited from solution by spin-coating method and was thermally cured. Finally a calcium (150 Å)/aluminum (2000 Å) bilayer cathode was thermally evaporated on top of the display [34]. We removed the PLED-active layers from display contact pads using organic solvents. The top and cross-section views of the fabricated 3- and 4-a-Si:H TFTs AM-PLED pixel are shown in Figure 9.5 and Figure 9.6, respectively. In both displays, the light is emitted from the backside through the glass substrate.

In 4-a-Si:H TFTs 100 dpi AM-PLED, the aperture ratio (AR) of the pixel was $\sim 22\%$, which was defined as the ratio of the light-emitting pixel_PLED area ($77 \times 185 \mu\text{m}^2$) to the whole pixel area ($254 \times 254 \mu\text{m}^2$). The AR of the pixel was reduced to $\sim 10\%$ in 4-a-Si:H TFTs 200 dpi AM-PLED; pixel_PLED area and the whole pixel area were $24 \times 65 \mu\text{m}^2$ and $127 \times 127 \mu\text{m}^2$, respectively.

9.4 ELECTRICAL PROPERTIES AND STABILITIES OF THE a-Si:H TFTs

Figure 9.7a shows an example of a-Si:H TFT transfer characteristics in linear regime with different W/L ratios and an example of a-Si:H TFT characteristics in saturation regime with $W/L = 170 \mu\text{m}/6 \mu\text{m}$. A threshold voltage (V_{th}) of $10 \sim 11$ V, a field-effect mobility (μ) of $0.2 \sim 0.3 \text{ cm}^2/(\text{V s})$, a subthreshold swing slope of 0.8 dec/V , and a current ON/OFF ratio of larger than 10^6 for V_{GS} from -10 to 30 V were obtained from these curves for a-Si:H TFTs. These devices were used in 4-a-Si:H TFTs AM-PLEDs. The electrical properties of a-Si:H TFTs used in 3-a-Si:H TFTs AM-PLEDs are described in Ref. [18].

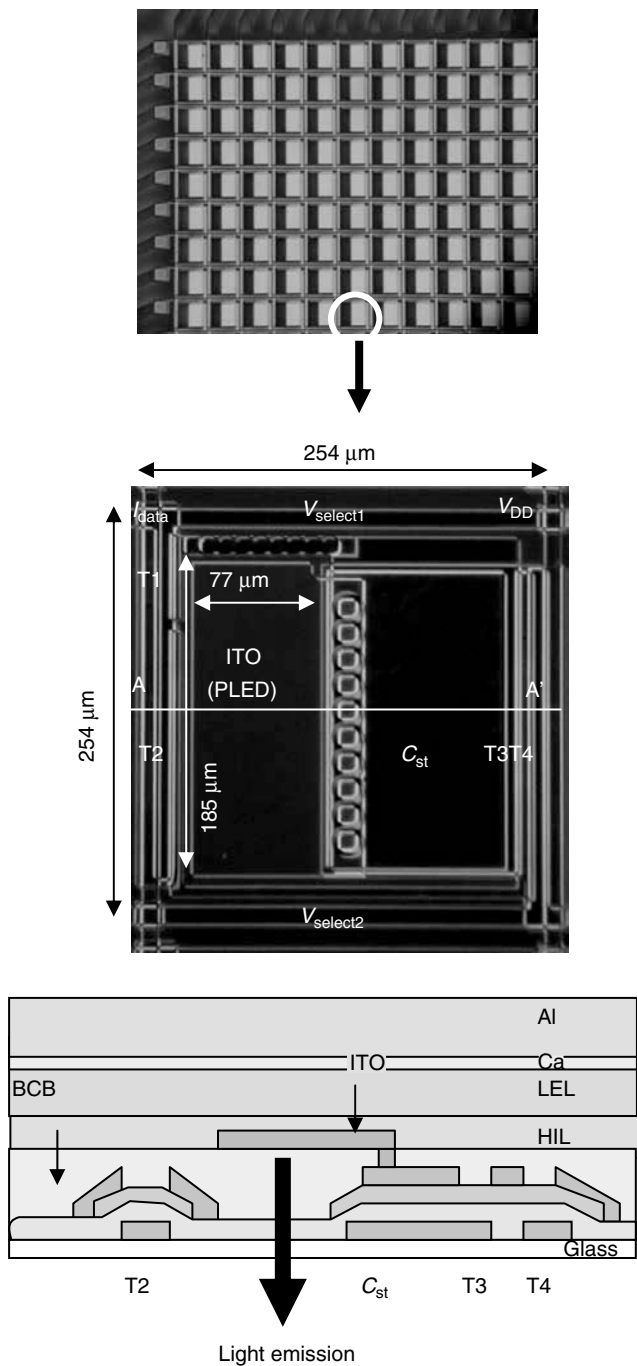


FIGURE 9.6 Top and cross-section views of the fabricated 4-a-Si:H TFTs pixel electrode circuits are shown. This pixel electrode circuit was used in 100 dpi AM-PLED. (From Hong, Y., Nahm, J.-Y., and Kanicki, J., *IEEE J. Selected Top. Quantum Electron. Org. Light-Emitting Diodes*, 10, 1, 2004. With permission.)

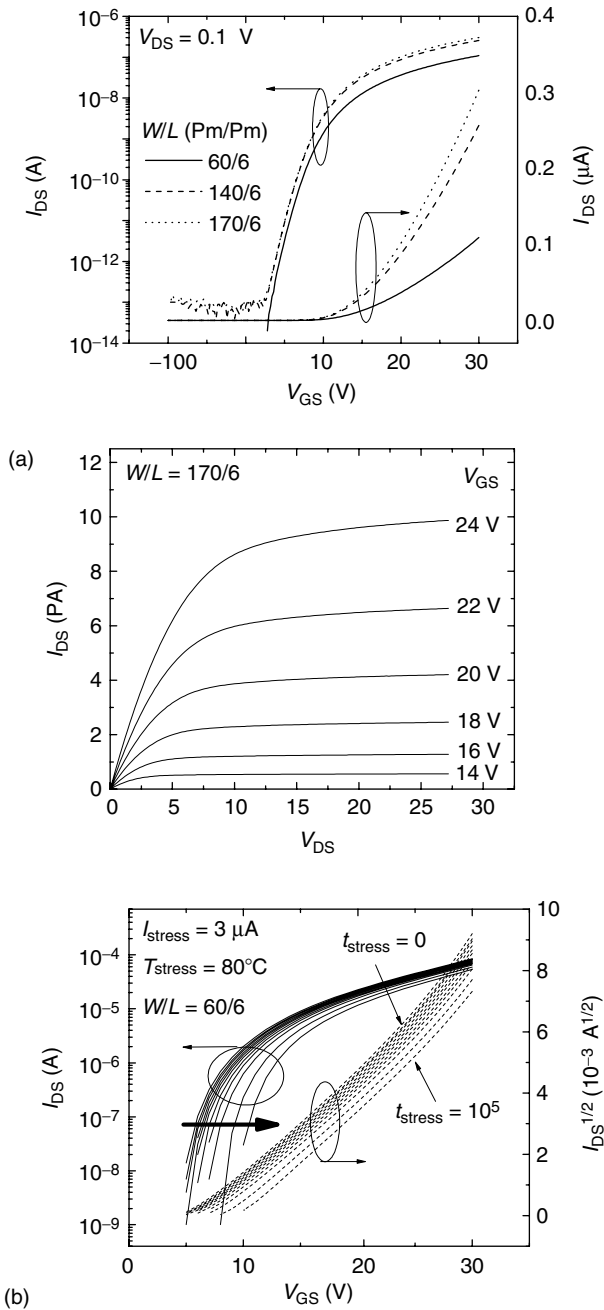


FIGURE 9.7 Measured characteristics of fabricated a-Si:H TFTs. (a) Transfer characteristics at $V_{DS}=0.1$ V for TFTs with different gate width, (b) an example of I_{DS} – V_{GS} characteristics for current–temperature–stress (CTS) measurements, (c) extracted ΔV_{th} versus stress time at RT and 80°C, and (d) Cadence Spectre simulation of pixel electrode circuit for threshold voltage shift of a-Si:H TFTs are shown. (From Hong, Y., Nahm, J.-Y., and Kanicki, J., *IEEE J. Selected Top. Quantum Electron. Org. Light-Emitting Diodes*, 10, 1, 2004. With permission.)

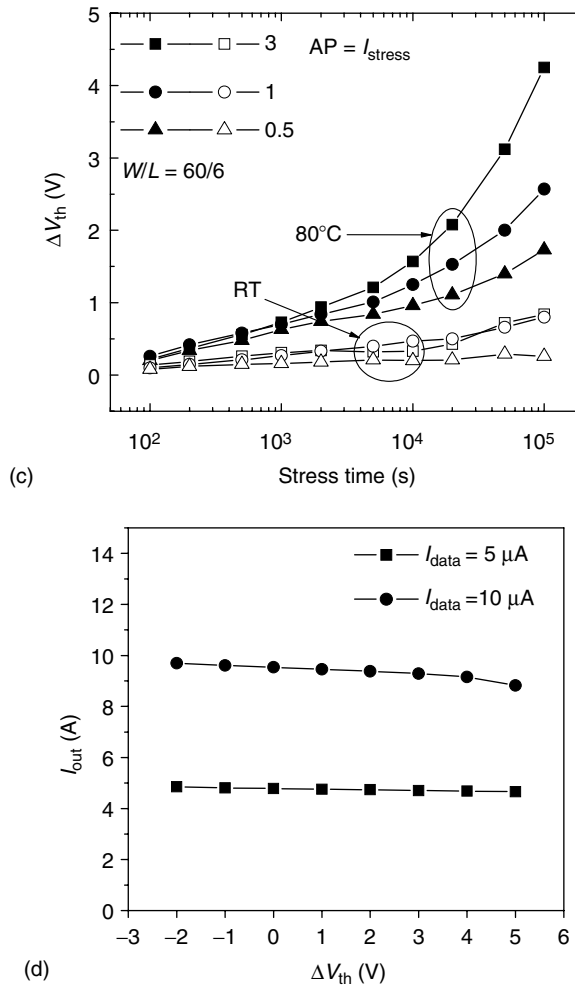


FIGURE 9.7 (continued)

To investigate the impact of T3 threshold voltage shift on 4-a-Si:H TFTs pixel electrode (Figure 9.4), the current–temperature–stress (CTS) of a-Si:H TFT ($W/L = 60 \mu\text{m}/6 \mu\text{m}$) was performed for different stress and current levels at room temperature (RT) and 80°C . During CTS, the drain and gate electrodes of a-Si:H TFT were electrically connected (the TFT remained in a deep saturation regime during electrical stressing) and a constant stress current was applied to the drain electrode. At several selected stress times, the stress was interrupted and drain-to-source current (I_{DS}) versus gate-to-source voltage (V_{GS}) characteristics in saturation regime were measured at a given stress temperature. Figure 9.7b shows an example of I_{DS} – V_{GS} characteristics measured during CTS at 80°C . The TFT threshold voltage was then extracted by fitting the experimental $\sqrt{I_{DS}}$ – V_{GS} characteristics to the following relation, using the MOSFET gradual channel approximation in saturation regime:

$$I_{DS} = \frac{1}{2} \mu C_{ins} \frac{W}{L} (V_{GS} - V_{th})^2,$$

where μ , C_{ins} , W , and L are field-effect mobility, gate insulator capacitance, channel width, and channel length of TFT, respectively.

Figure 9.7c shows the TFT threshold voltage shifts ($\Delta V_{\text{th}} = V_{\text{th}} - V_{\text{th0}}$, where V_{th0} and V_{th} threshold voltages of the TFT extracted from the $I_{\text{DS}}-V_{\text{GS}}$ characteristics measured before and after CTS) at RT and 80°C for stress currents of 0.5, 1, and 3 μA . At RT, the threshold voltage shift was less than 1 V for 3 μA stress current after 10^5 s of stress time while the threshold voltage shifted by as much as ~ 5 V at 80°C for the same CTS conditions. The change in field-effect mobility for the TFTs after CTS was within $\pm 5\%$ from its initial value. Based on this data, it was concluded that the threshold voltage shift of the TFTs will have the most significant effect on the operation stability of the pixel electrode circuit. If it is assumed that the amount of TFT threshold voltage shift in CTS is associated with the stress current per TFT gate width for TFTs with the same gate length, ~ 5 V threshold voltage shift of the driving TFT ($W/L = 172 \mu\text{m}/6 \mu\text{m}$) is expected for a stress current (or a continuous I_{data}) of $\sim 9 \mu\text{A}$ ($= 3 \mu\text{A}/60 \times 172$) at 80°C. This current level corresponds to a continuous pixel luminance of $L_{\text{pixel}} = \sim 45 \text{ cd/m}^2$ for red monochromatic AM-PLED, which was extracted from Figure 9.11c.

Using Cadence Spectre simulation [23], it was shown that the I_{out} of 4-a-Si:H TFTs pixel circuit can be maintained constant even for device threshold voltage shift as large as 5 V (Figure 9.7d). The simulation result showed that after ΔV_{th} of 5 V, I_{out} decreased by ~ 0.1 and $\sim 0.7 \mu\text{A}$ for $I_{\text{data}} = 5$ and $10 \mu\text{A}$, respectively. Based on Figure 9.11c, these current reductions correspond to ~ 2 and $\sim 7\%$ reduction of the pixel luminance when each pixel is continuously illuminated (red light) at ~ 25 and 50 cd/m^2 , respectively. This threshold voltage shift and pixel luminance decrease can be considered as the worst case for 4-a-Si:H TFTs pixel electrode circuit. Better threshold voltage compensation can be achieved through optimization of the pixel electrode circuit design and electrical performance of a-Si:H TFTs.

To investigate the impact of T3 threshold voltage shift on 3-a-Si:H TFTs pixel electrode circuit (Figure 9.3a), we performed the DC bias–temperature–stress (BTS) of a-Si:H TFT under the pixel electrode circuit operation conditions, which are $V_{\text{GS}} = 10 \text{ V}$ and $V_{\text{DS}} = 5.5 \text{ V}$ [25]. Two different stress temperatures, RT and 80°C were used for a stress period of $2 \times 10^4 \text{ s}$ (Figure 9.8a). The threshold voltage shift was extracted from TFT characteristics in the linear regime using the usual MOSFET equation. The variation of ΔV_{th} ($= V_{\text{th}} - V_{\text{th0}}$, where V_{th0} and V_{th} are threshold voltages of TFT extracted from the $I_{\text{DS}}-V_{\text{GS}}$ characteristics measured before and after BTS) versus stress time is shown in Figure 9.8a (inset). For this pixel circuit operation conditions, the maximum threshold voltage shift was 0.3 V at RT and 1.2 V at 80°C. Small subthreshold slope changes were observed during BTS at RT and 80°C. No significant field-effect mobility change was observed during the a-Si:H TFT stress period.

Considering the ΔV_{th} of a-Si:H TFT T3, the output current density (J_{out}) reduction has been calculated using a Cadence Spectre simulation for 3-a-Si:H TFTs pixel electrode circuit. Figure 9.8b shows the output current density changes with ΔV_{th} for three different gray scales (V_{data} of 5, 10, and 15 V). It can be concluded from this figure that the current compensation in 3-a-Si:H TFTs pixel circuit was not effective at the lower V_{data} . The current density was reduced by up to 45% for $V_{\text{data}} = 5 \text{ V}$. From the simulated data, it was concluded that this pixel circuit cannot fully compensate for ΔV_{th} at low V_{data} (i.e., low gray levels) without significant pixel circuit modifications. In normal applications, we need to control the AM-OLED luminance reduction to level below 3 to 5% at all gray levels.

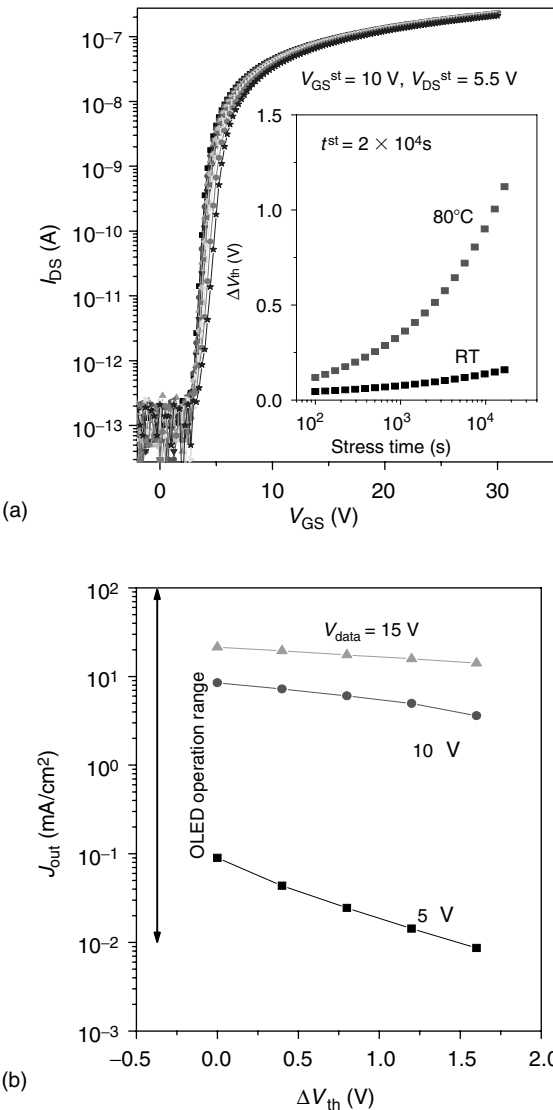


FIGURE 9.8 (a) An example of the BTS data for driver a-Si:H TFT. The inset shows the threshold voltage and subthreshold slope shift versus the stress time. (From Kim, J.-H., Lee, D., and Kanicki, J., *Proc. 22nd Int. Display Res. Conf.*, 601, 2002. With permission.) (b) The output current density changes versus threshold voltage shifts of a-Si:H TFT driver for our pixel electrode circuit. (From Kim, J.-H., Lee, D., and Kanicki, J., *Proc. 22nd Int. Display Res. Conf.*, 601, 2002. With permission.)

9.5 ELECTRICAL PROPERTIES OF THE A-Si:H TFT PIXEL ELECTRODE CIRCUITS

9.5.1 VOLTAGE-DRIVEN 3-A-Si:H TFTs PIXEL ELECTRODE CIRCUIT

An example of measured a-Si:H TFT driver characteristics and calculated load lines with $(V_{AR} + V_{PLED})$ and without voltage drop across the active resistor is shown in Figure 9.9a [26]. The crossing point between I_D – V_{DS} and load lines represents output current (I_{out}) of the pixel

electrode circuit. By adding an active resistor, the output current level is reduced but, at the same time, better current stability of the pixel circuits is realized. In this pixel electrode circuit, an active resistor forces the a-Si:H TFT driver to operate in linear regime for V_{data} larger than 5 V. In this operating regime, the output current level drifts associated with the a-Si:H TFT driver and PLED characteristics shifts can be reduced in comparison with the a-Si:H TFT driver, operating in saturation regime. However, as indicated above only partial compensation for an initial I_{out} decrease can be realized with this pixel electrode circuit.

The variation of the output current of the pixel electrode circuit with V_{GS} of the driver TFT is shown in Figure 9.9b. V_{scan} of 20 V and V_{DD} ranging from 10 to 35 V were applied

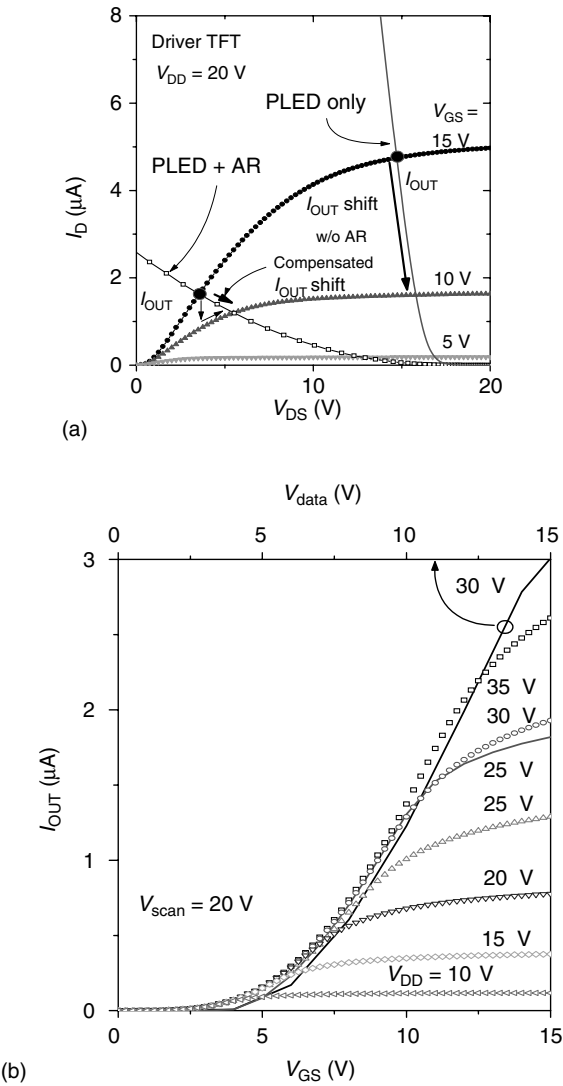


FIGURE 9.9 (a) The load lines of 3-a-Si:H TFT pixel circuit for $V_{\text{DD}} = 20\text{ V}$. The open symbol and solid line represent the load line with $(V_{\text{AR}} + V_{\text{PLED}})$ and without (V_{PLED}) active resistor. (From Kim, J.-H. and Kanicki, J., *SID Tech. Dig.*, 34, 18, 2003. With permission.) (b) Measured (symbol lines) and simulated (solid lines) pixel electrode output current versus input data voltage characteristics ($V_{\text{data}} = V_{\text{GS}} + V_{\text{OLED}}$). (From Kim, J.-H. and Kanicki, J., *SID Tech. Dig.*, 34, 18, 2003. With permission.)

during output current measurements. The current density between 2 and 50 mA/cm² was achieved for the pixel electrode AR of 45% and the PLED area of 7500 μm². The simulated curves for $V_{DD} = 25$ and 30 V are also shown in Figure 9.9b for V_{data} , ranging from 0 to 15 V; in this simulation, $\mu = 0.5$ cm²/(Vzs) and $V_{th} = 1.76$ V were used. The measured and simulated current–voltage transfer characteristics showed similar behavior with a small deviation. Based on this pixel electrode circuit performance, the output current density up to 100 mA/cm² can be achieved.

9.5.2 CURRENT-DRIVEN 4-A-Si:H TFTs PIXEL ELECTRODE CIRCUIT

To analyze the electrical performance of the 4-a-Si:H TFTs pixel electrode circuit, the electrical characteristics of the circuit without PLED were measured by applying ground (GND) to the ITO (source of T3) (Figure 9.4 and Figure 9.10a). A semiconductor parameter analyzer (HP 4156A) with a pulse generator expander (HP 41501A) was used to apply I_{data} , V_{DD} , $V_{select1}$, and $V_{select2}$ to the pixel electrode circuit as shown in Figure 9.10a. It is noted that during this study, for the one pixel electrode circuit analysis, 0–40 V with duty ratio 40% (40 ms select time and 60 ms deselect time) signals were used for $V_{select1}$ and $V_{select2}$ to guarantee that an appropriate data signal is stored during select time after a peak current flows for all the data current levels. Since a constant (not pulsed) current was applied as a data signal, a peak current flow was observed during the select time transition as discussed in the next section, which increases the data storage settling time during select time. Therefore, if a pulsed current signal is used for this pixel electrode circuit, the signal duty ratio can be further reduced and this reduction will be sufficient to operate higher resolution a-Si:H TFT AM-PLEDs. As the number of lines increases, charge leakage can be critical during the long frame time. However, previously reported simulation results [23] showed that low OFF-current of switching a-Si:H TFT did not cause any significant charge leakage during the frame time for 60 Hz, VGA (640 × 480) operation.

In this experiment, a combination of an operational amplifier (National Semiconductor LM741C) and an oscilloscope (HP 54615B) was used to measure the current flow at the source of T3, which is denoted as I_{out} in Figure 9.4. The operational amplifier provides virtual GND for the source of T3 and directs the current flow from the source of T3 through a 100 kΩ resistor (R). The voltage drop across the resistor was measured ($V_{measured}$) and displayed as a waveform on the oscilloscope display. The current flow (I_{out}) at the source of T3 was calculated by $V_{measured}/R$. It should be noted that LM741C has an input bias current of 80 nA (typical at RT) and 0.5–0.8 μA (maximum depending on temperature). Therefore, the voltage drop across R was first measured when $I_{data} = 0$ A, which was found to be $\sim +10$ mV. This voltage level can correspond to DC current of ~ 100 nA, flowing into the operational amplifier at zero data current. This zero-data-current voltage was added to the $V_{measured}$ for I_{data} of 1 ~ 6 μA to accurately calculate I_{out} . An example of measured signal waveforms for $I_{data} = 1, 4$, and 6 μA, when $V_{DD} = 30$ V is shown in Figure 9.10b. At $I_{data} = 1$ μA, I_{out} is close to I_{data} during select and deselect times. However, at $I_{data} = 4$ and 6 μA, I_{out} is close to I_{data} during select time while I_{out} is lower than I_{data} during deselect time. It is speculated that this I_{out} reduction during deselect time is associated with an operating point change of the pixel electrode circuit. A peak current flow was observed, especially for large I_{data} , during select time transitions, which is caused by the leftover charges from the previous frame time. To remove this effect, a current-sink type approach [27] or a current driver reset function [28] can be used.

The measured I_{out} versus I_{data} characteristics for different V_{DD} values (20, 25, 30 V) are shown in Figure 9.10c, where solid and open symbols correspond to I_{out} measured during select and deselect times. The peak current flow for I_{out} during the select time transition is excluded in Figure 9.10c. For the deselect time I_{out} values, the median values with error bars

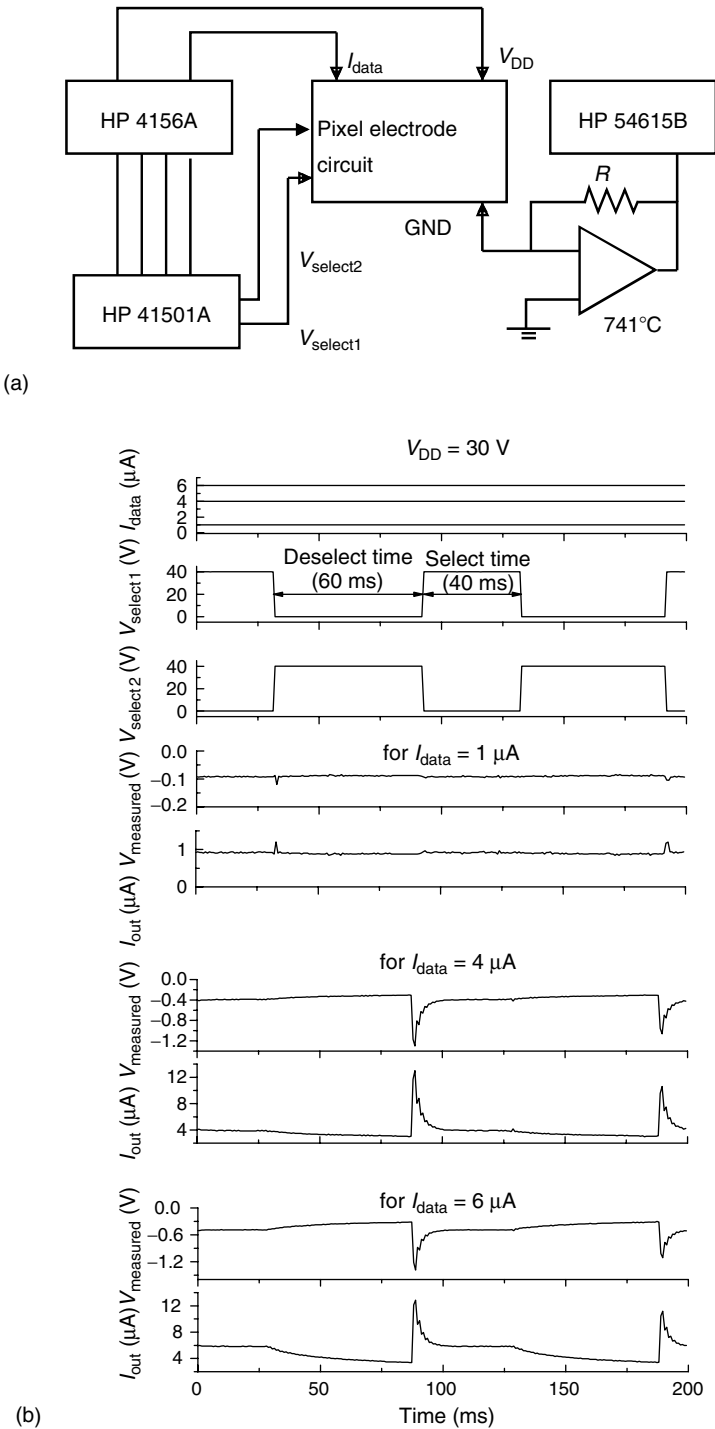


FIGURE 9.10 Pixel electrode circuit measurement results. (a) Measurement setup, (b) an example of measured waveforms for $I_{data} = 1, 4,$ and $6 \mu A$ for $V_{DD} = 30$ V, and (c) $I_{out}-I_{data}$ characteristics for $V_{DD} = 20, 25,$ and 30 V are shown. (From Hong, Y., Nahm, J.-Y., and Kanicki, J., *IEEE J. Selected Top. Quantum Electron. Org. Light-Emitting Diodes*, 10, 1, 2004. With permission.)

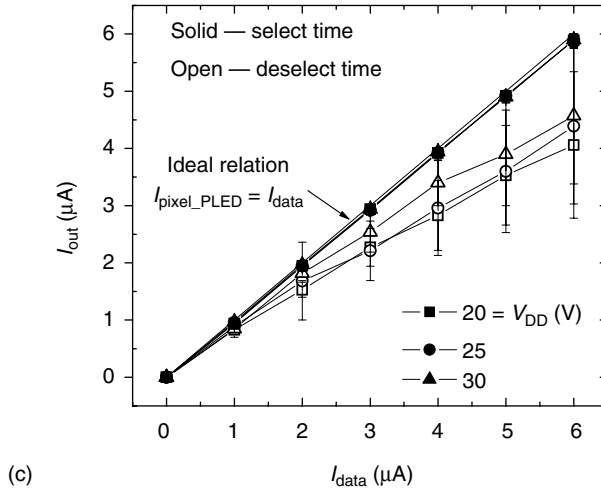


FIGURE 9.10 (continued)

are plotted to represent the I_{out} change during deselect time. The select time I_{out} values are very close to the I_{data} levels for different V_{DD} values. However, the deselect time I_{out} values deviate from the ideal curve (solid line) at higher I_{data} current levels. This deviation is consistent with the simulation data [23] and corresponds to the pixel electrode circuit operating point change during deselect time, which will be further discussed below. In this study, V_{DD} greater than 30 V is not considered since T4 operates in the saturation regime during deselect time when $V_{\text{DD}} > 30$ V due to the high threshold voltage (10 ~ 11 V) of a-Si:H TFTs used in this work. A good linear relationship between I_{out} and I_{data} up to ~1, ~2, and ~3 μA has been achieved for $V_{\text{DD}} = 20, 25$, and 30 V, respectively.

9.5.3 OPTOELECTRONIC CHARACTERISTICS OF CURRENT-DRIVEN 4-A-Si:H TFTs PIXEL ELECTRODE CIRCUIT

The optoelectronic characteristics of the pixel_PLED were extracted from the typical PLED optoelectronic characteristics independent of the pixel electrode circuit. Figure 9.11a shows the typical PLED current density and luminance versus voltage (J_{PLED} , L_{PLED} versus V_{PLED}) characteristics. The device structure of a typical red PLED ($2.54 \times 2.54 \text{ mm}^2$) fabricated by the authors on flexible plastic substrates is also included. The device consists of a HIL and a LEL. PEDOT doped with PSS was used as HIL, and red-light-emitting polyfluorene copolymer [29] represents LEL. A calcium–aluminum (Ca–Al) bilayer was used for the cathode. The PLED turn-on voltage and turn-on current density, defined at luminance of 1 cd/m^2 , are ~2.5 V and ~0.9 mA/cm^2 , respectively. The maximum light emission and power efficiencies of 0.53 cd/A and 0.27 lm/W are obtained at corresponding 1000–1300 cd/m^2 and 50 cd/m^2 . From these PLED optoelectronic characteristics, the pixel_PLED optoelectronic characteristics for the 100 dpi monochromatic red-light-emitting 4-a-Si:H TFTs AM-PLED have been estimated. Assuming that the PLED current density and luminance versus voltage characteristics do not change with the PLED size, which was experimentally verified, the pixel_PLED $I_{\text{pixel_PLED}}$ versus $V_{\text{pixel_PLED}}$ and pixel luminance (L_{pixel}) characteristics were calculated by using the following equations:

$$V_{\text{pixel_PLED}} = V_{\text{PLED}} \quad (9.1)$$

$$I_{\text{pixel_PLED}} = J_{\text{PLED}} \times A_{\text{pixel_PLED}} \quad (9.2)$$

$$L_{\text{pixel}} = \frac{L_{\text{PLED}} \times A_{\text{pixel_emission}}}{A_{\text{pixel}}} \quad (9.3)$$

where $A_{\text{pixel_PLED}}$, $A_{\text{pixel_emission}}$, and A_{pixel} are the effective pixel current-flowing area ($106.6 \times 185 \mu\text{m}^2$), the pixel light-emitting area ($77 \times 185 \mu\text{m}^2$), and the total pixel area ($254 \times 254 \mu\text{m}^2$), respectively. The difference between $A_{\text{pixel_PLED}}$ and $A_{\text{pixel_emission}}$ comes from overlap between the pixel_PLED ITO electrode and the T3 source, as shown in Figure 9.4. The calculated pixel_PLED optoelectronic characteristics are shown in Figure 9.11b and c. The extracted L_{pixel} versus $I_{\text{pixel_PLED}}$ characteristics can be described by the following equation by fitting extracted data in two different $I_{\text{pixel_PLED}}$ ranges:

$$L_{\text{pixel}} \propto I_{\text{pixel_PLED}}^{\alpha} \quad (\alpha = 1.2 \pm 0.1) \quad (9.4)$$

A slight deviation from the linear relationship was observed at lower luminance levels ($<2 \text{ cd/m}^2$) in Figure 9.11c. This deviation comes from a fluctuation in J_{PLED} versus V_{PLED} measurement at lower voltages ($<2.5 \text{ V}$), where smaller V_{PLED} steps (0.2 V) are applied as shown in Figure 9.11a.

9.6 A-Si:H TFT AM-PLEDs

9.6.1 100 DPI CURRENT-DRIVEN 4-A-Si:H TFTs AM-PLED

To analyze 100 dpi AM-PLED pixel operation load lines for T4 and pixel_PLED were produced during deselect time. Figure 9.12a shows the measured $I_{\text{DS_T3}}$ versus $V_{\text{DS_T3}}$ characteristics for several $V_{\text{GS_T3}}$ and T4/pixel_PLED load lines for several V_{DD} (20, 25, 30 V). To produce the load lines, the $I_{\text{pixel_PLED}}$ versus $V_{\text{pixel_PLED}}$ characteristics were used in combination with the $I_{\text{DS_T4}}$ versus $V_{\text{DS_T4}}$ characteristics. For a given I_{data} , $I_{\text{DS_T4}} = I_{\text{DS_T3}} = I_{\text{pixel_PLED}} = I_{\text{data}}$ and $V_{\text{DD}} = V_{\text{DS_T4}} + V_{\text{DS_T3}} + V_{\text{pixel_PLED}}$ during deselect time. Therefore, T4/pixel_PLED load lines were produced by plotting I_{data} versus $V_{\text{DS_T3}} (= V_{\text{DD}} - V_{\text{DS_T4}} - V_{\text{pixel_PLED}})$. The crossing points A, B, C and A', B', C' represent the normal operating points and the operational I_{data} range for the 4-a-Si:H TFTs AM-PLED pixel circuit. From Figure 9.12a, I_{data} operational limits of ~ 6 , ~ 7 , and $\sim 8 \mu\text{A}$ can be obtained for $V_{\text{DD}} = 20, 25$, and 30 V , respectively, which correspond to 23, 27, and 31 cd/m^2 pixel luminance values in Figure 9.11c. It is noted that these pixel luminance values were extracted for red PLED with an emission efficiency of $\sim 0.53 \text{ cd/A}$ and for 100 dpi 4-a-Si:H TFTs AM-PLED with AR of $\sim 22\%$. Therefore, by implementing a PLED with higher efficiency and increasing the AR of the AM-PLED by using a top emission pixel_PLED structure, this pixel electrode circuit should be able to produce much higher pixel luminance values. In addition, if the pixel circuit design and process are further optimized, the a-Si:H TFT AM-PLED pixel I_{data} operational range can be further increased.

To demonstrate a-Si:H TFT technology, a monochromatic red-light-emitting display ($0.5 \times 0.5 \text{ in.}^2$) using 100 dpi 4-a-Si:H TFTs AM-PLEDs with 50×50 pixels was fabricated. Here, 100 dpi represents the display resolution since the display has 50 dots (monochromatic pixels) for each row and column line. In this display, the pixel_PLED structure is the same as the one shown in the insert of Figure 9.11a. In this a-Si:H TFT AM-PLED, the cathode electrodes for each pixel were connected, and the polymer layers were removed from the contact pads with solvent.

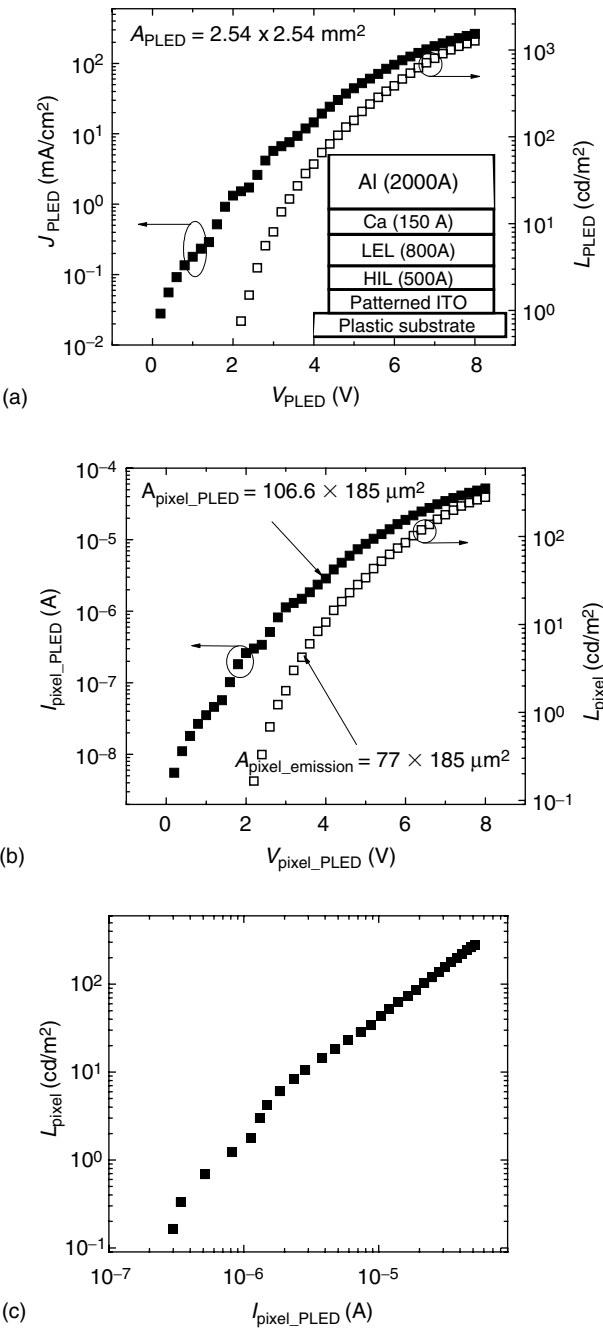


FIGURE 9.11 A 100 dpi AM-PLED pixel optoelectronic characteristics. (a) Optoelectrical characteristics of a typical red PLED fabricated in our laboratory on flexible plastic substrates, (b) and (c) extracted optoelectrical properties of pixel_PLED. (From Hong, Y., Nahm, J.-Y., and Kanicki, J., *IEEE J. Selected Top. Quantum Electron. Org. Light-Emitting Diodes*, 10, 1, 2004. With permission.)

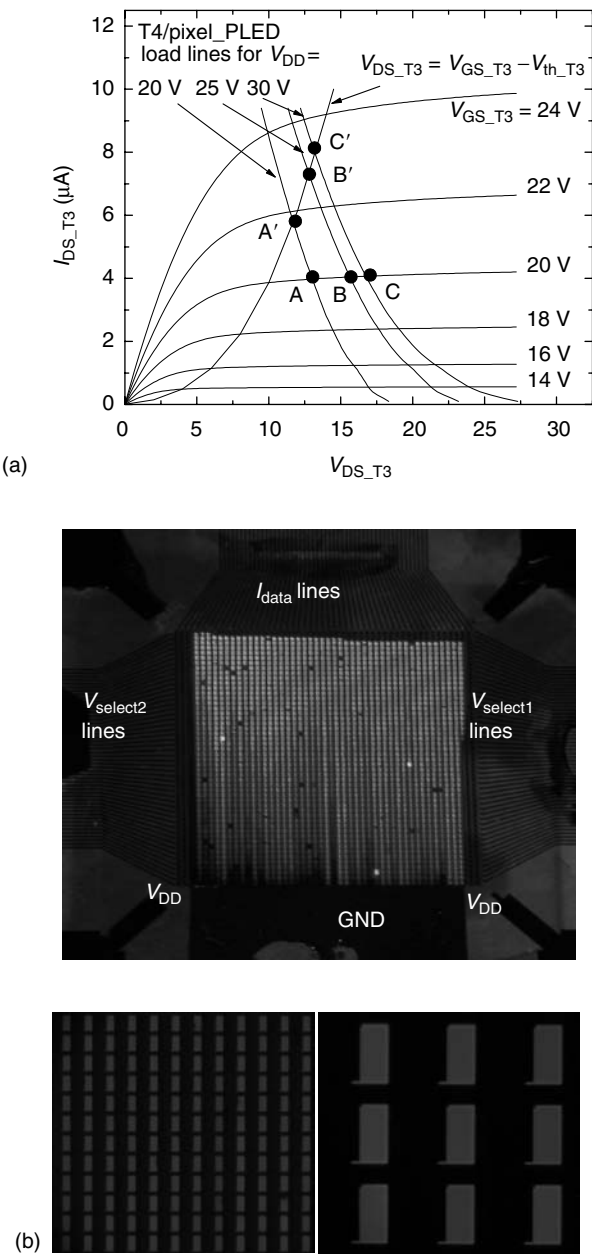


FIGURE 9.12 (a) I_{DS_T3} versus V_{DS_T3} characteristics for several V_{GS_T3} and T4/pixel_PLED load lines for $V_{DD} = 20, 25$, and 30 V are shown. The operating points for AM-PLED pixel changed from A, B, and C to A', B', and C' as I_{data} increases. (b) Top view of illuminated 4-a-Si:H TFTs 100 dpi AM-PLED and magnified images of pixel light emission. The light emission yield was about 70% for this display. (From Hong, Y., Nahm, J.-Y., and Kanicki, J., *IEEE J. Selected Top. Quantum Electron. Org. Light-Emitting Diodes*, 10, 1, 2004. With permission.)

For display evaluation, 0–15 mA was applied through the I_{data} lines to measure the display luminance at different data current levels. Figure 9.12b shows the demonstration of monochromatic red-light emission from a 100 dpi 4-a-Si:H TFTs AM-PLED when the data current is 5 mA. A magnified image of discrete pixel light emission is also included in Figure 9.12b.

The optoelectrical characteristics of the display have been measured using an integrating sphere and a calibrated photodetector connected to a radiometer [30]. First, the total luminous flux from the AM-PLED was measured for different I_{data} . Then, the AM-PLED luminance was calculated from the measured display luminous flux. For a Lambertian emitter, the luminance (L) can be calculated from the measured luminous flux (Φ) by using the following equation:

$$L = \frac{\Phi}{\pi \times A} \quad (9.5)$$

where A is the area of the light emitter. It has been experimentally verified that our AM-PLED is a Lambertian emitter [1]. By considering the pixel light emission yield of 0.7, the light-emitting display area A is $1.27 \text{ cm} \times 1.27 \text{ cm} \times 0.7 = 1.12 \times 10^{-4} \text{ m}^2$. The calculated AM-PLED luminance is plotted versus I_{data} in Figure 9.13a. The initial light emission was observed at I_{data} of 20 μA , and a-Si:H TFT AM-PLED luminance of up to 20 cd/m^2 at I_{data} of 15 mA was measured.

From the pixel_PLED optoelectrical characteristics shown in Figure 9.11c, the a-Si:H TFT AM-PLED luminance of a fully illuminated display can be estimated by assuming that there is no current flow through the pixels without light emission. First, the total display I_{data} required for AM-PLED (50 \times 50 pixels) with 70% light emission yield can be calculated by using the following equation:

$$\text{Total display } I_{\text{data}} = I_{\text{pixel_PLED}} \times 50 \times 50 \times 0.7 \quad (9.6)$$

The 70% illuminated AM-PLED luminance at a given calculated total display I_{data} is equal to L_{pixel} at the corresponding $I_{\text{pixel_PLED}}$. This estimated display luminance versus the total display I_{data} is also plotted in Figure 9.13a. The estimated AM-PLED luminance is larger by about a factor of 2 in comparison with the a-Si:H TFT AM-PLED luminance calculated from the measured luminous flux. This difference in display performances can be related to the nonuniform pixel light emission in certain areas of the fabricated display and the wave-guided light loss through the a-SiN_x:H and BCB layers and thicker glass substrate in comparison with the typical PLEDs on plastic substrates that have been used in this data extraction [1].

V_{data} was also measured at the I_{data} lines of the pixel electrode circuit for various I_{data} during select time (Figure 9.4). The variation of V_{data} with I_{data} is shown in Figure 9.13b. This measured voltage is related to the required compliance voltage of the current driver that supplies I_{data} . For example, to apply I_{data} up to 15 mA for a-Si:H TFT AM-PLED, the current driver should have a capacity of at least 37 V for the compliance voltage (estimated from Figure 9.13b).

In Figure 9.13c, the EL spectra of the red-light-emitting a-Si:H TFT AM-PLED and PLED are shown. EL peak positions at 654 and 653 nm, and full-width-at-half-maximum (FWHM) of 101 and 105 nm were obtained, for the a-Si:H TFT AM-PLED and PLED, respectively. From the obtained EL spectra, Commission Internationale de l'Eclairage (CIE) color coordinates [31] were calculated for AM-PLED and PLEDs, as shown in the inset of Figure 9.13c, and were found to be (0.67, 0.33) and (0.67, 0.32), respectively. These very

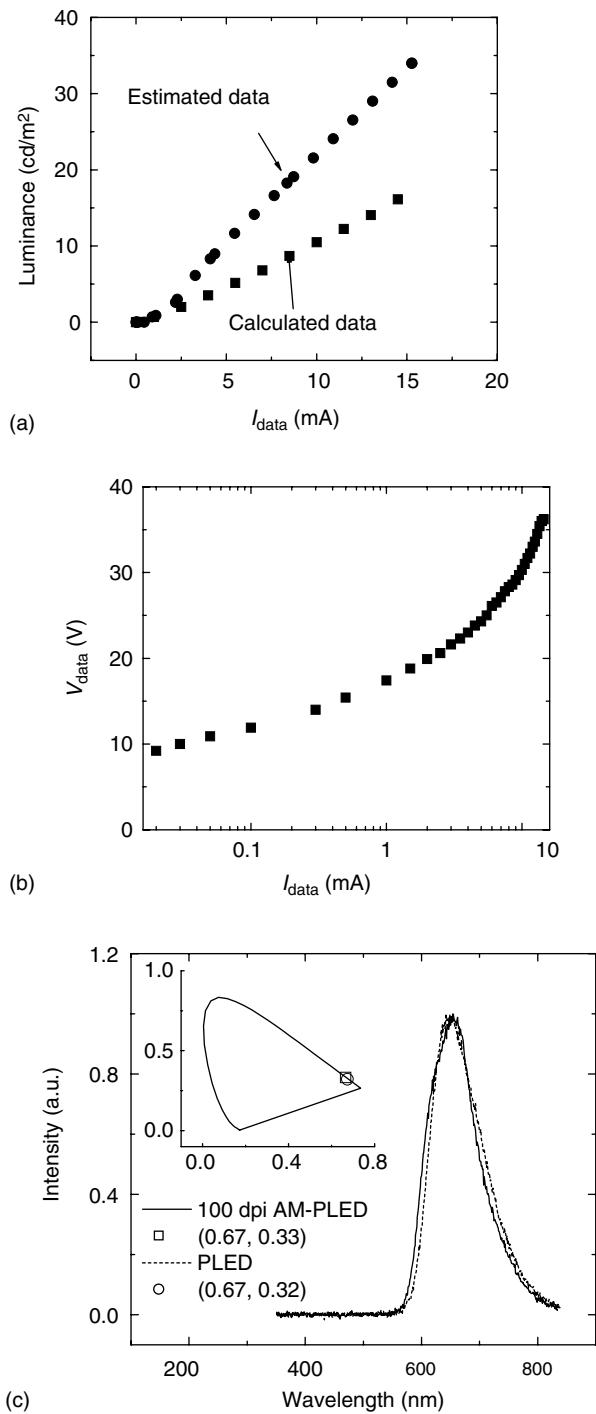


FIGURE 9.13 Optoelectronic characteristics of AM-PLED. (a) Calculated display luminance and estimated display luminance versus I_{data} characteristics, (b) measured V_{data} evolution with the I_{data} , and (c) PLED and AM-PLED electroluminescent (EL) spectra are shown. The CIE color coordinates of the PLED and AM-PLED are also shown in the inset of this figure. (From Hong, Y., Nahm, J.-Y., and Kanicki, J., *IEEE J. Selected Top. Quantum Electron. Org. Light-Emitting Diodes*, 10, 1, 2004 With permission.)

similar color coordinates indicate that the PLED EL characteristics can be used to define the CIE color coordinates for the full-color a-Si:H TFT AM-PLED.

9.6.2 200 DPI CURRENT-DRIVEN 4-A-Si:H TFTs AM-PLED

Higher resolution a-Si:H TFT AM-PLEDs were also fabricated by Hong et al. [32]. Figure 9.14a shows an image of the red-light-emitting 200 dpi a-Si:H TFT AM-PLED for data current of 25 mA; the magnified image of the light-emitting pixels is also included in this figure. The display size was $0.5 \times 0.5 \text{ in.}^2$ (100×100 pixels) and the pixel AR was about 10%; and $\text{AR} = \text{pixel_PLED } (24 \times 65 \text{ } \mu\text{m}^2) \text{ area/whole pixel } (127 \times 127 \text{ } \mu\text{m}^2) \text{ area}$. For this display, we measured up to 1.1×10^{-2} lumen when the data current was equal to 25 mA. We calculated the display luminance (L_{display}) by considering the display area and the fabrication yield (75%) of the light-emitting pixels: $A = 1.27 \text{ cm} \times 1.27 \text{ cm} \times 0.75 = 1.215 \times 10^{-4} \text{ m}^2$. The evolution of L_{display} with I_{data} is shown in Figure 9.14b and for data current of 25 mA, we obtained $L_{\text{display}} = 30 \text{ cd/m}^2$. In addition, if we take into consideration the pixel PLED area, e.g., pixel AR = 10%, we can calculate the effective light emission luminance (L_{emission}) for $A = 1.27 \text{ cm} \times 1.27 \text{ cm} \times 0.75 \times 0.1 = 1.215 \times 10^{-5} \text{ m}^2$. The variation of L_{emission} versus effective current density (defined as data current and total effective current-flowing area of the AM-PLED) is shown in Figure 9.14c; L_{emission} up to 300 cd/m^2 was obtained for 115 mA/cm^2 . The effective light emission efficiency of the a-Si:H TFT AM-PLED can be defined as the ratio of effective light emission luminance to effective current density. Its variation with the current density is also shown in Figure 9.14c. For the studied displays, we obtained a maximum effective light emission efficiency of about 0.3 cd/A at 115 mA/cm^2 . In Figure 9.14c, the luminance and light emission efficiency of the red-PLEDs ($2 \times 3 \text{ mm}^2$) are shown. The PLED had a luminance of about 720 cd/m^2 at 110 mA/cm^2 and a maximum light emission efficiency of about 0.71 cd/A at 31 mA/cm^2 (which corresponds to 220 cd/m^2). As shown in Figure 9.14c, the effective light emission efficiency of the AM-PLED is lower in comparison with the light emission efficiency of the PLEDs by a factor of 3 to 4 for the current density ranging from 80 to 110 mA/cm^2 . It is speculated that this difference is due to leakage current through defective AM-PLED pixels that do not contribute to light emission.

In Figure 9.14d, the EL spectra of the red-light-emitting AM-PLED and PLEDs are shown. From the EL spectra, we extracted their peak positions located at 644 and 653 nm, and their FWHM values of 95 and 105 nm for AM-PLED and PLEDs, respectively. From these spectra, we also calculated CIE color coordinates for AM-PLED and PLEDs, as shown in the inset of Figure 9.14d, which were (0.66, 0.33) and (0.68, 0.32), respectively. The blue shift of the AM-PLED EL spectrum is responsible for the decrease of CIE- x and smaller FWHM value of EL spectrum produces an increase of CIE- y color coordinates.

9.6.3 200 DPI VOLTAGE-DRIVEN 3-A-Si:H TFTs AM-PLED

Beside current-driven a-Si:H TFTs AM-PLED, the voltage-driven a-Si:H TFTs AM-PLED was also fabricated. To test the unit, whole display without packaging and driver electronics was illuminated (Figure 9.15a). The display size is 0.7 in. diagonal with 100×100 pixels. A very uniform green light intensity among pixels across the display under the microscope was observed (Figure 9.15a). There are however a few line defects in the V_{DD} bus lines or data signal bus lines and some pixel defects (bright spots).

The optoelectrical characteristics of 3-a-Si:H TFTs AM-PLED have been measured using the same method as outlined above [30]. To light up the whole display, we continuously applied a DC signal (30 V) to all the scan lines and V_{data} the signal was varied from 0 to 30 V for different gray scales. All the measurements have been performed in the air at RT [24].

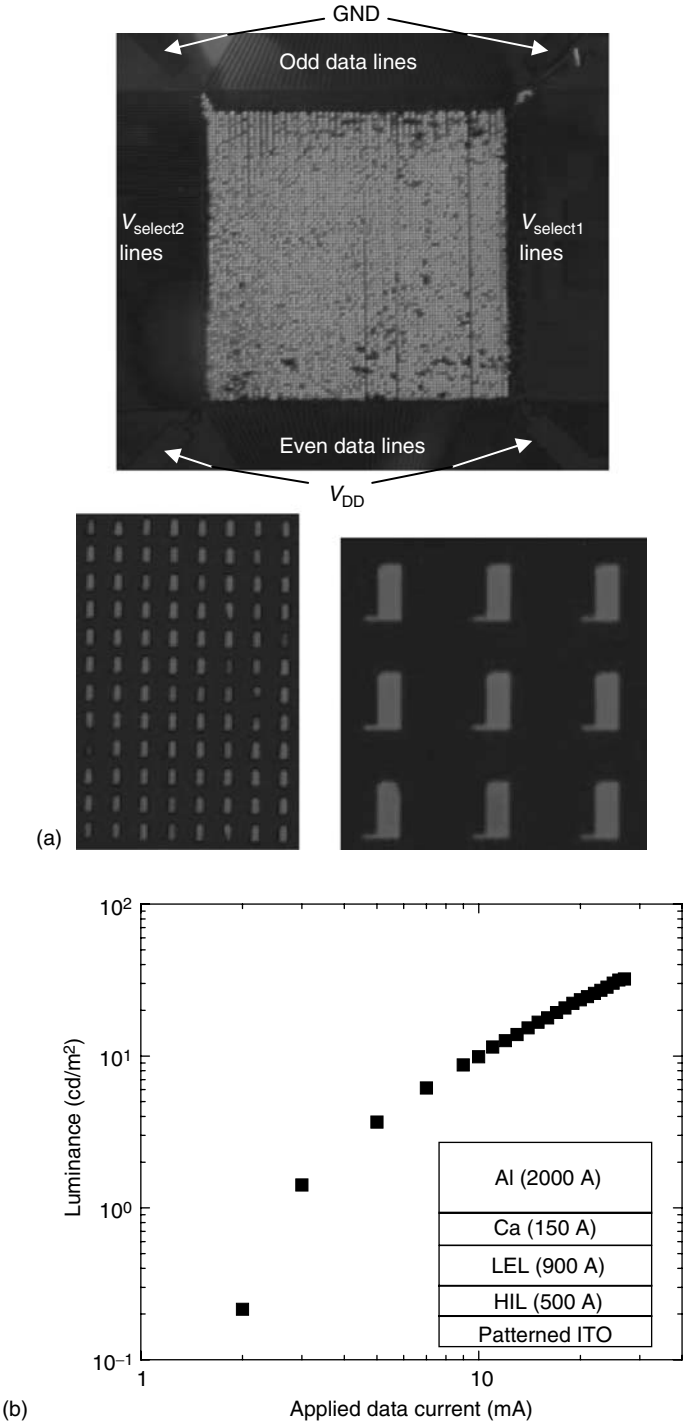


FIGURE 9.14 (a) Top view of illuminated 4-a-Si:H TFTs 200 dpi AM-PLED. Magnified images of the light-emitting pixels are also shown. (b) The luminance (L_{display}) versus applied data current of 4-a-Si:H TFTs 200 dpi AM-PLED is shown. The structure of the organic polymer light-emitting device is also included in this figure.

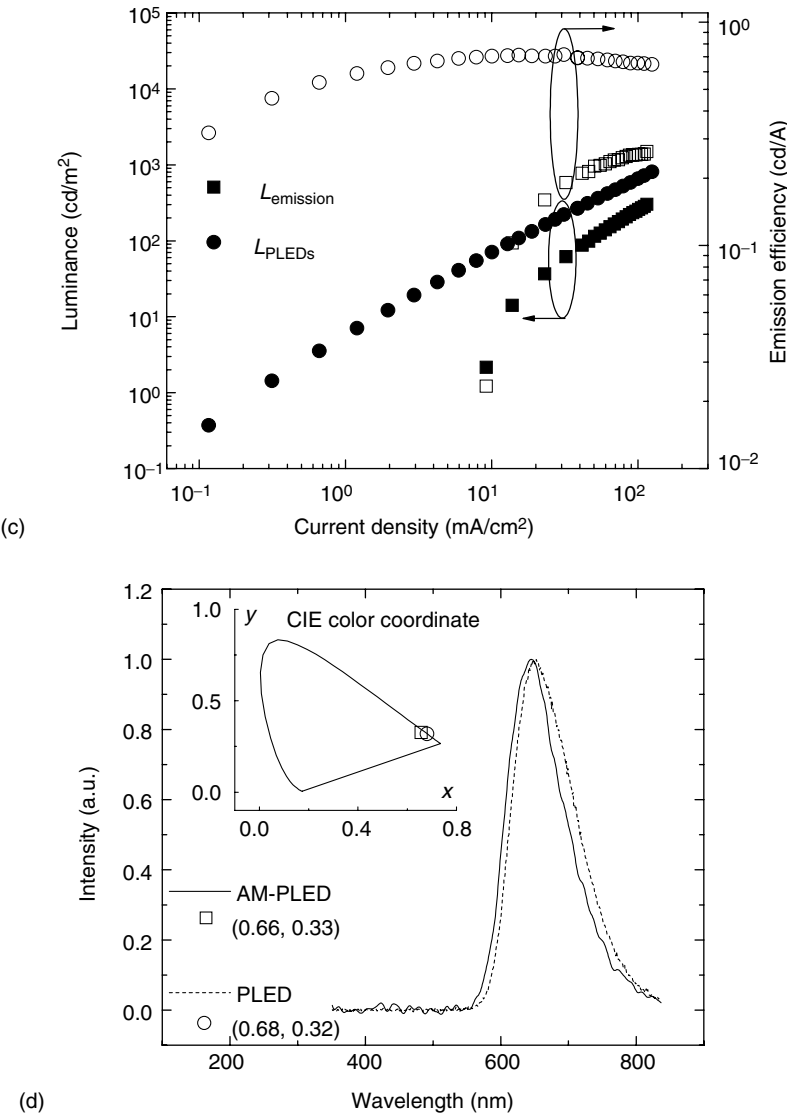


FIGURE 9.14 (continued) (c) The effective light emission luminance (solid square, L_{emission}) and effective light emission efficiency (open square) versus effective current density of 4-a-Si:H TFTs 200 dpi AM-PLED are shown. The evolution of luminance (solid circle, L_{PLED}) and light emission efficiency (open circle) versus effective current density of the red PLED are also shown. (d) Electro-luminescent (EL) spectra and CIE color coordinates of 4-a-Si:H TFTs 200 dpi AM-PLED (solid line) and PLED (dashed line) are shown. (From Hong, Y., Nahm, J.-Y., and Kanicki, J., *Appl. Phys. Lett.*, 83, 3233, 2003. With permission.)

Figure 9.15b shows the current and luminance versus data voltage characteristic of the monochromatic green-light-emitting display. The initial green light emission is observed when V_{data} is about 4 ~ 5 V. This data voltage is considered to be a turn-on data voltage that is closely related to the green PLED turn-on voltage and V_{DS} of the switching TFT (T1) and the V_{GS} of the driving TFT (T3) during selection time. Up to 2×10^{-2} lumen at $V_{\text{data}} = 30$ V was obtained. The display luminance was estimated from the optical flux, assuming that the AM-PLED has Lambertian emission (it was checked experimentally that PLED luminance

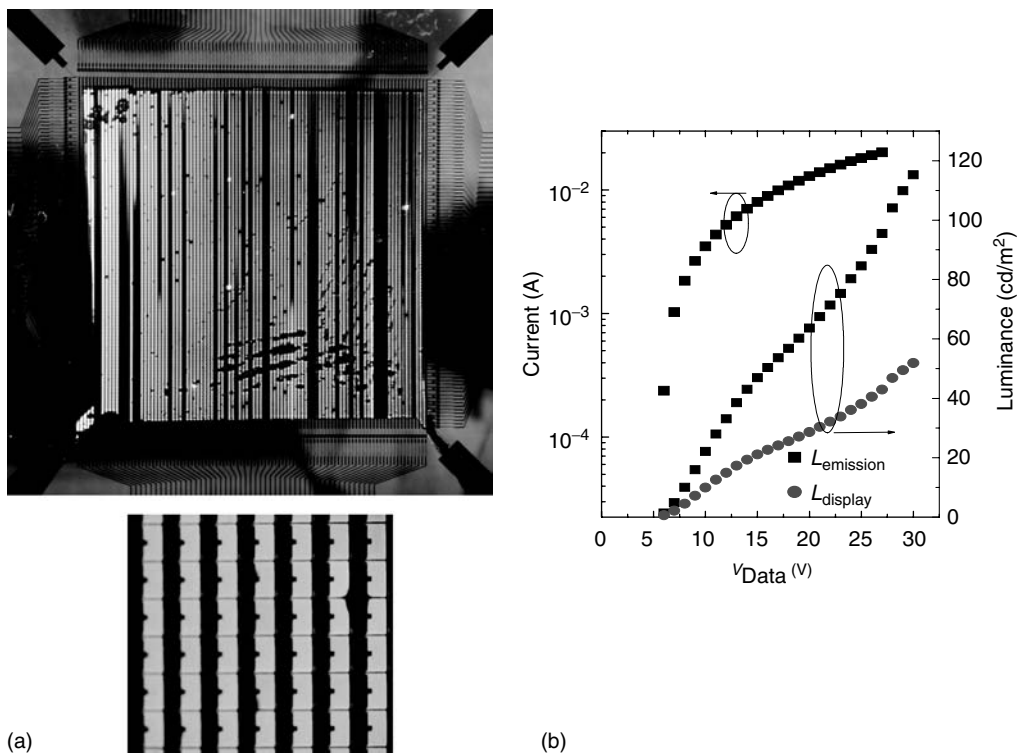


FIGURE 9.15 (a) Top view and blowup of illuminated AM-PLED is shown. The bright area on the left is glare from the room light. The PLED was about $120 \times 62.5 \mu\text{m}$ for pixel size of $127 \times 127 \mu\text{m}$. The fill factor was about 45%. (b) Measured current and luminance versus data voltage of 3-a-Si:H TFTs AM-PLED are shown. (From Kim, J. H., Hong, Y., and Kanicki, J., *IEEE Electron Device Lett.*, 24, 451, 2003. With permission.)

was constant over the whole angular domain under consideration). The total display area of $1.27 \text{ cm} \times 1.27 \text{ cm} = 1.62 \times 10^{-4} \text{ m}^2$ results in the display luminance:

$$L_{\text{display}} = \frac{\Phi}{\pi \times 1.6 \times 10^{-4}} \quad (9.7)$$

However, we also need to consider the actual light-emitting area to calculate the effective luminance of the light-emitting areas (L_{emission}), which can be expressed as $A_{\text{emission}} = \text{total number of pixels} \times \text{yield of emitting pixels} \times \text{PLED area in each pixel}$. For this 200 dpi AM-PLED, this area is $A_{\text{emission}} = 4.74 \times 10^{-5} \text{ m}^2$, where the yield of emitting pixels ($\sim 65\%$) was estimated from Figure 9.15a.

The estimated luminance values (L_{display} and L_{emission}) at maximum luminous flux are about 50 and 120 cd/m^2 , respectively. These values can be increased similarly through optimization of a-Si:H TFTs AM-PLED design and fabrication methods.

9.7 CONCLUSIONS

We described technology of 100 and 200 dpi, 3- and 4-a-Si:H TFTs pixel electrode circuits that can be used for current- and voltage-driven AM-PLEDs. Their optoelectronic properties were

also discussed in detail. We would also like to indicate that experimental results described in this chapter do not represent the optimum performance that can be expected for the a-Si:H TFTs AM-PLED technology. The display performance can be improved tremendously when a higher efficiency pixel_PLED, a higher AR, top emission pixel_PLED structure, and improved pixel electrode circuit design [33] and fabrication processes are used [35]. For example, IDTech, Chi Mai Optoelectronics, and IBM Corp. clearly showed that the a-Si:H TFTs can be used for large area AM-OLEDs [9]. Finally, the experimental data described in this chapter demonstrate clearly that future a-Si:H TFTs AM-PLED technology could challenge today's poly-Si TFTs AM-PLED technology. This will become especially true when it is desirable to fabricate AM-OLEDs on plastic substrate over large areas. Such development can open up two exciting possibilities. The first is the manufacturing of lightweight flexible displays that are less prone to breakage than devices on glass substrates and are not restricted to flat surfaces. The second is the use of in-line continuous processing for the manufacturing of large screens at low cost.

ACKNOWLEDGMENTS

This work was supported by an NIH grant. The authors would like to thank Dr. I. French at Philips Research Laboratory, U.K., for assistance with plasma enhanced chemical vapor deposition (PECVD) of different TFT layers. The authors also would like to thank Professor R. Hattori at Kyushu University, Japan, Dr. Y. He, Dr. J.-Y. Nahm, Dr. J.-H. Kim, Dr. S. Martin, Mr. D. Li, and Ms. S. Lee at the University of Michigan, Ann Arbor, United States, for their technical assistance during this project. The results presented in this chapter could not be achieved without their hard work and strong belief in a-Si:H TFT technology. The organic polymers used in this research were provided by Dow Chemical Corp. One of us (J.K.) acknowledges Mr. Aaron Johnson for critical reading of this manuscript.

REFERENCES

1. S. Lee, A. Badano, and J. Kanicki, Monte Carlo modeling of organic polymer light-emitting devices on flexible plastic substrates, *Proc. SPIE*, 4800, 156–163, 2002.
2. G.E. Jabbour, S.E. Shaheen, M.M. Morrell, B. Kippelen, N.R. Armstrong, and N. Peyghambarian, Aluminum composite cathodes: a new method for the fabrication of efficient and bright organic light-emitting devices, *Opt. Photon. News*, 10 (4), 24, 1999.
3. J.W. Allen, Organic electroluminescence and competing technologies, *J. Lumin.*, 60–61, 912, 1994.
4. D.E. Mentley, State of flat-panel display technology and future trends, *Proc. IEEE*, 90, 453–459, 2002.
5. http://www.tmdisplay.com/tm_dsp/press/2002/04-16a.htm
6. <http://wwwnl.kodak.com/US/en/corp/display/sanyoFlat.jhtml>
7. S. Terada, G. Izumi, Y. Sato, M. Takahashi, M. Tada, K. Kawase, K. Shimotoku, H. Tamashiro, N. Ozawa, T. Shibasaki, C. Sato, T. Nakadaira, Y. Iwase, T. Sasaoka, and T. Urabe, A 24-inch AM-OLED display with XGA resolution by novel seamless tiling technology, *SID Tech. Dig.*, 34, 1463–1465, 2003.
8. <http://www.samsungsdi.co.kr/>
9. T. Tsujimura, Y. Kobayashi, K. Murayama, A. Tanaka, M. Morooka, E. Fukumoto, H. Fujimoto, J. Sekine, K. Kanoh, K. Takeda, K. Miwa, M. Asano, N. Ikeda, S. Kohara, S. Ono, C.-T. Chung, R.-M. Chen, J.-W. Chung, C.-W. Huang, H.-R. Guo, C.-C. Yang, C.-C. Hsu, H.-J. Huang, W. Riess, H. Riel, S. Karg, T. Beierlein, D. Gundlach, S. Alvarado, C. Rost, P. Mueller, F. Libsch, M. Mastro, R. Polastre, A. Lien, J. Sanford, and R. Kaufman, A 20-inch OLED display driven by super-amorphous-silicon technology, *SID Tech. Dig.*, 34, 6–9, 2003.
10. C.C. Wu, S.D. Theiss, G. Gu, M.H. Lu, J.C. Sturm, and S. Wagner, Integration of organic LED's and amorphous Si TFT's onto unbreakable metal foil substrate, *IEDM Tech. Dig.*, 957–959, 1996.

11. M.H. Lu, E. Ma, J.C. Sturm, and S. Wagner, Amorphous silicon TFT active-matrix OLED pixel, *Proc. LEOS '98*, 130–131, 1998.
12. J.-J. Lih, C.-F. Sung, M.S. Weaver, M. Hack, and J.J. Brown, A phosphorescent active-matrix OLED display driven by amorphous silicon backplane, *SID Tech. Dig.*, 34, 14–17, 2003.
13. J. Kanicki and S. Martin, Hydrogenated amorphous silicon thin-film transistors, in *Thin-Film Transistors*, C.R. Kagan and P. Andry, Eds., Marcel Dekker, New York, 2003.
14. J.L. Sanford and F.R. Libsch, TFT AMOLED pixel circuits and driving methods, *SID Tech. Dig.*, 34, 10–13, 2003.
15. Y. He, R. Hattori, and J. Kanicki, Electrical reliability of two- and four-a-Si:H TFT pixel electrode circuits for active-matrix OLEDs, *SID Tech. Dig.*, 31, 354–357, 2000.
16. Y. Hong, J.-Y. Nahm, and J. Kanicki, 100 dpi 4-a-Si:H TFTs active-matrix organic polymer light-emitting display, *IEEE J. Selected Top. Quantum Electron. Org. Light-Emitting Diodes*, 10, 1–10, 2004.
17. J.-H. Kim and J. Kanicki, Amorphous silicon thin-film transistors-based active-matrix organic light-emitting displays, *SID Tech. Dig.*, 614–617, 2002.
18. J.-H. Kim and J. Kanicki, Amorphous silicon thin-film transistors-based active-matrix organic light-emitting displays for medical imaging, *Proc. SPIE*, 4681, 314–321, 2002.
19. J.L. Sanford and F.R. Libsch, Vt compensation performance of voltage data AMOLED pixel circuits, *Proc. IDRC*, 38–41, 2003.
20. Y. He, R. Hattori, and J. Kanicki, Improved a-Si:H TFT pixel electrode circuits for active-matrix organic light-emitting displays, *IEEE Trans. Electron Devices*, 48, 1322–1325, 2001.
21. S.K. Bhowmick and B. Mazhari, An improved four TFT circuit for active-matrix organic light emitting diode (OLED) display, *SID Tech. Dig.*, 33, 606–609, 2002.
22. C.-Y. Chen and J. Kanicki, High-performance a-Si:H TFT for large-area AMLCDs, *Proc. 26th Eur. Solid State Dev. Reas. Conf.*, 1023–1031, 1996.
23. J. Kanicki, J.-H. Kim, J. Nahm, Y. He, and R. Hattori, Amorphous silicon thin-film transistors based active-matrix organic light-emitting displays, *Proc. Asia Display/IDW '01*, 315–318, 2001.
24. J.H. Kim, Y. Hong, and J. Kanicki, Amorphous silicon thin-film transistors-based organic polymer light-emitting displays, *IEEE Electron Device Lett.*, 24, 451–453, 2003.
25. J.-H. Kim, D. Lee, and J. Kanicki, Three amorphous silicon thin-film transistors-based active-matrix organic polymer light-emitting displays, *Proc. 22nd Int. Display Res. Conf.*, 601–604, 2002.
26. J.-H. Kim and J. Kanicki, 200 dpi 3-a-Si:H TFTs voltage-driven AM-PLEDs, *SID Tech. Dig.*, 34, 18–21, 2003.
27. Y. Hong, R. Hattori, and J. Kanicki, Novel poly-Si TFT pixel electrode circuits and current programmed active-matrix driving methods for AMOLEDs, *SID Tech. Dig.*, 33, 618–621, 2002.
28. R. Hattori, Y. Kuroki, and J. Kanicki, Analog-circuit simulation of the current-programmed active-matrix pixel electrode circuits based on poly-Si TFT for organic light-emitting displays, *Proc. AM-LCD*, 223–226, 2001.
29. Y. Hong and J. Kanicki, Organic polymer light-emitting devices on flexible plastic substrates for AM-OLED, *Proc. Asia Display/IDW '01*, 1443–1446, 2001.
30. Y. Hong and J. Kanicki, Integrating sphere CCD-based measurement method for organic light-emitting devices, *Rev. Sci. Instrum.*, 74, 3572–3575, 2003.
31. J.W.T. Walsh, *Photometry*, Constable & Company Ltd., London, 1958.
32. Y. Hong, J.-Y. Nahm, and J. Kanicki, Opto-electrical properties of 200 dpi four amorphous silicon thin-film transistors active-matrix organic polymer light-emitting display, *Appl. Phys. Lett.*, 83, 3233–3235, 2003.
33. Y.-C. Lin, H.-P.D. Shieh, and J. Kanicki, A novel current-scanning a-Si:H TFTs pixel electrode circuit for AM-OLEDs, *IEEE Trans. Electron. Devices*, 52, 1123–1131, 2005.
34. J. Kanicki, S.-J. Lee, Y. Hong, and C.-C. Su, Optoelectronic properties of poly(fluorine) co-polymer light-emitting devices on a plastic substrate, *Journal of the SID*, 13/12, 993–1002, 2005.
35. A. Badano, M.J. Flynn, and J. Kanicki, High-fidelity medical imaging displays, SPIE Press, *Tutorial Texts in Optical Engineering*, volume T63, 2004 (ISBN 0-8194-5191-6).

10 Microstructural Characterization and Performance Measurements

Zhigang-Rick Li and Jeff Meth

CONTENTS

10.1	Microstructural Characterization Techniques.....	617
10.1.1	Transmission Electron Microscopy	618
10.1.2	Scanning Electron Microscopy	618
10.1.3	Dual Beam Microscopy	621
10.1.4	Scanning Probe Microscopy	621
10.1.5	Laser Scanning Confocal Microscopy	622
10.1.6	Electron Spectroscopy for Chemical Analysis	622
10.1.7	Raman Spectroscopy	623
10.1.8	Secondary Ion Mass Spectrometry	623
10.2	Performance Measurement Techniques.....	624
10.2.1	Human Vision, Light, and Color.....	624
10.2.2	Basic OLED Measurement and Efficiency	626
10.2.3	Getting on the Same Energy Scale	629
10.2.4	Lifetime Measurements.....	632
	Acknowledgments	633
	References	633

The development and manufacture of organic light-emitting diodes (OLEDs) have demanded the use of the most advanced microstructural characterization techniques and sophisticated performance measurement devices [1–14]. In this chapter, we will briefly describe these techniques and devices and review how scientists and engineers utilize them to improve the performance of OLEDs.

10.1 MICROSTRUCTURAL CHARACTERIZATION TECHNIQUES

In the last century, many microstructural characterization techniques have been developed, such as electron microscopy, atomic tunneling microscopy, photoelectron spectroscopy, Raman spectroscopy, etc. The structure of the OLED-based displays is such that many pixels are arranged orderly in the x - y plane. The size and number of pixels determine the resolution and size of the display. Along the z -axis, several layers are stacked on each other. These layers

are made up of very different materials, varying from soft, organic to hard, inorganic materials. Many of the layers are ultrathin, in the range of nanometers. The microstructure of the layers and the interfaces between them strongly influences the performance of the device [15]. Also, the presence of included defects, such as submicron-sized particles, critically degrades the diode's lifetime. Advanced microstructural characterization techniques have been providing the required structural information about the OLED in the recent years.

10.1.1 TRANSMISSION ELECTRON MICROSCOPY

Transmission electron microscopy (TEM) is a powerful and mature microstructural characterization technique. The principles and applications of TEM have been described in many books [16–20]. The image formation in TEM is similar to that in optical microscopy, but the resolution of TEM is far superior to that of an optical microscope due to the enormous differences in the wavelengths of the sources used in these two microscopes. Today, most TEMs can be routinely operated at a resolution better than 0.2 nm, which provides the desired microstructural information about ultrathin layers and their interfaces in OLEDs. Electron beams can be focused to nanometer size, so nanochemical analysis of materials can be performed [21]. These unique abilities to provide structural and chemical information down to atomic-nanometer dimensions make it an indispensable technique in OLED development. However, TEM specimens need to be very thin to make them transparent to electrons. This is one of the most formidable obstacles in using TEM in this field. Current versions of OLEDs are composed of hard glass substrates, soft organic materials, and metal layers. Conventional TEM sample preparation techniques are no longer suitable for these samples [22–24]. Recently, these difficulties have been overcome by using the advanced dual beam (DB) microscopy technique, which will be discussed later.

TEM has been used in OLED development in recent years. Indium–tin oxide (ITO) is commonly used as a transparent conducting electrode in displays. To achieve required properties, in particular low resistivity, ITO films must be either directly deposited on a heated substrate, or postannealed at high temperature, which prevent from using most inexpensive plastic substrates. Carcia et al. examined the microstructure of the ITO films grown by radio frequency (RF)-magnetron sputtering on polyester at room temperature [25]. Figure 10.1 shows a high resolution TEM image of ITO thin film on polyester substrate in cross-sectional view. It is found that crystalline features formed only near the air interface and are not uniform throughout the film thickness. Phosphorescent dye-doped films were studied in detail by Noh et al. [26]. The TEM results indicate that the formation of aggregates may impact the performance of the devices. Park et al. reported that a dramatic increase in photostability of a blue light-emitting polymer was achieved by the addition of gold nanoparticles [27]. The TEM was used to characterize the microstructure of polymers doped with gold nanoparticles. They found that the sizes of gold nanoparticles in polymer films are in the range of 5–10 nm only.

10.1.2 SCANNING ELECTRON MICROSCOPY

The scanning electron microscope (SEM) is another important and widely used electron beam instrument for the microstructural characterization of materials [28]. A modern SEM is very easy to use and its images are usually easy to interpret as well. The SEM has significant advantages over optical microscopy, with nanometer resolution, three-dimensional appearance due to the large depth of the view, and elemental composition analysis ability because of backscattering imaging (BSI) and energy dispersive spectroscopy (EDS). The SEM, like TEM, also uses a high-energy electron beam focused on the sample. In the case of SEM,

however, it provides microstructural information about the surface or the materials near the surface. An important advantage of SEM over TEM is that it can accommodate a relatively large OLED sample with modest sample preparation. Recently, environmental SEM has been developed and can be used to observe wet samples [29,30].

Using modern SEM with nanometer resolution, one can detect foreign particles on the substrate. Existence of subparticles on ITO films would severely impact the performance of the OLED. The SEM image of such a particle with size larger than $30\text{ }\mu\text{m}$ is shown in Figure 10.2, compared with the distance between cathode and anode of usually less than 200 nm . This kind of defects can generate visible dark spots or nonemissive areas. Do et al. used SEM and other microstructural characterization techniques to study degradation processes of Al electrodes in the unprotected OLEDs [31]. They concluded that one of the most crucial factors of the degradation process in those devices was deformation of metal and organic layers due to heat, gas evolution, and oxidation caused by applied voltage. Examples of utilization of SEM in the development of OLED were also reported by several other groups [32–34], and we expect SEM will be widely used in the commercial scale production of OLEDs.

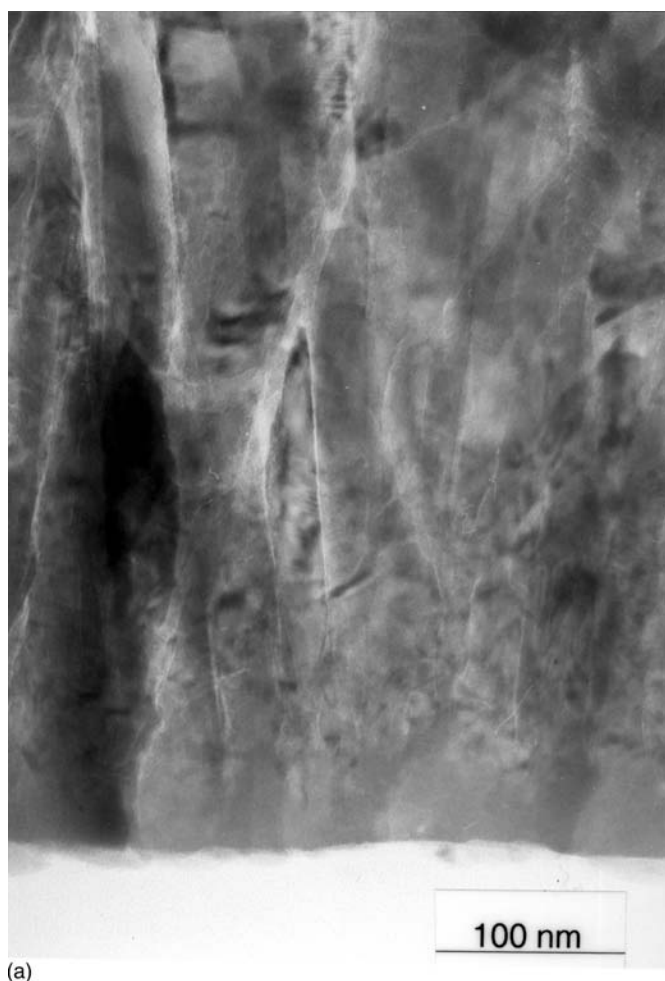
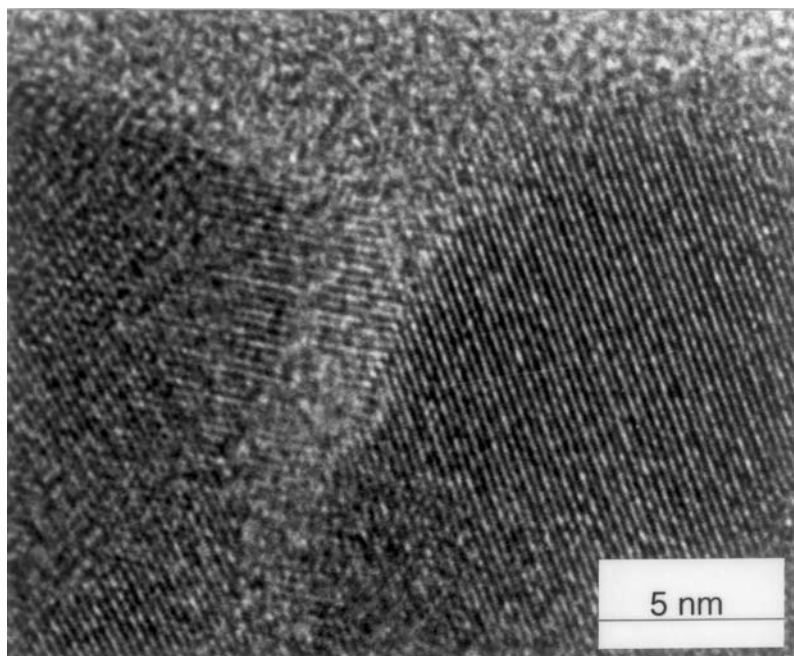


FIGURE 10.1 (a) Lower magnification TEM images of ITO thin film on polyester substrate in cross-sectional view. (b) atomic-resolution image of ITO film near the surface showing the crystalline feature.

(continued)



(b)

FIGURE 10.1 (*continued*)

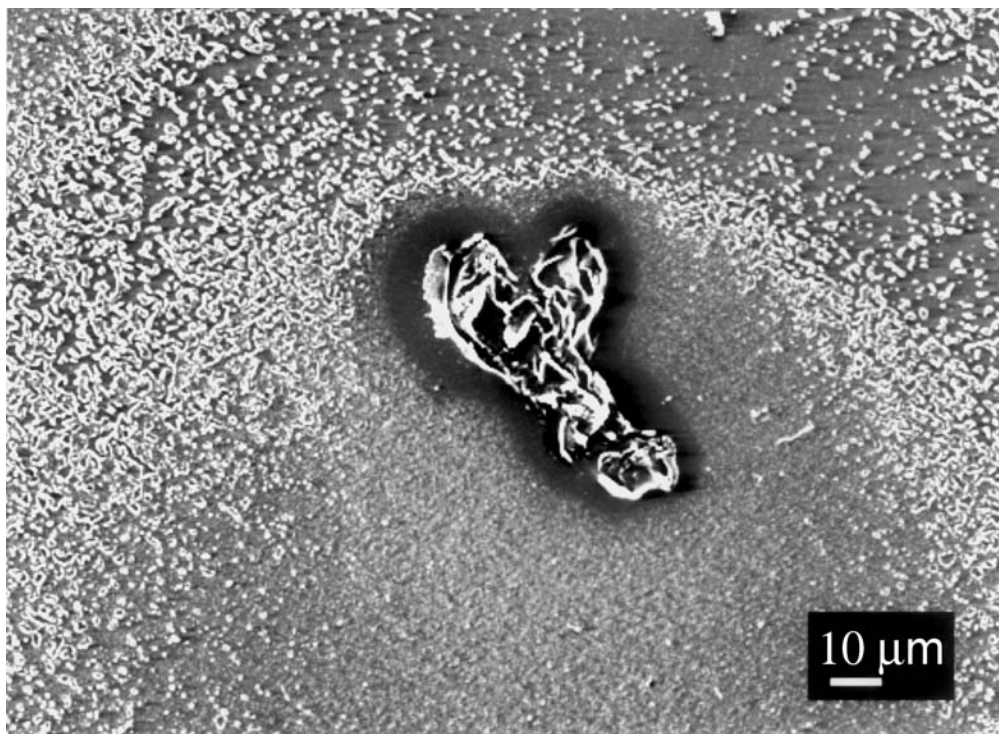


FIGURE 10.2 SEM image of small particle on ITO anode layer.

10.1.3 DUAL BEAM MICROSCOPY

Recently, a new kind of microscopy, DB microscopy, has been used in the material characterization and development [35]. The unique combination of scanning electron beam and focused ion beam (dual beam) technologies working jointly on a single platform can greatly expand the application range to include *in situ* modification (etch and deposition) of materials, which other electron microscopy techniques lack. The DB microscopy technique overcomes the limits of top-surface imaging and provides a three-dimensional, subsurface view of materials. The site-specific analysis ability of DB microscopy makes it a very useful technique in OLED development. Often, fabricated OLEDs contain many defects such as subparticles on the surface. By using DB microscopy, these defects can be effectively located and then analyzed in great detail. Another important use of DB microscopy is to prepare ultrathin samples for TEM, as mentioned before, so we can maximally explore the capacities of ultrahigh resolution TEM [36].

The OLED is composed of hard and soft layers so that the conventional cross-sectional TEM sample preparation techniques cannot be applied. Figure 10.3 is a first DB microscopy-prepared TEM image of an OLED in cross-sectional view [37]. The glass substrate, ITO, organic layers, and Al cathode are indicated in the image. The microstructure and interfaces of all these layers can be well studied now. The nanometer-sized spots in organic layers are indium-rich particles. We believe the combination of DB microscopy and TEM will greatly advance the OLED research and development in the near future.

10.1.4 SCANNING PROBE MICROSCOPY

Scanning probe microscopy (SPM) is a relatively new class of microstructural characterization technique that probes materials on micrometer to subnanometer scale [38]. The SPM includes atomic force microscopy (AFM), scanning tunneling microscopy (STM), and tens of other related imaging techniques. Each SPM uses a sharp probe to scan the surface of the sample, point-by-point and line-by-line, to form an image of the surface. The simplest map is of three-dimensional topography. Other maps distinguish regions that are physically or

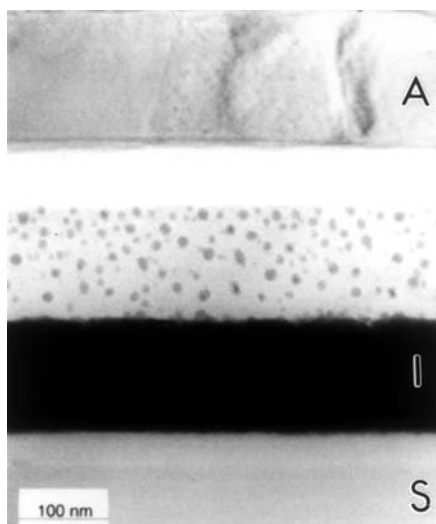


FIGURE 10.3 DB microscopy-prepared TEM image of an OLED in cross-sectional view. The glass substrate (S), ITO (I) anode, organic layers, and Al (A) cathode are clearly seen in the image.

chemically different from one another, revealing information about electrical, mechanical, magnetic, optical, and many other properties of the materials. Unlike electron microscopy, which requires vacuum and, often, some sample preparation, most of the SPM works in air and even in a liquid, with minimal or no sample preparation. The SPM measures surfaces in all the three dimensions: x , y , and z . Lateral topographic resolution for most SPM scanning techniques is typically 2 to 10 nm, and vertical resolution is typically better than 0.1 nm, far superior to the SEM. The SPM is the most powerful tool for surface metrology in our time. However, there are several limitations for SPM. For example, the sample must not have local variations in surface height of tens of micrometers.

There are many publications reporting how SPM was used to characterize the surface of organic materials in OLEDs [39–42]. Halls et al. used AFM to study the surface morphology of polyfluorene composites [40]. In 1996, Cumpston and Jensen investigated the failure mechanism in OLEDs [41]. The circular, nonemissive dark spot defects were imaged and analyzed, and the formation of such defects was explained based on AFM results. The nature of the interface between the light-emitting layer and the metal electrode is of importance in determining device performance. Ahn and Lee studied the effects of annealing of polythiophene derivative for polymer light-emitting diodes (PLEDS) [42]. The AFM images clearly indicate the differences in roughness of the films before and after annealing at four different temperatures.

10.1.5 LASER SCANNING CONFOCAL MICROSCOPY

Laser scanning confocal microscopy (LSCM) becomes a valuable tool for characterizing biological and other materials [43,44]. In conventional fluorescence microscopy, much of the structural detail that could otherwise be resolved is obscured due to the contribution of fluorescence from regions outside the plane of focus. By using a pinhole restricting the collection of light from out-of-focus regions, confocal microscopy provides both significantly higher lateral- and vertical-resolution images. The plane of focus (Z -plane) is selected by a computer-controlled fine-stepping motor that moves the microscope stage up and down. Typical focus motors can adjust the focal plane in as little as 0.1 μm increment. A three-dimensional reconstruction of a specimen can be generated by stacking the two-dimensional optical sections collected in series. The LSCM is a nondestructive microstructure characterization technique, which can directly generate, with and without applying the voltage, both electroluminescent and fluorescent images of the organic films in encapsulated OLEDs. We believe more applications of LSCM in the OLEDs will be found in the near future.

10.1.6 ELECTRON SPECTROSCOPY FOR CHEMICAL ANALYSIS

Electron spectroscopy for chemical analysis (ESCA), also known as x-ray photoelectron spectroscopy (XPS) was developed in the 1960s [45,46]. This technique is sensitive to 0.05–0.5 atomic percentage or a fraction of a monolayer with sampling depth on the order of 10 nm. In ESCA, the kinetic energies of photoelectrons excited by x-rays are measured using an energy analyzer. The most commonly used x-ray sources are Al $K\alpha$ (1486.6 eV, with 0.85-eV line width) and Mg $K\alpha$ (1253.6 eV, with 0.7-eV line width) x-rays. By measuring the kinetic energies, one can calculate the electron binding energies, which are characteristic of the atoms from which the electrons originate and the chemical state or oxidation state of the atom. An ESCA spectrum is a plot of the number of emitted electrons versus binding energy. The peak areas can be used to determine the surface elemental composition. Hence, ESCA can provide both chemical binding information and elemental concentration. The ESCA detects all

elements in the periodic table except hydrogen and helium. Different from SPM, ESCA is carried out in ultrahigh vacuum (UHV) conditions.

The ESCA has been heavily used in characterization of interfaces existing in the OLED [47–53]. By the oxygen plasma treatment of ITO anode, its working function can change, which impacts the performance of the OLED significantly [11]. Milliron et al. found that the oxygen plasma treatment of ITO generates a new type of oxygen species using ESCA technique, which could be responsible for the change in the working function. Addition of poly(3,4-ethylene dioxythiophene)–poly(styrene sulfonate), referred to as PEDOT–PSS, on ITO can significantly improve the lifetime of PLEDs [50]. However, the indium contamination of the polymers has become a new issue. Wong et al. used ESCA to measure indium incorporation in the emissive polymer layer [51]. Schlattmann et al. reported that PLEDs, prior to operation, contain high concentrations of metal impurities of indium and aluminum, indicated by ESCA depth profiling data and Rutherford backscattering spectroscopy (RBS) results [53,54]. Degradation-induced changes in the structural and optical properties of the polyfluorene-based blue PLEDs are examined using ESCA and other techniques by Bliznyuk et al. [52]. Two primary mechanisms of degradation, photooxidation of the polymer matrix and aggregate formation, are identified. These findings are helping researchers and engineers to further improve the lifetimes of the OLEDs.

10.1.7 RAMAN SPECTROSCOPY

Raman spectroscopy comprises the family of spectral measurements made on molecular media based on inelastic scattering of monochromatic radiation [55–57]. During this process, energy is exchanged between the photon and the molecule such that the scattered photon is of higher or lower energy than the incident photon. The difference in energy is associated with a change in the population of the rotational or the vibrational energy levels of the molecule. In 1930, Raman received the Nobel Prize in Physics for the discovery that bears his name. Raman spectroscopy can be used for routine qualitative and quantitative measurements of both inorganic and organic materials, and it is successfully employed to solve complex analytical problems such as determining chemical structures. Gases, vapors, aerosols, liquids, and solids can be analyzed by this technique.

Several excellent examples [58–61] using Raman spectroscopy in the field were illustrated. Kim et al. studied the nature of nonemissive black spots in the PLEDs [58]. In their devices, PEDOT–PSS as a hole-transporting layer was spin-coated on the top of the treated ITO, and Ca was used as a cathode with an Al capping layer. Micro-Raman as a nondestructive technique delivers valuable chemical and structural information with submicron resolution from the surface films as well as from the buried layers. Kim et al. demonstrated how micro-Raman spectroscopy could be used to yield new insight into organic device degradation through spectroscopic cross-mapping of the active layer in the working devices. Raman spectra were taken spot-by-spot across the black spots. On the basis of the micro-Raman results, they concluded that the nonemissive disks are characterized by a localized electrochemical reaction with reduction of the normal doped PEDOT–PSS to the dedoped material and oxidation of the active metal.

10.1.8 SECONDARY ION MASS SPECTROMETRY

Today, secondary ion mass spectrometry (SIMS) is frequently used for analysis of trace elements in solid materials, especially in semiconductors and in thin films [62,63]. Primary beam species useful in SIMS include Cs^+ , O_2^+ , O^+ , Ar^+ , and Ga^+ at energies from 1–30 keV. The bombarding primary ion beam produces monatomic and polyatomic particles of sample

material and resputtered primary ions, along with electrons and photons. The secondary particles carry negative, positive, and neutral charges, and they have kinetic energies that range from zero to several hundred electronvolts. During SIMS analysis, the sample surface is slowly sputtered away. When the sputtering rate is extremely slow, the entire analysis can be performed while removing less than a tenth of an atomic layer. This extremely slow sputtering mode is called static SIMS. Monitoring the secondary ion count rate of selected elements as a function of time leads to depth profiles, or dynamic SIMS. Ion images show secondary ion intensities as a function of location on sample surfaces. Ion images can be acquired in two operating modes, called ion microscope or stigmatic imaging, and ion micro-beam imaging or raster scanning. Ion microscopy requires a combination ion microscope and mass spectrometer capable of transmitting a mass selected ion beam from the sample to the detector without loss of lateral position information. Image detectors indicate the position of the arriving ions.

Chua et al. studied lifetime issue in OLED by SIMS [64]. In their devices, a thin 3-nm-thick parylene layer is deposited by chemical vapor deposition at room temperature on the ITO-coated glass substrate to form a bilayer anode of an OLED. The SIMS depth profiling was taken for C, In, O, Ag, and Ca (cathode materials) in the normal and the modified device structures at the bright and the dark nonemissive areas in electrically stressed devices. The device was taken out from the evaporator after cathode deposition and electrically stressed at a constant voltage. The position of dark spots formed in the active area was monitored. The sample was then loaded into the SIMS chamber for analysis. Chua et al. found that the parylene film not only reduces the occurrence of the dark spots, acting as a barrier for oxygen diffusion from either the ITO or the atmosphere and stabilizing the migration of the electrodes during electrical stress, but also improves the injection of the holes from the anode.

10.2 PERFORMANCE MEASUREMENT TECHNIQUES

Characterizing the performance of the OLED devices requires an understanding of how the device functions and how the performance is measured. First, we discuss the subjective visual response in relation to the objective emission of light. Then we describe basic measurements and efficiency calculations. Next, we describe energy levels in OLED devices. Finally, we discuss the lifetime measurements.

10.2.1 HUMAN VISION, LIGHT, AND COLOR

One primary distinction that needs to be made is the difference between physical units and human eye units [65,66]. Physical units are watts, meters, and steradians (solid angle). These units exist independently of the human eyeball. The human eye is sensitive to a small range of wavelengths (400–700 nm), and it is not uniformly responsive across the spectrum. This response is known as the photopic response. It is a fixed function of wavelength, and has been standardized over the years for the average human. Not all people have the same photopic response. As people have rods and cones, there are really two human response curves. The so-called black and white vision, which we use under low lighting conditions, is the scotopic response curve provided by the rods. Under normal lighting conditions, we see colors due to the cones in the eye. The response curve of the cones is the photopic response, and is applicable for the OLEDs. If we take a physical unit, then convolve it with the photopic response, we get the corresponding human eye unit. Table 10.1 clarifies the analogy.

In human eye units, watt becomes lumen. At 555 nm, the peak sensitivity of the photopic response, there are 683 lm/W. A watt is a joule per second, and a photon has energy in units of joules. A watt tells us how many photons per second are coming out of the OLED. A lumen

TABLE 10.1
Summary of Photometric Quantities and Associated Units

Quantity	Physical Name	Physical Units	Human-Eye Name	Human-Eye Units
Flux	Radiant flux	W	Luminous flux	lm
Flux density	Irradiance	W/m ²	Illuminance	lm/m ²
Flux density per solid angle	Radiance	W/(m ² sr)	Luminance	lm/(m ² sr) (cd/m ²) (nit)
Flux per solid angle	Radiant intensity	W/sr	Luminous intensity	lm/(sr cd)

tells us how many of those photons we actually see, accounting for the wavelength sensitivity of the eye.

The candela (cd) is equal to a lumen per steradian. A steradian is the measure of solid angle. A sphere has 4π sr on its surface area. This stems from the fact that the surface area of a sphere, $SA = 4\pi r^2$. The surface area divided by r^2 gives the total solid angle of the sphere. Similarly, to calculate the solid angle of a piece of a sphere's surface, one takes the area of interest, and divides by the radius squared. This gives the solid angle in steradians. A steradian is dimensionless because it is the ratio of two areas.

It is easy to understand watts, the number of photons per second, and lumens, the weighted number of photons per second that we can see. Radiance is more confusing. Imagine that there are a certain number of photons generated by a point source per second. These photons then travel out in all directions (in the isotropic case). The number of photons per second per solid angle is the radiant intensity. If you hold a piece of paper a distance away from the light source (thus fixing the distance and the area) that paper is irradiated with irradiance. If you measure the light coming off the paper, you are measuring the radiance of that piece of paper. Irradiance refers to what is impinging on a surface. Radiance refers to what is emitting from a surface.

Radiant intensity can be described as the amount of power (watt) heading in your direction, i.e., per steradian, from a light source. The total amount of power emitted by the source is the radiant flux (watt). If you integrate the radiant intensity over all solid angles, you get the total radiant flux. If it is weighted by the photopic response, then it is the luminous intensity and the luminous flux.

The candela is the amount of visible light coming in your direction from the OLED. The OLED pixels are small and flat, and have a fixed area. When you look at it, there is a certain amount of light coming out of the OLED in your direction. When this amount of light, in cd, is divided by the area of the OLED, you get the luminance of the OLED in cd/m².

Color is a subjective perception of optical stimuli [67]. There has been much work aimed at objectifying our visual experience [68]. For describing information on a visual screen, color is projected onto a two-dimensional plane known as the chromaticity diagram, standardized by the Commission International de l'Eclairage (CIE). This objectification enables the industry to develop standards. To produce a full-color display, it is generally accepted that three colors are needed. For an emissive display, red, blue, and green are the primary colors. For a reflective display, cyan, magenta, and yellow are the primary colors. The three colors form a triangle in color space. Any color inside this triangle can be reproduced by the display. Pushing the vertices of this triangle to the edge of the color space increases the fill factor, thus increasing the gamut of colors that can be reproduced. One advantage of the OLED technology is that the emitted colors are quite pure, which corresponds to a large fill factor. Generally, with only one green emitter, it is difficult to capture the full range of greens in a natural scene on a display, or to capture subtle distinctions in skin tone. There are certain

aspects to color that are not fully understood, as demonstrated by Land's famous set of experiments. The colors generated from the OLED depend on the energy differences between the excited and ground states of emissive molecules and can be largely tailored or tuned by modifying the chemical structure [3,5,10,14,15,69,70].

10.2.2 BASIC OLED MEASUREMENT AND EFFICIENCY

The primary OLED measurement is the current density–voltage–luminance (J – V – L) family of curves with an example illustrated in Figure 10.4. One applies a fixed voltage to a device, and then measures the resulting current and light output. The current is converted to current density to account for the lateral area of the OLED. The light output is measured by a commercial luminance meter [66]. In a typical curve, there is a subthreshold region, a turn-on region, and a saturated region. In the subthreshold region, the current is primarily ohmic through the device, and no light is emitted. In the turn-on region, the space-charge density is sufficiently large enough across the entire device to generate current and light output. However, many of these charges are occupying trap states. In this region, the current density is proportional to some high power of the voltage (8–12), and the luminance increases dramatically with voltage. The transition between subthreshold and turn-on occurs at the turn-on voltage. After the traps are filled, one reaches the saturation regime. A steady state of space-charge current exists in the device.

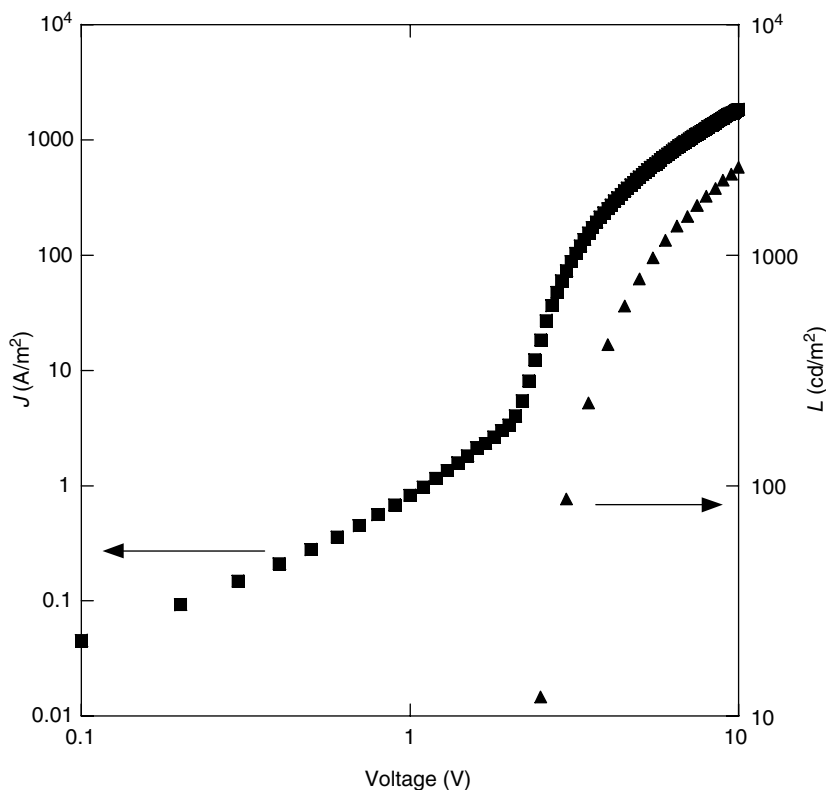


FIGURE 10.4 J – V – L family of curves of OLED.

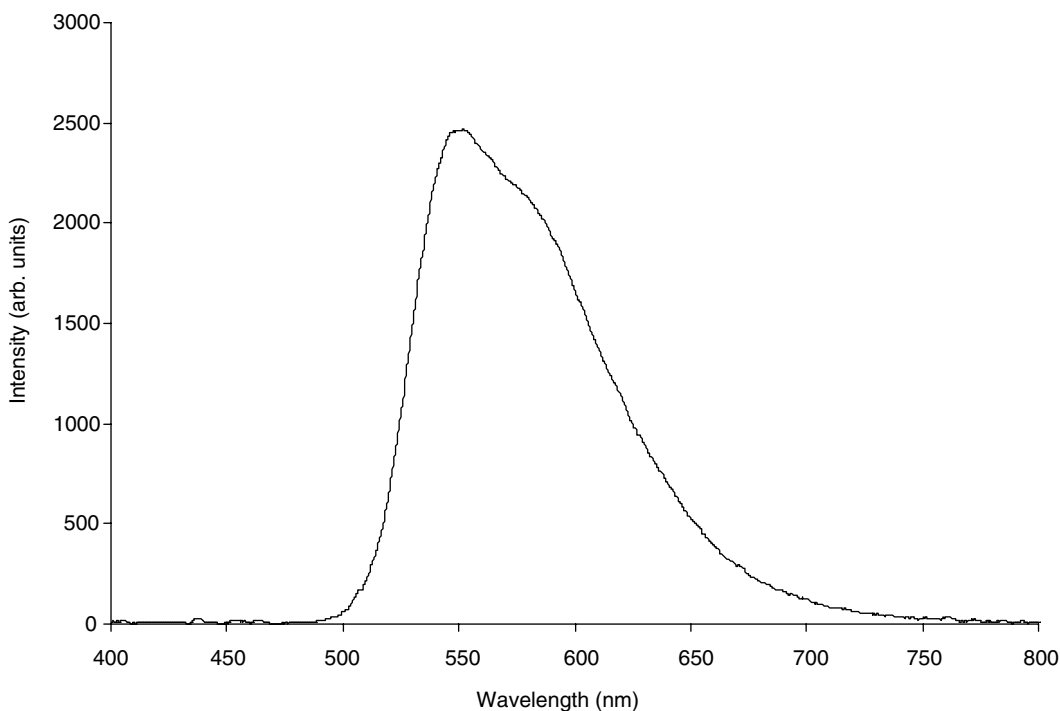


FIGURE 10.5 A typical electroluminescence spectrum from a PLED, comprising an ITO anode, a Baytron-P (Bayer) buffer layer, a PDY-131 (Covion) emitting layer, and an ytterbium cathode. The peak at 550 nm is associated with the emission from the polymeric excited state to the ground state, without exciting any vibrations. The shoulder at 580 nm is associated with relaxation to the vibrationally excited ground state. Higher overtones in the Franck–Condon progression, along with trapped states, account for the tail into the red spectrum of an OLED.

The optical and electronic properties of organic materials are described in several review papers [4,7,14,71,72]. The absorption and photoluminescent (PL) emission generated by ultraviolet light reflect intrinsic properties of organic materials. The absorption and PL spectra of many important organic materials for OLEDs were measured and reported [10,14,73,74]. The differences between photoluminescence and electroluminescence (EL) have been pointed out by several authors [4,5,10,14]. The EL spectrum (see Figure 10.5), the emitted light from OLED, as a function of wavelength, can be converted into CIE coordinates.

Important electrical informations about OLEDs, such as charge transport, charge injection, carrier mobility, etc., can be obtained from bias-dependent impedance spectroscopy, which in turn provides insight into the operating mechanisms of the OLED [14,15,73,75–78]. Campbell et al. reported electrical measurements of a PLED with a 50-nm-thick emissive layer [75]. Marai et al. studied electrical measurement of capacitance–voltage and impedance–frequency of ITO/1,4-*bis*-(9-anthrylvinyl)-benzene/Al OLED under different bias voltage conditions [76]. They found that the current is space-charge limited with traps and the conductivity exhibits power-law frequency dependence.

The impedance of PLEDs can be viewed in many different formats: G – B , R – X , or as a function of frequency (see Figure 10.6). The diode in this example was ITO/PEDOT–PSS/Alkoxy-PPV/Ca/Al, measured from 10^2 to 10^7 Hz, with forward bias from 0 to 5 V.

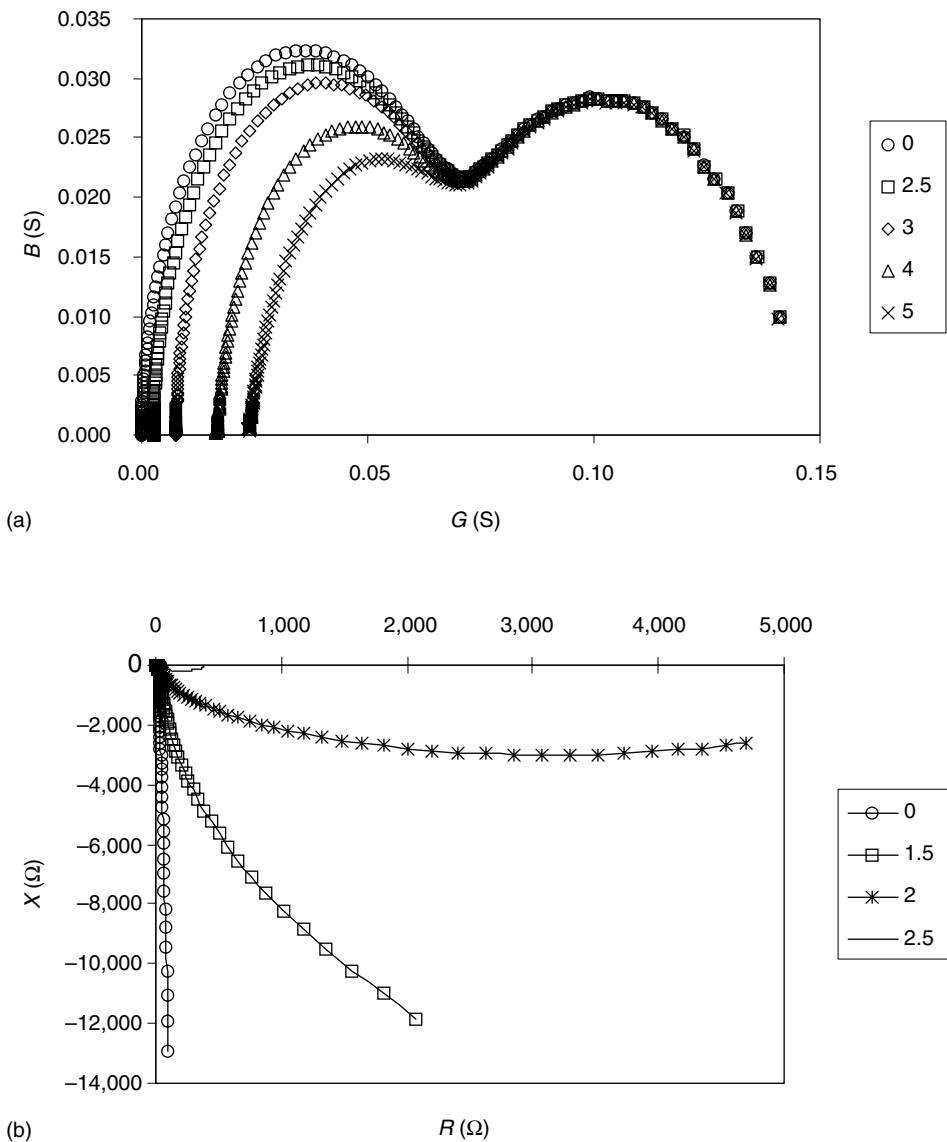


FIGURE 10.6 Impedance of an ITO/PEDOT-PSS/Alkoxy-PPV/Ca/Al LED. The bias voltage is indicated in the legend: (a) admittance of the diode, showing sensitivity above threshold voltage; (b) impedance of the diode, showing sensitivity below threshold voltage. The threshold voltage of this device was 2.5 V.

The R - X plot shows the most variation in the subthreshold region, while the G - B plot shows the most variation above threshold. One sees from the G - B plot that the high frequency response of the diode is independent of bias (>1 MHz). To fit the data, one models each material phase or interface as a parallel R - C combination. These combinations are then added in series, and an overall series resistance and series inductance are added. For the data in Figure 10.6, three R - C elements are used. One R - C element is associated with the Schottky barrier. Another is associated with the high frequency bias-independent arc, which we believe is associated with the capacitance of the alkoxy-PPV. The thinness of the film

produces a relatively large capacitance, which, along with its large resistance, leads to a high frequency relaxation. The third is associated with the AC conductivity of the PEDOT-PSS. This third R-C can be modeled more accurately as a lossy, amorphous semiconductor using the pair approximation, which is equivalent to the well-known Z_{ARC} model in the impedance literature, but the increased accuracy comes at the expense of an added parameter, which is eschewed to simplify the analysis. Changes induced by aging can be followed by changes in these elements.

There are three principal efficiency measurements in OLED: external quantum efficiency, luminous efficiency, and power efficiency [13].

Although one would prefer to know the internal quantum efficiency, it is only possible to measure the external quantum efficiency. Much of the light generated by an OLED is wave-guided out from the edges of the device.

The OLED emits a certain number of photons per second. The energy of one photon is $E = h\nu$. The energy of N photons is $E_N = Nh\nu$, with units of joules. Therefore, by knowing how many optical watts are generated by the OLED, one can calculate the number of photons per second, as long as the frequency (or wavelength) is known. The number of photons per second equals the light output in watts divided by $h\nu$: $N_\phi = W/h\nu$.

The current determines the number of electrons that pass through the device per second. As $1\text{ A} = 1\text{ C/s}$, the number of electrons per second equals the current divided by e : $N_e = I/e$. Knowing the device area allows one to use current density instead.

The external quantum efficiency is given by $\eta = N_\phi/N_e = We/(h\nu \cdot I)$.

The luminous efficiency is the simplest to calculate. It is the ratio of the luminance (cd/m^2) to the current density (A/m^2), and has units of cd/A . Finally, the power efficiency is the ratio of the light output in lumens divided by the electrical input in watts. For reference, a typical incandescent light bulb is $\sim 15\text{ lm/W}$, while a fluorescent light bulb is $\sim 60\text{ lm/W}$.

Complications here arise from two areas. First, the OLED is not necessarily a sharp line emitter. It is necessary to weight the output by the emission spectrum to get the number of photons. Second, the emission is not isotropic. A model needs to be constructed for the OLED emission geometry to relate the external quantum efficiency to the internal quantum efficiency. That model will take into account the fact that light only goes out from one side of the OLED, because there is a relatively thick metal electrode on the back surface that reflects the light. The model will also account for the fact that the ITO-coated glass has a finite thickness, and that light emitted at a wide angle will be totally internally reflected at the glass-air interface, and will exit the device from the edge of the glass. This model will be geometry dependent, and not device dependent, so it will be a fixed factor for all the devices [79].

Efficiency measurement results of OLEDs can be found in many published papers [3,4,7,8,11,12,14,15,80–83]. Mahon assessed the efficiencies of 2.2-in. active-matrix OLEDs made by Samsung with a polycrystalline-Si backplane and Universal Display's phosphorescent red and green materials system [83]. Figure 10.7 shows a power consumption simulation for a 2.2-in. full-color OLED display using UDC's phosphorescent OLEDs, small-molecule fluorescent devices, and polymer OLEDs along with a comparison of the power consumed by an active-matrix liquid crystal display (AMLCD) backlight. The use of phosphorescent OLED technology leads to a 100 cd/m^2 display consuming only 50 mW , compared with $110\text{--}130\text{ mW}$ for other OLED technologies and the AMLCD backlight.

10.2.3 GETTING ON THE SAME ENERGY SCALE

In OLEDs, the positive and the negative charges are injected from the anode and the cathode, respectively. These charges then move through hole and electron transport layers, and meet in

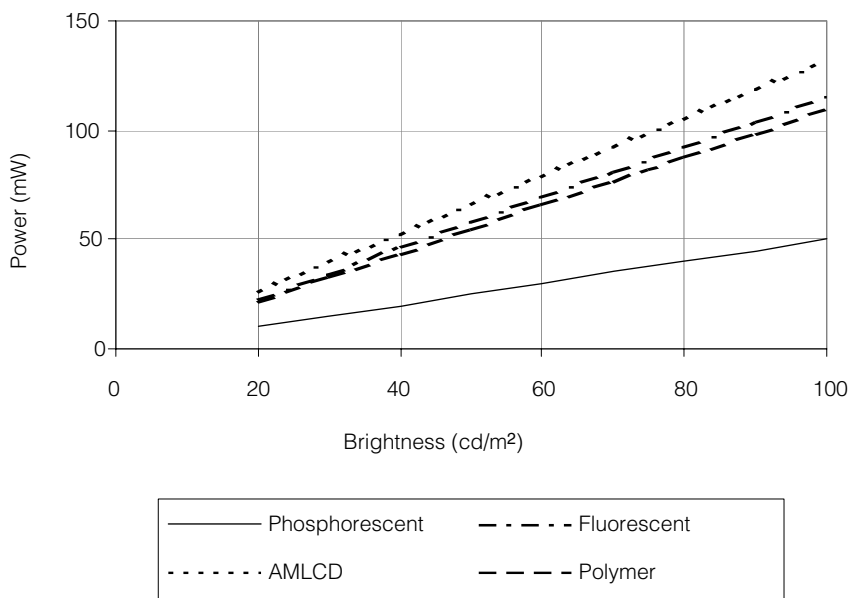


FIGURE 10.7 Power consumption simulation for a 2.2-in. full-color OLED display using Universal Display's phosphorescent OLEDs, small-molecule fluorescent devices, and polymer OLEDs along with a comparison of the power consumed by an active-matrix liquid crystal display backlight. $R:G:B = 3:6:1$, 50% polarizer efficiency, and 30% of pixels lit. (From Mahon, J.K., *Adv. Imaging*, June, 28, 2003. With permission.)

the emissive layer, creating a bound exciton. Radiative recombination of these excitons results in light emission. The electronic structure of the electrodes, transport layers, and emissive layers must be carefully considered when designing for high performance [4,6–8,14,15,73]. The relative positions of the highest occupied molecular orbitals (HOMOs) and the lowest unoccupied molecular orbitals (LUMOs) of these organic layers ultimately govern the efficiencies, turn-on voltages, and emission spectrums, etc. [14,15,84–98].

It is important to clarify how the HOMO and the LUMO energies are related to quantities like the work function and the vacuum energy. An energy level diagram relating photoelectron spectroscopy (PES) and cyclic voltammetry (CV) measurements is shown in Figure 10.8. We choose the zero point of energy to correspond to the vacuum energy. This is the energy of an electron, in vacuum, not near any other particles, and having no kinetic energy. This is the zero energy vacuum state. It is important to be aware of the surface dipole term to avoid confusion.

When working with metal electrodes, the energy of the electrons in the metal is lower than the vacuum level by the work function of the metal, which tends to be 3–5 eV. Work functions of some materials relevant to LED devices are collected in Table 10.2 [11]. The work function can vary depending upon the crystal facet from which emission is measured (or if the metal is amorphous), and sample preparation details. The photoelectric (PE) effect is exploited in XPS (ESCA) or UPS to measure the work function. It is very critical to realize that, in these experiments, what is measured is the energy required to remove an electron to a point just outside the surface of the solid, not to infinity. At this range, the dipolar forces at the surface are still active, and one can learn about surface dipoles in the material.

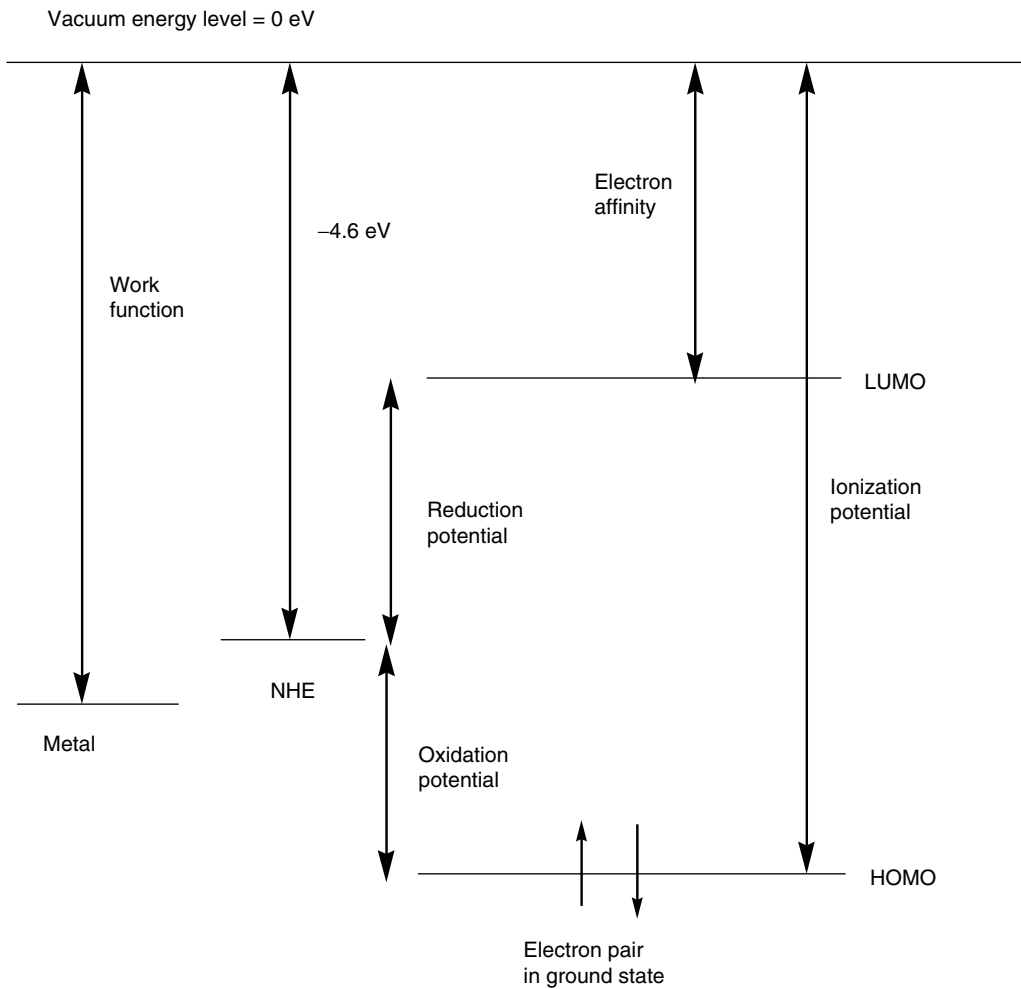


FIGURE 10.8 Energy level diagram relating PES and CV measurements.

TABLE 10.2
Work Functions of Some Materials Relevant to LED Devices. The Work Function Can Vary Depending upon the Crystal Facet from Which Emission Is Measured, and Sample Preparation Details

Material	Work Function, ϕ (eV)
Calcium	2.9
Magnesium	3.7
Aluminum	4.3
Silver	4.3
ITO	4.5–5.0
Polyaniline	4.4–5.0
Gold	4.8–5.4

The ionization potential of a molecule is the energy from the ground state of the molecule (HOMO) to the vacuum level. It is measured using UPS or XPS. The electron affinity of the molecule is the energy from the vacuum level to the LUMO. It is measured using inverse photoelectron spectroscopy (IPES) [15]. The values obtained in the gas phase are different from those obtained in the solid state, and shifts due to amorphous versus crystalline regions can be noticed.

CV is the electrochemical method for determining energy levels of molecules. In CV, the reduction potential is the voltage necessary to add an electron into the LUMO. The oxidation potential is the energy necessary to take an electron out of the HOMO. The sum of the absolute values of the oxidation potential and the reduction potential corresponds to the optical transition energy. The potentials measured by CV are measured relative to the Standard Calomel Electrode (SCE) or the Normal Hydrogen Electrode (NHE). The NHE is at -4.6 eV compared to the zero vacuum level [97]. This very important link helps connect chemistry and physics. CV measurements are usually performed in solution, so there can be an additional shift of the energy levels upon going from solution to the solid state.

10.2.4 LIFETIME MEASUREMENTS

One of the major issues related to the OLED is the long-term stability. A normal cathode ray tube (CRT) can last for about 100,000 h, or about 12 years of continuous operation, and most other display technologies can also operate for more than 50,000 h. In the early stages of OLED development, the short lifetime of OLEDs of only tens of hours made them impractical. Burrows et al. [99] introduced a simple encapsulation technique to protect OLEDs from the deleterious effects of the atmosphere, and demonstrate a greatly enhanced lifetime. This technique was widely adopted. Many studies of degradation mechanisms have been studied and proposed [4–7,98–115]. Xu pointed out that the typical OLED degrades in two separate and distinct ways [100]. The first is the intrinsic degradation, a gradual decrease in luminance of the display phosphors that occurs during the operation. The other is the aging problem known as dark spot degradation, which is characterized by circular, nonemissive areas that gradually cover a pixel. One of the major problems today is the fact that the blue light-emitting materials employed in OLEDs age much more rapidly than red and green ones, which makes the overall lifetime of the displays too short to be widely used in our daily life.

The basic OLED performance such as brightness decay, i.e., lifetime to 50% of initial brightness, can be measured with a direct current (DC) or pulsed-constant light-current-voltage test [101]. This test uses forward bias constant sourcing with high-speed voltage and light measurement during a single pulse. Pulsed testing of long-term characteristics requires continuous pulse trains with sample measurements at regular intervals of minutes or hours. Modular J – V – L systems can include a calibrated luminescence meter for calibrated light measurements, but a photometer alone will work in most applications because percentage change from initial brightness is sufficient. The relationship of increasing the voltage to decreasing light over time is also of interest in calculating end-of-life efficiencies.

Today, many red and green OLEDs have lifetimes exceeding 10,000 h (see one example in Table 10.3). Instead of testing the OLED at room temperature, an accelerated experiment may be useful. The operational lifetime of PLED was studied at several temperatures (25–85°C) by Parker et al. [110]. They found the changes in luminance were significantly accelerated at higher temperatures. From the lifetime data at several temperatures, the OLED lifetime at room temperature can be readily estimated.

Otsuka Electronics Company produces an OLED panel lifetime evaluation system [102]. Their system can measure the historical change of chromaticity, luminance, current, voltage of OLED panel emitted for a long period under the preset condition of constant voltage,

TABLE 10.3

Performance of Several OLEDs Made by UDC. Both Luminous Efficiency and Luminance Were Measured at 1 mA/cm². Initial Luminance for Red Is at 300 cd/m² and 600 cd/m² for Green in Lifetime Test

Name	RD07	RD61	GD29	BD14	BD30
Color	Red	Red	Green	Light blue	Blue
CIE (<i>x</i> , <i>y</i>)	0.65, 0.35	0.61, 0.38	0.30, 0.65	0.14, 0.37	0.14, 0.23
Luminous efficiency (cd/A)	12	22	24	16	10
Luminance (cd/m ²)	120	220	240	160	100
Lifetime (h)	15,000	15,000	13,000	N/A	N/A

Source: From Mahon, J.K., *Adv. Imaging*, June, 28, 2003. With permission.

constant current or designated luminance value (initial value) in the constant temperature environment. Furthermore, a maximum of 100 samples can be measured individually at the same time under different measurement conditions.

In conclusion, we have presented many microstructural characterization and performance measurement techniques, together with examples of how to use these techniques to improve the performance of OLEDs. Seeing the enormous progress recently, we expect more and more OLED-related products will be used in our daily life.

ACKNOWLEDGMENTS

We would like to thank L. Zhang, R. McLean, L. Liang, D. Howell, T. Liang (DuPont), X. Dong (Eli Lilly), and Q. Sun (Koch) for their valuable discussion.

REFERENCES

1. C.W. Tang and S.A. VanSlyke, Organic electroluminescent diodes, *Appl. Phys. Lett.*, 52:913–915, 1987.
2. J.H. Burroughes, D.D. Bradley, A.R. Brown, R.N. Marks, K. Mackay, R.H. Friend, P.L. Burns, and A.B. Holmes, Light-emitting diodes based on conjugated polymers, *Nature*, 347:539–541, 1990.
3. Y. Yang, Polymer electroluminescent devices, *MRS Bulletin*, 22:31–38, 1997.
4. A. Dodabalapur, Organic light emitting diodes, *Solid State Commun.*, 102:259–267, 1997.
5. M.T. Bernius, M. Inbasekaran, J. O'Brien, and W. Wu, Progress with light-emitting polymers, *Adv. Mater.*, 12:1737–1750, 2000.
6. L.R. Sheats, H. Antoniadis, M. Hueschen, W. Leonard, J. Miller, R. Moon, D. Roitman, and A. Stocking, Organic electroluminescent devices, *Science*, 273:884–888, 1996.
7. R.H. Friend, R.W. Gymer, A.B. Holmes, J.H. Burroughes, R.N. Marks, C. Taliani, D.D. Bradley, D.A. Dos Santos, J.L. Bredas, M. Logdlund, and W.R. Salaneck, Electroluminescence in conjugated polymers, *Nature*, 397:121–128, 1999.
8. D. Neher, Polyfluorene homopolymers: conjugated liquid-crystalline polymers for bright blue emission and polarized electroluminescence, *Macromol. Rapid Commun.*, 22:1365–1385, 2001.
9. G. Gustafsson, Y. Cao, G.M. Treacy, F. Klavetter, N. Colaneri, and A.J. Heeger, Flexible light-emitting diodes made from soluble conducting polymers, *Nature*, 357:477–479, 1992.
10. A. Kraft, A.C. Grimsdale, and A.B. Holmes, Electroluminescent conjugated polymers — seeing polymers in a new light, *Angew. Chem., Int. Ed. Engl.*, 37:402–428, 1998.

11. J.S. Kim, M. Granstrom, R.H. Friend, N. Johansson, W.R. Salaneck, R. Daik, W.J. Feast, and F. Cacialli, Indium–tin oxide treatments for single- and double-layer polymeric light-emitting diodes: the relation between the anode physical, chemical and morphological properties and the device performance, *J. Appl. Phys.*, 84:6859–6870, 1998.
12. H. Becker, H. Spreitzer, W. Kreuder, E. Kluge, H. Vestweber, H. Schenk, and K. Treacher, Advances in polymers for PLEDs: from a polymerization mechanism to industrial manufacturing, *Synth. Met.*, 122:105–110, 2001.
13. S.R. Forrest, D.D.C. Bradley, and M.E. Thompson, Measuring the efficiency of organic light-emitting devices, *Adv. Mater.*, 15:1043–1048, 2003.
14. S. Miyata and H.S. Nalwa, Eds., *Organic Electroluminescent Materials and Devices*, Gordon and Breach, Amsterdam, 1997.
15. W.R. Salaneck, K. Seki, A. Kahn, and J. Pireaux, Eds., *Conjugated Polymer and Molecular Interfaces*, Marcel Dekker, New York, 2002.
16. J.W. Cowley, *Diffraction Physics*, 2nd ed., North-Holland, New York, 1981.
17. D.B. Williams and C.B. Carter, *Transmission Electron Microscopy*, Plenum Press, New York, 1996.
18. P. Hirsch, A. Howie, R.B. Nicholson, D.W. Pashley, and M.J. Whelan, *Electron Microscopy of Thin Crystals*, 2nd ed., Kreiger Huntington, New York, 1977.
19. G. Thomas, *Transmission Electron Microscopy of Metals*, Wiley & Sons, New York, 1962.
20. Z.G. Li, Ed., *Industrial Applications of Electron Microscopy*, Marcel Dekker, New York, 2002.
21. J. Liu, M. Pan, and G. Spinnler, Coherent electron nanodiffraction from clear silver nano particles in a UHV STEM, in *Microscopy Society of American Proceedings*, 1983, pp. 1058–1059.
22. J. Bravman, R. Anderson, and M. McDonald, Eds., Specimen preparation for transmission electron microscopy of materials (I), *MRS Symp. Proc.*, Vol. 115, Pittsburgh, 1988.
23. J. Bravman and R. Sinclair, The preparation of cross-section specimens for transmission electron microscopy, *J. Electron. Microsc. Tech.*, 1:53–61, 1984.
24. Z.G. Li, P. Carcia, and P. Donohue, Microstructure of LaB₆-based thick film resistors, *J. Mater. Res.*, 7:2225–2229, 1992.
25. P.F. Carcia, R.S. Mclean, M.H. Reilly, Z.G. Li, L.J. Pillione, and R.F. Messier, Low-stress indium–tin-oxide thin films rf magnetron sputtered on polyester substrates, *Appl. Phys. Lett.*, 81:1800–1802, 2002.
26. Y.Y. Noh, C.L. Lee, and J.J. Kim, Energy transfer and performance in phosphorescent dye doped polymer light emitting diodes, *J. Chem. Phys.*, 118:2853–2864, 2003.
27. J.H. Park, Y.T. Lim, O.O. Park, and Y.C. Kim, Enhancement of photostabilities in blue-light-emitting polymers doped with gold nanoparticles, *Macromol. Rapid Commun.*, 24:331–334, 2003.
28. J.I. Goldstein, D.E. Newbury, P. Echlin, D.C. Joy, A.D. Roring, C.E. Lyman, C. Fiori, and E. Lifshin, *Scanning Electron Microscopy and X-Ray Microanalysis*, 2nd ed., Plenum Press, New York, 1992.
29. J.S. Shah and A. Beckett, A preliminary evaluation of moist environment ambient temperature scanning electron microscopy (MEATSEM), *Micron*, 10:13–23, 1979.
30. G.D. Danilatos, Design and construction of an atmospheric or environmental SEM, *Scanning*, 4:9–20, 1981.
31. L.M. Do, E.H. Han, Y. Niidome, and M. Fujihira, Observation of degradation processes of Al electrodes in organic electroluminescence devices by electroluminescence microscopy, atomic force microscopy, scanning electron microscopy, and Auger electron spectroscopy, *J. Appl. Phys.*, 76:5118–5121, 1994.
32. M.S. Weaver, L.A. Michalski, K. Rajan, M.A. Rothman, J.A. Silvernail, and J.J. Brown, Organic light emitting devices with extended operating lifetimes on plastic substrates, *Appl. Phys. Lett.*, 81:2929–2931, 2002.
33. G.L. Frey, K.J. Reynolds, R.H. Friend, H. Cohen, and Y. Feldman, Solution-processed anodes from layer-structure materials for high efficiency polymer light-emitting diodes, *Am. Chem. Soc.*, 125:5998–6007, 2003.
34. R.K. Kasim, M. Pomerantz, and R.L. Elsenbaumer, A simple method for fabricating polymeric light-emitting diodes, *Chem. Mater.*, 10:235–237, 1998.
35. S. Rubanov and P.R. Munroe, Applications of focused ion beam using FEI DualBeam DB235, *Microsc. Microanal.*, 9(Suppl. 2):884–885, 2003.

36. L.A. Giannuzzi, J.L. Brown, S.R. Brown, R.B. Irwin, and F.A. Stevie, Focused ion beam milling and micromanipulation lift-out for site specific cross-sectional TEM specimen preparation, *Mater. Res. Soc. Symp. Proc.*, 480:19–27, 1997.
37. Z.G. Li, Applications of microscopy in Organic Light-Emitting Diode Research and Development, *Proc. Microscopy and Microanalysis*, 1352–1353, 2004.
38. B.D. Ratner and V.V. Tsukruk, Eds., *Scanning Probe Microscopy*, Oxford University Press, New York, 1998.
39. A.C. Morteani, A.S. Dhoot, J.S. Kim, C. Silva, N.C. Greenham, C. Murphy, E. Moons, and R.H. Friend, Barrier-free electron-hole capture in polymer blend heterojunction light-emitting diodes, *Adv. Mater.*, 15:1708–1712, 2003.
40. J.M. Halls, A.C. Arias, J.D. MacKenzie, W.S. Wu, M. Inbasekaran, E.P. Woo, and R.F. Friend, Photodiodes based on polyfluorene composites: influence of morphology, *Adv. Mater.*, 12:498–502, 2000.
41. B.H. Cumpston and K.F. Jensen, Electromigration of aluminum cathodes in polymer-based electroluminescent devices, *Appl. Phys. Lett.*, 69:3941–3943, 1996.
42. T. Ahn and H. Lee, Effects of annealing of polythiophene derivative for polymer light emitting diodes, *Appl. Phys. Lett.*, 80:392–394, 2002.
43. C.J.R. Sheppard and D.M. Shotton, *Confocal Laser Scanning Microscopy*, Springer-Verlag, New York, 1997.
44. J. Pawley, Ed., *The Handbook of Biological Confocal Microscopy*, IMR Press, Madison, 1989.
45. D.B. Briggs and M.P. Seah, *Auger and X-Ray Photoelectron Spectroscopy*, Wiley & Sons, New York, 1990.
46. C.R. Brundle, C.A. Evans, and S. Wilson, *Encyclopedia of Materials Characterization*, Butterworth-Heinemann, Boston, 1992.
47. T. Kugler, M. Logdlun, and W.R. Saneck, Photoelectron spectroscopy and quantum chemical modeling applied to polymer surfaces and interfaces in light-emitting devices, *Acc. Chem. Res.*, 32:225–234, 1999.
48. P.K.H. Ho, J.S. Kim, J.H. Burroughes, H. Becker, S.F.Y. Li, T.M. Brown, F. Cacialli, and R.H. Friend, Molecular-scale interface engineering for polymer light-emitting diodes, *Nature*, 404:481–484, 2000.
49. K.M. Vaeth and K.F. Jensen, Selective growth of poly(*p*-phenylene vinylene) prepared by chemical vapor deposition, *Adv. Mater.*, 11:814–820, 1999.
50. D.J. Milliron, I.G. Hill, C. Shen, and A. Kahn, Surface oxidation activates indium tin oxide for hole injection, *J. Appl. Phys.*, 87:572–576, 2000.
51. K.W. Wong, H.L. Yip, Y. Luo, K.Y. Wong, W.M. Lau, K.H. Low, H.F. Chow, Z.Q. Gao, W.L. Yeung, and C.C. Chang, Blocking reactions between indium–tin oxide and poly (3,4-ethylene dioxithiophene): poly(styrene sulphonate) with a self-assembly monolayer, *Appl. Phys. Lett.*, 80:2788–2790, 2002.
52. V.N. Bliznyuk, S.A. Carter, J.C. Scott, G. Klärner, R.D. Miller, and D.C. Miller, Electrical and photoinduced degradation of polyfluorene based films and light-emitting devices, *Macromolecules*, 32:361–369, 1999.
53. A.R. Schlattmann, D.W. Floet, A. Hilberer, F. Garten, P.J.M. Smulders, T.M. Klapwijk, and G. Hadzioannou, Indium contamination from the indium–tin-oxide electrode in polymer light-emitting diodes, *Appl. Phys. Lett.*, 69:1764–1766, 1996.
54. M.P. de Jong, L.J. van Ijzendoorn, and M.J.A. de Voigt, Stability of the interface between indium–tin-oxide and poly(3,4-ethylenedioxythiophene)/poly(styrenesulfonate) in polymer light-emitting diodes, *Appl. Phys. Lett.*, 77:2255–2257, 2000.
55. C.V. Raman and K.S. Krishnan, The optical analog of the Compton effect, *Nature*, 121:711–711, 1928.
56. C.V. Raman and K.S. Krishnan, The production of new radiations by light scattering, *Proc. R. Soc. London*, 122:23–34, 1929.
57. T. Hirschfeld and D.B. Chase, FT-Raman spectroscopy: development and justification, *Appl. Spectrosc.*, 40:133–137, 1986.
58. J.S. Kim, P.K.H. Ho, C.E. Murphy, N. Baynes, and R.H. Friend, Nature of non-emissive black spots in polymer light-emitting diodes by *in-situ* micro-Raman spectroscopy, *Adv. Mater.*, 14:206–209, 2001.
59. L.A. Cury, L.O. Ladeira, and A. Righi, Large blue shift in the absorption spectra of BEH-PPV films containing gold nanoparticles, *Synth. Met.*, 139:283–286, 2003.

60. M. Ariu, D.G. Lidzey, and D.D.C. Bradley, Influence of film morphology on the vibrational spectra of dioctyl substituted polyfluorene (PFO), *Synth. Met.*, 111–112:607–610, 2000.
61. S. Garreau, G. Louarn, J.P. Buisson, G. Froyer, and S. Lefrant, *In-situ* spectroelectrochemical Raman studies of poly(3,4-ethylenedioxythiophene), *Macromolecules*, 32:6807–6812, 1999.
62. J.C. Vickerman and D. Briggs, *TOF-SIMS: Surface Analysis by Mass Spectrometry*, IM Publications and Surface Spectra Limited, London, 2001.
63. J.C. Vickerman, A. Brown, and N.M. Reed, *Secondary Ion Mass Spectrometry: Principles and Applications*, Oxford University Press, New York, 1989.
64. S.J. Chua, L. Ke, R.S. Kumar, and K. Zhang, Stabilization of electrode migration in polymer electroluminescent devices, *Appl. Phys. Lett.*, 81:1119–1121, 2002.
65. A. Ryer, *Light Measurement Handbook*, International Light, Newburyport, MA, 1997.
66. P.A. Keller, *Electronic Display Measurement*, Wiley & Sons, New York, 1997.
67. S. Sherr, *Electronic Display*, 2nd ed., Wiley & Sons, New York, 1993, pp. 1–78.
68. R.S. Berns, *Billmeyer and Saltzman's Principles of Color Technology*, 3rd ed., Wiley & Sons, New York, 2000.
69. I.S. Millard, High-efficiency polyfluorene polymers suitable for RGB applications, *Synth. Met.*, 111–112:119–123, 2000.
70. Y. Kawamura, S. Yanagida, and S.R. Forrest, Energy transfer in polymer electrophosphorescent light emitting devices with single and multiple doped luminescent layers, *J. Appl. Phys.*, 92:87–93, 2002.
71. G. Hadzioannou and P.F. van Hutten, Eds., *Semiconducting Polymers*, Wiley & Sons, New York, 2000.
72. M. Pope and C.E. Swenberg, *Electronic Processes in Organic Crystals and Polymers*, 2nd ed., Oxford University Press, New York, 1999.
73. N.C. Greenham and R.H. Friend, Semiconductor device physics of conjugated polymers, *Solid State Phys.*, 49:32–62, 1995.
74. P.L. Burn, A.B. Holmes, A. Kraft, D.D.C. Bradley, A.R. Brown, R.H. Friend, and R.W. Gymer, Chemical tuning of electroluminescent copolymers to improve emission efficiencies and allow patterning, *Nature*, 356:47–49, 1992.
75. I.H. Campbell, D.L. Smith, and J.P. Ferraris, Electrical impedance measurements of polymer light emitting diodes, *Appl. Phys. Lett.*, 66:3030–3032, 1995.
76. F. Marai, S. Romdhane, L. Hassine, M. Majdoub, and H. Bouchriha, Static and dynamic electrical investigations on AVB polymer light emitting diodes, *Synth. Met.*, 132:117–122, 2003.
77. H.C.F. Martens and H.B. Brom, Frequency-dependent electrical response of holes in poly(*p*-phenylene vinylene), *Phys. Rev. B*, 60:R8489–R8492, 1999.
78. H.C.F. Martens, J.N. Huiberts, and H.B. Brom, Simultaneous measurement of electron and hole mobilities in polymer light-emitting diodes, *Appl. Phys. Lett.*, 77:1852–1853, 2000.
79. N.C. Greenham, R.H. Friend, and D.D.C. Bradley, Angular dependence of the emission from a conjugated polymer light-emitting diode — implications for efficiency calculations, *Adv. Mater.*, 6:491–494, 1994.
80. A.W. Grice, D.D.C. Bradley, M.T. Bernius, M. Inbasekaran, W.W. Wu, and E.P. Woo, High brightness and efficiency blue light-emitting polymer diodes, *Appl. Phys. Lett.*, 73:629–631, 1998.
81. Y.H. Niu, Q. Hou, and Y. Cao, High efficiency polymer light-emitting diodes with stable saturated red emission based on blends of dioctylfluorene–benzothiadiazole–dithienylbenzothiadiazole terpolymers and poly[2-methoxy,5-(2-ethylhexoxy)-1,4-phenylene vinylene], *Appl. Phys. Lett.*, 82:2163–2165, 2003.
82. W. Zhu, Y. Mo, M. Yuan, W. Yang, and Y. Cao, Highly efficient electrophosphorescent devices based on conjugated polymers doped with iridium complexes, *Appl. Phys. Lett.*, 80:2045–2047, 2002.
83. J.K. Mahon, The OLED technology platform: strengthening the promise, *Adv. Imaging*, June:28–32, 2003.
84. A.J. Campbell, D.D.C. Bradley, and H. Antoniadis, Quantifying the efficiency of electrodes for positive carrier injection into poly(9,9-dioctylfluorene) and representative copolymers, *J. Appl. Phys.*, 89:3343–3351, 2001.

85. M.A. Baldo, A. Lamansky, P.E. Burrows, M.E. Thompson, and S.R. Forrest, Very high-efficiency green organic light-emitting devices based on electrophosphorescence, *Appl. Phys. Lett.*, 75:4–6, 1999.
86. F.C. Chen, G. He, and Y. Yang, Triple exciton confinement in electrophosphorescent polymer light-emitting diodes, *Appl. Phys. Lett.*, 82:1006–1008, 2003.
87. H. Kobayashi, S. Kanbe, S. Seki, H. Kiguchi, M. Kimura, I. Yudasaka, S. Miyashita, T. Shimoda, C.R. Towns, J.H. Burroughes, and R.H. Friend, A novel RGB multicolor light-emitting polymer display, *Synth. Met.*, 111–112:125–128, 2000.
88. Q. Huang, J. Cui, H. Yan, J.G.C. Veinot, and T.J. Marks, Small molecule organic light-emitting diodes can exhibit high performance without conventional hole transport layers, *Appl. Phys. Lett.*, 81:3528–3530, 2002.
89. C. Adachi, M.A. Baldo, M.E. Thompson, and S.R. Forrest, Nearly 100% internal phosphorescent efficiency in an organic light-emitting device, *J. Appl. Phys.*, 90:5048–5050, 2001.
90. R.B. Fletcher, D.G. Lidzey, D.D.C. Bradley, S. Walker, M. Inbasekaran, and E.P. Woo, High brightness conjugated polymer LEDs, *Synth. Met.*, 111–112:151–153, 2000.
91. E. Bellmann, S.E. Shaheen, R.H. Grubbs, S.R. Marder, B. Kippelen, and N. Peyghambarian, Organic two-layer light-emitting diodes based on high-T_g hole-transporting polymers with different redox potentials, *Chem. Mater.*, 11:399–407, 1999.
92. S.A. Carter, J.C. Scott, and P.J. Brock, Enhanced luminance in polymer composite light emitting devices, *Appl. Phys. Lett.*, 71:1145–1147, 1997.
93. K.J. Reynolds, G.L. Frey, and R.H. Friend, Solution-processed niobium diselenide as conductor and anode for polymer light-emitting diodes, *Appl. Phys. Lett.*, 82:1123–1125, 2003.
94. D. Sainova, T. Miteva, H.G. Nothofer, and U. Scherf, Control of color and efficiency of composite light emitting diodes based on polyfluorenes blended with hole-transporting molecules, *Appl. Phys. Lett.*, 76:1810–1812, 2000.
95. T.W. Lee and O.O. Park, The effect of different heat treatments on the luminescence efficiency of polymer light emitting diodes, *Adv. Mater.*, 12:801–804, 2000.
96. M.M. Alam and S. Jenekhe, Polybenzobisazoles are efficient electron transport materials for improving the performance and stability of polymer light emitting diodes, *Chem. Mater.*, 14:4775–4780, 2002.
97. A.J. Bard and L.R. Faulkner, *Electrochemical Methods*, Wiley & Sons, New York, 1980.
98. L.S. Hung and C.H. Chen, Recent progress of molecular organic electroluminescent materials and devices, *Mater. Sci. Eng., R*, 39:143–222, 2002.
99. P.E. Burrows, V. Bulovic, S.R. Forrest, L.S. Sapochak, D.M. McCarty, and M.E. Thompson, Reliability and degradation of organic light-emitting devices, *Appl. Phys. Lett.*, 65:2922–2924, 1994.
100. G. Xu, Fighting OLED degradation, *Inform. Display*, 19:18–21, 2003.
101. C. Cimico, Electro-Optical Characterization of Organic LEDs, *Photonics Spectra*, July: 66–68, 2003.
102. Website: <http://www.photal.co.jp/>
103. H. Aziz, Z. Popvic, S. Xie, A.M. Hor, N.X. Hu, and C. Tripp, Humidity-induced crystallization of tris(8-hydroxyquinoline) aluminum layers in organic light-emitting devices, *Appl. Phys. Lett.*, 72:756–758, 1998.
104. J. McElvain, H. Antoniadis, M.R. Hueschen, J.N. Miller, D.M. Roitman, J.R. Sheats, and R.L. Moon, Formation and growth of black spots in organic light-emitting diodes, *J. Appl. Phys.*, 10:6002–6007, 1996.
105. J.C. Scott, J.H. Kaufman, P.J. Brock, R. DiPietro, J. Salem, and J.A. Goitia, Degradation and failure of MEH-PPV light-emitting diodes, *J. Appl. Phys.*, 79:2745–2752, 1996.
106. M. Fujihira, L.M. Do, A. Koike, and E.M. Han, Growth of dark spots by interdiffusion across organic layers in organic electroluminescent devices, *Appl. Phys. Lett.*, 68:1787–1789, 1996.
107. J.S. Kim, R.H. Friend, and F. Cacialli, Improved operational stability of polyfluorene-based organic light-emitting diodes with plasma-treated indium–tin-oxide anodes, *Appl. Phys. Lett.*, 74:3084–3086, 1999.
108. N.C. Greenham, S.C. Moratti, D.D.C. Bradley, R.H. Friend, and A.B. Holmes, Efficient light-emitting diodes based on polymers with high electron affinities, *Nature*, 365:628–630, 1993.

109. P.E. Burrows, S.R. Forrest, T.X. Zhou, and L. Michalski, Operating lifetime of phosphorescent organic light-emitting devices, *Appl. Phys. Lett.*, 76:2493–2495, 2000.
110. I.D. Parker, Y. Cao, and Y. Yang, Lifetime and degradation effects in polymer light-emitting diodes, *J. Appl. Phys.*, 85:2441–2447, 1999.
111. S. Karg, J.C. Scott, S.R. Salem, and M. Angelopoulos, Increased brightness and lifetime of polymer light-emitting diodes with polyaniline anodes, *Synth. Met.*, 80:111–117, 1996.
112. S.A. Carter, M. Angelopoulos, S. Karg, J. Brock, and J.C. Scott, Polymeric anodes for improved polymer light-emitting diode performance, *Appl. Phys. Lett.*, 70:2067–2069, 1997.
113. S.H. Kim, Y. Chu, T. Zyung, L.M. Do, and D.H. Hwang, The growth mechanism of black spots in polymer EL device, *Synth. Met.*, 111–112:253–256, 2000.
114. S.F. Lim, L. Ke, W. Wang, and S.J. Chua, Correlation between dark spot growth and pinhole size in organic light-emitting diodes, *Appl. Phys. Lett.*, 78:2116–2118, 2001.
115. B.H. Cumpston, I.D. Parker, and K.F. Jensen, *In situ* characterization of the oxidative degradation of a polymeric light emitting devices, *J. Appl. Phys.*, 81:3716–3720, 1997.

11 Patent Position of Emerging Companies in Organic Light-Emitting Materials

Manxue Wang

CONTENTS

11.1 Eastman Kodak	640
11.2 Cambridge Display Technology	644
11.3 Universal Display Corporation	646
11.4 Dow Chemical	646
11.5 Covion	648
11.6 Idemitsu Kosan	649
11.7 DuPont	652
11.8 Summary	653
Acknowledgments	653
References	653

Since a research group at Eastman Kodak [1] reported the discovery of an organic light-emitting diode (OLED) in 1987, more than 100 companies worldwide have directed their research and development resources to explore the attractive attributes of a new generation of OLEDs such as broad viewing angle ($\sim 165\text{--}170^\circ$), lightweight, low driving voltage (5–10 V), high luminous efficiency, a brighter image without backlights ($>100\text{ cd/m}^2$), potentially low cost and long life, and possibly full-color displays. According to the projection of iSuppli/Stanford Resources [2], the fast-growing flat-panel display market, now dominated by liquid crystal display (LCD) and plasma display panel technologies, will lose a significant share to the OLED technology in a few years. There have been challenges to develop better materials for OLEDs. The multiple layer structure of OLEDs requires materials with different functions for each layer, ranging from emitters to hole transporters. However, out of the five layers of materials, light-emitting materials are the most important, yet the most difficult to create, for devices with better color hues and longer lives. Efforts have been made to explore more robust emitters, especially for blue color, before they can compete with LCDs. That is why almost 25% of the OLED patents are on the subject of electroluminescent materials; this is based on the analysis of all the International Patent Classification codes associated with patents dealing with OLED technology in the World Patent Index [3]. A full study of the patent estates of all active participants in OLED technique is beyond the scope of this

chapter. This chapter will focus only on the analysis of the intellectual property (IP) of the seven emerging companies: Eastman Kodak, Cambridge Display Technology (CDT), Universal Display Corporation (UDC), Dow Chemical, Covion, Idemitsu Kosan (IK), and DuPont on the OLED emitting materials. The technology of each of these companies is discussed in more detail below.

11.1 EASTMAN KODAK

Eastman Kodak pioneered the development of small-molecule OLED technology and has been involved in OLED technology since the mid-1980s. It has established a broad base of IP and manufacturing expertise. To form the light-emitting layer, Kodak uses a single component, the organic host material, or a multicomponent material consisting of a host material and one or more components of fluorescent dyes or electron-trapping agents as dopants.

Among the host materials that are suitable for use in forming thin film, the most well-known group from Kodak is metal (Al, Mg, Li, Ga, Zn) complexes of 8-hydroxyquinolate derivatives. The aluminum complex (AlQ, Figure 11.1) alone is also the most commonly used material for emitting green color. Another group claimed by Kodak is benzenoid compounds formed from polycyclic hydrocarbons. The preferred structures are anthracene derivatives such as 9,10-diarylanthracene (Figure 11.2).

Kodak claimed a variety of dopants and approaches for small-molecule OLED devices emitting red, green, blue, and white color. The dopants could be any fluorescent or phosphorescent dyes or pigments. The dyes reported by Kodak include coumarin, dicyanomethylenepyrans and thiopyrans, polymethine, oxybenzanthracene, xanthene, pyrylium and thiapyrylium, carbostyryl, and perylene. Approaches to red OLED devices were to use red fluorescent dopants in the electroluminescent layer, e.g., 4-dicyanomethylene-4*H*-pyran (DCM) derivatives such as DCJTb (Figure 11.3) and DCMM (Figure 11.4), or phthalocyanine derivatives (Figure 11.5) and the corresponding metal complexes.

Examples of green-emitting materials as light emitters are coumarin derivatives such as C-545T (Figure 11.6) or AlQ doped with quinacridone derivatives (Figure 11.7).

Blue emitters have been the most challenging to prepare. Aluminum complexes of mixed ligands of 8-hydroxyquinolate anion (Figure 11.8) or μ -oxo bis-aluminum complexes led to blue-emitting luminescent compositions. Blue dopants containing arylamines, coumarins, stilbenes, distyrylstilbenes, derivatives of anthracene, tetracene, perylene, and other conjugated benzenoids, with a blue host such as 9,10-bis(3',5'-diaryl)phenylanthracene emit in the blue region because the band gap of the host is large enough to affect the energy transfer to these commonly available fluorescent dyes. Other blue-emitting materials comprise benzazoles (Figure 11.9), perylene derivatives, e.g., 2,5,8,11-tetra-*tert*-butylperylene (TBP, Figure

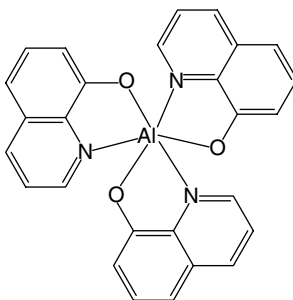


FIGURE 11.1 AlQ.

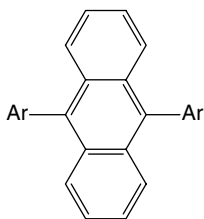


FIGURE 11.2 9,10-Diarylanthracene.

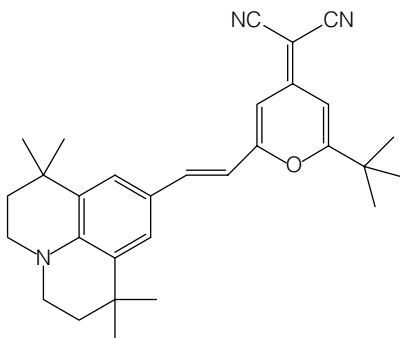


FIGURE 11.3 DCJTB.

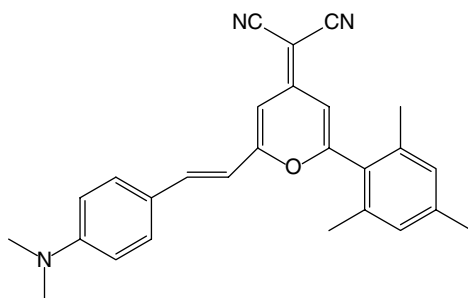
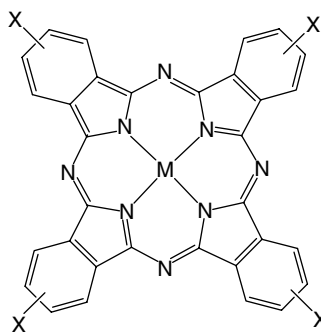


FIGURE 11.4 DCMM.



M = 2H, Mg, Li, Na, Ca, Zn, Al, Ga, In

FIGURE 11.5 Phthalocyanine derivatives.

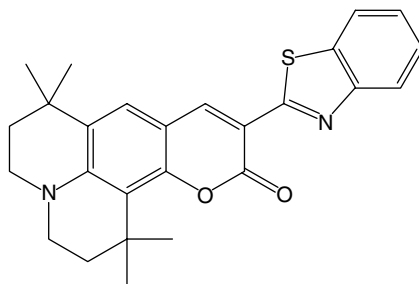


FIGURE 11.6 C-545T.

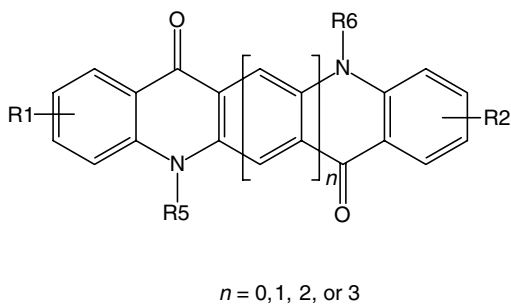


FIGURE 11.7 Quinacridone derivatives.

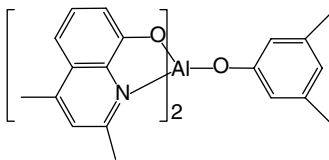
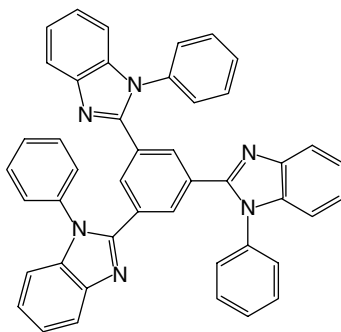
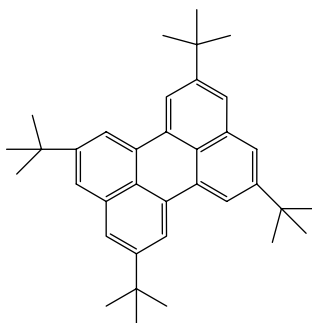
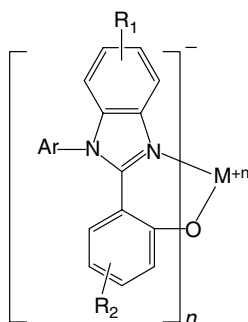
FIGURE 11.8 AlQ₁Q₂.

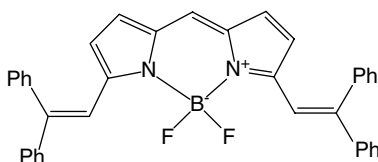
FIGURE 11.9 Benzazoles.

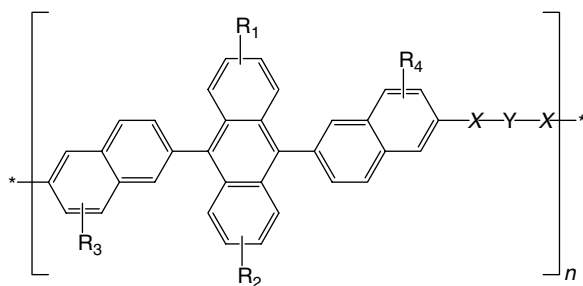
**FIGURE 11.10** TBP.**FIGURE 11.11** Metal complexes of *N*-aryl-2-benzimidazolyphenol.

11.10), and organometallic compounds derived from *N*-aryl-2-benzimidazolyphenol ligands (Figure 11.11).

The methodology to prepare white electroluminescent materials is to use hosts and dopants with complementary colors. One of Kodak's patents claimed white-emitting OLED devices containing a host material emitting blue-green light and a guest component emitting red light. The host materials are aluminum complexes of 8-quinolinolato ligands and the dopants are dipyrromethene difluoroborate complexes (Figure 11.12). Another approach is to combine red and blue fluorescent materials in an appropriate concentration with a single host material in a single layer to emit white light.

Recently, Kodak claimed several new polymeric light-emitting materials. U.S. 6,361,887, claimed polymer light-emitting diode (PLED) devices using 9,10-diarylanthracene-based light-emitting polymers (Figure 11.13 and Figure 11.14). Functionalized 9,10-di-(2-naphthyl) anthracene was polymerized with other monomers through the formation of, e.g., ester, ether, amide, or carbon-carbon bonds, to afford the desired polymeric emitters. In U.S. 6,329,086, PLED devices having arylamine moieties were claimed (Figure 11.15).

**FIGURE 11.12** Dipyrromethene difluoroborate complex.



X: Linking group

Y: Comonomer

FIGURE 11.13 Naphthylanthracene-based polymer.

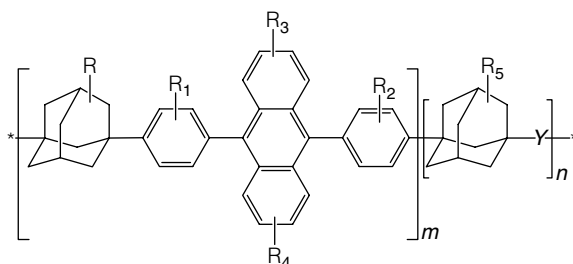


FIGURE 11.14 9,10-Diphenylanthracene-based polymer structure.

Table 11.1 lists the U.S. patent numbers and the titles granted to Eastman Kodak on the OLED emitting materials.

11.2 CAMBRIDGE DISPLAY TECHNOLOGY

CDT, based in Cambridge, U.K., was founded after initial work done at the Cambridge University. Researchers in Cambridge discovered that poly(*p*-phenylenevinylene) (PPV, Figure 11.16) and its derivatives can be used as emitters to construct OLEDs, which were the first examples of PLEDs [4]. The invention has brought flat-panel displays to the verge of commercialization.

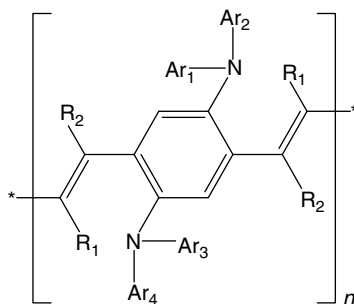


FIGURE 11.15 Triarylamine-based polymer.

TABLE 11.1
Patent Numbers and Titles of the U.S. Patents on the OLED Emitting Materials Granted to Eastman Kodak

Serial No.	PN	Title
1	U.S. 6,361,887	Electroluminescent devices having naphthylanthracene-based polymers
2	U.S. 6,268,072	Electroluminescent devices having phenylanthracene-based polymers
3	U.S. 6,020,078	Green organic electroluminescent devices
4	U.S. 5,972,247	Organic electroluminescent elements for stable blue electroluminescent devices
5	U.S. 5,904,961	Method of depositing organic layers in organic light emitting devices
6	U.S. 5,935,720	Red organic electroluminescent devices
7	U.S. 5,908,581	Red organic electroluminescent materials
8	U.S. 5,755,999	Blue luminescent materials for organic electroluminescent devices
9	U.S. 5,683,823	White light-emitting organic electroluminescent devices
10	U.S. 5,645,948	Blue organic electroluminescent devices
11	U.S. 5,593,788	Organic electroluminescent devices with high operational stability
12	U.S. 5,554,450	Organic electroluminescent devices with high thermal stability
13	U.S. 5,550,066	Method of fabricating a TFT-EL pixel
14	U.S. 5,409,783	Red-emitting organic electroluminescent device
15	U.S. 5,405,709	White light emitting internal junction organic electroluminescent device
16	U.S. 5,294,870	Organic electroluminescent multicolor image display device
17	U.S. 5,294,869	Organic electroluminescent multicolor image display device
18	U.S. 5,151,629	Blue emitting internal junction organic electroluminescent device (I)
19	U.S. 5,150,006	Blue emitting internal junction organic electroluminescent device (II)
20	U.S. 5,141,671	Mixed ligand 8-quinolinolato aluminum chelate luminophors
21	U.S. 5,061,569	Electroluminescent device with organic electroluminescent medium
22	U.S. 5,059,861	Organic electroluminescent device with stabilizing cathode capping layer
23	U.S. 5,047,687	Organic electroluminescent device with stabilized cathode
24	U.S. 4,769,292	Electroluminescent device with modified thin film luminescent zone
25	U.S. 4,885,211	Electroluminescent device with improved cathode
26	U.S. 4,720,432	Electroluminescent device with organic luminescent medium
27	U.S. 4,539,507	Organic electroluminescent devices having improved power conversion efficiencies
28	U.S. 4,356,429	Organic electroluminescent cell
29	U.S. 4,973,694	Benzofuran dyes containing a coumarin nucleus
30	U.S. 4,950,950	Electroluminescent device with silazane-containing luminescent zone
31	U.S. 4,948,893	Novel benzofuran dyes
32	U.S. 4,900,831	Novel benzofuran dyes

Polymeric materials invented by CDT are conjugated homo- or copolymers. Examples are poly(arylenevinylene)s, $[\text{ArCR}_1=\text{CR}_2]_n$, polymers with triarylamine and triazine groups (Figure 11.17), and fused thiophenes as structural repeating units (Figure 11.18).

A blue light-emitting electroluminescent device was claimed with an emission layer comprising a polymer matrix and a chromophoric component, which was either blended with or covalently attached to the polymer matrix. The chromophoric components were

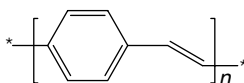


FIGURE 11.16 PPV.

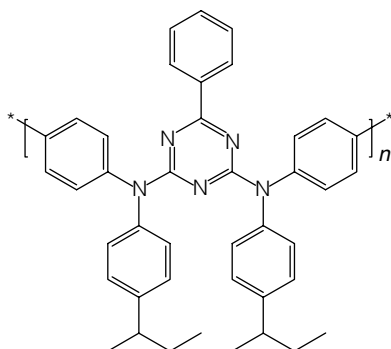


FIGURE 11.17 Polymer with triazine and triarylamine moiety.

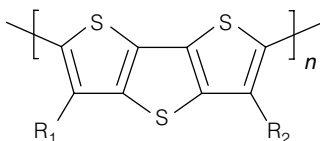


FIGURE 11.18 Polymers derived from fused thiophenes.

selected from stilbene or distyrylbenzene and the polymer matrix can be poly(methylmethacrylate), polycarbonate, or polystyrene.

In October 2002, CDT acquired the OLED technology from Oxford-based Opsys, which is known for its dendritic materials development. As of July 2003, no patents have been granted to Opsys.

Table 11.2 lists the U.S. patent numbers and the titles granted to CDT on the OLED emitting materials.

11.3 UNIVERSAL DISPLAY CORPORATION

UDC, founded in 1994, is located in Ewing, New Jersey since 1999. It has collaborated with researchers from Princeton University and the University of Southern California to develop OLED technology. Although there are only six U.S. patents granted to UDC as of July 2003, it has built one of the strongest IP portfolios in the area of OLEDs through licensing patents from Motorola, Princeton University, and the University of Southern California. It has developed electrophosphorescent dopants based on metalloporphyrins (Figure 11.19), which will potentially improve the power conversion efficiency by threefold compared to the widely used fluorescent dopants.

The U.S. patents granted to UDC are listed in Table 11.3.

11.4 DOW CHEMICAL

Dow used the Suzuki coupling process to synthesize a variety of fluorene-based homopolymers and copolymers that are able to emit the three primary LED colors: red, green, and blue. Structural representations of these polymers are shown in Figure 11.20. The U.S. patents granted to Dow Chemical on OLED emitting materials are listed in Table 11.4.

TABLE 11.2
Patent Numbers and Titles of the U.S. Patents on the OLED Emitting Materials
Granted to CDT

Serial No.	PN	Title
1	U.S. 6,559,256	Polymers for use in optical devices
2	U.S. 6,512,082	Polymers, their preparation and uses
3	U.S. 6,498,049	Display devices
4	U.S. 6,423,428	Conjugated copolymers for use in luminescent devices
5	U.S. 6,403,809	Compounds for electronic devices
6	U.S. 6,395,328	Organic light emitting diode color display
7	U.S. 6,340,732	Conjugated polymers
8	U.S. 6,353,072	Polymer preparation from boron derivative functional group-containing monomers
9	U.S. 6,340,732	Conjugated polymers
10	U.S. 5,965,979	Manufacture of organic light emitting devices
11	U.S. 5,807,627	Electroluminescent devices
12	U.S. 5,747,182	Manufacture of electroluminescent devices
13	U.S. 5,653,914	Electroluminescent device comprising a chromophoric polymeric composition
14	U.S. 5,514,878	Polymers for electroluminescent devices
15	U.S. 5,672,678	Semiconductive polymers for use in luminescent devices
16	U.S. 5,512,654	Semiconductive polymers for use in luminescent devices
17	U.S. 5,425,125	Optical device incorporating semiconductive conjugated polymer
18	U.S. 5,401,827	Semiconductive polymers for use in luminescent devices
19	U.S. 5,399,502	Method of manufacturing of electroluminescent devices
20	U.S. 5,328,809	Patterning of semiconductive polymers
21	U.S. 5,247,190	Electroluminescent devices

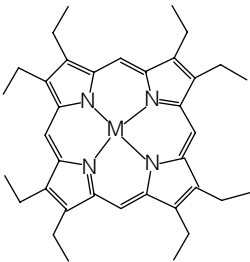


FIGURE 11.19 Typical metal complex of octaethylporphyrin.

TABLE 11.3
Patent Numbers and Titles of the U.S. Patents Granted to UDC

Serial No.	PN	Title
1	U.S. 6,597,111	Protected organic optoelectronic devices
2	U.S. 6,596,443	Mask for patterning devices
3	U.S. 6,576,351	Barrier region for optoelectronic devices
4	U.S. 6,569,697	Method of fabricating electrodes
5	U.S. 6,537,688	Adhesive sealed organic optoelectronic structures
6	U.S. 6,407,408	Method for patterning devices

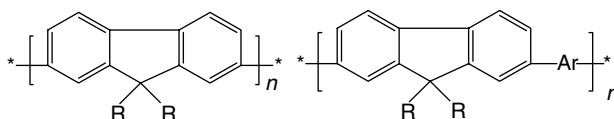


FIGURE 11.20 Fluorene-based homopolymers and copolymers.

TABLE 11.4
Patent Numbers and Titles of the U.S. Patents on the OLED Emitting Materials Granted to Dow Chemical

Serial No.	PN	Title
1	U.S. 6,593,450	2,7-Aryl-9-substituted fluorenes and 9-substituted fluorene oligomers and polymers
2	U.S. 6,353,083	Fluorene copolymers and devices made therefrom
3	U.S. 6,309,763	Fluorene-containing polymers and electroluminescent devices therefrom
4	U.S. 6,255,449	Fluorene-containing polymers and compounds useful in the preparation thereof
5	U.S. 6,255,447	2,7-Aryl-9-substituted fluorenes and 9-substituted fluorene oligomers and polymers
6	U.S. 6,169,163	Fluorene-containing polymers and compounds useful in the preparation thereof
7	U.S. 5,962,631	2,7-Aryl-9-substituted fluorenes and 9-substituted fluorene oligomers and polymers
8	U.S. 5,948,552	Heat-resistant organic electroluminescent device
9	U.S. 5,777,070	Process for preparing conjugated polymers
10	U.S. 5,708,130	2,7-Aryl-9-substituted fluorenes and 9-substituted fluorene oligomers and polymers

11.5 COVION

Covion, existing since 1992, originated from Hoechst AG's central research and development project and was established as a single lawful entity on April 1, 1999. It is now 100% owned by Avecia since January 1, 2002. Covion focuses on organic semiconductor materials, and the majority of light-emitting materials they develop are polymers. Partially conjugated polymers from Covion are either poly(spirobifluorene) (Figure 11.21) or polymers having fused nitrogen-containing heterocycle and arylenevinylene moieties (Figure 11.22). Ordered poly(arylenevinylene) terpolymers (Figure 11.23), and also poly(arylenevinylene) with good solubility properties in organic solvents (Figure 11.24), were claimed. Covion also claimed nonpolymeric 9,9'-spirobifluorene derivatives with good solubility and improved film-forming properties (Figure 11.25) as electroluminescent materials. The U.S. patents granted to Covion on OLED technology are listed in Table 11.5.

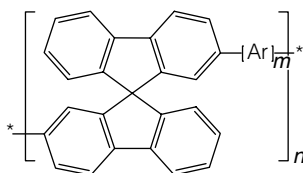


FIGURE 11.21 Poly(spirobifluorene).

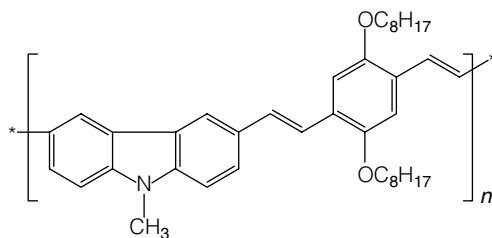


FIGURE 11.22 Polymer having fused nitrogen-containing heterocycle.

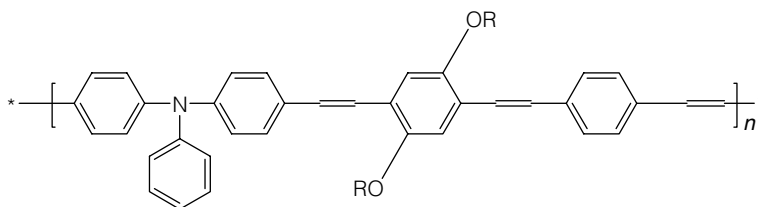


FIGURE 11.23 Poly(arylenevinylene) terpolymer with triarylamine moiety (generic).

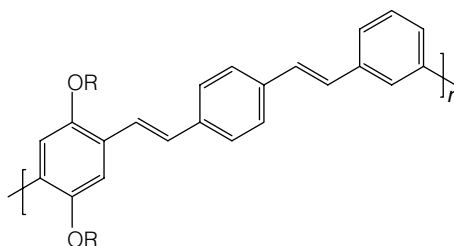


FIGURE 11.24 Poly(arylenevinylene) (generic).

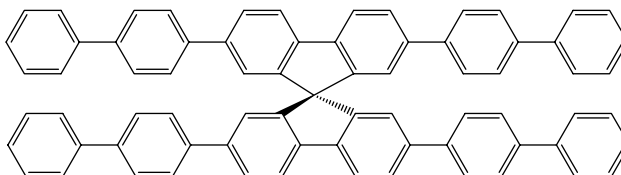


FIGURE 11.25 9,9''-Spirobifluorene derivative.

11.6 IDEMITSU KOSAN

The Japanese company IK has developed a wide variety of methodologies to improve color purity, lifetime, luminous brightness, and luminous efficiency, etc. IK uses either single-component or multicomponent materials in the electroluminescent layer. For single-component materials, the commonly used emitting materials are fused benzene rings such as anthracene derivatives (Figure 11.26), pentacene (Figure 11.27), or stilbene-based compounds (Figure 11.28), or heterocyclics such as an oxadiazole or thiadiazole compound (Figure 11.29), or a

TABLE 11.5
Patent Numbers and Titles of the U.S. Patents Granted to COVION

Serial No.	PN	Title
1	U.S. 6,476,265	Method for producing aryl oligoamines
2	U.S. 6,414,431	Thin film electrode for planar organic light-emitting devices and method for its production
3	U.S. 6,361,884	Partially conjugated polymers with spiro centers and their use as electro-luminescent materials
4	U.S. 6,316,591	Ordered poly(arylenevinylene) terpolymers, method for the production and the use thereof as electroluminescent materials
5	U.S. 6,040,069	Electroluminescence device with emission of polarized light
6	U.S. 5,874,179	Nitrogen-containing polymers as electroluminescent materials
7	U.S. 5,840,217	Spiro compounds and their use as electroluminescence materials

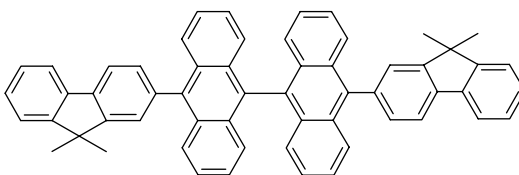


FIGURE 11.26 Anthracene derivative.

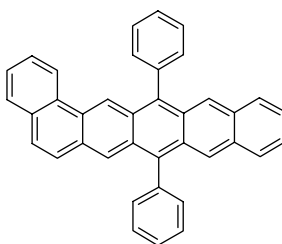


FIGURE 11.27 Pentacene derivative.

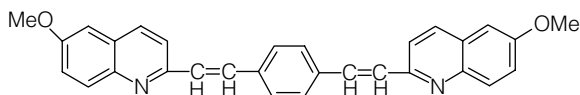


FIGURE 11.28 Stilbene derivative.

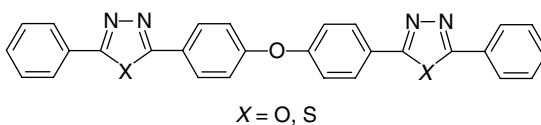


FIGURE 11.29 Oxadiazole or thiadiazole derivative.

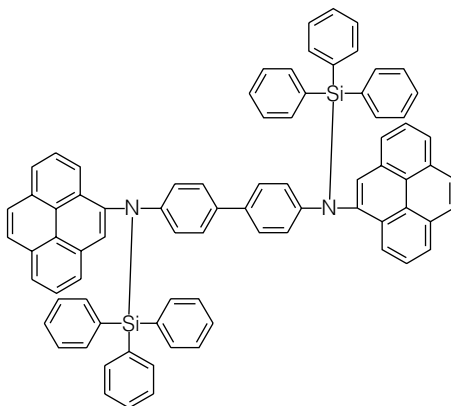


FIGURE 11.30 Silanamine derivative.

silanamine compound with substituted arylene substituents (Figure 11.30). It also used AIQ dimer and a dimerized or oligomeric styryl compound (Figure 11.31). For multicomponent materials, one of the components is one of the above-mentioned materials. Other components in the multicomponent emitting materials can be a reducing dopant such as Li, a fluorescent substance, or a charge injection assistant to improve the charge injection property of the device. To reduce production process cycle time, a light-emitting layer comprising one ingredient with both electronic carrier units and hole carrier units and another ingredient as the recombination site-forming substance is used. IK also claimed multiple emitting-layer methods. When stilbene or distyryl derivatives were used in the emitting layer, the metal chelates of an oxine such as metal complexes of 8-hydroxyquinoline derivatives were added as another layer functioned as the adhesion-improving layer. A device with two or more organic light-emitting layers using distyrylarylene doped with a fluorescent material of the same type or color as emitting materials was claimed. IK claimed use of a fluorescence transformation medium or membrane to convert the color emitted from the OLED to another color and the use of this technique for multicolored display devices. For example, a red-color light-emitting element was obtained using red-color fluorescence conversion film and a blue-emitting organic electroluminescence element. Coloring materials employed that are able to convert one color to another were stilbene-type or coumarin-type coloring matters, which transform ultraviolet or violet light into blue light; coumarin-type or Basic Yellow for transformation of blue into green; and cyanine-type, pyridine-type, xanthene-type, or other fluorescent dyes for transformation of blue to green light into orange to red light.

IK also claimed polymeric emitting materials comprising a polyimide, polyamideimide, polyurea, or polyazomethine with a dye component such as phthalocyanine, porphyrin, triphenylamine, oxadiazole moieties; or polycarbonate with a diarylvinylene arylene skeleton or styrylamine core.

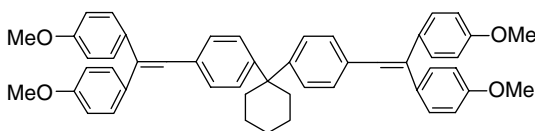


FIGURE 11.31 Styryl compound.

TABLE 11.6
Patent Numbers and Titles of the U.S. Patents on the OLED Materials Granted to Idemitsu Kosan

Serial No.	PN	Title
1	U.S. 6,541,129	Organic electroluminescence device and phenylenediamine derivative
2	U.S. 6,534,199	Organic electroluminescence device and organic light emitting medium
3	U.S. 6,515,182	Arylamine compound and organic electroluminescence device
4	U.S. 6,509,109	Organic electroluminescent device
5	U.S. 6,489,489	Organic electroluminescent device
6	U.S. 6,489,046	Organic electroluminescence device
7	U.S. 6,486,601	Organic luminescence device with reduced leakage current
8	U.S. 6,464,898	Fluorescence conversion medium and display device comprising it
9	U.S. 6,455,176	Fluorescence-reddening membrane and red-emitting device using same
10	U.S. 6,416,888	Organic electroluminescent device and method of manufacture thereof
11	U.S. 6,406,804	Organic electroluminescent device
12	U.S. 6,224,966	Organic electroluminescent device
13	U.S. 6,221,517	Fluorescence-reddening membrane and red-emitting device
14	U.S. 6,214,481	Organic electroluminescent device
15	U.S. 6,124,024	Organic electroluminescent device
16	U.S. 6,074,734	Organic electroluminescence device, organic thin film, and triamine compound
17	U.S. 5,891,554	Organic electroluminescence device
18	U.S. 5,837,166	Organic electroluminescence device and arylenediamine derivative
19	U.S. 5,705,284	Thin film electroluminescence device
20	U.S. 5,536,949	Charge injection auxiliary material and organic electroluminescence device containing the same
21	U.S. 5,516,577	Organic electroluminescence device
22	U.S. 5,505,985	Process for producing an organic electroluminescence device
23	U.S. 5,466,392	Organic electroluminescence device and compound having an aluminum complex structure
24	U.S. 5,443,921	Thin film electroluminescence device and process for production thereof
25	U.S. 5,427,858	Organic electroluminescence device with a fluorine polymer layer
26	U.S. 5,389,444	Organic electroluminescence device
27	U.S. 5,366,811	Organic electroluminescence device
28	U.S. 5,358,788	Organic electroluminescence device containing a silanamine compound
29	U.S. 5,336,546	Organic electroluminescence device
30	U.S. 5,307,363	Organic optical gain device and method of exciting the same
31	U.S. 5,126,214	Electroluminescent element
32	U.S. 5,121,029	Electroluminescence device having an organic electroluminescent element

Table 11.6 lists the U.S. patent numbers and the titles granted to Idemitsu Kosan on the OLED materials.

11.7 DUPONT

DuPont is an active player in OLED technology. Polymers used in devices as emitting materials are poly(*p*-phenylenevinylene), poly(arylenevinylene)s, poly(*p*-phenylene), poly(arylene)s, polyquinolines, and polyfluorenes. In some cases, an anionic surfactant such as lithium nonylphenoxy ether sulfate was added to the above-mentioned polymeric emitters

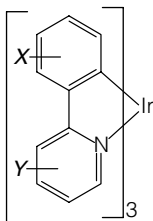


FIGURE 11.32 2-Arylpolyrpyridine ligands

to improve the electrical properties of the polymers. It has a few patent applications using organometallics having 2-arylpolyrpyridine ligands (Figure 11.32) as emitters. An example is in the Patent Cooperative Treaty (PCT) application (WO 2002002714) using electroluminescent iridium compounds with fluorinated phenylpyridines, phenylpyrimidines, and phenylquinolines.

11.8 SUMMARY

This study concentrates only on patents directly issued to Eastman Kodak, CDT, UDC, Dow Chemical, Covion, IK, and DuPont without the consideration of patent reassignments. If licensed patents are taken into account, the patent landscape of these companies will change significantly. The patents listed for each company are only a part of the IP portfolio in the OLED arena.

ACKNOWLEDGMENTS

The author is grateful to Edward S. Wilks and Olga Grushin for their help and their valuable comments.

REFERENCES

1. Tang, C.W. and VanSlyke, S.A., Organic electroluminescent diodes, *Appl. Phys. Lett.*, 51:913–915, 1987.
2. *Chemical & Engineering News*, August 26, 2002, p. 10.
3. Wang, M. Unpublished results.
4. Burroughes, J.H., Bradley, D.D.C., Brown, A.R., Marks, R.N., Mackay, K., Friend, R.H., Burns, P.L., and Holmes, A.B., Light-emitting diodes based on conjugated polymers, *Nature*, 347:539–541, 1990.

Index

A

- Absorption, linearly polarized, 451, 457
- Achiral dyes, 471–472
- ACPEL technology, *see* Alternating current phosphor electroluminescent displays
- Active matrix liquid crystal display (AMLCD), 17–18
- Active matrix organic light-emitting diode (AMOLED)
 - display panel, 30
 - displays, emitting pixels in, 28
 - for graphic and motion picture applications, 34–35
 - monochrome, 28
 - performance simulation for full-color, 32–34
 - power consumption of, 33–34
- Adhesion layer, 460
- ADN, blue host, 337, 356–357, 366, 420
- Aggregate formation, in LPPP, 223
- Aggregation, 59, 158
 - prevention of, 337, 541
 - in solid state, 90–91, 157, 173, 175, 222, 346
 - in solution, 59, 158
- Alignment
 - layers, 461–468, 470
 - near surface, 461
 - techniques, 470
 - uniaxial, 452, 456
- Alkoxy-substituted PPV, 58–62
 - dihexyloxy substituted PPV (DH-PPV), 58–59
 - methoxy/2-ethylhexyloxy (MEH-PPV), 59–60
 - monoalkoxy-PPV, 61
 - oligoethyleneoxy-substituted PPV, 62
 - (*S*)-2-methylbutoxy- substituted PPV, 60–61
 - tetraalkoxy-substituted PPV, 61
- Alkyl-substituted PPVs, 62–63
- ALQ, 640
- Alq₃, chemical structure of, 419
- Alternating current phosphor electroluminescent (ACPEL) displays, 579–580
- Alternating PF copolymers, 146–148
 - color tuning in, 160–169
 - with spiro-bifluorene moiety, 155
- Aluminum-doped zinc oxide (AZO), 302, 483, 504–507, 521
- Ambipolar device, 143
- America Organic Semiconductor, LLC, 297
- AMOLED, *see* Active matrix organic light-emitting diode
- AMPLED, cross-section views of the device structures of, 28
- Anionic copolymerization, 57
- Anionic ether sulfates, 23
- Anisotropy
 - factor, 456, 473
 - optical, 456, 458, 461–462, 464
- Annealing of polymer film, 124
- Anode materials, 521
 - for OLEDs, 302–303
- Anode modification for enhancing OLED performance
 - color tuning with graded indium tin oxide thickness, 502–504
 - indium tin oxide surface treatment and modification, 494–502
 - non-indium tin oxide anode for OLEDs, 504–507
- Antisymmetric excitons, 6
- Aperture ratio, 30, 32, 548, 596
- Arbitrary multilayer thin-film system, 519
- Architecture, helical supramolecular, 471
- Aromatic ring-substituted PFs, 128–129
- Arrangement, helical, 471
- Aryl-substituted PPVs, 64–69
- a-Si:H TFT AM-PLEDs
 - 3- and 4-a-Si:H TFTs AM-PLEDs fabrication steps, 595–596
 - 100 DPI current-driven 4-a-Si:H TFTs AM-PLED, 606–611
 - 200 DPI current-driven 4-a-Si:H TFTs AM-PLED, 611
 - 200 DPI voltage-driven 3-a-Si:H TFTs AM-PLED, 611–614
- a-Si:H TFT pixel electrode circuits for AM-OLEDs
 - current-driven 4-a-Si:H TFTs pixel electrode circuits, 592–595
- a-Si:H TFT pixel electrode circuits for AM-OLEDs

voltage-driven 3-a-Si:H TFTs pixel electrode circuits, 588–592
 voltage-driven 1- or 2-a-Si:H TFTs pixel electrode circuits, 584–588
 Aspect ratio, 457, 464–465, 468
 Au2MDP, chemical structure of, 427

B

Balancing charge transport/injection, 71, 170, 177–178, 334, 420–421
 Band-gap
 control of, 190
 in PTs, 190
 effect of structure on, 7, 200
 electrochemical, 333–334
 optical, 118
 of PPVs, 63
 substituents effect on, 63
 very low, 201–202
 Benzazoles, 642
 Benzothiazoles, 464
 Beryllium chelate, electron transport, 326
 Binaphthyl, 89, 158, 208, 210, 220
 Binaphthyl-linked thiophene block copolymers, 208, 210
 Bipolar host, 333
 Bis(2-(2-hydroxyphenyl)benzothiazolate)zinc (II) Zn(BTZ)₂, 326, 368
 Bis(2-(2-hydroxyphenyl)-pyridine)beryllium (Beq₂), electron transport, 326
 Bis-(8-hydroxyquinoline)zinc (II) (Znq₂), 326
 4,4'-bis[*N*-(1-naphthyl-1)-*N*-phenyl-amino]-biphenyl (α-NPD), hole transport, 312–313
 4,4'-bis[(*p*-methyloxysilylpropyl-phenyl)phenylamino]biphenyl (TPD-Si₂OMe), self-assemble hole transport, 307
 4,4'-bis[(*p*-trichlorosilylpropyl-phenyl)phenylamino]biphenyl (TPD-Si₂Cl), self-assemble hole transport, 307
 Black spot formation, 578
 Blending, of polymers, 422, 439–440
 with dialkoxy-PPV, 211, 213
 in LPPP, 223
 MEH-PPV, 59–60
 in PFs, 144–145
 Blend system, energy transfer mechanism in, 425
 Block copolymers, 92–97, 159–160, 199–200, 210, 220
 binaphthyl-linked thiophene, 208, 210
 of conjugated PPVs, 92–97
 light-emitting thiophene, with conjugation break, 199–200
 of PPVs, 95

Blodgett, 457
 Blue dopants, 640
 Blue emissions, 4, 17, 85, 91, 124–133, 137, 141–142, 146, 151, 153, 155–159, 351, 354, 356–358, 369, 386, 438, 441, 466, 469, 528, 550
 in polyfluorenes, 124–128
 in PPVs, 64, 85
 Blue emitters, 7
 Blue-emitting materials, 640
 Blue fluorescent emitters
 anthracene series, 355–358
 aromatic amine blue emitters, 362
 distyrylarylene series, 350–355
 heterocyclic compounds, other, 358
 metal chelates, 363–365
 organosilicon blue emitters, 362–363
 spiro-linked blue emitters, 358–362
 Blue phosphorescent dopants, 377–379
 phenylpyrazole complexes, 378–379
 phenylpyridine complexes, 377–378
 Boron-containing LEP polymers, 242–244
 BpyRe, chemical structure of, 422
 Brightness, display, 543, 545, 557
 Btp₂Ir, chemical structure of, 422

C

Calcium acetylacetonate, 311–312
 Calcium (Ca), 57
 electrode, 459
 Cambridge Display Technology (CDT), 47, 64, 124, 164, 310, 640, 644–646, 653
 Candela (cd), 625
 Carbazole
 -containing LEP polymers, 228–233
 substituted PF copolymers, 146–147
 Carbazole-3,6-diyl polymers, chemical structure of, 437
 4,4'-bis(9-carbazoyl)-biphenyl (CBP), hole transport host, 335–337, 380
 Carrier-confining layers, 187
 Carrier mobility, 6, 16, 199, 203, 488, 493, 627
 Cathode interfacial materials, for OLEDs, 309–310
 Li/Cs dopant with BCP and Li-quinolate complexes, 311
 LiF, CsF, 310
 M₂O, 310–311
 organic polymer surfactants, 311–312
 Cathode materials, 420
 for OLEDs, 301–302
 Cesium fluoride (CsF), 81, 230, 310–311, 420–421
 Chain rigidities, 457
 Charge density, 16, 626

- Charge injection, 10, 13, 22, 303, 305, 307, 336, 374, 384, 386, 414, 420, 528, 531, 534, 537–538, 568, 571, 627, 651–652
- Charge recombination, 301, 317, 462
- Charge transport, 312, 317, 331, 336, 362, 417, 420–421, 528, 531, 537–538, 541–542
- Charge trap, 353, 382
- Chemical oxidative polymerization, 185–187
- Chemical vapor deposition (CVD), for PPVs, 53
- Chiral matrices, 471–472
- Chiral nematic liquid crystals (CNLC), 471
- Chlorine precursor route (CPR), 56, 247–248
- Chromaticity diagram, PPLEd, 433, 625
- CIE color coordinates, 13, 17, 355–356
- Circularly polarized luminescence, 470–471
- from achiral dyes doped in chiral matrices, 471–472
 - from conjugated polymers, 472–474
 - other systems, 474
- CNLC, *see* Chiral nematic liquid crystals
- Color-from-blue approach, 33
- Color instability, 124, 140, 161
- Color space, 625
- Color stability of polymer, 128, 139–140, 147, 161
- Color tuning, 98, 159, 175, 181, 192, 214, 374, 427, 502–504
- in light-emitting thiophene homopolymers, 192–199
 - in PFs
 - doping with low molar-mass fluorescent dyes, 159–160
 - random (statistical) copolymers, 169–177
 - with three or more comonomer units, 177–178
 - in PPV block copolymers, 95
- Communication systems, 452
- Comonomers, chemical structure of, 439
- Composite hole transport material, 317, 319
- Conductive nanorods, 573
- Conjugated polymer(s), 2
- molecular structures of, 3
 - in PLED, 4–9
- Conjugated polymers as host materials
- polycarbazoles, 436–438
 - polyfluorenes, 428–432
 - poly(*P*-phenylenes), 432–436
 - polythiophenes, 438
- Conjugated PPVs
- block copolymers, 92–97
 - with twists, meta-links, and sp-hybridized atoms in backbone, 89–92
- Conjugation
- break, by meta-linkage, 150
 - break, by saturated moiety, 344
 - break, by twist, 89–90
 - effective length of, 89–90, 93, 97, 120–121, 158, 173, 184, 188, 190–192, 199–200, 203, 210, 213, 239
 - effect of, 89–97
- Conjugation chain, regularity in, 55
- Contrast ratio, 32, 518, 588
- Copper phthalocyanine (CuPc), 305–306, 539
- Coumarin, 339, 464, 541–542, 550
- dye, green dopant, 339
- Covion 647–648, 650
- Covion PDY, 13, 16
- CY film, optical absorption, photoluminescence and electroluminescence (circle) of, 14
 - luminous efficiency, 15
 - operation lifetimes of two PLEDs made with, 17
- CP emission, 453, 471, 474
- CPR, *see* Chlorine precursor route
- Cross-linkable triarylamine polymer, 145
- Cross-linked PF, 139, 141–142
- Cross-linking, 307, 317, 464
- Crystallinity, of polymers, 328, 464, 485
- Crystals, inorganic, 451
- C-545T, green fluorescent dopant, 339–343
- Cu4MDP, chemical structure of, 427
- Current density voltage luminance, 506, 537, 626
- Current ON/OFF ratio, 596
- Current-voltage transfer characteristic, 603
- CV, *see* Cyclic voltammetry
- CVD, *see* Chemical vapor deposition
- Cyclic voltammetry (CV), 51, 330, 632
- Cyclodextrin rings, 88
- Cyclophane moiety, in PF copolymers, 158–159
- ## D
- Data storage
- optical, 452, 471
 - systems, 472
- DB1
- asymmetric blue dopant, 353–354
 - deep blue, 353–354
- DCJ, red fluorescent dopant, 343–344
- DCJTB, 641
- red fluorescent dopant, 344–346, 366, 383–385, 391
- DCM
- chemical structure of, 422
 - red fluorescent dopant, 343–346, 366, 382–383
- DCMM, 641
- Defects in a polymer
- fluorenone type, 124–128
 - ketone type, 222–223
 - keto type, 126

- non-conjugated, 92
 - tolane-bisbenzyl (TTB)-type, 55, 65–67, 75
 - Deformation, pseudoaffine, 458
 - Degradation, 23, 377, 385, 394
 - intrinsic, 632
 - OLEDs, 385, 394, 535, 537, 545
 - Dendrimers, electrophosphorescent, 443–444
 - Dendron-containing monomer, 130–131
 - synthesis, 130
 - Dendrons and dendrimers, 365, 389, 415, 420, 427, 431, 433–434, 441, 463, 470, 528, 540, 542, 569
 - Device architecture, of OLEDs, 568–569
 - Device efficiency, 11, 312, 328, 365, 528, 541–542
 - with CuPc, of OLED, 305
 - PPLED, 443–444
 - Device fabrication
 - alternative organic deposition techniques, 536
 - anode preparation, 532–533
 - deposition of cathode, 536
 - deposition of organic layers, 533–536
 - encapsulation of organic light-emitting device, 537
 - Device instability, 134
 - Device lifetime, 2, 303, 306–307, 384, 392, 537, 539
 - Device operation
 - encapsulation of organic light-emitting device, 537–539
 - improved efficiency through doping, 542–543
 - improving device efficiency, 540
 - improving internal quantum efficiency, 541–542
 - improving power efficiency, 543
 - lifetime, 545
 - outcoupling, 543–545
 - Device stability, 60
 - Dexter, energy transfer, 7, 332, 415–417, 428, 435, 444
 - process, 416–417
 - Diaminoanthracene, green fluorescent dopant, 341–342
 - 9,10-Diarylanthracene, 641
 - Dichroic ratio, 119, 456, 462, 465, 467–468, 458459
 - linear, 456
 - polarized EL, 468
 - Diels–Alder reaction, 64
 - 3,7-Dimethyloctyl group, substitution in PPV, 60
 - Diphenyldi(o-tolyl)silane (UGH1), host, 336
 - 4,7-Diphenyl-1,10-phenanthroline (Bphen), hole blocking, 311
 - Displays, stereoscopic, 471
 - Display technology, flat panel, 25, 452
 - Dissymmetry factor, 456, 472–474
 - Distyrylarylene (DSA)
 - amino-substituted, 351
 - blue fluorescent, 350, 550
 - host, 350
 - Distyryl-based compound, blue host, 337
 - Dopants, ionic, 569
 - Dow Chemicals, 123–124, 129, 142, 149, 164, 259, 646
 - Drive voltage, 310, 531, 543, 588
 - Dual beam (DB) microscopy, 620
 - Dual-carrier thin-film devices, 12
 - Dual-function utility of MEH-PPV device, 21
 - DuPont, 25–26, 29–30, 35, 297, 365, 372, 652–653
 - Dyes, doping with low molar-mass fluorescent, 159–160
- ## E
- Eastman Kodak, 640–645
 - EHO-OPPE, 458–460
 - EHO-PPP, chemical structure of, 434
 - EL, *see* Electroluminescence
 - Electrical properties and stabilities of the a-Si:H TFTs, 596–601
 - Electrical properties of the a-Si:H TFT pixel
 - electrode circuits
 - current-driven 4-a-Si:H TFTs pixel electrode circuit, 603–605
 - optoelectronic characteristics of current-driven 4-a-Si:H TFTs pixel electrode circuit, 605–606
 - voltage-driven 3-a-Si:H TFTs pixel electrode circuit, 601–603
 - Electrical short, 306, 533
 - Electric conductivity, temperature dependence of, 9
 - Electric field
 - components, 454
 - vector, 454–455
 - Electrode's work function, 13
 - Electroluminescence (EL), 1, 6, 297, 528, 538, 541–543
 - in light emitting thiophene homopolymers, 187
 - linearly polarized, 452, 457–469
 - phenomenon, discovery of, 1
 - polarized, 119, 456, 650
 - regioregularity effect on, in PT, 187, 190–192
 - spectra, 380, 423, 538
 - spectrum, from PLED, 627
 - Electroluminescence (EL) efficiency
 - in alkyl substituted PPV, 60–61
 - in anthracene substituted PPV, 68
 - electron-withdrawing and donating substituents effect, 70
 - in end-capped PF, 140

- and molecular orbital levels, 69–70
 - in PPV copolymers, 74–76
 - in silyl substituted PPV, 63–64
 - in substituted PPV homopolymers, 57, 60–61
 - Electroluminescent LC polymer architectures, 466
 - Electroluminescent oligothiophenes, 203–204
 - Electrolysis, controlled potential, 57
 - Electromagnetic waves, Maxwell's framework, 454
 - Electromer, 369–370
 - Electron
 - blocking, *fac*-tris(1-phenylpyrazolato-*N*, *C2''*)iridium (III) (Irppz), 389–390
 - blocking material, 300, 382–390
 - donor, 304, 344
 - injecting materials
 - in device architecture, 569
 - print-based OLED manufacturing, 572–573
 - injection, 10–11, 15, 23, 302–305, 309–312, 322, 326, 346, 531, 539
 - barriers, 23
 - material, 304
 - migration, 573, 624
 - mobility, 323–324, 327–329, 386, 539
 - transport, 529, 532, 539–540
 - Electron spectroscopy for chemical analysis (ESCA), 622–623
 - Electron transport, 10–11, 296–300, 322–331, 333–334, 336, 365, 368, 386, 391
 - host, 333–334
 - layer (ETL), 10, 528–529, 537–539, 543
 - in device architecture, 569
 - materials, for OLEDs, 59, 322–323
 - fluorine-substituted electron transport materials, 328–329
 - metal chelate electron transport materials, 323–326
 - 4*n*- π and boron-based electron transport materials, 330
 - oxadiazole and triazole transport materials, 328
 - print-based OLED manufacturing, 572–573
 - silole, 329–330
 - thiophene-*S,S*-dioxides as, 205–207
 - TPBI and N-containing aromatic transport materials, 326–328
 - Electrophosphorescence, photophysical aspects of
 - exciton transfer processes, 415–417
 - singlet–triplet excitons ratio, 414–415
 - Electrophosphorescent dendrimers, 443–444
 - Electrophosphorescent fluorene copolymers,
 - chemical structure of, 443
 - Electropolymerization, 185–187
 - EL in organic material, 1
 - Elliptically polarized, 454–454
 - Emission
 - linearly polarized, 451–453
 - polarization, 456
 - spectrum, 324, 332–333, 344, 353–354, 368, 381, 417, 428, 441, 456, 544, 550
 - Encapsulation, 7, 531, 537, 545, 555, 577–579
 - End-capped polyfluorenes, 139–143
 - with oxadiazole moieties, 142
 - with POSS, 140
 - with styrene group, 141–142
 - with triarylamine moieties, 140, 142
 - End-capping, 55, 59, 128, 134, 139, 141, 146, 175, 178, 244
 - reagents, 55–56
 - Energy barrier, 10, 13, 300, 312–313, 322, 356, 539
 - Energy dispersive spectroscopy, 618
 - Energy efficiency, 452, 555
 - Energy level, 13, 15, 304, 308, 312, 314, 316, 319–320, 322–323, 326, 329, 332–336, 338, 351, 378, 380, 383, 386–387, 390, 430, 539, 630–632
 - Energy of triplet, 320, 333–336, 338, 380, 417, 429–431, 436–438, 444, 542
 - Energy transfer, 332–333, 338, 342, 346, 348–349, 353, 368, 380, 382–383
 - Dexter, 7, 332, 416–417, 428, 435
 - Förster, 7, 351, 417–418, 426–429, 434–435
 - in PF, 160
 - Environmental SEM, 619
 - Epitaxial growth, 470
 - Epitaxial processes, 462
 - ESCA, *see* Electron spectroscopy for chemical analysis
 - ETL, *see* Electron, transport layer
 - Excimers, 340, 369–370, 381–382, 537, 556
 - emission of, 379–380
 - formation, 146
 - Excitons, 6–7, 332, 349, 386, 537, 540–542, 546
 - singlet-to-triplet ratio, 542
 - External quantum efficiency (ECE), 13, 19, 388, 413, 421, 529, 542–545, 556, 629
- F**
- Failure mechanism, 622
 - FeCl₃, 304, 308
 - Field-effect mobility, 588–589, 592–594, 596, 600
 - Films, Langmuir–Blodgett, 464, 536, 547
 - Flat-panel displays
 - AMOLED for graphic and motion picture applications, 34–35
 - full-color AMPLD modules, 30–32

monochrome AMPELEDs made with solution-processible polymers, 29–30

performance simulation for full-color AMOLEDs, 32–34

PMOLED displays *versus* AMOLED displays, 26–29

SMOLEDs and PLEDs as emitter elements in flat-panel displays, 25–26

Flexible OLEDs, electrode for

- on Al-laminated plastic foils, 510–516
- indium tin oxide anode on flexible substrates, 507–509
- on polymer-reinforced ultrathin glass sheets, 510

Flexible plastic display, 550

Flexographic printing, 577

Fluorenone defects, 124–128

Fluorescence, yellow-green, of PPV, 51–52

Fluorescent

- blue dopant, 338
- dopant, 528, 542
- doping, 528
- dyes, low molar-mass, 159–160
- emission, 6, 414
- green dopant, 339–343
- host, 414–415, 444
- lighting, 555
- red dopant, 343–349

Fluorine (F), 99

Fluorine-substituted polymers, 72, 328

Fluorocarbon polymer, 304, 307–308

Förster energy transfer, 7

- mechanism, 417
- in PF, 160

Frenkel excitons, 416

Friction deposition, 457, 461–462

Full-color AMOLEDs, performance simulation for, 32–34

Full-color displays, 2, 4, 12, 25–26, 550–552

G

Gallium arsenide phosphide (GaAsP), 1

Gaq3, 323–324

GE, 464

Gel permeation chromatography (GPC), 99

Gen-5 panel-size panels, 30

Gilch method, 64, 247–248; *see also* Chlorine precursor route

- end-capping modification of, 55
- mechanism of formation of TBB in, 66
- for PPVs, 54–56, 247–248

Glass-transition temperature (T_g), 64, 69, 71–72, 100–117, 132, 135, 137, 141, 145–146,

151–152, 155–157, 161, 220, 312–318, 320, 322–323, 328, 330–331, 337–338, 353, 357, 362, 387, 460, 465, 468, 531

PF copolymers, 146

PF dendrimers, 132

PPV, monosubstituted, 64

Gold (Au), 16, 20, 24, 143, 145, 234, 302, 341, 427, 461, 470, 507, 570, 618, 631

Gravure printing, 577

Green fluorescent dopants

- coumarin dyes, 339
- diaminoanthracene compounds, 341
- heterocyclic green dopants, other, 341–342
- indeno[1,2,3-cd]perylene, 340–341
- metal chelates, 343
- quinacridones, 339–340

Green phosphorescent dopants, 372–375

- benzimidazole iridium complexes, 374–375
- phenyl pyridine iridium complexes, 372–374

Guest-host system, 331–333, 335, 347, 391, 457–458, 464

Guest molecules, 7, 332–333, 336, 415–417, 423, 435, 458

H

Halide scavenger, 371

Handness, 472, 474

Head-to-head (HH) coupling, effect on PT, 187

Heck-coupling polymerization

- of PPV copolymers, 57
- for PPVs, 248–249

Helicenes, 474

Highest occupied molecular orbital (HOMO), 414

High work function, 12, 23, 301, 531

Hole blocking

- BAIq, 11, 324–325, 331, 334, 340–341, 351, 377, 389
- BCP, 348, 356, 358, 360, 369–370, 375, 379–381, 386–391, 393
- boron compounds, 387
- material, 298, 300, 334, 386–389

Hole conductor, 312

Hole injection, 8, 10–11, 297, 300, 302–312, 322, 390, 539

- materials, 300, 303–312, 540
- for print-based OLED manufacturing, 569–570
- materials, for OLEDs, 303–304
- conducting polymers, 305–306
- doping the hole transport materials, 308–309
- fluorocarbon polymers, 307–308
- inorganic hole injection materials, 308
- organic–inorganic interface, 304–305

- porphyrinic metal complexes, 305
 - SAM-TPD, 307
 - Hole injection layer (HIL), 528, 532
 - Hole migration, 301
 - Hole mobility, 314, 320, 323, 384, 539
 - Hole transport, 10–11, 296–297, 300–301, 305, 307–308, 312–319, 333, 341, 348, 358, 386, 390
 - host, 334–336
 - materials, for OLEDs
 - phenylazomethines, 321
 - triarylamines, 312–320
 - triphenylmethanes, 320
 - for print-based OLED manufacturing, 569–570
 - properties of PF, 137–138
 - triarylamine-based materials, 146, 149–150
 - Hole transport layer (HTL), 10, 528–529, 537–539, 543–544, 568
 - HOMO, *see* Highest occupied molecular orbital
 - Homopolymers, light-emitting thiophene
 - emission color tuning in, 192–199
 - PT as red-light emitters, 187–190
 - regioregularity effect on electroluminescence, 190–192
 - Host–guest molecular system, 415
 - Host materials, nonconjugated polymers as, 417–428
 - HTL, *see* Hole transport layer
 - Hydrogen bonding, 340
 - Hydroxyethyl methyl methacrylate (HEMA), 467
- I**
- Ide 102, blue dopant, 353
 - Idemitsu Kosan (IK), 649–652
 - Impression printing process, 577
 - Incandescent lighting, 555
 - Indium tin oxide (ITO), 419, 459, 483–507, 568, 595
 - electrode, 7, 47, 296
 - Initiators, phenolic, 55
 - Ink-jet printing, 88, 216, 306, 536, 552, 568, 573–574, 576–577
 - Inks
 - of EL polymers, 569–571
 - LEP, 575–576
 - printable transparent conductive, 570
 - silver-based, 573
 - Inq3, 323–324
 - Integrated shadow mask (ISM), 547
 - Interface, 10–11, 13, 15, 17, 20, 76, 244, 299, 303–305, 308–314, 357, 369, 386–387, 394, 464, 494–495, 498, 500, 507, 516, 537–539, 543, 569, 618, 620–622, 628
 - dipole, 304, 387
 - Internal quantum efficiency, 6, 414–415, 540–543
 - Inverse photoelectron spectroscopy (IPES), 632
 - Ionic conductivity, 21–22
 - Ionic dopants, 569, 571–572
 - Ionization potential (IP), 145, 175, 207, 313, 429, 539, 631–632
 - Ir(Bu-ppy)₃, chemical structure of, 434
 - Ir(DcO-ppy)₃, chemical structure of, 434
 - Ir(DMO-ppy)₃, 431
 - Iridium complex(es)
 - heteroleptic, 377
 - homoleptic, 378
 - phenylisoquinoline, 375–376
 - phenylpyrazole, 378
 - phenylpyridine, 368–369, 377–378, 392, 543
 - synthesis, 370–372
 - Iridium-containing polymers, chemical structure of, 439
 - Iridium triplet complex, 430, 443
 - Ir(mppy)₃, chemical structure of, 422
 - Ir(Ocppy)₃, chemical structure of, 422
 - Ir(ppy)₃, chemical structure of, 419
 - ITO, *see* Indium tin oxide
 - ITO–hole-transporting layer (HTL) interface, 494
 - ITO pattern and cathode pattern of a seven-segment display, 27
- J**
- Joule heating, 322–328
- K**
- Ketone defects, 126, 222–223
 - Knoevenagel-coupling route, 56, 249–250
 - Knoevenagel polycondensation, 56
 - Kumada cross-coupling method, 186
- L**
- Ladder-type poly(*p*-phenylene) (LPPP), 7, 222–224
 - Langmuir, 53, 225, 234, 457, 536
 - Langmuir–Blodgett, 53, 225, 234, 457, 536
 - Langmuir–Blodgett films, 536
 - Lanthanide triplet complex, 298, 369, 414, 436
 - Laser, 16–17, 57–58, 63, 223, 339, 343, 348, 485, 528, 541, 547, 551–552, 557
 - Laser scanning confocal microscopy (LSCM), 622
 - Layer, monomolecular, 464
 - LCD, *see* Liquid crystal displays

- LCD projectors, 452
- LEC, *see* Light-emitting electrochemical cell architecture
- LEP, *see* Light-emitting polymers
- LEPs, commercial availability of, 259
- Lewis acid, 233, 304
- Li-doped, 311
- Lifetime, 528, 531, 537, 539, 542–543, 545–546, 548–550, 553, 555–556
- of emission, 377
- measurements, of OLEDs, 632–633
- Ligand, 153, 168–169, 323–325, 362–365, 368–379, 427, 434–435, 439, 441, 542, 640, 643, 645, 653
- Light
- circularly polarized, 451
- elliptically polarized, 454–455
- linearly polarized, 451–454, 469, 471
- polarized chromatic, 451–452
- polarized directly generated, 452
- Light-emitting diodes (LED), 1, 413
- degradation, 385
- emitting linearly polarized light, 452, 469
- lifetime, 34
- Light-emitting electrochemical cell architecture, 568–569
- Light-emitting electrochemical cells (LEC), 20–22, 24, 59, 74, 88, 93, 199, 215, 229, 429, 568–569, 571–572, 579
- dynamic junction in, 22
- with frozen junction operation, 22
- PT for, 200
- under pulsed operation with mean field, 22
- Light-emitting organic layer, printability of, 570–572
- Light-emitting polymer (LEP) devices
- encapsulation of, 577–579
- Light-emitting polymers (LEPs), classes of
- boron-containing polymers, 242–244
- carbazole-containing polymers, 228–233
- ladder type poly-*p*-phenylenes, 222–224
- oxadiazole polymers, 238–242
- oxazole polymers, 238–242
- PF, *see* Polyfluorenes
- phosphorus-containing polymers, 242–244
- poly(N-heterocycle)s, related, 233–238
- poly(phenylene ethynylene)s, 225–227
- poly-*p*-phenylenes, 214–222
- poly(pyridine)s, 233–238
- PPV, *see* Poly(*p*-phenylene vinylene)
- PT, *see* Polythiophenes
- silicon-containing polymers, 242–244
- substituted polyacetylenes, 227–228
- thiadiazole polymers, 238–242
- Light-emitting thiophene block copolymers, 199–200
- Light-emitting thiophene homopolymers
- emission color tuning in, 192–199
- PT as red-light emitters, 187–190
- regioregularity effect on electroluminescence, 190–192
- Linearly polarized photo- and electroluminescence
- Langmuir–Blodgett technique, 464
- LEDS emitting linearly polarized light, 469
- orientation of liquid-crystalline light-emitting materials, 464–469
- orientation of nonliquid-crystalline materials on orienting substrates, 462–464
- rubbing and friction deposition, 461–462
- tensile deformation, 457–461
- Li-NPTEOS-type compounds, 23
- Liquid-based processing, 567
- Liquid crystal
- chiral nematic, 471–472
- cholesteric, 471–472
- Liquid crystal displays (LCD), 365, 451–452, 461, 464, 471–472, 504, 507, 516, 528, 545, 548, 550, 557, 583–584, 588, 639
- backlit, 452
- twisted nematic, 472
- Liquid electroluminescent cells (LEC), 429
- Lithium fluoride (LiF), 61, 64, 72, 135, 148–150, 157, 163, 165, 170, 206, 211, 213, 233, 303, 309–311, 317, 354, 357–358, 364–368, 373, 377, 381, 384, 386, 389, 391, 393, 429, 439–440, 443, 469, 495, 516, 531, 572
- Lithium salts, 572
- Lower work-function electrode, 57
- Lowest unoccupied molecular orbital (LUMO), 414
- energy level, 13
- Low-molecular-weight liquid crystals, 464
- Low work function, 10, 12, 22–23, 69, 76, 87, 126, 177, 516, 531, 569, 572
- LPPP, *see* Ladder-type poly(*p*-phenylene)
- LPPP, chemical structure of, 436
- LSCM, *see* Laser scanning confocal microscopy
- Luminescence, circularly polarized, 457, 469–474
- Luminophores, helically arranged, 471
- Luminous efficiency, 629
- LUMO, *see* Lowest unoccupied molecular orbital
- ## M
- Marcus inversion region, 416
- Marcus theory, 416

- Materials, nonliquid-crystalline, 462–463
Matrix, chiral, 451, 471
Mauguin regime, 472
Maxwell's framework, 454
McCullough method, 186
 of preparation of regioregular HT poly(3-alkylthiophenes), 256–257
 for PT, 186
 for regioregular HT poly(3-alkylthiophenes), 256–257
Medical applications, 452
MEH-PPV, *see* Methoxy/2-ethylhexyloxy PPV
Mesogen, dislike, 466
Metal-catalyzed-coupling reactions, 185–187
 for PT, 185–187
Metal-catalyzed polycondensation, *see* Metal-catalyzed-coupling reactions
Metal chelate, 323–326, 328–329, 343, 348, 350, 363–365, 368, 651
 electron transport material, 323–326
Metallorganic electrophosphorescent polymers, 438–443
Methoxy/2-ethylhexyloxy PPV (MEH-PPV), 2–3, 5–7, 12–13, 16–19, 21, 25, 55, 58–60, 63–64, 67–69, 73, 76–78, 87, 90, 175, 202, 210, 235, 239–240, 259, 308, 324, 327, 415, 458–459
Microcavity, 16, 203, 502–504, 514–515, 548, 550
Mobility of charge carriers, 309
Molecular weight
 control of, 55–56, 123, 139, 156, 571, 576
 in end-capped PF, 139
 determination of, 59, 99, 122–124, 131, 171, 255–256, 259
 effect of, 59, 64, 69, 71, 81, 149, 152, 155, 178, 184–185, 188, 453, 457–458, 462, 464
 estimation of PF, 99
 solvent effects on, 2
Molecules
 form-anisotropic, 451, 456–458
 uniaxially oriented, 451–453, 457–469, 471
Monochromatic OLED displays, manufacturing, 30
Monochrome AMPLDs with solution-processible polymers, 29–30
Multiplexing operation of a four-digit segmental display, 27

N
Nanochemical analysis, 618
Naphthylanthracene-based polymer, 644
N-aryl-2-benzimidazolylphenol, metal complexes of, 643
Nematic, 9
Ni-catalyzed reaction, 123
Nile Red, 365–366
 chemical structure of, 425
Ni(0)-mediated polymerization, 188
NIR emission, 81, 98, 168, 192, 197, 205, 213
N,N'-Dicarbazoyl-3,5-benzene (mCP), host, 335, 337, 377, 390
N,N-diphenyl-*N,N*-bis(3-methylphenyl)-1,1-biphenyl-4,4-diamine (TPD), 149–150, 162, 164, 187, 206, 225, 307, 309, 312–317, 540
Nomarski microscopy, 531
Nomenclature, 454
Nonconjugated polymers as host materials, 417–428
Nonconjugated PPV
 block copolymers, 92–97
 containing oligo(phenylene vinylene) pendant substituents, 97–98
Nonemissive area, 619, 624, 632
Nonionic process, for PPV polymerization, 56
NPF-6, electron transport, 328–329

O
Odd-even effect, 473
Offset printing, 577
OLED, *see* Organic light-emitting diodes
OLED emitting materials, U.S. patents granted on
 Cambridge Display Technology (CDT), 644
 Covion, 650
 Dow Chemical, 646
 Eastman Kodak, 645
 Idemitsu Kosan, 652
 Universal Display Corporation (UDC), 646
OLED panel lifetime evaluation system, 632–633
OLEDs, microstructural characterization techniques, 617
 dual beam microscopy, 620
 electron spectroscopy for chemical analysis, 622–623
 laser scanning confocal microscopy, 622
 Raman spectroscopy, 623
 scanning electron microscopy, 618–620
 scanning probe microscopy, 620–622
 secondary ion mass spectrometry, 623–624
 transmission electron microscopy, 618
OLEDs, performance measurement techniques, 624
 human vision, light, and color, 624–626
 lifetime measurements, 632–633
 measurement and efficiency, 626–632

- Oligoethyleneoxy-substituted PPVs, 62
 - Oligomers, 49–50, 97, 120, 146, 184, 201, 203–205, 211, 225, 229, 252, 257, 313, 453, 464, 468–469
 - Oligo-2,5-thienylenevinylenes (OTV), 211, 213
 - Oligothiophenes, electroluminescent, 203–204
 - Onset voltage, 122, 459, 461
 - Optical destructive electrode for high contrast OLEDs
 - black cathode, 516–517
 - gradient refractive index anode, 517–522
 - Organic electroluminescence (OEL)
 - devices, 1, 32
 - ink, 569–571, 573
 - Organic-inorganic polymers, with POSS segments, 140
 - Organic light-emitting devices, 1–4
 - Organic light-emitting diodes (OLED), 330–331
 - anode materials for, 302–303
 - with a black cathode, 517
 - cathode interfacial materials for, 309–310
 - Li/Cs dopant with BCP and Li–quinolate complexes, 311
 - LiF, CsF, 310
 - M₂O, 310–311
 - organic polymer surfactants, 311–312
 - cathode materials for, 301–302
 - competition and markets for print-based, 579–580
 - device architecture of, 568–569
 - device structure, 297–300
 - schematic of multilayer, 300
 - display panel, power consumption of, 34
 - electron blocking materials, 389–390
 - electron transport materials, 322–323
 - fluorine-substituted electron transport materials, 328–329
 - metal chelate electron transport materials, 323–326
 - 4n- π and boron-based electron transport materials, 330
 - oxadiazole and triazole transport materials, 328
 - silole, 329–330
 - TPBI and N-containing aromatic transport materials, 326–328
 - function of layers of
 - charge recombination, 301
 - electron and hole injection from cathode and anode, 300–301
 - electron and hole migration through electron and hole transport layers, 301
 - hole blocking materials for, 386–389
 - hole injection materials for, 303–304
 - conducting polymers, 305–306
 - doping the hole transport materials, 308–309
 - fluorocarbon polymers, 307–308
 - inorganic hole injection materials, 308
 - organic–inorganic interface, 304–305
 - porphyrinic metal complexes, 305
 - SAM-TPD, 307
 - hole transport materials
 - phenylazomethines, 321
 - triarylaminines, 312–320
 - triphenylmethanes, 320
 - light emitting materials, fluorescent dopants, 338
 - blue fluorescent emitters, 349–365
 - green fluorescent dopants, 339–343
 - red fluorescent dopants, 343–349
 - white fluorescent organic light-emitting diodes, 365–369
 - light emitting materials, host–guest molecules, 330–333
 - light emitting materials, host materials
 - electron transport hosts, 333–334
 - fluorescent blue host materials, 337–338
 - hole transport hosts, 334–336
 - polymer hosts, 338
 - silane compound host materials for blue and white phosphorescent organic light-emitting diodes, 336–337
 - light emitting materials, phosphorescent dopants, 369–370
 - blue phosphorescent dopants, 377–379
 - green phosphorescent dopants, 372–375
 - red phosphorescent dopants, 375–377
 - synthesis of iridium complexes, 370–372
 - white phosphorescent organic light-emitting diodes, 379–382
 - operating mechanism
 - charge recombination, 301
 - electron and hole injection from cathode and anode, 300
 - electron and hole migration through electron and hole transport layers, 301
 - performance of the three primary color materials and device structures, 390–391
 - blue emitters and device structures, 393–394
 - green emitters and device structures, 392–393
 - red emitters and device structures, 391–392
 - pixel elements in PM displays, 28
 - sensitizers in, 385–386
 - stabilizers in, 382–385
 - structure, multilayer small molecule, 11
- Organic-metal interface, 304
- Organic phosphor materials, 571

- Organic photovoltaics, 567
Organic semiconductors, advantages of, 5
Organic solar cell, 348, 557
Organic vapor phase deposition (OVPD), 536
Organosiloxane, 307
Orientation
 layers
 conductive, 469
 photoaligned, 462
 methodologies, 453
 methods, 451
 uniaxial, 456–457, 462
OTV, *see* Oligo-2,5-thienylenevinylenes
Oxadiazole, 461, 463
1,3,4-Oxadiazole, electron transport, 60, 69, 71,
 142, 150, 152, 208, 328, 420, 440–441
Oxadiazole groups, 71, 84–85
 in PF, 150–153
Oxadiazole LEP polymers, 238–242
Oxadiazole-thiophene copolymers
 electrochemical and optical properties, 208, 213
Oxazole LEP polymers, 238–242
OXD-7, 204
 chemical structure of, 419
Oxidative coupling reaction, 122
 of PF homopolymers, 122
Oxidative defects, 223
Oxinoid complex, 331
Oxygen
 deficiency, 487, 492, 495
 plasma, 494–498, 533, 623
 treatment, 494–498, 623
 vacancy, 492, 495
P
PA, *see* Polyacetylenes
PANI, *see* Polyaniline
Parylene, 304, 624
P3AT, *see* Poly(3-alkyl)thiophene
Pauli exclusion principle, 414
PDHF, chemical structure of, 434
PDOF, chemical structure of, 422
PEDOT, *see* Polyethylenedioxythiophene
PEDOT-PSS, *see* Poly(ethylenedioxythiophene)-
 polystyrene sulfonate
Perylene, blue dopant, 338, 340–341, 348,
 355–357, 384, 386, 640
PF, *see* Polyfluorenes
Phenolic initiators, 55
Phenylazomethine dendrimer, 321
Phenylene-thiophene copolymers, 207–209
2-(5-Phenyl-1,3,4-oxadiazoyl)phenolatolithium
 (LiOXD), electron injection, 311
Phenyl-PPV, synthesis by dehydrogenation, 58
PhLPPP, chemical structure of, 436
Phosphorescent, 7, 10, 159, 229–230, 245,
 297–299, 320, 327, 331, 333–338, 369, 372,
 375–381, 385–387, 391–394, 413–445, 579,
 588, 618, 629–630, 640
 blue dopant, 334, 336, 338, 378, 380
 dendrimers, 443–444
 dopants, 369–371, 422
 blue dopant, 334, 336, 338, 377–380, 640
 green dopant, 372–375
 photophysical parameters of, 422
 red dopant, 375–377, 382
 emitters, 7, 331, 386, 392, 394
 green dopant, 372–375
 OLEDs, white, 379–382
 OLED technology, 629
 polyfluorenes, chemical structure of, 444
Phosphorescent polymer light-emitting diodes
 (PPLED), 413–414
 chemical structures of, 423
 configuration, multilayer, 419
Phosphor materials, organic, 571
Phosphorus-containing LEP polymers, 242–244
Photoalignment
 layer, 464, 470
 step, 468
Photo- and electroluminescent polymers, chemical
 structure of, 459
Photoconductivity, 5–6, 19
Photoexcitation, 2, 59, 233, 414
Photoisomerization, 472
Photoluminescence (PL), 5, 127
 circularly polarized, 454–457
 linearly polarized, 451, 454–469
Photonic stop-band, 472
Photooxidation, 125, 132, 623
Photophysical aspects of electrophosphorescence
 exciton transfer processes, 415–417
 singlet–triplet excitons ratio, 414–415
Photopic response, 540, 624–625
Photopumped solid-state lasing, 17
Photovoltaics, 223, 528, 557
PhqIr, chemical structure of, 422
Phthalocyanine derivatives, 641
p-i-n device, 13, 311
 architecture, 568–569, 571
Pinhole-free PPV thin films, 53
Pitch length, 471–472
PL, *see* Photoluminescence
Planarity, of polymer backbone, 184, 195
Planar PLEC in interdigitated cell configuration, 23
Planar PLED, in interdigitated cell
 configuration, 23

- Plasma, 32, 35, 122, 302, 304, 307–308, 341, 484, 494–498, 504, 507–508, 512, 533, 568, 595, 623
oxygen, 533
- PLEC, *see* Polymer light-emitting electrochemical cell
- PLED, *see* Polymer light-emitting diodes
- PL molecules, chiral, 451
- PMOT, chemical structure of, 438
- PMPLED
cross-section views of the device structures of, 28
- Polarization, 454
absolute, 455
circular, 472, 474
direction, absolute, 455
ratio, 126, 241, 456, 463, 466
right-handed, 454
- Polarized chromatic light, 451–452
- Polarized LEDs, performance of, 470
- Polarized light, elliptically, wave representation of, 455
- Polarized photoluminescence, linearly and circularly, 454–457
- Polarized polymer light-emitting diodes (PLED), 202–203
- Polarizer(s), 30–32, 453, 458, 460, 467, 469, 471, 516, 630
dichoric, 452
photoluminescent, 289, 451
- Polyacene, red fluorescent, 343, 348–349
- Polyacetylenes (PA), 4
electronic and molecular structures of, 5
substituted, 227–228
- Poly(3-alkyl)thiophene (P3AT), 2
- Polyaniline (PANI), 3, 7–9, 11, 16, 59, 61, 63, 66, 70, 75, 146, 155, 233–234, 239, 304–306, 568, 570, 631
CSA
infrared electric conductivity of, 8–9
optical transmission spectra, 8
- Polyblends, thin films of PANI–CSA complex in, 7
- Polycarbazoles, in PPLED, 436–438
- Polycarbonate, 201, 206, 308, 321, 458, 646, 651
- Polyelectrolytes, PPV, 88–89
- Polyethylene, 4–5, 216, 239, 458, 507, 510, 530, 569
electronic and molecular structures of, 5
- Polyethylenedioxythiophene (PEDOT), 3, 13–14, 57, 60–61, 67, 69–77, 80–81, 85, 87, 89, 92, 94, 98, 121–122, 130, 139–145, 149–157, 162, 165–166, 168–169, 172, 174, 178–179, 183, 205–206, 211, 213, 220, 223, 230, 233, 235–237, 240, 420–443, 468–470, 512–515, 568, 596, 605
- Poly(ethylenedioxythiophene)-polystyrene sulfonate (PEDOT-PSS), 7–8, 59, 295, 304–305, 307, 319, 354, 359, 469, 568, 570, 573, 623, 627–629
optical transmission spectra of, 8
- Polyethylene terephthalate (PET), 530
- Polyfluorenes (PF), 3, 7, 181–184
aromatic ring-substituted, 128–129
based polyelectrolytes, 178–181
blends with other polymers, 144–145
color tuning in
alternating copolymers, 160–169
doping with low molar-mass fluorescent dyes, 159–160
random (statistical) copolymers, 169–177
with three or more comonomer units, 177–178
copolymers, *see* Polyfluorene copolymers
electronic properties, 120–122
end-capping groups in, 139–143
homopolymers, 122–124
optical properties, 120–122
physical properties of, 100–119
polymerization
Ni-catalyzed reaction, 123
oxidative coupling reaction, 122
Suzuki-coupling method, 124, 252–253
Yamamoto method, 123, 253–255
in PPLED, 428–432
pure blue emission contamination, 124–128
side-chain modifications in, 129–139
stability and phase behavior, 99, 119–120
synthesis of PF monomers, 250–252
three dimensional, 144
triphenylamine substituted, 137–139
- Polyfluorene copolymers, 145–159
alternating, 146–147
carbazole substituted, 146–147
with interrupted conjugation, 157
with oxadiazole pendant groups, 152
random, 146–147
with triarylamine and fluorene compounds, 148–149
with triarylamine compounds, 148–149
with triphenylamine and oxadiazole pendant groups, 151–152
- Polyhedral oligomeric silsesquioxane (POSS) group, 140
- Polyimide, 234, 304, 317–318, 651
rubbed, 461
- Polymer(s)
emitters, luminance–voltage plots of, 19
hairy-rod, 464–465

- hosts, 458
 - photophysical parameters of, 422
- laser diodes, 16–17
- light-emitting electrochemical cell (PLEC), 20
- morphology, solvent effects on, 4–5
- optocoupler, 24–25
- photoaddressable, 467
- RGB emitters, CIE coordinates of, 20
- solubility, 58–59, 65, 68, 93, 132, 185, 357, 571–572, 647–648
- Polymerization
 - by Knoevenagel reaction, 346
 - method, effect on polymer properties, 188–190
 - of PF homopolymers
 - Ni-catalyzed reaction, 123
 - oxidative coupling reaction, 122
 - Suzuki-coupling synthesis, 124
 - Yamamoto method, 123
 - of PFs
 - Suzuki-coupling synthesis, 252–253
 - synthesis of PF monomers, 250–252
 - Yamamoto method, 253–255
 - of PPVs by
 - chemical vapor deposition (CVD), 53
 - chlorine (bromine) precursor route, 247–248
 - chlorine precursor route, 56
 - by Diels–Alder reaction, 64
 - electrolysis, controlled potential, 57
 - Gilch method, 54–56, 247–248
 - Heck-coupling route, 56–57, 248–249
 - Knoevenagel-coupling route, 249–250
 - Knoevenagel polycondensation, 56
 - nonionic route, 56
 - ring-opening metathesis polymerization, 54
 - thermoconversion (Wessling–Zimmerman route), 53, 245–247
 - Wittig or Wittig–Horner condensation, 57
 - of PTs by
 - chemical oxidative polymerization, 185–187
 - electropolymerization, 185–187
 - Kumada cross-coupling method, 186
 - McCullough method, 186
 - for regioregular HT poly(3-alkylthiophenes), 256–257
 - metal-catalyzed-coupling reactions, 185–187
 - Ni(0)-mediated polymerization, 188
 - polymerization of thiophene monomers with FeCl₃, 255
 - Rieke-nickel-catalyzed polymerization, 259
 - Rieke-zinc (Zn*)-mediated method, 186, 257–259
 - by Ullmann reaction with Cu powder, 188
 - Yamamoto method, 255–256
 - yield, 55
- Polymer light-emitting diodes (PLED), 2, 26
 - conjugated polymers in, 4–9
 - energy band structure of, 13
 - light intensity in, 18
 - L–V and I–V characteristics of, 14
 - sandwich configuration, 10
 - structures, processes, and performance, 10–18
- Polyoxyethylene tridecyl ether, 312
- Poly(phenylene ethynylene)s (PPE), 225–227
- Poly(*p*-phenylene) (PPP), 7, 214–222; *see also*
 - Ladder type poly-*p*-phenylenes
 - containing naphthalene and anthracene moieties, 220
 - in PPLED, 432–436
 - rubbed, 463
- Poly(*p*-phenylene vinylene) (PPV), 5, 51–52, 98
 - absorption and electroluminescence of, 6
 - chemical structure modification in, 58
 - conjugated copolymers
 - with electron donor and aryl substituents, 73–81
 - with electron-withdrawing substituents, 81–87
 - conjugation control
 - conjugated and nonconjugated block copolymers, 92–97
 - conjugated systems with twists, meta-links, and sp-hybridized atoms in backbone, 89–92
 - nonconjugated polymer, 97–98
 - polyelectrolytes, 88–89
 - polymerization, methods for
 - anionic copolymerization, 57
 - chemical vapor deposition (CVD), 53
 - chlorine precursor route, 56
 - electrolysis, controlled potential, 57
 - Gilch polycondensation, 54–56
 - Heck-coupling polymerization, 56–57
 - Knoevenagel polycondensation, 56
 - nonionic route, 56
 - ring-opening metathesis polymerization, 54
 - thermoconversion (Wessling–Zimmerman route), 53
 - Wittig or Wittig–Horner condensation, 57
 - polymerization by
 - chlorine (bromine) precursor route, 247–248
 - Gilch polymerization, 247–248
 - Heck-coupling route, 248–249
 - Knoevenagel-coupling route, 249–250
 - Wessling–Zimmerman (thermoconversion) route, 245–247
 - structure, 644–645
 - substituted homopolymers of, 57–58

- alkoxy-substituted PPV, 58–62
- alkyl-substituted PPV, 62–63
- aryl-substituted PPV, 64–69
- PPV homopolymers with electron-withdrawing and donating substituents, 69–73
 - silyl-substituted PPV, 63–64
- Poly(pyridine)s containing polymer, 233–238
- Polypyrroles (PPY), 3, 7, 304–306
- Polystyrenes, 7, 63, 99, 123, 140, 145, 151, 201, 235, 239, 247, 249, 254, 306–311, 370, 418, 441, 458, 461, 568, 646
- Polytetrafluoroethylene (Teflon), 246–247, 249, 257, 304, 308, 340, 462
- Polythiophenes, 2–3
 - helical organizations of, 473
 - in PPLEd, 438
- Polythiophenes (PT), 184
 - blends, 200–202
 - electroluminescent oligothiophenes, 203–204
 - HH coupling effect, 187
 - for light-emitting electrochemical cells, 200
 - light-emitting thiophene block copolymers with conjugation break, 199–200
 - light-emitting thiophene homopolymers
 - emission color tuning in, 192–199
 - PT as red-light emitters, 187–190
 - regioregularity effect on electroluminescence, 190–192
 - polymerization
 - chemical oxidative, 185–187
 - electropolymerization, 185–187
 - by Kumada cross-coupling method, 186
 - by McCullough method, 186
 - McCullough method of preparation of
 - regioregular HT poly(3-alkylthiophenes), 256–257
 - metal-catalyzed-coupling reactions, 185–187
 - Rieke-nickel-catalyzed polymerization, 259
 - Rieke-zinc (Zn^{*})-mediated polymerization, 257–259
 - of thiophene monomers with FeCl₃, 255
 - Yamamoto polymerization, 255–256
 - regioregular polymers of, 190–192
 - for structured and polarized polymer light-emitting diodes, 202–203
 - thiophene copolymers with other conjugated moieties
 - with aromatic moieties, 207–208
 - with heteroaromatic moieties, 208–213
 - thiophene-*S,S*-dioxides as emissive and electron transport moieties, 205–207
 - unsubstituted, 185
- Polyvinylcarbazol (PVK), 568
- Polyvinylchloride, 201, 458
- Porphyrine, 87
- Porphyrinic metal complex, 303, 305–306
- POSS, *see* Polyhedral oligomeric silsesquioxane group
- Postdeposition treatment, 485
- Power consumption, 10, 25–26, 29–30, 32–35, 507, 547, 549, 584, 588, 629–630
- Power efficiency, 10, 26, 30, 32–33, 35, 69, 81, 165, 175, 178, 182, 311, 339, 341–342, 345–346, 356, 358, 362–363, 366, 370, 377–378, 380, 382, 384–385, 391–393, 419, 421, 427, 429, 436, 441, 443, 445, 540–541, 543, 546, 556, 584, 629
 - in AMPLED, 30
- PPE, *see* Poly(phenylene ethynylene)s
- PPEP, chemical structure of, 438
- PPP, *see* Poly-*p*-phenylenes
- PPV, *see* Poly(*p*-phenylene vinylene)
- PPV copolymers, conjugated
 - with electron donor and aryl substituents, 73–81
 - with electron-withdrawing substituents, 81–87
 - cyano-substituted, 81–83
- PPV homopolymers with electron-withdrawing and donating groups, 69–73
- PPY, *see* Polypyrroles
- Primary colors, 17, 30, 331, 379, 390, 452, 625
- Print-based manufacturing of OLEDs
 - materials for
 - electron injecting materials, 572–573
 - electron transporting materials, 572–573
 - hole-injecting materials, 569–570
 - hole transporting materials, 569–570
 - light-emitting organic layer materials, 570–572
 - technologies, 573
 - ink-jet printing, 573–574
 - roll-to-roll printing, 577–578
 - screen printing, 574–576
- Print-based manufacturing technologies, 573
 - ink-jet printing, 573–574
 - roll-to-roll printing processes, 577–578
 - screen printing, 574–576
- Projection systems, 471
- PT, *see* Polythiophenes
- PtOX, chemical structure of, 422
- Purity
 - of colors, 181, 191, 339, 341, 349, 386, 433, 542, 649
 - of blue emission, 140, 169, 245, 351, 356–357, 378, 389
 - of green emission, 363
 - or red emission, 345
 - of materials, 7, 413, 573

PVK, *see* Polyvinylcarbazol
PVK, chemical structure of, 419

Q

Quarter-wave plate, 471

Quenching

- aggregate, 369–370
 - aggregation-induced, 216
 - charge transfer, 208
 - of emission
 - amplification of, 223
 - by defects, 222–223
 - in devices, 11
 - by functional groups and fragments, 126
 - intermolecular, 158
 - in multicomponent blends, 137–138
 - suppression of, 139, 142
 - interchain-fluorescent, 66
 - site, 309, 538
 - triplet–triplet, 369–370
- Quinacridone, 642
- fluorescent, 339–341, 384, 640
 - green dopant, 339–340

R

- Radiance, 625
- Radiant intensity, 625
- Radiative decay, 332, 413–416, 537–538
- Radiative recombination of excitons, 630
- Raman spectroscopy, 623
- Random PF copolymers, 146–148
- color tuning in, 169–177
 - with spiro-fluorene moieties, 156
- Rare earth metal, red fluorescent, 391
- Recombination, 7, 10–11, 21, 125, 140, 145, 301, 317, 336, 366, 414, 418, 420, 429, 452, 462, 500, 537, 630, 651
- Recycling mirror, 474
- Red fluorescent dopants
- DCM series, 343–346
 - metal chelates, 348–349
 - polyacenes red emitters, 348
 - push–pull red emitters, 346–348
- Red-light emitters, 187–190
- Red phosphorescent dopants, 375–377
- 2-benzo[b]thiophen-2-yl-pyridine iridium complexes, 375
 - phenylisoquinoline iridium complexes, 375–377
- Reflection band, 472
- Regioregularity
- of polymer, 122, 162, 193, 198, 213, 258

- effect of, on electroluminescence in PT, 186–187, 190–193
 - of polymerization process, 122
- Regioregular polymers, of PT, 190–192, 197
- Resonance regime, 472
- Rieke-nickel-catalyzed polymerization, 259
- for PT, 259
- Rieke-zinc method, for PT, 186
- Rieke-zinc (Zn*)-mediated method, 186, 257–259
- Ring-opening metathesis polymerization (ROMP), 54
- for PPV, 54
- Roll-to-roll printing, 568, 577–578
- Rubbing, 457, 470
- alignment, 461–462
- Ru(Ph2phn)₃, chemical structure of, 422
- ## S
- SbCl₅, 304
- Scanning electron microscopy (SEM), 618–620
- Scanning probe microscopy (SPM), 620–622
- Schottky diodes, 2
- Scratches, mechanical, 462
- Screen printing, 574–577
- Secondary ion mass spectrometry (SIMS), 623–624
- Security features, 451
- Self-assembled monolayer, 23, 498
- Self-assembled silane compound, 303
- SEM, *see* Scanning electron microscopy
- Sensitizers, 19, 346, 382–383, 385–386, 425
- Ir(ppy)₃, 385–386, 424
- Shadow mask, 12, 24, 30, 512, 532–533, 536, 547, 551–552, 557
- Sheet polarizers, dichroic, 452, 458
- Sheet resistance, 487, 494–496, 498, 508, 512, 520, 595
- Silicon-containing polymers, 242–244, 270
- Silole compound, electron transport, 329–330
- Silver-based ink, 573
- Silver nanoparticle inks, 573
- Silyl-substituted PPV, 63–64
- SIMS, *see* Secondary ion mass spectrometry
- Si₃N₄, 304
- Single-layer LED emitting polarized light
- architecture of, 453
- Single nozzle head, 557
- Singlet–triplet
- energy gap, 436
 - ratio of excitons, 60, 414–415, 439
- SiO₂, 59, 223, 304, 308, 346, 530, 533, 570
- nanoparticles, 59

Small molecule organic light-emitting diodes (SMOLED), 2

Solution-processible organic semiconductors
AMOLED for graphic and motion picture applications, 34–35

full-color AMOLED modules, 30–32

monochrome AMOLEDs, 29–30

performance simulation for full-color

AMOLEDs, 32–34

PMOLED displays *versus* AMOLED displays, 26–29

SMOLEDs and PLEDs as emitter elements in flat-panel displays, 25–26

Solvent effects

on emission, 58, 138–139, 152, 179, 206, 248, 250–251, 571

on molecular weight, 2, 55, 69, 72, 123, 147, 170, 178, 576

on polymer morphology, 4–5, 58, 67, 119–120, 131, 141, 155, 157, 180, 235, 244, 247, 252, 255–256, 312, 318, 420, 458, 571–574, 576

Solvent evaporation rate, 571, 576

Space charge density, 626

Spin-cast devices, 570–571

Spin coating, 12

Spin-orbital coupling, 184

Spin-symmetric excitons, 6

Spin symmetry, 6

Spiro-anthracene substituted PF, 135

Spiro-fluorenes, 135

Spiro-linked, blue emitter, 358, 361

SPM, *see* Scanning probe microscopy

Stabilizer, rubrene, 346, 366, 382–384, 391

Stainless steel foil substrate, 584

Starburst triarylamine, 316

Steric effects, 193

Steric hindrance, 214–215

Stress relaxation, 486

Stretch alignment, 461

Structure

hairy-rod, 466

patterned, 203, 468

pixilated, 468

rodlike, 468

Styrene-containing PF, 141–142

Subparticle, 619–620

Substituents effect

on band gap

in PPPs, 215–216

in PPV, 63

on charge transport properties, 71, 85, 122, 145, 161, 178, 317, 362

on device efficiency, 528, 540

on emission wavelength, 78, 325

on HOMO and LUMO levels

in PPVs, 62, 72

in PT, 190

on HOMO/LUMO or redox potentials, 121, 306, 390

on quenching, 340, 372

on reactivity, 124, 344

on solubility

in PFs, 132, 135, 138

in PPVs, 65

on solubility/processability, 65, 68, 155

on stability, 64

on TBB defects in PPV, 75

Surface

dipole model, 495

modification, 307, 498, 500, 577

morphology, 485, 494, 622

treatment, 302, 494–502, 521, 530, 570

Suzuki-coupling synthesis, 124, 252–253

of PF homopolymers, 124

for PFs, 252–253

Switches, photochemical, 471

T

TAZ, chemical structure of, 419

TBB, *see* Tolane-bisbenzyl defects

TBP, blue fluorescent dopant, 355–356, 358, 640, 643

TCO, *see* Transparent conducting oxides

TEM, *see* Transmission electron microscopy

Temperature dependence of electric conductivity, 9

Tensile alignment, 461

Tensile deformation, 457–461

4-Tert-butylbenzyl chloride, 55

Tetrafluorotetracyanoquinodimethane (F4-

TCNQ), p-i-n, 304, 308–309, 357, 393, 543

(2,2,6,6-Tetramethylpiperidyl-1-oxyl (TEMPO)), 55

2,5,8,11-Tetra-tert-butylperylene (TBP), 640, 643

Thermal annealing, in PPV, 56

Thermal stability

of fluorene homo- and copolymers, 99

of silyl-substituted PPVs, 64

Thermochromism, 184, 197

in PT films, 184

Thermoconversion (Wessling–Zimmerman route)

method, 245–247

germylated-PPVs, 64

for PPVs, 53, 245–247

Thiadiazole, 152, 164, 178, 238–242, 348, 649–650
polymers, 238–242

- Thickness uniformity, 485
- Thin-film conformability, 584
- Thin-film polymer devices, novel devices and functions in
- dual-function polymer device and display matrices, 18–20
 - optocouplers made with semiconducting polymers, 24–25
- PLED and PLEC in surface cell configuration, 23–24
- PLED with stable cathode electrode, 22–23
- polymer light-emitting electrochemical cells, 20–22
- Thin-film-transistor (TFT), 28
- Thiophene copolymers
- with aromatic moieties, 207–208
 - with heteroaromatic moieties, 208–213
- Thiophene rings, types of coupling of, 185–186
- Three dimensional (3D) polyfluorenes (PF), 144
- Threshold voltage, 170, 534, 548, 588–594, 596, 598–601, 605, 628
- Tolane-bisbenzyl (TBB) defects, in polymer, 55
- in PPV copolymers, 75
 - solvent effect on formation, 67
 - substituents effect, 65–66
- TPBI, electron transport, 326–327, 334, 342, 348, 356–358, 373, 385–387, 389, 392, 420, 432, 443
- Transmission electron microscopy (TEM), 618
- Transparent conducting oxides (TCO), 483–484
- Transparent conducting thin films
- indium tin oxide (ITO)
 - composition and surface electronic properties, 492–494
 - electrical properties, 487–489
 - optical properties of, 489–492
 - preparation, 484–485
 - structural properties, 485–487 - transparent conducting oxides (TCO), 483–484
- Transport layer, 10–11, 162, 239, 297, 301, 311–312, 363, 462–463, 528, 534, 538, 543, 570, 629–630
- Trapping of charge or excitons, 140, 174, 342, 351, 353, 382, 384, 417–418, 426–427, 430, 443, 445
- Triarylamine
- compound, 148, 312, 314
 - as end-cappers, 140
 - as hole transport materials, 137, 139–140, 142, 148–149, 204, 235, 296–297, 312, 358, 441
 - in main polymer chain, 140, 237, 644
 - as side groups, 149
- Triazole, 334, 338
- 1,2,4-Triazole, electron transport, 328, 334
- Triphenylamine, 309, 313–314, 316, 373
- substituted PFs, 137–139
- Triphenylmethane, 312, 320
- Triplet exciting, 7, 331–333, 385, 537, 542
- Triplet excitons, 7
- Triplet-triplet annihilation, 337, 349, 546
- Tris(4-bromophenyl)aminium
- hexachloroantimonate (TBAHA), 308–309
- 4,4',4''-tris(N,N-diphenylamino)triphenylamine (TDATA), hole transport, 309, 316
- 1,3,5-tris(*N*-phenylbenzimidazol-2-yl)benzene (TPBI)
- electron transport, 326–327, 334, 342, 348, 373, 386–387, 389, 420, 432, 443
 - hole blocking material, 334, 386–389
- Tris(quinolinolate)aluminum (III) Alq₃, 7, 11, 148–150, 165, 203, 227–228, 296–297, 303, 309–317, 321, 323–334, 339–349, 351, 353–359, 362–366, 368–370, 375, 379, 381–393, 419–424, 539–542
- Tuning, of color
- in light-emitting thiophene homopolymers, 192–199
 - in PFs
 - alternating copolymers, 160–169
 - doping with low molar-mass fluorescent dyes, 159–160
 - random (statistical) copolymers, 169–177
 - with three or more comonomer units, 177–178 - in PPV block copolymers, 95
- Turn-on-current density, 605
- Turn-on voltage, 24, 47, 61, 63–64, 67, 69, 71, 73–74, 80–81, 83–85, 95, 97–98, 130, 132, 139, 146, 149–154, 157, 162, 164–166, 172, 175–176, 191, 198, 203, 206, 245, 314, 317, 345, 358, 362, 365, 373–374, 383, 387, 429–432, 442, 474, 506, 613, 630
- U
- UHMW-PE, 458, 460
- Ullmann reaction, 188
- Ultraviolet photo electron spectroscopy (UPS), 304–306, 308–309, 324
- UNIAX, 2, 11, 16, 26
- Universal Display Corporation, 646, 648
- UV ozone exposure, 533
- V
- Vacuum deposition, 12
- Vacuum level, 77, 191, 304, 306, 308, 322, 333, 382–383, 538, 630, 632

Vapor-deposited organic light-emitting devices, 527–528
architecture, 529
 alternative device architectures, 531–532
 anode, 530
 cathode, 531
 organic materials, 530–531
displays
 active addressing schemes, 548–550
 full-color displays, 550–552
 passive addressing schemes, 545–550
future generation
 displays and beyond, 557
 flexible displays, 553–555
 lighting, 555–557
Vibronic structure, of emission band, 122–123, 171, 191, 197, 378, 394
Vision, black and white, 624

W

Water-soluble polymers, 88, 97, 178, 180–181, 225
Wavelength-dependent transmittance, 489, 508
Wessling–Zimmerman route, *see*
 Thermoconversion method

White, fluorescent, 379
White electroluminescent material, 643
White-emitting LEDs, 201, 223, 227, 244–245, 424, 432, 439, 441, 643
White phosphorescent organic light-emitting diodes, 379–382
Wittig–Horner condensation, 57
Work function, 10, 12–13, 15, 18, 22–23, 57, 67, 69, 72, 76, 87, 121–122, 126, 145, 149, 164, 177, 215, 234, 301, 441, 494–495, 506–507, 516–517, 520, 531, 533, 539, 568–569, 572, 630–631
 of materials relevant to LED devices, 631

X

X-ray photoelectron spectroscopy (XPS), *see*
 Electron spectroscopy for chemical analysis

Y

Yamamoto method, 123, 253–256
 for PFs, 253–255
 homopolymers, 123
 for PT, 255–256

Related Titles

Organic Electroluminescence

Zakya H. Kafafi, Naval Research Lab, Washington, D.C.

ISBN: 0824759060

Organic Photovoltaics

Sam-Shajing Sun, Norfolk State University, Norfolk, Virginia

ISBN: 082475963X

Organic Light-Emitting Diodes: Principles, Characteristics and Processes

Jan Kalinowski, Technical University of Gdansk, Poland

ISBN: 0824759478

New advances offer flexible, low-cost fabrication methods for light-emitting materials, particularly in display technologies. As researchers continue to develop novel applications for these materials, feasible solutions for large-scale manufacturing are increasingly important. **Organic Light-Emitting Materials and Devices** covers all aspects of organic light-emitting diodes (OLEDs), focusing on the unique characteristics of electroluminescent materials, device structures, and fabrication technologies.

Written by internationally recognized experts across several fields, this book compiles information on the synthesis, properties, and device performance of nearly 1,000 organic small molecule- and polymer-based electroluminescent materials. It also investigates practical manufacturing techniques for OLED fabrication as well as methods used for microstructural characterization, performance measurement, and defect analysis. Later chapters discuss the patent status of the currently employed organic light-emitting materials, potential applications of OLEDs, and the challenges facing future developments from both academic and industrial perspectives.

Combining organic materials synthesis with device physics and engineering, this single source of information—

- Summarizes the history, fundamental physics, structural design, and potential applications of OLED devices
- Enables quick access to the functions and applications associated with a comprehensive list of electroluminescent materials
- Highlights current research on fluorescent and phosphorescent polymer LEDs, polarized OLEDs, and transparent OLEDs
- Discusses techniques for solving real-world research problems, assessing performance, and failure analysis
- Compares ink jet printing and vapor phase deposition technologies for thin films preparation
- Explores the application of amorphous silicon (*a*-Si) based backplane for organic light-emitting displays

Incorporating the latest research on hundreds of light-emitting organic materials, **Organic Light-Emitting Materials and Devices** reflects the current understanding of molecular design in the field and reveals the most stable and efficient electroluminescent materials as well as the vast potential for future applications.



Taylor & Francis

Taylor & Francis Group
an informa business

A CRC PRESS BOOK
www.taylorandfrancisgroup.com

6000 Broken Sound Parkway, NW
Suite 300, Boca Raton, FL 33487

270 Madison Avenue
New York, NY 10016

2 Park Square, Milton Park
Abingdon, Oxon OX14 4RN, UK

DK3689

ISBN 1-57444-574-X



9 781574 445749